5/1

NASA Tech Briefs

National
Aeronautics and
Space
Administration

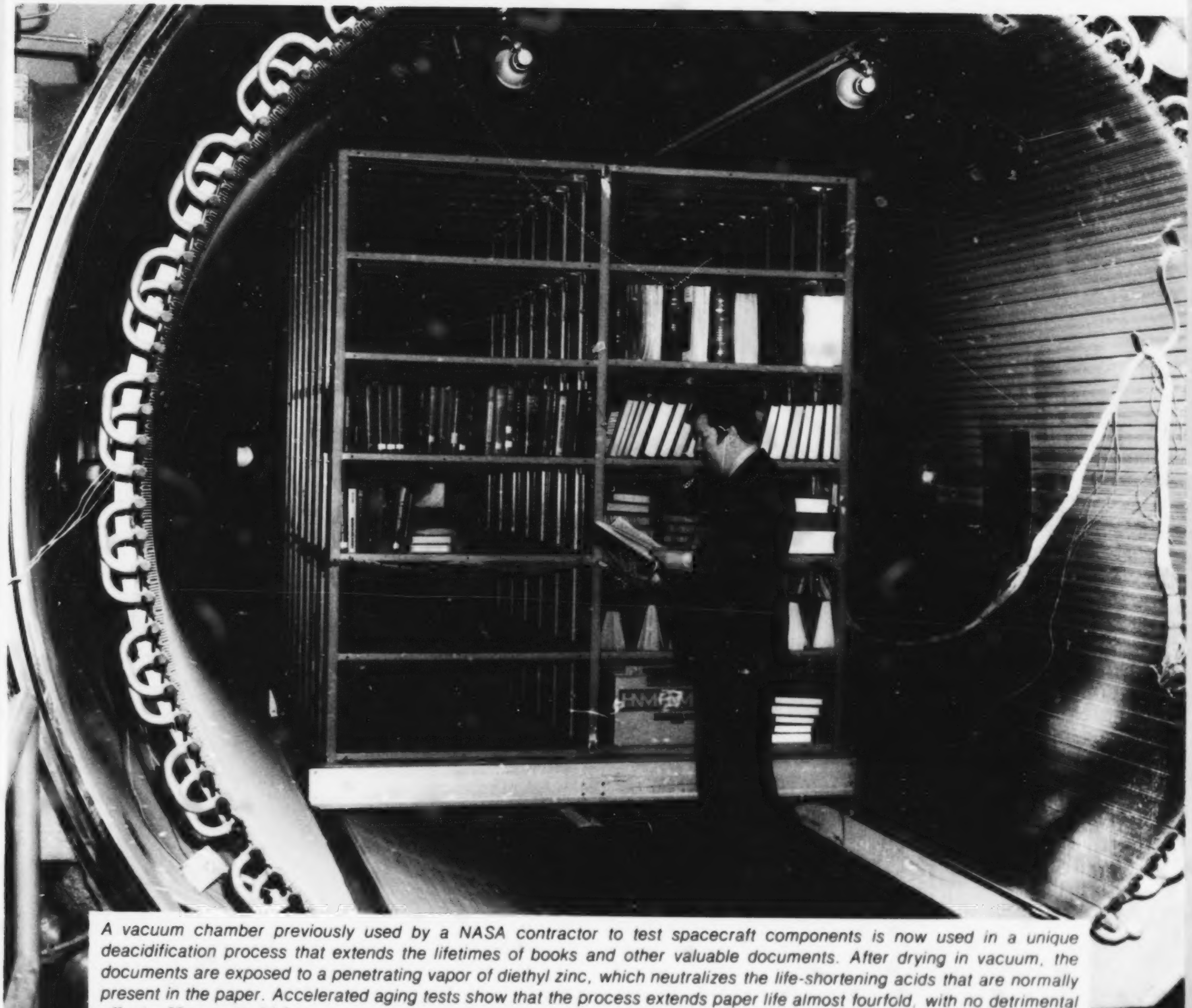

A vacuum chamber previously used by a NASA contractor to test spacecraft components is now used in a unique deacidification process that extends the lifetimes of books and other valuable documents. After drying in vacuum, the documents are exposed to a penetrating vapor of diethyl zinc, which neutralizes the life-shortening acids that are normally present in the paper. Accelerated aging tests show that the process extends paper life almost fourfold, with no detrimental effects. [See page A1.]

Vol. 5, No. 1

SPRING 1980

NAS 1.29/3:

About the NASA Technology Utilization Program

The National Aeronautics and Space Act of 1958, which established NASA and the United States civilian space program, requires that "The Administration shall provide for the widest practicable and appropriate dissemination of information concerning its activities and the results thereof."

To help carry out this objective, NASA's Technology Utilization (TU) Program was established in 1962. Now, as an element of NASA's Technology Transfer Division, this program offers a variety of valuable services to help transfer aerospace technology to nonaerospace applications, thus assuring American taxpayers maximum return on their investment in space research; thousands of spinoffs of NASA research have already occurred in virtually every area of our economy.

The TU program has worked for engineers, scientists, technicians, and businessmen; and it can work for you.

NASA Tech Briefs

Tech Briefs is published quarterly and is free to engineers in U.S. industry and to other domestic technology transfer agents. It is both a current-awareness medium and a problem-solving tool. Potential products . . . industrial processes . . . basic and applied research . . . shop and lab techniques . . . computer software . . . new sources of technical data . . . concepts . . . can be found here. The short section on New Product Ideas highlights a few of the potential new products contained in this issue. The remainder of the volume is organized by technical category to help you quickly review new developments in your areas of interest. Finally, a subject index makes each issue a convenient reference file.

Further Information on Innovations

Although some new technology announcements are complete in themselves, most are backed up by Technical Support Packages (TSP's). TSP's are available without charge and may be ordered by simply completing a TSP Request Card found at the back of this volume. Further information on some innovations is available for a nominal fee from other sources, as indicated. In addition, Technology Utilization Officers at NASA Field Centers will often be able to lend necessary guidance and assistance.

Patent Licenses

Patents have been issued to NASA on some of the inventions described, and patent applications have been submitted on others. Each announcement indicates patent status, if applicable.

Other Technology Utilization Services

To assist engineers, industrial researchers, business executives, city officials, and other potential users in applying space technology to their problems, NASA sponsors Industrial Applications Centers. Their services are described on page A6. In addition, an extensive library of computer programs is available through COSMIC, the Technology Utilization Program's outlet for NASA-developed software.

Applications Program

NASA conducts applications engineering projects to help solve public-sector problems in such areas as safety, health, transportation, and environmental protection. Applications teams, staffed by professionals from a variety of disciplines, assist in this effort by working with Federal agencies and health organizations to identify critical problems amenable to solution by the application of existing NASA technology.

Reader Feedback

We hope you find the information in *NASA Tech Briefs* useful. A reader-feedback card has been included because we want your comments and suggestions on how we can further help you apply NASA innovations and technology to your needs. Please use it; or if you need more space, write to the Director, Technology Transfer Division, P. O. Box 8256, Baltimore/Washington International Airport, Maryland 21240.

NASA Tech Briefs

National
Aeronautics and
Space
Administration

SPRING 1980
Volume 5, Number 1

NASA TU Services A3 Technology Utilization services that can assist you in learning about and applying NASA technology.

New Product Ideas A9 A summary of selected innovations of value to manufacturers for the development of new products.

Tech Briefs
1 Electronic Components and Circuits
19 Electronic Systems
29 Physical Sciences
43 Materials
57 Life Sciences
61 Mechanics
77 Machinery
93 Fabrication Technology
117 Mathematics and Information Sciences

Subject Index 123 Items in this issue are indexed by subject; a cumulative index will be published yearly.

COVERS: Further information on the Paper Preservation Process can be found in U.S. Patent No. 3,969,549, a copy of which can be obtained for 50 cents from the Commissioner of Patents and Trademarks, Washington, D.C. 20231. To obtain more information about the Seismic Testing Facility, Circle 83 on the TSP Request Card at the back of this issue of NASA Tech Briefs.

About This NASA Publication

NASA Tech Briefs, a quarterly publication, is distributed free to qualified U.S. citizens to encourage commercial application of U.S. space technology. For information on publications and services available through the NASA Technology Utilization Program, write to the Director, Technology Transfer Division, P. O. Box 8757, Baltimore/Washington International Airport, Maryland 21240.

"The Administrator of National Aeronautics and Space Administration has determined that the publication of this periodical is necessary in the transaction of the public business required by law of this Agency. Use of funds for printing this periodical has been approved by the Director of the Office of Management and Budget."

Change of Address

If you wish to have NASA Tech Briefs forwarded to your new address, use one of the Subscriptions cards enclosed in the back of this volume of NASA Tech Briefs. Be sure to check the appropriate box indicating change of address.

Communications Concerning Editorial Matter

For editorial comments or general communications about NASA Tech Briefs, you may use the Feedback card in the back of NASA Tech Briefs, or write to: The Publications Manager, Technology Transfer Division (ETD-6), NASA Headquarters, Washington, DC 20546. Technical questions concerning specific articles should be directed to the Technology Utilization Officer of the sponsoring NASA Center (addresses listed on page A4).

Acknowledgements

NASA Tech Briefs is published quarterly by the National Aeronautics and Space Administration, Technology Utilization Branch, Washington, DC: Administrator: **Robert A. Frosch;** Director, Technology Transfer Division: **Floyd I. Roberson;** Publications Manager: **D. W. Orrick.** Prepared for the National Aeronautics and Space Administration by **Logical Technical Services Corp.**: Editor-in-Chief: **Graham L. Gross;** Art Director: **Ernest Gillespie;** Managing Editor: **Jay Kirschenbaum;** Senior Editor: **Donald Blattner;** Chief Copy Editor: **Oden Browne;** Staff Editors: **Jerry Rosen, Ted Selinsky, George Watson;** Graphics: **Concetto Auditore, Luis Martinez, Pat McDermond;** Editorial & Production: **Richard Johnson, Rose Giglietti, Beth Rogers, Vincent Susinno, John Tucker, Ernestine Walker.**

This document was prepared under the sponsorship of the National Aeronautics and Space Administration.. Neither the United States Government nor any person acting on behalf of the United States Government assumes any liability resulting from the use of the information contained in this document, or warrants that such use will be free from privately owned rights.

NASA
TU SERVICES

READEX FICHE

NASA TECHNOLOGY UTILIZATION NETWORK

★ TECHNOLOGY UTILIZATION OFFICERS

Charles C. Kubokawa
Ames Research Center
Code AU: 240-2
Moffett Field, CA 94035
(415) 965-5333

Gussie Anderson
Hugh L. Dryden Flight Research Center
Code OD/TU Office - Room 2015
Post Office Box 273
Edwards, CA 93523
(805) 258-3311, Ext. 787

Donald S. Friedman
Goddard Space Flight Center
Code 702.1
Greenbelt, MD 20771
(301) 344-6242

John T. Wheeler
Lyndon B. Johnson Space Center
Code AT-3
Houston, TX 77058
(713) 483-3809

Raymond J. Cerrato
John F. Kennedy Space Center
Code PT-STA-1
Kennedy Space Center, FL 32899
(305) 867-2780

John Samos
Langley Research Center
Mail Stop 139A
Hampton, VA 23665
(804) 827-3281

Harrison Allen, Jr.
Lewis Research Center
Mail Code 7-3
21000 Brookpark Road
Cleveland, OH 44135
(216) 433-4000, Ext. 6422

Aubrey D. Smith
George C. Marshall Space Flight Center
Code AT01
Marshall Space Flight Center, AL 35812
(205) 453-2224

D. W. Orrick
NASA Headquarters
Code ETD-6
Washington, DC 20546
(202) 755-2244

John H. Warden
NASA Pasadena Office
4800 Oak Grove Drive
Pasadena, CA 91103
(213) 354-6420

Gilmore H. Trafford
Wallops Flight Center
Code OD
Wallops Island, VA 23337
(804) 824-3411, Ext. 201

● INDUSTRIAL APPLICATIONS CENTERS

Aerospace Research Applications Center
1201 East 38th Street
Indianapolis, IN 46205
E. G. Buck, director
(317) 264-4644

Computer Software Management and Information Center (COSMIC)
Suite 112, Barrow Hall
University of Georgia
Athens, GA 30602
(404) 542-3265

Kerr Industrial Applications Center
Southeastern Oklahoma State University
Durant, OK 74701
Robert Oliver, director
(405) 924-0121, Ext. 413

NASA Industrial Applications Center
LIS Building
University of Pittsburgh
Pittsburgh, PA 15260
Edmond Howie, director
(412) 624-5211

New England Research Applications Center
Mansfield Professional Park
Storrs, CT 06268
Daniel Wilde, director
(203) 486-4533

North Carolina Science and Technology Research Center
Post Office Box 12235
Research Triangle Park, NC 27709
Peter J. Chenery, director
(919) 549-0671

Technology Applications Center
University of New Mexico
Albuquerque, NM 87131
Stanley Morain, director
(505) 277-3622

Western Research Applications Center
University of Southern California
University Park
Los Angeles, CA 90007
Robert Mixer, acting director
(213) 741-6132

■ STATE TECHNOLOGY APPLICATIONS CENTERS

NASA/University of Florida
State Technology Applications Center
311 Weil Hall
University of Florida
Gainesville, FL 32611
Ronald J. Thornton, director
Gainesville: (904) 392-6760
Orlando: (305) 275-2706
Tampa: (813) 974-2499

NASA/University of Kentucky
State Technology Applications Program
109 Kinkead Hall
University of Kentucky
Lexington, KY 40506
William R. Strong, manager
(606) 258-4632

◆ PATENT COUNSELS

Robert F. Kempf
Asst. Gen. Counsel for patent matters
NASA Headquarters
Code GP-4
400 Maryland Avenue, S.W.
Washington, DC 20546
(202) 755-3954

Darrell G. Brekke
Ames Research Center
Mail Code: 200-11A
Moffett Field, CA 94035
(415) 965-5104

Paul F. McCaul
Hugh L. Dryden Flight Research Center
Code OD/TU Office - Room 2015
Post Office Box 273
Edwards, CA 93523
(213) 354-2734

John O. Tresansky
Goddard Space Flight Center
Mail Code: 204
Greenbelt, MD 20771
(301) 344-7351

Marvin F. Matthews
Lyndon B. Johnson Space Center
Mail Code: AM
Houston, TX 77058
(713) 483-4871

James O. Harrell
John F. Kennedy Space Center
Mail Code: SA-PAT
Kennedy Space Center, FL 32899
(305) 867-2544

Howard J. Osborn
Langley Research Center
Mail Code: 279
Hampton, VA 23665
(804) 827-3725

Norman T. Musial
Lewis Research Center
Mail Code: 500-311
21000 Brookpark Road
Cleveland, OH 44135
(216) 433-4000, Ext. 346

Leon D. Wofford, Jr.
George C. Marshall Space Flight Center
Mail Code: CC01
Marshall Space Flight Center, AL 35812
(205) 453-0020

Monte F. Mott
NASA Pasadena Office
Mail Code: 180-601
4800 Oak Grove Drive
Pasadena, CA 91103
(213) 354-2700

▲ APPLICATION TEAMS

William N. Fetzner, director
Advisory Center for Medical Technology and Systems
University of Wisconsin
1500 Johnson Drive
Madison, WI 53706
(608) 263-2735

Edmund R. Bangs, director
IIT Research Institute
10 West 35th Street
Chicago, IL 60616
(312) 567-4191

Doris Rouse, director
Research Triangle Institute
Post Office Box 12194
Research Triangle Park, NC 27709
(919) 541-6256

Tom Anyos, director
SRI International
333 Ravenswood Avenue
Menlo Park, CA 94026
(415) 326-6200, Ext. 2864

Eugene Schmidt, program coordinator
Stanford University School of Medicine
Cardiology Division
Biomedical Technology Transfer
703 Welch Road, Suite E-4
Palo Alto, CA 94304
(415) 497-5353

David MacFadyen, project director
Technology + Economics
2225 Massachusetts Avenue
Cambridge, MA 02140
(617) 491-1500

TECHNOLOGY UTILIZATION OFFICERS

Technology transfer experts can help you apply the innovations in NASA Tech Briefs.

The Technology Utilization Officer at each NASA Field Center is an applications engineer who can help you make use of new technology developed at his center. He brings you NASA Tech Briefs and other special publications, sponsors conferences, and arranges for expert assistance in solving technical problems.

Technical assistance, in the form of further information about NASA innovations and technology, is one of the services available from the TUO. Together with NASA scientists and engineers, he can often help you find and implement NASA technology to meet your specific needs.

Technical Support Packages (TSP's) are prepared by the center TUO's. They provide further technical details for articles in NASA Tech Briefs. This additional material can help you evaluate and use NASA technology. You may receive most TSP's free of charge by using the TSP Request Card found at the back of this issue.

Technical questions about articles *in NASA Tech Briefs are answered in the TSP's. When no TSP is available, or you have further questions, contact the Technology Utilization Officer at the center that sponsored the research [see page A4].*

NASA INVENTIONS AVAILABLE FOR LICENSING

Over 3,500 NASA inventions are available for licensing in the United States — both exclusive and nonexclusive.

Nonexclusive licenses for commercial use of NASA inventions are encouraged to promote competition and to achieve the widest use of inventions. They must be used by a negotiated target date but are usually royalty-free.

Exclusive licenses may be granted to encourage early commercial development of NASA inventions, especially when considerable private investment is required. These are generally for 5 to 10 years and usually require royalties based on sales or use.

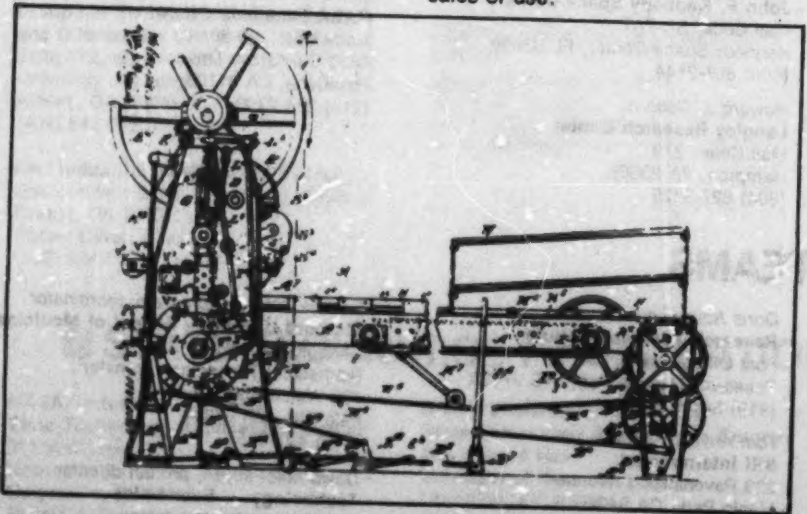

Additional licenses available include those of NASA-owned foreign patents. In addition to inventions described in NASA Tech Briefs, *"NASA Patent Abstract Bibliography"* (PAB), containing abstracts of all NASA inventions, can be purchased from National Technical Information Service, Springfield, VA 22161. The PAB is updated semiannually.

Patent licenses for Tech Briefs *are frequently available. Many of the inventions reported in NASA Tech Briefs are patented or are under consideration for a patent at the time they are published. The current patent status is described at the end of the article; otherwise, there is no statement about patents. If you want to know more about the patent program or are interested in licensing a particular invention, contact the Patent Counsel at the NASA Field Center that sponsored the research [see page A5]. Be sure to refer to the NASA reference number at the end of the Tech Brief.*

APPLICATION TEAMS

Technology-matching and problem-solving assistance to public-sector organizations

Application engineering projects are conducted by NASA to help solve public-sector problems in such areas as safety, health, transportation, and environmental protection. Some application teams specialize in biomedical disciplines; others, in engineering and scientific problems. Staffed by professionals from various disciplines, these teams work with other Federal agencies and health organizations to identify critical problems amenable to solution by the application of existing NASA technology.

Public-sector organization *representatives can learn more about application teams by contacting a nearby NASA Field Center Technology Utilization Office [see page A4].*

INDUSTRIAL APPLICATIONS CENTERS

Computerized access to nearly 10 million documents worldwide

Computerized information retrieval from one of the world's largest banks of technical data is available from NASA's network of Industrial Applications Centers (IAC's). The IAC's give you access to 1,800,000 technical reports in the NASA data base and to more than 10 times that many reports and articles found in 140 other computerized data bases.

The major sources include:

- *750,000 NASA Technical Reports*
- *Selected Water Resources Abstracts*
- *NASA Scientific and Technical Aerospace Reports*
- *Air Pollution Technical Information Center*
- *NASA International Aerospace Abstracts*
- *Chem Abstracts Condensates*
- *Engineering Index*
- *Energy Research Abstracts*
- *NASA Tech Briefs*
- *Government Reports Announcements*

and many other specialized files on food technology, textile technology, metallurgy, medicine, business, economics, social sciences, and physical science.

The IAC services range from tailored literature searches through expert technical assistance:

- *Retrospective Searches:* Published or unpublished literature is screened, and documents are identified according to your interest profile. IAC engineers tailor results to your specific needs and furnish abstracts considered the most pertinent. Complete reports are available upon request.
- *Current-Awareness Searches:* IAC engineers will help design a program to suit your needs. You will receive selected monthly or quarterly abstracts on new developments in your area of interest.
- *Technical Assistance:* IAC engineers will help you evaluate the results of your literature searches. They can help find answers to your technical problems and put you in touch with scientists and engineers at appropriate NASA Field Centers.

Prospective clients *can obtain more information about the services offered by NASA IAC's by contacting the nearest IAC [see page A4] or by checking the IAC box on a TSP Request Card in this issue.*

STATE TECHNOLOGY APPLICATIONS CENTERS

Technical information services for industry
and state and local government agencies

Local government and industry in Florida and Kentucky can utilize the services of NASA's State Technology Applications Centers (STAC's). The STAC's differ from the Industrial Applications Centers described on page A7, primarily in that they are integrated into existing state technical assistance programs and serve only the host state, whereas the IAC's serve multistate regions.

Many data bases, including the NASA base and several commercial bases, are available for automatic data retrieval through the STAC's. Other services such as document retrieval and special searches are also provided. (The STAC's normally charge a fee for their services.)

To obtain information *about the services offered by NASA STAC's, write or call the STAC in your state [see page A4].*

COSMIC®

An economical source of computer programs
developed by NASA and other government agencies

A vast software library is maintained by COSMIC — the Computer Software Management and Information Center. COSMIC gives you access to approximately 1,600 computer programs developed for NASA and the Department of Defense and selected programs for other government agencies. Programs and documentation are available at reasonable cost.

Available programs range from management (PERT scheduling) to information science (retrieval systems) and computer operations (hardware and software). Hundreds of engineering programs perform such tasks as structural analysis, electronic circuit design, chemical analysis, and the design of fluid systems. Others determine building energy requirements and optimize mineral exploration.

COSMIC services go beyond the collection and storage of software packages. Programs are checked for completeness; special announcements and an indexed software catalog are prepared; and programs are reproduced for distribution. Customers are helped to identify their software needs; and COSMIC follows up to determine the successes and problems and to provide updates and error corrections. In some cases, NASA engineers can offer guidance to users in installing or running a program.

Information about programs *described in NASA Tech Briefs articles can be obtained by completing the COSMIC Request Card at the back of this issue. Just circle the letters that correspond to the programs in which you are interested.*

NEW PRODUCT IDEAS

NEW PRODUCT IDEAS are just a few of the many innovations described in this issue of NASA Tech Briefs and having promising commercial applications. Each is discussed further on the referenced page in the appropriate section in this issue. If you are interested in developing a product from these or other NASA innovations, you can receive further technical information by requesting the TSP referenced at the end of the full-length article or by writing the Technology Utilization Office of the sponsoring NASA center (see page A4). NASA's patent-licensing program to encourage commercial development is described on page A6.

Multiband Microstrip Antenna

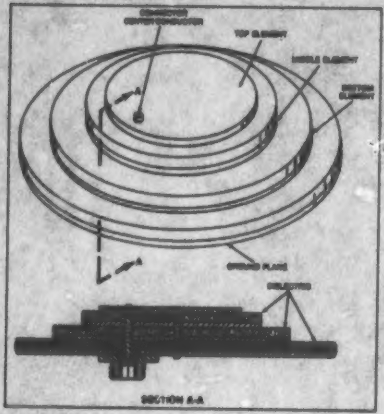
CONNECTOR CENTER CONDUCTOR
TOP ELEMENT
MIDDLE ELEMENT
BOTTOM ELEMENT
A
A
GROUND PLANE
DIELECTRIC
SECTION A-A

A compact, multiband microstrip antenna transmits and receives elliptically and circularly polarized radiation. The antenna consists of layers of elliptical disks separated by dielectric substrates. Each disk operates at a frequency determined by its size and the dielectric constant of the substrate. In principle, any number of elements may be included in a stack; if the sizes of the elements are close to each other in value, the individual frequency bands can be made to overlap, to yield a single broadband antenna. Standard microstrip techniques, involving sequential removal of material from a stack of conductors and insulators, can be used to build it.
(See page 3.)

Photoelectrochemical Cell With Nondissolving Anode

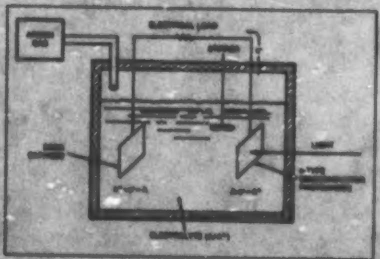
ELECTRICAL LOAD
LIGHT

Improved electrolytic photovoltaic cells have efficiencies comparable to those of the best silicon solar cells but are potentially less expensive to manufacture. The cells consist of a light-sensitive n-type semiconductor anode and a metallic cathode immersed in an electrolytic solution. Sunlight strikes the anode and establishes a current between the two electrodes. The reversible redox cells produce no chemical change in the electrolyte and stabilize the n-type semiconducting anode against dissolving. The cell can produce more than 500 mW of power per cm^2 of anode area at an output voltage of 0.4 V.
(See page 31.)

Cable-Splice Detector

A cable-splice detector has possible uses in aerial cable-car systems, in equipment handling in mines, boreholes, and undersea operations, and in other applications where moving steel cable must be measured, monitored, or controlled. Developed for the San Francisco cable-car system, the detector consists of a Hall-effect magnetic sensor that is located close to the cable. Magnetic markings on the cable are converted to electrical signals. The signals are filtered, amplified, and counted to actuate an alarm when a splice approaches a cable car.
(See page 63.)

Tubing Cutter for Tight Spaces

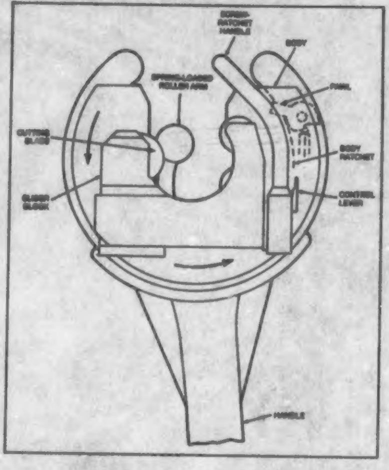
SCREW-RATCHET HANDLE
BODY
SPRING-LOADED ROLLER ARM
PAWL
CUTTING BLADE
BODY RATCHET
SLIDER BLOCK
CONTROL LEVER
HANDLE

A new tubing cutter requires only a few short swings of its handle to rotate its cutting edge a full 360° around a tube. It is ideal for cutting tubing installed in a confined space that would prevent the free movement of a conventional cutter. The cutter is snapped onto the tube and held in place by a spring-loaded clamp. A screw ratchet advances the cutting wheel until it contacts the tube. After each full rotation about the tube, the screw ratchet is turned so that the cutting blade penetrates deeper into the tube for the next cut.
(See page 84.)

Mechanical End Joint for Structural Columns

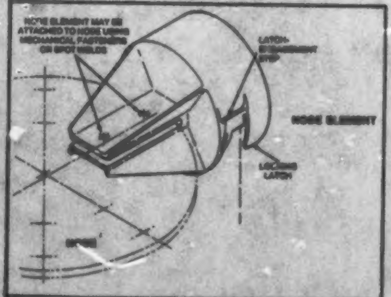
NOSE ELEMENT MAY BE ATTACHED TO NODE USING MECHANICAL FASTENERS OR SPOT WELDS
LATCH-ENGAGEMENT STOP
NODE ELEMENT
LOCKING LATCH

A connector for tubular struts permits the construction of lightweight frames without the use of tools or assembly equipment. The two main components are a node fitting and a strut element. To produce a structurally sound joint from the two components, they are alined approximately and pushed together. The design accommodates reasonable axial and rotational misalinement of nodes and struts. Also, individual columns can be inserted and removed between fixed nodes without affecting the integrity of the remaining structure. All joint components are interchangeable.
(See page 81.)

Fast-Response Atmospheric-Pollutant Monitor

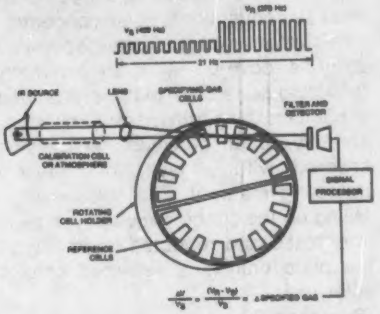
V_R (370 Hz)
V_S (400 Hz)
21 Hz
IR SOURCE
LENS
SPECIFIED-GAS CELLS
FILTER AND DETECTOR
CALIBRATION CELL OR ATMOSPHERE
SIGNAL PROCESSOR
ROTATING CELL HOLDER
REFERENCE CELLS
$\frac{\Delta V}{V_S} = \frac{(V_R - V_S)}{V_S}$ = ΔSPECIFIED GAS

A fast-response infrared spectrometer measures atmospheric CO, CH_4, and HCl over a range of 1 to 12 ppm. With some modifications it could measure other pollutants and use natural light as a source. A cell filled with the sample to be measured filters out the spectral lines of interest. The infrared beam passes through a rotating cell holder that produces chopped signals at two frequencies. The difference in signal amplitudes depends on the amount of test gas in the sample. Signal-processing circuitry amplifies and separates the test-gas and reference signals.
(See page 48.)

Self-Energized Screw Coupling

A novel threaded coupling carries its own store of rotational energy. Originally developed to ease the task of astronauts assembling structures in space, the coupling can offer the same advantages in other hazardous operations, such as underwater and in and around nuclear reactors. It could also be adapted to robotics. The coupling consists of two parts: a screw portion and a receptacle. When the screw portion is inserted into the receptacle and given a slight push by the operator, trigger pins release a ratchet, allowing the energy stored in springs to rotate the screw into a nut in the receptacle.
(See page 82.)

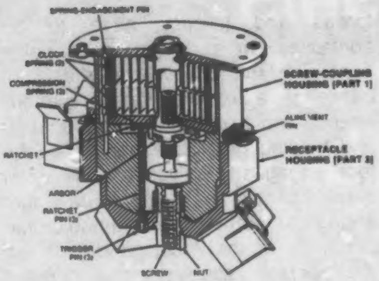
SPRING-ENGAGEMENT PIN
CLOCK SPRING (3)
COMPRESSION SPRING (3)
RATCHET
ARBOR
RATCHET PIN (3)
TRIGGER PIN (3)
SCREW
NUT
SCREW-COUPLING HOUSING (PART 1)
ALINEMENT PIN
RECEPTACLE HOUSING (PART 2)

Precision Filament Cutter

An automated filament cutter precisely chops filaments of glass, graphite, plastic, and other materials into fibers for use in composites and other applications. The cutter uses a movable blade that is pushed and pulled across a fixed blade. Because the mass of the movable blade is small and the stroke is short, operation is fast, and wear and energy consumption are low. Also, the push/pull motion of the blade speeds up operation by cutting on both forward and return movements. An operator selects the fiber length and chopping rate. After each cut, a blast of air blows the filament away so it can be collected.
(See page 79.)

Detecting a Coal/Shale Interface

A prototype coal/shale interface detector, which is intended to be used with a longwall shearer, determines when a cut has pierced through a coal layer. The detector combines the output of two optical reflectometers with that of a penetrometer. An accelerometer measures the hardness of the material struck by the penetrometer ram, while the reflectometers measure the reflectivity of the surface on both sides of the penetrometer. The signals are then combined in a voting circuit that indicates "coal" or "shale," depending on the information supplied by the three sensors. The penetrometer distinguishes between coal and shale by the differences in the accelerometer waveforms for the two materials.
(See page 47.)

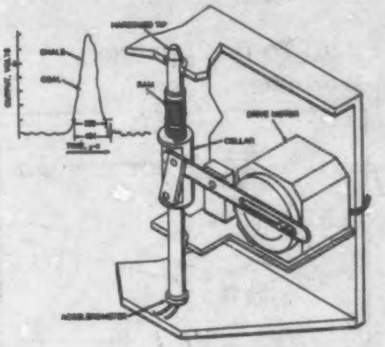
HARDENED TIP
SHALE
COAL
RAM
DRIVE MOTOR
COLLAR
ACCELEROMETER

Immersible Broadband Acoustic Transducer

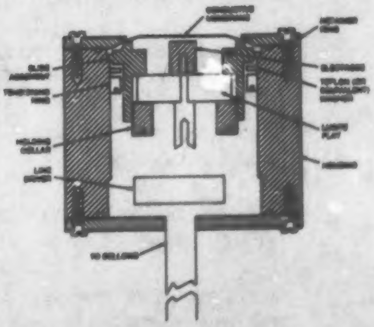

A broadband capacitive electrostatic transducer (ESAT) has been developed for use in liquids. Tests made with the transducer indicate that it may be useful as a broadband acoustic receiver with a predictable

frequency response. Since it measures the absolute displacement amplitudes of ultrasonic waves in liquids, it may be used as a calibrator for other transducers and as a probe for the nondestructive study and characterization of materials. The ESAT basically consists of a thin conductive membrane stretched over a metallic housing. Ultrasonic waves incident on the membrane cause it to vibrate and generate a signal proportional to the wave amplitude. The entire assembly is sealed for immersion in a liquid.
(See page 67.)

Zero-Torque Spanner Wrench

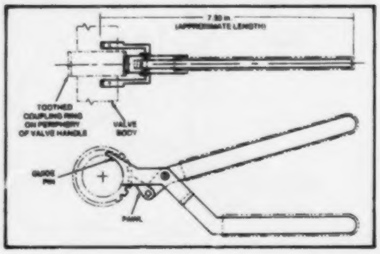

A proposed spanner wrench converts the gripping action of a hand to rotary motion. It does so without imparting reactive moments or forces on the part being turned or on the operator. The new wrench should be useful in undersea operations and other delicate work where reactive forces and torques have to be controlled. In a design for a valve tightening, the tool resembles a cross between a conventional spanner wrench and a pliers. Through locating and holding pins, one handle of the tool engages the valve body. The second handle has a ratchet pawl that engages a toothed coupling ring on the periphery of the valve handle. When the operator squeezes the handles together, the valve handle rotates with respect to the valve body.
(See page 90.)

Compact, Super Heat Exchanger

A compact, super heat exchanger uses porous media as a means of enhancing heat transfer through the walls of cooling channels, thereby lowering the wall temperature. Porous media within the cooling channel increase the internal surface area from which heat can be transferred to the coolant. Comparison data show that the wall has a lower temperature and the coolant has a higher temperature when a porous medium is used within a heat exchanger. The porous media can be sintered powdered metal, metal fibers, woven wire layers, or any porous metal having the desired permeability and porosity.
(See page 70.)

New Mounting Improves Solar-Cell Efficiency

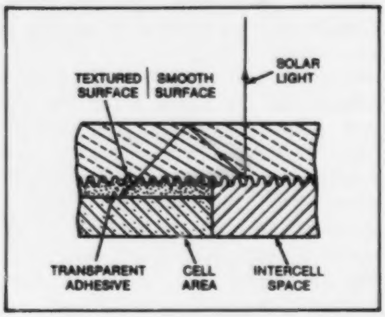

A new method of mounting and encapsulating solar cells boosts output by about 20 percent by trapping and redirecting solar radiation. This is done without the increased module depth needed for equivalent performance by conventional solar concentrators. When mounted, the solar-cell array is covered with an internally reflecting plate. The plate is attached to each cell by a transparent adhesive, and the space between the cells is covered with a layer of diffusely reflecting material. The solar energy falling on the space between the cells is diffused and reflected internally by the plate until it is reflected onto a solar cell.
(See page 32.)

Patent Licenses Recently Granted by NASA for Commercial Use of NASA-Owned Inventions

The patent licenses listed below are just a few of those recently awarded by NASA as part of its program to encourage the commercial application of its new technology. For information on how you may obtain nonexclusive or exclusive license for the commercial use of NASA inventions, see page A6 of this issue.

- A nonexclusive license to Fiber Materials, Inc., Biddeford, Maine, for U.S. Patent No. 4,072,532, covering an invention entitled "Hi-Temperature Resistant Cermet & Ceramic Compositions."

- A nonexclusive license to Foray Industries, Houston, Texas, for U.S. Patent No. 3,856,534, entitled "Anti-Fog Composition."

- A nonexclusive license to Pressure Systems, Hampton, Virginia, for U.S. Patent No. 4,111,058, entitled "Electronically Scanned Pressure Sensor Module With In Situ Calibration Capability."

- A nonexclusive license to Aerolab, Laurel, Maryland, for U.S. Patent No. 3,952,590, entitled "Apparatus for Reducing Aerodynamic Noise in a Wind Tunnel."

- A nonexclusive license to International Technology Corp., Satellite Beach, Florida, for U.S. Patent No. 4,087,975, entitled "Ocean Thermal Plant."

- A nonexclusive license to Hexcel Corp., San Francisco, California, for U.S. Patent Application Serial No. 839,963, entitled "Mixed Diamines for Lower Melting Addition Polyimide Preparation & Utilization."

Electronic Components and Circuits

Hardware, Techniques, and Processes

3 Multiband Microstrip Antenna
4 Simple Circuit Monitors "Third Wire" in ac Lines
5 Simple Buck/Boost Voltage Regulator
6 Independent Synchronizer for Digital Decoders
7 Multichannel Coincidence Circuit
8 Universal Odd-Modulus Frequency Divider
9 Detecting Short Circuits During Assembly
10 Continuous Control of Phase-Locked-Loop Bandwidth
11 Photocapacitive Image Converter
12 Crossed-Grid Charge Locator

Books and Reports

13 Semiconductor Step-Stress Testing
14 JANTX1N2970B Zener Diode
14 JANTX1N2989B Zener Diode
14 JANTX1N3016B Zener Diode
14 JANTX1N3031B Zener Diode
15 JANTX1N5622 Diode
15 JANTX1N5623 Switching Diode
15 JANTX2N2060 Dual Transistor
15 JANTX2N2219A Dual Transistor
16 JANTX2N2369A Transistor
16 JANTX2N2432A Transistor
16 JANTX2N2484 Transistor
16 JANTX2N2605 Transistor
17 JANTX2N2905A Transistor
17 JANTX2N2920 Dual Transistor
17 JANTX2N2945A Transistor
17 JANTX2N3637 Transistor
18 JANTX2N3811 Dual Transistor
18 JANTX2N4150 Transistor
18 JANTX2N4856 Field-Effect Transistor

Multiband Microstrip Antenna

An antenna composed of stacked elliptical disks operates over broadband or multiple frequency bands.

Lyndon B. Johnson Space Center, Houston, Texas

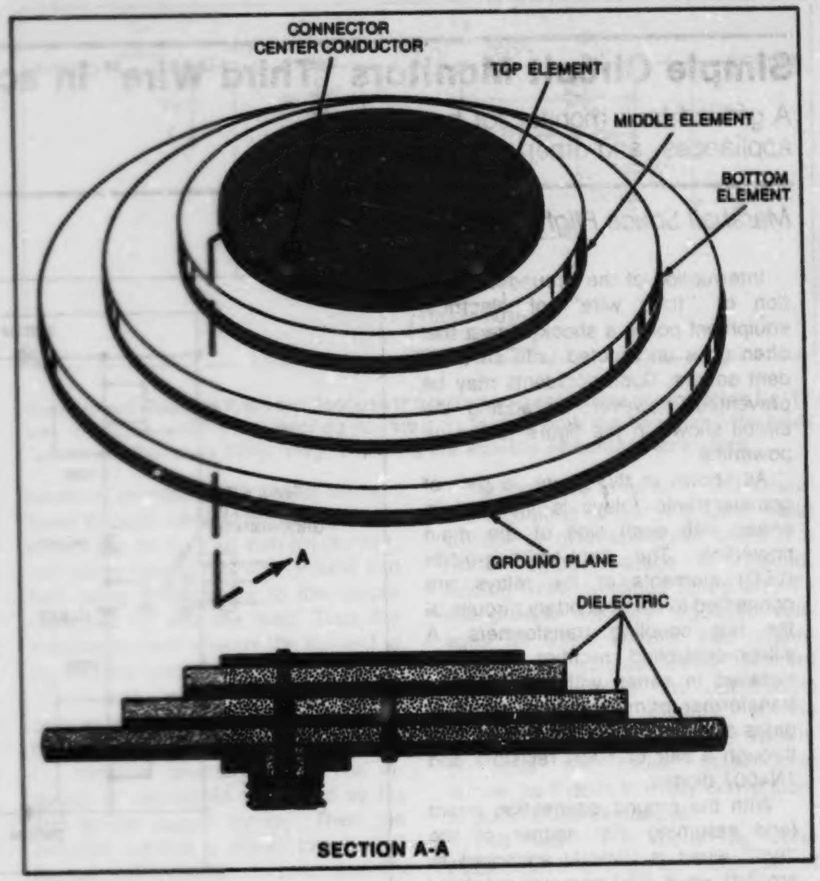

The Microstrip Construction is shown in these views of a three-element elliptical laminated antenna. Standard microstrip techniques, involving sequential removal of material from a stack of conductors and insulators, can be used to build it.

A compact, multiband (or broadband) microstrip antenna consists of layers of elliptical disks separated by dielectric substrates (see figure). Each disk operates at the frequency determined by its size and the dielectric constant of the substrate. A single-element antenna of this type is described in "Low-Profile Communications Antenna" (MSC-16683) on page 345 of *NASA Tech Briefs*, Vol. 4, No. 3. [Also see related article, "Low-Cost Dual-Frequency Microwave Antenna" (MSC-16100), on page 513 of Vol. 1, No. 4.]

The eccentricities of the antenna elements are all within the same range, so that the sizes of the individual elements vary approximately as do their semimajor axes. To achieve an operating frequency f, the semimajor axis, a, of an antenna element is given by

$$a = kc/f\sqrt{\varepsilon}$$

where ε is the relative dielectric constant of the substrate layer, c is the speed of light, and k is an empirical constant ranging from 0.27 to 0.29. Consequently, by decreasing the semimajor axis of the ellipse, the operating frequency is made larger.

Left (right) circularly polarized radiation results if the feedpoint is located on a line at a 45° angle measured counterclockwise (clockwise) from a semimajor axis. Maintaining a 10- to 20-percent limitation on the eccentricity of an antenna element insures that the element can receive and transmit circularly polarized radiation.

For the three-element antenna shown, the disks are positioned above the ground plane in the order of length of semimajor axis, with the element with the smallest semimajor axis on top. The center conductor of the coupling connector contacts the top antenna element only. The outer conductor is attached to the bottom of the ground plane. A conducting pin passes through the center of each disk, except for the top element.

In the three-element antenna, the middle element is the ground plane for the top element, and the dielectric space is the electromagnetic cavity for the top element. At the same time, the top and middle elements are capacitively coupled. Thus, signals received by the middle element are coupled through the top element to the connector. Similarly, the bottom element is the ground plane for the middle element; and the signals it receives are capacitively coupled in turn to the middle element, to the top element, and to the connector. In the transmit mode, signals are fed through the connector to the top element and are capacitively fed to the lower elements.

The electric currents generated in the antenna elements are generally concentrated on their peripheries and are zero at their geometric centers. Consequently, no loss in signal strength or operating efficiency results from linking the lower elements at

(continued on next page)

their centers. In principle, any number of elements may be included, with all but the top element being electrically joined at their geometric centers to the ground plane. Moreover, if the sizes of the elements are close to each other in value, the individual frequency bands can be made to overlap, to yield a single broadband antenna.

This work was done by I-Ping Yu of Lockheed Electronics Co., Inc., for **Johnson Space Center.** *For further information, Circle 1 on the TSP Request Card.*

This invention is owned by NASA, and a patent application has been filed. Inquiries concerning nonexclusive or exclusive license for its commercial development should be addressed to the Patent Counsel, Johnson Space Center [see page A5]. Refer to MSC-18334.

Simple Circuit Monitors "Third Wire" in ac Lines

A ground-fault monitor for handtools, appliances, and other electrical equipment

Marshall Space Flight Center, Alabama

Interruption of the ground connection or "third wire" of electrical equipment poses a shock hazard that often goes undetected until an accident occurs. Such accidents may be prevented, however, by adding the circuit shown in the figure to the ac powerline.

As shown in the figure, a pair of optoelectronic relays is installed in series with each side of the main powerline. The light-emitting-diode (LED) elements of the relays are connected to the secondary circuits of the two coupling transformers. A silicon-controlled rectifier (SCR) is installed in series with each of the transformer primaries, and the SCR gates are coupled to the ground wire through a pair of 100K resistors and 1N4007 diodes.

With the ground connection intact (and assuming that neither of the "hot" wires is directly anchored to ground), each SCR gate will reach its trigger voltage once during each cycle. This will occur when the corresponding hot lead is below ground potential.

Each SCR will thus be "on" and will pass current through the corresponding transformer primary once during each cycle. The voltages thus induced in the transformer secondaries, after smoothing by the 500-µF capacitor, will keep the relays energized with a steady dc voltage.

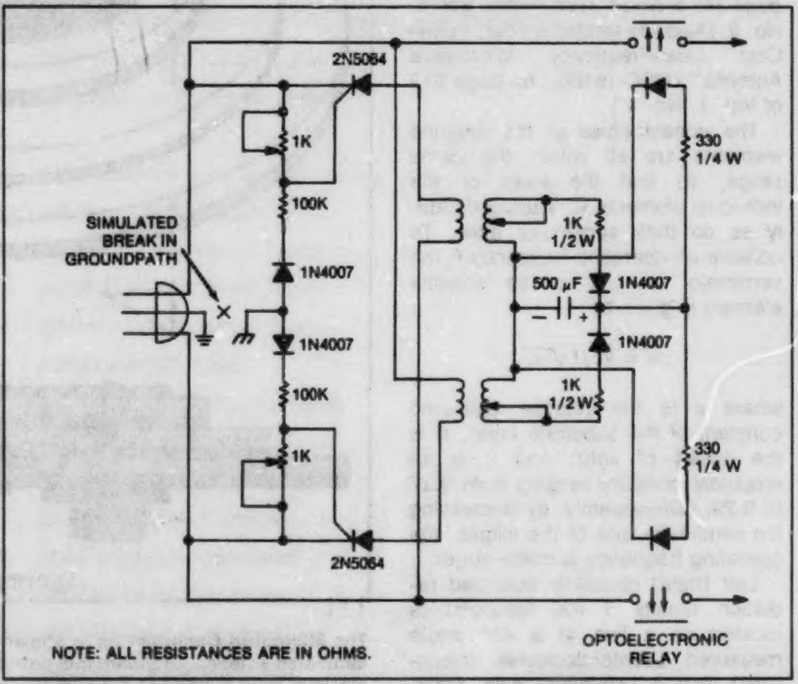

The Ground-Fault Monitor, originally developed to reduce shock hazard from an ultrasonic extensometer used to check bolt-tightening tension on the main engine of the Space Shuttle, includes optoelectronic relays in series with each of the main powerlines. The relays are closed unless the ground connection breaks or is disconnected. The variable resistors in the primary circuit trim the SCR trigger voltage.

Should the ground connection break, no current will flow through the 100K resistors, and the SCR's will not fire. This will deenergize the relays and open the main power connections.

This work was done by T. T. Kojima and D. E. Stuck of Rockwell International Corp. for **Marshall Space Flight Center.** *No further documentation is available.*
MFS-19457

Simple Buck/Boost Voltage Regulator

New circuit, with fewer components, operates more efficiently and reliably.

Goddard Space Flight Center, Greenbelt, Maryland

A new "buck/boost" voltage regulator requires fewer components than previous regulators of this type. It uses a single inductor/transformer combination to buck or boost the input voltage as it rises or falls, maintaining essentially-constant output voltage. The new regulator can handle input variations ranging from as low as one-half the output voltage to as high as the maximum rated voltage of the input transistor.

Using only one pulse-width modulator for both bucking and boosting, the regulator operates at high efficiency (90 percent in contrast to 80 percent for previous versions). In addition, the circuit subjects its switching transistors to a maximum voltage no greater than the input voltage or the output voltage, whichever is higher. These conservative operating conditions increase the lifetime of the transistors.

Potential uses for the regulator are in power sources for solar arrays, fuel cells, and thermionic generators. In a version designed for the 28-Vdc power supply aboard the Space Shuttle, the output is regulated to ±1 percent, for input voltages ranging from 21 to 35 volts.

The regulator (see figure) uses inductor L_2 and a capacitor C_2 for energy storage. C_2 keeps the output voltage constant over a complete pulse-width-modulation cycle, and L_2 maintains a net dc magnetic field. The combination of L_2 and transformer T_1, tapped as shown, provides the buck and boost voltages. The N_1 and N_2 windings of L_2 have an equal number of turns.

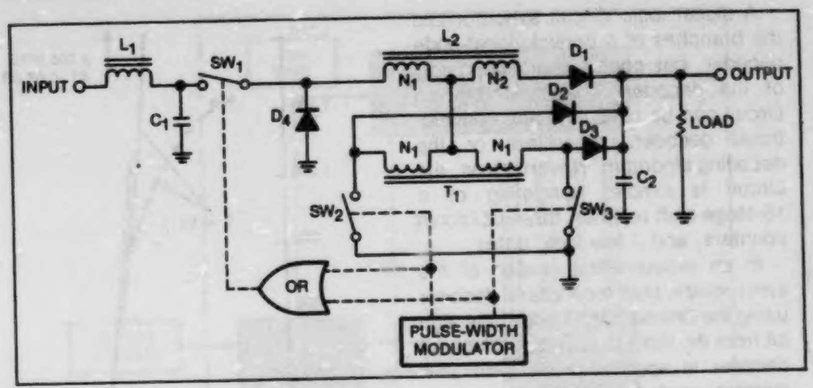

Component Count Is Reduced because the inductor/transformer combination L_2/T_1 and the pulse-width modulator do double duty, aiding both the boost and the buck functions. Switches SW_1, SW_2, and SW_3 are actually switching transistors.

When switches (actually transistors) SW_1 and SW_2 are closed (conducting), power diodes D_1, D_2, and D_4 become reverse-biased, and current flows through winding N_1 of L_2 to the center tap of T_1. The current divides, half going through SW_2 to ground and half going through D_3 to the output capacitor C_2 and the load. Thus the inductor current is twice the current to C_2 and the load.

However, when all switches are open (nonconducting), D_1 and D_4 become forward-biased, and D_2 and D_3 become reverse-biased. The inductor is connected to ground by D_4 and to the output by D_1. Then the inductor current is equal to one-half the original inductor current, and C_2 and the load receive the same amount of current as when SW_1 and SW_2 were closed.

The pulse-width modulator opens and closes SW_2 and SW_3 and, through an OR gate, opens and closes SW_1 in synchronism with SW_2 and SW_3. The pulse-width modulator adjusts the "on" time of the switches as necessary to regulate the output voltage.

Adding more turns to T_1 will extend the regulating range to a lower input voltage or give additional boost if a higher output voltage is needed. Adding more windings to L_2 and T_1 will provide auxiliary regulated voltages for other circuits that require isolation or voltage levels different from the output of the buck/boost voltage regulator. Overlap of the conduction period of the boost switches does not cause catastrophic failure, as it does in many conventional buck/boost regulators.

This work was done by John Paulkovich and G. Ernest Rodriguez of **Goddard Space Flight Center.** *For further information, Circle 2 on the TSP Request Card.*

This invention is owned by NASA, and a patent application has been filed. Inquiries concerning nonexclusive or exclusive license for its commercial development should be addressed to the Patent Counsel, Goddard Space Flight Center [see page A5]. Refer to GSC-12360.

Independent Synchronizer for Digital Decoders

Circuit maintains synchronization at low signal-to-noise ratios.

Lyndon B. Johnson Space Center, Houston, Texas

A digital logic circuit synchronizes the branches of a convolutional-code decoder, but operates independently of the decoder. The synchronizing circuit can be used with any convolutional decoder, regardless of the decoding algorithm. Nevertheless, the circuit is simple, consisting of a 15-stage shift register, three up/down counters, and a few logic gates.

In an experimental version of the synchronizer built for a Viterbi decoder using the Odenwalder 7 code, the sign bit from the input to each branch of the decoder is applied to a 15-bit shift register, and the modulo-2 sum is formed of the register 1st, 3d, 12th, 14th, and 15th stages. A second modulo-2 sum is formed of the contents of the 8th, 10th, and 11th stages, and a third modulo-2 sum is formed of the 5th and 6th stages.

The parity checks are used as an indicator of correct or incorrect node synchronization. If all three parity checks agree, an up/down counter is incremented. If the first two checks agree but the third disagrees, the same up/down counter is decremented. In any other situation, the counter is neither incremented nor decremented.

The process is repeated when the next bit is read into the shift register, but with a second up/down counter, and is repeated once more with the third input bit and a third up/down counter. The sequence starts again with the fourth input bit.

The up/down counter associated with the properly-framed code sequence is more likely than the other two counters to be augmented and less likely to be decremented when the polarity is correct. Correct node synchronization is thus determined by observing which of the counters first reaches predetermined positive and negative threshold values. Since a negative threshold crossing indicates an inverted decoder input, node synchronization and sign ambiguities are resolved simultaneously.

In tests the synchronizer maintained synchronization at signal-to-noise ratios as low as -3 dB (see figure). In contrast, a conventional branch synchronizer (one based on comparisons of "unanimity" and "nonunanimity" counters) was limited to signal-to-noise ratios above 1.4 dB.

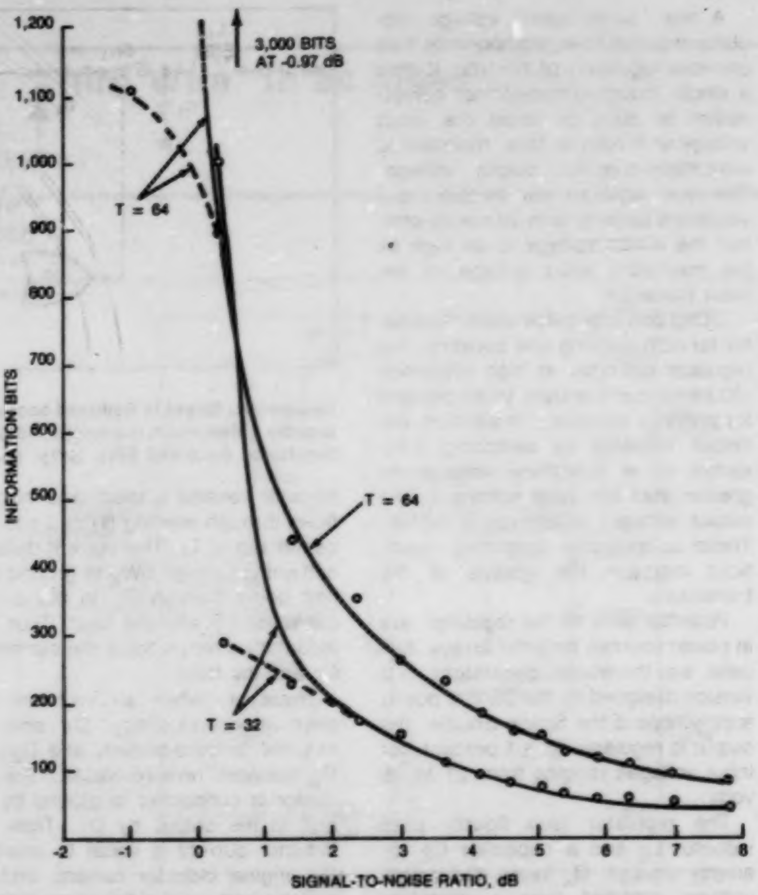

Plot of New Synchronizer Performance shows the average synchronization delay, in information bits, as a function of signal-to-noise ratio for up/down-counter thresholds of 32 (in black) and 64 (in color). The dashed lines indicate the synchronization delay to the first acceptance; the solid lines, the delay to the first correct acceptance. In both cases, the synchronizer was able to retain synchronization at all signal-to-noise ratios exceeding -3 dB.

This work was done by Jack J. Stiffler of Raytheon Co. for **Johnson Space Center.** *For further information, Circle 3 on the TSP Request Card.*
MSC-16723

Multichannel Coincidence Circuit

Circuit records coincidences between pulses in two or more channels.

Langley Research Center, Hampton, Virginia

The digital circuit shown in the block diagram in Figure 1 looks for coincidences between pulses in a primary channel and those in one or more secondary channels. When two consecutive coincidence events are found, the circuit records the elapsed time (the interval time) between the leading edges of the pulses in the primary channel.

The coincidence timer has already been built for two channels of data pulses, and a three-channel version is being developed. It has been tested with both simulated and actual data sources. Originally used in a laser velocimeter to determine the time between velocity measurements, the circuit can also be used to measure time intervals in other instruments that receive data at irregular rates from two or more sources.

The timer considers a pulse of the primary channel to be coincident with one of the secondary channel pulses if both occur within a predetermined timespan or "aperture" (see Figure 2); the coincident pulses do not necessarily have to overlap as long as their leading edges are less than 1 aperture time apart.

As seen in the block diagram, the circuit is divided into three major functions:

- The *interval-time measurement subcircuit* contains binary counters, temporary data storage, and data output devices to generate a digital number related to the time between coincident pulses.
- The *measurement-control subcircuit* controls the operation of the counters, storage, and output devices.
- The *system-control and timing-sequence generator* oversees routine timing and control.

The measurement of the interval time is made from the leading edges of the pulses in the primary data channel. Since it cannot be known if the time measurement after one coincidence is valid until a second coincidence event is recorded (and this is not certain until the completion

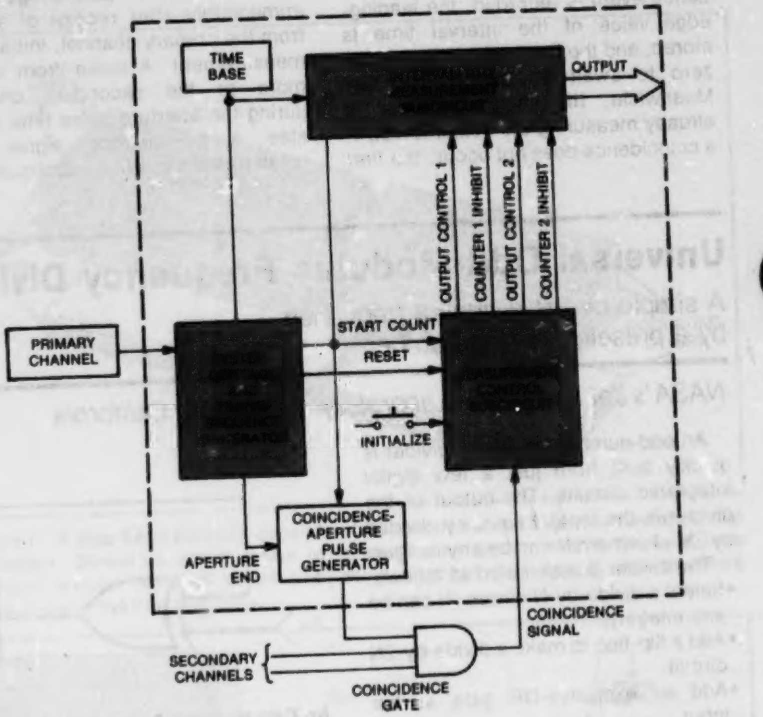
TIME BASE
MEASUREMENT
OUTPUT
OUTPUT CONTROL 1
COUNTER 1 INHIBIT
OUTPUT CONTROL 2
COUNTER 2 INHIBIT
PRIMARY CHANNEL
START COUNT
RESET
INITIALIZE
GENERATOR
COINCIDENCE-APERTURE PULSE GENERATOR
APERTURE END
COINCIDENCE SIGNAL
SECONDARY CHANNELS
COINCIDENCE GATE

Figure 1. **The Coincidence Circuit consists of three major blocks: Binary counters and latches are in the interval-time measurement subcircuit, the timing pulses originate in the measurement-control subcircuit, and routine timing is generated in the timing-sequence generator.**

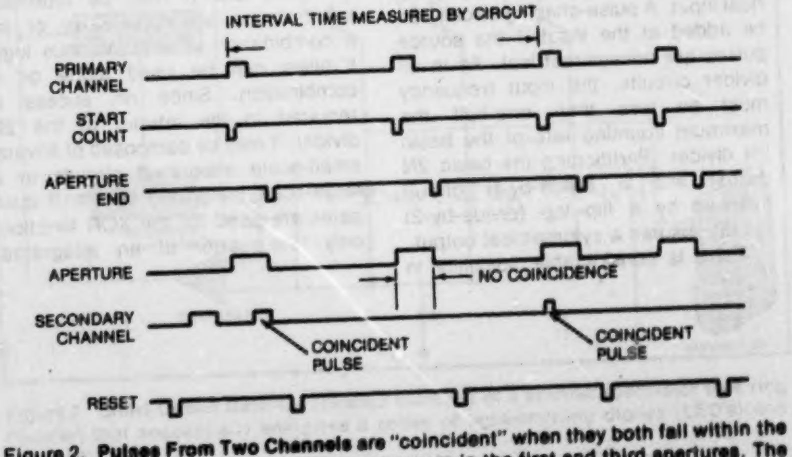
INTERVAL TIME MEASURED BY CIRCUIT
PRIMARY CHANNEL
START COUNT
APERTURE END
APERTURE
NO COINCIDENCE
SECONDARY CHANNEL
COINCIDENT PULSE
COINCIDENT PULSE
RESET

Figure 2. Pulses From Two Channels are "coincident" when they both fall within the same aperture period. Here, coincidence occurs in the first and third apertures. The "interval time" is thus the time between the leading edges of the first and third pulses in the primary channel.

of the aperture time for the second coincidence), two binary counters are required. While the counter making the current measurement continues its count until after the second coincidence aperture has ended, the second binary counter has already begun to measure the next interval. If a coincidence event is recorded, the leading-edge value of the interval time is stored, and the first counter is reset to zero to await a new input pulse. Meanwhile, the second counter is already measuring the next interval. If a coincidence does not occur, the first counter continues its measurement, and the second counter is reset.

A fixed series of pulses, consisting of start-count, aperture-end, and reset signals, is supplied to the coincidence-interval measurement subcircuit from the measurement-control subcircuit. The start-count pulse, generated immediately after receipt of a pulse from the primary channel, initiates the measurement. A pulse from one or more of the secondary channels during the aperture pulse time generates a coincidence signal. The measurement-control subcircuit continuously reads the count value on the active counter; when the coincidence signal is received, the count value that existed at the leading edge of the primary channel pulse is transferred to the output bus.

This work was done by James I. Clemmons, Jr., of **Langley Research Center.** *For further information, Circle 4 on the TSP Request Card.*

Inquiries concerning rights for the commercial use of this invention should be addressed to the Patent Counsel, Langley Research Center [see page A5]. Refer to LAR-12531.

Universal Odd-Modulus Frequency Divider

A simple circuit divides a frequency by a preselected odd number.

NASA's Jet Propulsion Laboratory, Pasadena, California

An odd-number frequency divider is quickly built from just a few digital integrated circuits. The output of the divider is the input frequency divided by 2N - 1, where N can be any integer.

The divider is assembled as follows:

- Select a divide-by-N circuit (N can be any integer).
- Add a flip-flop to make a divide-by-2N circuit.
- Add an exclusive-OR gate at the input.

The output frequency of the resulting circuit is $F_{out} = F_{in}/(2N - 1)$, where F_{in} is the input frequency (see figure).

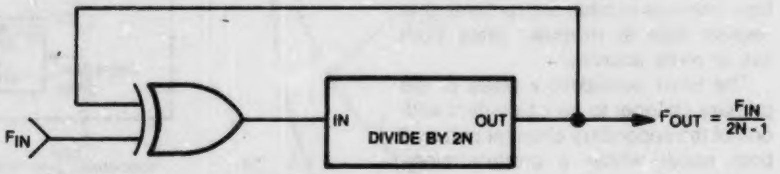

An **Odd-Number Frequency Divider** comprises an exclusive-OR gate and a 2N divider. The 2N divider consists of an N divider and a divide-by-2 flip-flop.

The divider produces symmetrical output pulses and requires a symmetrical input. A pulse-shaping circuit can be added at the input if the source pulses are nonsymmetrical. As in all divider circuits, the input frequency must be less than one-half the maximum counting rate of the basic 2N divider. Partitioning the basic 2N divider into a divide-by-N circuit followed by a flip-flop (divide-by-2) circuit ensures a symmetrical output.

There is considerable flexibility in choosing the basic 2N divider. It can be assembled from binary, binary-coded-decimal, twisted-ring, or other counters; and it may be internally synchronous, use ripple carry, or use a combination of both. Various logic families can be used alone or in combination. Since no access is required to the interior of the 2N divider, it may be composed of several small-scale integrated circuits or a large-scale integrated circuit. If quad gates are used for the XOR function, only one-quarter of an integrated-circuit chip is needed.

This work was done by Alexander Engel of Caltech for **NASA's Jet Propulsion Laboratory.** *For further information, Circle 5 on the TSP Request Card.*

This invention has been patented by NASA [U.S. Patent No. 3,906,374]. Inquiries concerning nonexclusive or exclusive license for its commercial development should be addressed to the Patent Counsel, NASA Resident Legal Office-JPL [see page A5]. Refer to NPO-13426.

Detecting Short Circuits During Assembly

Shorts between bus bars can be identified and eliminated as soon as they occur.

Ames Research Center, Moffett Field, California

A short-circuit detector indicates when and where a short occurs while electronic equipment is being wired. The detector is intended for use on power and ground bus bars (Figure 1) on computers and similar complex hardware. Ordinarily the bus bars are tested for shorts only after leads have been attached. Since the bus bars often have hundreds or even thousands of terminals, testing them for shorts — and a few shorts are bound to occur no matter how careful the wirer is — can be tedious and time consuming. Moreover, the equipment can be damaged if it is energized before the shorts are corrected.

The new detector sounds a buzzer to inform the wirer that a terminal is short-circuited immediately after a wire connection is made. The detector also shows the wirer, by illuminating light-emitting diodes (LED's), which bus bar conducting planes are shorted. It is then easy to make a correction by disconnecting and rewiring the affected terminals.

The short-circuit detector (Figure 2) is attached to the bus-bar assembly by a connector containing sockets for plugs on each of the bus bars to be tested. An oscillator in the detector feeds a train of positive pulses to a ring counter, and the ring counter in turn produces a corresponding positive pulse on each of its output leads (1 through n) in sequence. The output pulses bias transistors 1 through n and LED's 1 through n so that they briefly become conductive in sequence. If the oscillator frequency is 1 hertz, the LED's glow in sequence for 0.5 second.

The emitters of the transistors are connected to the pins on the bus bars. Thus, each transistor turns on when the corresponding bus bar is energized. Potentiometer R_1 is adjusted so that it produces a reference voltage that is slightly greater then the voltage across resistor R_2. R_1 and R_2 connect to separate input terminals on a comparator.

(continued on next page)

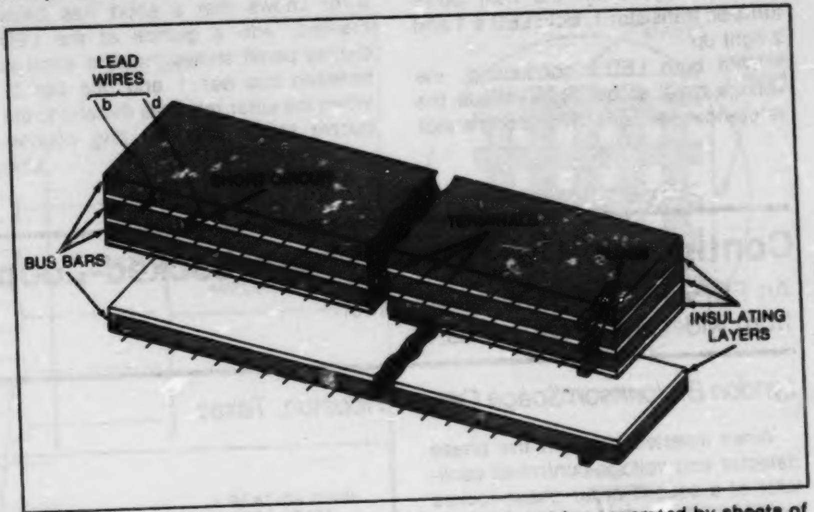

Figure 1. A **Bus-Bar Assembly** consists of conductive strips separated by sheets of insulation. Operators attach wires to terminal pins on the strips. Here, a wire wrapped around terminal d on bus bar 1 touches bus bar 2 and therefore short-circuits the two bus bars.

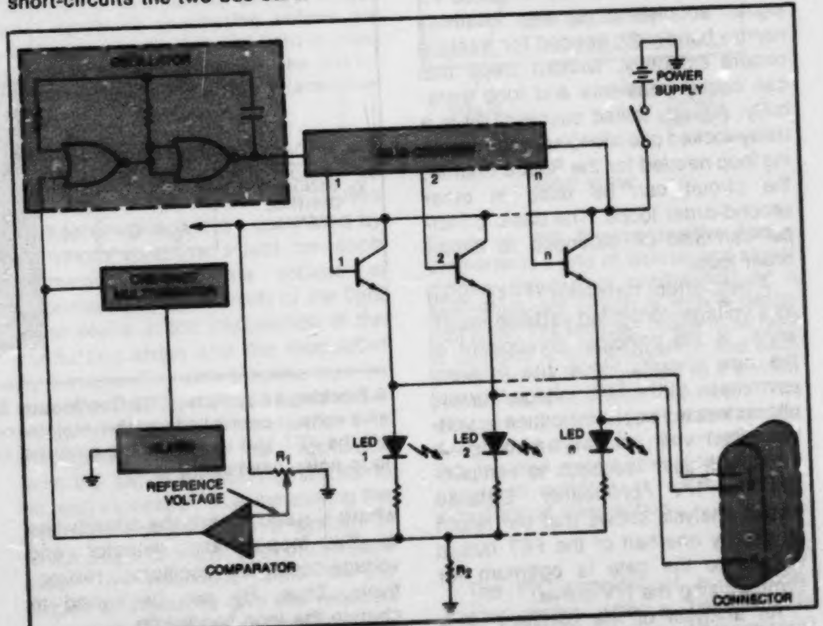

Figure 2. **Short-Circuit Detector** consists basically of a scanner (oscillator plus ring counter) that sequentially energizes a series of light-emitting diodes (LED's) and bus bars.

The detector continuously scans the bus bars until a short circuit occurs. For example, if a wire on one terminal of bus bar 1 touches bus bar 2 (as shown in Figure 1), bus bars 1 and 2 will be short-circuited. When this happens, the anode of LED 2 is connected to the anode of LED 1. Consequently, when the next pulse turns on transistor 1, both LED's 1 and 2 light up.

With both LED's conducting, the voltage drop across R_2 exceeds the reference voltage. The comparator then generates a positive output that stops the oscillator and triggers the one-shot multivibrator, which activates the alarm buzzer. With no pulses from the oscillator, the ring counter keeps transistor 1 on and LED's 1 and 2 as well.

As soon as the buzzer sounds, the wirer knows that a short has been created, and a glance at the LED display panel shows that the short is between bus bar 1 and bus bar 2. When the wirer removes the short, the buzzer stops, and the ring counter continues to scan.

This work was done by Gorden J. Deboo of ***Ames Research Center.*** *For further information, Circle 6 on the TSP Request Card.*

This invention is owned by NASA, and a patent application has been filed. Inquiries concerning nonexclusive or exclusive license for its commercial development should be addressed to the Patent Counsel, Ames Research Center [see page A5]. Refer to ARC-11116.

Continuous Control of Phase-Locked-Loop Bandwidth

An FET circuit smooths the transition from wideband to narrow band.

Lyndon B. Johnson Space Center, Houston, Texas

When inserted between the phase detector and voltage-controlled oscillator of a second-order phase-locked loop, the filter circuit shown in the figure allows continuous electronic control of the loop bandwidth. Change from the wide bandwidth required for signal acquisition to the relatively narrow bandwidth needed for tracking occurs smoothly, without steps that can cause transients and loop instability. Already tested successfully in a delay-locked pseudonoise-code tracking loop needed for the Space Shuttle, the circuit can be used in other second-order loops. The basic principle can also be extended to higher order loops.

A field-effect transistor (FET), used as a voltage-controlled variable resistance, is the principal component of the new circuit. Since the inherent asymmetry of the FET voltage/current characteristic would introduce a voltage offset when tracking an ac signal, the circuit uses feedback to compensate for I/V nonlinearity. Detailed circuit analysis shows that the return of exactly one-half of the FET output voltage to the gate is optimum for symmetrizing the I/V curve.

An analysis of the behavior of a "perfect" second-order phase-locked loop containing the new circuit shows that the loop bandwidth is given by

$$B = \frac{K_\phi K_V (R_1 + R_2)}{4R_2} + \frac{1}{4(R_1 + R_2)C}$$

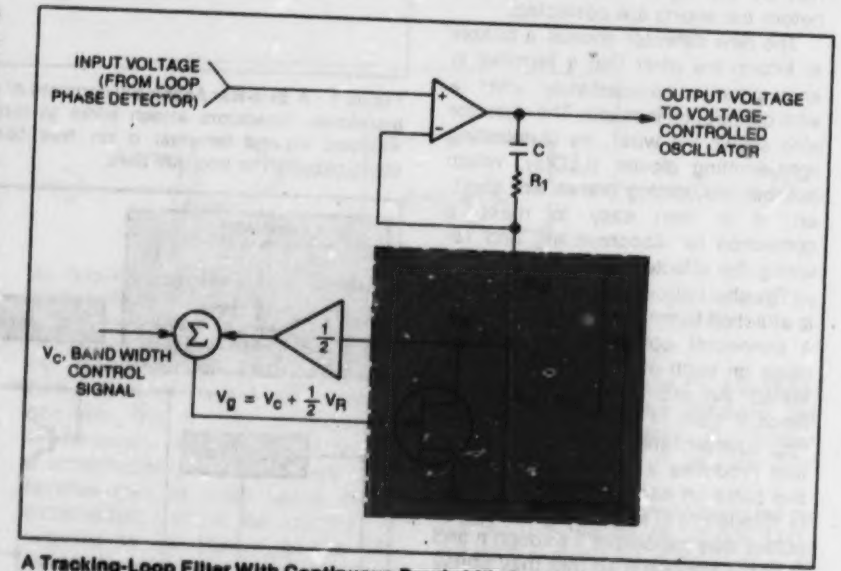
INPUT VOLTAGE (FROM LOOP PHASE DETECTOR)
+
-
OUTPUT VOLTAGE TO VOLTAGE-CONTROLLED OSCILLATOR
C
R_1
Σ
$\frac{1}{2}$
V_c, BAND WIDTH CONTROL SIGNAL
$V_g = V_c + \frac{1}{2} V_R$

A Tracking-Loop Filter With Continuous Bandwidth Control is made by using an FET as a voltage-controlled variable resistance. Decrease of the control voltage V_c turns off the FET and increases the effective value of R_2 from R_W to R_N, narrowing the loop noise bandwidth.

where K_ϕ and K_V are the sensitivities of the loop phase detector and voltage-controlled oscillator, respectively. Thus, R_2 can be varied to change the loop bandwidth.

For the circuit shown, the control voltage is held sufficiently positive to insure that the FET is on and $R_2 = R_W$ until the loop is locked. When a signal is acquired, V_c is decreased until the FET is switched off and R_2 equals R_N. A transition period of 40 milliseconds was used for the circuit tested for the Shuttle; the bandwidth was varied between 320 Hz for acquisition and 20 Hz for tracking.

This work was done by Gary W. Motal and James C. Vanelli of Lockheed Electronics Co., Inc., for ***Johnson Space Center.*** *For further information, Circle 7 on the TSP Request Card.*
MSC-16684

Photocapacitive Image Converter

Solid-state converters yield high sensitivity at high information-retrieval speed.

Langley Research Center, Hampton, Virginia

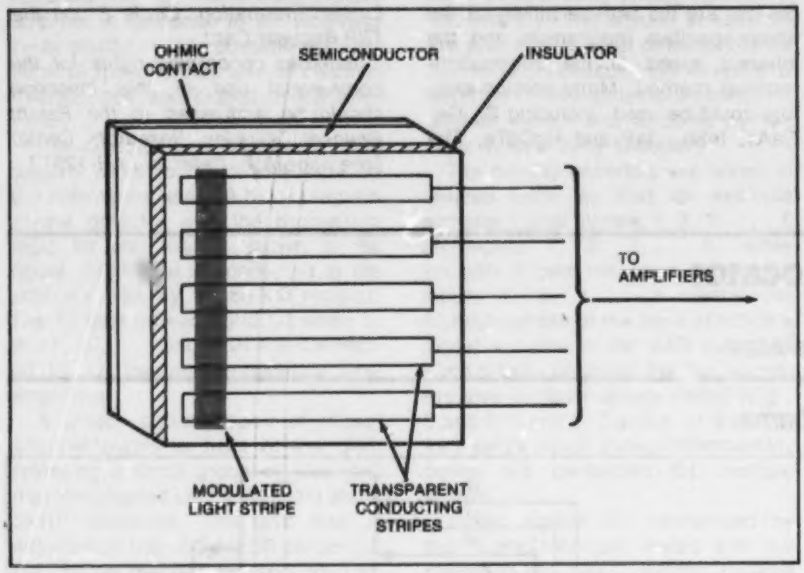

Figure 1. CAPICON Photocapacitive Image Converter is an insulated semiconductor structure with a depletion layer over which transparent conducting stripes are placed. An image is focused on the surface, and a modulated stripe of light is used to read out data. As the readout light stripe sweeps across the device, the photocapacitively generated voltage at each light-stripe/conducting-stripe intersection relates to the intensity of the focused image.

A sensitive, fast, solid-state imaging converter has been suggested that functions in a photocapacitive mode. Two configurations of this device have been proposed. The CAPICON version (Figure 1) reads an entire scene by sweeping a modulated light stripe across a surface of transparent conducting stripes. The PIC version (Figure 2) reads a scene by imaging it on a grid pattern of transparent conducting stripes.

The CAPICON is constructed by applying a back ohmic contact to a semiconductor wafer, applying a thin insulating layer on the front surface, and then depositing the transparent conducting stripes on the insulating layer. The ohmic contact material is chosen so that the semiconductor is in depletion when no bias is applied. An image of the scene being viewed is focused on the front surface. In regions where the light is brighter, the depletion layer is thinned more than in darker regions. A stripe of modulated light, which is perpendicular to the conducting stripes, is next focused on the surface of the device. This causes modulated voltage to be generated by the photocapacitive effect on each conducting stripe; the voltage is proportional to the intensity of the light in the scene at the intersection of the conducting stripe and the modulated light stripe. The entire scene can be read by sweeping the modulated stripe across the surface of the device. This arrangement permits the information from the set of conducting stripes to be read in parallel, thus increasing the data rate compared to a system in which a spot is swept over the surface area. The minimum width of the stripes is chosen to give the required resolution. Minimum separation between stripes is chosen so that crosstalk between them is negligible. This requires their separation to be larger than the depletion layer thickness, typically a few microns. Thus, the ultimate resolution is a few microns.

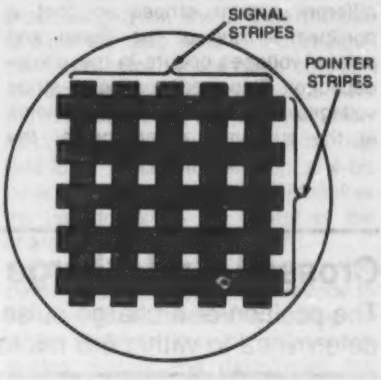

TOP VIEW

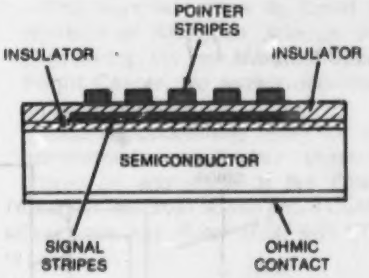

SIDE VIEW

Figure 2. PIC Photocapacitive Image Converter is a grid of pointer and signal stripes (transparent conductors) on a semiconductor structure with a depletion layer. The focused image to be read is chopped at one frequency, and each pointer stripe is connected to a current source at a unique frequency. The voltage from each signal stripe can be analyzed to determine the intensity of the focused image (photocapacitively generated voltage) at each pointer/signal stripe intersection.

The PIC consists of a semiconductor wafer with a back ohmic contact and two layers of transparent conducting stripes separated by an insulator on the front. The two layers of stripes are fabricated in a grid pattern. A light chopper is used to modulate the focused light falling on

(continued on next page)

the image converter so that the thickness of the semiconductor depletion layer is modulated at the chopper frequency. One set of stripes, the pointer stripes, is used to sense the intensity of the voltage signal generated at a given spot on the signal stripe. Current generators of different frequencies are connected to the different pointer stripes so that a nonlinear mixing of the signal and pointer voltages occurs in the photocapacitor. This produces signal-stripe voltages with frequency components at the sum and difference of the modulating and current-generating frequencies. Each signal stripe is connected to a processing circuit that measures the amplitude of the Fourier component of the signal at the frequency equal to the sum of the two frequencies. In this way the image pattern on each stripe is determined.

The main advantages of these devices are the high sensitivity of the photocapacitive mechanism and the inherent speed of the information-retrieval method. Many semiconductors could be used, including Si, Ge, GaAs, InSb, GaP and HgCdTe. The different materials will have different spectral regions where they are most sensitive. The fabrication of both devices should be relatively simple and inexpensive.

This work was done by William E. Miller of **Langley Research Center** *and Arden Sher and Y. H. Tsuo of the College of William and Mary. For further information, Circle 8 on the TSP Request Card.*

Inquiries concerning rights for the commercial use of this invention should be addressed to the Patent Counsel, Langley Research Center [see page A5]. Refer to LAR-12513.

Crossed-Grid Charge Locator

The position of a charge pulse is determined to within 6.5 micrometers.

Marshall Space Flight Center, Alabama

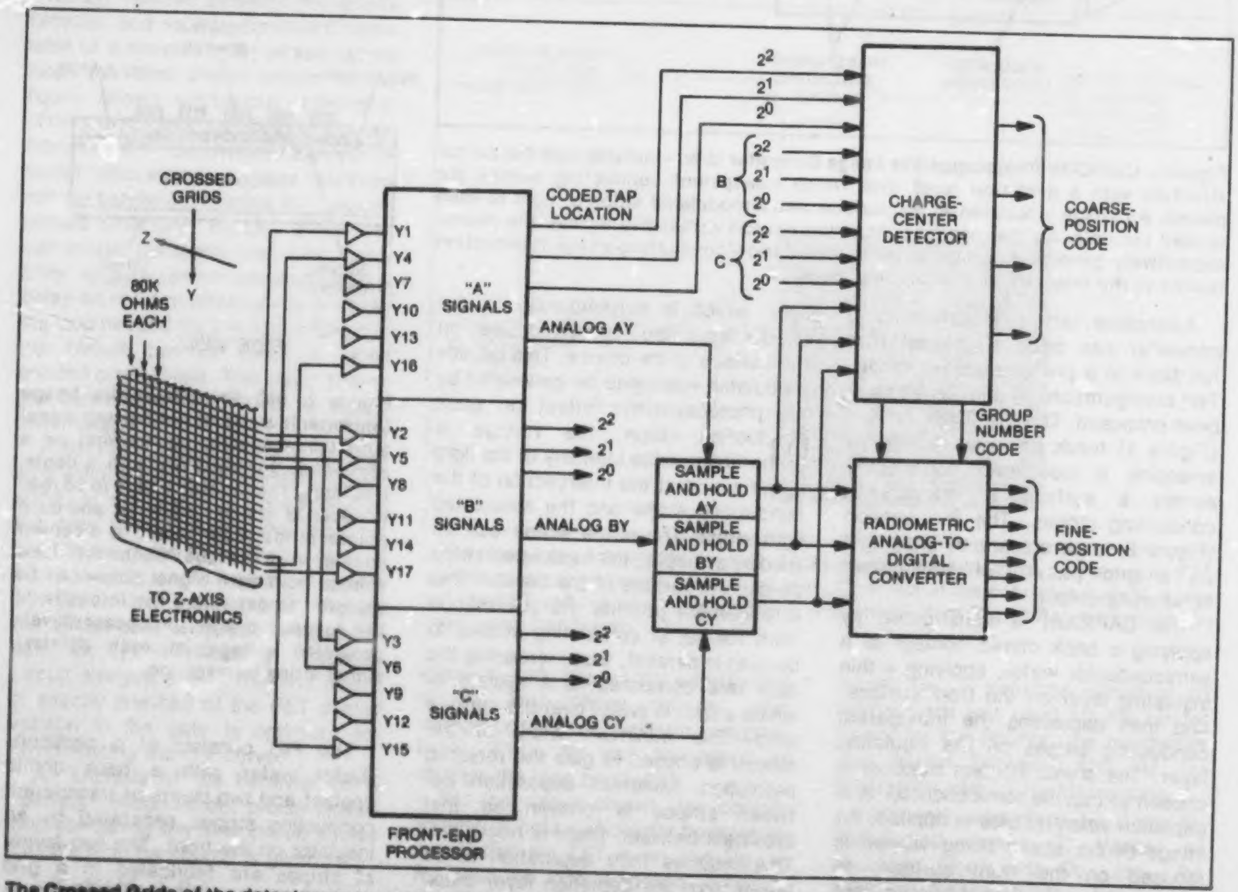
CROSSED GRIDS
Z
Y
80K OHMS EACH
TO Z-AXIS ELECTRONICS
Y1
Y4
Y7
Y10
Y13
Y16
Y2
Y5
Y8
Y11
Y14
Y17
Y3
Y6
Y9
Y12
Y15
"A" SIGNALS
"B" SIGNALS
"C" SIGNALS
FRONT-END PROCESSOR
CODED TAP LOCATION
ANALOG AY
ANALOG BY
ANALOG CY
2^2
2^1
2^0
B
C
SAMPLE AND HOLD AY
SAMPLE AND HOLD BY
SAMPLE AND HOLD CY
CHARGE-CENTER DETECTOR
COARSE-POSITION CODE
GROUP NUMBER CODE
RADIOMETRIC ANALOG-TO-DIGITAL CONVERTER
FINE-POSITION CODE

The Crossed Grids of the detector are tapped at 17 of the 129 wires in each grid. The wires in the vicinity of a charge cloud develop voltages that are processed, using priority encoders, to develop coarse- and fine-position codes. The coarse code is the 4-bit location of the tap nearest the center of the charge; the fine code is obtained by interpolating the signal strengths between taps.

A digital processor at the output of a crossed grid of closely spaced wires determines the position of a cloud of electrons to within 6.5 micrometers. The system is part of a high-resolution imager in the focal plane of an X-ray telescope. In this application it locates the center of the electron pulse released by a microchannel-plate ampifier in response to an incoming X-ray photon. Other possible applications of the detector are in electron microscopes and closed-circuit television.

The detector grid consists of 129 parallel wires for each axis, spaced 0.2 millimeters apart. A block diagram of the detector and the processing logic for one axis is shown in the figure. Each wire is connected to the adjacent wire by an 80-k Ω resistor. The 17 taps on each grid (at wires 1, 9, 17, 25, . . . and 129) are connected to 17 low-input-impedance preamplifiers.

A photon strikes a pair of microchannel plates in front of the grid, releasing a small group of electrons that is multiplied until it contains about 3×10^7 electrons. The grid bias is adjusted so that roughly 50 percent of the charge reaches the second grid. When this cloud of electrons arrives in the vicinity of the grid, it charges the wires in that region and is absorbed in the inputs of the nearest preamplifiers.

The processing circuit eliminates ambiguities that can arise when a large cloud, centered on a tapped wire, develops appreciable signals in the two adjacent preamplifiers. The set of 17 taps is divided into three subsets, A, B, and C, the signals of which are processed separately in the front-end processor. The five or six signals of each of these sets are summed to develop analog pulses AY, BY, and CY. The signals in each set are also sent to level detectors in the front-end processor. The outputs of each set of level detectors connect to latches, which are followed by two eight-input priority encoders.

The priority encoders are wired in reverse order so that for example encoder 1 gets signals 1, 2, 3, . . . 6 on inputs 1, 2, 3, . . . 6, while encoder 2 gets the same signals on inputs 6, 5, 4, . . . 1. Since the highest number of the input at which a signal appears in the 3-bit output of each priority encoder, the two encoders give complementary codes (e.g., 0 and 6, 1 and 5, 2 and 4, or 3 and 3) for a single signal. Noncomplementary codes are generated for multiple signals.

Single signals are recognized by their complementary codes and are classified as "valid" events, suitable for further processing, while multiple signals (noncomplementary codes) are classified as "invalid" events. The outputs from subsets A, B, and C are combined so that a valid event can be negated by an invalid event. The 3-bit-coded tap location of a valid event from each set is sent to the charge-center detector.

The three analog signals representing the sum of the charges of all elements of each set are sent through sample-and-hold circuits that maintain the signal level for the rest of the processing cycle. The outputs of these circuits are also sent to the charge-center detector, where three comparators determine the set of taps with the largest analog signal. This information, together with the 3-bit tap location, is used to develop a 4-bit "coarse-position" code that identifies the tap closest to the center of the charge cloud.

The charge-center detector also develops a 2-bit group-number code to be sent to a ratiometric analog-to-digital converter that interpolates the analog signals and determines the "fine position" of the charge center. The arithmetic for the algorithm is done by operational amplifiers.

This work was done by David C. Harrison of American Science and Engineering, Inc., for **Marshall Space Flight Center.** *No further documentation is available.*

Inquiries concerning rights for the commercial use of this invention should be addressed to the Patent Counsel, Marshall Space Flight Center [see page A5]. Refer to MFS-25170.

Books and Reports

These reports, studies, and handbooks are available from NASA as Technical Support Packages (TSP's) when a Request Card number is cited; otherwise they are available from the National Technical Information Service.

Semiconductor Step-Stress Testing

An extensive test program documents the behavior of discrete diodes and transistors under power and temperature overstress.

The behavior of discrete semiconductor components under temperature and power stress above the manufacturer's ratings is the subject of an extensive test program now underway for Marshall Space Flight Center. Twenty reports documenting some of the results of this program were described in the previous issue of *NASA Tech Briefs.* [See "Semiconductor Step-Stress Testing" (MFS-25329) on page 474 of Vol. 4, No. 4.] Described below are 19 additional reports in this series.

Details of the test program are given in the article cited above. Briefly, the effects of severe overstress on commercially available devices, including bipolar transistors, diodes, and field-effect transistors (FET's), were determined from measurements on samples obtained from various manufacturers. In broad outline, the test procedures are the same for all components. They differ in particulars, such as electrical parameters measured, for the different kinds of devices tested.

For the power-stress tests, a sample population is stressed at levels that increase in steps from half maximum rated power (MRP) to 1.75 MRP. The temperature-stress measurements are carried out in two groups. In the first group, the measurements are made in 160-hour steps starting at 75° C and increasing

(continued on next page)

in 25° C increments to 300° C. In the other group, the steps are for 16 hours duration each, commencing at 150° C and increasing in 25° C intervals to 300° C.

For all units, data are presented as graphs showing cumulative failures (in percent) for the temperature-stress group and as tables showing how the electrical parameters changed during each test phase. An analysis of the test results and the reasons for failures are given in the concluding sections of the reports. Throughout the reports, and in the following articles, the power-stress sample population is referred to as "Group I," the first temperature-stress population is "Group II," and the second temperature-stress population is "Group III."

Each of the reports described below titled "Step Stress Testing Program," presents the test procedures, results, and conclusions for one tested device. Persons wishing information about a particular unit can order the report for that device by circling the appropriate number on the TSP Request Card at the back of this issue of NASA Tech Briefs.

[*These reports were prepared to document work supported by the United States Government. They are intended solely as a vehicle for the presentation of test results and are not to be construed as an endorsement or a criticism of the companies mentioned or of their products.*]

JANTX1N2970B Zener Diode

The effects of power and temperature overstress

The testing proved strenuous for sample lots manufactured by General Semiconductor and Siemens. The Group I and Group II tests for both manufacturers were stopped due to excessive failures, although the General Semiconductor diodes underwent more hours of testings in each case.

In Group II, the predominant failure mode was detachment of the cathode lead. Failure analysis revealed that all analyzed samples failed due to the effects of excess heat. The separation of the tubulations was caused by extreme heat acting on the glass and the metal tube.

While the dice of the General Semiconductor devices were destroyed by alloying with the connecting metal, the Siemens dice were still functional and were within endpoint limits when tested by external probing of the die-lidded samples. Possibly, this difference is due to deeper junctions on the Siemens parts.

Since the General Semiconductor units had only one failure under Group III testing, only the Siemens lot underwent failure analysis. The analyzed samples were subjected to heat and power beyond their stress limits, which caused destructive damage to their internal structures. The protective junction coating charred, leading to excess leakage. The die and internal lead-attach metal melted, and the second nickel plate used on the dice peeled and separated with the connecting bonding metal. In addition, all the dice were shorted (probably due to "thermal runaway"), and two of the devices had cracks or chipouts. The die fell out of one device when it was touched.

This work was done by the Special Products Division of DCA Reliability Laboratory for **Marshall Space Flight Center**. *To obtain a copy of the report, Circle 9 on the TSP Request Card. MFS-25260*

JANTX1N2989B Zener Diode

The effects of power and temperature overstress

Zener diodes manufactured by Siemens and General Semiconductor were tested. All three stress groups proved detrimental to both sample lots. In Group I and Group III testing, the devices were electronically intact but damaged mechanically. Electrical readings were obtained by probing the die. The bonded die connections were damaged and the cathode detached when the part was opened. This suggests that the diodes failed due to excessive temperature.

The failure mode in the Group II testing for both manufacturers was "visual catastrophic." The failed parts had cracked glass and detached cathodes caused by the excessive temperature, which also resulted in the disconnection of the internal wire lead.

This work was done by the Special Products Division of DCA Reliability Laboratory for **Marshall Space Flight Center**. *To obtain a copy of the report, Circle 10 on the TSP Request Card. MFS-25261*

JANTX1N3016B Zener Diode

The effects of power and temperature overstress

Sample lots from Motorola and Siemens were tested. Both experienced large failure rates throughout all three stress tests. The failure mode common to all three groups was the I_R maximum-limit failure and the Zener-breakdown-voltage (B_V) maximum-limit failure. In some cases the I_R failures were shorted devices, and the B_V failures were opened devices.

In Group I testing, the diodes from both sample lots failed due to the thermal effects of excess power. In some cases the internal lead-bonding metal melted and flowed up the silver lead wire, which in turn disconnected from the die. Other devices failed due to shorting of the junction, probably caused by alloying with the melted metal at elevated temperatures.

Many devices in the Group II and Group III testing failed due to overheating. In some cases, probe testing of the dice after opening the packages showed shorts. The most probable cause of the shorts is alloying of the molten die metal into the silicon.

This work was done by the Special Products Division of DCA Reliability Laboratory for **Marshall Space Flight Center**. *To obtain a copy of the report, Circle 11 on the TSP Request Card. MFS-25262*

JANTX1N3031B Zener Diode

The effects of power and temperature overstress

Motorola and Siemens diodes were tested. The Motorola lot experienced one failure in Group I testing and no failures in Group III. Both the Siemens and Motorola diodes failed due to exposure to excessive temperatures, which, in many cases, melted the metal on the die connections.

The electrical test results suggest that the long dwell time of the molten metal caused the metal to alloy with the silicon dice, thus shorting out their junctions. Some of the Siemens devices also had electrical leakage of the glass in the glass-to-metal seal. The glass was conductive when probed either internally or externally, with the internal conductivity being somewhat greater.

This work was done by the Special Products Division of DCA Reliability Laboratory for **Marshall Space Flight Center**. *To obtain a copy of the report, Circle 12 on the TSP Request Card.*
MFS-25263

JANTX1N5622 Diode

The effects of power and temperature overstress

All three test groups were detrimental to diodes from Semtech and Micro Semiconductor. In each case, testing was halted before the process was completed.

The failure mode of the three Semtech lots was due to excessive reverse bias leakage. Failure analysis revealed this to be due to excessive conductivity in the external paint. When the conductivity was interrupted by sanding the paint, the reverse leakage fell to acceptable levels.

The Micro Semiconductor Group I diodes also had a failure mode of excessive I_R leakage. Failure analysis showed that this was caused by damaged silicon induced by the stress test. The analyzed diodes still showed a characteristic forward breakdown curve, indicating that they were not totally destroyed, but had resistive pathways (damage sites) in parallel with the junctions.

The Micro Semiconductor diode failure modes in Group II and Group III testing were the loss of leads due to the melting of connecting metal and cracked and broken glass. The excessive glass breakage is due to residual glass strain, which was not annealed out. The strain can be seen with polarized light.

This work was done by the Special Products Division of DCA Reliability Laboratory for **Marshall Space Flight Center**. *To obtain a copy of the report, Circle 13 on the TSP Request Card.*
MFS-25280

JANTX1N5623 Switching Diode

The effects of power and temperature overstress

The three Semtech lots produced two catastrophic failures. The testing of each Micro Semiconductor lot had to be stopped because the 50-percent-failures limit was reached.

Since both Semtech failures were due to excessive reverse-leakage current, only one diode underwent failure analysis. The analysis showed that the reverse-leakage-current failure was due to surface contamination, which was driven out of the glass under the high temperature and bias of the step-stress test.

The Micro Semiconductor diodes failed because of detaching leads. During Group I testing, one diode cracked in half. Failure analysis on this group showed that the glass of the analyzed diodes cracked due to the high junction temperatures reached in the stress testing. The leads fell off where the lead-bonding material exceeded its melting temperature.

The Group II diodes that were analyzed met all the specified limits for reverse-leakage current. Those that could be tested for V_F met the limit. It was noticed that the diodes that were missing paint were quite sensitive to light, which caused a large increase in the leakage measurement.

This work was done by the Special Products Division of DCA Reliability Laboratory for **Marshall Space Flight Center**. *To obtain a copy of the report, Circle 14 on the TSP Request Card.*
MFS-25281

JANTX2N2060 Dual Transistor

The effects of power and temperature overstress

The tested units were manufactured by Raytheon and Motorola. The Motorola sample lot showed signs of weakness in Group I testing; the Raytheon lot lost the majority of its devices in Group II.

The Motorola units in Group I experienced a decline in h_{FE}, while the collector/base leakages remained within specification limits. Such a loss of h_{FE}, without any evidence of surface leakage or low breakdown voltage, suggests a change in emitter efficiency. The migration of gold or other impurities possibly continued under high-power operation with consequent loss of h_{FE}.

All of the failures in Group II testing for Raytheon experienced some marked loss of h_{FE}. There is no significant bulk or surface leakage on these parts. This implies that the h_{FE} falloff is due only to a loss of emitter efficiency. The loss of injection efficiency, in turn, is due to the migration of gold and intermetallics under the influence of heat and bias, with a consequent loss of bulk silicon lifetime.

This work was done by the Special Products Division of DCA Reliability Laboratory for **Marshall Space Flight Center**. *To obtain a copy of the report, Circle 15 on the TSP Request Card.*
MFS-25251

JANTX2N2219A Dual Transistor

The effects of power and temperature overstress

These tested units were manufactured by Texas Instruments and National Semiconductor. In Group I testing, the Texas Instruments sample lot developed two catastrophic failures in 2,500 hours of testing; the National Semiconductor lot reached the 50-percent-failures limit 450 hours before the end of the testing.

The Group II testing failure analysis discovered that many Texas Instruments parts had clumps of silicon scattered over the dice. Gold/aluminum intermetallic contamination could also be seen on many of the units. The National Semiconductor parts showed no consistent failure mode, although, like the Texas Instruments sample lot, many of the National Semiconductor parts showed signs of gold/aluminum intermetallic contamination.

This work was done by the Special Products Division of DCA Reliability Laboratory for **Marshall Space Flight Center**. *To obtain a copy of the report, Circle 16 on the TSP Request Card.*
MFS-25252

JANTX2N2369A Transistor

The effects of power and temperature overstress

National Semiconductor and Raytheon transistors suffered a loss of gain, while generally continuing to maintain good junction quality with low leakage. A loss of emitter efficiency is the probable cause of the decline in gain. The loss of emitter efficiency is in turn due to the migration of gold and possibly other impurities, resulting in a loss of minority-carrier lifetime. In some cases the migration proceeded further, so that the junctions became excessively leaky, and all of the gain was lost.

Contaminant films were seen on the dice and wires of some of the devices of both manufacturers, but the nature and source were not determined. However, the material was not easily removed by water or alcohol. The rise of emitter forward voltage (VB_{EO}) in some devices, as compared to the collector forward drop, confirmed the rise in silicon resistivity.

This work was done by the Special Products Division of DCA Reliability Laboratory for **Marshall Space Flight Center**. *To obtain a copy of the report, Circle 17 on the TSP Request Card.*
MFS-25254

JANTX2N2432A Transistor

The effects of power and temperature overstress

Crystalonics and Texas Instruments were the manufacturers of these units. The Crystalonics sample lot showed no catastrophic failures in Group I. The transistors from Texas Instruments experienced six catastrophic failures toward the end of the testing. The durability of the Crystalonics lot became more apparent in the Group II (temperature-stress) testing. Although the Crystalonics lot experienced a greater total number of catastrophic failures, it was able to complete the entire Group II testing.

The Texas Instruments lot had to be stopped at the +225° C temperature step with a total of eight catastrophic failures. The majority of these were h_{FE} failures. This could indicate a change in emitter injection efficiency due to a diffusion of gold into the base under heat and bias over many hours.

In Group III, the Texas Instruments lot had 10 failures, and the Crystalonics lot had 8. Failure analysis showed that many of the failures developed weak emitter/base junctions. The high temperatures of the stress tests liberated sufficient contaminant within the devices so that both sample lots exhibited base inversions. The formation of gold/silicon intermetallics probably expedited the migration of contaminants by chemical attack on the oxide near the junctions.

This work was done by the Special Products Division of DCA Reliability Laboratory for **Marshall Space Flight Center**. *To obtain a copy of the report, Circle 18 on the TSP Request Card.*
MFS-25255

JANTX2N2484 Transistor

The effects of power and temperature overstress

Transistors manufactured by Raytheon had no failures in Group I; a Teledyne sample lot suffered only one failure during Group I testing.

In the Group II (temperature-stress) process, both sample lots had to be stopped at the +250° C step, 1,280 hours into testing. The Raytheon sample lot showed 9 out of 10 failures at the +250° C step of the process. The Teledyne lot showed a more even distribution of failures starting from the +200° C step, through the +250° C step, where (like the Raytheon lot) the job was stopped because the reject rate exceeded 50 percent of the sample lot.

Both lots develop aluminum/gold intermetallic formations ("purple plague") at the +250° C step. This could possibly be caused by the high temperature stress. The Raytheon samples all suffer from excess leakage, which can reasonably be ascribed to the movement of impurities, resulting from excess die temperature. On the Teledyne samples, the gold flowed away from the wires into the aluminum. This extreme attack on the gold may be due to an unusually high proportion of silicon doping in the aluminum metalization.

The Raytheon sample lot had failures in Group III. One failure came early in the testing at the +150° C step, due to a $V_{CE(SAT)}$ limit failure. Three more failures occurred at the +275° C step of the process, due to two I_{CBO} leakage failures and one h_{FE} limit failure. A Teledyne failure, which came at the last step (+300° C), was due to an excessive I_{CBO} leakage.

This work was done by the Special Products Division of DCA Reliability Laboratory for **Marshall Space Flight Center**. *To obtain a copy of the report, Circle 19 on the TSP Request Card.*
MFS-25253

JANTX2N2605 Transistor

The effects of power and temperature overstress

Group II and Group III testing proved to be the most detrimental of the three groups. Samples from Raytheon and National Semiconductor exhibited several microamperes of hysteresis in the BV_{CEO} curve trace. The pattern suggests the presence of contamination. The flow of metal from the gold leads and the intermetallics is one source of such contaminants.

The hysteresis currents in the base can inject base current that is not part of the known drive. Because of this, the h_{FE} will be high. At the same time, the contaminant may reduce emitter efficiency by reducing the lifetime of holes in the base. This tends to lower the h_{FE}.

Thus, the migration of contaminants during burn-in can have two opposite effects on the h_{FE} reading, and the net result depends upon which effect predominates in the individual sample at the moment of failure. When carried to extremes, gold migration in the base region will develop surface and junction-leakage problems and collector/emitter shorts. Possibly these failures could have been delayed to higher stress levels if aluminum wires were used in place of gold, thus removing the fast-migrating gold from the surface of the die.

This work was done by the Special Products Division of DCA Reliability Laboratory for **Marshall Space Flight Center**. *To obtain a copy of the report, Circle 20 on the TSP Request Card.*
MFS-25150

JANTX2N2905A Transistor

The effects of power and temperature overstress

Thirteen Motorola and Texas Instruments parts tested were destroyed by handling, and 31 others failed for a variety of other reasons. The most common of these was intermetallic formations due to temperature stress.

Visual inspection of one failed Texas Instruments unit in Group I revealed some areas of abraded metalization. One Motorola device was destroyed by electrical overstress.

In Group III testing, one Motorola unit lost most of its current gain without exhibiting any other junction anomalies sufficient to explain that loss. This suggests that the beta falloff was due to a loss of emitter injection efficiency, specifically a loss of hole lifetime and/or mobility. Such a change could be induced by the drifting of impurities under the influence of the high power and temperature. The increase in collector/emitter breakdown voltages upon opening the packages and the hysteresis seen on those measurements are evidence that contamination was indeed present within the packages.

Four Texas Instruments samples failed in Group III due to thermal overstress, which caused gold/aluminum intermetallics to form and which degraded the collector/base junctions. The excess die temperature and intermetallic attack on the oxide allowed metallic impurities to contaminate the oxide and thus degrade the transistor characteristics. The emitter/base junctions did not degrade because the higher boron concentration of the emitter diffusions "gettered" the impurities at the emitter/base junction.

This work was done by the Special Products Division of DCA Reliability Laboratory for **Marshall Space Flight Center**. *To obtain a copy of the report, Circle 21 on the TSP Request Card.*
MFS-25256

JANTX2N2920 Dual Transistor

The effects of power and temperature overstress

The only stress test that did any notable damage to the Fairchild and National Semiconductor lots was the Group II (temperature-stress) test. Many of the failures showed a marked loss of gain. There was no significant bulk or surface leakage on these parts. This would imply that the h_{FE} falloff was due only to a loss of emitter efficiency. The loss of efficiency, in turn, was due to the migration of gold and intermetallics under the influence of heat and electrical bias.

Since Group I does not reach the high junction temperatures of Group II, and since Group III does not reach the long time steps of Group II, could explain why there were not as many failures in the Group I and Group II testings.

This work was done by the Special Products Division of DCA Reliability Laboratory for **Marshall Space Flight Center**. *To obtain a copy of the report, Circle 22 on the TSP Request Card.*
MFS-25258

JANTX2N2945A Transistor

The effects of power and temperature overstress

For the Raytheon and Teledyne parts, only Group III was detrimental to both manufacturers' sample lots. The Raytheon sample lot was stopped 160 hours before the completion of the testing because half the lot failed the h_{FE} limits. Failure analysis showed that the samples for Raytheon have extensive gold/aluminum intermetallic formations. The absence of shorts, opens, and junction leakage suggests that the loss of h_{FE} was caused by a reduction in emitter efficiency.

The Teledyne samples experienced similar contaminations; and although testing of the lot was not stopped, it ended up having more catastrophic failures than the Raytheon lot. The fact that the reject rate in the Group III testing was slight compared to the Group II testing suggests that time was a factor. Group III testing reaches high temperatures, as does Group II, but the devices are held at these high temperatures 10 times longer in Group II than in Group III.

This work was done by the Special Products Division of DCA Reliability Laboratory for **Marshall Space Flight Center**. *To obtain a copy of the report, Circle 23 on the TSP Request Card.*
MFS-25259

JANTX2N3637 Transistor

The effects of power and temperature overstress

The testing of transistors manufactured by Transitron had to be stopped during Groups I and II. Motorola lots completed the entire test times in all three groups.

The Transitron devices have two different geometries, and the Motorola units have yet a third type. Transitron uses a rectangular layout and a butterfly pattern. The rectangular layout is superior to the butterfly pattern because it employs "field-plate" extension of the emitter metalization over the base/emitter junction. This is intended to reduce the tendency of p-channel transistors toward surface inversion. The Motorola chip appears to have a longer emitter periphery than either of the Transitron parts. This design is superior for minimizing h_{FE} falloff, increasing collector current, and reducing the emitter current density.

This work was done by the Special Products Division of DCA Reliability Laboratory for **Marshall Space Flight Center**. *To obtain a copy of the report, Circle 24 on the TSP Request Card.*
MFS-25264

JANTX2N3811 Dual Transistor

The effects of power and temperature overstress

Sample lots from National Semiconductor and Motorola held up well during the Group I (power-stress) testing. The Group II testing for National Semiconductor stopped at the 225° C step. Although the Motorola lot showed a higher total number of rejects, the majority of the failures occurred at the last step of the Group II testing.

Failure analysis showed that the National Semiconductor devices are constructed with gold-ball-bonded internal wires, while the Motorola devices have ultrasonically-bonded aluminum internal wires. This difference in construction may be the reason for the difference in performance between the two sample lots.

Hysteresis or leakage was a problem with a majority of the National Semiconductor parts. This pattern suggests the presence of contamination in (or on) the base diffusion. The flow of metal from the gold leads and the intermetallics, because of the stress, was one source of such contaminants. Possibly the National Semiconductor lot failures could have been postponed to higher stress levels if aluminum wires had been used instead of gold.

This work was done by the Special Products Division of DCA Reliability Laboratory for **Marshall Space Flight Center**. *To obtain a copy of the report, Circle 25 on the TSP Request Card.*
MFS-25265

JANTX2N4150 Transistor

The effects of power and temperature overstress

In Group I testing, a General Semiconductor sample lot had to be stopped 500 hours into the 125-percent maximum-rated-power step. A Transitron lot completed the entire testing with a total of seven failures. In Group II and Group III testings, Transitron experienced one catastrophic failure in each test, and General Semiconductor experienced six and seven, respectively.

The General Semiconductor samples had surface inversions and leakage due to contamination. Bare junction areas and the extremely high temperature contributed to the contamination vulnerability of these devices. There is a voltage threshold on these devices at which the inversion and drift of I_{CBO} are triggered. The leakage continues to increase over many seconds.

One Transitron failure had low-resistance contacts to emitter, collector, and base. This suggests that changes in the bulk silicon, such as an increase in base resistivity caused by the migration of gold under the heat and bias of the stress test, were the cause.

This work was done by the Special Products Division of DCA Reliability Laboratory for **Marshall Space Flight Center**. *To obtain a copy of the report, Circle 26 on the TSP Request Card.*
MFS-25267

JANTX2N4856 Field-Effect Transistor

The effects of power and temperature overstress

The Group II and Group III stress tests were the most detrimental of the three groups for transistors manufactured by Teledyne and Texas Instruments. Because of the similar failure mode observed in both groups, failure analysis was performed on samples from the Group II testing only.

The failure analysis pointed out that the majority of the devices exhibited, in various degrees, the effects of surface charges and metal migration. In one Texas Instruments sample, the aluminum had melted. This resulted in shorting the source and drain junctions. Aluminum/silicon eutectic melts at approximately 577° C, which indicates the extreme junction temperature reached by these samples.

This work was done by the Special Products Division of DCA Reliability Laboratory for **Marshall Space Flight Center**. *To obtain a copy of the report, Circle 27 on the TSP Request Card.*
MFS-25269

Electronic Systems

Hardware, Techniques, and Processes

21 Microprocessor-Controlled Data Synchronizer
22 Voltage Controller/Current Limiter for ac
23 Microprocessor Control for Phase-Lock Receiver
24 Improved Code-Tracking Loop
25 Multipath Star Switch Controller
26 Microprocessor-Based Detector for PSK Commands
27 Online Assessment of a Distributed Processor

Microprocessor-Controlled Data Synchronizer

A versatile receiver processes data at
a variety of rates and code formats.

Lyndon B. Johnson Space Center, Houston, Texas

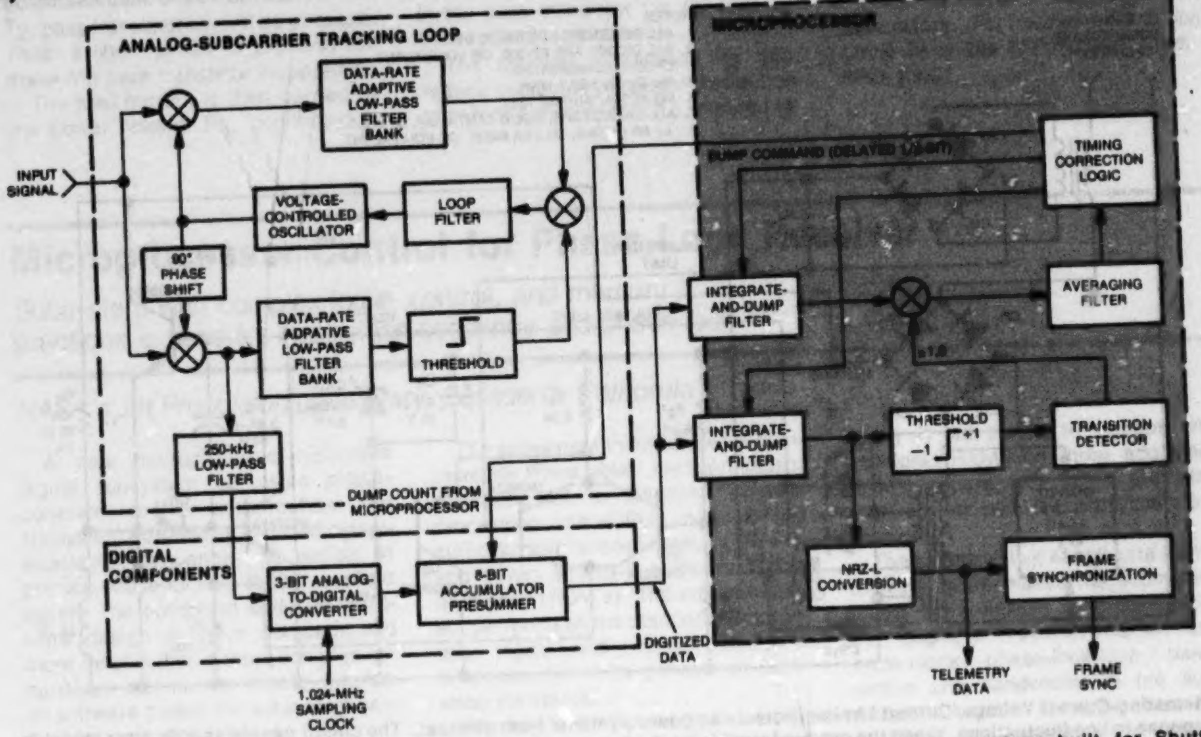
ANALOG-SUBCARRIER TRACKING LOOP
DATA-RATE ADAPTIVE LOW-PASS FILTER BANK
INPUT SIGNAL
VOLTAGE-CONTROLLED OSCILLATOR
LOOP FILTER
90° PHASE SHIFT
DATA-RATE ADPATIVE LOW-PASS FILTER BANK
THRESHOLD
250-kHz LOW-PASS FILTER
DUMP COUNT FROM MICROPROCESSOR
DIGITAL COMPONENTS
3-BIT ANALOG-TO-DIGITAL CONVERTER
8-BIT ACCUMULATOR PRESUMMER
1.024-MHz SAMPLING CLOCK
DIGITIZED DATA
MICROPROCESSOR
DUMP COMMAND (DELAYED 1/2-BIT)
TIMING CORRECTION LOGIC
INTEGRATE-AND-DUMP FILTER
AVERAGING FILTER
±1.0
INTEGRATE-AND-DUMP FILTER
THRESHOLD
+1
−1
TRANSITION DETECTOR
NRZ-L CONVERSION
FRAME SYNCHRONIZATION
TELEMETRY DATA
FRAME SYNC

The Microprocessor Accepts Digital Data from the front end of the telemetry receiver. A prototype built for Shuttle communications handles phase-shift-keyed modulated signals coded in biphase-L, biphase-M, biphase-S, NRZ-L, NRZ-M, or NRZ-S data at 1, 2, 4, 8, or 16 kb/s. Signal loss is less than 1.5 dB for signal-to-noise levels ranging from 2 to 11 dB at a minimum average bit-transition density of 12-1/2 percent (64 transitions per 512 bit periods). Signal acquisition typically occurs within 2,000 bit periods with 90 percent probability.

Telemetry data in a variety of rates and formats are processed by a versatile receiver designed around a custom bit-slice microprocessor. A prototype, built for 1.024-MHz communications between the Space Shuttle orbiter and a payload deployed up to 10 miles (16 km) away, handles phase-shift-keyed signals in any of six codes at rates varying between 1 and 16 kb/s. The receiver can be reprogramed to new rates and formats by changing the programs that control the processor.

As shown in the block diagram, the received signal is filtered and demodulated by analog circuitry, and the demodulated signal is digitized. Among the functions performed by the microprocessor on the digitized signal are:

- bit detection,
- NRZ-L conversion,
- frame synchronization (with programable word length),
- bit-sync acquisition and tracking,
- error-curve normalization,
- lock detection,
- half-bit-ambiguity resolution, and
- data-rate tracking.

The receiver program, stored in read-only memory on the microprocessor chip, is not written in standard assembly language. Instead, a language that is suited to parallel data transfers among the processor registers is used. (Much of the microprocessor operation is handled in parallel, allowing high-speed processing at minimum power consumption.) The language is intermediate between a high-level language and more conventional assembly languages. The mnemonics also simplify program revisions.

This work was done by Sam W. Houston, Donald R. Martin, and Larry R. Stine of TRW, Inc., for ***Johnson Space Center.*** *Further information may be found in the copyrighted article "Microprocessor Bit Synchronizer for Shuttle Payload Communications" from the IEEE Transactions on Communications, Copyright IEEE. To obtain a copy of the article, along with other documentation, Circle 28 on the TSP Request Card.*
MSC-18535

Voltage Controller/Current Limiter for ac

A circuit protects ac power
systems from overload failures.

NASA's Jet Propulsion Laboratory, Pasadena, California

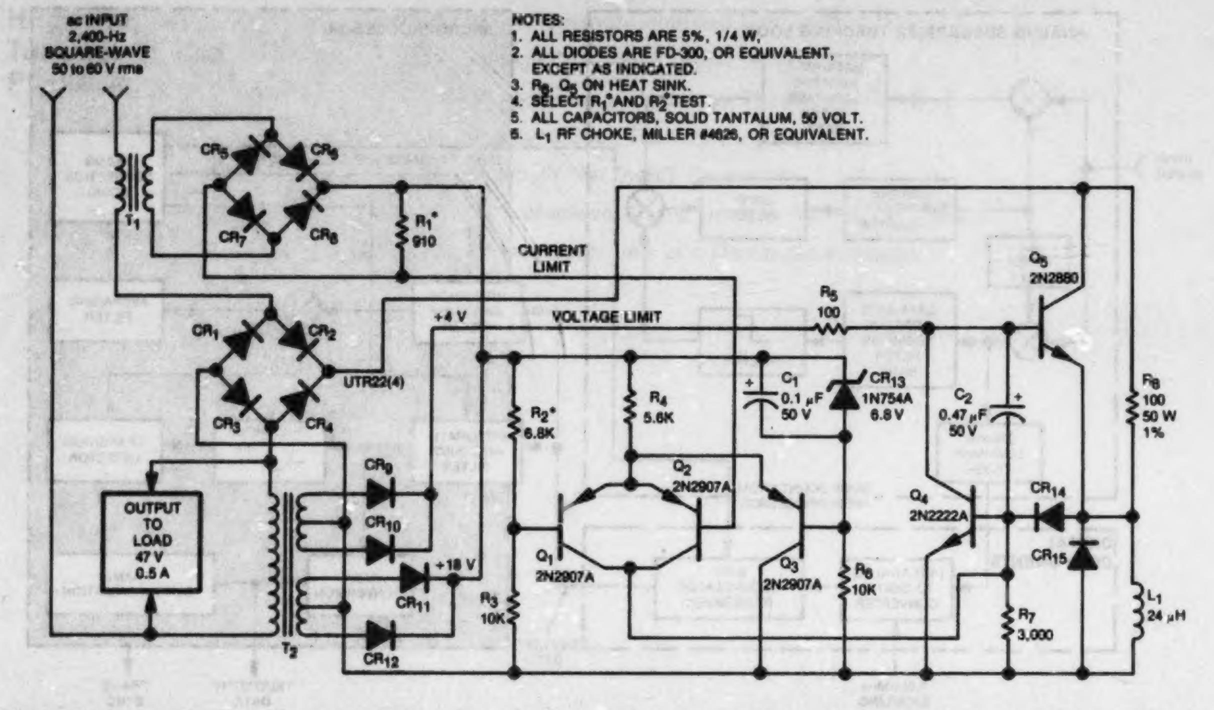
ac INPUT
2,400-Hz
SQUARE-WAVE
50 to 60 V rms
NOTES:
1. ALL RESISTORS ARE 5%, 1/4 W.
2. ALL DIODES ARE FD-300, OR EQUIVALENT, EXCEPT AS INDICATED.
3. R8, Q5 ON HEAT SINK.
4. SELECT R1* AND R2* TEST.
5. ALL CAPACITORS, SOLID TANTALUM, 50 VOLT.
6. L1 RF CHOKE, MILLER #4626, OR EQUIVALENT.
T1
CR5
CR6
CR7
CR8
R1*
910
CURRENT
LIMIT
CR1
CR2
CR3
CR4
UTR22(4)
+4 V
VOLTAGE LIMIT
R5
100
Q5
2N2880
OUTPUT
TO
LOAD
47 V
0.5 A
CR9
CR10
CR11
+18 V
CR12
T2
R2*
6.8K
R3
10K
R4
5.6K
C1
0.1 μF
50 V
CR13
1N754A
6.8 V
C2
0.47 μF
50 V
R8
100
50 W
1%
Q2
2N2907A
Q1
2N2907A
Q3
2N2907A
R6
10K
Q4
2N2222A
CR14
CR15
R7
3,000
L1
24 μH

Alternating-Current Voltage/Current Limiter protects ac power systems from overload. The circuit generates a dc error signal in response to line fluctuations. When the overload level is reached, transistor Q_5 is cut off, dumping power into the power resistor R_8 and inductor L_1 branch. Excess power is dissipated in R_8, and the current rise time is limited by the L_1, limiting power to the load.

A voltage- and current-limiting circuit uses feedback to prevent excessive transients and current and voltage fluctuations in ac power systems. Positioned between the source and the load, the circuit limits power-surge and short-circuit currents to 150 percent or less of their steady-state levels. In addition, it regulates the ac output voltage to a constant level and "soft starts" the load.

Basically the circuit generates dc error signal in response to current or voltage fluctuations on the line. This signal is applied to a pass transistor that is cut off when the line current or voltage exceeds a set limit. A closed-loop feedback is formed to limit the overload.

The circuit (see figure) uses a full-wave bridge rectifier (diodes CR_1 through CR_4) that converts ac line current to dc current. Power transistor Q_5 is the pass transistor and is mounted on a heat sink. The ac line current is "sensed" by current transformer T_1 with a 100:1 current stepdown ratio. The current transformer output is converted into a dc voltage through a full-wave diode bridge (CR_5 through CR_8) and resistor R_1. This voltage, which represents ac current, is compared with a reference voltage (CR_{13}) in a modified differential-amplifier circuit (Q_2, Q_3).

The output load voltage is "sensed" by transformer T_2, which also feeds dc power for the operation of the differential amplifier and base-drive current for the pass transistor (Q_5). This signal is fed into the differential amplifier (Q_1) through the resistor divider network (R_2, R_3).

Transistor Q_4 generates additional amplifier gain and reduces the power requirement for the differential amplifier. Inductor L_1 and capacitor C_2 provide high-frequency rolloff and prevent high-frequency oscillation when the limiter circuit goes into limiting action.

The inductor L_1 also limits current rise time (di/dt) via feedback through transistor Q_4 and diode CR_{14}. Capacitor C_1 is used to reduce voltage- and current-limit set points by slow buildup of reference voltage during initial power turn-on. Capacitor C_1 thus provides a gradual buildup of reference voltage during initial power turn-on and prevents current surges that may exceed limit during this transition period. The controlled voltage and current buildup soft starts the load devices.

There is also unique short-circuit protection. If the output load is short-circuited and develops little or no voltage, transformer T_2, which is across the load, will have little or no secondary output voltage. Since the pass transistor (power transistor Q_5) obtains its base drive from transformer T_2, pass transistor Q_5 will be at cutoff. Thus, a short circuit at the load will make the pass transistor inoperative.

The load current is then carried by the power resistor R_8, connected in parallel with the pass transistor. This approach completely eliminates the danger of thermal runaway of the pass transistor and consequently failure of the control circuit, as tested in the most severe conditions of current limiting. Resistor R_8 also drastically reduces maximum power dissipation in the pass transistor Q_8 by sharing the rectified load current.

The addition of resistor R_8 can reduce maximum transistor dissipation to only one-third as much compared to that without the resistor. With the short-circuit current determined only by R_8, the maximum allowable current level in the illustrated circuit is set at 100 percent of normal load current to reduce circuit dissipation and to increase reliability.

This work was done by Ta Tzu Wu of Caltech for **NASA's Jet Propulsion Laboratory.** *For further information, Circle 29 on the TSP Request Card.*
NPO-13061

Microprocessor Control for Phase-Lock Receiver

Subsystem with complex logic, control, and memory functions is used for acquisition sequence and phase lock.

NASA's Jet Propulsion Laboratory, Pasadena, California

A new microprocessor-controlled digital subsystem optimizes phase-coherent receiver performance. The subsystem controls an involved signal-acquisition sequence and assists in precise phase-locking to the received signal. The combined software/hardware design is more compact and more reliable than a more complex all-hardware alternative. Heavy reliance on software makes the subsystem very flexible to modifications.

The subsystem is incorporated into the NASA standard-TDRSS (Tracking and Data Relay Satellite System) user transponder. Its major functions include: (a) the selection of 1 of a family of 85 sets of pseudorandom-noise (PN) codes used to spread the received and transmitted signals, (b) the selection of one of several possible command data rates, (c) automatic configuration modification to receive a nonspread signal with an alternate data rate when such signal is detected, and (d) the selection of various receiver configurations and transmitter modulation data and PN-spreading code formats in response to control-command inputs.

The subsystem incorporates a commercially available microprocessor consisting of a standard control-processing unit (CPU), one 32-by-8 static random-access memory (RAM), and seven 512-by-8 static read-only memories (ROM's). The microprocessor performs all the standard sequencing, logic, and control functions characteristic of its general performance standards.

The key to the operation lies in the software programs, which include system and code-generator initialization routines and executive routine, utility subroutines, control sequence routines for each of the receiver acquisition states, a control-command decoding routine, and lookup tables for code-generator configuration versus code-set numbers. Programable ROM's have been used during transponder development to facilitate possible modifications of the subsystem.

Additional ROM's, RAM's, and I/O (input/output) buffers can be paralleled on the bidirectional data bus for further subsystem expansion. The multilayered printed-wiring memory board is adaptable to accept one additional RAM and three additional ROM's. Spare I/O bytes are also available for possible subsystem expansion.

The extensive use of software rather than hardware makes the subsystem much more flexible to modification. For example, receiver carrier and code-clock phase-lock-loop bandwidths and bandwidths in the suppressed carrier detector can be switched as necessary to match requirements during each step of the acquisition sequence. Steps can also be added as necessary in the acquisition sequence to extend the input-signal dynamic range by testing for false code lock on an autocorrelation side lobe.

This work was done by Lansing M. Carson and James R. Shaner of Motorola, Inc., for **NASA's Jet Propulsion Laboratory.** *For further information, Circle 30 on the TSP Request Card.*
NPO-14438

Improved Code-Tracking Loop

A new delay-locked loop is unaffected by gain imbalance.

Lyndon B. Johnson Space Center, Houston, Texas

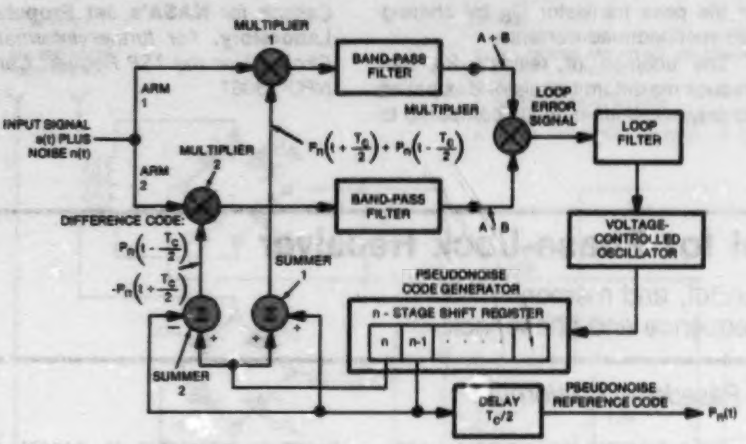
MULTIPLIER 1
BAND-PASS FILTER
A + B
ARM 1
INPUT SIGNAL s(t) PLUS NOISE n(t)
MULTIPLIER
LOOP ERROR SIGNAL
LOOP FILTER
$P_n\left(t+\frac{T_c}{2}\right)+P_n\left(t-\frac{T_c}{2}\right)$
MULTIPLIER 2
ARM 2
BAND-PASS FILTER
A – B
DIFFERENCE CODE:
$P_n\left(t-\frac{T_c}{2}\right)$
$-P_n\left(t+\frac{T_c}{2}\right)$
VOLTAGE-CONTROLLED OSCILLATOR
SUMMER 1
PSEUDONOISE CODE GENERATOR
n - STAGE SHIFT REGISTER
n
n-1
1
SUMMER 2
DELAY $T_c/2$
PSEUDONOISE REFERENCE CODE
$P_n(t)$

The New Delay-Locked Loop tracks pseudonoise codes without introducing dc timing errors due to gain imbalance between arms 1 and 2. Summer 1 applies the sum of the early and late codes to multiplier 1; summer 2 applies the difference between the early and late codes to multiplier 2.

An improved delay-locked loop (DLL) is insensitive to gain imbalance between its signal-processing arms and therefore eliminates dc timing errors. Loop tracking performance is equivalent to that of previous DLL circuits. The delay-locked loop is used for tracking pseudonoise codes in digital receivers.

The new circuit is arranged so that "early" and "late" reference codes pass in a combined form through both arms instead of through separate arms. Since each arm acts on both codes, differences in gain between the two arms cannot cause a timing offset at their outputs.

In the previous DLL, the received signal and its noise component are applied to the two signal-processing arms, each of which contains a multiplier and a square-law detector. One multiplier receives a late reference code from the last stage (n) of the shift register in a pseudonoise code generator; the other multiplier receives an early reference code from the next-to-last stage (n-1) of the shift register. Unless both arms have exactly equal gains, which is difficult to ensure, the loop error signal will have a dc offset or bias, and a timing error in the pseudonoise reference code will result.

In the new DLL (see figure), the received signal and noise are applied to both arms, as in the previous circuit; however, instead of receiving just the late reference code, multiplier 1 receives the late code plus the early code, and multiplier 2 receives the early code minus the late code. Multiplier 1 forms a sum product signal by multiplying the reference code sum with the incoming signal. Multiplier 2 forms a difference product signal by multiplying the reference code difference with the incoming signal. Any gain imbalance between multipliers 1 and 2 therefore has an equal effect on the data in stage n and stage n-1 of the shift register.

After going through a band-pass filter, the contents of arm 1 represent the product of the data portion S(n) of the incoming signal and the sum reference code. Similarly, after filtering, the contents of arm 2 represent the product of S(n) and the difference reference code.

The products are furnished to a multiplier, which forms an error signal. After filtering, the error signal is applied to a voltage-controlled oscillator, which provides the input to the shift register in the pseudonoise generator.

Often, a tau-dither loop is used instead of a delay-locked loop because of the gain imbalance problem. The new DLL not only is insensitive to gain imbalance but can accommodate weaker input signals; for equal tracking performance, the tau-dither loop requires a 1-dB greater signal-to-noise ratio than the new DLL.

This work was done by David T. LaFlame of Hughes Aircraft Co. for ***Johnson Space Center.*** *For further information, Circle 31 on the TSP Request Card.*

This invention is owned by NASA, and a patent application has been filed. Inquiries concerning nonexclusive or exclusive license for its commercial development should be addressed to the Patent Counsel, Johnson Space Center [see page A5]. Refer to MSC-18035.

Multipath Star Switch Controller

A function control method is proposed for multiple computer data-processing systems.

NASA's Jet Propulsion Laboratory, Pasadena, California

A proposed star switch concept is a means for a number of parallel computers to scan several common-network-connected data stations at a maximum rate. This is accomplished by using "leapfrog" sequencing to bypass any port already being serviced by another computer. A combination of functional logic techniques is used to raise the number of possible data paths in the system without installing additional connective hardware.

The output address for each path is held in individual hold registers. For internal switching of the timing control lines, their control logic is multiplexed so that only one path is in the process of being established at any one time. This avoids input-port collision between data paths. The address systems are asynchronous as to positions between systems but are otherwise synchronized to the same internal service clock.

The figure shows the concept for two sequencers X and Y. Each sequencer is implemented using a 4-bit hold register and a 4-bit adder connected end around. The second vector connected to the adder during normal operation is a constant 1. When using this sequencer implementation, a "leapfrog" operation becomes very simple. Two binary coincidence circuits are connected, one between X (the output of register X) and Y + 1 (the output from the adder in the end-around circuit) and one between Y and X + 1.

The outputs from the coincidence circuits are cross-coupled to the (2^1) terms of the second vectors in each adder. When the (2^1) term is turned on, the (2^0) term is turned off.

A sequencer leapfrogs only when the other sequencer is one step ahead and quiescent. All connections are cross-coupled so that when any one of the two sequencers is ahead one step, the second sequencer will leapfrog as they may alternate on being ahead because of their being randomly halted.

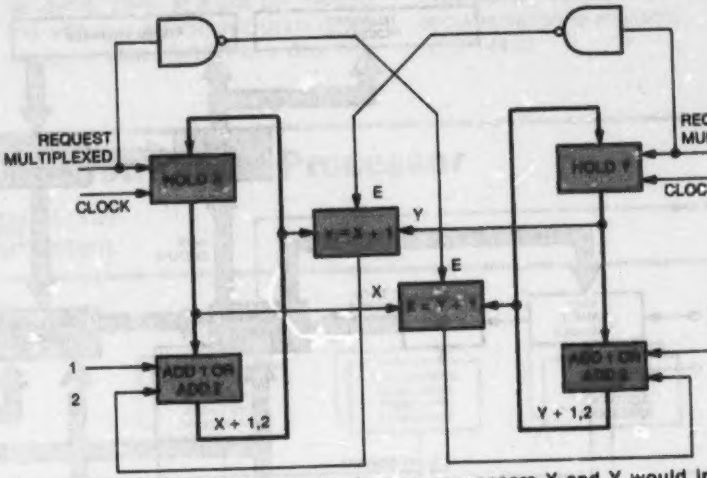

A Proposed Star Switch Controller for two sequencers X and Y would incorporate each sequencer using a 4-bit hold register and a 4-bit adder connected end around. The scheme would permit a number of parallel computers to scan a number of common-network-connected stations at a maximum rate, using "leapfrog" sequencing to bypass any part already being serviced by another computer.

For a three-sequencer system any two out of three sequencers are first cross-coupled in the same manner as for the two-sequencer system shown in the figure. In addition, any two sequencers halted at adjacent positions must be detected. When this occurs and the third is adjacent and operating, both the (2^0) and (2^1) terms of the fixed vector of the adder are energized so that it will advance three positions; i.e., leapfrog the two adjacent and quiescent sequencers.

A two-path system is only slightly more complex than a single-path system. Thus, a two-path system for a 16-port star switch controller would be cost-effective if the added bandwidth were required or the increased reliability were desired. A multiple-path system, however, becomes exponentially more complex. The triple-path system is yet manageable, but it may not be a cost-effective design for a 16-port system, although for a 32-port system it probably would.

This work was done by Tage O. Anderson of Caltech for ***NASA's Jet Propulsion Laboratory.*** *For further information, Circle 32 on the TSP Request Card.*

This invention has been patented by NASA [U.S. Patent No. 3,916,380]. Inquiries concerning nonexclusive or exclusive license for its commercial development should be addressed to the Patent Counsel, NASA Resident Legal Office-JPL [see page A5]. Refer to NPO-13422.

Microprocessor-Based Detector for PSK Commands

Command-detector unit operates over a wide range of data rates and signal levels in a space environment.

NASA's Jet Propulsion Laboratory, Pasadena, California

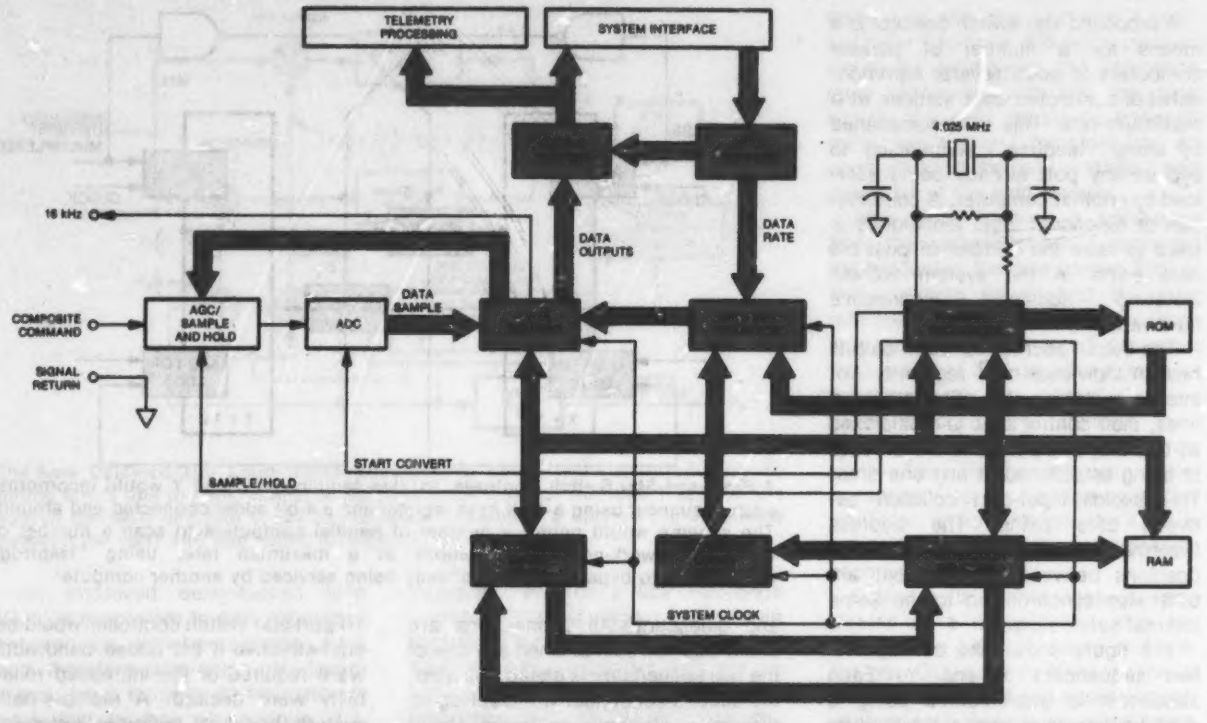

The Command Detector shown here as a block diagram consists of signal conditioning, read-only memory, random-access memory, and a digital processor. The entire command-detector unit fits on a single multilayer printed-wiring board. The components shown in color constitute the digital processor.

Command signals radioed to a spacecraft can be processed efficiently in a microprocessor-controlled command-detector unit (CDU) designed to be part of a standard transponder. The CDU is a coherent demodulator for binary phase-shift-keyed (PSK) signals on a 16-kHz subcarrier; it is readily adaptable to nine data rates ranging from 7.8 to 2,000 bits per second and can accommodate input levels over a 40-dB range. A comfortable performance margin is achieved through the power-and-weight-saving approach of digital signal processing using radiation-shielded CMOS custom large-scale integration (LSI).

Functionally, the command detector consists of a data-coherent automatic gain control (AGC), a sample-and-hold (S/H) circuit, an analog-to-digital converter (ADC), a second-order data-aided subcarrier tracking loop, a data-transition bit-synchronization loop, and a lock detector. Structurally, the detector consists (see figure) of the signal conditioning (AGC, S/H, and ADC), read-only memory (ROM), random-access memory (RAM), and a digital processor that uses a metal-gate CMOS technology.

The data-coherent AGC consists of logarithmic-linear digitally controlled attenuation with dynamic range in excess of 40 dB. Its loop performance (e.g., noise jitter and settling time) is determined by the AGC loop algorithm and coefficients stored in ROM. Upon receipt of the appropriate command from the digital processor, the sample-and-hold circuit freezes the analog input to the 8-bit successive-approximation analog-to-digital converter and holds it constant over the conversion time.

Unlike typical analog or digital data-aided loops — requiring mixers, filters, and analog-to-digital converters in both in-phase and quadrature synchronization channels — the sinusoidal subcarrier tracking loop implements the two synchronization channels with sample accumulators within the digital processor. The sample rate is constant over all data rates, resulting in design economy without compromised performance. A second-order subcarrier loop is in the demodulator algorithm in ROM, with ROM-resident loop coefficients selected to minimize steady-state phase jitter.

The data-transition bit-synchronization loop is driven by the contents of another dedicated sample accumulator within the digital processor. The loop resolution needs only to be accurate to within a subcarrier cycle to provide effective bit-synchronization resolution of 1/64 of a subcarrier cycle. Thus, at 8 bits per second, the effective bit-synchronization resolution is about 8×10^{-6} of a data bit.

The lock detection algorithm and coefficients are also ROM-resident, allowing complete flexibility in tailoring the demodulator to meet performance requirements.

This work was done by James Durden and Stephen W. Klare of Motorola, Inc., for **NASA's Jet Propulsion Laboratory.** *No further documentation is available.*
NPO-14440

Online Assessment of a Distributed Processor

Test sequence determines the operational readiness of a multicomputer test system.

John F. Kennedy Space Center, Florida

An operational readiness test (ORT) checks out a computer complex composed of many minicomputers. Developed for the Space Shuttle prelaunch checkout, the ORT software performs morning "wakeup" testing as well as testing before and after launch to determine the readiness of the checkout complex. This approach to online assessment of a distributed processor should interest the users of similar equipment in other applications.

The prelaunch-checkout complex consists of up to 64 minicomputers connected via a common data buffer (CDBFR) — a bipolar solid-state memory — to each other, to a central data system, and to peripheral equipment (see figure). The ORT software system allows a test engineer to run a complete readiness test on the complex from one console.

The ORT first makes a "rollcall" to determine the operability of:

- the peripheral equipment directly connected to the "host" minicomputer (the host minicomputer console is the one used by the test engineer),
- the minicomputers available through the CDBFR,
- the special peripheral units available within the CDBFR, and
- the peripheral units directly connected to the minicomputers.

The system then tests all minicomputer subsystems simultaneously in their operational modes.

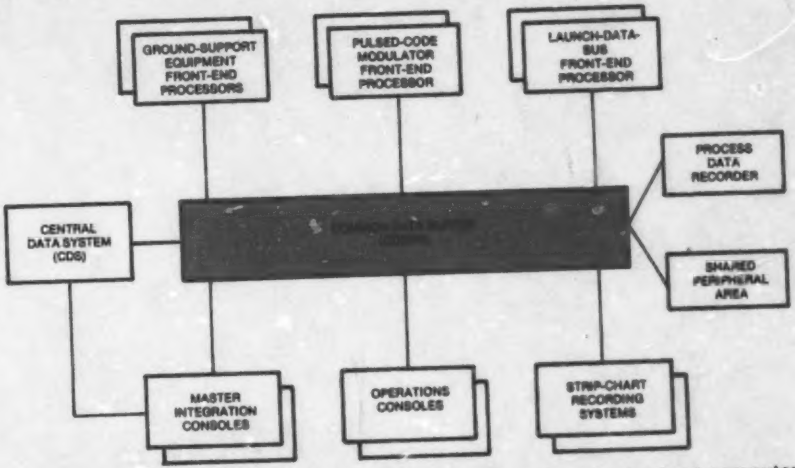
GROUND-SUPPORT EQUIPMENT FRONT-END PROCESSORS
PULSED-CODE MODULATOR FRONT-END PROCESSOR
LAUNCH-DATA-BUS FRONT-END PROCESSOR
PROCESS DATA RECORDER
CENTRAL DATA SYSTEM (CDS)
COMMON DATA BUFFER (CDBFR)
SHARED PERIPHERAL AREA
MASTER INTEGRATION CONSOLES
OPERATIONS CONSOLES
STRIP-CHART RECORDING SYSTEMS

A **Common Data Buffer** links the many elements of a prelaunch-checkout computer complex and gives the operational-readiness-test (ORT) software system access to the various minicomputers and their peripherals.

The ORT sequences, which are integrated into the rest of the prelaunch-checkout system, are based on run tables derived from the hardware configuration used during an actual launch. The test engineer can edit the tables in real time so that the test sequence accommodates changing hardware configurations and matches the configurations available at test time. Editing also allows the engineer to test any single peripheral unit or minicomputer.

The ORT system loads the prelaunch-checkout computers with instructions and data, either from disk storage or via the CDBFR. Test results are returned to the host minicomputer and displayed. On completion of a test, the affected subsystem is restored to its original condition, ready for use. To prevent a failed subsystem from halting a test sequence, the ORT uses an automatic "watchdog" timer to terminate a given test after a preset interval; it then moves on to the next test in the sequence.

(continued on next page)

To minimize testing time, the subsystems are tested in parallel. With this scheme, a complete system rollcall can be done in about 15 minutes.

This work was done by L. F. Ehrlich of IBM Corp. for **Kennedy Space Center.** *To obtain a copy of a report describing the ORT system in more detail [program listing is not included], Circle 33 on the TSP Request Card.*

Inquiries concerning rights for the commercial use of this invention should be addressed to the Patent Counsel, Kennedy Space Center [see page A5]. Refer to KSC-11124.*

Physical Sciences

Hardware, Techniques, and Processes

31 Photoelectrochemical Cell With Nondissolving Anode
32 New Mounting Improves Solar-Cell Efficiency
33 Energy-Saving Thermostat
34 Rotatable Prism for Pan and Tilt
34 Ultraviolet Spectrometer/Polarimeter
35 An Adjustable Solar Concentrator
36 Large-Volume Multiple-Path Nuclear-Pumped Laser
37 Extracting Energy From Natural Flow

Books and Reports

38 Twelve Solar-Heating/Cooling Systems: Design and Development
38 Solar-Heating and Cooling System Design Package
38 Benefit Assessment of Solar-Augmented Natural-Gas Systems
39 Air-Cooled Solar-Collector Specification
39 Indoor Tests of the Concentric-Tube Solar Collector
39 Evacuated-Tube Solar Collector — Performance Evaluation
40 Glycol/Water Evacuated-Tube Solar Collector
40 Thermosyphon Heat Exchanger
40 Controller for Solar-Energy Systems
41 Controller and Temperature Monitor for Solar Heating
41 Inhibiting Corrosion in Solar-Heating and Cooling Systems

Computer Programs

41 Numerical Tracing of Electron Trajectories
42 NASA Charging Analyzer Program

Photoelectrochemical Cell With Nondissolving Anode

New cell may be an economical alternative to silicon solar cell.

Langley Research Center, Hampton, Virginia

An improved electrolytic photovoltaic cell converts solar energy to electricity without electrode decomposition. Cell efficiencies up to 15 percent have been measured, which are comparable to those of the best silicon solar cells. However, the costs of materials and fabrication for electrolytic cells are potentially less than for silicon cells.

Previous efforts to build practical electrolytic solar cells were hampered because the anode would dissolve in the electrolyte under the influence of the incident Sunlight. The new cell employs electrolytes that overcome this tendency.

The cell consists of a light-sensitive n-type semiconductor anode and a metallic cathode both immersed in an electrolytic solution (see figure). The cathode and the anode are electrically interconnected by an external load. Sunlight passing through the transparent container strikes the anode. The incident photons excite the anode, which establishes a current between the two electrodes.

The anode materials tested were CdS, CdSe, CdTe, GaP, GaAs, and InP; and the tested electrolytes were Na_2X/X_n, where X is S, Se, or Te. Results show that the CdS and CdSe are the most stable anode materials and that all the anode materials are stable in the Na_2Te/Te_n. Some of the other electrode/electrolyte combinations are also successful.

A key element of these cells is that the reversible redox systems employed not only result in no net chemical change in the electrolyte but also stabilize the n-type semiconductor photoelectrode to photoanodic dissolution. Presumably, the electrolyte additive is capable of undergoing photoinduced oxidation at the semiconductor electrode at a rate that completely overwhelms the general photoanodic dissolution reaction of the small-band-gap n-type semiconductors.

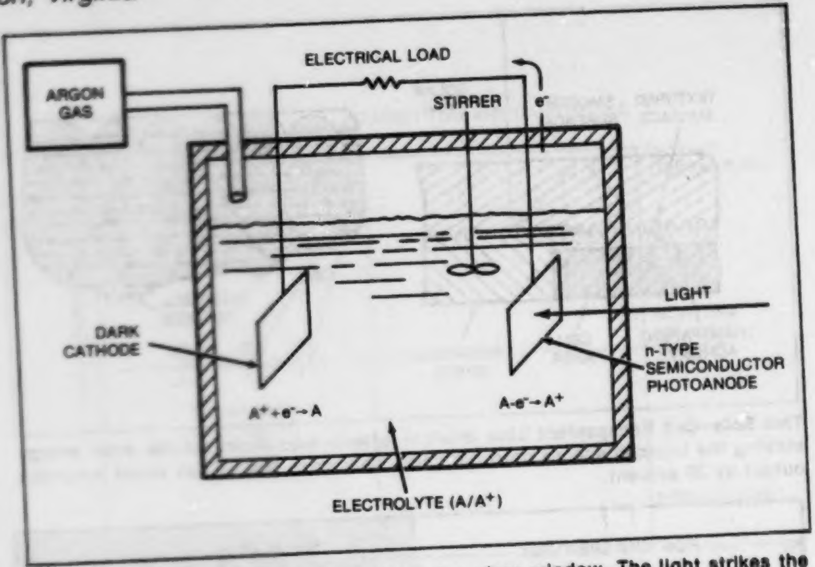

Photochemical Cell admits Sunlight through a glass window. The light strikes the semiconductor anode, which begins to conduct. A sodium compound (represented by A) oxidizes at the anode and is reduced at the cathode in a continuous cycle.

The cell can produce more than 500 mW of power per cm^2 of anode area at an output voltage of about 0.4 V. The anode has been operated at current densities as high as 16 mA/cm^2 with no deterioration.

Both single-crystal and less-costly polycrystalline semiconductors have been used as the anode. The stability of the anode is not affected by the crystal structure, although the single-crystal type is more efficient.

Argon fed over the electrolyte prevents the electrode from being oxidized by air and gently circulates the solution. Low electrolyte concentrations are circulated by using a motor-driven stirrer between the anode and cathode.

This work was done by Arthur B. Ellis, Steven W. Kaiser, and Mark S. Wrighton of the Massachusetts Institute of Technology for **Langley Research Center.** *For further information, Circle 34 on the TSP Request Card.*

Title to this invention has been waived under the provisions of the National Aeronautics and Space Act [42 U.S.C. 2457(f)], to the Massachusetts Institute of Technology, 77 Massachusetts Ave., Cambridge, MA 02139.
LAR-12591

New Mounting Improves Solar-Cell Efficiency

Solar-cell modules are modified to maximize solar-energy collection.

NASA's Jet Propulsion Laboratory, Pasadena, California

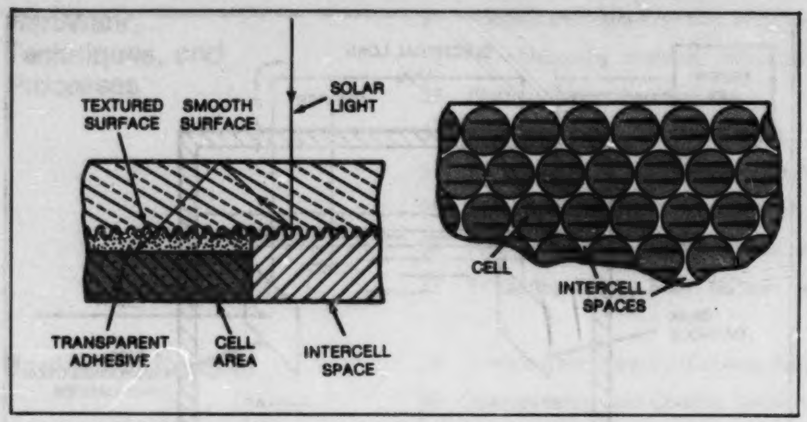

This Solar-Cell Encapsulant uses internal reflection to direct all the solar energy striking the intercell spaces onto the cells. This extra energy can boost solar-cell output by 20 percent.

Aperture Diameter (mm)	Short-Circuit Current at 100 mW/cm² and 28° C (mA)
53	672
64	752
76	792
89	812
102	823

Illumination Test Results show an increase in current for an increase in "intercell" space. Interpolation of these results indicates that for a typical interspace area equal to 55 percent of cell area, there is a 20 percent enhancement of short-circuit current.

A tested method of mounting and encapsulating solar cells traps solar radiation falling on intercell spaces and redirects it onto the cell surfaces by repeated internal reflection. This added energy can boost output by about 20 percent without increasing the module depth as is required with conventional concentrators for solar-cell arrays.

When mounted, the solar-cell array is covered with an internally reflecting plate (see figure) made from commercially-available highly transparent material. (Its outer surface is smooth, and the inner surface in contact with the module is textured.) The plate is attached to each cell by a transparent adhesive. The space between cells is covered with a layer of diffusely reflecting material.

Solar energy falling on the spaces between cells is diffused and reflected internally by the plate until it is reflected onto a solar cell. In a test of the technique, a single cell with a diameter of 53 mm was mounted as shown in the figure, with a surrounding "white space." The cell was covered with an opaque plate having a cutout the same size as the cell, and the output was measured. Plates with larger cutouts were then placed over the cell to measure the contribution of energy falling on varying amounts of intercell space. The results, as shown in the table, indicate that light falling on the "intercell" space is redirected to the cell.

This work was done by Neal F. Shepard, Jr., of General Electric Co. for **NASA's Jet Propulsion Laboratory.** *For further information, Circle 35 on the TSP Request Card.*

This invention has been patented by NASA [U.S. Patent No. 4,162,928]. Inquiries concerning nonexclusive or exclusive license for its commercial development should be addressed to the Patent Counsel, NASA Resident Legal Office-JPL [see page A5]. Refer to NPO-14467.

Energy-Saving Thermostat

Control unit and method for two-stage heating system

Langley Research Center, Hampton, Virginia

A new energy-and-cost-saving thermostat establishes a basic control concept for a two-stage heating system. It is based on a night-setback thermostat that controls a heating system according to a preprogramed schedule. The room set-point temperature schedule incorporates the desired room temperature, the time to reach the desired temperature (or target time), and the outside-air (OSA) temperature. The control turns heat off and on, according to building needs, in such a way as to reduce the amount of second-stage heating, which in two-stage systems such as heat pumps is the more-expensive resistance electrical heating.

The main purpose of the thermostat is to lower the temperature at night and to turn on the heat at the latest time necessary to have a room heated up at a chosen hour in the morning.

The second objective of the thermostat is to control second-stage heating. A typical setback thermostat initiates a large temperature set point adjustment in the morning. If after this adjustment there is still a large difference between the desired set point and actual room temperatures as could be expected the second stage is turned on even though the more-efficient first stage could raise the temperature, given enough time. In the new system, the thermostat room set-point temperature is preprogramed to rise gradually, allowing the heat pump used in the first stage to raise the room temperature. This saves considerable energy costs by reserving expensive second-stage resistance electrical heating for periods too cold for the first stage alone.

The diagram shows the desired temperature set point versus time. If the actual room temperature closely follows the adjusting set-point temperature, the second stage will not activate.

The control can be mechanical, electrical, electronic, pneumatic, or a microprocessor. A mechanical device has already been designed, and Langley Research Center is installing a microprocessor version in a building equipped with a heat pump. Sufficient data will be taken to evaluate the effectiveness of the concept.

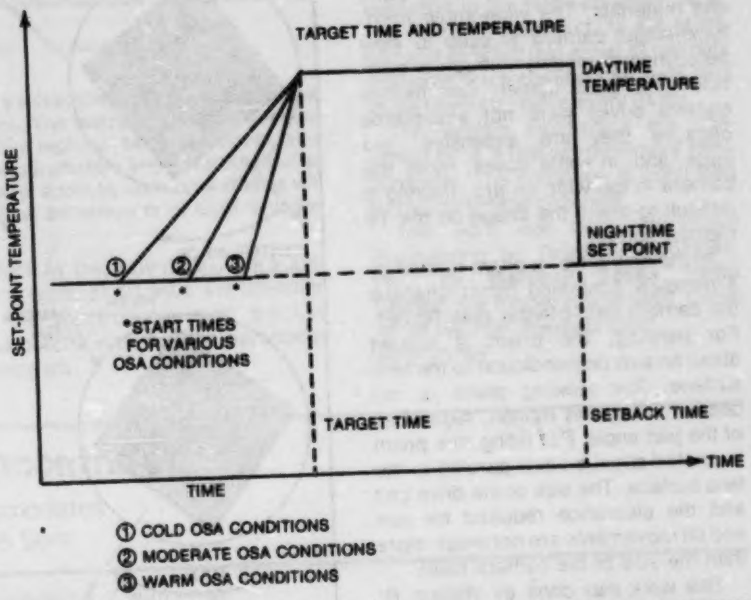

Set-Point-vs.-Time chart shows how the time required for the first (heat-pump) stage of a two-stage heating system to raise room temperature to a desired level varies with the outside-air (OSA) temperature. The new thermostat adjusts the turn-on time accordingly and reduces the amount of expensive second-stage (electrical-resistance) heating required.

The thermostat will be programed with the desired space temperature and a minimum setback temperature. A target time will be set corresponding to working hours in the building. A variable room set-point temperature will be a function of the outside-air temperature and time period before target time. If the room temperature rises above the variable set-point temperature, the heating unit shuts off; if the room temperature drops below the set-point temperature, first-stage heating is activated.

Only if the room temperature drops several degrees further below the set-point temperature is the expensive second stage activated. Correctional factors are to be included for cases where it is determined that the second-stage operation is more cost- and energy-effective than prolonged first-stage-only operation, such as when extremely-cold outside-air temperatures are encountered and the heat-pump coefficient of performance is low.

This work was done by Ronald N. Jensen of **Langley Research Center.** *No further documentation is available.*

Inquiries concerning rights for the commercial use of this invention should be addressed to the Patent Counsel, Langley Research Center [see page A5]. Refer to LAR-12450.

Rotatable Prism for Pan and Tilt

Compact, inexpensive drive changes the field-of-view of a TV camera.

Langley Research Center, Hampton, Virginia

A stationary television camera has been adapted so that it can pan and tilt with the aid of low-cost stock parts and materials. The wide-angle fixed-focal-length camera is used to view aerodynamic models through a porthole in a wind tunnel. Commercial camera drives were not acceptable because they are expensive, too large, and, in some cases, move the camera in too wide an arc, making it difficult to orient the image on the TV monitor screen.

In the new drive, a prism rotated by a remotely controlled motor changes the camera field-of-view (see figure). For panning, the prism is rotated about an axis perpendicular to the lens surface. The viewing plane is not disoriented by this motion, regardless of the pan angle. For tilting, the prism is rotated about an axis parallel to the lens surface. The size of the drive unit and the clearance required for pan and tilt movements are not much more than the size of the camera itself.

This work was done by William B. Ball of **Langley Research Center.** *No further documentation is available.*
LAR-12368

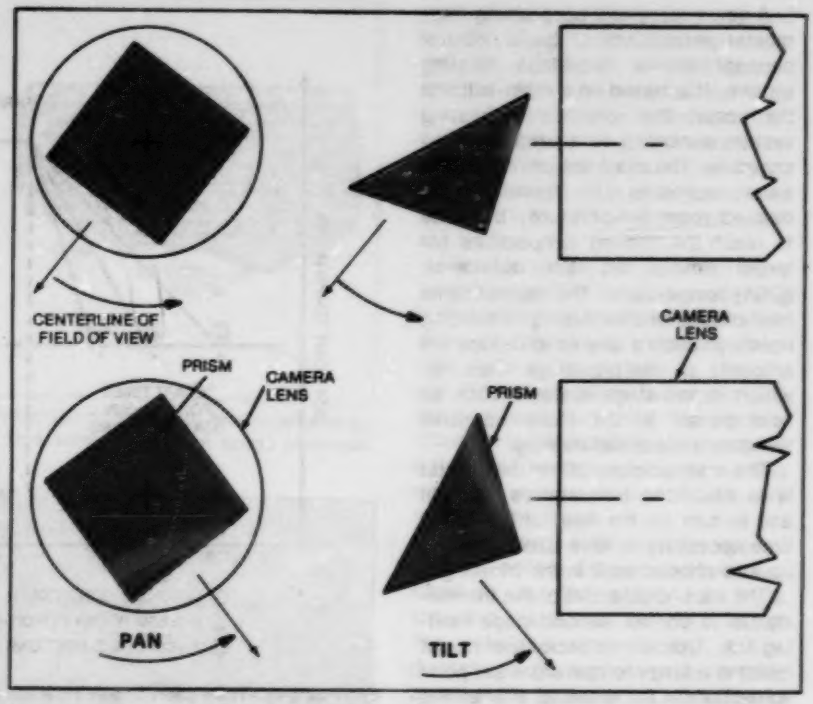

Panning Effect (left) is produced by rotating the camera and prism about the lens axis. The image is tilted by rotating the prism around an axis parallel to the lens (right).

Ultraviolet Spectrometer/Polarimeter

A combined instrument package for ultraviolet studies of solar radiation and of Earth's atmosphere

Marshall Space Flight Center, Alabama

A satellite instrument package has been developed to study solar ultraviolet radiation, particularly from flares and active regions, and to measure the constituents of Earth's atmosphere at the satellite dawn and dusk. The package consists of a telescope, a spectrometer with a polarimeter, five detectors, and the necessary electronics. The ultraviolet spectral range can be observed from 1,150 to 3,600 Å, with emphasis on the region from 1,150 to 2,000 Å. The instrument is controlled by a minicomputer that can interact with the data stream to modify the observation program.

The package is an improved version of a previously-used telescope/spectrometer system. Its major feature is the polarimeter that will allow all four Stokes parameters to be determined, giving the first such data down to about 1,200 Å. Data on possible mechanisms that produce linear and circular polarization effects will also be collected.

The telescope (see figure) is an aplanatic Gregorian with an ellipsoidal primary and a hyperboloidal secondary. This design limits the irradiation of the secondary mirror. By reducing the irradiance, ultraviolet damage to the mirror is prevented, and the instrument sensitivity is preserved. The telescope positioning range is 256 by 256 arc-seconds, and it can make rectangular rasters anywhere within this field.

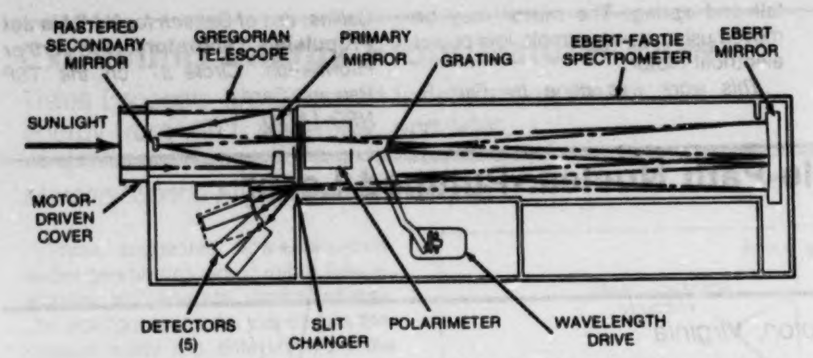
RASTERED SECONDARY MIRROR
GREGORIAN TELESCOPE
PRIMARY MIRROR
GRATING
EBERT-FASTIE SPECTROMETER
EBERT MIRROR
SUNLIGHT
MOTOR-DRIVEN COVER
DETECTORS (5)
SLIT CHANGER
POLARIMETER
WAVELENGTH DRIVE

Improved Satellite Instrument Package consists of a telescope, a spectrometer with a polarimeter, five detectors, and control electronics. The instrument is designed to study solar ultraviolet radiations involving the active regions, flares, Sunspots, and corona. The polarimeter will determine four Stokes parameters and possible mechanisms for producing linear and circular polarizations. In addition, aeronomy studies will be performed using density measurements of various constituents of Earth's upper atmosphere.

The Ebert-Fastie spectrometer includes entrance slits, an Ebert mirror, a grating with its wavelength drive, and exit slits with small mirrors to deflect the light to the detectors. There are several types of slit sets: the intensity slits, the spectroscopy slits, the Lyman-α corona slits, and the aeronomy entrance slit.

The polarimeter is located behind the spectrometer entrance slit and consists of two retarders (wave plates), a linear polarizer, and drive mechanisms to insert, extract, and rotate the wave plates. In addition, the spectrometer grating, although not part of the polarimeter, participates in polarization measurement as a partial linear polarizer.

The detectors are photomultipliers operating in the pulse-counting mode. The detector pulse outputs are amplified and directed into either of two data channels. Each channel can send data to the telemetry twice every 64 ms.

The system electronics are controlled by a 4,096-word-memory minicomputer. The computer is controlled by two command channels.

This work was done by Brown Engineering of Teledyne Industries, Inc., for **Marshall Space Flight Center.** *For further information, Circle 36 on the TSP Request Card. MFS-25298*

An Adjustable Solar Concentrator

This simple low-cost concept accommodates daily and seasonal movements of the Sun.

NASA's Jet Propulsion Laboratory, Pasadena, California

A proposed solar concentrator uses a fixed cylindrical converging lens, a movable parabolic mirror, and a conventional linear collector to accommodate daily and seasonal changes in the Sun's position. The arrangement could efficiently collect solar energy at a high temperature without costly tracking equipment. Solar rays incident on the lens are focused onto the mirror that in turn focuses them onto the collector. The collected heat is taken up by water or other working fluid.

A system would consist of several modules (see figure), each with its long axis in the east/west direction so that solar energy is focused equally well throughout the day. Seasonal changes in the Sun's position are accommodated by the movable mirror. The mirror slides on rails orthogonal to its long axis. During the winter, the mirror is moved up to

(continued on next page)

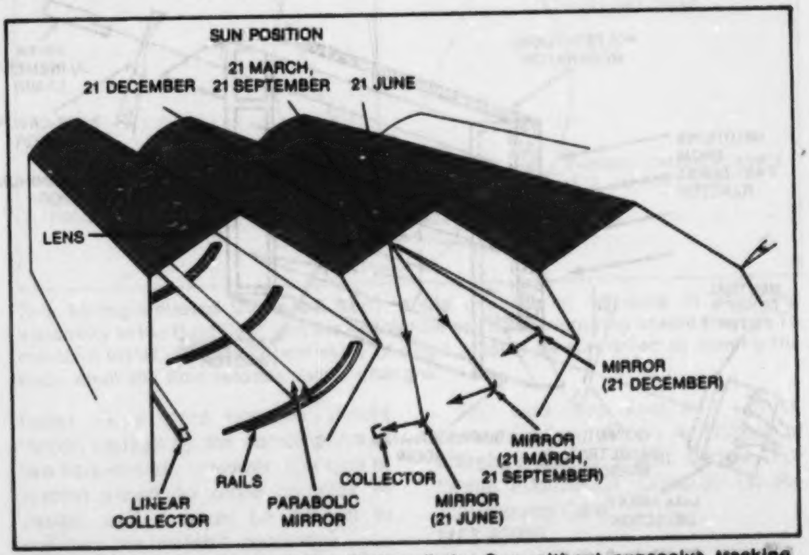
SUN POSITION
21 DECEMBER
21 MARCH, 21 SEPTEMBER
21 JUNE
LENS
MIRROR (21 DECEMBER)
MIRROR (21 MARCH, 21 SEPTEMBER)
RAILS
COLLECTOR
MIRROR (21 JUNE)
LINEAR COLLECTOR
PARABOLIC MIRROR

An Adjustable Solar Concentrator "follows" the Sun without expensive tracking devices. Each module, as shown above, contains a cylindrical converging lens with its long axis lying east/west. It collects solar energy throughout the day regardless of the Sun's angle. Seasonal adjustments are made by moving the parabolic mirror up or down, depending on the month.

accept the rays at low angles; and during the summer, it is moved down to accommodate the high angles. Intermediate positions are used in the fall and spring. The mirror may be moved using a very simple low-power electrical motor.

This work was done by Earl R. Collins, Jr., of Caltech for **NASA's Jet Propulsion Laboratory.** *For further information, Circle 37 on the TSP Request Card.*
NPO-14710

Large-Volume Multiple-Path Nuclear-Pumped Laser

Mirrors increase laser-cavity path length.

Langley Research Center, Hampton, Virginia

The output of a nuclear-pumped laser has been increased by using multiple optical reflections to enlarge the lasing-mode volume. The new design requires a lower thermal neutron flux and uses the flux more efficiently by increasing the total area available for neutron capture. The flux needed for lasing approaches that available from a steady-state reactor. Outputs over 100 watts have been reached with ^{3}He/Ar (1.79 μm) at 600 torr and a flux of 3×10^{16} neutrons/cm^{2}-s.

The laser, as outlined in Figure 1, is made of aluminum cover plates on a stainless-steel frame with a polyethylene neutron moderator on the front and back. Emitted coherent light is reflected back and forth by flat aluminum or gold mirrors on the inside of the frame. Dielectric-coated mirrors outside the frame and close to the Brewster angle windows complete the optical cavity.

A He/Ne laser is used to aline the internal and external mirrors. By varying the angle of the external dielectric-coated mirrors, the number of reflections (and thus the optical path length) can be varied.

Neutrons from a fast-burst reactor are moderated by the polyethylene. These thermalized neutrons enter the optical cavity, which contains ^{3}He and a minority-species gas, causing ^{3}He(n,p)^{3}H nuclear reactions to occur. The reactions produce charged particles with a high kinetic energy that ionize and excite the gas mixture to produce an energy-state population inversion in the minority species.

The resulting photon flux is amplified in the optical cavity and escapes through the output mirror in the form of a laser beam. A typical output is shown in Figure 2.

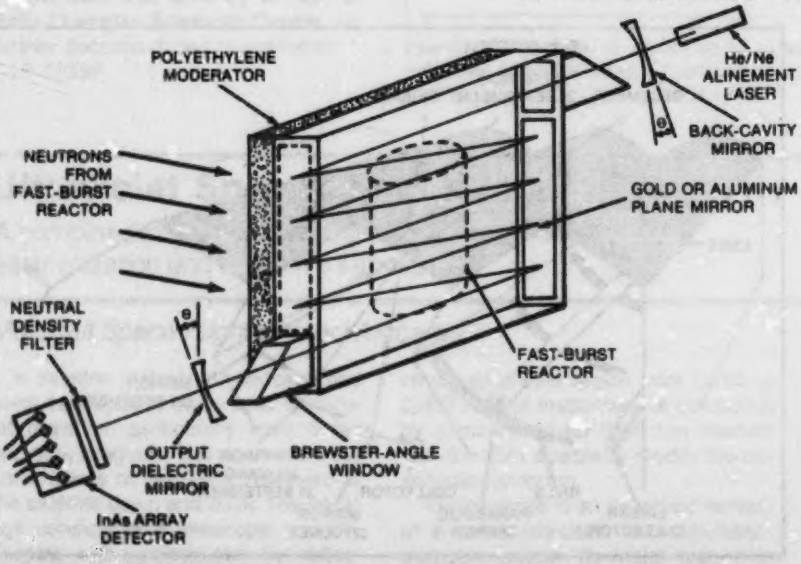

Figure 1. Multiple-Path Laser produces a greater output for a given size and neutron flux by replacing the conventional quartz tube with a multiple-reflection cavity. Tested versions are about 40 by 30 by 3 cm with a 5-cm-thick moderator layer front and back. By using transparent cover plates, it should be possible to make a similar laser that is homogeneously pumped by photons.

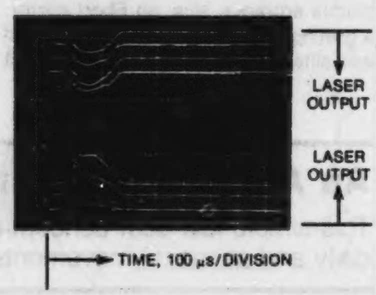

Figure 2. Typical Output from a multiple-path laser is shown for a ^{3}He-and-1-percent-Ar gas at 800 torr. Lasing (1.79 μm) was sensed by an InAr array detector. Peak thermal flux was 2.9×10^{16} neutrons/cm^{2}-s, and lasing-threshold thermal flux was 8.9×10^{15} neutrons/cm^{2}-s.

This work was done by Frank Hohl of **Langley Research Center** *and Russell J. De Young of Miami University. For further information, Circle 38 on the TSP Request Card.*

This invention is owned by NASA, and a patent application has been filed. Inquiries concerning nonexclusive or exclusive license for its commercial development should be addressed to the Patent Counsel, Langley Research Center [see page A5]. Refer to LAR-12592.

Extracting Energy From Natural Flow

Three concepts are proposed for extracting the energy from wind, waterflow, and tides.

Marshall Space Flight Center, Alabama

Three suggested flow-energy-converter geometries would utilize flow instability to generate usable energy. The configurations developed in a theoretical study are different from the traditional approach of driving the energy-generating machinery directly with natural flow sources, such as wind, waterflow, and tides. Fluid-flow instability, generally a problem in conventional engineering, is used because it is more efficient in developing a lift than the direct flow. The proposed converters would respond to one of the three instability modes: vortex excitation motion, galloping or plunging motion, and flutter.

The first converter is a spring-mounted cylinder that would oscillate at extremely high amplitudes in response to the vortex excitation. It would respond when the fluid-flow velocity past it reached a critical Strouhal reduced system frequency or reduced velocity value. This reduced velocity could be readily changed to stay tuned to the unstable conditions that generate the extreme cylinder motion. The cylinder movement can be readily converted to usable energy by conventional means, such as magnet/coil interaction.

A possibly even more effective system very much like the first except for the D-shaped cylindrical body (see figure) would respond to the galloping instability. The movement of the body would depend on the flow critical angle-of-attack α. The value of α could be maintained by turning the body when the approach flow velocity would change. This configuration is more attractive than the vortex motion because the oscillations would increase with the flow speed. Again usable energy can be extracted from the oscillation by conventional means as in the first case.

A third converter would respond to flutter — a more complex violent motion caused by the combination of two frequencies. However, this type of system would be more complex to design, and it would be difficult to maintain the unstable conditions.

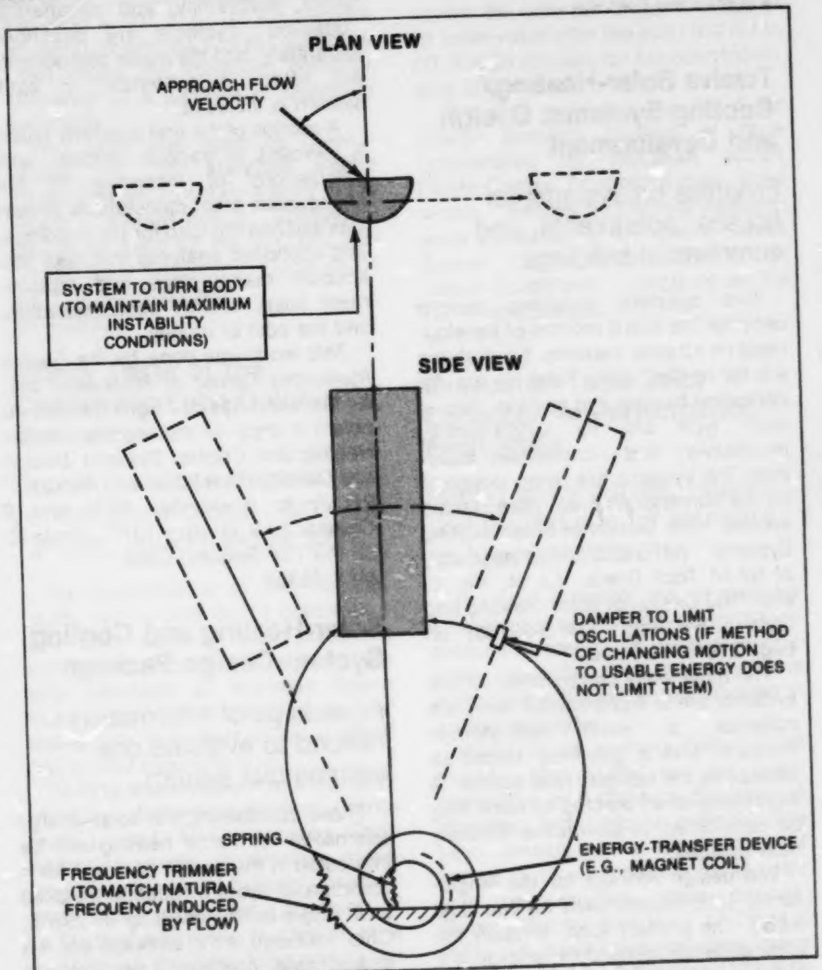
PLAN VIEW
APPROACH FLOW VELOCITY
SYSTEM TO TURN BODY (TO MAINTAIN MAXIMUM INSTABILITY CONDITIONS)
SIDE VIEW
DAMPER TO LIMIT OSCILLATIONS (IF METHOD OF CHANGING MOTION TO USABLE ENERGY DOES NOT LIMIT THEM)
SPRING
FREQUENCY TRIMMER (TO MATCH NATURAL FREQUENCY INDUCED BY FLOW)
ENERGY-TRANSFER DEVICE (E.G., MAGNET COIL)

This **Spring-Mounted D-Shaped Body** would oscillate in response to galloping instability in the fluid flow, and the oscillation can be converted to usable energy. To maintain instability, the critical value of angle α could be controlled by turning the body when the flow velocity vector changes.

This work was done by Leon M. Dellonback and Gilbert A. Wilhold of **Marshall Space Flight Center.** *For further information, Circle 39 on the TSP Request Card.*
MFS-23989

Books and Reports

These reports, studies, and handbooks are available from NASA as Technical Support Packages (TSP's) when a Request Card number is cited; otherwise they are available from the National Technical Information Service.

Twelve Solar-Heating/Cooling Systems: Design and Development

Progress on systems for houses, apartments, and commercial buildings

Two quarterly progress reports describe the first 6 months of development on 12 solar systems. Six systems are for heating alone, and six are for combined heating and cooling. Two of each type are for single-family, multifamily, and commercial buildings. The systems are being designed for the Minneapolis area. [See related articles "The Design of Solar-Heating Systems" (MFS-25108) on page 209 of *NASA Tech Briefs*, Vol. 4, No. 2, and "The Design of Solar-Heating and Cooling Systems" (MFS-25106) on page 210 of that issue.]

The most likely components for the systems are a liquid-cooled flat-plate collector, a water heat-storage medium, and a gas-fired forced-air furnace as the auxiliary heat source. A heat pump or an electric furnace may be considered as alternative auxiliary heat sources.

The design concept for the single-family solar system calls for two fluid loops. The primary loop, through the solar collector, gives up its energy in a heat exchanger to a secondary loop. The secondary loop incorporates a heat-storage water tank and heats domestic hot water and air for space heating.

The multiple-family system also has two fluid loops. It will heat 12 apartments through coils in the individual apartments, and it heats domestic water through a central heat exchanger.

The commercial-building system is similar but larger, being sized for a one-story, 32,500-ft^2 (3,019-m^2) structure — twice the floor area of the apartment house.

The reports discuss the basic requirements for the systems and present reasons for selecting the system configurations. The single-family, multifamily, and commercial "baseline" systems are described separately, and the major components are listed. A schematic of each system is included.

A section of the first quarterly report is devoted to tradeoff studies, with calculations of insolation in the Minneapolis area, calculations of heat loss and heating load for the buildings, and economic analyses that take into account maintenance and replacement costs, energy cost escalation, and the cost of money.

This work was done by the Energy Resources Center of Honeywell Inc. for **Marshall Space Flight Center.** *To obtain a copy of the reports, "Solar Heating and Cooling Systems Design and Development [Quarterly Report]," 9 July to 9 October 1976 and 9 October to 9 January 1977, Circle 40 on the TSP Request Card.*
MFS-25358

Solar-Heating and Cooling System Design Package

A package of information needed to evaluate one commercial system

Those considering the solar-energy alternative for home heating will be interested in the design package for a commercial system recently installed in a single-family dwelling in Akron, Ohio. Included in the package are the design data brochure, performance specifications, a hazards analysis, a spare-parts list, and detailed drawings. The documentation can help to assess the suitability of the system for a proposed installation.

The system in the Akron Metropolitan Housing Authority home combines a solar-heating unit with a heat pump for summer cooling and backup heat when solar energy is not available. The heat pump also stores offpeak electricity (supplied by utilities at reduced cost) for use during peak hours.

Using Akron solar-insolation levels, the system supplies 35 percent of the average total heating load (based on reasonable expected-load requirements). Potable water at 140° F (60° C) is delivered at a minimum of 5 gal/min (0.32 l/s). The maximum electrical power required to drive the solar portion of the system is 0.7 kW or less, and to drive the complete system, it is no more than 1.2 kW.

The system uses 546 ft^2 (50.7 m^2) of air flat-plate collectors and 27,000 lb (12,000 kg) of rock storage. It includes all the necessary control equipment, air-handling hardware, pumps, and electrical accessories.

This work was done by the Solaron Corp. for **Marshall Space Flight Center.** *To obtain a copy of the package, "System Design Package for a Solar Heating and Cooling System," Circle 41 on the TSP Request Card.*
MFS-25393

Benefit Assessment of Solar-Augmented Natural-Gas Systems

A study details how solar-energy-augmented systems can reduce natural-gas consumption.

A benefit assessment of solar-augmented natural-gas systems has been prepared as a starting point for a more extensive future project. It reveals how solar energy might be effectively utilized to reduce natural-gas consumption by 40 to 70 percent. Technology and economic factors are examined for five applications at less than 350° F (175° C).

For the first area, hot-water systems, the total solar-energy cost is presently estimated at about $14/MBtu ($0.01/MJ) for a single-family unit in a Sunny climate. In mixed climatic zones with frequent rainfall, energy costs are about $21/MBtu ($0.02/MJ). Future improvements are expected to lower energy costs to around $5.50/MBtu ($0.005/MJ) for the Sunny climatic regions.

The second area investigated is solar-assisted, gas, heat pumps for hot water and heating and cooling space. The authors estimate that the mass-produced solar components could be marketed at about $9,000, and the projected annual household-gas savings would be about 76 MBtu ($80.2x10^3$ MJ) for a Sunny climate.

In the third area examined, solar energy is collected and stored (e.g., in a water tank) and is then used to heat space directly, to heat water, or to drive a chiller. Currently, direct solar heating and cooling systems do not appear generally competitive with conventional energy systems.

Efficient application of solar energy to industrial processes is limited to temperatures below 350° F (175° C). Examples include hot water or hot air for the food, paper, and chemical industries and water for carwashing, curing concrete, textile processing, laundries, and uranium mills. Such industries consume about 35 percent of industrial natural gas, which could in theory be replaced with solar energy.

Finally, energy savings may be realized on solar-assisted appliances, including furnace water heaters, stoves, dryers, heat pumps, and the like. These items are subject to further investigation before an optimum hybrid system is designed for each one.

This work was done by Edgar S. Davis, Robert L. French, and Robert L. Sohn of Caltech for **NASA's Jet Propulsion Laboratory.** *To obtain a copy of the report, Circle 42 on the TSP Request Card.*
NPO-14568.

Air-Cooled Solar-Collector Specification

Report contains information for evaluating a collector for space heating and cooling.

A short report (17 pages) summarizes performance specifications for a 72-element concentric-tube collector, versions of which have been described in several previous articles in *NASA Tech Briefs.* [See, for example, "Design Review of a Liquid Solar Collector" (MFS-25140) on page 212 of Vol. 4, No. 2.] While much of the material in this document has been covered previously, this report summarizes the essential performance data and includes assembly and installation drawings. It thus can be useful as a quick reference for information on this collector.

The collector will convert at least 1,050 Btu/ft^2 ($10.3x10^6$ J/m^2) per day under precisely stated conditions, including a 30° F (-1.1° C) ambient temperature and the Sun at equinox. A chart shows the minimum collector efficiency as a function of operating conditions.

This work was done by Owens-Illinois, Inc., for **Marshall Space Flight Center.** *To obtain a copy of the report, "Owens-Illinois Subsystem Design Package for the SEC-601 Air-Cooled Solar Collector," Circle 43 on the TSP Request Card.*
MFS-25336

Indoor Tests of the Concentric-Tube Solar Collector

Report describes thermal performance tests on the 12-tube, liquid-filled version.

The performance of the 12-tube, liquid-filled version of the concentric-tube solar collector (see preceding article) was recently evaluated using a solar simulator at Marshall Space Flight Center. The test procedures and results are documented in a report that is now available.

Testing was in accord with ASHRAE (American Society of Heating, Refrigerating, and Air-Conditioning Engineers) standards. Parameters measured were thermal efficiency, incident-angle modifier, and time constant.

Thermal efficiency is plotted as a function of the inlet temperature for simulated solar-flux levels of 250 and 300 Btu/h-ft^2 (788 and 945 J/s-m^2). The measurements range between about 52 percent at 85° F (29° C) inlet temperature to about 40 percent at 200° F (93° C).

The incident-angle modifier measures the change in efficiency as the Sun tracks from east to west across the sky. It is determined by tilting the collector at 10°, 20°, 30°, 40°, and 50° with respect to the direction of normal incidence and recording the efficiency. From a value of 1.0 at normal incidence, the incident-angle modifier drops to a minimum of 0.81 at a tilt angle of 40°. It rises to about 0.85 at 50°.

The time constant reflects how rapidly the temperature differential across the collector drops to 0.368 of its initial value after the solar flux is cut off. It is 20 minutes for the concentric-tube collector.

This work was done by the Solar Energy Systems Division of Wyle Laboratories for **Marshall Space Flight Center.** *To obtain a copy of the report, "Results of Thermal Performance Evaluation of the Owens-Illinois Sunpak Liquid Solar Collector at Indoor Conditions," Circle 44 on the TSP Request Card.*
MFS-25390

Evacuated-Tube Solar Collector — Performance Evaluation

Report gives curves, tables, and procedures for standard and special tests.

A report presents the procedures and results of thermal performance tests on a commercial evacuated-tube solar collector. Two models of the eight-tube collector were evaluated in a solar simulator.

Water is the working fluid in both models. One model has an outlet manifold 1 inch (2.54 centimeters) in diameter with copper orifices. The other version has a manifold 1-1/4 inches (3.18 centimeters) in diameter with heat-resistant glass orifices. Gross collector area is 17.17 ft^2 (1.6 m^2). The overall external dimensions are 48 by 51.5 by 7.8 inches (121.9 by 130.8 by 19.8 centimeters).

The collectors were subjected to standard thermal performance tests in which ambient air temperature, fluid inlet and outlet temperatures, solar flux, waterflow rate, and efficiency were measured.

The collectors also underwent other special tests. These included:

- a time-constant test to determine

(continued on next page)

how fast the water cools when insolation stops,

- an incident-angle modifier test to determine the variation in collected energy as the Sun moves from east to west, and
- a "hot-fill" test to determine whether the tubes will break if they are accidentally filled with hot water.

This work was done by Wyle Laboratories for **Marshall Space Flight Center.** *To obtain a copy of the report, "Indoor Test for Thermal Performance of the Sunmaster Evacuated Tube [Liquid] Solar Collector," Circle 45 on the TSP Request Card.*

MFS-25339

Glycol/Water Evacuated-Tube Solar Collector

A report on performance of the 8-tube and 10-tube models

The performance of two multitube commercial solar collectors is detailed in a new test report. One collector has 8 tubes with parabolic-trough reflectors; the other has 10 tubes with vee-trough reflectors. Both types use a mixture of 35 percent glycol as the working fluid. The report covers indoor tests made with a solar simulator. The collectors were tested with and without a manifold furnished by the manufacturer as optional equipment.

Each of the tubular elements is glass, with an evacuated jacket and an absorbent coating on the outside of the inner wall. The working fluid travels through a serpentine tube that is in conductive contact with the inner wall. Thus, the fluid loop is not breached if the vacuum jacket is broken. The collectors measure 57.25 by 48 by 3.25 inches (145.4 by 121.9 by 8.2 centimeters). Gross collector area is about 17.4 square feet (1.62 square meters).

The report describes conditions, equipment, and procedures for the tests. It presents data on stagnation tests (temperature rise of noncirculating working fluid), thermal efficiency as a function of inlet temperature and other conditions, time-constant tests (the cooling of working fluid after insolation ends), and incident-angle modifier tests (the variation of efficiency with position of the Sun). Flux maps show the insolation at three points in each collector tube.

The eight-tube collector performs well when the insolation angle is 90°; it is somewhat less efficient when the incidence angle departs from the normal by more than 20°. In fact, the 8-tube version is less efficient at these angles than the 10-tube collector.

For solar cooling, the efficiency of the 10-tube collector is 28 percent, and for the 8-tube collector it is 26 percent. For space heating and water heating, the efficiencies are considerably higher, as expected. Data were also gathered for the 10-tube collector on thermal efficiency with plastic covers.

This work was done by Wyle Laboratories for **Marshall Space Flight Center.** *To obtain a copy of the report, "Indoor Test for Thermal Performance of the G.E. TC-100 Liquid Solar Collector Eight- and Ten-Tube Configuration," Circle 46 on the TSP Request Card.*

MFS-25337

Thermosyphon Heat Exchanger

A report on the final development of a pumpless liquid-to-air heat exchanger

A new report summarizes the final development, testing, and certification for use of a pumpless liquid-to-air heat exchanger for solar-heating systems. The report complements documentation released previously, described in "Passive Heat Exchanger for Solar Heating" (MFS-23914) and "Passive Heat Exchanger — Installation Package" (MFS-23930) on page 214 of *NASA Tech Briefs*, Vol. 3, No. 2.

Water from the storage tank of a residential or commercial solar-heating system flows through finned tubes in the heat exchanger. From there, it returns to the tank. A blower forces air across the fins, transferring the heat from the exchanger to the room. Resistive heating elements can be added to the storage tank for backup heating.

Since the water density increases on cooling, a natural convective flow, or "thermosyphon," is set up in a vertical pipe, which eliminates the need for a pump in the water loop. The exchanger is therefore simpler and less susceptible to failure than many forced-flow units.

The heat exchanger fan is rated at 1,640 ft^3/min (774 l/s). It is operated by a 6.5-A (full-load), 115-Vac motor. The heat output is 35,000 Btu/h (10,250 W) when the water temperature is 120° F (49° C) and the entering air temperature is 70° F (21° C). When the water temperature is 160° F (71° C), up to 74,000 Btu/h (21,680 W) are delivered.

This work was done by James D. Hankins of **Marshall Space Flight Center.** *To obtain a copy of the report, "Development, Testing and Certification of the Sigma Research, Maxi-Therm S-101 Thermosyphon Heat Exchanger," Circle 47 on the TSP Request Card.*

MFS-25389

Controller for Solar-Energy Systems

Prepackaged unit includes electronic and hydronic modules.

A new report describes the operation and final development and testing of a computerized control unit for solar-heating and cooling systems. The prepackaged controller includes the electronics and "plumbing" needed to oversee the operation of a solar-energy system. The components are modular, which allows the configuration to be altered and adapted to different solar-energy systems.

The controller only requires field connection of pipes, power, and sensors. It is programed to receive input on user-defined variables, such as insolation level, room and outside temperatures, the time of day and date, and the storage-tank temperature. When the data are processed to define the appropriate operating mode, pumps, fans, valves, and switches are set to place the system in that mode. Among possible modes are heating from collectors, storing energy, and heating from storage.

Where required, the user has access to the controller through a portable printer. Access features include a 32-hour programable file of selected data, a printout of all input and output, and program editing. Field loading of software changes is possible through an ASCII-compatible data channel.

The controller electronics are based around a microprocessor. Both ROM (read-only memory) and RAM (random-access memory) are used for program storage.

This work was done by James D. Hankins of **Marshall Space Flight Center.** *To obtain a copy of the report, "Development and Testing of the Sunkeeper Control Corporation Integrated Programmable Electronic Controller and Hydronics Package — Final Report," Circle 48 on the TSP Request Card.*
MFS-25386

Controller and Temperature Monitor for Solar Heating

A new report describes the final development and certification for public use.

The 77-171 controller is a differential thermostat with relay output for controlling a solar-heating or cooling system. It can be used with or without the 77-180, a temperature monitor that displays the indoor, outdoor, and storage temperatures. Both units, available commercially, were recently tested and certified for public use. A summary of their final development is described in a new report that is available on request.

The design package for these units is described in a previous article in *NASA Tech Briefs*. [See "Controller for Solar Heating — Design Package" (MFS-25009) on page 61 of Vol. 4, No. 1.] The new report contains a summary of their operation and performance specifications. It also references other applicable documents.

A brief summary of the background of the development program for these units is given in the report. The summary describes how this program meshes with the larger solar-energy development program managed by NASA and the Department of Energy. The larger program is part of the national effort to implement aspects of the Solar Heating and Cooling Act of 1974.

This work was done by James D. Hankins of **Marshall Space Flight Center.** *To obtain a copy of the report, "Development and Testing of the Solar Control Corporation Modular Controller and Solarstat Subsystem," Circle 49 on the TSP Request Card.*
MFS-25387

Inhibiting Corrosion in Solar-Heating and Cooling Systems

Water additives were tested in a 1-year study.

The initial phase of a program to evaluate corrosion-inhibiting additives for solar-heating and cooling systems is described in a 16-page report. A followup to this work is described in "Corrosion Inhibitors for Solar-Heating and Cooling Systems" (MFS-25023) on page 525 of *NASA Tech Briefs*, Vol. 3, No. 4.

The initial study tested 12 inhibitors, 4 of which were also evaluated in the followup. The 12 include commercial products recommended for automotive cooling systems along with several special formulations based on sodium salts.

Water, containing selected corrosive additives, was the test medium. Specimens of aluminum, steel, stainless steel, and copper were immersed at 80° C in solutions of the corrosive water mixed with the inhibiting agents. After 1 year of exposure, the specimens were removed, cleaned, and weighed.

Four of the formulations showed good promise as inhibiting agents (although the followup study revealed problems with two of these in protecting thin aluminum specimens). Others showed varying degrees of promise, depending on the temperature range and the particular metal exposed.

This work was done by G. E. DeRamus, Jr., and T. S. Humphries of **Marshall Space Flight Center**. *To obtain a copy of the report, "Corrosion Inhibitors for Solar Heating and Cooling Systems," Circle 50 on the TSP Request Card.*
MFS-23763

Computer Programs

These programs may be obtained at very reasonable cost from COSMIC, a facility sponsored by NASA to make new programs available to the public. For information on program price, size, and availability, circle the reference letter on the COSMIC Request Card in this issue.

Numerical Tracing of Electron Trajectories

For analysis and design of electron-imaging systems

The TRAJEC computer program aids the analysis and design of electron imaging systems. TRAJEC can integrate the path of a relativistic electron through a region of nonuniform, static electromagnetic fields to an accuracy of 1 micrometer in 10 centimeters. A fourth-order Runge-Kutta method with error estimation (a Kutta-Merson procedure) is used to integrate the motion equations. The force evaluation uses a third-order Legendre interpolation of the electrical potential.

The program easily interfaces with various forms of user-defined electric potentials and magnetic fields. It may be implemented interactively so that the analyst might freely experiment with combinations of trajectories and gain insight into the aberrations inherent in the imaging system under study. Several methods are provided for analyzing the imaging properties of the device under study.

The trajectory of a single electron injected from any point with arbitrary initial velocity may be studied. Lines of electrons may be studied to test linear imaging properties. TRAJEC also allows for studies of Monte Carlo point sources of electrons to simulate the characteristic emissive properties of photocathode materials and their effects on the images produced. TRAJEC has been used to evaluate

(continued on next page)

and modify designs for an imaging device used on the NASA Space Telescope.

The TRAJEC program is written in FORTRAN IV for batch or interactive execution and has been implemented on a DEC PDP-10 with a central memory requirement of 14K of 36-bit words and on a CDC 6000-series machine with a central memory requirement of 37K (octal) of 60-bit words. TRAJEC has also been utilized on PDP-11, CYBER 70, and CYBER 170-series machines. TRAJEC was developed in 1979.

This program was written by T. N. Delmer and T. C. Stephens of Science Applications, Inc., for **Goddard Space Flight Center.** *For further information, Circle A on the COSMIC Request Card.*
GSC-12535

NASA Charging Analyzer Program

Dynamic simulation of electrostatic charging of 3D objects

NASCAP (NASA Charging Analyzer Program) is able to predict how an object made of conducting sections, which may be entirely or partially covered with thin dielectric films, responds to a specified charged-particle environment with or without solar illumination. The environments of interest are those found in the Earth's magnetosphere and in a ground-based test chamber designed to simulate spacecraft charging effects. When Sunlight is present, shadowing is taken fully into account. NASCAP divides the spacecraft charging problems into two sections: (1) the tendency of materials to accumulate and emit charge when subjected to plasma environment and (2) the consequent response of the charged-particle envronment to the electrostatic field of an object. Both of these sections are treated in sufficient detail to simulate the charging of a complex satellite.

NASCAP includes formulations for electron backscatter and secondary emission, photoelectron emission, and proton-generated secondary electron emission. Dielectric constants and finite conductivity are also taken into account.

The response of the charged-particle environment to the electrostatic field of an object requires the calculation of the electric potentials on and near complex objects and the determination of how those potentials influence charged-particle trajectories. The electrostatic potential about the satellite or in the test tank is calculated by NASCAP, by using a finite-element formulation of Poisson's equation.

The computational space consists of an arbitrarily large number of nested cubic meshes. The resulting set of linear equations is solved using the Conjugate Gradient technique. The satellite or test object is defined within the innermost mesh and may have surfaces normal to any of the 26 cubic symmetry directions. It consists of one or more conductors that may be covered with thin dielectric layers. The conductors may be floating, held at fixed potentials, or biased relative to one another.

The net charge accumulation by each surface cell of the satellite is calculated in the presence of the electrostatic and magnetostatic fields about the satellite and specified environmental characteristics. In the ground test case, the incident flux is determined by forward trajectories from an electron source. In the space case, the incident flux of electrons and ions at surfaces is determined using the reverse trajectory sampling method. The ambient plasma may be isotropic and Maxwellian.

NASCAP has facilities for extensive graphical output, including several types of object display plots, potential contour plots, space charge density contour plots, current density plots, and particle trajectory plots.

NASCAP is written in FORTRAN V for batch execution and has been implemented on the 1100-series computer with a central memory requirement of approximately 62K of 36-bit words.

This program was written by J. J. Cassidy III, J. M. Harvey, I. Katz, and M. J. Mandell of Systems, Science & Software for **Lewis Research Center.** *For further information, Circle B on the COSMIC Request Card.*
LEW-12973

Materials

Hardware, Techniques, and Processes

45 Containerless Materials Processing in the Laboratory
46 Measuring Coal Deposits by Radar
47 Detecting a Coal/Shale Interface
48 Fast-Response Atmospheric-Pollutant Monitor
49 Fire Tests for Airplane Interior Materials
50 REDOX Electrochemical Energy Storage
51 Additive Improves Engine-Oil Performance
52 Drilling Side Holes From a Borehole
53 Corrosion-Resistant Ceramic Thermal-Barrier Coating
54 Reducing Static Charges in Fluidized-Bed Reactions
55 Transferring Small Samples of Viscous Liquid

Books and Reports

56 Coal Conversion and Synthetic-Fuel Production

Computer Programs

56 Underground Coal Mining

Containerless Materials Processing in the Laboratory

Drop tube makes possible the preparation of exotic materials.

Marshall Space Flight Center, Alabama

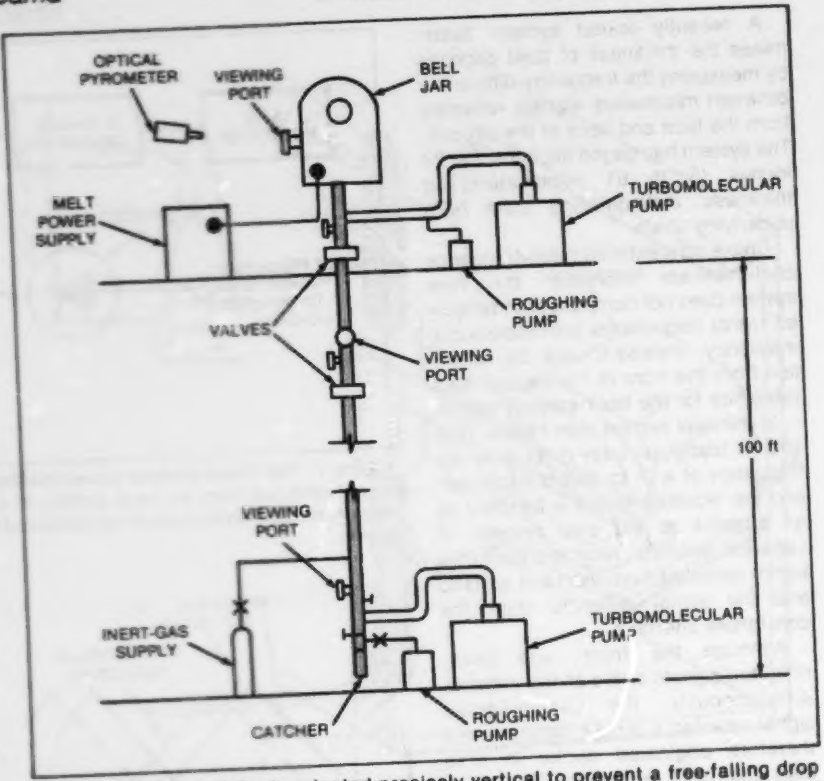

The 100-Foot Drop Tube is oriented precisely vertical to prevent a free-falling drop from hitting the tube walls. An inert-gas supply, evacuation pumps, viewing ports, and flexibility in the choice of melt technique allow precise control and monitoring of the solidification.

Containerless, zero-gravity materials processing, usually considered possible only in space, can now be carried out in the laboratory, using a drop tube developed at Marshall Space Flight Center. The apparatus makes possible various metastable and supercooled structures that cannot be reached easily by conventional processing. Among such structures are single crystals of high-temperature metals, bulk samples of metastable alloys and compounds, amorphous and glassy materials, and high-temperature superconductors.

The absence of a container means reduced possibility for contamination; and zero gravity implies an absence of convection currents and sedimentation, both of which disturb the uniformity of a molten sample as it solidifies. The net effect is to encourage homogeneity and supercooling, which allow the development of unusual new structures and better-quality conventional structures.

The apparatus (see figure) is similar to towers previously used to prepare spherical lead shot; however, it has substantial improvements that allow more precise control of the sample composition, shape, and environment. As shown, the primary component is a vertical stainless-steel drop tower. Samples are melted in a bell jar at the top of the tower, and the molten drops fall through the 100-foot (30.4-meter) tower to a detachable receiving chamber or "catcher" at the bottom. If the melt temperature and tower atmosphere are properly controlled, the drops are completely solidified when they reach the catcher.

The tower can be evacuated by a turbomolecular pump and a mechanical roughing pump. An inert-gas supply allows backfilling with a low-pressure inert gas. The progress of the drop as it falls can be photographed and monitored through viewing ports in the bell jar and along the tube. An optical pyrometer measures the melt temperature.

There is considerable flexibility in the method of melting and releasing the sample. One approach is to suspend it as a solid from a fine wire, then to melt it by electron bombardment or laser heating until it drops from the wire. Another technique is to melt the sample in a crucible fitted with a capillary tube. Drops of molten material form and are released from the end of the capillary.

This work was done by Lewis L. Lacy, Daniel B. Nisen, Thomas J. Rathz, and Michael B. Robinson of **Marshall Space Flight Center.** *For further information, Circle 51 on the TSP Request Card.*

Inquiries concerning rights for the commercial use of this invention should be addressed to the Patent Counsel, Marshall Space Flight Center [see page A5]. Refer to MFS-25242.

Measuring Coal Deposits by Radar

Thickness is measured directly as a frequency difference, eliminating the need for a local oscillator.

Marshall Space Flight Center, Alabama

A recently tested system determines the thickness of coal deposits by measuring the frequency difference between microwave signals reflected from the face and back of the deposit. The system has gaged deposits 2 to 24 inches (5 to 61 centimeters) in thickness, distinguishing them from underlying shale.

Unlike conventional radio-frequency coal-thickness monitors, the new system does not compare both reflected signal frequencies with the source frequency. Instead it uses the reflection from the front of the deposit as a reference for the back-surface signal.

In the new system (see Figure 1), a 100-Hz triangular wave modulates the frequency of a 2- to 4-GHz oscillator, and the resultant signal is beamed by an antenna to the coal deposit. A separate antenna receives both the signal reflected from the front surface and the signal reflected from the coal/shale interface.

Although the front- and back-reflected signals arrive at the antenna simultaneously, the back-reflected signal traveled a longer distance and therefore originated earlier in time than the front reflection. The back reflection therefore has a lower frequency than the front-surface signal (see Figure 2), and the frequency difference is a measure of the extra travel time. The two signals are combined in a mixer diode to generate the difference frequency, and this signal is used to give a readout of the thickness of the coal layer.

The new system avoids several difficulties inherent in previous radar coal-thickness monitors. In a conventional system, the two received reflections are mixed with the local oscillator signal, and the composite signal is processed to determine the range to the front and the range to the back of the deposit. The thickness is then found by subtraction.

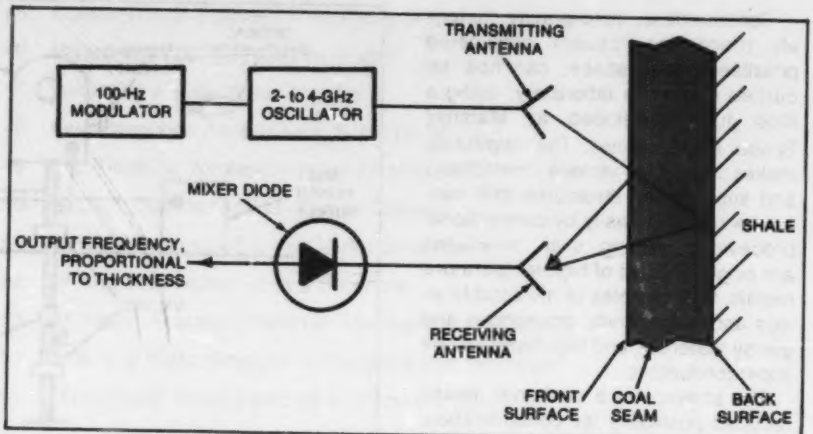

Figure 1. The **Front-Surface Local-Oscillator Radar** compares the frequency of the signal reflected from the back surface of a coal deposit with that reflected from the front surface. Previous systems compared both signals to a separate local-oscillator signal.

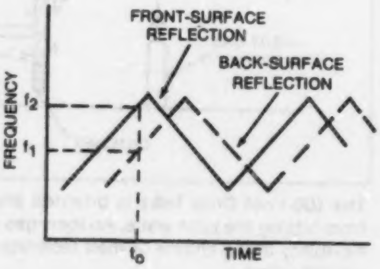

Figure 2. **Reflections From the Front and Back** of a coal deposit, received at time t_0, have different frequencies (f_1 and f_2) because they originate at different times from the frequency-modulated transmitter. The frequency difference represents the travel time through the coal and hence its thickness. The displacement between the curves is exaggerated in this figure.

In contrast, the mixer output in the new radar is a direct measure of thickness; only a frequency-to-thickness conversion is needed. Moreover, masking of the weak back reflection by the strong front reflection is greatly reduced, since the two reflections are not detected separately but in combination. Another benefit of the new system is that it is not sensitive to extraneous reflections from targets between the transmitting antenna and the coal surface, since no target information is generated until the front-surface reflection arrives at the mixer.

This work was done by Thomas A. Barr of **Marshall Space Flight Center.** *No further documentation is available.*
MFS-23922

Detecting a Coal/Shale Interface

The depth of cut is determined by combining penetrometer and reflectometer measurements.

Marshall Space Flight Center, Alabama

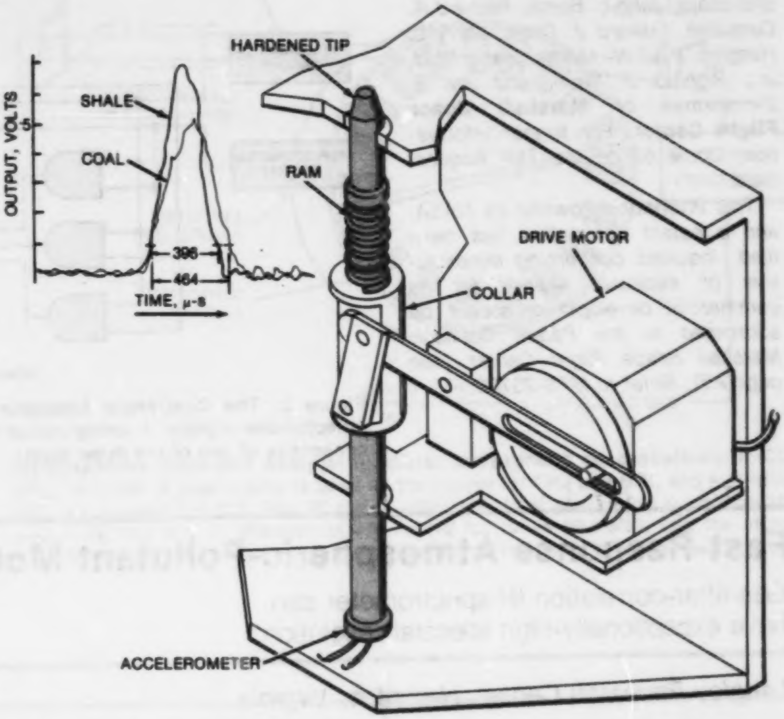

Figure 1. The **Penetrometer Portion** of the coal/shale interface detector includes a motor-driven ram with an accelerometer at the back end. Representative accelerometer outputs for coal and for shale are shown in the inset. The coal signal is identified by its broader width and lower height as compared to the shale signal.

A prototype coal/shale interface detector combines the outputs of two optical reflectometers with that of a penetrometer. Eventually, it will be used on a longwall shearer to determine when the cut has pierced through the coal layer. Tests on the prototype in a mine show that the basic design is workable.

In the prototype, an accelerometer measures the hardness of the material struck by the penetrometer ram, while the reflectometers measure the reflectivity of the surface on both sides of the penetrometer. The signals are then combined in a voting circuit that indicates "coal" or "shale" depending on the information supplied by the three sensors.

As shown in Figure 1, one end of the penetrometer ram is hardened for striking the mine wall. The accelerometer is attached to the opposite end of the ram. The ram shaft is reciprocally driven by a spring attached to a supporting collar, and the collar is moved by linked, pivoted arms driven by a motor. As the ram strikes the mine wall, the spring compresses, preventing the impact head from damaging the surface.

The penetrometer distinguishes between coal and shale by the differences in the accelerometer waveforms for the two materials. As shown in the inset to Figure 1, the spike corresponding to shale is taller and sharper than that for coal, because shale is usually harder than coal. (There can be exceptions to this qualitative result, which is why the penetrometer output is compared to the reflectometer signals.) Discriminating circuitry can distinguish between the two signal characteristics.

The reflectometers are standard commercial units. Each includes a light source and a light-sensitive switch that trips when the reflected light exceeds a preset threshold.

The detection circuitry is shown in Figure 2. One threshold detector is biased at 6 volts, which for the prototype is the maximum accelerometer output when the ram is impacted against coal. The triggered one shot that follows the threshold detector is normally in its high state, but it goes low when the 6-volt level is exceeded (i.e., when shale is encountered).

The accelerometer output is also applied to a threshold detector that puts out a high state when the input exceeds 1 volt. At the 1-volt level (see Figure 1), the signal width is 464 microseconds for coal and 396 microseconds for shale.

A cutoff of 450 seconds is selected to distinguish a coal pulse from a shale pulse. A 450-microsecond one shot that triggers on the leading edge of the pulse is applied to the disable input of a one shot that triggers on the pulse trailing edge. Thus, the second one shot fires only if the initial pulse width exceeds 450 microseconds. Ultimately, the AND gate output of the penetrometer is enabled only if the accelerometer pulse amplitude is between 1 and 6 volts and the pulse width exceeds 450 microseconds. Of course, these values are unique to the particular penetrometer selected and would vary with impact frequency and amplitude.

The penetrometer AND gate output is supplied to the voting circuit along

(continued on next page)

with the reflectometer outputs, which are at logical "1" for low-light conditions (for coal). The voting circuit output is high only if two of the three inputs indicate the presence of coal. In this case, the coal indicating light is turned on. If the voting circuit output is low, the "shale" light is activated.

This work was done by Peter H. Broussard, John L. Burch, Richard A. Campbell, Edward J. Drost, Jerry L. Hudgins, Paul W. Morris, Harry Reid, Jr., Richard J. Stein, and Joe E. Zimmerman of **Marshall Space Flight Center.** *For further information, Circle 52 on the TSP Request Card.*

This invention is owned by NASA, and a patent application has been filed. Inquiries concerning nonexclusive or exclusive license for its commercial development should be addressed to the Patent Counsel, Marshall Space Flight Center [see page A5]. Refer to MFS-23720.

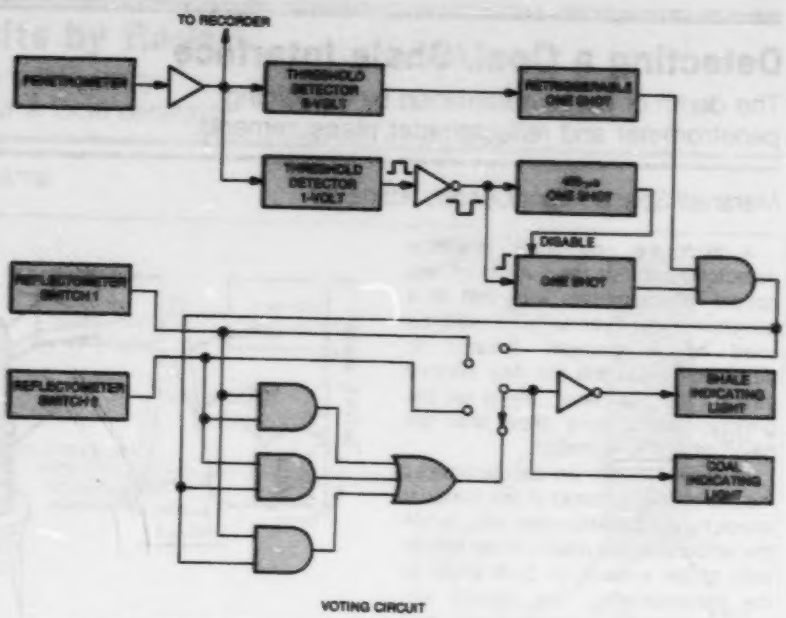

Figure 2. The **Coal/Shale Detection Circuit** processes the penetrometer and reflectometer signals. A voting circuit indicates "coal" or "shale" according to the consensus of two of the three inputs.

Fast-Response Atmospheric-Pollutant Monitor

Gas-filter-correlation IR spectrometer can have exceptionally-high spectral resolution.

Langley Research Center, Hampton, Virginia

A fast-response spectrometer has been used successfully to measure atmospheric CO, CH_4, and HCl over the range of 1 to 12 ppm. The instrument employs a modification of recent nondispersive infrared techniques, chosen for their greater resolution compared to dispersive measurements. The tested field version is relatively compact and includes its own IR source. With additional development and appropriate modifications, a similar spectrometer could measure other pollutants and use natural light as a source.

The nondispersive measurement requires no prisms or gratings. A cell filled with the gas to be measured is used to filter out selectively the spectral lines of interest. The amount of IR radiation passing through the gas-filled cell is compared to that passing through the atmosphere and an empty cell. The difference between the amounts of radiation transmitted varies with the amount of gas (of interest) in the atmosphere.

The main components of the instrument are shown in the illustration. Radiation from an IR source is focused to pass through one of several cells on a rotating disk. Ten of these cells are specifying cells; they are filled with either pure CO, CH_4, or HCl gas to attenuate the IR signal as strongly as possible at their absorption spectrum wavelengths. Nine of the cells are reference cells; they may be evacuated or may contain a nonabsorbing gas. Chopped signals are produced with an amplitude difference depending on the amount of test gas in the atmosphere (the greatest difference being when none of the gas is present).

The transmitted radiation intensity is measured by a detector that is preceded by a narrow-band-pass filter, which passes only a small part of the absorption band of interest. The filter reduces the effects of interfering gases and source variations with wavelength. The magnitude of ΔV (the change in signal for the specifying and reference cells) depends on the concentration of gas in the atmosphere. Signal ΔV is divided electronically by V_S (the detector output when the specifying cell is in the light path). Since V_S does not vary with gas concentration in the atmosphere, this procedure can be used to eliminate output-signal variations due to fluctuations in the IR source.

The signal-processing circuitry amplifies and separates the specifying and reference cell signals based upon their different frequencies. It adjusts to a null signal for a zero concentration of the test gas and divides the output signal by V_S. Varying integration times and input voltage control are used to adjust sensitivity to span a range of gas concentrations. Output is displayed on panel meters and monitored by a strip-chart recorder.

The instrument is zeroed electronically and calibrated with a standard calibration cell containing a known amount of the gas of interest. The lowest detectable concentration for CO, CH_4, and HCl is about 5 ppm with a 1-meter light path and 1-second time constant. Placing the IR source farther away and increasing the signal-integration time constant can greatly lower the minimum detectable concentration. (Field tests were made with a 50-m light path.)

Although other atmospheric constituents can interfere with this type of measurement, tests have shown these effects on CO, CH_4, and HCl measurements to be negligible at the concentrations normally present in the atmosphere.

This work was done by Daniel I. Sebacher of **Langley Research Center.** *Further information may be found in NASA TP 1113 [N78-13408/NSP], "A Gas Filter Correlation Monitor for CO, CH_4, and HCl" [$4.50]. A copy may be purchased [prepayment required] from the National Technical Information Service, Springfield, Virginia 22161.*
LAR-12317

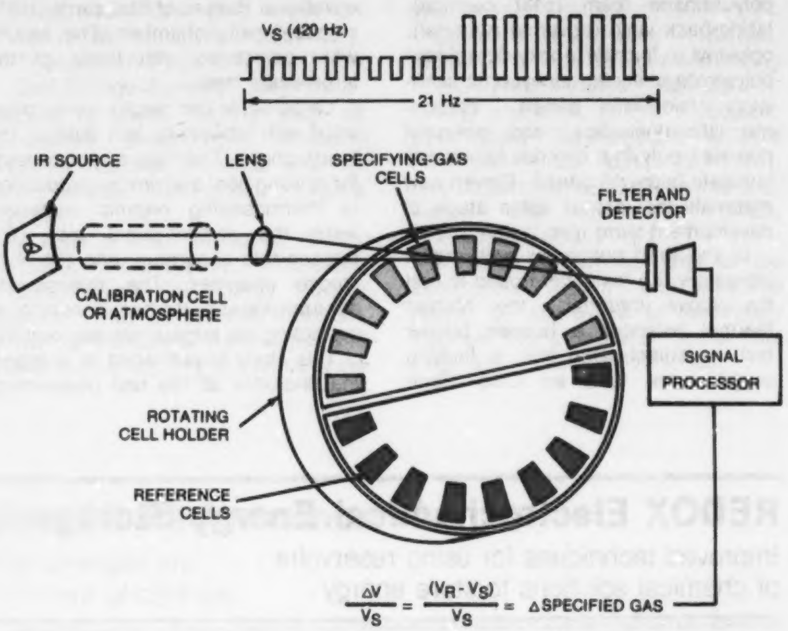

Nondispersive Trace-Gas Analyzer measures atmospheric concentrations of CO, CH_4, and HCl. A quartz lamp is used as the source for CH_4 and HCl, and a glowing SiC rod is used for CO. The IR signal after near-total absorption by gas in the specifying cell (V_S) is chopped at 420 Hz (42 rps times 10 cells), and the signal passing through the atmosphere (or calibration cell), V_R, is chopped at 378 Hz.

Fire Tests for Airplane Interior Materials

Selecting laboratory fire tests for accurate ranking of aircraft materials according to safety

Lyndon B. Johnson Space Center, Houston, Texas

A study conducted by Johnson Space Center identified reliable laboratory fire tests for evaluating the safety of airplane interior materials. Many of the existing laboratory procedures have been inaccurate in predicting how the materials would perform in actual aircraft fires, making it difficult to rank the materials according to safety. New large-scale simulated fire tests were performed in a salvaged airliner fuselage, and the results were compared with some modern laboratory tests. The conclusions are that several laboratory tests can be used to rank the materials according to heat and smoke production rates. None of the existing tests, however, is accurate in characterizing the toxic gas emissions.

The study detailed in a report, "Development of Fire Test Methods for Airplane Interior Materials," was conducted in four phases. The first involved a series of tests performed in a salvaged jetliner fuselage to determine the best methods of simulating postcrash and in-flight fires. Two "design" fire sources were selected: One simulating a crash used Jet A fuel ignited in the fuselage midsection, and the other simulating in-flight fire used a pair of polyethylene trash bags filled with paper towels, paper cups, and polystyrene glasses also ignited inside the fuselage. The characteristics of each were recorded and used as reference for a new quartz-lamp propane burner simulator that could duplicate each of the two conditions in the large-scale tests.

In the second phase, large panels of each test material were lined against the fuselage sidewall and tested one by one under each of the two conditions. The heat from the lamps and the burner was closely controlled. A total of five existing (baseline)

(continued on next page)

materials was tested, which included polyurethane foam (seat cushion), fabric-back vinyl (covering material), polyvinyl fluoride/epoxy-fiberglass/polyamide phenolic honeycomb sandwich (sidewall panel), carbonate (thermoplastic), and polyvinyl fluoride/ polyvinyl chloride/aluminum laminate (sidewall panel). Eleven new materials that are at some stage of development were also tested.

In the third phase six well-known laboratory fire tests were used to test the above materials: the Mettler thermal balance, a bunsen burner test, a radiant-panel test, a limiting oxygen-index test, an Ohio State University release-rate apparatus, and a National Bureau of Standards (NBS) smoke-density chamber. The results were compared with those of the large-scale tests.

Large-scale test results were correlated with laboratory test data in the fourth phase. The most accurate tests for ranking heat and smoke production of thermosetting organic materials were the radiant-panel test, the release-rate apparatus, and the NBS smoke chamber. The release-rate apparatus stands the best possibility of predicting the large-scale test results.

This study is published in a report that includes all the test parameters and other technical details about the tests. The test setups are illustrated in great detail.

This work was done by Everett A. Tustin of The Boeing Co. for **Johnson Space Center.** *Further information may be found in NASA CR-14568 [N79-19112/NSP], "Development of Fire Test Methods for Airplane Interior Materials" [$11.75]. A copy may be purchased [prepayment required] from the National Technical Information Service, Springfield, Virginia 22161.*
MSC-18478

REDOX Electrochemical Energy Storage

Improved techniques for using reservoirs of chemical solutions to store energy

Lewis Research Center, Cleveland, Ohio

A REDOX electrochemical storage system utilizes the oxidation and reduction reactions of two fully soluble REDOX couples to store and deliver electrical charge. Early developments in this technology were reported in *NASA Tech Briefs*, Vol. 1, No. 1, p. 78, "REDOX — Electrochemical Energy Storage" (LEW-12220). Recently, several advances have been made in this area, and prototypes have been built and tested.

The REDOX couples currently used are acidified chloride solutions of chromium (Cr^{+2}/Cr^{+3}) and iron (Fe^{+2}/Fe^{+3}). Reactant solutions are stored in tanks outside the power conversion section in which the charging and discharging reactions take place at inert electrodes. This separation of power conversion from storage is an important system design advantage. The solutions are pumped through the porous electrodes separated by a highly-selective ion-exchange membrane. The membrane prohibits the passage of iron and chromium ions and yet allows easy passage of chloride and hydrogen ions. The reactant solutions are currently 1.0 molar in iron chloride and chromium chloride and 2.0 normal in hydrochloric acid. The electrodes are highly-porous carbon felt. The chromium electrode is inexpensively catalyzed to make the chromium reactions reversible and efficient. The power conversion unit consists of a stack of cells connected together in parallel hydraulically and in series electrically. These stacks closely resemble fuel-cell batteries and water electrodialysis equipment. There are no particular temperature requirements, and operating conditions vary from -18° to +60° C. The system is 99 percent ampere-hour efficient and 75 percent watt-hour efficient. It is estimated that over a span of 25 to 30 years only a 25-percent capacity loss could occur.

Recent achievement of advancements in the ion-exchange membrane separators and electrocatalyst technologies has brought this energy-storage concept to the point where complete systems have been designed, built, and tested. Several novel features (rebalance cell, open circuit voltage cell, and trim cells) have been conceived and incorporated into complete REDOX systems that greatly enhance their ability to be kept in proper charge balance, to be capable of internal voltage regulation, and to be treated as true multicell systems rather than as many cells that are wired together.

Applications of a REDOX system will include remote power systems that are supplied either by solar-photovoltaic arrays or wind turbine generators, in traditional utility systems to reduce the need for peaking generators, and in load leveling for industry. At present, the technical requirements for solar-photovoltaic systems have been met. The development program presently underway is expected to achieve a lowered membrane resistivity that will meet electric utility requirements.

The present cost estimate for a REDOX storage system is the sum of about $325/kW of power required plus $51/kWh of storage capacity. This estimate is based on a power density of 80 watts/ft^2 (861 watts/m^2) in the power conversion section. For a 10-kW, 400-kWh application, the REDOX storage system would cost $24,000, half that of a lead-acid rechargeable battery system. A reasonable quantity market for REDOX systems will reduce the unit cost and would stimulate enough demand for chromium chemicals to warrant the use of proved low-cost large-scale manufacturing processes. Although no detailed cases have been analyzed, it is estimated that REDOX cost could then be reduced to approximately $163/kW plus $20/kWh in sizes from stand-alone isolated installations to utility-sized storage. This would amount to about $9,360 for the 10-kW, 400-kWh application, less than one quarter the lead-acid battery system cost.

This work was done by Lawrence H. Thaller of **Lewis Research Center.** *Further information may be found in:*

NASA TM-X-71540 [N74-21688/NSP], "Electrically Rechargeable REDOX Flow Cell" [$4], and NASA TM-79186 [N79-26505/NSP], "Recent Advances in REDOX Flow Cell Storage Systems" [$4].

Copies of these reports may be purchased [prepayment required] from the National Technical Information Service, Springfield, Virginia 22161.

A copy of AIAA Terrestrial Energy Systems Conference 70-0989, "REDOX Flow Cell Energy Storage System," may be obtained from the American Institute of Aeronautics and Astronautics, Inc., 1290 Avenue of the Americas, New York, New York 10019.

Copies of U.S. Patent 4,159,366, "Electrochemical Cell for Rebalancing REDOX Flow Systems" [filed June 9, 1978], and U.S. Patent 3,996,064, "Electrically Rechargeable REDOX Flow Cell" [filed August 22, 1975], may be obtained at cost from the U.S. Patent and Trademark Office, Washington, D.C. 20231.

Inquiries concerning rights for the commercial use of this invention should be addressed to the Patent Counsel, Lewis Research Center [see page A5]. Refer to LEW-13398.

Additive Improves Engine-Oil Performance

Engine wear and the frequency of oil changes are reduced by low concentrations of tricresyl phosphate.

Goddard Space Flight Center, Greenbelt, Maryland

Tricresyl phosphate (TCP) is a well-known "extreme pressure additive" for engine oil that substantially reduces the wear rate and may extend the interval between oil changes. It does this by reacting with the fresh metal surfaces that are created as the engine parts slide past each other to form a phosphate film coating that inhibits further wear. In addition to its use as an engine additive, TCP has also been found to give substantial performance improvements in ball bearings installed in spacecraft. NASA is now considering it as an additive for all diesel and motor-vehicle engine crankcases.

TEST CONDITIONS	CONCENTRATION OF METAL (ppm/h×10^{-2})					
	Fe	Al	Cu	Cr	Sn	SiO_2
Eight 250-h Changes (Without TCP)	7.75	1.60	1.25	0.60	0.55	5.35
Eight 250-h Changes (With TCP)	5.70	0.50	1.49	0.50	0.40	3.25
Percent Change	-26.5	-68.8	+19.4	-16.7	-27.3	-39.3
Three 500-h Changes (With TCP)	3.00	0.53	0.60	0.20	0.73	1.54
Percent Change From Values Without TCP	-61.3	-66.9	-52.0	-66.7	+32.7	-71.2

The **Wear Rate of Engine Oil** is reduced by TCP additive, as evidenced by the lowered metallic content of the used oil.

The accompanying table shows the results of chemical analyses of crankcase oil changes in diesel-electric generators both with and without TCP. Eight changes, each after 250 hours with no additive, are compared with eight changes, each after 250 hours, and three changes, each after 500 hours, with 5 percent by volume TCP. Except for the tin content, the origin of which is still being investigated, the metallic and SiO_2 concentration rates were significantly lower in the samples with TCP. By these tests, the oil-change interval was extended from 250 hours to 2,000 hours without a significant increase in wear rates.

In another study, commercial 10W30 oil gave one-tenth the wear and had less degradation when mixed with 5 percent TCP, suggesting its potential for use in other lubrication applications.

This work was done by Alfred J. Babecki and Hugh C. Fletcher of **Goddard Space Flight Center.** *No further documentation is available.*
GSC-12327

Drilling Side Holes From a Borehole

Novel machine concept would take long horizontal stratum samples from a narrow vertical hole.

NASA's Jet Propulsion Laboratory, Pasadena, California

A proposed machine for drilling horizontal holes in the earth surrounding a borehole could take samples extending a few meters into the strata. Such samples will yield important data for geological studies, oil surveys, and geothermal energy surveys. The machine could also drill holes for drainage or ventilation in coal mines.

The conventional method of taking side samples is to use an explosive to drive a small sampling vessel into the borehole wall. However, since the vessel penetrates only a short distance into the wall of the borehole, the samples are likely to have been contaminated by drilling mud, distorted by the borehole drilling, and lacking in normal stratum fluids. In contrast, the new drilling machine takes samples that extend deep into the strata.

In order to take long horizontal samples from the confines of a hole 6 inches (21.2 centimeters) in diameter, a folding structure drives and advances the drilling tool. As shown in Figure 1, the rotating drill bit is advanced by a shaft composed of interlocking half-cylindrical shells, drawn from vertical storage bins. The machine is enclosed in a steel tube 30 feet (10 meters) in length, which contains pumps, motors, and a feed mechanism. The enclosure is lowered to the required depth and fixed in place by packing rings.

The feed mechanism moves upper and lower chains of half-cylindrical shells from their vertical tracks. As segments of the two chains turn horizontal, they mate to form a rigid hollow thrust tube that pushes the drill bit into the bore wall. A worm gear furnishes the motive force for the advance, driving a set of racks on the segments.

The drilling head is rotated by an extensible, flexible hollow shaft that engages an expandable drill bit stored in a magazine. (The bits are short-life tools selected to suit the stratum being

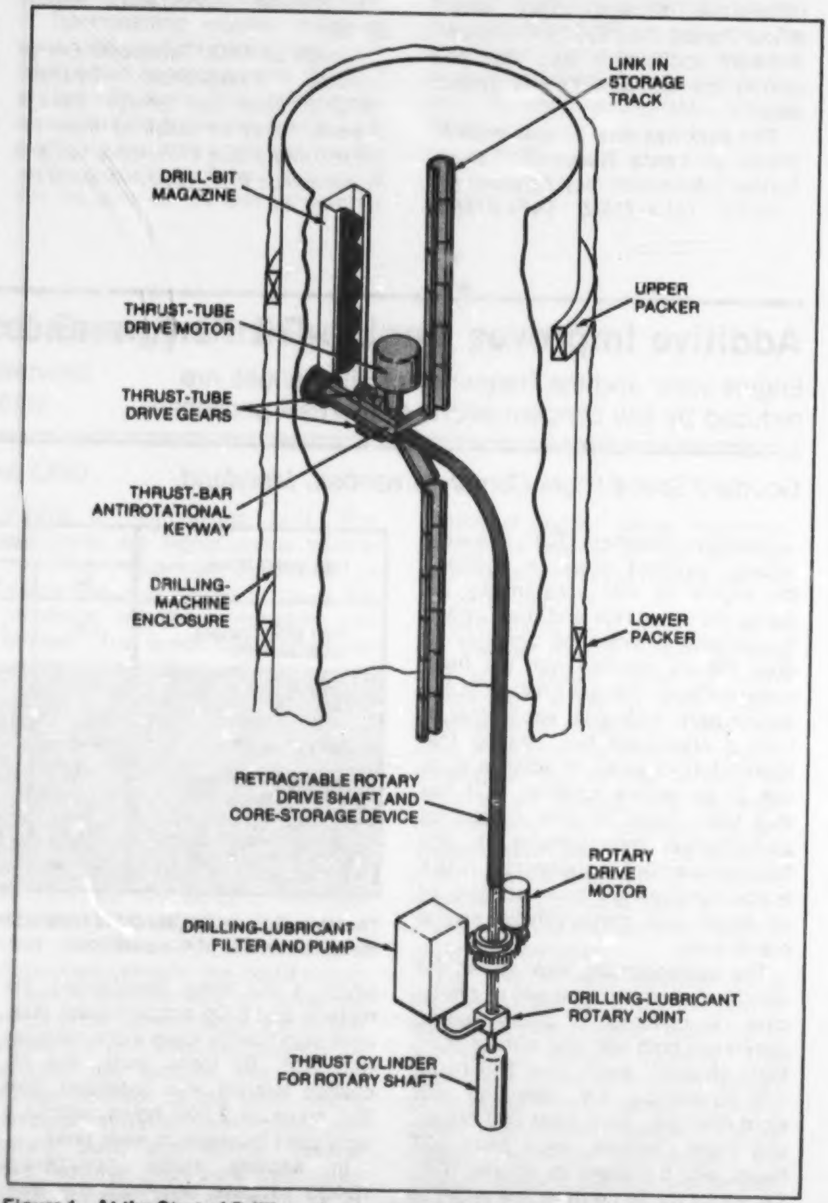
LINK IN STORAGE TRACK
DRILL-BIT MAGAZINE
UPPER PACKER
THRUST-TUBE DRIVE MOTOR
THRUST-TUBE DRIVE GEARS
THRUST-BAR ANTIROTATIONAL KEYWAY
DRILLING-MACHINE ENCLOSURE
LOWER PACKER
RETRACTABLE ROTARY DRIVE SHAFT AND CORE-STORAGE DEVICE
ROTARY DRIVE MOTOR
DRILLING-LUBRICANT FILTER AND PUMP
DRILLING-LUBRICANT ROTARY JOINT
THRUST CYLINDER FOR ROTARY SHAFT

Figure 1. **At the Start of Drilling, the thrust tube has been formed from the first links in the upper and lower chains of half-cylindrical shells. The thrust tube has engaged a drill bit and pressed it through a hole in the enclosure against the bore wall. The rotary shaft is inserted in the thrust tube and turns the drill bit.**

drilled.) The flexible rotary shaft fits inside the thrust tube. Composed of segmented, slip-jointed rings in a flexible sheath, the rotary shaft holds a stratum sample in its hollow center and carries lubricating fluid for the drill bit in the space between the segments and the sheath (see Figure 2). The rotary shaft is turned by a ring gear and motor and is advanced and retracted by a hydraulic cylinder. One rotary shaft is needed for each sample to be taken.

After the sample has been taken, the rotary shaft and the thrust tube are retracted into their vertical storage positions. The expendable drill bit is left in the hole. The drilling sequence is then repeated for other strata in the borehole. Measuring instruments can be inserted in the completed hole to record dimensional data and other information.

For drilling secondary horizontal ventholes from primary vertical vents in coal mines, multiple drilling mechanisms would be installed in the machine. It is estimated that four holes 1.25 inches (3.2 centimeters) in diameter and 8 feet (2.4 meters) deep could be drilled simultaneously in 1 hour.

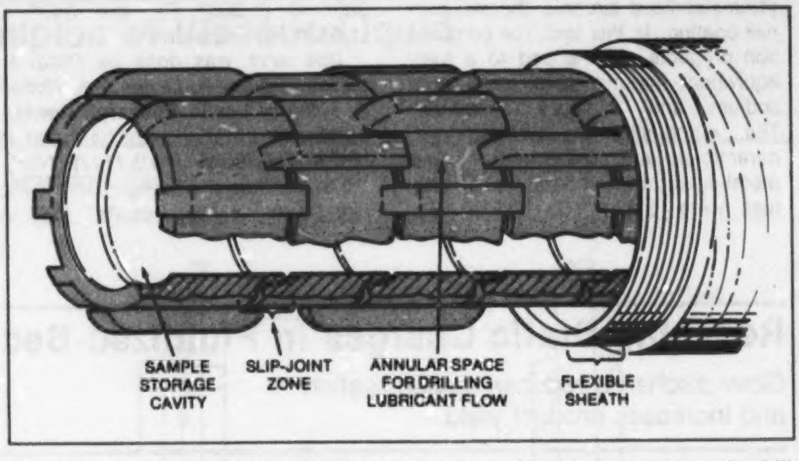

Figure 2. This **Flexible Rotary Shaft** comprising articulated segments turns the drill bit. The fins transmit rotation from one segment to the next, within a sheath. The hollow core of the shaft stores stratum samples a few meters long.

This work was done by Earl R. Collins, Jr., of Caltech for **NASA's Jet Propulsion Laboratory.** *For further information, Circle 53 on the TSP Request Card.*

Inquiries concerning rights for the commercial use of this invention should be addressed to the Patent Counsel, NASA Resident Legal Office-JPL [see page A5]. Refer to NPO-14465.

Corrosion-Resistant Ceramic Thermal-Barrier Coating

Coating for air-cooled components of gas-turbine engines better resists corrosion by fuel and air impurities.

Lewis Research Center, Cleveland, Ohio

A simple, two-layer thermal-barrier coating system that offers improved resistance to hot corrosion from fuel and air impurities has been identified for use on air-cooled components of gas-turbine engines. The coating system consists of an MCrAlY (where M is nickel, cobalt, or iron) alloy bond-coat layer and a highly-adherent, insulating, calcium silicate ceramic outer layer. The MCrAlY bond coating and the calcium silicate layer may both be deposited by plasma spraying in an air environment without the necessity of a special cover gas. The thickness of the bond coat can range from 0.008 cm (0.003 in.) to 0.018 cm (0.007 in.), and that of the calcium silicate ceramic layer may range from 0.012 cm (0.005 in.) to 0.051 cm (0.020 in.) or more. The calcium silicate coating can be polished to reduce aerodynamic frictional losses.

Ceramic coatings have low thermal conductivities and therefore impose a thermal barrier between high-temperature combustion gases and air-cooled metal parts such as the combustors, turbine blades, and vanes of power-generating turbines or the cooled components of other heat engines. As a result, the working parts can operate at reduced metal temperatures. Alternatively, increased gas temperatures or decreased coolant flows may be attained. These features provide the potential for increased engine performance, reduced fuel consumption, use of less costly materials or fabrication procedures, and increased life and durability of cooled engine components. Improved corrosion resistance is an additional attribute of the calcium silicate-based thermal-barrier coating. It offers potential to allow firing of power-generating turbines with lower-grade, corrosive fuels.

When the NASA-developed calcium silicate/MCrAlY coating was evaluated in an industrial/utility gas-turbine combustion simulation program sponsored by the Department of Energy, it was found to be more resistant to spalling in a corrosive environment than previous thermal-barrier coatings. This coating completed 675 1-hour test cycles before spalling on the leading edge compared to 80 1-hour cycles for 12 percent by weight

(continued on next page)

yttria-stabilized zirconia thermal-barrier coating. In this test, the combustion products were doped to a fuel-equivalent impurity level of 5 ppm sodium and 2 ppm vanadium. The combustion-gas temperature, ceramic-surface temperature, and metal-substrate temperature in this test were 1,370° C (2,500° F), 980° C (1,800° F), and 840° C (1,550° F), respectively.

This work was done by Philip E. Hodge, Stanley R. Levine, and Robert A. Miller of **Lewis Research Center.** *Further information may be found in NASA TM-79005 [N79-11179/NSP], "Thermal Barrier Coatings: Burner Rig Hot Corrosion Test Results" [$6]. A copy may be purchased [prepayment required] from the National Technical Information Service, Springfield, Virginia 22161.*

Inquiries concerning rights for the commercial use of this invention should be addressed to the Patent Counsel, Lewis Research Center [see page A5]. Refer to LEW-13088.

Reducing Static Charges in Fluidized-Bed Reactions

Glow discharge reduces agglomeration and increases product yield.

Ames Research Center, Moffett Field, California

Fluidized-bed reaction systems involving suspended particles often suffer unfaborable effects on their hydrodynamics due to agglomeration of the particles, caused by static charges on their surfaces. The addition of moisture or a conductive coating such as graphite on the particles can reduce the static charge, but these techniques can interfere with the chemical reactions in some processes. A new approach, ionizing the gas used to suspend the particles, introduces no foreign substances into the reaction chamber and has been shown in one case to increase the reactant-loading capacity sixfold over that in a static process, onto the same area as the diffuser plate.

The apparatus shown in the figure was used for the disproportionation of calcium peroxide diperoxyhydrate to calcium superoxide. Dry nitrogen gas is introduced at the bottom of the funnel-shaped reaction chamber to suspend the particles and create the fluidized bed. The gas is ionized by a ring-shaped high-voltage electrode (a power meter and impedance-matching circuit are not shown) to which a 5-W pulsed RF voltage is applied at 13.56 MHz.

A glow discharge makes the gas conductive enough to neutralize the static charge from the suspended particles. The particles can then react while suspended in the flowing gas stream.

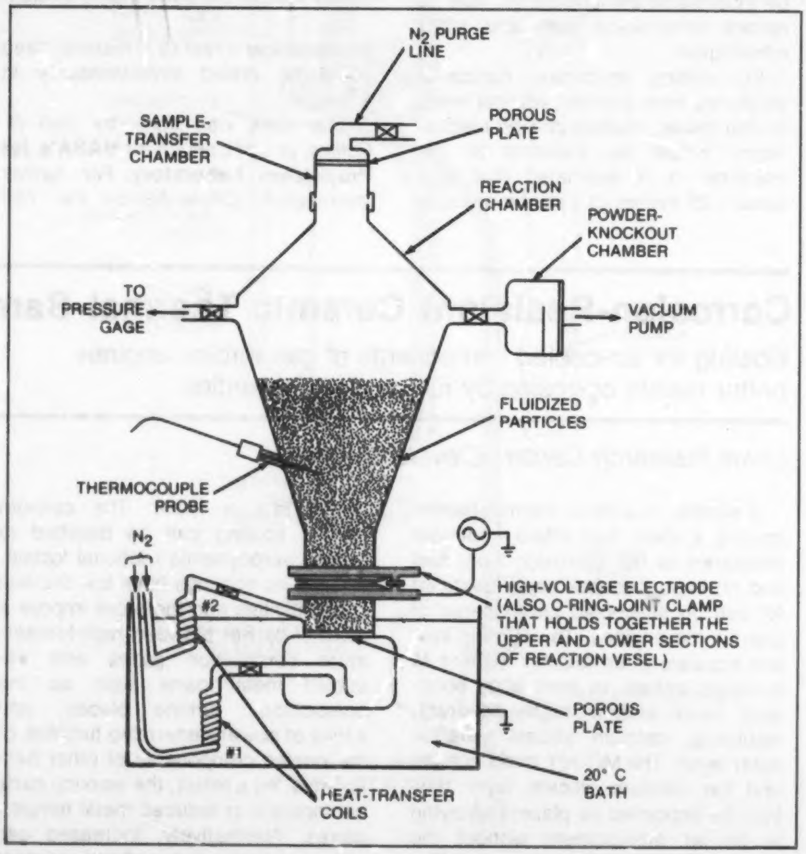

RF Glow Discharge Apparatus for a fluidized-bed reaction system ionizes the fluidizing gas to make it sufficiently conductive to neutralize static charge on the particles. In the apparatus above, the O-ring-joint pinch clamp is the high-voltage electrode.

This work was done by Theodore Wydeven of **Ames Research Center,** *E. Vernon Ballou and Peter C. Wood of San Jose State University Foundation, and LeRoy A. Spitze of San Jose State University. For further information, Circle 54 on the TSP Request Card.*

This invention is owned by NASA, and a patent application has been filed. Inquiries concerning nonexclusive or exclusive license for its commercial development should be addressed to the Patent Counsel, Ames Research Center [see page A5]. Refer to ARC-11245.

Transferring Small Samples of Viscous Liquid

Bubble-free samples are obtained for chemical analysis.

Lyndon B. Johnson Space Center, Houston, Texas

A simple technique for filling a small syringe with a viscous liquid almost completely avoids trapped air bubbles.

The sample is first drawn into an auxiliary syringe (see figure) that is large enough to avoid bubbles or allow them to be removed easily. The needle of this large syringe is used to fill the reservoir of a smaller, sample syringe from which the plunger has been removed. After the plunger is reinserted, the syringe is turned needle up, while the plunger is depressed to force out trapped air and reach the desired sample volume.

This technique makes it easy to handle and control a quantity of sample as small as 1 microliter. Such samples are often transferred by using syringes, but the vacuum created when the liquid is drawn through the hollow needle creates bubbles as the liquid reaches the barrel. It was necessary to clear the bubbles by inverting the syringe, tapping or otherwise coaxing the bubbles to rise to the needle entry, and then ejecting sufficient liquid to clear the barrel and needle of bubbles. Avoiding the bubble contamination becomes progressively more difficult for smaller syringes or for very viscous samples.

With the new technique, fewer bubbles are generated during the initial fill, and these are expelled when the plunger is reinserted. The method is thus simpler and more effective than the old approach.

This work was done by Bruce W. Miller, Shirley M. Mitchell, and John N. Olney of Rockwell International Corp. for **Johnson Space Center.** *No further documentation is available. MSC-18533*

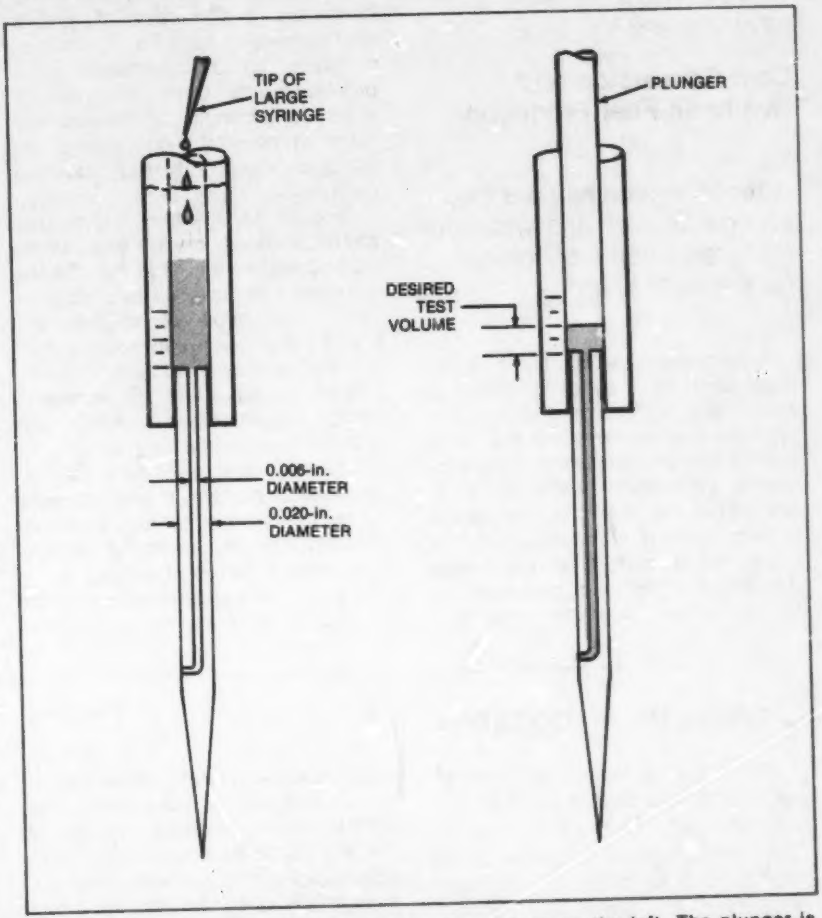

The **Viscous Fluid Is Directly Inserted** into the syringe on the left. The plunger is removed so that the fluid can be poured in or forced in from a larger auxiliary syringe. As shown on the right, the reinserted plunger forces out the air bubbles until the desired sample-volume mark is reached.

Books and Reports

These reports, studies, and handbooks are available from NASA as Technical Support Packages (TSP's) when a Request Card number is cited; otherwise they are available from the National Technical Information Service.

Coal Conversion and Synthetic-Fuel Production

A report evaluates potential coal gasification and synthetic-fuel production technologies for the near future.

A comprehensive report on a recent study identifies analytic techniques to design and implement a coal-based synthetic-fuel complex, viable coal gasification and utilization technologies for the 1985-to-1990 time frame, and the potential synthetic-fuel market in the southeastern United States. The first of five chapters is an overview of the entire study and presents the status quo and future technical and economic potentials of the coal technology.

Chapter II describes analysis methodologies, modeling capabilities, and supporting technology development required to conduct and monitor conceptual and practical designs for coal conversion facilities. The subject is focused on coal gasification and is organized into three sections: (1) engineering design and development, (2) environmental management, and (3) supporting technology development.

Chapter III identifies, evaluates, and recommends models and analysis methodologies that address the requirements established in chapter II. Three categories of models and analysis methods are investigated: (1) steady-state flowsheet simulators, (2) gasifier models, and (3) economic models broken down into costing and financial evaluations.

Chapter IV discusses potential coal gasification processes and identifies those most likely to be ready for commercial operation in the 1986-to-1990 period. Seven processes out of 100 studied are suggested as possible candidates for commercial operation (1,000 to 2,000 tons of coal/day/gasifier). Each of these is characterized by the product gas composition, byproducts, gasifier efficiency, the type of coal used, and several other factors.

Chapter V characterizes potential industrial users of coal conversion products. Major national, regional, and also specific industries in Northern Alabama are identified as potential customers for medium-Btu gas (MBG).

Two appendix sections conclude the report. The first is a catalog of 105 coal gasification systems listed alphabetically according to the manufacturers. The last is a catalog of models and analytical methodologies for coal conversion facilities.

This work was done by Rodney Bradford of **Marshall Space Flight Center** *and W. T. Atkins, Ronald M. Bass, Richard Dascher, Joseph Dunkin, Nina Luce, William Seward, and Dennis Warren of BDM Corp. To obtain a copy of the report, "Coal Conversion Processes and Analysis Methodologies for Synthetic Fuels Production," Circle 55 on the TSP Request Card.*
MFS-25330

Computer Programs

These programs may be obtained at very reasonable cost from COSMIC, a facility sponsored by NASA to make new programs available to the public. For information on program price, size, and availability, circle the reference letter on the COSMIC Request Card in this issue.

Underground Coal Mining

Closed-network queue model

Over the last 8 years, underground coal-mining productivity has declined by almost half, while the cost of coal has risen. With coal recognized as an important future energy source, it is essential that a better understanding of all aspects of coal productivity be developed. Almost all coal mining in the United States is mined with the aid of mechanical systems. Recent studies have shown that equipment at the work face is down about a quarter of the time. Since the equipment within a continuous-mining system is essentially linked in series with the workface machinery, downtime for the continuous system can be considerably more than a quarter of the time.

A new computer program that models coal-mining production, equipment failure, and equipment repair represents an underground mine as a collection of work stations that alternately require servicing by a production crew and a repair crew. Each crew is drawn from a respective pool of homogeneous crews. This interaction is modeled as a closed network of two queues in series and is solved as a classic Markov finite-state birth-and-death process. As such, the model is applicable to any cluster of processes that operate and fail independently but share pools of production and repair resources.

The model projects equipment availability and productivity based on the number of work stations, production crews, and repair crews and the equipment reliability parameters of "mean time between failure" and "mean time to repair." The sensitivity of productivity to these variables is readily derivable, suggesting appropriate areas for research and development, as well as indicating the proper balance of labor and equipment in advanced mining systems.

This program is written in FORTRAN IV for batch execution and has been implemented on a UNIVAC 1108 with a central memory requirement of approximately 14K of 36-bit words. This network queue modeling program was developed in 1978.

This program was written by Gerrie M. Hill of Caltech for **NASA's Jet Propulsion Laboratory.** *For further information, Circle C on the COSMIC Request Card.*
NPO-14704

Life Sciences

Hardware, Techniques, and Processes

59 Temperature Controller for Hyperthermia Device
60 Measuring Water Properties From a Moving Boat

Temperature Controller for Hyperthermia Device

Biomedical appliance measures and controls temperature in tumor.

Langley Research Center, Hampton, Virginia

A temperature controller was developed to support a research program investigating hyperthermia as an antineoplastic treatment modality. It closely controls temperature in the local region of a tumor in a live subject. Extensive laboratory investigations involving both leg and lung tumors in mice show that the controller is capable of maintaining a given temperature to within ±0.2° C. To allow its use by biomedical workers with little training on complex electronic systems, the controller has as few front-panel control functions as is practical. Furthermore, it is expandable for the treatment of several subjects simultaneously.

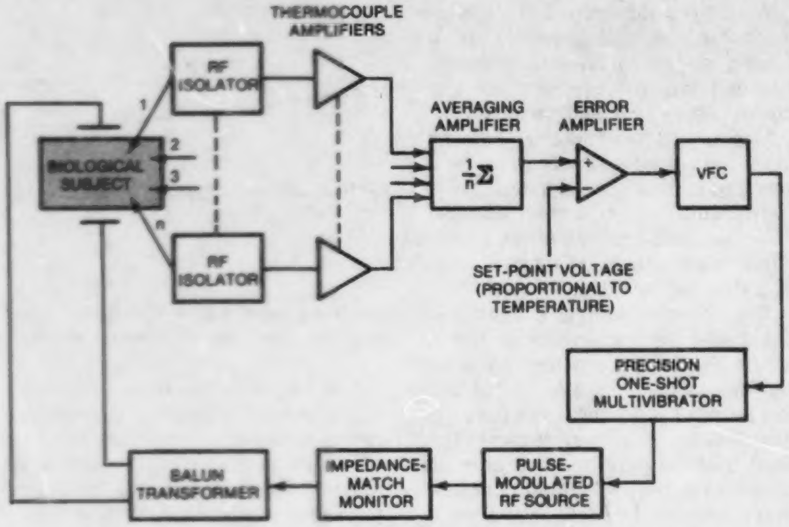

Single-Channel Hyperthermia Temperature Controller continuously monitors a subject's temperature and compares it to a target value. If the measured temperature is too high, no RF energy is applied, and the temperature drops off naturally. If the measured temperature is too low, a voltage proportional to the temperature error is generated in the error amplifier and applied to a voltage-to-frequency converter (VFC), which produces a square-wave signal with a frequency that is proportional to the input voltage. This in turn drives a precision one-shot multivibrator that produces a train of fixed-width, variable-duty-cycle pulses. This signal pulse-modulates an RF power source that provides the energy required to raise the local temperature of the subject. An impedance-match monitor allows a gross assessment of the degree to which the RF energy supplied by the generator is utilized to heat the subject. A balun transformer provides a broadband transformation from an unbalanced power source to an inherently balanced load; i.e., the subject. At the lower frequencies (≅10 MHz) the balun transformer can be eliminated.

Tissue is heated by pulsed radiofrequency energy applied directly to the subject through ohmic contacts. Special applicators efficiently couple the device to the leg and thoracic regions of mice, using a conductive jelly similar to EKG grease. For the critical temperature measurements in the region of the tumor, medical-grade thermocouples (enclosed in a hypodermic needle) give the best temperature measurements. These probes are inserted subcutaneously near the tumor or, in some cases, into the tumor. At the power levels used in this investigation, no problem associated with the potential rectifying characteristic of the junction of dissimilar metals was encountered. The junction of the thermocouple probe is electrically insulated from the hypodermic needle.

The configuration illustrated shows a closed-loop system in which the subject's temperature is continuously monitored and compared to a target temperature. RF energy is supplied as needed to heat the tissue. A multiple-subject version of the hyperthermia appliance was also developed and differs from the one illustrated here in that a single temperature measurement per subject is made with measurements sequentially applied to the controller through a multiplexer. The output of the power source is multiplexed accordingly, applying heat to the subject whose temperature is being measured. The impedance-match monitor was modified to operate in a sampling mode and can be switched to read any one of the several channels.

Extensive investigations thus far have been limited to radio frequencies in the region of 30 MHz. However, the system has been tested at frequencies ranging from 10 to 100 MHz with no significant degradation in performance.

This work was done by Richard H. Couch, Chase P. Hearn, and James B. Williams of **Langley Research Center.** *For further information, Circle 56 on the TSP Request Card.*

Inquiries concerning rights for the commercial use of this invention should be addressed to the Patent Counsel, Langley Reserach Center [see page A5]. Refer to LAR-12528.

Measuring Water Properties From a Moving Boat

Batch analyzer is modified
for continuous flow.

Langley Research Center, Hampton, Virginia

A modified commercial instrument measures the characteristics of a flowing stream of water. Originally intended for measurement on stationary water in a sample chamber, the instrument has now been adapted to measuring water scooped up by a submerged tube on a moving boat (see figure). The water analyzer measures such characteristics as pH, temperature, dissolved oxygen, conductivity, and turbidity.

The collector tube is shaped and attached to the boat so that its inlet is at the required depth for sampling. The tube is connected to a chamber that passes the flowing water from the tube over the instrument sensors. The new chamber replaces the original sensor chamber, which did not allow measurements on continuous flow. If required, water samples can be taken from the tube outlet for later analysis in a laboratory.

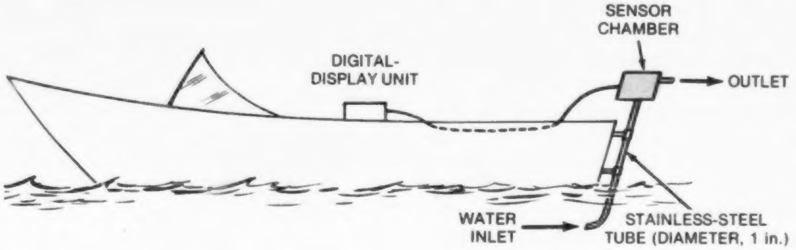

The **Tube Inlet Below the Boat** diverts a stream of water through the sensor chamber. The measured values appear on the remote digital-display unit.

The height of the sensor chamber above the water is fixed so that the ram pressure at a boat speed of 12 to 15 mi/h (19 to 24 km/h) is sufficient to force the water through the chamber. [A pressure of about 1/2 lb/in.^{2} per foot of elevation (3.4×10^6 N/m^2 per meter) is necessary.] A valve may be placed in the tube to regulate the waterflow.

This work was done by Ashby G. Lawson of **Langley Research Center.** *No further documentation is available.*
LAR-12325

Mechanics

Hardware, Techniques, and Processes

63 Cable-Splice Detector
64 LVDT Gage for Fracture-Toughness Tests in Liquid Hydrogen
65 Tension-Mode Loading for Bend Specimens in Cryogens
66 Modified Displacement Gage for Cryogenic Testing
67 Broadband Electrostatic Acoustic Transducer for Liquids
68 Eddy-Current Sensor Measures Bolt Loading
69 Multiple-Creep-Test Apparatus
70 Compact, Super Heat Exchanger

Books and Reports

71 Applications of Remote-Sensing Imagery

Computer Programs

72 Equations of Motion for Coupled N-Body Systems
72 Viscous Characteristics Analysis
73 Transonic Airfoil Design Code
73 Improved Multielement Airfoil Analysis
74 Aircraft Equilibrium Spin Characteristics
74 Flow Field in Supersonic Mixed-Compression Inlets
74 Shell Theory Automated for Rotational Structures
75 Three-Dimensional Potential Flow
75 Full-Coverage Film Cooling
76 Disturbance Amplification Rates

Cable-Splice Detector

An inexpensive sensor and electronic circuit reduce maintenance costs and improve the safety of San Francisco cable cars.

Ames Research Center, Moffett Field, California

A magnetic detector, originally developed to warn gripmen on San Francisco cable cars when a spliced section of cable is passing, could have other applications where moving steel cable must be measured, monitored, or controlled. Developed following a request by San Francisco city officials to a NASA Applications Team (see inside front cover), the splice detector has possible uses in aerial cable-car systems and equipment handling in mines, boreholes, and undersea operations.

In the San Francisco cable-car system, the car operator controls a lever that engages the grip mechanism with the moving underground cable; however, cable breakage at a splice has been a major problem. Such failures can occur when a spliced section [each of which is 72 feet (21.9 m) in length] is gripped, causing individual cable strands to tear. The separated cable strands can also entwine around the grip and drive the car uncontrollably into other vehicles.

To prevent such mishaps, the splice detector sounds a buzzer when a splice approaches the car. It is activated by a Hall-effect proximity sensor that produces a linear voltage proportional to magnetic-field intensity. The sensor is attached to the bottom of the grip mechanism, 1/4 to 1 inch (0.6 to 2.5 centimeters) from the cable.

The cable contains five magnetized spots ahead of the splice. The spots are spaced 10 feet (3 meters) apart, and the last spot precedes the splice by 42 feet (12.8 meters). For a cable speed of 14 ft/s (4.3 m/s), the spot separation corresponds to 0.7 second, and the splice separation corresponds to 3 seconds.

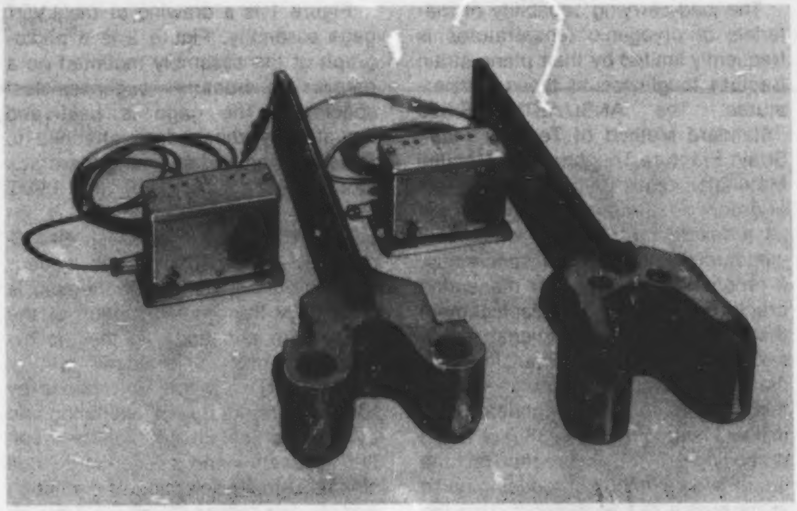

The **Cable-Splice Detector** consists of a Hall-effect magnetic sensor, which is located about 1/2 to 1 in. from the cable. Magnetic markings on the cable are converted to electrical signals by the sensor. The electrical signals are filtered, amplified, converted to pulses, and counted to actuate an audible alarm or light when a splice approaches a cable car.

The sensor produces voltage pulses as the magnetic spots pass it. The pulses are counted, and when at least three pulses are accumulated in rapid sequence, the circuit sounds an alarm. A 12-volt battery (such as that found in household smoke detectors) powers the circuit and alarm.

In tests on cable cars, the detector worked faultlessly, provided that the cable contains no spurious magnetism and the spots are strongly magnetized. To insure these conditions, the entire length of the cable is demagnetized and the spots are remagnetized every 3 days.

Located in the main cable house, the demagnetizer is a commercial "growler" that erases magnetic noise from the cable. The magnetizer, also in the cable-car house, rotates a horseshoe magnet around the steel cable at five places separated from the splice and from each other by the requisite distances.

For reliability testing and splice monitoring, three detectors similar to those on the cable cars are also in the cable house (one detector for each of the three cable-car lines). Each detector indicates passage of a splice by lighting a 40-watt bulb and a single buzzer shared by the three detectors. An electronic timer measures the interval after the last splice indication for each of the cable-barn detectors. If the cable must be shut down, the timer readings can be read to locate the current positions of the splices.

This work was done by Robert D. Lee, Ernest J. Iufer, and Angelo Giovannetti of **Ames Research Center.** *For further information, Circle 57 on the TSP Request Card.*
ARC-11291

LVDT Gage for Fracture-Toughness Tests in Liquid Hydrogen

LVDT displacement gage can be calibrated at room temperature.

Lewis Research Center, Cleveland, Ohio

The load-carrying capability of materials at cryogenic temperatures is frequently limited by their plane-strain fracture toughness at those temperatures. The ANSI/ASTM E-399 "Standard Method of Test for Plane Strain Fracture Toughness of Metallic Materials" requires the measurement of crack-mouth-opening displacement as a function of applied load using standardized precracked specimens. It recommends a gage for measuring crack-mouth-opening displacement that incorporates conventional resistance strain gages as sensing elements. One problem encountered with this gage for fracture toughness tests in liquid hydrogen (at -423° F or 20 K) is boiling of the hydrogen on the strain-gage elements, producing noise in the output signal and obscuring the test record.

An alternative crack-mouth-opening displacement gage incorporating a linear-variable differential transformer (LVDT) has been developed for use in fracture toughness tests in liquid hydrogen.

Figure 1 is a drawing of the LVDT gage assembly. Figure 2 is a photograph of the assembly mounted on a precracked fracture toughness test specimen. The gage is held and actuated by knife edges attached to the specimen and spanning the crack mouth. Prior to testing, the LVDT movable core is positioned by an adjustment screw to establish electrical null. As the specimen is loaded, crack-mouth-opening displacement is sensed by the relative motion of the LVDT core and body as they follow separation of the knife edges.

The LVDT output is determined by the level of primary coil excitation and by the electrical phase angle between the primary and secondary coil signals. Proper selection of excitation and phase angle can produce a match in outputs at any two temperatures; e.g., room temperature and liquid hydrogen temperature. This allows gage calibration and periodic verification at room temperature rather than in liquid hydrogen. Figure 3 illustrates the technique for obtaining dual-temperature calibration. Gage output is plotted for the two selected temperatures as a function of phase angle at a given excitation level. The intersection of the two curves establishes the phase angle where the output is identical at both temperatures. Changing the excitation level shifts the curves and their intersection.

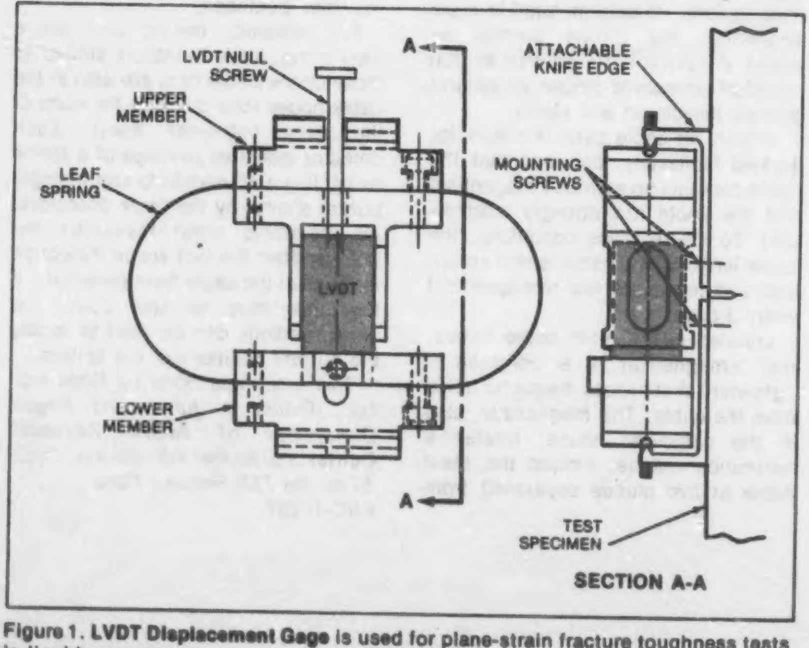

Figure 1. **LVDT Displacement Gage** is used for plane-strain fracture toughness tests in liquid cryogens.

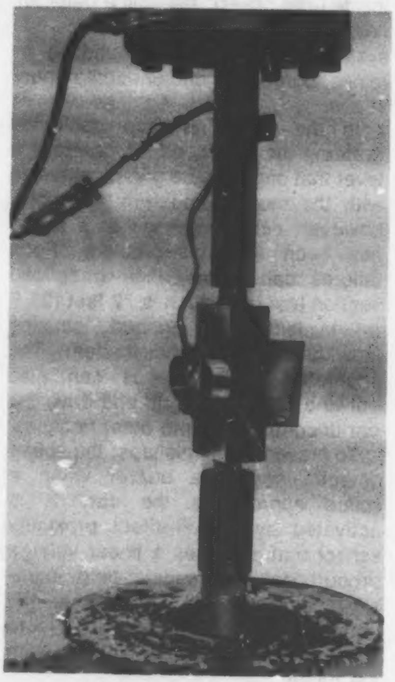

Figure 2. **Displacement Gage** is shown mounted on a test assembly.

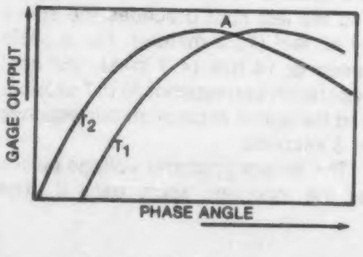

Figure 3. **Gage Output Versus Phase Angle** is plotted at temperatures T_1 and T_2 for a given displacement and excitation.

Although this gage is particularly well suited for use in cryogenic liquids, it can also be used at moderately elevated temperatures and can be encapsulated for use in corrosive or hostile environments. An encapsulated gage has been used commercially for stress corrosion cracking testing of materials in nuclear reactor environments.

This work was done by William S. Pierce and John L. Shannon, Jr., of **Lewis Research Center.** *No further documentation is available.*
LEW-13038

Tension-Mode Loading for Bend Specimens in Cryogens

Fixture allows fracture-toughness tests on standard bend specimens.

Lewis Research Center, Cleveland, Ohio

Material performance at cryogenic temperatures is frequently controlled by the plane-strain fracture toughness at those temperatures. The selection of a test specimen for determining the toughness is sometimes constrained by certain factors such as product size and configuration and crack-plane orientation. A problem arises when the necessary standard test specimen (ANSI/ASTM E-399) is incompatible with available test equipment; e.g., when only a bend specimen will do and the available equipment is suited only for tensile testing. For this particular situation, a test fixture has been developed that permits the use of tension-mode loading for fracture-toughness tests on standard bend specimens. The fixture is compatible with cryostats designed for tension testing.

Figure 1 shows the special load fixture prior to final assembly. The test specimen is centered and held in position on the support (reaction load) rollers by use of spacer blocks and wire clips. The V-block below the specimen alines the load-application roller (not shown). Figure 2 shows the load fixture assembled, with the load-application roller in place (below the specimen).

This work was done by William S. Pierce and John L. Shannon of **Lewis Research Center.** *No further documentation is available.*
LEW-13040

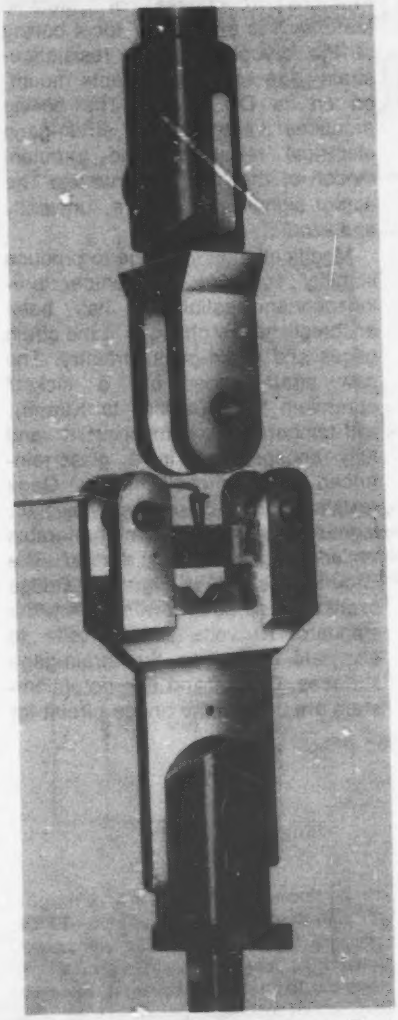

Figure 1. **Load Fixture Prior to Final Assembly**

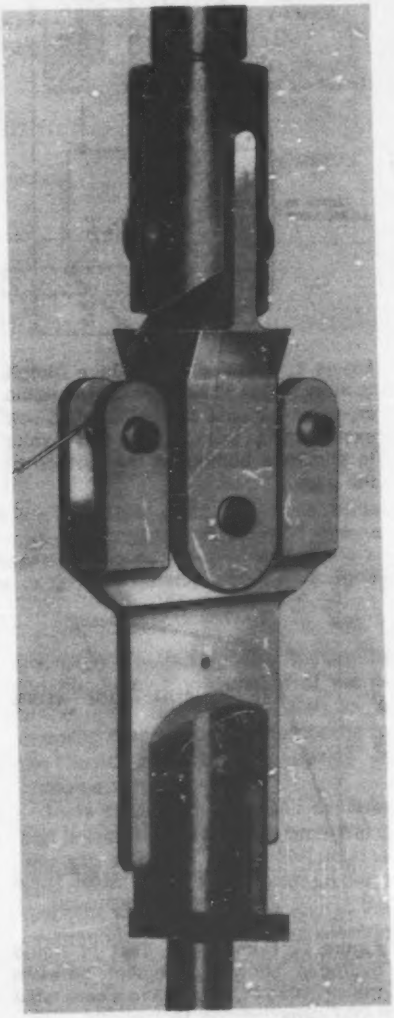

Figure 2. **Assembled Load Fixture**

Modified Displacement Gage for Cryogenic Testing

ANSI/ASTM E-399 clip-in gage for fracture toughness testing is made more stable in liquid hydrogen.

Lewis Research Center, Cleveland, Ohio

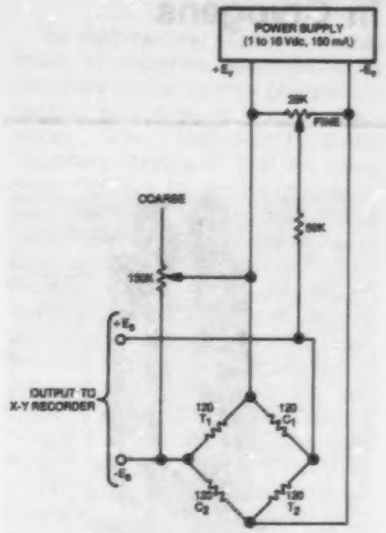

Figure 1. **Modified Strain-Gage Circuit** is more stable when immersed in liquid cryogens because the standard 10-volt excitation has been lowered to 1.5 volts to eliminate boiling on the surface of the gage.

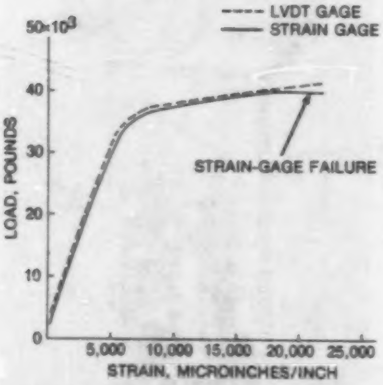

Figure 2. **Comparison Test** in liquid hydrogen shows agreement between the modified DCB gage and a calibrated LVDT gage.

Cryogenic temperatures can adversely affect the performance of electrical/mechanical measurement devices. The double-cantilever-beam (DCB) clip-in displacement gage described in ANSI/ASTM E-399 "Standard Test Method for Plane-Strain Fracture Toughness of Metallic Materials" is affected by local boiling of the cryogen on the resistance-strain-gage sensory elements mounted on its DCB arms. The boiling produces variations in strain-gage electrical resistance and turbulent motion of the gage as a whole. The output signal is, therefore, unsteady and erratic.

Modification of the gage to produce stability, accuracy, and temperature-independent calibration has been accomplished by changes in the strain gages and strain-gage circuitry. The new strain gages are a nickel/chromium alloy (similar to Karma), self-temperature compensated and fully encapsulated in a glass-reinforced epoxy-phenolic resin. Gage resistance is 120 ohms; however, higher resistance gages are preferable to reduce gage heating further. The circuitry is shown in Figure 1. Bridge excitation has been lowered from the standard 10 volts to 1.5 volts to eliminate boiling on the strain-gage surfaces. Coarse and fine potentiometers are used in the bridge circuit for output signal balancing. This circuit is capable of balancing the bridge over the entire useful range of the gage.

Sensitivity of the modified gage is 0.0333 millivolt per volt per 0.001 inch displacement. This sensitivity results in a 50X magnification at a recorder sensitivity of 1.0 millivolt per inch and 1.5 volts excitation. For higher magnification, the signal was increased by a dc amplifier with a 10X multiplier.

Calibration showed that the modified gage is linear within 0.0001 inch over the displacement range from 0.200 to 0.250 inch. Comparison tests of the modified DCB gage and a calibrated LVDT-type gage mounted on the same smooth tensile specimen gave essentially, identical results at both room temperature and liquid hydrogen temperature. The liquid hydrogen test results are shown in Figure 2.

This work was done by William S. Pierce of **Lewis Research Center.** *Further information may be found in NASA TN-D-3724 [N67-10749/NSP], "Design and Use of Displacement Gage for Crack-Extension Measurements" [$5]. A copy may be purchased [prepayment required] from the National Technical Information Service, Springfield, Virginia 22161.*
LEW-13039

Broadband Electrostatic Acoustic Transducer for Liquids

Capacitive transducer with predictable frequency response can be used to calibrate piezoelectric transducers.

Langley Research Center, Hampton, Virginia

A broadband capacitive electrostatic acoustic transducer (ESAT) has been developed for use in a liquid environment at megahertz frequencies. The ESAT is useful in the calibration of standard commercially available transducers and in pulsed or continuous-wave spectral analysis techniques for ultrasonic nondestructive-evaluation characterization of materials. The ESAT has a known electroacoustic transfer function and can be used to measure absolute ultrasonic-wave displacement amplitudes.

No previous transducer has all of these attributes. The dielectric capacitive transducer has a bandwidth and an electroacoustic transfer function comparable to the ESAT, but it cannot measure absolute displacement amplitudes. Capacitive airgap hydrophones are useful only in the kilohertz range. Piezoelectric, magnetostrictive, and electromagnetic transducers do not have the bandwidth and the desirable electroacoustic transfer characteristics of the ESAT, and they cannot measure absolute amplitude. Existing airgap capacitive transducers used in the megahertz range are not liquid-immersible.

The ESAT basically consists of a thin conductive membrane stretched over a metallic housing. The membrane functions as the ground plate of a parallel-plate capacitor; the other plate is a dc-biased electrode. An ultrasonic wave incident on the membrane causes it to vibrate and vary the membrane-electrode gap spacing; an electrical signal is generated proportional to the wave amplitude. The entire assembly (see Figure 1 and equivalent circuit in Figure 2) is sealed for immersion in a liquid. Calibration of the ESAT with incident ultrasonic waves of constant displacement amplitude from 1 to 15 MHz reveals a decrease in output signal with increasing frequency, independent of membrane tension. This is due to a coupling reaction of the membrane to the liquid in which the device is immersed.

Tests made with the ESAT indicate that it may be useful as a broadband acoustic receiver with a predictable frequency response. Its broadband response is especially beneficial to the calibration of standard piezoelectric transducers and in spectrum analysis techniques. In addition, relative ultrasonic attenuation measurements as a function of frequency are improved

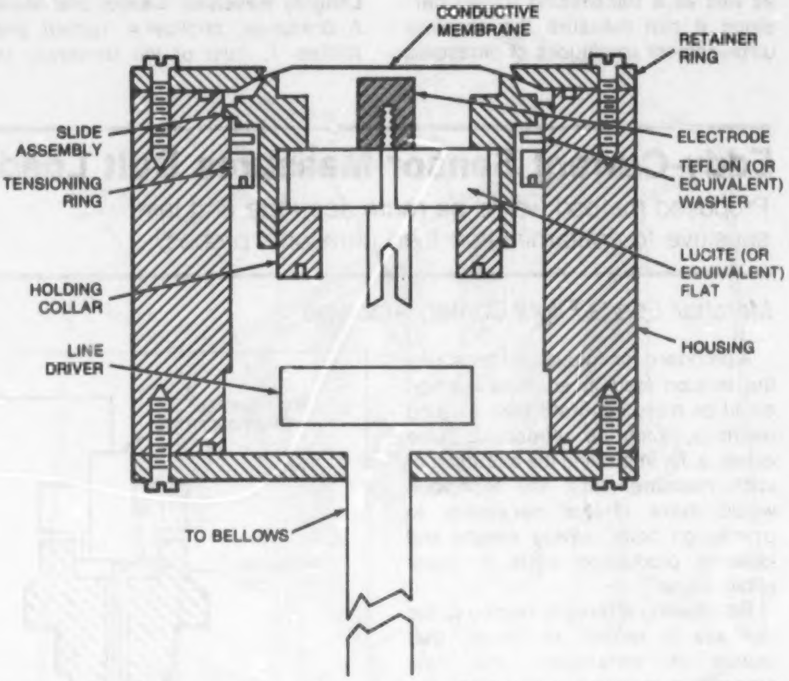

Figure 1. **Electrostatic Acoustic Transducer** is a broadband device that is sealed to allow immersion in water. The electrically grounded membrane forms a parallel-plate capacitor with the electrode, with a gap of about 10 micrometers. Ultrasonic waves incident on the membrane cause it to vibrate, producing a signal from the electrode.

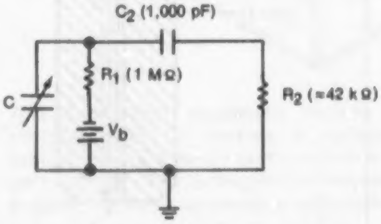

Figure 2. An **Equivalent Circuit of the ESAT** includes C, its capacitance, V_b the dc bias voltage (typically 100 volts), R_1 a large resistor used to prevent damage to the ESAT in case of arc-over, and C_2 a blocking capacitor to the load resistance R_2 (amplifier).

(continued on next page)

with the ESAT because of the repeatability and predictability of its frequency response as compared to conventional damped transducers. The device may be made of different materials and other sizes and shapes to accommodate specific situations. It may be used as a receiving transducer as well as a transmitting transducer. Since it can measure the absolute displacement amplitudes of ultrasonic waves in liquids, it may be used as a calibrator for other transducers and as a probe for the study and characterization of materials where absolute displacement amplitude is important.

This work was done by John H. Cantrell, Jr. [National Research Council], and Joseph S. Heyman of **Langley Research Center** *and Mack A. Breazeale, Michael A. Torbett, and William T. Yost of the University of Tennessee. For further information, Circle 58 on the TSP Request Card.*

This invention is owned by NASA, and a patent application has been filed. Inquiries concerning nonexclusive or exclusive license for its commercial development should be addressed to the Patent Counsel, Langley Research Center [see page A5]. Refer to LAR-12465.

Eddy-Current Sensor Measures Bolt Loading

Proposed method would be more accurate and less sensitive to contamination than ultrasonic probes.

Marshall Space Flight Center, Alabama

A proposed technique for measuring the tension load in an installed bolt could be more accurate than existing methods, such as ultrasonic pulse echoing. By improving the accuracy of such measurements, the technique would make it less necessary to overdesign bolts, saving weight and lowering production costs in many applications.

Bolt loading is directly related to the increase in length, or strain, that occurs on installation. The new proposal is to measure this strain by recording the displacement of a metal wire welded to the bottom of a hole along the axis of the bolt (see figure). A conventional eddy-current transducer could measure this displacement with an accuracy of about 0.0002 in. (0.05 mm). Strain (or load) values would be read directly on a digital display.

Although the required drilling and welding would be difficult and would make bolt manufacturing more complex, the needed technology does exist. Any increase in the cost to make a bolt could be offset by other production and assembly cost savings, particularly in specialty applications.

An existing bolt-load measurement, used with some success on the Shuttle main engine, is to record the time for an ultrasonic pulse to travel the length of the bolt and return. However, the accuracy of this approach is affected by dirt, oil, and other contamination in the bolthole. For each bolt size and type, it also requires a "standard" bolt for which the ultrasonic response is known at different loading levels. In contrast, the new technique is not sensitive to contamination, and it does not require a calibrated set of standard bolts. [Also see "Bolt-Tension Indicator" (MFS-19324) on page 88.]

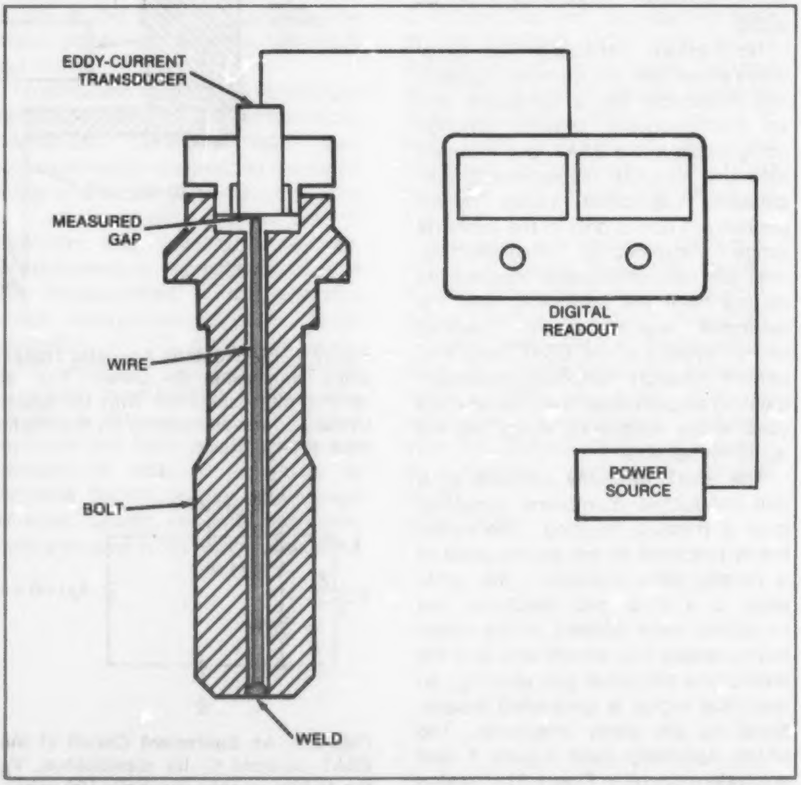

A Thin Wire Target welded to the bottom of a hole down the center of a bolt is the key element in a new proposal for measuring bolt loading. As the bolt stretches under load, changes in the gap between the target and the eddy-current sensing coil are measured and displayed on the digital readout.

This work was done by M. E. Burr of Rockwell International Corp. for **Marshall Space Flight Center.** *No further documentation is available.*
MFS-19486

Multiple-Creep-Test Apparatus

Simplified apparatus uses new fixtures, each supporting three samples at once.

Goddard Space Flight Center, Greenbelt, Maryland

An economical creep-testing apparatus measures flexural, compression, and shear creep of sodium iodide scintillation material. The tests are used to determine the mechanical properties of sodium iodide to design the scintillator support systems.

The apparatus (see figure) consists of a frame resting on a 4- by 6-ft (1.2- by 1.8-m) isolation table that prevents transient vibration. The heart of the apparatus is a new set of fixtures; each accommodates three samples and tests flexural, compression, or shear creep. The fixtures use a series of rods and plates that transfers a single load to all three samples at once.

The advantage of handling three samples simultaneously is that the number of loads used in any series of tests is reduced to one-third, making the apparatus more economical and compact. In addition, the samples in any given fixture are subjected to the same load. The fixtures are expandable to carry more samples by adding more rods and plates in series.

The current design accommodates 4 flexure, 3 compression, and 4 double-shear fixtures and can handle up to 24 fixtures for a maximum of 72 tests. Each vertical sample motion is independently recorded via millivolt printout from a dc-dc linear variable differential transformer responsive with a range of 0.020 in. (0.51 mm) and a sensitivity of 0.02 mil (5.1 μm). An acrylic cover protects from dust and inadvertent disturbances and retains low humidity inside.

This work was done by Carl L. Haehner of **Goddard Space Flight Center.** *For further information, Circle 59 on the TSP Request Card.*
GSC-12561

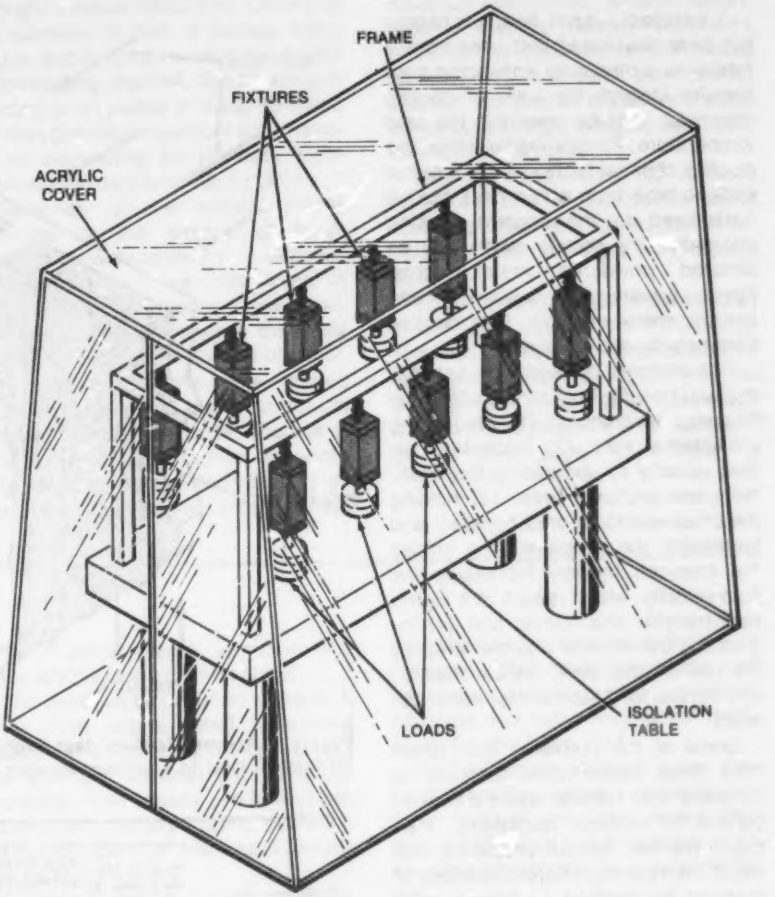

This Creep-Test Apparatus utilizes fixtures that can test three samples simultaneously for flexture, compression, or double-shear creep. Each fixture designed for a specific test requires a single load transferring identical forces to each sample. The arrangement reduces the amount of loads to one-third of the amount used on conventional apparatus that tests each sample separately.

Compact, Super Heat Exchanger

Porous medium enhances heat transfer.

Lewis Research Center, Cleveland, Ohio

A compact, super heat exchanger has been developed that uses porous media as a means of enhancing heat transfer through the walls of cooling channels, thereby lowering the wall temperature. Porous media within the cooling channel increase the internal surface area from which heat can be transferred to the coolant passing internally. The porous media can be sintered powdered metal, metal fibers, woven wire layers, or any porous metal having the desired permeability and porosity.

Conventional methods for enhancing heat transfer in channels utilize the following techniques: (1) roughening the internal wall; (2) increasing the fluid velocity by decreasing the channel cross-sectional area; (3) holding the cross-sectional area constant and increasing the pressure drop across the channel, thereby increasing the fluid velocity, which results in a higher heat-transfer coefficient; and (4) increasing the internal channel area by the use of fins, pins, helical inserts, and the like for heat-transfer enhancement.

Some of the problems that result from these conventional methods to increase heat transfer include lack of control of surface roughness, low-cycle thermal fatigue problems that result from joining different sections of material by welding or brazing, the difficulty of machining suitably sized channels in thin walls and confined spaces, and the difficulty of machining fins in small channels.

Figure 1 shows the physical model of a compact, super heat exchanger that is composed of a two-dimensional channel packed with porous media. The channel is exposed to the external heat flux $q_0(x)$ on one wall and $q_1(x)$ on the other wall. The heat flux is dissipated by the thermal capacity of a coolant flowing at the rate $\dot{m}$ through the porous medium in the channel.

Calculations were made to determine the cooling effectiveness of porous materials in the coolant passage of the heat-exchanger model.

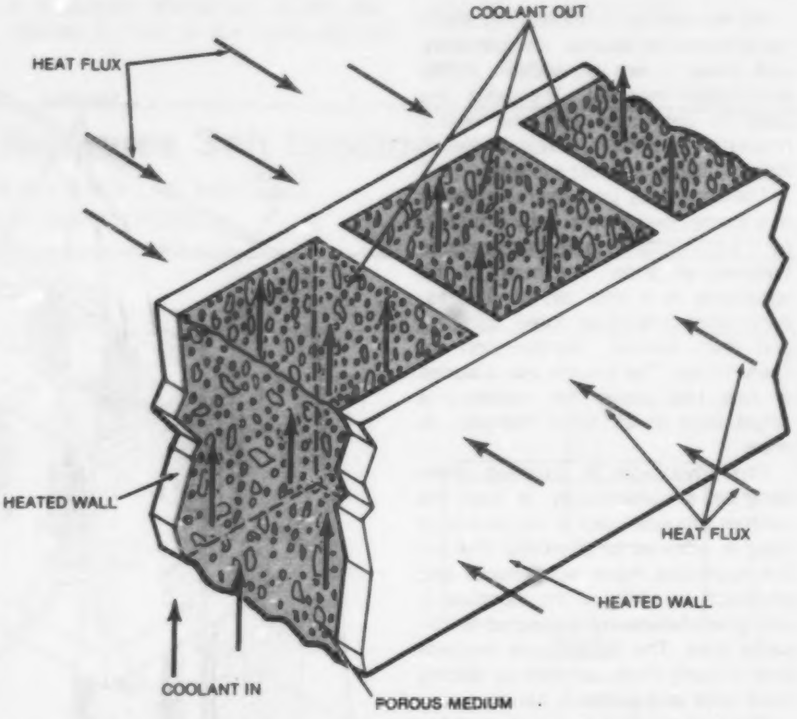

Figure 1. **Porous-Medium Heat Exchanger** has a large internal surface area for the transfer of heat to a coolant flowing through the porous material.

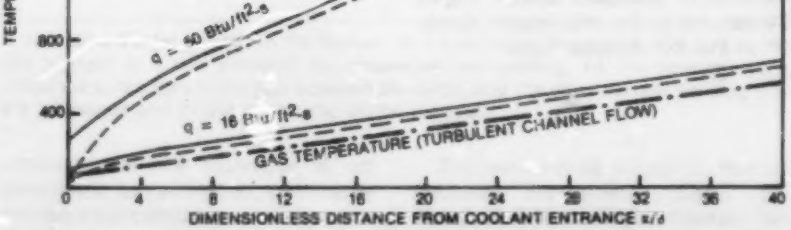

Figure 2. **Comparison Data** show that the wall has a lower temperature and the coolant gas has a higher temperature when a porous medium is used within a heat exchanger.

Figure 2 shows the result of the effects of porous media in a coolant channel. For this channel configuration and a maximum allowable wall temperature of 2,000° F (1,093° C), the wall heat flux with turbulent channel coolant flow is 16 Btu/ft^2-s (180x10^3 W/m^2). However, if the channel is packed with porous material, the wall flux can be increased to 50 Btu/ft^2-s (570x10^3 W/m^2). Thus, for a fixed wall-surface temperature, the effect of porous material is to increase the heat flux capability by over three times. On the other hand, if the heat flux is held at 16 Btu/ft^2-s, the effect of the porous material in the channel is to reduce the wall temperature from 2,000° to about 700° F (1,093° to 371° C).

The heat exchanger may be constructed by forming a body of the porous metal matrix into the desired shape. The cooling channel is then formed over the porous metal matrix by electroforming or sputtering. Both the density of the matrix and the diameter of the channel may be selected to provide the desired heat transfer and the cooling-fluid flow rate appropriate to the heat flux variations along the channel.

As an alternative, the heat exchanger may be constructed by first forming the cooling channel and then filling it with sintered metal powder, metal fibers, or the like. The unit is then heated to a temperature high enough to cause bonding or welding of the contents to form a porous metal matrix and to bond or weld the matrix to the cooling channel. The bonding or welding at all points of metal-to-metal contact provides maximum heat transfer by eliminating the normally high-thermal-resistance contact points.

Selection of the porous media depends on the amount of heat-transfer enhancement desired. Another factor to be considered in material selection relates to the structural requirements between the inner and outer walls of the cooling channel. In some applications, the porous material may serve as a structural support with the aid of ribs. The use of ribs will produce a higher enhancement factor because the ribs act as fins and are able to conduct more heat to the porous material where the heat is then transferred away by the coolant.

An important advantage in using this method of fabrication is that no distortion of the porous material occurs. As a result, prefabrication permeability and porosity characteristics are maintained. Another advantage is that no contact resistance exists at the interface of the porous material. In addition, the cooling channel structure is of one-piece construction, light weight, low cost, and high strength.

This work was done by Anthony Fortini and John M. Kazaroff of **Lewis Research Center.** *For further information, Circle 60 on the TSP Request Card.*

This invention has been patented by NASA [U.S. Patent No. 4,108,241]. Inquiries concerning nonexclusive or exclusive license for its commercial development should be addressed to the Patent Counsel, Lewis Research Center [see page A5]. Refer to LEW-12441.

Books and Reports

These reports, studies, and handbooks are available from NASA as Technical Support Packages (TSP's) when a Request Card number is cited; otherwise they are available from the National Technical Information Service.

Applications of Remote-Sensing Imagery

Aircraft and satellite imagery benefit land-development projects.

A compilation of reports discusses the usefulness of aircraft and satellite data for land-development projects. The type of imaging available and the means for analyzing it can answer some vital questions about future land development.

Remote-sensing images of the Earth are obtained using either conventional photographic cameras, scanners, or radars mounted on aircraft or satellites. The collected data are filed with different governmental agencies and are available to the general public.

The data can be analyzed using anything from sophisticated to simple equipment or with only the naked eye. For example, Landsat data may be analyzed with costly color-additive viewers and density slicers, but information sufficient for many applications can be found visually.

Landsat images are available as 70-mm and 9- by 9-in. (23- by 23-cm) positives and 9- by 9-in. and 30- by 30-in. (75- by 75-cm) prints produced in 1:500,000 or 1:250,000 scale. Three major signature categories can be determined with a naked eye: land use, biological, and geological/hydrological aspects.

The satellite images carry a lot of information about the extent of flood hazard areas, useful data for planning regional and urban developments. ERTS (Earth Resources Technology Satellites) images may be used to map the flood hazard areas. The cost of using these data for flood hazard mapping is just a few cents per kilometer of river that is being examined.

Program development and applications of remotely sensed data are also described by the Geological Survey of Alabama. This organization acquires remotely sensed data covering Alabama and has a substantial reference file about the land.

Remote-sensing imagery is also useful in estimating erosion and sedimentation rates in strip-mined areas. One lake is presented as an example of an accelerated erosion in a strip-mined area.

Lithologic mapping is also presented since it is an integral part of the proper land use. Although lithologic mapping involves regular fieldwork, it is significantly aided by aerial photographs.

The final section presents three methods how to determine the scale of a given view. The appendix includes maps of Alabama showing areas covered by various types of imagery and filed with the Geological Survey of Alabama.

This work was done by Travis H. Hughes of the University of Alabama for **Marshall Space Flight Center.** *To obtain a copy of the report, "Application of Remote Sensing for Planning Purposes," Circle 61 on the TSP Request Card.*
MFS-25107

Computer Programs

These programs may be obtained at very reasonable cost from COSMIC, a facility sponsored by NASA to make new programs available to the public. For information on program price, size, and availability, circle the reference letter on the COSMIC Request Card in this issue.

Equations of Motion for Coupled N-Body Systems

Complex systems modeled as a topological tree of idealized bodies

The dynamic characteristics of a complex system, such as a satellite or spacecraft, are best analyzed through a simulation model. The model must have the same dynamic characteristics as the complex system while lending itself to mathematical quantification. Idealized rigid bodies, point masses, and symmetric wheels are readily adapted to mathematical modeling; flexible bodies are more complex. However, if deformations are assumed to be small and if the laws of linear elasticity are applicable, their characteristics can be simulated by their natural modes and frequencies of vibration. A computer program, NBOD2, developed to help analyze spacecraft attitude dynamics, may be applied to a large class of problems involving coupled N-body systems. The program derives and solves numerically the equations of motion for any system that can be modeled as a topological tree of coupled rigid bodies, terminal flexible bodies, point masses, and symmetrical momentum wheels.

A topological-tree model of the dynamic system is used to derive vector-dyadic equations of motion for the system. To insure that the relative motion between contiguous bodies in the user-derived tree model is constrained kinematically, NBOD2 assumes that contiguous rigid and flexible bodies are connected by physically-realizable 0-, 1-, 2-, or 3-degrees-of-freedom gimbals. These gimbals prohibit relative translational motion while permitting up to 3 degrees of relative rotational freedom at hinge points.

Point masses may have 0, 1, 2, or 3 degrees of relative translational freedom, and symmetric momentum wheels have a single degree of rotational freedom relative to the body in which they are embedded. Flexible bodies must be at the end of limbs. They may possess several degrees of vibrational freedom in addition to the degrees of freedom associated with the connection gimbals. Data defining the elastic characteristics of the flexible bodies must be supplied by the user. These data can be obtained by using such programs as NASTRAN. A support program is provided for processing NASTRAN data into a format compatible with NBOD2. Program NBOD2 uses a Eulerian nested-body approach to derive the complete set of nonlinear equations of motion in a vector-dyadic format. These equations may be presented directly on a line printer for review, or they may be solved numerically; and a user-specified set of system state variables may be output.

This program is written in FORTRAN IV for batch execution and has been implemented on an IBM 360-series computer with a central memory requirement of approximately 270K of 8-bit bytes. NBOD2 was developed in 1978.

This program was written by Harold P. Frisch of **Goddard Space Flight Center.** *For further information, Circle D on the COSMIC Request Card.*
GSC-12407

Viscous Characteristics Analysis

Aid for supersonic-combustor development considers combustion and diffusion effects.

Investigations of the hydrogen-fueled supersonic combustion ramjet engine have delineated several technological problem areas. One area, the analysis of the injection, turbulent mixing, and combustion of hydrogen, requires accurate calculation of the supersonic combustion-flow fields. This calculation has proved difficult because of an interesting phenomenon: Temperature transitions in the flow field cause a change from supersonic to subsonic flow in the combustion field.

A first computer program was developed to use viscous characteristics theory to analyze supersonic combustion-flow fields with embedded subsonic regions (adjacent to boundaries). A second improved program was developed to consider both combustion and diffusive effects. It is intended to be used as a practical design tool for two-dimensional and axisymmetric supersonic-combustor development. (The first program is not presently available from COSMIC but is described in the documentation for LAR-12598, the second program.)

This second program has proved useful in the analysis of such problems as determining the flow field of a single underexpanded hydrogen jet, the internal flow of a gas-sampling probe, the effects of fuel-injector strut shape, and the effects of changes in combustor configuration. None of these problems have subsonic regions, and thus the subsonic capabilities of the program have not been tested rigorously.

Both combustion and diffusive effects can alter significantly the wave pattern in a supersonic field and can generate significant pressure gradients in the axial and radial directions. The induced pressure, in turn, substantially influences the ignition delay and reaction times as well as the velocity distribution. To analyze accurately the flow fields, the effects of finite-rate chemistry, mixing, and wave propagation must be linked to one another properly.

Viscous characteristics theory has been used in the past to describe flows that are pure supersonic; however, the interacting pressure effects in the combustor often cause the development of shock waves and embedded subsonic regions. Numerical investigation of subsonic regions (not adjacent to boundaries) awaits a new procedure that is valid within the subsonic region and can be coupled with the standard viscous characteristics procedure in the supersonic region.

Combustion and geometry shock waves, as well as expansion waves, are determined in the present program. The basic governing equations used are the viscous-inviscid equations, similar to those employed in higher-order boundary-layer analyses, with finite-rate chemistry terms included. In addition, the Rankine-Hugoniot and Prandtl-Meyer relations are used to compute shock and expansion conditions.

The program can handle up to 20 simultaneous shock waves. Chemistry terms are computed for a seven-species eight-mechanism hydrogen-and-air reaction scheme. Inputs consist of a physical description of the combustor and flow-determination parameters. Output includes detail flow-parameter values at selected points within the flow field.

This computer program is written in FORTRAN IV for batch execution and has been implemented on a CDC CYBER 175 with a central memory requirement of approximately 117K (octal) of 60-bit words. The program was developed in 1978.

This program was written by Renaldo V. Jenkins of **Langley Research Center.** *For further information, Circle E on the COSMIC Request Card.*
LAR-12598

Transonic Airfoil Design Code

Aid in design of shockless airfoils

Supercritical wing technology is expected to have a significant influence on the next generation of commercial aircraft. The use of supercritical wings could economize fuel consumption by reducing drag. An effective approach to the design of supercritical wings is through the development of shockless airfoils. In the past, the design of shockless airfoils was based on hodograph methods, which required extensive trial and error work. A recent computer program makes it possible to assign the velocity as a function of arc length and to obtain a shockless airfoil that nearly achieves the desired pressure distribution. It should enable engineers to design families of transonic airfoils for use on aircraft wings and could be useful for similar design problems, such as for turbine and compressor blades in cascade.

In gas dynamics, the partial differential equation for the velocity potential describing the isentropic flow of a compressible fluid can be derived from a variational principle. This principle asserts that the integral of the pressure over the flow field is stationary in its dependence on the velocity potential. Designing an airfoil for which the speed has been assigned as a function of arc length consists of solving a nonlinear boundary-value problem interrelating the map function and the stream function.

The solution is calculated iteratively between the map function and the stream function until a flow is determined that fits the prescribed pressure data. An exact solution cannot be expected to exist for transonic flows. However, a shockless flow is almost always obtained if there is one that closely approximates the given data.

The displacement thickness of the boundary layer is calculated from the inviscid pressure distribution by the momentum integral method of Nash and Macdonald. The displacement is subtracted from the airfoil coordinates, which are provided with a slightly-open trailing edge. The criterion of Stratford is used to impose a pressure distribution on the trailing edge of the upper surface that just avoids separation so that there is no loss of lift.

This program is written in FORTRAN IV for batch execution and has been implemented on a CDC-6000 series computer with a central memory requirement of approximately 135K (octal) of 60-bit words. This program was developed in 1977.

This program was written by Frances Bauer, Paul Garabedian, and David Korn of New York University for **Langley Research Center.** *For further information, Circle F on the COSMIC Request Card.*
LAR-12460

Improved Multielement Airfoil Analysis

Revised flow model produces results closer to experiment.

A great deal of attention has been given to the use of multielement airfoil designs, due to their high-lift capabilities. The flow around high-lift airfoils is characterized by many different inviscid and viscous flow regions. In particular, the existence of confluent boundary layers and regions of separated flow distinguishes the high-lift airfoil problem from the aerodynamic problem of standard airfoils at cruise speed.

To analyze high-lift airfoils effectively, it is necessary to compute accurately the various flow regions, including the outer potential flow, ordinary laminar and turbulent boundary layers, viscous wakes, and the confluent boundary layer. It is also necessary to predict the transition from laminar to turbulent boundary-layer flow and the onset of boundary-layer separation. The NASA/Lockheed Multielement Airfoil Analysis Program was one of the first attempts at numerically analyzing the complex viscous flow about slotted airfoils and has received worldwide usage. A recent evaluation of the Multielement Airfoil Computer Program has resulted in a major revision of the flow model. Comparisons between computed results and experimental data indicate that this version is more reliable than the older (1969) version.

The flow about a high-lift airfoil is computed assuming that the flow is attached to the airfoil surface and that the flow is two-dimensional and subcritical. The effect of the viscous flow is represented by a surface transpiration method, which uses an equivalent distribution of sources along the airfoil surface and the wake centerline to model the boundary layer and wake displacement effects. The flow model of the potential core utilizes the standard laminar and turbulent boundary-layer calculations with the addition of the lag-entrainment method of Green. The onset of separation of the confluent boundary layer is predicted by a modified version of Goradia's method with the power-law velocity profile replaced by Coles' two-parameter velocity profile. Drag prediction is based on the method of Squire and Young. The flow in the slot between adjacent airfoil components is calculated as an integral part of the overall flow computation. The airfoil to be analyzed may contain as many as 10 components with either negative or positive overlap.

(continued on next page)

This computer program is written in FORTRAN IV and Assembler for batch execution and can only be implemented on a CDC CYBER 175 with a central memory requirement of approximately 62K of 60-bit words. This version of the Multielement Airfoil Analysis Program was developed in 1978.

This program was written by G. W. Brune and J. W. Manke of The Boeing Co. for **Langley Research Center.** *For further information, Circle G on the COSMIC Request Card.*
LAR-12489

Aircraft Equilibrium Spin Characteristics

Solutions to equations of motion include spin characteristics.

Determination of the equilibrium spin characteristics of an aircraft is an essential part of the analysis step. The SPINEQ program was developed to provide analytic solutions to the nonlinear equations of motion for equilibrium spin conditions. These equations of motion require that the aircraft move along a helical trajectory with a constant angular velocity. Stability characteristics are also determined by linearization of the equations of motion about the equilibrium spin condition.

The solutions obtained by SPINEQ satisfy the requirement that a steady developed spin occurs if the equilibrium points are stable. Solutions having linear representations that are unstable either correspond to oscillatory spin conditions or are not actually developed spin conditions. The realism of the solutions is dependent on the accuracy of the aerodynamic data supplied to the program.

Inputs include aerodynamic coefficients, flight conditions, control settings, and solution control parameters. SPINEQ can be used to study the sensitivity of spin equilibrium conditions to variations in selected aerodynamic or inertial data. It can also be used in evaluating the adequacy of aerodynamic data in the spin region when accompanying experimental spin tests are available. Outputs include all values used in attaining convergence and the final state variables. With some alterations, SPINEQ could be employed to compute equilibrium conditions for steady maneuvers.

This program is written in FORTRAN IV for batch execution and has been implemented on a CDC CYBER 173 with a central memory requirement of approximately 10K (octal) of 60-bit words. SPINEQ was documented in 1978.

This program was written by William M. Adams, Jr., of **Langley Research Center.** *For further information, Circle H on the COSMIC Request Card.*
LAR-12502

Flow Field in Supersonic Mixed-Compression Inlets

Program uses 3-D method of characteristics.

The flow field in the supersonic portion of a mixed-compression aircraft inlet at nonzero angle of attack is calculated based on the method of characteristics for steady three-dimensional flow. The results of the computer program agree with those produced by the two-dimensional method of characteristics when axisymmetric flow fields are calculated. Except in regions of high viscous interaction and boundary-layer removal, the results agree well with experimental data obtained for three-dimensional flow fields.

The flow field in a variety of axisymmetric mixed-compression inlets can be calculated using the program. The bow shock wave and the internal shock-wave system are calculated using a discrete shock-wave fitting procedure. The internal flow field can be calculated either with or without the discrete fitting of the internal shock-wave system. The influence of molecular transport can be included in the calculation of the external flow about the forebody and in the calculation of the internal flow when internal shock waves are not discretely fitted.

The viscous and thermal diffusion effects are included by treating them as correction terms in the method of characteristics procedure. Dynamic viscosity is represented by Sutherland's law, and thermal conductivity is represented as a quadratic function of temperature. The thermodynamic model used is that of a thermally and calorically perfect gas.

The program assumes that the cowl lip is contained in a constant plane and that the centerbody contour and cowl contour are smooth and have continuous first partial derivatives. This program cannot calculate subsonic flow, the external flow field if the bow shock wave does not exist entirely around the forebody, or the internal flow field if the bow flow field is injected into the annulus. Input to the program consists of parameters to control execution, to define the geometry, and the vehicle orientation. Output consists of a list of parameters used, solution planes, and a description of the shock waves.

This program is written in FORTRAN IV for batch execution and has been implemented on a CDC 6000-series machine with a central memory requirement of 110K (octal) of 60-bit words when it is overlaid. This flow analysis program was developed in 1978.

This program was written by Allan R. Bishop of **Lewis Research Center** *and Joe D. Hoffman and Joseph Vadyak of Purdue University. For further information, Circle J on the COSMIC Request Card.*
LEW-13279

Shell Theory Automated for Rotational Structures

Numerical integration package for analysis of shells of revolution

Many structures, such as aircraft bodies, spacecraft, submarines, and storage tanks, can be analyzed efficiently by using shell theory. Several methods are currently available to solve the equations derived from shell theory. The program STARS (Shell Theory Automated for Rotational Structures) incorporates the method of numerical integration into a package of programs that use Love-Reissner first-order shell theory numerically to analyze shells of revolution.

The programs in the STARS package can perform static, buckling, vibration, and plastic analyses on thin shells of revolution subjected to distributed loads, concentrated line loads, and thermal strain. A wide range of shell-wall cross sections and combinations of geometric shapes can be effectively handled by these programs.

The structure under study is divided into numerous shell regions. Each region must be a singly connected shell. The regions are further subdivided into several shell segments, each being free to have its own geometric shape. Stiffness matrices obtained for each segment are coupled to determine regional stiffnesses. The regional stiffness matrices are reduced and coupled to form the stiffness matrix of the total structure.

In the linear analysis of unsymmetrically loaded shells, the partial differential equations of shell theory are reduced to first-order differential equations and are solved using a Runge-Kutta method of numerical integration. STARS may also be used for nonlinear analysis of axisymmetric loaded shells. These plastic, large deformation cases are analyzed by a special solution iteration scheme. The user supplies STARS with segment geometric data, segment orientation and coupling data, joint freedom data, and structural material data. Output from STARS includes stresses, displacements, plastic strains, and vibration and buckling results.

The STARS package is written in FORTRAN IV for batch execution and has been implemented on a UNIVAC 1108 with a central memory requirement of 53K of 36-bit words when segmented. The STARS package was developed in 1975.

This program was written by John Key of **Marshall Space Flight Center** *and V. Sval Gonas, H. Levine, and P. Ogilvie of Grumman Aerospace Corp. For further information, Circle K on the COSMIC Request Card.*
MFS-23027

Three-Dimensional Potential Flow

Geometry package for generation of input data

It is important that the aerodynamicist be able to study the effects of configuration changes on lift, load distributions, local pressures, and flow angles. A new computer program calculates viscous effects on the lifts and pressure distributions of arbitrary three-dimensional configurations. It combines a panel method that calculates potential flow about arbitrary three-dimensional lifting configurations with a two-dimensional boundary-layer method, which is used in a strip-theory sense. The program performs all the necessary calculations without user intervention once the configuration and flow regime are given. A geometry package for input data generation reduces the user-supplied configuration data required by an order of magnitude. Calculated inviscid and viscous lift and pressure distributions agree well with experimental data for a variety of wings and wing/fuselages having both conventional and supercritical airfoil sections.

The basic procedure for combining an inviscid-flow method and a boundary-layer method is independent of dimensionality and speed regime. The program couples a three-dimensional lifting potential-flow program and a simplified finite-difference program for calculating compressible laminar and turbulent boundary layers with a program that simulates the effect of the boundary layer on the flow. Alternate subroutines allow the boundary layer to influence the potential flow by a displacement of the surface coordinates or by a simulated surface blowing. The program computes an initial potential-flow solution; then it solves the two-dimensional boundary-layer equations along strips in the stream direction and generates a distribution of displacement thickness over the body surface. This displacement is used either to generate a new set of geometry coordinates or to calculate a simulated blowing velocity over the original body surface. The final potential-flow calculation is made with the chosen boundary-layer procedure producing the simulated viscous flow.

This program is written in FORTRAN IV for batch execution and has been implemented on a CDC CYBER 175 with a central memory requirement of approximately 250K (octal) of 60-bit words using the overlay capability. The potential flow program was developed in 1977 with updates and geometry package development occurring in 1978.

This program was written by N. Douglas Halsey and John L. Hess of McDonnell Douglas Corp. for **Langley Research Center.** *Further information on this technology may be found in NASA TM-80088 [N79-31142/NSP], "Comparison of Three-Dimensional Panel Methods with Strip Boundary-Layer Simulations to Experiment" [$5.25]. A copy may be purchased [prepayment required] from the National Technical Information Service, Springfield, Virginia 22161. For further information on the computer program, Circle L on the COSMIC Request Card.*
LAR-12623

Full-Coverage Film Cooling

Coolant flows and metal temperatures for blades and vanes

A computer program, called FCFC, has been developed to calculate coolant flow and wall temperatures of a full-coverage film-cooled vane or blade. Full-coverage film cooling is an effective way of protecting turbine components from the hostile environment of high gas temperature and pressure encountered in a gas-turbine engine. Full-coverage film cooling permits higher operating temperatures and pressures than conventional cooling, resulting in greater overall cycle efficiency.

FCFC combines previous experiments and analyses of full-coverage film cooling into an overall analytical procedure. Vane or blade metal temperatures are calculated for the blade-shell inner and outer surfaces.

(continued on next page)

These temperatures are average values for a shell outer-surface area associated with each film-cooling-hole row. Heat-transfer calculations are one-dimensional through the wall and neglect conduction from adjacent areas. A thermal barrier coating may be specified on the shell outer surface. When a coating is specified, the program also calculates the outer-surface temperature of the ceramic coating.

The program inputs consist of the blade or vane internal-chamber geometry (hole sizes and hole spacing); coolant supply temperature and pressure; and main-stream-gas heat-transfer coefficients and pressure, velocity, and temperature distributions. The physical properties of the coolant and the thermal conductivities of the metal and the ceramic coating are input as functions of temperature. The coolant-flow coefficients for the impingement and film-cooling holes are input as a function of mach number. Outputs summarize the geometric data; calculated coolant flows, pressure, and temperatures; and the calculated metal-coating temperatures.

FCFC is written in FORTRAN V for batch execution and has been implemented on a UNIVAC 1100-series computer with a central memory requirement of 22K of 36-bit words. This program development was completed in 1978.

This program was written by Peter L. Meitner of the U.S. Army Research & Technology Laboratories for **Lewis Research Center.** *For further information, Circle M on the COSMIC Request Card.*
LEW-13249

Disturbance Amplification Rates

Tapered laminar-flow control wings with suction

The computer program SALLY computes the incompressible linear stability characteristics and integrates the amplification rates of boundary-layer disturbances on swept and tapered wings. For some wing designs, boundary-layer disturbances can significantly alter the wing performance. This is particularly true for swept and tapered laminar-flow control wings, which incorporate suction to prevent boundary-layer separation.

The first step in calculating the disturbance amplification rates is to solve numerically the compressible laminar-boundary-layer equation with suction for the swept and tapered wing. A two-point finite-difference method solves the governing continuity, momentum, and energy equations. A similarity transformation is used to remove the wall normal velocity as a boundary condition and to place it into the governing equations as a parameter. Thus the awkard nonlinear boundary condition is avoided.

The resulting compressible boundary-layer calculations are used to compute the incompressible linear stability characteristics. The local disturbance growth is obtained from temporal stability theory and is converted into a local growth rate for integration. The local growth rates are integrated in the direction of the local group velocity, and the logarithmic disturbance-amplitude ratio is obtained as a function of chordwise distance. This disturbance-amplitude ratio is a measure of the growth of linear disturbances within the boundary layer and can serve as a guide in transition prediction.

This program is written in FORTRAN IV and Assembler for batch execution and has been implemented on a CDC CYBER 70-series computer with a central memory requirement of approximately 67K (octal) of 60-bit words. SALLY was developed in 1979.

This program was written by Andrew J. Srokowski of **Langley Research Center,** *Steven A. Orszag of Cambridge Hydrodynamics, Inc., and Tuncer Cebeci and Kalle Kaups of McDonnell Douglas Corp. For further information, Circle N on the COSMIC Request Card.*
LAR-12556

Machinery

Hardware, Techniques, and Processes

79 Precision Filament Cutter
80 Automatic Connector for Structural Beams
81 Mechanical End Joint for Structural Columns
82 Self-Energized Screw Coupling
82 Automatic Shutoff Valve
83 Vise Holds Specimens for Microscope
84 Tubing Cutter for Tight Spaces
85 Aluminum-Encased Lead Mallet
85 Clamshell Door System
86 Measuring Ball-Bearing Loads
87 Retaining a Sleeve on a Shaft
88 Compact Positioning Flange
88 Bolt-Tension Indicator
89 Dual-Mode Actuator
90 Zero-Torque Spanner Wrench
91 Drill-Motor Holding Fixture

Books and Reports

92 Self-Acting Shaft Seals

Precision Filament Cutter

Digital control lets an operator choose the fiber length and chopping rate.

Langley Research Center, Hampton, Virginia

The machine illustrated in the figure chops filaments of glass, graphite, plastic, or other material into fibers for use in composites and other applications. The fiber length and the chopping rate can be selected independently, and fiber length is accurate to within 0.2 millimeter of the length setting. A prototype has undergone successful operational tests and is in continuous use at Langley Research Center.

For a 10-millimeter fiber length, a single chop sequence requires 33 milliseconds. Longer fibers require an additional 0.8 millisecond per millimeter. Thus the maximum chopping rate for 10-millimeter fibers is 30 cuts per second; for 15-millimeter fibers it is 27 chops per second. The operator can select slower rates.

The machine contains a fixed blade, a double-edged moving blade actuated by opposed solenoids, a motor-driven precision indexing mechanism, and fixtures for guiding the filaments to the blades (see figure). Logic circuits control the indexing motor, the solenoids, and an air jet for dispersing the cut filaments.

An operator selects the fiber length and the chopping rate by adjusting controls on the front panel. The drive motor advances a length of multifilament tow according to the length setting. When the fiber is in position between the blades, the logic circuit actuates a solenoid, pulling the movable blade over the fixed blade and snipping off the filaments. The motor again advances a length of tow, and the circuitry actuates the opposite solenoid, pulling the other edge of the movable blade over the fixed blade. The sequence repeats automatically until the machine is turned off. After each cut, a blast of air blows the filament away so it can be collected.

Because the mass of the movable blade is small and the stroke is short, operation is fast, and wear and energy consumption are low. The push/pull motion of the blade speeds up operation by cutting on both forward and return movements.

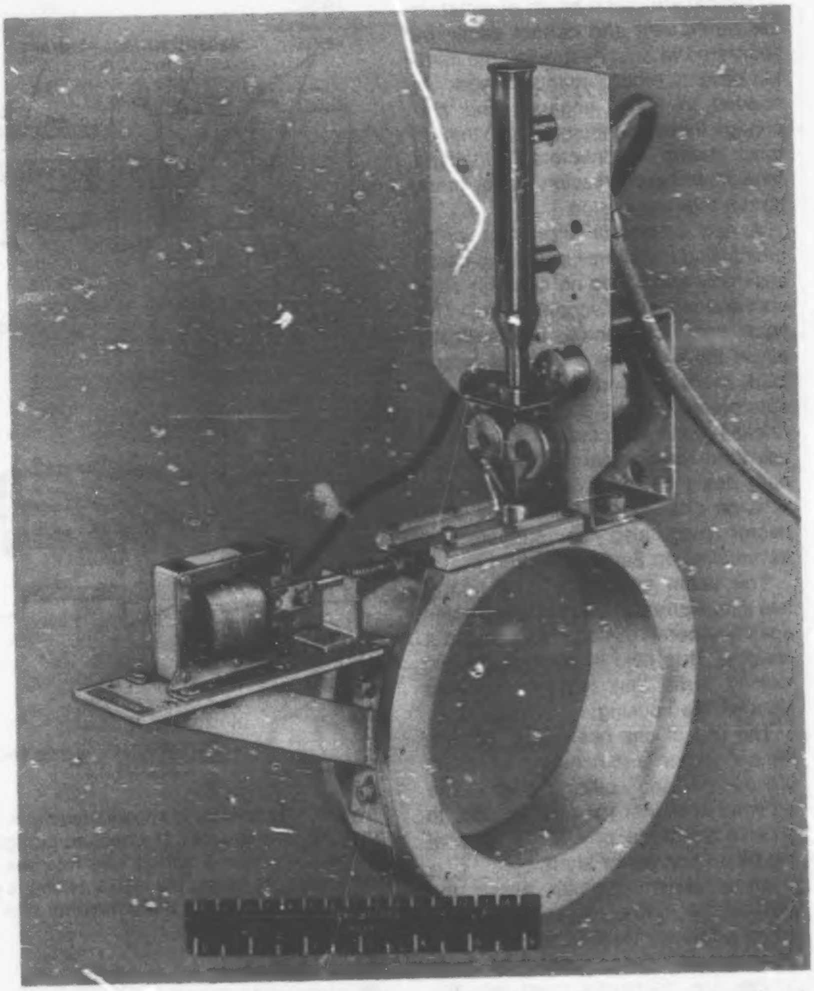

The **Push/Pull Blade** in this prototype filament cutter chops a length of multifilament tow as it is drawn back and forth over a fixed blade (not visible). The drive motor advances a precise length of tow each time the blade moves. Only one solenoid is used in this prototype; the final version will have two.

This work was done by Austin D. McHatton and Arthur L. Newcomb, Jr., of **Langley Research Center** *and Gregory Schluge of Bionetics Corp. For further information, Circle 62 on the TSP Request Card.*

This invention is owned by NASA, and a patent application has been filed. Inquiries concerning nonexclusive or exclusive license for its commercial development should be addressed to the Patent Counsel, Langley Research Center [see page A5]. Refer to LAR-12564.

Automatic Connector for Structural Beams

A novel beam connector allows quick alinement, connection, and disconnection.

Marshall Space Flight Center, Alabama

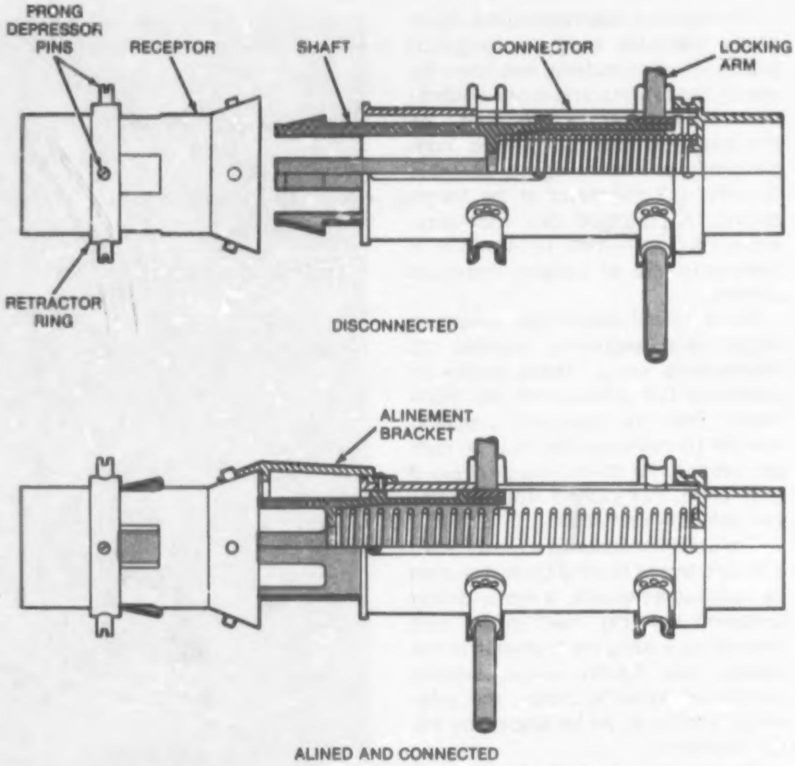

The **Beam Connector** is shown disconnected and connected. When the locking arms move out of their slots, the hooked prongs are pushed out of the connector housing by the compressed spring and into the receptor, where they lock into slots. To disconnect the beam, the retractor ring is pushed along the receptor slots to depress the connector prongs; the connector can then be retracted by the actuating levers.

Typical structural-beam connectors are permanent and cannot easily be separated without destroying the joint. Moreover, much manual work is needed to aline, engage, and disengage these connectors; and, though most beam connectors withstand tension and compression loads, many do not tolerate torsion.

A new connector allows for longitudinal and transverse structural-beam assembly and needs no tools for easy connection or disconnection. The lightweight connector automatically alines the beams and absorbs torque loads, tension, and compression. Its automated trigger engagement and release make the connector faster to use than many others. Though originally designed for in-space assembly of large orbiting structures, the connector may also be suitable for assemblies on Earth as well.

The beam connector (see figure) has a four-prong shaft that is retracted against a compression spring within a housing. It is held in position by two locking arms that rest in recessed slots on the housing.

The end of one beam is fitted with the connector; a matching receptor is placed on the other beam. The receptor is cylindrical and has slots to receive the three or more prongs of the beam connector shaft.

An alinement bracket alines the axes of the connector and receptor. When a release lever is actuated, the compressed spring expands and pushes the connector shaft into the receptor. The prongs, which have engagement hooks, snap and lock into the receptor slots to complete the connection. The lever can be remotely actuated, mechanically or electrically, for fully automated connection.

To disconnect the beam, a simple release, consisting of a sliding ring with a prong depressor, is used. The retractor ring is pushed along the slots of the receptor to depress the connector prongs. The connector can then be retracted by the actuating levers and secured, and the beams can be separated.

This work was done by Georg F. von Tiesenhausen of **Marshall Space Flight Center.** *For further information, Circle 63 on the TSP Request Card.*

Inquiries concerning rights for the commercial use of this invention should be addressed to the Patent Counsel, Marshall Space Flight Center [see page A5]. Refer to MFS-25134.

Mechanical End Joint for Structural Columns

Lightweight, side-entry system assembles without tools.

Langley Research Center, Hampton, Virginia

A column-end joint system that connects tubular struts in various lightweight skeletal-framework structures consists of two main components (see figure):

1. A node fitting with attached mechanical-joint halves at locations required by individual structures; and
2. Strut elements with machined joint halves attached to ends, with length adjustments made.

To produce a structurally sound joint from the two components, the two parts are alined approximately and pushed together. As the integral semicircular tongues enter their mating grooves, their tapered form compensates for small longitudinal misalinement. The radial alinement pins engage stops on the mating joint half to compensate for small radial misalinement. During this assembly sequence, the locking latches contact and subsequently ride the crests of the semicircular tongues until the tongues mate with their corresponding grooves. At that time the pawls on the locking latches engage their corresponding latch-engagement steps.

A small transverse force is required to effect this joint due to the wedge action of the engaging faces. Normal finger pressure is adequate. The node fitting, along with its joint-node elements, could be produced as a single piece; material could be cast or molded metal or filament-reinforced or thermoformed plastic.

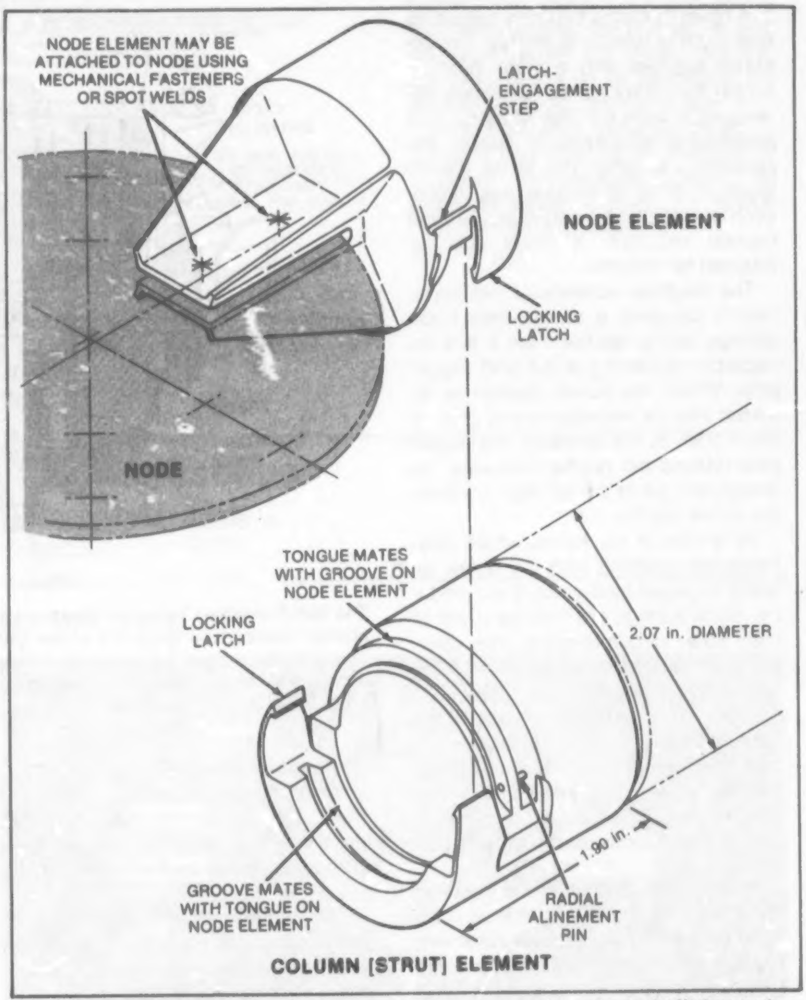
NODE ELEMENT MAY BE ATTACHED TO NODE USING MECHANICAL FASTENERS OR SPOT WELDS
LATCH-ENGAGEMENT STEP
NODE ELEMENT
LOCKING LATCH
NODE
TONGUE MATES WITH GROOVE ON NODE ELEMENT
LOCKING LATCH
2.07 in. DIAMETER
1.90 in.
GROOVE MATES WITH TONGUE ON NODE ELEMENT
RADIAL ALINEMENT PIN
COLUMN [STRUT] ELEMENT

Mechanical End-Joint System for structural columns consists of a node fitting and a strut element. The node and node-element shown are typical; they may be varied to meet specific requirements.

Previous methods of making such structural connections have utilized mechanical fasteners, threaded fittings, or welding operations. When assembly is in situ, such procedures are time consuming and costly, and the resulting joints are normally heavy. Some prior joint systems do not permit struts to be inserted or removed between fixed nodes without taking the nodal joint apart.

The new arrangement circumvents this restriction and permits the construction of skeletal frameworks without the use of tools or assembly equipment. Node fittings can be custom designed easily for various degrees of column fixity without affecting operative joint fixtures, and the design accommodates reasonable axial and rotational misalinement of nodes and struts. Individual columns can be inserted and removed between fixed nodes without affecting the integrity of the remaining structure, and all operative joint components are interchangeable. In addition, this joint system is lightweight and mass producible, and it contains no moving parts.

This work was done by Harold G. Bush of **Langley Research Center** *and Richard E. Wallsom of Vought Corp. For further information, Circle 64 on the TSP Request Card.*

Inquiries concerning rights for the commercial use of this invention should be addressed to the Patent Counsel, Langley Research Center [see page A5]. Refer to LAR-12482.

Self-Energized Screw Coupling

A spring-loaded threaded fastener is actuated by just a push.

Marshall Space Flight Center, Alabama

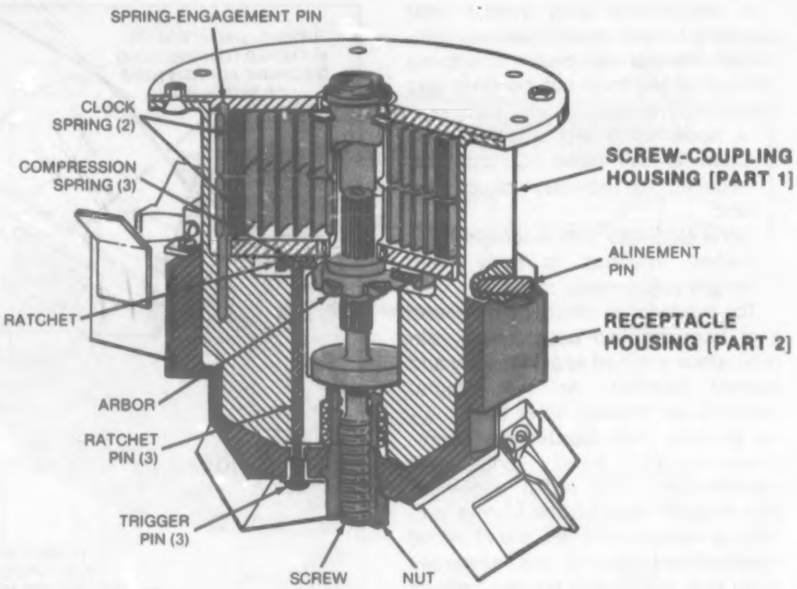

The Self-Energized Threaded Coupling has two clock springs that carry the rotational energy needed to engage the screw and nut. The adapter is disengaged by manually resetting the screw. A square-nosed speed wrench is inserted in one of two holes on opposite sides of the coupling, and the screw is turned until the ratchet reengages the arbor. At that point the coupling can be demated.

A novel threaded coupling carries its own store of rotational energy. The operator supplies only a small push to trigger the rotary motion. Originally developed to ease the task of astronauts assembling structures in space, the coupling can offer the same advantages in other hazardous operations, such as underwater and in and around nuclear reactors. It could also be adapted for robotics.

The coupling consists of two parts: Part 1 contains a screw, two clock springs, and a ratchet. Part 2 is a receptacle containing a nut and trigger pins. When the screw portion is inserted into the receptacle and given a slight push by the operator, the trigger pins release the ratchet, allowing the energy stored in the springs to rotate the screw into the nut.

As shown in the figure, which illustrates the coupling with the screw already engaged by the nut, the cylindrical clock springs are held by a pin at their outer circumference. The other ends of the springs power a rotating arbor that it attached to the screw.

Three compression springs load the ratchet so that it bears against the arbor, preventing the arbor from turning. The ratchet also has three sliding pins that extend through the body of the coupling and protrude through its bottom surface.

As the screw portion of the coupling is inserted into the receptacle, it is rotated by the operator until an alinement pin falls into a slot. This alines the three trigger pins so that they bear against the sliding pins. A slight force causes the trigger pins to depress the sliding pins, disengaging the ratchet from the arbor. This allows the arbor to rotate, and the energy stored in the springs is expended in rotating the screw into the nut.

The rotation stops when the midflange of the screw bears against the seating surface in the coupling. The energy remaining in the springs assures positive locking.

This work was done by Alan E. LeFever and Raymond S. Totah of Rockwell International Corp. for **Marshall Space Flight Center.** *No further documentation is available.*

Inquiries concerning rights for the commercial use of this invention should be addressed to the Patent Counsel, Marshall Space Flight Center [see page A5]. Refer to MFS-25340.

Automatic Shutoff Valve

A cellulose-sponge-activated valve bars water from the vent line.

Lyndon B. Johnson Space Center, Houston, Texas

A relatively-simple shutoff valve proposed for the Space Shuttle wastewater-tank vents is activated by a cellulose-sponge disk. The sponge absorbs incoming water and expands with enough force to shut the valve. This direct mechanical action is expected to be more reliable than an electrically-activated solenoid valve.

Preshaped sponge disks are prepared by first wetting and compressing them to about one-eleventh of the

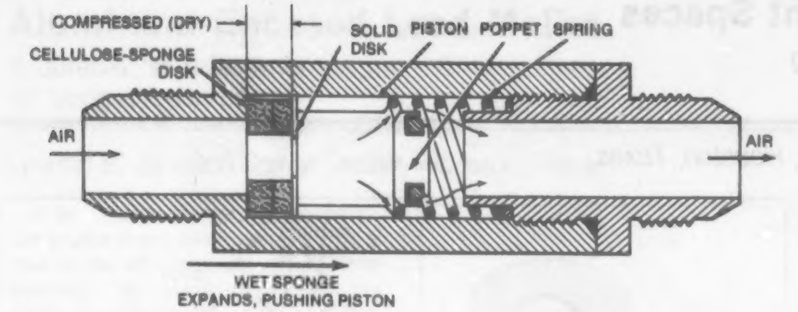

Cellulose-Sponge-Activated Valve prevents water from entering the air vent system. The sponge disk absorbs moisture and expands, driving a spring-loaded piston against a plunger and shutting off the valve. When the water recedes, the piston squeezes the sponge back to its original shape and opens the valve.

original dry thickness [e.g., 1-3/8 in. to 1/8 in. (3.5 cm to 0.3 cm)] for vacuum drying to a "permanent" thickness. Samples of wet finished disks are reported to expand from 1/8 in. (0.3 cm) to 3/4 in. (1.9 cm), developing 5 lb/in.^{2} (34.5x10^3 N/m^2) pressure — sufficient to close the valve.

The dry disk (see figure) is inserted into the valve cavity and is backed up by a solid disk that drives a spring-loaded piston. When the sponge is dry, spring force keeps the piston open, allowing air to escape through the vent. When water enters the system, the sponge expands, overcoming the spring force and driving the piston against the plunger to shut the valve. When the water recedes, the valve opens up by squeezing the sponge dry to its original shape.

This work was done by Scott F. Hawkins and Charles W. Overbey of Rockwell International Corp. for **Johnson Space Center.** *No further documentation is available.*
MSC-19385

Vise Holds Specimens for Microscope

A convenient, miniature, spring-loaded mechanism holds specimens for scanning electron microscope.

Lyndon B. Johnson Space Center, Houston, Texas

A simple vise (see figure) made from three components holds specimens for display in a scanning electron microscope. The specimen is secured with a jawlike structure without being cemented and can be easily reused after the analysis.

The vise consists of a studded aluminum angle and a threaded mating nesting angle. The specimen is simply inserted between the two, and a spring-loaded screw is tightened into the nesting angle until the spring becomes tight enough to depress the aluminum angle against the specimen. When the specimen is secured, the vise is inserted into the microscope mount. The stud at the bottom fits the standard mounts.

The vise eliminates a more involved method of using conductive adhesives to secure the samples. Samples cemented to flat studs with silver paint are more difficult to remove.

This work was done by Walter N. Greule of Rockwell International Corp. for **Johnson Space Center.** *No further documentation is available.*
MSC-18690

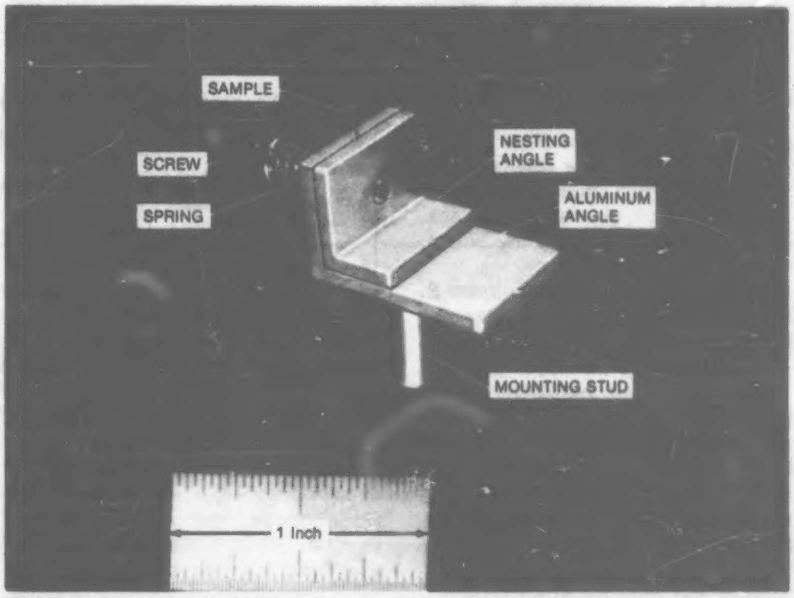

Miniature Spring-Loaded Vise holds specimens for scanning electron microscope analysis. A wire specimen shown is held in a jawlike structure formed by two mating angles. A spring-loaded screw driven into the nesting angle tightens the grip.

best copy available

best copy available

Tubing Cutter for Tight Spaces

Two-ratchet handtool cuts tubing in confined installations.

Lyndon B. Johnson Space Center, Houston, Texas

A new tubing cutter requires only a few short swings of its handle to rotate its cutting edge a full 360° around a tube. It is therefore useful for cutting tubing that has been installed in a confined space that would prevent the free movement of a conventional cutter.

The essential parts of the new cutter are seen in the figure. The cutting blade is mounted on a slider block that travels on a screw ratchet. A spring-loaded roller clamps the cutter on the tube until the blade is advanced to make the first cut. The blade, slider block, and clamping roller form a unit that is mounted on a ratchet in the main body of the cutter.

To use the cutter, the operator snaps it onto the tube, where it is held in place by the spring-loaded roller. Then the screw ratchet is rotated to advance the cutting wheel until it contacts the tube. After each full rotation of the body, the screw ratchet is turned so that the cutting blade penetrates deeper into the tube for the next cut.

A powered version of the tubing cutter would add a motorized drive to the basic unit shown. The motor could be made part of the cutter, or a fitting could be added to take power from a conventional drill motor. An automated advance of the slider block, synchronized with the cutting action, could also be designed.

This work was done by Anthony S. Girala of **Johnson Space Center.** *For further information, Circle 65 on the TSP Request Card.*

This invention is owned by NASA, and a patent application has been filed. Inquiries concerning nonexclusive or exclusive license for its commercial development should be addressed to the Patent Counsel, Johnson Space Center [see page A5]. Refer to MSC-18538.

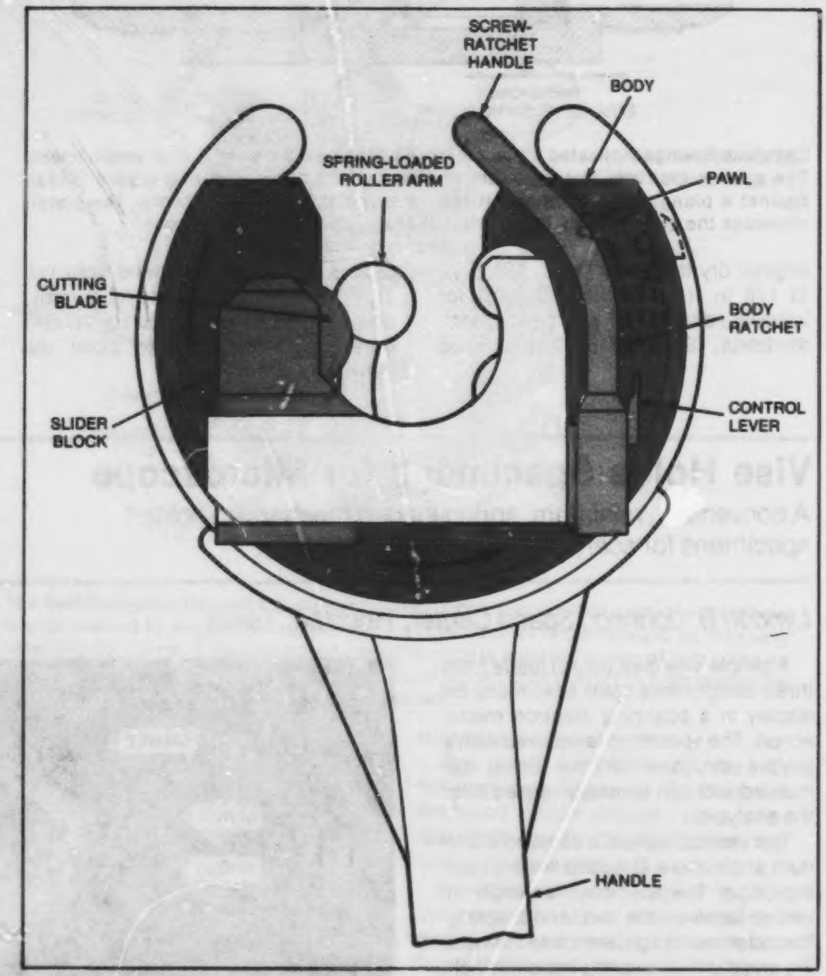

This Tubing Cutter is held on a tube by the spring-loaded clamp. The cutting wheel is advanced until it contacts the tube by moving the screw-ratchet handle. An existing model cuts titanium, iron/nickel alloys, or plastic tubing, 1/2 to 1 in. (1.2 to 2.5 cm) in diameter. It can be redesigned for other tubing materials and sizes.

Aluminum-Encased Lead Mallet

A durable, safe hammer for general shop use

Lyndon B. Johnson Space Center, Houston, Texas

A lead mallet for general shop use has an aluminum casing surrounding a lead core to retain its shape and balance. The aluminum casing reduces the amount and rate at which lead expands at the striking surface, greatly increasing the mallet service life. The casing also improves safety by eliminating major changes in balance and reducing the flaking of lead particles.

The mallet head, as shown, can be fabricated from aluminum tube. The handle can be made from heavy-wall pipe and either welded or flared to the head at the top end. The handle is also welded to the inside of the head shell at the handle end. If the handle is flared, a steel pin is installed perpendicular to the handle, inside the head shell; and the lead is cast around it. The pin prevents rotation of the handle. By melting out and recasting the head, shops can easily refurbish the mallets when the head is worn out.

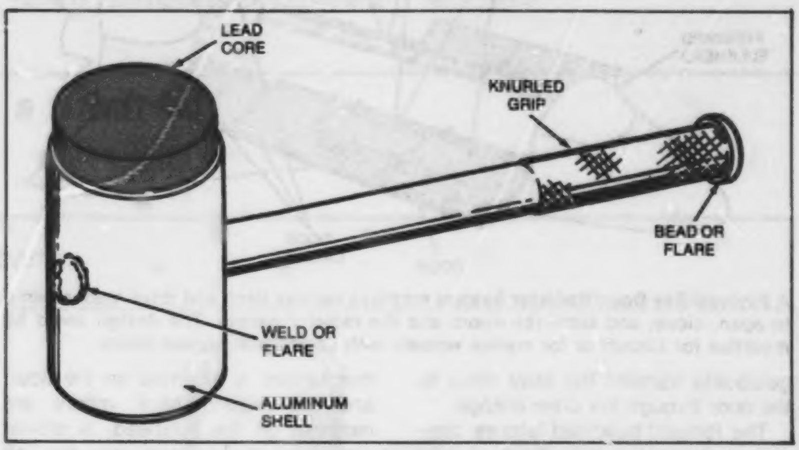

The Lead Core of the mallet is encased in aluminum. The knurled handle can be either welded or flared to the head at the top end. The handle is also welded to the inside of the head shell at the handle end.

Nonferrous soft hammers (plastic, lead, and aluminum) are widely used throughout industry to strike a workpiece without distorting it. Thus, the aluminum-encased lead mallet should find wide use.

This work was done by Floyd Chin and Ira F. Pardue of Rockwell International Corp. for **Johnson Space Center.** *No further documentation is available.*
MSC-18529

Clamshell Door System

Mechanisms that open, close, and latch large clamshell doors

Lyndon B. Johnson Space Center, Houston, Texas

A new system designed for the Space Shuttle orbiter consists of mechanisms that open, close, and latch the payload-bay doors and radiator panels under various gravity and temperature environments. It incorporates a remotely-controlled "zipper latch" operated by a mechanical sequence that accommodates thermal and structural deflections and misalinements in the doors. The entire system could be modified for commercial jetliners and marine vessels with underwater access doors.

The doors as shown in the illustration are opened, closed, and latched sequentially by electromechanical actuators controlled either manually from the onboard control panel or automatically from the onboard computer. There are four basic subelements: the door drive actuator, the forward bulkhead latches, the aft bulkhead latches, and the centerline latches.

Enclosed by the doors are radiator panels that are deployed to a predetermined position once the doors are opened. Basically these are two-sided radiative surfaces that dissipate accumulated heat from the orbiter systems. They are opened, closed, and latched by electromechanical actuators operated manually from the onboard control panel. The radiator mechanisms comprise two basic subelements: the radiator drive actuator and the radiator latches.

Two actuator systems, one on each side of the orbiter, open the doors. Each operates a "half door" at six points along the hinge line. Six

(continued on next page)

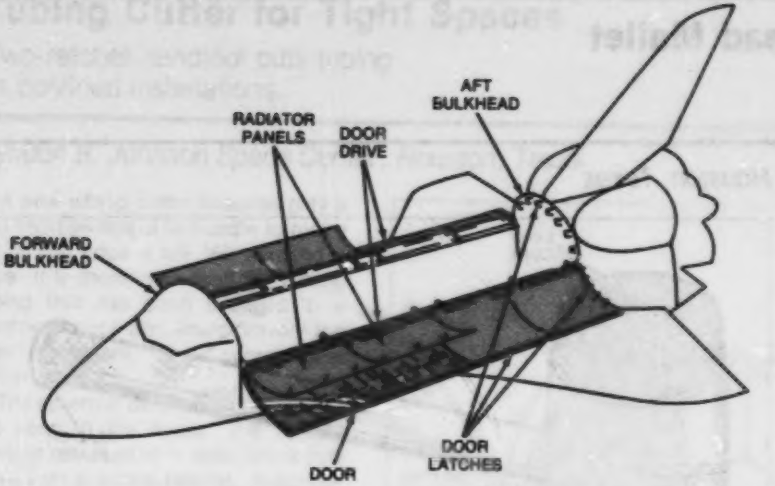

A Payload-Bay Door/Radiator System employs various latch and drive mechanisms to open, close, and latch the doors and the radiator panels. The design could be modified for aircraft or for marine vessels with underwater access doors.

gearboxes transmit the drive force to the door through the drive linkage.

The forward bulkhead latches consist of right-hand (four latches) and left-hand (four latches) gangs. The mechanism is mounted on the door, and the mating hook rollers are mounted on the bulkhead. A similar arrangement is used on the aft bulkhead latches.

The upper centerline latches connect the right- and left-hand doors along the upper centerline. There are four gangs of these (four latches each). The active latches are on the right-hand door, and the mating rollers are on the left-hand door.

The actuator system for the radiator mechanism drives the radiator panels to a position 35.5° away from the bay door. The drive system is similar to that of the bay door. Each radiator incorporates 12 latches in two groups of 6. Each group is driven by a single electromechanical unit.

The opening, closing, and latching follow specific sequences, and the status of each is monitored on a CRT in the cockpit. The ganged latches are mechanically sequenced in a "zippering effect," which helps to overcome thermal and mechanical distortion.

This work was done by Dean R. Helbie of Rockwell International Corp. for **Johnson Space Center.** *For further information, Circle 66 on the TSP Request Card.*
MSC-18468

Measuring Ball-Bearing Loads

A tool that measures the contour of the wear path aids in bearing design.

Marshall Space Flight Center, Alabama

The dynamic load on a ball bearing is difficult to predict accurately. It can sometimes be measured while the bearing is in service; however, for low- or high-temperature bearings and bearings in confined spaces, such measurements are difficult at best.

A simple diagnostic for characterizing the bearing load has been to remove the bearing race and measure the width of the wear path. Very often the width can be related to the load magnitude and direction, and load imbalances can be identified.

Recent experience with ball bearings on turbopumps for NASA's Space Shuttle shows that the contour of the wear-path boundary contains even more precise information about the load than does the width. A simple tool that measures the boundary has been used successfully for bearing-load estimates and bearing design. Shown in the figure, the tool measures the height

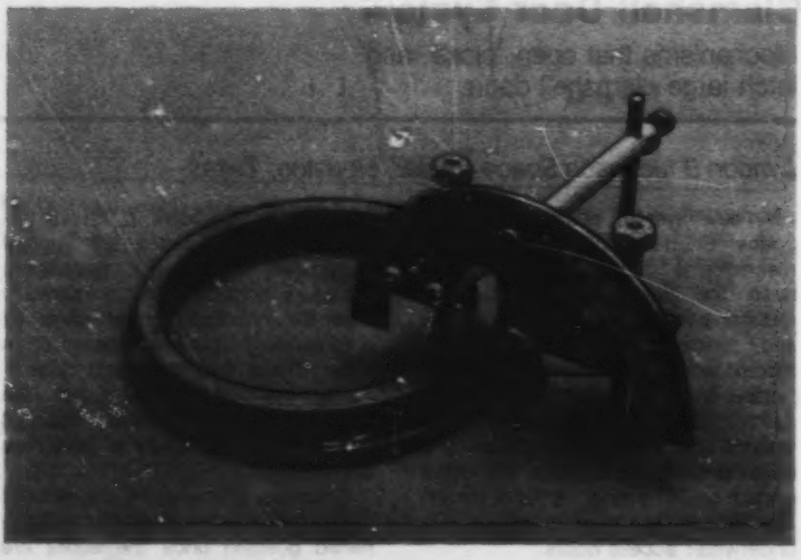

The Ball-Bearing Load Path Boundary is measured as an angular deflection of the pointer as the bearing race is rotated.

of the path perimeter as the horizontal bearing race is rotated manually. The height is read as an angle measurement. A set of interchangeable disks allows the pivot of the pointer to be located at the center of the raceway curvature. Leveling screws are adjusted to position the disk perimeter in the raceway. The tool can be used on the inner or outer race to measure both the upper and lower edges of the wear path.

Among bearing-load parameters that can be determined by interpreting the angle measurements are: whether the load is purely radial, purely axial, or a combination; whether it is stationary radial or rotating radial; and whether a rotating radial load is synchronous or asynchronous with the fundamental rotation frequency of the bearing.

This work was done by M. F. Butner of Rockwell International Corp. for **Marshall Space Flight Center.** *For further information, Circle 67 on the TSP Request Card.*
MFS-19505

Retaining a Sleeve on a Shaft

A fastener secures the sleeve to the shaft.

Marshall Space Flight Center, Alabama

The method used for holding the heat-shield retainer in place on the main injector of the Space Shuttle main engine may easily be adapted to many sleeve-on-shaft applications. A fastener was designed to keep a metal sleeve from slipping axially on a moving shaft.

The design (see figure) includes a slotted snapring fastener, a machined groove on the shaft, and a closely fitting sleeve. Before the sleeve is installed, the fastener is expanded and slipped over the shaft until it engages a groove. After the sleeve is slid into position, the fastener tabs are bent to lock it into position. To remove the sleeve, the procedure is reversed.

This work was done by Richard Pessin of Rockwell International Corp. for **Marshall Space Flight Center.** *No further documentation is available.*

Inquiries concerning rights for the commercial use of this invention should be addressed to the Patent Counsel, Marshall Space Flight Center [see page A5]. Refer to MFS-19518.

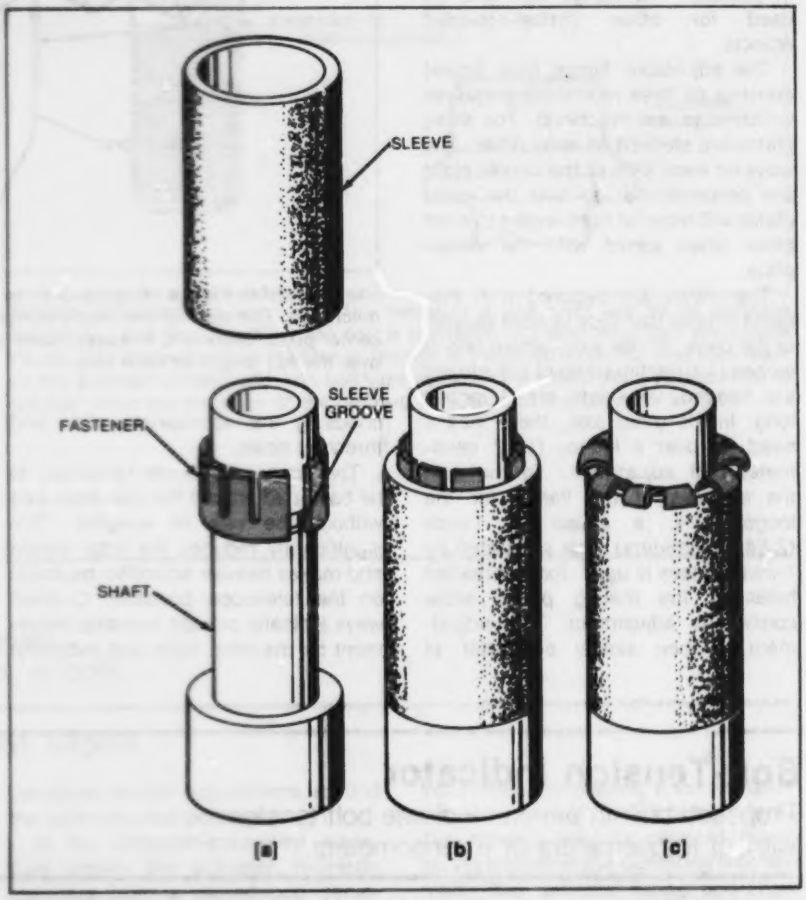

Slotted Snapring Fastener is held in place by the shaft groove (a). When the sleeve is positioned on the shaft (b), the fastener tabs are bent (c), locking the sleeve in place and preventing it from slipping along the shaft axis.

Compact Positioning Flange

A flange originally developed for a balloon-borne telescope allows easy repositioning of the center of gravity of gimbal-mounted objects.

Lyndon B. Johnson Space Center, Houston, Texas

A compact adjustable flange simplifies repositioning of the center of gravity of a balloon-borne telescope. Prior to development of the flange, counterbalancing was required because the center of gravity of the telescope was not along the elevation axis. Furthermore, since the elevation gimbal is inside the azimuth gimbal on this telescope, any mass added in elevation required additional weights in azimuth. The flange can also be used for other gimbal-mounted objects.

The adjustable flange (see figure) consists of three aluminum plates on which ways are machined. The three plates are stacked on each other. The ways on each side of the center plate are perpendicular so that the outer plates will move at right angles to each other when joined with the center plate.

The plates are secured with machine screws that slide in slots parallel to the ways. In one axis, where only 3 inches (7.6 centimeters) of adjustment are needed, the slots are 3 inches long. In the other axis, there was a need for over 6 inches (15.2 centimeters) of adjustment. To maintain the stiffness of the flange for the longer axis, a series of 1-inch (2.54-centimeters) slots separated by 1-inch bridges is used. Extra threaded holes in the mating plates allow continuous adjustment. The adjustment is then simply a matter of choosing the appropriate slots and threaded holes.

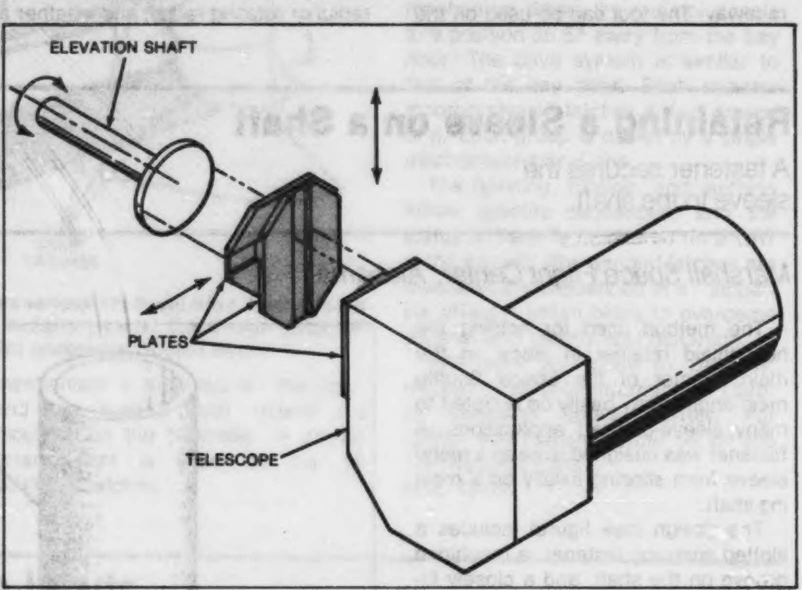

The **Adjustable Flange** consists of three aluminum plates on which ways have been machined. The outer plates move at right angles to each other when joined to the center plate. Slots and threaded holes (not shown) in the plates allow adjustment over the full length of each axis.

The flange allows the telescope to be balanced around the elevation axis without the use of weights. This significantly reduces the total weight and makes heavier scientific payloads on the telescope possible. Crossed ways typically provide two-axis movement on machine tools and industrial equipment. In this application, the overall thickness of the ways has been reduced significantly to minimize shifting of the centerline of the telescope along the elevation axis.

This work was done by Sonne L. Hooper of Kentron Hawaii, Ltd., for ***Johnson Space Center.*** *No further documentation is available.*
MSC-14876

Bolt-Tension Indicator

Proposed built-in pin can indicate bolt tension without torquemeters or extensometers.

Marshall Space Flight Center, Alabama

A proposed bolt has a built-in pin that indicates bolt tension. As the bolt is tightened, the pin is pulled into the bolt by the stretching bolt shaft. The amount of the pin remaining above the top of the bolt would correspond to the tension on the bolt. This pin-indicator bolt would be a more-accurate tension indicator than a torquemeter and would be less expensive than using an electronic extensometer.

The pin (see illustration) would be retained in the bolt by interference fit at the bottom of a hole step-drilled inside the bolt shaft. The length of the pin would be chosen according to the bolt design limits. The pinhead would be marked by two steps, corresponding to minimum and maximum acceptable tensions. As the bolt is tightened and the pin pulled in, the first step on the pinhead would become flush with the bolthead to indicate a minimum tension limit. Further tightening to the maximum allowable design limit will pull the top of the pin flush with the bolthead.

The counterbore inside the bolthead would be filled by elastic material to dampen pin vibration and prevent contamination. Initially, finished bolts could be "coarse" tightened with a torque wrench. A fine adjustment would follow by further tightening and observing the position of the pin ends relative to the bolt faces. These can be checked using a flat gage block to feel the steps extending above the bolt surface. When, as is often the case, the tension is set somewhere between the minimum and maximum limits, any part of the pin extending above the bolt can be filed off.

The proposed method would be particularly convenient for assembly in field locations without electronic and other specialized instruments. The installed bolts can be rapidly rechecked for any loss in tension by simply going over them with the flat gage block. [Also see "Eddy-Current Sensor Measures Bolt Loading" (MFS-19486) on page 68.]

This work was done by Kenneth L. Wilson of Rockwell International Corp. for **Marshall Space Flight Center.** *No further documentation is available. MFS-19324*

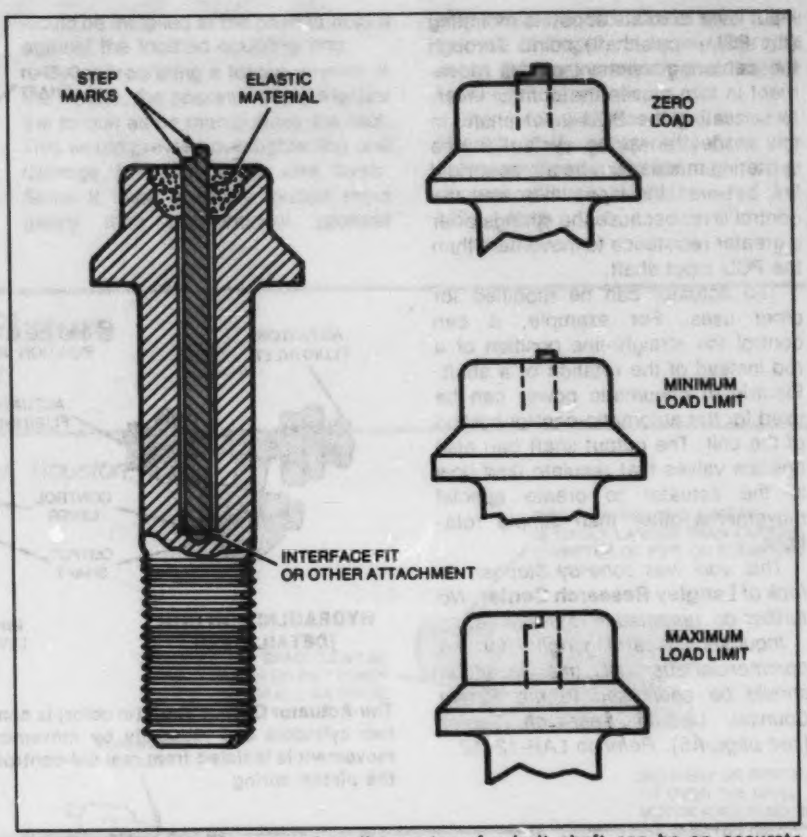

Tension-Indicating Pin secured to the center of a bolt shaft can be an accurate indicator of bolt tension. When the bolt is tightened, the stretching bolt shaft pulls the pin into the center hole. Minimum tension is indicated when the first step mark on the pinhead is flush with the bolthead surface. Maximum allowable tension is reached when the top edge of the pinhead is flush with the bolthead surface.

Dual-Mode Actuator

Compact mechanism functions under automatic control, manual control, or both.

Langley Research Center, Hampton, Virginia

The compact actuator shown in the figure accepts inputs from a person, a computer, or both in combination. It was developed as a retrofit to be attached to the spoiler position control unit (PCU) of existing aircraft where it is controlled by the pilot or by a computerized flight-control system. In the dual mode, the pilot can place the spoiler at an initial setting while the computer makes adjustments around the pilot-selected position.

In the computer-controlled mode, fluid enters the actuator hydraulic cylinders from a closed-loop servosystem. The computer controls the direction and amount of actuator movement and monitors its position. The hydraulic cylinder moves the control lever, thus rotating the PCU input lever and causing a corresponding movement of the aircraft spoilers. The control lever is resisted by a spring system in the centering mechanism, that deflects during operation and returns the mechanism to the zero position when hydraulic power is removed.

In the manual mode, movement of a control system by the pilot causes the

(continued on next page)

input lever to rotate about its mounting (the PCU input shaft) point. Through the centering mechanism this movement in turn moves the control lever, thus rotating the PCU input shaft. In this mode the spring system in the centering mechanism becomes a rigid link between the input lever and the control lever because the springs offer a greater resistance to movement than the PCU input shaft.

The actuator can be modified for other uses. For example, it can control the straight-line position of a rod instead of the rotation of a shaft. Electric or pneumatic power can be used for the automatic-control portion of the unit. The output shaft can also operate valves that regulate fluid flow in the actuator to create special movements other than simple rotations.

This work was done by Stephen C. Irick of **Langley Research Center.** *No further documentation is available.*

Inquiries concerning rights for the commercial use of this invention should be addressed to the Patent Counsel, Langley Research Center [see page A5]. Refer to LAR-12412.

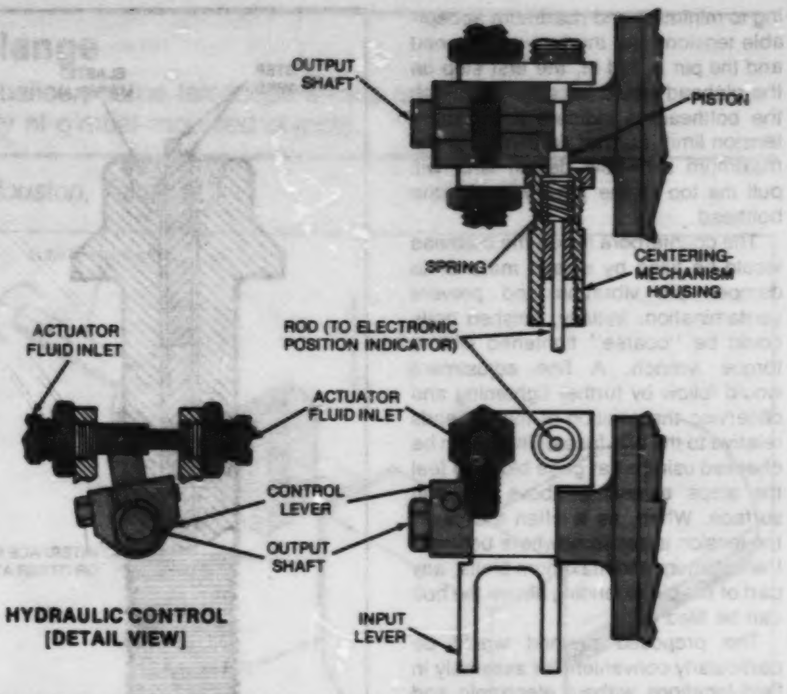
OUTPUT SHAFT
PISTON
SPRING
CENTERING-MECHANISM HOUSING
ROD (TO ELECTRONIC POSITION INDICATOR)
ACTUATOR FLUID INLET
ACTUATOR FLUID INLET
CONTROL LEVER
OUTPUT SHAFT
INPUT LEVER
HYDRAULIC CONTROL [DETAIL VIEW]

The **Actuator Output Shaft** (in color) is controlled automatically by hydraulic fluid in two cylinders and manually by movement of the input lever. Automatic-control movement is isolated from manual-control movement by adjustment of the force on the piston spring.

Zero-Torque Spanner Wrench

With this proposed tool, a coupling is rotated by simply tightening a grip.

Lyndon B. Johnson Space Center, Houston, Texas

A proposed spanner wrench converts the gripping action of a hand to rotary motion. It does so without imparting reactive moments or forces on the part being turned or on the operator.

The tool was originally proposed for use by astronauts in the weightless environment of outer space. Conventional spanner wrenches are difficult to manipulate in zero gravity because they generate moments and forces that rotate and push the astronaut's body. Because it eliminates this problem, the new wrench should also be useful in undersea operations and in other delicate work where reactive forces and torques have to be controlled.

In a design for valve tightening (see figure), the tool resembles a cross between a conventional spanner

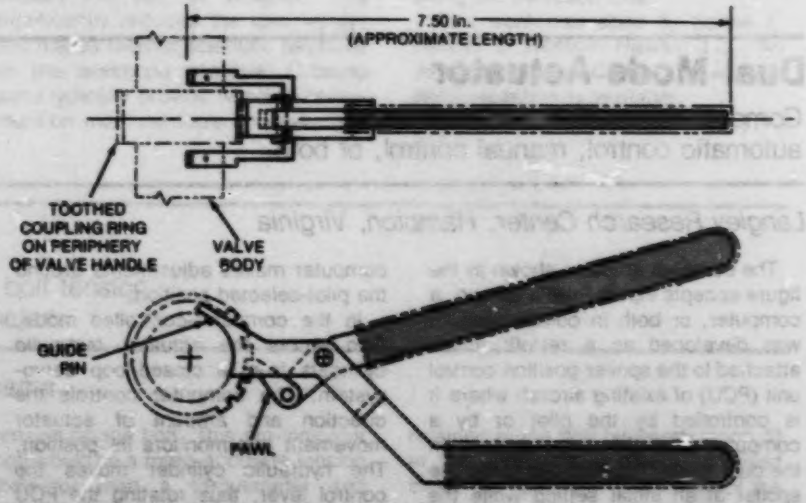
7.50 in.
(APPROXIMATE LENGTH)
TOOTHED COUPLING RING ON PERIPHERY OF VALVE HANDLE
VALVE BODY
GUIDE PIN
PAWL

No Unbalanced Moments or Forces are created when rotating the valve handle with this proposed spanner wrench. It thus prevents damage to lightweight shafts, which can be bent or broken when turned with a conventional spanner wrench.

wrench and a pliers. Through locating and holding pins, one handle of the tool engages the valve body. The second handle has a ratchet pawl that engages a toothed coupling ring on the periphery of the valve handle.

Two springs would be used in the tool. One would open the handle grips when they are released, and the other would be installed at the pawl to hold it against the toothed coupling ring.

By incorporating a torque wrench in the handle, the operator could monitor the torque as he manipulates the tool. This would prevent overtightening and damage to valve seats and seals. Since it imparts rotary motion more gently than conventional spanner wrenches, the tool would also allow the use of larger rotary handles and shafts than are presently practical for lightweight assemblies.

This work was done by Morley V. Friedell of Martin Marietta Corp. for **Johnson Space Center.** *No further documentation is available.*
MSC-14843

Drill-Motor Holding Fixture

Fixture prevents bit breakage and helps improve drilling accuracy.

Lyndon B. Johnson Space Center, Houston, Texas

A simple fixture prevents bit breakage and improves accuracy when drilling items that are too large or too awkward to be clamped in a drill press. As shown in the figure, a drill motor is mounted on a furniture clamp fitted with a 3/4-in. (1.9-cm) pipe. The pipe length and diameter are chosen to suit the size of the item being drilled.

The motor mount includes a short length of pipe that slides along the pipe on the furniture clamp. Hose clamps are used to attach the motor to the fixture.

As the hole is being drilled, the operator turns the handle on the furniture clamp. This slides the short length of pipe on the drillholder along the pipe on the furniture clamp, advancing the bit. At the same time, the fixture alines the bit so that it is perpendicular to the surface being drilled. Previously, the drill motor was hand-held, which often resulted in skewed holes and broken drill bits.

This work was done by Eldon N. Chartier and Lee N. Culp of Rockwell International Corp. for **Johnson Space Center.** *No further documentation is available.*
MSC-18582

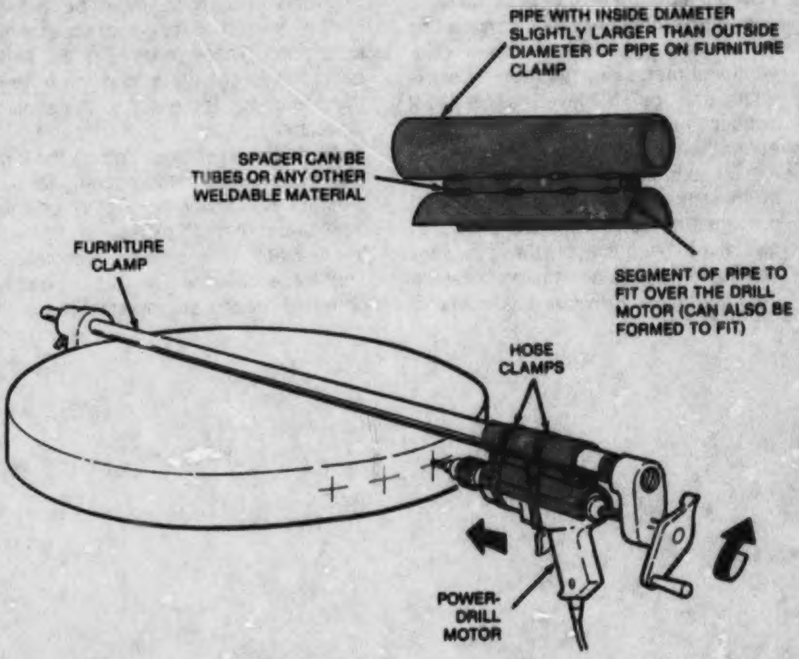
PIPE WITH INSIDE DIAMETER SLIGHTLY LARGER THAN OUTSIDE DIAMETER OF PIPE ON FURNITURE CLAMP
SPACER CAN BE TUBES OR ANY OTHER WELDABLE MATERIAL
FURNITURE CLAMP
SEGMENT OF PIPE TO FIT OVER THE DRILL MOTOR (CAN ALSO BE FORMED TO FIT)
HOSE CLAMPS
POWER-DRILL MOTOR

The **Drillholder** advances the drill motor as the bit pierces the edge of the disk. It is being used to drill 3/8-inch (0.93-cm) holes in iron/nickel alloy disks.

Books and Reports

These reports, studies, and handbooks are available from NASA as Technical Support Packages (TSP's) when a Request Card number is cited; otherwise they are available from the National Technical Information Service.

Self-Acting Shaft Seals

Operating principles and design

A paper has been published that reviews the operating principle and design of the self-acting shaft seal and also points out the effects of adverse operating conditions. By incorporating thrust-bearing geometry into a conventional face seal, nonrubbing operation can be achieved. This seal concept has been termed the "self-acting" seal, since the mechanism is similar to a self-acting thrust bearing in that the mating faces lift out of contact (the seal ring rides on a thin gas film) because of the pressure developed by relative motion between the seal faces. Previous studies have demonstrated that the self-acting seals can operate at advanced aircraft engine conditions and have lower leakage rates than labyrinth seals; thus they are attractive from the standpoint of efficiency.

The design of a self-acting seal requires that nonrubbing operation be achieved at all operating conditions (e.g., takeoff and cruise). Therefore, a crucial design consideration is the thickness of the gas film that separates the sealing faces.

To determine film thicknesses and associated leakage in a self-acting seal, the axial forces acting on the seal head (assembly of the primary ring and its carrier) must be determined over the range of operating conditions. These forces are the self-acting lift force, the spring force, and the pneumatic force due to the sealed pressure.

An analysis requires finding the film thickness for which the opening forces balance the closing forces. When this equilibrium film thickness is known, the leakage rate can be calculated. This force balance analysis is readily obtained for the steady-state case in which the seat face has zero runout with respect to the shaft centerline.

Elements of the analysis used to obtain seal performance predictions are described and evaluated. These elements are:

- Primary seal-pressure gradient
- Self-acting geometry and lift force
- Closing forces
- Equilibrium film thickness
- Performance maps
- Inlet effects

Elements of adverse operating conditions for seals are also described and evaluated. These elements are:

- Effect of nonparallel sealing faces
- Effect of seat face runout

The mathematical models for obtaining a seal force balance and the equilibrium operating film thickness are outlined in the paper.

This work was done by Lawrence P. Ludwig of **Lewis Research Center.** *Further information may be found in NASA TM-73856 [N78-19513/NSP], "Self-Acting Shaft Seals"* **[$6]**. *A copy may be purchased [prepayment required] from the National Technical Information Service, Springfield, Virginia 22161.*
LEW-13229

Fabrication Technology

Hardware, Techniques, and Processes

95 Verifying Root Fusion in Electron-Beam Welds
96 X-Ray Technique Verifies Weld-Root Fusion
96 Etchant for Incoloy-903 Welds
97 Chemical-Milling Solution for Invar Alloy
97 Eliminating Underbead Fissuring in Superalloys
98 Ion-Beam Cleaning for Cold Welds
99 Coatings for Hybrid Microcircuits
100 Placement Technique for Semicustom Digital LSI Circuits
101 A General Logic Structure for Custom LSI's
102 Jig for Assembling Large Composite Panels
103 Shaping Graphite/Epoxy Stiffeners
104 Flush-Mounting Technique for Composite Beams
104 Examining Graphite Reinforcement in Composites
105 Cryogenic Machining of Polyurethane Foam
105 "Grinding" Cavities in Polyurethane Foam
106 Alumina Barrier for Vacuum Brazing
106 Connector Heat Shield
107 Foam-Filled Cushions for Sliding Trays
108 Ion-Beam Etching Enhances Adhesive Bonding
109 Room-Temperature Adhesive for High-Temperature Use
110 Easily-Assembled Helical Heater
110 Microprocessor Systems for Industrial-Process Control
111 Wire Harness Twisting Aid
112 Adjustable Base for Centering Staked Bearings
112 Safely Splicing Glass Optical Fibers
113 Knife-Edge Seal for Vacuum Bagging
114 A Precoat Prevents Ceramic Stopoffs From Spalling

Books and Reports

114 Should We Industrialize Space?
115 Cost Models and Economical Packaging of LSI's
115 Automated Ion Implantation for IC's
115 An Automated Photolithography Facility for IC's
116 Models of MOS and SOS Devices

Verifying Root Fusion in Electron-Beam Welds

Ultrasonic equipment and recorder verify that the back side of the joint is welded.

Marshall Space Flight Center, Alabama

A new technique assures adequate penetration of an electron-beam weld to the back side (root) of the joint. A magnetostrictive wire waveguide inserted in the joint root is monitored by ultrasonic equipment using an x-y recorder. As the joint is welded, signals on the recorder indicate where the penetration is incomplete. The method is particularly valuable when the back side of the joint is inaccessible to conventional inspection after the welding. It is more accurate than most standard ultrasonic and X-ray inspection methods.

An electrical pulse applied to the transducer shown in the figure generates an ultrasonic signal in the magnetostrictive wire waveguide. This ultrasonic wave propagates in the thin rod (extensional mode of propagation). The portion of the wire in the weld joint is about 0.020 in. (0.51 mm) in diameter and may be of the same material as the sample. The wire is placed in a groove (slightly larger than the wire) at the root of the joint. As the welding head moves along the part, the end of the wire is melted and fused if the joint is adequately penetrated. Because of the difference in acoustic impedance between the liquid and solid phases, the ultrasonic signal is reflected, detected by the transducer, and amplified by the receiver. The time of arrival of this signal is measured. An analog position signal, representing the welding-head position and the propagation time (time of flight) of the signal, is differentiated and recorded on an x-y recorder.

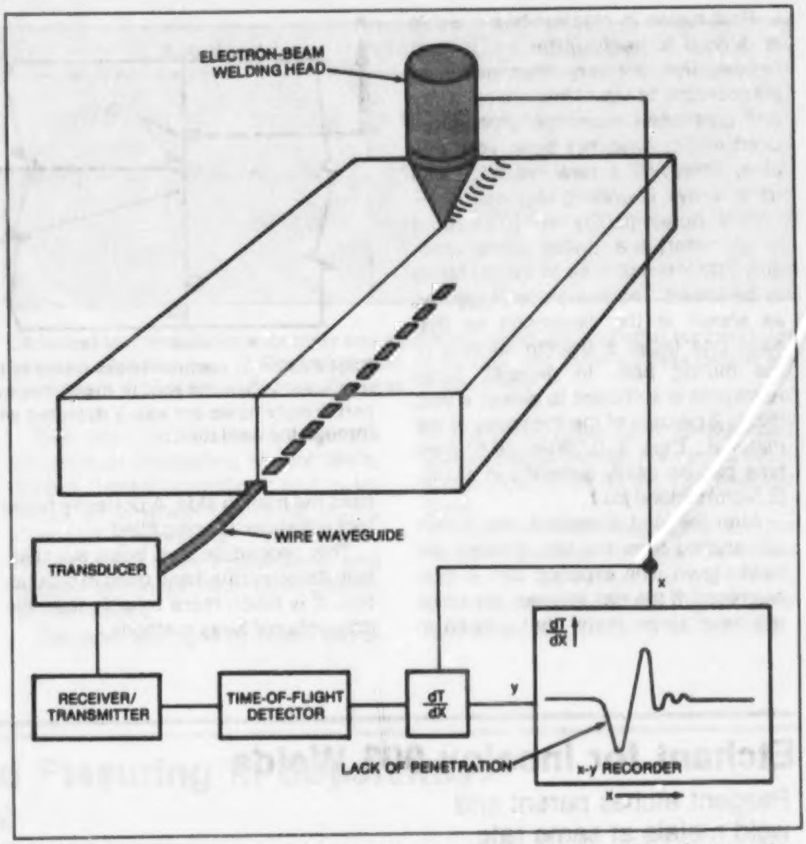

Monitoring Apparatus verifies root fusion in electron-beam welds. A magnetostrictive wire waveguide inserted in the back side of the joint transmits ultrasonic signals to the point where the weld is fully penetrated. The reflected signal is time-detected (similar to radar) and is fed to the x-y recorder. When the joint below the welding head is completely penetrated, the recorder indicates a steady signal. The point where the penetration is incomplete is indicated by a large signal on the recorder.

For an acceptable weld, the x-y output is very nearly constant. In an area where the joint is not fully penetrated and the wire is not melted, a large reflected signal is received from the area where the wire was last fused. This signal remains constant with time until the beam melts the wire. The length of time that the signal is constant is directly related to the length of the unfused zone, and its position can be located from the x position of the recording.

The method permits a determination of penetration depth in preweld samples without the time-consuming opening of the vacuum chamber of the electron-beam welder and sectioning of the sample.

This work was done by F. L. Becker, Steve Doctor, and R. E. Kleint of Rockwell International Corp. for **Marshall Space Flight Center.** *No further documentation is available.*
MFS-19499

X-Ray Technique Verifies Weld-Root Fusion

X-ray inspection of small holes shows whether the root is welded.

Marshall Space Flight Center, Alabama

Root fusion in electron-beam welds is difficult to verify. After the joint is welded, the root very often becomes inaccessible to visual inspection. X-ray and ultrasonic inspection procedures used earlier have not been very reliable; however, a new method, also using X-rays, is working very well.

Tiny holes [0.020 in. (0.51 mm) in diameter] are drilled perpendicularly into the root area of the surfaces to be joined. The holes are staggered as shown in the illustration so that each one faces a smooth surface of the mating part. In general, X-ray resolution is sufficient to detect a void that is 2 percent of the thickness of the material. Thus a 0.020-in. (0.51-mm) hole can be easily detected in a 1-in. (2.5-cm) welded joint.

After the joint is welded, the X-rays are applied from the top, through the weld crown. The exposed film is then examined. If the root is fused, the holes will have some metal that poured in from the mating side. A perfectly fused root will show all holes filled.

This procedure has been successfully demonstrated and used in production. It is much more reliable than the conventional X-ray methods.

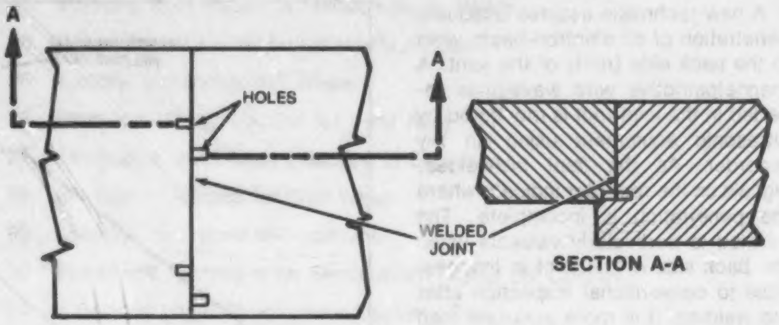

Root Fusion in electron-beam welds is inspected using predrilled small holes in the root area. When the root is fused, the holes are filled with material from the mating part. Empty holes are easily detected with X-rays applied from the weld crown down through the weld root.

This work was done by R. E. Kleint of Rockwell International Corp. for **Marshall Space Flight Center.** *No further documentation is available.*
MFS-19468

Etchant for Incoloy-903 Welds

Reagent etches parent and weld metals at same rate.

Marshall Space Flight Center, Alabama

When etching the surface of a weld area to reveal the underlying grain structure, it is important that the reagent not "overetch" and disguise the microstructure being examined. The etchant should also remove both the welded metal and the parent metal at the same rates. Often, a different etchant is used for each phase to prevent preferential etching.

When the welded material is Incoloy-903 (an iron/nickel alloy), a lactic/nitric/hydrochloric acid formulation can be used successfully. The reagent etches welded specimens uniformly without overetching. It exposes the grain structure of both the welded metal and the parent metal in fused Incoloy-903 joints.

The reagent composition is shown in the table. The proportions may be altered slightly to improve the ability to reveal particular, finely dispersed constituents. The reagent was developed for autogenous Incoloy-903 welds, in which pieces of the same metal are fused without the addition of a filler metal.

1 part	lactic acid ($CH_3CHOHCOOH$)	90-percent concentration
1 part	nitric acid (HNO_3)	70-percent concentration
4 parts	hydrochloric acid (HCl)	37-percent concentration

The Etchant Formulation for Incoloy-903 welds satisfactorily etches both weld and parent metal. It must be freshly mixed for each application.

This work was done by Joseph A. Gerstmeyer of Rockwell International Corp. for **Marshall Space Flight Center.** *No further documentation is available.*
MFS-19378

Chemical-Milling Solution for Invar Alloy

Excellent surface finishes and tolerances are possible with two nitric/hydrofluoric formulations.

Marshall Space Flight Center, Alabama

Two chemical-milling solutions for Invar (and equivalent alloys) give excellent surface finishes with none of the problems that plagued previous formulations. A finish of 125 μin. (3.17 μm) is possible with solution A (see table) if milling is done at 135° to 145° F (57° to 63° C). For finishes of 85μin. (2.16 μm), solution B is used. The latter has essentially the same composition as solution A, except for an additional 7 percent of phosphoric acid.

An effective chemical-milling solution is needed for Invar, because this 36-percent-Ni/Fe alloy is very often chosen for dimension-critical components because of its low thermal-expansion coefficient at temperatures up to 400° F (204° C). With the discovery of the two formulations, chemical milling can now complement conventional machining and electric-discharge machining when fabricating precise parts with high surface finishes and tolerances.

Solution A		Solution B	
HF (70 percent)	5.8 oz/gal	HF (70 percent)	5.8 oz/gal
HNO_3 (40 to 42 °Bé)	40 oz/gal	HNO_3 (42 °Bé)	40 oz/gal
H_2O	balance	H_2PO_4 (75 percent)	10 to 13 oz/gal
		H_2O	balance

Chemical-Milling Solutions for Invar and equivalent alloys are applied at temperatures between 135° and 145° C. Control ranges, etch rates, and other process details are available in the Technical Support Package for this article.

The new formulations eliminate problems of channeling at root fillets, dishing, island formation, and overhangs, all of which can occur during chemical processing. Previous attempts to use dilute hydrochloric acid (recommended for Invar) gave unsatisfactory results.

This work was done by Walter Batiuk of The Perkin-Elmer Corp. for **Marshall Space Flight Center.** *For further information, Circle 68 on the TSP Request Card.*

Inquiries concerning rights for the commercial use of this invention should be addressed to the Patent Counsel, Marshall Space Flight Center [see page A5]. Refer to MFS-25365.

Eliminating Underbead Fissuring in Superalloys

Reduced weld velocity eliminates underbead fissuring in superalloys.

Marshall Space Flight Center, Alabama

Severe underbead cracking had occurred in weld overlays of Incoloy-903, Incoloy-88, and Inconel-718. This problem was eliminated by carefully controlling the welding-speed parameter.

The weld parameters that produce high-integrity superalloy welds under overlay conditions (piling metal upon itself) were found to differ from those used for conventional welds (metal put in a recessed groove). The thermal and metallurgical properties of these overlays are critically tied to stress/strain and time/temperature threshold characteristics determined by the inherited strength and microstructure of the prior weld bead. The weld microstructure (grain size and segregation) is principally determined by the rate and direction of solidification. Each successive weld bead will tend to nucleate and solidify in a similar fashion as the previous underbead. Results show that weld velocity is critically associated with solidification rates and thermal gradients.

The upper limits of the weld velocity (travel speed) were established to eliminate the underbead fissuring. A maximum weld velocity of 4 in./min (10.2 cm/min) was applied to Incoloy-88 and Inconel-718 overlays, and a maximum travel speed of 3 in./min (7.8 cm/min) was used for Incoloy-903 overlay work. These limits are below the commonly used rates and keep the thermally induced forces to below crack-inducing levels on the grain boundaries of the heat-affected zone of the previous weld bead.

This work was done by R. D. Betts of Rockwell International Corp. for **Marshall Space Flight Center.** *No further documentation is available.*
MFS-19460

Ion-Beam Cleaning for Cold Welds

Ion-beam cleaning results in strong bonds with minimal deformation.

Lewis Research Center, Cleveland, Ohio

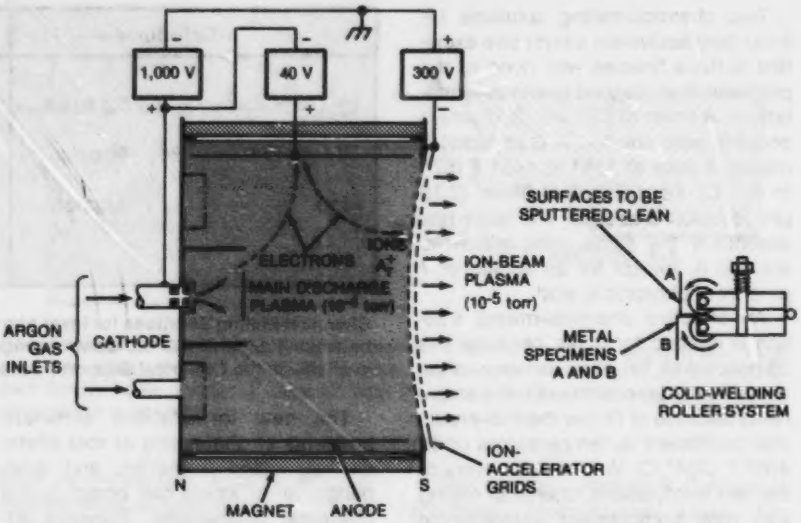
1,000 V
40 V
300 V
ARGON GAS INLETS
CATHODE
ELECTRONS
IONS A_r^+
MAIN DISCHARGE PLASMA (10^{-4} torr)
ION-BEAM PLASMA (10^{-5} torr)
SURFACES TO BE SPUTTERED CLEAN
A
B
METAL SPECIMENS A AND B
COLD-WELDING ROLLER SYSTEM
ION-ACCELERATOR GRIDS
N
S
MAGNET
ANODE

Electron Bombardment Ion Source and Roller System are used to clean metal surfaces and cold-weld them together with minimal deformation.

A variation of cold welding has been developed that utilizes an ion beam to clean mating metal surfaces prior to joining in a vacuum environment. High-quality solid-state welds are produced with minimal deformation (<1 percent).

In theory, if you bring two perfectly-clean metal surfaces into intimate contact so that the atoms of one surface are sufficiently close to the atoms of the other surface, the interatomic force-of-attraction becomes effective across the interface, and a solid-state weld is obtained. Theoretically, such a weld can be as strong as the parent metals involved.

In reality, metal surfaces are not "clean" but are contaminated with oxides, nitrites, water vapor, organics, and the like, so that sufficiently-intimate metal-to-metal contact cannot be readily established. The effectiveness of an oxide layer to interrupt or prevent metal-to-metal bonds has been shown to exist down to one or two monolayers of coverage. Oxide monolayers are extremely tenacious and especially difficult to remove from most metal surfaces. They are stable even at vacuum levels below their bulk vapor pressure. Thus, an effective cleaning method is necessary to remove completely the oxide or contamination layer in order to obtain a high-quality cold weld with minimal deformation.

In conventional practice it is possible to achieve reliable cold welding in aluminum, as well as some other materials, for many applications by applying sufficient pressure to cause plastic flow of the material at the interface of the pieces to be welded. By using welding dies or indenters to cause plastic flow, the oxide layers at the interface are broken up and dispersed, allowing clean underlying metal to squeeze through to the interface for clean metal-to-metal bonding. Additionally, under plastic flow the atomic contact and registry between the two metals are greatly increased. Thus a good solid-state weld is formed.

Past studies have shown that for conventional cold welding of aluminum, no welding was detected with less than 40 percent deformation. At about 70 percent deformation, however, the weld strength approached the strength of the parent metal, which had been thinned by the same amount.

Such plastic flow and deformation, however, have several drawbacks. First, the temper of the metal is increased by cold-working in the bond area so that it is less ductile than the parent metal, and second, the strength of the bond will eventually equal the strength of the thinned metal that resulted from the deformation.

The ion-beam cold-welding method overcomes these drawbacks by removing the oxide layer to expose clean metal that can be cold-welded with greatly reduced pressures so as not to cause gross deformation and thinning of the material at the weld. A minimal amount of deformation is necessary since most metal surfaces are not atomically flat. When two metal surfaces are brought together, the actual contact surface may be only a small portion of the apparent contact area of high points or spots, called asperities. The deformation process requires a loading force to cause sufficient elastic deformation and plastic flow of the surface asperities to increase the actual contact area at the interface to achieve a high-quality cold weld. With ion-beam cleaning, high-quality cold welds were observed in aluminum with deformation of less than 1 percent.

The ion-beam source used for cleaning is based on the technology developed by NASA for ion-propulsion space applications. A schematic diagram of the ion source modified for inert-gas ion-beam cleaning with the metal specimens and roller system is shown in the figure. The ion-beam source and roller system are mounted in a vacuum tank with a pressure range from 10^{-6} to 10^{-4} torr.

The ion-beam source operates as follows: Argon, an inert gas that is easily ionized, is introduced into the cylindrical main discharge chamber.

There the argon atoms are bombarded by electrons and ionized as they flow through the discharge chamber. The electrons are emitted from the cathode and accelerated to anode potential with an energy of the order of 40 eV. At the discharge operating pressure the electrons must travel an average distance of 1 meter before encountering an ionizing collision with an argon atom. Thus a magnetic field is applied in order to increase the electron mean path and enhance the ionization process within the limited dimension of the discharge chamber. Argon ions from the discharge plasma as they approach the acceleration grids are extracted and accelerated through the large number of small holes in the grids by the electrostatic field associated with the high voltages applied to the grid elements. These ions are directed onto the surface of the material to be sputter-cleaned, typically with an energy of 1,000 eV and with a current density of 1 mA/cm^2.

When a 1,000-eV ion beam bombards a metal surface, it imparts sufficient energy to break any chemical bond between the surface and near-surface atoms. All metals can be sputtered by this process, and in general the sputter removal rate is in the range of quite a few atomic layers per second for an ion-beam current density of 1 mA/cm^2.

The roller system used to cold-weld the ion-beam-cleaned surfaces is also shown in the figure. Metal specimens are inserted between the two steel rollers at one end and are separated and bent outward as indicated schematically. This configuration exposes both mating surfaces to a normal incident ion beam for sputter cleaning. The surfaces were mounted approximately 10 cm from the ion-beam source. After ion-beam-cleaning the exposed mating surfaces, the rollers were rotated to pull the specimens through. Rotational torque was applied manually from outside the vacuum chamber through a vacuum shaft feedthrough.

The force between the rollers was controlled by the spring compression, which was approximately 670 N (150 lb) maximum for 0.25 mm separation. Typically, metal specimens were cut from 0.127 mm foil into 25-mm-wide strips with a length of 12 to 15 cm for test purposes. Welding occurred down the center of the strips where the upper roller forced the specimens together. Work was limited in scope to low-yield-strength material due to the limitation of the experimental fixture used to apply pressure at the ion-beam-cleaned interface.

The following low-yield-strength materials were successfully cold-welded using the ion-beam cleaning technique and the experimental fixture: aluminum to aluminum, copper to copper, copper to aluminum, copper to nickel, and silver to iron. These materials could not be pulled apart in peel tests; instead, the base metal failed adjacent to the weld. Photomicrographs of as-welded and heat-treated-weld specimens demonstrated that metal-to-metal bonding had been achieved.

This work was done by Bernard L. Slater of **Lewis Research Center.** *Further information may be found in NASA TM-78933 [N78-27257/NSP], "Use of Ion Beam Cleaning to Obtain High Quality Cold Welds with Minimal Deformation" price [$5]. A copy may be purchased [prepayment required] from the National Technical Information Service, Springfield, Virginia 22161.*

This invention is owned by NASA, and a patent application has been filed. Inquiries concerning nonexclusive or exclusive license for its commercial development should be addressed to the Patent Counsel, Lewis Research Center [see page A5]. Refer to LEW-12982.

Coatings for Hybrid Microcircuits

Tests show the efficacy of protective coatings, but indicate problems with PIND tests.

Marshall Space Flight Center, Alabama

Leak Test	MIL-STD-883A (Fine and Gross)
PIND Test	
Electrical Test	
Stabilization Bake	24 hours at 150° C
Thermal Cycling	MIL-STD-883A (-65° to +150° C, 100 cycles)
Thermal Shock	MIL-STD-883A (0° to 100° C)
Mechanical Shock	MIL-STD-883A — Condition B
Acceleration	MIL-STD-883A — Condition A
High-Temperature Storage	168 hours at 125° C
Final Electrical	
External Visual	

Coated and Uncoated Microcircuits were subjected to the tests listed here. The leak test and the electrical test were performed after each of the environmental tests.

Uncoated hybrid microcircuits are vulnerable to electrical failures due to loose solder and other metal particles that cause shorts. In tests of two coating materials to prevent such failures — parylene and silicone, the only electrical failures were in uncoated control samples.

Although the coatings protect microcircuits from contamination by particles, there is the danger that the coating may entrap contamination that will degrade circuit performance over the long term. The tests showed, however, that particle entrapment need not be a concern.

(continued on next page)

A group of 30 microcircuits was subjected to the tests listed in the table. One-third of the units were coated with silicone and one-third with parylene; one-third were left uncoated.

The particle-impact noise detection (PIND) test produced contradictory results that raise doubts about its reliability as a failure predictor. In a PIND test, a packaged microcircuit is shaken while sensitive microphones listen for sounds from loose particles within the package. Although such sounds were detected in PIND tests of parylene-coated microcircuits, none of these circuits failed the electrical tests.

The high incidence of misleading PIND failures is probably a result of the parylene-coating process. Part of the microcircuit surface is masked during coating; when the masking material is removed, a small amount of the nonconducting coating material is dislodged. In small quantities, however, the loose coating particles are harmless.

Failures of uncoated microcircuits were also not predicted reliably by PIND testing. Only one-fourth of the electrical failures in uncoated specimens were anticipated in PIND test results.

This work was done by D. L. Kinser of Vanderbilt University for **Marshall Space Flight Center.** *For further information, Circle 69 on the TSP Request Card.*
MFS-25292

Placement Technique for Semicustom Digital LSI Circuits

An automated cell-placement technique modified to speed up new LSI circuit fabrication

Marshall Space Flight Center, Alabama

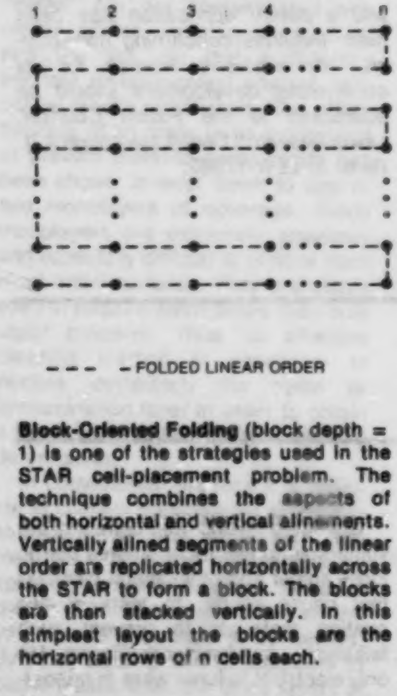

Block-Oriented Folding **(block depth = 1) is one of the strategies used in the STAR cell-placement problem. The technique combines the aspects of both horizontal and vertical alinements. Vertically alined segments of the linear order are replicated horizontally across the STAR to form a block. The blocks are then stacked vertically. In this simplest layout the blocks are the horizontal rows of n cells each.**

An automated placement technique that has been used with several LSI (large-scale integration) circuits was modified for new LSI technology developed at the Marshall Space Flight Center. The technique called STAR, for standard transistor array, uses a prefabricated transistor understructure and a comprehensive library of digital logic cells to fabricate semicustom LSI circuits efficiently. This technology is intended for small lots of special-purpose IC's and is generally less expensive than customized fabrication.

The STAR system was developed for bulk-metal CMOS technology, although its organization is adaptable to other technologies. The LSI cell placement is based on a linear ordering/folding technique.

Linear ordering produces a one-dimensional chain in which the total interconnection length is nearly minimum (considering the cell width). The folding methods (see example in figure) rely on the assumption that the linear order represents a near-optimum one-dimensional cell placement with respect to the total interconnection distance. The strategy is to decrease the distance between the connected cells or to place a higher percentage of cells in juxtaposition than specified in the linear order.

The entire placement technique is carried out via computer program (CAPSTAR) developed as an integral part of a system of programs for the STAR technology.

This work was done by B. D. Carroll and G. W. Cox of Auburn University for **Marshall Space Flight Center.** *For further information, Circle 70 on the TSP Request Card.*
MFS-25324

A General Logic Structure for Custom LSI's

A proposed concept to reduce the cost and complexity of producing custom LSI's

NASA's Jet Propulsion Laboratory, Pasadena, California

A proposed approach to fabricating custom LSI (large-scale integration) circuits would use a general logic structure (GLS) composed of standardized circuit arrays. Custom LSI's would be made by defining cut and contact points in the basic GLS mask set.

An approximation of the logical equivalent of a programed NMOS GLS is shown in the figure. Each of the m column lines may be formed into two or more NOR gates from physically disjoint partitions of the n implicant rows. A gate is created by connecting pulldown transistors at desired implicant rows to a column and connecting the column to a pullup resistor. The output of the NOR gate may be taken anywhere on the column segment on which the gate is built. Pullup resistors are located periodically along each column. This permits a column to be cut and formed into several independent NOR gates.

A NOR gate output may be connected to any unused implicant row that it crosses. The connection is made by forming a contact point at the desired row-and-column intersection. The formation of multiple contact points allows the NOR output to be transmitted to different locations within the structure.

Implicant rows may be cut into several segments. Each segment can be used to transmit a different implicant. In this way, for example, an implicant row carrying an input term may be cut after the last pulldown transistor that uses it. The segment after the cut can then be reused to transmit a NOR output.

In general the GLS structure consists of two types of rows: One row type transmits implicant terms; the other row is connected to ground. Transistors are created at the intersection of a column and implicant row where the implicant is needed in the NOR function. Transistor channels form a switchable path from columns to the ground row. Pulldown transistors are enchancement-mode devices. The channels of these transistors conduct when a positive gate-to-source voltage is present. Pullup resistors are implemented by depletion-mode transistors that are shorted from gate to source.

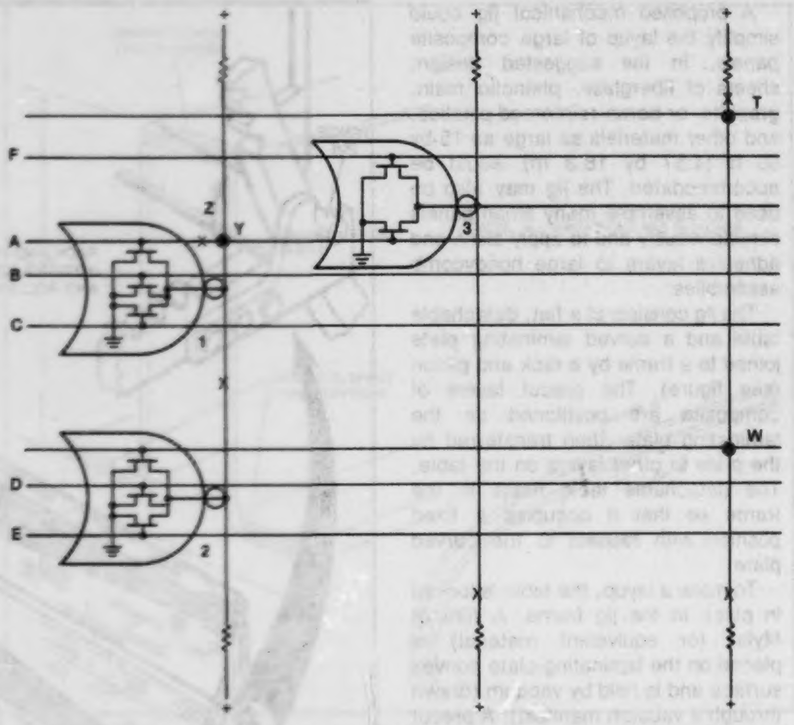

The General Logic Structure for custom LSI shows contact points indicated by a dot and cuts by an X. NOR gate 1 forms the result $\overline{A+B+C}$. The implicant row carrying input A is cut at Z, and a contact point is created at Y. This connects gate 1 output to the implicant row freed by cut Z. Gate 1 output is then available as an input to NOR gate 3. Gate 3 is connected to an unused implicant row, which in turn is connected at T to a column. Contact W places the output of gate 3 on an implicant row, which makes it available to the input of gate 2.

The GLS can also be used to form shift registers by using a multiplexer in front of a flip-flop. In this configuration the register may be continually clocked. The multiplexer determines whether a left or right shift, load, or no operation is to occur on the next clock transition.

The GLS may be designed using an interactive color graphics system. A user could specify the function to be mapped, design guidelines, and analysis to be performed. By viewing the GLS created by the computer, or the results of an analysis, the user could suggest other mapping approaches or request changes be made.

This work was done by Michael W. Sievers of Caltech for **NASA's Jet Propulsion Laboratory.** *For further information, Circle 71 on the TSP Request Card.*

This invention is owned by NASA, and a patent application has been filed. Inquiries concerning nonexclusive or exclusive license for its commercial development should be addressed to the Patent Counsel, NASA Resident Legal Office-JPL [see page A5]. Refer to NPO-14410.

Jig for Assembling Large Composite Panels

Composite layers are accurately positioned by a mechanical jig.

Langley Research Center, Hampton, Virginia

A proposed mechanical jig could simplify the layup of large composite panels. In the suggested design, sheets of fiberglass, phenolic resin, graphite- or boron-reinforced plastics, and other materials as large as 15 by 60 ft (4.57 by 18.3 m) would be accommodated. The jig may also be used to assemble many small panels simultaneously and to apply skins and adhesive layers to large honeycomb assemblies.

The jig consists of a flat, detachable table and a curved laminating plate joined to a frame by a rack and pinion (see figure). The precut layers of composite are positioned on the laminating plate, then transferred by the plate to other layers on the table. The detachable table nests in the frame so that it occupies a fixed position with respect to the curved plate.

To make a layup, the table is locked in place in the jig frame. A film of Mylar (or equivalent material) is placed on the laminating-plate convex surface and is held by vacuum (drawn through a vacuum manifold). A precut sheet of the preimpregnated material of the first composite layer is applied to the film, within an outline scribed on the plate. The prepreg resin temporarily bonds the composite sheet to the film.

The laminating plate is raised to vertical, then lowered face down on the table. Registration between the curved plate and the flat table is ensured by engagement of the rack and pinion. With the plate positioned on the table, the vacuum is cut off, releasing the layer and the film. The film can then be peeled off the layup, leaving the new layer in place.

The transfer procedure is repeated until the composite panel is complete. Then, the table is released and wheeled away from the fixture so that the composite can be cured.

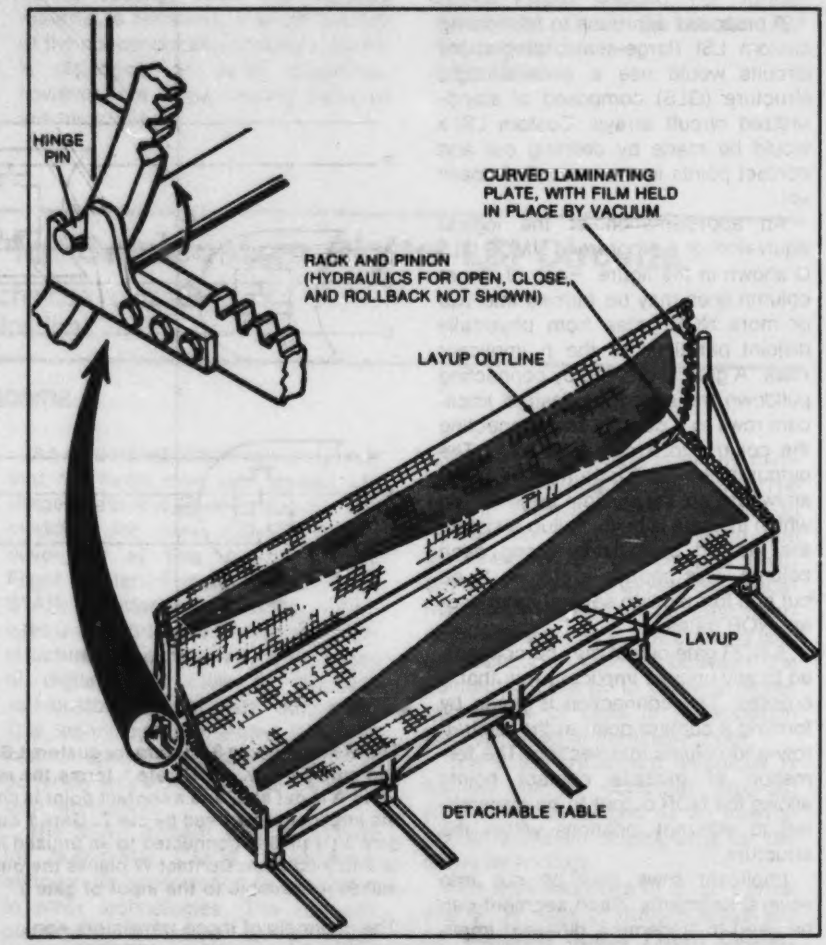
HINGE PIN
CURVED LAMINATING PLATE, WITH FILM HELD IN PLACE BY VACUUM
RACK AND PINION (HYDRAULICS FOR OPEN, CLOSE, AND ROLLBACK NOT SHOWN)
LAYUP OUTLINE
LAYUP
DETACHABLE TABLE

The Curved Plate of the Bonding Jig deposits a resin-impregnated layer on the table in a precise location, without disturbing other layers. After the layer is deposited, the vacuum chuck releases the film backing, and the film is peeled off the layup.

This work was done by John T. Watts of McDonnell Douglas Corp. for **Langley Research Center.** *For further information, Circle 72 on the TSP Request Card.*
LAR-12394

Shaping Graphite/Epoxy Stiffeners

A simple procedure produces long curved laminates without wrinkles or voids.

Lyndon B. Johnson Space Center, Houston, Texas

A method of shaping graphite-fiber-reinforced/epoxy parts eliminates wrinkles and voids and reduces fabrication time. Originally developed to make ribs (Figure 1) for the Space Shuttle payload-bay doors, the method may also find use in the fabrication of strong lightweight structural members in cars, trucks, and other vehicles.

A fixture shaped like the upper cap and lower flange of the rib is utilized (Figure 2). Twenty-five to thirty-eight layers of graphite/epoxy tape, 1 inch (2.5 centimeters) wide, are laid on each cap and flange of the fixture. Bleeder cloth covers the strips, and the fixture is placed in a vacuum bag and inserted in an oven at 175° F (79° C) for 15 to 20 minutes. The heat and external pressure on the vacuum bag shape the tape stacks smoothly around the contours of the fixture. (The stacks also retain their shape when they are removed from the fixture.) The caps and flanges are then interleaved with plies of graphite/epoxy fabric, 13 mils (0.33 millimeter) in thickness, to complete the rib.

Previously, layers of tape were shaped and applied by hand with the aid of a laminating adhesive. However, this method produced unacceptable ribs because of wrinkles and voids in the tape stacks.

This work was done by Jim L. Cupp of Rockwell International Corp. for **Johnson Space Center.** *For further information, Circle 73 on the TSP Request Card.*
MSC-18494

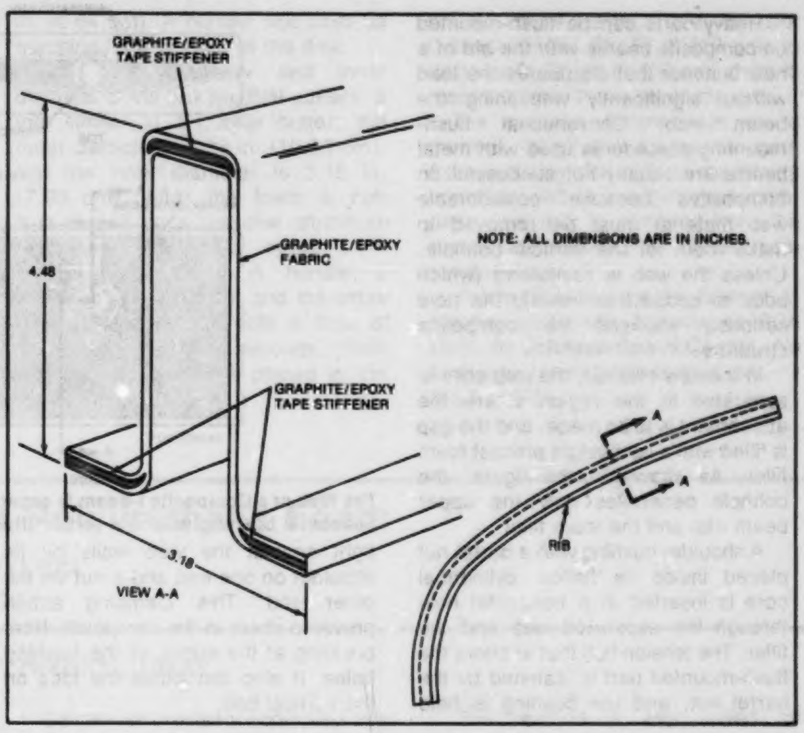
GRAPHITE/EPOXY TAPE STIFFENER
4.48
GRAPHITE/EPOXY FABRIC
NOTE: ALL DIMENSIONS ARE IN INCHES.
GRAPHITE/EPOXY TAPE STIFFENER
A
A
RIB
3.18
VIEW A-A

Figure 1. **Graphite/Epoxy Stiffeners** (in color) are embedded in the cap and flanges of a long, curved channellike rib.

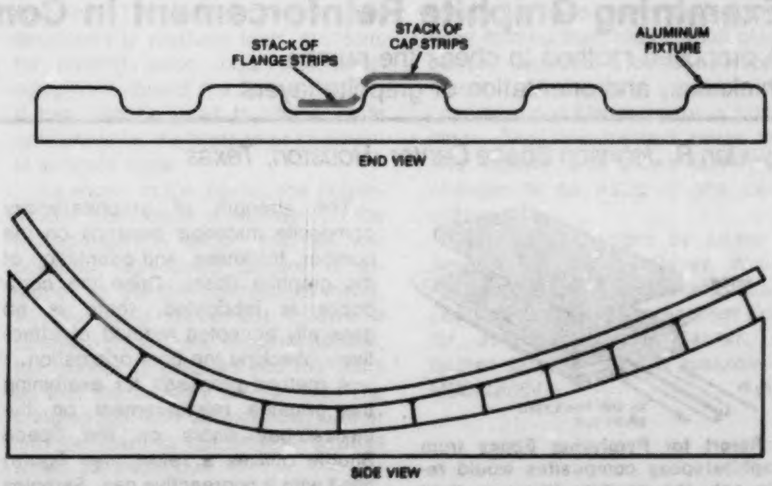
STACK OF CAP STRIPS
STACK OF FLANGE STRIPS
ALUMINUM FIXTURE
END VIEW
SIDE VIEW

Figure 2. The **Shaping Fixture** contains ridges and grooves shaped like the cap and flanges of the rib and following the same longitudinal curve. Layers of graphite/epoxy tape are stacked on the ridges and in the grooves. The layup is vacuum-bagged in an oven to form caps and flanges free of wrinkles and voids.

Flush-Mounting Technique for Composite Beams

Tension bolts are retained by a transverse bushing.

Langley Research Center, Hampton, Virginia

Heavy parts can be flush-mounted on composite beams with the aid of a new fastener that distributes the load without significantly weakening the beam web. Conventional flush-mounting procedures used with metal beams are usually not successful on composites because considerable web material must be removed to make room for the vertical bolthole. Unless the web is reinforced (which adds to production costs), the hole seriously weakens the composite structure.

In the new method, the web core is separated in the region where the attachment is to be made, and the gap is filled with a lightweight precast foam filler. As shown in the figure, the bolthole penetrates only the upper beam cap and the foam filler.

A shoulder bushing with a barrel nut placed inside its hollow cylindrical core is inserted in a horizontal hole through the separated web and the filler. The tension bolt that anchors the flush-mounted part is fastened by the barrel nut, and the bushing is held tight against the web walls by its shoulder on one end and a nut on the other end. This clamping action prevents fibers in the composite from buckling at the edges of the bushing holes. It also distributes the load on the vertical bolt.

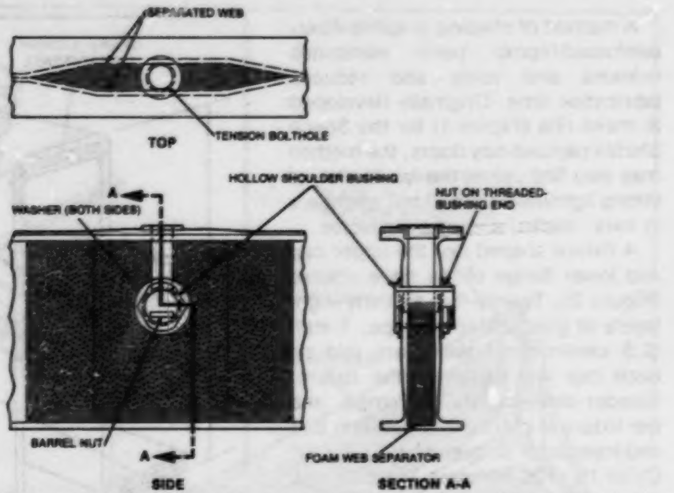

The Web of a Composite I-Beam is separated and filled with foam. A barrel nut in the horizontal bushing retains a vertical flush-mounting bolt.

This work was done by Thomas C. Harman and Bruce F. Kay of United Technologies Corp. for **Langley Research Center.** *For further information, Circle 74 on the TSP Request Card.*
LAR-12389

Examining Graphite Reinforcement in Composites

A proposed method to check the number, thickness, and orientation of graphite layers

Lyndon B. Johnson Space Center, Houston, Texas

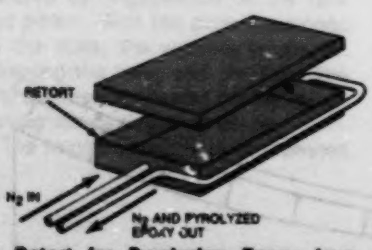

A Retort for Pyrolyzing Epoxy from graphite/epoxy composites would retain only the graphite fibers in their original orientation. The retort is placed in a furnace; the nitrogen inlet and outlet tubes extend through an opening in the furnace.

The strength of graphite/epoxy composite materials depends on the number, thickness, and orientation of the graphite fibers. Once the composite is fabricated, there is no generally accepted method of effectively checking the fiber orientation.

A method proposed for examining the graphite reinforcement on the payload-bay doors on the Space Shuttle utilizes a retort (see figure) filled with a nonreactive gas. Samples of graphite/epoxy compound would be placed in the retort, which would be tightly closed, purged with nitrogen gas, and heated in a furnace at 1,000° F (540° C) for 2 to 3 hours.

After several hours, the epoxy is pyrolyzed and carried away through the retort exhaust by a continuous flow of nitrogen gas. The retort is then cooled and opened. The graphite fibers remain and are easily separated to check the number, thickness, and orientation of the layers.

This work was done by Robert E. Sanders and Clyde I. Yates of Rockwell International Corp. for **Johnson Space Center.** *No further documentation is available.*
MSC-19594

Cryogenic Machining of Polyurethane Foam

Complex configurations can be machined in low-density foam.

Lyndon B. Johnson Space Center, Houston, Texas

A method for precisely machining low-density polyurethane foam in thin cross sections begins by cooling foam to cryogenic temperatures. Once "frozen," the foam is machined as if it were any other solid material. Developed to make foam lens seals on the Space Shuttle closed-circuit television cameras, the technique could also be used to make vibration dampers, mounting cushions, and other parts.

The Shuttle lens seal calls for a low-density[1.0 to 2.0 lb/ft^3 (16 to 32 kg/m^3)] closed-cell polyurethane foam disk with a cross section of 0.25 in. (0.64 cm). A narrow slot must be machined in the edge of the disk.

The outer diameter and inner diameter of the disk are first cut with a tool similar to a cookie cutter; the outer diameter is 4.25 in. (10.80 cm), and the inner diameter is 3.15 in. (7.99 cm). After the foam is cut, it is placed on a massive aluminum machining fixture; a cover plate keeps it in place. A handle is attached to the fixture, and the entire assembly is lowered into a tank of liquid nitrogen for 60 seconds. Upon removal, the fixture is placed in the chuck of a lathe, and a slot 0.05±0.005 in. (0.127±0.013 cm) in width by 0.485 in. (1.232 cm) deep is machined into the edge of the disk.

The massive fixture acts as a thermal "sink" that keeps the foam frozen during the entire machining operation. When machining is complete, the disk is removed from the fixture and allowed to reach room temperature.

This work was done by Edward A. Moshey and Peter Prychka of RCA Corp. for **Johnson Space Center.** *No further documentation is available.*
MSC-18572

"Grinding" Cavities in Polyurethane Foam

Foam blocks are cut by a grinding tool on a conventional milling machine.

Lyndon B. Johnson Space Center, Houston, Texas

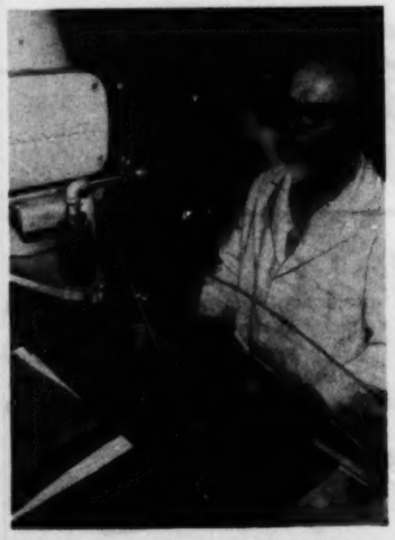

A Grinding Tool Removes Material from a foam block as the milling-machine table moves in the pattern established by a template.

Cavities of precisely controlled size and shape can be cut into blocks of polyurethane foam by a grinding tool installed in a conventional milling machine. The cutting method was developed to produce foam cushions for holding loose tools and small equipment aboard the Space Shuttle. It can also be used to shape foam containers for the storage or shipment of delicate items.

As shown in the figure, the polyurethane foam block is mounted on the milling-machine table, and an air-powered high-speed grinder is attached to the milling-machine head. As the table movement follows a template cut with the required pattern, the grinder is pressed into the foam so that the cavities are formed. The grinding tool can be extended further into the foam to cut smaller cavities within the initial cut.

The method is well suited for prototype or midsize production runs and can easily be adapted to computer control for mass production. Previously, shaped-cavity foam blocks were formed from many small blocks bonded together around a wooden mandrel. Alternatively, a hot wire was used to scoop pieces of foam from a block. The new method saves time and material and allows last-minute changes to be made in the cavity shape.

This work was done by James R. Brower, Raymond E. Davey, William F. Dixon, Paula H. Robb, and Paul P. Zebus of Rockwell International Corp. for **Johnson Space Center.** *No further documentation is available.*
MSC-18564

Alumina Barrier for Vacuum Brazing

Aluminum oxide "paper" protects tooling and improves brazed-joint quality.

Lyndon B. Johnson Space Center, Houston, Texas

Thin sheets of alumina-enriched paper prevent the workpiece from attaching to the tooling in brazing operations. Used in fluxless vacuum brazing of stainless-steel parts (Figure 1), the paper acts as a barrier that prevents the brazing alloy from bonding to the tooling. Because of the high chemical stability of alumina (aluminum oxide), the paper does not react with the parts or the tooling, even at the high temperatures and pressures required for brazing.

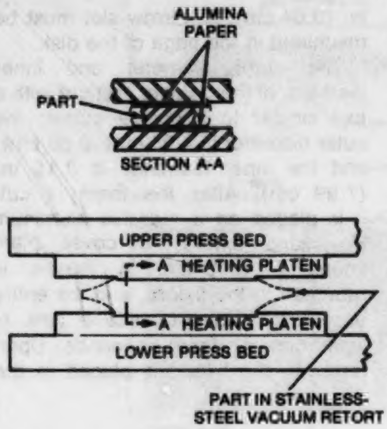

Figure 1. A **Sheet of Alumina Paper** is placed between the parts to be brazed and the heating platens of the press.

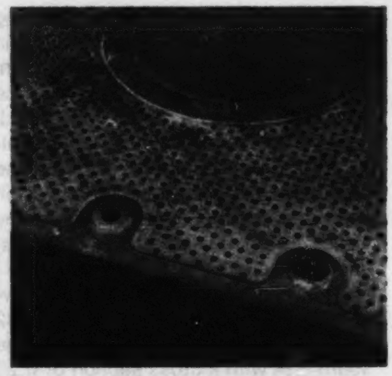

Figure 2. This **Perforated Heat Exchanger** was assembled, using alumina paper as a barrier between the braze alloy and the heating platens of the vacuum-brazing press. Note the smooth fillets.

The alumina barrier is especially useful in brazing parts with perforated or otherwise irregular surfaces, since it prevents the brazing alloy from extruding through the perforations and contacting the platens of the brazing press. Unlike other common barrier materials (various powders and solids), the alumina paper does not disintegrate in the press. Because the paper does not outgas, there is no contamination of the braze alloy, ensuring a uniform reliable joint without voids. As seen in the section of stainless-steel heat exchanger shown in Figure 2, the paper helps to form a smoothly-contoured regular fillet at the edges of the brazed pieces. On the heat exchanger, used on the vertical stabilizer of the Space Shuttle, the brazing was so successful it eliminated the need for a 130-inch (3.3-meter) peripheral closeout weld.

This work was done by Charles S. Beuyukian of Rockwell International Corp. for **Johnson Space Center.** *No further documentation is available.*
MSC-18528

Connector Heat Shield

Polytetrafluoroethylene protects coated electrical connectors during soldering.

Lyndon B. Johnson Space Center, Houston, Texas

The use of heat sinks and shields to protect electronic components during soldering is widely known. Often overlooked, however, is the susceptibility of plated electrical connectors to heat blistering. A blistered connector secured in place with epoxy potting will eventually corrode, requiring replacement. The cost of this relatively simple problem can be substantial, once the circuit is in operation.

The connectors can be protected against heat damage by wrapping them with polytetrafluoroethylene tape (e.g., Mystik Tape No. 7503 or equivalent) before soldering. The tape can be removed easily after the contacts are joined.

This method was used in soldering connectors to stainless-steel solenoid housings. Earlier, a polytetrafluoroethylene coating was used as the protection. However, this coating is difficult to remove after soldering.

This work was done by Shirley Clarke of Wright Components, Inc., for **Johnson Space Center.** *No further documentation is available.*
MSC-16282

Foam-Filled Cushions for Sliding Trays

Tubular dampers absorb vibrations.

Lyndon B. Johnson Space Center, Houston, Texas

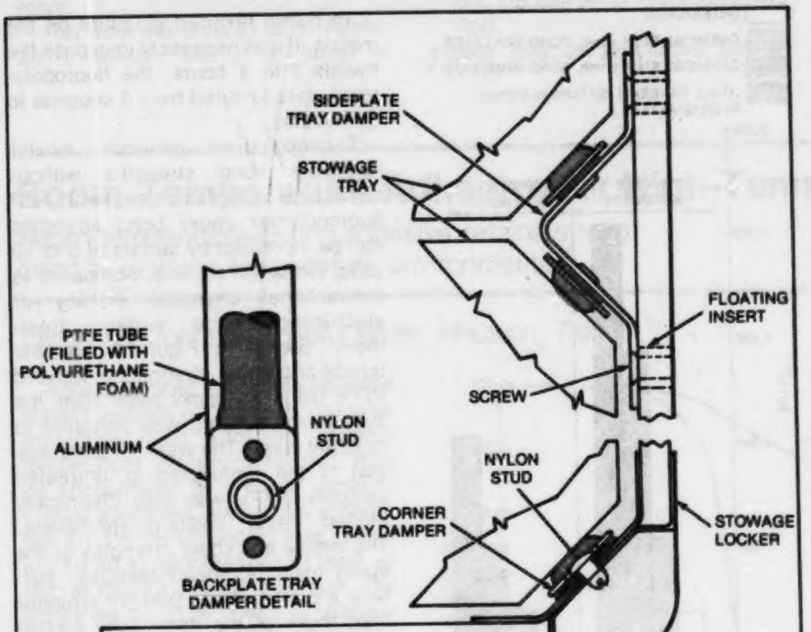
SIDEPLATE TRAY DAMPER
STOWAGE TRAY
FLOATING INSERT
PTFE TUBE (FILLED WITH POLYURETHANE FOAM)
SCREW
NYLON STUD
ALUMINUM
NYLON STUD
CORNER TRAY DAMPER
STOWAGE LOCKER
BACKPLATE TRAY DAMPER DETAIL
LOCKER END DETAIL
STOWAGE TRAY DAMPERS
STOWAGE LOCKER

Foam-Filled PTFE Tubes are fastened to the inside of stowage lockers by snap-in nylon studs. The configuration shown accommodates two stowage trays. With the sideplate dampers removed, the locker can accommodate one double-sized stowage tray. The PTFE tubes used for stowage trays on the Space Shuttle are 0.375 in. (0.95 cm) in diameter.

The cushioning of polyurethane foam and the durability of PTFE are combined in vibration dampers for sliding trays aboard the Space Shuttle. Consisting of polyurethane foam inside a PTFE tube, the dampers are fastened to the inside of modular "lockers" that hold the plastic trays. Each foam-filled tube offers a low-friction sliding surface that cushions vibrations, absorbs misalinements and manufacturing tolerances, and prevents accidental movement of the tray during normal crew operations. Possible uses for the dampers are in the packaging of components for shipping and in doors for lockers, refrigerators, automobiles, and other vehicles.

As shown in the figure, the PTFE tubes containing polyurethane foam are fastened to an aluminum strip prior to their installation in the lockers. The dampers are held in place by snap-in nylon studs, which permit easy installation.

This work was done by Samuel B. Nahin and Paula H. Robb of Rockwell International Corp. for ***Johnson Space Center.*** *No further documentation is available.*
MSC-18565

Ion-Beam Etching Enhances Adhesive Bonding

Ion-beam etching is superior to chemical etching for both metals and plastics.

Lewis Research Center, Cleveland, Ohio

Electron bombardment by an argon ion-beam source was used to etch various metals and fluoropolymers, which were then adhesively joined to themselves. Bond-strength tests on the fluoropolymers showed that there was a substantial improvement in bond strength over current state-of-the-art chemical-etching techniques. Two of the metals also showed substantial bond-strength improvement over untextured metals.

The materials tested were: fluorinated ethylene propylene (FEP), polytetrafluoroethylene (PTFE), perfluoroalkoxy (PFA), and polychlorotrifluoroethylene (CTFE), graphite, nickel, titanium, and type 304 stainless steel.

The metals and fluoropolymers were exposed to Ar ions of 0.5 to 1.0 keV at ion current densities of 0.2 to 1.5 mA/cm^2 for various exposure times. The resulting surface texture is in the form of needles or spires with vertical dimensions that may range from tenths to hundreds of micrometers, depending on the selection of beam energy, ion current density, and etch time. The bonding of textured surfaces was accomplished by ion-beam texturing mating pieces of either metals or fluoropolymers and applying a bonding agent, which flows around the microscopic conelike structures.

The 30-cm ion source used was developed from electric propulsion technology; it operates at beam energies between 300 and 1,500 eV. For the fluoropolymer samples, the source ion energy was 750 eV; for metal specimens, in the range 950 to 1,200 eV. The fluoropolymers and graphite samples were placed in a holder, and the surface to be textured was oriented normal to the ion beam 23 cm from the source-grid plane. The nickel, stainless-steel, and titanium samples were placed in the same position as the fluoropolymers with an additional tantalum target located above them at a 45° angle relative to the metals to provide seeding and sustain surface texturing.

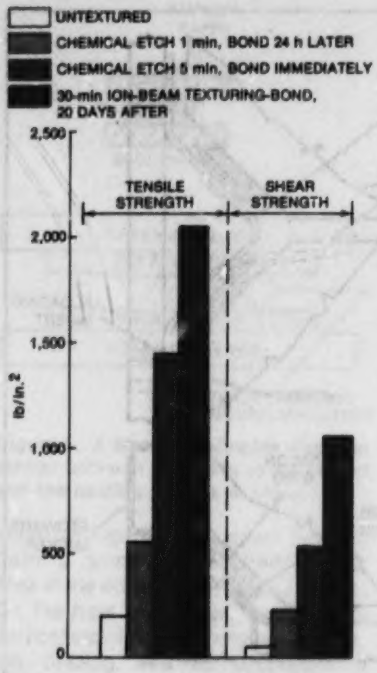

Figure 1. **Epoxy-Bonded PTFE has greater tensile and shear strengths after ion-beam texturing (the bulk tensile strength of PTFE is from 2,000 to 5,000 psi).**

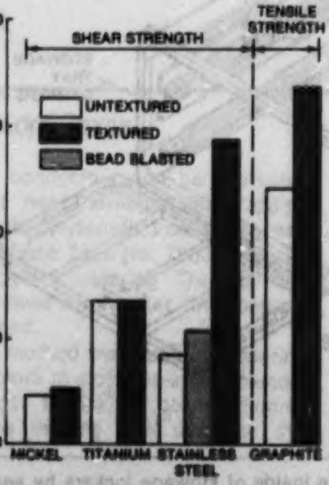

Figure 2. Epoxy-Bonded Metals and Graphite show, in some cases, greater tensile and shear strengths when textured by an ion beam.

To obtain textured structure on the metals, it was necessary to expose the metals 3 to 4 hours; the fluoropolymers were textured from 5 seconds to 30 minutes.

Fluoropolymers generally exhibit negligible bond strengths without some type of surface treatment. FEP fluoropolymer epoxy bond strengths can be increased by factors of 5 to 10 using ion-beam etching, compared to conventional chemical etching or electrical-discharge surface treatment. Shown in Figure 1 are the tensile and shear strengths of bonded PTFE using an epoxy resin after the surface for bonding was prepared in different ways. The weakest bond was that of the untextured or untreated samples. PTFE was also chemically etched using sodium/naphthalene. The tensile and shear strengths of the epoxy-resin ion-beam-textured surface are 46 and 100 percent stronger than those of the chemically etched surface. PTFE, FEP, and PFA exhibited about the same shear and tensile strengths when bonded with the epoxy resin. CTFE exhibited the highest bond strengths.

As shown in Figure 2, the shear strength of the textured stainless-steel bond improved by a factor of 3 over untextured stainless steel. Exposure to an ion beam did not texture nickel or titanium sufficiently to change the bond strength of these metals. Bond strength of carbon was helped only a little by ion-beam texturing.

Surface features similar to the polymers are also obtained by ion-beam texturing Kapton. Furthermore, all the fluoropolymers tested showed that ion-beam texturing produced bond strengths superior to those achieved with conventional surface treatments.

Chemically etched fluoropolymers must be bonded immediately after the surface treatment to attain maximum bond strength. Also, the chemical etchant residue must be thoroughly cleaned from the substrate to avoid a continuous deterioration of the bond, and environmental safeguards must be observed because of the deleterious effects of the chemicals used. The bond strength of ion-beam-etched fluoropolymers is not a function of shelf life; bonding may be done hours, days, or months after surface treatment.

This work was done by B. A. Banks, M. J. Mirtich, and J. S. Sovey of **Lewis Research Center.** *Further information may be found in:*

NASA TM-79004 [N79-12909/NSP], "Adhesive Bonding of Ion Beam Textured Metals and Fluoropolymers" [$4]; and

NASA TM-78888 [N78-24358/NSP], "Ion Beam Sputter Etching and Deposition of Fluoropolymers" [$4].

Copies may be purchased [prepayment required] from the National Technical Information Service, Springfield, Virginia 22161.

This invention is owned by NASA, and a patent application has been filed. Inquiries concerning nonexclusive or exclusive license for its commercial development should be addressed to the Patent Counsel, Lewis Research Center [see page A5]. Refer to LEW-13028.

Room-Temperature Adhesive for High-Temperature Use

Room-temperature-curing adhesive retains strong bond in extreme temperature environments.

Lyndon B. Johnson Space Center, Houston, Texas

Adhesives used in bonding reusable surface-insulation tiles to metallic substrates must withstand extreme temperature environments that may be encountered by the tile surface. Typical adhesives used in this application are the thermosetting type, which are cured at temperatures at least as high as those expected in service, and adhesives cured by chemical reaction in controlled humidity. One chemically curing adhesive requires careful weighing and thorough mixing of catalyst for proper cure. Its service temperature range is between -170° F (-113° C) to 500° F (262° C).

A significant improvement is obtained with polyphenylquinoxaline (PPQ). PPQ cures at room temperatures and withstands temperature extremes between -300° F (-186° C) and 750° F (402° C). Laboratory studies have shown that PPQ used with chloroform as solvent produces the best bond capable of withstanding both mechanical and thermal stresses (see figure).

Basically the PPQ-chloroform solution is sprayed or brushed onto a precleaned metal substrate. The other adherent, typically a porous material to permit quick solvent evaporation, is brought into contact with the PPQ film. The solvent is then allowed to evaporate at room temperature, leaving a strong bond. Evaporation of the solvent may be speeded up by the application of vacuum and/or elevated temperature.

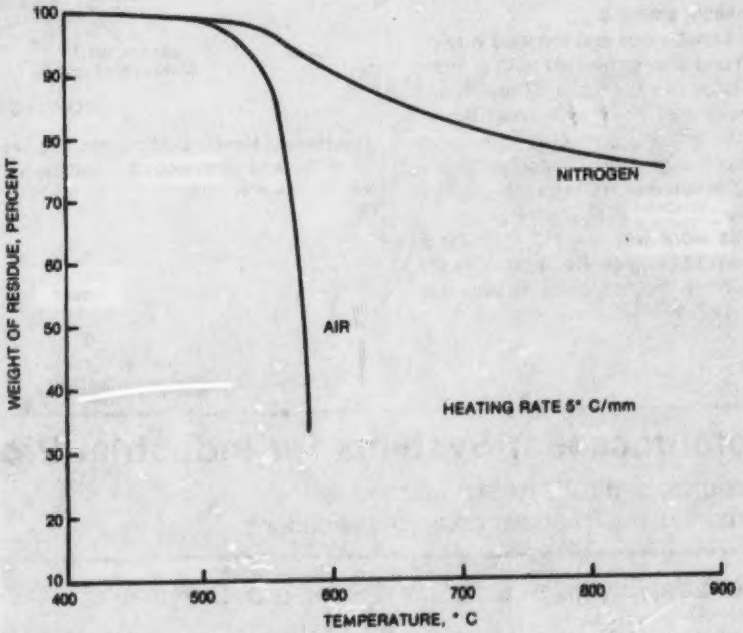

Excellent Thermal Stability of PPQ is demonstrated by thermogravimetric analysis as the polymer is heated. Decomposition in air or nitrogen does not begin until the temperature exceeds about 440° C.

This work was done by Jon L. Brooks, William L. Hill, and Charles R. Rousseau of Rockwell International Corp. for **Johnson Space Center.** *For further information, Circle 75 on the TSP Request Card.*
MSC-16930

Easily-Assembled Helical Heater

A rugged, compact coil heater

Langley Research Center, Hampton, Virginia

A rugged, low-current heater is assembled from readily available materials. The helical heater element is Inconel (or equivalent alloy) 0.004 in. (0.1 mm) in diameter with a resistance of 38 ohms per foot (125 ohms per meter). In a design for heating biological samples on the Viking lander, the total coil resistance is 195 ± 10 ohms, and the inner diameter of the coil is only 0.015 in. (0.38 mm).

Each end of the helical coil passes through a ceramic spool (see figure). The coil and spools are covered with 0.045-in. (1.14-mm) clear PTFE heat-shrinkable sleeving.

The heater coil and the lead wire on each end are terminated with a crimp clip made of steel tubing. The coil and the wire are joined with silver braze, and the splice is protected with epoxy adhesive or silicon elastomer before being covered with the crimp clip and sleeve.

This work was done by Donald E. Pizzeck of **Langley Research Center.** *No further documentation is available. LAR-11712*

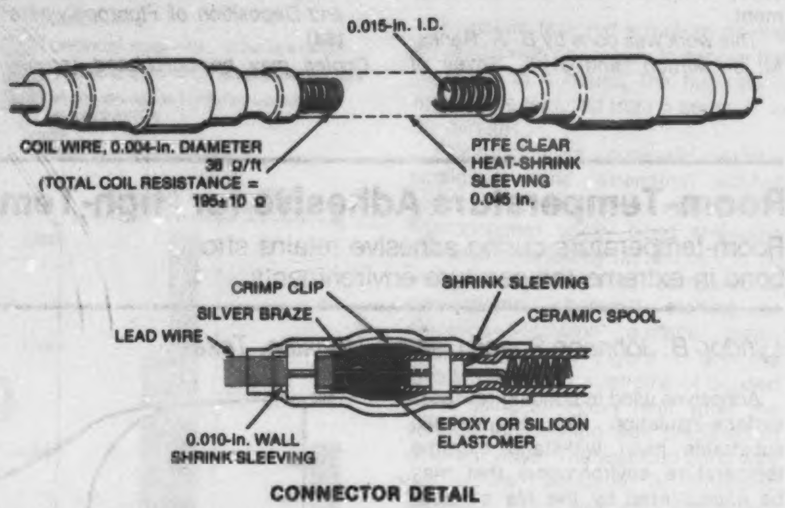

The **Helical Heater Coil** passes through a ceramic spool at each end. Silver braze joins the lead wires and coil, and the splices are covered with epoxy, a crimp sleeve, and shrink sleeving.

Microprocessor Systems for Industrial-Process Control

Spacecraft control systems as models for future industrial-process control applications.

NASA's Jet Propulsion Laboratory, Pasadena, California

Several promising spacecraft control systems are possible models for future industrial-process controls. Two versions have been examined: One uses minicomputers, and the other uses microprocessors. Both systems utilize distributed microprocessor architecture characterized by a number of microprocessors that are each dedicated to one subsystem. Each microprocessor (or minicomputer) is structured to control sensors and actuators of the subsystem, to collect data, and to maintain synchronization. This approach might be adapted for controlling complex packaging machinery, a steel-rolling plant, an automobile assembly line, and similar processes.

The first example, The Unified Data System (UDS), is an experimental breadboard system equipped with six minicomputers. Each minicomputer has 8,192 16-bit words and an average execution time of about 2.5 μs. It includes a ground computer with a CRT (cathode-ray-tube) display and, on the spacecraft, a processor that exerts overall spacecraft mission control. A format processor collects telemetry data in fixed-length blocks from other processors and moves the data to a modulation/demodulation subsystem computer. Another processor controls a television camera, and a data-storage subsystem computer controls a tape recorder.

The computers operate synchronously and are all interconnected with a set of three independent data buses. Each bus can transfer data at 1 megabit per second. The ground, command, and format processors are each equipped with a bus control and constitute the so-called "high-level modules." The others without the bus controllers constitute "terminal modules."

The UDS is synchronized using a single interrupt that occurs simultaneously on all processors every 2.5 ms. During the interrupt, each processor examines a list of things to be done during that interval. Any function is performed in a small fraction of the interval.

The system timing is obtained from its TV camera operation as reference. A special UDS design language is used in conjunction with the camera signals to control the timing.

A second example currently under development will be based on commercially available microprocessors with an 8-bit capacity using a different bus arrangement also capable of transferring data at 1-MHz rates in packets of up to 32 words (32-bit words) in length. This version will use a modified software arrangement permitting several programs to be operated concurrently in a single microprocessor.

This work was done by Fred H. Lesh of Caltech for **NASA's Jet Propulsion Laboratory.** *For further information, Circle 76 on the TSP Request Card.*
NPO-14661

Wire Harness Twisting Aid

Handtool and spacers separate and control the wires as they are twisted into a harness.

Lyndon B. Johnson Space Center, Houston, Texas

Long wire bundles are twisted into uniform spiral harnesses by the apparatus shown in the figure. The twisting aid uses a hand-held sliding tool, spacers, control tubes, a wire plate, and a slow-turning bench motor to twist a group of wires into a tight spiral harness. The handtool and spacers separate the wires as they are twisted by the bench motor.

To make a harness, individual wires are fed through the tubes and spacers, which are secured with tape to a table. They are then fed through the hand-held sliding tool and secured at the wire plate to the motor.

The sliding tool is held firmly and pulled along the wires away from the motor. This generates smooth twists in the wires between the motor and the sliding tool. As the spiral length increases, the operator continues to move the sliding tool away from the motor. One at a time the individual spacers are encountered and pushed toward the end of the wires. The sliding tool will be the last member off the wire bundle when the entire length of wires is smoothly twisted.

Besides reducing cost and improving the appearance of the harness, the technique produces wire harnesses that generate less radio-frequency interference when conducting current than do irregularly twisted cables. The tooling aid is ideal for prototype work and low-production runs.

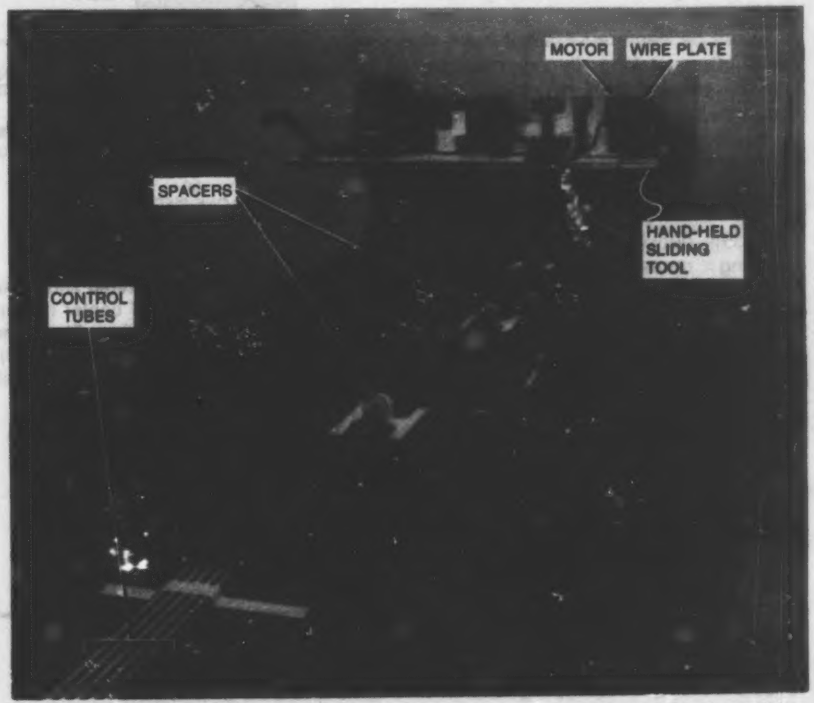

The Hand-Held Sliding Tool, spacers, and control tubes separate the wires while they are twisted by a bench motor into a harness. Smooth twists are generated between the motor and sliding tool by pulling the tool along the wires and away from the motor.

This work was done by Emil J. Casey, Curtis C. Commadore, and Mel E. Ingles of Rockwell International Corp. for **Johnson Space Center.** *No further documentation is available.*
MSC-18581

Adjustable Base for Centering Staked Bearings

A new base compensates for dimensional differences between the parts.

Lyndon B. Johnson Space Center, Houston, Texas

Bearings are normally staked into their housings with a conventional roller staking tool. As the tool is rotated around a flange on the race to stake the bearing, the bearing race and the housing are supported by a flat fixed locator base (see figure, left). For best results, the race must be centered with respect to the housing. If it is not, the misalined bearings are likely to fail under load.

Because slight dimensional differences in widths often occur between the housing and the bearing race during their manufacture, the bearings may not be centered if a flat base is used. One staking flange may be slightly smaller than the other; and when the roller swaging tool is applied to the longer flange, the race may be shifted off center, as in the figure, left.

A new adjustable base prevents that shift (see figure, right). The difference in widths between the race and the housing is measured and divided by 2. Part 1 of the base is then adjusted to support the race at the proper height so that it is staked on center with respect to the housing. The base is adjusted separately for each flange.

This work was done by Leo A. Berson of Rockwell International Corp. for **Johnson Space Center.** *No further documentation is available.*
MSC-19660

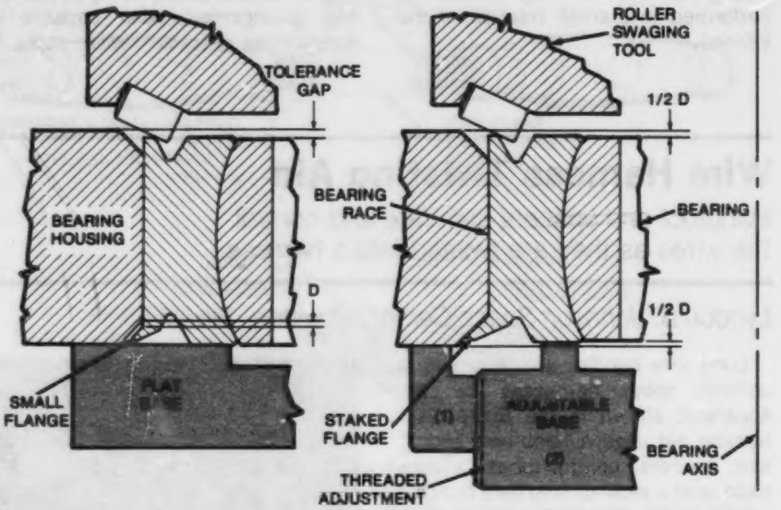

(a)
STANDARD ONE-PIECE BASE (NO EQUALIZATION FOR D, SMALL FLANGE SLIDES DOWN ON TURNOVER)

(b)
NEW ADJUSTABLE BASE (ADJUSTED TO EQUALIZE FOR 1/2 D, FULL FLANGE HELD TIGHT ON TURNOVER)

If the **Bearing Race Is Centered** and staked with the assistance of a flat base (left), the bearing may be set off center if there is a dimensional difference between the housing and the bearing race. The offset occurs when the roller swaging tool is applied to the top flange. The new adjustable base (right) prevents the shift by supporting the race and housing separately.

Safely Splicing Glass Optical Fibers

A fusion field-repair technique for use in flammable environment.

John F. Kennedy Space Center, Florida

A safer fusion splicing method for optical glass fibers can be used in explosive gas atmospheres. Splicing equipment is inside a box pressurized with inert-gas atmosphere. The method designed for fieldwork replaces earlier methods that use an unprotected electric arc not suitable for a flammable environment.

The new splicing apparatus includes:

a. V-groove vacuum chucks mounted on xyz micromanipulators for accurately positioning the fiber ends to be fused;
b. A high-voltage dc power supply to produce an arc between two tungsten electrodes for fusion of the butt-joint region of fibers;
c. A microscope to observe the joint alinement and fusion;
d. A means of monitoring optical transmission through the joint for

accurate fiber alinement before fusion; and

e. A gastight box containing inert gas under pressure and enclosing the electrodes, fiber holders, and micropositioners with feedthroughs for the electrical wiring and fibers.

A successfully-tested prototype unit uses a 0-to-10-kV dc power supply with current output from 0 to 20 mA. A 10X to 100X magnification microscope and high-resolution micropositioners are included. The fibers are fused in a 12- by 6- by 6-in. (30- by 15- by 15-cm) inert-gas box. Micromanipulator and other control knobs inside the box are projected into rubber sheaths, forming sealed, easily operated controls.

Other equipment necessary to produce a good splice joint includes: a fiber cutting tool, coating material, coating stripper (e.g., acetone), protective sleeve, vacuum pump, about 50 ft (15 m) of high-voltage power cable, an optical generator and receiver, a digital voltmeter, and lock-in amplifier.

About 2 ft (60 cm) of fiber ends are necessary for splicing. Typically, a single fiber is spliced. Typically, a single fiber is spliced at a time from a fiber-bundle tape. After the fibers are spliced, they are taken outside the box and laid on the splice housing one at a time until the entire bundle is finished. The spliced joints are tested with the optical transmitter and receiver for minimum optical energy loss across the joints.

This work was done by K. Korbelak of General Cable Corp. for **Kennedy Space Center.** *No further documentation is available.*
KSC-11107

Knife-Edge Seal for Vacuum Bagging

No adhesive, tape, or sealing groove is needed.

Marshall Space Flight Center, Alabama

In an improved clamping method for high-temperature vacuum bagging, a cam-actuated knife edge holds the perimeter of the film bag against a rubber cushion (see figure). This allows the bag to be quickly installed and removed, without using tape, adhesives, or tedious stripping procedures. Moreover, no permanent modifications to the aluminum baseplate are necessary, in contrast to a previous approach in which a sealing groove was machined in the aluminum surface.

To implement the method, which has been used for vacuum-bagging and cure cycles above 400° F (204° C), the rubber cushion is bonded to the baseplate with a high-temperature cement. The cushion is also a high-temperature-resistant material. The cam-actuated clamps are bolted to aluminum angle stock at approximately 22-in. (55-cm) intervals.

The sealing surface is a 0.005-in. (0.013-cm) knife edge that is machined on the vertical side of the angle stock. After the vacuum-bagging sheet is spread over the work with its edges draped over the rubber cushion, the clamps are used to force the knife edge against the bag and the cushion. This creates a tight seal that is effective at high temperatures.

This work was done by Joseph A. Rauschl of Rockwell International Corp. for **Marshall Space Flight Center.** *No further documentation is available.*
MFS-24049

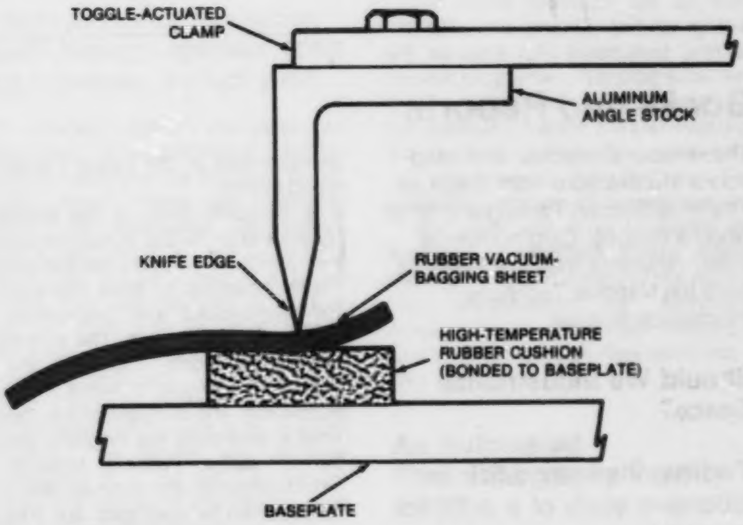
TOGGLE-ACTUATED CLAMP
ALUMINUM ANGLE STOCK
KNIFE EDGE
RUBBER VACUUM-BAGGING SHEET
HIGH-TEMPERATURE RUBBER CUSHION (BONDED TO BASEPLATE)
BASEPLATE

A Tight Seal is formed by clamping a vacuum-bagging sheet between a knife edge and a rubber cushion. Several cam-actuated clamps are spaced along the periphery of the sheet.

A Precoat Prevents Ceramic Stopoffs From Spalling

Nickel-alloy precoat secures ceramic stopoff to the metal surface.

Marshall Space Flight Center, Alabama

Ceramic stopoff materials, such as zirconium oxide, aluminum oxide, and boron nitride, are used to protect areas from unintentional brazing. However, if applied directly to the metal surface, these materials tend to spall during the brazing process. The problem is easily corrected using a nickel-alloy precoat (e.g., Nichrome or Inconel X, or equivalent) before the ceramic is applied. The precoat improves the ceramic adhesion and makes the ceramic more tolerant to any deformation.

The precoat is applied with a plasma gun. The prepared metal surface is sprayed with the alloy to a film thickness of 0.002 to 0.003 in. (0.05 to 0.08 mm). The covered surface is then coated with the ceramic, using the same procedure. The thickness (same as the precoat) of the ceramic coat and its texture can be varied to accommodate heavy tooling by changing the mesh size of the precoat.

Before the precoat, the metal surface is usually grit-blasted, which is the best and the cheapest method for most heavy-duty applications (e.g., in brazing machinery components). Fine aluminum oxide or silicon carbide can be used for light grit blasting. Furnace cleaning and abrasive cleaning can also be used to prepare the surface prior to plasma application. The coating easily adheres to an extremely-thin precoat sheet, as long as the sheet surface is oxide-free.

The stopoff coating does not interfere with the brazing process. When used in a vacuum, the coating does not contaminate the pumping system.

The process has been successfully used in brazing tubes inside the Space Shuttle main-engine nozzle. It is 100 percent reliable and totally controllable. The ceramics are more durable stopoffs than the conventional cloth-type materials.

This work was done by Alex Brennan of Rockwell International Corp. for **Marshall Space Flight Center.** *No further documentation is available.*
MFS-19495

Books and Reports

These reports, studies, and handbooks are available from NASA as Technical Support Packages (TSP's) when a Request Card number is cited; otherwise they are available from the National Technical Information Service.

Should We Industrialize Space?

Two reports summarize an extensive study of a complex question.

Whether or not to make a commitment to space industrialization is a question enmeshed with complex social, economic, and political issues. Space offers the possibility for benefits in the areas of energy, resources, services, and human activity; but the costs are large, and the risks, as with any venture into the unknown, are substantial. Since much of the reward would not be realized for several years, even if a program is immediately initiated, the issue is further complicated by uncertainties in the future course of world events.

A 20-month study of this question, sponsored by NASA, is summarized in two companion reports that can help to clarify the issues for those interested in the implications and possibilities of space industrialization. The effects of diminishing world resources and of expected changes in world markets, population, and technology are considered in assessing the industrial potential of space. Possible benefits of industrialization are outlined, and specific hardware concepts are treated along with cost estimates. A section of one report deals with possible legal implications.

In general, the reports try to project world needs over the next 30 to 50 years (with admitted uncertainty) and to correlate them with space opportunities. The opportunities are broken down into the broad categories of *services*, *products*, *energy*, and *human activities*. Each category is subdivided into numerous specific examples. Among over 100 *service* opportunities are:

- electronic mail,
- personal "wrist radio,"
- disaster warning relay,
- nuclear fuel locator, and
- forest-fire detection.

Products opportunities include:

- isoenzyme production in zero gravity,
- radioisotope separation,
- materials processing, and
- integrated-circuit manufacturing.

Opportunities in the *energy* area include:

- solar/electrical conversion,
- fusion,
- nuclear waste disposal, and
- night illumination for special applications.

In the area of *human activities*, space industrialization offers a diversity of new careers and new challenges, and space colonization is a possibility intimately linked with space industrialization.

This work was done by G. W. Driggers of Science Applications, Inc., and C. L. Gould of Rockwell International Corp. for **Marshall Space Flight Center.** *To obtain copies of the reports, "Space Industrialization," Circle 77 on the TSP Request Card.*
MFS-23963

Cost Models and Economical Packaging of LSI's

New developments in cost modeling and packaging hybrid microcircuits

A report, an extension of an earlier study [see "Cost Savings in LSI Fabrication" (MFS-25079) on page 580 of *NASA Tech Briefs*, Vol. 4, No. 4], presents recent developments in cost modeling and economical packaging of LSI hybrid microcircuits. The mathematical cost models that were developed for hybrid microelectronic subsystems have been refined and expanded. Improvements have also been made in the tape chip carrier (TCC) technology — a promising low-cost technique for packaging the LSI chips.

The report discusses the mathematical cost models that will be used in estimating the costs of developing and fabricating the microcircuits. Earlier models have been expanded to include rework terms related to substrate fabrication, nonrecurring developmental and manufacturing operations, and prototype production. Sample computer programs have been written to demonstrate how these cost models are applied. The programs will analyze the total development and manufacturing costs, calculate the cost variations when nonconventional technologies, such as TCC; become more widely used, and examine the behavior of the cost functions relative to the production volume.

These modeling techniques were also expanded to evaluate the total manufacturing costs of fully-assembled printed-wiring boards (PWB's). This is an important step leading to models that will handle a large variety of electronic technologies and yield comparative costs of the various development and manufacturing approaches. The models will not only indicate cost reductions but will clearly identify areas requiring technological improvements to reduce the costs.

The second part of the report discusses the development of LSI packaging utilizing the TCC technology, particularly in the areas of tape processing, wafer bumping, and inner/outer lead bonding. One section is devoted to studies and laboratory efforts to show the feasibility of interconnecting the LSI chips using the TCC and semiautomatic wire-bonding technology.

The report includes a number of cost plots and hardware illustrations. The appendix sections include references and sample program runs.

This work was done by R. P. Himmel, R. G. Ravetti, C. W. Rothrock, S. M. Stuhlbarg, and P. J. Zulueta of Hughes Aircraft Co. for **Marshall Space Flight Center.** *To obtain a copy of the report, "Design, Processing and Testing of LSI Arrays Hybrid Microelectronics Task," Circle 78 on the TSP Request Card.*
MFS-25359

Automated Ion Implantation for IC's

A semiconductor fabrication facility reduces operator costs and increases product yield.

A 24-page report discusses an automated ion-implantation facility being developed at the Marshall Space Flight Center. [Also see following article "An Automated Photolithography Facility for IC's" (MFS-25073).] This facility will be a part of a larger system that will process IC's from start to finish with minimal human intervention. The chips will be transported automatically from one processing station to another, eliminating the damage that occurs from manual handling. The facility will produce ultrareliable IC's that will function for 25 years or longer in spaceflights and other critical applications.

The facility will use four types of carriers according to the processing function: (a) an aluminum carrier designed for all regular IC operations, (b) a polypropylene carrier for processing in chemical solutions and caustic agents, (c) quartz boats for processing IC's in high-temperature environments, and (d) an interface for the other three to flip-transfer the wafer loads from one carrier type to another.

The facility will incorporate a commercially-available ion implanter modified for loading and unloading with an air-track input and output, respectively. Its continuously-variable energy output of 20 to 200 keV can generate ion-beam currents in excess of 40 μA using boron, phosphorus, or arsenic.

A 200-keV accelerator will be used. Its power supply will operate the cold-cathode ion source and also will include provision for operating optional hot-cathode and RF ion sources.

Three complete gas-handling systems will be used to supply dry nitrogen for backfilling the implantation chamber and system, dry air for operating electropneumatic valves, and liquid nitrogen as a cold trap for a high-speed oil-diffusion pump. The implanter will be furnished with two identical oil-diffusion pumping systems. These will control the electropneumatic valves and maintain the necessary vacuum and venting during the process cycles.

The entire operation will be controlled from a console, and the system will be more fully automated with an implant programer. The programer will receive command signals to interrupt the beam and initiate a wafer-indexing function until all the wafers receive the ion dose preset in the integrator. The integrator will have 15 current ranges.

This work was done by Bobby W. Kennedy of **Marshall Space Flight Center.** *To obtain a copy of the report, "Ion Implantation for Automatic Processing of Integrated Circuits," Circle 79 on the TSP Request Card.*
MFS-25193

An Automated Photolithography Facility for IC's

A facility for fully automated production of IC's

A 35-page report discusses various subsystems that will constitute a new fully-automated photolithography facility for the processing of IC's. [Also see preceding article "Automated Ion Implantation for IC's" (MFS-25193).] This facility being developed at the

(continued on next page)

Marshall Space Flight Center will be a part of a larger system that will process the IC's from start to finish with minimal human intervention. A number of carriers will be used to transport the chips from one station to another, eliminating the damage that occurs from manual handling. The facility will produce ultrareliable IC's that will last 25 years or longer in spaceflights and other critical applications.

The reported facility consists of an automatic scrubber, photoresist coater and developer, mask aliner, IR (infrared) bake, and inspection stations. The heart of the facility is the wafer carrier system. Four distinct carriers are utilized, depending on the nature of wafer processing. There is a standard aluminum carrier for all regular operations, a polypropylene carrier for areas with chemical solutions and caustic agents, quartz boats for high-temperature environments, and an inverting carrier for flip-transferring the wafers from one carrier system to another. Each carrier can handle 25 wafers at a time, the wafer diameter being 3 in. (7.5 cm).

An automatic in-line scrubber cleans the wafers with high-speed brush and solvent prior to other processing. This program-controlled station scrubs the wafers without creating mechanical stresses.

A single-head photoresist-coater and developer station is program-controlled and may include nitrogen purge, a spray wash, spin drying, precoating, and photoresist coating in its photoresist-coating cycle. A develop cycle may include various solvent washes and developer rinses with spin drying.

The automatic mask-aliner station alines the mask with the wafers using an optical-scanning computer control. The alined wafers are exposed to ultraviolet light for printing the pattern on the wafers and are then fed to the developer station.

The hard-bake IR station processes the coated wafers in 1 to 4 min and in 4 to 7 min after developing. The station includes a nitrogen purge available from two built-in nozzles.

The inspection station equipped with a micromanipulator includes a microscope to examine the wafers under low and high magnifications. A pantograph with template is also available for quick inspection. Acceptable wafers are returned to the wafer carrier by foot-switch command, while the rejects are sent to a holding position.

The report includes a number of illustrations showing various optical schemes for detecting and alining the chips. Photographs of the facility are also included.

This work was done by Bobby W. Kennedy of **Marshall Space Flight Center.** *To obtain a copy of the report, "Photolithography for Automatic Processing of Integrated Circuits," Circle 80 on the TSP Request Card.*
MFS-25073

Models of MOS and SOS Devices

A report on progress in the processing of metal-oxide-semiconductor and silicon-on-sapphire IC's

A quarterly report on trends and techniques for space-base electronics describes progress in three programs:

1. The development of a dc sputtering machine for aluminum and aluminum alloys,
2. The development of two-dimensional computer models of metal-oxide-semiconductor (MOS) transistors, and
3. The development of a computer program for calculating the redistribution diffusion of dopants in silicon-on-sapphire (SOS) films.

The sputtering machine can accommodate eight wafers for aluminum deposition. It rotates the wafers through three sputter-gun positions and two mask positions. The sputtering chamber opens into a clean bench located in a clean room.

The finite-element method of analysis was investigated as a means of modeling MOS transistors. Although the finite-element method is reportedly convenient in treating nonrectangular geometries and irregular boundaries, it produced disappointing results in the study; its accuracy was no better than that of the finite-difference method.

An MOS algorithm has been developed on the assumption that mobile carriers are included in an infinitesimally thin layer of charge at the silicon/silicon dioxide interface. The algorithm proceeds in an iterative fashion to solve simultaneously a one-dimensional current equation and Poisson's equation. The solution yields the potential distribution from which current is calculated as a function of the gate, drain, and body voltages.

The MOS model as it stands neglects generation/recombination mechanisms and therefore cannot treat impact-avalanche and bulk-generated leakage currents. However, it is likely that such effects can be treated by adding another iterative loop to the algorithm.

The SOS redistribution diffusion computer program is intended to produce curves showing the effects of diffusion time and temperature on junction depth, sheet resistance, and integrated ion-implanted impurity dose. These data have been generated for boron and phosphorus redistribution in nitrogen, dry oxygen, and steam ambients for SOS films in ⟨111⟩ crystal orientation. (The report furnishes the data in an appendix.)

The program contains three basic mathematical models: (1) an implantation profile, (2) an oxidation model, and (3) a diffusivity model. It was developed to account for both thin and thick oxides, but at present is limited to thin oxides because the simulation of both thick and thin oxides requires that a warped grid system be incorporated in the program — a modification that would demand considerable additional effort.

This work was done by J. D. Gassaway, Q. Mahmood, and J. D. Trotter of Mississippi State University for **Marshall Space Flight Center.** *To obtain a copy of the report, "Trends and Techniques for Space Base Electronics," Circle 81 on the TSP Request Card.*
MFS-25153

Mathematics and Information Sciences

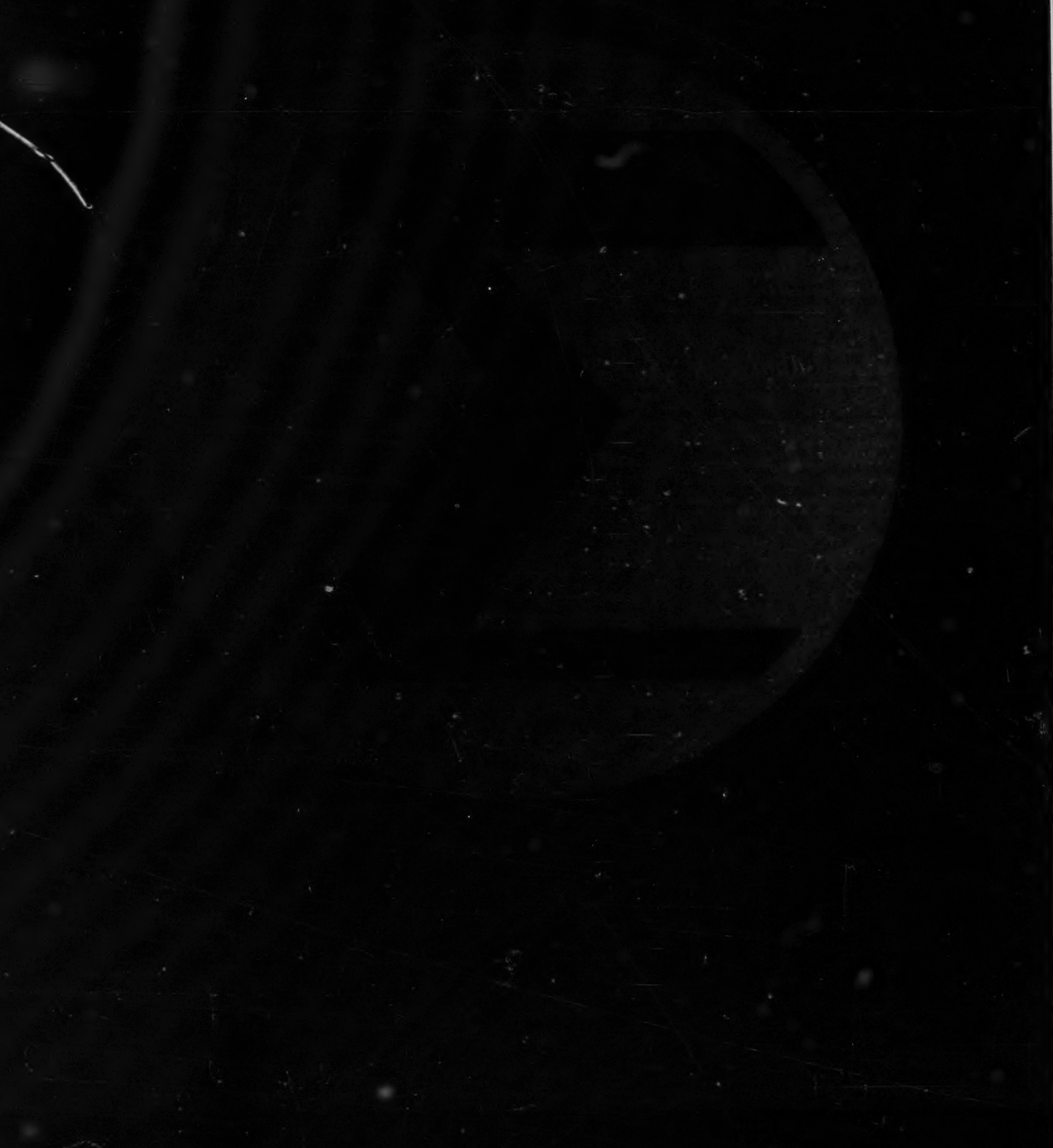

Hardware, Techniques, and Processes

119 Efficient Telemetry Format

Computer Programs

119 User's Guide to SFTRAN
120 Goddard Mission Analysis System
121 Software Design and Documentation Language
121 Estimation of Incomplete Multinomial Data
121 Automated Flow-Chart System
122 Systems Improved Numerical Differencing Analyzer

Efficient Telemetry Format

A proposed format promises to simplify ground processing of spacecraft data.

NASA's Jet Propulsion Laboratory, Pasadena, California

A recently-proposed telemetry format can organize spacecraft data from various sources into autonomous blocks. Each block would begin with a standard synchronization code, and contain a block-type identification, measurement-time information, and a data set from a particular source. Because all the blocks would be autonomous and would contain all the information needed for processing and routing, the processing at the receiving end (ground station) would be less complicated than in a time-multiplexed system. Thus, the complexity and cost of ground processing equipment could be reduced.

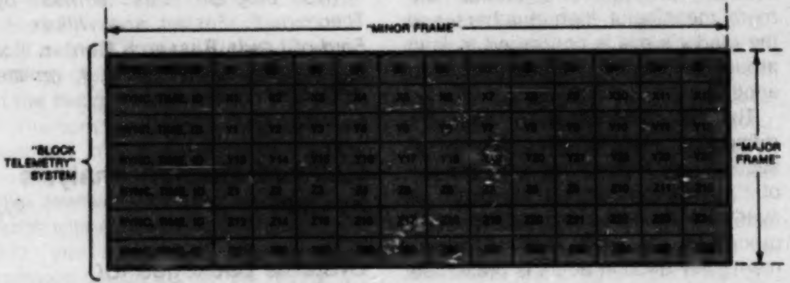

A Proposed Telemetry Data Format organizes data from various sources into autonomous blocks. Four spacecraft data sources are represented here by E, x, y, and z. In the "blocked" system, only one or several minor frames must be received, depending on the set, to reconstruct the data set. This approach is less error-prone and is more compatible with the packet-organized ground systems than the currently-used time-multiplexed transmission format.

In the new format, complete data sets from each source are assembled into autonomous blocks via onboard buffering. The telemetry formats are assembled by sequentially transmitting the blocks from each source, and data mode changes are accommodated by changing the order or frequency of transmission of the block stream. Because of the standard-length blocks, much of the data can be edited, and format changes become readily apparent. Any errors in the transmission block would affect only one source. In effect the data are preprocessed, simplifying the function of the central processing computer to determine the received-block type and process the data set as a batch.

The proposed format is illustrated using simple data sources E, x, y, and z representing, for example, spacecraft engineering data, scatterometer data, microwave radiometer data, and altimeter data, respectively. For each source, the data samples (E1 through E6, x1 through x12, etc.) are assumed to define completely the output of that source for one cycle of its operation.

In a "blocked" system, as shown, each minor frame is devoted to data from one specific source; some onboard source buffering is thus implied. The minor frame contains all or part of the data set. In order to reconstruct the set, it is only necessary to receive one E, x, two y, or three z minor frames. A missing minor frame creates an error in one set of source data only, whereas in a conventional system, all sets would be disrupted.

This work was done by Edward Greenberg and Adrian J. Hooke of Caltech for **NASA's Jet Propulsion Laboratory.** *For further information, Circle 82 on the TSP Request Card. NPO-13679*

Computer Programs

These programs may be obtained at very reasonable cost from COSMIC, a facility sponsored by NASA to make new programs available to the public. For information on program price, size, and availability, circle the reference letter on the COSMIC Request Card in this issue.

User's Guide to SFTRAN

Programing language has been expanded and improved.

SFTRAN, a structured-programing language, has been given additional language features, has had some operating limitations removed, and has been designed to run more efficiently. In addition, the concepts of modularity and top-down development have been extended to the area of task management, and a set of command-level procedures has been provided for this purpose. Thus, the programer is able to select one of several jobs, and one of several parts of that job, and to invoke one of several operations to be performed on that part. This is done by simple brief statements, freeing the programer of bothersome details of an operational nature in order to concentrate his attention on those areas where his skill and effort are of a maximum benefit.

SFTRAN (Structured FORTRAN) is a programing language combining the two principles of "GO-TO-less" programing and stepwise refinement. A more appropriate description of "GO-TO-less" programing might be "avoidance of numbered statements." When

(continued on next page)

this concept is employed, program flow is controlled by constructs, or structures, that imply a certain flowchart function; the name given each construct is selected to be suggestive of its function. A principal benefit of "GO-TO-less" programing is that the resulting code is easier to read because the structure names are more meaningful than numbers and the reader's eye is not forced to leap around the page or from one page to another.

The second principle of stepwise refinement involves the process of successively refining one's description of the solution method in terms of evermore primitive components or processes. At each level of refinement, only enough detail is presented to make the method clear. Anything of a complicated nature is merely referred to, with its precise definition postponed until later. Sometimes called top-down programing, this technique is another that results in an easier-to-read code. Only a few ideas need be kept in mind at each level of description; and the important ones can be put first, at the top, where they belong.

The combined techniques have more to offer than merely good readability. They also provide a natural sequence of steps to be taken in the programing process and replace much of the *art* of programing with a methodology that is easy for the novice to learn and very efficient in the hands of the experienced. In addition, a high degree of program modularity is obtained, which means the code produced can be easily changed, extended, or adapted for other uses.

SFTRAN was created by John T. Flynn (NASA's Jet Propulsion Laboratory, Pasadena, California) for the specific purpose of providing a language suitable for structured programing. Flynn's implementation of an SFTRAN language was a precompiler that translated from SFTRAN to FORTRAN. This permitted a great degree of simplification in the precompiler program, as it only had to recognize the few special structures that control program flow. Also, by translating to FORTRAN, the benefits of program portability were automatically obtained. The new SFTRAN precompiler retains all of Flynn's original structures in addition to the improvements described above.

This program is written in SFTRAN for use on the UNIVAC 1100 computer and is also written in SFTRAN for use on the IBM 360 computer (reference LEW-13165).

This program was written by Theodore E. Fessler and William F. Ford of **Lewis Research Center.** *For further information, Circle P on the COSMIC Request Card.*
LEW-13172

Goddard Mission Analysis System

Systems packages for controlling many dynamic modules

In conventional mission analysis systems, requirements to meet varying user demands have been met by developing large, cumbersome systems encompassing many options or by developing many small, individually tailored systems that require significant setup and deck-handling time between runs. The Goddard Mission Analysis System (GMAS) is a collection of software modules that can be readily configured by the user to solve a wide variety of specific mission analysis problems.

The setup time and machine resources required to analyze a particular problem are greatly decreased through the dynamic-execution-time loading of modules in a user-specified sequence. The GMAS design is based on the philosophy that multiple options and variably-sized data areas can be most effectively provided through dynamic allocation, rather than through a planned overlay structure. The user can command the full potential of the GMAS with a simple control language, similar to a programing language, that defines data and controls the order in which load modules are executed.

The GMAS includes modules for performing a large selection of standard mission analysis procedures. One may modify existing modules or add new modules to enhance the abilities of GMAS without modifying the GMAS control structure because the load modules are identified through the input control language. The GMAS could also be used to control the processing of user-supplied modules that are not necessarily mission analysis oriented.

The major components of GMAS are the executive and the dynamic load modules and the dynamic arrays. The GMAS executive is primarily responsible for interpretation of user-control directives and data management. The executive passes control to user-designated utility load modules after having prepared user-specified and default data for the utilities. The executive also controls the dynamic assignment and release of core space for user-specified modules and data areas.

The dynamic load modules represent the applications software to be used in specific problem solutions. They may consist of the GMAS library of standard routines along with user-developed libraries of routines. Each dynamic load module is a separate group of subroutines that, when loading during GMAS execution, can be executed to solve part of the assigned problem and then be deleted from core. Dynamic-load-module input and output can be transferred through out-of-core files or through user-specified dynamic arrays located in a core area separate from the executive and any dynamic load modules. GMAS also contains a graphics executive system for providing interactive graphics in the form of tables, plots, and displayed messages for the IBM 2250, IBM 2260, and Anagraph 6600.

The GMAS is written in FORTRAN IV and Assembler for batch or interactive execution on an IBM 360-series computer system. The executive component, which is always resident in core, has a central memory requirement of approximately 220K of 8-bit bytes. The GMAS was developed in 1977.

This program was written by Francis E. McGarry of **Goddard Space Flight Center.** *For further information, Circle R on the COSMIC Request Card.*
GSC-12392

Software Design and Documentation Language

Processor and methodology for using structured programing

The Software Design and Documentation Language (SDDL) supports the design and documentation of complex software. It comprises (1) a design and documentation language for expressing design concepts, with forms and syntax that are simple, unrestrictive, and communicative; (2) a processor that can take design specifications written in this language and produce an intelligible, informative, and machine-reproducible documentation; and (3) a methodology for effectively using the language and processor to create well-structured, top-down programs and documentation.

The SDDL syntax is based on concepts of structured programing that have been expanded in scope to accommodate the communication requirements of software design. The SDDL syntax supports the top-down development of the design as a hierarchy of modules that specify the important concepts of the program. Each module represents a design abstraction and contains only as much detailed information as is needed to communicate its own intent and purpose. Lower level detail is represented by other modules; i.e., abstractions; and the interrelationships between the modules are expressed by module-invocation statements. The details of each module are expressed in terms of iterations, conditional branches, and sequences.

In addition to the syntax for specifying design concepts, SDDL also provides extensive controls over actions of the processor. These include the capability to add or delete any keywords used to express the concepts described above, to supply title pages, to control formatting (e.g., page width and length, indentation, page eject, page headings, line, and page numbering), and to specify the means by which identifiers and names in the document will be caught and cross-referenced.

The SDDL processor reformats and prints the design specifications with indentation, flow lines, and page reference numbers that provide a two-dimensional representation superior to flow charts. In addition the processor checks for logic errors and summarizes important design information as a Table of Contents, a Module Hierarchy report (i.e., "calls to" and "calls from"), or Cross-Reference Listings of identifiers and names used in the design.

The combination of a language that supports the expression of design concepts and a processor that supplies machine-reproducible documentation with enhanced information content makes iterative, incremental, software design a practical reality.

Documentation provided with SDDL contains an introduction to the concepts, a description of the syntax, and a methodology for effective use of language and processor. The SDDL processor is written in the SIMSCRIPT II.5 Programing Language and is currently implemented on UNIVAC, IBM, and CDC machines.

This program was written by Henry Kleine of Caltech for **NASA's Jet Propulsion Laboratory.** *For further information, Circle S on the COSMIC Request Card.*
NPO-14610

Estimation of Incomplete Multinomial Data

For classification of multinomial data when observations are incomplete

At times during the collection of multinomial data, an observation may be only partially classified. Each such partially classified observation is observed to fall in one of two or more selected categories but cannot be further classified into a single category. A computer program was developed to estimate the multinomial cell probabilities from such incomplete data.

The data are assumed to be randomly incomplete; the estimation criterion is the minimization of risk for quadratic loss. The estimators are the classical maximum-likelihood estimate, the Bayesian posterior mode, and an approximate Bayesian posterior mean. For both Bayesian estimators, the conjugate prior for the multinomial distribution (the Dirichlet) is assumed. The program performs Monte Carlo simulation studies on small- and medium-size samples to assess which estimate — the maximum-likelihood, posterior mode, or approximate posterior mean — best minimizes risk for specified values of the probability vector. For trinomial samples the program can also assess how well each of these functions approximates the exact posterior mean and how well a Taylor-series function approximates elements of the posterior covariance matrix. Various properties of the estimators can be evaluated. This program should prove useful in any project involving the collection of multinomial data where observations are sometimes incomplete.

This program is written in FORTRAN IV and Assembler for batch execution and has been implemented on the CDC CYBER 173 with a central memory requirement of approximately 112K (octal) of 60-bit words. This estimator program was documented in 1978.

This program was written by Karen R. Credeur of **Langley Research Center.** *For further information, Circle T on the COSMIC Request Card.*
LAR-12593

Automated Flow-Chart System

Accurate flow chart produced for FORTRAN programs

The TAMU Flow-Chart System will produce a flow chart of any program written in the FORTRAN language. With your program as input, TAMU generates, as line-printer output, a detailed representation of the action taken as each program statement is executed.

Each statement in a flow-charted program is displayed within a symbol that represents the program action during processing of the enclosed statement. Symbols available include: subroutine, function, and entry statements; arithmetic statements; input

(continued on next page)

and output statements; arithmetical and logical IF statements; subroutine calls with or without argument list returns; computed and assigned GO TO statements; DO statements; STOP and RETURN statements; and CONTINUE and ASSIGN statements. Comment cards within the source program may be suppressed or may be displayed and associated with a succeeding source statement. Each symbol is annotated with a label (if present in the source code), a block number, and the statement-sequence number. Program flow and options within the program are represented by line segments and direction indicators connecting symbols.

This program is written in COBOL for batch execution and has been implemented on an IBM 370-series computer with a central memory requirement of approximately 380K of 8-bit bytes. It was developed in 1977.

This program was written by William Woodford of **Goddard Space Flight Center.** *For further information, Circle U on the COSMIC Request Card.*
GSC-12514

Systems Improved Numerical Differencing Analyzer

SINDA program for CDC computers

The program SINDA (Systems Improved Numerical Differencing Analyzer) solves physical problems governed by diffusion-type equations that can be modeled by lumped-parameter representation. Previously available only to UNIVAC users [see *NASA Tech Briefs*, Vol. 1, No. 4, page 658 (MSC-13805)], the SINDA program has now been adapted for use on CDC machines.

The system is most widely used as a general thermal analyzer with resistor/capacitor network representations, but it may be adapted to a wide range of problems represented by differential equations, such as Fourier, Poisson, or Laplace equations. SINDA can solve numerically most any set of ordinary differential equations which may be used to represent the transient behavior of a lumped-parameter system, or any set of nonlinear algebraic equations, which might represent the steady-state conditions of a physical system.

For flexibility, SINDA offers numerical solution techniques including finite-difference formulations of the explicit method, such as the forward-difference explicit approximation, the Dufort-Frankel approximation, the exponential approximation, and the alternating-direction approximation. Also available are formulations of the implicit method, such as the backward-difference implicit approximation and the Crank-Nicholson approximation. Many physical problems, particularly those in thermal analysis, can be readily analyzed with the SINDA system.

The SINDA system consists mainly of a preprocessor and a subroutine library. The preprocessor accepts programs written in the SINDA language and converts them into standard FORTRAN programs. The SINDA language is designed for working with lumped-parameter representations and finite-difference solution techniques. The SINDA library consists of a large number of prewritten FORTRAN subroutines that perform a variety of commonly needed actions. The user may call these subroutines from the user's SINDA language program, thus greatly reducing the programing efforts required to solve many problems.

Most of the subroutines in the SINDA library were developed for use in solving thermal analysis problems. As a thermal analyzer, SINDA can handle such interrelated complex phenomena as sublimation, diffuse radiation within enclosures, transport delay effects, sensitivity analysis, and thermal network error correction. Special subroutines are included in the SINDA library to facilitate the thermal analysis of systems incorporating fluid flow networks. SINDA can easily account for pumps, valves, and heat exchangers during a thermal analysis. The user-written SINDA language program determines the input data required and the information that is produced as output by the program.

This program is written in FORTRAN IV and Assembler and has been implemented on a UNIVAC 1100-series computer operating under EXEC 8 with a central memory that varies depending on input but never exceeds 65K of 36-bit words. For plotted output, a Stromberg-Carlson SC 4020 plotter is required. The SINDA program was developed in 1971 with the fluid capability added in 1975. SINDA was adapted to the CDC computer in 1978. The CDC version has been implemented on a CDC CYBER 175 operating under NOS with a central memory requirement of approximately 175K (octal) of 60-bit words.

This program was written for **Johnson Space Center.** *For further information, Circle V on the COSMIC Request Card.*
MSC-18597

SUBJECT
INDEX

ACTUATORS
Dual-mode actuator
page 89 LAR-12412
ADDITIVES
Additive improves engine-oil performance
page 51 GSC-12327
ADHESIVE BONDING
Ion-beam etching enhances adhesive bonding
page 108 LEW-13028
ADHESIVES
Room-temperature adhesive for high temperatures
page 109 MSC-16930
AERODYNAMIC DRAG
Improved multielement airfoil analysis
page 73 LAR-12489
Three-dimensional potential flow
page 75 LAR-12623
AERODYNAMIC STABILITY
Aircraft equilibrium spin characteristics
page 74 LAR-12502
Disturbance amplification rates
page 76 LAR-12556
AGGLOMERATION
Reducing static charges in fluidized-bed reactions
page 54 ARC-11245
AIR POLLUTION
Fast-response atmospheric-pollutant monitor
page 46 LAR-12317
AIRCRAFT HYDRAULIC SYSTEMS
Dual-mode actuator
page 89 LAR-12412
AIRCRAFT SAFETY
Fire tests for airplane interior materials
page 49 MSC-18476
AIRFOILS
Improved multielement airfoil analysis
page 73 LAR-12489
Transonic airfoil design code
page 73 LAR-12460
ALIGNMENT
Adjustable base for centering staked bearings
page 112 MSC-19660
ANODES
Photoelectrochemical cell with nondissolving anode
page 31 LAR-12591
ATTITUDE CONTROL
Aircraft equilibrium spin characteristics
page 74 LAR-12502
AUTOMATIC CONTROL VALVES
Automatic shutoff valve
page 82 MSC-19385
AVALANCHE DIODES
JANTX1N2970B Zener diode
page 14 MFS-25260
JANTX1N2989B Zener diode
page 14 MFS-25261
JANTX1N3016B Zener diode
page 14 MFS-25262
JANTX1N3031B Zener diode
page 14 MFS-25263

BALL BEARINGS
Measuring ball-bearing loads
page 86 MFS-19505
BANDWIDTH
Continuous control of phase-locked-loop bandwidth
page 10 MSC-16864
BEAMS [SUPPORTS]
Automatic connector for structural beams
page 80 MFS-25134
Mechanical end joint for structural columns
page 81 LAR-12482
BEARINGS
Adjustable base for centering staked bearings
page 112 MSC-19660
BOLTS
Bolt-tension indicator
page 66 MFS-19324
Eddy-current sensor measures bolt loading
page 68 MFS-19486
BOUNDARY LAYER STABILITY
Disturbance amplification rates
page 76 LAR-12556
BRAZING
Alumina barrier for vacuum brazing
page 106 MSC-16528
BUS CONDUCTORS
Detecting short circuits during assembly
page 9 ARC-11116

CARBON FIBER REINFORCED PLASTICS
Examining graphite reinforcement in composites
page 104 MSC-19594
CERAMIC COATINGS
A precoat prevents ceramic stopoffs from spalling
page 114 MFS-19495
Corrosion-resistant ceramic thermal-barrier coating
page 53 LEW-13068
CHARGE DISTRIBUTION
Crossed grid change locator
page 12 MFS-25170
NASA charging analyzer program
page 42 LEW-12973
CHECKOUT EQUIPMENT
Online assessment of a distributed processor
page 27 KSC-11124
CHEMICAL MACHINING
Chemical-milling solution for invar
page 97 MFS-25365
CIRCUIT PROTECTION
Voltage controller/current limiter for ac
page 22 NPO-13081
Simple circuit monitors "third wire" in ac lines
page 4 MFS-19457
CLAMPS
Drill-motor holding fixture
page 91 MSC-18582
Vise holds specimens for microscope
page 83 MSC-18660
CLEANING
Ion-beam cleaning for cold welds
page 98 LEW-12982
COAL
Detecting a coal/shale interface
page 47 MFS-23720
Measuring coal deposits by radar
page 48 MFS-23922
Underground coal mining
page 56 NPO-14704
COAL GASIFICATION
Coal conversion and synthetic-fuel production
page 58 MFS-25330
COATINGS
Coatings for hybrid microcircuits
page 99 MFS-25292
COINCIDENCE CIRCUITS
Coincidence-interval measuring circuit
page 7 LAR-12531
COLD WELDING
Ion-beam cleaning for cold welds
page 98 LEW-12982
COLUMNS [SUPPORTS]
Automatic connector for structural beams
page 80 MFS-25134
Mechanical end joint for structural columns
page 81 LAR-12482
COMPONENT RELIABILITY
JANTX1N2970B Zener diode
page 14 MFS-25260
JANTX1N2989B Zener diode
page 14 MFS-25261
JANTX1N3016B Zener diode
page 14 MFS-25262
JANTX1N3031B Zener diode
page 14 MFS-25263
JANTX1N5622 diode
page 15 MFS-25250
JANTX1N5623 switching diode
page 15 MFS-25261
JANTX2N2060 dual transistor
page 15 MFS-25251
JANTX2N2219A dual transistor
page 15 MFS-25252
JANTX2N2369A transistor
page 16 MFS-25254
JANTX2N2432A transistor
page 16 MFS-25255
JANTX2N2484 transistor
page 15 MFS-25253
JANTX2N2605 transistor
page 16 MFS-25150
JANTX2N2905A transistor
page 17 MFS-25258
JANTX2N2920 dual transistor
page 17 MFS-25256
JANTX2N2945A transistor
page 17 MFS-25259
JANTX2N3637 transistor
page 17 MFS-25264
JANTX2N3811 dual transistor
page 18 MFS-25265
JANTX2N4150 transistor
page 18 MFS-25267
JANTX2N4856 field-effect transistor
page 18 MFS-25269
COMPOSITE MATERIALS
Examining graphite reinforcement in composites
page 104 MSC-19594
Flush-mounting technique for composite beams
page 104 LAR-12389
Jig for assembling large composite panels
page 102 LAR-12394
Shaping graphite/epoxy stiffeners
page 103 MSC-18494
COMPUTER PROGRAMMING
Automated flow-chart system
page 121 GSC-12514
CONNECTORS
Automatic connector for structural beams
page 80 MFS-25134
Mechanical end joint for structural columns
page 81 LAR-12482
CONTAINERLESS MELTS
Containerless materials processing in the laboratory
page 45 MFS-25242
CONTROLLERS
Controller and temperature monitor for solar heating
page 41 MFS-25387
Controller for solar-energy systems
page 40 MFS-25386
COOLING
Compact, super heat exchanger
page 70 LEW-12441
CORE SAMPLING
Drilling side holes from a borehole
page 52 NPO-14485
CORROSION RESISTANCE
Corrosion-resistant ceramic thermal-barrier coating
page 53 LEW-13088

Inhibiting corrosion in solar-heating and cooling systems
page 41 MFS-23763
COST ANALYSIS
Cost models and economical packaging of LSI's
page 115 MFS-25369
COUPLINGS
Self-energized screw coupling
page 82 MFS-25340
CRACKING
Eliminating underbead fissuring in superalloys
page 97 MFS-19460
CREEP TESTS
Multiple-creep-test apparatus
page 69 GSC-12561
CRYOGENIC EQUIPMENT
Cryogenic machining of polyurethane foam
page 105 MSC-18572
LVDT gage for fracture toughness tests in liquid hydrogen
page 64 LEW-13038
Modified displacement gage for cryogenic testing
page 66 LEW-13039
Tension-mode loading for bend specimens in cryogens
page 65 LEW-13040
CRYSTALLIZATION
Containerless materials processing in the laboratory
page 45 MFS-25242
CURING
Knife-edge seal for vacuum bagging
page 113 MFS-24049
CUTTERS
Precision filament cutter
page 79 LAR-12564
Tubing cutter for tight spaces
page 84 MSC-18536

DATA LINKS
Multipath star switch controller
page 25 NPO-13422
DATA TRANSMISSION
Efficient telemetry format
page 119 NPO-13679
DECODERS
Independant synchronizer for digital decoders
page 6 MSC-16723
DEMODULATORS
Microprocessor-based detector for PSK commands
page 26 NPO-14440
DIFFERENCE EQUATIONS
Systems improved numerical differencing analyzer
page 122 MSC-18597
DIODES
JANTX1N2970B Zener diode
page 14 MFS-25260
JANTX1N2999B Zener diode
page 14 MFS-25261
JANTX1N3016B Zener diode
page 14 MFS-25262
JANTX1N3031B Zener diode
page 14 MFS-25263
JANTX1N5622 diode
page 15 MFS-25280
JANTX1N5623 switching diode
page 15 MFS-25281
DISPLACEMENT MEASUREMENT
LVDT gage for fracture toughness tests in liquid hydrogen
page 54 LEW-13038
Modified displacement gage for cryogenic testing
page 66 LEW-13039
DOORS
Clamshell door system
page 85 MSC-18468
DRILLING
Drilling side holes from a borehole
page 52 NPO-14155
Drill-motor holding fixture
page 91 MSC-18582

EDDY CURRENTS
Eddy-current sensor measures bolt loading
page 68 MFS-19486
ELECTRIC CONNECTORS
Connector heat shield
page 106 MSC-16282
ELECTRICAL GROUNDING
Simple circuit monitors "third wire" in ac lines
page 4 MFS-19457
ELECTROACOUSTIC TRANSDUCERS
Broadband electrostatic acoustic transducer for liquids
page 67 LAR-12465
ELECTROCHEMICAL CELLS
REDOX electrochemical energy storage
page 50 LEW-13398
ELECTRON BEAM WELDING
Verifying root fusion in electron-beam welds
page 95 MFS-19499
X-ray technique verifies weld-root fusion
page 96 MFS-19488
ELECTRON TRAJECTORIES
Numerical tracing of electron trajectories
page 41 GSC-12535
ELECTRONIC PACKAGING
Placement technique for semicustom digital LSI circuits
page 100 MFS-25324
ENERGY CONSERVATION
Energy-saving thermostat
page 33 LAR-12450
ENERGY CONVERSION
Extracting energy from natural flow
page 37 MFS-23989
ENERGY CONVERSION EFFICIENCY
New mounting improves solar-cell efficiency
page 32 NPO-14467
ENERGY POLICY
Coal conversion and synthetic-fuel production
page 56 MFS-25330
Underground coal mining
page 56 NPO-14704
ENERGY STORAGE
REDOX electrochemical energy storage
page 50 LEW-13398
ENGINES
Additive improves engine-oil performance
page 51 GSC-12327
EQUATIONS OF MOTION
Equations of motion for coupled N-body systems
page 72 GSC-12407
ESTIMATING
Estimation of incomplete multinomial data
page 121 LAR-12593
ETCHANTS
Etchant for Incoloy-903 welds
page 96 MFS-19378
ETCHING
Ion-beam etching enhances adhesive bonding
page 108 LEW-13026
EXTENSOMETERS
Bolt-tension indicator
page 88 MFS-19324
Eddy-current sensor measures bolt loading
page 68 MFS-19486
FASTENERS
Flush-mounting technique for composite beams
page 104 LAR-12339
Self-energized screw coupling
page 82 MFS-25340
FIBERS
Precision filament cutter
page 79 LAR-12564
FIELD EFFECT TRANSISTORS
JANTX2N4856 field-effect transistor
page 18 MFS-25269
FILM COOLING
Full-coverage film cooling
page 75 LEW-13249
FLAMMABILITY
Fire tests for airplane interior materials
page 49 MSC-18476
FLANGES
Compact positioning flange
page 88 MSC-14876
FLIGHT CONTROL
Dual-mode actuator
page 89 LAR-12412
FLIGHT HAZARDS
Fire tests for airplane interior materials
page 49 MSC-18476
FLOW CHARTS
Automated flow-chart system
page 121 GSC-12514
FLOW CHARACTERISTICS
Flow field in supersonic mixed-compression inlets
page 74 LEW-13279
Improved multielement airfoil analysis
page 73 LAR-12460
Viscous characteristics analysis
page 72 LAR-12598
FLUID POWER
Extracting energy from natural flow
page 37 MFS-23989
FLUIDIZED BED PROCESSORS
Reducing static charges in fluidized-bed reactions
page 54 ARC-11245
FOAMS
Foam-filled cushions for sliding trays
page 107 MSC-18565
FRACTURE STRENGTH
LVDT gage for fracture toughness tests in liquid hydrogen
page 64 LEW-13038
Modified displacement gage for cryogenic testing
page 66 LEW-13039
Tension-mode loading for bend specimens in cryogens
page 65 LEW-13040
FREQUENCY DIVIDERS
Universal odd-modulus frequency divider
page 8 NPO-13426

GAS HEATING
Benefit assessment of solar-augmented natural-gas systems
page 38 NPO-14568
GAS TURBINE ENGINES
Full-coverage film cooling
page 75 LEW-13249
GIMBALS
Compact positioning flange
page 88 MSC-14876
GLASS FIBERS
Safe splicing of glass optical fibers
page 112 KSC-11107
GRINDING [MATERIAL REMOVAL]
"Grinding" cavities in polyurethane foam
page 105 MSC-18584

HAMMERS
Aluminum-encased lead mallet
page 85 MSC-18529
HARNESSES
Wire harness twisting aid
page 111 MSC-18581
HEAT EXCHANGERS
Compact, super heat exchanger
page 70 LEW-12441
Thermosyphon heat exchanger
page 40 MFS-25389
HEAT RESISTANT ALLOYS
Eliminating underbead fissuring in superalloys
page 97 MFS-19460
HEAT SHIELDING
Connector heat shield
page 106 MSC-16282
HEATING EQUIPMENT
Air-cooled solar-collector specification
page 39 MFS-25336
An adjustable solar concentrator
page 35 NPO-14710
Benefit assessment of solar-augmented natural-gas systems
page 38 NPO-14568
Controller and temperature monitor for solar heating
page 41 MFS-25387
Controller for solar-energy systems
page 40 MFS-25386
Evacuated-tube solar collector — performance evaluation
page 39 MFS-25339
Glycol/water evacuated-tube solar collector
page 40 MFS-25337
Indoor tests of the concentric-tube solar collector
page 39 MFS-25390
Inhibiting corrosion in solar-heating and cooling systems
page 41 MFS-23763
Solar-heating and cooling system design package
page 38 MFS-25393
Solar-heating/cooling systems: design and development
page 38 MFS-25368
Thermosyphon heat exchanger
page 40 MFS-25389
HELICAL WINDINGS
Easily-assembled helical heater
page 110 LAR-11712
HOLDERS
Drill-motor holding fixture
page 91 MSC-16582
HYPERTHERMIA
Temperature controller for hyperthermia device
page 59 LAR-12526

IMAGE CONVERTERS
Photocapacitive image converter
page 11 LAR-12513
IMAGERY
Applications of remote-sensing imagery
page 71 MFS-25107
IMAGING TECHNIQUES
Numerical tracing of electron trajectories
page 41 GSC-12535
INDUSTRIAL PLANTS
Microprocessor systems for industrial-process control
page 110 NPO-14861
INFORMATION RETRIEVAL
Photocapacitive image converter
page 11 LAR-12513
INSTRUMENT ORIENTATION
Compact positioning flange
page 88 MSC-14876
INTEGRATED CIRCUITS
An automated photolithography facility for IC's
page 115 MFS-25073
Automated ion implantation for IC's
page 115 MFS-25193
Coatings for hybrid microcircuits
page 99 MFS-25292
Cost models and economical packaging of LSI's
page 115 MFS-25359
Models of MOS and SOS devices
page 116 MFS-25153
Placement technique for semicustom digital LSI circuits
page 100 MFS-25324
ION BEAMS
Ion-beam cleaning for cold welds
page 98 LEW-12982
Ion-beam etching enhances adhesive bonding
page 108 LEW-13028
ION EXCHANGE MEMBRANE ELECTROLYTES
REDOX electrochemical energy storage
page 50 LEW-13385
ION IMPLANTATION
Automated ion implantation for IC's
page 115 MFS-25193
IRON ALLOYS
Chemical-milling solution for Invar
page 17 MFS-25365

JIGS
Jig for assembling large composite panels
page 102 LAR-12394
JOINTS [JUNCTIONS]
Automatic connector for structural beams
page 80 MFS-25134
Mechanical end joint for structural columns
page 81 LAR-12482

LAMINATES
Jig for assembling large composite panels
page 102 LAR-12394
Shaping graphite/epoxy stiffness
page 103 MSC-18494
LARGE SCALE INTEGRATION
A general logic structure for custom LSI's
page 101 NPO-14410
An automated photolithography facility for IC's
page 115 MFS-25073
Automated ion implantation for IC's
page 115 MFS-25193
Coatings for hybrid microcircuits
page 99 MFS-25292
Cost models and economical packaging of LSI's
page 115 MFS-25359
Models of MOS and SOS devices
page 116 MFS-25153
Placement technique for semicustom digital LSI Circuits
page 100 MFS-25324
LASERS
Large-volume multiple-path nuclear-pumped laser
page 36 LAR-12592
LATCHES
Clamshell door system
page 85 MSC-18468
LITHOGRAPHY
An automated photolithography facility for IC's
page 115 MFS-25073
LOAD TESTS
Measuring ball-bearing loads
page 86 MFS-19505
LOGIC DESIGN
A general logic structure for custom LSI's
page 101 NPO-14410
LOOPS
Eliminating DLL timing errors
page 24 MSC-18035
LUBRICATING OILS
Additive improves engine-oil performance
page 51 GSC-12327

MACHINING
Cryogenic machining of polyurethane foam
page 105 MSC-18572
MAGENTIC TRANSDUCERS
Cable-splice detector
page 63 ARC-11291
MANY BODY PROBLEM
Equations of motion for coupled N-body systems
page 72 GSC-12407
MATERIALS HANDLING
Transferring small samples of viscous liquid
page 55 MSC-18533
MAXIMUM LIKELIHOOD ESTIMATES
Estimation of incomplete multinomial data
page 121 LAR-12593
MEDICAL EQUIPMENT
Temperature controller for hyperthermia device
page 59 LAR-12526
METAL BONDING
Room-temperature adhesive for high temperatures
page 109 MSC-16930
METAL OXIDE SEMICONDUCTORS
Models of MOS and SOS devices
page 116 MFS-25153
METAL-METAL BONDING
Ion-beam cleaning for cold welds
page 98 LEW-12982
MICROSCOPES
Vise holds specimens for microscope
page 83 MSC-18590
MILLING [MACHINING]
Chemical-milling solution for Invar
page 97 MFS-25365
"Grinding" cavities in polyurethane foam
page 105 MSC-18564
MINES [EXCAVATIONS]
Underground coal mining
page 56 NPO-14704
MINING
Detecting a coal/shale interface
page 47 MFS-23720
Measuring coal deposits by radar
page 46 MFS-23922
MISSION PLANNING
Goddard mission analysis system
page 120 GSC-12392
MONITORS
Fast-response atmospheric-pollutant monitor
page 48 LAR-12317
MOUNTING
Compact positioning flange
page 88 MSC-14876
Flush-mounting technique for composite beams
page 104 LAR-12389
New mounting improves solar-cell efficiency
page 32 NPO-14467
MULTIPROCESSING [COMPUTERS]
Online assessment of a distributed processor
page 27 KSC-11124

NUCLEAR REACTIONS
Large-volume multiple-path nuclear-pumped laser
page 36 LAR-12592

NUMERICAL ANALYSIS
Systems improved numerical differencing analyzer
page 122 MSC-18597

OPTICAL COMMUNICATION
Safe splicing of glass optical fibers
page 112 KSC-11107

OPTICAL TRACKING
An adjustable solar concentrator
page 35 NPO-14710

PACKAGING
Cost models and economical packaging of LSI's
page 115 MFS-25359

PANORAMIC SCANNING
Rotatable prime for pan and tilt
page 34 LAR-12388

PENETROMETERS
Detecting a coal/shale interface
page 47 MFS-23720

PHASE LOCKED SYSTEMS
Continuous control of phase-locked-loop bandwidth
page 10 MSC-18584

Microprocessor control for phase-lock receiver
page 23 NPO-14436

PHASE SHIFT KEYING
Microprocessor-based detector for PSK commands
page 26 NPO-14440

PHOTOVOLTAIC CELLS
Photoelectrochemical cell with nondissolving anode
page 31 LAR-12591

PIPES [TUBES]
Tubing cutter for tight spaces
page 84 MSC-18536

POLARIMETERS
Ultraviolet spectrometer/polarimeter
page 35 MFS-25298

POLLUTION MONITORING
Measuring water properties from a moving boat
page 60 LAR-12325

POLYQUINOXALINES
Room-temperature adhesive for high temperatures
page 109 MSC-18830

POLYURETHANE FOAM
Cryogenic machining of polyurethane foam
page 105 MSC-18572

"Grinding" cavities in polyurethane foam
page 105 MSC-18564

POROUS MATERIALS
Compact, super heat exchanger
page 70 LEW-12441

POSITION LOCATION
Crossed grid charge locator
page 12 MFS-25170

POSITIONING DEVICES [MACHINERY]
Drill-motor holding fixture
page 91 MSC-18582

POTENTIAL FLOW
Three-dimensional potential flow
page 75 LAR-12623

POWER LIMITERS
Voltage controller/current limiter for ac
page 22 NPO-13081

PRODUCTION ENGINEERING
Microprocessor systems for industrial-process control
page 110 NPO-14881

PROGRAMMING LANGUAGES
Software design and documentation language
page 121 NPO-14610

User's guide for SFTRAN
page 119 LEW-13172

PROTECTIVE COATINGS
A precoat prevents ceramic stopoffs from spalling
page 114 MFS-19495

Aluminia barrier for vacuum brazing
page 85 MSC-18528

RADAR MEASUREMENT
Measuring coal deposits by radar
page 46 MFS-23922

RADIATION DETECTORS
Crossed grid charge locator
page 12 MFS-25170

RECEIVERS
Microprocessor control for phase-lock receiver
page 23 NPO-14436

REMOTE SENSORS
Applications of remote-sensing imagery
page 71 MFS-25107

RESISTANCE HEATING
Easily-assembled helical heater
page 110 LAR-11712

RETAINING
Retaining a sleeve on a shaft
page 87 MFS-19518

RIBS [SUPPORTS]
Shaping graphite/epoxy stiffeners
page 103 MSC-18494

SAFETY DEVICES
Cable-splice detector
page 63 ARC-11291

SCREWS
Self-energized screw coupling
page 82 MFS-25340

SEALS [STOPPERS]
Knife-edge seal for vacuum bagging
page 113 MFS-24049

Self-acting shaft seals
page 92 LEW-13229

SEMICONDUCTOR DEVICES
JANTX1N2970B Zener diode
page 14 MFS-25260

JANTX1N2988B Zener diode
page 14 MFS-25261

JANTX1N3016B Zener diode
page 14 MFS-25262

JANTX1N3031B Zener diode
page 14 MFS25263

JANTX1N5622 diode
page 15 MFS-25280

JANTX1N5623 switching diode
page 15 MFS-25281

JANTX2N2060 dual transistor
page 15 MFS-25251

JANTX2N2219A dual transistor
page 15 MFS-25252

JANTX2N2369A transistor
page 16 MFS-25254

JANTX2N2432A transistor
page 16 MFS-25255

JANTX2N2484 transistor
page 16 MFS-25253

JANTX2N2905 transistor
page 16 MFS-25150

JANTX2N2905A transistor
page 17 MFS-25256

JANTX2N2920 dual transistor
page 17 MFS-25258

JANTX2N2946A transistor
page 17 MFS-25259

JANTX2N3637 transistor
page 17 MFS-25264

JANTX2N3811 dual transistor
page 18 MFS-25265

JANTX2N4150 transistor
page 18 MFS-25267

JANTX2N4856 field-effect transistor
page 18 MFS-25269

SEQUENCING
Multipath star switch controller
page 25 NPO-13422

SHAFTS [MACHINE ELEMENTS]
Retaining a sleeve on a shaft
page 87 MFS-19518

Self-acting shaft seals
page 92 LEW-13229

SHAPERS
Shaping graphite/epoxy stiffeners
page 103 MSC-18494

SHELL THEORY
Shell theory automated for rotational structures
page 74 MFS-23827

SHORT CIRCUITS
Detecting short circuits during assembly
page 9 ARC-11116

Voltage controller/current limiter for ac
page 22 NPO-13081

SIGNAL PROCESSING
Eliminating DLL timing errors
page 24 MSC-18035

SLEEVES
Retaining a sleeve on a shaft
page 87 MFS-19518

SLICING
Precision filament cutter
page 79 LAR-12564

SOFTWARE
Software design and documentation language
page 121 NPO-14610

SOLAR CELLS
Photoelectrochemical cell with nondissolving anode
page 31 LAR-12591

SOLAR ENERGY
Air-cooled solar-collector specification
page 39 MFS-25336

An adjustable solar concentrator
page 35 NPO-14710

Benefit assessment of solar-augmented natural-gas systems
page 38 NPO-14566

Controller and temperature monitor for solar heating
page 41 MFS-25367

Controller for solar-energy systems
page 40 MFS-25366

Evacuated-tube solar collector — performance evaluation
page 39 MFS-25339

Glycol/water evacuated-tube solar collector
page 40 MFS-25337

Indoor tests of the concentric-tube solar collector
page 39 MFS-25390

Inhibiting corrosion in solar-heating and cooling system
page 41 MFS-23763

New mounting improves solar-cell efficiency
page 32 NPO-14467

Solar-heating and cooling system design package
page 38 MFS-25393

Solar-heating/cooling systems: design and development
page 38 MFS-25358

Thermosyphon heat exchanger
page 40 MFS-25369

SPACE MANUFACTURING
Should we industrialize space?
page 114 MFS-23963

SPALLING
A precoat prevents ceramic stopoffs from spalling
page 114 MFS-19495

SPECIMENS
Vice holds specimens for microscope
page 83 MSC-18690

SPECTROSCOPIC TELESCOPES
Ultraviolet spectrometer/polarimeter
page 35 MFS-25298

SPIN STABILIZATION
Aircraft equilibrium spin characteristics
page 74 LAR-12502

SPLICING
Cable-splice detector
page 63 ARC-11291
Safe splicing of glass optical fibers
page 112 KSC-11107

STATIC ELECTRICITY
Reducing static charges in fluidized-bed reactions
page 54 ARC-11245

STATISTICAL ANALYSIS
Estimation of incomplete multinomial data
page 121 LAR-12580

STOWAGE [ONBOARD EQUIPMENT]
Foam-filled cushions for sliding trays
page 107 MSC-18565

STRUCTURAL ANALYSIS
Shell theory automated for rotational structures
page 74 MFS-23627

STRUCTURAL MEMBERS
Automatic connector for structural beams
page 80 MFS-25134
Mechanical end joint for structural columns
page 81 LAR-12482

SUPERSONIC INLETS
Flow field in supersonic mixed-compression inlets
page 74 LEW-13279

SURFACE FINISHING
Chemical-milling solution for invar
page 97 MFS-25365

SWAGING
Adjustable base for centering staked bearings
page 112 MSC-19660

SWITCHING
Multipath star switch controller
page 25 NPO-13422

SYNCHRONIZERS
Independent synchronizer for digital decoders
page 6 MSC-16723
Microprocessor-controlled data synchronizer
page 21 MSC-18535

SYNTHETIC FUELS
Coal conversion and synthetic-fuel production
page 56 MFS-25330

SYRINGES
Transferring small samples of viscous liquid
page 55 MSC-18533

TECHNOLOGY ASSESSMENT
Should we industrialize space?
page 114 MFS-23963

TELEMETRY
Efficient telemetry format
page 119 NPO-13679
Microprocessor-controlled data synchronizer
page 21 MSC-18535

TELEVISION CAMERAS
Rotatable prism for pan and tilt
page 34 LAR-12388

TEMPERATURE CONTROL
Energy-saving thermostat
page 33 LAR-12450
Temperature controller for hyperthermia device
page 59 LAR-12528

TENSILE TESTS
Tension-mode loading for bend specimens in cryogens
page 65 LEW-13040

THERMAL CONTROL COATINGS
Corrosion-resistant ceramic thermal-barrier coating
page 53 LEW-13088

THERMAL DIFFUSION
Systems improved numerical differencing analyzer
page 122 MSC-18597

THERMOSIPHONS
Thermosyphon heat exchanger
page 40 MFS-25389

THERMOSTATS
Energy-saving thermostat
page 33 LAR-12450

TIME MEASUREMENT
Coincidence-interval measuring circuit
page 7 LAR-12531

TOOLS
Aluminum-encased lead mallet
page 85 MSC-18529
Tubing cutter for tight spaces
page 84 MSC-18538
Zero-torque spanner wrench
page 90 MSC-14843

TORQUE
Bolt-tension indicator
page 86 MFS-19324
Eddy-current sensor measures bolt loading
page 66 MFS-19486
Zero-torque spanner wrench
page 90 MSC-14843

TRANSDUCERS
Broadband electrostatic acoustic transducer for liquids
page 67 LAR-12465

TRANSISTORS
JANTX2N2060 dual transistor
page 15 MFS-25251
JANTX2N2219A dual transistor
page 15 MFS-25252
JANTX2N2369A transistor
page 16 MFS-25254
JANTX2N2432A transistor
page 16 MFS-25255
JANTX2N2484 transistor
page 16 MFS-25253
JANTX2N2605 transistor
page 16 MFS-25150
JANTX2N2905A transistor
page 17 MFS-25256
JANTX2N2920 dual transistor
page 17 MFS-25258
JANTX2N2945A transistor
page 17 MFS-25259
JANTX2N3637 transistor
page 17 MFS-25264
JANTX2N3811 dual transistor
page 18 MFS-25265
JANTX2N4150 transistor
page 18 MFS-25267
JANTX2N4858 field-effect transistor
page 18 MFS-25269

TRANSMISSION EFFICIENCY
Efficient telemetry format
page 119 NPO-13679

TRANSONIC FLOW
Transonic airfoil design code
page 73 LAR-12460

TURBULENCE
Extracting energy from natural flow
page 37 MFS-23860

TWISTING
Wire harness twisting aid
page 111 MSC-18581

ULTRASONIC TESTS
Broadband electrostatic accoustic transducer for liquids
page 67 LAR-12465
Verifying root fusion in electron-beam welds
page 95 MFS-19499

ULTRAVIOLET SPECTROMETERS
Ultraviolet spectrometer/polarimeter
page 35 MFS-25298

USER MANUALS [COMPUTER PROGRAMS]
User's guide for SFTRAN
page 119 LEW-13172

VACUUM APPARATUS
Knife-edge seal for vacuum bagging
page 113 MFS-24049

VALVES
Automatic shutoff valve
page 82 MSC-19385

VIBRATION DAMPING
Foam-filled cushions for sliding trays
page 107 MSC-18565

VISCOUS FLOW
Viscous characteristics analysis
page 72 LAR-12598

VISCOUS FLUIDS
Transferring small samples of viscous liquid
page 55 MSC-18533

VOLTAGE REGULATORS
Simple buck/boost voltage regulator
page 5 GSC-12360

WATER QUALITY
Measuring water properties from a moving boat
page 60 LAR-12325

WEAR INHIBITORS
Additive improves engine-oil performance
page 51 GSC-12327

WEAR TESTS
Measuring ball-bearing loads
page 86 MFS-19505

WEIGHTLESSNESS
Containerless, zero-gravity materials processing — in the laboratory
page 45 MFS-25242

WELDING
Eliminating underbead fissuring in superalloys
page 97 MFS-19460
Etchant for Incoloy-903 welds
page 96 MFS-19378
Verifying root fusion in electron-beam welds
page 95 MFS-19499
X-ray technique verifies weld-root fusion
page 96 MFS-19468

WIRE WINDING
Wire harness twisting aid
page 111 MSC-18581

WIRING
Simple circuit monitors "third wire" in ac lines
page 4 MFS-19457

WRENCHES
Zero-torque spanner wrench
page 90 MSC-14843

X RAY INSPECTION
X-ray technique verifies weld-root fusion
page 96 MFS-19468

National Aeronautics and
Space Administration

Washington, D C
20546

Official Business
Penalty for Private Use $300

Postage and Fees Paid
National Aeronautics and
Space Administration
NASA 451

Director, Technology Transfer Division
P. O. Box 8757
Baltimore/Washington International Airport, MD 21240

National Aeronautics and
Space Administration

Washington, D C
20546

Official Business
Penalty for Private Use $300

Postage and Fees Paid
National Aeronautics and
Space Administration
NASA 451

Director, Technology Transfer Division
P. O. Box 8757
Baltimore/Washington International Airport, MD 21240

National Aeronautics and
Space Administration

Washington, D C
20546

Official Business
Penalty for Private Use $300

Postage and Fees Paid
National Aeronautics and
Space Administration
NASA 451

Director, Technology Transfer Division
P. O. Box 8757
Baltimore/Washington International Airport, MD 21240

TECH BRIEFS SUBSCRIPTIONS

☐ Please place me on the subscription list for NASA Tech Briefs (issued quarterly).
☐ I wish to change the delivery address for my current subscription.

SPRING 1980

1. Please check any of the following that describe your organization:
   - ☐ Federal Government
   - ☐ State Government
   - ☐ Municipal Government
   - ☐ University/College
   - ☐ Secondary School
   - ☐ Trade/Vocational School
   - ☐ Manufacturing
   - ☐ Sales
   - ☐ Research
   - ☐ Consulting
   - ☐ Medicine
   - ☐ Professional Society
   - ☐ News Media
   - ☐ Information Sciences/Library
2. Please check the number of employees in your organization: ☐ Under 25 ☐ 25-100 ☐ 100-500 ☐ Over 500
3. Please indicate if your position is one of the following: ☐ Owner or Chief Executive Officer ☐ Administrator/Manager ☐ Scientist ☐ Engineer ☐ Other ______

[PLEASE PRINT]

NAME ______ TITLE ______

COMPANY & ______ PHONE ______

STREET ADDRESS ______ CITY ______ STATE ______ ZIP ______

TECH BRIEFS SUBSCRIPTIONS

☐ Please place me on the subscription list for NASA Tech Briefs (issued quarterly).
☐ I wish to change the delivery address for my current subscription.

SPRING 1980

1. Please check any of the following that describe your organization:
   - ☐ Federal Government
   - ☐ State Government
   - ☐ Municipal Government
   - ☐ University/College
   - ☐ Secondary School
   - ☐ Trade/Vocational School
   - ☐ Manufacturing
   - ☐ Sales
   - ☐ Research
   - ☐ Consulting
   - ☐ Medicine
   - ☐ Professional Society
   - ☐ News Media
   - ☐ Information Sciences/Library
2. Please check the number of employees in your organization: ☐ Under 25 ☐ 25-100 ☐ 100-500 ☐ Over 500
3. Please indicate if your position is one of the following: ☐ Owner or Chief Executive Officer ☐ Administrator/Manager ☐ Scientist ☐ Engineer ☐ Other ______

[PLEASE PRINT]

NAME ______ TITLE ______

COMPANY & ______ PHONE ______

STREET ADDRESS ______ CITY ______ STATE ______ ZIP ______

FEEDBACK — YOUR COMMENTS

WE NEED YOUR HELP!

SPRING 1980

Our ultimate goal is to provide you with solutions to your day-to-day technical problems. Are we meeting that goal? Tell us how Tech Briefs has helped you, or how it can be made more useful. We are especially interested in brief descriptions of specific instances where Tech Briefs has either helped you solve a problem or been applied to your product line.

______

______

______

______

If you need more space, write us a letter at the address on the front of this card.

[PLEASE PRINT]

NAME ______ TITLE ______

COMPANY ______ PHONE ______

STREET ADDRESS ______ CITY ______ STATE ______ ZIP ______

TSP REQUESTS

Please send me the Technical Support Package (TSP)
for the Tech Brief articles circled below:

SPRING
1980

☐ I would like information about NASA's Industrial Applications Centers and other NASA TU services.

I am requesting these TSP's for:

☐ Current Awareness
☐ Product Development
☐ Other ______________
☐ Process Improvement
☐ Problem Solving

Approximately how many TSP's have you requested from NASA in the last five years?

☐ 0 to 10 ☐ 11 to 25 ☐ over 25

[PLEASE PRINT]

NAME ______________
TITLE ______________
COMPANY & STREET ADDRESS ______________ PHONE ______________
CITY ______________ STATE ______ ZIP ______

1	2	3	4	5	6	7	8	9	10	11	12	13	14	15	16
17	18	19	20	21	22	23	24	25	26	27	28	29	30	31	32
33	34	35	36	37	38	39	40	41	42	43	44	45	46	47	48
49	50	51	52	53	54	55	56	57	58	59	60	61	62	63	64
65	66	67	68	69	70	71	72	73	74	75	76	77	78	79	80
81	82	83													

TSP REQUESTS

Please send me the Technical Support Package (TSP)
for the Tech Brief articles circled below:

SPRING
1980

☐ I would like information about NASA's Industrial Applications Centers and other NASA TU services.

I am requesting these TSP's for:

☐ Current Awareness
☐ Product Development
☐ Other ______________
☐ Process Improvement
☐ Problem Solving

Approximately how many TSP's have you requested from NASA in the last five years?

☐ 0 to 10 ☐ 11 to 25 ☐ over 25

[PLEASE PRINT]

NAME ______________
TITLE ______________
COMPANY & STREET ADDRESS ______________ PHONE ______________
CITY ______________ STATE ______ ZIP ______

1 2 3 4 5 6 7 8 9 10 11 12 13 14 15 16
17 18 19 20 21 22 23 24 25 26 27 28 29 30 31 32
33 34 35 36 37 38 39 40 41 42 43 44 45 46 47 48
49 50 51 52 53 54 55 56 57 58 59 60 61 62 63 64
65 66 67 68 69 70 71 72 73 74 75 76 77 78 79 80
81 82 83

COSMIC REQUESTS

SPRING
1980

I would like price and availability information about the computer program(s) circled below

A B C D E F G H J K L M N P R S T U V

Please send me further information about software and services available from COSMIC. I am particularly interested in programs in the following areas: ______________

[PLEASE PRINT]

NAME ______________ TITLE ______________
COMPANY & STREET ADDRESS ______________ PHONE ______________
CITY ______________ STATE ______ ZIP ______

National Aeronautics and
Space Administration

Washington, D.C.
20546

Official Business
Penalty for Private Use $300

Postage and Fees Paid
National Aeronautics and
Space Administration
NASA 451

Director, Technology Transfer Division
P. O. Box 8757
Baltimore/Washington International Airport, MD 21240

NASA

National Aeronautics and
Space Administration

Washington, D.C.
20546

Official Business
Penalty for Private Use $300

Postage and Fees Paid
National Aeronautics and
Space Administration
NASA 451

Director, Technology Transfer Division
P. O. Box 8757
Baltimore/Washington International Airport, MD 21240

NASA

National Aeronautics and
Space Administration

Washington, D.C.
20546

Official Business
Penalty for Private Use $300

Postage and Fees Paid
National Aeronautics and
Space Administration
NASA 451

COSMIC
Computer Software Management and Information Center
Suite 112, Barrow Hall
Athens, GA 30602

NASA

National Aeronautics and
Space Administration

Washington, D.C.
20546

Official Business
Penalty for Private Use $300

THIRD-CLASS BULK

THIRD-CLASS BULK RATE
POSTAGE & FEES PAID
NASA
WASHINGTON, D.C.
PERMIT No. P-154

NASA

A commercial seismic testing facility, shown here ready for testing of a 25-ton diesel generator, evolved from related work by a NASA contractor on the Saturn V launch vehicle. The Saturn V had to be tested for its ability to withstand launch vibration. Similarly, massive equipment, such as that used in nuclear power generating stations, is tested [at lower frequencies] for Earthquake resistance. [See page A1.]

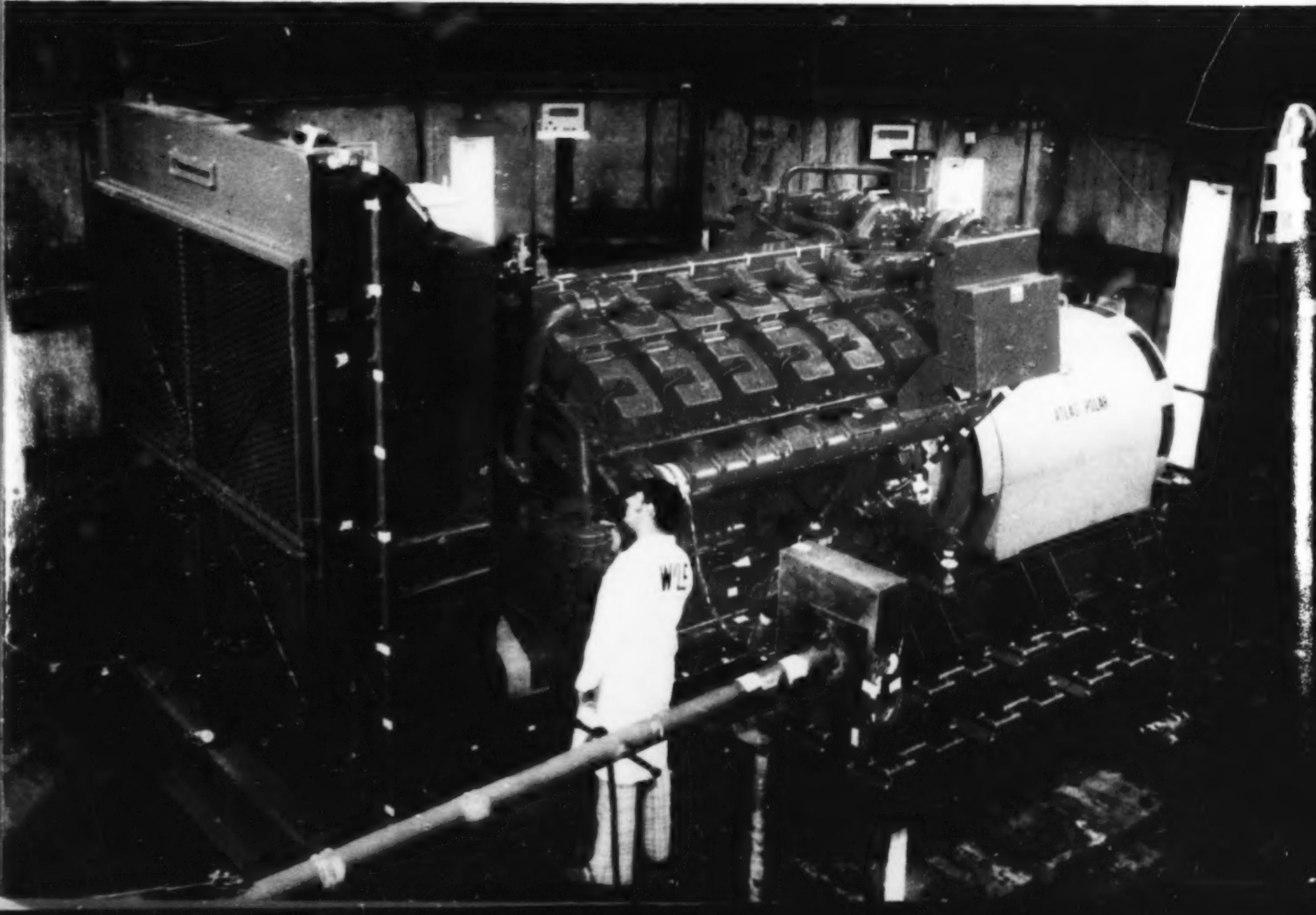

5/2

NASA Tech Briefs

National
Aeronautics and
Space
Administration

[illegible] LIBRARY

**Have You Requested
The 1978 NASA Tech Briefs Index?
[See Page A2.]**

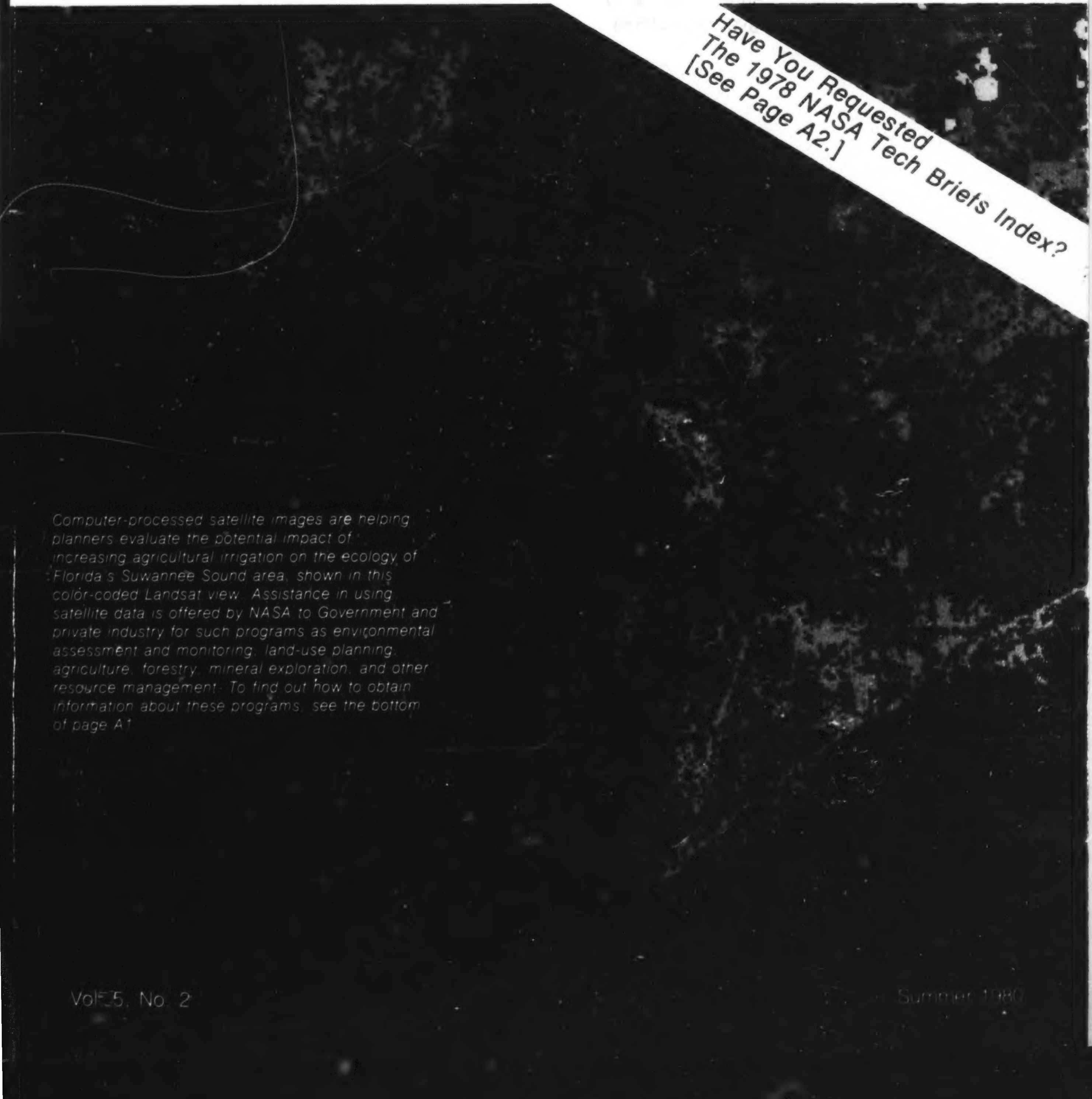

Computer-processed satellite images are helping planners evaluate the potential impact of increasing agricultural irrigation on the ecology of Florida's Suwannee Sound area, shown in this color-coded Landsat view. Assistance in using satellite data is offered by NASA to Government and private industry for such programs as environmental assessment and monitoring, land-use planning, agriculture, forestry, mineral exploration, and other resource management. To find out how to obtain information about these programs, see the bottom of page A1.

Vol. 5, No. 2

Summer 1980

About the NASA Technology Utilization Program

The National Aeronautics and Space Act of 1958, which established NASA and the United States civilian space program, requires that "The Administration shall provide for the widest practicable and appropriate dissemination of information concerning its activities and the results thereof."

To help carry out this objective, NASA's Technology Utilization (TU) Program was established in 1962. Now, as an element of NASA's Technology Transfer Division, this program offers a variety of valuable services to help transfer aerospace technology to nonaerospace applications, thus assuring American taxpayers maximum return on their investment in space research; thousands of spinoffs of NASA research have already occurred in virtually every area of our economy.

The TU program has worked for engineers, scientists, technicians, and businessmen; and it can work for you.

NASA Tech Briefs

Tech Briefs is published quarterly and is free to engineers in U.S. industry and to other domestic technology transfer agents. It is both a current-awareness medium and a problem-solving tool. Potential products . . . industrial processes . . . basic and applied research . . . shop and lab techniques . . . computer software . . . new sources of technical data . . . concepts . . . can be found here. The short section on New Product Ideas highlights a few of the potential new products contained in this issue. The remainder of the volume is organized by technical category to help you quickly review new developments in your areas of interest. Finally, a subject index makes each issue a convenient reference file.

Further Information on Innovations

Although some new technology announcements are complete in themselves, most are backed up by Technical Support Packages (TSP's). TSP's are available without charge and may be ordered by simply completing a TSP Request Card found at the back of this volume. Further information on some innovations is available for a nominal fee from other sources, as indicated. In addition, Technology Utilization Officers at NASA Field Centers will often be able to lend necessary guidance and assistance.

Patent Licenses

Patents have been issued to NASA on some of the inventions described, and patent applications have been submitted on others. Each announcement indicates patent status, if applicable.

Other Technology Utilization Services

To assist engineers, industrial researchers, business executives, city officials, and other potential users in applying space technology to their problems, NASA sponsors Industrial Applications Centers. Their services are described on page A7. In addition, an extensive library of computer programs is available through COSMIC, the Technology Utilization Program's outlet for NASA-developed software.

Applications Program

NASA conducts applications engineering projects to help solve public-sector problems in such areas as safety, health, transportation, and environmental protection. Applications teams, staffed by professionals from a variety of disciplines, assist in this effort by working with Federal agencies and health organizations to identify critical problems amenable to solution by the application of existing NASA technology.

Reader Feedback

We hope you find the information in *NASA Tech Briefs* useful. A reader-feedback card has been included because we want your comments and suggestions on how we can further help you apply NASA innovations and technology to your needs. Please use it; or if you need more space, write to the Director, Technology Transfer Division, P. O. Box 8757, Baltimore/Washington International Airport, Maryland 21240.

NASA Tech Briefs

National
Aeronautics and
Space
Administration

SUMMER 1980
Volume 5, Number 2

NASA TU Services
A3 Technology Utilization services that can assist you in learning about and applying NASA technology.

New Product Ideas
A9 A summary of selected innovations of value to manufacturers for the development of new products.

Tech Briefs
131 **Electronic Components and Circuits**

147 **Electronic Systems**

159 **Physical Sciences**

177 **Materials**

185 **Life Sciences**

189 **Mechanics**

211 **Machinery**

229 **Fabrication Technology**

249 **Mathematics and Information Sciences**

Subject Index
257 **Items in this issue are indexed by subject; a cumulative index will be published yearly.**

COVERS: The photographs on the front and back covers illustrate developments by NASA and its contractors that have resulted in commercial and nonaerospace spinoffs. To find out more about the application of satellite images [Regional Remote-Sensing Applications Program], Circle 100 on the TSP Request Card at the back of this issue of NASA Tech Briefs. To find out more about the metalized products, Circle 101.

About This NASA Publication

NASA Tech Briefs, a quarterly publication, is distributed free to qualified U.S. citizens to encourage commercial application of U.S. space technology. For information on publications and services available through the NASA Technology Utilization Program, write to the Director, Technology Transfer Division, P. O. Box 8757, Baltimore/Washington International Airport, Maryland 21240.

"The Administrator of National Aeronautics and Space Administration has determined that the publication of this periodical is necessary in the transaction of the public business required by law of this Agency. Use of funds for printing this periodical has been approved by the Director of the Office of Management and Budget."

Change of Address

If you wish to have NASA Tech Briefs forwarded to your new address, use one of the Subscriptions cards enclosed in the back of this volume of NASA Tech Briefs. Be sure to check the appropriate box indicating change of address.

Communications Concerning Editorial Matter

For editorial comments or general communications about NASA Tech Briefs, you may use the Feedback card in the back of NASA Tech Briefs, or write to: The Publications Manager, Technology Transfer Division (ETD-6), NASA Headquarters, Washington, DC 20546. Technical questions concerning specific articles should be directed to the Technology Utilization Officer of the sponsoring NASA Center (addresses listed on page A4).

1978 Index

Readers who wish to request a copy of the 1978 Index to NASA Tech Briefs may still do so by Circling 102 on the TSP Request Card at the back of this issue.

Acknowledgements

NASA Tech Briefs is published quarterly by the National Aeronautics and Space Administration, Technology Utilization Branch, Washington, DC: Administrator: **Robert A. Frosch;** Director, Technology Transfer Division: **Floyd I. Roberson;** Publications Manager: **D. W. Orrick.** Prepared for the National Aeronautics and Space Administration by **Logical Technical Services Corp.**: Editor-in-Chief: **Jay Kirschenbaum;** Art Director: **Ernest Gillespie;** Assistant Editor: **Jerome Rosen;** Chief Copy Editor: **Oden Browne;** Staff Editors: **Donald Blattner, Ted Selinsky, George Watson:** Graphics: **Concetto Auditore, Luis Martinez;** Editorial & Production: **Richard Johnson, Rose Giglietti, Beth Rogers, Vincent Susinno, John Tucker, Ernestine Walker.**

This document was prepared under the sponsorship of the National Aeronautics and Space Administration.. Neither the United States Government nor any person acting on behalf of the United States Government assumes any liability resulting from the use of the information contained in this document, or warrants that such use will be free from privately owned rights.

NASA
TU SERVICES

NASA TECHNOLOGY UTILIZATION NETWORK

★ TECHNOLOGY UTILIZATION OFFICERS

Charles C. Kubokawa
Ames Research Center
Code AU: 240-2
Moffett Field, CA 94035
(415) 965-5333

Gussie Anderson
Hugh L. Dryden Flight Research Center
Code OD/TU Office - Room 2015
Post Office Box 273
Edwards, CA 93523
(805) 258-3311, Ext. 787

Donald S. Friedman
Goddard Space Flight Center
Code 702.1
Greenbelt, MD 20771
(301) 344-6242

John T. Wheeler
Lyndon B. Johnson Space Center
Code AT-3
Houston, TX 77058
(713) 483-3809

Raymond J. Cerrato
John F. Kennedy Space Center
Code PT-STA-1
Kennedy Space Center, FL 32899
(305) 867-2780

John Samos
Langley Research Center
Mail Stop 139A
Hampton, VA 23665
(804) 827-3281

Harrison Allen, Jr.
Lewis Research Center
Mail Code 7-3
21000 Brookpark Road
Cleveland, OH 44135
(216) 433-4000, Ext. 6422

Aubrey D. Smith
George C. Marshall Space Flight Center
Code AT01
Marshall Space Flight Center, AL 35812
(205) 453-2224

D. W. Orrick
NASA Headquarters
Code ETD-6
Washington, DC 20546
(202) 755-2244

John H. Warden
NASA Pasadena Office
4800 Oak Grove Drive
Pasadena, CA 91103
(213) 354-6420

Gilmore H. Trafford
Wallops Flight Center
Code OD
Wallops Island, VA 23337
(804) 824-3411, Ext. 201

● INDUSTRIAL APPLICATIONS CENTERS

Aerospace Research Applications Center
1201 East 38th Street
Indianapolis, IN 46205
E. G. Buck, director
(317) 264-4644

Computer Software Management and Information Center (COSMIC)
Suite 112, Barrow Hall
University of Georgia
Athens, GA 30602
(404) 542-3265

Kerr Industrial Applications Center
Southeastern Oklahoma State University
Durant, OK 74701
Robert Oliver, director
(405) 924-0121, Ext. 413

NASA Industrial Applications Center
LIS Building
University of Pittsburgh
Pittsburgh, PA 15260
Edmond Howie, director
(412) 624-5211

New England Research Applications Center
Mansfield Professional Park
Storrs, CT 06268
Daniel Wilde, director
(203) 486-4533

North Carolina Science and Technology Research Center
Post Office Box 12235
Research Triangle Park, NC 27709
Peter J. Chenery, director
(919) 549-0671

Technology Applications Center
University of New Mexico
Albuquerque, NM 87131
Stanley Morain, director
(505) 277-3622

Western Research Applications Center
University of Southern California
University Park
Los Angeles, CA 90007
Robert Mixer, acting director
(213) 741-6132

■ STATE TECHNOLOGY APPLICATIONS CENTERS

NASA/University of Florida
State Technology Applications Center
311 Weil Hall
University of Florida
Gainesville, FL 32611
Ronald J. Thornton, director
Gainesville: (904) 392-6760
Orlando: (305) 275-2706
Tampa: (813) 974-2499

NASA/University of Kentucky
State Technology Applications Program
109 Kinkead Hall
University of Kentucky
Lexington, KY 40506
William R. Strong, manager
(606) 258-4632

◆ PATENT COUNSELS

Robert F. Kempf
Asst. Gen. Counsel for patent matters
NASA Headquarters
Code GP-4
400 Maryland Avenue, S.W.
Washington, DC 20546
(202) 755-3954

Darrell G. Brekke
Ames Research Center
Mail Code: 200-11A
Moffett Field, CA 94035
(415) 965-5104

Paul F. McCaul
Hugh L. Dryden Flight Research Center
Code OD/TU Office - Room 2015
Post Office Box 273
Edwards, CA 93523
(213) 354-2734

John O. Tresansky
Goddard Space Flight Center
Mail Code: 204
Greenbelt, MD 20771
(301) 344-7351

Marvin F. Matthews
Lyndon B. Johnson Space Center
Mail Code: AM
Houston, TX 77058
(713) 483-4871

James O. Harrell
John F. Kennedy Space Center
Mail Code: SA-PAT
Kennedy Space Center, FL 32899
(305) 867-2544

Howard J. Osborn
Langley Research Center
Mail Code: 279
Hampton, VA 23665
(804) 827-3725

Norman T. Musial
Lewis Research Center
Mail Code: 500-311
21000 Brookpark Road
Cleveland, OH 44135
(216) 433-4000, Ext. 346

Leon D. Wofford, Jr.
George C. Marshall Space Flight Center
Mail Code: CC01
Marshall Space Flight Center, AL 35812
(205) 453-0020

Monte F. Mott
NASA Pasadena Office
Mail Code: 180-601
4800 Oak Grove Drive
Pasadena, CA 91103
(213) 354-2700

▲ APPLICATION TEAMS

William N. Fetzner, director
Advisory Center for Medical Technology and Systems
University of Wisconsin
1500 Johnson Drive
Madison, WI 53706
(608) 263-2735

Edmund R. Bangs, director
IIT Research Institute
10 West 35th Street
Chicago, IL 60616
(312) 567-4191

Doris Rouse, director
Research Triangle Institute
Post Office Box 12194
Research Triangle Park, NC 27709
(919) 541-6256

Tom Anyos, director
SRI International
333 Ravenswood Avenue
Menlo Park, CA 94026
(415) 326-6200, Ext. 2864

Eugene Schmidt, program coordinator
Stanford University School of Medicine
Cardiology Division
Biomedical Technology Transfer
703 Welch Road, Suite E-4
Palo Alto, CA 94304
(415) 497-5353

David MacFadyen, project director
Technology + Economics
2225 Massachusetts Avenue
Cambridge, MA 02140
(617) 491-1500

TECHNOLOGY UTILIZATION OFFICERS

Technology transfer experts can help you apply the innovations in NASA Tech Briefs.

The Technology Utilization Officer at each NASA Field Center is an applications engineer who can help you make use of new technology developed at his center. He brings you NASA Tech Briefs and other special publications, sponsors conferences, and arranges for expert assistance in solving technical problems.

Technical assistance, in the form of further information about NASA innovations and technology, is one of the services available from the TUO. Together with NASA scientists and engineers, he can often help you find and implement NASA technology to meet your specific needs.

Technical Support Packages (TSP's) are prepared by the center TUO's. They provide further technical details for articles in NASA Tech Briefs. This additional material can help you evaluate and use NASA technology. You may receive most TSP's free of charge by using the TSP Request Card found at the back of this issue.

Technical questions about articles *in NASA Tech Briefs are answered in the TSP's. When no TSP is available, or you have further questions, contact the Technology Utilization Officer at the center that sponsored the research* [*see page A4*].

NASA INVENTIONS AVAILABLE FOR LICENSING

Over 3,500 NASA inventions are available for licensing in the United States — both exclusive and nonexclusive.

Nonexclusive licenses for commercial use of NASA inventions are encouraged to promote competition and to achieve the widest use of inventions. They must be used by a negotiated target date but are usually royalty-free.

Exclusive licenses may be granted to encourage early commercial development of NASA inventions, especially when considerable private investment is required. These are generally for 5 to 10 years and usually require royalties based on sales or use.

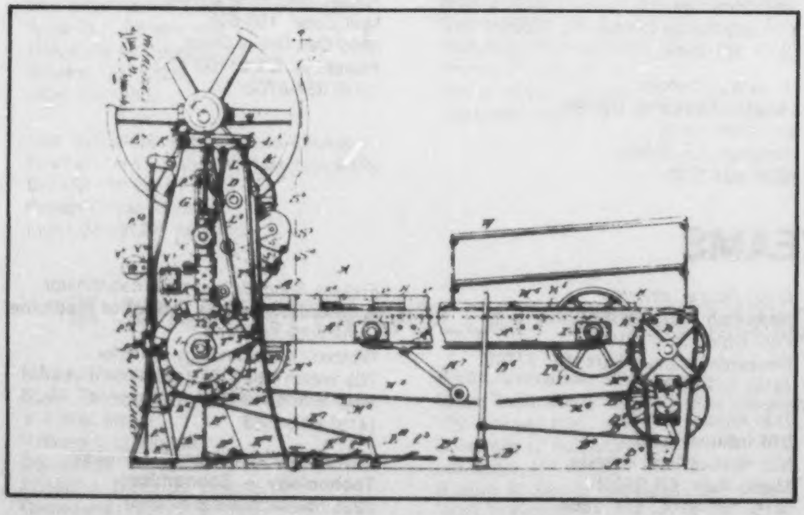

Additional licenses available include those of NASA-owned foreign patents. In addition to inventions described in NASA Tech Briefs, *"NASA Patent Abstract Bibliography"* (PAB), containing abstracts of all NASA inventions, can be purchased from National Technical Information Service, Springfield, VA 22161. The PAB is updated semiannually.

Patent licenses for Tech Briefs *are frequently available. Many of the inventions reported in NASA Tech Briefs are patented or are under consideration for a patent at the time they are published. The current patent status is described at the end of the article; otherwise, there is no statement about patents. If you want to know more about the patent program or are interested in licensing a particular invention, contact the Patent Counsel at the NASA Field Center that sponsored the research* [*see page A5*]. *Be sure to refer to the NASA reference number at the end of the Tech Brief.*

APPLICATION TEAMS

Technology-matching and problem-solving assistance to public-sector organizations

Application engineering projects are conducted by NASA to help solve public-sector problems in such areas as safety, health, transportation, and environmental protection. Some application teams specialize in biomedical disciplines; others, in engineering and scientific problems. Staffed by professionals from various disciplines, these teams work with other Federal agencies and health organizations to identify critical problems amenable to solution by the application of existing NASA technology.

***Public-sector organization** representatives can learn more about application teams by contacting a nearby NASA Field Center Technology Utilization Office [see page A4].*

INDUSTRIAL APPLICATIONS CENTERS

Computerized access to nearly 10 million documents worldwide

Computerized information retrieval from one of the world's largest banks of technical data is available from NASA's network of Industrial Applications Centers (IAC's). The IAC's give you access to 1,800,000 technical reports in the NASA data base and to more than 10 times that many reports and articles found in 140 other computerized data bases.

The major sources include:
- *750,000 NASA Technical Reports*
- *Selected Water Resources Abstracts*
- *NASA Scientific and Technical Aerospace Reports*
- *Air Pollution Technical Information Center*
- *NASA International Aerospace Abstracts*
- *Chem Abstracts Condensates*
- *Engineering Index*
- *Energy Research Abstracts*
- *NASA Tech Briefs*
- *Government Reports Announcements*

and many other specialized files on food technology, textile technology, metallurgy, medicine, business, economics, social sciences, and physical science.

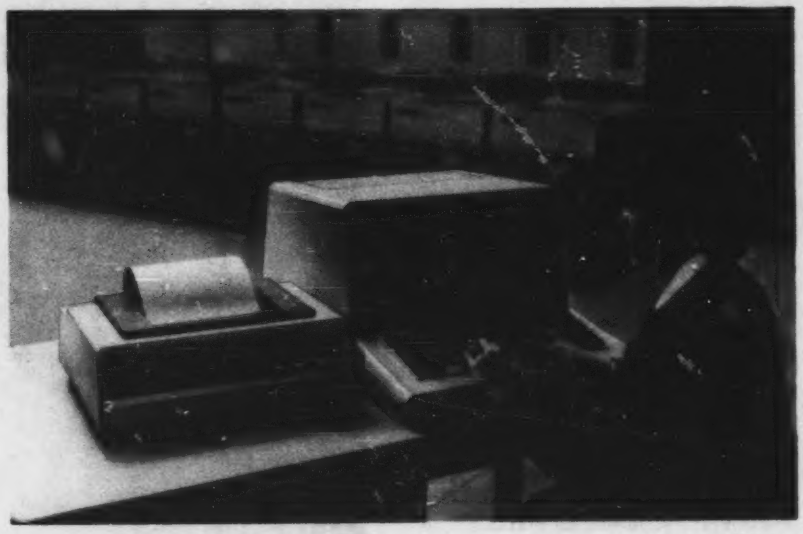

The IAC services range from tailored literature searches through expert technical assistance:

- *Retrospective Searches:* Published or unpublished literature is screened, and documents are identified according to your interest profile. IAC engineers tailor results to your specific needs and furnish abstracts considered the most pertinent. Complete reports are available upon request.
- *Current-Awareness Searches:* IAC engineers will help design a program to suit your needs. You will receive selected monthly or quarterly abstracts on new developments in your area of interest.
- *Technical Assistance:* IAC engineers will help you evaluate the results of your literature searches. They can help find answers to your technical problems and put you in touch with scientists and engineers at appropriate NASA Field Centers.

***Prospective clients** can obtain more information about the services offered by NASA IAC's by contacting the nearest IAC [see page A4] or by checking the IAC box on a TSP Request Card in this issue.*

STATE TECHNOLOGY APPLICATIONS CENTERS

Technical information services for industry
and state and local government agencies

Local government and industry in Florida and Kentucky can utilize the services of NASA's State Technology Applications Centers (STAC's). The STAC's differ from the Industrial Applications Centers described on page A7, primarily in that they are integrated into existing state technical assistance programs and serve only the host state, whereas the IAC's serve multistate regions.

Many data bases, including the NASA base and several commercial bases, are available for automatic data retrieval through the STAC's. Other services such as document retrieval and special searches are also provided. (The STAC's normally charge a fee for their services.)

To obtain information *about the services offered by NASA STAC's, write or call the STAC in your state [see page A4].*

COSMIC®

An economical source of computer programs
developed by NASA and other government agencies

A vast software library is maintained by COSMIC — the Computer Software Management and Information Center. COSMIC gives you access to approximately 1,600 computer programs developed for NASA and the Department of Defense and selected programs for other government agencies. Programs and documentation are available at reasonable cost.

Available programs range from management (PERT scheduling) to information science (retrieval systems) and computer operations (hardware and software). Hundreds of engineering programs perform such tasks as structural analysis, electronic circuit design, chemical analysis, and the design of fluid systems. Others determine building energy requirements and optimize mineral exploration.

COSMIC services go beyond the collection and storage of software packages. Programs are checked for completeness; special announcements and an indexed software catalog are prepared; and programs are reproduced for distribution. Customers are helped to identify their software needs; and COSMIC follows up to determine the successes and problems and to provide updates and error corrections. In some cases, NASA engineers can offer guidance to users in installing or running a program.

Information about programs *described in NASA Tech Briefs articles can be obtained by completing the COSMIC Request Card at the back of this issue. Just circle the letters that correspond to the programs in which you are interested.*

NEW PRODUCT IDEAS

NEW PRODUCT IDEAS are just a few of the many innovations described in this issue of NASA Tech Briefs and having promising commercial applications. Each is discussed further on the referenced page in the appropriate section in this issue. If you are interested in developing a product from these or other NASA innovations, you can receive further technical information by requesting the TSP referenced at the end of the full-length article or by writing the Technology Utilization Office of the sponsoring NASA center (see page A4). NASA's patent-licensing program to encourage commercial development is described on page A8.

Flared-Tube Attachment Fitting

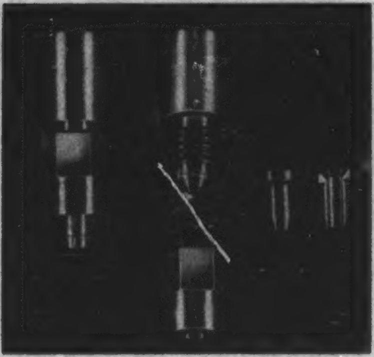

Tubes can be flared first, then attached to valves and other flow-line components, with a new fitting that can be disassembled and reused. The installed fitting can be disassembled so that the parts can be inspected. It can be salvaged and reused without damaging the flared tube; and the tube can be coated, tempered, or otherwise treated after it has been flared, rather than before, as was previously required. The fitting consists of a threaded male portion with a conical seating surface, a hexagonal nut with a hole larger than the outer diameter of the flared end of the tube, and a split ferrule.
(See page 213.)

Automatic Thermal Switches

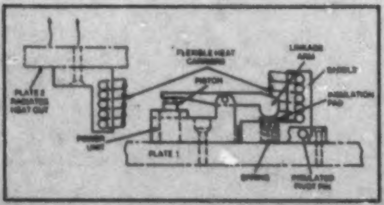

Two new automatic switches control heat flow from one thermally conductive plate to another. One switch permits heat flow to the outside; the other limits heat flow. Mechanically simple and reliable, the switches can be used in almost any situation in which temperature can be controlled by regulating heat flow. In one switch, heat on a conductive plate activates a piston that forces a saddle against the plate. Heat carriers then conduct the heat to a second plate that radiates it away. After the temperature in the first plate drops, the piston contracts and a spring breaks thermal contact with the plate. In the second switch, the action is reversed.
(See page 191.)

UV Actinometer Film

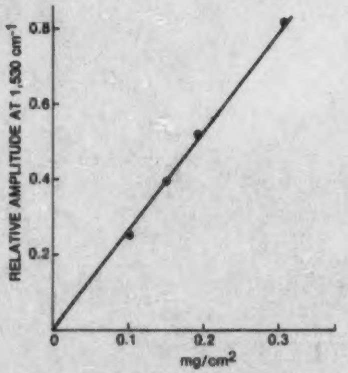

Cumulative UV radiation can be measured by a proposed low-cost polymer film that is unaffected by visible light. Useful for virtually any surface, the film can help paint and plastics manufacturers determine how well their products stand up aginst UV radiation. The proposed actinometer film uses a photochemically sensitive compound that changes its chemical composition in response to solar UV radiation. The extent of this chemical conversion depends on the length of the exposure and can be measured by examining the film samples with a spectrophotometer. The film can be exposed from several seconds up to a month.
(See page 165.)

Tube-Flare Inspection Tool

The flare angle and symmetry of tube ends can be checked by a simple tool that consists of two stainless-steel pins bonded to a rubber plug. The primary function of the tool is to inspect tubes before they are installed, thereby eliminating the expense and inconvenience of repairing leaks caused by imperfect flares.

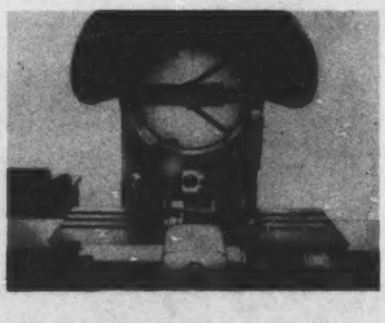

Measuring hole tapers, countersink angles, and bearing-race angles are other possible uses. The tool is used with an optical comparator. The axis of the tool is alined with the centerline of the tube. The shadow of the seated pins on the comparator screen allows the operator to verify that the flare angle is within tolerance.
(See page 213.)

Direct-Current Converter for Gas-Discharge Lamps

Metal/halide and similar gas-discharge lamps can be powered from a low-voltage dc source, using a small efficient converter. The converter can be useful wherever 60-cycle ac power is not available or where space and weight allocations are limited. Possible applications are in offshore platforms, mobile homes, and emergency lighting. Several design innovations give the new supply high reliability and an efficiency of up to 75 percent. The instantaneous high voltage available

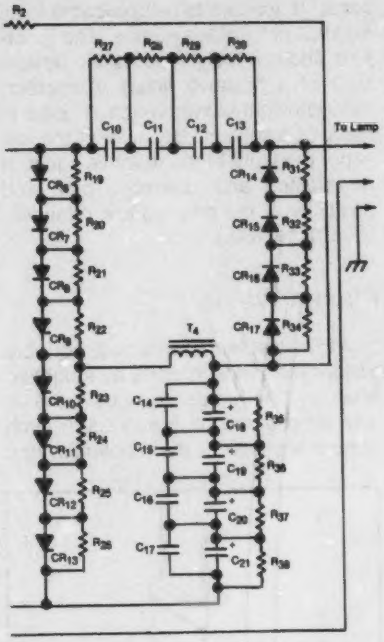

R7
R27
R28
R29
R30
C10
C11
C12
C13
To Lamp
CR6
CR7
CR8
CR9
CR10
CR11
CR12
CR13
R19
R20
R21
R22
R23
R24
R25
R26
CR14
CR15
CR16
CR17
R31
R32
R33
R34
T4
C14
C15
C16
C17
C18
C19
C20
C21
R35
R36
R37
R38

with the circuit makes the lamp less likely to "blow out" because of transients in the power source. The circuit also stabilizes the lamp current, thus eliminating the need for an external "ballast."
(See page 140.)

Camera Add-On Records Time of Exposure

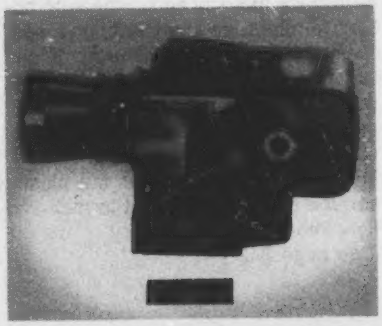

A compact module attached to a camera contains all the electronics and optics needed to print the time a photograph is taken on the edge of that photograph. The module can be used wherever it is necessary to document the exact time a photo is taken. The module includes an eight-digit LED display that continuously shows the time to an accuracy of a hundredth of a second. The normally blanked display is unblanked when the camera shutter switch is activated. Light from the display is reflected off two flat mirrors, through a focusing lens, into the camera, and onto the film.
(See page 168.)

Electrofluidic Accelerometer

An electrofluidic accelerometer senses components of a linear or angular acceleration field. A typical application of such an accelerometer is as an active controlling element in an airplane autopilot. In contrast to conventional accelerometers, an electrofluidic accelerometer is lightweight, small, inexpensive, rugged, and requires little power. It consists of two temperature sensors on opposite sides of a heating element. The sensors detect the temperature gradient created by an acceleration field on the fluid; and when the device is accelerated, the gradient changes because of the buoyant force on the hotter (thus lighter) portion of the fluid.
(See page 201.)

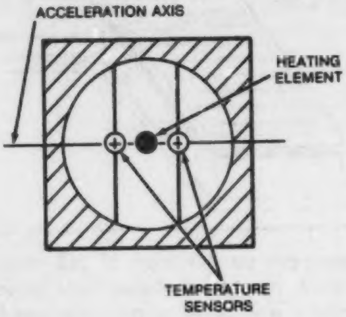

ACCELERATION AXIS
HEATING ELEMENT
TEMPERATURE SENSORS

Handtool Assists in Bundling Cables

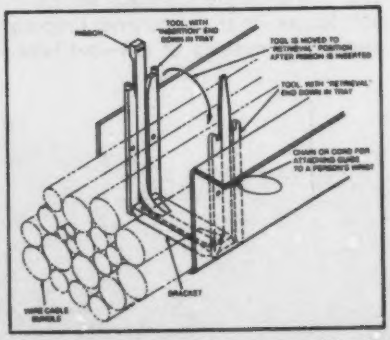

RIBBON
TOOL, WITH "INSERTION" END DOWN IN TRAY
TOOL IS MOVED TO "RETRIEVAL" POSITION AFTER RIBBON IS INSERTED
TOOL, WITH "RETRIEVAL" END DOWN IN TRAY
CHAIN OR CORD FOR ATTACHING GUIDE TO A PERSON'S WRIST
BRACKET
WIRE CABLE BUNDLE

A simple tool makes it possible to bundle electrical cables in a channel or "tray" without requiring that the cables be lifted out of the tray. The procedure for bundling is faster and less awkward than the old method of lifting the cables for wrapping. Used with commercially-available plastic ribbons that tie the cables together, the tool guides the ribbon along a tray wall, through a bracket at the bottom of the tray, and up the opposite wall. One end of the ribbon locks in the other end, securing the cable bundle.
(See page 225.)

Bayonet Plug With Ramp-Activated Lock

A matched pair of washers with broad surface ramps is the locking mechanism in a new bayonet plug. It can be used where threaded fasteners and springs are impractical because of extreme temperatures or other environmental incompatibility. The matched pair of ramped washers is placed on the plug and the bayonet inserted. The inner slot of one washer matches the contour of the plug; this washer is stationary. The inner slot of the second washer is circular. When the second washer is rotated, the washers push against the bayonet plug, locking it in place. A retaining wire secures the plug.
(See page 218.)

Fluorescent Radiation Converter

A new fluorescent radiation converter uses an optically transparent substrate. One side of the substrate is coated with a plastic film containing fluorescent organic dyes that absorb optical radiation at one wavelength and emit it at a longer one. The coating is formulated to respond to specific wavelengths. The emitted radiation is reflected internally inside the substrate, amplifying the intensity that reaches the radiation detector.

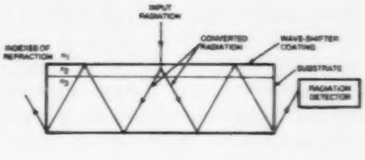

The converter can be made in several sizes and shapes; round or square bars coated all around their lengths are useful in converting relatively intense radiation and transmitting it through the substrate over lengthy distances.
(See page 166.)

A Linear Magnetic Motor and Generator

In a proposed linear magnetic motor and generator, suitable for remote and hostile environments, magnetic forces drive a reciprocating shaft along its axis. The actuator shaft is located in the center of a cylindrical body and may be supported by either contacting or noncontacting bearings. When the device operates as a bidirectional motor, the drive coil selectively adds and subtracts magnetic flux to and from the flux paths to produce the forces that drive the actuator back and forth along the axis. When the actuator is driven by an external reciprocating engine, the device becomes an ac generator.
(See page 226.)

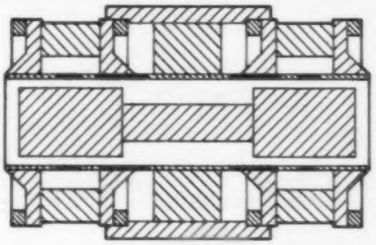

"Peeled-Film" Solar Cells

Proposed "peeled-film" solar cells could be lighter and less expensive than conventional cells. The GaAs cells would be deposited on a GaAs substrate coated with a thin etchable layer that would allow the completed cell film to be peeled away from the substrate. At an estimated conversion efficiency of 18 percent, an array of such cells would deliver about 1 kW of electricity per kilogram of cell material. A blanket of these cells would deliver energy at a power-to-weight ratio about 4 times that of conventional 2-mil (0.5-mm) silicon solar cells. In addition, GaAs solar cells have better radiation resistance than silicon cells.
(See page 135.)

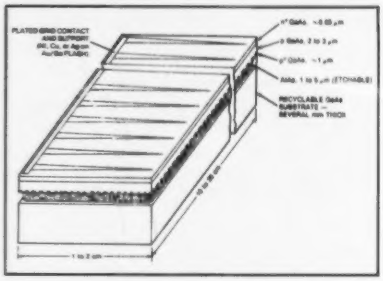
PLATED GRID CONTACT AND SUPPORT (Ni, Cu, or Ag on Au/Ge FLASH)
n+ GaAs
p GaAs, 2 to 3 µm
p+ GaAs, ~1 µm
AlAs, 1 to 5 µm (ETCHABLE)
RECYCLABLE GaAs SUBSTRATE — SEVERAL mm THICK
1 to 2 cm

Plasticizer for Polyimide Composites

The problem of maintaining good prepreg tack and drape has been solved by a new modification of an addition polyimide. Tack and drape are the ability of the prepreg to adhere to adjacent plies and to conform to a desired shape during the layup process. This alternate approach will allow both longer life of the polymer prepreg and the processing of low-void laminates. It appears to be applicable to all addition polyimide systems. The modified addition polyimide takes advantage of a reactive liquid plasticizer, monoethylphthalate, which is used in place of a solvent. Because of the low vapor pressure of the reactive liquid, it is retained and, thereby, tack and flexibility of the prepreg are retained.
(See page 180.)

Plastic Welder

A low-cost, self-contained, portable welder joins plastic parts by induction heating. The welder can be used in any atmosphere or in a vacuum, with almost any type of thermoplastic; and the plastic components can be joined in situ. Possible uses are in the aerospace industry and in the automobile, furniture, and construction industries. The low power requirements can be easily met by battery or solar power. In the welder, a toroidal inductor transfers magnetic flux through the thermoplastic to a screen. The heated screen causes the plastic surface on either side of it to melt and flow into it to form the joint.
(See page 242.)

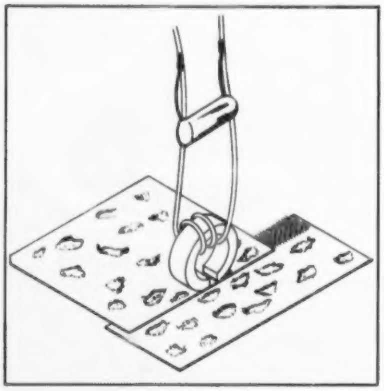

Electronic Components and Circuits

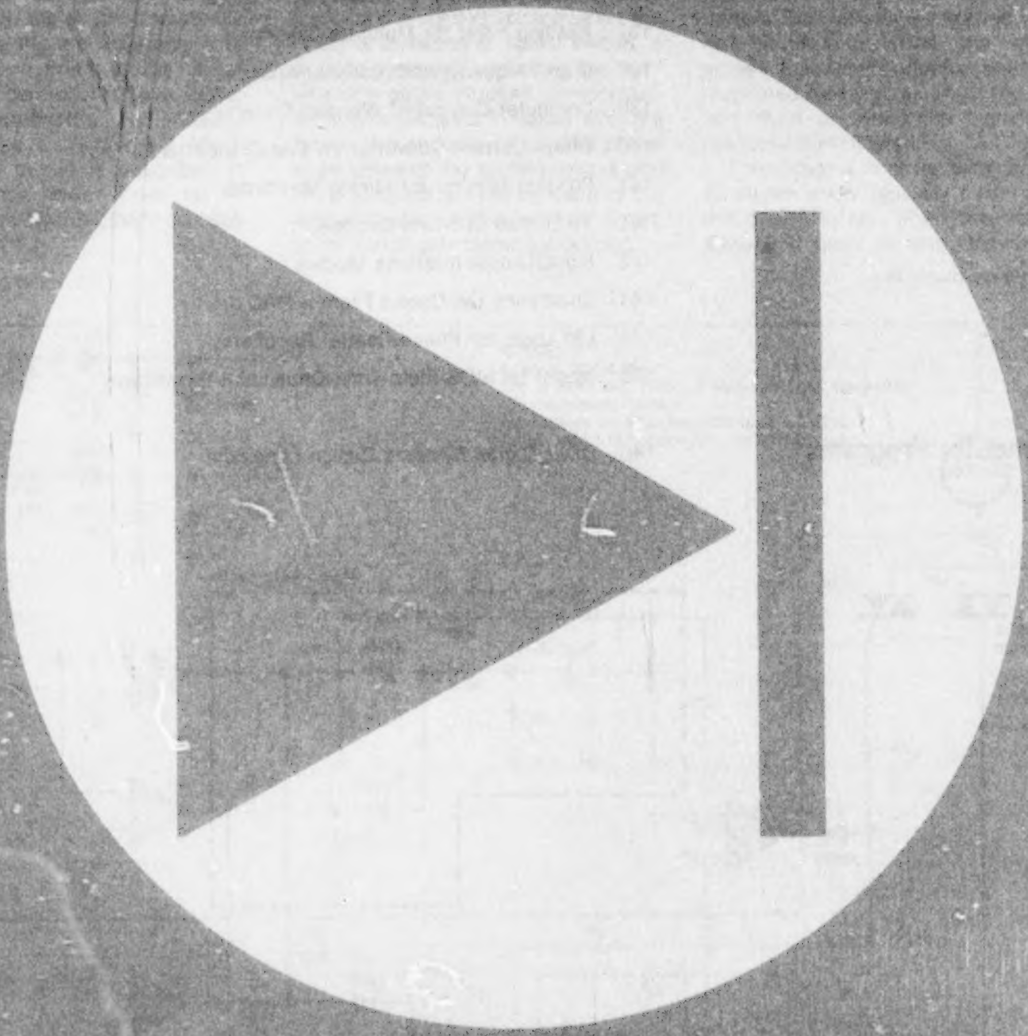

Hardware, Techniques, and Processes

133 Improved Power-Factor Controller
134 Energy Saving in ac Generators
135 "Peeled-Film" Solar Cells
136 Temperature-Compensating dc Restorer
137 Aliasing Filter for Multirate Systems
138 Dual-Frequency Bidirectional Antenna
139 Computer-Controlled Warmup Circuit
140 Direct-Current Converter for Gas-Discharge Lamps
141 Position Monitor for Mining Machines
141 11-Line to 512-Line Decoder
143 Input/Output Interface Module
144 Smoothing the Output From a DAC
144 LSI Logic for Phase-Control Rectifiers
145 Model for MOS Field-Time-Dependent Breakdown

Computer Programs

146 DDL: Digital Systems Design Language

Improved Power-Factor Controller

Two improvements increase energy savings in ac motors without sacrificing performance.

Marshall Space Flight Center, Alabama

An improved power-factor controller for ac motors saves more energy, yet is simpler and less expensive than the original circuit. Motor performance is unaffected by the modifications. [The first *NASA Tech Briefs* article on the power-factor controller, "Save Power in AC Induction Motors" (MFS-23280), appeared on page 179 of Vol. 2, No. 2. An improved circuit is described in "Fast-Response Power Saver for Induction Motors" (MFS-23988) on page 6 of Vol. 4, No. 1.]

The power-factor controller, in either its original or improved form, reduces ac losses in an induction motor by lowering the applied voltage when the motor is unloaded or lightly loaded. It does so by phase-controlling the "on" time of a gate-controlled semiconductor switch installed in series with the motor. The circuit monitors the phase angle between the applied voltage and the lagging current (an indicator of the level of loading) and adjusts the timing of the switch gate signal accordingly.

In the original circuit, the voltage across a high-power resistor in series with the motor was used to sense the current. This resistor is removed in the new circuit and instead, the voltage across the semiconductor switch is monitored (see figure). Thus, the cost and effort of wiring the high-power resistor are eliminated.

The voltage across the semiconductor switch is low, typically 1 volt, when the switch is on. When the current through it goes to zero, the switch

(continued on next page)

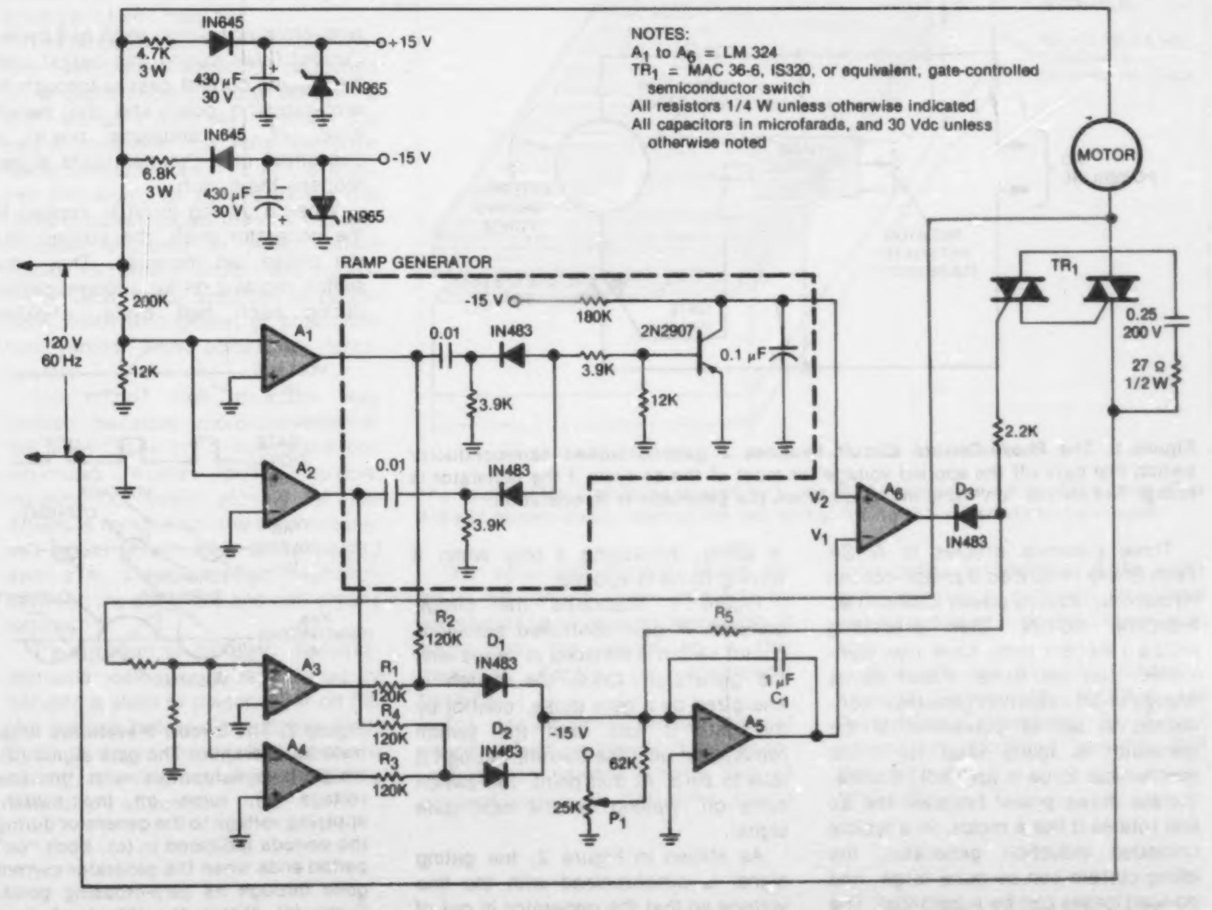
IN645
4.7K
3 W
430 μF
30 V
IN965
+15 V
IN645
6.8K
3 W
430 μF
30 V
IN965
-15 V
RAMP GENERATOR
-15 V
180K
0.01
IN483
3.9K
2N2907
0.1 μF
12K
3.9K
200K
120 V
60 Hz
12K
A1
A2
0.01
IN483
3.9K
MOTOR
TR1
0.25
200 V
27 Ω
1/2 W
2.2K
V2
V1
A6
D3
IN483
R2
120K
D1
IN483
R5
1 μF
C1
A3
R1
120K
R4
120K
A4
R3
120K
D2
IN483
-15 V
62K
A5
25K
P1

NOTES:
A_1 to A_6 = LM 324
TR_1 = MAC 36-6, IS320, or equivalent, gate-controlled semiconductor switch
All resistors 1/4 W unless otherwise indicated
All capacitors in microfarads, and 30 Vdc unless otherwise noted

In the Improved Power-Factor Controller, A_6 delivers a gate pulse that turns on the semiconductor switch. The voltage across the switch, an indicator of the motor current, is fed back to op-amps A_3 and A_4. Resistor R_5 adds feedback of the gate pulse.

automatically shuts off, and the voltage rises to almost the full line voltage. This abrupt rise marks the zero-crossing point of the current.

The time interval between the current and voltage zero crossings is a measure of the phase angle. The circuit associated with op-amps A_3 and A_4, resistors R_1, R_2, R_3, and R_4, and diodes D_1 and D_2 develops a positive voltage proportional to this interval at the inverting input to A_5. A negative voltage from potentiometer P_1 is also fed to this input. Thus, the output voltage of A_5, a measure of how much the phase angle departs from a preselected value set by P_1, is an error signal that can be used to control the turn-on point of the switch. This voltage (V_1) is compared with ramp voltage V_2 at A_6, and the output of A_6 delivers the gate pulse.

Resistor R_5 is also an improvement not present on the original circuit. It adds a small amount of positive feedback of the gate signal to the inverting input of A_5. This further decreases the switch "on" time when the motor is unloaded, without sacrificing full-load performance. In tests, no-load savings were increased by over 70 percent by adding just this one resistor.

This work was done by Frank J. Nola of **Marshall Space Flight Center**. *For further information, Circle 1 on the TSP Request Card.*

Inquiries concerning rights for the commercial use of this invention should be addressed to the Patent Counsel, Marshall Space Flight Center [see page A5]. Refer to MFS-25323.

Energy Saving in ac Generators

Circuit cuts no-load losses, without sacrificing full-load power.

Marshall Space Flight Center, Alabama

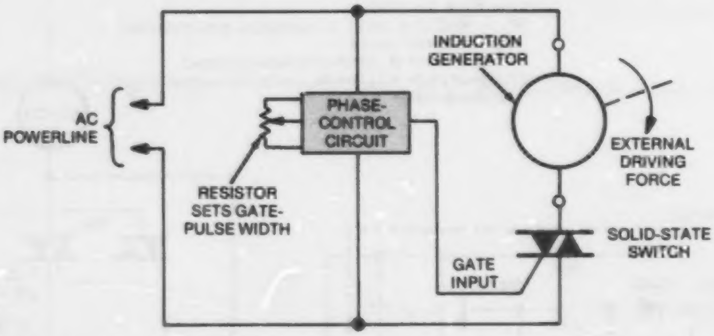

Figure 1. The Phase-Control Circuit includes a gate-controlled semiconductor switch that cuts off the applied voltage for most of the ac cycle if the generator is idling. The switch "on" time increases when the generator is in operation.

Three previous articles in *NASA Tech Briefs* described a phase-control circuit that reduces power losses in ac induction motors. (See preceding article.) Recent tests have now confirmed that the same circuit saves energy in an induction generator connected to an ac powerline. If the generator is idling (that is, if no mechanical force is applied), it nonetheless draws power because the ac line rotates it like a motor. In a typical unloaded induction generator, the idling current can be quite large, and no-load losses can be substantial. The circuit reduces the losses by lowering the applied voltage when the generator is idling, increasing it only when a driving force is applied.

Figure 1 illustrates the circuit concept. A gate-controlled semiconductor switch is installed in series with the generator. Once the switch is energized by a gate pulse, control by the gate is lost, and the switch remains on until the current through it falls to zero. At that point, the switch turns off, waiting for the next gate signal.

As shown in Figure 2, the gating signal is synchronized with the line voltage so that the generator is out of the circuit except for a short period that begins just before the voltage zero-crossing point in each half cycle. Current flows during this period until the lagging current passes through its zero-crossing point and the switch turns off. No additional power is consumed until the next gate signal reopens the switch.

When a driving force is applied to the generator shaft, the current and the phase lag increase. Thus, the switch remains on for a longer period during each half cycle, allowing

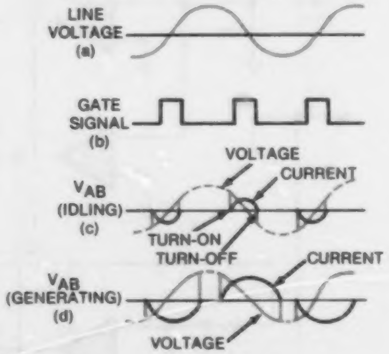

Figure 2. The Circuit Waveforms illustrate its operation. The gate signal (b), which is synchronous with the line voltage (a), turns on the switch, applying voltage to the generator during the periods indicated in (c). Each "on" period ends when the generator current goes through its zero-crossing point. Curve (d) shows the increased "on" time registered when the generator is driven.

energy from the generator to be transferred to the ac line. If the current and phase lag increase sufficiently, the switch can remain on for a full cycle.

Using this method for a 1/2-horsepower (746-watt) induction generator driven by a dc motor, idling losses were reduced from 210 watts to 70 watts, with no sacrifice in performance when the generator is driven at full output.

This work was done by Frank J. Nola of **Marshall Space Flight Center.** *For further information, Circle 2 on the TSP Request Card.*

Inquiries concerning rights for the commercial use of this invention should be addressed to the Patent Counsel, Marshall Space Flight Center [see page A5]. Refer to MFS-25302.

"Peeled-Film" Solar Cells

Proposed GaAs cells would be lighter and more economical than conventional cells.

NASA's Jet Propulsion Laboratory, Pasadena, California

Proposed "peeled-film" solar cells could be lighter and less expensive than conventional cells. At an estimated conversion efficiency of 18 percent, an array of such cells would deliver about 1 kW of electricity per kilogram of cell material.

The proposed GaAs n^+p cell structure (see figure) would be deposited on a GaAs substrate coated with a thin, etchable AlAs layer. When the cell is complete, the AlAs interlayer would be etched away, and the 4-μm cell film would be peeled away. The GaAs substrate could then be reused. Possible etchants of AlAs, which would not attack GaAs, are hydrofluoric acid, redox solutions of potassium iodide with iodine, or potassium ferricyanide plus potassium ferrocyanide.

The n^+pp^+ cell structure was chosen because more-conventional Al(Ga)As/GaAs p^+n heteroface cell structures would require special masking to avoid etching of the Al(Ga)As layer. Also, the conventional cell would "curl" after being peeled away since there is a slight mismatch between the substrate and cell crystal lattices.

The problem of handling the ultrathin solar cells would be reduced by bonding a glass or plastic layer on the top surface before the etching step. Such a layer might also prevent curling, allowing use of the Al(Ga)As heteroface structure.

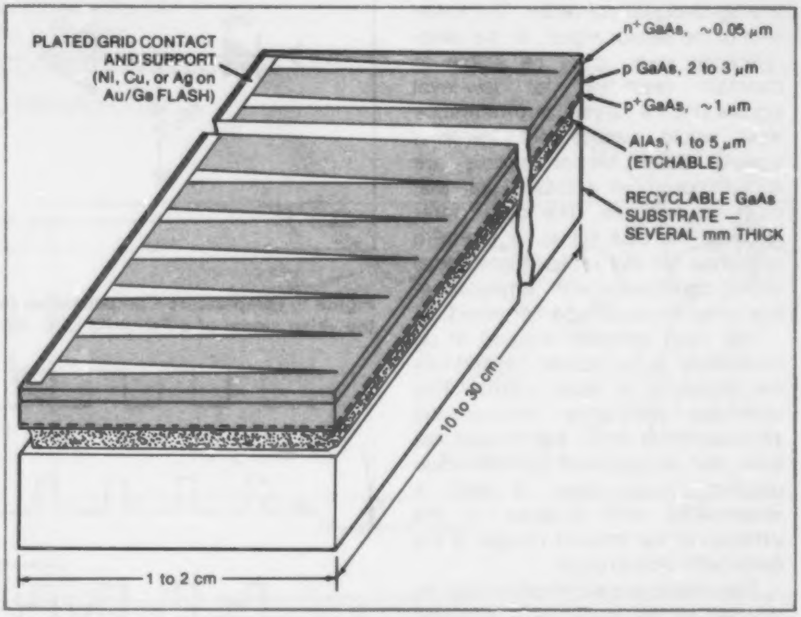
PLATED GRID CONTACT AND SUPPORT (Ni, Cu, or Ag on Au/Ge FLASH)
n^+ GaAs, ~0.05 μm
p GaAs, 2 to 3 μm
p^+ GaAs, ~1 μm
AlAs, 1 to 5 μm (ETCHABLE)
RECYCLABLE GaAs SUBSTRATE — SEVERAL mm THICK
10 to 30 cm
1 to 2 cm

The **Peeled-Film Cell** is separated from the GaAs substrate by an AlAs layer. The AlAs is etched away, freeing the cell and allowing the substrate to be reused.

The solar-cell blanket would be given an ohmic back contact by electroplating or vacuum deposition. It could then be placed on a thin metalized Kapton (or equivalent) backing.

The peeled-film solar-cell blanket would deliver energy at a power-to-weight ratio roughly 4 times that of conventional 2-mil (0.5-mm) silicon solar cells. In addition, GaAs solar cells have better radiation resistance and temperature stability than silicon cells.

This work was done by Richard J. Stirn of Caltech for **NASA's Jet Propulsion Laboratory.** *For further information, Circle 3 on the TSP Request Card.*
NPO-14734

Temperature-Compensating dc Restorer

Circuit provides stable reference restoration
in addition to temperature compensation.

Langley Research Center, Hampton, Virginia

In a closed-loop computerized control system, analog-to-digital converters may be used to condition analog sensor signals. These analog-to-digital converters have a fixed operating range that determines the limits of the sensor signals. In order to improve resolution, the sensor signals are set equal to the operating range of the analog-to-digital converter. The lower limit of the sensor signal, or the zero-reference level, must be stable to maintain resolution for low-level signals since a varying zero-reference level would swamp out low-level signals. Some sensor signals are superimposed on a bias signal that must be removed. The dc restorer removes the bias signal. If the zero reference for the sensor signal level varies significantly with temperature, this effect must also be corrected.

The most common method of dc restoration is to couple capacitively the signal to a diode clamp. This technique adequately restores the zero-reference level, but it does not solve the temperature compensation problem. Furthermore, it adds a temperature drift because of the variation of the forward voltage of the diode with temperature.

The temperature-compensating dc restorer shown in Figure 1 provides stable zero-reference restoration and compensates for temperature variations. It was developed for an autonomous Earth-observation experiment aboard the Space Shuttle. CCD cameras are used as sensors; their outputs are digitized and recorded on magnetic tape for later evaluation.

When light strikes the image sensor elements, a packet of electrons proportional to the incident light is generated at each sensing element. ØH clocking sequentially delivers the charge packets to a gated charge integrator, which produces an output signal proportional to the input charge (see Figure 2). The ØR clock resets the charge integrator prior to the arrival of the next charge packet. A portion of the ØR clock is coupled

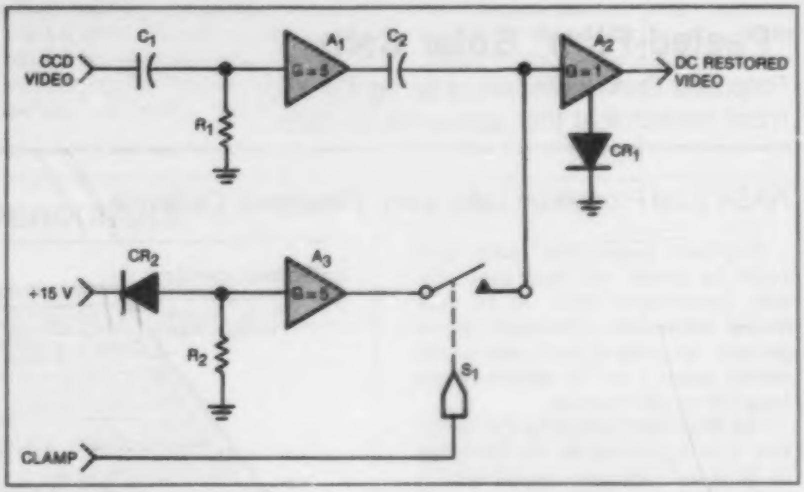

Figure 1. **Temperature-Compensating dc Restorer** circuit was designed to condition the video signal of a Fairchild CCD 202 area-image sensor.

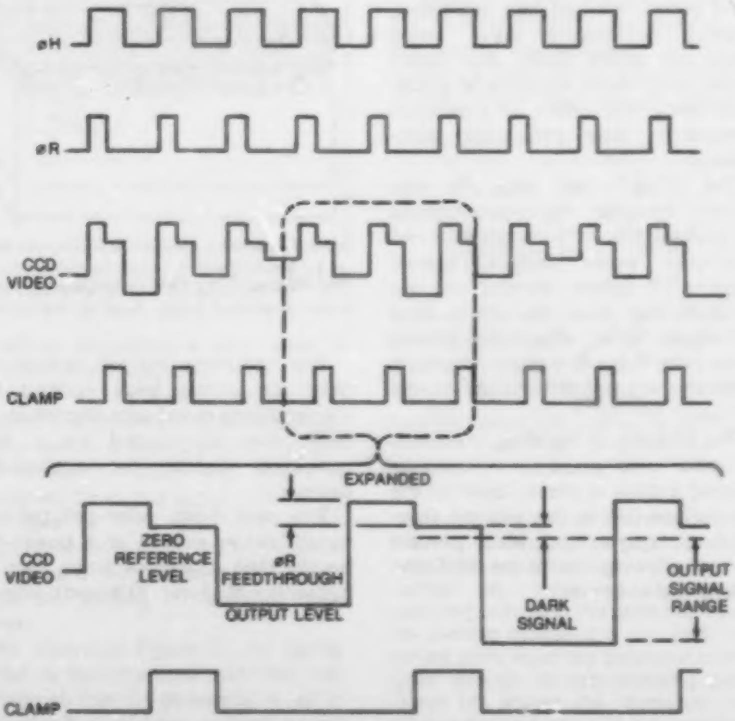

Figure 2. **Timing Diagram** of CCD 202 video output appears as a pulse-amplitude-modulated data stream.

through to the video output. Following the ØR feedthrough is a reference-level pedestal for the output video pulse.

Although it was designed for solid-state optical sensors, the temperature-compensating dc restorer could be adapted to any sensor with bias and temperature drift similar to those described; e.g., in closed-loop computerized process-control systems. While closed-circuit TV applications do not require the output to be digitized for display on a TV monitor, this circuit would be advantageous if the observer did not have access to the monitor controls to adjust for reference-level changes. Possible TV monitor applications include traffic and security surveillance systems, where cameras are subject to environmental extremes, as in unheated warehouses or outdoors.

This work was done by H. M. Thomas of Martin Marietta Corp. for **Langley Research Center.** *For further information, Circle 4 on the TSP Request Card.*

Inquiries concerning rights for the commercial use of this invention should be addressed to the Patent Counsel, Langley Research Center [see page A5]. Refer to LAR-12549.

Aliasing Filter for Multirate Systems

Adding a rolloff filter is an inexpensive way of reducing aliasing in digital control systems.

Lyndon B. Johnson Space Center, Houston, Texas

Digital control systems operating at single or multiple sampling rates are susceptible to foldback, or "aliasing," for signals above the half-sampling frequency. A rolloff filter operating at the faster sample rate (or rates) of a system with a 2:1 rate ratio gives infinite attenuation at the half-sample rate of the fast-rate loop. Tested successfully on the Space Shuttle primary flight-control system, the filter technique could be applied to other multirate sampled-data systems.

Three methods have previously been used to reduce or at least account for the effects of aliasing:

1. analyzing the high-frequency effects in the sampled-data domain,
2. using a faster sample rate such that all significant dynamics are within the half-sample-rate bandwidth, and
3. using a digital filter operating at the lower sampling frequency and accepting the degradation of the lower frequency characteristics.

Compared to these approaches, the rolloff filter is a relatively-inexpensive software function that eliminates aliasing without requiring an extensive foldback analysis, as in method 1.

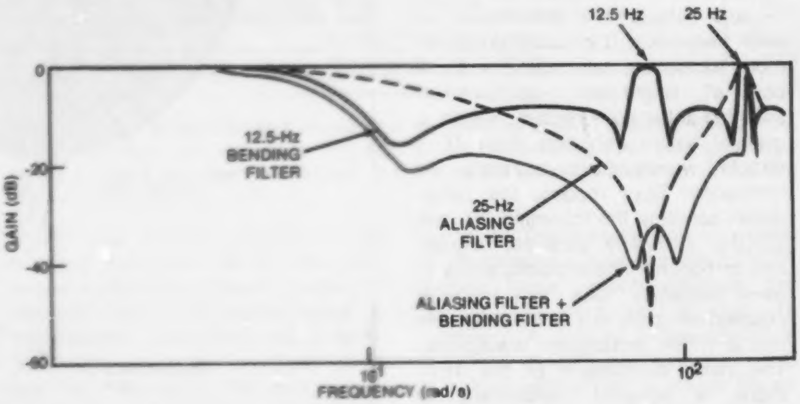

A 25-Hz Rolloff Filter reduces aliasing in the Shuttle flight-control system. The solid curve in black is the response of a 12.5-Hz bending filter. The dashed curve is the characteristic of the added rolloff filter. The response of the combination, shown in color, has increased attenuation in the vicinity of 12.5 Hz.

The Shuttle flight-control system experiences significant bending modes over (at least) the range from 2 to 12-1/2 Hz. Core limitations in the central-processing unit required that a 25-Hz rate-fill function in the attitude-control loop be reduced to 12-1/2 Hz; however, aliasing was a potential problem because of high-frequency bending-mode foldback.

As shown in the figure, adding the 25-Hz rolloff filter between the rate gyro and the 12.5-Hz bending filter increases the attenuation at 12.5 Hz. The end-to-end transfer function is virtually insensitive to dynamics in the vicinity of 12.5 Hz, and the impact on the low-frequency dynamics is minimal.

This work was done by John F. L. Lee of Honeywell Inc. for **Johnson Space Center.** *For further information, Circle 5 on the TSP Request Card.*
MSC-18472

Dual-Frequency Bidirectional Antenna

Simultaneous two-way communication at 20 and 30 GHz is possible with a versatile paraboloid-dish antenna.

Goddard Space Flight Center, Greenbelt, Maryland

A versatile communications antenna transmits left-circularly-polarized or right-circularly-polarized signals at one frequency and simultaneously receives either polarization at another frequency. Developed for two-way communications between the Space Shuttle and a ground station, the antenna includes a parabolic reflector, a feed horn, a waveguide network, and a single-axis gimbal mounting.

The waveguide network separates the two frequency components — 20 GHz and 30 GHz in the Shuttle system — and selects one polarization at each frequency. It includes an orthomode transducer, two diplexers, and a pair of single-pole, double-throw solenoid-actuated switches. Using a gradual finline transition from TE_{11} circular waveguide to separate the orthogonal TE_{11} modes, the transducer converts the incoming 20- and 30-GHz circularly polarized signals into orthogonal linear polarizations at each frequency. One TE_{11} mode is coupled vertically out of the main line into a WR34 rectangular waveguide. The other component of the TE_{11} mode is coupled horizontally to another WR34 waveguide. Identical diplexers separate the 20- and 30-GHz signals in each arm.

A 90° hybrid reconstitutes the circularly-polarized 20-GHz wave from the two 20-GHz linear components, and another hybrid does the same for the 30-GHz signal. Phase trimmers between the output arms of the diplexers and the hybrids compensate for phase deviations that can arise from minor differences in waveguide dimensions. The two waveguide switches select either sense of polarization at each frequency.

Small grooves in the flared section of the feed horn adjust the impedance relationships to give nearly-equal field amplitudes in the E- and H-planes. The flare angle is 53.0°, and the corrugations are 0.150 inch (0.38 centimeter) deep.

An iterative numerical procedure established the optimum reflector shape. The reflector has different curvatures in two perpendicular planes: In one plane it is parabolic; in the other, it is distorted to give the required far-field pattern.

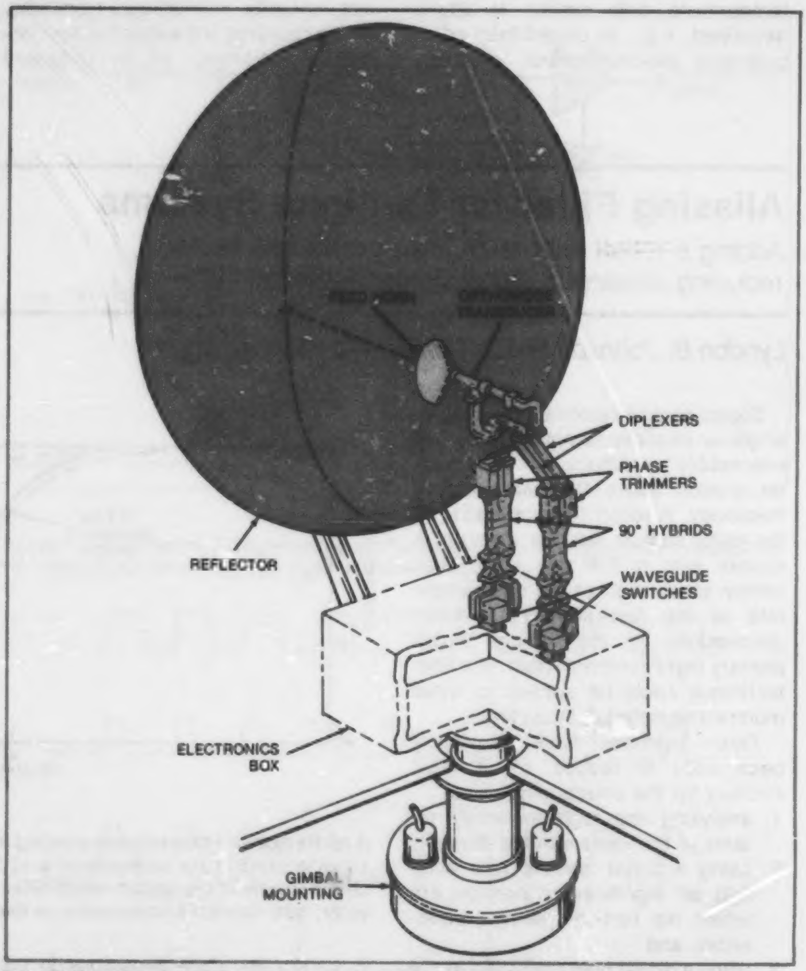

This **Bidirectional Antenna** transmits at 20 GHz and receives at 30 GHz. Peak system gain at 20 GHz is 29.8 dB; at 30 GHz, gain is 32.3 dB. The nominal paraboloid-dish reflector focal length is 14.76 in., with an f/D = 0.5. The edge of the dish subtends an angle of 53° with the position of the feed horn. The actual dish departs slightly from a true paraboloid of revolution.

The feed horn is located 14.76 inches (37.49 centimeters) from the vertex of the reflector. It is displaced 2.40 inches (6.10 centimeters) from the central axis of the dish in the direction of maximum edge elevation.

The antenna and its electronics are positioned by a single-axis gimbal driven by a stepper motor. The gimbal drive is run open loop, with its position indicated by a potentiometer output. The system resolution and accuracy are better than 1°.

This work was done by W. H. Kummer of Hughes Aircraft Co. for **Goddard Space Flight Center.** *For further information, Circle 6 on the TSP Request Card.*
GSC-12501

Computer-Controlled Warmup Circuit

Filament of high-power radio transmitter can be brought to operating temperature automatically.

NASA's Jet Propulsion Laboratory, Pasadena, California

A special circuit automatically heats the filament of a klystron tube to operating temperature, relieving a human operator of the 15-minute task of slowly turning the knob of a variable transformer to maintain current at its maximum safe level while filament temperature (and resistance) increases. The warmup controller circuit, which was developed for the klystron transmitting tubes used in Deep-Space Network stations, is activated by a pushbutton. It thus reduces the operator's role to a one-step command and is compatible with various forms of computer control.

The klystron filament floats at the beam potential, which can be as high as 70 kV, so an isolation transformer is used to deliver ac filament power. Filament current and voltage are sensed through windings on the isolation transformer. The power to the isolation transformer is supplied by a motor-driven variable transformer that is controlled, in turn, by a circuit board.

Figure 1 is a photograph of the Local Control Console (LCC), and Figure 2 is a block diagram of the warmup controller. When the user issues a warmup command (RAISE) at the LCC, the circuit applies power to the variable transformer via a solid-state relay and turns the motor on in the "up" direction. The motor continues to run until the maximum programed current limit or the operating voltage limit is reached. When the filament is cold and the resistance low, the current limit will always be reached first; so the controller will pulse the motor every few seconds, maintaining the current at the limit as the filament warms up. When the filament reaches 70 percent of its operating voltage, a 20-minute timer is started. After 20 minutes the filament-ready signal closes the beam voltage interlock, allowing dc operating voltages to be applied to the klystron. When the filament is hot and current limiting no longer occurs, the filament voltage is regulated to within ±0.1 volt.

Figure 1. **Automatic Control** of heater power to a klystron filament is furnished by the circuit board. After the operator pushes the RAISE button on the console panel, the filament temperature is raised to the operating level at a rate that prevents excessive filament current or voltage.

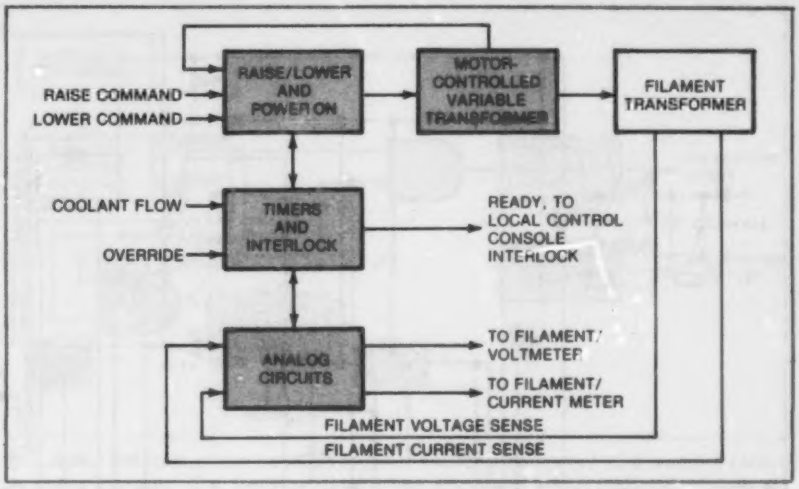

Figure 2. This **Block Diagram** shows how the warmup control circuit monitors the filament current and voltage of the high-power transmitting tube and governs a motor to raise or lower the voltage from a variable transformer that drives the filament transformer.

A filament shutdown can be initiated by three events: (1) a "down" command from the operator, (2) a failure of the cooling system, or (3) a power failure for more than a few seconds. The operator can command a shutdown by pressing the LOWER button twice, which changes the circuit mode from "up" to "halt" to "down." A cooling failure forces a "down" mode, but only after a 1-minute time delay. A power failure longer than 5 seconds causes the circuit to reset, removing filament power and mechanically lowering the variable transformer setting when power returns. The variable transformer must be turned all the way down before it can be raised again.

An override function allows either manual or external computer control. When override is enabled, the RAISE and LOWER buttons at the LCC control the motor that is connected to the variable transformer. (The control is constrained by the current and voltage limits set by switches in the filament supply chassis.) This feature allows an operator or a computer to control the filament power directly.

This work was done by John J. Daeges of Caltech for **NASA's Jet Propulsion Laboratory.** *For further information, Circle 7 on the TSP Request Card.*
NPO-14815

Direct-Current Converter for Gas-Discharge Lamps

No ballast is required with a new dc supply for metal/halide and other gas-discharge lamps.

Lyndon B. Johnson Space Center, Houston, Texas

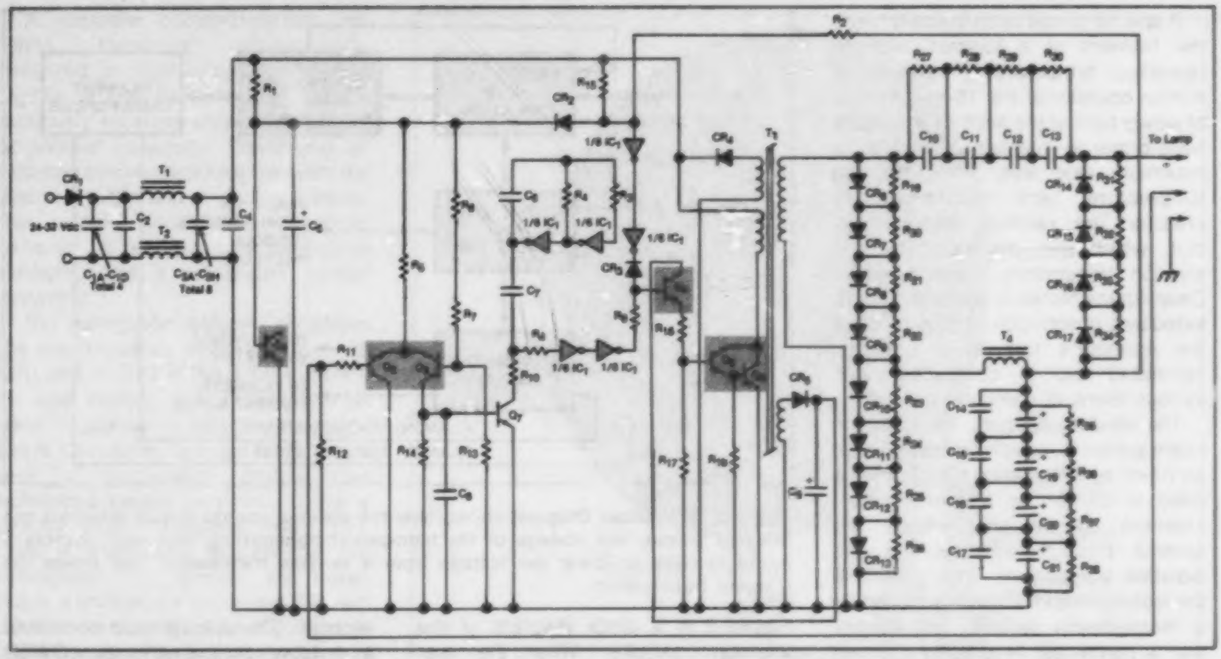

The Lamp Power Supply consists of a high-frequency inverter switched by a waveform generator, a current-regulating loop, and associated circuitry driven by direct-current sources. Prototypes are used at power levels of 175 watts for mercury-vapor lamps doped with halides of sodium and scandium. The lamps contain argon as a start gas.

Metal/halide and similar gas-discharge lamps can be powered from a low-voltage dc source, using the small efficient converter shown in the figure. The circuit also stabilizes the lamp current, thus eliminating the need for an external "ballast," a standard component with conventional ac-powered lamps. The prototype converter can be useful wherever 60-cycle ac power is not available or where space and weight allocations are limited. (It was developed for discharge lamps aboard the Space Shuttle.) Possible terrestrial applications are in offshore platforms, mobile homes, and emergency lighting.

Several design innovations give the new supply high reliability and an efficiency of up to 75 percent. The heart of the circuit is a 20-kHz power-switching inverter (a "forward converter") that changes the input dc power to high-voltage alternating current, which is then rectified and integrated to supply direct current to the lamp.

The forward converter is the middle portion of the circuit, shown in the figure. It instantaneously develops the high starting voltages (typically 1,200 V for the Shuttle lamps) necessary to turn the lamp on. It is a rapid-response circuit that is inherently efficient because the single output transistor (Q_6) is either fully on or fully off at all times.

A lamp-current control loop is formed with transistors Q_2, Q_3, and Q_7 sensing the lamp current and feeding signals back to the waveform generator that controls the inverter duty cycle. The inverter duty cycle is thus lengthened or shortened to compensate for changes in the lamp current.

The instantaneous high voltages available with the circuit make the lamp less likely to "blow out" because of transients in the power source. The high voltages also reduce restart times to about 5 minutes if the lamp is shut off and then reenergized. (Typical restart times for conventional ac-powered lamps are 10 to 15 minutes.) In addition, whereas conventional power sources require a three-electrode lamp, for which the third electrode is a starting electrode, the new supply can directly energize simpler, two-electrode lamps.

This work was done by P. Lutus of ILC Technology for **Johnson Space Center.** *For further information, Circle 8 on the TSP Request Card.*

Inquiries concerning rights for the commercial use of this invention should be addressed to the Patent Counsel, Johnson Space Center [see page A5]. Refer to MSC-18407.

Position Monitor for Mining Machines

A simple circuit at the output of an incremental transducer records the progress of a longwall shearer.

Marshall Space Flight Center, Alabama

Faced with the problem of monitoring the forward progress of a longwall shearer (a coal-mining machine), engineers under contract to Marshall Space Flight Center developed a simple digital circuit that could have applications in other harsh environments. Shown in the figure, the circuit attaches to the output of a rotary-motion transducer and develops a pulse for rotation equivalent to each 5-foot (1.5-m) increment of forward progress of the machine. A reset pulse is derived after the shearer has moved 1,000 feet (304 meters). In contrast to mechanical shaft encoders, the electronic circuit can be easily packaged to withstand the shock and vibration of the mining machine as it cuts across the coal seam.

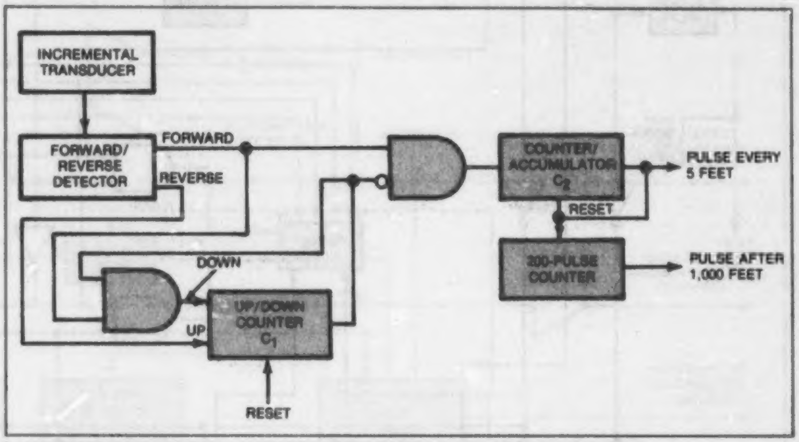

This **Block Diagram** of the position monitor could be converted to a working circuit by using standard IC's. Increments of 5 feet along a 600-foot (182-meter) path are resolved to within 0.06 in. (0.15 cm) by the system.

The circuit delivers pulses only when true forward progress has been made. If the mining machine should reverse direction, as happens periodically, the pulses cease until the point of maximum forward progress is returned to and exceeded.

Referring to the figure, the stream of pulses from the transducer (e.g., optoelectronic or magnetic) is channeled along one of two paths, depending on whether the machine is moving forward or backward. Forward-motion pulses clock the "down" input of an up/down counter/accumulator (C1) and also the input of another counter/accumulator (C2), which delivers one output pulse when the number of input pulses corresponds to 5 feet of forward motion. Reverse-motion pulses clock the "up" input of C1.

When the C1 output is reset to "0," AND gate 1 prevents pulses from reaching the "down" input, while AND gate 2 allows forward-motion pulses to reach C2. In this mode, the forward motion is continuously monitored.

If the machine should reverse direction, no pulses reach C2, and C1 is incremented to a count that corresponds to the net backward motion. When forward progress resumes, AND gate 1 prevents pulses from reaching C2 until "down" pulses decrement C1 back to its "zero" state. When this happens, the AND gate 2 is reopened and normal operation resumes.

This work was done by Joseph Lubich of Benton Corp. for ***Marshall Space Flight Center.*** *No further documentation is available.*

Inquiries concerning rights for the commercial use of this invention should be addressed to the Patent Counsel, Marshall Space Flight Center [see page A5]. Refer to MFS-25342.

11-Line to 512-Line Decoder

CMOS decoder is assembled from standard 4-line to 16-line decoder/demultiplexer IC's.

Lyndon B. Johnson Space Center, Houston, Texas

The matrix of logic integrated circuits shown is an 11-line to 512-line parallel decoder assembled from standard 4-line to 16-line decoders. It can be expanded by adding more 4-line to 16-line decoders. The matrix may also be used to generate 256 latched-on or latched-off logic signals instead of 512 discrete unlatched signals. By using conventional CMOS IC's, the circuit consumes only about 30 milliwatts.

An input word to the decoder consists of two groups of bits: nine numerical bits and two execute bits. The binary word comprised of bits A_0 through A_8 designates which of the 512 discrete outputs will change from

(continued on next page)

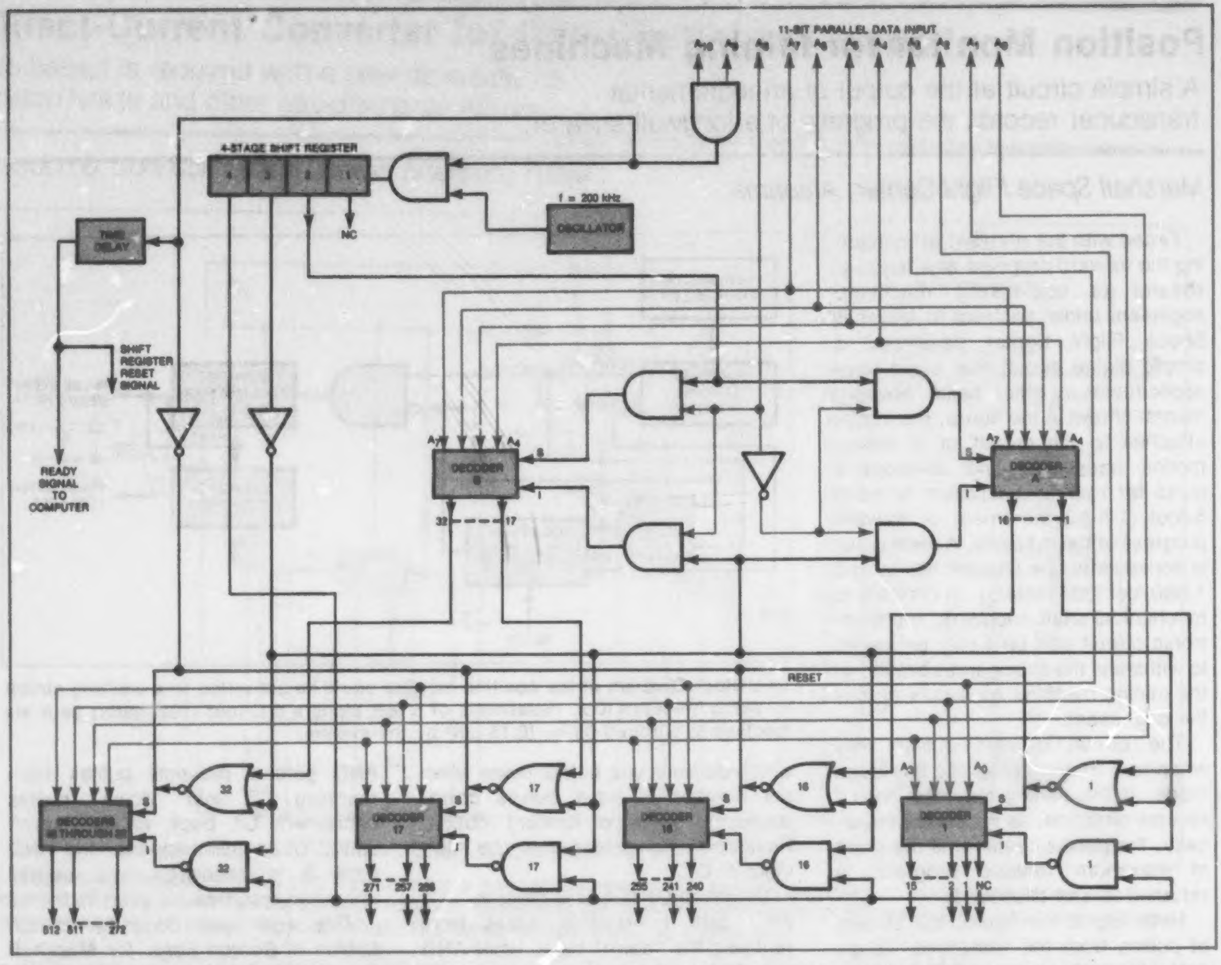
11-BIT PARALLEL DATA INPUT
A_{10}
A_9
A_8
A_7
A_6
A_5
A_4
A_3
A_2
A_1
A_0
4-STAGE SHIFT REGISTER
4
3
2
1
NC
f = 200 kHz
OSCILLATOR
TIME DELAY
SHIFT REGISTER RESET SIGNAL
READY SIGNAL TO COMPUTER
A_7
A_4
S
DECODER B
I
32
17
DECODER A
16
1
RESET
DECODERS 18 THROUGH 32
32
512
511
272
DECODER 17
17
271
257
256
DECODER 16
16
255
241
240
A_3
A_0
DECODER 1
1
15
2
1
NC

11-Line to 512-Line Decoder Is Composed of complementary metal-oxide-semiconductor integrated circuits. Pairs of output signals can be wired as latch-on and latch-off commands, to remember the most recent output state after the input is switched off.

a 0 to a 1. The execute bits A_9 and A_{10} turn the decoder "on" when both are 1's.

When a valid 11-bit word is presented to the matrix, the two 1's in the execute group enable a 200-kHz clock oscillator that starts a four-stage shift register (see figure). Shift register position 1 is held for roughly one clock period to allow the 11-bit input data to settle. When the shift register reaches position 2, it generates a strobe signal that enters data bits A_4 through A_7 into decoder blocks A and B. If A_8 is 0, the data enter block A; if A_8 is 1, data enter block B.

Data bits A_0 through A_3 are connected to the input terminals of decoders 1 through 32. When the shift register is stepped to position 3, it switches off the inhibit line from decoder block A. This enables the appropriate decoder so that it produces a logic "1" at the output terminal corresponding to the word at bits A_0 through A_8. The output of the selected decoder is enabled when the shift register reaches position 4.

This work was done by Wilson N. Miller of Rockwell International Corp. for **Johnson Space Center.** *For further information, Circle 9 on the TSP Request Card.*
MSC-19751

Input/Output Interface Module

Module stores up to 4 consecutive changes on each of 16 I/O lines.

Lyndon B. Johnson Space Center, Houston, Texas

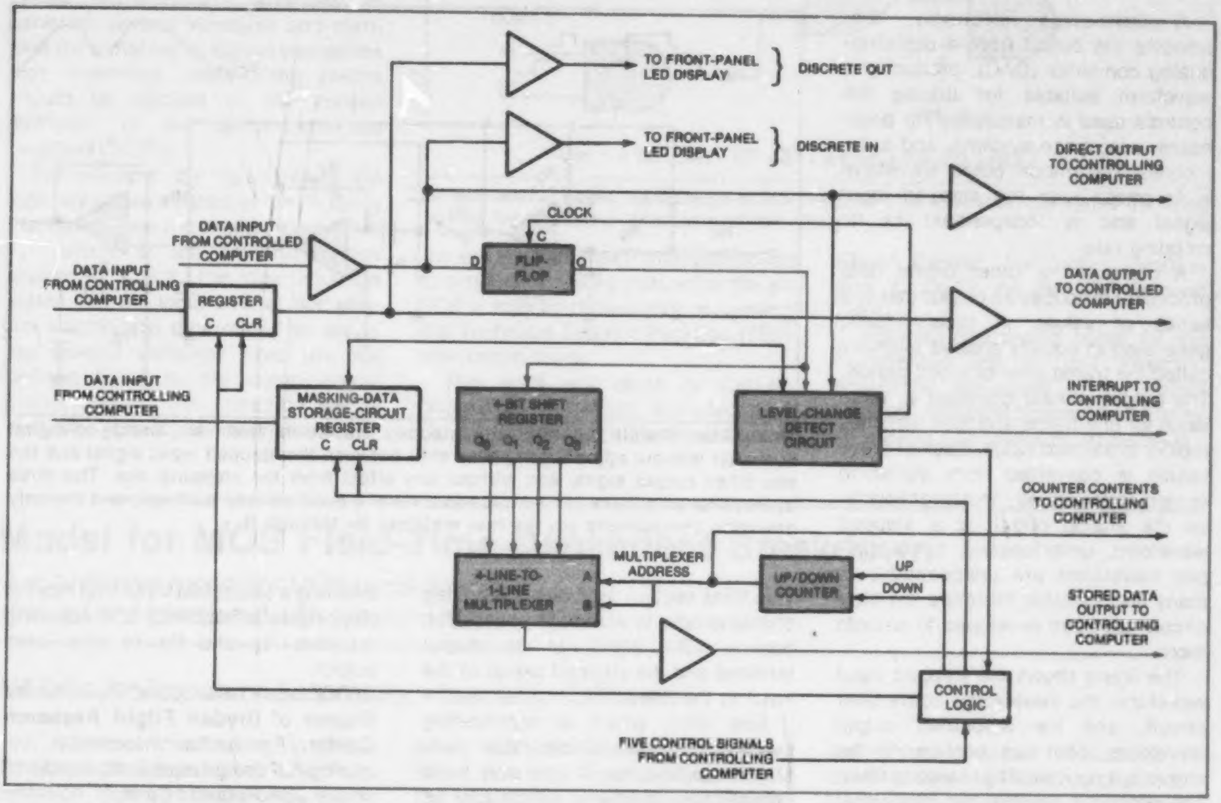
TO FRONT-PANEL LED DISPLAY
DISCRETE OUT
TO FRONT-PANEL LED DISPLAY
DISCRETE IN
DIRECT OUTPUT TO CONTROLLING COMPUTER
CLOCK
C
DATA INPUT FROM CONTROLLED COMPUTER
D
FLIP-FLOP
Q
DATA INPUT FROM CONTROLLING COMPUTER
REGISTER
C CLR
DATA OUTPUT TO CONTROLLED COMPUTER
DATA INPUT FROM CONTROLLING COMPUTER
MASKING-DATA STORAGE-CIRCUIT REGISTER
C CLR
4-BIT SHIFT REGISTER
Q_0 Q_1 Q_2 Q_3
LEVEL-CHANGE DETECT CIRCUIT
INTERRUPT TO CONTROLLING COMPUTER
COUNTER CONTENTS TO CONTROLLING COMPUTER
MULTIPLEXER ADDRESS
4-LINE-TO-1-LINE MULTIPLEXER
A
B
UP/DOWN COUNTER
UP
DOWN
STORED DATA OUTPUT TO CONTROLLING COMPUTER
CONTROL LOGIC
FIVE CONTROL SIGNALS FROM CONTROLLING COMPUTER

One of Sixteen I/O Circuits is shown in this simplified diagram. The circuit stores up to 4 changes in state in each of the 16 circuits.

An input/output module that transfers up to 16 parallel logic signals between computer systems is useful in computer-to-computer operations, such as flight simulation, and in industrial process control. The module detects level changes in any of its 16 input lines, transfers these to its output lines, and generates interrupts when level changes are detected.

As shown in the simplified block diagram of 1 of the 16 lines, the module contains a counter and a shift register that stores up to 4 changes in state per line. When the maximum number of changes has been reached, the controlling computer can retrieve the stored data by decrementing the count. The computer has access at all times to the current value of all 16 signals and to the contents of the counter.

The I/O module is packaged in a rack-mounted chassis 3.5 inches (8.9 centimeters) high and 21 inches (53.3 centimeters) deep. It fits into a standard 19-inch-wide (48.3-centimeter) console. The module uses standard TTL logic.

This work was done by Emin M. Ozyazici of Rockwell International Corp. for ***Johnson Space Center.*** *For further information, including logic diagrams of the I/O module, Circle 10 on the TSP Request Card.*
MSC-18180

Smoothing the Output From a DAC

A simple filter conditions the waveform from a digital-to-analog converter for use in control systems.

Dryden Flight Research Center, Edwards, California

A three-stage electronic filter smooths the output from a digital-to-analog converter (DAC), producing a waveform suitable for driving the controls used in manufacturing processes, aerospace systems, and automobiles. The smooth output waveform is in phase with the stepped input signal and is independent of its stepping rate.

A computer or other digital data processor produces an output that is a series of values in binary form, generated at equally spaced intervals called the frame time or clock period. The output is held constant at each value for one frame and then switches rapidly to the next value. Each of these values is converted from digital to analog form virtually instantaneously, so the analog output is a stepped waveform. Unfortunately, such stepped waveforms are unacceptable in many applications; therefore the filter circuit has been developed to smooth them.

The figure shows the stepped input waveform, the three-stage active filter circuit, and the smoothed output waveform. The first section of the circuit is a noninverting low-pass filter. The second is an inverting stage that passes a narrow frequency band centered at the stepping frequency (frame rate), with sharp cutoff on either side of that narrow band. The third section adds the noninverted output of the first section to the inverted output of the second section. This third section includes a lead/lag characteristic to eliminate phase shift between the signal at its output terminal and the stepped signal at the input to the filter.

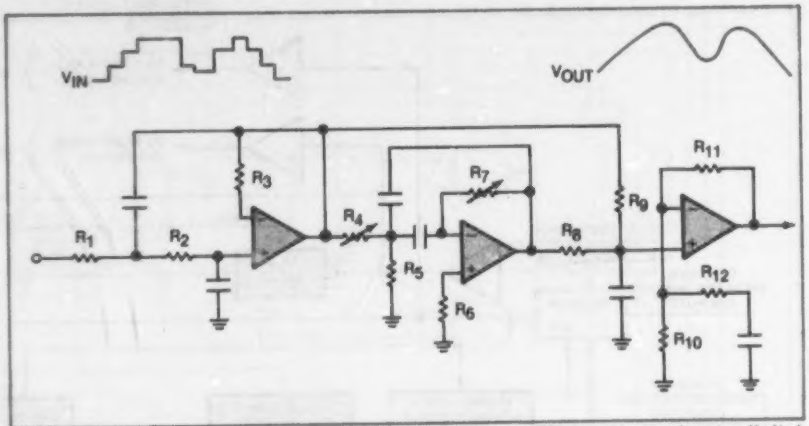

This **Filter Circuit** smooths the stepped waveform from an analog-to-digital converter without appreciable phase shift between the stepped input signal and the smoothed output signal and without any effect from the stepping rate. The three operational amplifiers can be three-fourths of a quad op-amp package, and the only precision components are the four resistors R_8 through R_{11}.

This filter, which is noninverting overall, has several desirable constructional features. It uses only three operational amplifiers, which can be three-fourths of a quad op-amp package. Nearly all of the components can have tolerances as large as 5 percent; the only exceptions are the four resistors R_8 through R_{11}. Precision capacitors are not required. Calibration is easily done by simply injecting a sinusoidal input that has the stepping-rate frequency and adjusting resistors R_4 and R_7 to give zero output.

This work was done by Charles Wagner of **Dryden Flight Research Center.** *For further information, including full design equations, Circle 11 on the TSP Request Card.*

This invention is owned by NASA, and a patent application has been filed. Inquiries concerning nonexclusive or exclusive license for its commercial development should be addressed to the Patent Counsel, Dryden Flight Research Center [see page A5]. Refer to FRC-11025.

LSI Logic for Phase-Control Rectifiers

Large-scale-integrated components reduce the size of control circuitry.

Marshall Space Flight Center, Alabama

The signals for controlling a phase-controlled rectifier circuit are generated by combinatorial logic that can be implemented in large-scale integration (LSI). The LSI circuit saves space, weight, and assembly time compared to previous controls that employ one-shot multivibrators, latches, and capacitors. The LSI logic functions by sensing the three phases of the ac power source and by comparing actual currents with the intended currents.

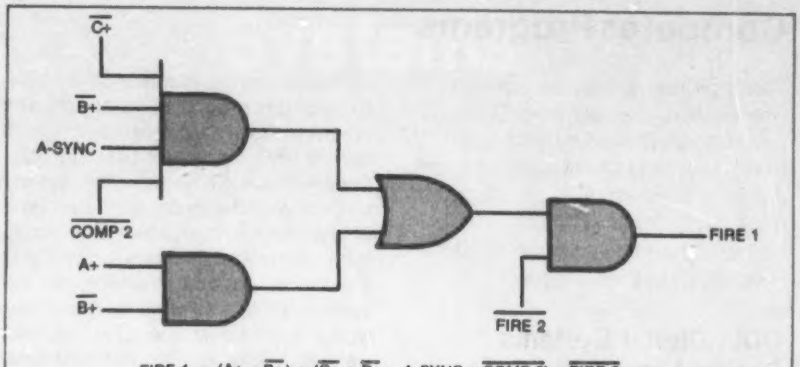

$$\text{FIRE 1} = (A+ \bullet \overline{B+}) + (\overline{C+} \bullet \overline{B+} \bullet \text{A-SYNC} \bullet \overline{\text{COMP 2}}) \bullet \overline{\text{FIRE 2}}$$

Combinatorial Logic, using large-scale-integrated components, generates the firing pulses for a phase-controlled rectifier circuit.

The LSI components required for the logic operations are:

- operational amplifiers (for integrating waveforms and for comparing magnitudes),
- inverters,
- AND gates, and
- OR gates.

These elements are arranged to generate several variables and combine the variables in logical operations that determine when firing pulses should be applied to the control terminals of six silicon-controlled rectifiers (SCR's).

For example, the figure shows the logic equation and part of the circuitry that determines the signal called "Fire 1," which is the control voltage applied to SCR 1. The logic equation states that the logic level at that control electrode is determined by applying several variables (that are not defined here) to the combinatorial circuit shown. The complete circuit diagram, showing the formation of all the variables and their interconnection to produce the firing pulses for the six SCR's, may be obtained by requesting the Technical Support Package (TSP) referenced below.

This work was done by Carlisle Dolland of Airsearch Manufacturing Co. of California for **Marshall Space Flight Center.** *For further information, Circle 12 on the TSP Request Card.*

Inquiries concerning rights for the commercial use of this invention should be addressed to the Patent Counsel, Marshall Space Flight Center [see page A5]. Refer to MFS-25208.

Model for MOS Field-Time-Dependent Breakdown

A quantitative model for MOS breakdown is derived and correlated with experiments.

NASA's Jet Propulsion Laboratory, Pasadena, California

A dominant mechanism in MOS time-dependent breakdown is sodium emission from the metal/oxide interface, which occurs during the application of a positive gate bias. This breakdown is related to the clustering of the emitted ions at localized defect sites at the oxide/silicon interface. Therefore, much smaller ion densities than normally associated with ion-charge stabilities can initiate breakdown.

The existing physical model describing this breakdown in terms of a single trapping energy has been extended to include the effect of a range of ion-trapping energies, leading to a logarithmic time dependence and a Schottky field dependence for breakdown to occur. The initial breakdowns have been related to a Fowler-Nordheim field dependence. Experimental data on MOS breakdown probability, enhanced by implantation damage, have been obtained and correlated with the predicted time and field dependencies. The results can be applied to evaluate the reliability of an MOS process.

The theoretical analysis indicates that the breakdown probability is

$$P_1(t,F) = B \ln(t/t_0)$$

where t is the elapsed time after a field F is applied. The parameter t_0, the time delay until onset of breakdown is related exponentially to the trapping energy barrier, which is lowered by a factor proportional to the square root of the applied field (Schottky field dependence); and the coefficient B is proportional to the area of the silicon interface, the defect density per unit area, the density of trapped ions, the effective ion-capture cross section, the Boltzmann constant, and the temperature.

The logarithmic time-dependent breakdown probability does not include the effects of initial breakdowns at localized defects. These are characterized by a Fowler-Nordheim field dependence given by the probability

$$P_0(F) = b \exp(-a/F)$$

where a and b are constants. The total probability P(t,F) of breakdown is therefore

$$P(t,F) = P_0(F) + P_1(t,F).$$

The modified model was verified by testing 24 wafers containing MOS capacitor arrays. The wafers were n-type silicon having 1- to 3-ohm-cm values, a 5-cm diameter, and a 100 orientation. A linear regression analysis of the tested initial breakdown and time-dependent breakdown probabilities correlated well with the model.

This work was done by Seung P. Li, Joseph Maserjian, and Simon Prussin of Caltech for **NASA's Jet Propulsion Laboratory.** *For further information, Circle 13 on the TSP Request Card. NPO-14701*

Computer Programs

These programs may be obtained at very reasonable cost from COSMIC, a facility sponsored by NASA to make new programs available to the public. For information on program price, size, and availability, circle the reference letter on the COSMIC Request Card in this issue.

DDL: Digital Systems Design Language

A block-oriented hardware description language

Hardware description languages are valuable tools in such applications as hardware design, system documentation, and logic design training. Just as software designers use high-level languages to express algorithms in concise language statements, digital hardware designers use hardware description languages to describe the system they are desiging.

The Digital Systems Design Language (DDL) is a convenient medium for inputting design details into a hardware-design automation system. A translator program and a simulator program allow hardware designers to benefit from the use of DDL. In DDL, the structural elements of the system are explicitly declared. At a lower level of description, functional and structural elements correspond directly to the actual physical elements of the system. DDL is suitable for describing digital systems at the gate, register transfer, and major combinational block level.

DDL is a "block-oriented" language that the designer can use to describe the functional specifications of a digital system. The blocks usually correspond to the natural divisions of the hardware being described. Thus a DDL description of a computer might have a major block called an "ALU," which contains a block called "adder," which consists of interconnected logic blocks called "full adders." The DDL language can describe parallel operations as well as synchronous and asynchronous behaviors.

The DDL translator program (DDLTRN) translates the user-supplied DDL description of a system into a set of Boolean equations and register-transfer statements. The output from DDLTRN is used as input for the DDL simulation program (DDLSIM). DDLSIM enables the designer to test and verify the design of the digital system. DDLSIM is a table-driven, event-oriented simulator. Time is treated as a discrete quantity and advance on an event-by-event basis. Through command statements, the response of the simulated system to a wide variety of input signals may be determined.

The DDLTRN and DDLSIM programs are written in FORTRAN IV for batch execution on the SEL-32 computer. Each program requires approximately 64K of 8-bit bytes on the SEL-32. These digital system design aids were developed in 1979.

This program was written by Sajjan G. Shiva of the University of Alabama at Huntsville for **Marshall Space Flight Center.** *For further information, Circle A on the COSMIC Request Card.*
MFS-25352

Electronic Systems

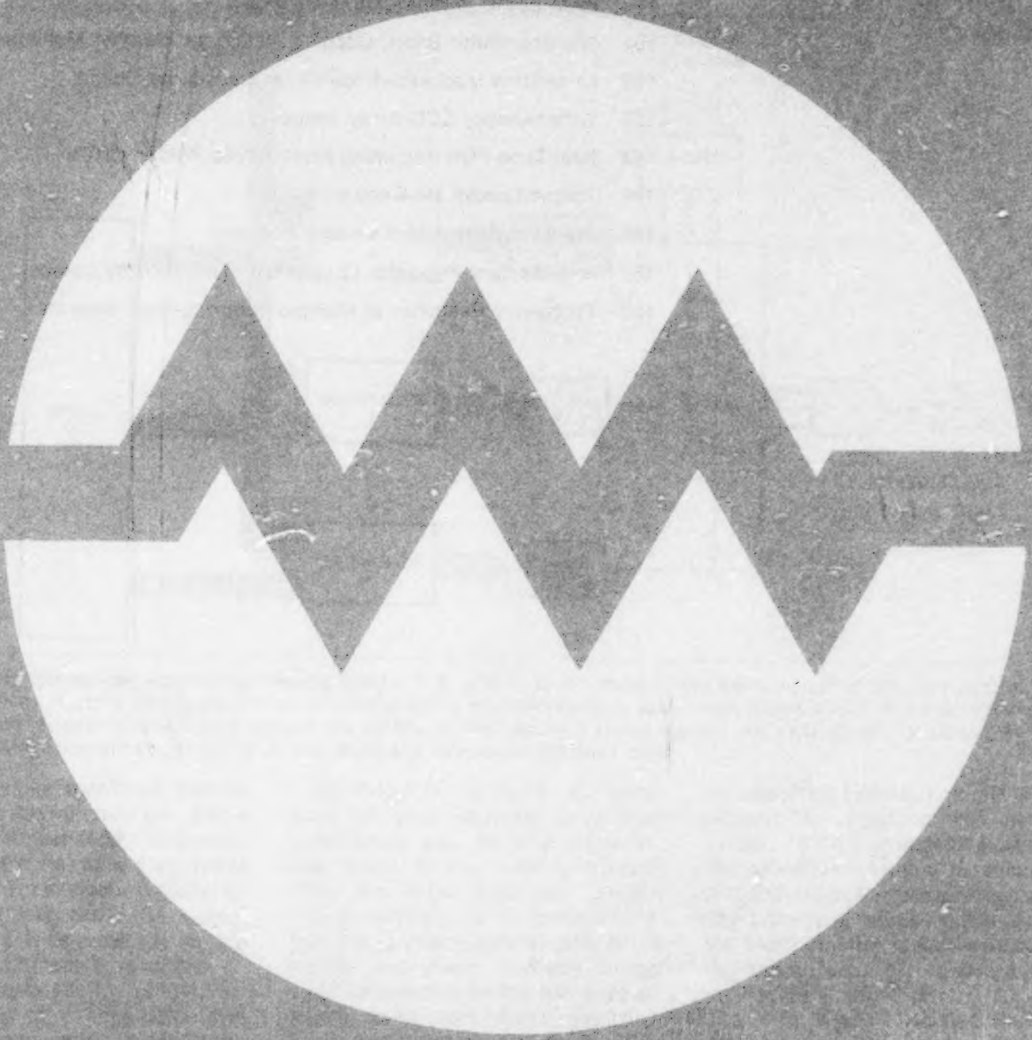

Hardware, Techniques, and Processes

149 RAM-Based Frame Synchronizer
150 RAM-Based Parallel-Output Controller
151 Microcomputer-Based Doppler System for Weather Monitoring
152 Linearizing Magnetic-Amplifier dc Transducer Output
153 Better-Quality CCD-Array Images
154 Real-Time Film Recording From Stroke-Written CRT's
155 Torque Control for Electric Motors
156 Frequency-Controlled Voltage Regulator
157 A Redundant Regulator Control With Low Standby Losses
158 Frequency Response of Multiple-Sampling-Rate Systems

RAM-Based Frame Synchronizer

A frame synchronizer for serial telemetry can be rapidly reconfigured for changing formats.

Goddard Space Flight Center, Greenbelt, Maryland

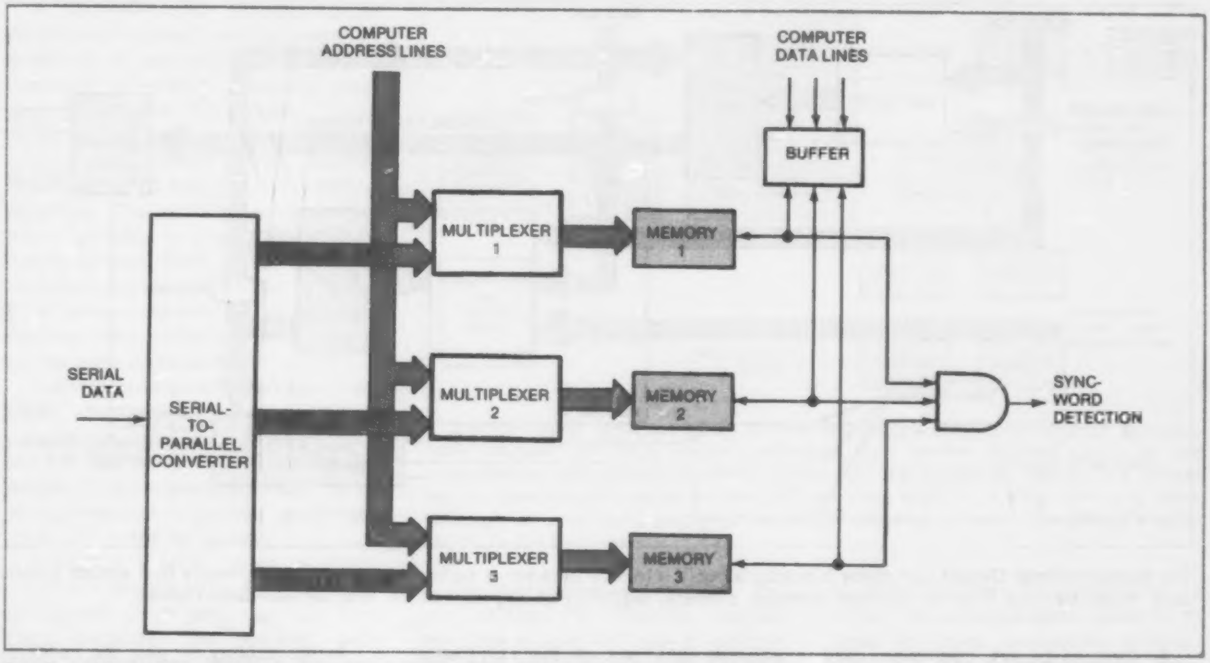

The **Sync-Word Recognizer,** containing memory blocks 1, 2, and 3, is the heart of the frame synchronizer. The synchronizer generates signals marking data-word boundaries (word sync), the beginning of each frame (frame sync), and the beginning of each paragraph (subframe sync). Also derived are search, check, and lock status signals. An existing unit is assembled from standard random-access memory elements and MOS and low-power-Schottky logic.

Random-access memories are the key elements in a versatile new frame synchronizer for serial-data telemetry. The use of memories makes it possible to reconfigure the system rapidly for changing formats and sync words, while offering wide flexibility in the specification of these parameters.

The memory-based frame synchronizer consists of a serial-to-parallel converter, sync-word recognizers, and control logic. The sync-word recognizers are segmented memory elements that are set up with the patterns of "1's" and "0's" necessary to identify the sync word, including its length and allowable bit error. A "true" output from any recognizer implies that there is a successful match between the parallel data and the sync-word segment.

As shown in the figure, the sync-word recognizer is made up of input multiplexers and memory elements. The inputs to the memory address lines are either from an external microprocessor, or a computer, or from the telemetry parallel data. In the control subsystem, memory arrays used as counters define the word bit length, frame word length, and paragraph frame length.

The frame synchronizer has an initialization mode and a processing mode. During initialization, the microprocessor or a computer loads the sync and format information into the memory-array elements, by memory mapping. When the memory modules are loaded, the frame synchronizer enters the processing mode. Incoming serial data are scanned continuously by presenting the data in parallel to the address line inputs of the memory arrays. A sync is detected by gating of the recognizer-memory data outputs and the control-subsystem counters. The processing mode continues until the memories are reaccessed by the microprocessor or computer to change the matrix format.

This work was done by James K. Niswander and Raymond J. Stattel of **Goddard Space Flight Center.** *For further information, Circle 14 on the TSP Request Card.*

This invention is owned by NASA, and a patent application has been filed. Inquiries concerning nonexclusive or exclusive license for its commercial development should be addressed to the Patent Counsel, Goddard Space Flight Center [see page A5]. Refer to GSC-12430.

RAM-Based Parallel-Output Controller

Selected bit strings in a serial-data link are extracted for processing.

Goddard Space Flight Center, Greenbelt, Maryland

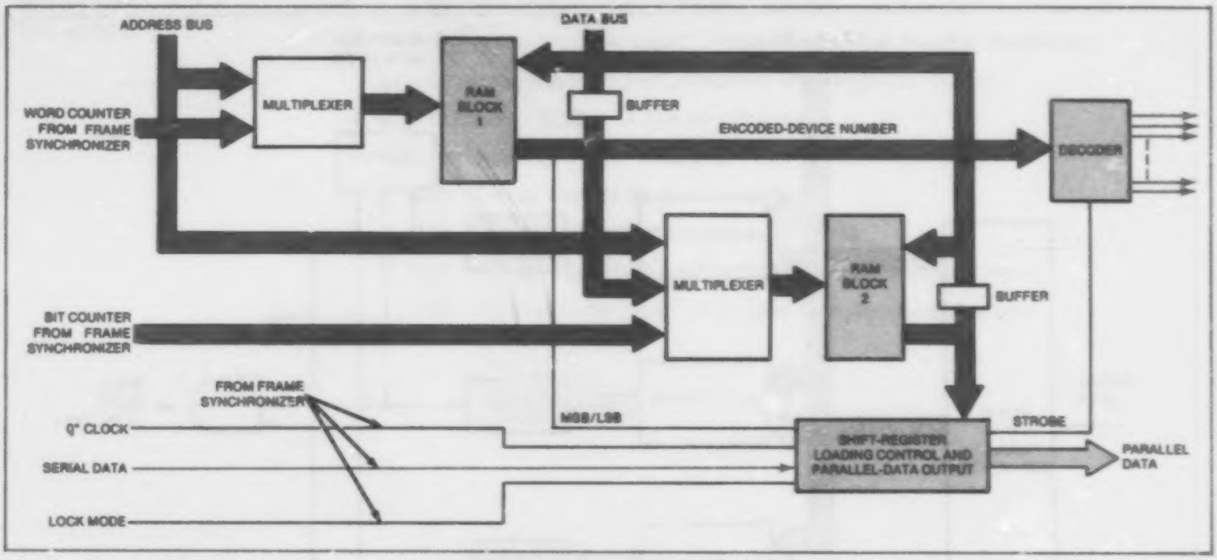
ADDRESS BUS
DATA BUS
WORD COUNTER FROM FRAME SYNCHRONIZER
MULTIPLEXER
RAM BLOCK 1
BUFFER
ENCODED-DEVICE NUMBER
DECODER
MULTIPLEXER
RAM BLOCK 2
BUFFER
BIT COUNTER FROM FRAME SYNCHRONIZER
FROM FRAME SYNCHRONIZER
0° CLOCK
SERIAL DATA
LOCK MODE
MSB/LSB
STROBE
SHIFT-REGISTER LOADING CONTROL AND PARALLEL-DATA OUTPUT
PARALLEL DATA

The **Memory-Based Output Controller** is a programable interface between a serial-data link and peripherals that accept parallel data. It can be used to drive displays, printers, plotters, digital-to-analog converters, and parallel-output ports.

A memory-based controller (see figure) selects bit strings from a stream of formatted serial data and directs the strings to peripherals as parallel data. It has several unique features:

- The configuration of the bit-string selector can be easily changed to accommodate changing formats. (This is especially useful for time-shared data links.)
- Any sequence of bits in a data word, or overlapping more than one word, can be selected for any peripheral.
- The data can be transferred either most-significant-bit first or least-significant-bit first.
- Costs are reduced below those of previous designs because of lowered parts count.

The output controller contains a block of random-access memory (RAM) that has at least as many address locations as the number of words in a paragraph. The word counter input from a frame synchronizer addresses the RAM block, which provides as its output: (1) an encoded peripheral device number and (2) a most-significant-bit first/least-significant-bit first (MSB/LSB) flag.

The encoded device number and the bit counter from a frame synchronizer are address lines to another RAM block, which contains start and stop flags to pick out the required bits from the specified word number(s). The MSB/LSB and start and stop flags, along with the serial data, go into a control block, which selectively fills a shift register to drive the parallel-data output bus. A strobe pulse is also generated, enabling a decoder to select the appropriate peripheral using the encoded device number.

A microcomputer sets the contents of the RAM blocks during an initialization phase, using the technique of memory mapping. After the RAM blocks are loaded, the output controller operates completely independently of the microcomputer. The speed of operation is limited only by the access times required for operation of the memories.

This work was done by James K. Niswander and Raymond J. Stattel of **Goddard Space Flight Center.** *For further information, Circle 15 on the TSP Request Card.*

This invention is owned by NASA, and a patent application has been filed. Inquiries concerning nonexclusive or exclusive license for its commercial development should be addressed to the Patent Counsel, Goddard Space Flight Center [see page A5]. Refer to GSC-12447.

Microcomputer-Based Doppler System for Weather Monitoring

A microcomputer processes satellite Doppler data to determine the locations of weather beacons.

Goddard Space Flight Center, Greenbelt, Maryland

A ground-based microcomputer processes Doppler data from weather satellites to determine geographical positions of weather beacons interspersed around the globe. These beacons, such as weather balloons and buoys, collect local weather information and transmit it to orbiting satellites. The satellites in turn relay this information to ground-based monitoring stations. Each station equipped with the microcomputer can print out both beacon location and accurate weather data collected from various points around the globe.

The microcomputer as shown in the block diagram includes a central processing unit (CPU), memory, and input/output peripherals. The CPU is a single large-scale-integration (LSI) microprocessor chip that addresses up to 2^{16} bytes of memory.

A built-in 1 MHz timing oscillator and clock driver eliminate the need for an external clock generator. The time base generates the required two-phase clock pulses. Address lines and read/write commands are set up during the first pulse period, and data are transferred (either read or write) during the second pulse.

Internally, the processor is organized into two sections. The instructions obtained from program memory are executed by implementing a series of data transfers in the register section of the chip. The lines that cause the data transfers are in the control section.

Most of the program execution occurs in the register section. Input data from the program memory, the data memory, or from peripheral devices appear during the last 100 ns of the second (or phase two) positive clock pulse. These data are simply transferred into the input-data latch for use during the next cycle.

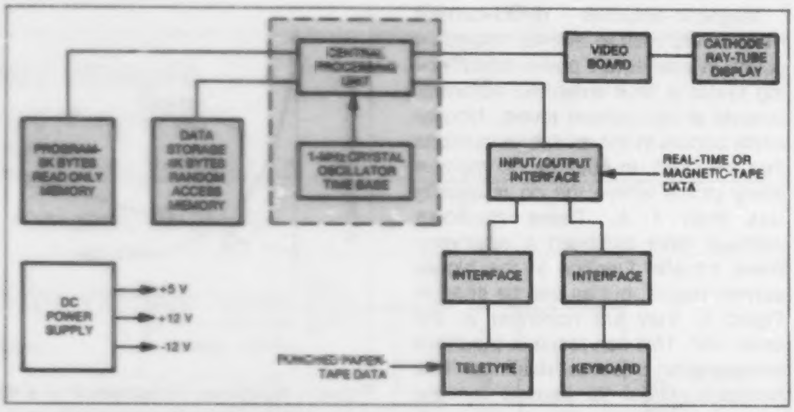

A Ground-Based Microcomputer determines geographical positions of beacons, using Doppler data from weather satellites. The system requires only 7 W and incorporates least-squares iteration to compute the positions. Results are printed out in alphanumerics either on the CRT or on the teletype. A 6502 CPU was used, although an equivalent processor could be substituted (with appropriate modification to the hardware).

The microcomputer memory section stores the satellite Doppler measurements in 4K bytes of random-access memory (RAM). The RAM has two distinct segments: the data storage and the working storage. Data are stored anytime the satellite passes over a radio beacon and can be loaded into the computer, using punched paper tape, via the teletype, magnetic tape, real-time satellite receiver tie, or by manual entry via the keyboard. The working storage segment is used for intermediate results in arithmetic operations for peripheral output data storage.

A position-location least-squares program is stored in read-only-memory (ROM) chips. These chips are permanently programed to compute beacon latitude and longitude positions either on a single or two successive satellite passes. A minimum of three Doppler measurements is needed for a single-pass solution, to solve for three unknowns: latitude, longitude, and frequency bias. Typically, however, about 15 data points are obtained per pass. That represents a 10-min observation inverval, and it takes about 20 s to compute a beacon position for that interval.

The microcomputer can be interfaced with a number of peripherals. One typical interface is with a keyboard and a cathode-ray-tube (CRT) display. The results are printed out in alphanumerics on the keyboard and on the CRT.

This work was done by Paul E. Schmid of **Goddard Space Flight Center** *and Joe J. Lynn of Old Dominion Systems, Inc. for further information, Circle 16 on the TSP Request Card.*
GSC-12448

Linearizing Magnetic-Amplifier dc Transducer Output

A diode corrects nonlinearity at small currents in
a magnetic-amplifier dc transducer circuit.

NASA's Jet Propulsion Laboratory, Pasadena, California

Magnetic-amplifier direct-current transducers used to monitor important points in spacecraft power-conditioning systems have exhibited nonlinear outputs at low current levels. Nonlinearity occurs in the miniature versions that are used, in quantity, to monitor many points where the dc is usually less than 1 A. These miniature versions have exhibited a relatively-linear transfer function in the higher current region, but as can be seen in Figure 1, they are nonlinear at the lower end. This can result in incorrect interpretation of actual readings. This nonlinear effect is caused by the magnetizing current, flowing through winding 6-5 and R_2, in parallel with R_1, and by the characteristics of the core material. The problem was corrected by adding a diode (CR_3) in series with the output stage between winding 6-5 and resistors R_2 in the circuit in Figure 2. The forward voltage drop of this diode minimizes the shunting effect on R_1 and reduces the magnetizing current flowing through R_2.

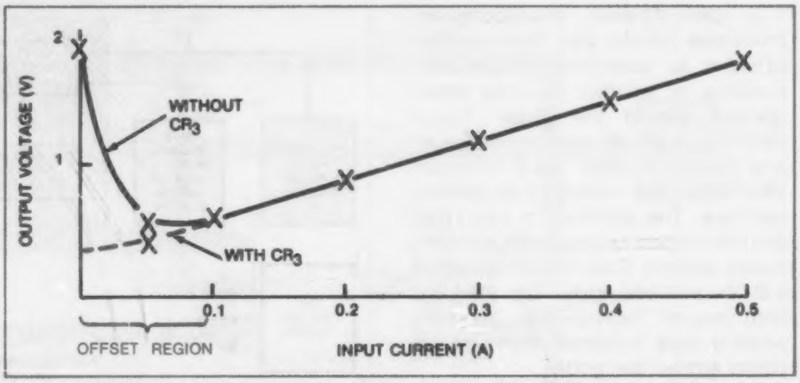

Figure 1. **Nonlinear Performance of a Magnetic-Amplifier dc Transducer** that occurs at low current levels is corrected by inserting a diode in series with the output stage.

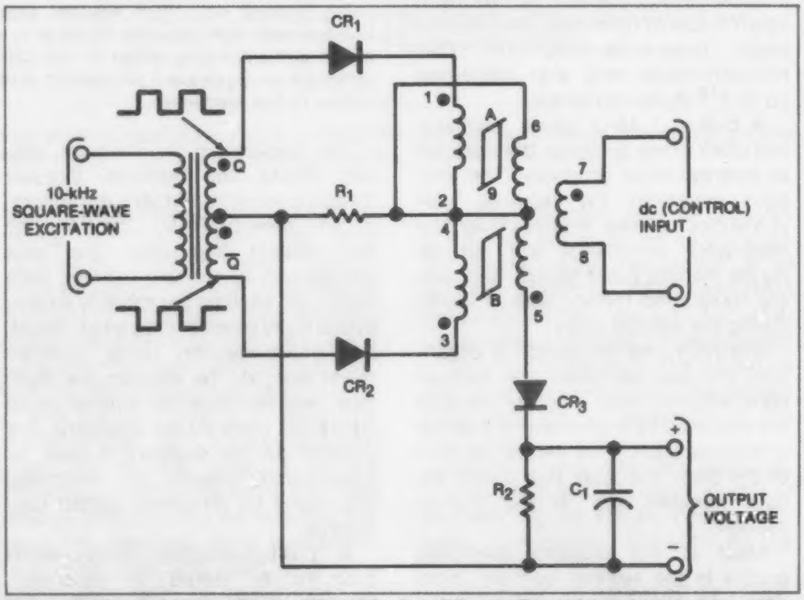

Figure 2. **Circuit Schematic of a Magnetic-Amplifier dc Transducer** shows where the diode is inserted to produce linear output at small current levels. The diode in series with the output stage corrects the nonlinear performance of the transducer in the offset region as shown on the graph.

The magnetic amplifier shown has the properties of a current transformer: The amplitude of the current in winding 5-6 equals the amplitude of the dc current being monitored (in winding 7-8), divided by the ratio of the turns of winding 5-6 to winding 7-8. During each respective Q and $\overline{Q}$, switching half cycle of the ac square-wave excitation applied sequentially to windings 1-2 and 3-4, the cores A and B each have two distinct operating phases: an unsaturated phase and a saturated one.

When a magnetic amplifier operates in the switching mode, desaturation can only occur if the voltage at the primary winding (e.g., 1-2) is of the same amplitude but of opposite polarity as the voltage across the secondary winding (e.g., 6-9). Hence the voltage that "resets" each of the cores in turn must not be allowed to reach a level that would overbias either core to produce saturation in the wrong direction. If this should occur with either core, both cores would thereafter remain saturated, defeating the desired switching action.

The diode drop (depending upon the number of diodes in series) in series with resistors R_2 and R_1 has a threefold effect: (1) It limits the indicating voltage that appears across R_2 to provide the output indication and linearizes in the offset region; (2) it limits the voltage needed to reset the cores and thus lessens the possibility of overbiasing in the wrong direction (which could produce reverse saturation); and (3) it gives leeway in selecting the value of R_1. After the value of R_1 is determined, the number of diodes used in series to produce the desired diode drop is determined experimentally.

Resistor R_1 is used to provide the desired transformer action. The value of R_1 must be a compromise, small enough to provide the return path for the magnetizing current instead of the alternate path through winding 6-5 yet high enough to minimize power loss.

This work was done by Satoshi Nagano of Caltech for **NASA's Jet Propulsion Laboratory.** *For further information, Circle 17 on the TSP Request Card.*

This invention is owned by NASA, and a patent application has been filed. Inquiries concerning nonexclusive or exclusive license for its commercial development should be addressed to the Patent Counsel, NASA Resident Legal Office-JPL [see page A5]. Refer to NPO-14617.

Better-Quality CCD-Array Images

Quadruple sampling increases the signal-to-noise ratio of charge-coupled-device imagers.

NASA's Jet Propulsion Laboratory, Pasadena, California

The quality of the image from an array of charge-coupled devices (CCD's) is improved by about 40 percent by a four-step sampling scheme. The scheme is easily implemented using simple logic circuits.

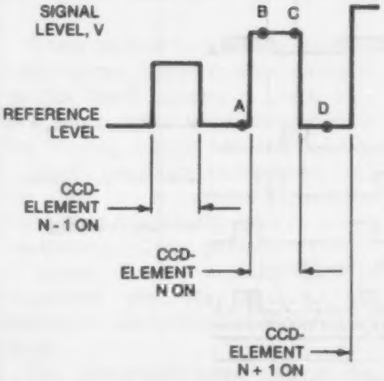

Figure 1. The **Signal From Contiguous Elements of a CCD Array** is sampled at points A, B, C, and D. The difference pairs $V_B - V_A$ and $V_C - V_D$ are added to double the signal level.

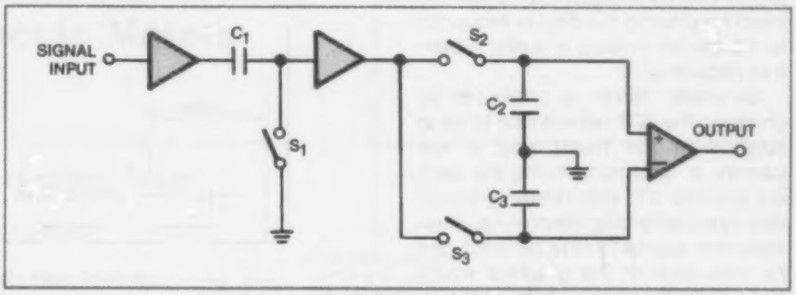

Figure 2. **Quadruple-Sampling Processor** is triggered by timing signals from the CCD array. The signals open and close electronic switches S_1, S_2, and S_3.

Previous CCD image processors used single or double sampling of the array output, as illustrated in Figure 1, which shows the signal derived from two contiguous CCD elements. In single sampling, only the signal level (B) during the "on" phase of each array element is measured; the "on" level and a reference level (B and A) are measured and subtracted in double sampling, improving the signal-to-noise level by a factor of 8 in one CCD imaging star tracker.

In quadruple sampling, the signal from each element in the array is sampled once before the element is clamped on, twice during the "on" period, and once again after the element is turned off. Thus, in Figure 1, one sample pair is taken at points A and B (as in double sampling), and another pair is taken at points C and D. The differences $V_B - V_A$ and $V_C - V_D$ are then added.

Adding the difference voltages effectively doubles the signal; and, since ideally the noise levels before and after the on period are uncorrelated, the noise increases only by a factor of $\sqrt{2}$, for an overall increase in signal-to-noise of $2/\sqrt{2}$, or 1.414, above its value if double sampling is used.

Figure 2 shows a simple implementation of a quadruple-sampling processor. Switch 1 clamps the reference level at time A, and switch 2 samples the signal at time B. Switch 1 also clamps the signal level at C; and the reference level is sampled at D with switch 3. The negative signal on capacitor C_3 is subtracted from the positive signal on capacitor C_2 by the differential amplifier, producing a net signal gain of 2. The timing signals to open and close the switches are easily derived from the CCD-array timing, using standard logic.

In practice, there is usually some correlation between the "before" and "after" noise levels. However, calculations for a worst-case noise spectrum in one star tracker showed the added noise to be only 11 percent above the uncorrelated noise level; and for a more typical noise spectrum, the added noise is only about 2 percent. Thus, the quadruple-sampling scheme should increase the overall signal-to-noise by about 40 percent above the level for double sampling, a prediction verified by measurements on the star-tracking imager.

This work was done by Steve D. Gaalema of Caltech for **NASA's Jet Propulsion Laboratory.** *For further information, Circle 18 on the TSP Request Card.*

This invention is owned by NASA, and a patent application has been filed. Inquiries concerning nonexclusive or exclusive license for its commercial development should be addressed to the Patent Counsel, NASA Resident Legal Office-JPL [see page A5]. Refer to NPO-14426.

Real-Time Film Recording From Stroke-Written CRT's

A simple method for phasing ensures flicker-free recordings.

Langley Research Center, Hampton, Virginia

Real-time simulation studies often require motion-picture film recording of the events directly from stroke-written cathode-ray tubes (CRT's). The main difficulty presented is the prevention of "flicker," which results from the lack of synchronization between the display sequence on the CRT and the shutter motion of the camera. A simple programmatic method has been devised for phasing the display sequence to the shutter motion, ensuring flicker-free recordings.

Generally, flicker is prevented by choosing the CRT refresh rate to be at least twice the frame rate of the camera or by synchronizing the camera and the CRT with relatively-expensive interconnecting electronics. However, this approach may be precluded by limitations of the graphics equipment or by the unavailability of the interconnectors. Most computer graphics systems operate on a priority interrupt basis: The graphical computations are interrupted at fixed intervals of time to display the image on the CRT. For flicker-free film recording at 24 frames/second, a display refresh rate of at least 60 Hz is required. However, at this refresh rate, too little time may be available for an acceptable update rate for the graphical computations.

In the new technique, a motion-picture camera with a synchronous ac motor, running at a fixed frame rate of 24 frames/second and a shutter speed of 1/60 second, is used. The refresh rate of the display is set at 24 Hz (five intervals of 1/120 second each). Since the camera and the graphics terminal are both connected to the same power system, they are fully synchronized. In order to record the image on film, the phase lag between the shutter motion and display sequence must be such that the CRT image is displayed during the interval in which the shutter is fully open.

In Figure 1, pulse train I is the camera shutter sequence; pulse trains II are the display sequences for fully invisible, partially visible, and fully visible images. The problem of phasing

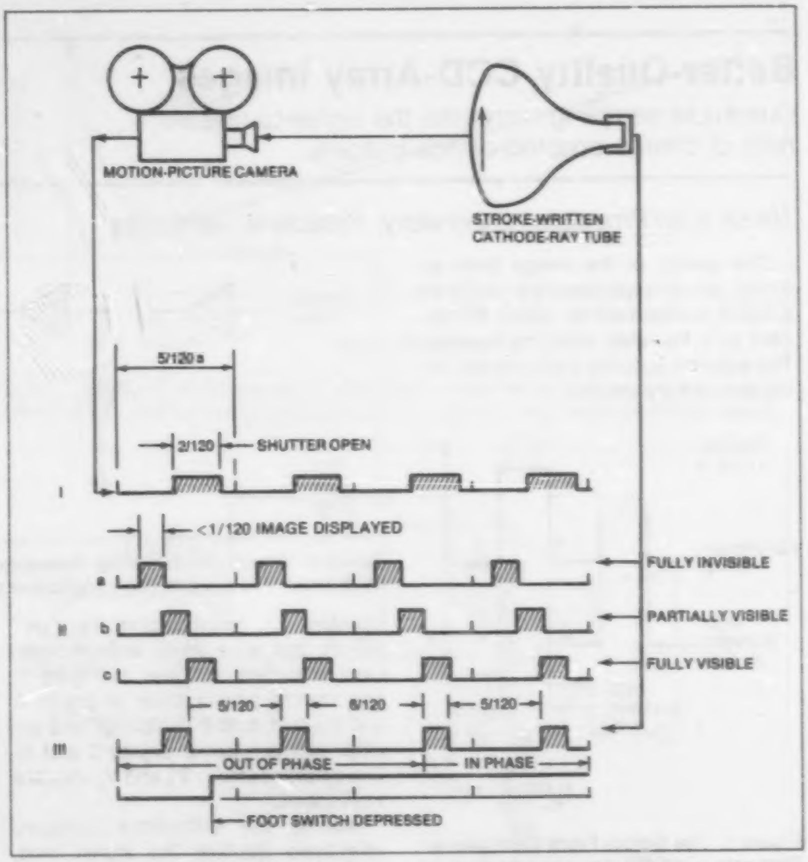

Figure 1. **Display Sequence** can be delayed by depressing a foot switch a sufficient number of times to phase the CRT image to the open shutter.

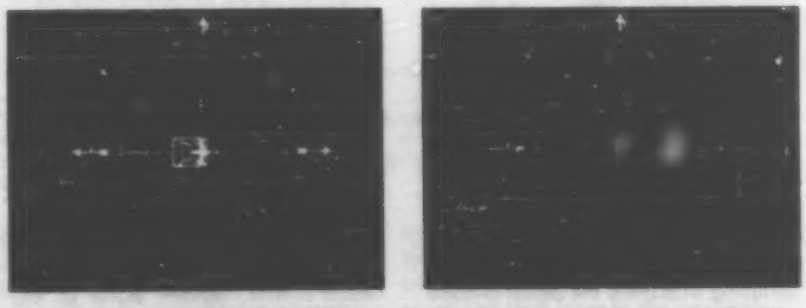

Figure 2. **Flicker-Free Phasing** is shown correctly in the single-frame image on the left. The image on the right, with incorrect phasing, shows an image only partly visible.

the camera and the graphics system is solved by programmatically delaying the display sequence. A simple foot switch, standard to most graphics systems, is used to initiate the delay. The number of 1/120-second intervals between interrupts is normally five. By depressing the foot switch, the display sequence is delayed by an interval of another 1/120 second, as shown in sequence III.

After releasing the foot switch, this process can be repeated, and the sequence is delayed by an additional 1/120 second. After pressing the foot switch five times, the phasing is again the same as at the start. While observing the image through the viewfinder with running camera, the foot switch is pressed several times until the image is fully visible. Figure 2 shows single frames from a motion picture made using both correct and incorrect phasing. This method requires that the viewfinder image is identical to the image recorded on film.

The motion-picture recordings obtained with this method are absolutely free of flicker, with an adequate computational update rate. The image appears only slightly dimmer than with the more-wasteful 60-Hz refresh rate.

This work was done by Robert L. Hunt of **Langley Research Center** *and Arthur J. Grunwald of the National Research Council. For further information, in the form of a film, 15 minutes long, taken using this technique, request film L-1266 from the NASA Langley Research Center, Film Lending Library, MS 425, Hampton, Virginia 23665.*

Inquiries concerning rights for the commercial use of this invention should be addressed to the Patent Counsel, Langley Research Center [see page A5]. Refer to LAR-12529.

Torque Control for Electric Motors

Torque output is varied to accommodate various loads.

Lyndon B. Johnson Space Center, Houston, Texas

A new method for adjusting electric-motor torque output to accommodate various loads utilizes a phase-lock loop to control a relay connected to the starting circuit. As the load is imposed, the motor slows down, and the phase lock is lost. The phase-lock signal then triggers the relay to power the starting coil and generate additional torque. Once the phase lock is recovered, the relay restores the starting circuit to its normal operating mode.

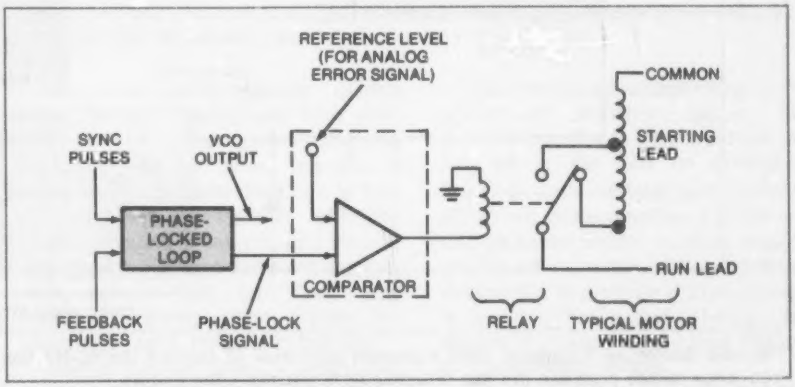

Motor Control Circuit uses a phase-locked loop to supply additional power to the motor shaft to accommodate various loads. When the load is applied, phase lock is lost, and a relay is triggered to feed power to the starting coil to generate the extra torque. When the phase lock is restored, the relay opens, and power is applied directly to the run lead.

The phase-lock loop controls the motor starting coil. This eliminates the centrifugal switch and insures maximum torque whenever the motor is started or whenever additional torque is needed to restore the phase lock. This approach gives more positive control than the timed application of a starting torque and can generate additional torque when the motor is at operating speed.

The phase-lock signal may serve as a digital indication of the phase lock or as an analog indication of a phase error. As shown in the figure, the signal can drive the relay directly; in the second case the signal is compared to a reference level corresponding to the desired maximum in-lock phase error, and the comparator controls the relay.

Motor drive signals on the run lead are applied to the starting coil when the relay is activated (loop out of lock) to produce extra torque. Motor drive signals are applied to the run lead of the motor when the relay is not activated (loop in lock). The method can save power because the running torque can match the load more closely, and additional torque (requiring additional power) is only generated when it is needed.

This work was done by Clement A. Berard of RCA Corp. for **Johnson Space Center.** *No further documentation is available.*
MSC-18635

Frequency-Controlled Voltage Regulator

Converting input ac to a higher frequency reduces size and weight and makes possible a unique kind of regulation.

NASA's Jet Propulsion Laboratory, Pasadena, California

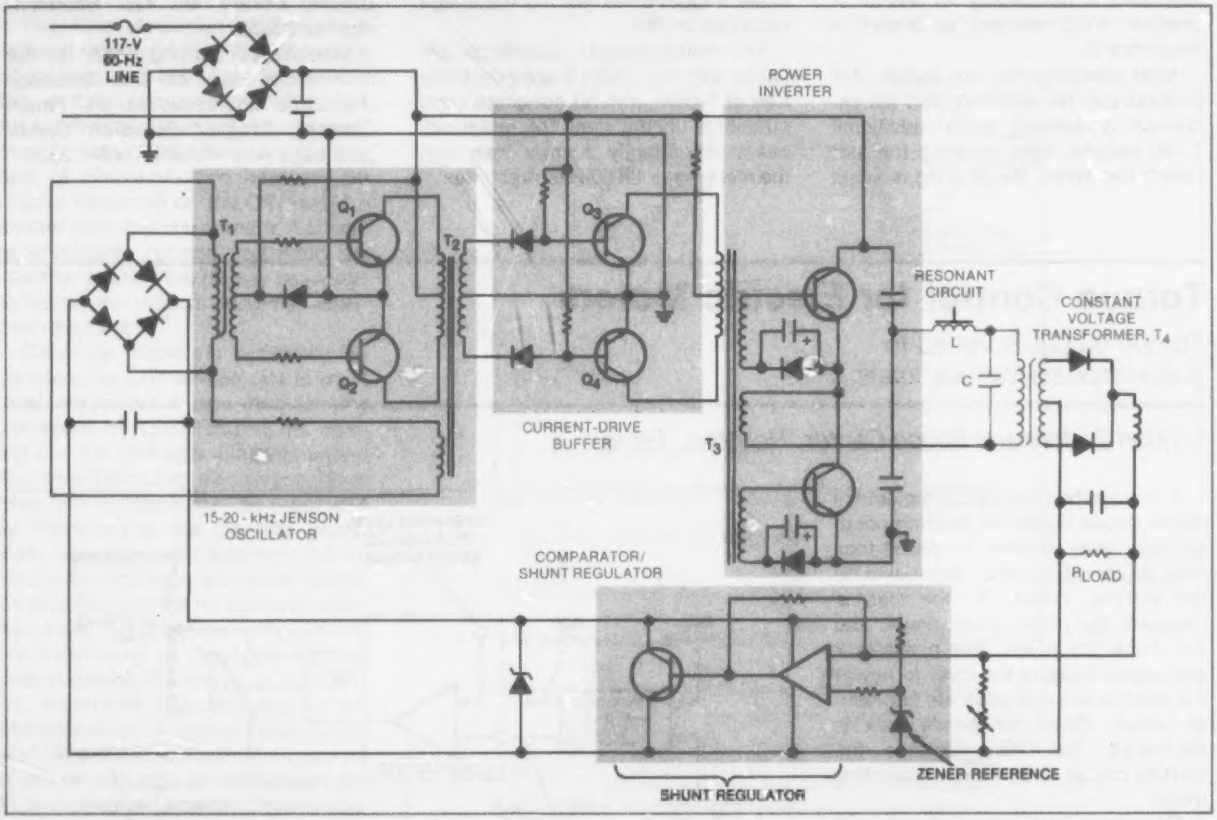

The new **Switching Regulator** uses a Jenson oscillator to convert the 60-Hz line voltage to 20 kHz. Stepping up to higher frequency makes possible the use of lightweight passive components.

A proposed power supply would be smaller and lighter than conventional supplies because it converts its ac line input to a much higher frequency before regulating it and rectifying it. At the higher frequency, the size and weight of the inductive and filter components are reduced by a factor of 100 or more; and since the conversion frequency is above the range of human hearing, the supply generates no audible noise. The supply also exploits the high-frequency conversion feature to regulate its output voltage in a novel way.

In the circuit (see figure), the 60-hertz, 117-volt line power is converted to a 15 to 20 kilohertz square wave. This signal drives a resonant circuit (inductor L and capacitor C) at the input to saturable-core transformer T_4. A feedback leg returns part of the load voltage to the oscillator to vary its frequency in response to output voltage changes.

By operating the circuit at a frequency near the resonant point of the LC circuit, the voltage input to transformer T_4 is made large enough to drive the transformer into saturation. At that point on its operating curve, the transformer is insensitive to voltage fluctuations at its input, and the voltage at its output is "hard-limited" to the required value.

In the saturation mode, the transformer voltage varies proportionally to its drive frequency, and this effect is used to regulate the circuit output. The error signal obtained by monitoring the load voltage is fed to one input of an op amp. The other input is a reference Zener diode. Any difference between these inputs is amplified and applied to a shunt regulator to vary the resistance across a bridge rectifier. Changes in the bridge impedance at the input to transformer T_1 adjust the oscillator frequency to compensate for changes in the load voltage. The ferroresonant circuit is inherently short-circuit proof.

This work was done by Colonel W. T. McLyman of Caltech for **NASA's Jet Propulsion Laboratory.** *For further information, Circle 19 on the TSP Request Card.*
NPO-13633

A Redundant Regulator Control With Low Standby Losses

A shunt regulator minimizes power-conditioning losses.

NASA's Jet Propulsion Laboratory, Pasadena, California

A new shunt regulator circuit for an outer-planet-spacecraft radioisotope thermoelectric generator minimizes power-conditioning losses. The unit consists of a bank of duplicate regulator control amplifiers and their associated shunt transistors connected across a power-supply line. Its high-gain circuitry arranged in a redundant configuration is very reliable and is characterized by low standby loss. The circuit can be used in other power-supply applications where size, weight, and reliability are important.

The unit is based on a simple regulator control amplifier designed to minimize the power losses. Regulated bus voltage is sampled and compared to a voltage reference; an error signal proportional to the difference is produced by the operational amplifier. This output error signal drives shunting transistors to maintain the regulated bus voltage.

Four of these control amplifiers and their shunt transistors are arranged as shown in the figure, forming a highly reliable regulator. Each circuit has a standby loss of approximately 15 mW nominal and 25 mW worst-case maximum. The shunt regulator controls a maximum of 600 W regulating the bus voltage through all the spacecraft operational modes. With approximately 60 mW of power in the four regulator control amplifiers, an efficiency of 99.99 percent is realized when the full 600-W source power is delivered to the load.

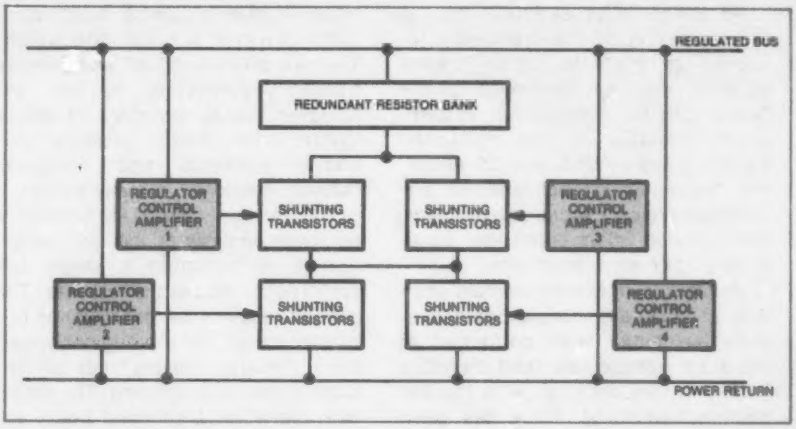

Shunt Regulator block diagram shows the arrangement of control amplifiers and their shunt transistors. Because each regulator control amplifier has high gain, only one of the four governs shunting at any time. This highly reliable circuit features a very low standby power loss.

Because each regulator control amplifier has a sufficiently high gain, only one of the four governs shunting operations at any time. The one in series with the controlling unit is fully on; the one in parallel with the controlling unit is fully off; and the one diagonal to the controlling unit is either fully off or fully on. This quad redundant configuration makes the regulator highly tolerant to failures.

Partial failures, short or open, are accommodated without affecting the regulator performance. Control is transferred automatically from the failed unit to either its series or parallel unit, depending upon the mode of failure (fully on or fully off).

The 21-V output voltage swing of the operational amplifier causes the shunting circuitry to translate from the fully off to the fully on condition. The large signal-voltage gain, typically 300 V/mV, of the amplifier and the 5:1 voltage-sense divider network require only 35 mV deviation on the regulated voltage bus to produce a 21-V change in the amplifier output. Hence, the regulation change versus load change is nearly immeasurable.

This work was done by Roman W. Andryczyk and Stephen R. Peck of General Electric Co. for **NASA's Jet Propulsion Laboratory.** *For further information, Circle 20 on the TSP Request Card.*
NPO-13165

Camera Add-On Records Time of Exposure

The time a photograph is taken is permanently recorded on the edge of the exposure by a compact electronics module that attaches to the camera case. A single-chip timing circuit drives an LED display, which is imaged on the film plane. The normally blanked display is unblanked when the shutter switch is activated.

(See page 168.)

Input/Output Interface Module

An input/output module detects level changes in any of its 16 inputs, transfers the changes to its outputs, and generates interrupts when the changes are detected. Up to four changes-in-state per line are stored for later retrieval by a controlling computer. Using standard TTL logic, the module fits in a 19-inch rack-mounted console.

(See page 143.)

Improved Power-Factor Controller

Power dissipation in an ac induction motor is reduced by an improved circuit that lowers the applied voltage when the motor is idling or only lightly loaded. Timing voltages in phase with the motor current are sensed across a gate-controlled semiconductor switch in series with the motor, rather than across a high-power resistor, as in an earlier version.

(See page 133.)

Frequency Response of Multiple-Sampling-Rate Systems

A new procedure makes a complex problem tractable.

Lyndon B. Johnson Space Center, Houston, Texas

An analytical procedure simplifies the prediction of the frequency response of multirate digital control systems. Although developed for the Space Shuttle flight-control system, which operates at two gyroscope sampling rates (12.5 and 25 hertz), the procedure is applicable to any multirate system describable by linear, constant-coefficient differential equations or difference equations.

Previously, frequency-domain analysis of multirate sampled-data systems has either been performed at the lower sample rate (and therefore limited in frequency range to the low sample frequency), or it has been performed at the higher sample rate by the use of a method that effectively increases the order of continuous- or higher-frequency piece parts by a factor of n in an n:1 multirate system. The new procedure also analyzes the frequency domain at the fast rate; however, it does so without increasing system order (which presents root-finding problems and computer-memory overloads in many cases).

The previous method for frequency-response analysis at the fast sample rate is to construct a single rate system operating at the fast rate. This method requires the construction of a "mirror image" of the original system (or n "mirror images" for an n:1 sample-rate-ratio system). The loop is then broken at a selected point, and the frequency-response characteristics of the enlarged system are determined.

The new procedure replaces the enlarged system with the computation of two separate frequency responses based on the original system. The two frequency responses are vector-summed at discrete frequencies to produce the total system frequency response at the faster sample rate. The advantage is a reduction in problem size and, consequently, the emergence of a problem that fits within many existing analysis tools and that does not present multiple-root determinaton problems.

This work was done by David K. Scharmack of Honeywell, Inc., for **Johnson Space Center.** *For further information, Circle 21 on the TSP Request Card.*
MSC-18473

Physical Sciences

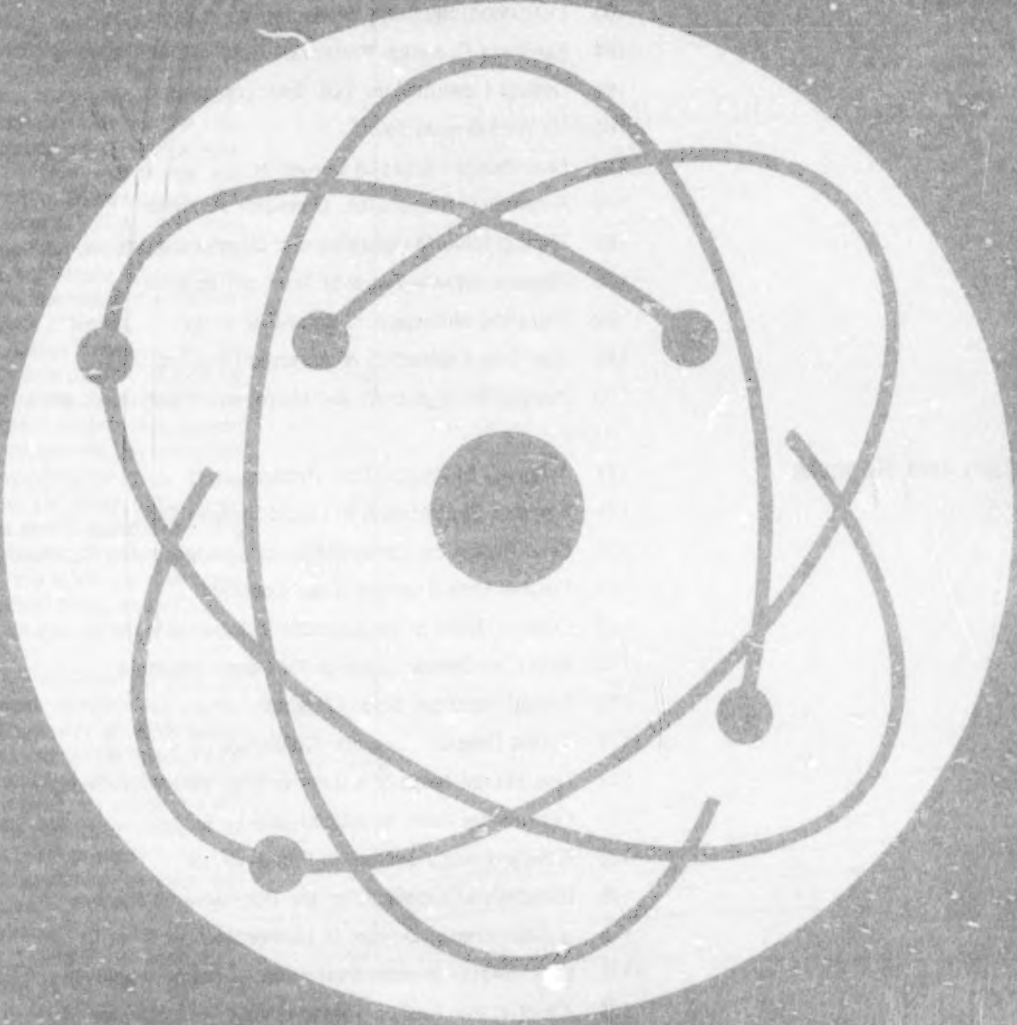

Hardware, Techniques, and Processes

161 An Equation of State for Liquids
162 High-Resolution Spectrometer/Interferometer
163 Instrument Remotely Measures Wind Velocities
164 Far-Field Radiation Pattern of Tunable Diode Lasers
164 Optical Calibrator for TDL Spectrometers
165 UV Actinometer Film
166 Fluorescent Radiation Converter
166 Automated Holographic Drop-Size Analyzer
167 Photographic Measurement of Droplet Density
168 Camera Add-On Records Time of Exposure
169 Improved Multispectral Solar-Cell Array
169 Low-Cost Calibration of Acoustic Locators
170 Integral Storage-Bulb and Microwave Cavity for Masers

Books and Reports

171 A Survey of Photovoltaic Systems
171 Thermal Stratification in Liquid-Storage Tanks
171 Final Report on Development of a Programable Controller
172 Fresnel Lens Tracking Solar Collector
172 Outdoor Tests of the Concentric-Tube Collector
173 Selective Optical Coatings for Solar Collectors
173 Finned-Absorber Solar Collector
173 A Test Program for Solar Collectors
174 Operational Tests of a Solar-Energy System in Georgia
174 Operational Tests of a Solar-Energy System — Florida Site
174 A Solar-Energy System in Pennsylvania
175 Installation Guidelines for the Pennsylvania System
175 A Solar-Energy System in Minnesota
175 Solar-Energy System Evaluation — Pennsylvania Site
175 A Hot-Water System Tested Onsite — Togus, Maine
176 A Reliable Solar-Heating System — Huntsville, Alabama
176 Solar-Heating and Cooling Demonstration Project

An Equation of State for Liquids

A closed expression for volume as a function of pressure and temperature has been verified for over 250 liquids.

NASA's Jet Propulsion Laboratory, Pasadena, California

While several equations of state are known for gases, much less success has been achieved in describing the pressure, volume, and temperature interrelationship for liquids. Recently, however, researchers at the Jet Propulsion Laboratory discovered a relatively simple equation that works well for a wide group of liquid metals, molten salts, polymeric liquids, and inert liquids. The equation can assist chemical engineers, solid-state researchers, and others with interest in the thermodynamic behavior of liquids.

The new equation is given in the figure, where it is also plotted for several representative pressure values. It contains two constant parameters, β_o and p_o, which are determined by fitting the equation to experimental data. Three other constants are taken either from tabulated data or are estimated using established schemes. These constants are v_c and T_c, the volume and temperature at the critical point, and v(0,0), a hypothetical volume of the liquid at $T = 0$.

In tests of the equation on data for 250 liquids near atmospheric pressure, only the behavior of water below about 140° C could not be fitted. For a few liquids, including organics, metallics, and fused salts, for which the v(T) response is known as a function of pressure, volumes predicted by the equation agree to within 1 percent with measured values.

The figure shows v(p,T) for $p/p_o = 0, 0.2, 0.5, 1, 2$, and 5. The monotonically increasing curve for $p/p_o = 0$ corresponds to behavior near atmospheric pressure. For higher pressures, the equation predicts a point of inflection in v(p,T) and decreasing slope above that point. This general behavior is known for all liquids for which sufficient data exist. The new equation is one of only a few closed-form expressions that predict the inflection point.

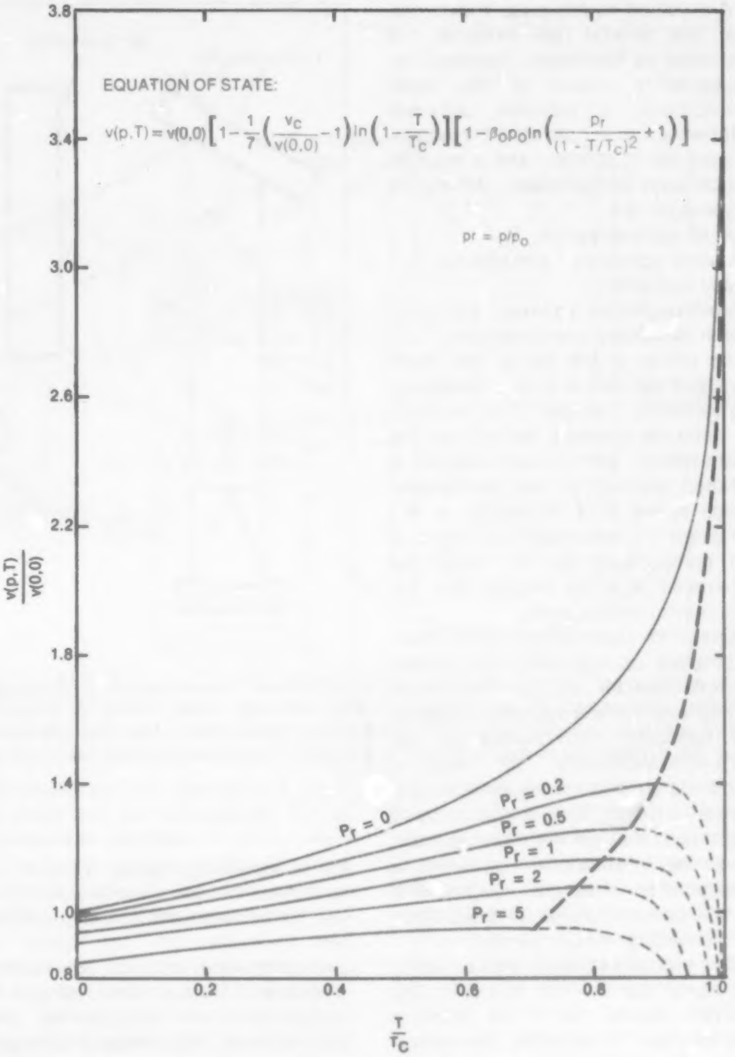

Equation of State for Liquids is plotted as v(p,T) for several values of pressure. The behavior in the region of dashed lines at the lower right, including the maximums of v(p,T), is not observed in real liquids, and the equation is not valid in this region.

This work was done by Robert F. Fedors, Robert F. Landel, and Jovan Moacanin of Caltech for **NASA's Jet Propulsion Laboratory.** *For further information, Circle 22 on the TSP Request Card.*
NPO-14821

best copy available

High-Resolution Spectrometer/Interferometer

Proposed design compensates for tilt errors and minimizes spectrum channeling.

NASA's Jet Propulsion Laboratory, Pasadena, California

A modified double-pass interferometer has several new features that maximize its resolution. Proposed for rocket-borne probes of the upper atmosphere, it includes cat's-eye retroreflectors in both arms, a wedge-shaped beam splitter, and a wedged optical-path compensator. Among its advantages are:

- full tilt compensation,
- minimal spectrum "channeling,"
- easy tunability,
- maximum fringe contrast, and
- even two-sided interferograms.

As shown in the figure, the basic configuration has only five freestanding elements: two flat "fold" mirrors, an entrance-aperture flat mirror, the beam splitter, and the compensator. A detailed analysis of the double-pass optics shows that the design is tilt-canceled — reasonable tilt errors of the components do not upset the superposition of the images from the two interferometer arms.

Spectrum channeling in some interferometers occurs when light makes multiple passes through the beam splitter and forms a spurious image of the foreoptics field-of-view on the cat's-eye secondary. This image is displaced by a small angle from that formed by light that makes only a single pass through the beam splitter. Thus, the interferogram becomes a superposition of several images, and an artificial modulation of the pattern — channeling — is observed.

This problem is eliminated by using a wedged beam splitter to deflect the spurious beams out of the detector field-of-view. To equalize the optical paths in both arms, the compensator is also wedged. For the proposed system, the required wedge angle is only 0.2°.

Because both the compensator and the beam splitter cover the input and the output of the cat's-eyes, precise matching of the wedge angles is not necessary. An analysis of the geometry shows that the total optical path through the wedge, including ingoing and outgoing rays, is the same, regardless of the wedge angle or of wedge rotation. Consequently, the tolerances on the wedge angles and their alinement are not particularly critical. In the proposed design the angles do not have to be matched to better than 5 arc-minutes out of 0.2°.

The optical configuration shown has the smallest practical angles of incidence on the mirrors and on the dielectric/air interfaces. Thus, polarization on reflection is minimal, and the loss of contrast due to such polarization is reduced.

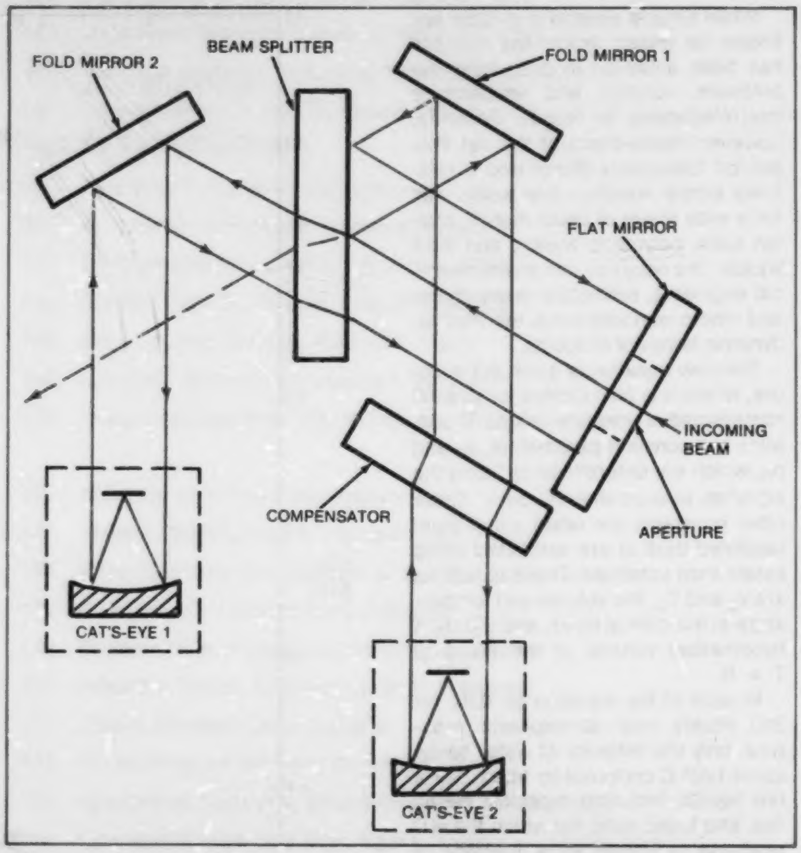

The **Interferometer Optics** has only five freestanding components (other than the cat's-eyes) that could be misalined by vibration or shock. By combining fold mirror 1 with the compensator in a single (Mangin) element, the number can be reduced to four.

This work was done by James B. Breckinridge, Robert H. Norton, and Rudolf A. Schindler of Caltech for **NASA's Jet Propulsion Laboratory.** *For further information, Circle 23 on the TSP Request Card.*

This invention is owned by NASA, and a patent application has been filed. Inquiries concerning nonexclusive or exclusive license for its commercial development should be addressed to the Patent Counsel, NASA Resident Legal Office-JPL [see page A5]. Refer to NPO-14448.

Instrument Remotely Measures Wind Velocities

Gas velocity is determined by measuring the Doppler shift of its spectrum.

NASA's Jet Propulsion Laboratory, Pasadena, California

A Doppler-shift spectrometer makes remote satellite measurements of atmospheric wind velocity and temperature at specified altitudes. As in a correlation spectrometer, the spectrum of a gas in a reference cell and the spectrum of the same gas in the atmosphere are correlated both in emission and absorption. Correlation, usually lost due to Doppler-shifted spectra because of relative velocities between the measured and reference gases, is retained by a mechanically-modulated cat's-eye assembly. Acoustic/optic or electro-optic devices have also been considered and show promise in this application.

As shown in the figure, light coming in through the telescope established the field-of-view of the instrument. The light is reflected off two cat's-eye assemblies that oscillate with opposed motions in a direction normal to their faces.

Each reflection from the cat's-eye primary mirrors induces a Doppler shift in frequency by an amount of $\delta\nu$, where $\delta\nu = 2\nu(v/c)$ and where v is the velocity of the mirror, c is the speed of light, and ν is the unshifted frequency. The use of two cat's-eyes increases the Doppler shift and also eliminates the motion of the center of mass of the assembly. The Doppler-shifted light is bent away from the cat's-eyes by a mirror and is directed through a gas-reference cell, deflected by another mirror through a spectral filter, and onto the detector.

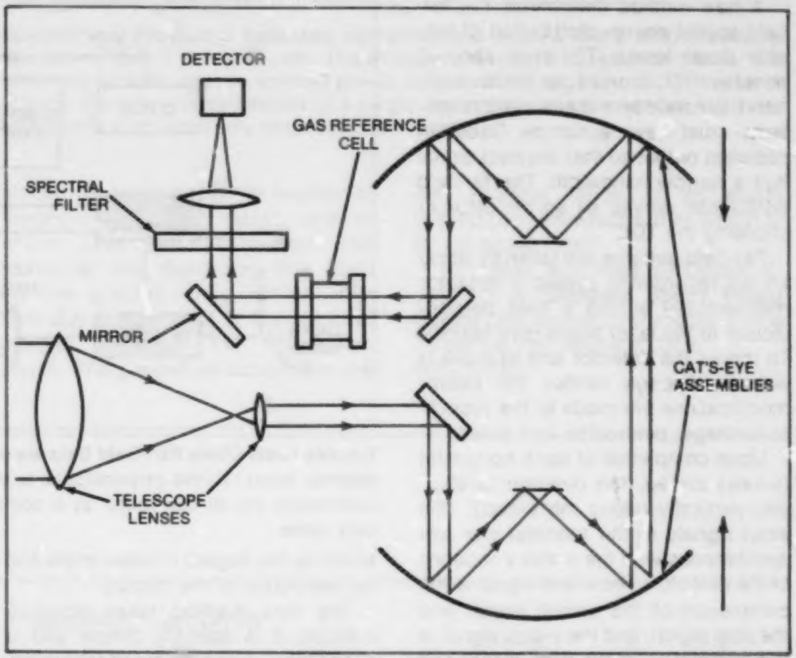

Doppler-Shift Spectrometer determines wind velocities of the atmosphere. The altitudes at which these velocities are measured can be determined using a radiometer and color filter-wheel combination or by changing gas pressure in the reference cell that corresponds to pressure of the same gas at the specific altitude.

At some instant the motion of the cat's-eye will cancel out the Doppler shift due to the relative motion of the instrument and the atmosphere. This canceled shift will be apparent in the signal in the detector.

The linear velocity of the cat's-eye assembly depends on the angular position of a rotating drive wheel. At the instant that the reference and atmospheric spectra are correlated, the angular position of the driver wheel is a measure of the atmospheric velocity. A suitable shaft encoder may be used to read out the shaft position.

This work was done by Jack S. Margolis, Daniel J. McCleese, Clay H. Seaman, and Michael S. Shumate of Caltech for **NASA's Jet Propulsion Laboratory.** *For further information, Circle 24 on the TSP Request Card.*

This invention is owned by NASA, and a patent application has been filed. Inquiries concerning nonexclusive or exclusive license for its commercial development should be addressed to the Patent Counsel, NASA Resident Legal Office-JPL [see page A5]. Refer to NPO-14524

Far-Field Radiation Pattern of Tunable Diode Lasers

An improved technique rapidly determines the far-field spatial energy distribution.

Langley Research Center, Hampton, Virginia

A new method determines the far-field spatial energy distribution of tunable diode lasers (TDL's) in about 3 minutes. TDL's used as local oscillators in heterodyne measurement systems must have a narrow Gaussian radiation output so that the beat signal has a narrow bandwidth. The far-field distribution serves as an indicator in choosing the TDL.

Far-field patterns are taken by using an x-y recorder to sweep a detector mechanically across a field perpendicular to the laser beam (see figure). To mount the detector and to move it without slippage across the beam, modifications are made to the recorder carriage, penholder, and cables.

Upon completion of each horizontal (x-axis) sweep, the detector is stepped vertically (along the y-axis). The input signals to the recorder pen are synchronous with the x and y motions of the detector: The x-axis signal is the summation of the sweep signal and the step signal, and the y-axis signal is the summation of the step signal and the detector output. By adding the step signal to the x-axis motion, the graphical display is displaced to the right or left after each sweep, making the pattern appear to be three-dimensional. The step amplitude determines the degree of skew angle and the resolution of the display.

The new method takes about 3 minutes. It is optically simple and is economical, using standard laboratory parts and equipment. It records automatically without operator control and is easily adaptable to computer control of input instructions and computer treatment of output data. The degree of data resolution is limited only by the width of the recorder pen, and data are repeatable.

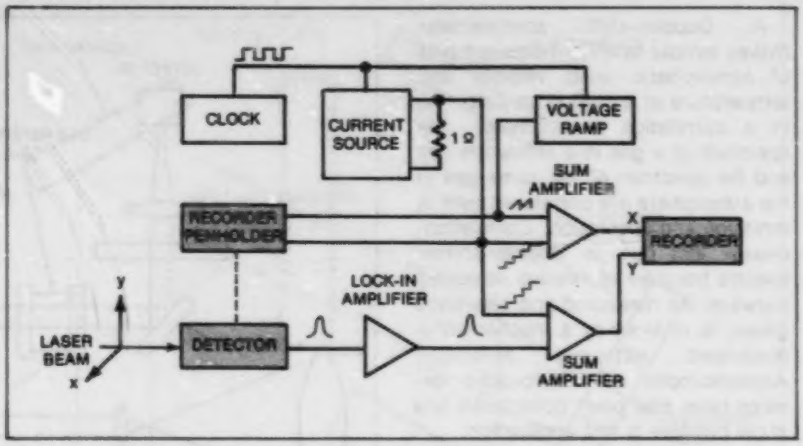

Tunable Laser Diode Far-Field Data are obtained by using an x-y recorder to sweep a detector across a field perpendicular to the laser beam. The sweep, step, and pen lift commands are all controlled by a common clock, with adjustable frequency and duty cycle.

This work was done by Thomas J. Lash of **Langley Research Center**. *For further information, Circle 25 on the TSP Request Card.*

Inquiries concerning rights for the commercial use of this invention should be addressed to the Patent Counsel, Langley Research Center [see page A5]. Refer to LAR-12631.

Optical Calibrator for TDL Spectrometers

Two etalons and a monochromator mode selector help calibrate the spectrometer in the selected laser mode.

Goddard Space Flight Center, Greenbelt, Maryland

Spectrometers using a tunable diode laser (TDL) source are difficult to calibrate in some laser modes. The frequency range of these modes does not include any frequency generated by standard molecular sources, leaving the spectrometer without the reference frequency.

A new approach of transferring and extending the absolute frequency calibration from one lasing mode to another spectrally isolated from the first resolves that problem. TDL's emit in many modes; each is approximately 1 cm^{-1} wide, distributed over a range of up to 200 cm^{-1}. If two Fabry-Perot etalons (see figure) of unequal lengths and a monochromator mode selector are arrayed in tandem within the laser path, they can be used to establish the number of fringes between any two spectral points separated by a large frequency interval.

The etalons are the germanium type: One is 1 in. (2.5 cm) long, and the other is 0.8 in. (2 cm) long, although other lengths and materials can be used. If the first has a 0.05-cm^{-1} free spectral range and the second a 0.0625-cm^{-1}, the two combined in tandem will cause the

fringes to coincide every 0.25 cm^{-1}. The fringes that coincide are the most intense and are clearly identified with the aid of the monochromator, displaying every fifth fringe of the longer etalon and every fourth fringe of the shorter one.

The Ebert monochromator mode selector has a 0.1-cm^{-1} calibration accuracy and easily resolves the 0.25-cm^{-1} spaced undulations of the combined fringe pattern. Thus, if a peak fringe of one laser mode is precisely calibrated, the precise frequency of a peak fringe in any other mode can be determined, provided the free spectral range of one of the etalons is known. In this way, the absolute calibration of one laser mode can be extended to other modes separated from the first by arbitrarily large spectral intervals.

This technique also accurately determines the free spectral range of an etalon. By establishing the number of fringes between two modes, both of which have been calibrated with molecular line standards, one finds the free spectral range with an error inversely proportional to the spectral interval between the calibration points. This procedure establishes the free spectral range of an etalon without prior knowledge of its length or its refractive index.

This work was done by Donald E. Jennings of **Goddard Space Flight Center.** *For further information, Circle 26 on the TSP Request Card.*
GSC-12562

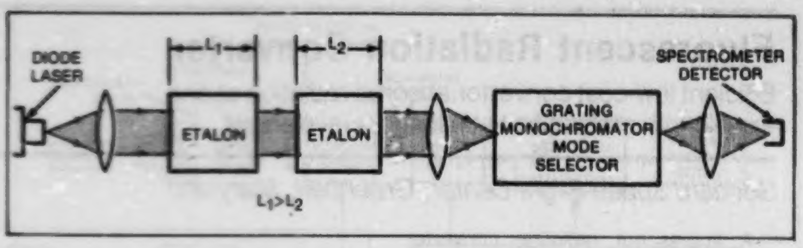

Spectrometer Frequency Calibrator comprises two etalons and a monochromator alined in tandem in the laser path. The arrangement is used to establish the number of fringes between any two spectral points separated by a large frequency interval. It extends the absolute calibration of a single laser mode to other modes separated from the first by arbitrarily large spectral intervals.

UV Actinometer Film

Low-cost polymer film measures cumulative UV radiation.

NASA's Jet Propulsion Laboratory, Pasadena, California

A proposed UV actinometer film using a photochemically sensitive compound changes its chemical composition in response to solar UV radiation. The extent of this chemical conversion depends on the length of the exposure and can be measured by examining the film samples with a spectrophotometer. The film can be exposed from several seconds up to a month. Paint and plastics manufacturers can use this film to determine total UV irradiance on their products to see how well they stand up against the UV radiation.

The film is cast from dichloromethane using polymethylmethacrylate containing 10 percent o-nitrobenzaldehyde (NBA). The NBA undergoes a photochemical rearrangement in response to the 300- to 430-nm UV region, forming o-nitrobenzoic acid. After the exposure to solar radiation, the film samples are mounted on 35-mm slides and examined with a spectrophotometer via absorption spectroscopy. The amount of remaining NBA is determined by observing the height of the 1,530-cm^{-1} band (see figure). This quantity is compared with the amount of NBA present prior to exposure. The difference between the two shows how much of the NBA has been converted and hence the cumulative UV irradiance responsible for this conversion.

It is important not to overexpose the NBA. If more than 50 percent of the NBA is converted, the film response loses linearity.

The film is unaffected by visible light. It can be used on any surface, in areas inaccessible to bulky instruments (e.g., radiometers), and can also measure solar ultraviolet radiation as a function of wavelength and bandwidth using appropriate filters. Although less sensitive than radiometers, the film needs no direct or hemispherical irradiance to work and, of course, no calibration — a frequent necessity with the radiometers.

This work was done by Clifford D. Coulbert and Amitava Gupta, of Caltech and James N. Pitts of the University of California, Riverside, for **NASA's Jet Propulsion Laboratory.** *For further information, Circle 27 on the TSP Request Card.*
NPO-14479

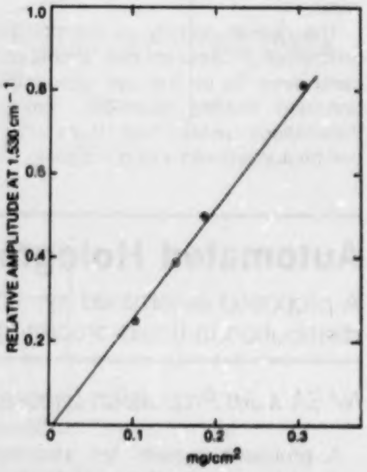

Calibration Curve for NBA shows the height of the absorptance band as a function of NBA density. This curve is used to determine the amount of NBA left on a film following its exposure to solar UV radiation. The amount, in turn, is used to compute the total solar UV irradiance on the film as a function of time.

Fluorescent Radiation Converter

Efficient low-cost converter absorbs radiation at one wavelength and emits it at a longer wavelength.

Goddard Space Flight Center, Greenbelt, Maryland

A fluorescent radiation converter (see figure) uses an undoped optically transparent substrate. One side of the substrate is coated with a plastic film containing fluorescent organic dyes that absorb optical radiation at one wavelength and emit it at a longer one. The emitted radiation is reflected internally inside the substrate, amplifying the intensity that reaches the radiation detector.

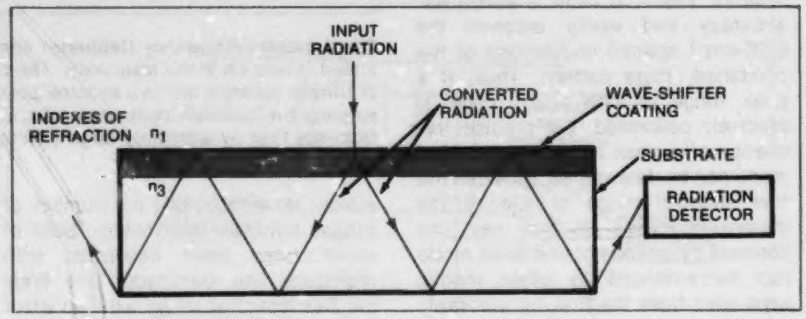

New Fluorescent Radiation Converter uses optically transparent substrate coated with a wave-shifter material. The wave-shifter coat absorbs radiation at one wavelength and emits it at a longer wavelength. Emitted radiation is more intense than the original input and is more easily detected.

The transparent substrate can be fused silica, glass, or polymethylmethacrylate. Its index of refraction must be greater than that of the surrounding medium to trap the emitted radiation.

The coating is formulated to respond to specific wavelengths. Typically, one liter of the coating solution contains 1,000 g of toluene or xylene solvent, 70 to 200 g of organic polymer (e.g., isobutyl methacrylate or ethylmethacrylate), and 0.2 to 25 g of at least one fluorescent organic dye. The organic polymer gives the coating the necessary adhesion and proper hardness.

The optical density of the coating within the fluorescent-dye absorption band depends on the dye concentration and coating thickness. Typical thicknesses are less than 10 μm, which can be applied with a single dipping.

The converters can be made in sizes and shapes other than the one illustrated. Round or square bars coated all around their lengths are useful in converting relatively intense radiation and transmitting it through the substrate over lengthy distances.

The new converter is also more efficient and economical than earlier models. Conventionally, substrates were doped with radiation conversion material, a more expensive process, which absorbed and scattered much of the emitted radiation, resulting in unnecessary losses.

This work was done by Walter Viehmann of **Goddard Space Flight Center**. *For further information, Circle 28 on the TSP Request Card.*

This invention is owned by NASA, and a patent application has been filed. Inquiries concerning nonexclusive or exclusive license for its commercial development should be addressed to the Patent Counsel, Goddard Space Flight Center [see page A5]. Refer to GSC-12528.

Automated Holographic Drop-Size Analyzer

A proposed automated system analyzes drop-size distribution in liquid-droplet-spray combustion fields.

NASA's Jet Propulsion Laboratory, Pasadena, California

A proposed system for studying particulate or droplet combustion spray fields uses a holographic camera for taking a "stop-motion" hologram of the combustion volume. The hologram is then reconstructed and viewed by a vidicon camera connected to a digital data-processing system that identifies the particles or droplets, determining their size and count, and displays a histogram of the drop-size distribution in the holographic field.

Two processes are involved: one to construct the hologram and the other to process data in the viewed field. A three-dimensional snapshop, or holoplate, is taken of the combustion volume containing the droplets. The holoplate is illuminated by a laser through an expanding collimating system of lenses to form a hologram. The hologram is a three-dimensional still picture translatable along one axis, as shown in the illustration.

The hologram is examined by a narrow depth-of-field vidicon camera fitted with a narrow-depth-of-field lens. By translating the hologram back and forth, different planes can be imaged by the camera. The camera is controlled by a two-dimensional translation mechanism and views only a small piece of the cross section of the field at a time.

The camera output is applied to an analog-to-digital converter (ADC) for digital processing by computer algorithms. The information may be processed via fast Fourier transform filter to eliminate the high-frequency noise while retaining the low-frequency information. Algorithms locate the droplets, which are then sized and stored. The size distributions are displayed on the output histogram.

This work was done by Samuel P. Feinstein and Michael A. Girard of Caltech for **NASA's Jet Propulsion Laboratory.** *For further information, Circle 29 on the TSP Request Card.*
NPO-14676

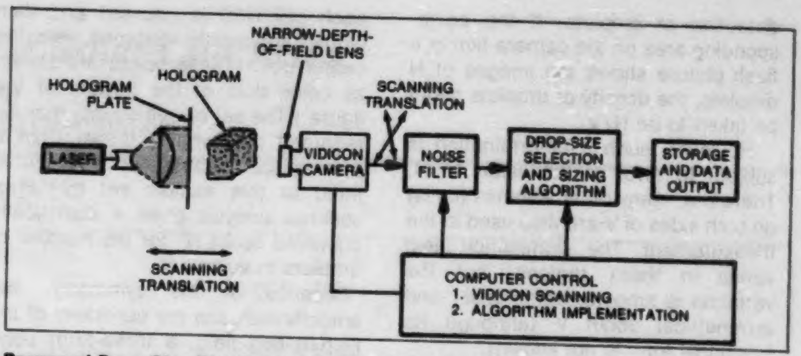
NARROW-DEPTH-OF-FIELD LENS
HOLOGRAM PLATE
HOLOGRAM
SCANNING TRANSLATION
LASER
VIDICON CAMERA
NOISE FILTER
DROP-SIZE SELECTION AND SIZING ALGORITHM
STORAGE AND DATA OUTPUT
SCANNING TRANSLATION
COMPUTER CONTROL
1. VIDICON SCANNING
2. ALGORITHM IMPLEMENTATION

Proposed Drop-Size-Distribution Analysis System can be used for studying particle or droplet distribution in a liquid-droplet-spray combustion field. A hologram of the combustion volume is examined by a vidicon camera, which feeds the data to a digital processing system. The system using algorithms produces a histogram of particle distribution according to size within the examined field.

Photographic Measurement of Droplet Density

Pollutant analysis, fine-particles research, and aerosol and cloud studies should benefit from new accurate method.

Marshall Space Flight Center, Alabama

The density of cloud droplets in an expansion chamber or static diffusion liquid chamber can be measured with an error of less than 3 percent by an improved photographic technique. Measurement of this density is one of the principal instrumentation requirements in laboratory studies of atmospheric physics; the newly achieved precision is a substantial advance over the 10-percent accuracy limitation in methods used in the past. The method should also be useful in pollutant analysis, fine-particles research, and aerosol studies.

The figure shows how the measurement is performed: Two identical flashlamps with projection lenses face each other from the ends of the chamber, and a camera in front focuses on a plane containing the common axis of the lamps. The lamp lenses produce a well-defined image of a slot at the center of the chamber. In the vicinity of this sharp image, it is possible to define a small test volume, V, where the illumination is uniform and above the threshold for the

(continued on next page)

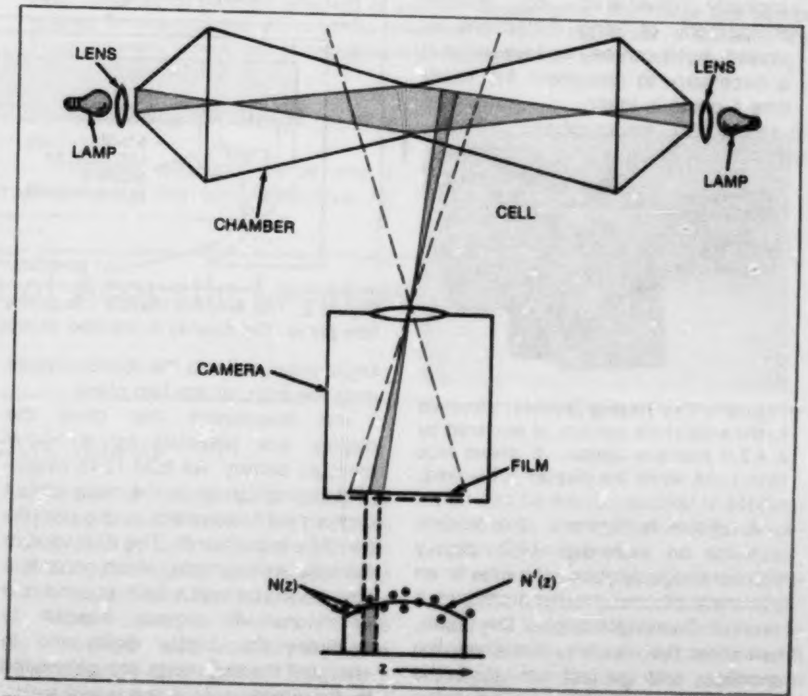
LENS
LAMP
LENS
LAMP
CHAMBER
CELL
CAMERA
FILM
N(z)
N'(z)
z

The Count of Droplet Images on a photographic film, in an area corresponding to a particular volume in an expansion chamber, may be in error. By counting images for many areas and drawing a smooth curve $N'(z)$, the most likely "true" count for the center volume, can be found.

detection of droplets. If the corresponding area on the camera film in a flash picture shows the images of N droplets, the density of droplets might be taken to be N/V.

However, such a determination is subject to error in the value of N. Therefore, many other volumes (cells) on both sides of V are also used in the measurement. The illumination field varies in these regions, but the variation is smooth, continuous, and symmetrical about V (although its functional form is not known).

On the flash photograph, the number of droplets in the images of each cell N(z) is counted and then plotted against the distance from the center cell. (These points are shown as color dots at the bottom of the figure.) The set of cell counts may be regarded as samples drawn from a symmetrical distribution. A curve fitted to this sample set by least-squares analysis gives a statistically improved count N′ for the number of droplets in volume V.

Because of the symmetry, the smoothness, and the continuity of the illumination field, a three-term polynomial generally will give a very satisfactory fit. If the number of cells is about 30 and three parameters describe the fitted curve, then N′ and V are found to within 2 percent, and their ratio, N′/V, is accurate to within 3 percent.

This work was done by W. C. Yager of General Electric Co. for **Marshall Space Flight Center.** *For further information, Circle 30 on the TSP Request Card.*

Inquiries concerning rights for the commercial use of this invention should be addressed to the Patent Counsel, Marshall Space Flight Center [see page A5]. Refer to MFS-25326.

Camera Add-On Records Time of Exposure

Module prints the time a photo is taken on the edge of the exposed film.

Langley Research Center, Hampton, Virginia

The compact module attached to the camera shown in Figure 1 contains all the electronics and optics needed to print the time a photograph is taken on the edge of that photograph. It was originally developed for in-flight photography of wing deflections in aircraft, but it can be used wherever it is necessary to document the exact time a photo is taken.

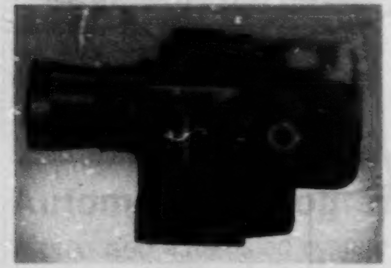

Figure 1. The Timing Module, attached to the side of the camera, is powered by a 4.2-V mercury battery. It draws less than 1 mA while the display is blanked.

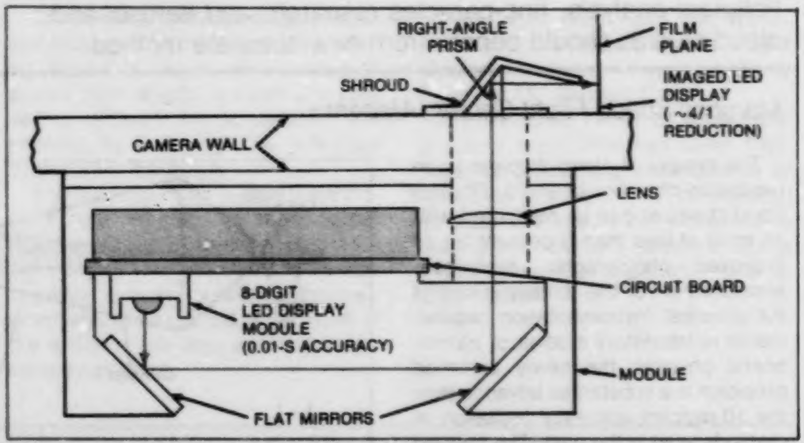
RIGHT-ANGLE PRISM
FILM PLANE
SHROUD
IMAGED LED DISPLAY (~4/1 REDUCTION)
CAMERA WALL
LENS
CIRCUIT BOARD
8-DIGIT LED DISPLAY MODULE (0.01-S ACCURACY)
MODULE
FLAT MIRRORS

Figure 2. The Module Optics image the seven-segment display on the edge of the film plane. The display is blanked except at the time the camera shutter is actuated.

As shown in Figure 2, the module includes an eight-digit LED display that continuously shows the time to an accuracy of one one-hundredth of a second. Two digits display the hours, two show the minutes, two show the seconds, and the last two show the fraction of a second. Leading zeros are blanked to conserve power.

Light from the display is reflected off two flat mirrors, through a focusing lens, and into the camera. A right-angle prism reflects the display image onto the edge of the film plane.

The electronics that drive the display are powered by a 4.2-V mercury battery. An ICM 7045 single-chip timing circuit is the main circuit component (equivalent timing circuits could be substituted). The IC is used in the split-timing mode, which records a time period between 0.01 second and 24 hours. All signals needed to multiplex the display digits and to energize the segments are generated by the timer.

The normally blanked display is unblanked when the camera shutter switch is actuated. A signal from the shutter switch triggers a monostable multivibrator, which turns on the display drivers for a short period at the time of exposure. The monostable pulse width is adjustable to accommodate a range of shutter speeds and ASA film ratings.

The unit can be adapted to other cameras besides the one shown. Most of the changes would be in reconfiguring the optics.

This work was done by E. Conrad Compton, Philip C. Kassell, Jr., and Charles W. Knight of **Langley Research Center.** *For further information, Circle 31 on the TSP Request Card.*
LAR-12635

Improved Multispectral Solar-Cell Array

Proposed optics may optimize solar collection efficiency and reduce cell overheating.

NASA Headquarters, Washington, D.C.

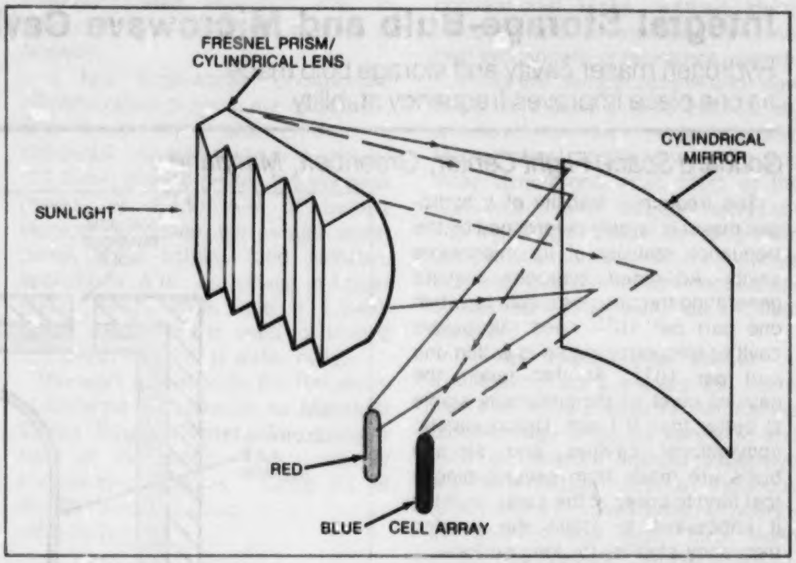

Proposed Solar-Collector System projects oval-shaped color-band images onto solar cells designed to be most efficient at specific wavelengths. The image size can be altered by changing the width of the reflecting mirror or the power of the lens. The image intensity is thus kept at an optimum level, preventing the cells from overheating.

A combined Fresnel prism/cylindrical lens along with a cylindrical reflector can be used to improve the efficiency of multispectral solar-cell arrays. These arrays consist of solar cells that have enhanced efficiencies at various single wavelengths. Previously these cells relied on a single type of optical dispersion/concentrator system which either resulted in cell overheating or poor energy concentration. The proposed system allows a more precise control over the dimension and distribution of the separated color bands onto the cell array.

The system (see figure) consists of a prism lens separating the incident solar energy into color components and focusing them on the reflector. The reflector projects each color band on the solar cells that operate most efficiently at that wavelength.

In essence the system combines the characteristics of both cylindrical and rotational optics to project oval images on the solar cells. The precise dimensions of the images may be controlled by varying the power of the Fresnel prism/cylindrical lens to match closely the specific requirements of the solar cells used. The arrangement would prevent cell overheating without significantly reducing the energy reaching each cell.

This work was done by Jerome J. Redmann of The Aerospace Corp. for **NASA Headquarters**. *For further information, Circle 32 on the TSP Request Card.*
HQN-10937

Low-Cost Calibration of Acoustic Locators

Piezoelectric-torch lighter makes calibration easier.

Langley Research Center, Hampton, Virginia

A standard method of checking the sensitivity and accuracy of acoustic-emission-signal locators is not the most convenient one. An acoustic transducer (pulser) used in this procedure simulates an acoustic-signal source. The pulser, connected via long cable to a module built into the locator, converts a module-generated fast-risetime voltage spike (about 30 V) to an acoustic spike. The locator is calibrated by determining the position of the pulser signal and comparing it with the actual pulser position.

A more convenient method is to use a modified commercially-available piezoelectric-torch lighter. This handheld lighter has a controlled spark gap that can be easily adjusted to produce repeatable short-duration high-amplitude voltage spikes.

The pulser and the lighter are coupled via a short coaxial cable, eliminating a long cable run, variations in cable attenuation, and a problem with the cable entangling with anything in its path.

(continued on next page)

The piezoelectric lighter is very reliable. It needs no batteries or external power and can be taken farther away unrestricted by the cable length.

Tests have shown that the lighter output is accurate within 1 percent. The nominal unloaded output of the spark generator is in the range of 4 to 6 kV. The combination cable/transducer loading limits the excitation pulse to the range of 350 to 400 V. Because of the spark, the lighter can only be used in nonexplosive environments.

This work was done by Robert F. Berry of **Langley Research Center.** *No further documentation is available.*
LAR-12632

Integral Storage-Bulb and Microwave Cavity for Masers

Hydrogen maser cavity and storage bulb made as one piece improves frequency stability.

Goddard Space Flight Center, Greenbelt, Maryland

The frequency stability of a hydrogen maser is largely determined by the frequency stability of its microwave cavity. Advanced hydrogen masers generating frequencies stable to within one part per 10^{15} need microwave cavities frequency stable to within one part per 10^{11}. At that level, the cavities must be dimensionally stable to better than 0.1 nm. Unfortunately, conventional cavities and storage bulbs are made from several pieces that tend to creep at the joints, making it impossible to attain the needed frequency stability for long periods.

A mechanically-stable integral storage-bulb/microwave cavity (see figure) made out of a single piece of fused quartz can solve that problem. The single-piece construction eliminates the joints, making the cavity dimensionally and hence frequency-stable. Fused quartz is used because of its low thermal expansion coefficient.

To form the high Q (36,000) microwave cavity, the bulb cavity is vacuum-coated with copper on the outside instead of on the inside as in conventional designs, allowing the cavity to be coated after the complete one-piece assembly is fabricated. The cavity wall thickness can be at least 16 mm without appreciably affecting the Q. The cavity can be trimmed to the proper frequency by lapping its ends to change its length and recoating it with copper. The storage-bulb section is 1 to 2 mm thick and coated with PTFE on the inside as in conventional designs.

A temperature-controlled aluminum shell enclosing the quartz storage-bulb/cavity enhances temperature stability. A hydrogen maser with an aluminum cavity showed a frequency coefficient of 4.5×10^{-14}/°C of room-temperature change. Using the same thermal design with the quartz cavity should therefore, yield a temperature coefficient of 1.8×10^{-15}/°C.

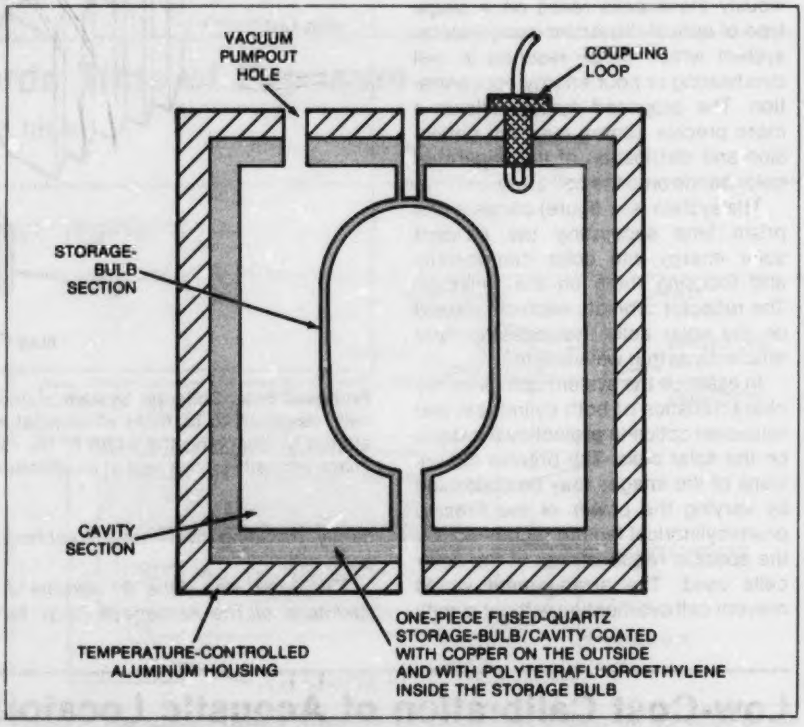
VACUUM PUMPOUT HOLE
COUPLING LOOP
STORAGE-BULB SECTION
CAVITY SECTION
TEMPERATURE-CONTROLLED ALUMINUM HOUSING
ONE-PIECE FUSED-QUARTZ STORAGE-BULB/CAVITY COATED WITH COPPER ON THE OUTSIDE AND WITH POLYTETRAFLUOROETHYLENE INSIDE THE STORAGE BULB

Integral Storage-Bulb and Microwave Cavity proposed for hydrogen masers can be built as one piece using fused quartz. The one-piece construction makes the assembly mechanically stable and therefore frequency-stable. This design can potentially attain a frequency coefficient of 1.3×10^{-15}/°C necessary for the future high-performance masers.

This work was done by Victor S. Reinhardt of **Goddard Space Flight Center.** *No further documentation is available.*
GSC-12542

Books and Reports

These reports, studies, and handbooks are available from NASA as Technical Support Packages (TSP's) when a Request Card number is cited; otherwise they are available from the National Technical Information Service.

A Survey of Photovoltaic Systems

A compilation of suppliers, product data sheets, and other documentation

The results of an extensive telephone survey of photovoltaic manufacturers are compiled in a 220-page report that is available on request. The three-part report includes a catalog of suppliers, data sheets on specific products, and typical operating, installation, and maintenance procedures.

Photovoltaic technology — converting Sunlight into electricity — was applied just over 20 years ago when small photovoltaic cells were used to power one of the first U.S. satellites. Since that time, photovoltaics have been intensively researched to make them attractive for everyday use. Cost has been the primary barrier; however, in areas where electricity is unavailable or prohibitively expensive, photovoltaics have become economical and practical.

Three U.S. companies accounted for 77 percent of the total domestic photovoltaic sales in 1978. One firm surveyed reported that state regulations requiring a 30-year warranty on photovoltaic products are limiting its marketing efforts. Lacking extensive test data and field experience, such a warranty would be impractical or impossible, the firm said.

Another company reported that there is little or no domestic market for the systems but that there is an export demand. However, trade barriers are severely hampering exports. The export demand comes from countries where electricity costs are many times higher than in the United States and in applications where conventional electricity is unavailable, such as offshore or in underdeveloped countries. Typical applications include offshore navigational aids and petroleum platforms; television, telemetry, and microwave transmitters and repeaters; and irrigation pumps. One manufacturer stated that he had sold several thousand units to recharge battery-operated television sets in weekend and summer cabins in Norway.

A few large-scale, photovoltaic demonstration projects are underway. One is in the Indian village of Schuchuli, Arizona, where a 768-ft^2 (71.3-m^2) array provides 3.5 kW peak power, or 2,380 A-h of battery storage, to power the village water pump, home lighting, and domestic appliances. A remote village in Upper Volta, West Africa, has a 1.8-kW power supply that is used to drive a 1,200-gal/h (1.2-l/s) water pump.

This work was done by the University of Alabama in Huntsville for **Marshall Space Flight Center.** *To obtain a copy of the report, "A Survey of Photovoltaic Systems," Circle 33 on the TSP Request Card.*
MFS-25397

Thermal Stratification in Liquid-Storage Tanks

A comprehensive literature survey

Thermal stratification in a solar-energy/liquid-storage tank can improve system performance by as much as 15 percent. Collector efficiency increases when the collector inlet fluid is drawn from the bottom of the storage tank, where the fluid is coolest; the warmest liquid is drawn from the top of the tank to satisfy the thermal load.

A comprehensive survey of the literature on thermal stratification is compiled in a report that is available on request. Following an introductory section (section 1), the 30-page report assesses thermal-stratification effects on the performance of several solar-energy systems. In section 3, theoretical and experimental studies of "thermocline" tanks are reviewed; and in section 4, a brief discussion on the applicability of stratification techniques to solar heating and cooling is presented. Conclusions are given in section 5; the appendix lists the surveyed thermal-stratification literature.

Several simulation studies have quantified the net effects of thermal stratification on the total system performance, using a one-dimensional storage-tank model. The model assumes simple geometric shapes of conventional tanks, without short-circuited-flow phenomena, internal heat exchangers, or resistance heaters.

Transient temperatures and flow fields have been studied theoretically and, to a lesser extent, experimentally. Mathematical models for one, two, and three dimensions exist. Most of the one-dimensional models represent liquid-storage tanks in long-term computer-simulation studies, while two- and three-dimensional models are concerned with transient flow and heat transfer.

Detailed experimental studies on thermocline tanks are scarce. Flows that commonly prevail in thermocline liquid-storage tanks are very slow and hard to measure without expensive experimentation. Some rigorous temperature measurements in operating liquid-storage tanks have been made; however, the thermal stratification inside tanks is usually very small. Several researchers have studied enhancing thermal stratification by passive devices.

This work was done by D. L. Christensen and S. M. Han of the University of Alabama in Huntsville for **Marshall Space Flight Center.** *To obtain a copy of the report, "Thermal Stratification of Solar Energy Liquid Storage Systems," Circle 34 on the TSP Request Card.*
MFS-25416

Final Report on Development of a Programable Controller

Microprocessor-based controller for solar-heating and cooling systems

The development of a sophisticated microprocessor-based controller for solar-heating and cooling systems is described in a new report. [Also see "Programable Controller for Solar Heating" (MFS-23915) on page 204 of *NASA Tech Briefs*, Vol. 3, No. 2.]

(continued on next page)

Analog data from flow sensors, temperature sensors, and other devices are accepted by the programable controller. It also receives digital input from relays and switches. Following a program stored in programable read-only memory, the microprocessor commands 16 optically-coupled output relays that operate pumps, fans, and valves.

A five-digit LED display automatically displays the input channels in sequence or shows the date or time. Fifty-two constants in the program equations can be set through a 16-key keyboard.

The most obvious application of the controller is in complex residential, commercial, and industrial solar-energy systems. It can also be used for debugging and checkout during prototype work and early development of new systems.

The 23-page report describes the background of the development program. It also summarizes the operation, performance, and applications of the controller.

This work was done by James D. Hankins of **Marshall Space Flight Center.** *To obtain a copy of the report, "Development and Testing of the Rho Sigma Incorporated Microprocessor Control Subsystem," Circle 35 on the TSP Request Card.*
MFS-25388

Fresnel Lens Tracking Solar Collector

A report on performance outdoors

A commercial tracking collector that uses acrylic Fresnel lenses to focus Sunlight on copper absorber tubes was recently evaluated outdoors at Marshall Space Flight Center. Performed in accord with ASHRAE (American Society of Heating, Refrigerating, and Air-Conditioning Engineers) standards, the tests are documented in a 16-page report that is available on request. All tests were done at the Marshall Space Flight Center solar house. [Also see "Concentrating Solar Collector — Performance Tests" (MFS-25086) on page 60 of *NASA Tech Briefs,* Vol. 4, No. 1.]

The collector array consists of seven panels at an angle of 32° to the horizontal. Each panel has four modules covered by 10.75 ft² (0.99 m²) of transparent acrylic plastic Fresnel lenses. The complete assembly consists of the panels, supporting framework, insulated fluid manifolding, and a tracking drive. The panels are spaced 10 ft (0.33 m) between centers. The copper absorber tube has a selective coating with 0.95 absorptivity and 0.12 emissivity.

The Sun tracker is powered by photovoltaic cells. Collector panels, linked by galvanized cable and pulleys, are driven by a bidirectional motor through a chain drive, a stainless-steel (Acme) screw, and a drive nut.

The test array was operated over 10 months for heating and cooling of the solar house. It was then monitored for approximately 2 months under clear weather. On days with intermittent cloud cover or a high-density cloud cover, the tracking mechanism would either lag or would not track at all. Thus, the data presented in the report were obtained from selected clear days when the collector array was tracking properly.

Array performance at high inlet temperatures drops significantly in comparison to the single-panel curve offered by the manufacturer. The heat losses are attributed to losses from the large manifold area and from possible weathering of the array during exposure of almost 1 year.

This work was done by the Solar Energy Systems Division of Wyle Laboratories for **Marshall Space Flight Center.** *To obtain a copy of the report, "Thermal Performance Evaluation of the Northrup Model NSC-01-0732 Concentrating Solar Collector Array at Outdoor Conditions," Circle 36 on the TSP Request Card.*
MFS-25418

Outdoor Tests of the Concentric-Tube Collector

The 72-element air-filled version is tested in a residential installation.

The 72-element, air-filled version of the concentric-tube solar collector recently underwent a 2-month performance evaluation at the Marshall Space Flight Center solar house. A summary of the test results, along with other relevant data, is presented in a 27-page report that is now available. Performed in accord with ASHRAE Standard 93-77 ("Method of Testing to Determine the Thermal Performance of Solar Collectors"), the tests included measurements of thermal efficiency, incident-angle modifier, and time constant. [See related article "Indoor Tests of the Concentric-Tube Solar Collector," (MFS-25390) on page 39 of *NASA Tech Briefs,* Vol. 5, No. 1.]

Thermal efficiency was measured at air inlet temperatures of 0°, 70°, 90°, and 110° F (-18°, 21°, 32°, and 43° C) above ambient, at an airflow rate of 2 ft³/min per ft² (0.01 m³/s per m²) of collector area. Results are presented in tables and graphically. The efficiency ranged between 43.6 percent at 75.3° F (24.1° C) inlet air temperature and 34.0 percent at 200.2° F (93.4° C).

Permanently tilted at the 45° slope of the roof, the collector was measured for incident-angle modifier by logging its efficiency when the direction of the incident solar radiation was approximately 15°, 30°, 45°, 60°, and 67.5° with respect to the direction at solar noon. An average of the measurements for three clear days is shown as a graph of incident-angle modifier versus incident angle. For this collector, the efficiency is actually about one-third greater at an incident angle of 60° than it is at normal incidence. A time constant (the time for the differential temperature to drop to 0.368 of its initial value) of 16.6 minutes was measured for the collector. It was determined by shading the collector, while maintaining a constant flow rate and inlet temperature.

This work was done by Wyle Laboratories for **Marshall Space Flight Center.** *To obtain a copy of the report, "Outdoor Test for Thermal Performance Evaluation of the Owens-Illinois Sunpak SEC-601 [Air] Solar Collector," Circle 37 on the TSP Request Card.*
MFS-25398

Selective Optical Coatings for Solar Collectors

Several chemical treatments and coatings are evaluated.

For best performance, the energy-absorbing surface of a solar collector should be characterized by a high ratio of solar absorptance to thermal emittance. Designers and users of solar-energy systems will therefore be interested in a new report on the optical characteristics of several chemical treatments and electrodeposited coatings for metal solar-absorbing surfaces. The moisture resistance of some of the coatings is also reported.

The coatings were produced by electroplating, by chemical conversion, and by anodizing (electrochemically converting a metal to its oxide). For proprietary processes, manufacturer's directions were followed; directions reported in the literature were followed for nonproprietary processes.

Optical measurements were made with a solar/infrared reflectometer or a ratio-recording spectrophotometer. The solar absorptance was determined by subtracting the solar reflectance from unity; the thermal emittance was determined by computing the difference between the infrared reflectance and unity. The moisture resistance was established by subjecting coated specimens to a relative humidity of 92 to 98 percent at a temperature of 95° to 100° F (35° to 38° C).

Of the coatings tested, black nickel showed the best combination of selective optical properties, although it was susceptible to degradation in high humidity. Electroplated black chrome has high solar absorptance, but its thermal emissivity varies between specimens and is quite high under some conditions. The black chrome also has very high moisture resistance. Black oxide coatings on copper and steel substrates showed the best combination of selective optical properties of any of the chemical conversion films.

This work was done by James R. Lowery of **Marshall Space Flight Center.** *To obtain a copy of the report, "Solar Absorption Characteristics of Several Coatings and Surface Finishes," Circle 38 on the TSP Request Card.*
MFS-23589

Finned-Absorber Solar Collector

Report presents the results of a performance evaluation.

You can use the TSP Request Card at the back of this issue of *NASA Tech Briefs* to obtain a report summarizing performance tests on a commercial solar collector. The tests are part of a continuing study of solar-heating systems and components for NASA and the Department of Energy.

The tested collector is flat-plate, with water as the heat-transfer fluid. Its cover is tempered antireflective glass (one layer). The black-coated heat-absorbing surface consists of collared aluminum fins bonded to copper tubing.

Standard ASHRAE (American Society of Heating, Refrigerating, and Air-Conditioning Engineers) requirements were followed. Parameters measured, under simulated conditions, were thermal efficiency and time constant. A 30-day stagnation test (exposure to simulated sunlight with no fluid flow) was also done. This is not a standard ASHRAE test. The collector absorptivity and heat-loss rate were measured before and after the 30-day exposure.

Test data are presented as graphs and tables. The report also summarizes the test procedures and a mathematical analysis of the results.

This work was done by the Solar Energy Systems Division of Wyle Laboratories for **Marshall Space Flight Center.** *To obtain a copy of the report, "Thermal Performance Evaluation of the Suncatcher SH-11 (Liquid) Solar Collector," Circle 39 on the TSP Request Card.*
MFS-25385

A Test Program for Solar Collectors

Rigorous environmental and performance tests qualify a solar collector for use in residential solar-energy systems.

Those using or testing solar collectors will be interested in a new report describing qualification tests on a particular commercial collector, described in a previous *NASA Tech Briefs* article. [See "Weathering of a Liquid-Filled Solar Collector" (MFS-25113) on page 60 of Vol. 4, No. 1.] Testing over a 7-month period examined pressurization effects, wind and snow loading, hail damage, solar and thermal degradation, the effects of pollutants, efficiency, and outgassing. The test procedures and results are summarized in tables, graphs, and text.

Some of the tests (pressure, loading, efficiency, hail, solar degradation, and outgassing) were done on a fully assembled collector. Coupon specimens of the absorber plate, cover glass, and other subcomponents were subjected to the pollutant and thermal-degradation tests.

Typical of the rigor with which this series was carried out is the test for thermal degradation. Coupon specimens of the essential collector subcomponents were each heated for at least 500 hours in a temperature-controlled chamber. Following the exposure, the specimens were tested for tensile strength or transmittance (for glass specimens). American Society for Testing Materials (ASTM) standards were applied in the tests. Unexposed specimens were also tested for comparison with the thermally treated samples.

This work was done by the Energy Resources Center of Honeywell Inc. for **Marshall Space Flight Center.** *To obtain a copy of the report, "Qualification Test Procedures and Results for Honeywell Solar Collector Subsystem, Single-Family Residence," Circle 40 on the TSP Request Card.*
MFS-25433

Operational Tests of a Solar-Energy System in Georgia

12-month performance of a hot-water heating system

A 73-page report describes the 1-year performance of a commercial solar-energy hot-water system. Installed in a public housing project in Macon, Georgia, the system is one of several at test sites throughout the country.

Silicone oil is the heat-exchange fluid in the tested system, designed to meet the needs of a family of four. A roll-bend heat exchanger is wrapped around the hot-water storage tank. The oil circulates through the exchanger and through flat-plate solar collectors. Auxiliary energy, to maintain a selectable minimum temperature in the storage tank, is supplied by a 4,500-watt resistance-heating element.

The manufacturer's specifications state that the system will supply up to 75 gallons (284 liters) of potable hot water per day at a temperature of 140° F (60° C), based on an average heating load of 1,313,000 Btu/month (1.385×10^9 J/month). Auxiliary hot-water requirements are 20 percent of the monthly load. The operating mode (collector-to-storage) begins when a differential controller recognizes a collector/storage-tank differential temperature of 20° F (11° C). The mode is terminated when the differential drops to 5° F (3° C). Both temperature settings are nominal.

For the test period, the incident solar-energy totaled 35.21×10^6 Btu (36.04×10^9 J) while the system was operating; the collected energy totaled 10.32×10^6 Btu (10.88×10^9 J), for an efficiency of 31 percent. Electrical-energy savings at the site were 8.98×10^6 Btu (9.47×10^9 J), after 1.34×10^6 Btu (1.41×10^9 J), required to operate the pump, are subtracted.

This work was done by the Federal Systems Division of IBM Corp. for ***Marshall Space Flight Center.*** *To obtain a copy of the report, "Solar Energy System Performance Evaluation -- Seasonal Report for SEMCO, Macon, Georgia," Circle 41 on the TSP Request Card.*
MFS-25420

Operational Tests of a Solar-Energy System — Florida Site

Projected annual electrical energy savings are above 10 million Btu.

The solar-energy hot-water system described in the preceding article has also been evaluated for performance at a test site in Loxahatchee, Florida. Results of these tests are available in a 76-page report.

Projected electrical energy savings at this site are above 10 million Btu (10.5 billion J) annually. Actual savings were less because the building was unoccupied for 8 months of the 11-month test period, and the hot-water load was abnormally low. Estimates based on results during the 3 months of nominal operation indicate that, during the summer, the system should deliver 90 percent of the hot-water load from solar energy.

The operating sequence for the system begins when the collector/storage-tank differential temperature exceeds 20° F (11° C). On one typical day (October 8, 1979), this occurred at 9:25 a.m., when the collector absorber plate was at 145° F (63° C). Collector-loop operation was continuous on that day until 4:31 p.m., when the absorber plate temperature was 165° F (73° C). At the time of turnoff, the storage tank was at approximately 166° F (75° C).

During the day, the incident solar energy was 135,000 Btu (142×10^6 J) of which 16,000 Btu (17×10^6 J) were supplied to meet the hot-water load. (The balance goes to replenishing the thermal-energy losses of the tank.)

This work was done by the Federal Systems Division of IBM Corp. for ***Marshall Space Flight Center.*** *To obtain a copy of the report, "Solar Energy System Performance Evaluation — Seasonal Report for SEMCO, Loxahatchee, Florida," Circle 42 on the TSP Request Card.*
MFS-25423

A Solar-Energy System in Pennsylvania

A specific case illustrates techniques that have general applicability.

A new report describes the development of a solar-heating system for a single-family residence at a site in Pennsylvania. The 143-page document, containing detailed drawings, performance specifications, cost tradeoff studies, and other material, can assist those planning similar systems in areas with comparable climate.

Components and design parameters were selected with the help of a computer simulation model, using weather and insolation data as inputs. The model computed the effect of collector area on the solar contribution to the total energy requirements of the dwelling. Using this information, an area of 504 ft^2 (47 m^2) was selected as a compromise between architectural constraints and the required solar contribution. The storage-tank temperature set points were also selected with the help of the computer simulation.

For an average heating load of 4.0×10^6 Btu per month (4.2×10^9 joules per month), the system will deliver 46.5 percent from solar energy. In addition, 52 gallons (197 liters) of potable hot water will be delivered at 140° F (60° C), or greater, assuming a delivery rate of 3 gallons per minute (11 liters per minute) and a recovery time of 0.75 h.

Included in the report are a spare parts list and an outline of the projected installation, operation, and maintenance manual. Over 30 drawings of the system and its subcomponents are supplied.

This work was done by the Energy Resources Center of Honeywell, Inc., for ***Marshall Space Flight Center.*** *To obtain a copy of the report, "Solar Energy Heating System Design Package for a Single-Family Residence at New Castle, Pennsylvania," Circle 43 on the TSP Request Card.*
MFS-25427

Installation Guidelines for the Pennsylvania System

Detailed installation, operation, and maintenance procedures

The installation of the solar-energy system described in the preceding article is documented in a new report. Included are procedures for filling and testing the entire system, along with installation guidelines for each major subsystem.

The 170-page report describes operating procedures, controls, cautionary procedures, and maintenance. Information is in the form of text, schematics, detailed drawings, and photographs. An appendix contains 113 pages of manufacturers' literature, organized into separate sections for each subsystem.

When space heating is required and solar energy is available, the collectors supply heat directly. Energy is transferred through a heat exchanger and a heating coil; a blower moves the building air across the coil. Thermal energy is stored by circulating water from the bottom of the storage tank through the heat exchanger. The water is returned to the top of the tank. When required, auxiliary energy is supplied by an electrical resistance-heating coil.

This work was done by the Energy Resources Center of Honeywell, Inc., for **Marshall Space Flight Center.** *To obtain a copy of the report, "Installation Guidelines for Solar Heating System, Single-Family Residence at New Castle, Pennsylvania," Circle 44 on the TSP Request Card.*
MFS-25424

A Solar-Energy System in Minnesota

Design of a system for a Minnesota residence

A companion report to that described in the preceding article discusses a system for a Minnesota residence. Using similar procedures, a final design was arrived at that will meet 45 percent of the total average heating load and will supply 40 gallons (151 l) of potable water at 140° F (60° C). The delivery rate is 3 gal/min (11 l/min), with a recovery time of 0.75 h. Optimum collector area for this site is 594 ft² (55 m²).

As in the report on the Pennsylvania site, this document contains detailed drawings, specifications, and cost tradeoff studies. Also included are an outline of the proposed installation, operation, and maintenance manual and an analysis of hazards.

This work was done by the Energy Resources Center of Honeywell, Inc., for **Marshall Space Flight Center.** *To obtain a copy of the report, "Solar Heating System Design Package for a Single-Family Residence at William O'Brien State Park, Minnesota," Circle 45 on the TSP Request Card.*
MFS-25428

Solar-Energy System Evaluation — Pennsylvania Site

An in-depth evaluation of an installed system

A solar-heating and hot-water system installed in a single-family residence in Tunkhannock, Pennsylvania, has been evaluated for performance in a 1-year test program. Results of the tests are available as an 32-page report.

Tested previously under simulated conditions [see "Test and Evaluation of a Solar-Heating System" (MFS-25001) on page 380 of NASA Tech Briefs, Vol. 4, No. 3], the system has now been evaluated onsite from two perspectives. The first is an overall view to determine the net energy savings for prevailing and long-term climatic conditions and heating loads. The second is an in-depth look at the performance of individual subsystems.

The Tunkhannock solar-energy system supplies space heating and domestic-hot-water preheating for a 1,000-ft² (92.9-m²) single-family residence. Solar energy is collected with flat-plate collectors, using air as the transport fluid. The collector array has a gross area of 208.5 ft² (19.36 m²). Energy is transferred to and from storage by a liquid-to-air heat exchanger.

Storage capacity is 240 gallons (909 liters) of water in the main tanks and 40 gallons (151 liters) in the domestic-hot-water tank. The system has five modes of operation: collector-to-space heating, storage-to-space heating, collector-to-storage, domestic-hot-water preheat, and collector-to-storage and auxiliary space heating.

During the 12-month test period, the daily average incident insolation in the plane of the collector array was 1,063 Btu/ft² (12.1×10^6 J/m²). Solar energy satisfied 17 percent of the total measured load, which is considerably below the design prediction of 39 percent. The reduction in overall system solar fraction was due primarily to the space-heating subsystem. The space-heating solar fraction was only 7 percent. However, the computations do not account for uncontrolled energy losses from duct leakage. These losses are substantial and considerably reduce the measured space-heating load.

If the uncontrolled losses of solar energy are considered, the heating solar fraction becomes approximately 18 percent. This is a significant improvement, but is only about one-half of the value needed.

This work was done by the Federal Systems Division of IBM Corp. for **Marshall Space Flight Center.** *To obtain a copy of the report, "Solar Energy System Performance Evaluation — Seasonal Report for Fern, Tunkhannock, Pennsylvania," Circle 46 on the TSP Request Card.*
MFS-25434

A Hot-Water System Tested Onsite — Togus, Maine

Performance close to design specifications was verified over a 1-year study.

A solar hot-water system described in several previous NASA Tech Briefs articles [see "Prototype Residential Solar-Energy System — Installation Package" (MFS-23956) on page 355 of Vol. 3, No. 3] has been evaluated during a 1-year onsite study. Described in a 69-page report that is now available, the study looked at the long-term operation of the system installed in a residential building in Togus, Maine.

Silicone fluid circulating through flat-plate collectors is the working

(continued on next page)

medium in this hot-water system. The water is preheated in a 120-gal (454-l) tank and is fed to a 40-gal (151-l) domestic-hot-water heater, which adds the balance of the energy. Solar power supplies about 51 percent of the hot-water energy.

Over the 1-year study, the system operated consistently well, experiencing no downtime. At the expected weather and hot-water load, the system operated very close to its design specifications.

This work was done by the Federal Systems Division of IBM Corp. for **Marshall Space Flight Center.** *To obtain a copy of the report, "Solar Energy System Performance Evaluation — Seasonal Report for IBM System 2, Togus, Maine," Circle 47 on the TSP Request Card.*
MFS-25435

A Reliable Solar-Heating System — Huntsville, Alabama

Silicone-liquid heat-exchange medium requires no freeze or stagnation protection.

The final report on a solar-heating demonstration project in Huntsville, Alabama, is rich in technical data, planning considerations, test and maintenance data, and other information. It can be a useful reference for those planning similar systems.

The solar facility installed at the Huntsville Senior Citizen Center is expected to supply 85 percent of the building hot-water requirements. A silicone fluid was chosen as the heat-transfer medium. Since this liquid can be pumped at temperatures as low as -121° F (-85° C) and generates very little vapor pressure when its temperature is elevated to 600° F (316° C), it requires no freeze protection and can operate with a simple closed-loop flow path. No special provisions for stagnation are necessary. These features simplify maintenance and improve system reliability.

The report describes the major subsystems and includes relevant manufacturer's product literature. Each of the operating modes (e.g., direct-solar, heat-from-storage, stored-solar) is explained in detail. Drawings and photographs of the system are included.

This work was done by the City of Huntsville for **Marshall Space Flight Center.** *To obtain a copy of the report, "Solar Heating and Hot Water System Installed at the Senior Citizen Center, Huntsville, Alabama," Circle 48 on the TSP Request Card.*
MFS-25431

Solar-Heating and Cooling Demonstration Project

Design, operation, and installation details of a solar-heating and cooling system

The Florida Solar Energy Center has retrofitted an office building, approximately 5,000 square feet (465 square meters) of area, with solar heating and air-conditioning. This demonstration project is viewed by hundreds of center visitors each day.

Information on the operation, installation, controls, and hardware for this system is contained in a report that is available on request. The 164-page document includes manufacturer's product literature and detailed drawings.

The major system subcomponents are:

- solar collectors,
- an absorption chiller,
- storage tanks (for hot water and chilled water), and
- controls and piping.

A ten-tube commercial evacuated collector supplies the high-temperature water (at 80° to 90° C) needed for the absorption chiller. Rated at 25 tons (2.2×10^5 N), the chiller is supplied with hot water from one storage tank and delivers its chilled water to another tank.

The system has operated without problems for almost 9 months. A count of the cooling hours from solar energy and of the total hours of space cooling indicates a solar fraction of between 50 and 60 percent during the summer.

This work was done by the Florida Solar Energy Center of the University of Florida for **Marshall Space Flight Center.** *To obtain a copy of the report, "Solar Heating and Cooling Demonstration Project at the Florida Solar Energy Center," Circle 49 on the TSP Request Card.*
MFS-25443

Materials

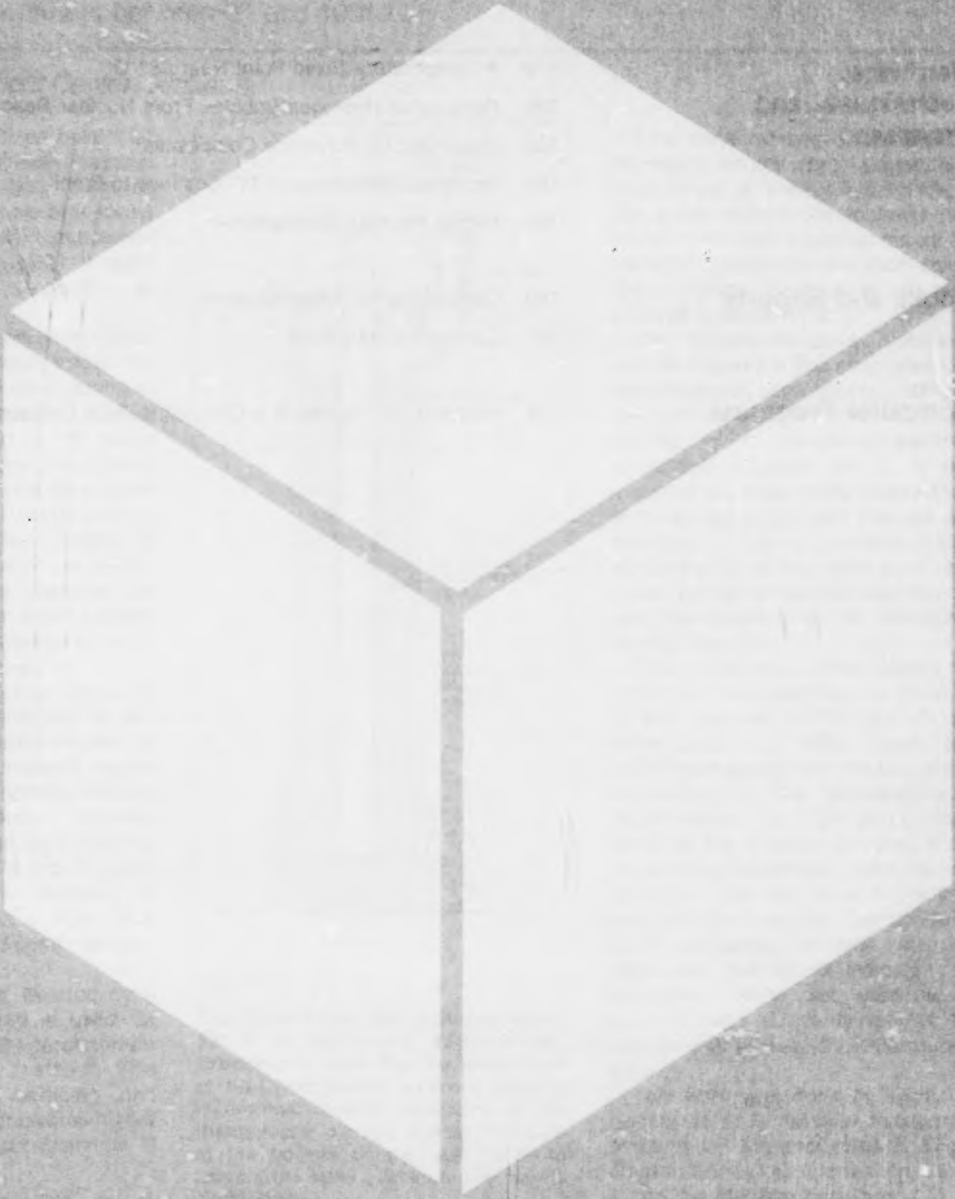

Hardware, Techniques, and Processes

179 A Temperature Fixed Point Near 58° C
180 Removal of Hydrogen Bubbles From Nuclear Reactors
180 Plasticizer for Polyimide Composites
181 Improved Adherence of TIC Coatings to Steel
182 Hybrid Polymer Microspheres

Books and Reports

183 Composites for Aeropropulsion
183 Lubrication Handbook

Computer Programs

184 Methane/Air Flames in a Concentric-Tube Combustor

A Temperature Fixed Point Near 58° C

The triple point of ultrapure succinonitrile could be used to calibrate thermometers between 0° and 100° C.

Marshall Space Flight Center, Alabama

A new secondary "fixed point" for defining the International Practical Temperature Scale has emerged from improved materials-processing methods for the organic substance succinonitrile [$CN(CH_2)_2NC$]. It has a reproducible triple point at 58.0810°±0.0004° C.

If adopted as a temperature standard, the new fixed point would improve the certainty of calibrations in the important temperature domain between 0° and 100° C. It would complement the primary fixed points of 0.010° and 100° C (the triple point and the boiling point of water) and the melting point of gallium metal at 29.770° C, the only other secondary fixed point in this range. Together, the secondary fixed points would bracket the clinically important temperature of 37° C (body temperature).

Techniques for preparing high-purity succinonitrile were developed as part of a study of the solidification of supercooled liquids (ultrapure liquids cooled to below their normal freezing points). The methods combine vacuum distillation and zone refining in a sealed system. To avoid recontamination, the pure material is directly transferred to a triple-point cell, where the fixed-point temperature is determined.

A mechanical pump isolated by a liquid-nitrogen cold trap is used for vacuum distillation of 99-percent-pure succinonitrile starting material. This step removes dust particles and impurities with vapor pressures higher or lower than that of succinonitrile at 80 to 90 C.

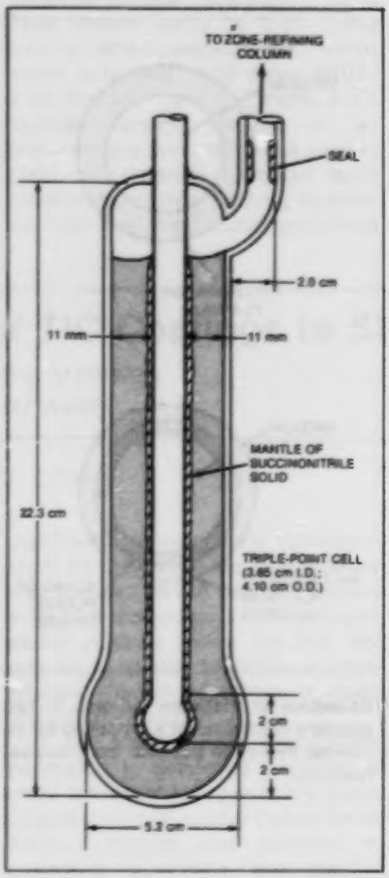
TO ZONE-REFINING COLUMN
SEAL
2.8 cm
11 mm
11 mm
MANTLE OF SUCCINONITRILE SOLID
22.3 cm
TRIPLE-POINT CELL (3.85 cm I.D.; 4.10 cm O.D.)
2 cm
2 cm
5.2 cm

The **Triple-Point Cell** contains about 300 g of high-purity succinonitrile. Experiments show that the lower 4 cm of the thermometer well are virtually isothermal, making placement of the thermometer not very critical. The bulb at the bottom of the well helps to prevent the solid succinonitrile mantle from slipping.

Final zone refining of the distilled material is done in three stages, with 30 passages of 3 zones in each stage. The purer half of the material produced after each stage serves as the starting material for the next stage. The resulting product is at least 99.9999+ percent pure.

The borosilicate-glass triple-point cell (see figure) is first evacuated and then filled with approximately 300 g of the purified succinonitrile. It is immersed in a variable-temperature water bath at about 58° C. A thermometer is placed in the oil-filled well at the center of the cell. The cell wall becomes coated with a mantle of solid succinonitrile at the triple point, and good thermal contact between the cell and the thermometer is maintained through the oil.

The triple-point temperature is determined by observing the behavior of the specimen in the cell. At the triple point, the solid, liquid, and gaseous phases of the material are in equilibrium. If the temperature is raised above the triple point, liquid forms at the expense of solid; if the temperature is lowered, more material solidifies. Both the liquidus (melting) and solidus (freezing) temperatures were measured to look for any hysteresis that would indicate contamination. None was observed to within 0.001° C, verifying that the sample was at least 99.9999 percent pure.

This work was done by Martin E. Glicksman of Rensselaer Polytechnic Institute for **Marshall Space Flight Center.** *For further information, Circle 50 on the TSP Request Card.*
MFS-25304

Removal of Hydrogen Bubbles From Nuclear Reactors

Palladium spheres could be used to absorb radioactive hydrogen.

Langley Research Center, Hampton, Virginia

During the recent crisis at the Three-Mile-Island nuclear electric-generating plant, a hydrogen bubble formed in Unit 2. It was considered dangerous since expansion would have uncovered the fuel rods from the core top down, causing further overheating of the core. The bubble was eventually reduced in size by allowing the radioactive hydrogen to escape into the containment building. This solution allowed additional radioactivity into the containment building and into the environment.

A novel method proposed for removing large hydrogen bubbles from the nuclear environment uses, in its simplest form, hollow spheres of palladium or platinum. At room temperature, palladium absorbs 900 times its own volume of hydrogen; when heated, it releases the hydrogen. A similar phenomenon occurs with platinum. The evacuated palladium or platinum spheres are introduced into the reactor with the cooling water where they rise to the top of the water and contact the hydrogen bubble. At low temperature, this contact results in the metal absorbing large volumes of hydrogen; and since the vapor pressure of hydrogen inside the spheres is initially zero, hydrogen also enters the vacuum of the spheres. At higher temperature, the metals absorb smaller volumes of hydrogen, but hydrogen passes through the metal more easily to the hollow of the sphere. Hydrogen will pass through the metal until the vapor pressure inside the sphere equals that outside the sphere.

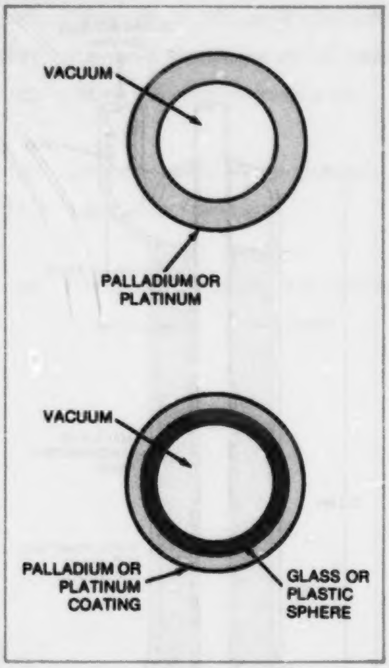

Palladium or Platinum Spheres in two possible configurations proposed for removing hydrogen bubbles from nuclear reactors

Such spheres cannot be used if an explosive mixture of hydrogen and oxygen is contained in the bubble. Platinum, in particular, would cause the mixture to explode. However, if the oxygen content is below the explosion limit, the metals will simply catalyze the formation of water from the hydrogen and oxygen. If the spheres are initially pressurized with pure oxygen, hydrogen entering through the metal shell will react with it to form water. Partially filling the spheres with water in this manner will cause them to sink. Gas-filled spheres, on the other hand, would sink only if critically balanced in buoyancy. Either method would result in the hydrogen bubble being reduced in size without letting more radioactivity outside the reactor.

An alternate technique would involve coating glass or plastic vacuum spheres with platinum and/or palladium and introducing these to the reactor. If the gas mixture is below the explosion limit, water will be formed, reducing the hydrogen bubble. The bubble can be completely removed by slowly adding oxygen to combine with the hydrogen to form water.

This work was done by Renaldo V. Jenkins of **Langley Research Center.** *No further documentation is available.*
LAR-12597

Plasticizer for Polyimide Composites

Liquid plasticizer makes prepregs tacky and drapable.

Langley Research Center, Hampton, Virginia

A new modification of a NASA-developed addition polyimide, LaRC-160, is an essentially-solventless, high-viscosity laminating resin that is synthesized from low-cost liquid monomers. The modified version takes advantage of a reactive liquid plasticizer, which is used in place of solvent, and helps to solve a major problem of maintaining good prepreg tack and drape, (or the ability of the prepreg to adhere to adjacent plies and conform to a desired shape during the layup process). This alternate approach will allow both longer life of the polymer prepreg and the processing of low-void laminates. This approach appears to be applicable to all addition polyimide systems. The reactive liquid that is used is monoethylphthalate (MEP), which is a liquid above 2° C that does not boil.

An added advantage to this material is that it has a very low vapor pressure at the temperatures that occur during normal fabrication (the laying up of prepreg in a shop area). This low vapor pressure allows essentially all of the MEP to be retained, and thereby, tack and flexibility of the prepreg are retained. When alcohol solvents are used, the solvents are so volatile at room temperature that they are rapidly lost to the atmosphere, leaving a brittle and dry prepreg with which it is impossible to work. High boiling alcohols, such as *n*-butyl alcohol have been tried; but these solvents cannot be removed during processing and, therefore, lead to cracked or voidy composite parts.

The MEP is normally used in place of 10 percent of the benzophenone tetracarboxylic diester diacid (BTDE). Hence a nominal formulation for a liquid system would be 2.00 moles 5-norbornene-2,3-dicarboxylic methylester acid (NE); 1.50 moles BTDE; 0.34 mole MEP; and 2.67 moles 4,4'-methylenedianiline (MDA), or an amine mixture such as the one used in LaRC-160. Graphite-reinforced laminates prepared from prepreg containing MEP had mechanical properties equal to the base LaRC-160 system both before and after aging at 600° F (315° C) for up to 500 hours.

This work was done by Terry L. St. Clair of **Langley Research Center** *and John M. Butler of Virginia Polytechnic Institute and State University. For further information, Circle 51 on the TSP Request Card.*

This invention is owned by NASA, and a patent application has been filed. Inquiries concerning nonexclusive or exclusive license for its commercial development should be addressed to the Patent Counsel, Langley Research Center [see page A5]. Refer to LAR-12642.

Improved Adherence of TiC Coatings to Steel

Use of a nitrogen-containing plasma improves adherence and reduces friction and wear.

Lewis Research Center, Cleveland, Ohio

A modified process for RF sputtering of titanium carbide coatings onto 440-C steel has resulted in improved adherence. A small partial pressure of nitrogen (~ 0.5 percent) during the first few minutes of deposition markedly improved adherence, friction, and wear properties when compared with coatings applied on sputter-etched surfaces, or oxidized surfaces, or in the presence of a small oxygen partial pressure. X-ray photoelectron spectroscopy and X-ray diffraction were used to characterize the resultant coatings.

Considerable interest in the use of hard coatings for wear resistance has prompted work on various coating methods. One of the most attractive methods is RF sputtering. Many different hard refractory compounds applied by sputtering have been studied for wear resistance. These studies have shown that coatings applied by sputtering can provide good wear protection and in many cases low friction. However, most coatings are limited not by coating properties but rather by the adherence of those coatings to the substrates. Failures generally occur at the coating/substrate interface.

Previous work showed that for certain refractory types of material, significant improvement in adherence could be obtained if the steel surface was oxidized before coating. Recent tests have shown that a small nitrogen partial pressure during the first few minutes of sputter deposition promoted shear strength adherence for metal and ceramic couples.

In the present work, tests were conducted to determine if adding a small amount of nitrogen to the argon plasma during RF sputter deposition of titanium carbide was effective in promoting adherence and thereby improving friction and wear performance. A further objective was to contrast the effectiveness achieved with nitrogen when compared with the adherence gains achieved by oxidation.

The sputtering was done in a commercial, radio-frequency diode apparatus that operated at 13.56 MHz. Titanium carbide coatings were applied to several 440-C steel disk specimens under a variety of conditions so that comparisons could be made of the effectiveness of nitrogen and oxygen partial pressures and substrate preoxidation. A range of oxygen and nitrogen partial pressures was employed.

The RF-sputtered films were evaluated in a pin-on-disk apparatus, which is often used for solid-film lubrication evaluation. The apparatus consisted of a pin loaded against a flat, rotating disk. The disk specimen was a 440-C bearing steel that had been RF sputter-coated with titanium carbide; the pin was 304 stainless steel. A strain gage measured the friction force. The combination of a 304 stainless-steel pin and a 440-C steel disk was chosen because the friction for this couple is very sensitive to any coating failure and transfer of the 304 steel to spalled regions accelerates the failure process.

The results obtained are shown in the figure. These results represent the best performance that was obtained for the particular gas listed. The oxidized substrates were prepared by furnace heating to 340°° C for 18 to 20 hours. This treatment produced a thin, reddish-cast oxide but did not soften the 440-C disk. Also shown for comparison on the figure are data for coatings applied directly to sputter-etched surfaces without any oxygen or nitrogen partial pressure.

Both nitrogen and oxygen partial pressures provide some improvement over the sputter-etched-only values; however, the oxygen partial pressure technique did not yield results as good as furnace oxidation. At 2 N (newtons)

(continued on next page)

load, both the coatings on the oxidixed 440-C steel disk and the coating prepared with an initial nitrogen partial pressure exhibited comparably low friction and wear.

At a high load of 5 N, only the sample prepared with nitrogen ran the entire 30 minutes without spalling. All other coatings, regardless of how prepared, failed, resulting in high friction and rider wear. The coating prepared with a nitrogen partial pressure ran without failure at loads of 10 N.

The friction and wear tests in conjunction with X-ray photoelectron spectroscopy and X-ray diffraction analyses yielded the following results:

- The addition of a small nitrogen partial pressure (~ 0.5 percent) during the initial stages of deposition (interface formation) yielded coatings with adherence, friction, and wear properties superior to coatings applied to oxidized surfaces or with an oxygen partial pressure instead of nitrogen.
- The improvement in adherence is related to the formation of an interface containing both titanium nitride and iron nitride.
- X-ray diffraction showed the RF-sputtered TiC coating done with a nitrogen partial pressure had a preferred orientation with the densest (111) planes parallel to the surface. In contrast, samples done with oxides present were more random in orientation.

This work was done by W. A. Brainard and D. R. Wheeler of **Lewis Research Center.** *Further information may be found in NASA TP-1377 [N79-15184/NSP], "Effect of Nitrogen-Containing Plasma on Adherence, Friction, and Wear of Radiofrequency-Sputtered Titanium Carbide Coatings" [$5]. A copy may be purchased [prepayment required] from the National Technical Information Service, Springfield, Virginia 22161.*

Inquiries concerning rights for the commercial use of this invention should be addressed to the Patent Counsel, Lewis Research Center [see page A5]. Refer to LEW-13169.

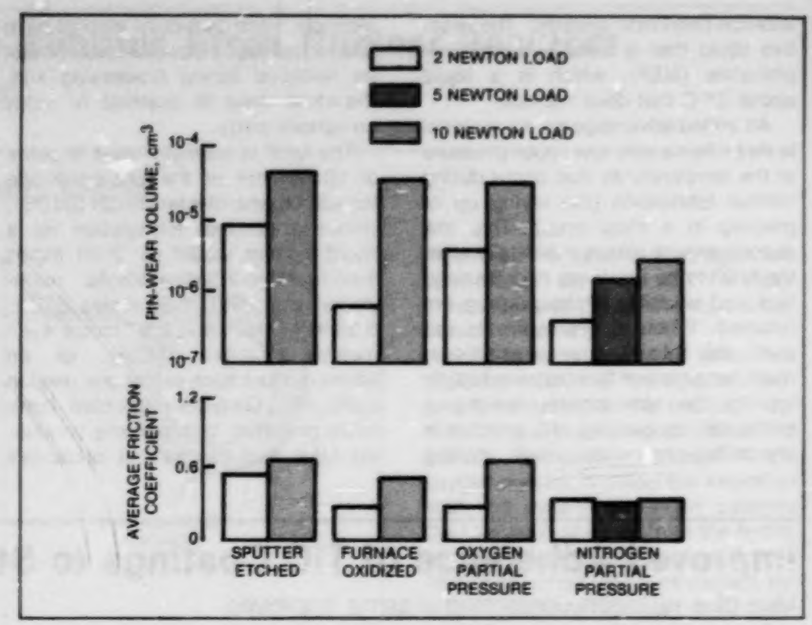

Average Friction Coefficient and Pin Wear Volume for 440-C steel disks sputtered with titanium carbide, sliding speed 25 cm-s^{-1}, 30-min run, N_2 atmosphere

---

Hybrid Polymer Microspheres

Tiny polymeric spheres with even smaller spheres attached to their surfaces may be used for separation.

NASA's Jet Propulsion Laboratory, Pasadena, California

Several techniques have been successfully tested for bonding polymeric spheres, typically 0.1 micron in diameter, to spheres with diameters up to about 100 microns. The hybrids are being developed as improved packing material for ion-exchange columns, filters, and separators.

The polymers, including latex and poly-HEMA (poly-hydroxymethylmethacrylate), are prepared as microspheres by exposing a mixture of reagents to ionizing radiation (to promote polymerization) and then washing and filtering the product. Solid and hollow glass spheres have also been used.

The polymeric spheres have attached carbonyl or other groups that are accepter sites for extracting antibodies, enzymes, and other large molecules from aqueous suspensions and solutions. To enhance the possibility for binding in such applications, it is preferable to use spheres with small diameters, since this maximizes the exposed surface area in a given volume. However, if the spheres are too small and densely packed, they impede the flow of liquid, which decreases the effectiveness of the separation process.

Compound spheres increase the effective surface area, while minimizing obstruction to the liquid flow. The initial experiments show that a stable hybrid consisting of a large sphere with many small spheres attached to its surface is formed by chemical bonding or electrostatic bonding.

In chemical bonding, glass spheres, typically 30 microns in diameter, are treated with silane or other agent that introduces functional groups to the glass surface. The smaller poly-HEMA spheres (0.1 to 1.0 micron in diameter) form stable bonds to the treated glass. A similar treatment is used to prepare hybrid spheres of poly-HEMA and polystyrene.

Small poly-HEMA spheres were also attached to glass spheres by electrostatic attraction. The smaller spheres are prepared with positively-charged dimethylamino surface groups. These form electrostatic bonds with the glass, which is negatively charged. Preliminary tests have also verified that some species of red blood cells can be extracted from an aqueous suspension by the glass/dimethylamino hybrids.

In another experiment, polyvinyl pyridine microspheres (5 microns in diameter), having amino groups on the surface, were mixed with magnetic microspheres (0.2 micron in diameter) with aldehyde groups on the surface. The hybrid has a polyvinyl pyridine nucleus and a magnetic coating on the surface. A magnetic field is used to handle and separate these spheres.

This work was done by Alan Rembaum of Caltech for **NASA's Jet Propulsion Laboratory**. *For further information, Circle 52 on the TSP Request Card.*
NPO-14462

Books and Reports

These reports, studies, and handbooks are available from NASA as Technical Support Packages (TSP's) when a Request Card number is cited; otherwise they are available from the National Technical Information Service.

Composites for Aeropropulsion

Status report details significant advances made in the past several years.

A report has been published that summarizes the status of composite materials for aeropropulsion.

Composite materials are increasingly of interest for a variety of applications. A large potential exists for strategic material conservation and energy savings with composite materials. Research efforts in this field have resulted in major strides in the development of materials as well as in improved design and analysis capability. This report details significant advances made in the past several years. The applications discussed deal primarily with composites used in the cold and hot sections of aircraft turbine engines. Also reported is the current status of composite structural analysis technology. Although this report is concerned primarily with NASA-funded research, it also includes other investigations. Specific composites are described for both low- and high-temperature usage.

The most-widely-used low-temperature [less than 350° F (177° C)] composites utilize an epoxy resin matrix and graphite fiber reinforcement. These materials exhibit good physical properties, low cost, and ease of processing into complex shapes. Use temperatures of nonmetallic composites could be extended up to 600° F (315° C) if improved polyimide resins can be used as matrix materials.

Metal matrix composites are emerging as potential materials for both low- and high-temperature applications. For the former, boron/aluminum composites and for the latter, tungsten-fiber-reinforced superalloys show considerable promise.

This report describes key advances made in the past several years and lists 47 references published from 1971 to 1979.

This work was done by G. M. Ault and J. C. Freche of **Lewis Research Center.** *To obtain a copy of the report, Circle 53 on the TSP Request Card.*
LEW-13438

Lubrication Handbook

A ready reference for many of the solid and liquid lubricants used in the space industry

A lubrication handbook is divided into two major parts: Part A describes solid lubricants and part B liquid lubricants used in the aerospace industry. The listed materials cover a broad application spectrum from manufacturing and ground support to missile and spacecraft hardware. The handbook can serve as ready reference in the design and maintenance service of industrial equipment.

More than 250 lubricants are covered in each section, with accompanying chemical and physical property data. The solid lubricants include bonded solid lubricants, dispersions, and composites; liquid lubricants include greases, oils, compounds, and fluids.

Part A of the handbook is divided into six major sections: Section I defines the solid lubricants and outlines their advantages and disadvantages. Section II lists the manufacturers in alphabetical order with their products and characterizes lubricant compatibility and usage tables for selected bonded solid lubricants and composite materials. Section III presents data sheets giving general composition and physical properties of selected lubricants; section IV presents data sheets listing manufacturer-supplied test and applications data. The data on selected solid film lubricants obtained from tests conducted by an independent laboratory are covered in section V. Section VI has three appendixes: one a glossary of terms, the second containing excerpts of solid lubricant applications, and the third describing test apparatus and procedures used in the laboratory evaluation of solid lubricants.

Part B consists of five sections: Section I instructs the reader on the use of part B, presents an index of all the liquid lubricants covered, and includes a series of charts describing the lubricant applications. A brief description of military specifications is given in section II, while section III presents data sheets listing physical and chemical properties of selected lubricants. Section IV shows the results of long-term evaluation of

(continued on next page)

selected grease lubricants. Section V contains three appendixes: one, a glossary of lubrication terms; two, a series of summaries of standard testing methods used to evaluate lubricating oils, greases, and fluids; and three, a detailed-conversion chart into international (SI) units.

The handbook is a valuable reference to designers, manufacturers, and maintenance crews of aerospace hardware. Much of the information is readily transferable to industrial and commercial hardware. It should be a welcome addition in any engineering library as well as to groups and individuals involved with mechanical systems.

This work was done by Midwest Research Institute for **Marshall Space Flight Center.** *To obtain a copy of the handbook, Circle 54 on the TSP Request Card.*
MFS-25158

Computer Programs

These programs may be obtained at very reasonable cost from COSMIC, a facility sponsored by NASA to make new programs available to the public. For information on program price, size, and availability, circle the reference letter on the COSMIC Request Card in this issue.

Methane/Air Flames in a Concentric-Tube Combustor

Hydrodynamics and chemistry of confined turbulent flames are predicted.

This computer program gives a realistic prediction of the hydrodynamics and chemical reaction in a reverse-flow two-concentric-tube combustor. Special attention is given to the formation of oxides of nitrogen in the combustion process.

The combustor geometry considered is a two-concentric-tube combustor. Concentric streams of fuel (methane) and air enter the inner duct and mix. At the end of the inner duct, the flow expands radially outward and reverses its flow. Combustion occurs in this flow reversal region. Oxides of nitrogen and other combustion products are formed as a result of the chemical reaction. The flow is two-dimensional, axisymmetric, steady, and turbulent. Heat transfer between the combustion products in the annular passage between the tubes and the reactant stream in the center tube is considered.

The analysis involves the mathematical formulation of the flow in terms of partial differential and auxiliary algebraic equations. These equations are used in their finite-difference form for obtaining numerical solutions. The solution procedure is incorporated in the computer program to produce profiles of velocity, temperature, and chemical species concentration throughout the combustor.

In this program two test cases were considered, cold flow (without chemical reaction) and hot flow. Possible modifications to this program include the use of more sophisticated heat transfer, chemical kinetics, and turbulence models.

This program is written in FORTRAN IV for batch execution and has been implemented on a UNIVAC 1100 computer with a central memory requirement of approximately 33K of 36-bit words. This combustor analysis program was developed in 1978.

This program was written by N. C. Markatos, D. B. Spalding, and S. K. Srivatsa of Concentration, Heat and Momentum Ltd. for **Lewis Research Center.** *For further information, Circle B on the COSMIC Request Card.*
LEW-13388

Life Sciences

Hardware, Techniques, and Processes

187 Testing EKG Electrodes On-Line

Books and Reports

187 Laser-Fluorescence Measurement of Marine Algae

Testing EKG Electrodes On-Line

A simple circuit verifies electrode-lead continuity and contact during an electrocardiograph recording.

Lyndon B. Johnson Space Center, Houston, Texas

A simple test instrument allows an electrocardiograph operator to check individual electrodes while they are attached to the subject. Simply by rotating a switch and observing a meter, the operator verifies that each electrode is not short-circuited or open-circuited and does not present excessive contact resistance at its interface with the skin. The instrument also makes it convenient to check electrode cables that are subject to frequent bending and wear, such as cables used on patients who are exercising.

After the patient is instrumented (that is, after the skin is smeared with electrode paste, the electrodes are placed on the skin, and the leads are attached to the electrodes), the cable from the EKG junction box is attached to the test instrument (see figure). A current-limited impedance meter is plugged into another connector on the instrument.

Rotary switches allow the operator to select any electrode lead and measure the impedance between it and another lead or between it and the cable shield. The impedance is read directly on the meter.

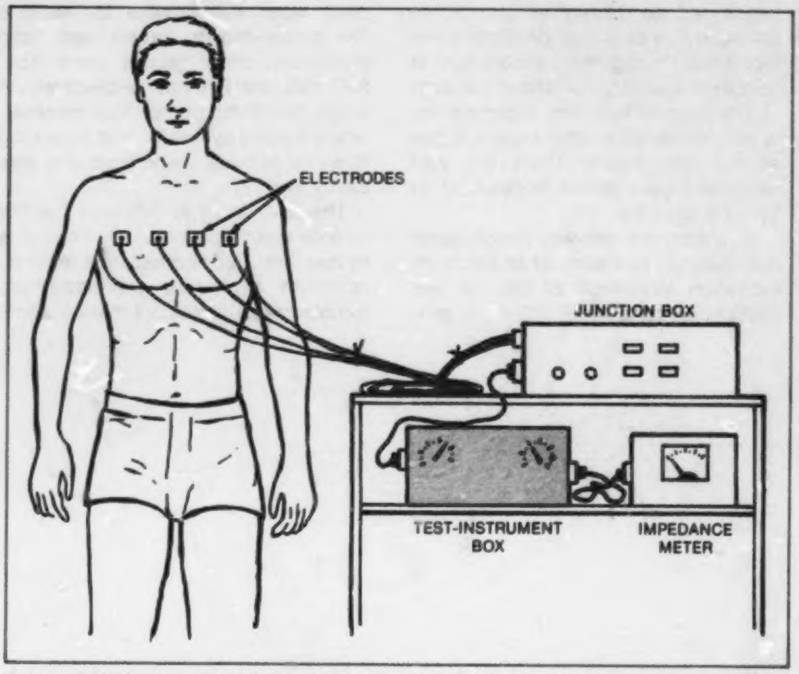

Rotary Switches on Test Instrument allow an EKG operator to select individual electrode pairs for impedance measurements. The instrument also contains operational amplifiers that condition the EKG signals. Two 4-gang, 12-position rotary switches interconnect 14 electrode leads and 1 shield in a prototype. Improved versions will do all switching with a single rotary switch.

An electrode-to-electrode impedance of less than 2,000 ohms is considered satisfactory, and a reading of 1,000 ohms is regarded as ideal. An open circuit, either in a lead or the junction box, shows up as infinite impedance. A short circuit appears as a zero reading. The electrode-to-shield impedance should be above 10 megohms.

This work was done by William G. Crosier and Gordon S. Rutt of Technology Inc., for **Johnson Space Center.** *For further information, Circle 55 on the TSP Request Card.*
MSC-18696

Books and Reports

These reports, studies, and handbooks are available from NASA as Technical Support Packages (TSP's) when a Request Card number is cited; otherwise they are available from the National Technical Information Service.

Laser-Fluorescence Measurement of Marine Algae

A thorough review of theory and experiment, plus some new information

Progress in the remote sensing of algae by laser-induced fluorescence is the subject of a comprehensive new report. Existing single-wavelength and four-wavelength systems are reviewed, and a new expression for the power received by an airborne sensor is derived. The result differs by as much as a factor of 10 from those previously reported. A detailed error analysis evaluates factors affecting the accuracy of laser-fluorosensor systems.

Measurements of the concentration and distribution of algae in bodies of

(continued on next page)

water are of ecological interest because they reflect chemical, thermal, and mechanical conditions in the marine environment. Algae presence is quantified by exciting the chlorophyll *a* pigment and detecting fluorescence at 685 nm.

Most algal species fall into one of four basic color groups: green, golden brown, red, and blue green; all contain chlorophyll *a* plus one or more other pigments. The pigments absorb light at specified wavelengths, and the energy is transferred between pigments toward chlorophyll *a*, where deexcitation at 685 nm occurs. There are also secondary deexcitation modes at other points in the cycle.

An airborne single-wavelength laser fluorosensor, operating at an optimum excitation wavelength of 600 nm and flying at an altitude of 500 m, is predicted to measure algae concentrations as low as 1 μg/liter. The calculations assume a 100-kW (peak power) laser.

Four-wavelength laser fluorosensors give information on the distribution of algae in the four color groups. In a system previously developed at Langley Research Center, the optimum laser wavelengths for exciting the golden-brown, green, red, and blue-green color groups were 454, 539, 598, and 618 nm, respectively. A single flashlamp pumps four symmetrically-placed dye cells, and a rotating aperture permits lasing from only one cavity at a time.

The error analysis indicates that the remote quantification of chlorophyll *a* by laser-induced fluorescence requires optimum excitation wavelength(s), remote measurement of marine attenuation coefficients, and instrumentation to reduce uncertainties in fluorescence cross sections. Without these additional measurements, the systems only give qualitative information about the presence of chlorophyll *a*, and the results of single-wavelength measurements are comparable to those of multiple-wavelength sensors.

This work was done by Edward V. Browell of **Langley Research Center**. *Further information may be found in NASA TND-8447 [N77-26480/NSP], "Analysis of Laser Fluorosensor Systems for Remote Algae Detection and Quantification" [$6]. A copy may be purchased [prepayment required] from the National Technical Information Service, Springfield, Virginia 22161.*
LAR-12282

Mechanics

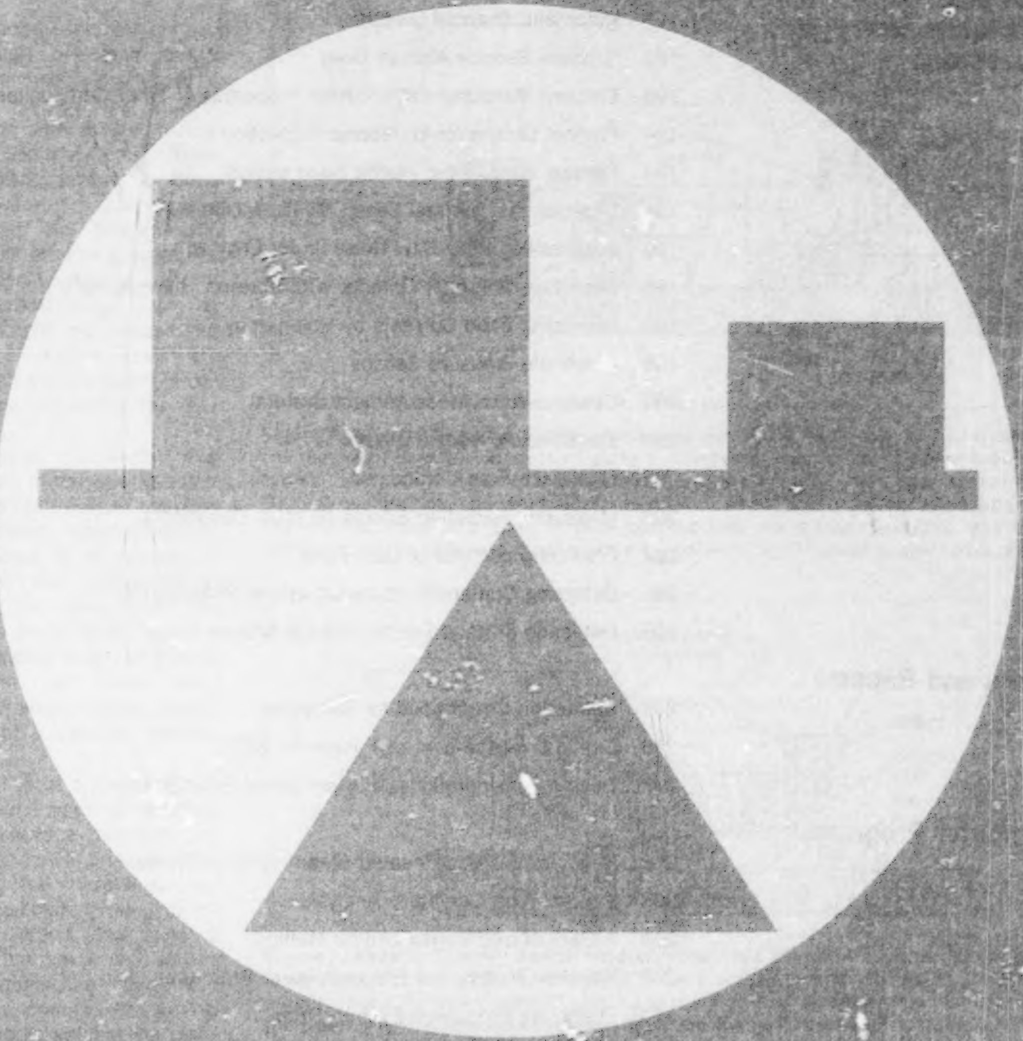

Hardware, Techniques, and Processes

191 Automatic Thermal Switches
192 Grooves Reduce Aircraft Drag
193 Efficient Measurement of Shear Properties of Fiber Composites
194 Fresnel Lenses for Ultrasonic Inspection
194 Passive Wing/Store Flutter Suppression
195 Changes in "Thermal Lens" Measure Diffusivity
196 Suppressing Buzz-Saw Noise in Jet Engines
196 Detection of Tanker Defects With Infrared Thermography
198 Recording Fluid Currents by Holography
199 Downhole Pressure Sensor
200 Oceanic-Wave-Measurement System
201 Electrofluidic Accelerometer
202 Flashback-Free Combustor
203 Measuring Radiation Effects on MOS Capacitors
204 Predicting Lifetime of Cast Parts
205 Detecting Contaminants by Ultraviolet Photography
205 Detecting Surface Faults on Solar Mirrors

Books and Reports

206 Refraction Corrections for Surveying
206 Digital Enhancement of X-Rays for NDT
207 Design Considerations for Mechanical Face Seals

Computer Programs

208 Regenerative Superheated-Steam Turbine Cycles
208 Stream-Tube Curvature Analysis
209 A Generalized Vortex Lattice Method
209 Vibration Modes and Frequencies of Structures
210 Predicting Propulsion-System Drag
210 Heat Conduction in Three Dimensions

Automatic Thermal Switches

Reliable and efficient switches control heat transfer from one area to another.

Goddard Space Flight Center, Greenbelt, Maryland

Two new switches control heat flow from one thermally conductive plate to another. One switch is activated to permit heat flow to the outside environment; the other is used to limit such heat flow. Both switches, developed for controlling payload temperatures in spacecraft, represent a practical answer to mechanically complex and less-reliable louvers that would close when facing the Sun and open when turned away from it. Mechanically simple and reliable, the switches can be used in almost any situation in which the temperature can be controlled by regulating the heat flow.

Figure 1 shows the switch that normally remains in the open position so long as the temperature of the plate (in contact with some internal system; e.g., the payload) it is resting on remains below the phase-change temperature of the power unit. The power unit has an internal reservoir containing a material (e.g., ammonia, deionized water, or some other material) that changes phase (liquid, solid, or gas) at a specific temperature.

When plate 1 is at a low temperature, the power-unit piston is retracted, and a spring biases a thermally-conductive switch saddle in an upward position, breaking the thermal contact with plate 1. When plate 1 heats up, the procedure is reversed. Heat expands the material in the power unit, forcing the piston up against the linkage arm. This force overcomes the spring, pressing the saddle against the plate. Heat is then transferred from plate 1 to plate 2 via flexible heat carriers (e.g., heat pipes). Plate 2 then radiates the heat to the outside.

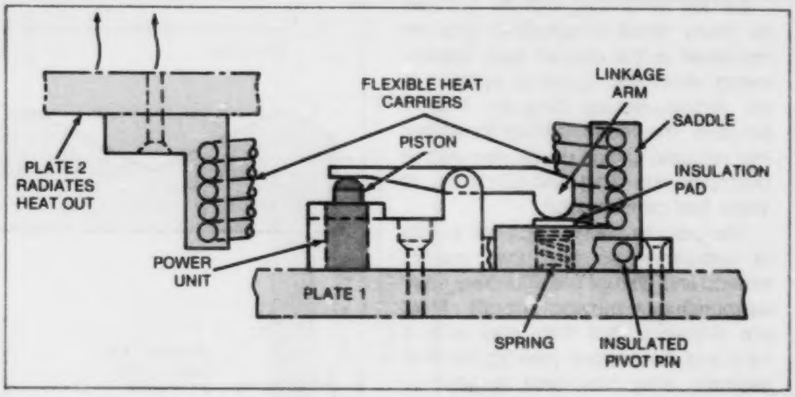

Figure 1. **Thermal Control Switch** eliminates excessive heat flow to the outside environment. Heat on conductive plate 1 (in thermal contact with some internal system) activates a piston that extends upward, forcing the saddle against plate 1. Flexible heat carriers conduct the heat to plate 2, which then radiates to the outside environment. After the plate 1 temperature drops, the piston contracts, and the spring forces the saddle to move clockwise, breaking the thermal contact with plate 1.

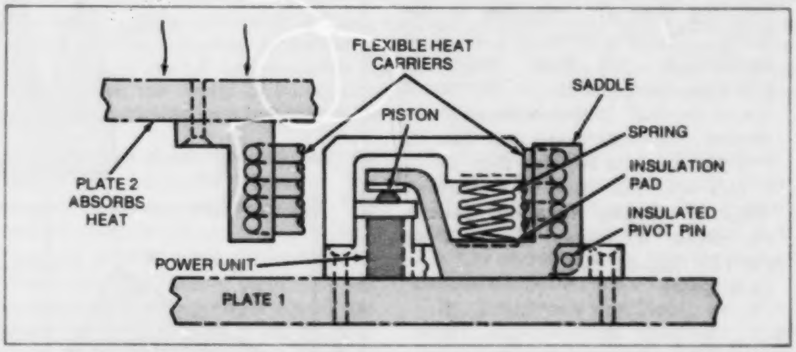

Figure 2. **Reverse Thermal Switch** regulates heat flow from the outside. The saddle remains in thermal contact with plate 1 until sufficient heat comes in from the outside (plate 2). When plate 1 heats up to a certain temperature, the heat extends the piston, forcing the saddle arm up, breaking the saddle contact with plate 1. As plate 1 cools, the piston contracts, and the spring forces the saddle counterclockwise into thermal contact with plate 1.

Figure 2 shows the switch used for preventing excessive heat flow to or from the outisde. The arrangement is similar; however, the switch action is reversed. When plate 1 is cold, the power-unit piston is retracted, and the spring biases the saddle to stay in contact with the plate. Heat coming in from plate 2 eventually warms up plate 1 to a level sufficient to activate the piston. The piston then forces the saddle arm upward, breaking the saddle contact with the plate and stopping the heat transfer.

Both switches are completely automatic and can be custom-designed to operate at specific temperatures. The material in the power unit determines at what temperatures the switches will trigger. The flexible heat carriers tolerate vibration and some relative displacement between the plates.

This work was done by Joseph W. Cunningham and Lawrence D. Wing of **Goddard Space Flight Center.** *For further information, Circle 56 on the TSP Request Card.*

This invention is owned by NASA, and a patent application has been filed. Inquiries concerning nonexclusive or exclusive license for its commercial development should be addressed to the Patent Counsel, Goddard Space Flight Center [see page A5]. Refer to GSC-12553.

Grooves Reduce Aircraft Drag

Tiny grooves in various cross-sectional shapes reduce aircraft fuel consumption.

Langley Research Center, Hampton, Virginia

Aerodynamic drag can be reduced by many small longitudinal grooves machined in the aircraft skin. Experiments show that grooves parallel to the airflow reduce drag by 4 to 7 percent. The reduced drag translates into reduced engine power required to overcome the drag and ultimately to lower fuel consumption.

The grooves confine incipient bursts of turbulence so that they cannot expand and disrupt the boundary layer surrounding a moving aircraft. Most are V-shaped, but they may take a variety of dimensions (see figure). For example, they may have rounded or sharp peaks and symmetrical or asymmetrical cross sections. Asymmetrical grooves of various cross-sectional geometries may be arranged in some regular sequences to optimize the aerodynamic performance.

The most effective dimensions for reducing drag are indicated in the figure. The dimensions are small in comparison with those tested in previous experiments. In terms of law-of-the-wall (turbulent-flow) coordinates, the heights are less than 30 and the spacings are less than 40.

This work was done by Michael J. Walsh of **Langley Research Center.** *For further information, Circle 57 on the TSP Request Card.*
LAR-12599

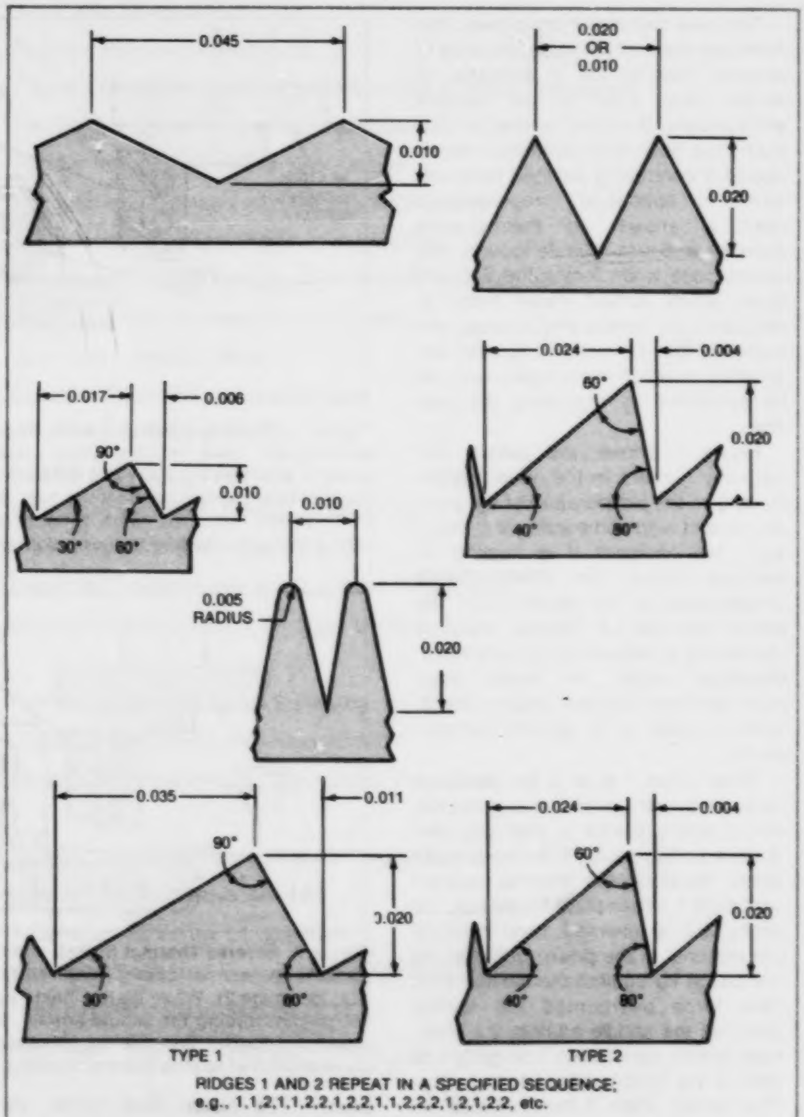
0.045
0.010
0.020
OR
0.010
0.020
0.017
0.006
90°
0.010
30°
60°
0.024
0.004
60°
0.020
40°
80°
0.010
0.005
RADIUS
0.020
0.035
0.011
90°
0.020
30°
60°
0.024
0.004
60°
0.020
40°
80°
TYPE 1
TYPE 2
RIDGES 1 AND 2 REPEAT IN A SPECIFIED SEQUENCE;
e.g., 1,1,2,1,1,2,2,1,2,2,1,1,2,2,2,1,2,1,2,2, etc.
NOTE: ALL DIMENSIONS ARE IN INCHES

Most Effective Groove Shapes are shown with dimensions. The grooves inhibit the turbulent bursting process, thus reducing aerodynamic drag and aircraft fuel consumption.

Efficient Measurement of Shear Properties of Fiber Composites

10°-off-axis tensile-test specimen is recommended as a standard for developing design data.

Lewis Research Center, Cleveland, Ohio

Efficient intralaminar (in-plane) shear characterization (shear stress/strain relationships) of unidirectional fiber composites has been hampered by the difficulty of producing a state of pure shear in practical laboratory test specimens. The simplest test specimen in use today is the three-point-bend short-beam shear test specimen (ASTM D-2344-72). While adequate for material quality control, this specimen is not suitable for generating design data because shear stress is not uniform throughout its thickness and only the fracture stress, not the total shear stress/shear strain history, is recorded. The best test specimen, a thin tube subjected to torsion, is too expensive and time consuming to be practical.

The new proposed method is to use a 10°-off-axis tensile specimen (fibers oriented 10° from the load direction) in conjunction with simple transformation equations for intralaminar shear characterization of fiber composites. The geometry, dimensions, end reinforcements, and instruments are shown in the figure.

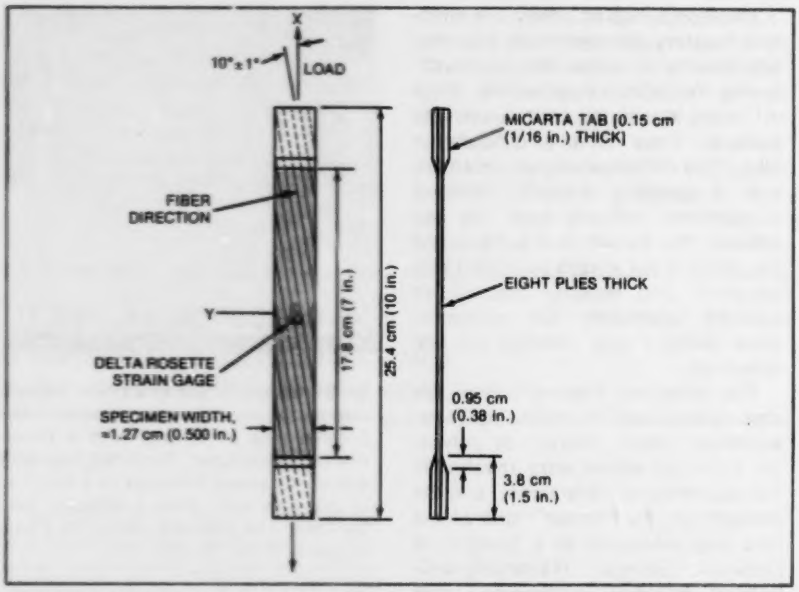

Test Setup is shown for the 10°-off-axis specimen recommended for developing data on the intralaminar shear characteristics of unidirectional fiber composites. The load is applied at a 10° angle with the fiber orientation, and the strain gage is placed midlength at the center of the specimen. Two, back-to-back delta-rosette strain gages are recommended to account for out-of-plane bending.

The procedures for generating the intralaminar shear properties, shear stress/strain curves, initial shear modulus, tangent shear modulus, secant shear modulus, fracture shear stress, and fracture shear strain are relatively straightforward.

Stress-vs.-strain curves are calculated from the outputs of three simultaneous strain-gage readings at increments of stress, using equations of the form:

$$\text{Intralaminar shear stress} = \text{coefficient}\ \frac{\text{tensile load}}{\text{specimen cross section}}$$

and

$$\text{Intralaminar shear strain} = \sum_{i=1}^{i=3} c_i \varepsilon_{gi}$$

where the c_i are coefficients and the ε_{gi} are strain-gage readings. Equations have been derived for rectangular-rosette and 60°-delta-rosette strain gages.

The initial shear modulus is determined from the slope of the initial tangent to the shear stress-vs.-strain curve. The shear modulus at any other point (tangent shear modulus) may be determined from the slope of the tangent to the curve at that point. The secant shear modulus is determined from the slope of a line connecting the origin with the fracture point. The ply intralaminar shear strength equals the shear stress calculated at the fracture load. The ply intralaminar fracture strain is the shear strain calculated at the fracture load.

Theoretical investigation of the technique showed, among other things, that for this tensile-test setup the major stress contribution to fracture is intralaminar shear, and the test will be sensitive to errors greater than 1° in fiber orientation. Experimental data indicated that at specimen midlength fracture strains and Poisson's (transverse) strains are higher at the edges than at the center for some materials, but most measurements are not overly sensitive to small variations in the strain-gage location.

Experimental data compared reasonably well with structural-axis shear strain as predicted by finite-element analysis. Experimental results from 10°-off-axis specimens for initial-tangent intralaminar shear moduli and fracture stresses are within the range of values reported in the literature.

Its consistency with theory and with other experimental methods, the variety of data yielded, and its relatively straightforward procedures suggest that the 10°-off-axis specimen be considered as a standard test for intralaminar shear characterization of unidirectional fiber composites.

This work was done by Christos C. Chamis and John H. Sinclair of **Lewis Research Center**. *Further information may be found in NASA TN-D-8215 (N76-22314/NSP), "10° Off-Axis Tensile Test for Intralaminar Shear Characterization of Fiber Composites" ($6.00). A copy may be purchased (prepayment required) from the National Technical Information Service, Springfield, Virginia 22161.*
LEW-13011

Fresnel Lenses for Ultrasonic Inspection

Fresnel lenses are easily coupled to the test object.

Lyndon B. Johnson Space Center, Houston, Texas

Ultrasonic Fresnel lenses are effective focusing elements with potential applications in ultrasonic "contact" testing for defects in materials. Since a Fresnel lens is flat (with a serrated surface), there is little difficulty in filling the lens/test-object interface with a coupling medium. With a conventional concave lens, the gap between the curved lens surface and the object is not always saturated with couplant; and residual trapped air severely attenuates the ultrasonic wave before it ever reaches the test specimen.

The ultrasonic Fresnel lenses are cast from epoxy in molds made of aluminum, brass, rubber, or polyester. Prototype lenses were attached to flat piezoelectric transducers, and the intensity on the "image" side of the lens was measured as a function of distance. Several reasonably-well-defined intensity maximums were recorded (see figure).

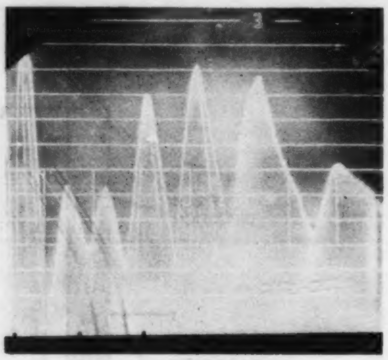

An **Ultrasonic Intensity Pattern** demonstrates the dynamic response of a flat Fresnel lens in contact with a piezoelectric transducer. The time exposure shows the sound intensity as a function of distance away from a reflector near the lens. The distance along the x-axis is about 10 in. (25 cm).

Although contact transducers have been used for inspection testing without a focusing lens, focusing is desirable because it increases the ultrasonic-wave intensity within the test object and thus improves the signal-to-noise ratio.

Ultrasonic beams focused by concave lenses are used successfully with immersion transducers, for which the test object is immersed in a water bath. However, for large objects, objects that are already installed, objects on production lines, and objects that can be damaged by water, contact testing is more practical than immersion.

This work was done by Calvin C. Kammerer of Rockwell International Corp. for **Johnson Space Center.** *No further documentation is available.*
MSC-18469

Changes in "Thermal Lens" Measure Diffusivity

A new double-beam method rapidly measures thermal diffusivity.

NASA's Jet Propulsion Laboratory, Pasadena, California

In an extension of the "thermal-lens" effect to new applications and better resolution, two laser beams combine to rapidly measure thermal diffusivity and other molecular dynamic properties. The new double-beam technique can handle very small samples, unlike classical techniques for measuring diffusivity; and it can be used for measurements on samples undergoing stress, making it applicable to data collection for structural engineering.

The thermal lens is set up when heat from an ultrashort burst of pulsed-laser energy introduces inhomogeneity in the refractive index of a

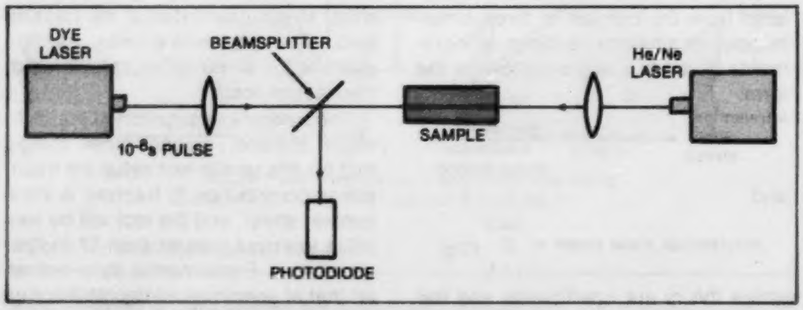

Two Laser Beams, one pulsed and one continuous, measure the thermal diffusivity and the properties of a test sample. The high-energy pulsed laser changes the sample refractive index, which is probed by the low-energy continuous beam. For opaque samples, the continuous beam can be reflected off the sample surface.

test sample. In the double-beam method, a low-power continuous laser probes the sample as it is heated by the high-energy pulse. The continuous beam monitors changes in the optical characteristics, which are related to temperature inhomogeneities and to microscopic dynamic processes. By varying the pulse width of the high-energy laser, it is possible to determine the relationship between the rate of formation of the thermal lens and lattice relaxation processes. The decay time of the lens is related to the thermal diffusivity.

The test setup shown in the figure has measured the thermal properties of polymethylmethacrylate. Using a dye laser with 10-nanosecond pulse width and variable wavelength (360 to 380 nanometers), less than 10^{-8} joule is deposited in the sample during each dye-laser pulse. Estimates of the temperature rise are about 10^{-3}° C or less.

A computer plot of the lens formation, generated by averaging 5,000 scans, took 10 minutes to complete. A trace of the lens decay yielded a value for the thermal diffusivity of 1.0×10^{-3} cm^2/s, in good agreement with measurements using classical methods.

This work was done by Amitava Gupta, Su-Don Hong, and Jovan Moacanin of Caltech for **NASA's Jet Propulsion Laboratory.** *For further information, Circle 58 on the TSP Request Card.*

This invention is owned by NASA, and a patent application has been filed. Inquiries concerning nonexclusive or exclusive license for its commercial development should be addressed to the Patent Counsel, NASA Resident Legal Office-JPL [see page A5]. Refer to NPO-14657.

Passive Wing/Store Flutter Suppression

Combination of passive and active elements suppresses aircraft-wing/store flutter by decoupling the vibration modes of the wing and store.

Langley Research Center, Hampton, Virginia

A passive flutter-suppression system has been developed to increase the flutter speed of aircraft wings that are adversely affected by the addition of large masses (stores) to the wings, such as external fuel tanks. Important features of the system are its effectiveness for large variations in the mass of the store as well as the unsensitivity of the system to large changes in the location of the store center-of-gravity.

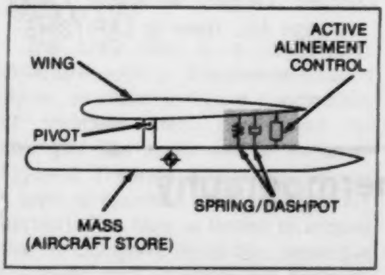

Figure 1. **Decoupler Pylon** used with aircraft wings carrying stores such as fuel pods uses active and passive elements to isolate the store pitch from wing modes.

As illustrated in Figure 1, the store is pivoted near the elastic axis of the wing. A spring and dashpot control the frequency and damping of the system. The manner in which this decoupler increases the flutter speed is shown in Figure 2, where wing frequencies are plotted against airspeed. Flutter usually involves the coupling of at least two vibration modes, one of which involves a torsional or pitching motion of the wing. For a rigidly mounted store, the variation of torsional and bending frequencies with airspeed is shown. When the frequencies of these two modes approach each other, a flutter instability may occur. If the store were mounted with a relatively soft spring as shown in Figure 1, the pitch mode of the store would be virtually decoupled from the wing, and a large increase in flutter speed would be found due to the initial wide separation of the torsion and bending frequencies as shown.

To avoid large static deflections normally associated with a low-frequency suspension system, a feedback control system is used to keep the mean deflection of the store alined with the wing chord.

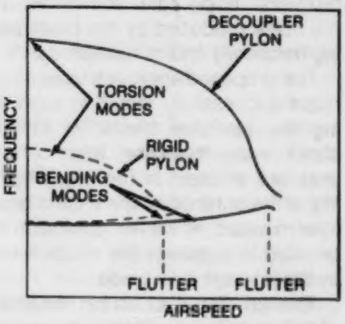

Figure 2. **Frequency Separation** provided by the decoupler pylon, compared to a rigidly attached store, produces a higher aircraft flutter speed.

This work was done by Jerome T. Foughner, Jr., and Wilmer H. Reed III of **Langley Research Center** *and Harry L. Runyan, Jr., of George Washington University. For further information, Circle 59 on the TSP Request Card.*

Inquiries concerning rights for the commercial use of this invention should be addressed to the Patent Counsel, Langley Research Center [see page A5]. Refer to LAR-12468.

Suppressing Buzz-Saw Noise in Jet Engines

Technique promises to reduct annoying fan noise.

Langley Research Center, Hampton, Virginia

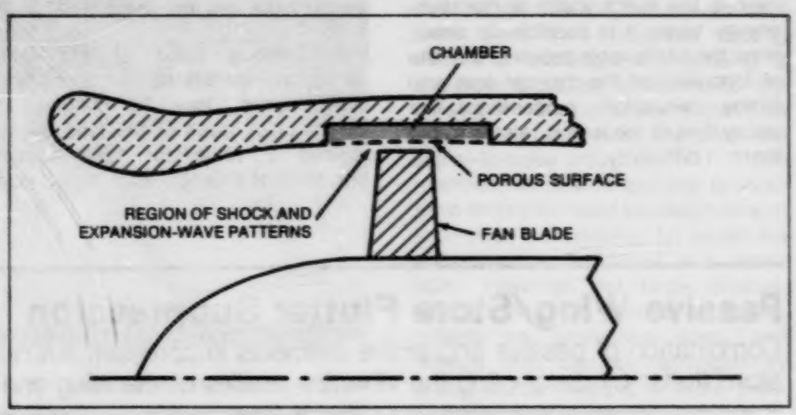

Buzz-Saw Noise produced by jet engines can be suppressed, if not entirely eliminated, by lining part of the engine duct wall with a porous surface. the combination of porous surface and the chamber above the turbofan blade tip would absorb the shock waves, suppressing the annoying aircraft shrill.

Buzz-saw noise, the most annoying noise component generated by turbofan engines, can be suppressed by installing a porous surface on the duct wall (see figure) directly above the engine fan-blade tip. The porous surface and its housing would reduce the shock-wave reflection from the wall and thus suppress the noise.

Turbofan engine fans produce both tonal and random noises. When the fan-blade tip is supersonic, the tonal noise dominates. Shock- and expansion-wave patterns that constitute the tonal noise are formed at the blade tips. This shock, together with the resulting interacting patterns, rotates inside the duct and propagates out as a strong pulse forming the so-called buzz-saw noise that dominates over the noise produced by the blade-passing frequency and its harmonics.

The proposed approach uses a technique successfully tested in suppressing the jet-noise shock in which a shock wave resulting from a large pressure gradient in the flow originating at the outer tip of the engine nozzle is eliminated. A similar approach can be used to suppress the shock formed by the jet-engine air blade.

The turbofan duct wall in the vicinity of the blade tip would include a porous surface that can suppress direct shock and expansion waves impinging on the wall. Waves reflected from the duct wall are suppressed due to absorption by the porous surface. A chamber behind the porous surface acts like a pressure stabilizer.

Aerodynamically, a shock impinging on the porous surface reflects as an expansion wave, while it reflects as a shock over the nonporous part of the surface. As it is reflected, the resulting interacting patterns (compression and expansion waves) cancel each other's contributions. This effect has been observed experimentally.

This work was done by Lucio Maestrello of **Langley Research Center.** *Further information may be found in NASA TM-78802 [N79-13820/NSP] "Initial Results of a Porous Plug Nozzle for Supersonic Jet Noise Suppression" [$5]. A copy may be purchased [prepayment required] from the National Technical Information Service, Springfield, Virginia 22161.*

Inquiries concerning rights for the commercial use of this invention should be addressed to the Patent Counsel, Langley Research Center [see page A5]. Refer to LAR-12645.

Detection of Tanker Defects With Infrared Thermography

IR scanner locates internal defects of LNG tank wall.

Langley Research Center, Hampton, Virginia

An infrared scanning technique for finding defects in the secondary barrier of a liquid natural gas (LNG) tank has been successfully tested on a ship under construction at the Newport News Shipbuilding and Dry Dock Company. The company is currently building a number of LNG tankers to transport Algerian LNG to the east coast of the United States. These ships must be constructed with exact care because of the volatility and hazardous nature of the fuel being transported. Langley Research Center was asked to assist in the detection of flaws by nondestructive methods to determine whether a defect existed in the secondary barrier of one tank of the first ship of the LNG tanker class being built at the shipyard.

The secondary barrier was located inside the tank wall. The tank itself was already assembled inside the ship. Therefore, a nonstandard, nondestructive evaluation method was required. Probe techniques were found usable, but the large internal surface area of the tank together with the small size of the defects made such methods inadequate. Ultrasonic techniques using computer enhancement to detect defects and their locations were proposed but were found unworkable since normal random ship noise would null or obscure the noise caused by a slight diffusion leak.

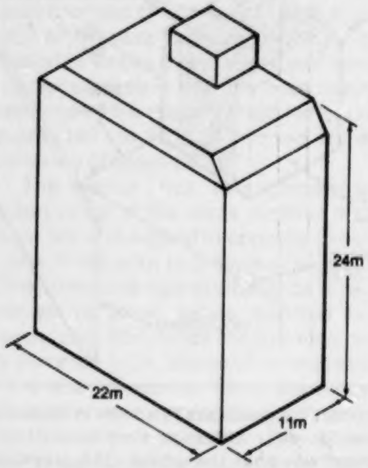

Figure 1. **Rectangular LNG Tank** with trapezoidal dome must be free of defects because of the hazardous nature of LNG.

The LNG tank is a rectangular structure with a trapezoidal-shaped dome, as shown in Figure 1, with walls of stainless steel corrugated for strength. The inside wall is shown in Figure 2. The inner wall of the tank has a layer of stainless steel (the primary barrier). The tank is tested to ensure that no cryogenic liquid can penetrate this layer, and all welds are finished, polished, and thoroughly examined to ensure leakproof conditions. There are additional layers of balsa, plywood, and insulation. The 3.4-mm plywood sheet *is called the secondary barrier* and forms a fuel-tight boundary between the stainless-steel wall and the outer mild-steel wall. The criteria for the tank to pass inspection require that neither the stainless-steel nor the mild-steel walls leak and that only a certain rate of diffusion of gas occurs across the secondary barrier.

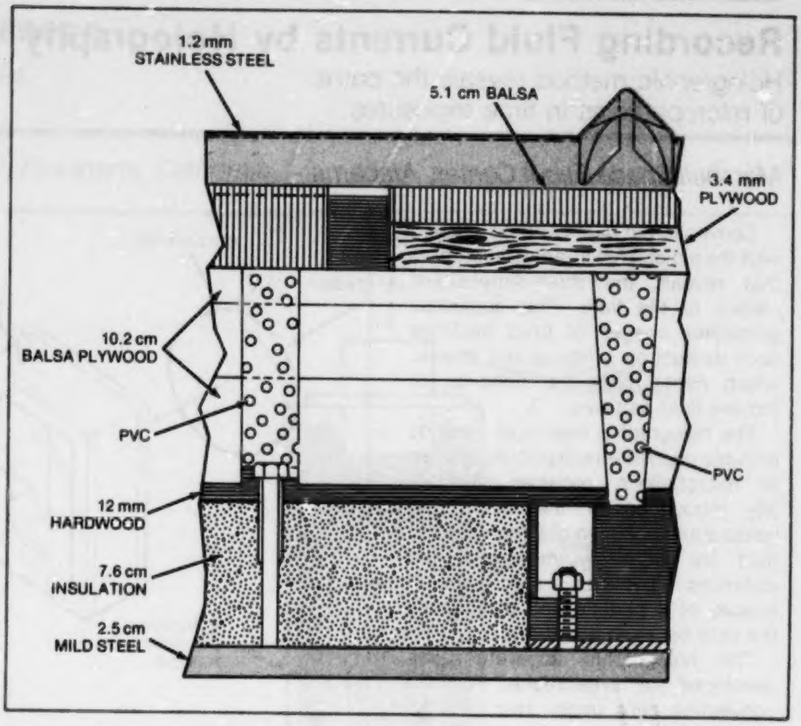

Figure 2. **LNG Tank Wall** consists of several layers that include steel and wood construction and insulation.

The equipment used for the infrared scans is commercially-available AGA 680 camera systems with 8°, 25°, and 45° lenses. These systems operate over a spectral range of 3 to 5.6 μm using a liquid-nitrogen-cooled InSb detector; they have a temperature resolution of 0.2 K at 303 K. If the regions between the primary and outer barriers of the tank wall are evacuated and very cold nitrogen gas is inserted into the outer area (between the outer wall and the secondary barrier) while the primary barrier is observed with the infrared scanner, the secondary barrier leakage will show as a cold spot on the primary barrier. To accentuate this effect, the inner wall is heated to 310 K or greater using a *large airhose* to bring in hot air.

Several defects were found. Even though none of the holes detected reached a total of integrated defect size of 2.5 cm in diameter in wall area of 1,280 m^2, (the criteria for tank acceptance required no hole larger than 2.5 cm diameter, which was exceeded in this tank) the infrared system was able to resolve them because of the diffusion and spreading effect at the primary boundary. These defects were confirmed by the use of ultrasonic and thermometer probe devices. Needed repairs were made at these areas.

The infrared technique has proved itself an efficient method of determining defects in this application with minimal expenditure of time and manpower. These tests could be repeated during the life of the tanker and make more complicated testing unnecessary. The tests also confirmed that the tank did not have any major defects, and the tank was certified.

This work was done by Andronicos G. Kantsios of **Langley Research Center.** *For further information, Circle 60 on the TSP Request Card.*
LAR-12655

Recording Fluid Currents by Holography

Holographic method reveals the paths of microparticles in time exposures.

Marshall Space Flight Center, Alabama

Convection in fluids can be studied with the aid of a holographic apparatus that reveals the three-dimensional motion of the fluid. The apparatus eliminates images of fixed particles such as dust on windows and lenses, which might mask the behavior of moving fluid particles.

The holographic flowmeter records multiple-exposure holographic images of "microballoon" particles intentionally introduced in the fluid. The velocity and direction of streams in the fluid are found by measuring the distances between reconstructed images of a particle and dividing by the time between exposures.

The holographic apparatus was developed for experiments on fluid convection cells under zero gravity. The principle is adaptable to the study of a variety of fluid processes — for example, electrochemical plating and combustion in automotive engines.

In the present form of the apparatus, microballoons (100-μm-diameter, neutrally-buoyant, hollow glass particles) are suspended in a water-filled cell that has four transparent plastic sides and two aluminum sides (see figure). One of the aluminum sides is heated while the other is cooled, so that convection currents are created in the water. A beam from a helium/neon laser passes through the cell and strikes a photographic film. A reference beam from the same laser also strikes the film, without passing through the cell. The two beams produce interference patterns that contain information about the positions of the microballoons in the cell.

The film is exposed four times; the first two exposures are separated by 2 seconds, the second and third by 8 seconds, and the third and fourth by 4 seconds. When the holographic image on the film is reconstructed, the multiple exposures show the successive positions of microballoons as they are moved by convection currents. The velocities of the microballoons are computed from the distances between successive images and the known interval between exposures.

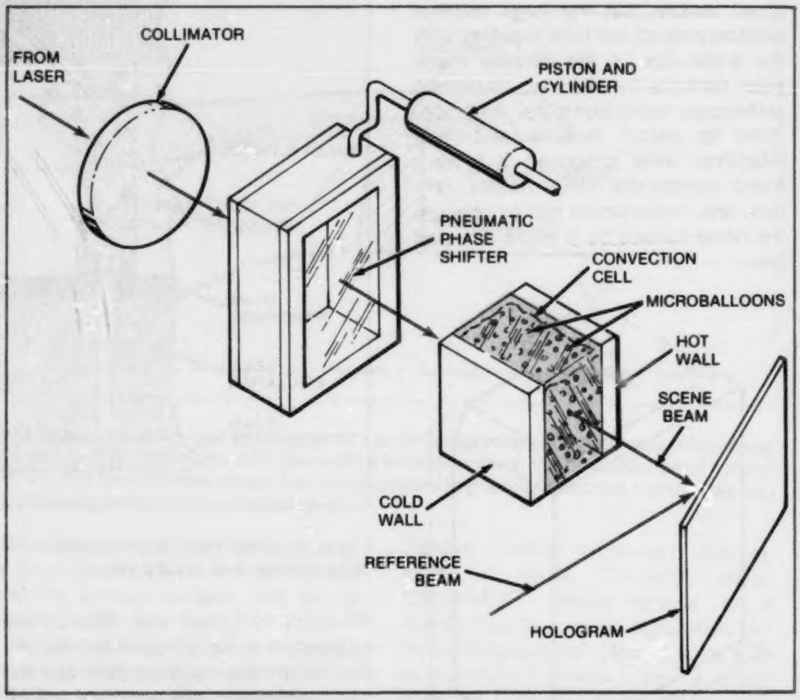

The Key to Noise-Free Recording of moving-particle positions is a shift in phase of the laser beam passing through the convection cell. Although simply rotating a glass plate from a plane normal to the beam will shift the phase, the proposed pneumatic phase shifter shown here would be more precise. Altering the pressure of the air in the shifter alters the phase of the light passing through it.

Between the second and third exposures, the beam passing through the cell is shifted in phase by 180°. This phase shift cancels images of fixed particles that may have been recorded on the film during the first two exposures. Without this background "noise," the moving particles are much easier to discern.

A simple glass microscope slide serves as the phase shifter. Rotation of the glass from a position normal to the scene beam to a new position 3° away from the normal changes the path of the beam by 1/2 wavelength, corresponding to a 180° phase shift.

In a planned phase shifter, the primary beam would be passed through an air cell before passing through the convection cell. The pressure in the air cell is varied by a piston, and the light passing through it is advanced or retarded in phase. A pressure change of 0.115 atmosphere (0.16×10^5 N/m^3) in a cell with windows separated by 1 cm is sufficient to shift the phase by 180°.

This work was done by Lee O. Heflinger and Ralph F. Wuerker of TRW, Inc., for **Marshall Space Flight Center.** *For further information, Circle 61 on the TSP Request Card.*
MFS-25373

Downhole Pressure Sensor

Pressure sensor for oil and gas wells
is not affected by temperature.

NASA's Jet Propulsion Laboratory, Pasadena, California

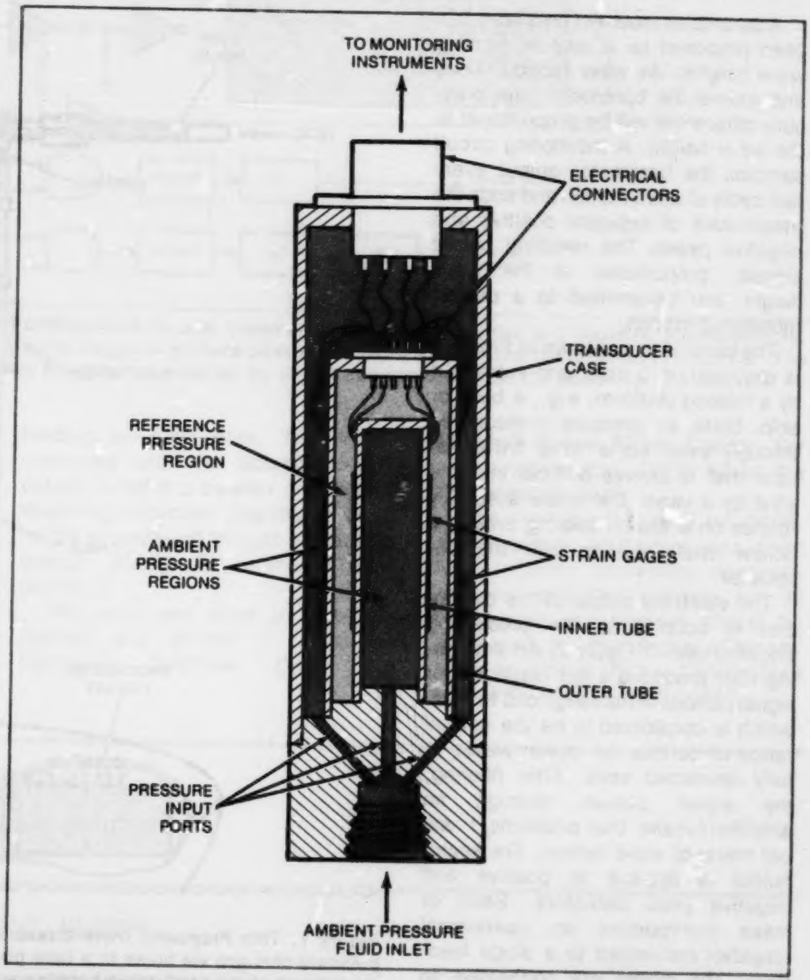

Proposed Pressure Sensor is unaffected by temperature changes. It utilizes strain gages to measure the downhole pressures in petroleum reservoirs. The inner and outer tubes are made of identical material and move in opposite directions in response to pressure. That doubles the displacement, making the instrument sensitive to relatively small pressure changes. The temperature effects are canceled because both tubes respond in the same way to any temperature change.

A proposed downhole pressure sensor remains accurate in spite of varying temperatures. Very accurate, sensitive, and stable downhole pressure measurements are needed for a variety of reservoir engineering applications, such as deep petroleum reservoirs, especially gas reservoirs, and in areas of high geothermal gradient.

Pressures in these applications may reach 15,000 psi (103.5×10^6 N/m^2), and instruments must measure pressure changes of less than 1 psi (6.9×10^3 N/m^2) occurring gradually over a period of weeks. The accuracy of conventional pressure sensors is too much affected by the relatively high temperatures (180° to 350° C) involved in the recovery of heavy oil.

The sensor has two concentric tubes made of the same material that contract and expand in opposite directions in response to pressure changes. The strain (see figure) difference is detected by strain gages mounted on each tube. Both tubes are mounted on a common base, and each is exposed to ambient pressure. Since the tubes have the same expansion coefficient, their relative motion is determined solely by the ambient pressure. Temperature changes affect both to the same extent, and the thermal effect is canceled.

If the ambient pressure is higher than the reference pressure, the outer tube contracts and the inner tube elongates; the ambient displacement produces twice the change of a sensor with a single tube. The opposite happens when the ambient pressure is lower than the reference. Small tube displacements are easily detected by the sensitive strain gages. These gages produce large indications for small pressure changes.

The electrical transducer for the sensor is a Wheatstone bridge with four active strain gages of the vacuum sputtered type. Since all four gages are subjected to identical strains from temperature effects, bridge output is not altered as a result of the temperature changes.

This work was done by C. Martin Berdahl of Caltech for **NASA's Jet Propulsion Laboratory**. *For further information, Circle 62 on the TSP Request Card.*
NPO-14729

Oceanic-Wave-Measurement System

An inexpensive system
accurately records wave heights.

Marshall Space Flight Center, Alabama

A barometer mounted on a buoy has been proposed as a way of sensing wave heights. As wave motion raises and lowers the barometer, the pressure differential will be proportional to the wave height. A monitoring circuit samples the barometer output every half cycle of wave motion and adds the magnitudes of adjacent positive and negative peaks. The resulting output signals, proportional to the wave height, are transmitted to a central monitoring station.

The barometer as shown in Figure 1 is mounted on a mast and supported by a floating platform; e.g., a buoy or ship. Static air pressure is measured through small holes in a horizontal tube that is always pointed into the wind by a vane. The entire assembly rotates on a sealed bearing around a hollow shaft feeding into the barometer.

The electrical output of the barometer is coupled to the processing circuit shown in Figure 2. An integrating filter produces a flat response for signal periods in the range of 5 to 20 s, which is considered to be the normal range of periods for ocean waves in fully developed seas. After filtering, the signal passes through an amplifier/scaler that produces 1 volt per meter of wave motion. The scaler output is applied to positive and negative peak detectors. Each of these incorporates an operational amplifier connected to a diode feedback. The diodes are connected so that each detector responds only to its portion of the cycle.

As a wave rises, a signal is fed to a holding circuit comprising capacitor C_1 and resistor R_1. This stored value, controlled by relay, is then applied to an isolation amplifier that feeds the signal to the differential amplifier. The latter combines the inputs from the positive and negative detectors to produce a signal corresponding to the peak wave height.

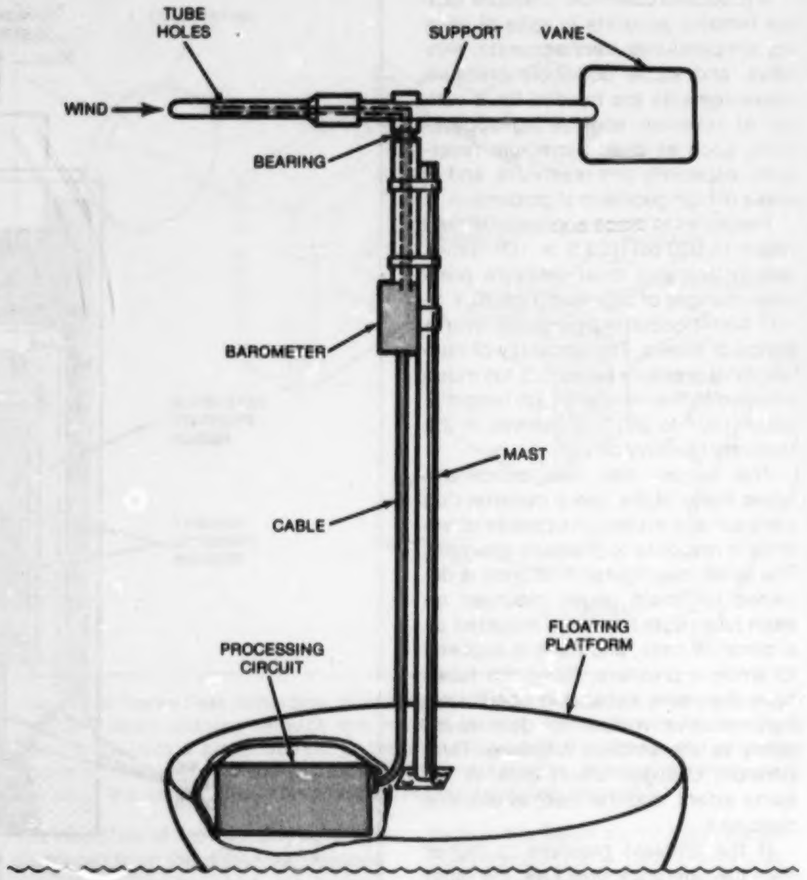

Figure 1. This Proposed Wave-Measurement System uses a barometer sensing pressure changes via holes in a tube pointed into the wind. Different air pressures are sensed as the platform is bobbing up and down with the waves. The signals are fed to an electronic processing circuit, which produces signals proportional to wave height.

Both peak detectors are timed by a circuit consisting of zero-crossing detector and Schmitt trigger. The zero-crossing detector responds only to the positive half of the barometer excursion cycle, activating the Schmitt trigger to produce a positive square-wave output with a period identical to the positive barometer cycle. The Schmitt trigger output is fed to two inverting-amplifier branches, each connected to the respective detector relay. Each relay is alternately energized by its inverting-amplifier branch. For example, the positive detector relay is energized during the initial 10 percent of the positive cycle, as determined by the RC constant of the first

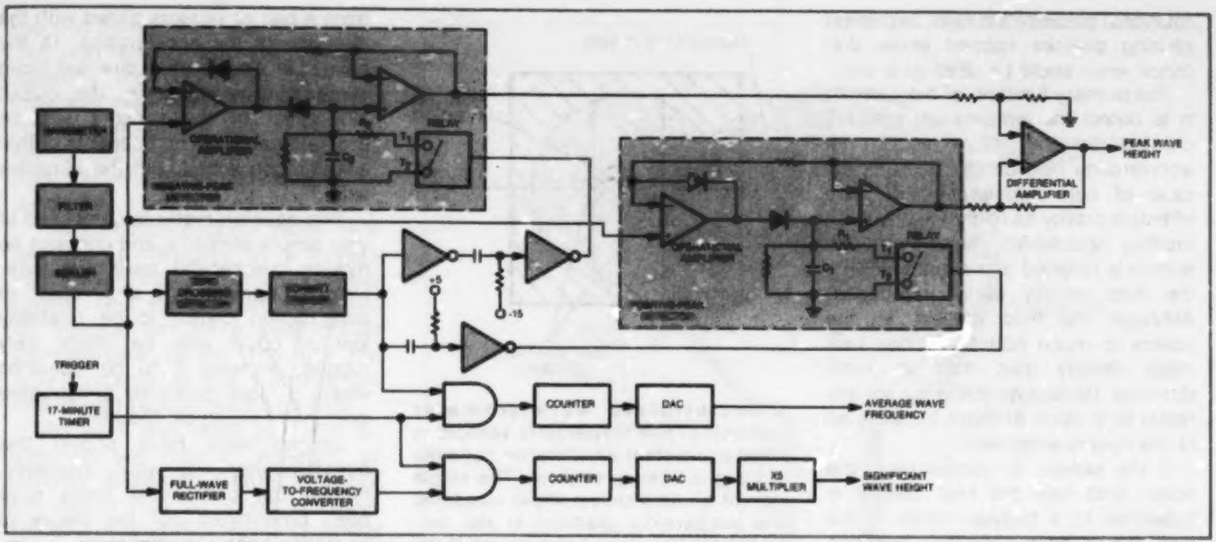

Figure 2. An **Electronic Processing Circuit** detects peak-to-peak barometer readings via positive and negative peak detectors. The detector outputs are synchronized by Schmitt trigger to produce peak wave-height output from the differential amplifier. The average wave frequency and significant wave height are processed by digital circuits shown on the bottom of the diagram.

amplifier branch, while the second relay is similarly energized during the trailing portion of the positive cycle via the double inverting branch. The storage capacitors are thus alternately discharged only during the short portion of the positive cycle, leaving sufficient time to recharge.

The average wave frequency is measured using a 17-min timer feeding an AND gate. This input, combined with the Schmitt trigger output, is fed to a counter and digital-to-analog converter. Significant wave height is measured through a separate branch during the same 17-min period.

This work was done by John F. Holmes and Ronald T. Miles of Computer Sciences Corp. for **Marshall Space Flight Center.** *For further information, Circle 63 on the TSP Request Card.*

This invention is owned by NASA, and a patent application has been filed. Inquiries concerning nonexclusive or exclusive license for its commercial development should be addressed to the Patent Counsel, Marshall Space Flight Center [see page A5]. Refer to MFS-23862.

Electrofluidic Accelerometer

Electrical sensors in a fluid measure thermal distributions caused by acceleration.

Langley Research Center, Hampton, Virginia

An electrofluidic accelerometer developed at Langley Research Center senses components of a linear or angular acceleration field and provides an analog signal as a direct function of each component. A typical application is as an active controlling element in an airplane autopilot.

Acceleration-measuring devices typically employ damped mass-and-spring systems to sense the acceleration; a strain gage, piezoelectric crystal, or optical sensors provide the output analog signal. Many devices are relatively complex and therefore relatively expensive. Also, some conventional accelerometers are delicate and can be easily broken or thrown out of calibration. In contrast, an electrofluidic accelerometer is lightweight, small, inexpensive, rugged, and requires little power.

The figure shows the basic arrangement of a single-axis electrofluidic accelerometer. In this basic form, a hollow chamber contains a gas or liquid. Suspended within the chamber are two, identical, small, temperature-sensing devices. The two sensors are spaced a few diameters apart along the housing axis, which is the sensitive axis for the device. A source of heat is required. This can be provided by a single, small filament midway between the sensors or by the sensors themselves if they generate heat as a byproduct of their operation, such as is the case with thermistors.

The illustrated arrangement is used to sense acceleration along a single axis. Additional pairs of sensors with properly oriented axes can sense other components of a linear acceleration field relative to the reference axes of the device. In the case of a

(continued on next page)

rotational acceleration field, two linear sensing devices spaced some distance apart could be used as a unit.

The primary function of the sensors is to detect the temperature gradient created by the influence of the acceleration field on the fluid. In the case of zero acceleration or zero effective gravity as might exist with an orbiting spacecraft, heat from the source is radiated and conducted into the fluid equally in all directions. Although the fluid closest to the source is much hotter and has less mass density than that at some distance, there is no tendency for this hotter fluid mass to move because all of the fluid is weightless.

If the sensor is accelerated, the hotter fluid near the heat source is subjected to a buoyant force in the direction of the acceleration because its mass reaction to the acceleration, or its weight, is less than that of the cooler and more dense fluid.

Therefore, the hotter fluid is forced away from the source in the direction of the acceleration, and the thermal gradient pattern is distorted. A finite output differential will be obtained from a pair of sensors alined with the direction of the acceleration. In the case of an acceleration directed along some intermediate axis, the output differential of the sensors will be proportional to the components of that acceleration alined with the sensitive axis.

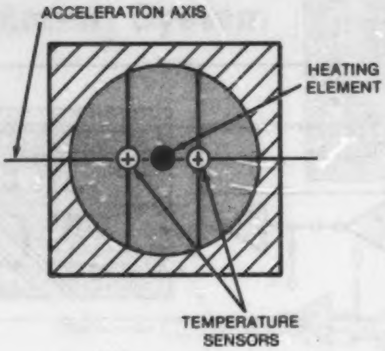

Electrofluidic Accelerometer consists of two temperature sensors in fixed equidistant positions on opposite sides of a heating element. The single pair of sensors shown above measures the temperature gradient in the surrounding fluid along a single axis. If the device is accelerated, the gradient changes because of the buoyant force on the hotter (thus lighter) portion of the fluid.

This accelerometer is composed of very simple elements and contains no moving mechanical parts. Its size, weight, complexity, and cost of construction appear to be relatively low. It could also be made very rugged, allowing it to be operated where a more delicately constructed instrument would be ill-suited.

Limited tests have shown this accelerometer will work. However, neither the operational limits have been determined nor the theory of operation been substantiated.

This work was done by Donald E. Hewes of **Langley Research Center.** *No further documentation is available.*

Inquiries concerning rights for the commercial use of this invention should be addressed to the Patent Counsel, Langley Research Center [see page A5]. Refer to LAR-12493.

Flashback-Free Combustor

All-zirconia construction prevents fuel in the supply line from igniting.

Langley Research Center, Hampton, Virginia

An all-zirconia combustion chamber for testing fuels prevents "flashback" — accidental extension of the flame into the fuel supply line. The chamber consists of a hemispherical injector on a base surrounded by a hemispherical cap (see figure). A fuel/air mixture feeding through the transition tube enters the chamber combustion cavity through 40 injector holes. The combustion products are exhausted through 25 holes in the cap. The cap has two additional ports for thermocouple and gas-sampling probes.

Previously, the injector was made of iron/nickel alloy or quartz. However, these materials passed enough heat through the injector wall to ignite the fuel/air mixture within the injector, particularly at or near stoichiometric fuel-to-air ratios. The zirconia-injector thermal resistance prevents the flashback without special cooling procedures (such as diluting the fuel/air mixture with nitrogen).

The zirconia injector operates at higher temperatures and lasts longer than the quartz injectors (which were superior to the nickel-alloy version). Moreover, zirconia is not subject to solid-state diffusion to the same extent as the quartz. The two materials, zirconia and quartz, tend to interdiffuse when in contact at high temperature, which degrades the ultimate lifetime of the quartz injector.

The combustor base, cap, and injector are cast from commercial zirconia powder. The injector is cast in two split molds — one for the core and one for the external surface. The molded injector is cured at 1,800° F (980° C). It is then placed in the combustor hemisphere, and the complete combustor assembly is cured at 3,000° F (1,650° C).

The combustor burns both gaseous and liquid fuels. Liquid fuels are supplied from closed vessels pressurized with nitrogen and are mixed by adjusting the flow rates from the individual reservoirs. The liquids are atomized in nozzles located close to the combustor to prevent high-boiling-point fractions from condensing in the supply line.

The combustion-cavity flame temperature is measured by a traversing iridium/iridium-rhodium thermocouple. Gas samples are withdrawn for analysis through a water-cooled stainless-steel probe. The NO and NO_X contents of the samples are determined by chemiluminescence.

This work was done by Swen G. Anderson and Noel T. Wakelyn of **Langley Research Center.** *Further information may be found in NASA TP-1472 [N79-28259/NSP] "Chemical Kinetic Modeling of Benzene and Toluene Oxidation Behind Shock Waves"* **[$6]**. *A copy may be purchased [prepayment required] from the National Technical Information Service, Springfield, Virginia 22161.*

Inquiries concerning rights for the commercial use of this invention should be addressed to the Patent Counsel, Langley Research Center [see page A5]. Refer to LAR-12666.

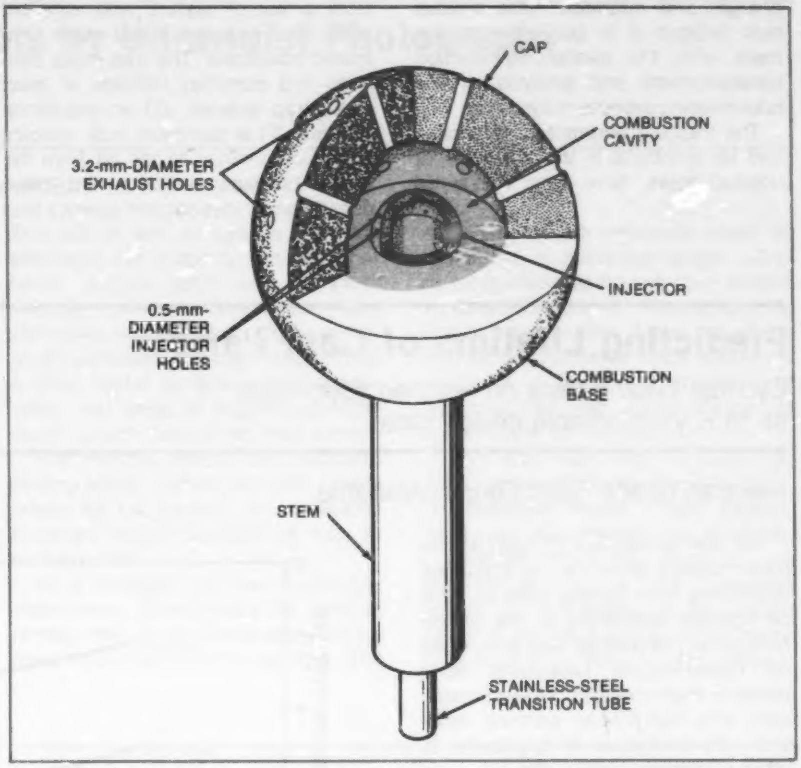
CAP
COMBUSTION CAVITY
3.2-mm-DIAMETER EXHAUST HOLES
INJECTOR
0.5-mm-DIAMETER INJECTOR HOLES
COMBUSTION BASE
STEM
STAINLESS-STEEL TRANSITION TUBE

All-Zirconia Combustor used for testing various fuels prevents flashbacks in the fuel supply line. A fuel/air mixture enters the combustion cavity through holes in a hemispherical injector. Combustion products leave the cavity through holes in the hemispherical cap.

Measuring Radiation Effects on MOS Capacitors

Avalanche injection combined with current/voltage technique give a more complete picture about irradiation charging.

NASA's Jet Propulsion Laboratory, Pasadena, California

A major problem of interpreting the effect of ionizing radiation on MOS capacitors stems from the fact that it is difficult to distinguish between the charge at the Si/SiO_2 interface and the charge in the bulk of the oxide. Conventional current-voltage (CV) techniques could not resolve that difference and have led to conflicting reports that shifts of flatband and threshold voltages follow either a square or cube dependence on the oxide thickness. The distinction, however, becomes clearer using electron-avalanche injections to obtain independent information on charge trapping in the oxide.

The electron-injection technique serves as a powerful probe of the resulting trapped-hole distribution after irradiation because it was determined that the electrons only annihilate the trapped holes. Other effects, such as other electron traps and interface state generation, are negligible in the injection range used.

In the avalanche injection, the MOS capacitors are pulsed to produce avalanche breakdown in the depletion region of Si. This process generates energetic minority carriers that are injected into the oxide, surmounting the barrier at the Si/SiO_2 interface. The holes are injected from n-type Si and the electrons from p-type Si. The voltage shift ΔV of the MOS CV curve due to the trapping of injected carriers is measured as a function of the total density of carriers injected per unit area.

The result for dry oxides indicates a distribution of dominant hole traps that tails off rapidly from the Si/SiO_2 interface with a characteristic distance between 150 and 200 A (Wet oxides suggest a value of about 400 A.) These results are consistent with results of previous etch-back photoemission studies.

A large set of data on the CV shift (in the form of effective sheet density of

(continued on next page)

charge) and interface state buildup near midgap is in qualitative agreement with the avalanche-injection measurements and analysis of the hole-trapping process in the oxide.

The trapping parameters for holes, and for electrons in the presence of trapped holes, have been measured from a set of wafers with different oxide thickness processed under controlled conditions. The trap cross sections and densities indicate at least three trap species: (1) an interfacial species; (2) a dominant bulk species that is determined to tail off from the silicon interface; and (3) a third, lower density and cross-section species that may be distributed throughout the bulk of the oxide.

This work was done by Mietek Bakowski, Richard H. Cockrum, Joseph Maserjian, and Nasser Zamani of Caltech for **NASA's Jet Propulsion Laboratory**. *For further information, Circle 64 on the TSP Request Card.*
NPO-14700

Predicting Lifetime of Cast Parts

Cyclical loading tests on notched specimens at 78 K yield reliable design data.

Marshall Space Flight Center, Alabama

The life expectancy of cast aluminum machine parts can be predicted accurately from fatigue tests at 78 K on notched specimens of the aluminum alloy. The method was developed for rocket-engine turbopump parts made of high-strength, heat-treatable alloy with high silicon content; however, the technique is applicable to other aluminum-casting alloys.

The notched specimens produce test results that more accurately reflect actual part performance than do the smooth specimens previously used. In addition, the test data are far less scattered with the notched specimens. Design curves based on the test data predict the lifetime of a part for any stress state and mean stress, over the range of stress concentrations spanned by the data.

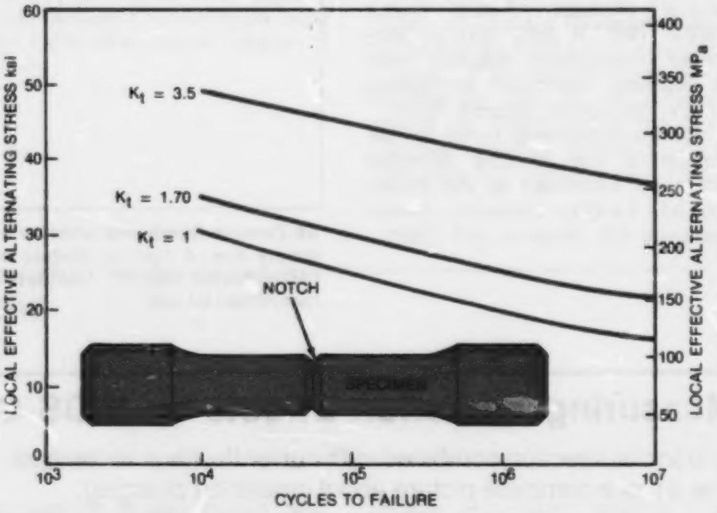

Part Lifetime Increases With Decreasing Stress and Stress Concentration. In this plot, the ratio of minimum to maximum cyclical axial load is -1.0. The values of K_t represent stress concentration, with K_t = 1 being the value for an unnotched, smooth specimen.

Specimens for the tests were taken from a sandcasting of a turbopump part and were machined and heat-treated like the part. A groove was cut around the specimen at its center (see figure). The radius at the bottom of the notch was selected to give the desired stress concentration. For example, with a 0.009-inch (0.229-mm) radius, the elastic stress concentration factor K_t is 3.5. The specimens were subjected to a sinusoidally-varying axial load until they fractured at the notch. The ratio of minimum to maximum alternating stress was -1 (that is, equal but opposite stress) for some specimens, 0 for others (stress alternated between zero and a maximum value without changing direction), and +0.5 for still others (the minimum stress was one-half the maximum). The specimens were cooled with liquid nitrogen to a temperature of -320° F (78 K) to accelerate failure and thus reduce the time required for the test.

The local effective alternating stress and the peak stress were calculated for each specimen from its geometry and loading. The results were plotted as stress versus cycles to failure.

The same procedure can be used to develop similar plots for other parts. The only difference is that the notch radius should be altered to correspond to the stress concentration in the part. From such plots, a designer can readily observe the influence of stress and stress concentration on operating life.

This work was done by R. A. Cooper of Rockwell International Corp. for **Marshall Space Flight Center.** *For further information, Circle 65 on the TSP Request Card.*
MFS-19549

Detecting Contaminants by Ultraviolet Photography

A simple technique could help prepare clean metal surfaces.

Marshall Space Flight Center, Alabama

The relatively high ultraviolet absorptivity of most organics as compared to metal is suggested as a basis for detecting traces of contamination. By photographing a metal surface in ultraviolet light, contaminants that might otherwise interfere with the adhesion of surface coatings or with welding and brazing, could be detected and removed. Real-time monitoring of the cleaning process is also possible if an ultraviolet-sensitive television camera is used instead of photographic film.

Most adhesives, solvents, lubricants (except 100-percent aliphatic hydrocarbon oils), and other potential contaminants absorb radiation in the range from about 2,400 to 2,800 Å. Skin oils as well as various polymers also have this property. On the other hand, metals such as aluminum strongly reflect radiation at these ultraviolet wavelengths. Consequently, an ultraviolet photographic print of a clear metal surface would appear white, and areas of organic contamination would show up as dark spots.

The method would use standard photographic techniques with quartz lenses for the camera. An ultraviolet floodlight would irradiate the area to be inspected.

In a variation of the technique, interference filters would be used to remove the visible spectrum, allowing parts to be inspected in daylight. The sensitivity of the technique could be enhanced if short-wavelength ultraviolet is used and the detection system is tuned to pick up fluorescence at longer wavelengths. Many absorbers that do not fluoresce in the visible do fluoresce in the ultraviolet portion of the spectrum and would appear as bright spots on the film.

This work was done by David W. Neiswander of Martin Marietta Corp. for **Marshall Space Flight Center.** *No further documentation is available.*

Inquiries concerning rights for the commercial use of this invention should be addressed to the Patent Counsel, Marshall Space Flight Center [see page A5]. Refer to MFS-25296.

Detecting Surface Faults on Solar Mirrors

Two tests determine the quality of spherical mirrors.

NASA's Jet Propulsion Laboratory, Pasadena, California

Two quality-control tests determine reflectivity and curvature faults of concave solar mirrors. These mirrors have relatively large radii of curvature anywhere from 10 to 500 ft (3 to 150 m) and concentrate solar energy to heat water boilers or other collector surfaces. Acceptable mirrors reflect between 85 to 95 percent of the incident solar energy and focus it into a "spot," or aperture, the size of the surface to be heated.

For economy, the mirrors are not fabricated with great precision, and they are tested without the sophisticated procedures used on high-quality optical-grade mirrors. However, to insure adequate quality control, special tests have been worked out for the production of these mirrors.

The first test, easily adaptable to mass production, tests the mirror reflectivity. A light source illuminates the entire mirror, and a photometer at

(continued on next page)

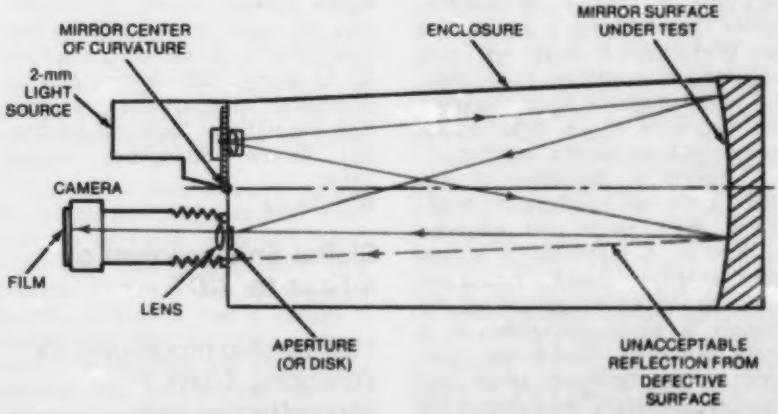
MIRROR CENTER OF CURVATURE
2-mm LIGHT SOURCE
ENCLOSURE
MIRROR SURFACE UNDER TEST
CAMERA
FILM
LENS
APERTURE (OR DISK)
UNACCEPTABLE REFLECTION FROM DEFECTIVE SURFACE

Curvature Defects in solar mirrors are easily revealed by photographing the mirror surface. A calibrated aperture placed in front of the camera lens admits rays reflecting only from acceptable areas of the mirror, blocking out the diverging rays reflected from the defective areas. The defects can pinpoint problems that may exist in production. The same photograph can be obtained using a calibrated disk instead of the aperture, except that, this time, only the defective areas would be exposed.

the mirror focusing point measures the reflected energy. The reflected intensity is compared with the incident.

The second test is used to study the rejected mirrors to identify possible faults in production. Curvature faults are detected by photographing the mirror surface or by examining it with the photometer. The mirror is mounted on a special frame at the end of a tunnellike enclosure (see figure). A large-aperture camera and a light source are at the other end.

Light from a 2-mm source illuminates the entire mirror and is reflected back into the camera. Rays reflected from a correctly curved surface pass at or near the camera axis; rays diverging from faulty surfaces enter through the edge of the camera lens or miss it entirely.

Some divergence is acceptable; e.g., a 3-min deviation from the "perfect" angle of reflection. A calibrated aperture or disk corresponding to acceptable deviation may be placed in front of the camera lens. If the aperture is used, rays reflecting from an acceptable surface will expose the film. The diverging rays will miss the aperture, leaving unexposed areas on the film. A disk would do just the opposite, producing the same pattern but showing the unexposed areas as acceptable and the exposed areas as faults. An assortment of apertures or disks can be used in one test.

This work was done by Maurice J. Argoud, Michael S. Shumate, Walter L. Walker, and Richard A. Zanteson of Caltech for **NASA's Jet Propulsion Laboratory**. *For further information, Circle 66 on the TSP Request Card.*
NPO-14684

Books and Reports

These reports, studies, and handbooks are available from NASA as Technical Support Packages (TSP's) when a Request Card number is cited; otherwise they are available from the National Technical Information Service.

Refraction Corrections for Surveying

A mathematical analysis for determining true range and elevation

Optical measurements of range and elevation angles are distorted by the refraction of Earth's atmosphere. Rather than following a straight-line path from source to target, light rays follow an arcing path that gives longer than actual range and larger elevation. The magnitude of the distortion increases with decreasing elevation.

A theoretical discussion of this effect, along with equations for determining exact range and elevation corrections, is presented in a new report. Potentially useful in optical site surveying and related applications, the analysis is easily programed on a pocket calculator. Input to the equations is the measured range and measured elevation; the output is the true range and true elevation.

The measured data are inserted in a set of three nonlinear differential equations that are derived by applying Snell's law of refraction and assuming that the atmospheric modulus of refraction (1 minus the index of refraction) decreases exponentially with altitude. The solution of the equations, by Runge-Kutta integration, yields the true range and elevation.

The report includes examples of solutions to the equations and tables of short-, medium-, and long-range corrections. For a measured range of 10 km and a measured elevation of -0.239°, the range correction is 4 meters and the elevation correction is 0.36 milliradian. This translates into a displacement of about 4 meters along the line of sight and a displacement of 3.6 meters in altitude. At 100 km, the displacements are 40 m and 36.7 m, respectively.

This work was done by William M. Lear of TRW, Inc., for **Johnson Space Center.** *Further information may be found in TM-80803 [N80-10907/NSP], "Refraction Corrections for Surveying" [$5]. A copy may be purchased [prepayment required] from the National Technical Information Service, Springfield, Virginia 22161.*
MSC-18664

Digital Enhancement of X-Rays for NDT

Step-by-step procedures for enhancing X-rays in nondestructive tests

A new report is virtually a "cookbook" for the digital processing of industrial X-rays. Computer techniques, previously used primarily in laboratory and developmental research, have been outlined and codified into step-by-step procedures for enhancing X-ray images. Those involved in nondestructive testing should find the report a valuable asset, particularly if visual inspection is the method currently used to process X-ray images. Whereas the eye has only limited capability to distinguish shades of gray and tends to distort the data, a computer "sees" typically 256 gray shades, without introducing inadvertent distortion.

While no actual software is included in the report, many of the required image-enhancement programs are generally available. (Some are available through COSMIC; see page A8 of this issue of *NASA Tech Briefs.*) Others are described in the report along with their arithmetic statements and algorithms.

The report gives step-by-step procedures for applying the software. For example, the process for deblurring an X-ray to recover edge information and detail is to digitize the image through video averaging to increase the signal-to-noise ratio, then to filter the image through a high-emphasis filter to boost the high spatial frequencies on the original image.

Another example is the method for improving the visibility of image detail and minimizing the effects of some shading nonlinearities. The procedure involves: digitizing, filtering by using a high-pass filter that suppresses the low spatial frequencies, redistributing the gray levels in the filtered image for optimum presentation to the eye by using a contrast stretch filter, and filtering with a low-pass filter to attenuate slightly the highest spatial frequencies if excessive "graininess" exists.

Also included in the report are methods for removing random noise by using a low-pass filter, extracting only edge information utilizing a nine-point gradient, and displaying small gray-level variations using a density slicer routine. Other procedures are for improving the contrast of the X-ray or a particular feature of the X-ray by using a contrast stretch filter and for minimizing the effect of shading nonuniformity by the use of the ramp and background masks and the linear combiner.

All the procedures were successfully tested. The first example mentioned was used to analyze a blurred X-ray of a pump. The second example was used to reveal information about defects in a Space Shuttle solid rocket motor.

This work was done by Robert L. Butterfield of **Kennedy Space Center.** *To obtain a copy of the report, Circle 67 on the TSP Request Card.*
KSC-11118

Design Considerations for Mechanical Face Seals

Two companion reports cover configuration and lubrication of the seals.

Two companion reports have been published that deal with design considerations for improving the performance of mechanical face seals, one of a family of devices used in the general area of fluid sealing of rotating shafts. One report deals with basic seal configuration and the other with lubrication of the seal.

Basic Configuration

Basically, a mechanical face seal prevents leakage of a fluid along a rotating shaft that passes through a housing or pressure vessel. Sealing is accomplished by a stationary (nonrotating) primary-seal ring that bears against the face of a mating ring (seat) mounted on the shaft. Axial loading, from the sealed pressure and from springs, maintains the contact between the primary ring and the mating ring. Sealing occurs at the primary-seal faces.

Four basic primary-seal assembly configurations and their parts nomenclature are identified: a rotating primary ring with the sealed liquid at either the outside diameter (O.D.) or the inside diameter (I.D.) and a nonrotating primary ring with the sealed liquid at either the O.D. or the I.D. Occasionally, counterrotating and differential speed applications are encountered where both the primary ring and the mating ring are rotating.

The most common configuration, especially in pumps, is the rotating primary ring configuration. Its principal advantage lies in the relative ease of attachment to straight shaft sections without affecting the seal face alinement. The primary ring assembly is easily attached to the shaft by setscrews, friction fits, or similar means that assemble directly on a smooth shaft diameter.

Nonrotating primary ring configurations are often found in applications where space is limited or where the rotating speeds are high. The principal advantage of the nonrotating primary ring is the absence of centrifugal forces on both the primary and secondary rings.

The rotating primary ring with the sealed liquid at the O.D. has a number of advantages compared to the rotating primary ring with the sealed liquid at the I.D.: (1) centrifugal force tends to retard leakage; (2) centrifugal force tends to centrifuge solid particles away from the primary seal and springs; thus there is a tendency to be self-cleaning; and (3) the sealed pressure tends to put the seal rings into compression.

The rotating primary ring I.D. configuration has advantages in that it is easier to install; and in sealing corrosive fluids, the seal can be designed so that metal parts do not come into contact with the corrosive fluid.

Three basic secondary-seal assembly configurations are described: compression packings, automatic packings, and bellows diaphragm. The principal feature of the compression packing system is that it utilizes a mechanical load on the packing. Automatic packings are all of those packing rings and devices that are self-energized by the sealed pressure and do not normally require an auxiliary load to maintain sealing contact. Bellows diaphragms have no sliding packing surfaces, thus eliminating friction; they also eliminate the need for separate springs since the bellows serves both the sealing and the face-loading functions.

The technique for seal pressure balancing and its application are described. The PV factor, an arbitrary mathematical relationship used to evaluate the severity of an application, is described and evaluated. Finally, the operating conditions for various applications of low-pressure seals and their failure mode are discussed.

Seal Lubrication

This report reviews the state-of-the-art of liquid-lubricated face seals and summarizes current thinking in regard to seal lubrication. Consideration is primarily given to that class of seals that operate on a full lubricating film.

Face seals operate with a fluid film separating the faces of the primary seals. Within this general class of lubrication there are four different modes of lubrication: Liquid Film Forces, either (a) hydrodynamic due to waviness and angular misalinement (low pressure) or (b) combined hydrodynamic and hydrostatic (low speed, moderate to high pressures); and Liquid/Vapor Film Forces, either (c) thermally induced phase change or (d) thermally induced phase change combined with hydrodynamic and hydrostatic forces.

The report also points out that the lubricating-film thickness is very small (in the range of 1 micron) and therefore small variations in the primary-seal geometry have a dramatic effect on the lubricating process. In general, these small variations in primary-seal geometry are due to unplanned effects of thermal gradients, pressure distortions, wear, etc., which complicate construction of seal performance models.

The report indicates that seal lubrication is a complex mechanism involving many possible primary-seal geometries, liquid vaporization, hydrodynamic forces, hydrostatic forces, inertia and secondary-seal friction. However complex, certain conditions must be met for satisfactory liquid film lubrication: (1) Balance of Axial Forces — the pressure in the fluid film (opening force) must equal the closing force; (2) Positive Axial Film Stiffness — a positive film stiffness is required for stable operation; that is, if the closing force increases for some reason (shock load, etc.), then an

(continued on next page)

increase in the opening force must accompany any decrease in film thickness; and (3) Balance of Moments — the restoring moment generated by the film must be sufficient to balance the moments due to secondary-seal friction, hydrostatic forces, etc.

Current thinking in regard to seal lubrication is reviewed: The effect of energy dissipation in the thin lubricating film separating the sealing faces is pointed out, and the results of vaporization due to heating are illustrated. Also, hydrodynamic lubrication is reviewed, and an inherent tendency for the seal to operate with angular misalinement is shown. Recent work on hydrostatic effects is summarized, and the conditions for seal instability are discussed. Four different modes of seal lubrication are postulated with the particular mode strongly a function of speed and pressure.

This work was done by Lawrence P. Ludwig of **Lewis Research Center** *and Harold F. Greiner of Sealol, Inc. Further information may be found in:*

NASA TM-73735 [N78-13439/NSP], "Design Considerations in Mechanical Face Seals for Improved Performance, I. Basic Configurations" [$5], and

NASA TM-73736 [N77-33518/NSP], "Design Considerations in Mechanical Face Seals for Improved Performance, II. Lubrication" [$5].

Copies of these reports may be purchased [prepayment required] from the National Technical Information Service, Springfield, Virginia 22161.

LEW-13146

Computer Programs

These reports, studies, and handbooks are available from NASA as Technical Support Packages (TSP's) when a Request Card number is cited; otherwise they are available from the National Technical Information Service.

Regenerative Superheated-Steam Turbine Cycles

PRESTO program aids design and analysis of steam turbines.

One of the most important factors in the design of base-load or peak-load powerplants is an accurate analysis of the steam-turbine cycles involved. Several engineering options available in the design of steam-turbine cycles can significantly increase the generating efficiency of these powerplants. Of particular interest are the reheat and regenerative steam-turbine cycles that utilize the superheated steam normally available from large fossil-fueled steam turbines.

The PRESTO computer program was developed to analyze the performance of a wide range of steam-turbine cycles with special attention given to regenerative superheated-steam turbine cycles. PRESTO can be used to model standard turbine cycles, including such features as process steam extraction, induction and feedwater heating by external sources, peaking, and high back pressure. Expansion line efficiencies, exhaust loss, leakages, mechanical losses, and generator losses are used to calculate the cycle heat rate and the generator output. PRESTO provides the power engineer with a flexible aid for the design and analysis of steam-turbine systems.

PRESTO calculates the expansion line efficiency as a function of volume flow, pressure ratio, initial pressure, initial temperature, and the governing-stage design. This expansion line calculation is used along with packing leakages, valve stem leakages, mechanical losses, exhaust losses, and generator losses to determine the heat rate and generator output.

The PRESTO user specifies the throttle steam thermodynamic properties, the preliminary conditions of the governing stage, system pressure relations, and condenser conditions, as well as the cycle configuration. PRESTO calculates the working parameters for the cycle and executes a performance analysis of the full steam-turbine cycle.

The PRESTO analysis is performed by an iterative procedure that calculates the system operating parameters. All iterations begin at the high-pressure end of the cycle and progress toward the condenser. The use of this iterative procedure allows PRESTO to handle easily such options as parallel or series external heat input, process steam extraction, regressive feedwater heating, and reheaters. PRESTO outputs include cycle heat rate, cycle efficiency, generator output, losses, and other useful system parameters.

This program is written in FORTRAN IV for batch execution and has been implemented on an IBM 360 with a central memory requirement of approximately 230K of 8-bit bytes. PRESTO was developed in 1979.

This program was written by L. C. Fuller and T. K. Stovall of Union Carbide Corp. for **Lewis Research Center**. *For further information, Circle C on the COSMIC Request Card.*

LEW-13392

Stream-Tube Curvature Analysis

Pressure distribution and flow field at transonic speeds

The Stream-Tube Curvature Analysis Program accurately calculates the inviscid pressure distribution and flow field, including viscous displacement effects, around an arbitrary axisymmetric ducted body at transonic speeds. This computerized flow-field analysis predicts the transonic flow around long and short high-bypass-ratio fan duct nacelles with inlet and outlet flows having appropriate aerothermodynamic properties. The program makes possible parametric studies for evaluating nacelle design criteria and selecting configurations for further experimental investigations.

The inviscid solution technique used is based on a stream-tube curvature method. Engineers frequently rely on one-dimensional compressible flow relationships for a first-order solution to ducted flow. The stream-tube curvature approach is similar except that a number of confluent stream tubes, with slightly different properties, are added together to obtain the total flow in the channel. This method exactly satisfies the inviscid equations of motion in the limit as the size of the individual stream tubes approaches zero.

The program utilizes an automatic grid refinement procedure and solves the flow-field equations with a matrix relaxation technique. The location of incipient turbulent boundary-layer separation is identified when the calculated pressure gradients indicate sufficient cause. Due to its significance to performance predictions, a boundary-layer displacement calculation is coupled with the inviscid analysis.

A compressible turbulent boundary-layer solution is computed using the method of Stratford and Beavers, with turbulent separation predicted by the method of Stratford. Inclusion of these effects allows accurate evaluation of all nacelle forces. The user only needs to supply the program with configuration data, boundary coordinates, and channel flow properties. Program outputs include solution history, flow data, and boundary-layer data. The predicted pressure distributions have been favorably compared with through-flow nacelle test results obtained in wind-tunnel tests.

This program is written in FORTRAN IV and COMPASS for batch execution and has been implemented on the CDC CYBER 175 with a central memory requirement of approximately 108K (octal) of 60-bit words. The Stream-Tube Curvature Analysis Program was developed in 1972 and most recently updated in 1975.

This program was written by D. R. Ferguson and J. S. Keith of General Electric Co. for **Langley Research Center.** *For further information, Circle D on the COSMIC Request Card.*
LAR-11535

A Generalized Vortex Lattice Method

Aerodynamic load distributions are calculated for subsonic and supersonic flows.

The several variations of the vortex lattice method that are currently available have proved to be practical and versatile theoretical tools for the aerodynamic analysis and design of planar and nonplanar configurations. The success of the method is due in great part to the relative simplicity of the numerical technique involved and to the accuracy of the results obtained; however, most of the available procedures are for subsonic flow applications. The VORLAX program was developed to incorporate a direct extension of the vortex lattice method into the supersonic flow regime, thus providing the analyst with a full flow-range capability.

VORLAX has the capability of calculating the aerodynamic load distributions at subsonic and supersonic speeds for arbitrary nonplanar configurations. It is also capable of the inverse process: namely, the computation of the surface warp required to achieve a given load distribution. Correlations with experimental data have shown good agreement in the overall force and moment coefficients due to lift and in the distribution of load coefficients.

If the discrete vortex lattice is considered as an approximation to the surface-distributed vorticity, the generalized principal part of the solution integral yields a residual term to the vorticity-induced velocity field. This term is incorporated into the velocity field generated by the discrete vortex lines, thus making the vortex lattice method valid for supersonic flows. Techniques for simulating nonzero-thickness lifting surfaces and fusiform bodies with vortex lattice elements are included in the VORLAX program. Thickness effects of winglike components are simulated by a double (biplanar) vortex lattice layer.

Fusiform bodies are represented by a vortex grid arranged on a series of concentric cylindrical surfaces to simulate volume displacement effects and to compute surface pressure distributions accurately. A special technique was developed for the VORLAX program to perform the analysis of sideslip effects. The technique uses a combination of the skewed-wing approach and the skewed free-stream approach. The formulation utilizes a first-order perturbation solution, which does not involve the geometrical complications of the skewed-wing approach. Inputs to VORLAX consist of data including configuration geometry, free-stream parameters, and solution-control parameters. Outputs include vortex element locations, pressure coefficients, circulation strengths, and computational parameters.

This program is written in FORTRAN IV and COMPASS for batch execution and has been implemented on a CDC CYBER 175 with a central memory requirement of approximately 217K (octal) of 60-bit words. The VORLAX program was developed in 1977.

This program was written by William M. Baker, Robert D. Elliott, and Luis R. Miranda of Lockheed Aircraft Corp. for **Langley Research Center.** *For further information, Circle E on the COSMIC Request Card.*
LAR-12636

Vibration Modes and Frequencies of Structures

Finite-element procedure for coupled mass and stiffness matrices

The program SUDAN, Substructuring in Direct Analysis, analyzes natural modes and frequencies of vibration of structural systems. Based on a direct method of analysis that employs a substructures methodology, the program is used with structures that may be represented as an equivalent system of beams, springs, and rigid bodies.

A finite-element stiffness technique, in combination with a lumped-mass method that allows nondiagonal masses, is used to generate the stiffness and mass matrices for each substructure in a system. User-written constraint equations are used to join analytically the mass and stiffness matrices of the substructures to form the coupled mass and stiffness matrices of the complete structure.

The resulting generalized eigenvalue problem is reduced to symmetric standard eigenvalue form and is solved for all the modes and frequencies of the system. Both the mass and stiffness matrices of the coupled system may be singular simultaneously, in contrast to the usual assumption that one or the other is nonsingular. The SUDAN program has been successfully applied to airframe-vibration analyses.

The program is written in FORTRAN IV and has been executed on CDC 6400/6600 and CYBER 173/175 computers. Only a relatively few changes would be required for conversion to other computers. Development of the public version of SUDAN was completed in 1978.

This program was written by Barbara J. Durling and Raymond G. Kvaternik of **Langley Research**

(continued on next page)

Center. *For further information, Circle F on the COSMIC Request Card.*
LAR-12647

Predicting Propulsion-System Drag

Axisymmetric nozzle afterbody pressure distributions and drag are predicted at subsonic speeds.

The drag-producing components of an airplane propulsion system are usually installed in areas where the flow field is extremely complex. High body slopes and long boundary-layer runs, especially in the afterbody nozzle region, result in strong viscous effects on the boattail drag. The viscous nature of the jet-exhaust plume further complicates the flow in this region. Because of these strong viscous interactions, most methods used for predicting the installed propulsion-system drag are limited to empirical techniques.

The DONBOL computer program analytically predicts the axisymmetric nozzle afterbody pressure distributions and drag. The predictions are based on a Neumann solution for inviscid external flow coupled with a modified Reshotko-Tucker integral boundary-layer technique, the control volume method of Presz for calculating flow in the separated region, and an inviscid one-dimensional solution for the jet-exhaust flow. Comparisons with experimental data indicate that the program accurately predicts the pressure distributions of boattail afterbodies for which the jet-exhaust plume can be simulated by a solid body. For other configurations, the nozzle pressure drag seems to be significantly underpredicted. This method is limited to subsonic free-stream mach numbers below those for which the flow over the body becomes sonic.

The DONBOL program is based on the assumption that the flow is composed of a viscous layer near the body, an inviscid external flow, and if present, an inviscid jet-exhaust flow. A Neumann solution for incompressible flow, along with a compressibility correction, is used to determine the inviscid external flow.

The inviscid boundary of the jet-exhaust flow is calculated based on one-dimensional isentropic flow theory. Properties of the viscous boundary layer, both attached and separated, and the location of any separation on the nozzle boattail are calculated using the method of Presz, King, and Bateau. The concept of a discriminating streamline is used to avoid singularities in the boundary-layer calculations. However, the boundary-layer displacement thickness, the discriminating streamline shape, and the inviscid jet boundary are functions of the pressure distribution along the body and the jet boundary.

The final flow solution is obtained by iterating between the inviscid outer-flow solution, the inviscid jet-plume solution, and the viscous boundary-layer solution until a specified degree of convergence occurs. Inputs include body geometry, solution-control parameters, free-stream conditions, and jet-exhaust conditions. Outputs include detailed information on the iterative calculations of the flow field.

This program is written in FORTRAN IV for batch execution on a CDC 6600 computer and has an overlaid central memory requirement of approximately 76K (octal) of 60-bit words. The DONBOL program was developed in 1979.

This program was written by Lawrence E. Putnam of **Langley Research Center**. *For further information, Circle G on the COSMIC Request Card.*
LAR-12619

Heat Conduction in Three Dimensions

Transient and steady-state solutions for complex geometries

A multidimensional heat-conduction program computes the transient temperature history and the steady-state temperatures of complex body geometries in three dimensions. Emphasis is placed on the type of problems associated with the Space Shuttle thermal protection system, but the program could be used in the thermal analysis of most three-dimensional systems.

The thermal model is subdivided into sections, or nodes, to a level of approximation that yields the required accuracy. Inputs to the program consist of a geometrical description of the physical system, the material properties, and selected boundary conditions. The boundary conditions account for heat flux, reradiation, radiation interchange, convection, fixed temperatures, and phase changes. The program will accommodate a thermal model with as many as 500 nodes, 4,000 conductors, 3,600 radiation-interchange conductors, and 75 of each type of boundary condition.

The program solves the differential equations describing the transient and steady-state behavior of the model using finite-difference techniques. For the transient analysis, the user may select either a forward-difference method, a midpoint-difference (Crank-Nicolson) method, a backward-difference method, or an alternating-direction method to solve the governing equations numerically. For the steady-state analysis, a modified backward-difference method is available. Program outputs are in the form of temperature-versus-time histories for each section of the thermal model.

The heat-conduction program is available for IBM and CDC machines: The IBM version is written in FORTRAN IV and OS Assembler for batch execution and has been implemented on an IBM 370-series computer with a central memory requirement of approximately 450K of 8-bit bytes. The CDC version is written in all-FORTRAN IV for batch execution and has been implemented on a CDC CYBER 170-series computer with a segmented memory requirement of approximately 230K (octal) of 60-bit words. This heat-conduction program was originally developed in 1976, with the latest update occurring in 1979.

This program was written by Thomas M. Danza, Lloyd W. Fesler, and Richard D. Mongan of Rockwell International Corp. for **Johnson Space Center**. *For further information, Circle H on the COSMIC Request Card.*
MSC-18616

Machinery

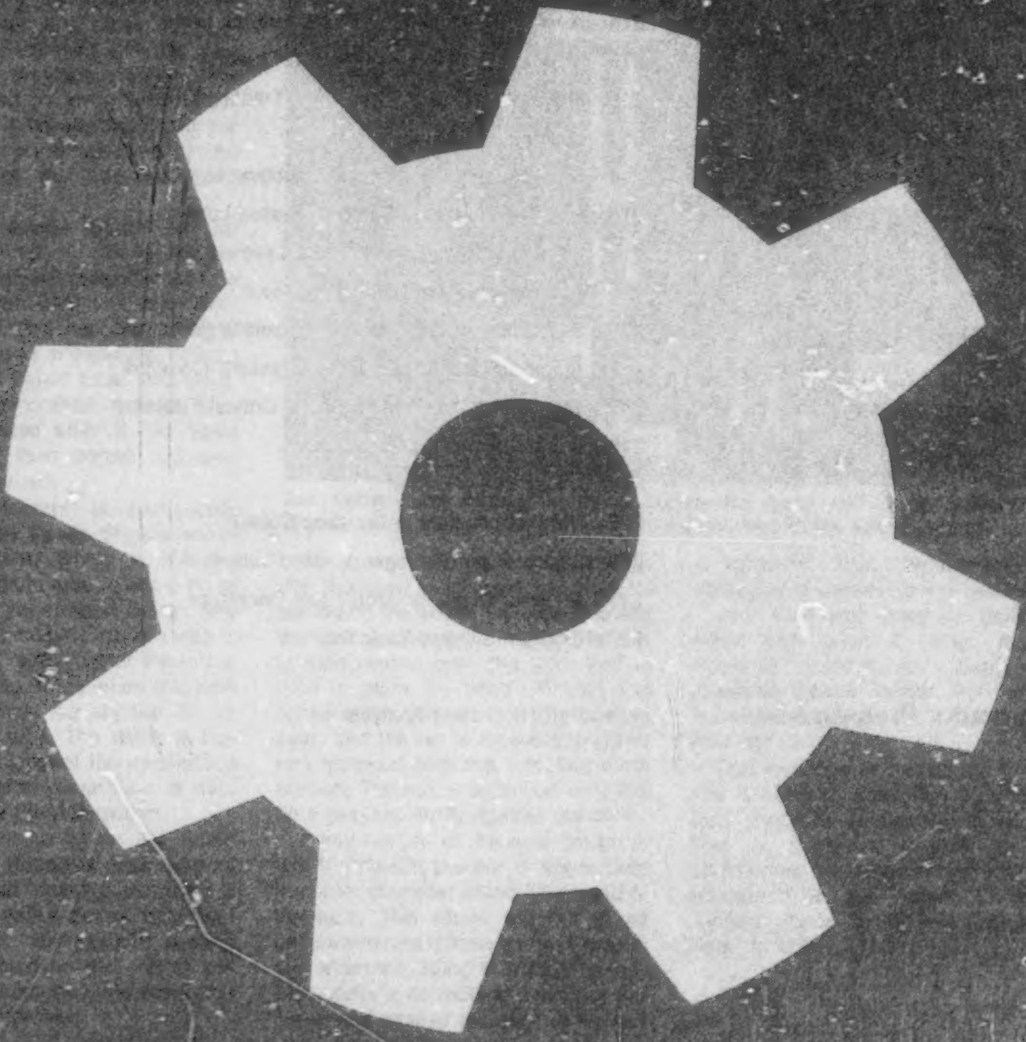

Hardware, Techniques, and Processes

213 Flared-Tube Attachment Fitting
213 Tube-Flare Inspection Tool
214 A Versatile Tunnel Acts as a Flexible Duct
215 Mechanical Hand for Gripping Objects
216 High-Performance, Multiroller Traction Drive
217 Locknut Preload Tool
218 Self-Adjusting Mechanical Snubbing Link
218 Bayonet Plug With Ramp-Activated Lock
219 Heat-Pipe Sensor for Remote Leveling
220 Automatic 35-mm Slide Duplicator
221 3-D Guidance System With Proximity Sensors
222 Automatic Connector Joins Structural Columns
222 Test Fittings for Dimensionally Critical Tubes
223 Electromechanical Slip Sensor
224 X-Ray Beam Pointer
225 Handtool Assists in Bundling Cables
225 Sleeve Puller Salvages Welded Tubes
226 A Linear Magnetic Motor and Generator
227 Cryogen-Storage-Tank Support

Computer Programs

228 Rotor Transient Analysis

Flared-Tube Attachment Fitting

Tubes are flared first, then installed, with a fitting that can be disassembled and reused.

Lyndon B. Johnson Space Center, Houston, Texas

A new fitting for attaching flared tubing to valves and other flow-line components is installed after the tube is flared. In previous designs, the fitting is placed on an unflared tube, then the tube is flared, and finally the tube and fitting are attached to the mating end of the flow-line component.

The new design offers several advantages: First, it allows the installed fitting to be disassembled so that the parts can be inspected; second, the fitting can be salvaged intact and reused or replaced without damaging the flared tube; and third, the tube can be coated, tempered, or otherwise treated after it has been flared, rather than before, as was previously required.

This last feature is particularly valuable for the Space Shuttle entry-air data system, where a silicide-coated columbium tube is attached to the nose-cap penetration fitting. The silicide (mostly columbium silicide) is a ceramic-like layer. Since the brittle coating tends to crack when the tube is flared, it must be applied on an already-flared tube. The ability to disassemble and inspect the connection and coating after installation is also required in the Shuttle system.

As shown in the figure, the fitting consists of a threaded male portion with a conical seating surface, a hexagonal nut with a central hole, and a split ferrule. The conical seating surface is formed on the end of the valve or other component to which the tube is to be attached.

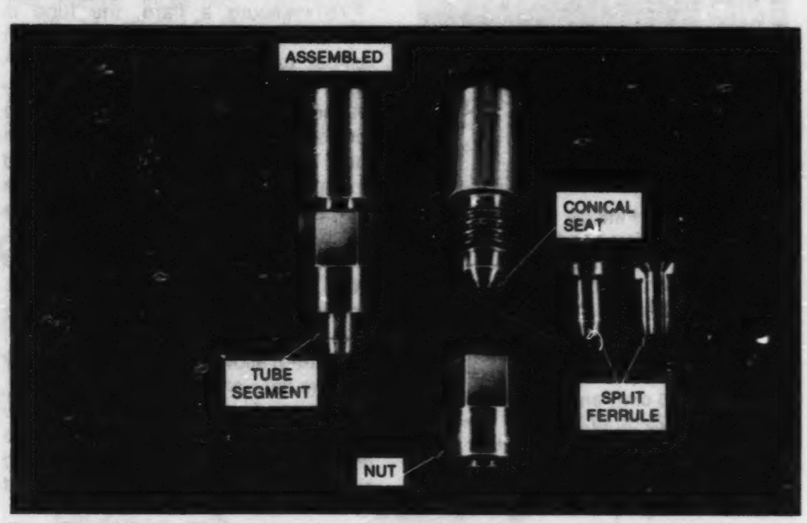

The **Flared-Tube Fitting** is shown assembled (left) and disassembled. The already-flared tube will be inserted through the hole in the hexagonal nut.

To connect the flared-tube end to the threaded male part, the nut is placed on the end of the tube and slid back along its length. The split ferrule is then nested over the flare and is held in place by hand. Finally, the flared end is placed over the conical seat, and the nut is moved into place and screwed onto the threaded male portion. The nut is tightened until the flare presses firmly against the seat.

A key feature of the new design is that the hole in the nut is larger than the outer diameter of the flared end of the tube. This allows the nut to be unscrewed and removed from the tube end when the fitting is disassembled. Also, there is no rubbing motion of the flared end against the seat as the nut is tightened. Thus, the possibility of damaging a coated tube is reduced.

This work was done by Innis D. Alkire and Julian P. King, Jr., of Rockwell International Corp. for **Johnson Space Center.** *For further information, Circle 68 on the TSP Request Card.*

This invention is owned by NASA, and a patent application has been filed. Inquiries concerning nonexclusive or exclusive license for its commercial development should be addressed to the Patent Counsel, Johnson Space Center [see page A5]. Refer to MSC-18416.

Tube-Flare Inspection Tool

Self-alining pins reveal the flare angle on an optical comparator.

Lyndon B. Johnson Space Center, Houston, Texas

A simple tool, consisting of two stainless-steel pins bonded to a rubber plug, checks flared tube ends for flare angle and symmetry. Its primary function is to inspect tubes before they are installed, thereby eliminating the expense and inconvenience of repairing leaks caused by imperfect flares. Other possible uses are in measuring hole tapers, countersink angles, and bearing-race angles.

(continued on next page)

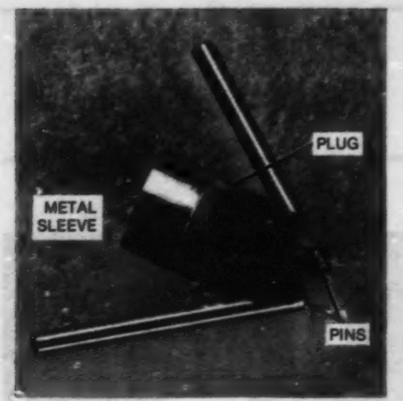

Figure 1. **Steel Pins on a Rubber Plug** conform to the flared end when the plug is inserted in a tube. The fixture dimensions for 1/4-in. (0.63-cm) tubing are: plug length, 1/2 in. (1.27 cm); plug diameter, 0.05 in. (0.13 cm) less than the maximum flare diameter; pin length length, 0.75 in. (1.9 cm); pin diameter, 0.062 in. (0.16 cm); and centerline hole diameter, 0.025 in. (0.063 cm). The tool dimensions can be scaled for other tube sizes.

As shown in Figure 1, the two stainless-steel pins rest in slots 180° apart on one end of the plug. Each pin is bonded with rubber cement at an angle of 45° with respect to the plug centerline. A metal sleeve is slipped over the rubber to prevent it from splitting after repeated use.

To measure a flare, the tube is clamped in a V-block on the table of an optical comparator. The shaft of a holding fixture is inserted in the centerline hole of the plug, and the axis of the tool is alined with the centerline of the tube. The comparator table is adjusted until the shadows of the tube and the tool are visible in the center of the comparator screen (Figure 2).

The rubber plug is gently engaged with the tube so that the rubber "gives" and the pins aline with the flare. The shadow of the seated pins on the screen allows the operator to verify that the flare angle is within tolerance. To check for any eccentricity, the operator slightly loosens the clamp holding the tube in the V-block and slowly rotates the tube. The range of movement of the pins is a measure of the symmetry of the flare.

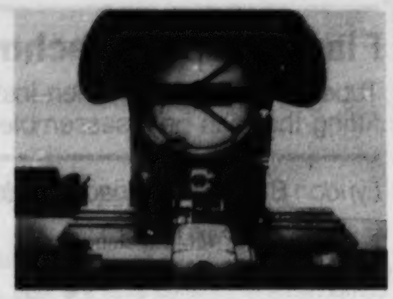

Figure 2. The **Shadows of the Pins** on an optical comparator screen reveal the angle of a flared tube.

The new tool does not demand any special operator skill. Only a few minutes are required for a measurement.

This work was done by Gerald E. Meunier of Rockwell International Corp. for **Johnson Space Center**. *No further documentation is available.*
MSC-19636

A Versatile Tunnel Acts as a Flexible Duct

Tunnel duct can be expanded, contracted, and bent

Marshall Space Flight Center, Alabama

A tunnel activated by a cable assembly can be expanded, contracted, and bent similar to a flexible duct without uncoupling at either end. The tunnel was developed to join a reusable space vehicle with a cargo module and could be modified to be used as a hydraulic or a pneumatic hose or duct connecting complex moveable joints in remote manipulators and earth-moving machinery.

Two sets of equal-length cables operated by a single winch control the tunnel length. The cables, guided through rings and pulleys, move in unison regardless of the way the tunnel is deployed.

As shown in the simplified illustration, the tunnel is a bellows tube structure sealed to the module and the vehicle, and the cables run inside it. The module slides on the vehicle tracks and is normally attached to the vehicle by pins inserted through clevis members.

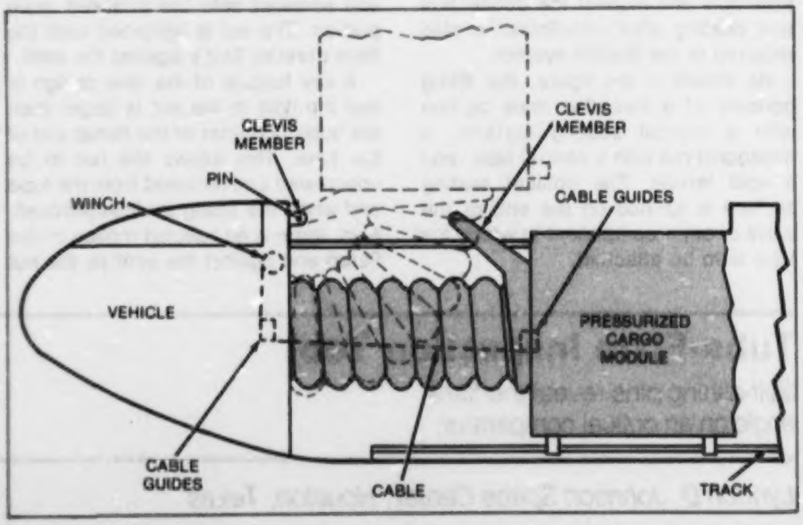

Flexible Tunnel joining a space vehicle with a pressurized cargo module can be contracted, expanded, or bent. The tunnel is inflated by air pressure, its length being controlled by a set of cables. It can be deployed in a straight line or at an angle, depending on how the cargo module is attached to the vehicle.

If the module is deployed in a straight line as shown in the figure, the pins are disconnected, and the cable is paid out. The cables loose, differential pressure (about 1 atm) applied from the module then inflates the tunnel to its maximum length. The tunnel length can be controlled by restraining forces of the cable system.

If the module is to be deployed above the vehicle, the cables are wound up to contract the tunnel until the clevis fixtures aline and the module is secured to the vehicle. The cables are again paid out, and the differential air pressure forces the cargo module upward over the vehicle.

The tunnel and its mechanism might also find applications in the airlines and marine industries. The design could be modified for underwater work.

This work was done by Newton D. Brown, Nicholas C. Costakos, and Gordon L. Jeppesen of Goodyear Aerospace Corp. for **Marshall Space Flight Center.** *For further information, Circle 69 on the TSP Request Card.*

This invention has been patented by NASA [U.S. Patent No. 3,952,976]. Inquiries concerning nonexclusive or exclusive license for its commercial development should be addressed to the Patent Counsel, Marshall Space Flight Center [see page A5]. Refer to MFS-22636.

Mechanical Hand for Gripping Objects

Remotely operated end effector can grip objects of different sizes and shapes.

Marshall Space Flight Center, Alabama

An improved end effector serves as a "hand" for a remote-manipulator spacecraft system to grasp objects of various sizes. The device has a built-in flexible wrist-joint "cartilage" for increased gripping force without significant strain on the mechanical connections.

Two identical jaws are used to grip objects (see figure). Each jaw has a set of laterally-spaced finger plates. The plates of one jaw are set off from the other so that they intermesh when the jaws are closed. An object is held by V-shaped notches running across each jaw. These notches allow objects as small as a wire or as large as the notch to be gripped firmly.

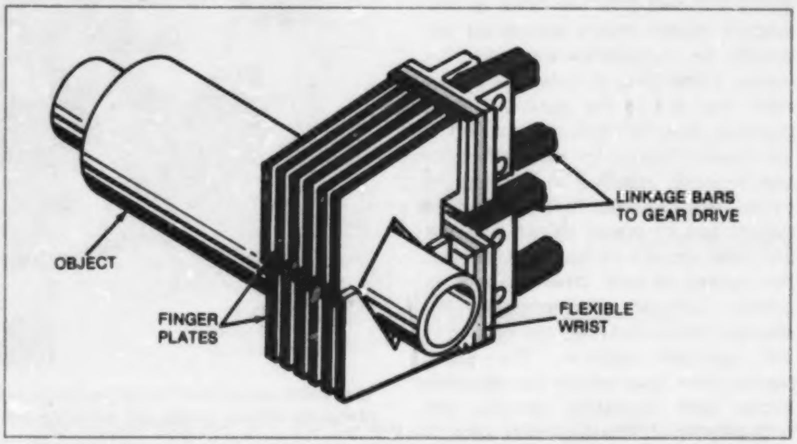

This End Effector has interlocking finger plates to grip the object. The end effector can grasp objects as small as wires and up to the size fitting the V-notches.

Each jaw is driven by a pair of parallel linkage bars coupled to the corresponding wrist joints by a pair of spaced pivots. The pivot support plate is separated from an integral finger backplate by a flexible material such as synthetic rubber. This material, held to the plates by rivets or brads, forms the flexible wrist joint.

The opposite ends of the parallel linkage bars attach to a pair of spaced plates enclosing a gear mechanism. Each inner linkage bar is rigidly joined to a gear plate, and the gear plates mesh with a bevel gear driven by an electric motor directly behind.

The end effector is guided toward a target object by a mechanical arm linked with the central control station. The object is approached with the jaws widely open. Once the jaws are alined with the object, the bevel gear is activated to close the jaws.

This work was done by Keith H. Clark and James D. Johnston of **Marshall Space Flight Center.** *For further information, Circle 70 on the TSP Request Card.*

This invention is owned by NASA, and a patent application has been filed. Inquiries concerning nonexclusive or exclusive license for its commercial development should be addressed to the Patent Counsel, Marshall Space Flight Center [see page A5]. Refer to MFS-23692.

High-Performance, Multiroller Traction Drive

High power at large gear ratios using sun-and-planet drives

Lewis Research Center, Cleveland, Ohio

A fixed-speed-ratio traction drive (NASVYTRAC) has been developed that can transmit high power across a large speed ratio using a compact cluster of rollers. This traction drive transmits power without gear teeth, through shear forces on the thin lubricant film that separates the drive rollers. An automatic loading mechanism regulates the normal load between rollers so that sufficient normal load is present to transmit the required torque without slip or overloading.

The traction drive, shown in the photo consists of a single-stage planetary roller with two rows of five stepped planet rollers contained between the concentric sun and ring rollers. Either the sun roller or the ring roller may act as the input or output member. Reaction torque is carried to the housing by a pair of rolling-element ball bearings installed in the second (outer) row of planet rollers. The first (inner) row of planet rollers and the sun roller require no bearings, so that the number of total drive bearings is greatly reduced. Furthermore, the reaction torque bearings are located in the optimum position, the outer planet-roller row, where the reaction forces and operating speeds are relatively small. The ring-roller assembly is positioned by its contact with the second row of planet rollers and is splined to the low-speed input/output shaft.

Because the planet rollers in the drive are in three-point contact with adjacent rollers, the roller cluster has a high degree of stability: The first row of planet rollers and the second row of planet rollers (to the extent of bearing internal clearance) will shift under load until a nearly-ideal force balance is established. Consequently, slight mismatches in roller dimensions or housing distortions under load or thermal gradients will have little effect on drive performance other than to cause a slight change in roller orientation. This greatly simplifies manufacturing tolerances.

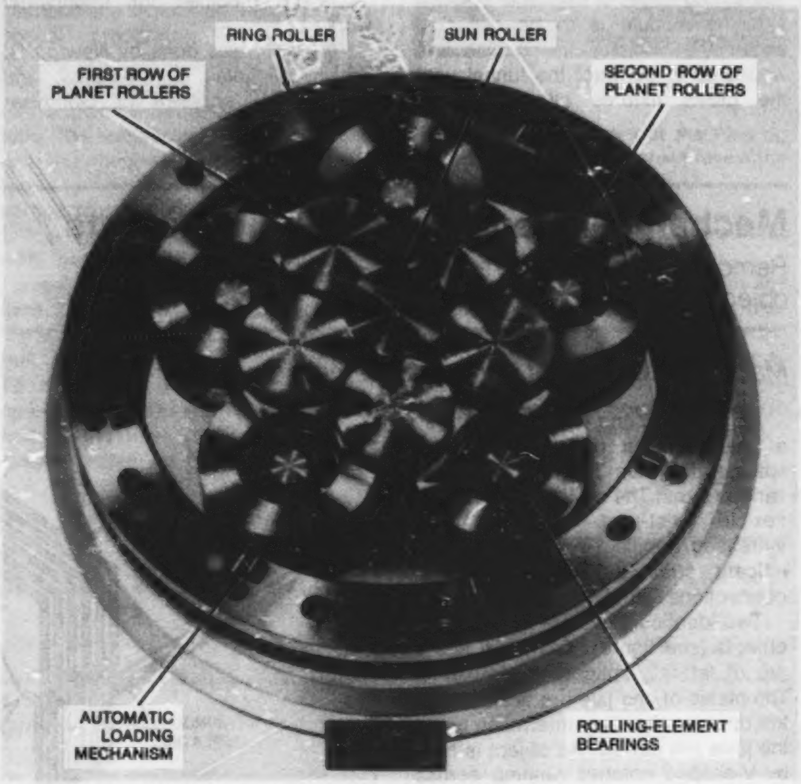
RING ROLLER
SUN ROLLER
FIRST ROW OF PLANET ROLLERS
SECOND ROW OF PLANET ROLLERS
AUTOMATIC LOADING MECHANISM
ROLLING-ELEMENT BEARINGS

Test Drive consists of a single-stage planetary roller with two rows of five stepped planetary rollers contained between concentric sun and ring rollers.

The number of planet-roller rows, the number of planet rollers in each row, and the relative diameter ratios at each contact are variables to be optimized according to the overall speed ratio and the uniformity of contact forces. In general, drives with two planet rows are suitable for speed ratios to about 35 to 1, and drives with three planet rows are suitable for ratios to about 150 to 1. The input or output member can be either the ring or the central roller depending on whether the speed is to be increased or decreased.

Although conventional oils can be used, traction fluid is preferred to lubricate and cool the rollers and to transfer torque. The traction fluid used is a synthetic, high-traction cycloaliphatic hydrocarbon fluid. The traction coefficient of the fluid is approximately 50 percent greater than conventional mineral oils, which permits a smaller drive to be used. The traction fluid readily becomes a glassylike substance as it is forced between the rollers under high pressure and therefore can transmit a large amount of traction without the rollers actually touching. At the same time, the lubricant forms a protective elastohydrodynamic film that separates the rollers and almost completely eliminates roller wear. This lubricant film, together with the multiple roller elements in highly loaded contact between the flexible ring and the sun roller, provides excellent torsional vibration damping characteristics and promotes quiet performance.

In comparison with conventional transmission gearing, this new traction drive provides large reduction ratios (up to 150:1) at high speeds in a single stage without differential action. This is unlike conventional gears that require a series of multiple gear meshes. The NASVYTRAC drive can be constructed to transmit 500 horsepower and higher and is quite capable of operating at speeds to 400,000 rpm (roller surface velocities greater than 50,000 fpm). The practical upper speed limit is generally dictated by the other driven or driving mechanical components (bearings, seals, couplings, etc.) in the system.

Parametric tests on a 14.7-to-1-ratio NASVYTRAC drive at speeds to 73,000 rpm showed peak efficiencies in excess of 95 percent. This compares quite favorably with conventional multistage gearing at equivalent speeds.

The NASVYTRAC drive is capable of transmitting in excess of 7 horsepower per pound of transmission weight, compared to today's best gearboxes, which transmit approximately 4 horsepower per pound.

This work was done by S. Lowenthal, D. A. Rohn, and E. Zaretsky of **Lewis Research Center,** *N. E. Anderson of the U.S. Army Research & Technology Laboratories, and A. Nasvytis of Transmission Research, Inc. Further information may be found in NASA TP-1378 [N79-13369/NSP], "Performance of a Nasvytis Multiroller Traction Drive" [$4.50]. A copy may be purchased [prepayment required] from the National Technical Information Service, Springfield, Virginia 22161.*

Inquiries concerning rights for the commercial use of this traction drive should be addressed to NASTEC, Inc., Mr. Richard C. Klein, President, 1700 Ohio Savings Plaza, 1801 East Ninth Street, Cleveland, Ohio 44114, Telephone: [216] 696-5157.
LEW-13347

Locknut Preload Tool

A small tool replaces a large torque wrench for turning locknuts.

Lyndon B. Johnson Space Center, Houston, Texas

Massive locknuts that fix the stroke of hydraulic actuators on the Shuttle engines could previously be turned only with a very large torque wrench — one that could supply the required 1,500 ft-lb (2.0×10^3 N-m) moment. With the assistance of the simple sleevelike tool shown in the figure, however, it now takes only about 150 ft-lb (199 N-m) to loosen the nuts, a torque small enough to be supplied by more common hand wrenches. Other advantages, such as reduced cost and weight, the ease of manipulation in the cramped space near the actuators, and portability, are also realized with the new tool.

Basically, the preload tool takes advantage of the hydraulic force of the actuator to "stretch" the threaded rod on which the locknut turns. This relieves some of the force on the nut, reducing the amount of torque needed to turn it.

As shown in the figure, the locknut fixes the stroke length of the actuator piston. (The actuator is one of two that control the orientation of each Shuttle engine.) To change the stroke length, the nut is loosened, the rod end is turned, and, when the proper length is set, the nut is retightened.

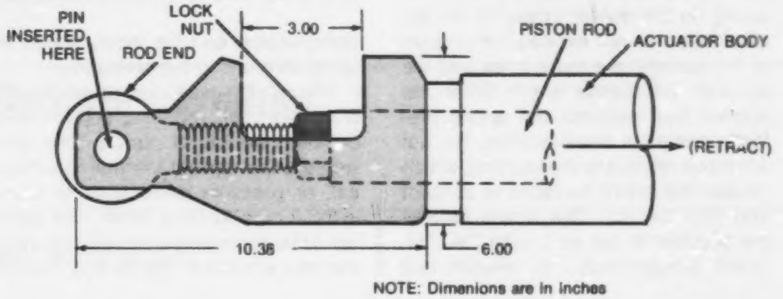

The Preload Tool fits over the rod end, as seen in this simplified drawing of the Shuttle actuator. When the piston rod is retracted, the threaded rod stretches, relieving some of the pressure on the locknut. The nut can then be turned by a small wrench through the cutout slot.

To turn the tightened nut, the preload sleeve is placed over the rod end, which has been removed from its clevis on the engine mount. The actuator is then gradually pressurized (retracted or extended) until the hole in the preload tool alines with a hole in the rod end bearing. Finally, a pin is inserted through the alined holes.

With the preload tool in place, the actuator is pressurized in the retraction direction. Since the rod end is pinned to the preload tool, the piston rod cannot move; and the rod stretches, relieving some of the pressure on the locknut. A small wrench inserted through the slot on the tool turns the nut, while a second wrench holds the piston rod to prevent it from turning.

This work was done by John E. Greenwood and Jerome F. Kauppi of Rockwell International Corp. for **Johnson Space Center.** *No further documentation is available.*
MSC-16153

Self-Adjusting Mechanical Snubbing Link

An all-mechanical shock-absorber concept has several advantages over hydraulic devices.

Lyndon B. Johnson Space Center, Houston, Texas

A proposed purely-mechanical load-support link will automatically adjust its length under light loads when the relative motion is slow. It will automatically lock at any position when the onslaught (acceleration) exceeds the design limits for which the link is set. The device will not leak oil or require periodic servicing and inspection common to hydraulic shock absorbers (snubbers).

The concept (see figure) consists of a threaded rod and a free-running nut. The nut is supported between two antifriction bearings held in position by two opposing preloaded springs. The nut flange has brake surfaces on each side, which are positioned just to clear the mating surfaces of the housing.

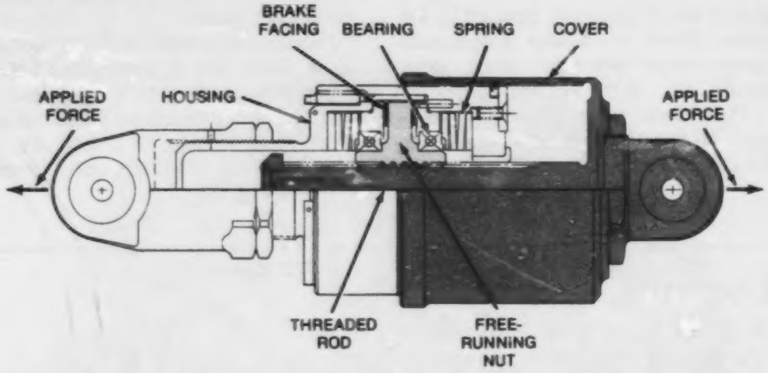

All-Mechanical Snubbing Link utilizes a threaded rod and a nut that rotates under applied low-magnitude loads. Under high loads, the nut moves left or right relative to the housing, until one brake surface bears against the facing surface. With the nut prevented from turning, the mechanism acts as a solid link. In a snubber proposed for the Space Shuttle, the preload springs are 500-lb (2,220-N) disk springs.

When opposing loads are applied to the link, the nut will rotate due to forces acting on the helical thread. If the applied loads do not exceed the preload of the springs, the nut rotates and the snubber will change length. When the applied load exceeds the spring preload (tension or compression), the nut will move relative to the housing, which causes the brake surfaces to contact and stop the nut. This action causes the snubber to act as a solid link. Different lockup forces for tension and compression can be incorporated by using different spring preloads.

The design was conceived for the Shuttle orbiter, requiring support links between structural panels. The links would allow normal thermal, mechanical, or pressure deflections to occur without high loading. When one panel would be exposed to high acceleration, the links would lock rigidly and transmit loads to other panels without free play.

The concept might be incorporated as a safety device on material handling systems or as an energy absorption device or a governor for machines or equipment.

This work was done by Earl V. Holman of Rockwell International Corp. for **Johnson Space Center.** *No further documentation is available.*
MSC-16134

Bayonet Plug With Ramp-Activated Lock

Plug and ramped washers are an effective lock at high temperatures.

Lyndon B. Johnson Space Center, Houston, Texas

A matched pair of washers with broad surface ramps is the locking mechanism in a new bayonet plug. It can be used where threaded fasteners and springs are impractical because of extreme temperatures or other environmental incompatibility.

The prototype locking mechanism was made for attaching silicon carbide-coated columbium tubes, which are subjected to temperatures up to 2,600° F (1,427° C) on the Space Shuttle nose cap. At such temperatures, it is difficult to retain complex shapes, such as thread forms. Typically, the silicon carbide coating cracks at the peaks and valleys of the threads, and the substrate columbium is attacked by oxidation. In contrast, the coating on the broad-surface ramps of the washers is much less susceptible to cracking.

The figure shows the plug fastened to a stepped flange that simulates a portion of the Shuttle nose cap. In (a) the main body of the plug extends through a hole in the flange. A lip (not visible) on the lower surface of the plug matches a bevel on the bottom of

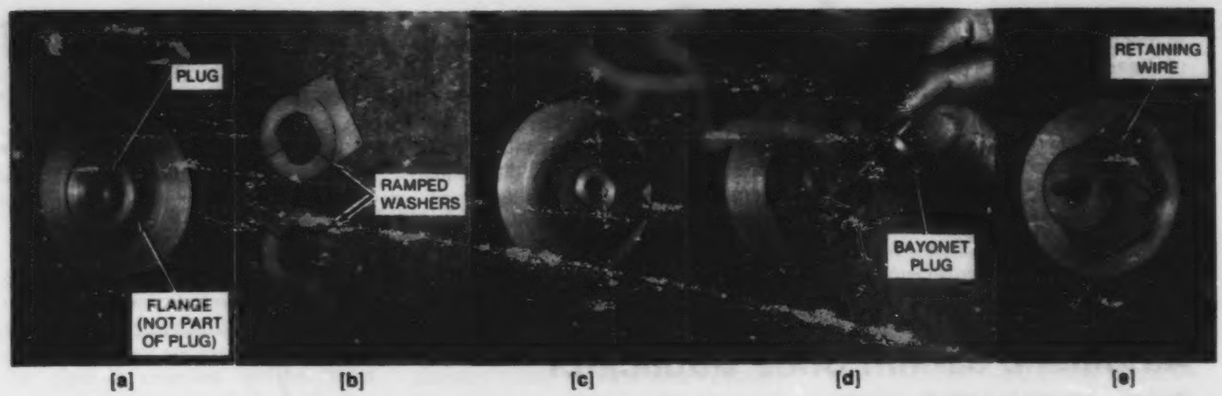

A Bayonet Plug With Ramped Washers locks at high temperatures that would deteriorate threaded fasteners. The plug was developed for attaching static-pressure probe tubes to the nose cap of the Space Shuttle. A lip on the inner plug holds the plug in place from below (the lip is not visible in these photos).

the flange. The matched pair of ramped washers shown in (b) is placed on the plug in (c), and in (d) the bayonet is inserted.

The inner slot of one washer matches the contour of the plug; this washer is stationary. The inner slot of the second washer is circular. When the second washer is rotated, the washers push against the bayonet plug, locking it in place. A retaining wire (e) secures the plug.

This work was done by Kenneth E. Wood of Rockwell International Corp. for **Johnson Space Center.** *For further information, Circle 71 on the TSP Request Card.*

This invention is owned by NASA, and a patent application has been filed. Inquiries concerning nonexclusive or exclusive license for its commercial development should be addressed to the Patent Counsel, Johnson Space Center [see page A5]. Refer to MSC-18526.

Heat-Pipe Sensor for Remote Leveling

A new system gives level readings in remote locations.

Goddard Space Flight Center, Greenbelt, Maryland

A heat-pipe sensor system permits remote leveling in inaccessible areas without actually "seeing" the object in question. Three thermocouples, on the ends and the middle of the heat pipe, are used to measure temperature differences that arise when the pipe is tilted. When the platform on which the pipe is resting is leveled, the three thermocouple recordings are identical. When the readings are unequal, the platform is leveled by remote control until the readings are identical. The sensor was successfully used on the International Ultraviolet Explorer satellite.

A conventional heat pipe with an axially grooved interior wall is used with ammonia as the working fluid. The pipe is equipped with two heaters and three thermocouples as shown in the illustration.

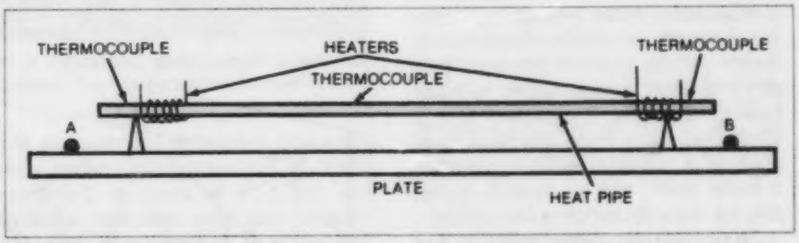

Proposed Remote-Readout Level Sensor uses a heat pipe equipped with two identical heaters and three monitoring thermocouples. When the platform on which the pipe is resting is level, all three thermocouples produce identical readings. If the platform is tilted, the higher end of the heat pipe would be warmer, and the platform must be leveled by remote control until all the temperature readings are identical.

Once the heaters are turned on, all thermocouples will record a slight rise in temperature. If the platform is level, all three temperature readings are identical. If for example point A is lower than B, the fluid will gravitate to A. The vapors concentrating at B will make that end warmer. This temperature difference will be recorded by the thermocouples, and the lower end will then be lifted by remote control until all the thermocouples have the same readings. The process would be reversed if point B would be lower than A.

(continued on next page)

The system could be easily modified to monitor a platform with two degrees of freedom. It need not be located directly on a platform but can be mounted on a gimbal controlling the platform level. The leveling accuracy is within ±0.25°, and no calibration is needed.

This system could effectively replace the frequently-calibrated expensive optical equipment that can be used only if the object is visible. It can function in cold, in vacuum, and in hot humid environments that produce nonlinear expansion and contraction in conventional level-monitoring equipment.

Other potential advantages include low cost, no moving parts, and operation in toxic environments (e.g., radioactive areas). The system can be customized to operate in steps from −320° F (−195° C) to +600° F (315° C).

This work was done by James P. Marshburn of **Goddard Space Flight Center**. *No further documentation is available.*
GSC-12095

Automatic 35-mm Slide Duplicator

Automatic duplicator is readily assembled from conventional equipment and parts.

Lewis Research Center, Cleveland, Ohio

An automatic 35-mm slide duplicator is easily assembled from conventional inexpensive photographic and electrical components. Duplicates of a series of slides can be exposed automatically without operator attention, eliminating the considerable manual handling and operator processing ordinarily required.

The slide duplicator consists of a conventional single-lens reflex camera and a conventional magazine slide projector electrically coupled through a control unit for automatic operation. The camera, equipped with a bellows extension unit and a 75- to 150-mm zoom lens, a battery-operated film winder, and a right-angle viewer for focusing, is mounted on a baseplate. The slide projector, with lens removed, is mounted with the lens aperture facing the camera. A filter holder is installed on the front of the slide projector to allow compensation for color balance changes. The control unit is assembled from three standard components: a presettable digital counter, a cycle timer, and an audible alarm, plus the requisite switches and cabling.

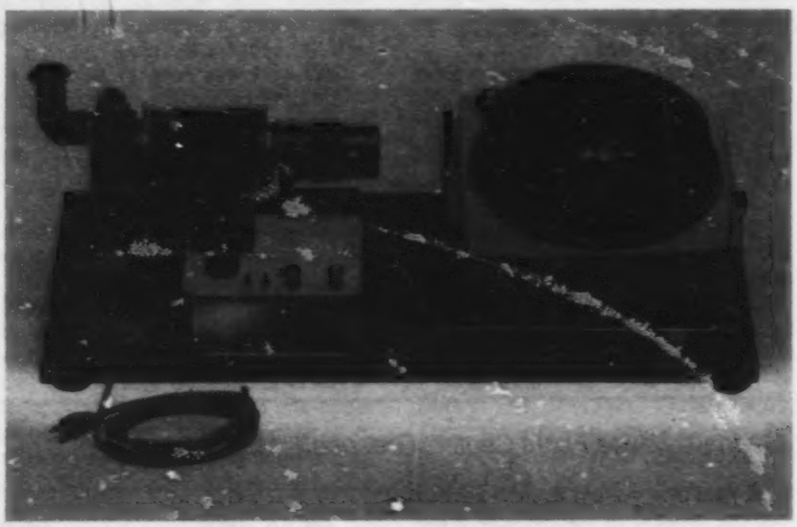

Automatic 35-mm Slide Duplicator is constructed from a conventional camera and slide projector and a control unit assembled from readily available parts.

To operate the slide duplicator, the counter is set to the number of slides to be duplicated, and the electric power is turned on. The timer automatically advances the projector magazine and injects the first slide into the aperture. Following a slight pause to allow the slide to stabilize, the timer initiates exposure and film winding. The cycle is automatically repeated with the next slide and continues through the entire series. At the end of the programed exposure sequence, the unit shuts off, and an audible alarm signals completion of the entire process.

This work was done by H. F. Seidel and R. E. Texler of **Lewis Research Center**. *For further information (schematic, parts list, and assembly instructions), Circle 72 on the TSP Request Card.*
LEW-13399

3-D Guidance System With Proximity Sensors

Proximity sensors help orient a mechanical claw with respect to target fixture.

NASA's Jet Propulsion Laboratory, Pasadena, California

A 3-D guidance system utilizes four proximity sensors on a remotely-controlled mechanical claw. The sensors feed pitch and range information to a manned control station indicating how the claw is oriented relative to a mating fixture it is about to grasp. The operator then alines the claw so that the fixture is grasped correctly. This system developed for coupling space vehicles can be used in other remote manipulators.

The sensors (see Figure 1) are mounted on the center square frame of the end effector of a four-claw grapple. Each sensor consisting of an LED source and a photodetector is aimed to sense the object parallel to the shaft (the roll axis) supporting the grapple. Thus four sensitive areas are established ahead of the claws. Using the claws to define four corners of a square, the sensors are mounted at midpoints of the sides of the square. Thus, two orthogonal lines connecting opposite pairs of sensors define the pitch-and-yaw axis of the system.

In the simplest arrangement, each sensor is operated in a two-state binary sensing mode, where a zero indicates a too far state while 1 indicates a too close state when the system is in the vicinity of the target (see Figure 2). The detection distances of sensors B and D are somewhat shorter than of A and C. Thus a success state when the claws are alined with the target is defined by A signaling 1, B a zero, C a 1, and D a zero. An all-zero state shows that the entire claw is too far from the target and an all-1 that it is too close.

A total of 16 combinations is possible (2^4) indicating various misalinements of yaw and pitch axes with respect to the target. One of the 16 states never occurs, when A and C are zero and B and D 1, because of the detection pattern setup.

A more precise alternative would involve three-state sensing. A signal with a value of 2 would indicate too close, 1 on target, and zero too far. Success would be defined by all 1's, and a total of 75 workable logic states would be possible, giving a more accurate feedback.

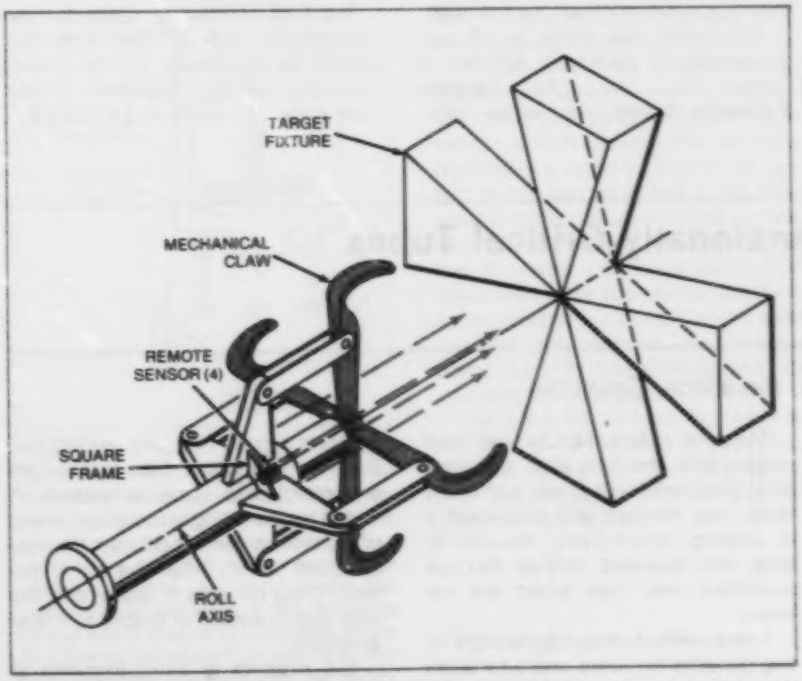

Figure 1. **Four Proximity Sensors** help to guide the mechanical claw into alinement with the target fixture. Digital signals are used to sense the target distance and to aline roll, pitch, and yaw with respect to the target before it is grasped.

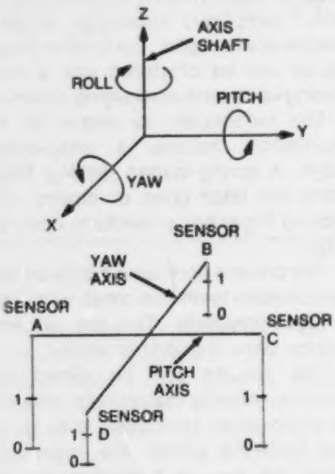

Figure 2. The **Sensors** are arranged to form the yaw-and-pitch axis of reference for guiding the claw. The sensors generate binary signals of 1 for too close and zero for too far. These signals are fed to the control operator guiding the claw. A similar more-precise alternative uses three states signaling 2 for too close, 1 on target, and zero for too far; and, an even more precise alternative uses continuous calibrated data from the sensors.

This work was done by Antal K. Bejczy of Caltech for **NASA's Jet Propulsion Laboratory**. *For further information, Circle 73 on the TSP Request Card.*

This invention is owned by NASA, and a patent application has been filed. Inquiries concerning nonexclusive or exclusive license for its commercial development should be addressed to the Patent Counsel, NASA Resident Legal Office-JPL [see page A5]. Refer to NPO-1452

Automatic Connector Joins Structural Columns

A connector snap-locks
over column ends.

Langley Research Center, Hampton, Virginia

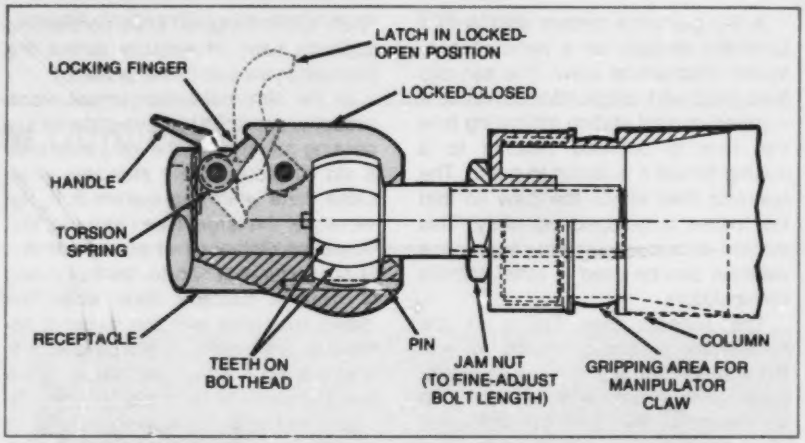
LATCH IN LOCKED-OPEN POSITION
LOCKING FINGER
LOCKED-CLOSED
HANDLE
TORSION SPRING
RECEPTACLE
TEETH ON BOLTHEAD
PIN
JAM NUT (TO FINE-ADJUST BOLT LENGTH)
GRIPPING AREA FOR MANIPULATOR CLAW
COLUMN

Automatic Connector snap-locks columns together to make a truss structure. An unlocked receptacle accepts a bolthead from a column end. When the two are together, the latch snaps over the bolt, locking it in place. The joint is rigidly locked and will not bend or twist.

A new connector developed for space application joins 20-m-long columns. At column intersections a latch snaps closed over a toothed bolthead mounted on the column end, forming a rigid joint that will not bend or twist. Developed for quick assembly and disassembly of large space structures, the connector could be used in conventional construction to install temporary structures or as a mechanical coupler. Up to nine receptacles can be clustered into a node joining up to nine converging columns.

The receptacle, as shown in the illustration, houses a snap-action latch. A spring-loaded locking finger holds the latch open or closed. The locking finger has a handle to open the latch.

The column end has a bolthead with sprocketlike teeth that mesh with a pin in the receptacle. This pin prevents torsion once the joint is locked.

The column can be alined and joined by remote manipulator claws or by some other convenient means. As the bolthead enters the receptacle from the top, a projection on the bolthead depresses the open latch. Once the dead center of the latch is passed, the spring-loaded finger locks the latch positively over the bolthead.

This work was done by G. G. Jacquemin of Lockheed Missiles & Space Co., Inc., for **Langley Research Center.** *For further information, Circle 74 on the TSP Request Card.*

Inquiries concerning rights for the commercial use of this invention should be addressed to the Patent Counsel, Langley Research Center [see page A5]. Refer to LAR-12578.

Test Fittings for Dimensionally Critical Tubes

Fittings prevent damage
to tube stubs.

NASA's Jet Propulsion Laboratory, Pasadena, California

Dimensional tolerances are frequently critical for tubes used in aerospace and aviation fluid-control equipment. These tubes can be easily damaged when components into which they lead are tested and calibrated. For instance, a small offset in the tube dimension can go unnoticed and eventually cause leakage at the manifold joints, creating an expensive repair problem once the component is put into operation.

Temporary test fittings that are slipped over the tube stub are available. However, if left in place after the tests, they interfere with final welding or brazing. Alternatively, integral fittings with face-seal O-rings that are machined onto tube stubs are too heavy.

A new method using a lightweight fitting protects the tubes and tube stubs during testing and through to the final welding. A threaded male fitting (see figure) is slipped over and welded to a dimensionally critical tube that in turn is connected to some component. A mated female fitting leading from a test or calibration instrument can then be attached at will. After the tests, the male fitting remains in place, and the tube stub is welded or brazed to a final assembly.

The male-fitting inner diameter is slightly larger than the outer diameter of the tube. The fitting is slipped on the

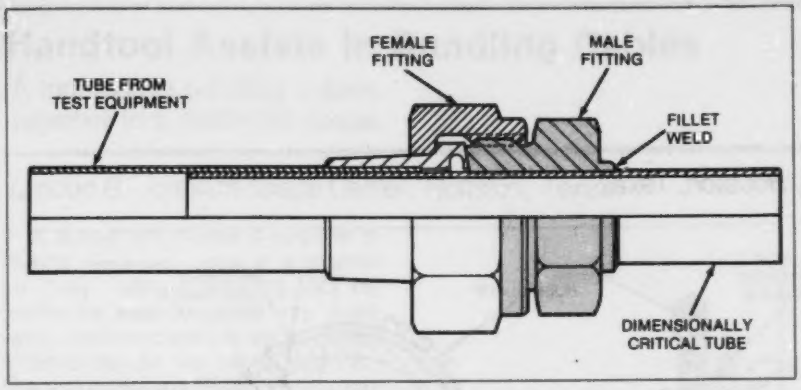

Male Threaded Fitting used as a test connector is welded to a tube stub. The fitting prevents damage to dimensionally critical tubes during the tests and is light enough to be left in place during the final assembly.

tube, positioned at some distance from the stub, and fillet-welded. The female fitting is tightened over the male fitting, forming a temporary leakproof seal. The dimensions of the female fitting and its tube are chosen to be somewhat larger to prevent contact with the tested tube, especially at the tube stub.

The new approach is adaptable to many types of components, including valves, transducers, and filters. It was applied in ground tests of Voyager 77; and despite numerous qualifications and calibration tests, not a single tube stub or weld had to be reworked.

This work was done by Ray Hagler of Caltech for **NASA's Jet Propulsion Laboratory.** *For further information, Circle 75 on the TSP Request Card.*
NPO-14399

Electromechanical Slip Sensor

New sensor indicates the direction of slip and slip rate of objects handled by remote manipulators.

NASA's Jet Propulsion Laboratory, Pasadena, California

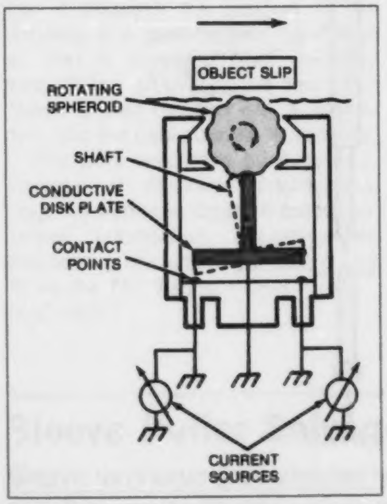

Slip Sensor uses a freely movable spheroid with a staggered pattern of indentations on its surface. The spheroid rotates in the direction of the slipping body, tilting a shaft with a conductive disk plate. The conductive plate assembly is bent toward the contact corresponding to the direction of slip and is flicked by the indentations at a rate corresponding to slip rate. The slip direction and rate can be determined using LED's arranged in a circular array or a microcomputer with a CRT display.

A new slip sensor system for teleoperator grasping manipulators detects the presence, direction, and rate of slip. Previous sensors were less versatile, detecting only the presence of slip.

The two basic components (see figure) are the sensor on the manipulator and a microcomputer located at a convenient remote location. The sensor incorporates a circular array of 16 contact points corresponding to 16 compass directions relative to the sensor. As the object slips in a certain direction, it rotates a spheroid that in turn tips a shaft in the appropriate direction. A disk base at the bottom of the shaft touches the appropriate contact points. A current flow at those contacts indicates the slip direction.

The spheroid surface has indentations that pulse the shaft at a rate proportional to the slip rate. This generates current pulses that are used to determine the slip rate.

The sensor signals can be direct raw analog LED displays or digitally processed signals on a graphics display. The analog display uses 16 LED's arranged in a circle corresponding to the contact points. A slip in any given direction will pulse the appropriate LED. Since an adjacent LED could also be firing, the operator would visually average out the direction of the slip. The rate of blinking indicates the slip rate.

A microcomputer can process these signals in real time to show the slip rate and direction on a CRT display. The signals are averaged, showing the data in eight compass directions. Slip rate is determined by the frequencies of steps on the display lines.

This work was done by Antal K. Bejczy and Sur Park of Caltech for **NASA's Jet Propulsion Laboratory.** *For further information, Circle 76 on the TSP Request Card.*
NPO-14654

X-Ray Beam Pointer

Pointer aims X-ray machine for weld radiographs.

Lyndon B. Johnson Space Center, Houston, Texas

A simple pointer (see figure) indicates the direction the beam will take from a portable X-ray machine. The pointer is an aid in making X-ray photographs of welded assemblies — for example, of complicated plumbing and valve systems.

A conventional, 36-in. (0.9 m) telescoping antenna serves as a pointer to aim the X-ray tube port. The antenna, welded onto a conventional 3-in. (7.6-cm) hose clamp that is tightened around the rotatable X-ray lead shield, extends radially outward.

Before the X-rays are taken, the antenna is extended, and the machine is alined so that the antenna points to the object and the X-ray film. Once alined, the antenna is collapsed and moved out of the way by turning the shield to open the X-ray tube port. The open port then faces the target exactly as the antenna pointed.

The pointer is inexpensive and constructed from readily available parts. A plumb bob used previously for vertical alinement and a yardstick used to visualize the X-ray paths at various angles were less convenient and not as accurate. The new pointer cuts the alinement time by one-half and virtually eliminates retakes necessitated by poor alinement. It is estimated that for 3,000 weld radiographs, the pointer will save 300 worker-hours and significant materials costs.

This work was done by C. W. Nelson of Beech Aircraft Corp. for **Johnson Space Center**. *For further information, Circle 77 on the TSP Request Card. MSC-18590*

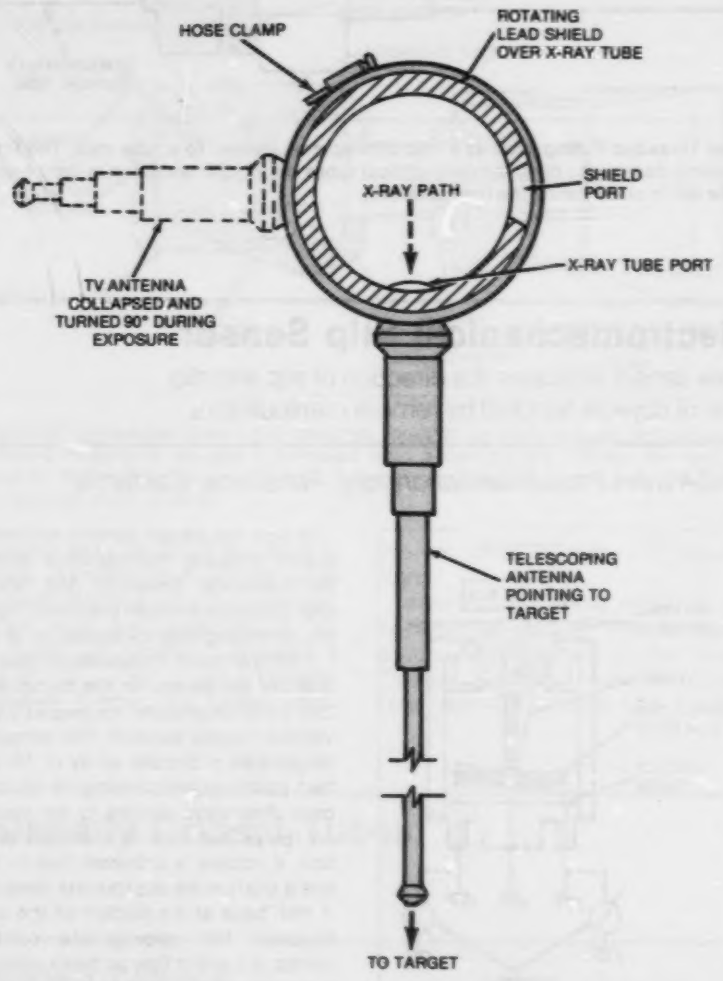
HOSE CLAMP
ROTATING LEAD SHIELD OVER X-RAY TUBE
SHIELD PORT
X-RAY PATH
X-RAY TUBE PORT
TV ANTENNA COLLAPSED AND TURNED 90° DURING EXPOSURE
TELESCOPING ANTENNA POINTING TO TARGET
TO TARGET

Telescoping Pointer shows the direction the X-ray beam will take when the tube shield is opened. Once alined, the pointer is rotated 90° out of the way, opening the X-ray tube port to face the target. The pointing mechanism is made of inexpensive parts.

Handtool Assists in Bundling Cables

A tool aids in bundling cables
together in a restricted space.

Lyndon B. Johnson Space Center, Houston, Texas

A simple tool makes it possible to bundle electrical cables in a channel or "tray" without requiring that the cables be lifted out of the tray. Used with commercially-available plastic ribbons that tie the cables together, the tool guides the ribbon along a tray wall, through a bracket at the bottom of the tray, and up the opposite wall. One end of the ribbon locks in the other end, securing the cable bundle. The procedure is faster and less awkward than the old method of lifting the cables for wrapping.

As shown in the illustration, one inserts the tool gently into the space between the cable and the tray wall, engaging it with a bottom bracket. The ribbon is then slid along a groove in the tool until it threads into the bracket. The operator removes the tool, reinserts it along the other wall so that it engages the bracket at the opposite end, and pushes the ribbon so that it emerges from the tray through the groove in the tool. The ribbon is then cinched with a special gun, and the cable bundle is secured.

This work was done by Eugene J. Stringer of Rockwell International Corp. for **Johnson Space Center.** *For further information, including an engineering drawing of the tool, Circle 78 on the TSP Request Card.*
MSC-18567

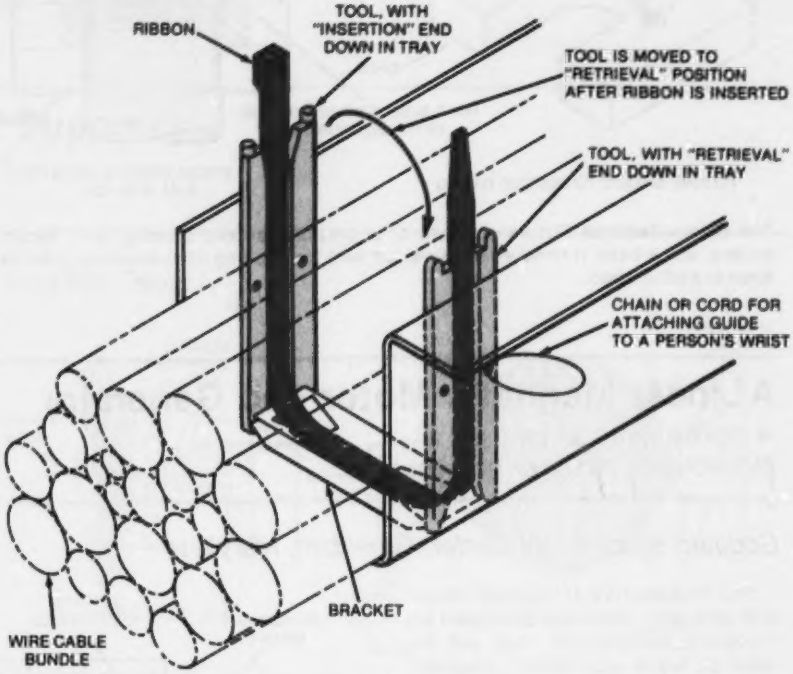
RIBBON
TOOL, WITH "INSERTION" END DOWN IN TRAY
TOOL IS MOVED TO "RETRIEVAL" POSITION AFTER RIBBON IS INSERTED
TOOL, WITH "RETRIEVAL" END DOWN IN TRAY
CHAIN OR CORD FOR ATTACHING GUIDE TO A PERSON'S WRIST
BRACKET
WIRE CABLE BUNDLE

The **Cable-Bundling Tool** helps to insert and then retrieve the ribbon that wraps the cables together. The two ends of the tool are slightly different: The "insertion" end is configured to guide the ribbon into the bottom bracket; the other end (the "retrieval" end) is shaped to guide the ribbon from the bracket into the tool groove. Thus, the tool is inverted when used for the retrieval step.

Sleeve Puller Salvages Welded Tubes

Sleeve remnants are removed nondestructively
so tubes can be reused.

Lyndon B. Johnson Space Center, Houston, Texas

The remnants of sleeves used in welded tube joints are removed without damaging the tube ends by a simple new fixture. Tubes can therefore be reused, saving time, labor, and material in many applications.

The welded tube is salvaged by first sawing through the sleeve and the weld. A half segment of the sleeve remains on each sawed-off section of tube. The end of one tube is then clamped on the fixture, a plug is inserted, and a pressure screw is advanced to push the tube out of the sleeve segment. The same procedure is repeated for the other tube section. The sleeves are removed without distorting or damaging the tubes, as often happens when the sleeves are removed by pliers or other handtools.

(continued on next page)

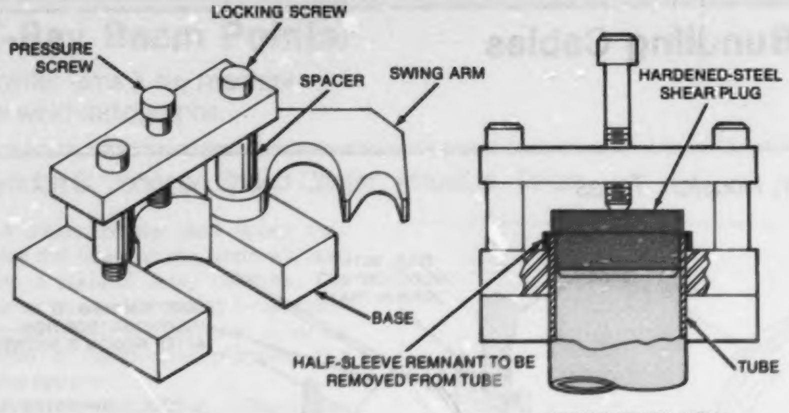
LOCKING SCREW
PRESSURE SCREW
SPACER
SWING ARM
BASE
HARDENED-STEEL SHEAR PLUG
HALF-SLEEVE REMNANT TO BE REMOVED FROM TUBE
TUBE

FIXTURE OPENED TO RECEIVE TUBING

CROSS SECTION, WITH TUBE IN PLACE

The Sleeve-Removal Fixture consists of a pressure screw, a swing arm, locking screws, and a base. It removes a sleeve remnant from tubing after a welded joint has been sawed through.

As shown in the figure, the fixture consists of a base, two locking screws, two spacers, a swing arm, and a pressure screw. The tube is placed in the cutout in the base, with the sleeve remnant resting on the base. The swing arm is closed around the tube and locked by tightening the two locking screws.

A hardened-steel shear plug, with outside diameter equal to that of the tube, is inserted in the tube end. When the pressure screw is advanced, it pushes the shear plug, which shears the tube segment out of the sleeve.

This work was done by James F. Weaver of Rockwell International Corp. for **Johnson Space Center**. *No further documentation is available.*
MSC-18686

A Linear Magnetic Motor and Generator

A device that can be used as bidirectional motor or ac generator

Goddard Space Flight Center, Greenbelt, Maryland

In a proposed linear magnetic motor and generator, originally developed for cryogenic refrigerators that will be used on future spacecraft, magnetic forces drive a reciprocating shaft along its axis. The actuator shaft, as shown in the figure, is located in the center of a cylindrical body. Support for the shaft may be provided by linear ball bushings, plain bearings, or by noncontacting means such as gas or magnetic bearings. The motor/generator could be applied in remote or hostile environments.

A drive coil between the two permanent-magnet structures controls the linear movement of the actuator. Each of the permanent-magnet structures establishes a flux path passing through the ends of the actuator. The permanent magnets are oriented so that their north poles face axially outward. When the motor/generator operates as a bidirectional motor, the drive coil selectively adds and subtracts magnetic flux to and from these flux paths and thus produces the forces that drive the actuator back and forth along the axis.

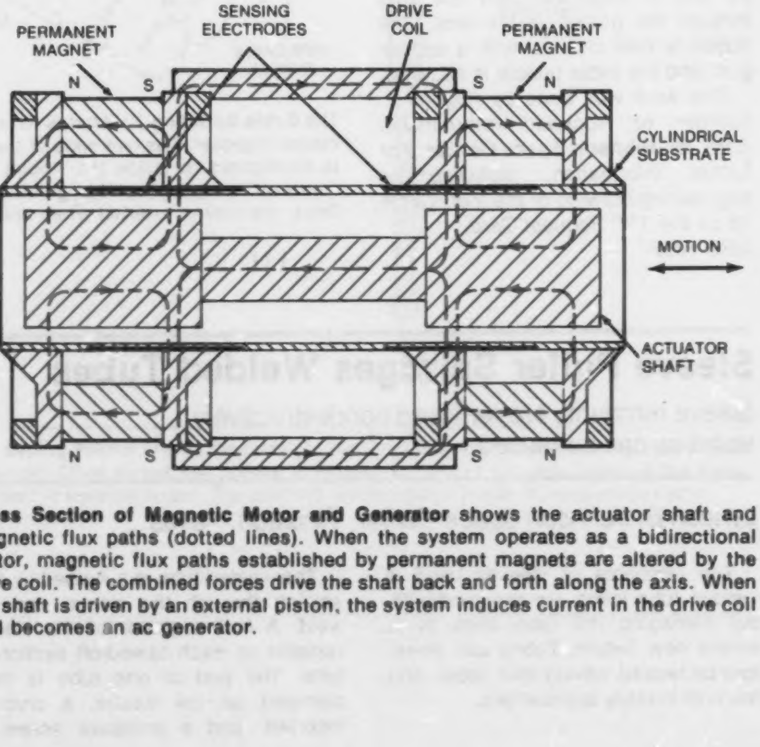

Cross Section of Magnetic Motor and Generator shows the actuator shaft and magnetic flux paths (dotted lines). When the system operates as a bidirectional motor, magnetic flux paths established by permanent magnets are altered by the drive coil. The combined forces drive the shaft back and forth along the axis. When the shaft is driven by an external piston, the system induces current in the drive coil and becomes an ac generator.

When the actuator is driven by an external reciprocating engine, the motor/generator becomes an ac generator. In this mode, the actuator coupled to the engine piston moving back and forth along the axis alters flux paths established by the permanent magnets. This induces alternating current within the coil, which can be connected to an external load.

A somewhat modified motor/generator is not cylindrical and has magnetic flux confined to the vertical plane. Its operation is similar to the one described.

This work was done by Philip A. Studer of **Goddard Space Flight Center.** *For further information, Circle 79 on the TSP Request Card.*

This invention is owned by NASA, and a patent application has been filed. Inquiries concerning nonexclusive or exclusive license for its commercial development should be addressed to the Patent Counsel, Goddard Space Flight Center [see page A5]. Refer to GSC-12518.

Cryogen-Storage-Tank Support

Proposed support isolates the tank from thermal and mechanical loads.

Lyndon B. Johnson Space Center, Houston, Texas

High-pressure helium cryogen tanks supported on structures that are subject to mechanical and thermal loading must be effectively isolated against structural deflection and thermal effects. This problem can be resolved using a proposed, statically determinate support, shown in the figure. The support would isolate the tank from the thermal and mechanical loading by its environment. The tank is supported by an independent mechanism at each end to accommodate changes in tank size due to temperature and pressure variations. This arrangement is self-alining from the beginning, accommodating manufacturing variations in the tank dimensions as the tank is installed.

On one end the tank is attached to a trunnion ring that can transfer a three-axis load and torque. To isolate the tank thermally, the ring is held away from the structure by titanium fittings. The opposite end of the tank is supported by an A-frame swing-link mechanism clamped around a hub on the tank end. This frame reacts to tank loads in the plane of the frame and allows tank pressure and thermal growth in a direction normal to the frame. The frame also has titanium links for thermal isolation.

This work was done by Gerald H. Wisdom of McDonnell Douglas Corp. for **Johnson Space Center.** *No further documentation is available.*
MSC-14848

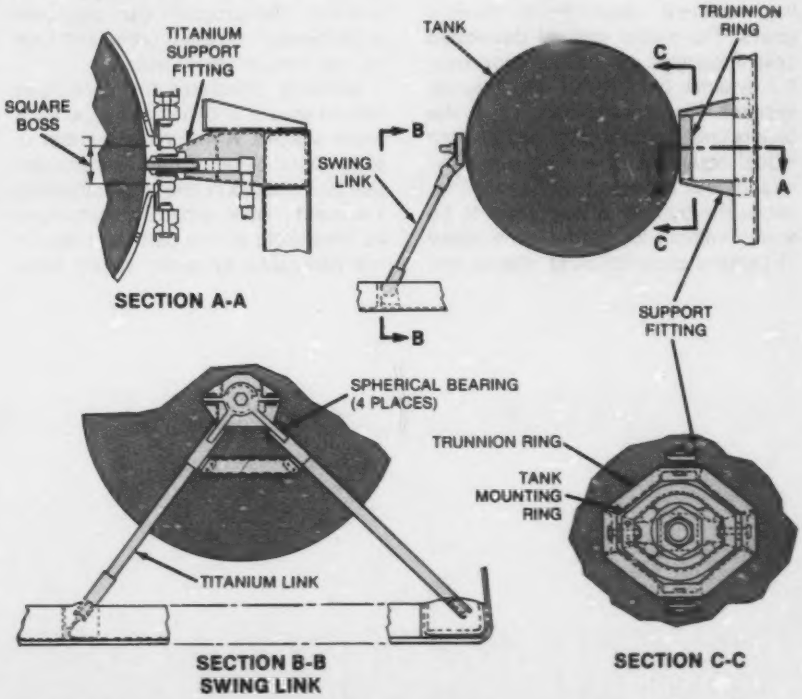

Proposed Tank Support would isolate a cryogen high-pressure helium tank from thermal and mechanical loads imposed on its support structures. This design, using a combination of well-known common mechanisms, would isolate the tank and allow for tank expansion and contraction due to temperature and pressure changes. A similar support method was already used on nitrogen tanks.

Computer Programs

These programs may be obtained at very reasonable cost from COSMIC, a facility sponsored by NASA to make new programs available to the public. For information on program price, size, and availability, circle the reference letter on the COSMIC Request Card in this issue.

Rotor Transient Analysis

Undamped modes approximate the dynamic behavior of rotors and bearings.

Two programs, Modal 1 and Modal 2, have been developed for calculating the transient response of flexible rotors. The modal method developed uses undamped modes to approximate the dynamic behavior of rotor/bearing systems. Modal transformation of the generalized equations of motion into modal equations of motion using the undamped modes significantly reduces the number of equations to be solved without losing the generalities of bearing cross-coupling effects and influence of gyroscopic moments. This reduction of degrees of freedom greatly reduces the computational effort and cost and thus makes possible the transient analysis of large, complex rotor systems.

Modal 1 is used to calculate the undamped critical speeds and their corresponding mode shapes, damped natural frequencies and their corresponding mode shapes, rotor unbalance response, and transient response of multimass rotor/bearing systems. Special capabilities of this program include asymmetric bearing, bearing rotational damping and stiffness effects, shaft residual bow, and disk skew effects.

Nonlinear bearing forces can also be calculated for each time step during transient analysis with bearing characteristics. The program can also generate plots of transient orbits and time vs. transient response plots.

Modal 2 calculates the undamped critical speeds and their corresponding mode shapes. A maximum number of eight speed cases of transient analysis can be obtained in one single analysis. Transient motion orbits and amplitude vs. time plots at one particular station are generated for every speed case. Fast Fourier transformation is used to produce frequency spectrum analysis for every speed case.

The application of modal analysis to uncouple the equations of motion simplifies stability, steady-state unbalance response, and transient response analysis of the system. Nonlinear stability of the system can be predicted by frequency spectra calculated from Fourier transformation of the transient solution. This analysis will provide designers with complete design information, such as critical speed and modes, amplification factors, stability, steady-state and transient forced response, and frequency spectrum of the system, without involving large-scale computational costs. The correlation of experimental data with modal analysis verified the use of modal analysis and numerical Fourier transformation.

These programs are written in FORTRAN IV for use on a CDC 6600 computer.

This program was written by P. E. Allaire, K. C. Choy, and E. J. Gunter of the University of Virginia for **Lewis Research Center.** *For further information, Circle J on the COSMIC Request Card.*
LEW-13230

Fabrication Technology

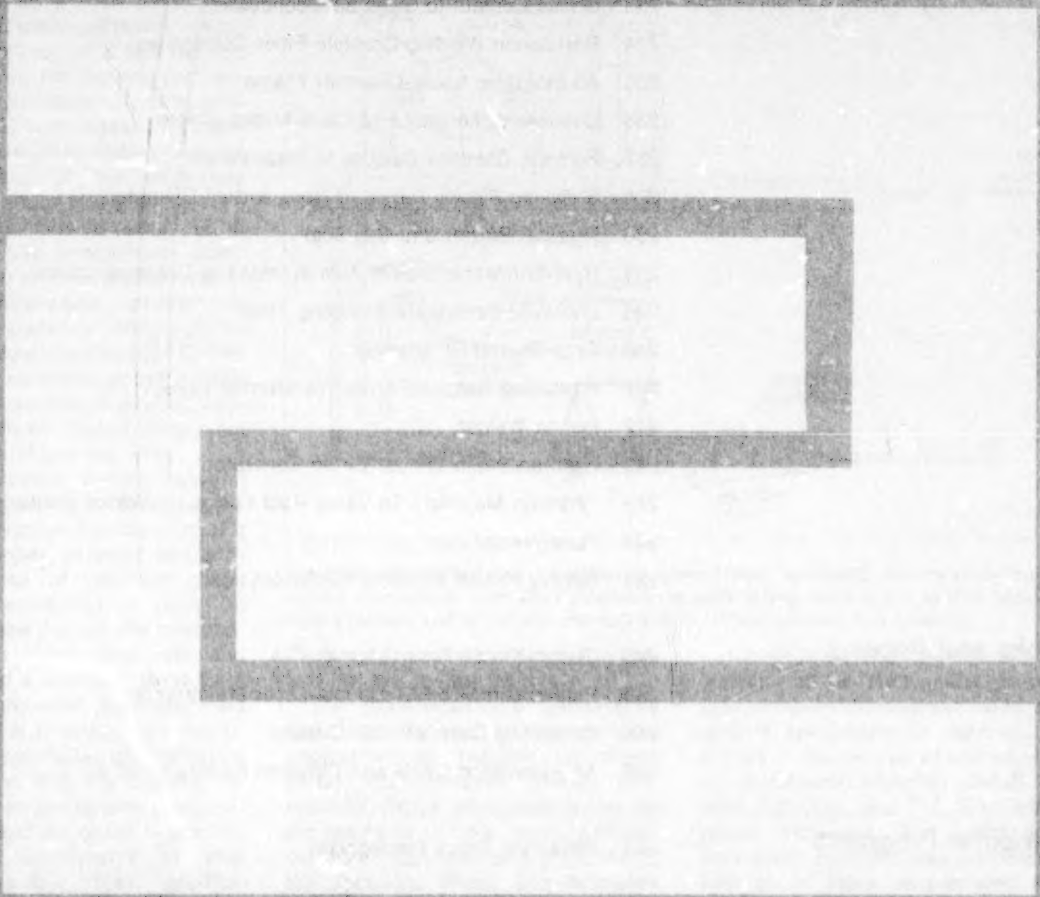

6

Hardware, Techniques, and Processes

231 Photonitride Passivating Coating for IC's
232 Double Metalization for VLSI
232 More-Reliable SOS Ion Implantations
233 Ohmic Contact to GaAs Semiconductor
234 Resistance Welding Graphite-Fiber Composites
235 All-Inorganic Spark-Chamber Frame
236 Controlling the Shape of Glass Microballoons
237 Forming Complex Cavities in Clear Plastic
237 Shrinking Plastic Tubing to Nonstandard Diameters
238 Thermal Barrier and Gas Seal
239 Heat-Shrinkable Sleeve Aids in Installing Universal Joints
240 Improved Particulate-Sampling Filter
240 Time-Shared RF Brazing
241 Producing Gapped-Ferrite Transformer Cores
242 Plastic Welder
243 Electron-Beam Welder Circle Generator
243 "Foreign Material" To Verify Root Fusion in Welded Joints
244 Tube-Welder Aids
244 Honing Fixture for Weld Electrodes

Books and Reports

245 Silicon Nitride Passivation of IC's
246 Progress in MOSFET Double-Layer Metalization
246 Optimizing Costs of VLSI Circuits
246 An Automated Oxide and Diffusion Facility for IC's

Computer Programs

247 Predicting Crack Propagation

Photonitride Passivating Coating for IC's

Increased reliability and simplified fabrication result from the postassembly preencapsulation passivation process.

Marshall Space Flight Center, Alabama

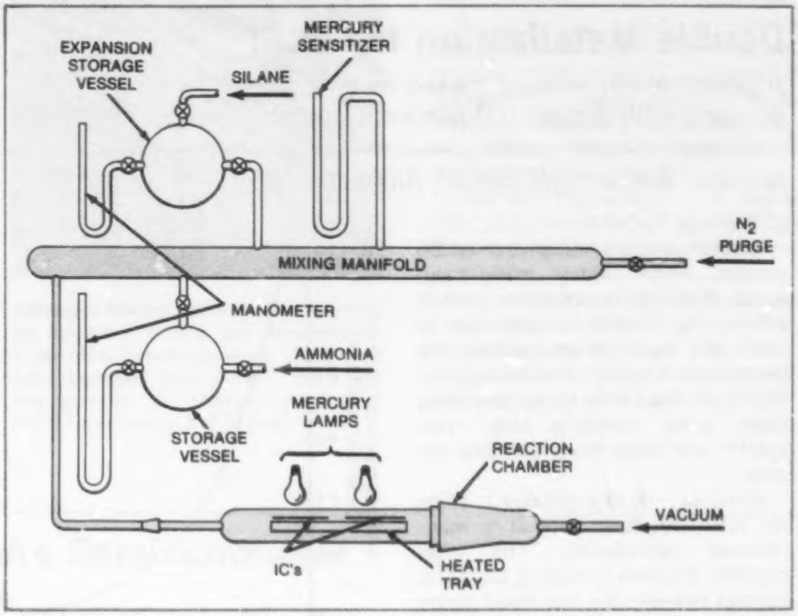

The **Photonitride Reaction Chamber** receives silane, ammonia, and mercury from a mixing manifold to form the silicon nitride passivating coating on the IC's. Mercury lamps initiate and terminate the reaction in which mercury is a catalyst.

The use of low-temperature photochemically-deposited silicon nitride (photonitride) as a final passivation layer over finished metalized semiconductor devices (MOS and bipolar) simplifies their fabrication and enhances their reliability. The photonitride layer is a barrier against moisture and the penetration of mobile ions into sensitive areas of the solid-state devices. The silicon nitride passivation process also inhibits corrosion due to moisture at wire interconnect sites, thus leading to their enhanced reliability. Low-temperature photonitride films are prepared at temperatures from 300° C downward to 100° C. The low temperature makes possible post-assembly passivation of devices containing relatively low-melting-point metalization and bonding wire.

The photonitride coating, several thousand angstroms in thickness, is applied in a reactor that consists of a reaction chamber, metered and controlled sources of reactant gases (silane and ammonia), a pump to move the gases through the chamber at a predetermined flow rate and pressure, and a mercury lamp as a source of ultraviolet radiation (see figure). In the process, the microcircuits to be passivated are placed on a heated tray, and the chamber is evacuated to an acceptable pressure. The flow of reactant gases is started, followed by adjustments of total pressure, gas-flow rates, gas-flow ratios, and substrate temperature.

When the complete system reaches equilibrium, the deposition of silicon nitride is initiated by transmitting ultraviolet radiation through fused-quartz windows that form the top of the deposition chamber. The deposition rate is directly proportional to the intensity of ultraviolet radiation impinging on the substrate surface and is terminated by turning off the mercury lamps positioned over the fused-quartz windows. A programable control panel allows the selection of automatic or manual operation and associated pneumatic and vacuum equipment to admit the reactant gases and remove the byproducts.

The low-temperature photonitride films are prepared by the mercury photosensitized reaction of silane (SH_4) and ammonia (NH_3). Only radiation that is absorbed, either by the reactants or by a mercury photosensitizer, can lead to a photochemical reaction. Silane and ammonia absorb radiation significantly only at wavelengths below 2,200 Å. The mercury lamp is the most convenient source of radiation for the chemical processes, but its frequency range is limited to a cutoff wavelength of about 2,000 Å. By saturating the reaction chamber with mercury vapor, the lamp limited-frequency range is overcome; the excited but un-ionized mercury atoms transfer their energy by collision to the chemical reactants within the system, generating free radicals that initiate chain reactions leading to the final silicon nitride product.

The electrical and mechanical compatibility of the photonitride process with microcircuits was examined with various semiconductor devices. Included in the devices examined were an operational amplifier; CMOS, bipolar Schottky, and TTL IC's; and a power transistor. The photonitride deposition process was compatible with all of these wire-bonded lead frame assemblies, with or without initial chip passivation. The survival after the application of photonitride to lead frame assemblies of devices with no chip passivation suggests the possibility of simplifying the device fabrication process by eliminating the chip passivation operation.

The ability of photonitride films to withstand flexure stresses helps to protect IC devices subjected to severe mechanical handling or circuit repair procedures. Tests indicate that leads 75 mils (1.90 mm) in length can be laterally displaced by more than 25 mils (0.63 mm) at the point of

(continued on next page)

maximum curvature without damage to the nitride film.

Significant advantages exist for the photochemical process over other processes, plasma and sputtering, for the deposition of silicon nitride on microelectronics. The advantages are low deposition temperature and zero stray radiation and ion levels, all of which can change device characteristics. [Also see related article, "Silicon Nitride Passivation of IC's" (MFS-25309), on page 245 of this issue.]

This work was done by T. C. Hall and J. W. Peters of Hughes Aircraft Co. for **Marshall Space Flight Center.** *For further information, Circle 80 on the TSP Request Card.*
MFS-25401

Double Metalization for VLSI

A postsintering process makes electrical contacts with almost 100 percent certainty.

Marshall Space Flight Center, Alabama

Very-large-scale integrated (VLSI) circuits, which contain many thousands of individual circuits on a small silicon chip, benefit from the use of two metal layers to interconnect the devices on the chip. The two layers, which are separated by an insulating oxide layer, conserve chip "real estate" and allow more functions per chip.

However, double-metalized chips for VLSI have been difficult to manufacture reproducibly. The most common problem is making electrical contact between the two metal layers through "vias" (holes) in the oxide insulating layer. The via contacts tend to have excessively high resistance, often to the point of being open circuits. The problem is worse when the number of vias is large (500 or more) and the via size is very small [less than 0.2 mil (5 millimeters) square]. A recently tested sintering procedure carried out after "wet chemistry" processes increased the yield of double-layer metal conductors to more than 98 percent.

The wafers containing the double-metalized chips are sintered (see figure) at 490° C. Apparently the aluminum metal layers react with an aluminum oxide film that remains in the via, breaking up the film so that it no longer impedes the electric current. Alternately, the recrystallization of both aluminum layers as they cool from the sintering temperature may mechanically disrupt the oxide film. At any rate, the yield of "good" small vias — that is, those with low contact resistance — increases dramatically.

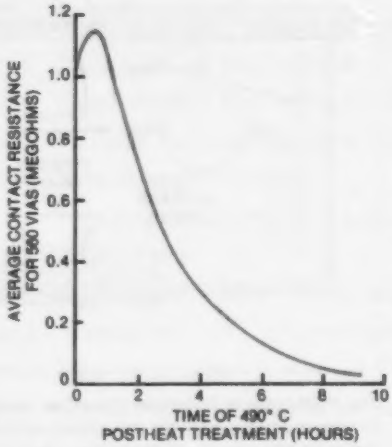

The **Effectiveness of Postheat Treatment** is clearly demonstrated by the drop in via resistance as a function of heating time. This result was obtained from 560 vias of 0.5 by 0.5 mil in size. The heat treatment usually eliminates most of the open circuits (contact resistance of more than 20 megohms).

The sintering technique was evaluated using 50 specimens. The specimens consisted of a double-layer structure containing 560 vias. The via size varied from 0.5 to 0.2 mil (0.013 to 0.005 mm) square, although only one size was used per specimen. Best results have demonstrated that the technique reduces the number of defective contacts to less than 2 percent — a very respectable figure in this relatively new technology.

This work was done by J. D. Trotter and Thomas E. Wade of Mississippi State University for **Marshall Space Flight Center.** *For further information, Circle 81 on the TSP Request Card.*

Inquiries concerning rights for the commercial use of this invention should be addressed to the Patent Counsel, Marshall Space Flight Center [see page A5]. Refer to MFS-25149.

More-Reliable SOS Ion Implantations

A conducting layer prevents static charges from accumulating during implantation of silicon-on-sapphire MOS structures.

Marshall Space Flight Center, Alabama

A method for preventing static charges from building up on silicon-on-sapphire (SOS) MOS structures during ion-implantation doping has improved yields for several LSI circuits. To dissipate the potentially destructive accumulations before they develop, a thin conducting path to ground is deposited prior to the start of the implantation. Either a very thin conducting film that is essentially transparent to the ions is deposited or a

(continued on next page)

thicker film is used, and gaps are etched in the regions to be doped.

In silicon-on-sapphire technology the silicon layer over the sapphire substrate is selectively etched to form electrically-isolated silicon islands. Then, relatively-heavy ion-implantation doses are applied to dope the MOS subelements to degenerate impurity concentrations on the order of 10^{20} cm^{-3}. The three exposures to an ion beam are required for an all-ion-implantation process: (1) polygate implantation; (2) n^+ implantation with a thick photoresist shield on the PMOS area; and (3) p^+ implantation with a photoresist shield on the NMCS area.

During the heavy source and drain implantations, charges build up on the silicon film. When they reach the breakdown level, the charge flows through neighboring silicon islands or through the sapphire substrate to the ground plate, often damaging the film (see figure) or cracking the sapphire wafer.

Two approaches to reduce charge buildup have been used. In the first, a relatively-thick conducting-shield film, such as aluminum, 1 μm in thickness, is deposited. The film is selectively etched to expose areas for implantation, yet it maintains a continuous electrical path for static charges to dissipate.

Damaged Silicon Films (darkened areas) on sapphire wafers are apparent on these MOS circuit elements. The silicon was damaged during heavy boron-ion implantation at dosages of 5×10^5 cm^{-2} and energies of 70 keV.

In the second approach, a thin conducting layer, such as 200 Å of aluminum, is deposited. Photoresist is used for shielding, as in the conventional process. The ion current passes through the thin aluminum layer to implant the underlying material.

Previous approaches to prevent charge buildup, such as simultaneously exposing the structure to charges of opposite sign, require extensive equipment modifications that are less practical and more expensive than depositing the conducting layer.

This work was done by D. S. Woo of RCA Corp. for **Marshall Space Flight Center**. *No further documentation is available.*

Inquiries concerning rights for the commercial use of this invention should be addressed to the Patent Counsel, Marshall Space Flight Center [see page A5]. Refer to MFS-25322.

Ohmic Contact to GaAs Semiconductor

Multimetallic layers produce stable, low-resistance contacts.

Langley Research Center, Hampton, Virginia

Reliable, low-resistance ohmic contacts to gallium arsenide (GaAs) semiconductor solar cells and lasers have been a constant problem. Often elaborate methods, such as extra p-type GaAs "capping layers," are used to make good contact.

A much easier and more reliable procedure has been developed for contacts to p-type GaAs and p-type GaAlAs devices. The contacts are made by evaporating a layer of magnesium (Mg) 20 to 75 Å thick, covered by a layer of titanium (Ti) 200 to 400 Å thick, covered by a layer of palladium (Pd) 200 to 400 Å thick, covered by a layer of silver (Ag) over 1,000 Å thick. The coating system is annealed at 375° to 475° C. Annealing times decrease from 45 to 10 minutes as the temperature increases. The contact metallurgy may be evaporated through a mask, or liftoff procedures may be used.

This method was used to make ohmic contacts to GaAlAs/GaAs solar cells that were grown by the "saturated-melt" liquid-phase epitaxy method. Slots were etched through the GaAlAs to the underlying GaAs by lithography. Then layers of 20 Å Mg, 300 Å Ti, 300 Å Pd, and 5,000 Å Ag were evaporated on the photoresist. Lifting off the photoresist leaves the metallic contacts in the slots. The contacts were annealed at 475° C for 10 minutes in vacuum.

The series resistance of these contacts has been too small to measure at 1 Sun intensity. Also, no leakage problems were encountered, presumedly due to the improved contacts and the lower density of Ga droplets in the saturated-melt epitaxy layers. On devices made by the etch-back-epitaxy process, this method of forming contacts has given contact resistances of 7×10^{-4} ohm-cm^2 or less.

The ohmic contact is stable and is expected to meet the 20-year-lifetime requirement at 150° C for GaAs combined photothermal/photovoltaic concentrators.

This work was done by Harold J. Hovel and Jerry M. Woodall of IBM Corp. for **Langley Research Center.** *No further documentation is available. LAR-12466*

Resistance Welding Graphite-Fiber Composites

High-strength joints are welded in a few seconds.

Lyndon B. Johnson Space Center, Houston, Texas

Carbon-reinforced thermoplastics, a family of lightweight materials that is finding increasing uses in homes and vehicles, are rapidly bonded together by resistance welding. In recent tests of several methods for joining composite beams for assembly in space, it was found that applying an electric current for a few seconds to melt the thermoplastic locally is the most promising approach. Among other tested methods, adhesive bonding and encapsulation are more time consuming and introduce additional material (the bonding agent) into the joint. Ultrasonic heating shows promise as a bonding method, but it can damage the graphite fibers in the composite.

For resistance welding, the graphite conducts sufficient current to heat and melt the thermoplastic in the vicinity of the joint. By using a spring-loaded electrode, such as that shown in Figure 1, pressure is applied as the thermoplastic softens; and the electrode follows the softening material to maintain contact.

In tests, three rods of graphite/polysulfone at 36 percent by weight of polysulfone were cut into 2-inch (5.08-cm) lengths and stacked as in Figure 2. The rods had square cross sections and were 0.08 in. (0.2 cm) on an edge. Welding was done with an applied force of 2, 3, 4, 5, or 6 lb (9, 13, 17, 22, or 27 N) and 30 to 35 volts dc across the joint. The total energy was 50, 75, or 90 joules, and typical heating times were about 2 seconds.

Excellent tensile strengths were measured for the resistance-welded joints. In the best samples, fibers were pulled from one member of the joint couple when the tensile limit was exceeded. Optimum joining conditions for the samples tested were 3 lb force at 90 joules and 4 lb at 75 joules. In both cases, the measured joint tensile strengths were above 8.3×10^6 N/m^2.

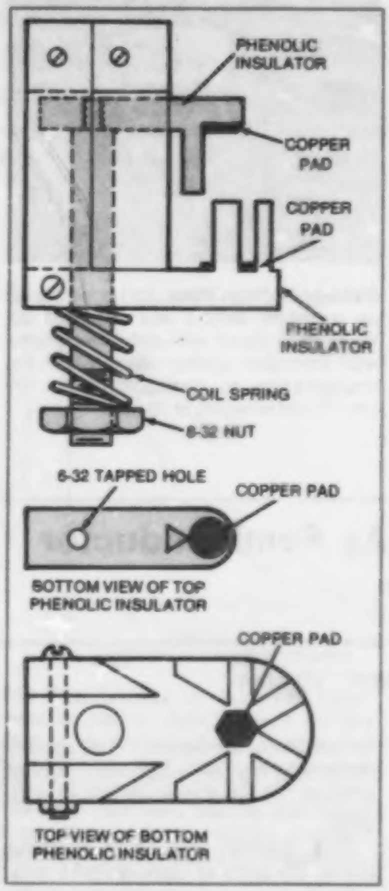

Figure 1. The **Resistance-Welding Electrode** would simultaneously apply heat and pressure to a joint. As the thermoplastic softens, the spring-loaded electrode follows the softening material to maintain contact. The electrode also holds the parts together during the cooling phase.

Resistance welding can be done in several configurations. In addition to the transverse arrangement of Figure 2, the joint can be heated longitudinally by connecting both power-source electrodes to the center rod and passing current until the thermoplastic softens. Heating by microwaves is also being considered. Thus far, little effort has been devoted to varying the joint surface condition or its size and shape; however, it is expected that optimization of these parameters will further improve the joint strength.

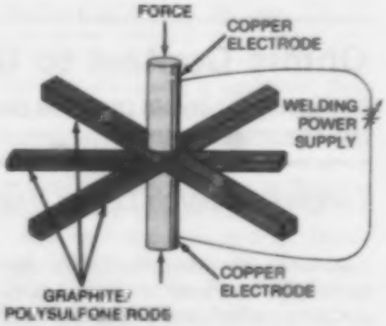

Figure 2. **Heat Is Applied** transverse to the joint to soften the thermoplastic. Since the joint interfaces offer higher resistance than the bulk, they reach softening temperature first.

This work was done by Richard T. Lamoureux of McDonnell Douglas Corp. for **Johnson Space Center.** *For further information, Circle 82 on the TSP Request Card.*
MSC-18534

All-Inorganic Spark-Chamber Frame

Outgassing is reduced by using ceramic and glass materials exclusively.

Goddard Space Flight Center, Greenbelt, Maryland

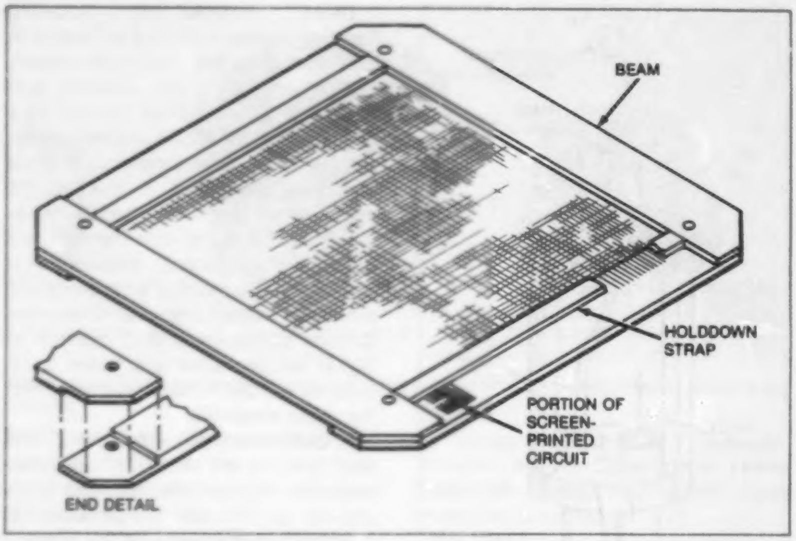

New **Spark-Chamber Frames** are assembled from four beams that are rabbeted at their ends. Ceramic or glass adhesives are used exclusively, and the printed circuit is applied by screen printing directly on the beams.

New spark-chamber frames, fabricated without organic-based adhesives or epoxy circuit boards, are less susceptible to contamination by outgassing than previous designs. The all-inorganic frames were developed for gamma-ray studies aboard spacecraft, where stable spark-chamber operation without gas refill is essential. They would offer the same advantage in terrestrial gamma-ray studies, in high-energy physics research, and other applications.

A typical spark chamber is assembled from 40 or 50 stacked frames, each containing hundreds of closely spaced wires (see figure). Within each frame, the wires lie in two adjacent parallel planes, in mutually perpendicular directions, forming a grid.

When a high-energy photon passes in the vicinity of one of the crosspoints of one of the grids, the locally-ionized filler gas conducts current between the two wires at the crosspoint. These wires define the x and y coordinates of the particle trajectory; the z coordinate is defined by the particular frame involved. The ends of the wires of each frame connect to circuits that record the coordinates of the trajectory.

The four ceramic or glass beams that form the edges of the square frame are bonded using a ceramic adhesive. The adhesive is selected for its low vapor pressure and for an expansion coefficient nearly equal to that of the frame material.

Wires are stretched across the frame between the opposing beams. A continuous wire is fed from a spool back and forth across the frame and is secured by holddown straps. After the straps are bonded over the wire with a ceramic adhesive, the continuous wire is cut, and the wire ends are connected to a printed circuit overlaid directly on the beams. The circuit is applied by screen-printing silver paste and firing the silver in place.

The frame is assembled on a special wire-wrapping/firing jig. The jig alines the beams while the ceramic adhesive is fired. Special combs attached to the jig guide the wire as it is wrapped on the frame. An automated wire-wrapping machine is used when attaching the wire.

A key element in the assembly of a satisfactory frame is the proper choice of materials. Effective compositions for the frame material, the wire, the bonding agent, the silver paste, and the jig have been identified and tested. Data on these materials, and other information, can be obtained by requesting the Technical Support Package referenced below.

This work was done by Thomas M. Heslin of **Goddard Space Flight Center.** *For further information, Circle 83 on the TSP Request Card.*

This invention is owned by NASA, and a patent application has been filed. Inquiries concerning nonexclusive or exclusive license for its commercial development should be addressed to the Patent Counsel, Goddard Space Flight Center [see page A5]. Refer to GSC-12354.

Controlling the Shape of Glass Microballoons

Percent yield of "perfect" glass microballoons is increased.

Marshall Space Flight Center, Alabama

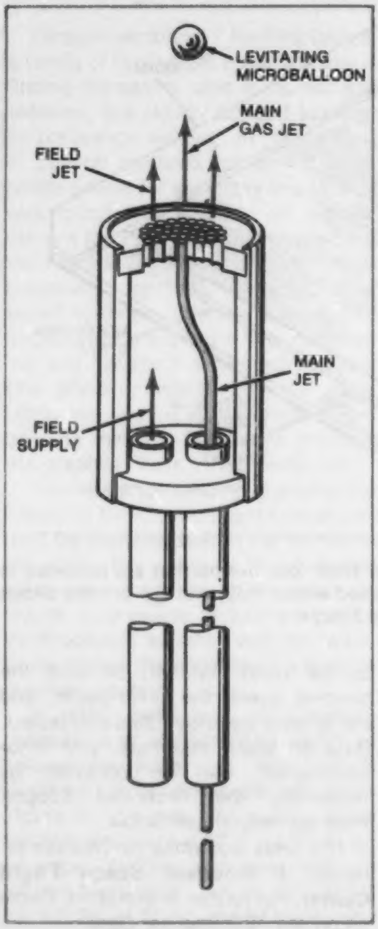

Improved Collimated-Hole Structure is made from a platinum/rhodium alloy, making it possible to increase the microlevitating furnace temperature limit to 1,450° C. The levitating gas jets are supplied by two lines: one feeding through the center hole, forming the main jetstream, to support and manipulate the suspended microballoon, and the other feeding the remaining holes to keep the microballoon in the center during the heat treatment. The new structure will speed up the remelting and reshaping of the microballoons, reducing the number of rejects for the laser fusion studies.

Glass microballoons encasing heavy hydrogen and used as targets in laser fusion studies must have a nearly perfect geometry and uniform wall thickness. Only a small fracton of a typical production lot is acceptable for use. Recently an economical method has been developed to improve the microballoon symmetry, using microlevitating furnaces that remelt and reshape the balloons suspended in gas. An analysis of this technology has produced further improvements: new furnace components that operate at higher temperatures and gases to be used for levitation that would not affect the glass materials.

A collimated-hole structure (CHS) was constructed from a refractory platinum/rhodium alloy that can operate at a furnace temperature of 1,450° C. This speeds up the shaping process. Stainless steel used previously limited the upper operating furnace temperature to 1,000° C. In the future, a tungsten CHS may be used. It will withstand furnace temperatures of 2,000° C, further speeding up the process.

The CHS configuration was also modified (see figure) using hexagonally-arranged jet holes for feeding the levitating gas. The central hole feeds the main jetstream, and the rest feed the field stream. The two flow velocities combine to suspend the microballoon and spin it on a horizontal axis, making it easier to manipulate it in a suspended state. The holes around the center are dimpled to stabilize the lateral-spinning microballoon.

Analysis of heat treatment revealed that oxygen fostered devitrification of the glass materials. Therefore, reducing gases (e.g., nitrogen or hydrogen) are recommended to eliminate this damage to the microballoon walls.

The furnaces, it was found, could also be improved using positive electronic sensing and control to maintain a constant pressure differential across the CHS when the furnace pressure and temperature are changing. This control will retain the microballoon in a stable levitating state.

This work was done by Stanley A. Dunn and Steven Gunter of Bjorksten Research Laboratories Inc. for **Marshall Space Flight Center.** *For further information, Circle 84 on the TSP Request Card.*

Inquiries concerning rights for the commercial use of this invention should be addressed to the Patent Counsel, Marshall Space Flight Center [see page A5]. Refer to MFS-25230.

Forming Complex Cavities in Clear Plastic

Lost-wax process is used
to mold plastic parts.

Lewis Research Center, Cleveland, Ohio

An increasing number of applications require the use of optically clear components. For example, these components are necessary for the efficient design of systems utilizing complex combustion and manifold systems. A technique has been developed that utilizes standard procedures developed for specialized metal casting. Complex internal cavities are readily formed in clear plastic parts by using elements of the "lost-wax" process.

The size and shape of the desired internal cavity are first replicated in a wax pattern. This pattern is then positioned in an assembly mold that conforms to the exterior requirements of the part. An inexpensive clear epoxy resin is cast into the mold and solidifies around the wax pattern. After curing of the epoxy, the wax is heated until it melts and is poured from the cavity. The figure shows the wax pattern, the assembly mold, and the finished casting. Substantial savings are obtainable utilizing this technique for the fabrication of parts with complex cavities.

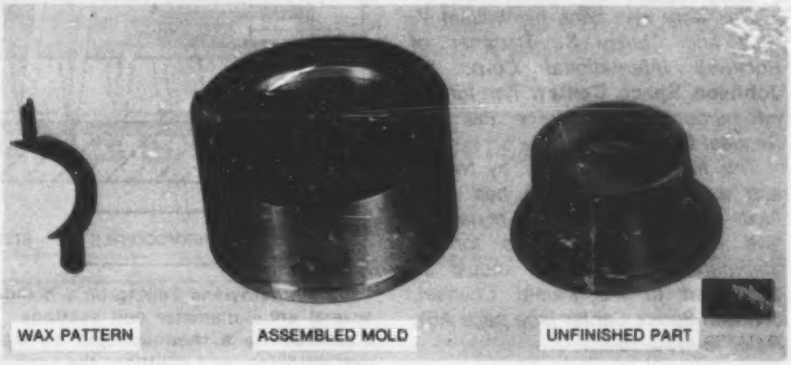

Economical Casting Process produces optically-clear plastic components of complex shapes.

This work was done by T. Riley, G. Matusik, and C. Casterline of **Lewis Research Center.** *No further documentation is available.*
LEW-13412

Shrinking Plastic Tubing to Nonstandard Diameters

Process allows larger-than-normal postshrink
diameters without splitting.

Lyndon B. Johnson Space Center, Houston, Texas

A new process allows heat-shrinkable plastic tubing to be shrunk to nonstandard sizes or to special contours. The new process for tetrafluoroethylene tubing minimizes temperature fluctuations and monitors the temperature to limit the shrinkage to a value greater than one-half the overexpanded diameter. Formerly, when shrinkage was restricted, the tube wall tended to split because it was too thin to resist the shrinking force at the shrink temperature.

The new method was originally used to prepare a seal for the cargo door of the Space Shuttle. A spring, which gives the seal its proper stiffness, is inserted into the shrunk tubing.

In the new shrinking method, the temperature of the tubing is monitored so that it can be removed from the oven at the proper time. A fiberglass-insulated thick-wall steel pipe is inserted in the shrinking oven to provide a uniform temperature enclosure (see figure). The tubing is slipped over an aluminum mandrel. The mandrel diameter is the same as the diameter required in the tubing. The mandrel is shorter than the tubing so that the ends of the tubing can be held partially closed by clamps that prevent the tubing from shrinking lengthwise. The tubing and mandrel are placed into a supporting coil of aluminum or steel wire. A thermocouple is positioned in the mandrel near one of its ends.

The assembly is slid into the hot steel pipe in the oven, with the thermocouple end nearest the oven door. The coil positions the mandrel and tubing at the center of the pipe.

The oven-temperature setting is kept at about 670° F (354° C) while the thermocouple temperature is monitored. When the thermocouple temperature reaches about 630° F (332° C), the mandrel and tubing are removed from the oven. The tubing will have shrunk to the desired diameter.

With the wire supporting coil and aluminum mandrel removed from the oven, a bolt of fiberglass is wrapped around the supporting coil so that cooling proceeds slowly. When the tube and mandrel have cooled, the

(continued on next page)

thin-tube mandrel is removed by chemical milling.

The method has been used to shrink 9-ft (2.74-m) lengths of 1.25-in. inner-diameter, 0.004-in. wall tubing to 0.75-in. inner-diameter, 0.008-in. wall (3.175-cm inner-diameter, 0.01-cm wall tubing to 1.9-cm inner-diameter, 0.02-cm wall).

This work was done by William V. Ruiz and Conley S. Thatcher of Rockwell International Corp. for **Johnson Space Center.** *For further information, Circle 85 on the TSP Request Card.*

This invention is owned by NASA, and a patent application has been filed. Inquiries concerning nonexclusive or exclusive license for its commercial development should be addressed to the Patent Counsel, Johnson Space Center [see page A5]. Refer to MSC-18430.

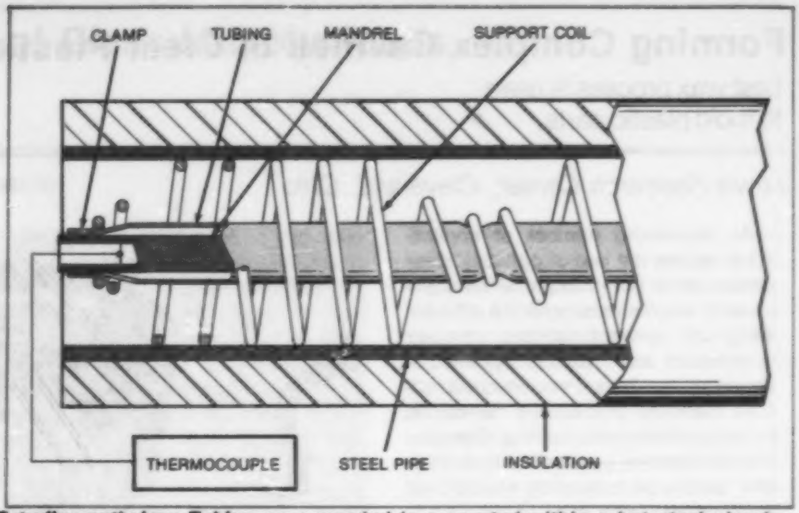

Tetrafluoroethylene Tubing on a mandrel is supported within a hot steel pipe by several small-diameter coil sections. The rising temperature of the mandrel is measured via a thermocouple so that the assembly can be removed without overshrinking (and splitting) the tubing.

Thermal Barrier and Gas Seal

Resilient baglike seal tolerates thousand-degree temperatures.

Lyndon B. Johnson Space Center, Houston, Texas

A high-temperature seal prevents gases from entering gaps between mating parts. The seal withstands temperatures of 2,300° F (1,260° C), or higher, and accommodates small changes in the gap size [width variations of about 0.06 inch (1.5 mm)] without losing its gas-barrier properties. At the same time, the seal maintains a smooth aerodynamic surface across the gap.

Developed for the Space Shuttle, where it closes the gap between the nose landing-gear doors and the forward fuselage, the seal may have high-temperature industrial uses as well, for example, in equipment for the liquefaction or gasification of coal.

As shown in the illustration, the seal contains alumina filler in a woven ceramic-fiber envelope. The alumina both insulates and seals, and the ceramic-cloth envelope stitched together with quartz thread holds the alumina in position between the sealed parts. A metal plate (made of a heat-

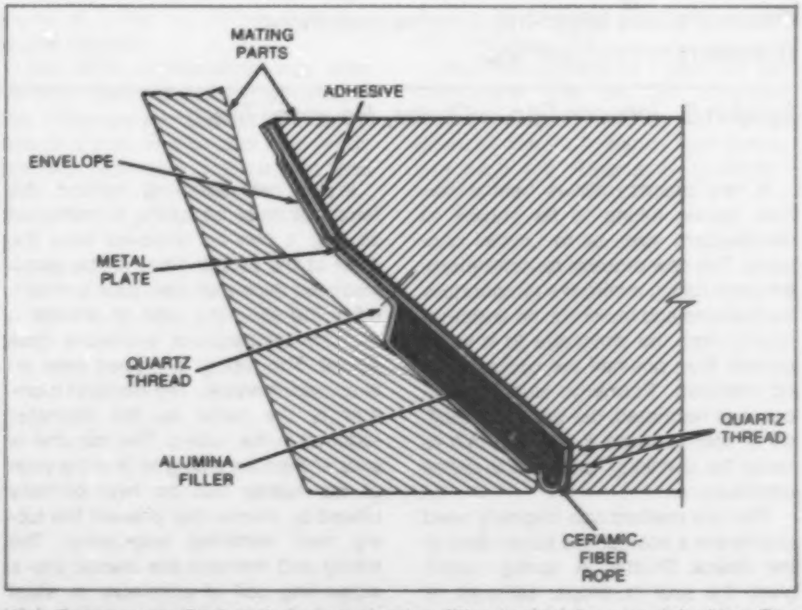

High-Temperature Seal includes an alumina filler backed by a metal plate. The alumina-filled envelope is easily handled and installed and can be used in high-temperature industrial processes, such as coal gasification and liquefaction.

resistant material such as nickel alloy) serves as the backbone and helps the seal hold its shape during fabrication, handling, and installation. A ceramic-fiber rope along the bottom of the plate furnishes a stiff rounded edge at the gap opening.

The materials were selected for their low thermal conductivity as well as their resistance to high temperatures. The plate side of the seal is bonded to the adjacent part with a high-temperature adhesive. The mating part then compresses the envelope and filler so that the gap is sealed. The seal changes its shape to conform to small changes in the gap width.

This work was done by John O. Kane and Milo Surbat of Rockwell International Corp. for **Johnson Space Center.** *For further information, Circle 86 on the TSP Request Card.*

This invention is owned by NASA, and a patent application has been filed. Inquiries concerning nonexclusive or exclusive license for its commercial development should be addressed to the Patent Counsel, Johnson Space Center [see page A5]. Refer to MSC-18390.

Heat-Shrinkable Sleeve Aids in Installing Universal Joints

Tubing stiffens the joint and protects it from contamination.

Lyndon B. Johnson Space Center, Houston, Texas

Heat-shrinkable tubing, normally used as electrical insulation on wire and cable, is now being applied in a new and quite different way — to "stiffen" universal joints so they can be attached to other structural members in confined spaces. This innovative technique, which saves considerable time and effort when assembling nonrigid parts, makes it unnecessary to use special holding fixtures or tools. In addition, the tubing also protects the joint from dust and other contamination.

The method was developed for attaching a universal joint on the end of a shaft to a spline fitting, where access to the spline is only through a small hole in a bulkhead (see figure). The tendency of the joint to "droop" under the pull of gravity makes it difficult to aline it with the spline.

To overcome this problem, assemblers place a length of heat-shrinkable tubing over the joint, as shown, and apply heat at the ends to shrink it in place. This stiffens the joint sufficiently so that it is easily alined with the spline. After the parts are joined, the sleeve remains in place as a shield against contamination. It is flexible enough so that it does not interfere with normal motion of the joint.

This work was done by William S. Green and Fredrick W. Thompson of Rockwell International Corp. for **Johnson Space Center.** *No further documentation is available.*
MSC-18685

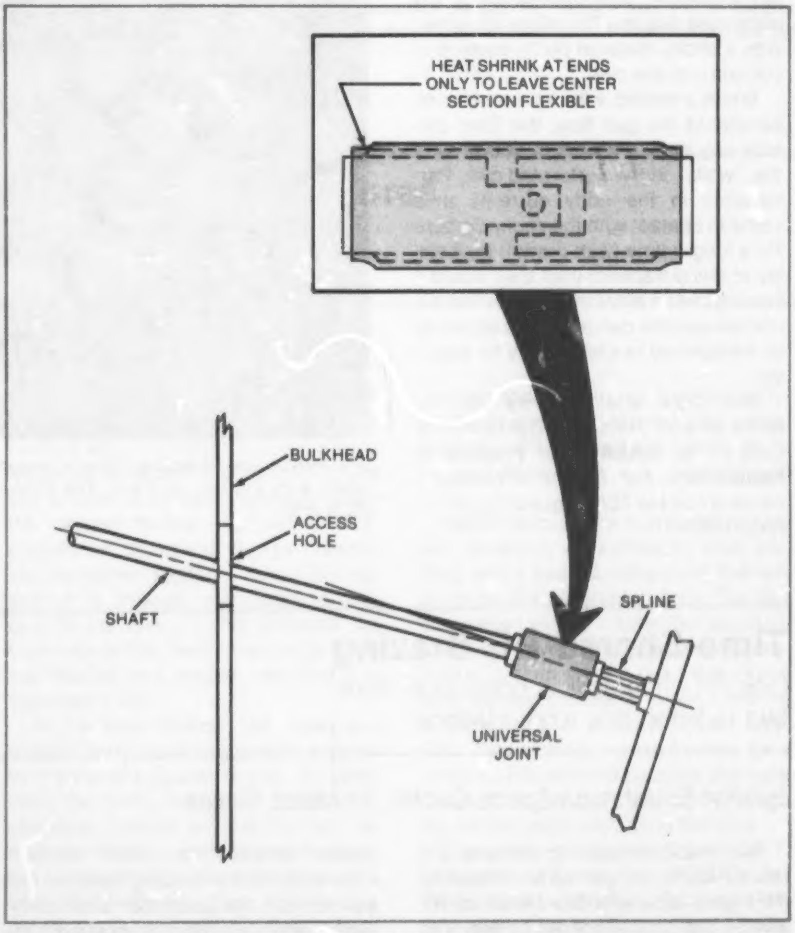

A Heat-Shrinkable Sleeve stiffens this joint so that it can be alined with a spline fitting. Previously, the unsleeved joint would droop, making it difficult to attach it to the splines.

Improved Particulate-Sampling Filter

Small surface indentations entrain a larger and more representative sampling.

NASA's Jet Propulsion Laboratory, Pasadena, California

A passive filter for sampling the particulates in a gas flow is more efficient because of its indented surface. When tested in the air-purge line of a planetary spacecraft, the indented surface trapped larger and more representative samples than did a petri-dish smeared with a smooth layer of adhesive. Potential applications of the improved filter are in air-quality monitoring at industrial sites, in mines, and in and around nuclear powerplants.

The new filter consists of a perforated aluminum disk backed by a flat plate (see figure). The plate is coated with a sticky material on its surface in contact with the disk.

When installed with its active area parallel to the gas flow, the filter creates tiny eddy currents in and around the "wells" in the perforated disk. Particulates in the eddy currents thus come in contact with the sticky surface for a longer time (with greater probability of being trapped) than they would if flowing over a smooth surface. The extracted sample can be analyzed onsite or transported to a laboratory for analysis.

This work was done by Alan R. Hoffman and Horst W. Schneider of Caltech for **NASA's Jet Propulsion Laboratory.** *For further information, Circle 87 on the TSP Request Card.*
NPO-14801

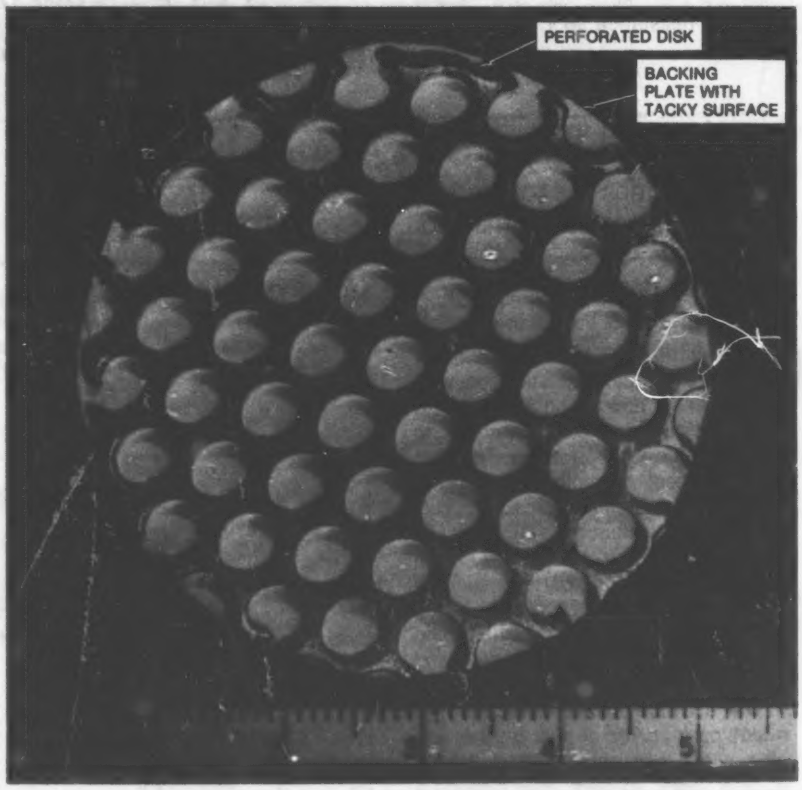

The **Particulate-Sampling Filter** is assembled from a perforated disk and a flat backing plate with a sticky surface. The thickness of the perforated disk is about 1/8 inch (0.31 cm).

Time-Shared RF Brazing

One RF generator is controlled from two independent work stations.

Lyndon B. Johnson Space Center, Houston, Texas

Two induction-brazing stations are served by a single radio-frequency (RF) generator with the aid of an RF switch and simple control boxes. The time-shared outlet increases the utilization and productivity of a costly RF power generator.

The two-station system was developed for brazing tubular joints on the Space Shuttle life-support system. Operators at the brazing stations use power from the generator alternately; while one operator is brazing, the other sets up a new workpiece.

A standard RF switch routes power from a 30-kilowatt generator to either of the stations. The switch is controlled by boxes at the brazing stations (see figure). When an operator turns on the control box and presses the "station select" switch on that box, the RF switch connects that station to the generator.

A light on each control box indicates which operator has control. When the generator has warmed up, a "ready" lamp lights up. Operator 1 pushes the "braze" button on control box 1, and RF energy flows to station 1. When the work is finished, operator 1 pushes the "stop" button. The generator is then available to operator 2, who pushes the buttons on control box 2 to braze at station 2.

Brazing may be stopped automatically, instead of manually, by a brazing-temperature controller at the station; or a timer in the RF switch housing may terminate a brazing operation automatically. The RF switch is air-operated with water-cooled contacts. If the switch loses air pressure, the generator is automatically prevented from transmitting power.

This work was done by John A. Stein and Maurice A. Vannasse of Rockwell International Corp. for **Johnson Space Center.** *For further information, Circle 88 on the TSP Request Card.*
MSC-18617

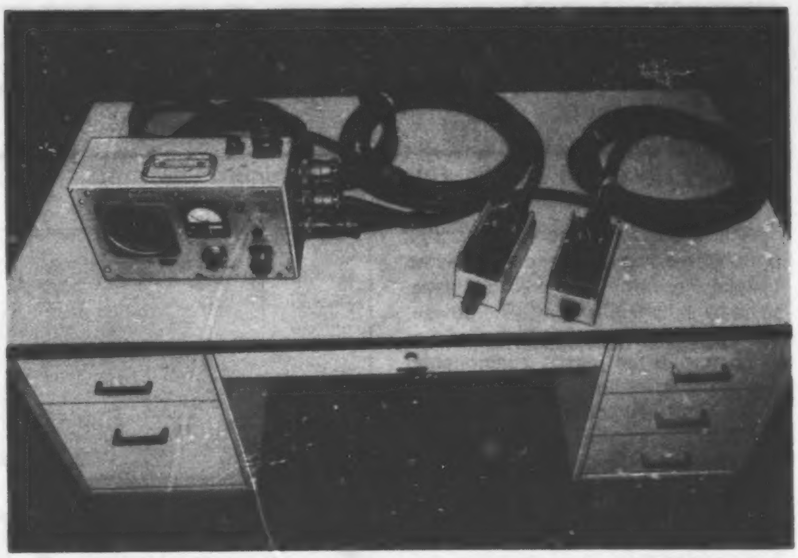

Control Boxes for Stations 1 and 2 connect to the RF switch and RF generator through a master control box (left). The master control must be turned on before the ancillary control boxes can be used.

Producing Gapped-Ferrite Transformer Cores

Improved manufacturing techniques make reproducible gaps and minimize cracking.

NASA's Jet Propulsion Laboratory, Pasadena, California

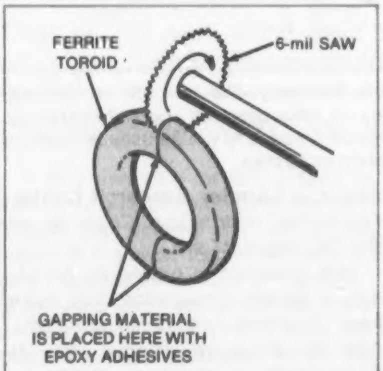

Molded Unfired Transformer Cores are cut with a thin saw and then fired. The hardened semicircular core sections are then bonded together, placed in an aluminum core box, and fluidized-coated. After the winding is run over the box, the core is potted. This economical method significantly reduces the number of rejects.

New fabricating techniques produce more-uniform ferrite toroidal core inductors with an airgap. In conventional methods, airgaps in transformer cores are produced by partly grinding away the central hollow sections of cup-shaped half cores and then by cementing the halves together. Since this operation is manual, the gaps are frequently not uniform and, because the cores are brittle, many crack apart during winding and potting, resulting in a high reject rate.

In the new method, the cores are molded from fine ferrite powder shaped by means of a volatile binder. As taken from the mold, the toroid is soft and chalklike. Instead of firing the mold to cure the binder, as is normally done, the cores are cut apart radially using a 6-mil (0.2-mm) saw (see figure). The halves are then fired to produce a hard semicircular core section. The toroid is formed when both halves are cemented together using commercially-available gapping material and epoxy adhesive. This allows the final core to be assembled with any required gap size.

Before potting, the cemented halves are placed in an aluminum core box filled with a sealing compound that will surround the assembled core. The box is covered with a washerlike epoxy/fiberglass cover and fluidized-coated. Wiring is then wound over the aluminum box that encases the core. Potting is performed in a conventional way, after the winding; however, this time stresses are relieved because the core is free to adjust itself within the damping compound surrounding the core.

This work was done by Colonel W. T. McLyman of Caltech for **NASA's Jet Propulsion Laboratory.** *For further information, Circle 89 on the TSP Request Card.*
NPO-14715

Plastic Welder

Induction heating is used to join plastic parts.

Langley Research Center, Hampton, Virginia

A low-cost, self-contained, and portable welding system developed at Langley Research Center joins plastic parts by induction heating. The device can be used in any atmosphere or in a vacuum, and the plastic components can be joined in situ.

Conventional methods used to join thermoplastics and composites include adhesives, fusing, and mechanical fasteners (e.g., using nuts and bolts or rivets). Adhesives are not reliable when parts are exposed to a vacuum, and fusing often deforms the plastic and causes it to flow around a joint. Mechanical fasteners require hole preparation and special hardware; riveting, if heat is used, can cause hole deformation; and nuts and bolts may require two people for assembly, especially with large sheets. Induction heating, however, causes little or no deformation at the joints, utilizes few component parts, and can be used with almost any type of thermoplastic.

A modified, wound, toroidal inductor core (see illustration) is used to transfer magnetic flux through the thermoplastic to a carbon steel screen. The airgap cut into the toroid diverts the path of the magnetic flux from the toroid to the screen.

Typically the metal screen would be cut into long strips 1/4 in. (0.64 cm) wide and sandwiched between sheets of plastic at a joint to join one sheet of plastic to another or to join a plastic sheet to a structural beam. The airgap of the toroid is placed on one of the plastic surfaces directly above the screen. When the toroid is energized, the alternating current produces inductive heating in the screen, causing the plastic surfaces on either side of the screen to melt and flow into the screen and forming the joint. The temperature of the screen is determined by such factors as the input power, number of coil windings, width of the airgap, and the frequency of the alternating current. The toroid is moved along the seam or joint at a controlled speed to produce optimum joining.

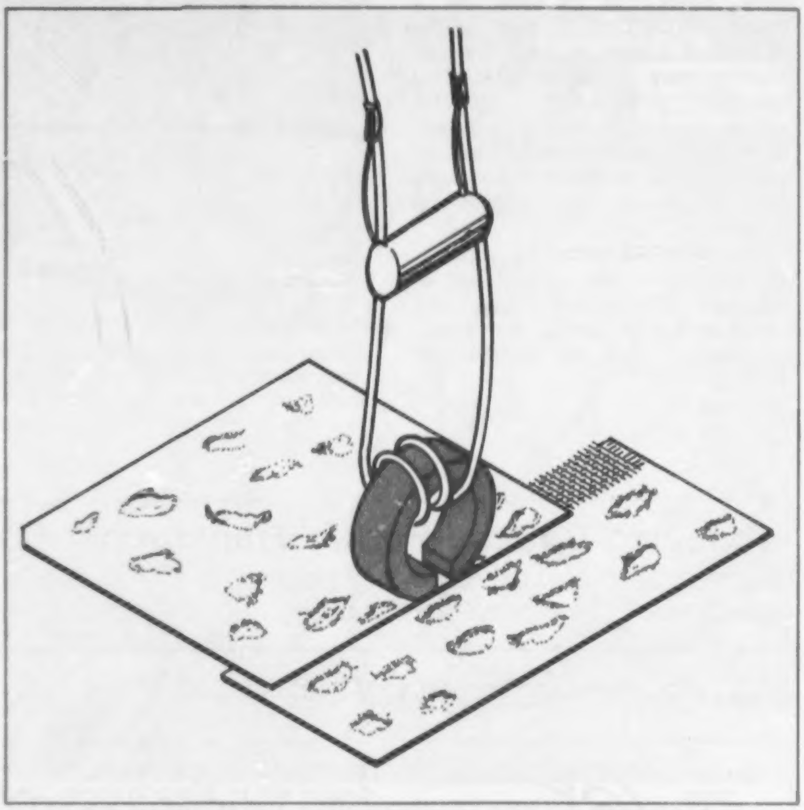

Inductive-Heating Welder joins plastic sheets thermally. The low, 25- to 100-watt, power required readily permits it to be battery- or solar-powered and self-contained. Various configurations of the plastic welder could be used in the aerospace industry and in the automobile, furniture, and construction industries.

This work was done by John D. Buckley, Robert L. Fox, and Robert J. Swaim of **Langley Research Center.** *For further information, Circle 90 on the TSP Request Card.*

This invention is owned by NASA, and a patent application has been filed. Inquiries concerning nonexclusive or exclusive license for its commercial development should be addressed to the Patent Counsel, Langley Research Center [see page A5]. Refer to LAR-12540.

Electron-Beam Welder Circle Generator

A generator rotates an electron beam and performs
other convenient functions during the welding process.

Marshall Space Flight Center, Alabama

Conventional electron-beam welders will not rotate the beam in a circular pattern. Circular or arc joints are usually welded by time-consuming techniques relying heavily on the operator's skill. A new circle generator automatically guides the beam in preset circular or elliptical patterns. The generator output is ac coupled to the welder deflection coil to preclude dc offset that could affect the beam alinement.

The generator utilizes two equal-amplitude sinusoidally varying signals set 90° out of phase (see control panel drawing). One signal controls the x-axis displacement, and the other controls the y-axis displacement. The method is identical to that used to produce the well-known Lissajous patterns on oscilloscopes. By varying the phase angle between the two signals, the beam can be made to describe either a circle or an ellipse.

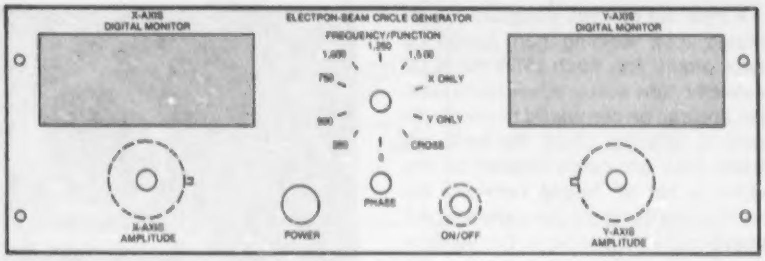

Electron-Beam Circle-Generator Panel has controls to set the beam in circular or elliptical patterns. The panel has x- and y-axis signal amplitude controls and permits phase adjustment between the two signals to weld circular or elliptical joints. A frequency selector on the panel controls the beam travel speed. Two digital readouts monitor the amplitudes of x- and y-axis inputs.

The welding speed can be varied with a frequency selector that ranges from 250 to 1,500 Hz in 250-Hz steps. The amplitudes of the x- and y-axes are varied by adjusting the phase shift. Both high- and low-range adjustments are available, and each axis can be controlled separately. A crosshair is provided for setup and beam alinements.

This work was done by Richard K. Burley of Rockwell International Corp. for **Marshall Space Flight Center.** *For further information, Circle 91 on the TSP Request Card.*
MFS-19441

"Foreign Material" To Verify Root Fusion in Welded Joints

A foil or thin wire at the weld root can
be used to verify weld penetration.

Marshall Space Flight Center, Alabama

A very thin wire, or foil, placed at the root of an electron-beam weld joint before the welding can verify the fusion of the weld root. The material (e.g., gold or zirconium) is "foreign" to the weld joint; and since only very small amounts are used, it does not affect the joint structure. When the weld is adequately penetrated, the material mixes with the weld, and traces of it diffuse to the top (the weld crown). A chemical analysis (e.g., spectroscopic) of samples taken from the weld crown will identify the foreign material and verify that the root has fused.

Weld roots are difficult to examine because the root is usually inaccessible to visual inspection. X-ray and ultrasonic inspection techniques, two commonly available methods, are not always reliable.

Using the new method, weld samples can be rapidly prepared without elaborate machining that could delay the production line. Any convenient handtool can be used to remove minute samples from the crown. Also spectroscopic analysis is highly sensitive so that a minimum amount of trace material can be used to avoid degrading the weld. The content of trace foil in the weld crown is predictable from the amount placed at the root and is accurately measurable by spectroscopic elemental analysis.

Currently, computer studies are being made to determine the optimum amount of material to be used without degrading the weld structure. Good results have been obtained using a gold/nickel alloy, which may be even better than gold in minimizing possible weld embrittlement.

This work was done by R. E. Kleint of Rockwell International Corp. for **Marshall Space Flight Center.** *For further information, Circle 92 on the TSP Request Card.*

Inquiries concerning rights for the commercial use of this invention should be addressed to the Patent Counsel, Marshall Space Flight Center [see page A5]. Refer to MFS-19496.

Tube-Welder Aids

Simple tools assist in setting up and welding tubes.

Lyndon B. Johnson Space Center, Houston, Texas

A new set of tools designed for repeated tube welding can speed up mass production. Each set is made for a specific tube size and weld-joint location and can be compared to templates used in lettering. Once the tools are made, they are easily slipped on the tubes to set an airgap between the welding head and the joint and to mark sleeve and joint positions. Conventional measurements are too slow for mass production and are prone to errors similar to sloppy hand lettering without a template.

The set, as shown in the photograph, includes an electrode locator, a sleeve cup, and a tube-locator cup. The electrode locator incorporates a sleeve that fits over the tube to be joined. The sleeve thickness matches the desired gap between the electrode and the weld joint. The electrode housing is simply slipped over the sleeve, and the electrode is lowered to touch the sleeve surface. This sets the gap, and the electrode is tightened in that position for repeated use without further readjustments.

The sleeve cup is simply slipped over the tube end like a cap. The cup in place, the tube is marked around the cup edge to show where one end of a welding sleeve will join the tube. The same procedure is repeated with a mating tube end to mark the other end of the welding sleeve.

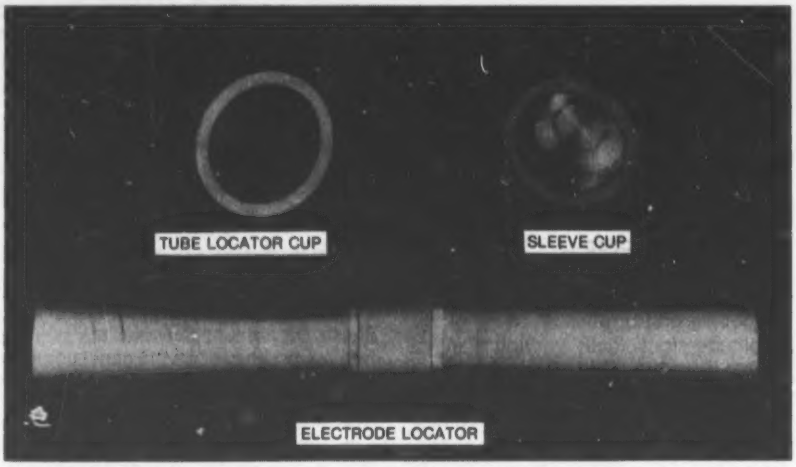

Tube-Welder Aids speed up mass-production tube welding. A set of such tools can be easily made to fit a given tube diameter. A finished set can be used repeatedly to fix the electrode-to-weld gap and to mark the sleeve and joint positions.

A somewhat similar tube-locator cup is also slipped over a tube end. Its edge marks a stop for a weld-locator tool moved flush against the cup. The weld-locator tool is clamped at that location to show the area where the tube is to be welded.

The tools can be readily made in most tube-manufacturing plants and will more than pay for themselves in a very short time in reduced labor costs and quality control.

This work was done by James F. Weaver of Rockwell International Corp. for **Johnson Space Center.** *For further information, Circle 93 on the TSP Request Card.*
MSC-18687

Honing Fixture for Weld Electrodes

A fixture for refacing electrodes mounts directly on the welding machine.

Marshall Space Flight Center, Alabama

Weld quality is improved by a honing fixture that attaches directly to the welding machine. Although developed for refacing the electrodes on a particular commercial welder (Unitek), the fixture could easily be adapted to other resistance welding machines.

The new fixture is used in lieu of manually refinishing the electrodes with emery paper or other abrasive. It produces uniformly flat, parallel electrodes, in contrast to the rounded and skewed faces and generally inconsistent results of the manual approach. Moreover, it does so in less time, which can translate into significant cost savings on production runs.

As shown in the figure, the honing fixture consists of a free-floating arm that travels along a cylindrical shaft. A special bracket attaches the shaft to the welding machine.

An abrasive stone is clamped in a slot on the free-floating arm. Thus, the fixture allows the operator to move the stone up and down between the electrodes. As long as the stone is flat and the fixture is properly alined, the flatness and parallelism of the electrode faces are assured.

This work was done by R. F. Nicholas and W. H. Schubert of Rockwell International Corp. for **Marshall Space Flight Center**. *To obtain drawings of the electrode honing fixture, Circle 94 on the TSP Request Card.*
MFS-19537

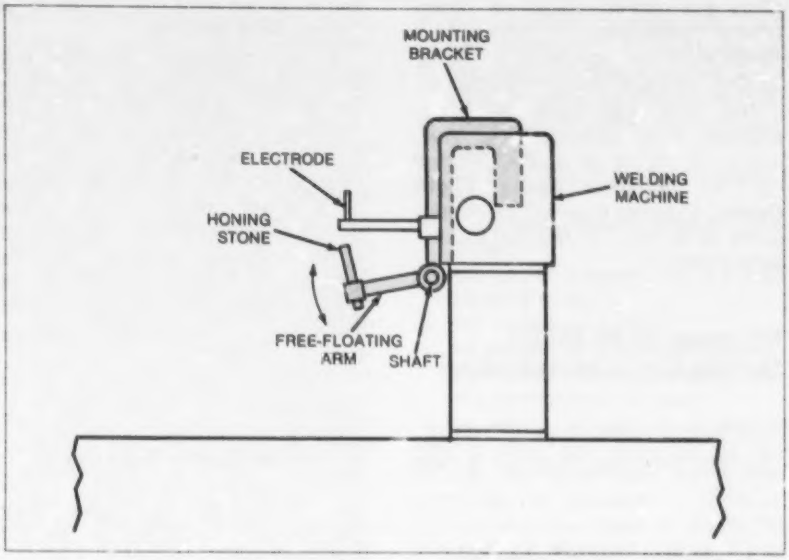

The **Honing Fixture** is installed on the welding machine by using a mounting bracket. The up and down movement of the stone against the electrode can be done manually, or a motor drive could be designed.

Books and Reports

These reports, studies, and handbooks are available from NASA as Technical Support Packages (TSP's) when a Request Card number is cited; otherwise they are available from the National Technical Information Service.

Silicon Nitride Passivation of IC's

A feasibility study looks at the effectiveness of a silicon nitride passivation coating against the effects of moisture and mobile ions.

A 49-page report evaluates the effectiveness of depositing low-temperature (100° to 300° C) silicon nitride protective layers on wire-bonded integrated circuits mounted on lead frame assemblies. A feasibility study evaluated the effectiveness of silicon nitride passivation in inhibiting the corrosion due to moisture at wire interconnect sites of plastic-molded integrated circuits. The study assessed the overall protection given a plastic-encapsulated device containing charge-sensitive microcircuits. A CMOS microcircuit was used in the study.

Two methods of silicon nitride passivation were studied: photonitride passivation and plasma nitride passivation. The devices were passivated (not to be confused with passivation of the chip alone) while still attached to the lead frames. After passivation and encapsulation, the devices were subjected to a sequence of accelerated electrical and environmental tests. The tests included temperature cycling, high-temperature electrical stress, and temperature and humidity exposure. Electrical parameter measurements were made of all devices initially and then at intervals in the course of each test.

From the tests it was concluded that photonitride passivation is compatible with all wire-bonded lead frame assemblies tested, with or without initial chip passivation, and that plasma nitride passivation of lead frame assemblies is possible only if the chip is passivated before assembly. The survival rate after the environmental-test sequence of devices with a coating of plasma nitride on the chip and a coating of either plasma nitride or photonitride over the assembled device is significantly greater than that of devices assembled with no nitride protective coating over either chip or lead frame. The majority of devices with unpassivated chips and with photonitride over the lead frames survived the environmental test sequence.

Moreover, the report concludes that plastic-encapsulated circuits incorporating a photonitride protective coating exhibit high survival rates. The survival of devices with no prior chip passivation suggests the possibility of simplifying the device fabrication process by eliminating the chip passivation operation.

In addition to descriptions of the passivation processes, the report includes several tables that summarize the results of the tests. There are also figures included that show the effects of flexing on the coatings.

(continued on next page)

[Also see related article on photonitride passivation, "Photonitride Passivating Coatings for IC's" (MFS-25401), on page 231 of this issue.]

This work was done by J. J. Erickson, F. L. Gebhart, T. C. Hall, and J. W. Peters of Hughes Aircraft Co. for **Marshall Space Flight Center.** *To obtain a copy of the report, Circle 95 on the TSP Request Card.*
MFS-25309

Progress in MOSFET Double-Layer Metalization

Theoretical and experimental studies are described in a new report.

A 237-page report describes a one-year research effort in VLSI fabrication. Four activities are described:

- a theoretical study of two-dimensional diffusion in SOS (silicon-on-sapphire);
- the setup of a sputtering system, furnaces, and photolithography equipment;
- experiments on double-layer metal; and
- an investigation of two-dimensional modeling of MOSFET's (metal-oxide-semiconductor field-effect transistors).

Computer simulations of various phosphorus and boron diffusions in SOS were completed using a diffusion program. The objective was to produce curves of the variation with diffusion time and temperature of the junction depth, sheet resistance, and integrated impurity dose. Data were generated for boron and phosphorus redistributed in nitrogen, dry oxygen, and steam ambients for <111> oriented SOS films, using a model that considers the implanted profile, oxidation, and diffusivity.

In place at the IC-fabrication facility are the furnaces, the photolithography apparatus, and other equipment for double-layer metalization. The only missing apparatus is an SiO_2 reactor.

Previous double-layer metalwork emphasized wet chemistry. By incorporating ultrasonic etching of the vias, premetal cleaning with modified buffered HF, phosphorus-doped SiO_2, and extended sintering, yields of 98 percent were obtained.

A two-dimensional modeling program has been written for the simulation of short-channel MOSFET's with nonuniform substrate doping. A key simplifying assumption is that the majority carriers can be represented by a sheet charge at the silicon dioxide/silicon interface. The program is not complete; however, the two-dimensional Poisson equation for the potential distribution has been solved. The status of other MOSFET simulations is summarized.

This work was done by J. D. Gassaway, J. D. Trotter, and T. E. Wade of Mississippi State University for **Marshall Space Flight Center.** *To obtain a copy of the report, "Trends and Techniques for Space Base Electronics," Circle 96 on the TSP Request Card.*
MFS-25239

Optimizing Costs of VLSI Circuits

Various costs of custom VLSI circuits are analyzed.

An 85-page report analyzes the costs of developing and producing low-production-volume, customized VLSI (very-large-scale integrated) circuits. A relationship is developed between the IC cost and an electronic system cost using IC cost models that are based on a design/fabrication approach. The emphasis of this report is in developing an understanding between the cost and volume for custom circuits that will be used by NASA. Reliability is one of the major cost components in these models.

The first of the five report sections states the purpose of this project, summarizes the new models, and presents a brief history of electronic system development. Examples are cited of how the systems have grown in complexity from tube technology to modern VLSI circuits that pack up to 75,000 transistors.

The second section presents a macroscopic model of electronic system cost. The electronic system is assumed to be partitioned into LSI chips composed of distinct subassemblies. The cost of the entire system is then related to the subassembly cost, the number of subassemblies being variable depending on the integration level.

A macroscopic model of MOS IC chip cost is presented in the third section. The model is developed for IC die cost in terms of manufacturing parameters and the degree of integration as it relates to the die area.

The fourth section discusses die and system cost curves for four cases: (1) a full-custom seven-mask-level CMOS LSI, (2) standard CMOS LSI, (3) semicustom CMOS LSI in double metal, and (4) semicustom CMOS LSI in a single metal.

Four appendix sections conclude the report. Three list some very useful reference literature; the fourth presents a basic-language computer program used in analyzing die and system costs.

The report has a number of plotted curves that show relationships among various cost and circuit parameters. Benefit-to-cost ratio, a popular decisionmaking tool in selecting the most economical system circuits, is also presented.

The presented analysis serves as a solid basis for future cost modeling. As the models become more precise, electronic systems manufacturers will be able to tailor an optimum mix of standard and customized IC's that would go into a particular system.

This work was done by Koy B. Cook, Jr., and David V. Kerns, Jr., of Auburn University for **Marshall Space Flight Center.** *To obtain a copy of the report, "Cost Optimization in Low Volume VLSI Circuits," Circle 97 on the TSP Request Card.*
MFS-25348

An Automated Oxide and Diffusion Facility for IC's

Totally-automated oxidation and diffusion facility for fabricating the IC's

A 34-page report discusses an IC fabrication facility developed at the Marshall Space Flight Center. [Also see related articles "An Automated Photolithography Facility for IC's" (MFS-25073) and "Automated Ion Implantation for IC's" (MFS-25193) on page 115 of *NASA Tech Briefs*, Vol. 5, No. 1.] The almost-entirely-automated oxide-growth and diffusion plant will be a part of an overall IC fabrication facility requiring virtually no labor other than process-control monitoring. The facility will produce ultrareliable IC's that will function for 25 years or longer in spaceflights and other critical applications.

The new system will process wafers arriving at the facility on an air track. The wafers will be automatically loaded into a furnace tube, processed, returned to the track, and sent to the next operation. The entire process will be controlled by a computer.

At this stage the system was already installed at the two three-stack furnaces and checked. The following diffusion and oxidation processes were demonstrated: (a) wet and dry oxidation for general use, (b) wet and dry oxidation for gate oxide, (c) boron diffusion, (d) phosphorus diffusion, and (e) sintering.

Part of the system incorporates state-of-the-art components and processes, such as the diffusion furnace and high-temperature-grown oxide. However, several major innovations have been demonstrated: (a) process controller specifically designed for semiconductor processing; (b) an automatic loading system to accept wafers from an air track, insert them into a quartz carrier, and place the carrier on a paddle for insertion into the furnace; (c) automatic unloading of the wafers back onto the air track; and (d) boron diffusion using diborane.

The system will perform oxidation and diffusion processes as required for PMOS processing. No experience is yet available on the productivity of the design; however, enough data have been gathered to suggest several improvements in future systems. These include a more-flexible real-time process controller with improved capacity, a simpler means of rotating the quartz carrier 90° and laying it on the paddle, boron diffusion using solid boron or boron tribromide, and an adjustable air track that would prevent the wafers from "hanging up."

The overall diffusion system consists of the following:

a. two existing commercially-available three-stack diffusion furnaces,
b. two special load stations that incorporate a wafer track and buffer tee,
c. two automatic wafer-boat elevation systems,
d. six automatic wafer-boat insertion systems,
e. a computer-based process controller,
f. two source cabinets for the gas-blending systems,
g. eight one-boat loaders,
h. six gas-blending assemblies, and
i. expendable materials (quartz, silicon carbide and the like).

The report includes a number of photographs and drawings of the facility. Operating details and parameters are also discussed.

This work was done by Bobby W. Kennedy of **Marshall Space Flight Center.** *To obtain a copy of the report, "Thermally Grown Oxides and Diffusions for Automatic Processing of Integrated Circuits," Circle 98 on the TSP Request Card.*
MFS-25357

Computer Programs

These programs may be obtained at very reasonable cost from COSMIC, a facility sponsored by NASA to make new programs available to the public. For information on program price, size, and availability, circle the reference letter on the COSMIC Request Card in this issue.

Predicting Crack Propagation

Flaw growth under load is predicted in two dimensions.

Structural flaws and cracks may grow under fatigue-inducing loads and, upon reaching a critical size, cause structural failure. The growth of flaws and cracks may occur at load levels well below the ultimate load-bearing capability.

The Advanced Crack Propagation Predictive Analysis Program, FLAGRO4, aids in predicting the growth of preexisting flaws and cracks. FLAGRO4 provides fracture mechanics analysts with a computerized method of evaluating the "safe crack-growth life" of structural components. FLAGRO4 could also be used to evaluate the damage tolerance of a structure.

The propagation of a crack is governed by the stress field in the vicinity of the crack tip. The "stress intensity factor" is defined in terms of the relationship between the stress field magnitude and the crack size. The propagation of the crack becomes catastrophic when the local stress intensity factor equals the fracture toughness of the material.

FLAGRO4 uses a two-dimensional model that predicts flaw growth in two directions independently, based on the calculation of stress intensity factors. The analyst may specify that the growth rate be controlled by Collipriest's equation, Forman's equation, Paries' equation, or by tabulated, user-supplied data. FLAGRO4 can model part-through, through, and corner cracks located on panels, on panel edges, at open holes, at pin-loaded holes, at pin-loaded lugs, and on tub or bar surfaces. The modeling of the crack growth may be continued until propagation becomes catastrophic. FLAGRO4 can accommodate part-through to through crack transitions, stress gradients across the width and thickness, cold-worked hole residual stresses, material property variations due to environmental changes, and Willenberg retardation.

Input to FLAGRO4 consist of initial crack definition (which can be defined automatically), rate-solution type, flaw type and geometry, material properties (if they are not in the built-in material table), load-spectrum data, load-stress functions, and design-limit stress levels. FLAGRO4 outputs include echoes of the inputs with any errors or warning messages and a life-history profile of the crack propagation.

(continued on next page)

FLAGRO4 is written in FORTRAN IV for batch execution and is available for CDC and IBM machines. The CDC version (MSC-18718) has been implemented on a CDC 6000-series machine with a central memory requirement of approximately 150K (octal) of 60-bit words. The IBM version (MSC-18721) has been implemented on an IBM 360-series machine with a central memory requirement of approximately 260K (octal) 8-bit bytes. The FLAGRO4 program was developed in 1979.

This program was written by Tianlai Hu of Rockwell International Corp. for **Johnson Space Center.** *For further information, Circle K on the COSMIC Request Card.*
MSC-18718 and MSC-18721

Mathematics and Information Sciences

Hardware, Techniques, and Processes

251 An Approximation to Student's t-Distribution
252 Low-Cost Landsat Processing System

Computer Programs

252 NASA PERT Time II
253 Linear Stochastic Optimal Control and Estimation Problem
254 Multiple Linear Regression Analysis
254 Structured FORTRAN Preprocessor
254 MBASIC Processor
255 Basic Cluster Compression Algorithm
255 System Time-Domain Simulation
256 Image-Based Information, Communication, and Retrieval

An Approximation to Student's t-Distribution

Three equations relate Student's t-distribution to the standard normal distribution.

Langley Research Center, Hampton, Virginia

During the development of a computer subroutine, an approximation to Student's t-distribution was needed that would be accurate for all degrees of freedom yet would not occupy much memory space. The set of equations in Figure 1 was tested and found to satisfy these requirements. They give a maximum error of less than 0.8 percent and a typical error of less than 0.01 percent.

Equation (1) expresses the t variable of Student's t-distribution as a function of the variable z of the standard normal distribution function and the number of degrees of freedom ν. The equation is thus a prescription for converting standard normal distribution tables to Student's t-distribution tables. In this approximation, t approaches z when ν is large, and t equals z for $\nu = \infty$.

Since no error estimates are given in the reference for equation (1), several values of t were computed and compared with exact values listed in a table of probability distributions. The comparison indicated that the approximation is excellent for degrees of freedom larger than 6. It is inadequate, however, for degrees of freedom equal to 1 and 2. Fortunately, equations (2) and (3) give exact solutions for these cases.

The three equations were used to calculate values of t for values of probability equal to 0.995, 0.99, 0.975, 0.90, 0.80, 0.70, and 0.60 for each degree of freedom up to 120. These levels of probability correspond to z values of 2.5758, 2.3263, 1.9600, 1.2816, 0.8420, 0.5240, and 0.2533, respectively. The calculated t values were compared with exact values, and the errors are shown in Figure 2. The table shows that the set of equations covers the entire range with excellent accuracy. Since the approximation for t in equation (1) monotonically approaches the exact values as ν goes to infinity, the error of the approximation is greater at any value of ν than it is for larger ν values.

$$t = z + \frac{g_1(z)}{\nu} + \frac{g_2(z)}{\nu^2} + \frac{g_3(z)}{\nu^3} + \frac{g_4(z)}{\nu^4} \qquad (1)$$

where

$$g_1(z) = \frac{1}{4}(z^3 + z)$$

$$g_2(z) = \frac{1}{96}(5z^5 + 16z^3 + 3z)$$

$$g_3(z) = \frac{1}{384}(3z^7 + 19z^5 - 15z)$$

$$g_4(z) = \frac{1}{92,160}(79z^9 + 776z^7 + 1,452z^5 - 1,920z^3 - 945z)$$

$$t = \cot[\pi(1 - P)] \qquad \text{for } \nu = 1 \qquad (2)$$

$$t = \sqrt{\frac{1}{2P(1 - P)} - 2} \qquad \text{for } \nu = 2 \qquad (3)$$

Figure 1. **Three Equations** approximate Student's t-distribution. Equation (1), used for $\nu > 2$, expresses the t variable in terms of the standard normal variable z. For $\nu = 1$ and 2, equations (2) and (3) express t exactly in terms of probability P. Equation (1) is listed in Handbook of Mathematical Functions, AMS 55, National Bureau of Standards, U.S. Government Printing Office (1964).

ν	PROBABILITY, P							
	0.60	0.70	0.80	0.90	0.95	0.975	0.99	0.995
1						0	0	0
2						0	0	0
3						0.005	-0.016	-0.044
4						0.001	-0.003	-0.004
5							-0.001	-0.002
6	MAXIMUM ERROR <0.0005							
7								
•								
•								
•								
120								

Figure 2. **The Error of the Approximation** (where error is the difference between true and approximate values for t) is tabulated for ν between 1 and 120 and for several probabilities.

This work was done by Donald R. Rummler and Columbus W. Stroud of **Langley Research Center.** *No further documentation is available.*
LAR-12238

Low-Cost Landsat Processing System

Study shows Landsat analysis system can be assembled at a relatively low cost.

Marshall Space Flight Center, Alabama

Many potential users of Landsat data, such as state agencies and universities, do not have enough funds to purchase an automated Landsat data-analysis system. Most commercial units cost between $400,000 and $1,000,000, and even the assembled low-cost systems can be from $75,000 to $100,000. A recent study, however, has shown that a small-scale analysis system can be put together for about $30,000 — an affordable price for many potential users.

The proposed system would consist of a central processing unit (CPU) and memory, a dual floppy disk and dual-drive magnetic tape, a console and interface, an output device, and an interactive display, all commercially available. The key components are shown on the block diagram.

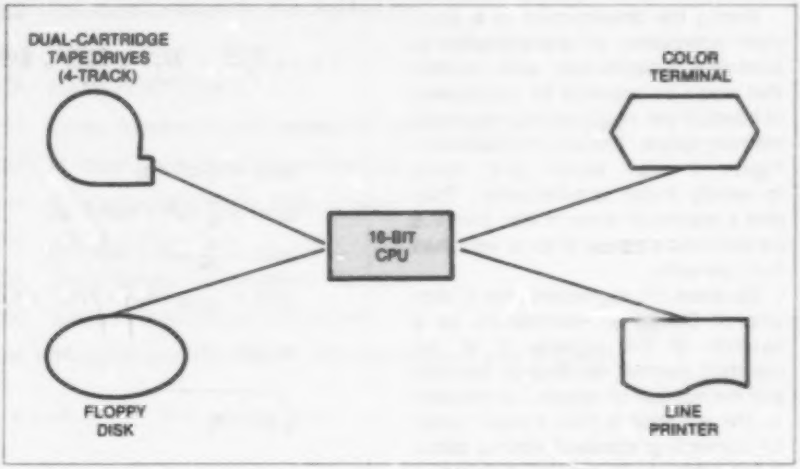

Small-Scale Landsat Data-Processing System can be assembled from commercially available components. The proposed system could be used by state agencies and universities that cannot afford expensive processing systems currently offered on the market.

The CPU would be a minicomputer with 32 kilowords of core memory. The floppy disk would have a 0.5-megabyte storage capacity. The magnetic-tape drive would be a 1,600-bits/in. (340-bits/cm), 4-track dual tape drive with 2.88 megabytes of storage capacity. The interaction display would be a 256- by 256-pixel display with a minimum of 6 bits of information per pixel (equivalent to a 64-color display). A cursor and zoom are highly-recommended display options that will make the analysis more accurate and convenient.

A number of processing programs written in FORTRAN IV is available for analyzing the Landsat data. Individual programs can process training-field selection, maximum-likelihood classification, linear classification, unsupervised classification, coordinate transformation, polygon extraction, rectification/sampling, and geographic data bases; and can also extract polygonal data that encompass parts of two Landsat scenes.

The proposed system can process Landsat data for subscene areas on a repetitive basis. With additional hardware enhancements, such as the floating-point processor and hardware multiply/divide, the system could process entire scenes of Landsat data in less than 2 days, not counting training-sample-selection time. Without these improvements, a full-scene classification for approximately 60 classes would take about 20 to 25 days of constant processing, assuming no equipment malfunction or power losses. The amount of time required for processing decreases linearly with the number of classifications desired (e.g., a full-scene classification with approximately 15 classes would take about a week of constant processing).

This work was done by Nickolas L. Faust, Nancy J. Hooper, and G. William Spann of Metrics, Inc., for **Marshall Space Flight Center.** *For further information, Circle 99 on the TSP Request Card.*
MFS-25336

Computer Programs

These programs may be obtained at very reasonable cost from COSMIC, a facility sponsored by NASA to make new programs available to the public. For information on program price, size, and availability, circle the reference letter on the COSMIC Request Card in this issue.

NASA PERT Time II

IBM 370 version of a versatile management tool

The planning and management of a large engineering project, where the interrelationships between activities and functional areas are numerous and involved, can become so complex that it is difficult to visualize as a whole. This potential problem readily lends itself to the employment of computerized data management systems. The Program Evaluation and Review Technique (PERT) is defined as a disciplined management technique involving computer processing.

NASA PERT Time II was developed as a computerized aid in the planning and control of project development variables, namely time and performance measurements. NASA PERT Time II can give the project manager an insight into current and future project development, as well as forewarning of potential problem areas. A formalized evaluation and planning system cannot replace good management; therefore, the usefulness of NASA PERT Time II is entirely dependent on analysis and judgment by the project manager. NASA PERT Time II can prove to be a very valuable aid, offering the project manager a better overview of the project as a whole.

The NASA PERT Time II program utilizes a modular technique. The module for computer system requirements is called a subnet; it is a subset or portion of a project-network activities. The program user will usually see this module as a "fragnet." A fragnet is defined as a meaningful portion of a project network. There is no significant difference between a subnet and a fragnet. A fragnet allows the user to represent project entities such as a subdivision of work, a contractor, an organization, a mission, a summary, or an integration network. Each fragnet will contain some events that are identical to events in other fragnets that make up the project network. These events are defined as interface events and identify the relations between fragnets.

Once all aspects of a project have been described in terms of fragnets, a control network is automatically generated. This control network is made up of control activities obtained by condensing all paths between control network events. Control network events are made up of interface events and all start and end events.

The program determines both expected and allowed dates for each control network event. Finally, the program generates reports on expected and allowed activity dates for fragnets specified by the user. As a project progresses, event and time variables in the fragnets and control network may be updated and new reports generated.

There are no well-defined limits on the size of the project that may be analyzed. The size of the project that may be analyzed depends mainly on the computer resources available and the level of detail used in the fragnets. The program is currently designed to handle a maximum of 50 fragnets with each fragnet containing a maximum of 2,160 activities, 2,000 events, and 500 starts, ends, and interfaces.

This program is written in FORTRAN IV and OS Assembler for batch execution and has been implemented on an IBM 370 with a minimum central memory requirement of approximately 350K of 8-bit bytes. (The original NASA PERT Time II program was developed in 1965 for use on the IBM 7094 and was adapted for use on the IBM 370 in 1979.)

This program was written by Ross C. Bainbridge, Frank Funicelli, Daniel J. Hirsch, Eugene A. Pallat, Elizabeth Ryan, and Joseph D. Walker of **Lewis Research Center** *and Hans Bremmer of Goddard Space Flight Center. For further information, Circle L on the COSMIC Request Card.*
LEW-13145

Linear Stochastic Optimal Control and Estimation Problem

IBM 360 version of LSOCE program

The linear stochastic optimal control and estimation problem (LSOCE) involves the design of controls for a linear time-invariant system that is disturbed by white noise in such a way as to minimize a performance index. These controls must be designed to use system measurements that are corrupted by white noise. The solution to the LSOCE problem is a Kalman filter coupled through a set of optimal regulator gains to produce the desired control signal.

The key to solving the LSOCE problem is the solution of the matrix Riccati differential equation. This equation occurs in solving for both the finite-time optimal linear regulator gains and the finite-time optimal linear estimator (Kalman filter) gains. A computer program, LSOCE, was developed to solve effectively the LSOCE problem for a wide range of practical applications. It has been used to design numerous control systems including the controls for supersonic inlets.

In solving the general LSOCE problem, it is helpful to study the infinite-time LSOCE problem in which the main equations to be solved use algebraic matrix Riccati equations. In practice, the solution of the algebraic equation is used in obtaining the solution to the more general differential equation. In this package, both the algebraic and differential equations are solved using an extension of the eigenvector method. For the infinite-time case, various system covariance matrices and mean-square values are computed as a measure of the control-system effectiveness.

The state-covariance matrix is obtained by solving the system Lyapunov equation, and the covariance of the error in system estimates is given by a Riccati equation. The program also offers the user the ability to solve common variations on the LSOCE problem including noise-free regulator problems and open-loop plant-covariance matrices problems. The LSOCE program is structured to handle any number of state variables and is restricted only by computer core availability. The program is currently dimensioned to handle up to 12 system state variables.

This program is written in FORTRAN IV for batch execution and has been implemented on an IBM 360 with a central memory requirement of approximately 77K of 8-bit bytes. The LSOCE program was originally developed in 1975 with the current version being released in 1979.

This computer program written in FORTRAN IV for use on the IBM 7094 computer, reference LEW-12505, and for use on the UNIVAC 1110/EXEC 8 computer, reference LEW-12540, was published previously in *NASA Tech Briefs*, Vol. 1, No. 4 page 657 (LEW-12540/LEW-12505).

This program was written by Lucille C. Geyser and F. K. Bruce Lehtinen of **Lewis Research Center.** *For further information, Circle M on the COSMIC Request Card.*
LEW-13206

Multiple Linear Regression Analysis

Rapid calculation of best-suited coefficients

A major problem in linear regression calculations is selection of the best set of coefficients. A computer program (MRA) for a multiple linear regression analysis automatically selects the best-suited set of coefficients. It uses an algorithm based on a procedure developed by Efroymson that proceeds one step at a time with statistical testing at each step. Since only the statistically most significant terms are considered, the best-suited coefficients can be calculated rapidly. The statistical testing incorporates a modification suggested by Draper and Smith to increase efficiency. The user need supply only the vectors of independent and dependent data and specify the confidence level required in the analysis.

The program uses a stepwise statistical procedure for relating a minimal set of variables to a particular set of observations. This is accomplished by introducing independent variables into the regression one at a time and ordering the selection of the next variable entered into the regression according to the magnitude of its partial correlation coefficient. The partial correlation coefficient gives the proportion of the variation of the dependent variable due to each of the independent variables not presently in the regression.

Once a variable has been added to the regression, all of the independent variables in the regression are tested for their statistical significance by calculating the added regression sum-of-squares due to each term. A variable that entered the regression at an earlier step may now prove to be statistically insignificant due to the influence of later terms. This insures that the final regression contains the statistically most significant set of coefficients.

This program is written in FORTRAN IV for batch execution and has been implemented on the NOVA 1200 with a core requirement of approximately 32K of 16-bit words. The MRA program was developed in 1977.

This program was written by Thomas R. Edwards of **Marshall Space Flight Center.** *For further information, Circle N on the COSMIC Request Card.*
MFS-23764

Structured FORTRAN Preprocessor

Structured-programing features simplify software design.

The NASA Structured FORTRAN Preprocessor was developed to assist programers in constructing reliable software. The preprocessor features "structured-programing" control structures that can be used to facilitate program design, coding, documentation, and debugging. The FORTRAN programer needs to learn only a few control statements to code his program in a structured format that is easy to debug and maintain. By freeing the programer from the flow constraints of standard FORTRAN, the preprocessor simplifies the design and coding of difficult logic flows and helps to improve software reliability.

The principal control structures supported by the preprocessor include the IF THEN ELSE, OR IF, DO WHILE, FOR, and TEST CASE statements. The first three are well-known structured-programing features that have previously been unavailable to the FORTRAN programer. With these features, codes can be structured without confusing the logical flow of the program with a large number of GO TO statements.

The FOR construct is a special iterative construct allowing code repetition by testing an index for a specified termination value. In the TEST CASE construct, the specified expression is checked for a match in the parameter string of a CASE statement. When a match is detected, the segment of code associated with the CASE statement is executed, and then execution is returned to the statement following the TEST CASE construct.

Input to the preprocessor may be a mixture of standard FORTRAN and structured control statements. The output is a standard FORTRAN program that is the logical equivalent of the input program and is ready for compilation and execution. During debugging, updating, and maintenance, the programers need to concern themselves only with the easy-to-follow structured program. Once any changes are made, the structured program is preprocessed and compiled again.

This software is written in ANSI FORTRAN and should be compatible with any machine supporting a FORTRAN compiler that accepts ANSI statements. The preprocessor has been implemented on an IBM 370-series computer with a central memory requirement of approximately 90K of 8-bit bytes. The preprocessor was developed in 1977.

This program was written by S. Austin, B. Buckles, and J. P. Ryan of Science Applications, Inc., for **Marshall Space Flight Center.** *For further information, Circle P on the COSMIC Request Card.*

Inquiries concerning rights for the commercial use of this invention should be addressed to the Patent Counsel, Marshall Space Flight Center [see page A5]. Refer to MFS-23813.

MBASIC Processor

UNIVAC and DEC-10 processors for a flexible efficient language

MBASIC, an advanced version of the BASIC language developed at Dartmouth College, is a high-level interactive computer language that reduces the time required to program a task for computer execution. Like BASIC and FORTRAN, MBASIC combines English and simple algebra to give instructions to the computer; however, MBASIC results in shorter, simpler programs that are easier to write and understand. In addition, practically all system commands needed for management information processing are available in MBASIC. This feature makes it unnecessary for MBASIC users to learn executive commands or to rewrite MBASIC programs to accommodate system changes. MBASIC should provide a powerful computing language for technical or management information processing and for scientific and engineering applications.

The conversational nature of MBASIC allows the user to interact with the program as it is being developed.

Each MBASIC statement is analyzed for errors as it is entered. Diagnostic error messages and versatile editing features make corrections quicker and easier. Any portion of a program may be executed before it is completely assembled. This ability is one of the fundamental design features of MBASIC and is the principal reason why MBASIC has truly conversational capabilities. Although individual statements may be syntactically correct, erroneous expressions can cause an interruption during program execution. If an interruption occurs, a diagnostic message is printed, and control is returned to the user. If necessary, the user may enter direct statements and execute them immediately. After program corrections have been made, execution can be resumed at any appropriate statement, including the statement in which the interruption occurred.

The power of MBASIC lies in its capacity to direct a computer to perform a large variety of complex tasks while the user supplies only a few simple English or algebraic instructions. The program instructions are written like sentences, resulting in a program that is easy to read and write. These instructions are combined into program modules that are written as paragraphs. Comments may be included to document module functions.

The outstanding features that contribute to the power of MBASIC include: multiple assignments in a single instruction; conditional, assignment, and repetitive statement modifiers; multiple statements in a single instruction; and excellent string-handling capabilities. Excellent array-handling capabilities are available, including assigning values while dimensioning, matrix algebra written like simple algebra, and combining simple and array expressions in a single instruction. The programer may use expressions to refer to statement numbers and may access magnetic tapes through terminals during program execution. The availability of these and other features leads naturally to a simplification of the program design process.

Two machine versions of the MBASIC processor are available, UNIVAC and DEC-10. The UNIVAC version is written in reentrant Assembler code for interactive execution under EXEC 8 and has a memory requirement of approximately 15K of 36-bit words. The UNIVAC MBASIC processor was developed in 1973. In 1977, an MBASIC processor was developed for use on the DEC System-10. The DEC-10 version is written in reentrant Assembler code for interactive execution under TOPS-10 and requires approximately 14K of 36-bit words. MBASIC is a trademark of the California Institute of Technology.

This program was written by R. Booth Hartley and Robert E. Holzman of Caltech for **NASA's Jet Propulsion Laboratory.** *For further information, Circle R on the COSMIC Request Card.*
NPO-14245

Basic Cluster Compression Algorithm

Feature extraction and data compression of Landsat data

The Basic Cluster Compression Algorithm (BCCA) program reduces the costs associated with transmitting, storing, distributing, and interpreting Landsat multispectral image data. This preprocessing algorithm uses feature extraction and data compression techniques to represent the information in the image data efficiently. The format of the preprocessed data allows simple lookup-table decoding and direct use of the extracted features. This reduces user computation needed for image reconstruction or computer interpretation of the image data.

The algorithm uses spatially local clustering to extract features from the image data to describe spectral characteristics of the data set. These features may be used to form a sequence of scalar numbers that define each picture element in terms of the cluster features. The sequence, called the feature map, may be represented efficiently by using source encoding concepts. It is possible to make various extensions on the Basic Cluster Compression Algorithm to obtain different types of compression characteristics.

The Basic Cluster Compression Algorithm was derived from the standard iterative approach to clustering. This approach requires only simple repetitive computations, and parallel processing can be used for very high data rates. The only user supervision required for the BCCA is the specification of the number of clusters desired. Initial cluster centers are selected to be well scattered throughout the set of all data vectors, and the BCCA is somewhat insensitive to the choice of initial cluster centers. Data vectors are assigned to clusters dependent on the relative distance between the data vector and the cluster center. The clustering is terminated whenever the clustering converges or whenever a specified number of iterations has been performed.

This program is written in FORTRAN IV for batch execution and has been implemented on an SEL 32/55 with a central memory requirement of approximately 27K of 32-bit words. The BBCA program was developed in 1977.

This program was written by Edward E. Hilbert and Jun-Ji Lee of Caltech for **NASA's Jet Propulsion Laboratory.** *For further information, Circle S on the COSMIC Request Card.*
NPO-14816

System Time-Domain Simulation

Complex systems can be simulated by engineers without extensive computer experience.

The System Time Domain (SYSTID) Simulation Program is a powerful tool for the transient simulation and analysis of complex systems. SYSTID requires little computer experience and has been used to simulate and analyze a wide range of systems, including communications systems and spacecraft power systems.

The analyst uses a free-form engineering-oriented language to input a topological "black-box" description of a system. SYSTID automatically generates the appropriate algorithms and proceeds with the simulation. The user has enormous flexibility in the representation of system elements;

(continued on next page)

any element may be defined in terms of the extensive SYSTID library of models, as a user-developed SYSTID model, or as a FORTRAN-coded algorithm. Models can be nested, and one can build a model library from a basic set. Furthermore the program can easily be linked to postprocessing routines for detailed analysis of the simulation results.

The basic SYSTID library consists mainly of routines that aid in the simulation of continuous functions. The technique of the bilinear z-transform representation of transform functions is used and may be defined in terms of poles and zeros or in terms of the classical functions, such as Bessel and elliptic functions.

SYSTID is designed to execute as a multipass processor in a batch or demand mode of operation. The first phase reads the user-input description of the system along with supporting models and performs a variety of error checks. This phase also formulates the FORTRAN algorithms corresponding to the system description. SYSTID can be viewed as a FORTRAN program generator that converts nonprocedural topological input into an executable computer program. If the first phase is completed successfully, the FORTRAN routines are compiled and linked with the SYSTID library and the simulation executed. For multiple simulations of the same system, the first phase needs to be completed only once. Simulation results are output as graphs and tables. Linking the simulation program to a postprocessor allows the user to access the time histories of any node or variable for further analysis.

The SYSTID program is written in FORTRAN IV for batch execution and has been implemented on a UNIVAC 1110 under control of EXEC 8, Level 31. The basic SYSTID system has a central memory requirement of approximately 60K of 36-bit words. This release of SYSTID was developed in 1977.

This program was written by Carroll T. Dawson, Theodore W. Eggleston, and Andy C. Goris of **Johnson Space Center;** *Mike Fashano and Dale Paynter of Hughes Aircraft Co.; and William H. Tranter of the University of Missouri — Rolla. For further information, Circle T on the COSMIC Request Card.*
MSC-18333

Image-Based Information, Communication, and Retrieval

IBIS/VICAR system combines video image processing and information management.

The IBIS/VICAR system is a powerful system for analyzing, manipulating, and managing image data. It combines the JPL IBIS (Image-Based Information System) geographic information management system and the JPL VICAR (Video Image Communication and Retrieval System) image-processing system. The IBIS/VICAR system has extensive general-purpose image-processing capabilities, and an information management system that accepts, converts, and operates on vector (graphical) and tabular data.

The system can be used to perform various image-processing functions on any type of digitized image data, including remotely sensed data such as Landsat multispectral scanner data. The image-processing functions available include picture comparison, picture expansion with noise elimination, convolution filtering, geometric transformations, Fourier transformations, and many other manipulation and enhancement procedures. In addition, the information management system handles image-related data and merges image data with other types of data files.

The IBIS system analyzes geographical problems by grouping selected functions from the IBIS library for investigation of a variety of spatial phenomena. Tabular and graphical data can be stored in registration with imagery data in the form of overlaid data planes. Information may be derived from simple associations and comparisons between two or more data files or from more complex procedures, including polygon overlay and spatial cross tabulation. The VICAR program library can be readily used to generate, input, output, and process image data for the IBIS system.

The IBIS/VICAR system, which requires minimal inputs, can be used by analysts with only elementary programing knowledge and a simple understanding of the system operation. The analyst calls for the automatic execution of one or more of the system programs, including the requisite image-data management services, through a set of command instructions. The flexible programs require that the user supply only the parameters specific to a particular application. Special-purpose input/output routines efficiently transfer image data with reduced memory requirements. New applications programs can be easily incorporated as they are developed.

The IBIS/VICAR system is a system of programs and control procedures written in FORTRAN IV, Assembler, and OS JCL for batch execution. The IBIS/VICAR system has been implemented on an IBM 360-series computer with a minimum central memory requirement of approximately 150K of 8-bit bytes. The IBIS/VICAR system was released in 1979.

This program was written by Nevin A. Bryant and Albert L. Zobrist of Caltech for **NASA's Jet Propulsion Laboratory.** *For further information, Circle U on the COSMIC Request Card.*
NPO-14893

SUBJECT INDEX

ABSORBERS [EQUIPMENT]
Self-adjusting mechanical snubbing link
page 218 MSC-16134

AC GENERATORS
Energy saving in ac generators
page 134 MFS-25302

ACCELEROMETERS
Electrofluidic accelerometer
page 201 LAR-12493

ACOUSTIC SIMULATION
Low-cost calibration of acoustic locators
page 169 LAR-12632

AERODYNAMIC DRAG
Grooves reduce aircraft drag
page 192 LAR-12599

AIR QUALITY
Improved particulate-sampling filter
page 240 NPO-14801

AIRCRAFT ENGINES
Composites for aeropropulsion
page 183 LEW-13438

ALGAE
Laser-fluorescence measurement of marine algae
page 187 LAR-12282

ALGORITHMS
Basic cluster compression algorithm
page 255 NPO-14816

ALIGNMENT
X-ray beam pointer
page 224 MSC-18590

ANGULAR ACCELERATION
Electrofluidic accelerometer
page 201 LAR-12493

ATMOSPHERIC REFRACTION
Refraction corrections for surveying
page 206 MSC-18664

AUGMENTATION
Digital enhancement of X-rays for NDT
page 206 KSC-11118

BASIC [PROGRAMMING LANGUAGE]
MBASIC processor
page 254 NPO-14245

BRAZING
Time-shared RF brazing
page 240 MSC-18617

BUBBLES
Removal of hydrogen bubbles from nuclear reactors
page 180 LAR-12597

BUNDLES
Handtool assists in bundling cables
page 225 MSC-18567

CALIBRATING
A temperature fixed point near 58° C
page 179 MFS-25304
Low-cost calibration of acoustic locators
page 169 LAR-12632
Optical calibrator for TDL spectrometers
page 164 GSC-12562

CAMERAS
Camera add-on records time of exposure
page 168 LAR-12635

CAPACITORS
Measuring radiation effects on MOS capacitors
page 203 NPO-14700

CASTINGS
Predicting the lifetime of cast parts
page 204 MFS-19549

CATHODE RAY TUBES
Real-time film recording from stroke-written CRT's
page 154 LAR-12529

CAVITIES
Forming complex cavities in clear plastic
page 237 LEW-13412

CHARGE COUPLED DEVICES
Better-quality CCD-array images
page 153 NPO-14426

CIRCLES [GEOMETRY]
Electron-beam welder circle generator
page 91 MFS-19441

COAL
Position monitor for mining machines
page 141 MFS-25342

COATINGS
Improved adherence of TIC coatings to steel
page 181 LEW-13169
Photonitride passivating coating for IC's
page 231 MFS-25401
Selective optical coatings for solar collectors
page 173 MFS-23589

COLUMNS [SUPPORTS]
Automatic connector joins structural columns
page 222 LAR-12578

COMBUSTION CHAMBERS
Flashback-free combustor
page 202 LAR-12686
Methane/air flames in a concentric-tube combustor
page 184 LEW-13388

COMPOSITE MATERIALS
Composites for aeropropulsion
page 183 LEW-13438
Efficient measurement of shear properties of fiber composites
page 193 LEW-13011
Plasticizer for polyimide composites
page 180 LAR-12642
Resistance welding graphite-fiber composites
page 234 MSC-18534

COMPUTER PROGRAMMING
DDL: digital systems design language
page 146 MFS-25352
MBASIC processor
page 254 NPO-14245
Structured FORTRAN preprocessor
page 254 MFS-23813

COMPUTERIZED SIMULATION
System time-domain simulation
page 255 MSC-18333

CONDUCTIVE HEAT TRANSFER
Heat conduction in three dimensions
page 210 MSC-18616

CONTACT RESISTANCE
Ohmic contact to GaAs semiconductors
page 233 LAR-12466

CONTAMINANTS
Detecting contaminants by ultraviolet photography
page 205 MFS-25296

CONTROLLERS
Final report on development of a programable controller
page 171 MFS-25388

CONVECTION
Recording fluid currents by holography
page 198 MFS-25373

CORROSION PREVENTION
Photonitride passivating coating for IC's
page 231 MFS-25401
Silicon nitride passivation of IC's
page 245 MFS-25309

COST ANALYSIS
Low-cost Landsat processing system
page 252 MFS-25396
Optimizing costs of VLSI circuits
page 246 MFS-25348

COUPLINGS
Automatic connector joins structural columns
page 222 LAR-12578
Flared-tube attachment fitting
page 213 MSC-18416

CRACK PROPAGATION
Predicting crack propagation
page 248 MSC-18718

CRYOGENIC EQUIPMENT
Cryogen-storage-tank support
page 227 MSC-14848

CURVATURE
Stream-tube curvature analysis
page 206 LAR-11536

DATA COMPRESSION
Basic cluster compression algorithm
page 255 NPO-14816

DATA PROCESSING EQUIPMENT
RAM-based parallel-output controller
page 150 GSC-12447

DECODERS
11-line to 512-line decoder
page 141 MSC-19751

DECOUPLING
Quasi-passive vibration decoupler
page 195 LAR-12468

DEFECTS
Detection of tanker defects with infrared thermography
page 196 LAR-12655

DIGITAL DATA
11-line to 512-line decoder
page 141 MSC-19751

DIGITAL FILTERS
Aliasing filter for multirate systems
page 137 MSC-18472

DIGITAL TO ANALOG CONVERTERS
Smoothing the output from a DAC
page 144 FRC-11025

DIMENSIONAL STABILITY
Test fittings for dimensionally critical tubes
page 222 NPO-14399

DIRECTIONAL ANTENNAS
Dual-frequency bidirectional antenna
page 138 GSC-12501

DISCONNECT DEVICES
Automatic connector joins structural columns
page 222 LAR-12578

DISTRIBUTION FUNCTIONS
An approximation to Student's t-distribution
page 251 LAR-12238

DOPPLER EFFECT
A microcomputer for Doppler data processing
page 151 GSC-12448
Instrument remotely measures wind velocities
page 163 NPO-14524

DRAG
Grooves reduce aircraft drag
page 192 LAR-12599
Predicting propulsion system drag
page 210 LAR-12619

DROPS [LIQUIDS]
Holographic drop-size analyzer
page 166 NPO-14676
Photographic measurement of droplet density
page 167 MFS-25326

DUCTS
A versatile tunnel acts as a flexible duct
page 214 MFS-22636

DYNAMIC CHARACTERISTICS
Frequency response of multiple-sampling-rate systems
page 156 MSC-18473

ELECTRIC GENERATORS
A linear magnetic motor and generator
page 226 GSC-12518

ELECTRIC MOTORS
Torque control for electric motors
page 155 MSC-18636

best copy available

ELECTRICAL FAULTS
Model for MOS field-time-dependent breakdown
page 145 NPO-14701
ELECTROCARDIOGRAPHY
Testing EKG electrodes on-line
page 187 MSC-18696
ELECTRODES
Testing EKG electrodes on-line
page 187 MSC-18696
ELECTRON BEAM WELDING
Electron-beam welder circle generator
page 91 MFS-19441
ELECTRONIC EQUIPMENT TESTS
Testing EKG electrodes on-line
page 187 MSC-18696
ENERGY CONVERSION EFFICIENCY
Energy saving in ac generators
page 134 MFS-25302
Improved power-factor controller
page 133 MFS-25323
ENERGY DISTRIBUTION
Far-field radiation pattern of tunable diode lasers
page 164 LAR-12631
EQUATIONS OF STATE
An equation of state for liquids
page 161 NPO-14821
EXPOSURE
Camera add-on records time of exposure
page 168 LAR-12835

FASTENERS
Bayonet plug with ramp-activated lock
page 218 MSC-18526
Handtool assists in bundling cables
page 225 MSC-18567
FATIGUE TESTS
Predicting the lifetime of cast parts
page 204 MFS-19549
FEEDBACK CONTROL
Temperature-compensating dc restorer
page 136 LAR-12549
FIELD EFFECT TRANSISTORS
Progress in MOSFET double-layer metalization
page 246 MFS-25239
FILTRATION
Improved particulate-sampling filter
page 240 NPO-14601
FITTINGS
Flared-tube attachment fitting
page 213 MSC-18416
Test fittings for dimensionally critical tubes
page 222 NPO-14399
FLAME PROPAGATION
Methane/air flames in a concentric-tube combustor
page 184 LEW-13388
FLARED BODIES
Flared-tube attachment fitting
page 213 MSC-18416
Tube-flare inspection tool
page 213 MSC-19836
FLASHBACK
Flashback-free combustor
page 202 LAR-12866
FLICKER
Real-time film recording from stroke-written CRT's
page 154 LAR-12529
FLOW DISTRIBUTION
A generalized vortex lattice method
page 209 LAR-12036
Stream-tube curvature analysis
page 208 LAR-11536
FLUID FLOW
Recording fluid currents by holography
page 198 MFS-2537
FLUORESCENCE
Fluorescent radiation converter
page 166 GSC-12528
FORMING TECHNIQUES
Forming complex cavities in clear plastic
page 237 LEW-13412
FORTRAN
Structured FORTRAN preprocessor
page 254 MFS-23813
FRACTURE MECHANICS
Predicting crack propagation
page 248 MSC-18718
FREQUENCY ANALYZERS
Frequency response of multiple-sampling-rate systems
page 156 MSC-18473
FREQUENCY CONTROL
Frequency-controlled voltage regulator
page 156 NPO-13633
FREQUENCY CONVERTERS
Fluorescent radiation converter
page 166 GSC-12528
FREQUENCY STANDARDS
Integral storage-bulb and microwave cavity for masers
page 170 GSC-12542
FRESNEL DIFFRACTION
Fresnel lens tracking solar collector
page 172 MFS-25419
Fresnel lenses for ultrasonic inspection
page 194 MSC-18469
FRICTION REDUCTION
Lubrication handbook
page 183 MFS-25156
FUEL INJECTION
Flashback-free combustor
page 202 LAR-12866

GALLIUM ARSENIDES
Ohmic contact to GaAs semiconductors
page 233 LAR-12466
GAPS
Producing gapped-ferrite transformer cores
page 241 NPO-14715
GASEOUS DIFFUSION
An automated oxide and diffusion facility for IC's
page 246 MFS-25357
GEOLOGICAL SURVEYS
Refraction corrections for surveying
page 206 MSC-18664
GLASS
Controlling the shape of glass microballoons
page 236 MFS-25230
GROOVING
Grooves reduce aircraft drag
page 192 LAR-12599
GUIDANCE SENSORS
3-D guidance system with proximity sensors
page 221 NPO-14521

HEAT PIPES
Heat-pipe sensor for remote leveling
page 209 GSC-12095
HEAT SHIELDING
Thermal barrier and gas seal
page 238 MSC-18390
HEAT TRANSFER
Automatic thermal switches
page 191 GSC-12553
Heat conduction in three dimensions
page 210 MSC-18616
HEATING
Computer-controlled warmup circuit
page 139 NPO-14815
HEATING EQUIPMENT
A hot-water system tested onsite — Togus, Maine
page 175 MFS-25435
A reliable solar-heating system — Huntsville, Alabama
page 175 MFS-25431
A solar-energy system in Minnesota
page 175 MFS-25423
A solar-energy system in Pennsylvania
page 173 MFS-25427
A test program for solar collectors
page 174 MFS-25433
Final report on development of a programable controller
page 171 MFS-25368
Finned-absorber solar collector
page 173 MFS-25366
Fresnel lens tracking solar collector
page 172 MFS-25419
Installation guidelines for the Pennsylvania system
page 175 MFS-25424
Operational tests of a solar-energy system in Georgia
page 174 MFS-25420
Operational tests of a solar-energy system — Florida site
page 174 MFS-25423
Outdoor tests of the concentric-tube collector
page 172 MFS-25398
Selective optical coatings for solar collectors
page 173 MFS-23569
Solar-heating and cooling demonstration project
page 176 MFS-25443
HIGH RESOLUTION
High-resolution double-pass interferometer
page 162 NPO-14448
HOLOGRAPHY
Holographic drop-size analyzer
page 166 NPO-14676
Recording fluid currents by holography
page 198 MFS-25373
HYDROGEN
Removal of hydrogen bubbles from nuclear reactors
page 180 LAR-12597

IMAGE ENHANCEMENT
Better-quality CCD-array images
page 153 NPO-14426
Digital enhancement of X-rays for NDT
page 206 KSC-11118
IMAGERY
Image-based information, communication, and retrieval
page 256 NPO-14693
Low-cost Landsat processing system
page 252 MFS-25396
INDUCTION MOTORS
Improved power-factor controller
page 133 MFS-25323
INFRARED INSPECTION
Detection of tanker defects with infrared thermography
page 198 LAR-12855
INSTALLATION MANUALS
Installation guidelines for the Pennsylvania system
page 175 MFS-25424
INSTALLING
Heat-shrinkable sleeve aids in installing universal joints
page 239 MSC-18685
INTERFACES
Input/output interface module
page 143 MSC-18180

INTERFEROMETERS
High-resoultion double-pass interferometer
page 162 NPO-14448

INVISCID FLOW
Stream-tube curvature analysis
page 208 LAR-11535

ION EXCHANGING
Hybrid microspheres
page 182 NPO-14462

ION IMPLANTATION
More-reliable SOS ion implantations
page 232 MFS-25322

JET ENGINES
Suppressing buzz-saw noise in jet engines
page 196 LAR-12645

JOINTS [JUNCTIONS]
Heat-shrinkable sleeve aids in installing universal joints
page 239 MSC-18885

KLYSTRONS
Computer-controlled warmup circuit
page 139 NPO-14815

LANDSAT SATELLITES
Image-based information, communication, and retrieval
page 256 NPO-14893
Low-cost Landsat processing system
page 252 MFS-25396

LARGE SCALE INTEGRATION
An automated oxide and diffusion facility for IC's
page 246 MFS-25357
Double metalization for VLSI
page 232 MFS-25149
LSI logic for phase control rectifiers
page 144 MFS-25208
More-reliable SOS ion implantations
page 232 MFS-25322
Optimizing costs of VLSI circuits
page 246 MFS-25348
Photonitride passivating coating for IC's
page 231 MFS-25401
Progress in MOSFET double-layer metalization
page 246 MFS-25239
Silicon nitride passivation of IC's
page 245 MFS-25309

LASER APPLICATIONS
Changes in "thermal lens" measure diffusivity
page 195 NPO-14657
Laser-fluorescence measurement of marine algae
page 187 LAR-12282

LASERS
Far-field radiation pattern of tunable diode lasers
page 164 LAR-12831

LENSES
Fresnel lenses for ultrasonic inspection
page 194 MSC-18469

LEVEL [HORIZONTAL]
Heat-pipe sensor for remote leveling
page 209 GSC-12095

LIFE [DURABILITY]
Predicting the lifetime of cast parts
page 204 MFS-19549

LIGHTING EQUIPMENT
Direct-current converter for gas-discharge lamps
page 140 MSC-18407

LINEARIZATION
Linearizing dc transducer output
page 152 NPO-14617

LIQUIDS
An equation of state for liquids
page 161 NPO-14821

LOCKS [FASTENERS]
Bayonet plug with ramp-activated lock
page 218 MSC-18526

LUBRICATION
Design considerations for mechanical face seals
page 183 LEW-13146
Lubrication handbook
page 183 MFS-25158

MACHINE ORIENTED LANGUAGES
DDL: digital systems design language
page 146 MFS-25352

MAGNETIC CORES
Producing gapped-ferrite transformer cores
page 241 NPO-14715

MANAGEMENT SYSTEMS
NASA PERT time II
page 252 LEW-13145

MANIPULATORS
Electromechanical slip sensor
page 223 NPO-14654
End effector for gripping objects
page 215 MFS-23692

MARINE TECHNOLOGY
Laser-fluorescence measurement of marine algae
page 187 LAR-12282

MASERS
Integral storage-bulb and microwave cavity for masers
page 170 GSC-12542

MATERIALS HANDLING
End effector for gripping objects
page 215 MFS-23692

MECHANICAL DRIVES
High-performance, multiroller traction drive
page 216 LEW-13347

MERCURY LAMPS
Direct-current converter for gas-discharge lamps
page 140 MSC-18407

METAL MATRIX COMPOSITES
Composites for aeropropulsion
page 183 LEW-13438

METAL OXIDE SEMICONDUCTORS
Measuring radiation effects on MOS capacitors
page 203 NPO-14700
Model for MOS field-time-dependent breakdown
page 145 NPO-14701

METAL SURFACES
Detecting contaminants by ultraviolet photography
page 205 MFS-25296

METALLIZING
Double metalization for VLSI
page 232 MFS-25149
Progress in MOSFET double-layer metalization
page 246 MFS-25239

METHANE
Methane/air flames in a concentric-tube combustor
page 184 LEW-13388

MICROPARTICLES
Controlling the shape of glass microballoons
page 236 MFS-25230

MICROWAVE EQUIPMENT
Computer-controlled warmup circuit
page 139 NPO-14815
Integral storage-bulb and microwave cavity for masers
page 170 GSC-12542

MINING
Position monitor for mining machines
page 141 MFS-25342

MIRRORS
Detecting surface faults on solar mirrors
page 205 NPO-14684

MOTORS
A linear magnetic motor and generator
page 226 GSC-12518

NOISE REDUCTION
Suppressing buzz-saw noise in jet engines
page 196 LAR-12645

NONDESTRUCTIVE TESTS
Digital enhancement of X-rays for NDT
page 206 KSC-11118

NONLINEARITY
Linearizing dc transducer output
page 152 NPO-14617

NOZZLE DESIGN
Predicting propulsion system drag
page 210 LAR-12619

NUCLEAR REACTORS
Removal of hydrogen bubbles from nuclear reactors
page 180 LAR-12597

NUTS [FASTENERS]
Locknut preload tool
page 217 MSC-16153

OCEAN SURFACE
Oceanic-wave-measurement system
page 200 MFS-23862

OPTICAL DATA PROCESSING
Better-quality CCD-array images
page 153 NPO-14426

OPTICAL EQUIPMENT
Optical calibrator for TDL spectrometers
page 164 GSC-12562

OPTICAL MEASUREMENT
Detecting surface faults on solar mirrors
page 205 NPO-14684

OXIDATION
An automated oxide and diffusion facility for IC's
page 246 MFS-25357

PARALLEL PROCESSING
Input/output interface module
page 143 MSC-18180

PARTICLE DENSITY
Photographic measurement of droplet density
page 167 MFS-25326

PARTICULATE SAMPLING
Improved particulate-sampling filter
page 240 NPO-14801

PASSIVITY
Photonitride passivating coating for IC's
page 231 MFS-25401
Silicon nitride passivation of IC's
page 245 MFS-25309

PERFORMANCE TESTS
A test program for solar collectors
page 174 MFS-25433
Operational tests of a solar-energy system in Georgia
page 174 MFS-25420
Outdoor tests of the concentric-tube collector
page 172 MFS-25396

PHASE CONTROL
LSI logic for phase control rectifiers
page 144 MFS-25208

PHOTOCHEMICAL REACTIONS
UV actinometer film
page 165 NPO-14479

PHOTOGRAPHIC MEASUREMENT
Photographic measurement of droplet density
page 167 MFS-25326

PHOTOGRAPHIC PROCESSING
Automatic 35-mm slide duplicator
page 220 LEW-13399
PHOTOGRAPHY
Camera add-on records time of exposure
page 188 LAR-12635
PHOTOVOLTAIC CELLS
A survey of photovoltaic systems
page 171 MFS-25397
PIEZOELECTRIC TRANSDUCERS
Low-cost calibration of acoustic locators
page 189 LAR-12632
PIPES [TUBES]
Flared-tube attachment fitting
page 213 MSC-18416
Shrinking plastic tubing to nonstandard diameters
page 237 MSC-18430
Sleeve puller salvages welded tubes
page 225 MSC-18686
Test fittings for dimensionally critical tubes
page 222 NPO-14399
Tube-flare inspection tool
page 213 MSC-18636
Tube-welder aids
page 244 MSC-18687
PLASTICIZERS
Plasticizer for polyimide composites
page 180 LAR-12642
PLASTICS
Forming complex cavities in clear plastic
page 237 LEW-13412
Plastic welder
page 242 LAR-12540
POLARIZED RADIATION
Dual-frequency bidirectional antenna
page 138 GSC-12501
POLYIMIDES
Plasticizer for polyimide composites
page 180 LAR-12642
POLYMERIC FILMS
UV actinometer film
page 165 NPO-14479
POSITION [LOCATION]
A microcomputer for Doppler data processing
page 151 GSC-12448
Position monitor for mining machines
page 141 MFS-25342
POWER EFFICIENCY
Energy saving in ac generators
page 132 MFS-25302
Improved power-factor controller
page 133 MFS-25323
POWER SUPPLY CIRCUITS
Frequency-controlled voltage regulator
page 156 NPO-13633
PRESSURE SENSORS
Downhole pressure sensor
page 199 NPO-14729
PROGRAMMING LANGUAGES
MBASIC processor
page 254 NPO-14245
PROJECT MANAGEMENT
NASA PERT time II
page 252 LEW-13145
PROPULSION SYSTEM CONFIGURATIONS
Predicting propulsion system drag
page 210 LAR-12619
PROXIMITY
3-D guidance system with proximity sensors
page 221 NPO-14621
PYLONS
Quasi-passive vibration decoupler
page 196 LAR-12468
RADIATION EFFECTS
Measuring radiation effects on MOS capacitors
page 203 NPO-14700
RADIATION MEASURING INSTRUMENTS
All-inorganic spark-chamber frame
page 235 GSC-12354
RADIO FREQUENCY HEATING
Time-shared RF brazing
page 240 MSC-18817
RANDOM ACCESS MEMORY
RAM-based frame synchronizer
page 149 GSC-12430
RAM-based parallel-output controller
page 150 GSC-12447
RECTIFIERS
LSI logic for phase control rectifiers
page 144 MFS-25206
REDUNDANT COMPONENTS
A redundant regulator control with low standby losses
page 157 NPO-13165
REGENERATION [ENGINEERING]
Regenerative superheated steam-turbine cycles
page 208 LEW-13392
REGRESSION ANALYSIS
Multiple linear regression analysis
page 234 MFS-23764
REMOTE HANDLING
End effector for gripping objects
page 215 MFS-23692
REMOTE SENSORS
Heat-pipe sensor for remote leveling
page 209 GSC-12095
REPRODUCTION [COPYING]
Automatic 35-mm slide duplicator
page 220 LEW-13399
REUSE
Sleeve puller salvages welded tubes
page 225 MSC-18686
ROTORS
Rotor transient analysis
page 228 LEW-13230

SEALS [STOPPERS]
Design considerations for mechanical face seals
page 183 LEW-13146
Thermal barrier and gas seal
page 238 MSC-18390
SHEAR PROPERTIES
Efficient measurement of shear properties of fiber composites
page 193 LEW-13011
SHOCK ABSORBERS
Self-adjusting mechanical snubbing link
page 218 MSC-18134
SHRINKAGE
Shrinking plastic tubing to nonstandard diameters
page 237 MSC-18430
SIGNAL PROCESSING
Smoothing the output from a DAC
page 144 FRC-11025
SILICON NITRIDES
Photonitride passivating coating for IC's
page 231 MFS-25401
Silicon nitride passivation of IC's
page 245 MFS-25309
SLEEVES
Heat-shrinkable sleeve aids in installing universal joints
page 239 MSC-18685
Sleeve puller salvages welded tubes
page 225 MSC-18686
SLIDING
Electromechanical slip sensor
page 223 NPO-14654
SOLAR CELLS
A survey of photovoltaic systems
page 171 MFS-25397
Improved multispectral solar-cell array
page 169 HQN-10937
Ohmic contact to GaAs semiconductors
page 233 LAR-12486
"Peeled-film" solar cells
page 135 NPO-14734
SOLAR ENERGY
A hot-water system tested onsite — Togus, Maine
page 175 MFS-25436
A reliable solar-heating system — Huntsville, Alabama
page 175 MFS-25431
A solar-energy system in Minnesota
page 175 MFS-25428
A solar-energy system in Pennsylvania
page 173 MFS-25427
A survey of photovoltaic systems
page 171 MFS-25397
A test program for solar collectors
page 174 MFS-25433
Detecting surface faults on solar mirrors
page 205 NPO-14664
Final report on development of a programable controller
page 171 MFS-25388
Finned-absorber solar collector
page 173 MFS-25385
Fresnel lens tracking solar collector
page 172 MFS-25419
Installation guidelines for the Pennsylvania system
page 175 MFS-25424
Operational tests of a solar-energy system in Georgia
page 174 MFS-25420
Operational tests of a solar-energy system — Florida site
page 174 MFS-25423
Outdoor tests of the concentric-tube collector
page 172 MFS-25398
Selective optical coatings for solar collectors
page 173 MFS-23589
Solar-heating and cooling demonstration project
page 176 MFS-25443
SPARK CHAMBERS
All-inorganic spark-chamber frame
page 235 GSC-12354
SPECTRAL ENERGY DISTRIBUTION
Improved multispectral solar-cell array
page 169 HQN-10937
SPECTROMETERS
High-resolution double-pass interferometer
page 162 NPO-14446
Optical calibrator for TDL spectrometers
page 164 GSC-12562
SPHERES
Hybrid microspheres
page 182 NPO-14462
STANDARDS
A temperature fixed point near 58° C
page 179 MFS-25304
STATIC DISCHARGERS
More-reliable SOS ion implantations
page 232 MFS-25322
STATISTICAL ANALYSIS
Multiple linear regression analysis
page 234 MFS-23764

STATISTICAL DISTRIBUTIONS
An approximation to Student's t-distribution
page 251 LAR-12238
STEAM TURBINES
Regenerative superheated steam-turbine cycles
page 208 LEW-13392
STEELS
Improved adherence of TiC coatings to steel
page 181 LEW-13169
STORAGE TANKS
Thermal stratification in liquid-storage tanks
page 171 MFS-25416
STOCHASTIC PROCESSES
Linear stochastic optimal control and estimation problem
page 253 LEW-13206
STRATIFICATION
Thermal stratification in liquid-storage tanks
page 171 MFS-25416
STRUCTURAL ANALYSIS
Predicting crack propagation
page 248 MSC-18718
STRUCTURAL MEMBERS
Automatic connector joins structural columns
page 222 LAR-12578
STRUCTURAL VIBRATION
Vibration modes and frequencies of structures
page 209 LAR-12647
STUDENT'S t-DISTRIBUTION
An approximation to Student's t-distribution
page 251 LAR-12238
SUPPORTS
Cryogen-storage-tank support
page 227 MSC-14848
SUPPRESSORS
Suppressing buzz-saw noise in jet engines
page 196 LAR-12645
SURFACE DEFECTS
Detecting surface faults on solar mirrors
page 205 NPO-14684
SWITCHES
Automatic thermal switches
page 191 GSC-12553
SYNCHRONIZERS
RAM-based frame synchronizer
page 149 GSC-12430
SYSTEMS ANALYSIS
System time-domain simulation
page 255 MSC-18333

TANKER SHIPS
Detection of tanker defects with infrared thermography
page 196 LAR-12665
TELECOMMUNICATION
Dual-frequency bidirectional antenna
page 138 GSC-12501
TELEMETRY
RAM-based frame synchronizer
page 149 GSC-12430
TEMPERATURE COMPENSATION
Temperature-compensating dc restorer
page 136 LAR-12549
TEMPERATURE CONTROL
Automatic thermal switches
page 191 GSC-12553
TEMPERATURE DISTRIBUTION
Heat conduction in three dimensions
page 210 MSC-18616
Thermal stratification in liquid-storage tanks
page 171 MFS-25416
TEMPERATURE SCALES
A temperature fixed point near 58° C
page 179 MFS-25304
THERMAL DIFFUSIVITY
Changes in "thermal lens" measure diffusivity
page 195 NPO-14657
THERMAL INSULATION
Thermal barrier and gas seal
page 238 MSC-18390
THERMOPLASTIC RESINS
Plastic welder
page 242 LAR-12540
Resistance welding graphite-fiber composites
page 234 MSC-18534
THERMOSTATS
Automatic thermal switches
page 191 GSC-12553
THIN FILMS
"Peeled-film" solar cells
page 135 NPO-14734
TIME SHARING
Time-shared RF brazing
page 240 MSC-18617
TIMING DEVICES
Camera add-on records time of exposure
page 168 LAR-12635
TITANIUM CARBIDES
Improved adherence of TiC coatings to steel
page 181 LEW-13169
TOOLS
Handtool assists in bundling cables
page 225 MSC-18567
Locknut preload tool
page 217 MSC-16153
Tube-flare inspection tool
page 213 MSC-19636
Tube-welder aids
page 244 MSC-18687
TORQUE
Locknut preload tool
page 217 MSC-16153
Torque control for electric motors
page 155 MSC-18635
TRACTION
High-performance, multiroller traction drive
page 216 LEW-13347
TRANSDUCERS
Linearizing dc transducer output
page 152 NPO-14617
TRANSFER TUNNELS
A versatile tunnel acts as a flexible duct
page 214 MFS-22636
TRANSFORMERS
Producing gapped-ferrite transformer cores
page 241 NPO-14715
TRANSIENT RESPONSE
Rotor transient analysis
page 226 LEW-13230
TURBINES
Regenerative superheated steam-turbine cycles
page 208 LEW-13392

ULTRASONIC TESTS
Fresnel lenses for ultrasonic inspection
page 194 MSC-18469
ULTRAVIOLET PHOTOGRAPHY
Detecting contaminants by ultraviolet photography
page 206 MFS-25296
ULTRAVIOLET SPECTROPHOTOMETERS
UV actinometer film
page 165 NPO-14479

VIBRATION MODE
Vibration modes and frequencies of structures
page 209 LAR-12647
VIBRATORY LOADS
Quasi-passive vibration decoupler
page 195 LAR-12468
VIDEO EQUIPMENT
Real-time film recording from stroke-written CRT's
page 154 LAR-12529
VOLTAGE CONVERTERS [DC TO DC]
Direct-current converter for gas-discharge lamps
page 140 MSC-18407
VOLTAGE REGULATORS
A redundant regulator control with low standby losses
page 157 NPO-13165
Frequency-controlled voltage regulator
page 156 NPO-13833
VORTEX SHEETS
A generalized vortex lattice method
page 209 LAR-12636

WATER WAVES
Oceanic-wave-measurement system
page 200 MFS-23862
WEATHER DATA RECORDERS
A microcomputer for Doppler data processing
page 151 GSC-12446
WELD TESTS
"Foreign material" to verify root fusion in welded joints
page 243 MFS-19496
WELDED JOINTS
Tube-welder aids
page 244 MSC-18687
WELDING
Electron-beam welder circle generator
page 91 MFS-19441
Plastic welder
page 242 LAR-12540
Resistance welding graphite-fiber composites
page 234 MSC-18534
WELLS
Downhole pressure sensor
page 199 NPO-14729
WIND VELOCITY MEASUREMENT
Instrument remotely measures wind velocities
page 163 NPO-14624

X RAY INSPECTION
Digital enhancement of X-rays for NDT
page 206 KSC-11118
X-ray beam pointer
page 224 MSC-18590

☆U.S. GOVERNMENT PRINTING OFFICE: 1980 311 450 4

National Aeronautics and
Space Administration

Washington, D.C.
20546

Official Business
Penalty for Private Use $300

NO POSTAGE
NECESSARY
IF MAILED
IN THE
UNITED STATES

BUSINESS REPLY MAIL

FIRST CLASS PERMIT NO. 12028 WASHINGTON, D.C.

POSTAGE WILL BE PAID BY ADDRESSEE

Director, Technology Transfer Division
P.O. Box 8757
Baltimore/Washington International Airport, MD 21240

NASA

National Aeronautics and
Space Administration

Washington, D.C.
20546

Official Business
Penalty for Private Use $300

NO POSTAGE
NECESSARY
IF MAILED
IN THE
UNITED STATES

BUSINESS REPLY MAIL

FIRST CLASS PERMIT NO. 12028 WASHINGTON, D.C.

POSTAGE WILL BE PAID BY ADDRESSEE

Director, Technology Transfer Division
P.O. Box 8757
Baltimore/Washington International Airport, MD 21240

NASA

National Aeronautics and
Space Administration

Washington, D.C.
20546

Official Business
Penalty for Private Use $300

NO POSTAGE
NECESSARY
IF MAILED
IN THE
UNITED STATES

BUSINESS REPLY MAIL

FIRST CLASS PERMIT NO. 12028 WASHINGTON, D.C.

POSTAGE WILL BE PAID BY ADDRESSEE

Director, Technology Transfer Division
P.O. Box 8757
Baltimore/Washington International Airport, MD 21240

NASA

TECH BRIEFS SUBSCRIPTIONS

SUMMER
1980

☐ Please place me on the subscription list for NASA Tech Briefs (issued quarterly).
☐ I wish to change the delivery address for my current subscription.

1. Please check any of the following that describe your organization:

☐ Federal Government
☐ State Government
☐ Municipal Government
☐ University/College
☐ Secondary School
☐ Trade/Vocational School
☐ Manufacturing
☐ Sales
☐ Research
☐ Consulting
☐ Medicine
☐ Professional Society
☐ News Media
☐ Information Sciences/Library

2. Please check the number of employees in your organization: ☐ Under 25 ☐ 25-100 ☐ 100-500 ☐ Over 500

3. Please indicate if your position is one of the following: ☐ Owner or Chief Executive Officer ☐ Administrator/Manager ☐ Scientist ☐ Engineer ☐ Other ______

[PLEASE PRINT]

NAME ______ TITLE ______
COMPANY & STREET ADDRESS ______ PHONE ______
CITY ______ STATE ______ ZIP ______

TECH BRIEFS SUBSCRIPTIONS

SUMMER
1980

☐ Please place me on the subscription list for NASA Tech Briefs (issued quarterly).
☐ I wish to change the delivery address for my current subscription.

1. Please check any of the following that describe your organization:

☐ Federal Government
☐ State Government
☐ Municipal Government
☐ University/College
☐ Secondary School
☐ Trade/Vocational School
☐ Manufacturing
☐ Sales
☐ Research
☐ Consulting
☐ Medicine
☐ Professional Society
☐ News Media
☐ Information Sciences/Library

2. Please check the number of employees in your organization: ☐ Under 25 ☐ 25-100 ☐ 100-500 ☐ Over 500

3. Please indicate if your position is one of the following: ☐ Owner or Chief Executive Officer ☐ Administrator/Manager ☐ Scientist ☐ Engineer ☐ Other ______

[PLEASE PRINT]

NAME ______ TITLE ______
COMPANY & STREET ADDRESS ______ PHONE ______
CITY ______ STATE ______ ZIP ______

FEEDBACK — YOUR COMMENTS

SUMMER
1980

WE NEED YOUR HELP!

Our ultimate goal is to provide you with solutions to your day-to-day technical problems. Are we meeting that goal? Tell us how Tech Briefs has helped you, or how it can be made more useful. We are especially interested in brief descriptions of specific instances where Tech Briefs has either helped you solve a problem or been applied to your product line.

If you need more space, write us a letter at the address on the front of this card.

[PLEASE PRINT]

NAME ______ TITLE ______
COMPANY & STREET ADDRESS ______ PHONE ______
CITY ______ STATE ______ ZIP ______

TSP REQUESTS

Please send me the Technical Support Package (TSP)
for the Tech Brief articles circled below:

SUMMER
1980

☐ I would like information about NASA's Industrial Applications Centers and other NASA TU services.

I am requesting these TSP's for:

☐ Current Awareness
☐ Process Improvement
☐ Product Development
☐ Problem Solving
☐ Other ______

Approximately how many TSP's have you requested from NASA in the last five years?

☐ 0 to 10 ☐ 11 to 25 ☐ over 25

[PLEASE PRINT]

NAME ______

TITLE ______

COMPANY ______ PHONE ______

& STREET ADDRESS ______

CITY ______ STATE ______ ZIP ______

1	2	3	4	5	6	7	8	9	10	11	12	13	14	15	16
17	18	19	20	21	22	23	24	25	26	27	28	29	30	31	32
33	34	35	36	37	38	39	40	41	42	43	44	45	46	47	48
49	50	51	52	53	54	55	56	57	58	59	60	61	62	63	64
65	66	67	68	69	70	71	72	73	74	75	76	77	78	79	80
81	82	83	84	85	86	87	88	89	90	91	92	93	94	95	96
97	98	99	100	101	102										

TSP REQUESTS

Please send me the Technical Support Package (TSP)
for the Tech Brief articles circled below:

SUMMER
1980

☐ I would like information about NASA's Industrial Applications Centers and other NASA TU services.

I am requesting these TSP's for:

☐ Current Awareness
☐ Process Improvement
☐ Product Development
☐ Problem Solving
☐ Other ______

Approximately how many TSP's have you requested from NASA in the last five years?

☐ 0 to 10 ☐ 11 to 25 ☐ over 25

[PLEASE PRINT]

NAME ______

TITLE ______

COMPANY ______ PHONE ______

& STREET ADDRESS ______

CITY ______ STATE ______ ZIP ______

1 2 3 4 5 6 7 8 9 10 11 12 13 14 15 16
17 18 19 20 21 22 23 24 25 26 27 28 29 30 31 32
33 34 35 36 37 38 39 40 41 42 43 44 45 46 47 48
49 50 51 52 53 54 55 56 57 58 59 60 61 62 63 64
65 66 67 68 69 70 71 72 73 74 75 76 77 78 79 80
81 82 83 84 85 86 87 88 89 90 91 92 93 94 95 96
97 98 99 100 101 102

COSMIC REQUESTS

SUMMER
1980

I would like price and availability information about the computer program(s) circled below.

A B C D E F G H J K L M N P R S T U

Please send me further information about software and services available from COSMIC. I am particularly interested in programs in the following areas: ______

______

______

[PLEASE PRINT]

NAME ______ TITLE ______

COMPANY ______ PHONE ______

& STREET ADDRESS ______ CITY ______ STATE ______ ZIP ______

National Aeronautics and
Space Administration

Washington, D.C.
20546

Official Business
Penalty for Private Use, $300

NASA

NO POSTAGE
NECESSARY
IF MAILED
IN THE
UNITED STATES

BUSINESS REPLY MAIL

FIRST CLASS PERMIT NO. 12028 WASHINGTON, D.C.

POSTAGE WILL BE PAID BY ADDRESSEE

Director, Technology Transfer Division
P.O. Box 8757
Baltimore/Washington International Airport, MD 21240

National Aeronautics and
Space Administration

Washington, D.C.
20546

Official Business
Penalty for Private Use, $300

NASA

NO POSTAGE
NECESSARY
IF MAILED
IN THE
UNITED STATES

BUSINESS REPLY MAIL

FIRST CLASS PERMIT NO. 12028 WASHINGTON, D.C.

POSTAGE WILL BE PAID BY ADDRESSEE

Director, Technology Transfer Division
P.O. Box 8757
Baltimore/Washington International Airport, MD 21240

National Aeronautics and
Space Administration

Washington, D.C.
20546

Official Business
Penalty for Private Use, $300

NASA

NO POSTAGE
NECESSARY
IF MAILED
IN THE
UNITED STATES

BUSINESS REPLY MAIL

FIRST CLASS PERMIT NO. 12028 WASHINGTON, D.C.

POSTAGE WILL BE PAID BY ADDRESSEE

COSMIC
Computer Software Management and Information Center
Suite 112, Barrow Hall
Athens, GA 30602

National Aeronautics and
Space Administration

Washington, D.C.
20546

Official Business
Penalty for Private Use $300

THIRD-CLASS BULK

THIRD-CLASS BULK RATE
POSTAGE & FEES PAID
NASA
WASHINGTON, D.C.
PERMIT No. P-154

NASA

Lightweight metalized plastic blankets are now a familiar sight at the finish lines of distance races, where runners use them to prevent loss of body heat. An outgrowth of early NASA work on metalization technology for spacecraft, the blankets are just one of a broad line of related products with industrial and consumer-oriented applications. [See the bottom of page A1.]

5/3

NASA Tech Briefs

National
Aeronautics and
Space
Administration

NEWARK PUBLIC LIBRARY

FEB 3 1981

U. S. GOVT. PUBS.
DEPOSITORY 376

The 1979 Index to NASA Tech Briefs Is Now Available. [See Page A2.]

Water hyacinth technology, an imaginative new approach to wastewater treatment, has emerged from research in a NASA application project. Shown here being harvested at a Florida demonstration site, water hyacinths purify wastewater by absorbing and metabolizing pollutants — at a fraction of the cost of conventional sewage treatment. Side benefits under study are the conversion of harvested hyacinths to fuel gas, fertilizer, and animal feed. [See the bottom of page A1.]

Vol. 5, No. 3

Fall 1980

NAS 1.29/3:

About the NASA Technology Utilization Program

The National Aeronautics and Space Act of 1958, which established NASA and the United States civilian space program, requires that "The Administration shall provide for the widest practicable and appropriate dissemination of information concerning its activities and the results thereof."

To help carry out this objective, NASA's Technology Utilization (TU) Program was established in 1962. Now, as an element of NASA's Technology Transfer Division, this program offers a variety of valuable services to help transfer aerospace technology to nonaerospace applications, thus assuring American taxpayers maximum return on their investment in space research; thousands of spinoffs of NASA research have already occurred in virtually every area of our economy.

The TU program has worked for engineers, scientists, technicians, and businessmen; and it can work for you.

NASA Tech Briefs

Tech Briefs is published quarterly and is free to engineers in U.S. industry and to other domestic technology transfer agents. It is both a current-awareness medium and a problem-solving tool. Potential products . . . industrial processes . . . basic and applied research . . . shop and lab techniques . . . computer software . . . new sources of technical data . . . concepts . . . can be found here. The short section on New Product Ideas highlights a few of the potential new products contained in this issue. The remainder of the volume is organized by technical category to help you quickly review new developments in your areas of interest. Finally, a subject index makes each issue a convenient reference file.

Further Information on Innovations

Although some new technology announcements are complete in themselves, most are backed up by Technical Support Packages (TSP's). TSP's are available without charge and may be ordered by simply completing a TSP Request Card found at the back of this volume. Further information on some innovations is available for a nominal fee from other sources, as indicated. In addition, Technology Utilization Officers at NASA Field Centers will often be able to lend necessary guidance and assistance.

Patent Licenses

Patents have been issued to NASA on some of the inventions described, and patent applications have been submitted on others. Each announcement indicates patent status, if applicable.

Other Technology Utilization Services

To assist engineers, industrial researchers, business executives, city officials, and other potential users in applying space technology to their problems, NASA sponsors Industrial Applications Centers. Their services are described on page A7. In addition, an extensive library of computer programs is available through COSMIC, the Technology Utilization Program's outlet for NASA-developed software.

Applications Program

NASA conducts applications engineering projects to help solve public-sector problems in such areas as safety, health, transportation, and environmental protection. Applications teams, staffed by professionals from a variety of disciplines, assist in this effort by working with Federal agencies and health organizations to identify critical problems amenable to solution by the application of existing NASA technology.

Reader Feedback

We hope you find the information in *NASA Tech Briefs* useful. A reader-feedback card has been included because we want your comments and suggestions on how we can further help you apply NASA innovations and technology to your needs. Please use it; or if you need more space, write to the Director, Technology Transfer Division, P. O. Box 8757, Baltimore/Washington International Airport, Maryland 21240.

NASA Tech Briefs

FALL 1980
Volume 5, Number 3

National
Aeronautics and
Space
Administration

NASA TU Services A3 Technology Utilization services that can assist you in learning about and applying NASA technology.

New Product Ideas A9 A summary of selected innovations of value to manufacturers for the development of new products.

Tech Briefs

265 Electronic Components and Circuits

275 Electronic Systems

295 Physical Sciences

317 Materials

333 Life Sciences

341 Mechanics

365 Machinery

381 Fabrication Technology

397 Mathematics and Information Sciences

Subject Index 401 Items in this issue are indexed by subject; a cumulative index will be published yearly.

COVERS: The photographs on the front and back covers illustrate developments by NASA and its contractors that have resulted in commercial and nonaerospace spinoffs. To find out more about the Water-Hyacinth Technology, Circle 89 on the TSP Request Card at the back of this issue of NASA Tech Briefs. [Also see the related article "Treating Domestic Wastewater With Water Hyacinths" on page 336.] To find out more about the Noise-Absorption Technology, Circle 90.

About This NASA Publication

NASA Tech Briefs, a quarterly publication, is distributed free to qualified U.S. citizens to encourage commercial application of U.S. space technology. For information on publications and services available through the NASA Technology Utilization Program, write to the Director, Technology Transfer Division, P. O. Box 8757, Baltimore/Washington International Airport, Maryland 21240.

"The Administrator of National Aeronautics and Space Administration has determined that the publication of this periodical is necessary in the transaction of the public business required by law of this Agency. Use of funds for printing this periodical has been approved by the Director of the Office of Management and Budget."

Change of Address

If you wish to have NASA Tech Briefs forwarded to your new address, use one of the Subscriptions cards enclosed in the back of this volume of NASA Tech Briefs. Be sure to check the appropriate box indicating change of address.

Communications Concerning Editorial Matter

For editorial comments or general communications about NASA Tech Briefs, you may use the Feedback card in the back of NASA Tech Briefs, or write to: The Publications Manager, Technology Transfer Division (ETD-6), NASA Headquarters, Washington, DC 20546. Technical questions concerning specific articles should be directed to the Technology Utilization Officer of the sponsoring NASA Center (addresses listed on page A4).

1979 Index

To obtain a copy of the 1979 Index to NASA Tech Briefs, Circle 91 on the TSP Request Card at the back of this issue.

Acknowledgements

NASA Tech Briefs is published quarterly by the National Aeronautics and Space Administration, Technology Utilization Branch, Washington, DC: Administrator: **Robert A. Frosch;** Director, Technology Transfer Division: **Floyd I. Roberson;** Publications Manager: **D. W. Orrick.** Prepared for the National Aeronautics and Space Administration by **Logical Technical Services Corp.:** Editor-in-Chief: **Jay Kirschenbaum;** Art Director: **Ernest Gillespie;** Assistant Editor: **Jerome Rosen;** Chief Copy Editor: **Oden Browne;** Staff Editors: **Donald Blattner, Ted Selinsky, George Watson:** Graphics: **Concetto Auditore, Conrad Carlock, Luis Martinez, Janet McCrie;** Editorial & Production: **Richard Johnson, Jeanne Bonner, Rose Giglietti, Marena Gutman, Kathi Norklun, Michael Stanton, Vincent Susinno, John Tucker, Ernestine Walker.**

This document was prepared under the sponsorship of the National Aeronautics and Space Administration.. Neither the United States Government nor any person acting on behalf of the United States Government assumes any liability resulting from the use of the information contained in this document, or warrants that such use will be free from privately owned rights.

NASA
TU SERVICES

NASA TECHNOLOGY UTILIZATION NETWORK

★ TECHNOLOGY UTILIZATION OFFICERS

Charles C. Kubokawa
Ames Research Center
Code AU: 240-2
Moffett Field, CA 94035
(415) 965-5151

Gussie Anderson
Hugh L. Dryden Flight Research Center
Code OD/TU Office - Room 2015
Post Office Box 273
Edwards, CA 93523
(805) 258-3311, Ext. 787

Donald S. Friedman
Goddard Space Flight Center
Code 702.1
Greenbelt, MD 20771
(301) 344-6242

John T. Wheeler
Lyndon B. Johnson Space Center
Code AT-3
Houston, TX 77058
(713) 483-3809

Raymond J. Cerrato
John F. Kennedy Space Center
Code PT-STA-1
Kennedy Space Center, FL 32899
(305) 867-2780

John Samos
Langley Research Center
Mail Stop 139A
Hampton, VA 23665
(804) 827-3281

Harrison Allen, Jr.
Lewis Research Center
Mail Code 7-3
21000 Brookpark Road
Cleveland, OH 44135
(216) 433-4000, Ext. 6422

Aubrey D. Smith
George C. Marshall Space Flight Center
Code AT01
Marshall Space Flight Center, AL 35812
(205) 453-2224

D. W. Orrick
NASA Headquarters
Code ETD-6
Washington, DC 20546
(202) 755-2244

John H. Warden
NASA Resident Office-JPL
4800 Oak Grove Drive
Pasadena, CA 91103
(213) 354-6420

Gilmore H. Trafford
Wallops Flight Center
Code OD
Wallops Island, VA 23337
(804) 824-3411, Ext. 201

● INDUSTRIAL APPLICATIONS CENTERS

Aerospace Research Applications Center
1201 East 38th Street
Indianapolis, IN 46205
John M. Ulrich, director
(317) 264-4644

Computer Software Management and Information Center (COSMIC)
Suite 112, Barrow Hall
University of Georgia
Athens, GA 30602
Harold G. Hale, Jr., director
(404) 542-3265

Kerr Industrial Applications Center
Southeastern Oklahoma State University
Durant, OK 74701
Robert Oliver, director
(405) 924-0121, Ext. 413

NASA Industrial Applications Center
701 LIS Building
University of Pittsburgh
Pittsburgh, PA 15260
Paul A. McWilliams, executive director
(412) 624-5211

New England Research Applications Center
Mansfield Professional Park
Storrs, CT 06268
Daniel Wilde, director
(203) 486-4533

North Carolina Science and Technology Research Center
Post Office Box 12235
Research Triangle Park, NC 27709
Peter J. Chenery, director
(919) 549-0671

Technology Applications Center
University of New Mexico
Albuquerque, NM 87131
Stanley Morain, director
(505) 277-3622

NASA Industrial Applications Center
University of Southern California
Denny Research Building
University Park
Los Angeles, CA 90007
Robert Mixer, acting director
(213) 743-6132

■ STATE TECHNOLOGY APPLICATIONS CENTERS

NASA/University of Florida State Technology Applications Center
311 Weil Hall
University of Florida
Gainesville, FL 32611
Ronald J. Thornton, director
Gainesville: (904) 392-6760
Orlando: (305) 275-2706
Tampa: (813) 974-2499

NASA/University of Kentucky State Technology Applications Program
109 Kinkead Hall
University of Kentucky
Lexington, KY 40506
William R. Strong, manager
(606) 258-4632

◆ PATENT COUNSELS

Robert F. Kempf
Asst. Gen. Counsel for patent matters
NASA Headquarters
Code GP-4
400 Maryland Avenue, SW.
Washington, DC 20546
(202) 755-3954

Darrell G. Brekke
Ames Research Center
Mail Code: 200-11A
Moffett Field, CA 94035
(415) 965-5104

Paul F. McCaul
Hugh L. Dryden Flight Research Center
Code OD/TU Office - Room 2015
Post Office Box 273
Edwards, CA 93523
(213) 354-2734

John O. Tresansky
Goddard Space Flight Center
Mail Code: 204
Greenbelt, MD 20771
(301) 344-7351

Marvin F. Matthews
Lyndon B. Johnson Space Center
Mail Code: AM
Houston, TX 77058
(713) 483-4871

James O. Harrell
John F. Kennedy Space Center
Mail Code: SA-PAT
Kennedy Space Center, FL 32899
(305) 867-2544

Howard J. Osborn
Langley Research Center
Mail Code: 279
Hampton, VA 23665
(804) 827-3725

Norman T. Musial
Lewis Research Center
Mail Code: 500-311
21000 Brookpark Road
Cleveland, OH 44135
(216) 433-4000, Ext. 346

Leon D. Wofford, Jr.
George C. Marshall Space Flight Center
Mail Code: CC01
Marshall Space Flight Center, AL 35812
(205) 453-0020

Monte F. Mott
NASA Resident Office-JPL
Mail Code: 180-601
4800 Oak Grove Drive
Pasadena, CA 91103
(213) 354-2700

▲ APPLICATION TEAMS

William N. Fetzner, director
Advisory Center for Medical Technology and Systems
University of Wisconsin
1500 Johnson Drive
Madison, WI 53706
(608) 263-2735

Edmund R. Bangs, director
IIT Research Institute
10 West 35th Street
Chicago, IL 60616
(312) 567-4191

Doris Rouse, director
Research Triangle Institute
Post Office Box 12194
Research Triangle Park, NC 27709
(919) 541-6256

Tom Anyos, director
SRI International
333 Ravenswood Avenue
Menlo Park, CA 94025
(415) 326-6200, Ext. 2864

Eugene Schmidt, program coordinator
Stanford University School of Medicine
Cardiology Division
Biomedical Technology Transfer
703 Welch Road, Suite E-4
Palo Alto, CA 94304
(415) 497-5353

David MacFadyen, project director
Technology + Economics
2225 Massachusetts Avenue
Cambridge, MA 02140
(617) 491-1500

TECHNOLOGY UTILIZATION OFFICERS

Technology transfer experts can help you apply the innovations in NASA Tech Briefs.

The Technology Utilization Officer at each NASA Field Center is an applications engineer who can help you make use of new technology developed at his center. He brings you NASA Tech Briefs and other special publications, sponsors conferences, and arranges for expert assistance in solving technical problems.

Technical assistance, in the form of further information about NASA innovations and technology, is one of the services available from the TUO. Together with NASA scientists and engineers, he can often help you find and implement NASA technology to meet your specific needs.

Technical Support Packages (TSP's) are prepared by the center TUO's. They provide further technical details for articles in NASA Tech Briefs. This additional material can help you evaluate and use NASA technology. You may receive most TSP's free of charge by using the TSP Request Card found at the back of this issue.

Technical questions about articles *in NASA Tech Briefs are answered in the TSP's. When no TSP is available, or you have further questions, contact the Technology Utilization Officer at the center that sponsored the research [see page A4].*

NASA INVENTIONS AVAILABLE FOR LICENSING

Over 3,500 NASA inventions are available for licensing in the United States — both exclusive and nonexclusive.

Nonexclusive licenses for commercial use of NASA inventions are encouraged to promote competition and to achieve the widest use of inventions. They must be used by a negotiated target date but are usually royalty-free.

Exclusive licenses may be granted to encourage early commercial development of NASA inventions, especially when considerable private investment is required. These are generally for 5 to 10 years and usually require royalties based on sales or use.

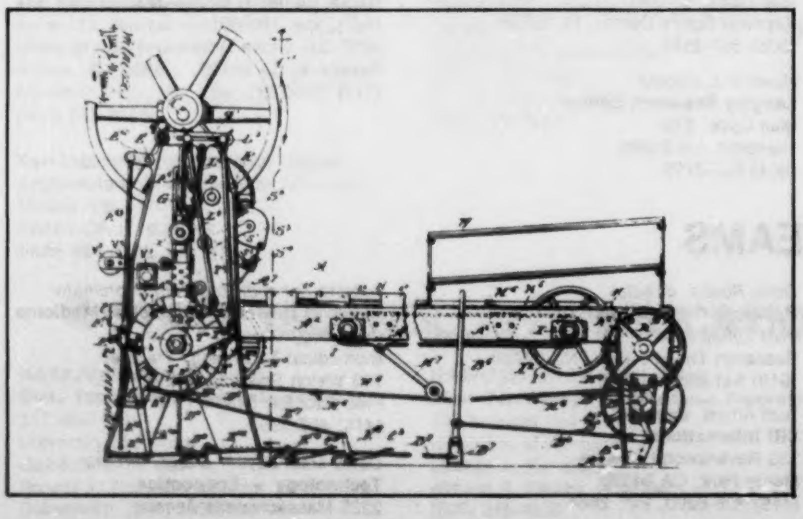

Additional licenses available include those of NASA-owned foreign patents. In addition to inventions described in NASA Tech Briefs, *"NASA Patent Abstract Bibliography"* (PAB), containing abstracts of all NASA inventions, can be purchased from National Technical Information Service, Springfield, VA 22161. The PAB is updated semiannually.

Patent licenses for Tech Briefs *are frequently available. Many of the inventions reported in NASA Tech Briefs are patented or are under consideration for a patent at the time they are published. The current patent status is described at the end of the article; otherwise, there is no statement about patents. If you want to know more about the patent program or are interested in licensing a particular invention, contact the Patent Counsel at the NASA Field Center that sponsored the research [see page A5]. Be sure to refer to the NASA reference number at the end of the Tech Brief.*

APPLICATION TEAMS

Technology-matching and problem-solving
assistance to public-sector organizations

Application engineering projects are conducted by NASA to help solve public-sector problems in such areas as safety, health, transportation, and environmental protection. Some application teams specialize in biomedical disciplines; others, in engineering and scientific problems. Staffed by professionals from various disciplines, these teams work with other Federal agencies and health organizations to identify critical problems amenable to solution by the application of existing NASA technology.

Public-sector organization *representatives can learn more about application teams by contacting a nearby NASA Field Center Technology Utilization Office [see page A4].*

INDUSTRIAL APPLICATIONS CENTERS

Computerized access to nearly
10 million documents worldwide

Computerized information retrieval from one of the world's largest banks of technical data is available from NASA's network of Industrial Applications Centers (IAC's). The IAC's give you access to 1,800,000 technical reports in the NASA data base and to more than 10 times that many reports and articles found in 140 other computerized data bases.

The major sources include:
- *750,000 NASA Technical Reports*
- *Selected Water Resources Abstracts*
- *NASA Scientific and Technical Aerospace Reports*
- *Air Pollution Technical Information Center*
- *NASA International Aerospace Abstracts*
- *Chem Abstracts Condensates*
- *Engineering Index*
- *Energy Research Abstracts*
- *NASA Tech Briefs*
- *Government Reports Announcements*

and many other specialized files on food technology, textile technology, metallurgy, medicine, business, economics, social sciences, and physical science.

The IAC services range from tailored literature searches through expert technical assistance:

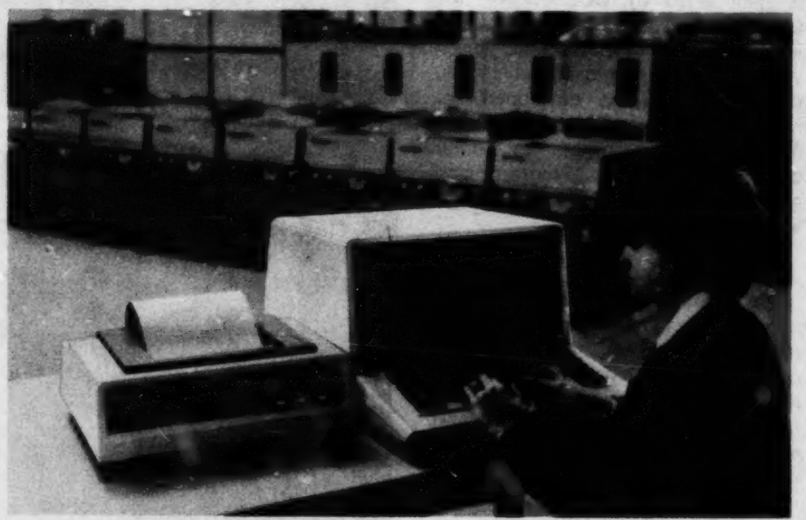

- *Retrospective Searches:* Published or unpublished literature is screened, and documents are identified according to your interest profile. IAC engineers tailor results to your specific needs and furnish abstracts considered the most pertinent. Complete reports are available upon request.
- *Current-Awareness Searches:* IAC engineers will help design a program to suit your needs. You will receive selected monthly or quarterly abstracts on new developments in your area of interest.
- *Technical Assistance:* IAC engineers will help you evaluate the results of your literature searches. They can help find answers to your technical problems and put you in touch with scientists and engineers at appropriate NASA Field Centers.

Prospective clients *can obtain more information about the services offered by NASA IAC's by contacting the nearest IAC [see page A4] or by checking the IAC box on a TSP Request Card in this issue.*

STATE TECHNOLOGY APPLICATIONS CENTERS

Technical information services for industry and state and local government agencies

Local government and industry
in Florida and Kentucky can utilize the services of NASA's State Technology Applications Centers (STAC's). The STAC's differ from the Industrial Applications Centers described on page A7, primarily in that they are integrated into existing state technical assistance programs and serve only the host state, whereas the IAC's serve multistate regions.

Many data bases,
including the NASA base and several commercial bases, are available for automatic data retrieval through the STAC's. Other services such as document retrieval and special searches are also provided. (The STAC's normally charge a fee for their services.)

To obtain information
about the services offered by NASA STAC's, write or call the STAC in your state [see page A4].

COSMIC®

An economical source of computer programs developed by NASA and other government agencies

A vast software library
is maintained by COSMIC — the Computer Software Management and Information Center. COSMIC gives you access to approximately 1,600 computer programs developed for NASA and the Department of Defense and selected programs for other government agencies. Programs and documentation are available at reasonable cost.

Available programs
range from management (PERT scheduling) to information science (retrieval systems) and computer operations (hardware and software). Hundreds of engineering programs perform such tasks as structural analysis, electronic circuit design, chemical analysis, and the design of fluid systems. Others determine building energy requirements and optimize mineral exploration.

COSMIC services
go beyond the collection and storage of software packages. Programs are checked for completeness; special announcements and an indexed software catalog are prepared; and programs are reproduced for distribution. Customers are helped to identify their software needs; and COSMIC follows up to determine the successes and problems and to provide updates and error corrections. In some cases, NASA engineers can offer guidance to users in installing or running a program.

Information about programs
described in NASA Tech Briefs articles can be obtained by completing the COSMIC Request Card at the back of this issue. Just circle the letters that correspond to the programs in which you are interested.

NEW PRODUCT IDEAS

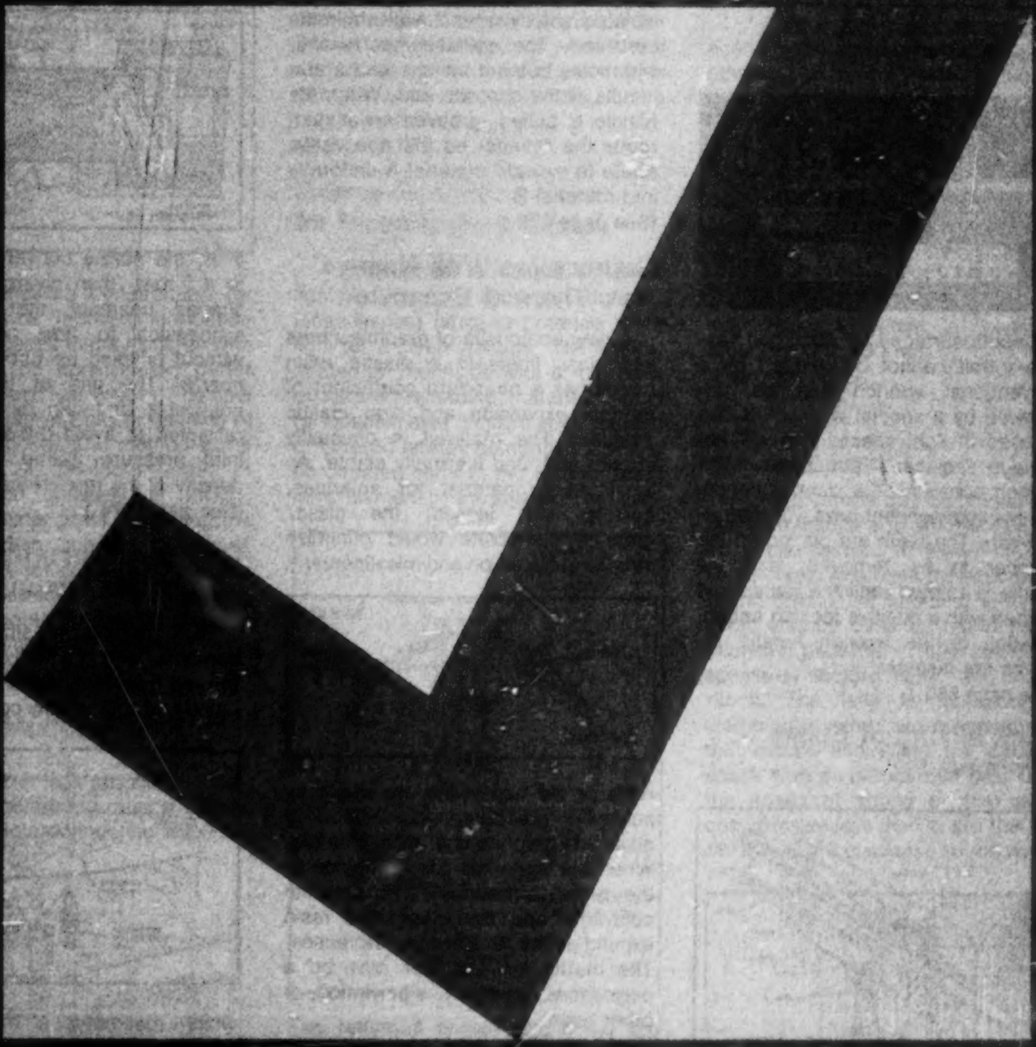

NEW PRODUCT IDEAS are just a few of the many innovations described in this issue of NASA Tech Briefs and having promising commercial applications. Each is discussed further on the referenced page in the appropriate section in this issue. If you are interested in developing a product from these or other NASA innovations, you can receive further technical information by requesting the TSP referenced at the end of the full-length article or by writing the Technology Utilization Office of the sponsoring NASA center (see page A4). NASA's patent-licensing program to encourage commercial development is described on page A8.

Wrench for Smooth or Damaged Fasteners

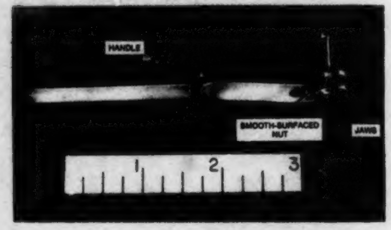
HANDLE
SMOOTH-SURFACED NUT
JAWS
1
2
3

Smooth-surfaced or damaged fasteners that cannot be gripped by a conventional wrench can be unscrewed by a special wrench. It can be used in tight spaces and will not damage adjacent structures. The wrench consists of a central handle and two independent jaws with serrated teeth. The teeth are placed on the fastener to be removed, and the handle is rotated until the fastener is gripped with a positive locking action. Rotation of the wrench handle removes the fastener.
(See page 380.)

Quick Mixing of Epoxy Components

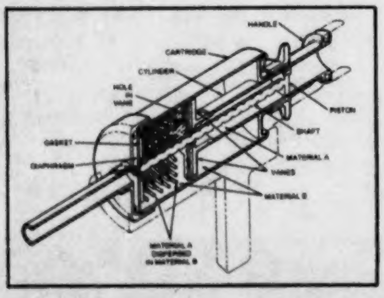
HANDLE
CARTRIDGE
CYLINDER
HOLE IN VANE
PISTON
SHAFT
GASKET
DIAPHRAGM
MATERIAL A
VANES
MATERIAL B
MATERIAL A DISPERSED IN MATERIAL B

Two materials would be mixed quickly, thoroughly, and in precise proportion by a proposed disposable cartridge. The cartridge would mix components of fast-curing epoxy resins, with no mess, just before they are used. It could also be used in the home and in industry for caulking, sealing, and patching. The materials (A and B) to be mixed are initially isolated by a cylindrical wall within the cartridge. The cylinder has vanes, with holes in them, at one end and a handle at the opposite end. When the handle is pulled, grooves on a shaft rotate the cylinder so that the vanes rotate to extrude material A uniformly into material B.
(See page 379.)

Composites With Nearly-Zero Thermal Expansion

A new composite of graphite fibers and glass fibers in a plastic resin matrix has a near-zero coefficient of thermal expansion and high elastic modulus. The material is unusually strong, stiff, and thermally stable. As a mounting material for antennas, mirrors, and lenses, the glass/graphite composite would minimize structural distortion and misalinement.

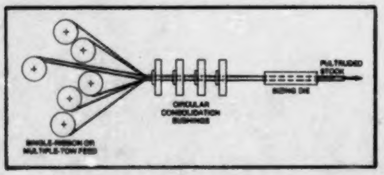
PULTRUDED STOCK
SIZING DIE
CIRCULAR CONSOLIDATION BUSHINGS
SINGLE-RIBBON OR MULTIPLE-TOW FEED

Rods of the composite are made by pulling a preimpregnated ribbon of glass and graphite fiber through a die. When the materials are combined in the proper proportion, the graphite contracts and the glass and resin expand as the temperature increases. The matrix for the fiber may be a polysulfone, an epoxy, a polyimide, or other resin.
(See page 323.)

Spraying Suspensions Uniformly

Coarse, multi-ingredient suspensions are sprayed on a surface smoothly and uniformly with the aid of a nozzle attachment for a commercial spray gun. The new nozzle attachment is contoured internally to suppress overspray and to prevent the spray from segregating. From its conical inlet, the nozzle converges smoothly to a throat, then diverges in a bell-shaped chamber that allows the suspension to flow uninterruptedly without building up turbulently in the nozzle. The end of the nozzle is adjustable and can be extended or retracted to avoid dripping when the inlet pressure, pump pressure, or density of the mixture changes.
(See page 374.)

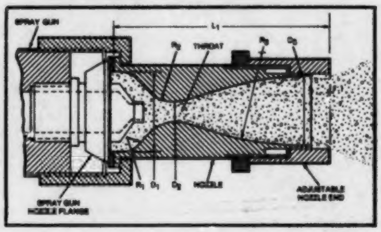
SPRAY GUN
L_1
R_2
THROAT
R_3
D_3
R_1
D_1
D_2
NOZZLE
SPRAY GUN NOZZLE FLANGE
ADJUSTABLE NOZZLE END

Contour-Measuring Tool for Composite Layups

With the help of a simple handtool, contours and complex shapes are formed from laminae of resin-impregnated fabric. The new contouring tool, which resembles a micrometer, is used to make paper templates prior to cutting the laminae. It consists of a yoke with a ballpoint pen at one extremity and a spindle and gage at the other. The handtool scribes a locus of constant thickness on a paper-covered model of the part. The paper is used as a template to cut the sheet of resin-impregnated fabric. Several such layers are stacked and cured to form a composite layup with the same shape as the original part.
(See page 383.)

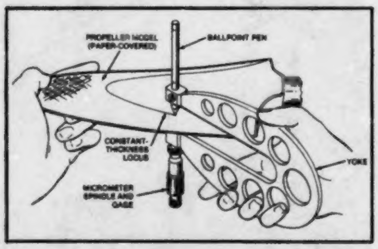
PROPELLER MODEL (PAPER-COVERED)
BALLPOINT PEN
CONSTANT-THICKNESS LOCUS
MICROMETER SPINDLE AND GAGE
YOKE

Lightweight Terminal Board

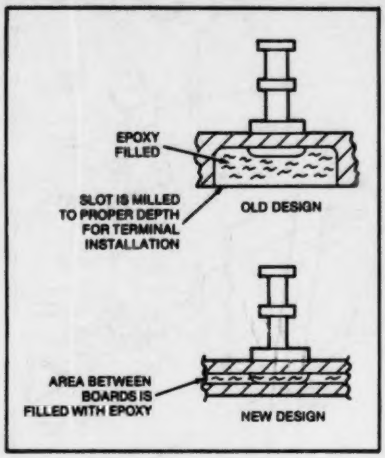
EPOXY FILLED
SLOT IS MILLED TO PROPER DEPTH FOR TERMINAL INSTALLATION
OLD DESIGN
AREA BETWEEN BOARDS IS FILLED WITH EPOXY
NEW DESIGN

A new sandwich construction for terminal boards reduces fabrication time and produces thinner boards with better insulation consistency, better appearance, and less weight. The new method also permits closer spacing of the terminal posts. The method starts with a thin (0.031-inch) sheet of polyimide and consists of drilling, inserting terminal posts, upsetting the ends, and then bonding a second sheet to the upset side as a continuous insulation member. The resulting sandwich is lighter and much cheaper than the single board.
(See page 392.)

Versatile Modular Scaffolds

Movable and fixed modular scaffolds can be tailored to most scaffolding needs by interconnecting only four basic structural elements: platforms, rails, vertical-support angles, and a stiffener. Standard nuts and bolts are used to join elements, simplifying construction and reducing costs. The scaffolds are rigid and can be made any length. They are stable on unlevel ground and can extend to well over 50 feet in height. The scaffolds allow for internal elevators and for wheels and air mounts so that the same elements can be used for a standing or a movable scaffold.
(See page 372.)

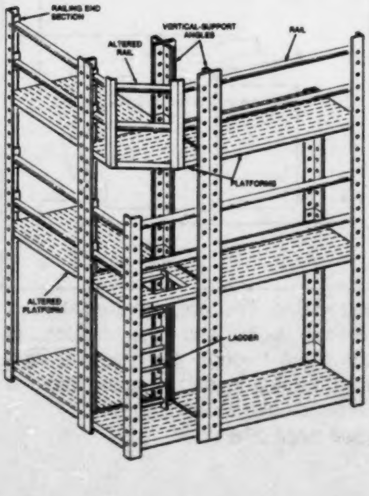
RAILING END SECTION
VERTICAL-SUPPORT ANGLES
ALTERED RAIL
RAIL
PLATFORMS
ALTERED PLATFORM
LADDER

Energy-Reduction Concept for Incandescent Lamps

A concept for a coated spherical light fixture may allow an ordinary incandescent lamp to produce more light for a given wattage. The fixture, coated on the inside with a thin layer of infrared-reflecting material, would be installed over the light bulb. Instead of infrared energy being lost, it would be directed back to the incandescent lamp filament by the selective coating.

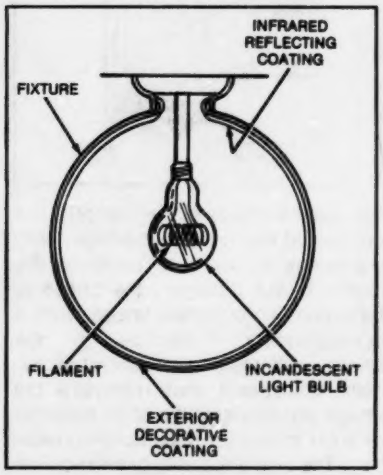
INFRARED REFLECTING COATING
FIXTURE
FILAMENT
INCANDESCENT LIGHT BULB
EXTERIOR DECORATIVE COATING

The reflected energy would aid the electric current in heating the filament and would allow a lower-wattage light bulb to produce the same amount of light as a higher wattage bulb in an ordinary light fixture.
(See page 304.)

Economical Ultraviolet Radiometer

Ultraviolet radiation from Sun and sky, integrated over the celestial hemisphere, is measured by an economical, cosine-corrected radiometer. Suitable for field use, the new radiometer has possible applications in testing materials for the effects of ultraviolet exposure and in studies of solar-cell degradation. It consists of a cup-shaped diaphragm and diffusing dome to obtain a cosine-corrected response, two filters that select the wavelength range, and a silicon solar cell. The two-component filter controls the response within a passband around 300 to 400 nm.
(See page 301.)

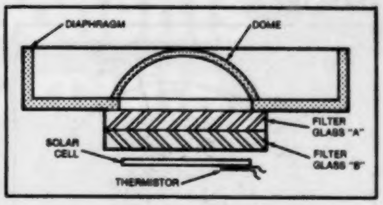
DIAPHRAGM
DOME
FILTER GLASS "A"
SOLAR CELL
FILTER GLASS "B"
THERMISTOR

Acoustic Lens

A fluorocarbon gas contained by a plastic membrane is an effective lens for sound waves. In tests, the lens substantially improved the accuracy of sound "maps" of turbulent airflow. It could also be used to record sound-intensity patterns in the design of speakers, lecture halls, and auditoriums. The lens is fabricated by clamping together two membranes of thin plastic and filling the enclosed space with a fluorocarbon gas. Since the speed of sound in the gas is considerably less than in air, the lens refracts and focuses the sound waves, analogous to focusing light by a glass lens. The focal length is adjusted simply by changing the gas pressure, which changes the lens curvature.
(See page 345.)

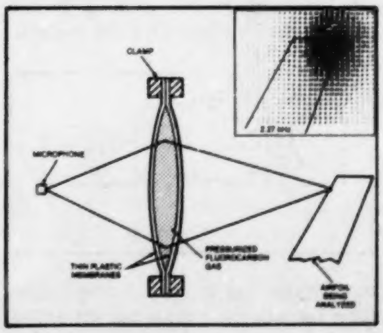
CLAMP
MICROPHONE
THIN PLASTIC MEMBRANES
PRESSURIZED FLUOROCARBON GAS
AIRFOIL BEING ANALYZED

Reshaping Tube Ends for Welding

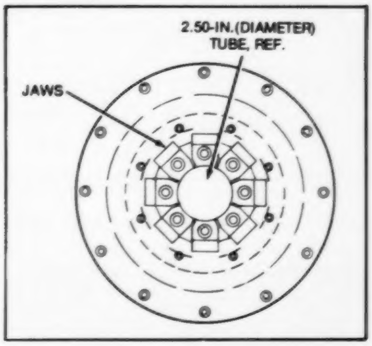
2.50-IN.(DIAMETER) TUBE, REF.
JAWS

Roundness is restored to tube ends prior to welding by a semiautomatic tool. The hydraulically operated tool can be mounted on a workbench and is small enough to be moved easily from one factory area to another. It consists of two major parts: an "expander" that opens up the out-of-round tube so that a plug can be inserted and a "crimper" that compresses the tube into shape around the plug. After using the expander, hydraulic pressure is applied, and the jaws of the crimper swage the tube around the plug so that it assumes the proper shape. The present design handles a range of tube sizes, from 1/4 to 2-1/2 in.
(See page 373.)

Torque-Wrench Extension

A torque-wrench extension makes it easy to install and remove fasteners that are beyond the reach of typical wrenches or are located in narrow spaces that prevent full travel of the wrench handle. At the same time the new tool reads the applied torque accurately. The wrench drive system, for torques up to 125 inch-pounds, uses two standard drive-socket extensions in an aluminum frame. The extensions are connected to a bevel gear that turns another bevel gear. The gears produce a 1:1 turns ratio through a 90° translation of the axis of rotation. The output bevel gear has a short extension that is used to attach a 1/4-inch drive socket.
(See page 378.)

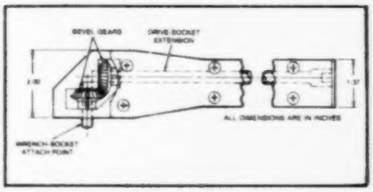
BEVEL GEARS
DRIVE-SOCKET EXTENSION
ALL DIMENSIONS ARE IN INCHES
WRENCH SOCKET ATTACH POINT

Four-Cell Solar Tracker

A very sensitive Sun tracker has four solar cells surrounded by a cylindrical mirror. When added to a declination-angle/hour-angle drive, it can orient a solar collector or a solar mirror accurately for maximum illumination. Signal conduction leads from the upper surfaces of the four cells are connected to a resistance bridge. With the image of the Sun falling on the center of the detector, the bridge is balanced. An offcenter image, with a corresponding imbalance in the bridge, will result in a servomechanism adjustment that recenters the image and reorients the solar collector or solar mirror for maximum illumination. The cylindrical mirror extends the acquisition angle of the device by reflecting the Sun image back onto the solar cells.
(See page 298.)

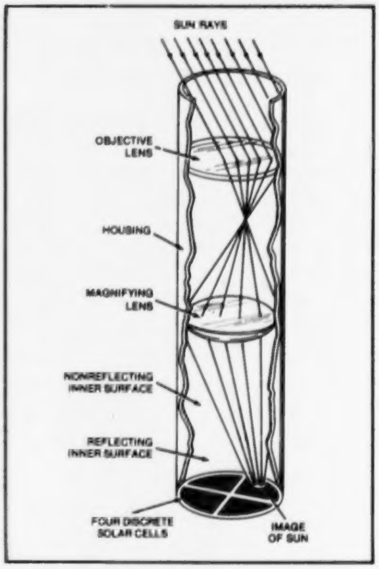
SUN RAYS
OBJECTIVE LENS
HOUSING
MAGNIFYING LENS
NONREFLECTING INNER SURFACE
REFLECTING INNER SURFACE
FOUR DISCRETE SOLAR CELLS
IMAGE OF SUN

Cleaving Machine for Hard Crystals

Hard crystalline materials such as lithium fluoride (LiF) are cleaved in thin sections by a new semiautomatic machine. The yield of undistorted LiF crystals is almost 100 percent, even when the cleaved section is only 1/32 inch thick. The machine contains a spring-activated hammer that limits the penetration of a blade and controls the shock that cleaves the crystal. A fixture with spring-loaded clamps precisely locates and holds the crystal, restraining it in an ideal position for cleaving. The crystal then splays apart.
(See page 367.)

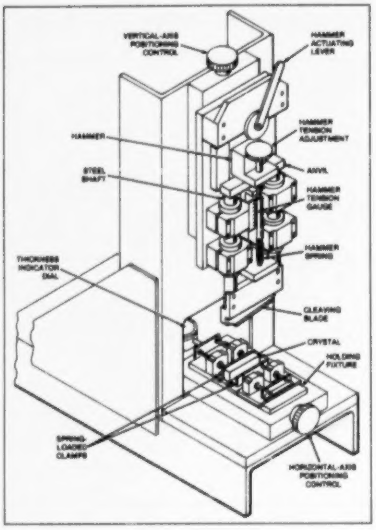
VERTICAL-AXIS POSITIONING CONTROL
HAMMER ACTUATING LEVER
HAMMER TENSION ADJUSTMENT
HAMMER
ANVIL
STEEL SHAFT
HAMMER TENSION GAUGE
HAMMER SPRING
THICKNESS INDICATOR DIAL
CLEAVING BLADE
CRYSTAL
HOLDING FIXTURE
SPRING-LOADED CLAMPS
HORIZONTAL-AXIS POSITIONING CONTROL

Compact Table-Tilting Mechanism

Optical components would be oriented precisely by a proposed motorized device for manipulating objects attached to a plane tilt table. The mechanism is compact, simple, and has low backlash. It consists of a drive motor, a rotatable disk, a rigid link, and a table. The motor rotates about a vertical axis, and the motion is converted through the disk and rigid link to rotation of the table about a perpendicular axis.
(See page 376.)

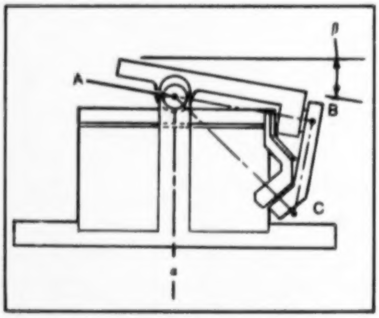

Electronic Components and Circuits

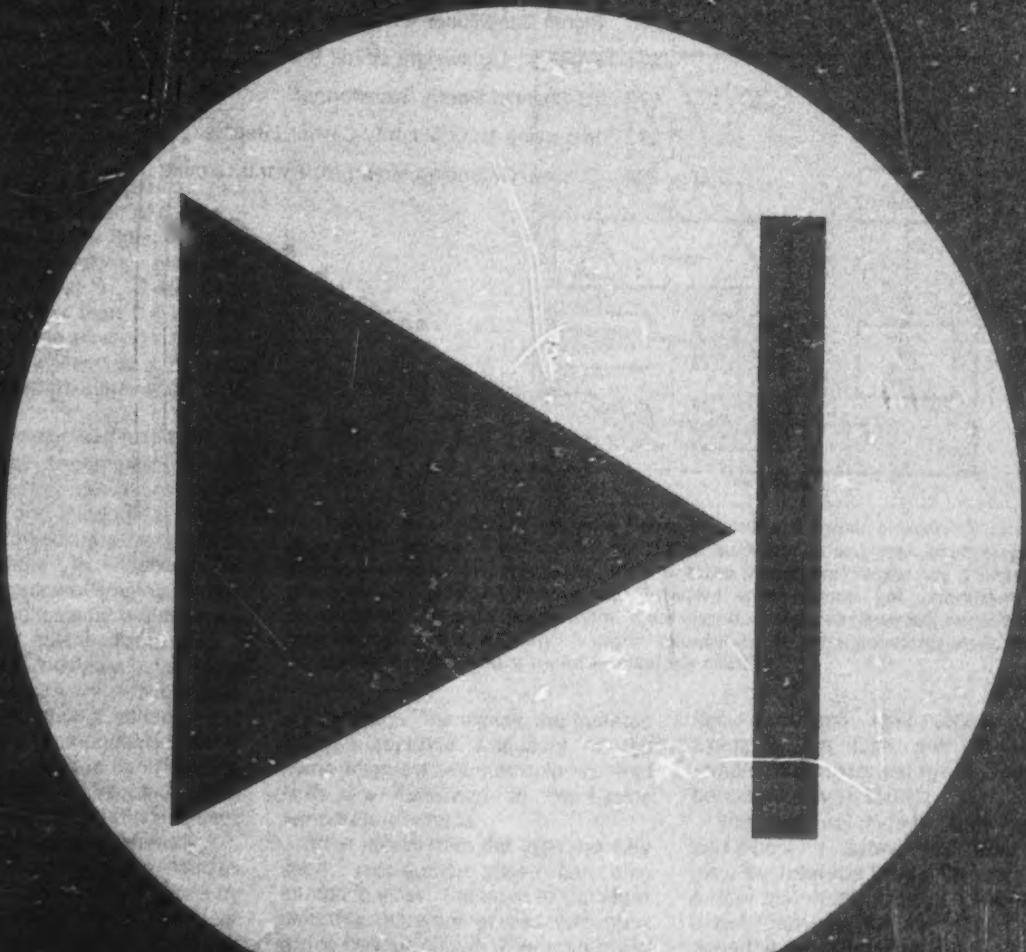

Hardware, Techniques, and Processes

267 Ultrastable Automatic Frequency Control
268 Fast Microwave Switching Power Divider
269 High-Power Solid-State Microwave Transmitter
270 Antenna Feed for Linear and Circular Polarization
270 Signal Conditioner for Nickel Temperature Sensors
271 Efficient, Lightweight dc/dc Switching Converter
273 28-Channel Rotary Transformer
273 Improving MOS Minority-Carrier Lifetime
274 Cooling/Grounding Mount for Hybrid Circuits

Ultrastable Automatic Frequency Control

The center frequency of a wideband AFC circuit drifts only a few hundredths of a percent per day.

Lyndon B. Johnson Space Center, Houston, Texas

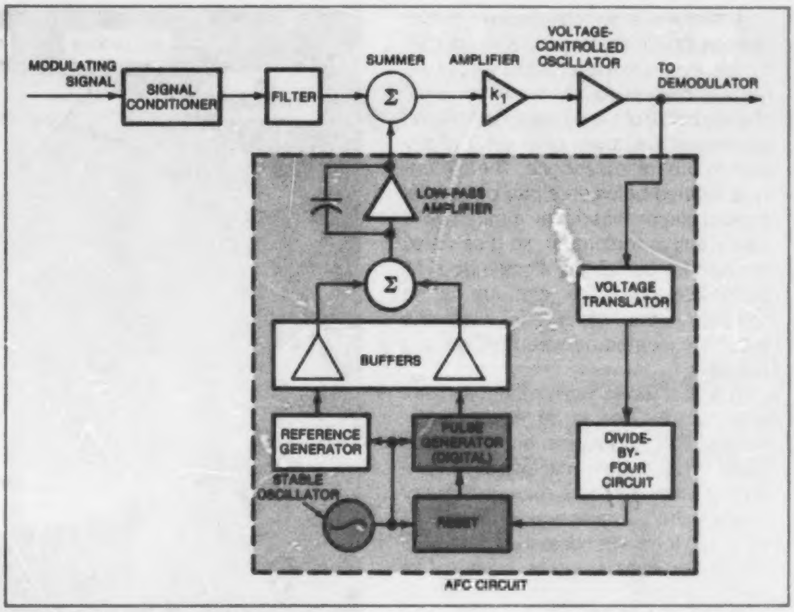

The improved **Automatic Frequency Control Circuit** is a negative-feedback loop that regulates a wideband FM voltage-controlled oscillator. Since the circuit responds only to relatively slow frequency drifts and the modulation signal has a high-pass characteristic, the AFC does not interfere with normal FM operation. The combination of the stable oscillator, reset circuit, and pulse generator constitutes a time-averaging discriminator. A digital counter in the pulse generator replaces the monostable multivibrator found in previous circuits.

Designers of FM modulators using a voltage-controlled oscillator (VCO) must minimize carrier-frequency drift while allowing for wide modulation-frequency deviations. Adding automatic frequency control (AFC) to the VCO is a standard solution to the carrier-drift problem; however, conventional AFC may not suffice when the stability requirements are very tight.

A new circuit adds several new features to conventional AFC. Originally developed for the Space Shuttle payload communications simulator, the circuit stabilizes a 1.7-MHz FM subcarrier to better than 0.4 percent over 24 hours, while allowing a modulation-frequency deviation of ±160kHz. The operating temperature range is 0° to 50° C.

The major elements of an AFC loop are a frequency discriminator, which converts frequency deviations to an error voltage, and a loop filter, which removes the modulating signal from the error voltage. In wideband FM receivers, a pulse-averaging circuit containing a monostable multivibrator is usually used as the discriminator. However, the monostable pulse width and voltage levels vary with changes in temperature, supply voltage, and external timing components. As a result, the error voltage can fluctuate even if the modulation frequency does not change. These fluctuations appear as a drift of the center frequency.

The new AFC (see figure) minimizes discriminator pulse-width variations by using a highly stable crystal oscillator and a digital counting circuit, rather than a monostable multivibrator. Variations in discriminator voltages are compensated for by adding a correction voltage, obtained by subtracting the discriminator output from a reference voltage. The signals are buffered through separate amplifiers on the same integrated-circuit chip, so that both are subjected to the same temperature effects.

If the pulses from the VCO are very short, propagation delay can also introduce error. The input to the reset circuit is therefore passed through a divide-by-four circuit. The input pulse width is quadrupled, and the propagation delay becomes insignificant.

The new AFC circuit has been built with transistor-transistor-logic (TTL) integrated circuits. Its performance has surpassed specifications; for example, the total drift at room temperature, recorded over a 24-hour period, is only ±100 Hz.

This work was done by Andy Furiga and Donald J. Sabourin of Motorola, Inc., for **Johnson Space Center.** *For further information, including detailed circuit drawings of the AFC, Circle 1 on the TSP Request Card.*

Inquiries concerning rights for the commercial use of this invention should be addressed to the Patent Counsel, Johnson Space Center [see page A5]. Refer to MSC-18679.

Fast Microwave Switching Power Divider

Power from a single input is divided among any 12 of 120 output terminals and is redistributed in 0.6 μs.

Goddard Space Flight Center, Greenbelt, Maryland

A microwave switching power divider has one input terminal and 120 output terminals. Power that is fed into the input terminal is divided equally (to within ±0.5 dB) among 12 of the output terminals and can be switched to any other set of 12 outputs in 0.6 microseconds. The circuitry is located between a pair of parallel ground planes that define a microwave cavity and is reciprocal, so it can also be used for combining signals from 12 ports into one. The circuitry is on opposite sides of a thin dielectric substrate located between the ground planes.

The fast switching divider/combiner was built for use in an electronically-steered S-band antenna, but it can also divide and switch microwave energy among other networks such as filters or phase shifters. The design is not restricted to 120 terminals nor to the selection of 12; other numbers can be used just as well.

As shown in the figure, the center conductor of a coaxial cable is connected to the center of a copper disk on the dielectric substrate. The outer conductor of the coaxial cable is connected to the ground planes (the top ground plane is not shown).

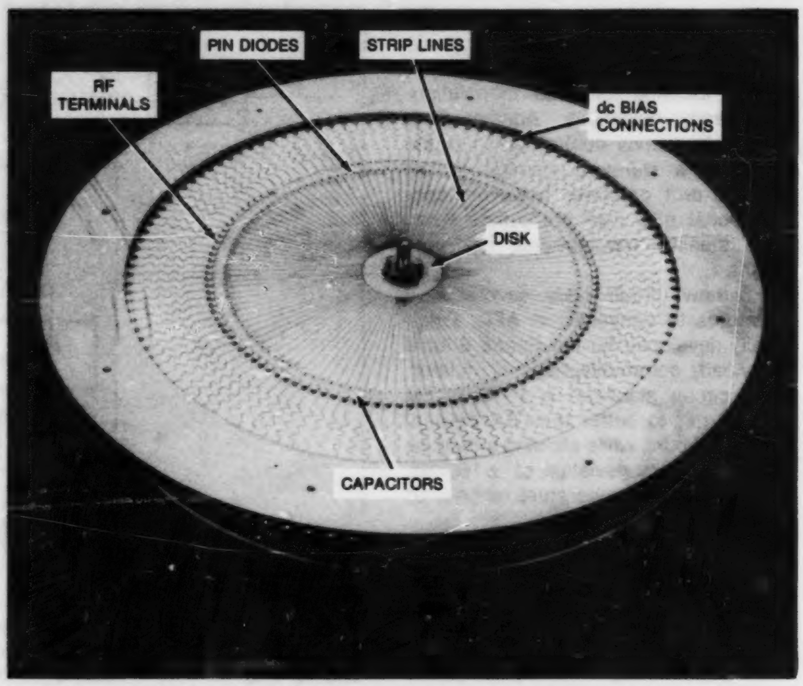

In this S-band **Switching Power Divider**, shown with one ground plane removed, microwave power from a coaxial line excites a disk that feeds many radial strip transmission lines. The 1.9-lb (0.87-kg) unit has an outer diameter of 22 cm.

Strip transmission lines are connected radially every 3° around the circumference of the disk; each line includes a PIN diode (for opening or closing the line) and a dc-blocking capacitor and tapers to 50 ohms impedance at its output terminal. A dc voltage applied to a diode biases it for conduction or nonconduction. The voltage is applied through an RF choke that presents very high impedance to the microwave signal; the choke isolates the microwave signal from the dc-blocking capacitor, and the capacitor keeps the dc voltage off the RF output cable.

The radius of the disk and the widths of the strip lines leaving it are chosen so that when 12 of the lines are closed and terminated in 50 ohms and the other 108 lines are open, the input impedance is also 50 ohms.

The PIN diodes have low insertion loss and high switching speed. A microprocessor or other source supplies dc bias current to switch the diodes.

Optimum power division (with respect to the uniformity of phase and amplitude) occurs when the output ports are symmetrically spaced about the circumference. The uniformity degrades slowly as the symmetric case is transformed (one port at a time) into the worst-case asymmetry where all the output ports are adjacent. Even this arrangement still gives good performance.

The switching divider/combiner built for the S-band antenna weighs only 865 grams, has an overall diameter of 22 cm, and is 3.3 cm high. The central disk has a radius of 1.24 cm, and the strip lines are 4.34 cm long.

This work was done by Russell W. Johnson and Ronald J. Stockton of Ball Corp. for **Goddard Space Flight Center**. *For further information, Circle 2 on the TSP Request Card.*

This invention is owned by NASA, and a patent application has been filed. Inquiries concerning nonexclusive or exclusive license for its commercial development should be addressed to the Patent Counsel, Goddard Space Flight Center [see page A5]. Refer to GSC-12420.

High-Power Solid-State Microwave Transmitter

Outputs from individual amplifier modules are phased and then combined in a multielement array feed antenna.

NASA's Jet Propulsion Laboratory, Pasadena, California

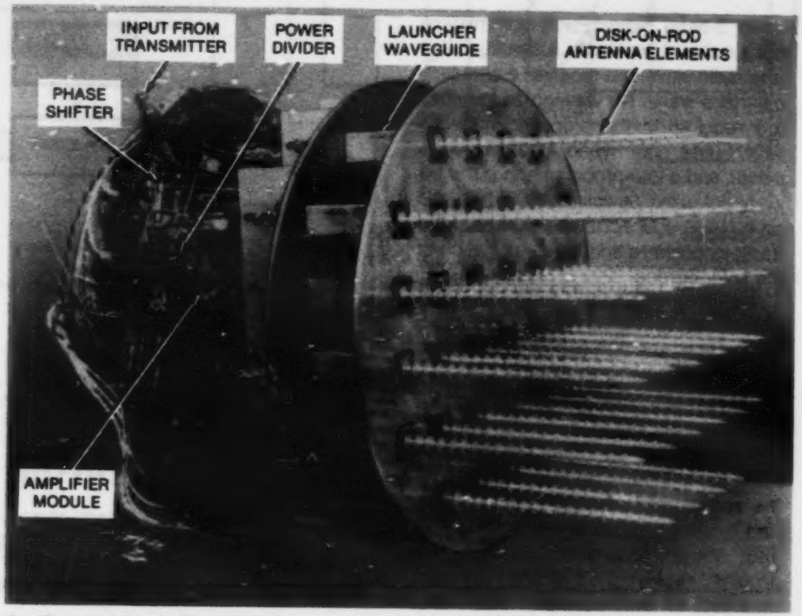

An Array of Radiating Elements, fed by paralleled solid-state amplifiers, combines its outputs to transmit a powerful signal from deep space to Earth. This arrangement gives solid-state reliability at a high power level.

Although solid-state microwave amplifiers are more reliable than traveling-wave tubes (TWT's), they do not normally measure up to the high power-output levels possible with a TWT. Solid-state reliability and high power are both realized, however, with a new multielement microwave transmitter. In the new design, an input microwave signal is divided among many low-power solid-state amplifiers and then recombined in the proper phase to transmit a high-power output.

In an X-band antenna built for transmissions from deep space, the input is divided among 32 solid-state amplifiers that drive an equal number of in-phase radiating elements. For microwave power input at 1.11 watts, the amplifier transmits an output power level of 22.09 watts, while dissipating 77.96 watts of dc power. The basic design can be scaled up or down in size and power-handling capability for applications such as radar and other small-angle scanning.

The photograph of the combiner shows the input port, the power divider, the line-stretcher phase shifters, the amplifier modules, and the array feed for recombining the amplified signal. The power divider (in this case, a combination of 4- and 8-way dividers) splits the input power 32 ways. The phase shifters equalize the phasing of the 32 separated signal paths prior to injection into the 32 radiating elements.

The solid-state amplifiers operate at X-band. Each is a three-stage microstrip configuration housed in an H-frame chassis. The amplifier input power is 20 milliwatts; its output is 750 milliwatts at 8.415 GHz, with a minimum gain of 15 dB and efficiency greater than 25 percent. The GaAs field-effect transistors selected for the three-stage amplifier are rated at 1/4, 1/2, and 1 watt, respectively, with a total dc input power of 2.9 watts maximum. By using fixed 3-bit phase shifters and variable line stretchers, the relative phase difference among 32 amplifiers at the final array assembly is held to 2.5°, which contributes less than a 0.01-dB loss to the array beam phase efficiency.

In the power amplifier module, the 3-bit phase shifter (45°, 90°, and 180°) is included on the microstrip to combine signals in phase in the array; the desired phase is selected during testing. Line-stretcher phase shifters, having phase shifts of about 90°, are located in the input circuit between the 32-way power divider and the inputs to the amplifiers. These shifters compensate for most of the residual phase differences between the amplifiers.

The output of each amplifier module is isolated by a ferrite circulator and third port load. This protects the amplifier output stage and minimizes the array mismatch loss in the event of an amplifier failure.

This work was done by James F. Boreham, Bruce L. Conroy, Richard B. Postal, and Donald G. Yenche of Caltech for **NASA's Jet Propulsion Laboratory.** *For further information, including details of mechanical design and construction, Circle 3 on the TSP Request Card.*

Inquiries concerning rights for the commercial use of this invention should be addressed to the Patent Counsel, NASA Resident Office-JPL, [see page A5]. Refer to NPO-14803.

Antenna Feed for Linear and Circular Polarization

Hybrid elements transmit linear polarization and receive circular polarization without switching losses.

NASA's Jet Propulsion Laboratory, Pasadena, California

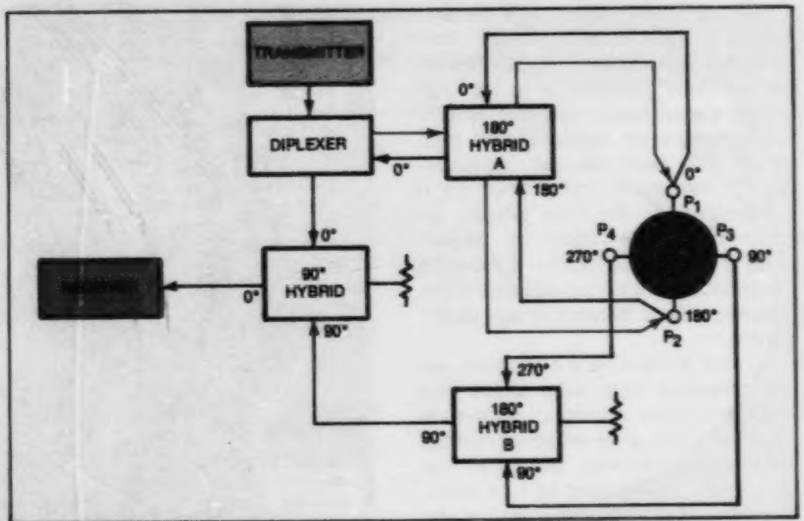

This Antenna System transmits a linearly-polarized microwave radio signal, yet a circularly-polarized incoming signal is received without polarization-mismatch losses. Other circuit arrangements are possible, using additional transmitters and receivers.

An S-band bidirectional communications network transmits a linearly-polarized radio wave and receives a circularly polarized wave. No waveguide switches are required in the proposed network, which uses only hybrid junctions, a diplexer, and a four-probe antenna. The linearly polarized downlink would be used on a NASA spacecraft for studies of the Earth ionosphere and for investigation of the solar corona.

A circularly-polarized radio wave consists of two orthogonal linearly polarized waves that are 90° out of phase. The NASA deep-space telecommunication links normally transmit and receive in circular polarization to avoid orientation problems. To meet the requirement for a linearly polarized downlink, the spacecraft antenna feed is modified to put all of the transmitted power into linear polarization only. The ground receiving antenna is also modified to automatically track and record the incoming plane of the linear polarization.

The figure shows an antenna feed with orthogonal coupling probes P_1, P_2, P_3, and P_4. In the transmit mode (color arrows), the diplexer connects the transmitter to 180° hybrid A, which excites probes P_1 and P_2 out of phase, producing a linearly polarized wave.

In the receive mode (black arrows), probes P_1 and P_2 are connected to 180° hybrid A; probes P_3 and P_4, 90° out of phase with P_1 and P_2, are connected to 180° hybrid B. The diplexer connects hybrid A to the 90° hybrid, and hybrid B delivers an orthogonal signal to the 90° hybrid; these two inputs are delivered in phase to the receiver.

The hybrids can be implemented as waveguide, strip-line, or coaxial components. Possible configurations are the 3-dB coupler, the "rat-race," and the "magic-tee."

This work was done by Dan A. Bathker and Boris L. Seidel of Caltech for **NASA's Jet Propulsion Laboratory.** *For further information, Circle 4 on the TSP Request Card.*

This invention is owned by NASA, and a patent application has been filed. Inquiries concerning nonexclusive or exclusive license for its commercial development should be addressed to the Patent Counsel, NASA Resident Legal Office-JPL [see page A5]. Refer to NPO-14810.

Signal Conditioner for Nickel Temperature Sensors

Simple circuit conditions sensor signal for readout on a strain-gage recorder.

Lyndon B. Johnson Space Center, Houston, Texas

A strain-gage monitor can be used to read the output of a 50-ohm nickel temperature sensor if the sensor output is first conditioned through a simple circuit. Shown in the figure, the signal conditioner saves time and reduces instrumentation costs when both strain and temperature are being measured in the same setup.

In the standard application of a strain-gage monitor, the gage is inserted in one arm of a Wheatstone bridge, and the monitor measures strain by recording the departures from bridge balance. With the new circuit, a 50-Ω nickel temperature sensor replaces the strain gage, and the readings of the monitor are related to the temperature of the sensor.

The circuit consists of a few resistors, a switch, and a "matching" network available commercially (Vishay Intertechnology, Inc., Micro-Measurements Division, Part # LST-10F-350B, or equivalent). The 50-Ω nickel temperature sensor is attached to two input terminals on the module, and the strain-gage recorder is attached to the output bulkhead connector. The bridge excitation voltage is applied through pins A and D (or A and F), and the bridge output is read between pins C and B (or C and E).

The matching network makes the 50-Ω temperature sensor look like one-half of a 350-Ω Wheatstone bridge at 70° F (21.1° C). It also linearizes the sensor output. With resistors R_1 and R_2 installed, the bridge is complete when the switch is in the "operate" mode. Resistors R_3 and R_4 are connected to the output when the switch is set to "zero" so that the bridge can be zeroed.

This work was done by Robert R. Walker of Rockwell International Corp. for **Johnson Space Center**. *No further documentation is available.*
MSC-18367

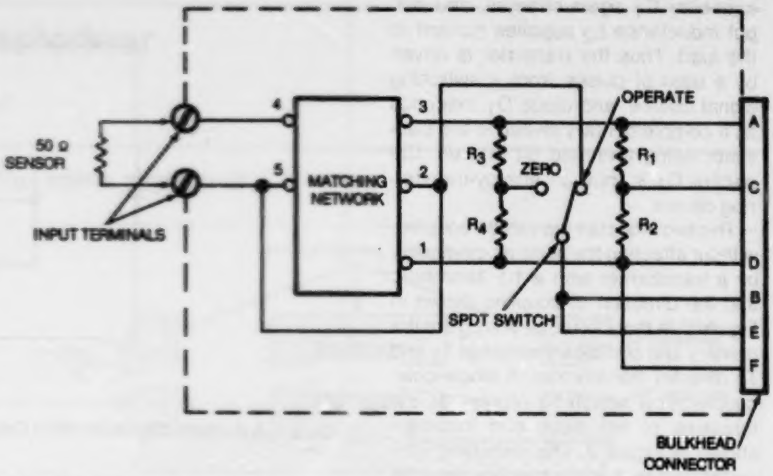

The Resistance of a Nickel Temperature Sensor, at the circuit input terminals, is converted to a strain reading on the recording equipment at the output. Resistors R_1 through R_4 are 350-Ω, ± 0.1 percent, wire-wound.

Efficient, Lightweight dc/dc Switching Converter

Efficient converters have the desirable input properties of a boost power stage and output properties of a buck power stage.

Lewis Research Center, Cleveland, Ohio

A dc-to-dc converter offers higher efficiency (95 as compared to 65 percent), lower output-voltage ripple, reduced EMI, and smaller size. As a general converter, the circuit output voltage is less than or larger than the input voltage, depending on the duty ratio of the transistor switch. New circuit arrangements allow both input and output currents to be nonpulsating, and capacitive energy transfer is used rather than the usual inductive energy transfer.

Variations of the fundamental circuit allow some important extensions not achievable with conventional switching converters.

In the basic circuit (Figure 1), a dc input voltage source (V_g) is connected to an input inductor L_1 that is connected to capacitor C_1. A switch S_1 alternately connects either the junction between L_1 and C_1 or the junction between C_1 and inductor L_2 to a common point between the source and the load. Inductor L_2 is connected in series with the load R. A filter capacitor C_2 is connected across the load.

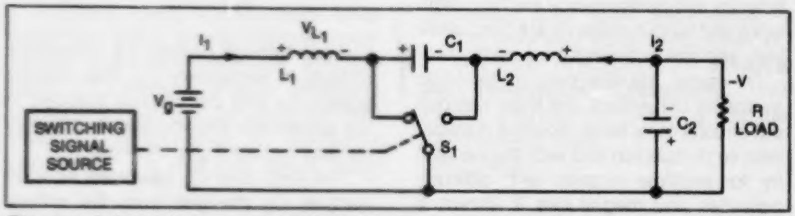

Figure 1. **A dc-to-dc Converter With Capacitive Energy Transfer**

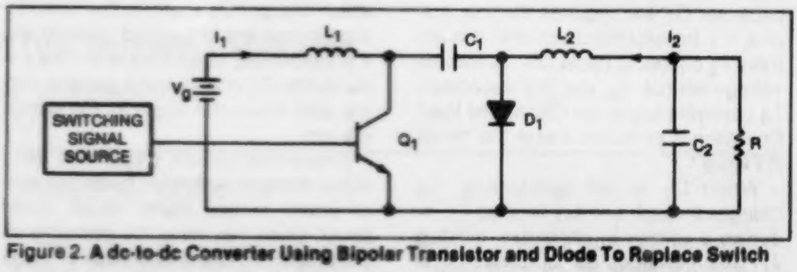

Figure 2. **A dc-to-dc Converter Using Bipolar Transistor and Diode To Replace Switch**

Switch S_1 can be implemented with a transistor and a diode (Q_1 and D_1 in Figure 2). The transistor is initally in its nonconductive state, and C_1 charges from the voltage source V_g through the inductance since diode D_1 is forward-biased. At that time the collector of the transistor is positive with respect to its emitter. When a switching pulse turns the transistor on, it becomes conductive. This grounds the side of the capacitor connected to the transistor. The diode is thus back-biased, and the capacitance discharges through the inductance L_2 into the load. When the switching pulse drops, the transistor is cut off, storage

(continued on next page)

capacitor C_1 again charges, and output inductance L_2 supplies current to the load. Thus the transistor is driven by a train of pulses from a switching signal source, and diode D_1 responds as a complementary switch to the transistor being switched off and on. Capacitor C_1 is thus an energy-transferring device.

The two inductances can be coupled, without affecting the basic dc coversion, by a transformer with a 1:1 turns ratio and the direction of coupling shown in Figure 3. In that circuit, L_1 and L_2 are the primary and secondary windings T_1 and T_2 of a 1:1 transformer. A single-pole, double-throw switch S_1 represents the functions of the diode and transistor shown in Figure 2. This switching converter (Figure 3) is the only one (besides the straightforward cascade-connected boost and buck converters) in which transformer coupling of the input and output inductances is possible. The input or the output current ripple can be reduced by an order of magnitude or more compared with the noncoupled counterparts. In fact, either input or output current ripple can be made zero. Also, instead of two cores for two noncoupled inductors, a single transformer core may be used. The switching converter in Figure 3 has the simplest possible structure (single 1:1 transformer, commutation capacitor C_1, and switch S_1); yet efficiency and performance are high (both input and output currents are nonpulsating), and size and weight are minimized.

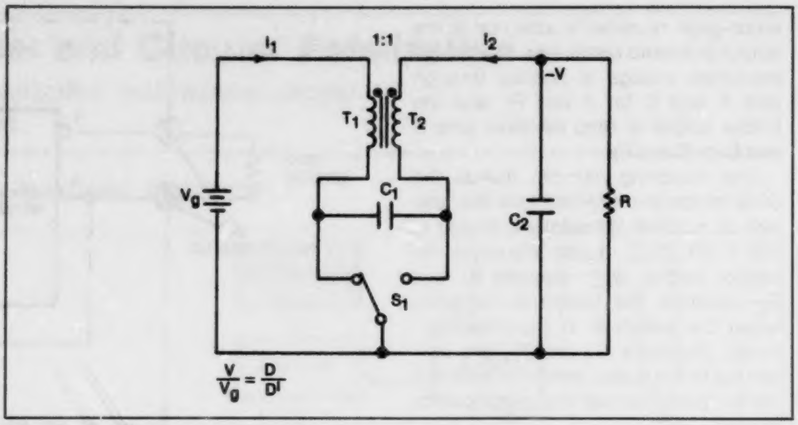

Figure 3. **A dc-to-dc Converter With Coupled Inductors**

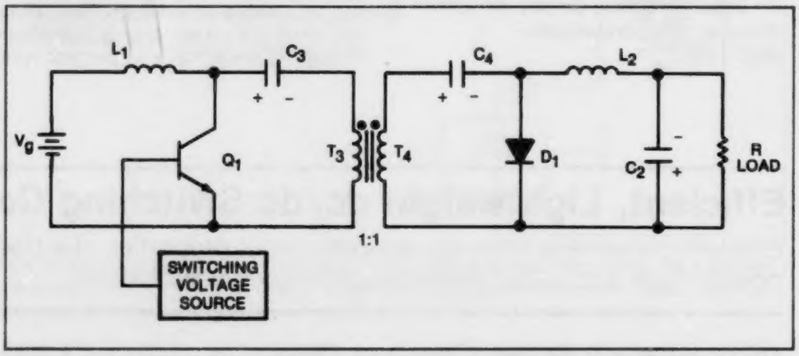

Figure 4. **Isolated dc-to-dc Converter**

In many applications of dc-to-dc switching converters, the input and output circuits must be dc isolated. A circuit with such isolation and with the capability for multiple outputs with different polarities and magnitudes is shown in Figure 4. The modification requires two capacitors C_3 and C_4 in place of the capacitor C_1 and requires the insertion of a 1:1 transformer such that the primary T_3 connects capacitor C_3 and the voltage source V_g, and the secondary T_4 connects capacitor C_4 and the load. Operation is similar to that of the circuit in Figure 1.

When Q_1 is not conducting, C_3 charges through primary winding T_3, inducing a voltage in secondary winding T_4, which charges up C_4. Diode D_1 is conductive at this time. When the transistor Q_1 becomes conductive, C_3 discharges through primary T_3, inducing a voltage in secondary T_4. The voltage acress C_4 and the voltage induced in the secondary winding add and supply current through L_2 to the load.

The next time Q_1 becomes nonconductive, C_3 charges from the voltage source V_g, causing current flow through T_3 and inducing a voltage across T_4, which charges C_4 again. At that time, L_2 supplies current to the load, maintaining a nonpulsating output current. The capacitance C_2 connected in parallel with the load filters the ripple in the output current.

These new circuits outperform each of the three so-far-known basic converter power stages (buck, boost, buck/boost) since they have the desirable input properties of the boost power stage and the desirable output properties of the buck power stage; yet they perform the general conversion function (increase or decrease of input voltage) of a conventional buck/boost power stage with considerably higher efficiency.

This work was done by S. Cuk and R. D. Middlebrook of the California Institute of Technology for **Lewis Research Center**. *Further information may be found in NASA CR-135174 (N78-29351/NSP), "Modeling, Analysis, and Design of Switching Converters" ($17). A copy may be purchased (prepayment required) from the National Technical Information Service, Springfield, Virginia 22161.*

Title to this invention has been waived under the provisions of the National Aeronautics and Space Act [42 U.S.C. 2457(f)] to the California Institute of Technology, Pasadena, California 91125.

LEW-12809

28-Channel Rotary Transformer

Each channel handles digital data at 1 megabaud.

NASA's Jet Propulsion Laboratory, Pasadena, California

A 28-channel transformer for a 6-year Jupiter mission has been proposed to transmit power and digital data across a rotating interface. Tests on transformer components for two channels showed clean transmission of a 1-MHz square wave.

Each channel uses a separate ferrite-core rotary transformer capable of a 1-megabaud (1-megabit-per-second) data rate. The torus-shaped transformers are spaced along the rotor like beads on a string (see figure); there is no inherent limit to the number of channels.

The rather large airgap in the transformer magnetic circuit, required for rotary motion, is contrary to conventional transformer design since it increases leakage inductance and magnetizing current. Fortuitously, the large gap also permits a simpler, single-ended data drive circuit. In a core with no airgap, the dc bias imposed by such a circuit could drive the core into saturation.

Special ferrite cores offering good high-frequency response are manufactured to tolerances of 1 mil (25 μm). In a prototype, the rotor and stator each had two 5-turn windings, allowing experiments with either 5 or 10 turns.

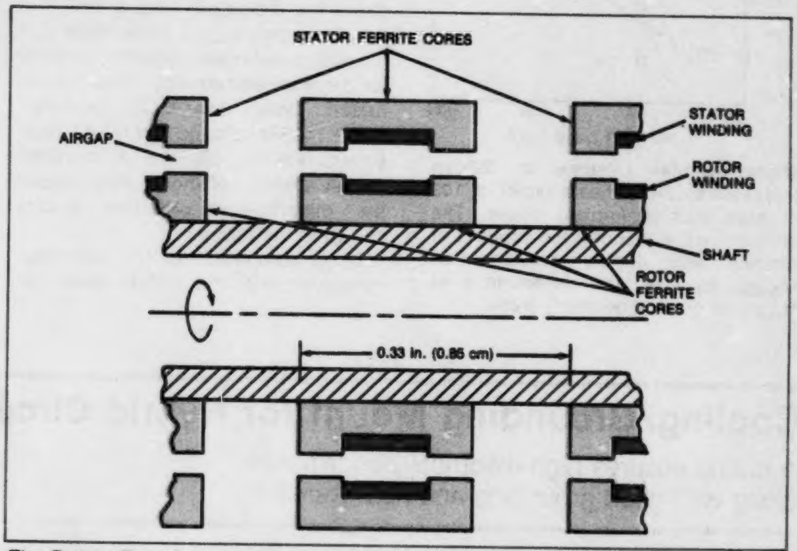

The **Rotary Transformer Array** has many parallel data channels, each with up to 1-megabaud data rate. The ferrite-cored transformers are spaced at 0.33-in. (0.85-cm) intervals along the rotor. The space between the transformers reduces crosstalk.

Previous rotary transformers have generally been single-channel units limited to end-of-shaft use at data rates of 15 kilobaud or less. Mechanical sliprings can also be used, but they require driving power to overcome contact friction, and they suffer gradual contact wear, noise, and bounce.

This work was done by Colonel W. T. McLyman of Caltech for **NASA's Jet Propulsion Laboratory.** *For further information, Circle 5 on the TSP Request Card.*
NPO-14861

Improving MOS Minority-Carrier Lifetime

Fluorine implantation can increase minority-carrier lifetime in silicon by a factor of 100.

NASA's Jet Propulsion Laboratory, Pasadena, California

Fluorine ion implantation can increase minority-carrier generation lifetime in silicon by a factor of up to 100 or so. In MOS (metal-oxide semiconductor) applications this can increase power efficiency by improving conduction when a voltage is applied across a pn junction.

Other findings of a study of the effects of fluorine as an impurity in silicon are as follows: Fluorine implantation does not increase microdefects at the silicon surface when thin oxide layers are grown; and fluorine appears to "getter" impurities at or near the silicon surface without adversely affecting MOS electrical parameters. Thus, there is no apparent need to remove fluorine often left on wafer surfaces after processing.

The effects of fluorine ion implantation were studied with a series of wafers from a ⟨100⟩ *n*-type, 1- to 3-Ω-cm Czochralski ingot. These were

(continued on next page)

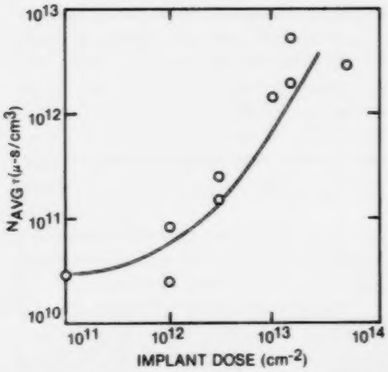

Minority-Carrier Lifetime in Silicon increases by more than a factor of 100 at high fluorine implant doses. The ordinate actually shows the product of lifetime and doping concentration N_{AVG}; however, the dependence of N_{AVG} on dose is relatively weak.

implanted at doses from 10^{11} to 5×10^{13} atoms per square centimeter. At the 150-keV ion kinetic energy used for implantation, the ions penetrate about 0.32 μm into the silicon.

Capacitor contact areas of 2×10^{-3} cm^2 were prepared on the wafers to permit measurements of capacitance versus voltage and versus time. (The capacitor dielectric was a 0.07-μm thermally-grown gate oxide layer.) A calculator-controlled system was used for these measurements. [See "Automated Tester for MOS Devices" (NPO-14088) on page 3 of *NASA Tech Briefs*, Vol. 3, No. 1.] A modified Zerbst analysis of these data yielded the minority-carrier-lifetime results shown in the figure.

Upon completion of the electrical measurements, the wafers were examined for microdefects. This required stripping off the capacitors to expose the base silicon surface. Etching showed no difference in the density of stacking faults and dislocation loops between implanted wafers and unimplanted controls; but such defects were formed below the surface at the depth of the fluorine ions. These deeper defects were detected by etching after growing (and then removing) an additional 1.1-μm oxide layer to expand the microdefects enough to reach the surface.

This work was done by Richard H. Cockrum, Seung P. Li, and Simon Prussin of Caltech for **NASA's Jet Propulsion Laboratory.** *For further information, Circle 6 on the TSP Request Card.*
NPO-14738

Cooling/Grounding Mount for Hybrid Circuits

A clamp ensures high electrical performance along with good grounding and heat transfer.

Lyndon B. Johnson Space Center, Houston, Texas

A new mounting for hybrid integrated-circuit modules allows extremely-short input and output connections so that the voltage standing-wave ratio (VSWR) is kept low. At the same time, the mounting ensures adequate grounding and efficient heat removal from the module.

The module is inserted in a rectangular clamp. The lead pins on the base of the module are inserted in a circuit board in the conventional way, and the circuit board is placed on a ground plane. Bosses on the ground plane pass through cutouts in the circuit board, and the clamp is attached to the ground plane by bolts (see figure).

Because the module leads are directly connected to the circuit board, VSWR is low and the circuit introduces no undue delay in processing a signal. Also, because the clamp is in close contact with the module and the ground plane, heat flows readily from the module to the metal plane, which serves as a sink for both heat and current.

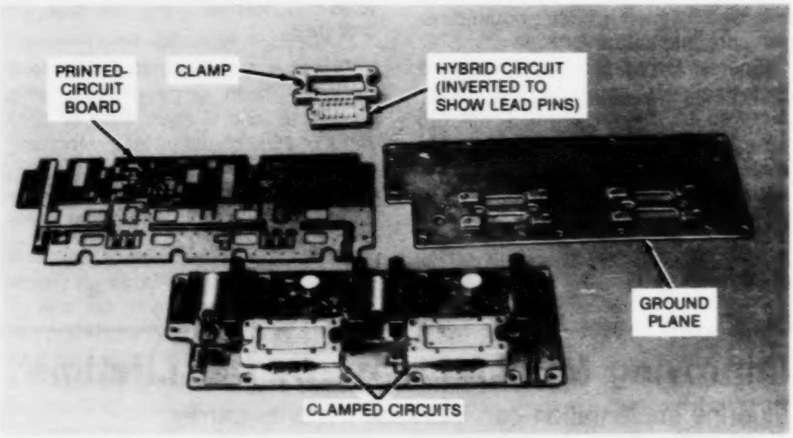

Rectangular Clamps Hold Hybrid Circuits on a printed-circuit board, in contact with a heat-conductive grounding plane. The assembled hybrid circuit, with clamps and ground plane in place, is an automatic-gain-control network for a first-stage intermediate-frequency amplifier.

The clamp mounting is superior to attaching ground straps to the module or connecting the module leads to the circuit board through jumpers.

This work was done by Bruce Bagstad, Robert Estrada, and Harold Mandel of TRW, Inc., for **Johnson Space Center.** *For further information, Circle 7 on the TSP Request Card.*
MSC-18728

Electronic Systems

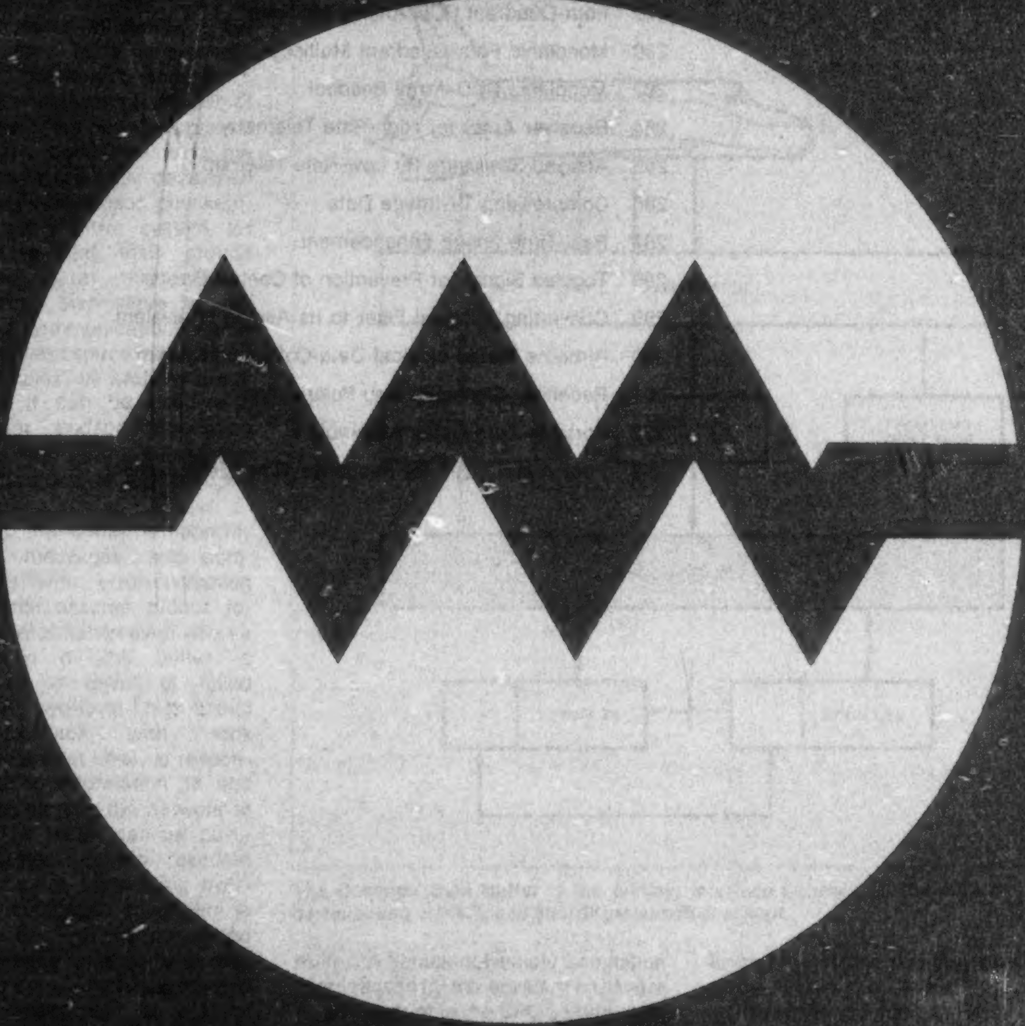

Hardware, Techniques, and Processes

277 Common Data Buffer
278 Simultaneous Disk Storage and Retrieval
279 Four-Quadrant CCD Analog Multiplier
280 Monolithic Four-Quadrant Multiplier
282 Monolithic CCD-Array Readout
284 Receiver Array for High-Rate Telemetry
285 Arrayed Receivers for Low-Rate Telemetry
286 Compressing TV-Image Data
287 Real-Time Image Enhancement
288 Toggled Signal for Prevention of Control Errors
289 Converting a Digital Filter to Its Analog Equivalent
290 Airborne Meteorological Data-Collection System
291 Receiving Signals of Any Polarization
292 Portable Zero-Delay Assembly
293 Photometer Used for Response Time Measurement

Common Data Buffer

Time-shared interface speeds data processing in a distributed computer network.

John F. Kennedy Space Center, Florida

The processing of information by a distributed network of computers proceeds much more efficiently if the network is linked by a time-shared data buffer (memory), access to which is sequenced such that each of the computers in the network appears to be the only computer using the buffer. Although originally developed as part of a 64-processor checkout, command, and control system for space vehicles and their ground facilities (see figure), the common data buffer can also serve as the interface and communications medium in a nonaerospace distributed computer complex. Its architecture is flexible, and it can be used with any computer and/or processing language, as long as the information interchange protocol is agreed upon by the users.

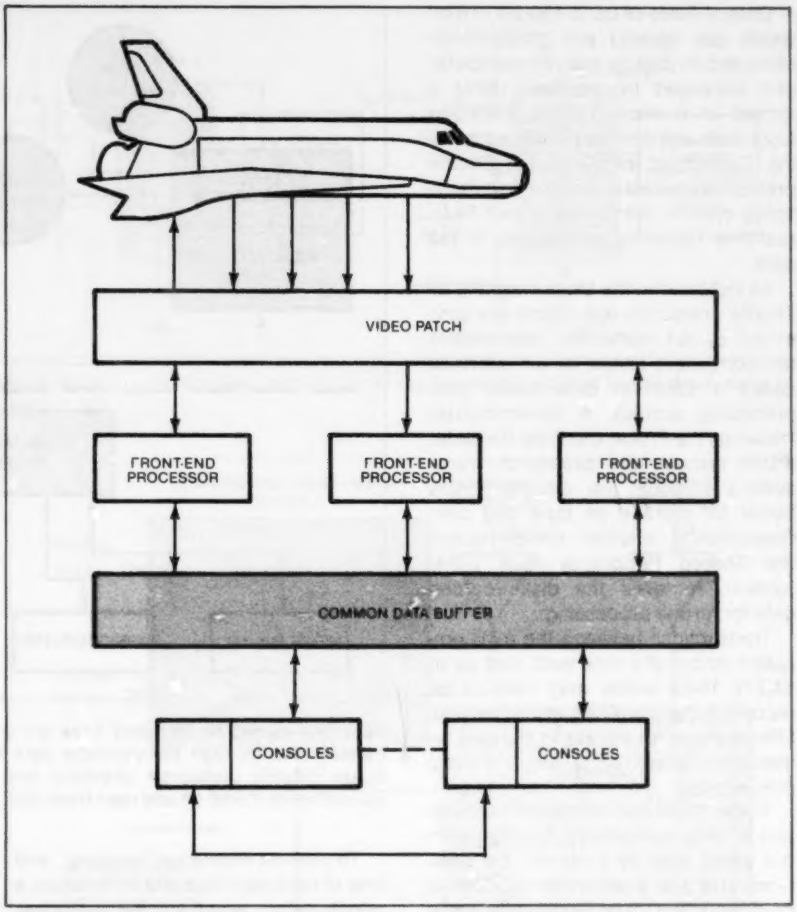

The **Common Data Buffer** is the primary interface between all the minicomputers participating in the Space Shuttle prelaunch checkout.

In operation, the buffer temporarily stores data, messages, and commands along with error-correcting information that assures proper retrieval of this information even when a certain portion of the buffer is inoperative as a result of failed hardware. A two-level high-speed scanning approach, with "look ahead" at the lowest level, is responsible for routing information to and from the computers in the network to the buffer. The buffer can be partitioned to protect certain reserved areas of memories from being overwritten by unauthorized computers in the network. Each of the connected central-processing units (CPU's) may have such an area, which is protected by address-validity logic to prevent accidental alteration of that memory.

A portion of the buffer is reserved for a series of "first-in, first-out" memory stacks supported by auxiliary hardware. These stacks allow any CPU to interrupt any other CPU in the network. Up to 64 interrupt vectors may be written to each stack, such that each CPU services, on a "first-come" basis, interrupts from each of the other CPU's connected to the buffer. A "stack-not-empty" condition is processed by the auxiliary hardware as an interrupt to the CPU belonging to the stack.

The buffer address structure and the memory are protected by an error-correcting code to protect and correct transactions to and from the buffer from noise or failed components. Bit-planar memory organization supports this feature. Redundant power is supplied to all components of the buffer, and certain critical timing and clock circuits have spare logic functions installed and may be selected by the flip of a switch.

This work was done by Frank Byrne of **Kennedy Space Center**. *For further information, including block diagrams and circuit descriptions that detail the operation of the system, Circle 8 on the TSP Request Card.*

This invention is owned by NASA, and a patent application has been filed. Inquiries concerning nonexclusive or exclusive license for its commercial development should be addressed to the Patent Counsel, Kennedy Space Center [see page A5]. Refer to KSC-11048.

Simultaneous Disk Storage and Retrieval

An efficient format handles simultaneous disk reads and writes.

John F. Kennedy Space Center, Florida

Data at rates of up to 150,000 16-bit words per second are concurrently recorded on disk by one minicomputer and accessed by another, using a format of memory blocks, buffering algorithm, and time-sequence addressing. Developed for the Space Shuttle prelaunch checkout, control, and monitoring system, the format allows near-real-time recording and access to the data.

As indicated in the block diagram, all Shuttle prelaunch operations are governed by 64 nominally independent minicomputers linked by an interface called a common data buffer (see preceding article). A minicomputer known as the Processed-Data Recorder (PDR) records the prelaunch transactions through the common data buffer for storage on tape and disk. Concurrently, another minicomputer, the Shared Peripheral Area (SPA) System, retrieves the disk-recorded data for further processing.

Transactions between the minicomputers occur at a rate such that up to 54,272 16-bit words may have to be recorded by the PDR each second. SPA requests for access to the data on disk may occur once every 77.222 milliseconds.

These rapid and concurrent storage and access requests are handled without losing data by selecting the data-block size and a buffering algorithm to hold incoming data temporarily while the SPA is reading from the disk. In addition, each of the addresses of the data on disk is quickly identified by a directory format that uses the times of start and end of each data request by the PDR as an index. Data are written sequentially, so all times of start and end for a data request are unique.

The PDR reads data in block sizes of 118 words and attaches a 10-word header, which describes and identifies the start and end times of all the data within a block. The data plus the header constitute a logical record of 128 words, which is the exact size of a sector on disk.

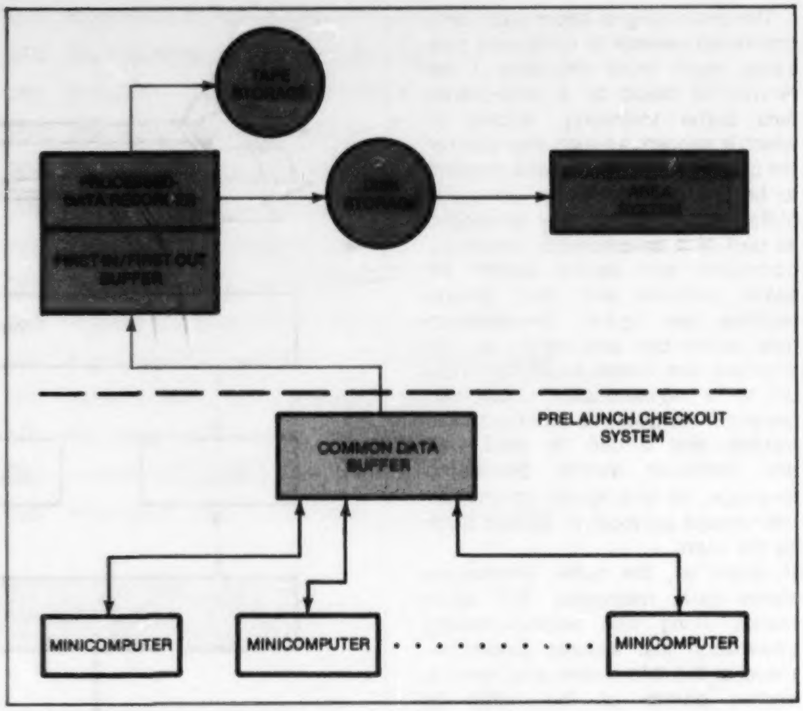

Data Transferred to Disk and Tape are a record of the minicomputer/minicomputer transactions through the common data buffer. In this simplified schematic of the Space Shuttle prelaunch checkout and control system, data at high rates are concurrently stored on and read from disk.

To prevent excessive "seeking" and loss of recorded data, the PDR issues a priority select, which lets the in-process SPA request complete and which allows subsequent requests come only from the PDR, until the PDR has finished writing all its backed-up data to disk. The PDR then lets the SPA begin a new request.

To allow the SPA to have access to the disk, the PDR has sufficient buffering area to hold all incoming data while the SPA request is being exercised. Also the algorithm for updating the directories minimizes "seeking" and does not interfere with the normal recording algorithm.

Although it was developed to handle a data rate of 54,000 words per second, the buffering algorithm has been tested successfully at data rates up to 68,000 words per second. A modified buffering algorithm to allow transfer of varying block sizes to disk has been tested at better than 150,000 words/second, and proposed modifications of the way the directory is recorded on disk should up the rate to 160,000 words/second.

This work was done by F. E. Levine of IBM Corp. for **Kennedy Space Center**. *For further information, Circle 9 on the TSP Request Card.*

Inquiries concerning rights for the commercial use of this invention should be addressed to the Patent Counsel, Kennedy Space Center [see page A5]. Refer to KSC-11167.

Four-Quadrant CCD Analog Multiplier

Sequential processing technique improves accuracy when multiplying CCD-array signals by a weighting function.

Langley Research Center, Hampton, Virginia

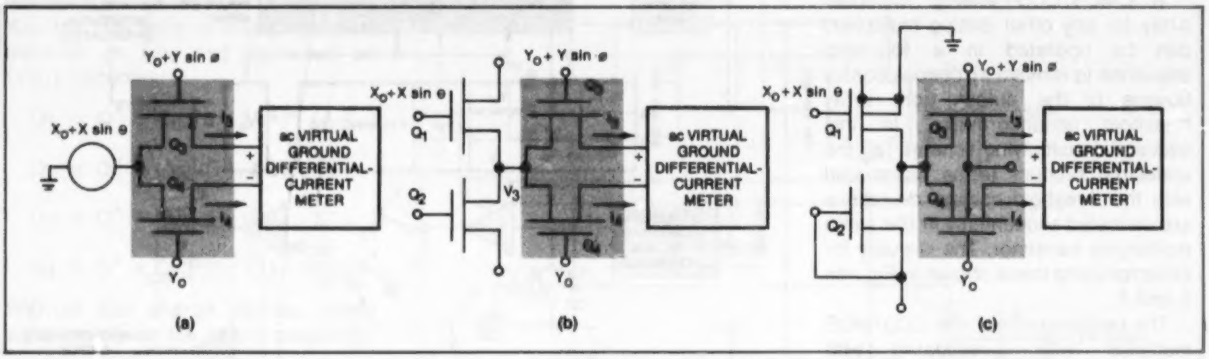

Y_o+Y sin ø
X_o+X sin θ
Q_3
Q_4
I_3
I_4
+
-
ac VIRTUAL GROUND DIFFERENTIAL-CURRENT METER
Y_o
(a)
Q_1
Q_2
V_3
(b)
(c)

Figure 1. **One Cell of an MOS Multiplier Array** is shown in its simplest form in (a); in (b) the signal applied to the drain node is buffered; a CMOS implementation is illustrated in (c).

The multiplication of each element of a charge-coupled-device (CCD) array by a weighting function is usually necessary to remove offsets brought about by the applied bias voltages. However, a constant weighting function is not always sufficiently general for applications such as vector/matrix products or sums of products for analog correlators. Often with such vector or matrix products, ac coupling is not convenient for removing constant or slowly varying offsets, since a single true four-quadrant sum of products is needed after the analog data have been distributed into the vector/matrix component locations.

Analog correlator multipliers use two schemes to cancel the undesired output contributions arising from the prerequisite biases. The first is spontaneous cancellation by multiple "nominally identical" devices; and the second is sequential cancellation, where the same devices are used repeatedly to form the multiple products. A single device then successively subtracts the products, eliminating the effects of MOS-array threshold nonuniformities.

The multiplication function can be performed with MOS transistors operating in the "triode" region. A diagram of a balanced multiplier is shown in Figure 1a. When the signals are derived from the floating gate of a CCD, the signal should be applied to the gate of the minimum-geometry MOS transistor to reduce parasitic signal loading. Furthermore, to avoid unwanted interaction, the signal from a floating gate should not be connected directly to the drains of Q_3 and Q_4.

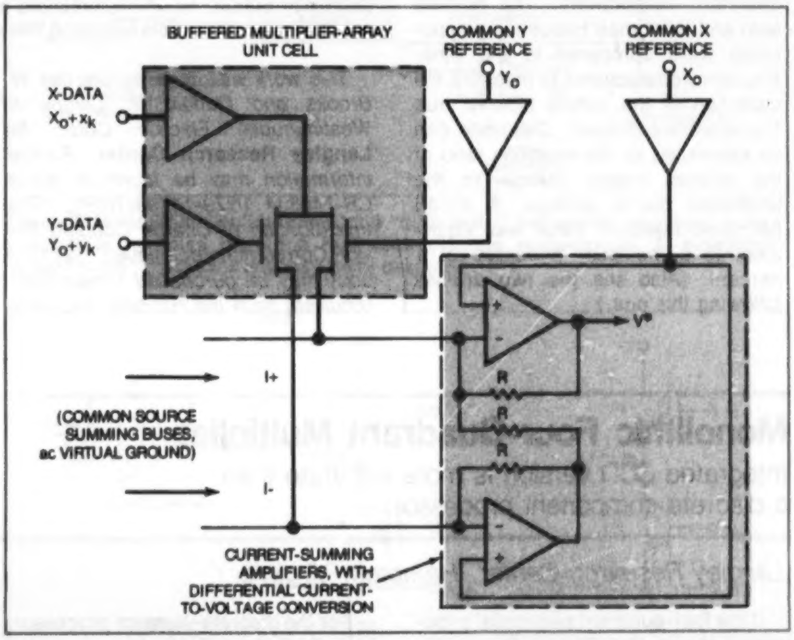

BUFFERED MULTIPLIER-ARRAY UNIT CELL
COMMON Y REFERENCE
COMMON X REFERENCE
Y_o
X_o
X-DATA
X_o+x_k
Y-DATA
Y_o+y_k
+
-
V*
R
R
R
I+
I-
(COMMON SOURCE SUMMING BUSES, ac VIRTUAL GROUND)
CURRENT-SUMMING AMPLIFIERS, WITH DIFFERENTIAL CURRENT-TO-VOLTAGE CONVERSION

Figure 2. **Current-Summing Amplifiers and a Differential Current-to-Voltage Converter** are connected to the CCD-array output. The output voltage is processed in a four-step sequence by the circuit of Figure 3.

One solution is to use a buffer with voltage gain, which can be either a source follower or an inverter. Figure 1b shows a balanced multiplier using a buffer to drive the drain node of the multiplier. For inverting buffers the unequal dc voltage levels of the two

(continued on next page)

signals may be inconvenient. For instance, if both signals are derived from CCD's on the same structure, it is desirable to have the two signals at the same dc level. This difficulty can be circumvented by using complementary MOS circuits as shown in Figure 1c.

A CMOS/CCD analog multiplier array (or any other analog multiplier) can be operated in a four-step sequence to remove erroneous contributions to the output from array threshold nonuniformities. In this sequential multiplying scheme, all the undesired product terms associated with the threshold voltage deviations are canceled sequentially in the same multiplying transistor. The circuitry for accomplishing this is shown in Figures 2 and 3.

The performance of the CCD/MOS multiplier was investigated with Fourier analysis. Two signals of different frequencies were applied to the drain (X-channel) and gate (Y-channel), respectively. The desired sum and difference frequency components were compared to the other frequency components to measure the distortion of the output from a true four-quadrant product. Distortion can be expressed as the rejection ratio of the desired output voltage to the undesired output voltage. A 40-dB harmonic rejection value was equivalent to a multiplier accuracy of 1 percent. (Also see the two articles following this one.)

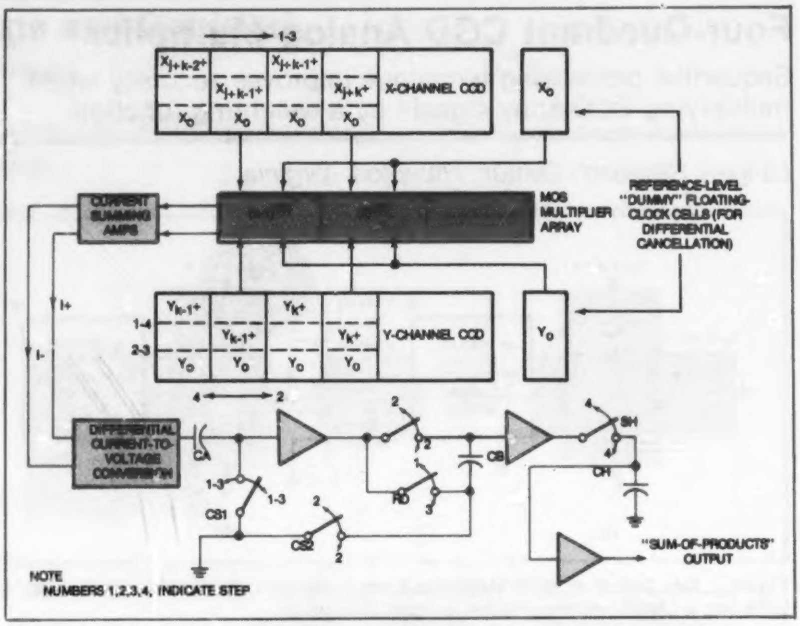

Figure 3. The **Four-Quadrant MOS Analog Multiplier Array** generates a "sum-of-products" output, in which threshold nonuniformity among the array elements is canceled. (See the article following this one for a summary of the circuit equations.)

This work was done by Charles W. Brooks and Donald R. Lampe of Westinghouse Electric Corp. for **Langley Research Center.** *Further information may be found in NASA CR-145334 [N79-14796/NSP], "The Investigation of Charge Coupled Device Correlation Techniques" [$11]. A copy may be purchased [prepayment required] from the National Technical Information Service, Springfield, Virginia 22161.*

Title to this invention has been waived under the provisions of the National Aeronautics and Space Act [42 U.S.C. 2457(f)] to the Westinghouse Electric Corp., 1310 Beulah Road, Pittsburgh, PA 15235.
LAR-12332

Monolithic Four-Quadrant Multiplier

Integrated CCD version is more accurate than a discrete component processor.

Langley Research Center, Hampton, Virginia

If the four-quadrant sequential processor shown in Figure 3 of the preceding article is implemented with discrete capacitors, resistors, switches, and operational amplifiers, its accuracy is limited by such factors as sample-and-hold (S/H) acquisition speed, S/H droop rate, and possible stray pickup by the card-mounted discrete components. Such problems would be eliminated, however, in a monolithic or integrated version incorporated on the same chips as the multiplier array.

For the discrete-element processor, four distinct products are generated sequentially in a perfectly uniform array of multiplying devices:

$$A = \sum_k (X_o + x_k) \cdot (Y_o),$$

$$B = \sum_k (X_o + x_k) \cdot (Y_o + y_k),$$

$$C = \sum_k (X_o) \cdot (Y_o + y_k),$$

$$D = \sum_k (X_o) \cdot (Y_o)$$

The ideal result then becomes:

$$Z = (B - A) + (D - C)$$

$$= \sum_k (x_k) \cdot (y_k)$$

A monolithic implementation of the part of the processor that is downstream of the current-to-voltage converter is shown in Figure 1. This version is for differential current summing; an analogous circuit has been designed for single-sided current summing. Both devices use the stabilized charge injection or filled/spill scheme.

The charge metered and read while switch $\emptyset_0$ is activated is given by $Q^* = (C_{IN})$. With the "differential" processor, if the current-summing-to-voltage converters have an effective offset or threshold difference of Δ, while the resultant output voltages are K±, the sequence of charge packets metered on C_{IN} and collected on C_{OUT} becomes:

$$Q_1 = Q^* + C_{IN}\left| \Delta + (A+) - (A-) \right|$$

$$Q_2 = Q^* + C_{IN}\left| (B-) - \Delta - (B+) \right|$$

$$Q_3 = Q^* + C_{IN}\left| \Delta + (C+) - (C-) \right|$$

$$Q_4 = Q^* + C_{IN}\left| (D-) - \Delta - (D+) \right|$$

With all four charge packets added algebraically on the output capacitor:

$$\begin{aligned} Q &= \sum_{1}^{4} Q_K \\ &= 4Q^* + C_{IN}(\delta A - \delta B + \delta C - \delta D) \end{aligned}$$

With the "single-sided" processor, the total charge added to C_{OUT} becomes:

$$\begin{aligned} Q &= Q_1 + Q_2 \\ &= 2Q^* + C_{IN}(A - B + C - C) \end{aligned}$$

Most multipliers generate product currents that are then combined in a way that eliminates the effects of array nonuniformities. Furthermore, the node into which the product currents flow often should be a virtual ground. Figure 2a shows this concept schematically, with the product current converted directly into a voltage by the operational amplifier and resistor R.

Simple monolithic approximations compatible with CCD fabrication are also illustrated in Figure 2, but they require appreciable bias currents from the current source Q_2 to increase the transconductance of the "grounded base" transistor Q_1 and thus better approximate a virtual ground. The techniques shown in Figures 2b and 2c convert the currents into voltages with a suitable bias for direct application to the input gates of the sequential processor. With transistor Q_1 operating in the saturation or "pentode" region, the actual current-to-voltage conversion is performed by resistor R, which must accurately be established and matched in duplicate at every location where differential current-to-voltage conversion occurs. For this reason it is preferable to have only one such pair of resistors per "sum-of-products" device, rather than one pair for each multiplier in the array.

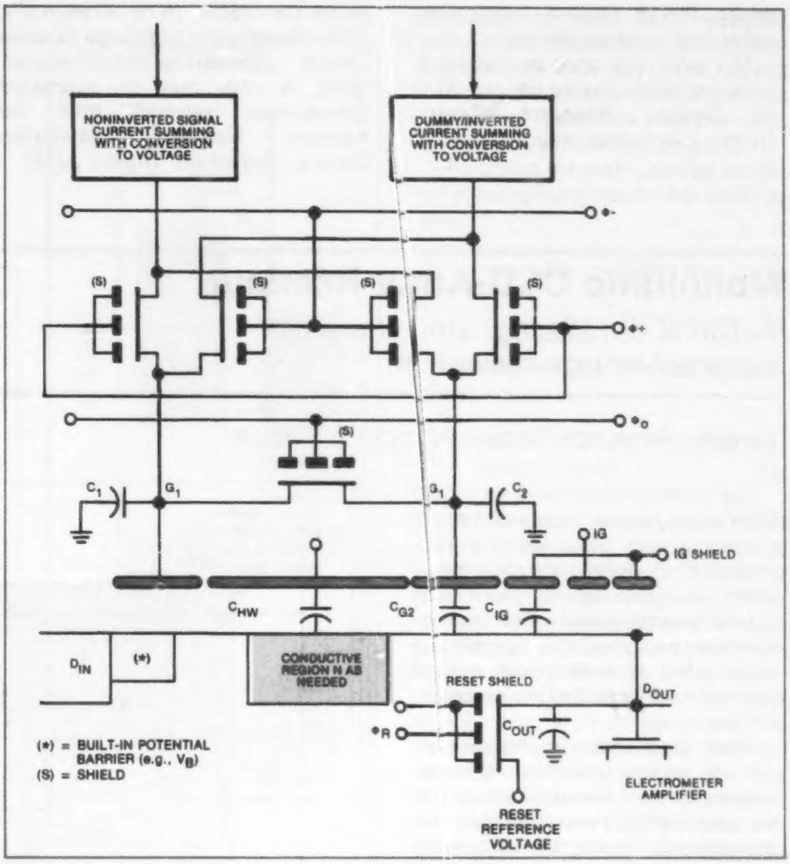
NONINVERTED SIGNAL CURRENT SUMMING WITH CONVERSION TO VOLTAGE
DUMMY/INVERTED CURRENT SUMMING WITH CONVERSION TO VOLTAGE
ø-
ø+
ø0
(S)
C1
G1
G1
C2
IG
IG SHIELD
CHW
CG2
CIG
DIN
(*)
CONDUCTIVE REGION N AS NEEDED
RESET SHIELD
øR
COUT
DOUT
ELECTROMETER AMPLIFIER
RESET REFERENCE VOLTAGE
(*) = BUILT-IN POTENTIAL BARRIER (e.g., VB)
(S) = SHIELD

Figure 1. **Monolithic Configuration** for a "differential" sequential processor is less susceptible to noise than one that uses discrete components. A monolithic "single-sided" processor has also been designed.

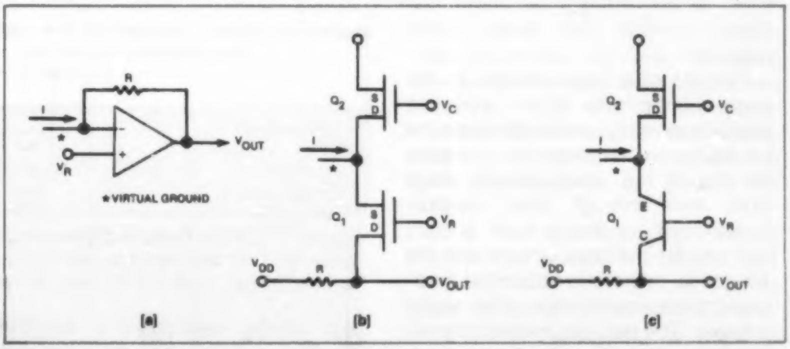
R
I
*
VR
VOUT
*VIRTUAL GROUND
Q2
S
D
VC
Q1
VR
VDD
R
VOUT
E
C
(a)
(b)
(c)

Figure 2. **Three Single-Sided Current-to-Voltage Converters** are compatible with CCD-array fabrication: (a) shows the circuit concept; (b) and (c) show MOS and MOS/bipolar implementations, respectively.

The schemes of Figures 2b and 2c have been computer-modeled. The results predict that the distortion added by the circuits, beyond that of the basic multiplier, is negligible. Since, typically, the distortion rejection performance of the CCD sequential processor well exceeds that of the multipliers, the complete monolithic

(continued on next page)

device should perform substantially better than previous devices.

This work was done by Donald R. Lampe of Westinghouse Electric Corp. for **Langley Research Center.** *Further information may be found in NASA CR-145334 [N79-14796/NSP], "The Investigation of Charge Coupled Device Correlation Techniques" [$11]. A copy may be purchased [prepayment required] from the National Technical Information Service, Springfield, Virginia 22161.*

Title to this invention has been waived under the provisions of the National Aeronautics and Space Act [42 U.S.C. 2457(f)] to the Westinghouse Electronic Corp., 1310 Beulah Road, Pittsburgh, PA 15235.
LAR-12330A

Monolithic CCD-Array Readout

Circuit is self-biasing, with differential current-to-voltage conversion.

Langley Research Center, Hampton, Virginia

The multiplying elements for a CCD MOS analog signal processor require a readout with dc-balanced virtual-ground input nodes, the dc bias of which is controlled by a voltage applied to another node. One conceptual and two simplistic forms of a single-sided or unbalanced readout are shown in Figure 2 of the preceding article.

Since most analog multipliers consist of counterbalancing elements, yielding currents that are subtracted to cancel threshold nonuniformities, it is desirable to obtain the differential current directly from noninteracting high-impedance current sources that are added in parallel. The high impedances can feed a high resistance, for converting small differential signal currents into large signal voltages.

The use of a large resistor in the single-sided circuits of the preceding article is severely limited because the full bias current needed to increase the G_M of the virtual-ground stage must flow through that resistor. Consequently, a pair of such circuits with smaller resistors, mated with the differential monolithic sequential processor, gives smaller differential signal voltages. The result is reduced signal-to-noise ratio or the need for a larger-area sequential processor to maintain the same ratio.

A possible CMOS circuit to subtract the two currents (canceling the dc bias components) and allow higher resistances to be used is illustrated in Figure 1. The circuit consists partly of a dc-balanced pair of virtual-ground stages. The remainder is the basic current-differencing part of the circuit and closely resembles a modified current mirror; i.e., the currents through transistors DXCS and NOCS, which are nominally matched, try to establish themselves at very nearly equality:

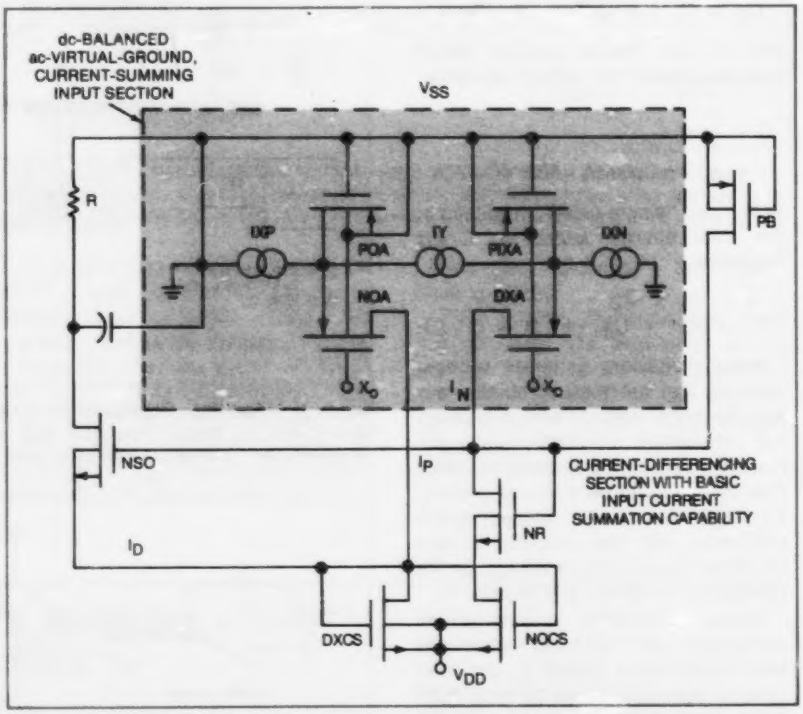

dc-BALANCED ac-VIRTUAL-GROUND, CURRENT-SUMMING INPUT SECTION
V_{SS}
R
IXP
IY
IXN
PB
POA
PIXA
NOA
DXA
X_0
I_N
X_0
NSO
I_P
CURRENT-DIFFERENCING SECTION WITH BASIC INPUT CURRENT SUMMATION CAPABILITY
NR
I_D
DXCS
NOCS
V_{DD}

Figure 1. **CMOS Current-Dfferencing Readout** consists of a dc-balanced pair of virtual ground stages (in color) and current-differencing circuit that is similar to a current mirror. I_D is the differential readout current.

$$I_D + I_P = I_N + \Delta I \qquad (1)$$

I_P and I_N are the signal (IXP, IXN, IY) plus bias currents for the two counterbalancing legs of the multiplier, as fed into their respective ac-virtual-ground nodes; ΔI is a fixed incremental offset current to enable readout of bipolar current differentials; and I_D is the differential readout current.

When a completely-quadruply-balanced triode multiplier cell replaces the test sources (IXP, IXN, IY), the circuit of Figure 2 results.

The transistors to the left of the dashed line are those belonging to the selected multiplier cell and need to be

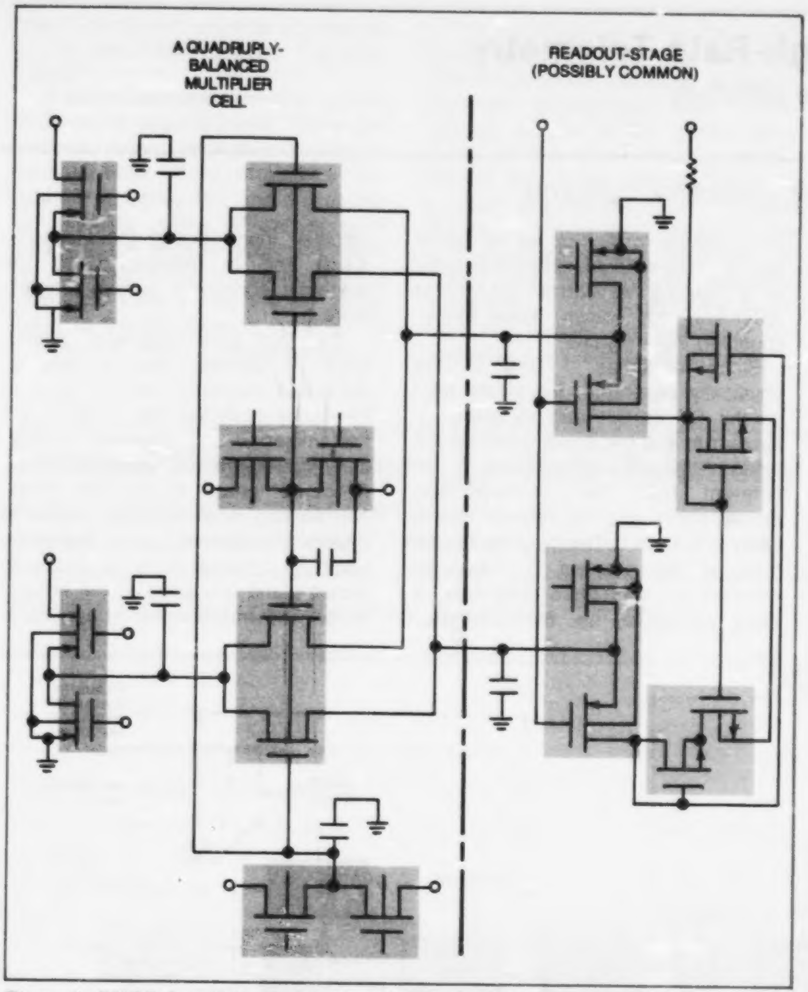
A QUADRUPLY-BALANCED MULTIPLIER CELL
READOUT-STAGE (POSSIBLY COMMON)

Figure 2. **CMOS Correlator Cell With Self-Bias and Differential Current-to-Voltage Readout** is shown in a form suitable for a monolithic implementation.

Feature	V_{DD}	CMRR (dB)	Differential Gain (dB)	V(48)	Equivalent Transconduction Sensitivity: Output Current Shift/Threshold Shift
Balanced, Higher Voltage	-15	72.9	-3.5	-2.116	N/A
Balanced	-12	49.6	-3.7	-1.762	N/A
0.2-V Increase in (NOA) Pinchoff	-12	36.1	-3.8	-1.580	6.46 μV
0.2-V Increase in (DXA) Pinchoff	-12	52.3	-3.5	-1.836	8.8 μV
0.2-V Increase in (DXCS) Threshold	-12	51.8	-5.7	-0.584	98.4 μV

CMOS Readout Circuit Sensitivity and Performance were calculated from a computer model.

duplicated for each such multiplier within the correlator chip. The remaining elements form part of the readout and may be scaled according to the number of multipliers involved as a single common readout stage.

Assuming the bias currents for the ac-virtual-ground stages are given by IB±:

$$I_P = (IB+) + (IXP) - (IY) \qquad (2)$$

$$I_N = (IB-) + (IXN) + (IY) \qquad (3)$$

Combining with the previous equation gives:

$$I_D = (\Delta I) + 2(IY) + |(IXN) - (IXP)| + |(IB-) - (IB+)| \qquad (4)$$

For MOS "triode" multipliers, IXP and IXN are the drain/source currents when a common signal is applied to both drains; any ac component of the common drain signal cancels, assuming that the matched pair of MOSFET triodes is truly identical.

Equation 4 indicates that the fixed bias current, ΔI, is comparable to the worst case of unbalance for the virtual-ground stage biases plus the unbalance between the nominally-matched multiplier MOSFET's plus the peak signal excursion. Consequently, the common-mode rejection ratio (CMRR) for this circuit is:

$$\text{CMRR} = \frac{IX_{IN}}{IX_{OUT}}$$

This parameter as well as other measures of performance have been modeled using the commercially-available ISPICE routine. The results, showing circuit CMRR, differential gain, and sensitivity, are given in the table.

This work was done by Dave L. Farnsworth, Donald R. Lampe, and Tom J. Shutt of Westinghouse Electric Corp. for **Langley Research Center.** *Further information may be found in NASA CR-145334 [N79-14796/NSP], "The Investigation of Charge Coupled Device Correlation Techniques" [$11]. A copy may be purchased [prepayment required] from the National Technical Information Service, Springfield, Virginia 22161. LAR-12376*

Receiver Array for High-Rate Telemetry

A proposed system improves the sensitivity of a telemetry station network.

NASA's Jet Propulsion Laboratory, Pasadena, California

An RF (radio-frequency) arraying system proposed for high-rate telemetry receiving stations promises to increase the receiver signal-to-noise ratio. [Also see the following related article "Arrayed Receivers for Low-Rate Telemetry" (NPO-14590).] The ratio will be improved in proportion to the number of the arrayed receivers. Marginal high-rate satellite telemetry signals, which are frequently lost due to system, atmosphere, and galactic noises, will come in more clearly.

A simplified setup using one primary and one slave receiver is shown in the illustration. Each is equipped with its own antenna to pick up an RF signal that is phase-modulated with telemetry or a ranging waveform. The other receivers, not shown, have corresponding input signals.

Since antennas 1 and 2 are physically separated, the phase shift on the RF carrier and square-wave subcarrier and the group delay on the data in the receiving system 2 are different from the corresponding phase shifts and modulation group delay in system 1. The combined noise from all the sources is measured relative to reference-temperature loads connected to the low-noise amplifier input (during the measurement) and is designated as the operating equivalent system temperature.

The first local oscillator signal, which is derived from a voltage-controlled oscillator (VCO_1) through frequency multiplier XM, is fed to the first mixer X and provides a noisy estimate (due to receiver noise) of the RF-carrier phase to the first mixer. The second local oscillator signal in system 1 is derived from a frequency standard common to all N receiving systems and is applied to the second mixer. The mixed signal is applied to

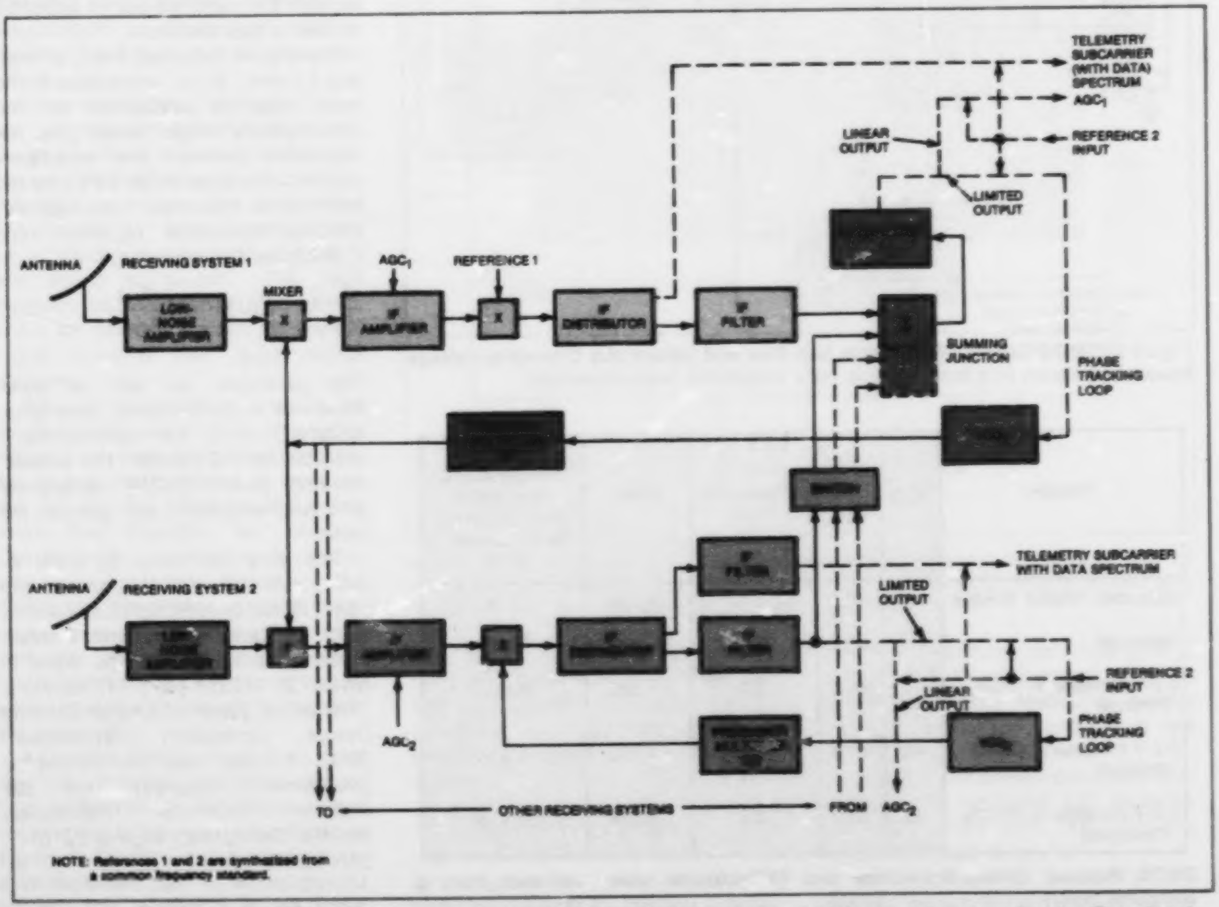
TELEMETRY SUBCARRIER (WITH DATA) SPECTRUM
AGC_1
LINEAR OUTPUT
REFERENCE 2 INPUT
LIMITED OUTPUT
ANTENNA
RECEIVING SYSTEM 1
AGC_1
REFERENCE 1
MIXER
LOW-NOISE AMPLIFIER
X
IF AMPLIFIER
X
IF DISTRIBUTOR
IF FILTER
SUMMING JUNCTION
PHASE TRACKING LOOP
TELEMETRY SUBCARRIER WITH DATA SPECTRUM
ANTENNA
RECEIVING SYSTEM 2
LIMITED OUTPUT
X
REFERENCE 2 INPUT
LINEAR OUTPUT
AGC_2
PHASE TRACKING LOOP
TO
OTHER RECEIVING SYSTEMS
FROM
AGC_2
NOTE: References 1 and 2 are synthesized from a common frequency standard.

RF Carrier Array uses two receiver systems to improve the signal-to-noise ratio of high-rate telemetry signals. The signals separately processed by each system are coherently combined at the summing junction to produce an improved signal-to-noise ratio. Two receivers improve the ratio by 2.7 dB; three receivers, by 4.1 dB; and four, by 4.6 dB.

the IF distribution amplifier and then to the IF filter that removes the sidebands.

A similar process occurs in system 2 up to the second mixer. There the second local oscillator signal is derived from VCO$_2$ through a frequency multiplier XQ, and it provides an estimate of the RF-carrier input phase to the second mixer in system 2. A phase shifter in series with a reference input 2 sets the RF phase equal to the RF phase of system 1 at the input to the summing junction.

The carrier-phase noise that is fed from system 2 into the summing junction is small (because of much-narrower closed-loop noise bandwidths) relative to the phase noise error on the first local oscillator. Carrier signals fed into the summing junction are coherent with a small differential phase jitter. The sum of the two coherent signals becomes an output with an improved signal-to-noise ratio as compared to the single receiving system. An additional improvement is made by arraying more receiver systems.

This work was done by Milton H. Brockman and Mahlon Easterling of Caltech for **NASA's Jet Propulsion Laboratory.** *For further information, Circle 10 on the TSP Request Card.*

This invention has been patented by NASA [U.S. Patent No. 4,186,347]. Inquiries concerning nonexclusive or exclusive license for its commercial development should be addressed to the Patent Counsel, NASA Resident Office-JPL [see page A5]. Refer to NPO-14579.

Arrayed Receivers for Low-Rate Telemetry

A proposed method to maintain a low detection threshold of low-rate telemetry receiving stations

NASA's Jet Propulsion Laboratory, Pasadena, California

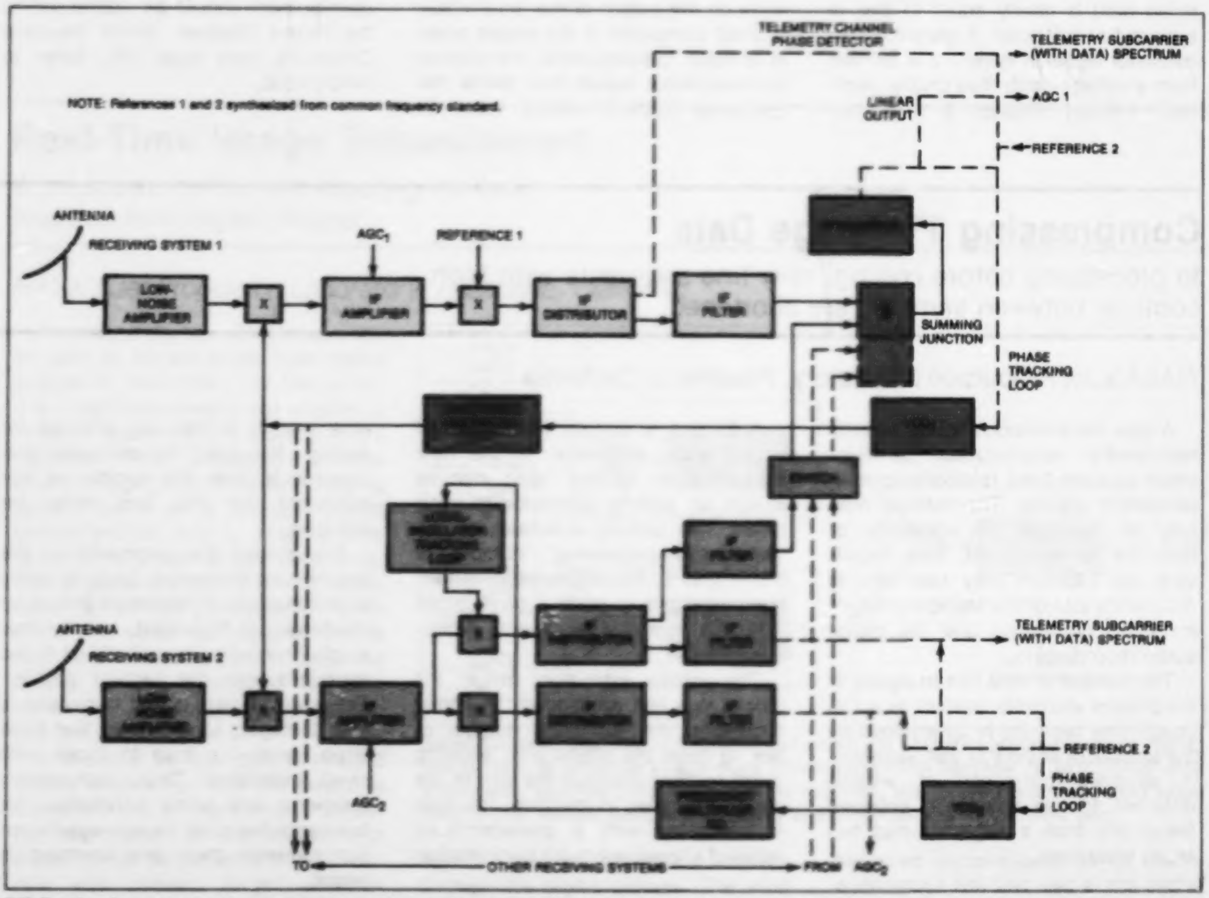
TELEMETRY CHANNEL PHASE DETECTOR
TELEMETRY SUBCARRIER (WITH DATA) SPECTRUM
NOTE: References 1 and 2 synthesized from common frequency standard.
LINEAR OUTPUT
AGC 1
REFERENCE 2
ANTENNA
RECEIVING SYSTEM 1
AGC$_1$
REFERENCE 1
LOW-NOISE AMPLIFIER
X
IF AMPLIFIER
X
IF DISTRIBUTOR
IF FILTER
SUMMING JUNCTION
PHASE TRACKING LOOP
SWITCH
LOCAL OSCILLATOR TRACKING LOOP
IF FILTER
ANTENNA
RECEIVING SYSTEM 2
TELEMETRY SUBCARRIER (WITH DATA) SPECTRUM
REFERENCE 2
PHASE TRACKING LOOP
AGC$_2$
TO
OTHER RECEIVING SYSTEMS
FROM
AGC$_2$

RF Carrier Array includes one master and one slave receiving systems to improve the overall signal-to-noise ratio. The system can be expanded to N slave systems to improve further the signal-to-noise ratio. This scheme reduces the detection threshold of low-rate telemetry signals transmitted from spacecraft, improving the overall communications efficiency.

(continued on next page)

An RF arraying system proposed for low-rate telemetry receiving stations [also see the preceding related article "Receiver Array for High-Rate Telemetry" (NPO-14579)] promises to increase the system signal-to-noise ratios. The scheme incorporates a local-oscillator tracking loop operating a 0.1-Hz bandwidth in a group of 1-Hz-bandwidth slave receivers.

A simplified scheme using one main and one slave receiver is shown in the illustration. Additional receiving systems can be added to improve further the signal-to-noise ratio of the station.

Both systems receive an RF signal phase modulated with telemetry and/or a ranging waveform. Receiving system 1 incorporates a low-noise amplifier, a mixer, an IF (intermediate frequency) amplifier, another mixer, an IF distribution amplifier, and a filter.

System 2 is similarly arranged up to the second mixer, and its signal-to-noise ratio is nearly equal to that of system 1 at that point. A second local-oscillator signal in system 2 is derived from a voltage-controlled crystal oscillator (VCO_2) through a frequency multiplier (XQ). The phase of the VCO_2 is modified by the differences in carrier phase plus any differences in carrier phase relative to system 1.

The second local-oscillator signal includes the estimate of the RF carrier input phase to the lower second mixer (system 2). The phase estimate is derived from a phase-locked loop with a closed-loop noise bandwidth that is a small fraction of the closed-loop noise bandwidth of the RF carrier-phase tracking loop in system 1. Hence the noise on the phase estimate is much less than that on the VCO_1 output.

When arraying many receiving systems, the cumulative phase noise at the summing junction is kept small relative to the phase noise in system 1 by including an additional second mixer (upper mixer) shown in system 2, with the second local oscillator fed to this additional second mixer through a narrow-band phase-locked local-oscillator tracking loop. The phase noise on the output of the local VCO_2 is small compared to the phase noise at its input. Consequently, the second local-oscillator signal that feeds the additional (upper) second mixer in system 2 has a very small amount of noise on its phase estimate.

System 2 has two second IF distribution amplifiers. The upper IF distribution amplifier accepts the output of the upper second mixer and in turn provides its output signal to the upper IF carrier filter (and to the telemetry IF channel) in system 2.

Additional filtering of the phase estimate in system 2 with subsequent coupling through the additional (upper) second mixer, IF distribution amplifier, and IF filter provide the near-maximum signal-to-noise ratio improvement for RF carrier arraying.

This work was done by Milton H. Brockman and Mahlon F. Easterling of Caltech for **NASA's Jet Propulsion Laboratory.** *For further information, Circle 11 on the TSP Request Card.*

This invention has been patented by NASA [U.S. Patent No. 4,186,347]. Inquiries concerning nonexclusive or exclusive license for its commercial development should be addressed to the Patent Counsel, NASA Resident Office-JPL [see page A5]. Refer to NPO-14590.

Compressing TV-Image Data

In processing before coding, only line segments with high contrast between samples are shortened.

NASA's Jet Propulsion Laboratory, Pasadena, California

A data compression method permits high-quality reconstruction of television pictures from relatively-narrow-bandwidth signals. The method may help to increase the capacity of television transmissions, both broadcast and cable. It may also help to reduce the size of the storage medium for video recordings and for digital audio recordings.

The number of data bits assigned to the picture elements (pixels) in a TV-image line segment is determined by the amount of activity in that segment. A segment composed of widely-different sample values is assigned fewer bits than a segment that has fewer variations.

A TV line is divided into 64 small data blocks, or pixels. In the new method (see figure), logic circuits assign an activity estimator to each block. The activity estimator is the "information-preserving" number of bits — that is, the estimated minimum number of bits to code a given block that will permit its exact reconstruction.

The activity estimators for all the blocks in a line are added. The total represents the estimated number of bits to code the entire line, allowing exact reconstruction of the part of the image contained in that line. The total is compared with a predetermined value of allowable bits for transmission of a line. If N bits are allowed for coding a line and if the estimator total exceeds N, then the number of bits estimated for the line must be reduced.

This means that segments of the line must be shortened. Logic circuitry determines which segments should be shortened, or truncated, and by how much. Truncation is applied first to the segments with the highest activity. The principle here is that truncation is less damaging to segments that have large transitions than to those with small transitions. Thus, high-activity segments are prime candidates for truncation because the average transition between their data samples is larger.

After data for a line have been preprocessed by selective truncation, the bits are applied to an adaptive variable-length coder (AVLC). The AVLC automatically selects the best of several optional codes for the line and encodes the line accordingly for transmission. The selection is based on the length of strings of zeros in the data stream; the longer the zero strings, the fewer the bits in the code.

The truncation during preprocessing means that the reconstructed image will have less detail than the original. However, when the data compression method was used on the Galileo satellite for pictures of Earth's surface, the image degradation was imperceptible.

This work was done by Edward E. Hilbert, Jun-Ji Lee, Robert F. Rice, and Alan P. Schlutsmeyer of Caltech for **NASA's Jet Propulsion Laboratory.** *For further information, Circle 12 on the TSP Request Card.*
NPO-14823

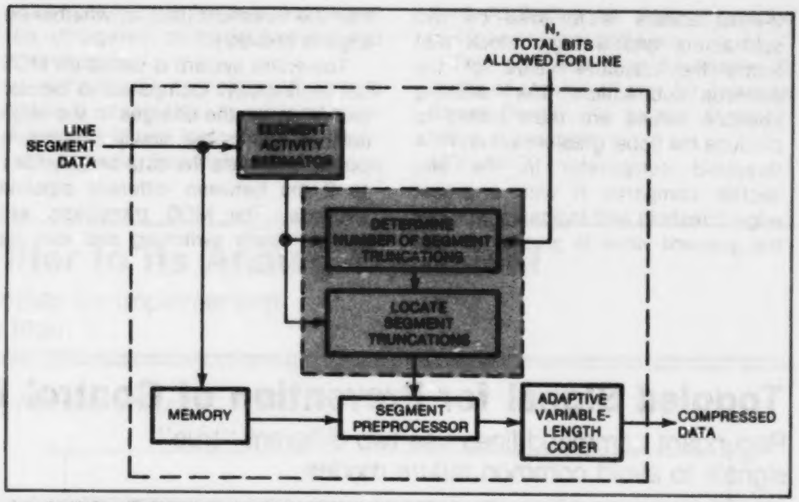
N,
TOTAL BITS
ALLOWED FOR LINE
LINE SEGMENT DATA
SEGMENT ACTIVITY ESTIMATOR
DETERMINE NUMBER OF SEGMENT TRUNCATIONS
LOCATE SEGMENT TRUNCATIONS
MEMORY
SEGMENT PREPROCESSOR
ADAPTIVE VARIABLE-LENGTH CODER
COMPRESSED DATA

An Activity Estimator Is Calculated for each segment of an image line. The estimator is used in conjunction with the allowable bits per line, N, to determine the number of bits needed to code each segment and which segments can best tolerate truncation. The preprocessed line data are then passed to the adaptive variable-length coder, which selects the optimum transmission code.

Real-Time Image Enhancement

A proposed method of extracting low-level features from digital images

NASA's Jet Propulsion Laboratory, Pasadena, California

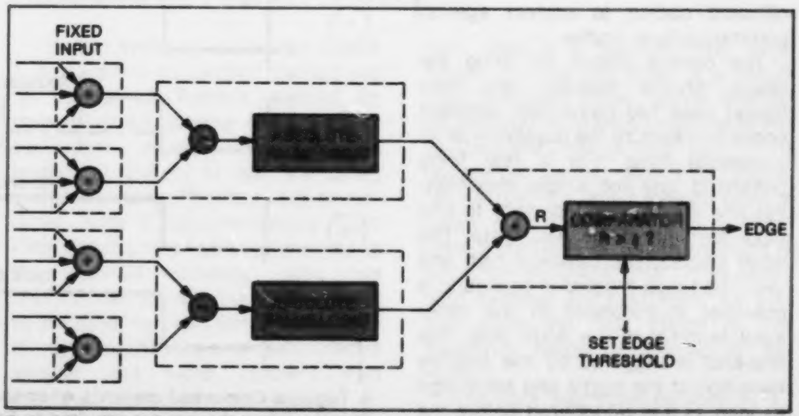

Sobel Gradient Operator is implemented on an LSI chip that processes input digital image data to produce image-edge information. The operator is partitioned into three parts, with the 3-input adder in the first part, the difference and absolute value cells in the second part, and an adder and a comparator in the third part.

A successfully tested technique can be used to extract edges from digital images in "real time" (30 frames/s). It is a pipelined system that employs a "vision" algorithm, the Sobel gradient operator. This processor accepts binary image data from an imaging system (such as a charge-coupled device and an A-to-D imaging converter) and produces an edge map. The edge processor is being fabricated on an n-MOS LSI chip. Such a system could be used to locate objects on a moving belt, in deep-sea mining, in coal mining, in real-time control of robotic planetary rovers, and the like.

A scene to be analyzed is imaged onto a photoarray, and the output is converted into an 8-bit binary number for each pixel of the image. For experimental purposes a 3-by-3 window was chosen; larger windows should work equally well. As the pixel values of the digitized picture are shifted through pixel buffers, the 3-by-3 window effectively moves through the digital picture. The pixel values from the window are then fed into the edge-enhancement pipeline. In this scheme the 3-by-3 window becomes discontinuous at the end of each image line and also at the end of each frame (blanking).

The operation is depicted in the illustration. The front section of four

(continued on next page)

3-input adders is followed by two subtracters and a logic block that forms the absolute value of the previous subtraction. The resulting absolute values are then added to produce the Sobel gradient value, R. A threshold comparator in the last section compares R with a preset edge threshold and indicates whether the gradient value is greater or less than the threshold (that is, whether an edge is present).

The entire system is based on MOS LSI technology. Compared to bipolar technologies, the charges in the MOS devices leak away slowly, making it possible to store the data reliably for 1 to 2 ms between different pipeline sections. The MOS transistors are symmetrically switching and can be used as simple on/off switches either to transmit or isolate data from section to section. Finally, the MOS design is more reliable because of reduced package count and reduced number of interconnections.

This work was done by Vincent S. Wong of Caltech for **NASA's Jet Propulsion Laboratory.** *For further information, Circle 13 on the TSP Request Card.*
NPO-14281

Toggled Signal for Prevention of Control Errors

Redundant command lines use two different "true" signals to avoid common failure modes.

Lyndon B. Johnson Space Center, Houston, Texas

Like a security vault that can be opened only when two keys are turned simultaneously, control-system functions can be protected against accidental excitation by using an AND gate that requires two high inputs to produce a high output. The activating command from the controlling logic circuit or controlling operator goes to the AND gate through two paths, so an erroneous high signal in one path cannot set the function into operation. Moreover, in analogy to keys of different shapes, the signals sent through the two paths can have different coding to protect against common failure modes.

The control circuit for firing the Space Shuttle reaction jets (see figure) uses two paths with different codes to minimize the possibility of an accidental firing. For a real firing command, one line simply goes high; this line is connected directly to one input terminal of the AND gate. The other line toggles between high and low. The toggled signal is applied to a one-shot multivibrator at the other input terminal of the AND gate. The one-shot is triggered by the positive transition of the toggle and stays high as long as it is retriggered before the monostable delay period ends. Thus both inputs to the AND gate are held high so the jets can operate.

A jet-firing command is generated in the computer and transmitted to a demultiplexer. The command is split along two paths in the demultiplexer, producing outputs from separate electronic cards.

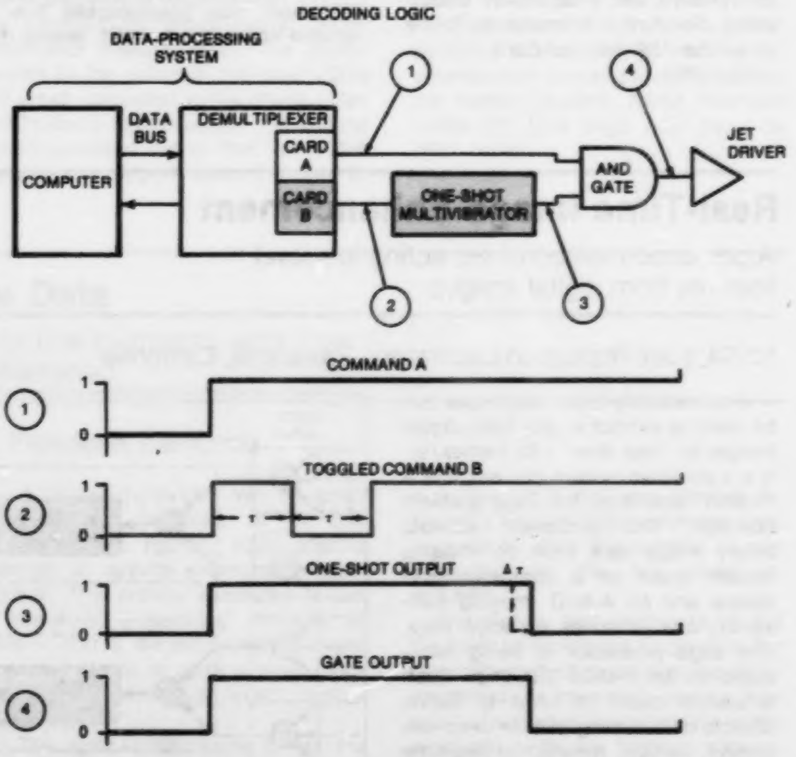

A Toggled Command prevents erroneous activation of reaction jets on the Space Shuttle. When the jets are required to fire, commands "A" and "B" combine to drive the AND gate high and turn them on. A failure in line "B" after two toggle pulses is illustrated by the graphs.

The one-shot in series with the toggle line, which has a delay of ($2\tau + \Delta\tau$), maintains the signal at a high level at the input to the AND gate. The one-shot retriggers before it has timed out, to maintain a continuous output as required to activate the jet driver. A failure in the toggle line after two pulses is illustrated by the graphs in the figure.

Failure modes upstream of the output cards still could cause both card outputs to fail high. However, firing a jet requires command line "B" to toggle between high and low with a period 2τ while "A" remains high. A failure that causes both "A" and "B" to go high simultaneously causes a single jet pulse. Since "B" does not drop back to zero, the one-shot cannot be retriggered, so the jet turns off and remains off.

In the Shuttle application, the single pulse is acceptable. In other applications, additional logic may be desirable to avoid the single pulse; e.g., a third ANDed input from a second multiplexer/demultiplexer.

This work was done by Charles E. Wyllie of Honeywell Inc. for **Johnson Space Center.** *No further documentation is available.*
MSC-18779

Converting a Digital Filter to Its Analog Equivalent

Two methods complement each other for implementing the analog equivalent of a digital filter.

Lyndon B. Johnson Space Center, Houston, Texas

Two proposed procedures for converting a digital filter into an analog filter could simplify the analysis of digital control systems. By converting to the continuous frequency domain, various mathematical techniques for analyzing the stability and response of analog systems can be brought to bear on a digital system.

Given a digital filter in the w-domain:

$$G(w) = \left(\frac{\nu_D}{\nu_N}\right)^2 \frac{w^2 + 2\zeta_N \nu_N w + \nu_N{}^2}{w^2 + 2\zeta_D \nu_D w + \nu_D{}^2}$$

where

$$w = \frac{z+1}{z-1} \text{ and } z = e^{St}$$

t = sampling period, seconds.

Then the equivalent S filter is obtained by:

1. Direct Conversion Method

$$G(S) = \left(\frac{\omega_D}{\omega_N}\right)^2 \frac{S^2 + 2\zeta_N \omega_N S + \omega_N{}^2}{S^2 + 2\zeta_N \omega_D S + \omega_D{}^2}$$

where

$$\omega_N = \frac{2}{t}\,\frac{\pi}{180}\,\tan^{-1}\nu_N \text{ radians per second}$$

$$\omega_D = \frac{2}{t}\,\frac{\pi}{180}\,\tan^{-1}\nu_D \text{ radians per second}$$

or by:

2. Inverse of Tustin's Method

$$G(S) = \left(\frac{\omega_D}{\omega_N}\right)^2 \frac{S^2 + 2\zeta_N \omega_N S + \omega_N{}^2}{S^2 + 2\zeta_D \omega_D S + \omega_D{}^2}$$

where

$$\omega_N = \frac{2}{t}\,\nu_N \text{ radians per second}$$

$$\omega_D = \frac{2}{t}\,\nu_D \text{ radians per second}$$

Figure 1. **The Analog Equivalent G[S] of a Digital Filter G[w]** can be obtained by two conversion schemes.

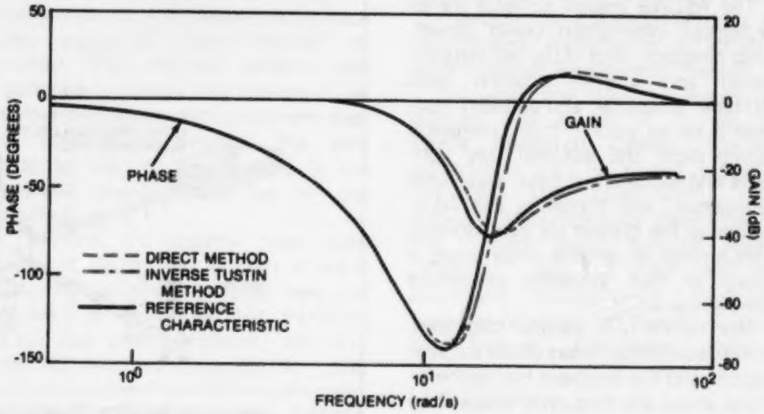

Figure 2. The reference **Response of a Banding Filter Is Matched** at low frequency by either the direct or inverse of Tustin's method. At frequencies above 10 radians per second, the direct method gives a better match. The curves are not drawn in the regions where they merge with the reference.

The two methods, outlined in Figure 1, are a direct conversion method and an inverse of Tustin's method for converting an analog filter into an equivalent digital filter. Tustin's method is already in use; the direct method is new. Together, the procedures form a complementary pair: Filters that cannot be implemented to the required accuracy using one method can usually be implemented by the other method. Both require only direct computations and are therefore simpler and more efficient than previous iterative techniques or methods that require "ad hoc" adjustment of filter parameters.

The procedures have been tested on low-frequency digital filters used in the Space Shuttle flight-control system. One is a banding filter (see Figure 2), and the other is a rolloff filter. For both cases, either method matches the reference response in the low-frequency range from zero to 10 radians per second. Above 10 radians per second, the direct method gives a better match for the banding filter, while the inverse of Tustin's method is better for the rolloff filter. In general, both methods are exercised; the one that gives the best match in the frequency range of interest is selected.

This work was done by John F. L. Lee of Honeywell Inc. for **Johnson Space Center.** *For further information, Circle 14 on the TSP Request Card.*
MSC-18587

Airborne Meteorological Data-Collection System

Aircraft position and weather data are collected, formatted, and relayed to ground from in-flight commercial jets.

Lewis Research Center, Cleveland, Ohio

An airborne data acquisition and communication system called ASDAR (Aircraft to Satellite Data Relay) has been developed as a result of a joint NASA/NOAA (National Oceanic & Atmospheric Administration) project to provide an improved source of meteorological data for weather forecasting.

The ASDAR system collects meteorological information (wind speed, wind direction, and static air temperature) and aircraft position data (latitude, longitude, and altitude) from wide-body jet aircraft instrumentation during flight and automatically converts and formats the data, adds time references, and transmits this information to the ground via synchronous meteorological satellite relay using a group of four satellites positioned around the world.

Much of the U.S. weather originates in the data-sparse areas of the tropical regions and the Southern Hemisphere. These areas are frequently crossed by many of the modern, wide-body jet aircraft of the B-747 and DC-10 types on regular routes. These aircraft contain navigation and data systems capable of providing latitude, longitude, altitude, wind speed, wind direction, and outside air temperature. Conventionally, the pilot records this information manually and submits it for use at the terminus of a flight. Conventionally, up to 24 hours may be required for a report to get into the weather data bank. Manual recording and data entry can be a source of errors making the data unusable or suspect.

The ASDAR system consists of a data acquisition and control unit to acquire, store, and format these data automatically; a transmitter to relay the formatted data via satellite to the ground; and a clock to time the data sampling and transmission periods. The data are relayed to the ground via NOAA Geostationary Operational Environmental Satellites (GOES) and then to the National Meteorological

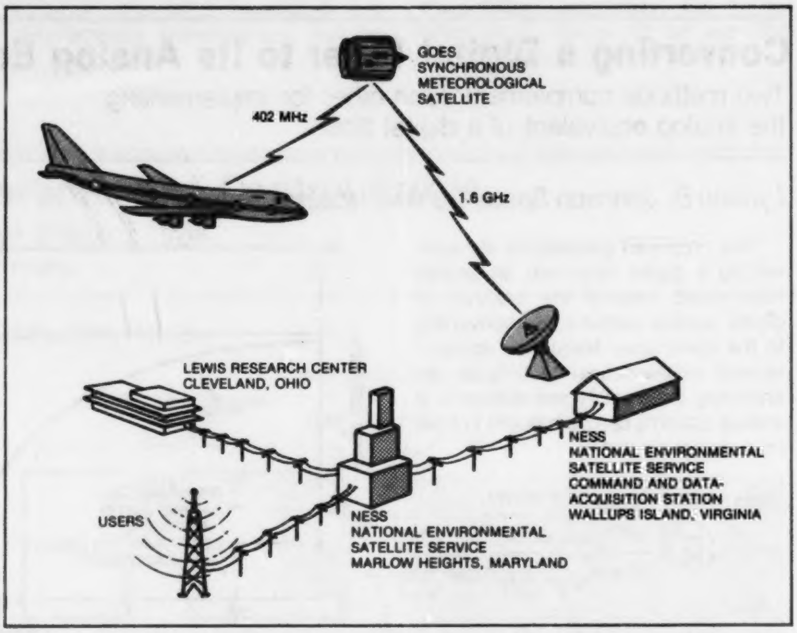
GOES
SYNCHRONOUS
METEOROLOGICAL
SATELLITE
402 MHz
1.6 GHz
LEWIS RESEARCH CENTER
CLEVELAND, OHIO
NESS
NATIONAL ENVIRONMENTAL
SATELLITE SERVICE
COMMAND AND DATA-
ACQUISITION STATION
WALLUPS ISLAND, VIRGINIA
USERS
NESS
NATIONAL ENVIRONMENTAL
SATELLITE SERVICE
MARLOW HEIGHTS, MARYLAND

Figure 1. **Aircraft-to-Satellite Meteorological Data** are relayed to the ground to aid in weather forecasting. In normal operation, eight complete sets of data are acquired over a 1-hour period and transmitted to the satellite at a precise time each hour.

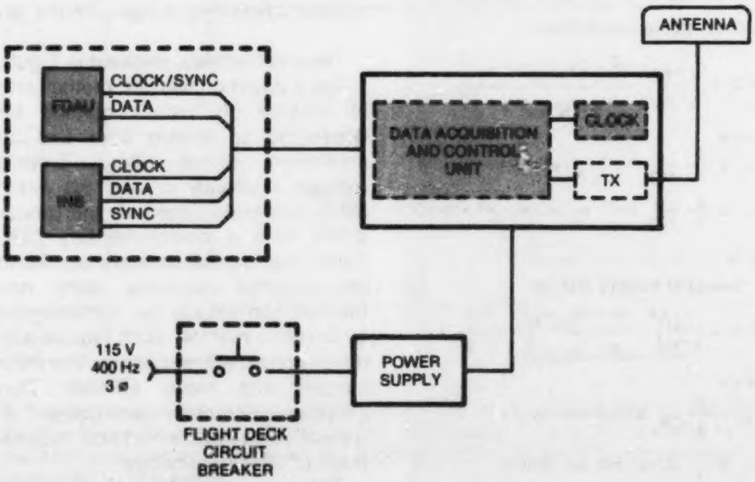
ANTENNA
FDAU
CLOCK/SYNC
DATA
INS
CLOCK
DATA
SYNC
DATA ACQUISITION AND CONTROL UNIT
CLOCK
TX
115 V
400 Hz
3 ø
POWER SUPPLY
FLIGHT DECK CIRCUIT BREAKER

Figure 2. The **Data Acquisition and Control Unit** (DACU) receives information from the aircraft Inertial Navigation System (INS) and the Flight Data Acquisition Unit (FDAU). A battery-powered clock determines the data sampling time and transmission time for the microprocessor-based controller.

Center to aid in weather forecasting (see Figure 1).

The B-747 aircraft in commercial airline service use an Inertial Navigation System (INS) and a Flight Data Acquisition Unit (FDAU) as standard avionics equipment. These two units serve as sources of the data necessary to provide the wind speed and direction and static outside air temperature at a specific latitude, longitude, and altitude. The INS provides latitude, longitude, wind direction, and wind speed as serial BCD (binary coded decimal) data. The FDAU system provides altitude and outside static air temperature in the form of PCM (pulse-code modulation) serial data. These data are the same as are normally manually reported by airline pilots in the form of aircraft reports. The ASDAR reports are formatted on board in a manner similar to these reports. As a result of the onboard formatting prior to transmission, the messages received on the ground require little processing to be suitable for insertion onto the Global Telecommunications System and, subsequently, into the weather data base.

The major elements of the ASDAR system are the electronics unit, the antenna, and the power supply. These are interconnected as shown in Figure 2. Data from the aircraft INS and FDAU are fed into the Data Acquisition and Control Unit (DACU). A battery-powered clock is included in the electronics unit with the DACU. The clock output is used by the microprocessor-based controller to determine the data sampling times and transmission times. In normal operations, eight complete sets of data are acquired over a 1-hour period and transmitted to the satellite at a precise time each hour. The DACU provides all the necessary scaling to the data and stores them in International Alphabet. At the appropriate time each hour, the DACU turns the transmitter on and delivers a biphase data signal to phase-modulate its carrier. The ASDAR system was designed to survive and operate in the below-deck electronic equipment area of commercial aircraft; the only external part of significance is the antenna mounted on top of the fuselage.

To date, 17 systems have been installed on the 747 aircraft of eight national and international airlines and on the U.S. Air Force C-141. Performance has been excellent, with the ASDAR fleet returning 800 to 1,000 data sets daily. The data have been consistently high-quality and are being used routinely to generate worldwide weather maps of significantly improved accuracy. Because it retrieves and transmits data automatically and is inherently accurate, ASDAR can require less labor than when collecting and processing data manually, as is now done.

ASDAR has other potential uses. It could locate aircraft precisely and could selectively reroute them in near-real time to conserve fuel by taking advantage of favorable winds. (NOAA has a plan underway to install ASDAR on hundreds of aircraft worldwide.) Slightly modified, ASDAR could help in the search for a downed aircraft by continuously transmitting its location on a separate emergency channel.

This work was done by James W. Bagwell and Bruce G. Lindow of **Lewis Research Center.** *Further information may be found in NASA TM-78992 [N78-33283/NSP], "An Airborne Meteorological Data Collection System Using Satellite Relay [ASDAR]"* [**$**5]. *A copy may be purchased [prepayment required] from the National Technical Information Service, Springfield, Virginia 22161.*

LEW-13346

Receiving Signals of Any Polarization

Two-channel detection accommodates linear, circular, and elliptical polarization in the same receiving unit.

NASA's Jet Propulsion Laboratory, Pasadena, California

Losses due to polarization mismatch are avoided with a radio receiver that handles signals of any polarization—linear, left- or right-circular, or elliptical. The polarization-diversity receiver employs an orthomode transducer, a device that breaks a signal down into two components—one with right-circular and the other with left-circular polarization—regardless of the polarization of the original signal. (Any polarization can be separated into left- and right-circular components.)

The components are processed separately in two receiver channels having approximately-equal time delay. Each channel is phase-locked to the same reference signal so that the signals to the phase detectors in both channels are in phase and add coherently when they are combined.

The polarization-diversity receiver is proposed for an Earth station for linearly-polarized telemetry transmissions from a spinning satellite [see "Antenna Feed for Linear and Circular Polarization" (NPO-14810) on page 270 of this issue of *NASA Tech Briefs*]. The telemetry signals are received at the ground station by a circularly polarized antenna. Because the linearly polarized signals are transmitted from a spinning source, the plane of polarization is continuously changing. Compensation for the changing plane of polarization comes from treating the linearly polarized wave as a superposition of two circularly polarized waves, allowing reception by a circularly polarized antenna.

The two outputs of the receiver orthomode transducer are fed to two RF amplifiers for low-noise amplification (see figure). From there, the signals proceed through the closed-loop receiver channels where they are phase-locked to the reference.

(continued on next page)

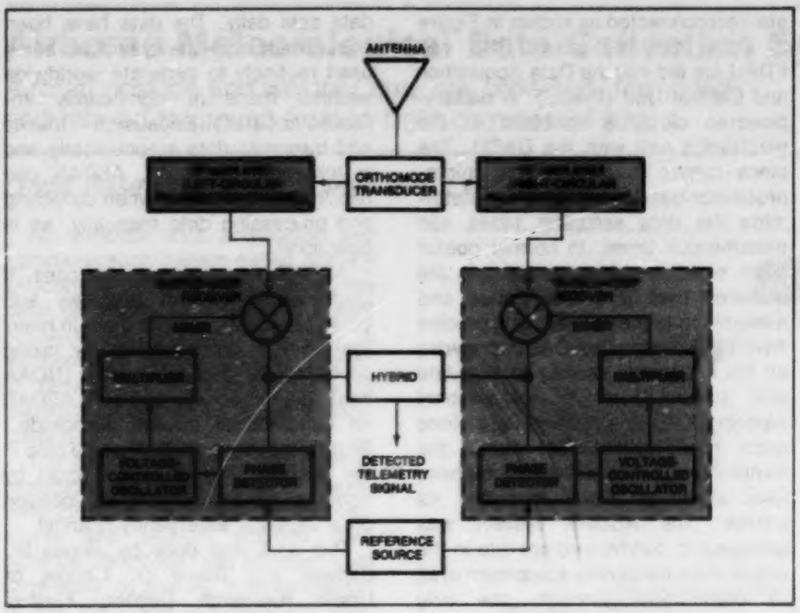

Separated into Left-Circular and Right-Circular Polarizations, a telemetry signal is detected in two channels, then recombined so that the data can be extracted. The two channels allow any polarization to be processed.

The synchronization source is derived from the Earth-station timing signals.

The gain in each channel must be controlled according to the polarization of the received signal. If the received signal is linearly polarized, both channels have equal gain. For circular polarization, one channel has zero gain; and for elliptical polarization, the ratio of the gains in the two channels is greater than zero but less than one. Under these conditions, the signal-to-noise ratio at the hybrid circuit is about the same as that of a receiver matched to the signal polarization when it is operated at a reasonable margin above threshold.

This work was done by John E. Ohlson, Boris L. Seidel, and Charles H. Stelzried of Caltech for **NASA's Jet Propulsion Laboratory.** *For further information, Circle 15 on the TSP Request Card. NPO-14836*

Portable Zero-Delay Assembly

The instrument accurately calibrates a translator for ground-station ranging-system time delay measurements.

NASA's Jet Propulsion Laboratory, Pasadena, California

A portable zero-delay device (PZDA) is the basic reference standard used to calibrate the time delays of an S- and X-band ground-station ranging system that has both transmit and receive paths. The PZDA is used to calibrate the delays of a station Doppler translator connected to an uplink sampling point and downlink signal-injection points into S- and X-band masers. After calibrating the translator path with the PZDA, the translator becomes the field instrument for measuring station time delays on a routine basis. For ground stations having antennas with severe multipath errors, the accuracy of the calibrated translator method is an order of magnitude better than that obtainable with calibrating instruments mounted on the surface of the antenna.

Before use in the field, the time delay of the PZDA is calibrated using a back-to-back method shown in the figure. The assembly on the right is under test; the one on the left is the comparison standard. The standard is also a portable zero-delay assembly, but the S-X isolators are reversed to permit reverse signal flow.

When the PZDA is used at each deep-space station, the calibration involves two measurements. In the first, the Doppler translator path between the uplink sampling and the maser injection points is replaced by the PZDA and its associated test cables and attenuators. With the assembly installed, ranging measurements are made and noted.

The second measurement consists of changing the delay path back to the normal translator path with the exception that the test cables and attenuators are connected in series with the normal translator-path cables. The adjustable attenuators of the PZDA are set to zero, and the fixed pads are replaced by pads of lower value to produce the same received-signal

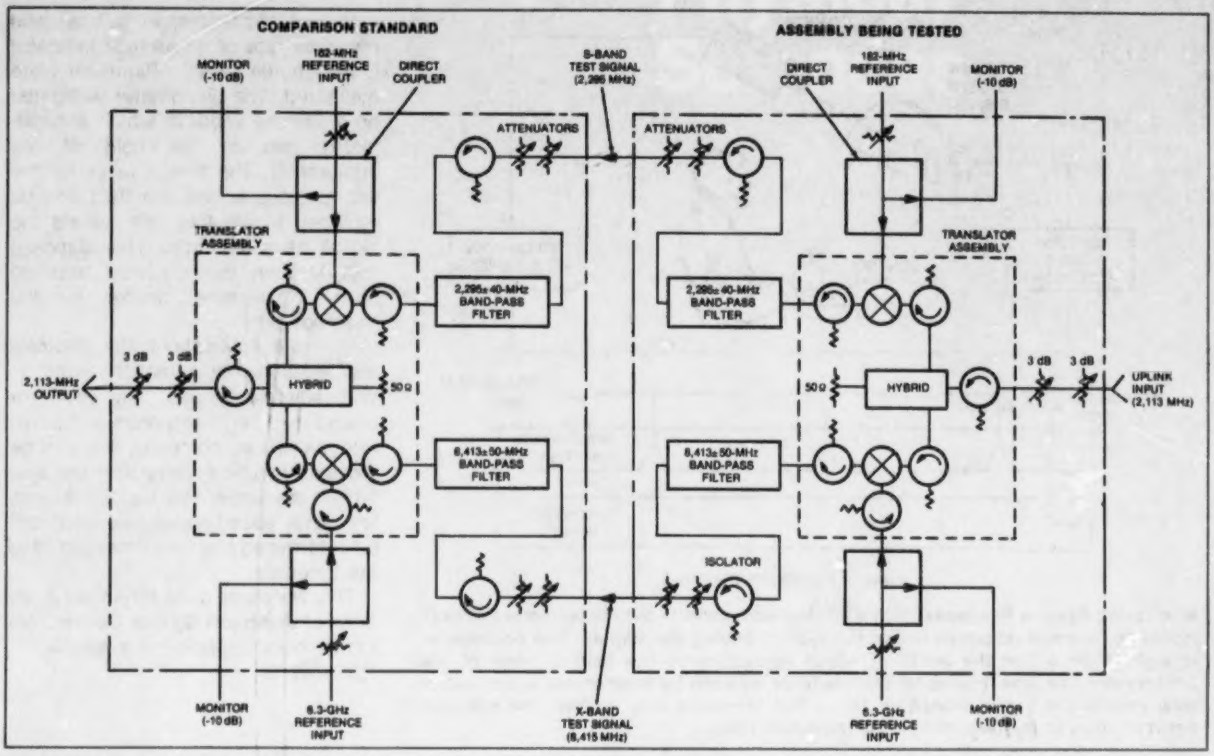
COMPARISON STANDARD
ASSEMBLY BEING TESTED
MONITOR (-10 dB)
182-MHz REFERENCE INPUT
DIRECT COUPLER
S-BAND TEST SIGNAL (2,295 MHz)
ATTENUATORS
ATTENUATORS
DIRECT COUPLER
182-MHz REFERENCE INPUT
MONITOR (-10 dB)
TRANSLATOR ASSEMBLY
2,295±40-MHz BAND-PASS FILTER
2,295±40-MHz BAND-PASS FILTER
TRANSLATOR ASSEMBLY
3 dB
3 dB
2,113-MHz OUTPUT
HYBRID
50Ω
50Ω
HYBRID
3 dB
3 dB
UPLINK INPUT (2,113 MHz)
8,415±50-MHz BAND-PASS FILTER
8,415±50-MHz BAND-PASS FILTER
ISOLATOR
MONITOR (-10 dB)
6.3-GHz REFERENCE INPUT
X-BAND TEST SIGNAL (8,415 MHz)
6.3-GHz REFERENCE INPUT
MONITOR (-10 dB)

Portable Zero-Delay Assemblies are calibrated by use of the back-to-back method. The comparison standard differs from the device being tested in that S-X isolators are reversed to permit signal flow in the reverse direction. After the calibration PZDA is used in the field to calibrate time delays of deep-space network ground-station ranging systems. This approach may also be used in calibrating microwave links in other communication systems transmitting large quantities of digital data.

levels as those of the first measurement. Range measurements are again made and noted. The translator-path delay can then be determined by subtracting the first measurement from the second and adding in the delay of the portable zero-delay assembly.

This work was done by Manuel M. Franco, Tommy Y. Otoshi, and Edward J. Serhal, Jr., of Caltech for **NASA's Jet Propulsion Laboratory.** *For further information, Circle 16 on the TSP Request Card.*
NPO-14671

Photometer Used for Response Time Measurement

A photometer measures the response time of a servocontrol system.

Lyndon B. Johnson Space Center, Houston, Texas

Measuring light intensities is the standard application of a photometer, but this sensitive optical instrument, with its extremely narrow field of view and fast response, can also be put to some less obvious uses. In tests of the servocontrol systems of space vehicles, for example, a photometer is used as a motion detector for measuring response speed and acceleration.

To measure the response time of a servocontrol system, the photometer senses output movement shortly after an operator activates a hand-controlled input. The time delay is measured on an X/T recorder. In this application (see figure) the output is the motion of attitude-indicator indices; however, the photometer could also be sighted on the cursor of a cathode-ray tube, on a meter pointer, or even a pencil mark on a piece of paper taped to an object.

When the photometer with a very small acceptance angle (2 minutes of arc) is sighted on an edge of the cursor, the cursor motion across the field of view changes the photometer output signal. The delay between the activation of the hand controller and the signal change is the system response time.

(continued on next page)

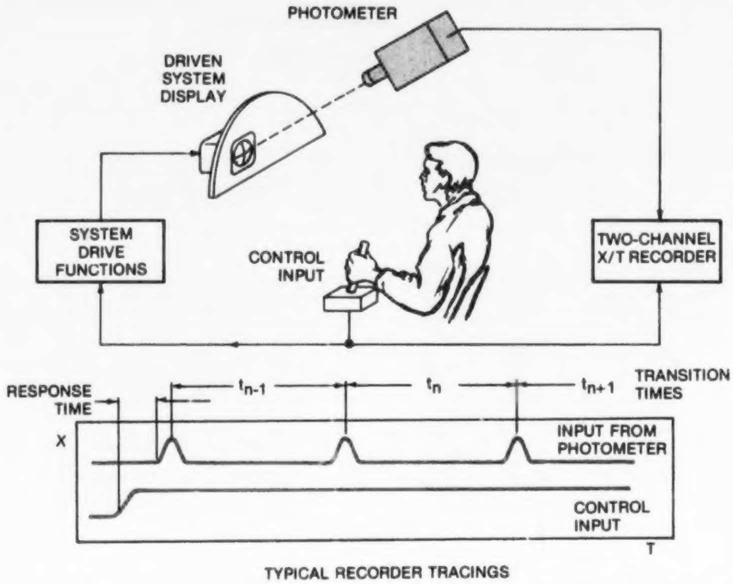
PHOTOMETER
DRIVEN SYSTEM DISPLAY
SYSTEM DRIVE FUNCTIONS
CONTROL INPUT
TWO-CHANNEL X/T RECORDER
RESPONSE TIME
t_{n-1}
t_n
t_{n+1}
TRANSITION TIMES
X
INPUT FROM PHOTOMETER
CONTROL INPUT
T
TYPICAL RECORDER TRACINGS

Monitoring System Response With a Photometer permits the measurement of both response time and response rate of the system driving the display. The photometer is sighted on a line the width of which approximates the field of view of the photometer. The time it takes for the line to be replaced by another line in the field of view equals the signal transition time. The response rate is then the distance between lines in degrees divided by transition time.

In use, both response time and response rate of an attitude indicator in the Shuttle Mission Simulator were measured. The photometer is sighted on a line the width of which approximates that of the field of the photometer. The time it takes for the line to move across the field and be replaced by another line equals the signal transition time. The response rate is then the distance between lines, in degrees, divided by the transition time.

In these applications the photometer is acting as a motion detector. With suitable targets, any open- or closed-loop servo response and servo rate, as well as computer lag, can be measured without perturbing the system. If the target has equally spaced lines on it, speed and acceleration can be determined from the times the lines are detected.

This work was done by Anibal J. da Silva of **Johnson Space Center.** *No further documentation is available.*
MSC-18712

Physical Sciences

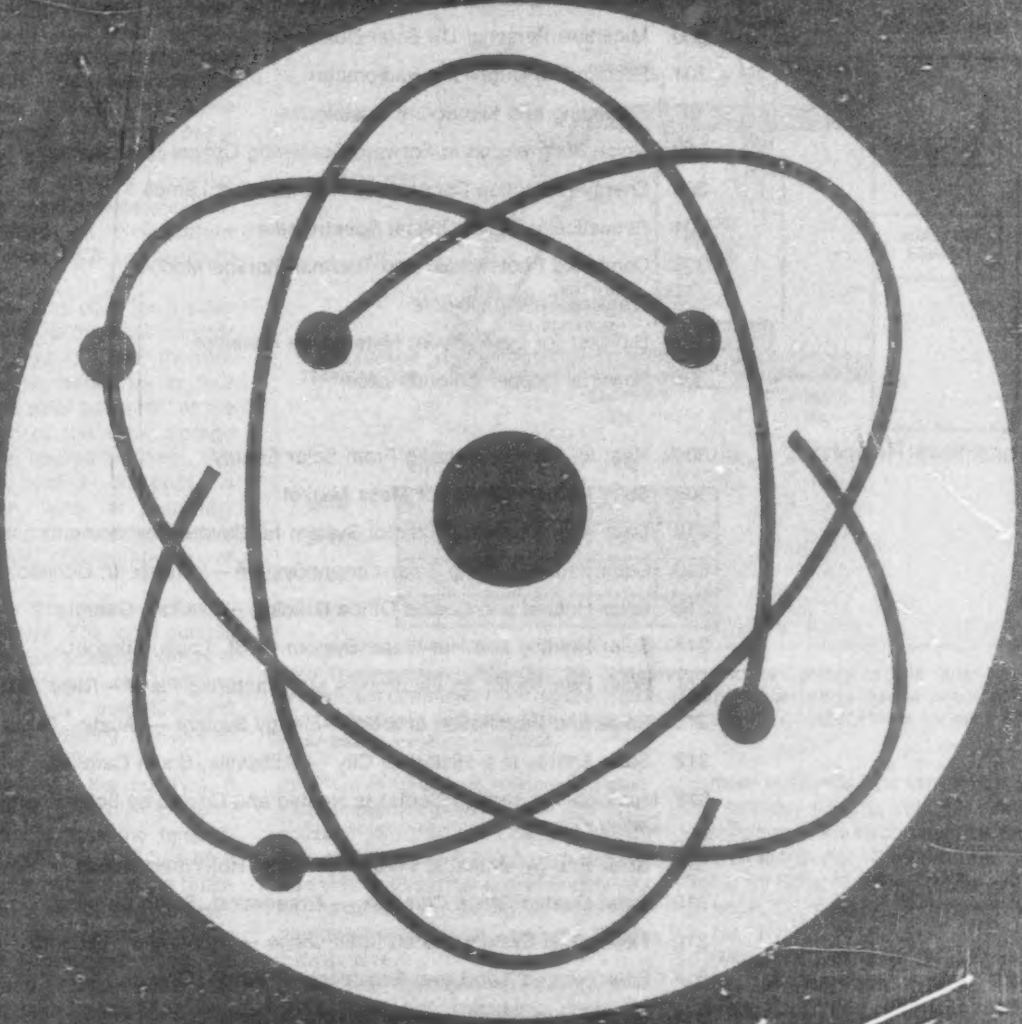

Hardware, Techniques, and Processes

297 Multiplexed Logic Controls Solar-Heating System
298 Four-Cell Solar Tracker
299 Offset Paraboloidal Solar Concentrator
300 Miniature Personal UV Solar Dosimeter
301 Economical Ultraviolet Radiometer
302 Predicting and Monitoring Duststorms
303 Noise Suppression in Forward-Scattering Optical Instruments
304 Energy-Reduction Concept for Incandescent Lamps
304 Acoustically-Tuned Optical Spectrometer
305 Combined Photovoltaic and Thermal-Storage Module
306 Tracking Falling Objects
307 Diplexer for Laser-Beam Heterodyne Receiver
308 Powerful Copper Chloride Laser

Books and Reports

309 Heat for Film Processing From Solar Energy
309 Solar Heater/Cooler for Mass Market
310 Data-Acquisition and Control System for Severe Environments
310 Commercial-Building Solar-Energy System — Stamford, Connecticut
310 Solar-Heated and Cooled Office Building — Dalton, Georgia
311 Solar-Heating and Hot-Water System — St. Louis, Missouri
311 Solar Heating for an Electronics Manufacturing Plant — Blue Earth, Minnesota
312 Costs and Description of a Solar-Energy System — Austin, Texas
312 Solar Energy in a Historical City — Abbeville, South Carolina
312 Municipal Recreation Center Is Heated and Cooled by Solar Energy — Dallas, Texas
313 Solar Energy Meets 50 Percent of Motel Hot-Water Needs — Key West, Florida
313 Solar-Heated Office Complex — Greenwood, South Carolina
314 Residential System Tested In an Office — Huntsville, Alabama
314 Solar-Heated Two-Level Residence — Akron, Ohio
314 Solar-Energy Workshop — Tucson, Arizona
315 Residential Solar Hot-Water System — Tempe, Arizona
315 Residential Solar-Heating Installation — Stillwater, Minnesota
315 Three-Story Residence With Solar Heat — Manchester, New Hampshire
316 A High School Is Supplied With Solar Energy — Dallas, Texas

Multiplexed Logic Controls Solar-Heating System

Inexpensive sensors and logic circuits select from four operating modes.

Marshall Space Flight Center, Alabama

A controller for solar heating uses inexpensive thermocouples as temperature sensors and uses simple logic circuits to select among four operating modes. The sensor signals are multiplexed through the same amplifier, instead of each being processed by separate amplifiers. Errors caused by differing amplifier characteristics are therefore avoided. Control is based on temperature differences (rather than on absolute temperatures).

The controller was built for a solar heater in which air is the heat-transfer medium (see figure). The thermocouples sense temperatures at four locations: at the solar collector, at the top and bottom of the rock storage bed, and at the heated building. The logic circuits control dampers, a circulating fan, and an auxiliary heater, arranging the heating system in one of four configurations, or modes:

- Mode 1 heats the building directly from the collector. The logic selects mode 1 when the collector temperature is greater than the building temperature by a predetermined amount and the building thermostat calls for heat.
- Mode 2 stores heat in the rock bed. It is selected when the collector temperature is higher than the temperature at the top of the rock bed by a predetermined amount and the building thermostat is not calling for heat.
- Mode 3 heats the building from the rock bed. It is selected when the temperature at the bottom of the rock bed is greater than the building temperature by a predetermined amount and the thermostat calls for heat.
- Mode 4 heats the building with the auxiliary heater. It is selected when the collector and rock bed temperatures are low and the thermostat calls for heat.

Copper/constantan thermocouples with high-voltage change with temperature — about 0.023 mV/°F (0.041 mV/°C) — produce relative temperature measurements that are accurate within 2° F (1.1° C). Unlike thermistors, the thermocouples do not require an external electrical power supply, do not have to be selected for matched characteristics, and are relatively inexpensive.

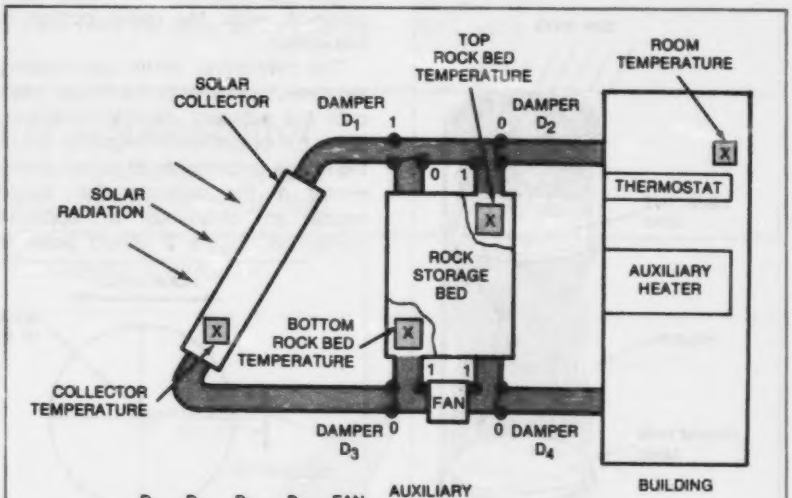

	D_1	D_2	D_3	D_4	FAN	AUXILIARY HEATER
MODE 1	0	1	1	1	ON	OFF
MODE 2	0	0	1	0	ON	OFF
MODE 3	1	1	0	1	ON	OFF
MODE 4	0	0	0	0	OFF	ON

Four Thermocouples Monitor the Temperatures at key points in this solar-heating system. On command from logic circuitry, dampers open and close to direct airflow. The table shows damper positions and fan and auxiliary heater status for each of the solar-heater operating modes.

The thermocouple outputs go to a multiplexer that alternately connects differential thermocouple voltages to an amplifier. Another amplifier and synchronized multiplexer connect the appropriate voltages representing preset temperature differences to a third amplifier, which compares the differential signals and provides mutliplexed outputs to the logic circuitry. The logic circuits decide on the proper operating mode and operate relays to control damper solenoids, the fan motor, and the auxiliary heating unit. [A detailed description of the circuit may be found in "Multichannel Temperature Controller for Solar Heating" (MFS-23775) on page 203 of *NASA Tech Briefs*, Vol. 3, No. 2.]

This work was done by James R. Currie of **Marshall Space Flight Center.** *For further information, Circle 17 on the TSP Request Card.*

This invention is owned by NASA, and a patent application has been filed. Inquiries concerning nonexclusive or exclusive license for its commercial development should be addressed to the Patent Counsel, Marshall Space Flight Center [see page A5]. Refer to MFS-25287.

Four-Cell Solar Tracker

A very sensitive tracking device for control of collector or mirror drives

NASA's Jet Propulsion Laboratory, Pasadena, California

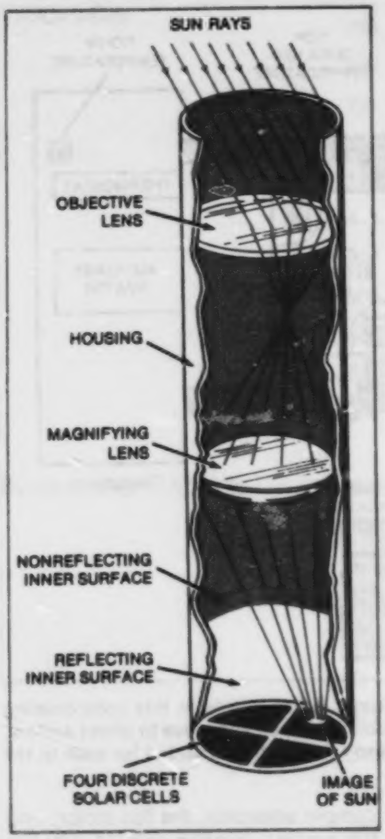
SUN RAYS
OBJECTIVE LENS
HOUSING
MAGNIFYING LENS
NONREFLECTING INNER SURFACE
REFLECTING INNER SURFACE
FOUR DISCRETE SOLAR CELLS
IMAGE OF SUN

Figure 1. This Sun Tracker, consisting of an optical telescope and four solar cells, generates signals that keep the cylinder pointed at the Sun throughout the day. Roughly 40 cm in length, it can properly orient solar collectors or mirrors for maximum energy collection.

A prototype Sun tracker has four solar cells surrounded by a cylindrical mirror. When added to a declination-angle/hour-angle drive, it can orient a solar collector or solar mirror accurately for maximum illumination.

Figure 1 shows the lenses and detectors. The objective lens gathers incoming light from the Sun; and the magnifying lens focuses a sharp image of the solar disk, magnifying its motion across the detectors to enhance sensitivity. The inside of the lower portion of the housing is polished, while the upper portion is blackened.

The cylindrical mirror surrounding the detectors reflects the image back onto the adjacent detector element, but is not of sufficient height to return the image to center or to reflect it to a sector of the detector that would cause an erroneous or opposite correction. Figure 2 shows possible Sun image positions with different pointing errors and illustrates the capability of the cylindrical mirror to accommodate overtravel or wide-angle acquisition.

Signal conduction leads from the upper surfaces of the four cells are connected to a resistance bridge. With the image of the Sun falling on the center of the detector, the bridge is

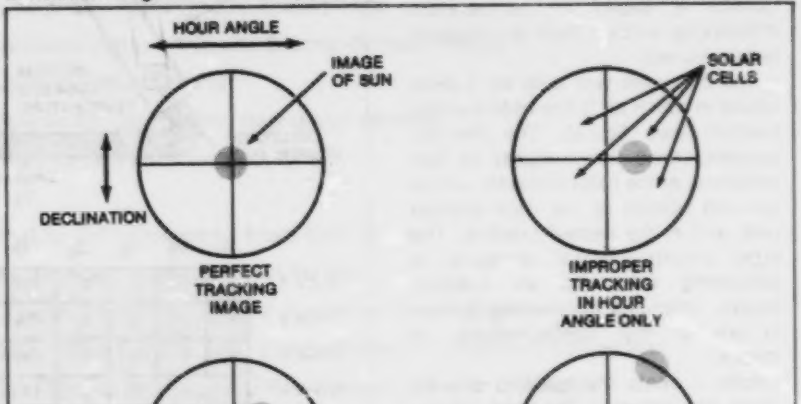
HOUR ANGLE
IMAGE OF SUN
DECLINATION
PERFECT TRACKING IMAGE
SOLAR CELLS
IMPROPER TRACKING IN HOUR ANGLE ONLY
IMPROPER TRACKING IN BOTH HOUR ANGLE AND DECLINATION
IMAGE APPROACHING CONDITION OF INABILITY TO DETECT ERROR
IMAGE
REFLECTED IMAGE
MIRROR UPPER BOUNDARY
OFF-DETECTOR IMAGE REFLECTED BACK BY CYLINDRICAL MIRROR
IMAGE OUTSIDE OF CYLINDRICAL MIRROR DOES NOT REAPPEAR ON DETECTOR

Figure 2. Each Solar Cell generates a voltage proportional to the part of the solar image it receives; the voltages drive servomotors that keep the image centered. Note how the mirrored portion of the cylinder extends the range of image excursion that can be corrected.

balanced. An offcenter image, with a corresponding imbalance in the bridge, will result in a servomechanism adjustment that recenters the image and reorients the solar collector or solar mirror for maximum illumination.

The sum of the voltages from the four cells remains nearly constant as long as no part of the Sun image moves off the circular boundary of the cells. When the light is reflected back to the detector array by the cylindrical mirror, the output falls off about 10 percent, which in most cases does not seriously affect tracking.

Standard electronic amplifier, comparator, and intensity measuring circuits may be used with the output signals from the detector to produce extremely close tracking. The detector may also be adapted to other types of tracking systems such as altitude/azimuth drives.

This work was done by C. Martin Berdahl of Caltech for **NASA's Jet Propulsion Laboratory.** *For further information, Circle 18 on the TSP Request Card.*
NPO-14811

Offset Paraboloidal Solar Concentrator

The new design increases solar gathering efficiency by 3 to 4 percent by eliminating shadowing and blocking of solar rays.

NASA's Jet Propulsion Laboratory, Pasadena, California

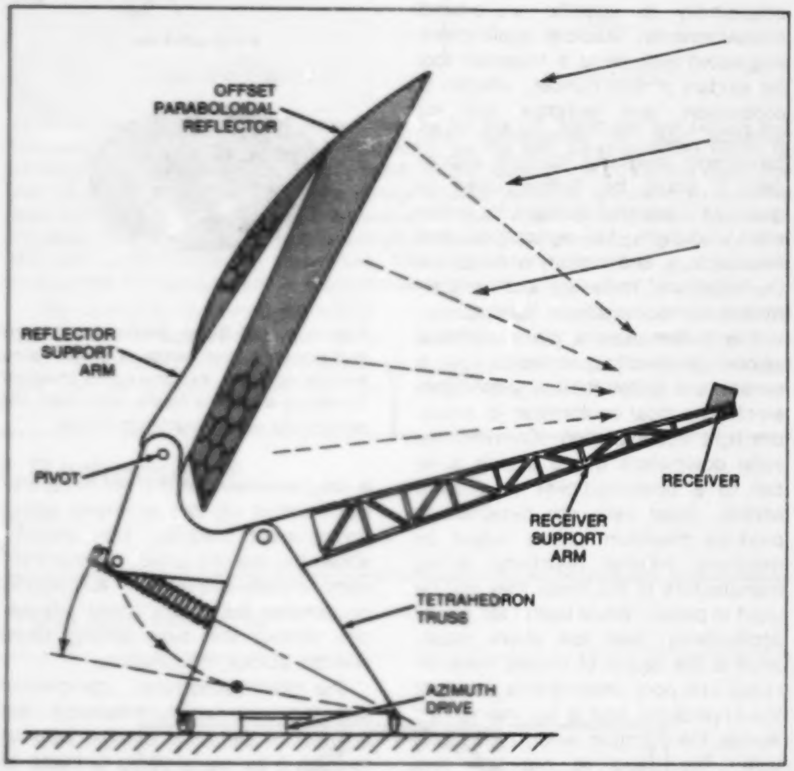

The Offset-Paraboloidal Reflector receives all of the incoming light and reflects it without obstruction to the receiver. Because the reflector can be folded toward the receiver, wind loading is reduced and maintenance is made easier.

A section of a conventional paraboloid, offset from its major axis, is used as a reflector in a solar concentrator. The offset paraboloid is 3 to 4 percent more efficient in gathering solar rays than a conventional paraboloid because neither the receiver nor its support interferes with the incoming rays as they pass from the Sun to the reflector to the receiver. In addition, the offset paraboloid has certain maintenance advantages.

In a conventional solar concentrator, the receiver is supported at the focus of a paraboloid by a structure that blocks some of the incoming light and some of the reflected light. The result is shadowing and a loss in concentrator efficiency.

The non-axisymmetric reflector, receiver, and support is illustrated in the figure. Two parallel arms extending from the base support the reflector. Two other arms extend from the base and join approximately at the focal point of the concentrator, where the receiver is mounted.

The paraboloid and receiver support arms are pivoted about the apex of a truncated tetrahedron-truss base. Wheels are mounted at the three corners of the base triangle of the tetrahedron. A bull gear on a low, short pedestal below ground level, at the center of the base triangle, provides azimuth drive. The concentrator may also be driven in azimuth through a cable wrapped around the pedestal with a pinion and drive attached to the tetrahedron base.

The entire concentrator support can be located either below or above ground level for waist-high servicing of the receiver. A pivot in the reflector support arms allows the reflector to be folded toward the receiver and stowed. Since wind loading on the stowed structure is reduced, the cost of building a foundation can be lowered. Moreover, the concentrator is easily cleaned and serviced in the stowed position.

This work was done by Edwin Y. Chow of Caltech for **NASA's Jet Propulsion Laboratory.** *For further information, Circle 19 on the TSP Request Card.*
NPO-14846

Miniature Personal UV Solar Dosimeter

Small light-powered meter measures accumulated radiation in the ultraviolet or other selected regions.

Langley Research Center, Hampton, Virginia

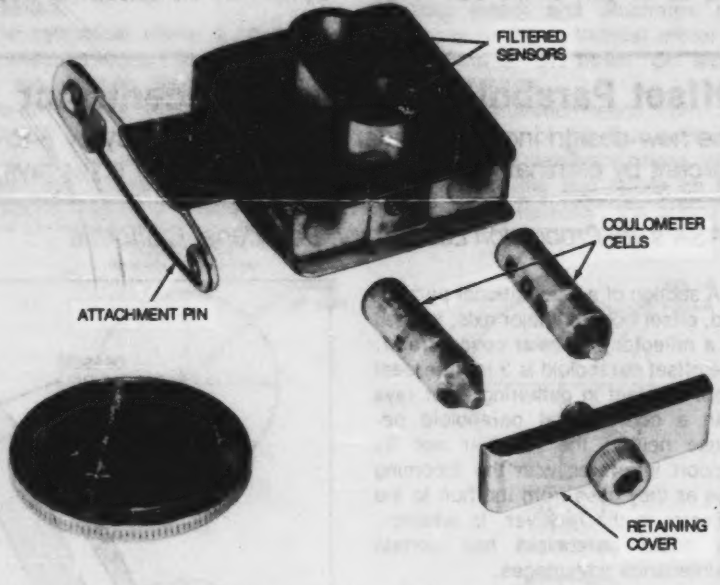

Figure 1. **UV Solar Dosimeter** currently undergoing tests was assembled from components that weigh 5 g and occupy 1.4 cm^3 exclusive of packaging. Under normal daylight, exposure over the band 250 to 400 nm was readily measurable on an hourly-to-a-weekly basis, with daily measurements being the best tradeoff between sensitivity and integration range.

A miniature integrating light meter originally developed for use in space has many other possible applications. Small enough to be worn unobtrusively, it can measure accurately the radiation dose accumulated for a few minutes or over a period of weeks. It can measure total light or selected wave bands, such as UV or IR.

The primary practical advantages of the dosimeter are its potentially low cost, small size, accuracy, and adaptability to specific wave-band measurements. Medical applications suggested include as a research tool for studies of skin cancer, vitamin D production, and jaundice and for possible use in conjunction with treatments involving Sunlight exposure. It could be further used to measure integrated Sunlight for solar-energy design, for agriculture and meteorology, and to study and monitor the stability of materials and environmental and occupational lighting.

The meter uses a planar-diffused silicon photovoltaic detector as a sensor and a commercially available electrochemical coulometer to measure light accumulation. Conventional solar dosimeters use a silicon solar cell or a photomultiplier tube as a sensor. Solar cells are designed to produce maximum power output by matching internal resistivity during manufacture to the loads they will be used to power. While useful for power applications, their low shunt resistance is the cause of limited dynamic range and poor linearity if a constant low-impedance load is not maintained across the junction when measuring light. The need to maintain this artificial load to insure operation in the short-circuit-current mode reduces sensitivity unless supplemented by external signal-conditioning electronics that make the meters too complex and bulky for a miniature personal meter.

In contrast, the photovoltaic detector has a shunt resistance on the order of megohms and behaves more nearly as an ideal current source under typical loading conditions for light measurement. Reasonable variations in load resistance within the measurement circuit will not adversely affect photocurrent linearity. This linearity allows the use of a small, inexpensive, commercially-available electrolytic coulometer for photocurrent integration without the desensitizing shunt resistor across the junction.

The electrochemical coulometer selected accurately measures the quantity of electrical charge passing through it by transferring a mass of silver directly proportional to the input charge. Since the plating and deplating of silver are the only electrochemical reactions taking place, the coulometer operates with virtually 100 percent charge efficiency. Total radiation is determined by measuring the time required to deplate the silver using a constant current source.

Since virtually all of the photocurrent is recorded linearly, the junction area required is reduced from several square centimeters to a few square millimeters, yet sensitivity is sufficient to allow optical filtration for wave-band selection.

Figure 1 shows a prototype dosimeter currently being tested, and Figure 2 is a schematic of the dosimeter and a cell-readout circuit. There is also commercially available equipment for automatic readout and reset of the cells.

The dosimeter can be used to detect selected wave bands by using filters. The pair of cells in Figure 2a is used to measure a selected band of UV radiation. One filter, Schott UG-11, blocks light in the visible and admits UV (250 to 400 nm) and IR (mostly 660 to 800 nm). The other filter, Schott WG-305, blocks UV from 250 to 320 nm, passes UV from 320 to 400 nm, and passes IR. The difference between the radiation accumulations in the cell with the first filter only and in the cell with both filters is the UV radiation over the wave band 250 to 320 nm. This example is of particular interest because it simulates the spectral response of human skin erythema and could be useful in clinical studies.

The coulometric cells currently retail for less than $5 and are accurate to within 2 percent. They can record up to 3,600 mA-s and are reusable indefinitely. The sensor can be larger or smaller, depending on the bandwidth and application desired. It was found that statistically significant readings of UV exposure in the 250-to-400-nm band can be obtained in open shade in 1 minute with only 5 mm^2 of filtered detector area per sensor.

The sensor is readily calibrated (relating mA-s reading to J/cm^2) in the laboratory using standard photometric procedures. The dosimeter should be packaged to allow the spring-loaded cells to be removed and replaced easily in the field. They can be read by removing the cell and using a circuit like that in Figure 2b. It would probably be most convenient to mail them to a central location.

This work was done by Richard R. Adams, Ian O. MacConochie, and Bordie D. Poole, Jr., of **Langley Research Center.** *For further information, Circle 20 on the TSP Request Card.*

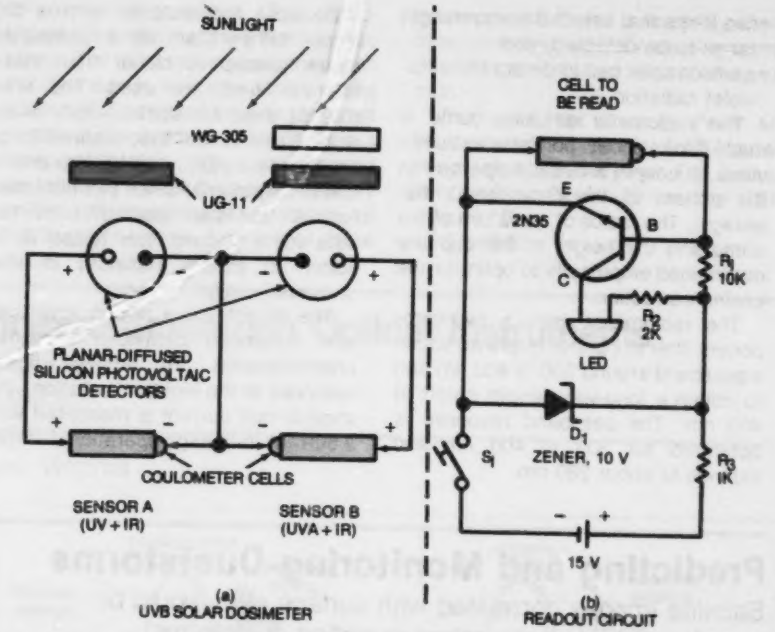

(a)
UVB SOLAR DOSIMETER

(b)
READOUT CIRCUIT

Figure 2. **Measurement and Readout Circuits** for the UV dosimeter are simple and inexpensive to build. The two-cell dosimeter, on the left, uses selective filters to allow measurement of a specific UV band. In the readout circuit on the right, the battery, R_3, and D_1 form a constant voltage source. When S_1 is closed, R_1 sets the read current through the cell to a constant 1 mA. When all the silver has been depleted, cell resistance increases abruptly, causing the transistor to conduct and the LED to light; then S_1 is opened. The product of the current and the time (monitored by a stopwatch) is proportional to the amount of silver transferred.

This invention is owned by NASA, and a patent application has been filed. Inquiries concerning nonexclusive or exclusive license for its commercial development should be addressed to the Patent Counsel, Langley Research Center [see page A5]. Refer to LAR-12469.

Economical Ultraviolet Radiometer

Compact cosine-corrected radiometer measures total ultraviolet insolation.

NASA's Jet Propulsion Laboratory, Pasadena, California

The simple, economical ultraviolet radiometer shown in the figure is suitable for field use. The new radiometer measures the ultraviolet radiation from Sun and sky, integrated over the celestial hemisphere. It has possible applications in testing materials for the effects of ultraviolet exposure and in studies of solar-cell degradation by ultraviolet.

The components of the radiometer include:

- a cup-shaped diaphragm and diffusing dome to obtain a cosine-corrected response,

(continued on next page)

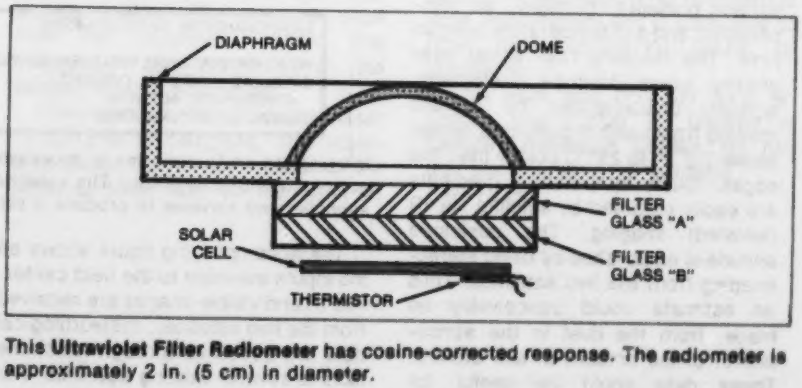

This Ultraviolet Filter Radiometer has cosine-corrected response. The radiometer is approximately 2 in. (5 cm) in diameter.

- two filters that select the wavelength range to be detected, and
- a silicon solar cell to detect the ultraviolet radiation.

The radiometer diffusing dome is made from sheet polytetrafluoroethylene. It covers a circular aperture in the bottom of the cup-shaped diaphragm. The radius of curvature of the dome and the height of the cup are determined empirically to optimize the cosine correction.

The radiometer uses a two-component filter to control response within a passband around 300 to 400 nm and to obtain a long-wavelength cutoff at 400 nm. The passband response is optimized for 300 to 400 nm and extends to about 280 nm.

Because the radiation arrives diffusely rather than as a collimated beam, absorptive rather than interference filters are used. The filter glasses used are commercially available. Glass A has the required long-wavelength cutoff near 400 nm and is chemically stable. Since this filter also has a low-level passband in the infrared. a second filter (glass B) is added to absorb radiation in that unwanted region.

The detector is a silicon solar cell with enhanced ultraviolet response characteristics. To achieve linear response to the incident radiation, the short-circuit current is measured with a current-to-voltage operational amplifier circuit. Its output may be fed to a data logger.

The solar-cell sensitivity varies a few percent over the temperature range expected in field use. To monitor temperature, a thermistor is attached to the back of the cell and connected to a bridge circuit. The thermistor data can be used to correct the radiometer readings for temperature.

This work was done by Clay H. Seaman of Caltech and Roger S. Estey of Kirk-Mayer, Inc., for **NASA's Jet Propulsion Laboratory.** *For further information, Circle 21 on the TSP Request Card.*
NPO-14843

Predicting and Monitoring Duststorms

Satellite images correlated with surface data would be transformed into color maps depicting duststorms.

NASA's Jet Propulsion Laboratory, Pasadena, California

A proposed duststorm-monitoring system combines surface data with stereoimage data from two geosynchronous satellites viewing the same area, or a geostationary satellite capable of providing stereoimages. The combined information would be processed at a field center, using correlation and image-enhancement algorithms. A series of maps generated this way would reveal the storm direction, warning areas in the path of the storm from zero to 24 hours before they are struck.

Duststorms are generally associated with large-scale meteorological events, such as rapidly-changing surface pressure, humidity, air temperature, and soil temperature over an area. The resulting high winds over eroding areas produce dustclouds, typically characterized by upward rotating fronts with a dustcloud center appearing 7° to 25° C colder than the edges. Such temperature gradients are easily recorded by satellite via IR (infrared) imaging. The dustcloud altitude is established by using stereoimaging from the two satellites. Thus an estimate could conceivably be made, from the dust in the atmosphere, of the amount of soil eroded. These data could be useful for agricultural productivity forecasts.

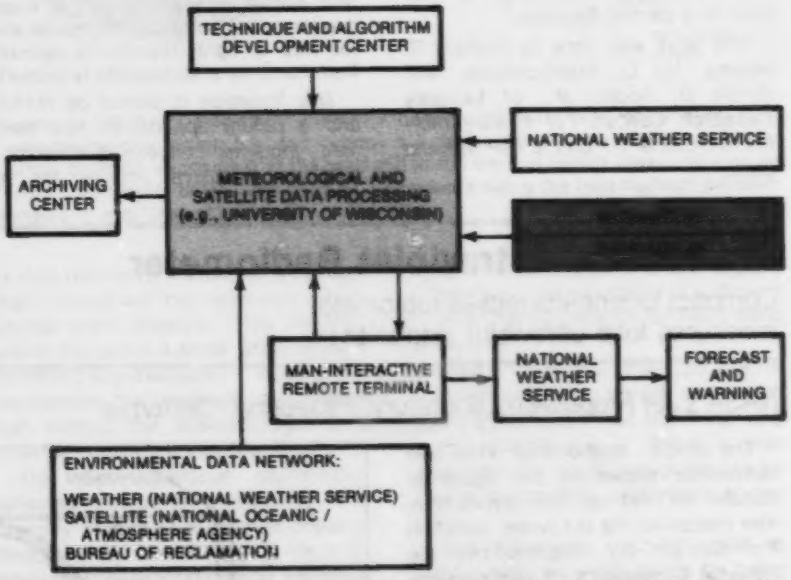
TECHNIQUE AND ALGORITHM DEVELOPMENT CENTER
NATIONAL WEATHER SERVICE
ARCHIVING CENTER
METEOROLOGICAL AND SATELLITE DATA PROCESSING (e.g., UNIVERSITY OF WISCONSIN)
MAN-INTERACTIVE REMOTE TERMINAL
NATIONAL WEATHER SERVICE
FORECAST AND WARNING
ENVIRONMENTAL DATA NETWORK:
WEATHER (NATIONAL WEATHER SERVICE)
SATELLITE (NATIONAL OCEANIC / ATMOSPHERE AGENCY)
BUREAU OF RECLAMATION

Information on Duststorms is processed by a terminal receiving signals from two geosynchronous satellites. The satellite information is correlated with that of other agencies and services to produce a series of maps of the storm area.

The accompanying figure shows all the inputs available to the field center. The IR and visible images are received from the two satellites; meteorological data are accessed through telephone links to several existing agencies. For example, the Data Archiving Center of the University of Wisconsin collects weather data from the Weather Service. The university also has its own meteorological data-processing system. In addition, the University of Wisconsin receives satellite data directly from two current geosynchronous satellites and archives the data for processing.

The visible-image data and the IR data can be combined and registered on a grid. The images would be validated by reference to surface-data maps provided by the other agencies and recorded on photographic plates.

As an alternative, the analog videotape-recorded frames may be digitized for further processing. The videoimage is transformed by a digitizer into pixels. The pixel value associated with the IR image is split into bands, using color codes corresponding to recorded temperature gradients. The result is a composite map of superimposed visual and infrared images clearly defining the temperature gradients of the duststorm area. A series of these maps produced over a relatively-short time period would indicate the storm direction and is used in predicting its path.

This work was done by Peter M. Woiceshyn of Caltech for **NASA's Jet Propulsion Laboratory.** *For further information, Circle 22 on the TSP Request Card.*
NPO-14277

Noise Suppression in Forward-Scattering Optical Instruments

Apertures and stops reduce noise due to light scattered by the instrument optics.

Langley Research Center, Hampton, Virginia

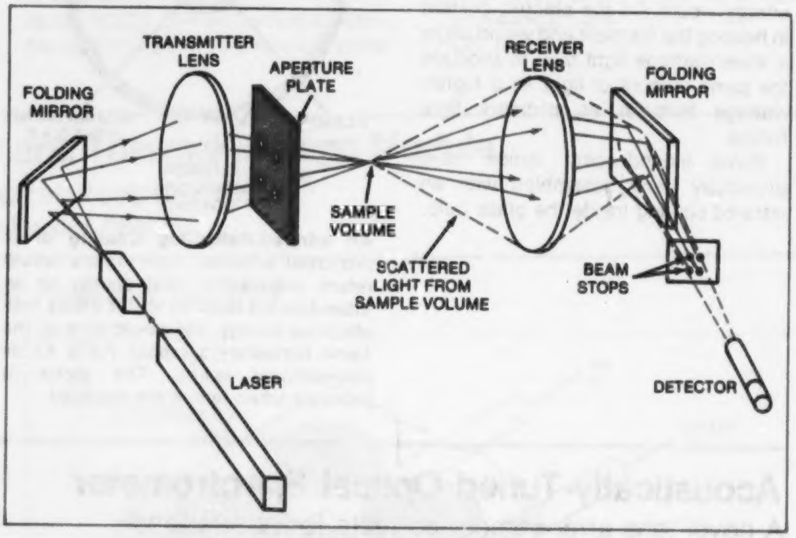

Apertures and Stops Reduce Noise due to scattered light in this laser velocimeter. The apertures and stops are placed and sized as if they were real, inverse images of each other in the receiver lens. Only light scattered from the sample volume reaches the detector.

Signal-to-noise ratio in forward-scattering optical instruments is increased by a combination of apertures and stops located at conjugate points in the receiver optics. Light scattered from the optics (such as from dust on the transmitter lens) is blocked, while light scattered from the sample volume is hardly affected.

The technique suppresses noise caused by scattered light in the forward-scattering laser velocimeter illustrated schematically in the figure. The transmitter optics cross and focus four laser beams at a point of interest in the sample region of a flow field. The receiver lens forms an image at the detector of light scattered from the sample.

The aperture plate next to the transmitter lens contains holes just large enough to pass the laser beams. Thus, it serves two functions: It is a baffle that stops stray light, and it is the aperture through which all light that passes through the transmitter optics must pass. The receiver lens, in addition to forming an image of the sample at the detector, also forms an image of the aperture plate at a plane that lies between the lens and the detector. If a stop plate that is the inverse of the aperture plate is placed in this plane, it will block the main laser beams and any undesired scattered light that passes through the aperture plate from the transmitter optics. The blockage of light scattered from the sample volume is minimal.

Development of a prototype laser velocimeter is complete. The noise-suppression technique increased the signal-to-noise ratio on the order of 15 dB. The technique is not restricted to laser velocimeters and is applicable to other forward-scattering optical instruments.

This work was done by John M. Franke and Luther R. Gartrell of **Langley Research Center.** *No further documentation is available.*
LAR-12730

Energy-Reduction Concept for Incandescent Lamps

Reusable infrared reflector proposed to maintain filament temperature and reduce power requirements

Lyndon B. Johnson Space Center, Houston, Texas

A concept for a coated, spherical light fixture may allow ordinary incandescent lamps to produce more light for a given wattage. The fixture, coated on the inside with a thin layer of infrared-reflecting material, would be installed over the light bulb (see figure). Instead of infrared energy being lost, it would be directed back to the incandescent lamp filament by the selective coating. The reflected energy would aid the electric current in heating the filament and would allow a lower-wattage light bulb to produce the same amount of light as a higher wattage bulb in an ordinary light fixture.

Some incandescent lamps have previously been assembled with an infrared coating inside the glass bulb. This scheme is costly, however, since the coating is expensive and has to be discarded when the bulb burns out. With the coating as part of a separate fixture, it can be used indefinitely over the lifetimes of many lamps.

The fixture must be spherical to reflect the infrared energy back to the filament of the light bulb. To make it more attractive, the fixture could have a decorative exterior coating. Work would have to be done to select the optimum reflective-coating material and thickness and to choose a compatible substrate.

This work was done by Kenneth H. Vorhaben of Lockheed Electronics Co., Inc., for **Johnson Space Center.** *No further documentation is available. MSC-18757*

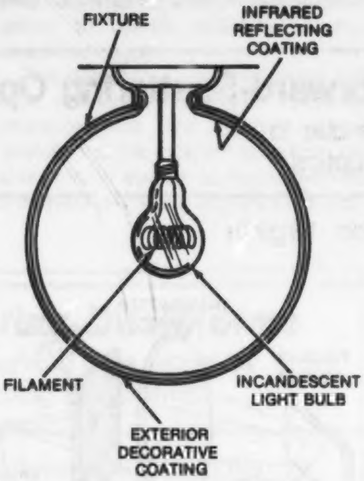

An **Infrared-Reflecting Coating** on a proposed spherical light fixture would return substantial heat energy to an incandescent lamp so that it draws less electrical energy, yet would glow at the same temperature (about 2,870 K) as conventional lamps. The globe is reusable when lamps are replaced.

Acoustically-Tuned Optical Spectrometer

A novel lens arrangement corrects for aberrations and gives a resolution of 0.7 seconds of arc.

NASA Headquarters, Washington, D.C.

A new imaging spectrometer can be electronically tuned to view an object at a selected wavelength between 6,500 and 14,000 angstroms. The spectrometer includes a two-element birefringent crystal in an acoustically-tunable optical filter (ATOF). Although such two-element ATOF devices are effective filters, they normally introduce severe optical aberrations when used for imaging; however, the new spectrometer corrects these aberrations with a cylindrical lens tilted away from the optical axis. The spectrometer combines 15-Å spectral resolution with a spatial resolution of 0.7 seconds of arc (as compared to 5 seconds of arc in a previous ATOF spectrometer).

The filter employs a pair of crossed calcite polarizers. One polarizer is placed at the filter input and the other at its output face. The acoustically tuned element between the polarizers is a birefringent calcium molybdate crystal (see figure). Acoustic waves generated by a radio-frequency voltage-controlled oscillator and a piezoelectric transducer propagate along the axis of the ATOF. Light from the object is polarized by the input polarizer and passes through the crystal in the same direction as the acoustic waves. The light interacts with the acoustically strained crystal in such a way that only a narrow range of wavelengths (determined by the acoustic frequency) is converted to the orthogonal polarization state. At the output end, the second polarizer passes the filtered wavelengths.

The ATOF actually consists of two pieces of calcium molybdate separated by an air gap at an angle of 28° with the normal to the optical axis. The purpose of the second piece is to redirect the light so that it emerges parallel to the axis. However, because

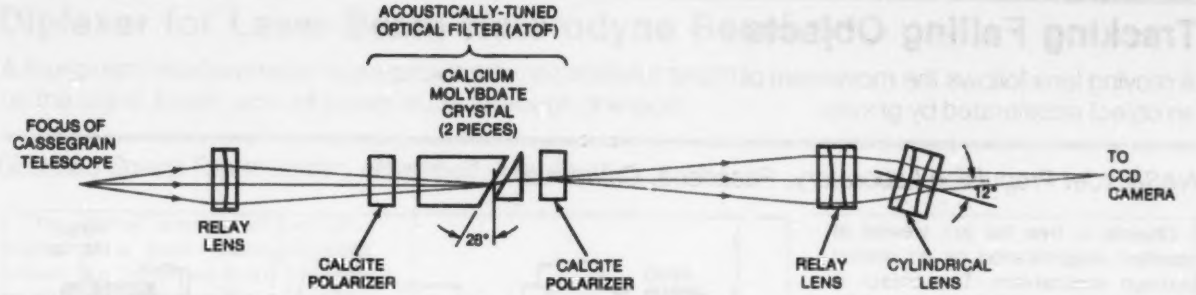
ACOUSTICALLY-TUNED OPTICAL FILTER (ATOF)
CALCIUM MOLYBDATE CRYSTAL (2 PIECES)
FOCUS OF CASSEGRAIN TELESCOPE
RELAY LENS
CALCITE POLARIZER
28°
CALCITE POLARIZER
RELAY LENS
CYLINDRICAL LENS
12°
TO CCD CAMERA

In an Imaging Acoustic/Optical Spectrometer, light from a telescope is relayed by a doublet lens to an acoustically-tuned optical filter. The selected wavelengths are relayed by a triplet lens to a charge-coupled-device camera. An intervening cylindrical lens, tilted at a 12° angle, corrects for astigmatism and coma introduced by the two-element birefringent crystal in the filter.

the rays are almost tangent to the 28° faces, severe astigmatism and coma are introduced.

A simple cylindrical lens could correct the astigmatism, but not the coma. However, if an achromatic cylindrical lens is tilted 12° from the optical axis, the off-axis aberration of the lens would compensate for the extreme coma and also correct the astigmatism.

The beam from the tilted cylindrical lens is directed to a charge-coupled-device (CCD) camera, which converts the light image to an electrical signal for recording and display on a screen.

This work was done by Edward Sklar of American Science and Engineering, Inc., for **NASA Headquarters.** *For further information, Circle 23 on the TSP Request Card.*
HQN-10924

Combined Photovoltaic and Thermal-Storage Module

Wax, a phase-change heat absorber, cools the module and stores energy for space and water heating.

NASA's Jet Propulsion Laboratory, Pasadena, California

A proposed photovoltaic module would use a phase-change heat-absorbing wax to reduce peak temperatures, thus increasing its electrical efficiency. In addition, the heat absorber could make the module more cost-effective by storing thermal energy for air and water heating.

The photovoltaic module normally operates at a cell temperature of 41° to 47° C. However, as the temperature increases, the open-circuit voltages decrease linearly by about 2.2 millivolts per °C, reducing the power output.

The aluminum box enclosing the photovoltaic module can incorporate a heat absorber that will limit the temperature rise. It has been found that eicosane, a wax having a melting point of 36.7° C (4° to 7° C less than the normal operating temperature of the module) reduces the module temperatures by about 5 percent and improves the diurnal power output by 2 to 2.5 percent.

Although reducing the photovoltaic module temperature by using a wax phase-change material makes the module more expensive, the added costs could be offset if the thermal energy stored in the material is utilized. This could be done by circulating building air or water to be heated through the thermal-storage area. At the wax melting point, more energy can be stored with about 15 percent less weight than with water.

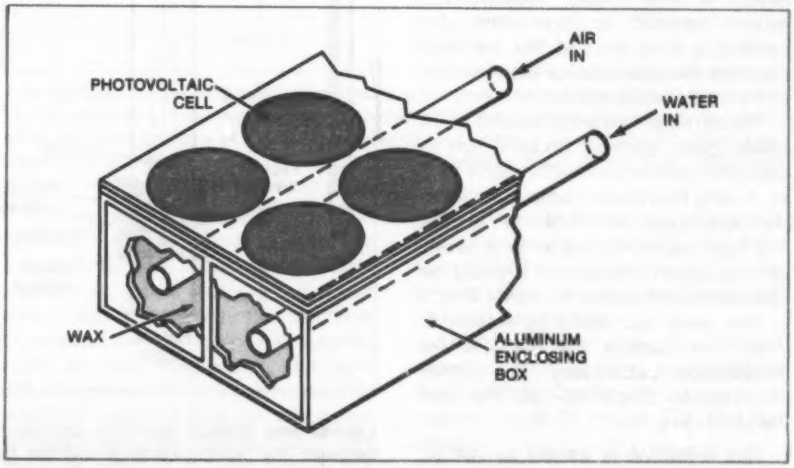

A Wax Phase-Change Heat Absorber reduces the photovoltaic module operating temperature while storing the latent heat of fusion. This heat can be used for water and space heating by passing conduits containing air or water through the module.

This work was done by James W. Stultz of Caltech for **NASA's Jet Propulsion Laboratory.** *For further information, Circle 24 on the TSP Request Card.*
NPO-14591

Tracking Falling Objects

A moving lens follows the movement of an object accelerated by gravity.

NASA's Jet Propulsion Laboratory, Pasadena, California

Objects in free fall are viewed at constant magnification by an optical carriage mechanism. The object is viewed continuously by a movie or TV camera for studies of the dynamics of free fall. A prototype is used in experiments on the formation of glass coatings on nuclear fuel pellets as they fall under the influence of gravity.

As shown in the figure, the system consists of an optical carriage on a vertical track and a fixed telescope that is attached to a camera. The carriage holds a lens that collimates rays of light reflected from the falling object. To have constant magnification, the distance from the object to the lens is equal to the focal length of the lens, and the telescope is focused at infinity.

The carriage travels on the vertical track, composed of an H-beam, as it falls with the object. Three wheels, with grooved edges to minimize rolling friction, guide the carriage along the beam. A small motor supplies the power needed to overcome the remaining drag so that the carriage matches the gravitational acceleration of the freely falling object.

The carriage has been used to track falling glass spheres about 2 cm in diameter over a vertical distance of 2 m. A long fluorescent lamp, parallel to the object path, illuminates the object. The light could be strobed for a series of stop-action images, or it could be operated continuously for movie films.

This work was done by Robert E. Frazer of Caltech for **NASA's Jet Propulsion Laboratory**. *For further information, Circle 25 on the TSP Request Card.*

This invention is owned by NASA, and a patent application has been filed. Inquiries concerning nonexclusive or exclusive license for its commercial development should be addressed to the Patent Counsel, NASA Resident Office-JPL [see page A5]. Refer to NPO-14813.

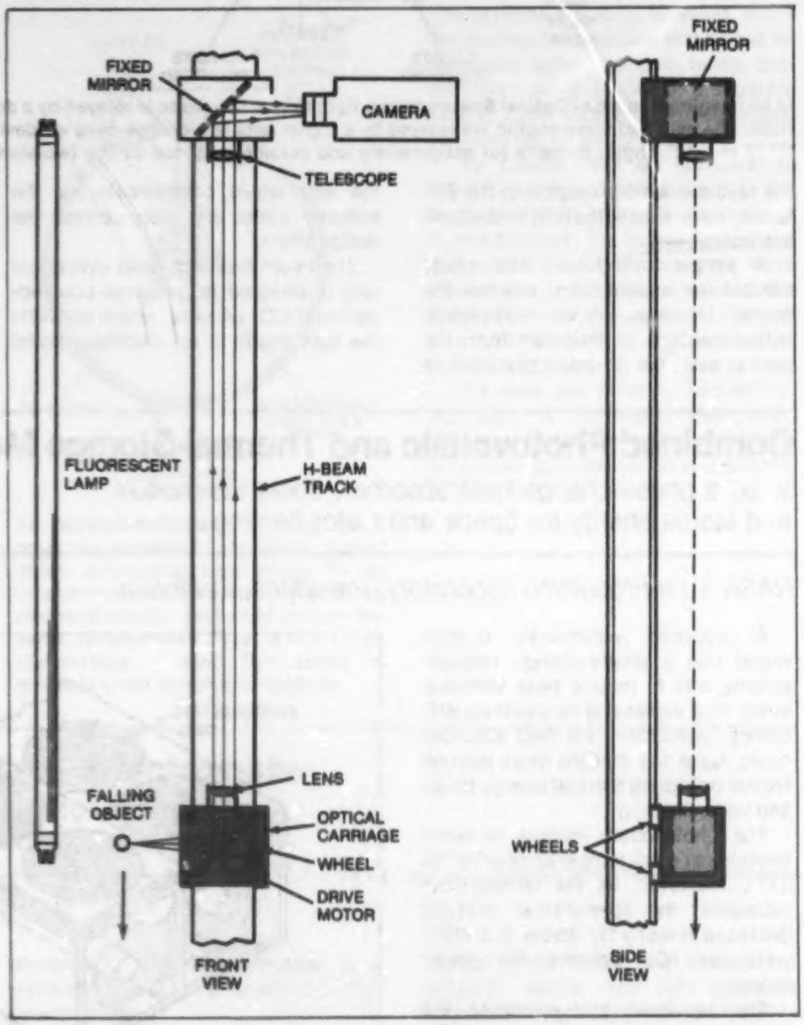

Lenses and Mirrors maintain constant magnification regardless of the distance between the moving carriage and the fixed telescope.

Diplexer for Laser-Beam Heterodyne Receiver

A four-prism interferometer superposes a local-oscillator beam on the signal beam, with all power output through one port.

Goddard Space Flight Center, Greenbelt, Maryland

The signal and local-oscillator beams of a laser communications system are combined in an interferometric diplexer that delivers all of the incident light energy to a single output port. The superposed beams, with phase fronts parallel, can then be directed onto a mixer to generate a difference frequency carrying the signal information, as in other heterodyne detection systems.

The three major advantages of the interferometric diplexer over laser-beam combiners used in the past are:

1. All of the power of the signal and local-oscillator beams emerges from one port, which is determined by the adjustable position of one of the prisms.
2. The output port is spatially separated from the input ports.
3. There is no limitation on how large the frequency difference between the two signals may be.

The diplexer, presently under construction, consists of four 90° prisms, as shown in the figure. The perpendicular faces of each prism are covered with either beam splitters or mirrors. Three of the prisms are fixed, but the top one can be translated along the direction of input beam 2.

Collimated beams entering at inputs 1 and 2 are split into two paths: One path propagates to the right and around the lower part of the configuration, and the other path propagates upward and around the upper part of the configuration. The two beams recombine at the second beam splitter, so both input beams contribute to both output ports. The path-length difference is adjusted by translating the movable prism.

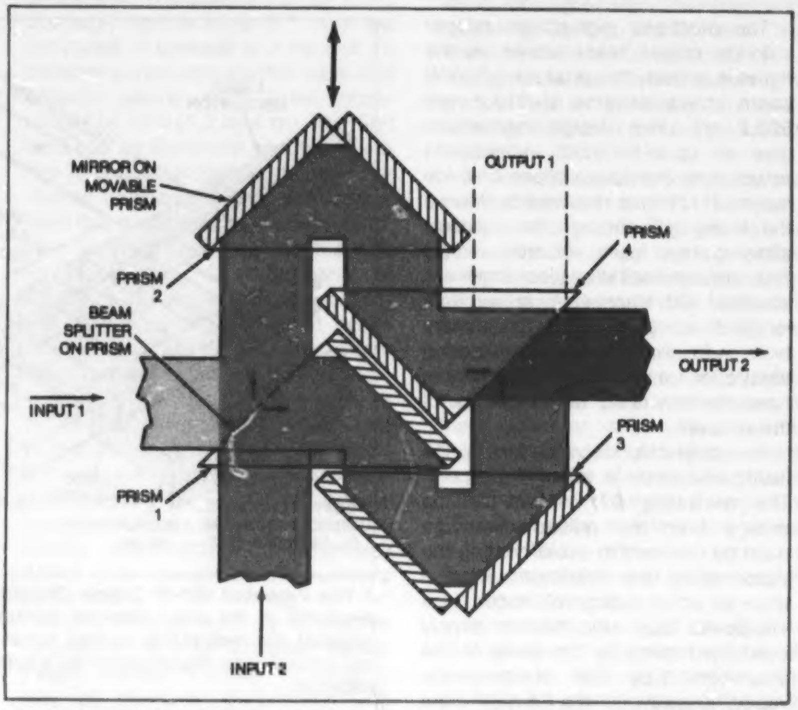

This **Diplexer for Laser Beams** superposes a local-oscillator beam on a signal beam. The movable prism can be positioned so that all of the incident energy in both beams emerges from just one of the two possible output ports — here, output 2. If an additional half wavelength is added to the path difference, then all the light exits from output 1 and no light emerges from output 2.

For each input frequency, the difference in path lengths can be adjusted to give constructive interference at either output port 1 or output port 2. To satisfy the condition of constructive interference simultaneously for both frequencies, the path difference is set at $c/2\Delta f$ (where c is the speed of light and Δf is the difference between the two frequencies). The movable prism is moved toward the fixed prisms for a large Δf value and is moved away for a small Δf. No limitation exists for large Δf values; but for low Δf, diffraction losses degrade the transmission function.

This work was done by Gerhard Koepf of Phoenix Corp. for **Goddard Space Flight Center**. *For further information, Circle 26 on the TSP Request Card.*
GSC-12589

Powerful Copper Chloride Laser

Flowthrough design avoids overheating in a 300-W laser amplifier.

NASA's Jet Propulsion Laboratory, Pasadena, California

The proposed high-power copper chloride pulsed laser shown in the figure is expected to produce a 300-W beam at wavelengths of 510.6 and 578.2 nm. Two design innovations give an up-to-thirtyfold increase in power over previous copper chloride lasers: (1) Heat is removed by flowing the lasing gas through the system, allowing larger lasing volumes; and (2) fast, uniform excitation discharges are obtained with transverse, rather than longitudinal, electrodes. Preliminary tests with experimental dissociating electrodes and pulsed discharges have demonstrated the feasibility of the concept.

In copper chloride vapor lasers, the lasing efficiency is about 1 percent. The remaining 99 percent of the energy from the pulsed discharge must be removed to avoid heating the vapor above the maximum temperature at which lasing will occur. In a low-power laser, the heat is simply conducted away by the walls of the small-bore tube that contains the vapor. However, the small tube volume has limited the output of previous copper chloride lasers to about 10 W. Large increases in power require amplifiers with cross sections too large to cool by conduction.

In the proposed laser, copper vapor and a buffer gas (e.g., helium) are pumped through the amplifier just fast enough to prevent its temperature from exceeding 3,000 K as it is heated by the pulsed discharge. (Above 3,000 K, certain excited copper states are overpopulated, and a population inversion cannot occur.)

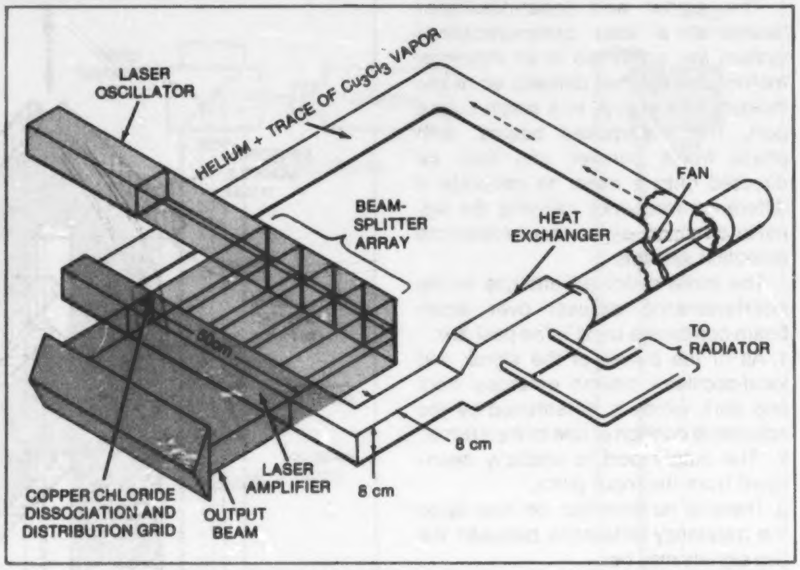

In this **Proposed 300-W Copper Chloride Laser,** a fast-rise-time transverse pulsed discharge in the laser amplifier pumps the lasing gas. Lasing occurs between resonant and metastable excited states in copper. Copper chloride is dissociated into ground-state copper atoms by a hollow-cathode grid at the entrance to the laser amplifier.

The design parameters of the proposed laser are based on experiments with hollow-cathode discharges (for dissociating copper chloride) and fast-rise-time pulse discharges (to produce a population inversion). Data from the hollow-cathode discharge work indicate that the copper chloride vapor is dissociated predominately into ground-state copper atoms. In the experiments with fast transverse pulse discharges, lasing occurred at buffer gas pressures between about 100 and 200 torr (1.3 to 2.6×10^5 N/m^2), pulse repetition rates between 1 and 2×10^4 Hz, and 8 to 10 kV peak voltage drop between the electrodes.

To create a population inversion between the resonant and metastable states of the copper atom that are involved in the lasing, the pumping must be fast. This is possible with low-inductance pulsed-discharge circuits that give an initial rate of current rise of about 10^{10} amperes per second and pulse widths of about 100 ns.

This work was done by Thomas J. Pivirotto of Caltech for **NASA's Jet Propulsion Laboratory.** *For further information, Circle 27 on the TSP Request Card.*

This invention is owned by NASA, and a patent application has been filed. Inquiries concerning nonexclusive or exclusive license for its commercial development should be addressed to the Patent Counsel, NASA Resident Office-JPL [see page A5]. Refer to NPO-14782.

Books and Reports

These reports, studies, and handbooks are available from NASA as Technical Support Packages (TSP's) when a Request Card number is cited; otherwise they are available from the National Technical Information Service.

Heat for Film Processing From Solar Energy

A commercial film-processing lab gets most of its hot-water energy from the Sun.

A solar water-heating system for a commercial building is described in a final report. Installed in the Iris Images photo laboratory in Mill Valley, California, the system furnishes 59 percent of the hot-water requirements for photographic film processing. The 120-page report describes the site and building, the solar-energy system, and problems and modifications. It analyzes performance and economics, and it supplies drawings and an operation and maintenance manual.

The system uses 640 ft^2 (60 m^2) of flat-plate collectors on the roof to produce 6 gallons of hot water per minute at at least 100° F (38° C) for 8 hours per day. The hot water is stored in tanks having a total capacity of 360 gallons (1,332 liters). The solar-heated water from the tanks passes through an auxiliary gas-fired heater, which adds heat if necessary to raise the water to the required temperature. The hot water is then piped to the film processors and to six sinks and two bathrooms.

The film processors require water at temperatures between 75° and 100° F (24° and 38° C), depending on the type of film being developed. The hot water from the solar panels and auxiliary heater is mixed with cold water to the desired temperature at each unit.

A low-temperature (less than 120° F, 49° C) industrial process such as film developing is an ideal application for solar heating. With a constant year-round daytime load, storage requirements are minimized and solar utilization is maximized. High collector efficiency can be expected because of the relatively-low hot-water temperature.

The solar collectors are not prefabricated, but instead were constructed on the site. The collector array faces due south and is tilted 36° from the horizontal. It consists of a bank of 12 collector panels and another bank of 4 collector panels, each panel measuring 4 by 10 ft (1.2 by 4 m). The first bank has an aluminum absorber plate that is bonded to copper tubing. The second bank has a copper absorber plate that is soldered to copper tubing. Both absorber plates are coated with flat black paint. A single panel of coated fiberglass covers the collectors. The report cautions that onsite fabrication is practical only where skilled, low-cost labor is available.

To prevent damage from freezing, a pump circulates water through the collector array whenever the temperature of either collector-bank absorber plate is below 36° F (2.2° C). If there is a power failure at freezing temperatures, the system automatically drains the collectors and exterior pipes.

This work was done by Interactive Resources, Inc., for **Marshall Space Flight Center.** *Further information may be found in DOE/NASA CR-161414 [N80-22781/NSP], "Solar Process Water Heat for the Iris Images Custom Color Photo Lab" [$10]. A paper copy may be purchased [prepayment required] from the National Technical Information Service, Springfield, Virginia 22161. The report is also available on microfiche at no charge. To obtain a microfiche copy, Circle 28 on the TSP Request Card.*
MFS-25444

Solar Heater/Cooler for Mass Market

Project aims for an affordable, easy-to-install system.

A 106-page report describes a project to design, build, and test a family of solar-heating/cooling systems for a mass market. Four basic systems were developed:

- Heating and Domestic Hot Water for Single-Family Dwellings;
- Heating and Domestic Hot Water for Commercial Buildings;
- Heating, Cooling, and Domestic Hot Water for Single-Family Dwellings; and
- Heating, Cooling, and Domestic Hot Water for Commercial Buildings.

The systems have been installed, or are planned for installation, in seven buildings scattered around the United States.

To keep manufacturing costs low, the systems use common parts and modular subsystems. To keep installation costs low, they are compatible with many types of heating, ventilating, and air-conditioning (HVAC) equipment and employ prepackaged controls and auxiliary units.

The solar collector for all systems has evacuated glass outer tubes, a metal reflector, and a heat-transfer fluid circulating in selectively-coated metal tubes. The control of fluid flow is based on a time average of insolation, as measured by an integrating sensor in the collector, rather than on instantaneous insolation; this reduces on/off cycling of the pump.

For heating, the fluid transfers its heat to water in a storage tank, which transfers its heat to forced air. For cooling, the stored water delivers its heat to a heat pump, which cools air or water circulating through the building.

The report describes the plan for the project, the systems and their components, the test sites, and performance. The text is complemented by detailed drawings and test data.

This work was done by the Space Division of General Electric Co. for **Marshall Space Flight Center.** *Further information may be found in DOE/NASA CR-161422 [N80-24746/NSP], "Solar Heating and Cooling System Design and Development [Final Report]" [$9]. A paper copy may be purchased [prepayment required] from the National Technical Information Service, Springfield, Virginia 22161. The report is also available on microfiche at no charge. To obtain a microfiche copy, Circle 29 on the TSP Request Card.*
MFS-25452

Data-Acquisition and Control System for Severe Environments

Evaluation test procedures and results

An evaluation test program on a commercial solar data-acquisition and control system is documented in a new report. The program measured the accuracy and performance of the system subcomponents, including the interface wiring unit, power controller, and tape recorder, in a severe environment.

One proposed installation site, at Frenchman's Reef in the Virgin Islands, is an uncontrolled enclosed area near surfaces with higher than ambient temperatures and high relative humidity. Also, the supply voltage in the area varies in magnitude and frequency. Test parameters were established as: temperature 0° to 50° C, relative humidity 0 to 90 percent, supply frequency 54 to 66 cycles/second, voltage 103 to 127 volts, and temporary voltage dropout 10 milliseconds.

The evaluation was conducted in an environmental chamber for controlling humidity and temperature. Initial tests established unit temperature recording accuracy. A custom solar simulator was used to provide a simulated collector system. Two computer programs were written: a program to exercise the discrete digital outputs at 5-minute intervals and a program executed at 30-minute intervals to test thermistor inputs and analog voltage channels. The second program also exercised internal counters, discrete inputs and discrete outputs, and printed the time and system status.

Although the data-acquisition and control system performed as expected at 100° F (38° C) and 87 percent humidity, it failed to operate at 120° F (49° C). In some cases, a failure might result in false triggering of output drivers unless special shutdown precautions are taken.

The report features test program descriptions, sample readouts, and test results. A summary of the custom solar system simulator is included.

This work was done by Wyle Laboratories for **Marshall Space Flight Center.** *Further information may be found in DOE/NASA CR-161449 [N80-25783/NSP], "Test Results on the Frenchman's Reef Solar Data Acquisition and Control System" [$5]. A paper copy may be purchased [prepayment required] from the National Technical Information Service, Springfield, Virginia 22161. The report is also available on microfiche at no charge. To obtain a microfiche copy, Circle 30 on the TSP Request Card.*
MFS-25471

Commercial-Building Solar-Energy System — Stamford, Connecticut

Electrical energy consumption is reduced by half for a 2-1/2-story office building.

An efficient distributed heat-pump system and an electrical boiler backup, together with an almost-completely-empty flat roof that faces nearly due south, made the Executive East office building in Stamford, Connecticut, very attractive for a solar-energy retrofit. Solar energy now replaces more than half the total electrical energy previously used for heating, and it eliminates all the electrical boiler capacity used during peak daytime hours. A 93-page final report on the project includes detailed drawings and photographs, the operation and maintenance manual, the acceptance test plan, and other pertinent information.

The Stamford office building has 25,000 square feet (2,300 square meters) of heated space in 2½ stories. Its aluminum and glass curtain wall construction is typical of office buildings built prior to the energy crisis. Located next to a major shopping center on a busy highway in Stamford, the building is oriented with its long axis pointing 5° west of south; the roof is flat and almost completely unobstructed. Zoning regulations restrict the construction of any nearby tall buildings that could block the Sunshine to the building.

Nearly 80 water-source heat pumps heat and cool the building. They are connected in series in a hydronic loop, which is always maintained between 75° and 85° F (24° and 29° C). When heating the building, a heat pump extracts heat from the hydronic loop. Prior to installation of the solar system, all the heat needed to maintain the loop temperature was supplied by two 75-kVA electric boilers.

One hundred and thirty-eight liquid flat-plate solar collectors, arranged in six rows, are mounted on the roof of the building. A polished aluminum reflector in front of each row increases the collected energy (by 46 percent during the winter). For protection against overheating or stagnation, the shutters are hinged and can be folded up as a shield for the collectors.

Solar energy is delivered to a 6,000-gallon (23,000-liter) stone-lined storage tank and, from there, to the building heat-pump loop. If the storage-tank temperature drops too low, the building loop can be heated by the electrical hot-water boilers.

This work was done by the Lutz-Sotire Partnership for **Marshall Space Flight Center.** *Further information may be found in DOE/NASA CR-161436 [N80-27800/NSP], "Solar Heating System Installed at Stamford, Connecticut" [$8]. A paper copy may be purchased [prepayment required] from the National Technical Information Service, Springfield, Virginia 22161. The report is also available on microfiche at no charge. To obtain a microfiche copy, Circle 31 on the TSP Request Card.*
MFS-25468

Solar-Heated and Cooled Office Building — Dalton, Georgia

A modern energy-efficient building is heated and cooled by solar energy.

Information on an energy-efficient Georgia office building equipped with solar heating and cooling is contained in a recently released report. Located on a 1.5-acre (6.1 x 10^3-m^2) lot near downtown Dalton, Georgia, the building is a modern two-story structure with 7,000 ft^2 (650 m^2) of office space and workspace. The energy collected in five rows of flat-plate solar collectors supplies a major fraction of the building heating and cooling demand, along with all of its modest domestic hot-water needs. Included in the 132-page final report are detailed drawings and photographs, manufacturer's literature, performance specifications, acceptance test data (the plan and results), and performance verification statements. The operation and maintenance manual is also included.

The building is constructed with many energy-conserving features. Its western and northwestern first-floor elevations are buried into the sloping contour of the lot, reducing the summertime afternoon Sun load and minimizing the cooling effect of the winter wind. The square shape of the building has minimal exterior wall area, which also reduces the heating and cooling load. The two-story design minimizes the roof area. Window area has also been kept to a minimum and is protected from the Sun by generous roof overhangs. All windows are operable so that natural ventilation is available. The double-glazed insulation is shaded to block direct Sunlight.

Heating for the building is by the direct flow of solar-heated water to an exchange deck in the central air handler. The building is cooled by the flow of chilled water to a separate exchange deck. For cooling, solar-heated water drives a 25-ton (88-kW) absorption chiller. The backup or supplementary supply of heated water to drive the chiller and for building heat is supplied by a conventional oil-fired boiler. A multizone central processor controls the system in each of its heating and cooling modes. Day and night periods of heating and cooling are regulated by a standard automatic timeclock and an overriding thermostat.

This work was done by the North Georgia Area Planning and Development Commission for **Marshall Space Flight Center.** *Further information may be found in DOE/NASA CR-161273 [N80-11555/NSP], "Solar Energy System Installed at the North Georgia APDC Office Building" [$10]. A paper copy may be purchased [prepayment required] from the National Technical Information Service, Springfield, Virginia 22161. The report is also available on microfiche at no charge. To obtain a microfiche copy, Circle 32 on the TSP Request Card.*

MFS-25451

Solar-Heating and Hot-Water System — St. Louis, Missouri

Sunlight supplies about half the heat-energy needs of a small office.

A solar-energy system of more modest size than those of the two preceding articles is described in a new report. The system, installed in a St. Louis office building, supplements the winter heating load for a 900-ft^2 (84-m^2) addition to the building and preheats the service hot water for the entire building. It includes 252 square feet (23.4 square meters) of "mildly-concentrating" commercial solar collectors and a 1,000-gallon (3,785-liter) energy-storage tank. The 67-page report contains a description of the system and its components, drawings and photographs, manufacturer's data, and other related material.

About 50 percent of building hot-water requirements and 45 percent of the space-heating needs of the addition are supplied by Sunlight. To maximize the collection efficiency, the tilt angle of the six solar collectors is variable and is adjusted seasonally. Energy is transferred to the 1,000-gallon storage tank through a tube-in-shell heat exchanger. Incoming city water is preheated in a smaller storage tank equipped with a heat exchanger.

This work was done by William Tao and Associates for **Marshall Space Flight Center.** *Further information may be found in DOE/NASA CR-161420 [N80-24744/NSP], "Solar Heating and Hot Water System Installed at St. Louis, Missouri — Final Report" [$7]. A paper copy may be purchased [prepayment required] from the National Technical Information Service, Springfield, Virginia 22161. The report is also available on microfiche at no charge. To obtain a microfiche copy, Circle 33 on the TSP Request Card.*

MFS-25453

Solar Heating for an Electronics Manufacturing Plant — Blue Earth, Minnesota

Space heating for a 97,000-square-foot plant is supplied partly by solar energy.

The heating system of a large manufacturing plant for tape recorders and other electronics in southern Minnesota has been refitted for solar energy as part of the Solar Heating and Cooling Demonstration Program. Described in detail in a 167-page final report, the system has been delivering space heat since February 1978.

The 97,000-square-foot (9,000-square-meter) building houses assembly areas, administrative offices, and a warehouse. It is constructed of steel, with 6 inches (15.2 cm) of fiberglass insulation between the steel skins. In cold weather, the space-heating load is 9 million to 12 million Btu (9.5×10^9 to 12.6×10^9 J) per day. There is little hot-water demand. Because it uses electric resistance heating, the plant was considered a good choice for adaptation to solar energy.

The 360 flat-plate solar collectors are mounted on a wood-and-concrete support structure adjacent to the building. Arranged in 10 rows of 36 collectors, each 4 by 8 feet (1.2 by 2.4 m), the solar array has a gross area of 11,520 square feet (1,071 square meters). Solar energy is stored as heat in a 20,000-gallon (75,000-l) water tank located inside the building.

The plant is heated by water-to-air heating coils in the nine already-existing air-handling units and three water-to-air heating coils. If the storage-tank temperature is insufficient to meet the heating requirements of a part of the building, the balance of the heat is supplied by electrical resistance heating. The system includes all the necessary control electronics for year-round operation. During the month of December 1978, solar energy supplied about 24.4 percent of the building space-heating load.

This work was done by Telex Communications, Inc., for **Marshall Space Flight Center.** *Further information may be found in DOE/NASA*

CR-161437 [N80-25786/NSP], "Solar Heating System Installed at Telex Communications, Inc., Blue Earth, Minnesota — Final Report" [$12]. A paper copy may be purchased [prepayment required] from the National Technical Information Service, Springfield, Virginia 22161. The report is also available on microfiche at no charge. To obtain a microfiche copy, Circle 34 on the TSP Request Card.
MFS-25469

Costs and Description of a Solar-Energy System — Austin, Texas

Heating and cooling system uses Fresnel-lens concentrating collectors.

The final report on a solar-energy system installed at the site of a Texas corporation includes a detailed breakdown of the costs of the project. Commercial concentrating solar collectors covered by acrylic Fresnel lenses are used in the heating and cooling system. The major system components are 36 concentrating collectors, a 1,500-gallon (5,700-l) thermal storage tank, an absorption cooler, a cooling tower, a heating coil, pumps, a heat exchanger, and backup heating and air-conditioning.

Each concentrating collector has a Fresnel lens [1 by 10 feet (0.3 by 3 meters)] to concentrate Sunlight onto a flattened copper absorber tube that has a black-chrome absorptive coating. A tracking mechanism focuses the Sunlight. Each collector has a pulley attached to a shaft at the lower end. A steel cable looped around the pulleys simultaneously rotates up to 20 collectors. A pair of photovoltaic cells senses the location of the Sun. An unbalanced output from these cells turns on a motor, which rotates the collectors through a gearbox and the cable.

A 3-ton (11 kW) lithium bromide air-conditioner provides space cooling. It requires 55,000 Btu/h ($58,000 \times 10^3$ J/h) heat input from solar-heated water to boil the water in the lithium bromide/water solution. The water vapor is passed over the condensing coils in the cooling tower, which extracts heat at the rate of 91,000 Btu/h ($96,000 \times 10^3$ J/h), for a net cooling rate of 36,000 Btu/h ($38,000 \times 10^3$ J/h).

The performance of this system is monitored by 47 sensors that measure temperature, flow rate, insolation, power, windspeed, and other parameters. Once every 5 minutes, the sensors are sampled, and the data are stored on cassette tape.

Component and installation costs are given for seven subsystems (e.g., collectors, storage tank, and controls). The costs of monitoring sensors, of installation, and of engineering are listed separately. The total of "essential" costs for the system installed in 1977 is $42,082.

This work was done by Radian Corp. for **Marshall Space Flight Center.** *Further information may be found in DOE/NASA CR-161442 [N80-25784/NSP], "Solar Heating and Cooling Demonstration Project at Radian Corporation, Austin, Texas — Final Report" [$6]. A paper copy may be purchased [prepayment required] from the National Technical Information Service, Springfield, Virginia 22161. The report is also available on microfiche at no charge. To obtain a microfiche copy, Circle 35 on the TSP Request Card.*
MFS-25472

Solar Energy in a Historical City — Abbeville, South Carolina

Direct-air solar heating does not alter building appearance.

A solar-heating system installed in the Abbeville, South Carolina, municipal building does not compromise approval of the building design by state and local historical societies. The flat-roofed two-story brick structure, which houses the police and fire departments and the recorder's court, is architecturally compatible with other buildings in this very old and historical city — a factor that was considered very seriously when planning the solar-energy system.

The system that met the architectural standards is a direct-air solar space-heating system with roof-mounted flat-plate collectors and a rock-storage bin. The collectors lie flat against the roof and are not visible from the ground. An air-handling unit coordinates the solar and backup heating systems by monitoring the temperatures of the outside air, the collector, the storage bin, and the building air. From these data, it controls the collection and distribution of solar heat.

"Natural" cooling modes supplement the building air-conditioning. Inside air is circulated through the rock-storage bin, allowing the rocks to absorb some of the heat from the air. When the outside air temperature drops below that of the rocks, the air handler circulates the outside air over the rocks to exhaust the heat to the outside.

Solar preheating of domestic hot water is possible when excess hot air in the collectors would be exhausted to the outside. At these times, water from a storage tank is circulated through a heat exchanger in the exhaust duct. Any additional heat required is supplied by an electric hot-water heater.

The 52-page final report on the system contains performance data, drawings, photographs, and other pertinent information. The installation manual for the air handler is included as an appendix.

This work was done by Gilliland-Bell Associates, Inc., for **Marshall Space Flight Center.** *Further information may be found in DOE/NASA CR-161443 [N80-25788/NSP], "Solar Heating and Hot Water System Installed at Municipal Building Complex, Abbeville, S.C. — Final Report" [$7]. A paper copy may be purchased [prepayment required] from the National Technical Information Service, Springfield, Virginia 22161. The report is also available on microfiche at no charge. To obtain a microfiche copy, Circle 36 on the TSP Request Card.*
MFS-25479

Municipal Recreation Center Is Heated and Cooled by Solar Energy — Dallas, Texas

A major fraction of heating, cooling, and domestic hot-water requirements is supplied by Sun energy.

The final report on the solar-heating and cooling facility at the North Hampton Park Recreation and Health Center, Dallas, Texas, chronicles the demonstration project from its inception in November 1975 through its completion in July of 1978. Other material in the 115-page document is a summary of the project performance, costs, operating modes, and data-acquisition system. An appendix contains manufacturer's product literature and over 20 pages of engineering drawings.

The North Hampton Park Recreation and Health Center is a single-story structure enclosing a gymnasium, locker area, and health-care clinic. It is surrounded by a recreational area and an athletic field. Total building area is 16,000 square feet (1,486 square meters) of which one-half is the gymnasium, which is conventionally heated and not part of the solar-energy demonstration project.

The solar-energy system is designed to supply 80 percent of the annual space heating, 48 percent of the annual space cooling, and 90 percent of the heat for domestic hot water. It includes a solar-collector loop, hot-water energy storage, a domestic hot-water system, an absorption chiller, and chilled water storage. The collector loop heat-transfer medium is an aqueous solution of 35 percent ethylene glycol.

The 238 commercial flat-plate solar collectors are roof-mounted in 29 arrays. A heat exchanger transfers the collected energy to a 6,000-gallon (22,000-liter) storage tank insulated with 4 inches (10 cm) of urethane.

Space cooling is partly supplied by using solar energy to operate a commercial absorption chiller. The chilled water is stored in a 2,000-gallon (7,600-liter) tank. The balance of space cooling is supplied by two vapor compression units.

Domestic supply water is preheated by heat exchangers on the hot side of the absorption-chiller condenser loop and the hot-water storage-tank loop. A conventional natural-gas heater supplies any additional energy needed for domestic hot water.

This work was done by Travis-Braun and Associates, Inc., for **Marshall Space Flight Center.** *Further information may be found in DOE/NASA CR-161444 [N80-26766/NSP], "Solar Energy Facility at North Hampton Recreation Center, Dallas, Texas — Final Report" [$10]. A paper copy may be purchased [prepayment required] from the National Technical Information Service, Springfield, Virginia 22161. The report is also available on microfiche at no charge. To obtain a microfiche copy, Circle 37 on the TSP Request Card.*
MFS-25478

Solar Energy Meets 50 Percent of Motel Hot-Water Needs — Key West, Florida

When occupancy is less than 50 percent, no auxiliary energy is needed.

A final report describes a solar domestic-water preheat system installed in a 148-room motel in Key West, Florida. The solar equipment meets 50 percent of the domestic hot-water needs when the motel is 100 percent occupied; equivalently, it supplies 100 percent of the hot water when occupancy is 50 percent. Prior to the installation of the solar-energy demonstration project, domestic hot water was heated by an oil-fired boiler feeding a 500-gallon (1,900-liter) storage tank.

The energy demand estimate for the motel is 6.81×10^8 Btu/year (7.18×10^{11} J/year) of which 3.19×10^8 Btu/year (3.36×10^{11} J/year) are to be supplied by solar energy. The system consists of 1,400 square feet (130 square meters) of flat-plate liquid solar collectors, storage tanks, a pump, a controller, and other hardware. Cold water in copper tubing is circulated through the collectors, and the heated water is stored. At times when no hot water is being used, the stored water is continuously passed through the collectors. When hot water is needed, it is either transferred directly to the boiler storage tank or through the boiler to the tank, depending on the water temperature.

This work was done by Quality Inn of Key West for **Marshall Space Flight Center.** *Further information may be found in DOE/NASA CR-161434 [N80-23774/NSP], "Solar Hot Water System Installed at Quality Inn, Key West, Florida — Final Report" [$5]. A paper copy may be purchased [prepayment required] from the National Technical Information Service, Springfield, Virginia 22161. The report is also available on microfiche at no charge. To obtain a microfiche copy, Circle 38 on the TSP Request Card.*
MFS-25454

Solar-Heated Office Complex — Greenwood, South Carolina

System meets 85 percent of heat requirements.

A Greenwood, South Carolina, office complex, completed in 1975, is 85-percent heated by solar energy. The system uses roof-mounted recirculating-water solar panels and underground hot-water energy storage. Aluminum-film reflectors increase the total solar flux captured by the panels. A thorough documentation of the project is contained in a recently-released final report.

Solar energy captured as heat and stored in the underground water tank is transferred to the building air at a coil located in the hot-air duct. A heat pump downstream of the coil and an electric resistance heater in the duct add additional heat when needed. Service water is heated by a single-wall, tube-bundle heat exchanger immersed in the storage tank. Its heat is augmented by an electric water heater.

Domestic city water mixed with a corrosion inhibitor is the heat-transfer fluid in the collector loop. The water is prevented from freezing by automatic drain-down instrumentation.

The solar-heated area of the office complex is 4,284 square feet (398 square meters). A total of 954 square feet (89 square meters) of collector area supplies 85 percent of the heating requirements of this area.

This work was done by W. E. Gilbert & Associates, Inc., for **Marshall Space Flight Center.** *Further information may be found in DOE/NASA CR-161435 [N80-23776/NSP], "Solar Heating System Installed At Blakedale Professional Center, Greenwood, S.C. — Final Report" [$6]. A paper copy may be purchased [prepayment required] from the National Technical Information Service, Springfield, Virginia 22161. The report is also available on microfiche at no charge. To obtain a microfiche copy, Circle 39 on the TSP Request Card.*
MFS-25458

Residential System Tested in an Office — Huntsville, Alabama

A system does not meet its design specifications if it is not matched with its application.

The difficulties in trying to adapt a residential solar-energy system to a commercial building are underscored by the results at one operational test site. Installed in a Huntsville office building, the system designed for a single-family residence supplied considerably less of the annual heat load than expected, although actual hardware problems were minimal. An 85-page report on the project discusses these observations and contains an abundance of design, performance, and test information.

There are two key differences between the office and residential applications. First, the space-heating demand at the office was more than the design value because the thermostat was not held at 70° F (21° C), as specified for the residence. Often the temperature was maintained at 76° F (24° C) during work hours. Second, the hot-water demands of an office are considerably less than those of a residence. Thus, much of the energy collected and stored during the summer went unused because relatively little hot water was used. In fact, it is estimated that if the solar equipment had been shut off during the late spring, summer, and early fall, energy savings would have increased by 21 percent for the year.

The system, which uses air solar collectors, is designed to supply 50 to 60 percent of the space-heating requirements of a single-family dwelling with 2,200 ft^2 (200 m^2) of floorspace. The hardware is described in more detail in "Prototype Solar-Heating System" (MFS-23916) on page 201 of *NASA Tech Briefs*, Vol. 3, No. 2.

This work was done by the Federal Systems Division of IBM Corp. for **Marshall Space Flight Center.** *Further information may be found in DOE/NASA CR-161464 [N80-25790/NSP], "Solar Energy System Performance Evaluation — Seasonal Report for IBM System 1A, Huntsville, Alabama" [$8]. A paper copy may be purchased [prepayment required] from the National Technical Information Service, Springfield, Virginia 22161. The report is also available on microfiche at no charge. To obtain a microfiche copy, Circle 40 on the TSP Request Card.*
MFS-25481

Solar-Heated Two-Level Residence — Akron, Ohio

Operational tests over a 1-year period

A report available on request describes a 1-year evaluation of a solar-heating and hot-water system for a two-level single-family residence in Akron, Ohio. The system uses flat-plate solar collectors with air as the heat transport medium. A rock-storage bin stores the collected energy. Backup heat is supplied by an air-to-liquid heat pump. [For more details about this system, see "Solar-Heating and Cooling System Design Package" (MFS-25393) on page 38 of *NASA Tech Briefs*, Vol. 5, No. 1.]

Solar energy satisfied 24 percent of the hot-water and space-heating load during the 1-year test. Gross electrical-energy savings were 9.03×10^6 Btu (9.52×10^9 J). Net savings, after 2.15×10^6 Btu (2.27×10^9 J) needed to operate the system are subtracted, were 6.88×10^6 Btu (7.26×10^9 J). If a 30-percent efficiency is assumed for power generation and distribution, then 22.92×10^6 Btu (24.18×10^9 J) of fuel were saved at the power-generating station.

This work was done by the Federal Systems Division of IBM Corp. for **Marshall Space Flight Center.** *Further information may be found in DOE/NASA CR-161465 [N80-25791/NSP], "Solar Energy System Performance Evaluation — Seasonal Report for Solaron-Akron, Akron, Ohio" [$8]. A paper copy may be purchased [prepayment required] from the National Technical Information Service, Springfield, Virginia 22161. The report is also available on microfiche at no charge. To obtain a microfiche copy, Circle 41 on the TSP Request Card.*
MFS-25480

Solar-Energy Workshop — Tucson, Arizona

A showplace for solar-energy utilization includes a complex solar-heating and cooling system.

A complex solar-heating and cooling system, tested onsite at the "Decade 80" house, Tucson, Arizona, supplied 93 percent of the building space-heat requirements between November 1978 and October 1979. As stated in a seasonal report on the project, solar energy saved 202 million Btu (213×10^9 J) of conventional energy sources during that period.

The Decade 80 house, a one-story single-family dwelling, is a showplace and workshop for solar-energy utilization. Superior construction techniques and quality materials were utilized, and a full-time maintenance staff was assigned to keep all systems operating.

An aqueous solution of propylene glycol is the heat-transfer medium in the flat-plate collector loop. The collected energy is transferred to an underground water-storage tank. The collector-to-storage loop also has a heat exchanger that diverts some heat to a swimming pool.

Two absorption-cycle water chillers operating in parallel supply space cooling. Heat from the storage tank is circulated through the generators of the chillers to activate the absorption cycle. The chilled water is pumped to heat exchangers in the building air-distribution system. When the available solar energy is not sufficient, a gas-fired boiler supplies the balance of the energy requirements.

Domestic hot water is circulated through a heat exchanger in the energy storage tank. Additional energy is supplied by electrical heating elements. The domestic water is continuously circulated between a small storage tank and the building plumbing, so that hot water is always available on demand.

This work was done by the Federal Systems Division of IBM Corp. for **Marshall Space Flight Center.** *Further information may be found in DOE/NASA CR-161450 [N80-25787/NSP], "Solar Energy System Performance Evaluation — Seasonal Report for Decade 80 House, Tucson,*

Arizona" [$9]. A paper copy may be purchased [prepayment required] from the National Technical Information Service, Springfield, Virginia 22161. The report is also available on microfiche at no charge. To obtain a microfiche copy, Circle 42 on the TSP Request Card.
MFS-25473

Residential Solar Hot-Water System — Tempe, Arizona

Domestic hot water for a single-story residence is heated by two 4- by 8-foot solar collectors.

A solar hot-water supply saved 5.54 million Btu (5.84 billion Joules) from June 1979 through January 1980 at the Agricultural Department residence at Arizona State University. Since hot-water consumption at the site was low, and consequently much of the solar energy went to make up standby losses, savings with increased usage would be significantly higher. The system is described along with test results in a report that is now available.

The commercial domestic hot-water system uses two 4- by 8-foot (1.2- by 2.4-meter) flat-plate collectors to heat water in either a preheat tank or a domestic hot-water tank, each with a capacity of 52 gallons (196 liters). Additional heat is supplied, if required, by an auxiliary electrical heating element in the domestic hot-water tank.

Energy from the solar collectors is supplied to the domestic hot-water tank whenever the tank temperature is less than 140° F (60° C) and more than 20° F (11° C) below the solar-collector outlet temperature. Should the tank temperature exceed 140° F, excess solar energy is routed to the preheat tank. The system protects against freezing by automatically circulating hot water through the collectors when the collector temperatures approach freezing. Total incident solar energy while the collector was operating during the 6-month period was 15.78 million Btu (16.64 billion Joules). Collected solar energy totaled 8.16 million Btu (8.61 Joules), for a collector efficiency of 52 percent.

This work was done by the Federal Systems Division of IBM Corp. for **Marshall Space Flight Center.** *Further information may be found in DOE/NASA CR-161466 [N80-26778/NSP], "Solar Energy System Performance Evaluation — Seasonal Report for Elcam Tempe, Arizona State University, Tempe, Arizona" [$7]. A paper copy may be purchased [prepayment required] from the National Technical Information Service, Springfield, Virginia 22161. The report is also available on microfiche at no charge. To obtain a microfiche copy, Circle 43 on the TSP Request Card.*
MFS-25490

Residential Solar-Heating Installation — Stillwater, Minnesota

Installer guidelines for each subsystem, including filling and testing

The 179-page "installation guidelines" for the single-family residential heating system at William O'Brien State Park in Stillwater, Minnesota, are now available. The design package for the system is described in "A Solar-Energy System in Minnesota" (MFS-25428) on page 175 of *NASA Tech Briefs*, Vol. 5, No. 2. Information on the operating procedures, controls, caution requirements, and routine and scheduled maintenance is included as written procedures, schematics, detailed drawings, and manufacturer's component data.

The system has 33 liquid flat-plate collectors, a 1,000-gallon (3,790-liter) steel water-storage tank, an auxiliary gas-fired furnace, a domestic hot-water preheater, and accessory pumps, piping, and control equipment. The glycol/water collector loop interfaces with a water-storage loop through a tube-and-shell heat exchanger. A domestic hot-water preheat coil transfers collected energy to the storage tank. A heat exchanger transfers solar-collector heat to the hot-water coil in the return air duct to supply building heat.

Solar-heated water is diverted to charge storage when the building heat demand is met. When available solar energy is inadequate, storage is tapped, or the auxiliary furnace is activated. The domestic hot water is continuously preheated and purged of excess energy.

This work was done by the Energy Resources Center of Honeywell, Inc., for **Marshall Space Flight Center.** *Further information may be found in DOE/NASA CR-161480 [N80-28861/NSP], "Installation Guidelines for Solar Heating System Single-Family Residence at William O'Brien State Park, Stillwater, Minnesota" [$12]. A paper copy may be purchased [prepayment required] from the National Technical Information Service, Springfield, Virginia 22161. The report is also available on microfiche at no charge. To obtain a microfiche copy, Circle 44 on the TSP Request Card.*
MFS-25504

Three-Story Residence With Solar Heat — Manchester, New Hampshire

Heat lost through ducts should be included for an accurate performance assessment.

The performance of a solar-energy system that heats the interior and the domestic hot water of a three-story dwelling on the New Hampshire Vocational Technical College campus is documented in a recently-released 78-page report. The system was evaluated from March 1979 to February 1980. During this period, the measured average outdoor ambient temperature was 53° F (12° C). When the net energy savings are adjusted for heat lost through ducts, but absorbed within the building, solar energy supplied 56 percent of the total measured load for space heating. Average building temperature was maintained at 69° F (21° C).

Compared to an oil-fired furnace efficiency of 60 percent, measurements based on the energy delivered to the space-heating subsystem show a net energy savings of only 14.52 million Btu (15.32 billion Joules). However, solar heat that is lost in delivery to the space-heating subsystem (e.g., through ducts) also contributes to building heat. Including this "unmeasured" contribution, the net savings total 50.48 Btu (53.25 billion Joules).

(continued on next page)

Solar energy is collected by 20 double-glazed flat-plate collectors, connected in parallel, with a total area of 805 square feet (75 square meters). Air is the heat-transfer medium. Thermal energy is stored by a rock bin holding approximately 720 cubic feet (20.4 cubic meters). Six operational modes include heating from the solar collectors, storing heat, heating from storage, auxiliary heating with an oil-fired furnace, summer venting, and hot-water preheating.

This work was done by the Federal Systems Division of IBM Corp. for **Marshall Space Flight Center.** *Further information may be found in DOE/NASA CR-161471 [N80-27802/NSP], "Solar Energy System Performance Evaluation — Seasonal Report for Contemporary-Manchester, Manchester, New Hampshire" [$8]. A paper copy may be purchased [prepayment required] from the National Technical Information Service, Springfield, Virginia 22161. The report is also available on microfiche at no charge. To obtain a* microfiche *copy, Circle 45 on the TSP Request Card.*
MFS-25499

A High School Is Supplied With Solar Energy — Dallas, Texas

All the domestic hot water and almost half of the annual building heating requirements are supplied.

An 85-page final technical report includes the details of installation, operation and maintenance, contract negotiation, and the acceptance test plan for a retrofit solar-energy system in a Dallas high school building. The system preheats 100 percent of the domestic hot water and supplies 47.5 percent of annual heating requirements for the three-story, concrete-frame, brick-masonry building with basement.

The building, 56 years old and in excellent structural condition, was recently air-conditioned with a 300-ton (1,100-kilowatt) chilled-water system. The new solar system is interconnected with the cooling system to convert it to a two-pipe heating and cooling system.

The flat-plate collectors are roof-mounted utilizing standard steel supports resting in pitch pans on the flat roof deck. The steam-radiation heating system for the building was abandoned, but the boilers supply steam as a backup heat source.

With the summer/winter switch indexed to "winter," three-way valves isolate the chiller from the heating loop. Water from the storage tanks either preheats the hot-water supply or is mixed with cooler water to supply water at 95° F (35° C) to the primary building heating-system pump. In the "summer" mode, the system operates in its normal cooling mode, and the solar storage supplies domestic hot water.

This work was done by the Dallas Independent School District for **Marshall Space Flight Center.** *Further information may be found in DOE/NASA CR-161482 [N80-29847/NSP], "Solar Heating and Domestic Hot Water System Installed at North Dallas High School" [$9]. A paper copy may be purchased [prepayment required] from the National Technical Information Service, Springfield, Virginia 22161. The report is also available on microfiche at no charge. To obtain a* microfiche *copy, Circle 46 on the TSP Request Card.*
MFS-25514

Materials

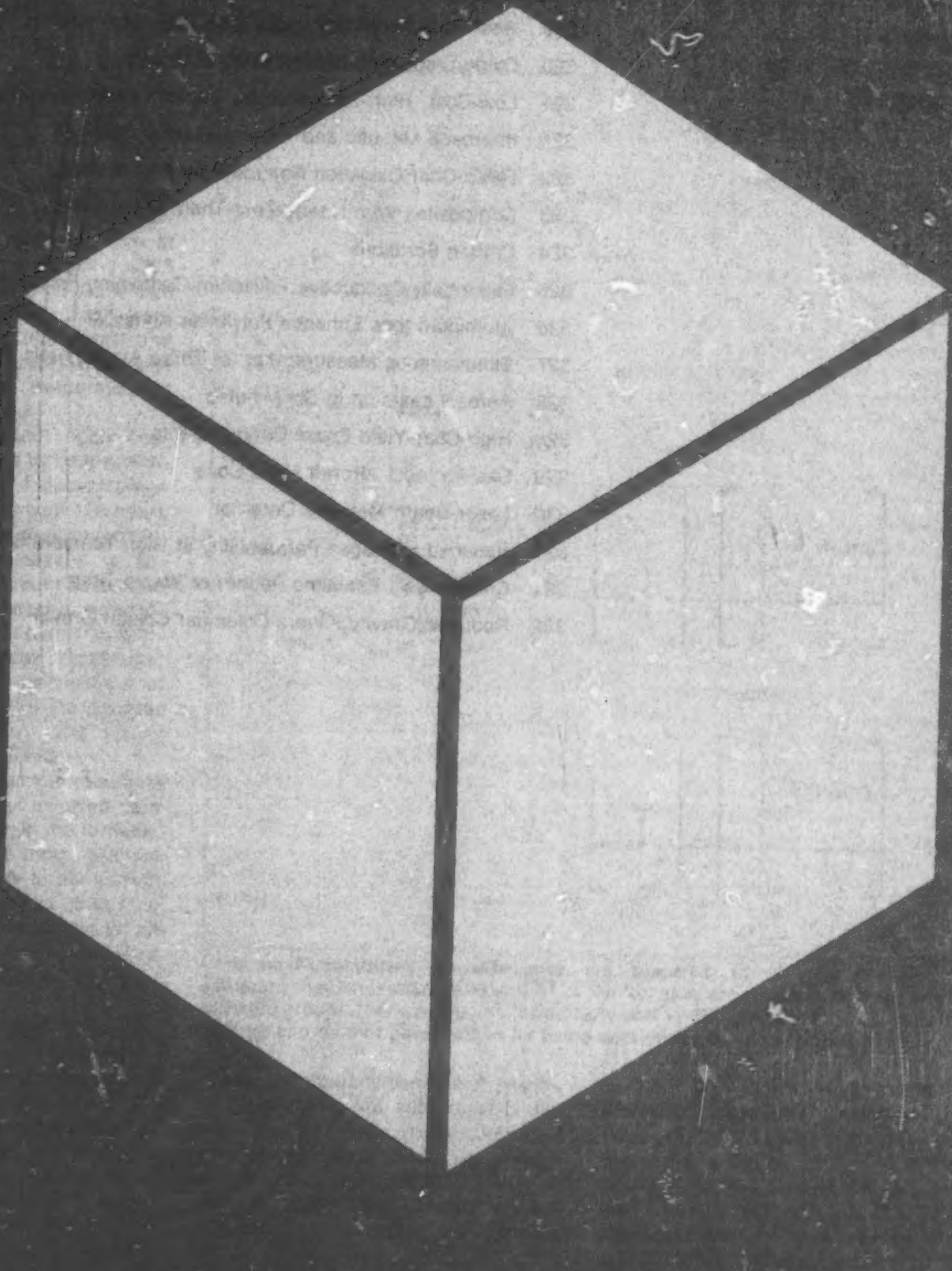

Hardware, Techniques, and Processes

319 Heat-Resistant Polyphosphazene Polymers
320 Oxide-Dispersion-Strengthened Superalloy
321 Low-Cost, High-Temperature, Duplex Coating for Superalloys
321 Improved Metallic and Thermal-Barrier Coatings
322 Resin-Char Oxidation Retardant for Composites
323 Composites With Nearly-Zero Thermal Expansion
324 Carbon Scrubber
325 Electrically-Conductive Palladium-Containing Polyimide Films
326 Aluminum Ions Enhance Polyimide Adhesive
327 Simultaneous Measurement of Three Atmospheric Pollutants
328 Aerosol Lasts up to Six Minutes
328 High-Char-Yield Epoxy Curing Agents
329 Cap Protects Aircraft Nose Cone
330 Laser-Beam Methane Detector
331 Reduced Hydrogen Permeability at High Temperatures
331 Chlorinolysis Reclaims Rubber of Waste Tires
332 Reduced Gravity Favors Columnar Crystal Growth

Heat-Resistant Polyphosphazene Polymers

Polymers of carboranyl-substituted polyphosphazene are stable at high temperatures and produce an insulating char upon pyrolysis.

Ames Research Center, Moffett Field, California

A new process synthesizes carboranyl-substituted polyphosphazenes and their thermal polymerization to heat-resistant polymers. The incorporation of carboranyl groups in the molecules of conventional polyphosphazenes greatly increases their thermal stability. Upon decomposition at extreme temperatures (about 1,000° C), the new polymers produce a high char yield that insulates other less-resistant materials from heat and flame. In contrast, unsubstituted polyphosphazene totally evaporates at about 400° C.

Carboranyl-substituted polyphosphazenes are prepared by heat-polymerizing a carboranyl halocyclophosphazene at 250° C for about 120 hours in the absence of oxygen and moisture. The cyclophosphazene is obtained by reacting a lithium carborane with, for example, hexachlorocyclotriphosphazene at ambient temperature, under anhydrous conditions. For greater stability in the presence of moisture, the chlorine of the polymer is replaced by aryloxy and alkoxy groups, such as CF_3CH_2O-.

The generalized chemical reactions and the compounds involved are illustrated in the figure. In the formula, R is either a hydrogen atom, a lower alkyl radical having up to six carbon atoms, or an aryl radical of up to nine carbon atoms; R^1 is an alkyl group, an aryl group, a halogenated homolog of these groups, or a mixture of any of these groups.

The following example illustrates the process. A solution of hexachlorocyclotriphosphazene (I) was added to phenyl-o-carborane and *n*-butyllithium dissolved in diethyl ether at 25° C. The reaction proceeded for 12 hours at 25° C in an anhydrous environment. The solvent was removed under reduced pressure, and the residue was heated at 80° C and 0.05 mm Hg to remove unreacted starting material. A subsequent increase in temperature to 120° C brought about the volatilization and condensation of phenylcarboranylpentachlorocyclotriphosphazene (II).

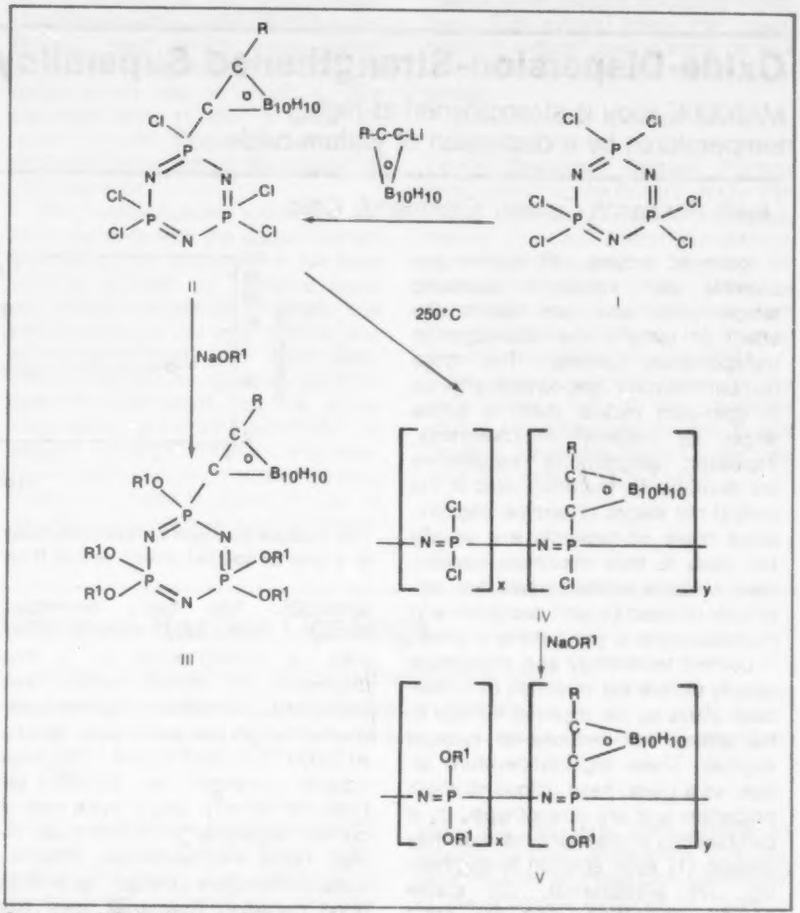

Carboranyl-Substituted Phosphazenes are prepared by heat-polymerizing a carboranyl halophosphazene. R and R^1 in the formulas are members of a number of different groups. In the polymeric formulas IV and V, the ratio of x to y is 2 to 1, the number and type of polymeric units being determined by the structure of II.

Phenylcarboranylpentachlorocyclotriphosphazene was subsequently dissolved in dry THF (tetrahydrofuran) and treated with a solution of sodium trifluoroethoxide in THF for 28 hours at 66° C. After the treatment, the solution was neutralized with concentrated hydrochloric acid and the product isolated by extraction with benzene and dried over magnesium sulfate. Upon filtration and removal of the solvent, phenylcarboranylpentatrifluoroethoxycyclotriphosphazene (III), an oily product, was obtained.

The phenylcarboranylcyclopentachlorotriphosphazene monomer (II) was polymerized by heating in an evacuated tube at 250° C for 120 hours. The next step in the process was chlorine replacement. The polymeric product (IV) was reacted with sodium trifluoroethoxide in boiling THF for 120 hours to yield the fluoroethoxy-substituted polymer (V). The product was concentrated and neutralized with hydrochloric acid and the precipitate filtered off, washed with water, and dried. A fractional precipitation of a

(continued on next page)

THF solution of the product into hexane and benzene gave V. A similar preparation process using methyl-o-carborane, in place of phenyl-o-carborane, yielded methylcarboranylcyclopentachlorotriphosphazene.

This work was done by Larry L. Fewell of **Ames Research Center** *and Harry R. Allcock, John P. O'Brien, and Angelo G. Scopelianos of Pennsylvania State University. For further information, Circle 47 on the TSP Request Card.*

This invention is owned by NASA, and a patent application has been filed. Inquiries concerning nonexclusive or exclusive license for its commercial development should be addressed to the Patent Counsel, Ames Research Center [see page A5]. Refer to ARC-11176.

Oxide-Dispersion-Strengthened Superalloy

MA6000E alloy is strengthened at high temperatures by a dispersion of yttrium oxide.

Lewis Research Center, Cleveland, Ohio

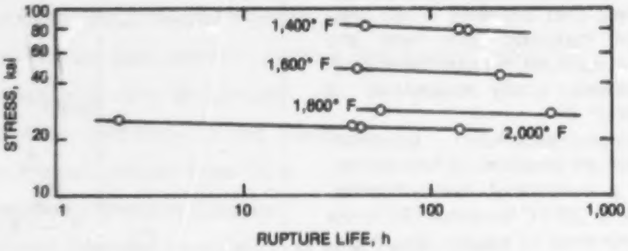

The **Rupture Strength of MA6000E Alloy** is shown for several operating temperatures as a plot of applied stress versus time to rupture.

Improved engine efficiencies are possible with increased operating temperatures and can lessen the effect of today's fuel shortage on transportation systems. The large number of aircraft gas-turbine engines in operation makes them a prime target for material improvements. Increased temperature capabilities are desirable for materials used in the critical hot stages of turbine engines, since these components are usually run close to their maximum capabilities. Material improvements are vigorously pursued by both designers and manufacturers of gas-turbine engines.

Current technology and economics usually dictate the selection of nickel-base alloys as the material for use in the critical hot sections of turbojet engines. These high-temperature alloys, as a class, have unique strength properties and are strengthened by a combination of mechanisms that may include (1) solid solution strengthening, (2) precipitation, (3) stable particle dispersion, and (4) grain structure control.

Until the recent development of mechanical alloying, it has not been possible to combine all of these mechanisms successfully together with oxide dispersion strengthening in one alloy system. A new alloy, MA6000E, has been developed through mechanical alloying. This alloy is strengthened by a fine dispersion of yttrium oxide, and possesses outstanding high-temperature-strength properties (see figure). At 2,000° F (1,090° C) the 1,000-hour rupture strength is 20,000 psi (138×10^6 N/m^2), about twice that of current high-strength nickel-base alloys. Good thermal-fatigue, intermediate-temperature strength, as well as good oxidation resistance give this alloy a unique combination of properties not available in any other material.

This work was done by Thomas K. Glasgow of **Lewis Research Center** *and Y. G. Kim, L. R. Curwick, and H. F. Merrick of Inco Research and Development Center. Further information may be found in:*

NASA CR-135150 [N77-22213/NSP], "Development of an Oxide Dispersion Strengthened Turbine Blade Alloy by Mechanical Alloying" [$7],

NASA CR-159493 [N80-13218/NSP], "Characterization of an Oxide Dispersion Strengthened Superalloy" [$6], and

NASA TM-79088 [N79-20180/NSP], "An Oxide Dispersion Strengthened Alloy for Gas Turbine Blades" [$5].

Copies of these reports may be obtained from the National Technical Information Service, Springfield, Virginia 22161.

LEW-13589

Low-Cost, High-Temperature, Duplex Coating for Superalloys

The high-temperature resistance to oxidation and corrosion of nickel-base alloys is substantially improved by a duplex silicon-slurry / aluminide coating.

Lewis Research Center, Cleveland, Ohio

Energy shortages and fuel substitutes place an increasing demand on power systems and their component materials. Efficient use of such systems can usually be improved by increased operating temperatures. These increased temperatures, however, cause accelerated material degradation in the form of oxidation, hot corrosion, and thermal fatigue. Nickel-base alloys that are widely used in critical sections of some power systems (i.e., turbojet engines) require protective coatings to extend their operating capabilities.

A new low-cost coating has been developed that exhibits significant protection for superalloys from high-temperature, high-gas-velocity oxidation, hot corrosion, and thermal fatigue. The coating is a duplex silicon-slurry/aluminide material approximately 0.01 inch (0.03 centimeter) thick. It was applied to the surface of two high-strength nickel-base alloys, NASA-TRW VI A and B-1900. Both alloys were tested at 2,000° F (1,090° C) in a cyclic oxidation rig test at mach 1. Hot corrosion tests [1,650° F (900° C), mach 0.3, with 5 ppm sea salt injection] were also run on the cooled B-1900 material.

Test results indicate substantial life improvements with the duplex silicon-slurry/aluminide coating over the base material as well as standard pack-cementation aluminide coatings. The performance of this new coating was somewhat different with each alloy, and it may not be quite as good, in specific applications, as the more-expensive platinum/aluminum or MCrAlY coatings. However, with additional characterization of alloy/coating interaction, suitable alloys should be identified that will give superior performance under severe operating conditions. This system offers the opportunity to reduce coating costs as well as to increase material operating capabilities.

This work was done by Stanley G. Young and Daniel L. Deadmore of **Lewis Research Center**. *Further information may be found in NASA TM-79178 (N79-29292/NSP), "An Experimental, Low-Cost, Silicon Slurry/Aluminum High-Temperature Coating for Superalloys" [$5]. A copy may be purchased [prepayment required] from the National Technical Information Service, Springfield, Virginia 22161.*

Inquiries concerning rights for the commercial use of this invention should be addressed to the Patent Counsel, Lewis Research Center [see page A5]. Refer to LEW-13497.

Improved Metallic and Thermal-Barrier Coatings

Low-thermal-conductivity two-layer ceramic coatings are efficient thermal barriers between cooled metallic components and high-temperature combustion gases.

Lewis Research Center, Cleveland, Ohio

Two-layer ceramic thermal-barrier systems (TBS) have been developed that are significantly improved, simple, and highly adherent. These TBS consist of an alloy bond coating and a thermal-barrier coating (TBC). In these systems, bond coatings are either M-Cr-Al-Yb (M $\equiv$ Ni, Co, or Fe), Ni-Al-Y, or improved M-Cr-Al-Y (M $\equiv$ Ni, Co, or Fe) compositions. The TBC is an improved $6Y_2O_3$ or $8Y_2O_3$ stabilized zirconia (composition in weight percent). These TBC's have very low thermal conductivity and therefore impart an efficient thermal barrier between cooled metalic components and high-temperature combustion gases. More importantly, they have significantly longer life than those reported earlier.

Metallic components could typically be combustors, blades, and vanes in aircraft engines or power-generating turbines, or any other cooled heat-engine component. The presence of the improved and more efficient two-layer coatings on cooled components can greatly reduce the metal substrate temperature or minimize coolant requirements.

Experimental evidence indicates that improvements in durability result chiefly from the optimization of the reactive metal (yttrium or ytterbium) content of the bond coating, replacement of yttrium by ytterbium, and optimization of the Y_2O_3 content of the zirconia. Optimization studies to date have also indicated that coating durability is sensitive to the concentrations of Cr and Al in the bond coating.

Moreover, experimental results indicate that the compositions of the bond coat and TBC are more critical in limiting coating adherence and life than the thermal expansion coefficient of the substrate material. In rigorous systematic cyclic furnace tests between 1,095° and 280° C, Ni-17.5Cr-6.6Al-0.14Yb coupled with ZrO_2-$6.1Y_2O_3$ or ZrO_2-$7.8Y_2O_3$ withstood 280 and 206 1-hour cycles, respectively; Ni-19.3Al-0.5Y/ZrO_2-$7.8Y_2O_3$ withstood 198 1-hour cycles; and Ni-25.7Cr-6.6Al-0.3Y/ZrO_2-$7.8Y_2O_3$ withstood 246 1-hour cycles. These results indicate that the improved ceramic thermal-barrier coatings are approximately four times superior to the previously reported Ni-16Cr-6Al-0.6Y/ZrO_2-$12Y_2O_3$ thermal-barrier system. In these studies ytterbium-containing bond coatings were found to be more oxidation resistant than

(continued on next page)

similar yttrium-containing bond coatings.

This work was done by Stephan Stecura of **Lewis Research Center**. *Further information may be found in:*

NASA TM-79206 [N79-29293/NSP], "Effects of Yttrium, Aluminum, and Chromium Concentrations in Bond Coatings on the Performance of Zirconia-Yttria Thermal Barriers" [$6]; and NASA TM-78976 [N78-31212/NSP], "Effects of Compositional Changes on the Performance of a Thermal Barrier Coating System" [$6].

Copies of these reports may be purchased [prepayment required] from the National Technical Information Service, Springfield, Virginia 22161.

Inquiries concerning rights for the commercial use of this invention should be addressed to the Patent Counsel, Lewis Research Center [see page A5]. Refer to LEW-13324.

Resin-Char Oxidation Retardant for Composites

Boron powder stabilizes the char, so that graphite fibers are retained.

Lewis Research Center, Cleveland, Ohio

An effective and simple method has been developed for retarding the oxidation of resin char formed in the burning of resin matrix/graphite fiber composites. The method consists of adding boron to the resin matrix by dispersion in the impregnation mixture applied to the graphite fiber. Addition of as little as 3 percent boron powder by weight effectively maintains the structural integrity of the composite and prevents release of the graphite fibers.

Char formed during the burning of resin matrix composites is a carbonaceous material that oxidizes rapidly in air at temperatures above 1,200° F (650° C). Elemental boron powder added to the composite as a filler material stabilizes the char as it is formed and protects it from oxidation. Resin matrix/graphite fiber composites modified by the addition of boron powder can be exposed to high thermal heat fluxes in air for prolonged periods of time and maintain their structural integrity. The char formed by the thermally decomposed resin is protected from oxidation in air and remains as a functional matrix material that cements the fibers together.

The effectiveness of boron powder as a char oxidation retardant has been demonstrated for both a typical low char forming resin and a typical high char forming resin. Test panels of a low char forming epoxy/graphite composite (HTS/3501-6), such as used in the aircraft industry today, and a high char forming polyimide/graphite composite (HTS/PMR-15) were made both with and without the boron powder filler. The test panels were burned in air by exposure to a radiative heat source of 5.3 Btu/ft^2-s (6.0×10^4 J/m^2-s) for a period of 35 minutes. Results are shown in Figures 1 and 2.

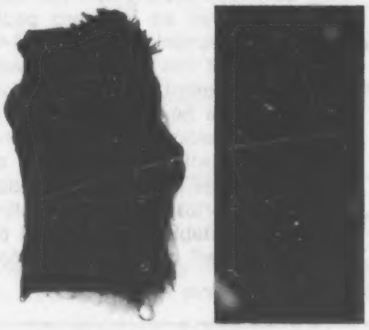
(a) UNFILLED (b) BORON-FILLED

Figure 1. **Graphite /Epoxy Laminates** burned in air by 5.3 Btu/ft^2-s radiation flux are stabilized by boron filler. In (a), the surface of the burned unfilled sample exhibits loose graphite fibers; whereas the surface of the burned boron-filled sample (b) is smooth, shiny, and free of loose graphite fibers.

Figure 1 shows photographs of two panels of the epoxy/graphite composite. The surface of the burned unfilled sample, Figure 1(a), consists of a deep mat of loose graphite fibers. The surface of the burned boron-filled sample, Figure 1(b), is smooth, shiny, and free of loose graphite fibers that are retained within the stabilized char filler material. Panels of the burned polyimide/graphite composite exhibited similar appearances. Both the unfilled epoxy and unfilled polyimide composites were reduced to piles of free graphite fibers after the burning tests were concluded. All boron-filled samples exhibited solid surfaces after burning with no visible free fibers.

Figure 2 shows the comparative resin weight loss for the unfilled and boron-filled (designated /B) epoxy/graphite and polyimide/graphite test panels. (The percent resin weight loss data for the unfilled samples are artificially high because they include a significant amount of fiber weight loss after the first 5 minutes.) Resin weight losses for both the unfilled and boron-filled samples were nearly identical for the first 3 minutes of burning. After 3 minutes, the unfilled samples continued to lose weight while the boron-filled samples stabilized.

Addition of the boron powder filler to resin matrix/graphite fiber composites

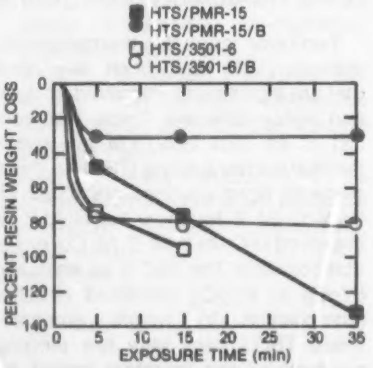

Figure 2. **Resin Weight Loss** of laminates during exposure to 5.3 Btu/ft^2-s thermal radiation in air is nearly identical for the first 3 minutes for both unfilled and boron-filled samples. After 3 minutes, the boron-filled samples (represented by graphs in color) stabilize.

has no significant effect on the mechanical properties of the materials. Density increases by about 1.5 percent. Boron powder addition is easily incorporated into conventional composite processing procedures with minimal modification or interruption.

These resin char oxidation retardant composites can be used in fire-sensitive environments where stringent burnthrough requirements are specified and where structural integrity when exposed to burning is essential.

This work was done by K. J. Bowles and R. E. Gluyas of **Lewis Research Center.** *Further information may be found in:*

NASA TM-79314 [N80-14196/NSP], "Burning Characteristics and Fiber Retention of Graphite/Resin Matrix Composites" [$5], and

NASA TM-79288 [N80-13171/NSP], "Improved Fiber Retention by the Use of Fillers in Graphite Fiber/Resin Matrix Composites" [$5].

Copies of these reports may be purchased [prepayment required] from the National Technical Information Service, Springfield, Virginia 22161.

Inquiries concerning rights for the commercial use of this invention should be addressed to the Patent Counsel, Lewis Research Center [see page A5]. Refer to LEW-13275.

Composites With Nearly-Zero Thermal Expansion

Graphite, glass, and resin composite is unusually strong, stiff, and thermally stable.

Lyndon B. Johnson Space Center, Houston, Texas

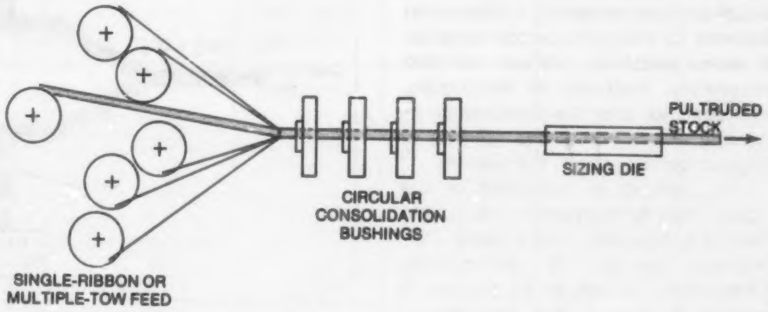
PULTRUDED STOCK
SIZING DIE
CIRCULAR CONSOLIDATION BUSHINGS
SINGLE-RIBBON OR MULTIPLE-TOW FEED

Glass/Graphite Fibers in a Resin Matrix Are Pulled through a sizing die, forming structural rods or bars. The process, which is economical and continuous, may be fed by a single ribbon of resin-impregnated fibers or by multiple reels that pass through a resin bath (not shown). The sizing die has a rectangular cross section or a circular cross section.

A new composite has a near-zero coefficient of thermal expansion and a high modulus of elasticity. The material thus combines exceptional dimensional stability over a wide temperature range with unusually high strength and stiffness.

The composite consists of graphite fibers and glass fibers in a plastic resin matrix. The constituents are inexpensive and lightweight, and the composite material is produced by an economical process — "pultrusion" (see figure).

Developed for large truss structures in space, the composite is also suited to applications in optics and communications. In the truss structures, the composite is used as narrow rods that overlap in an open lattice; where the rods overlap, they are joined by an encapsulant. As a mounting material for antennas, mirrors, and lenses, the glass/graphite composite can eliminate serious structural distortion.

The graphite fibers have a negative coefficient of thermal expansion, and the glass fibers and resin matrix have a positive coefficient; that is, the graphite contracts and the glass and resin expand as the temperature increases. When the materials are combined in the proper proportion, they produce a nearly thermally-inert composite material.

The matrix for the fiber may be a polysulfone, an epoxy, a polyimide, or other resin. The proportion of the constituents for a nearly thermally inert composite was found to be 14.2 percent glass fiber, 38.5 percent graphite fiber, and 47.3 percent resin (percentages by volume).

For maximum elastic modulus and zero thermal-expansion coefficient, it is important that the fibers be oriented in the same direction and that the glass fibers be uniformly distributed among the graphite fibers. To ensure these conditions, rods of the composite are made by pulling a preimpregnated ribbon of glass and graphite fiber through a die. The ribbon is just wide enough to fill an 0.08- by 0.08-inch (2- by 2-mm) sizing die. Four bushings precede the sizing die and consolidate the ribbon in steps. The bushings are heated to 750° F (399° C) and the sizing die is heated to 500° F (260° C). The pull rate varies from 6 to 20 inches/min (15 to 51 cm/min). As an alternative to preimpregnation, the fibers can be pulled through a resin bath as part of the pultrusion process.

The final product is only three-fifths as dense as aluminum, yet has an elastic modulus of 18 to 24 million psi (1.2 to 1.7×10^{11} N/m^2). The thermal-expansion coefficient can be adjusted negatively or positively by altering the proportions of glass and graphite and

(continued on next page)

by adding fibers at an angle to the main axis of the bars.

This work was done by Thomas J. Dunn of **Johnson Space Center** *and Anthony J. Cwiertny, Jr., Vernon L. Freeman, and Read Johnson, Jr., of McDonnell Douglas Corp. Further information may be found in NASA CR-160558 [N80-19144/NSP], "Development of a Composite Geodetic Structure for Space Construction"* **[$7]**. *A copy may be purchased [prepayment required] from the National Technical Information Service, Springfield, Virginia 22161.*
MSC-18724

Carbon Scrubber

Automated membrane separation is usod to remove inorganic carbon from samples to be analyzed for "total organic carbon."

Lyndon B. Johnson Space Center, Houston, Texas

An online flow system utilizes a pH-dependent equilibrium reaction and a semipermeable membrane to remove inorganic carbon from samples to be analyzed for total organic carbon. It was developed for use with automated water-analysis systems. Unlike other systems for inorganic carbon removal, it works passively, without complex machinery, methods, or techniques, and does not alter the composition or content of any nonionized species of organic compounds in the system.

The method is illustrated in the figure. A sample stream is divided into two equal streams. In one stream the aqueous solution is continuously mixed with a strongly acidic reagent to convert carbonate and bicarbonate ions to dissolved carbon dioxide gas. In the second stream the aqueous solution is continuously mixed with an alkaline reagent. The alkaline reagent converts carbon dioxide to carbonate and bicarbonate ions.

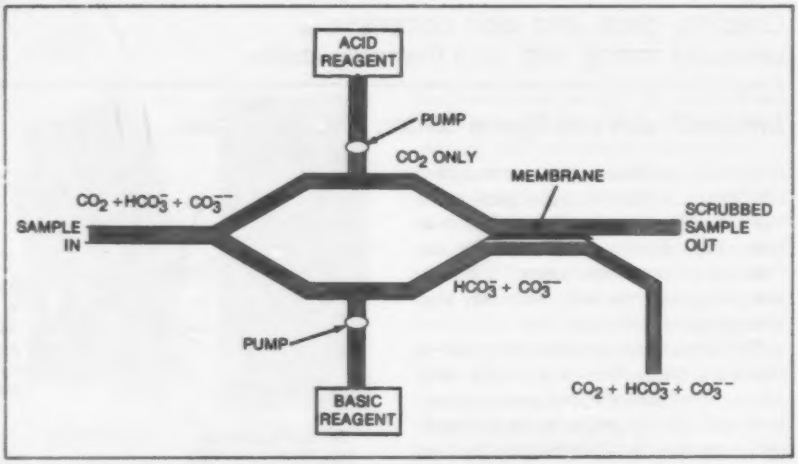

A **Semipermeable Membrane** separates two sample streams, one of which is treated with an acid reagent and the other with a base. Carbonate and bicarbonate ions are converted to dissolved CO_2 by the acid; the reverse process occurs in the basic stream. Only CO_2 is passed by the membrane, from the acid-treated stream to the base-treated stream. Thus, the acidic stream emerges free of all species of inorganic carbon.

The acidic and basic solutions then flow past opposite sides of a membrane permeable to dissolved carbon dioxide gas and impermeable to carbonate and bicarbonate ions. Since there is no carbon dioxide in the basic solution, the dissolved carbon dioxide in the acidic solution tends to flow across the membrane. After crossing the membrane, the carbon dioxide is converted to carbonate and bicarbonate ions and cannot recross. The process continues removing carbon dioxide from the acidic solution. The length of the membrane and the flow rate of each mixed stream determine the degree to which inorganic carbon is removed from the acidic solution. A sample stream containing 1,000 ppm of inorganic carbon prior to stripping was found to contain 1 ppm after 30 seconds of residence in the stripper.

The constant flows of alkaline and acid reagents are maintained by a pump. The use of a single pump, adding equal volumes of reagent to sample streams, results in equal dilution of the sample streams.

The semipermeable membrane used in the method is made from such material as silicone rubber, porous polypropylene, or porous tetrafluoroethylene. A typical acid reagent used in the scrubber is $H_2SO_4(NH_4)_2S_2O_8$, and a typical alkaline reagent used is NaOH.

When the inorganic carbon removal is complete, the alkaline stream contains all the inorganic carbon; and the acidic stream, free of inorganic carbon, can be measured for total organic carbon. The total organic carbon is oxidized in the acidic solution to form carbon dioxide, the concentration of which is monitored with a potentiometric electrode.

This work was done by Martin S. Frant of Orion Research Inc. for **Johnson Space Center.** *For further information, Circle 48 on the TSP Request Card.*
MSC-16531

Electrically-Conductive Palladium-Containing Polyimide Films

Addition of palladium reduces electrical resistivity.

Langley Research Center, Hampton, Virginia

A palladium complex has been added to a polyimide film to make it more conductive. Because polyimide films can be lightweight, thermally stable, and flexible, they are currently being considered as materials for large space structures. To dissipate electric charge in this application, the films should possess antistatic properties with an electrical resistivity of 10^8 to 10^{10} ohm-cm.

Linear condensation polyimides, however, are not conductive by nature, having electrical resistivities of the order of 10^{17} ohm-cm. Attempts to lower the resistivity have been made by doping the polymers with such metals as aluminum or with carbon microspheres. These approaches led to an unwanted increase in weight of the material, a much embrittled film, uneven dispersion of the additive throughout the film, and a degradation in thermal and mechanical properties.

The palladium polyimide film is prepared in four general steps: (1) the preparation of a polyamic acid in a polar solvent, (2) the addition of a soluble palladium complex salt, (3) fabrication of a thin film of the "palladium-polyamic acid" solution, and (4) thermal imidization of the film to the palladium-containing polyimide by heating at 300° C.

The polyamic acid solution is prepared by adding an equivalent amount of 3,3',4,4'-benzophenone tetracarboxylic acid dianhydride (BTDA) to a stirred solution of 4,4'-oxydianiline (ODA) in an amide solvent. The palladium-containing complex is then added using a 1:4 mole ratio of the metal species to the polymer. After several hours stirring, a viscous polymer is formed with the structure shown in the figure.

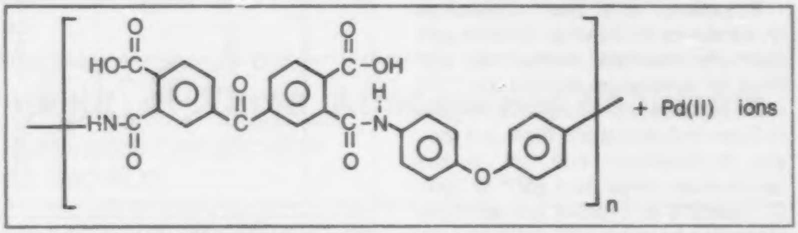

Palladium Polyimide Complex can be used to make a light, flexible film with sufficiently low resistivity to relieve space charging.

Film	Volume Resistivity[a] (ohm-cm)	Surface Resistivity (ohm)	Metal Content	T_g[b] (°C)
Polymer alone	1.0×10^{17}	1.0×10^{17}	0	282
Polymer + Li_2PdCl_4	2.0×10^6	9.5×10^5	0.17% Li 5.33% Pd	338
Polymer + $Pd[S(CH_3)_2]_2Cl_2$	very low[c] $<10^5$	very low[c] $<10^5$	0.23% S 7.02% Pd	343
Polymer + Na_2PdCl_4	2.3×10^{15}	———	1.36% Na 4.69% Pd	372
Polymer + $PdCl_2$	2.3×10^{11}	———	2.97% Pd	281

[a] Electrical resistivities were measured according to ASTM method of test D257-66.

[b] Glass transition temperatures determined by thermomechanical analysis at 5° C/min in static air

[c] Unmeasurable due to overloading at 10 volts

Test Data on Palladium-Containing Polyimide Films

The electrical conductivity of the polymer is entirely dependent upon the presence of palladium. The best results were obtained using Li_2PdCl_4 or $Pd[S(CH_3)_2]_2Cl_2$ as a source of the metal. As shown in the table, volume and surface resistivities of films containing these two complexes were dramatically lowered when compared to the polymer alone. A lesser decrease in electrical resistivity was achieved with other palladium salts. Good solubility of the palladium salt in the polyamic acid is necessary for achieving conductivity.

The lowered electrical resistivities of these palladium polyimide films were achieved without a loss in film flexibility and with a minimal increase in the weight of the film. Resistivities obtained (10^6 or lower) by the addition of Li_2PdCl_4 and $Pd[S(CH_3)_2]_2Cl_2$ should be low enough to relieve space-charging effects.

This work was done by Anne K. St. Clair of **Langley Research Center** *and T. A. Furtsch, and L. T. Taylor of Virginia Polytechnic Institute and State University. For further information, Circle 49 on the TSP Request Card. LAR-12629*

Aluminum Ions Enhance Polyimide Adhesive

Adding complexed aluminum ions raises the useful temperature of polyimide adhesive without embrittling it or reducing long-term stability.

Langley Research Center, Hampton, Virginia

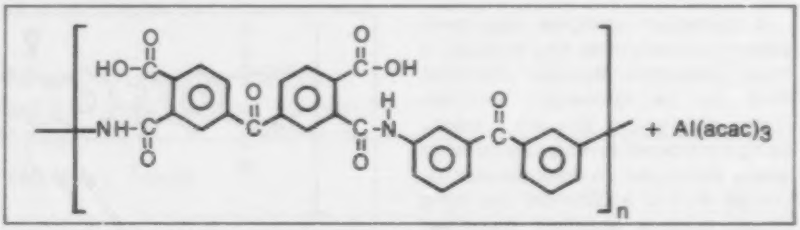

Structural Unit of Aluminum-Ion-Containing Polyimide

Polymer	T_g(°C)[a]	PDT(°C)[b]	RT	Lap Shear Strength (psi)[c]		
				250° C	275° C	300° C
With $Al(acac)_3$	271	555	2,380	1,890	1,640	700
Polymer alone	251	570	2,970	1,570	0	0

[a] Glass transition temperature determined by thermomechanical analysis at 5° C/min in static air

[b] Polymer decomposition temperature determined by thermogravimetric analysis at 2° C/min in air

[c] Lap shear tensile strength on titanium alloy determined according to ASTM D-1002 (CTM No. 26)

Test Data on a polymer formulated from BTDA and 3,3'-DABP with $Al(acac)_3$ are compared to those for the polymer without aluminum ions.

Polyimides have been considered as adhesives for bonding titanium and thermally resistant composites and films for aerospace applications. The room-temperature adhesive strengths of linear polyimides are high, but they are thermoplastic and fail in the temperature range from 250° to 300° C. Attempts to improve the adhesive properties have generally reduced the long-term thermal stability of these resins.

Previous modifications that have improved the adhesive properties of linear polyimides include polymer preparation from isomeric meta-oriented aromatic diamines, polymer preparation in certain water- or alcohol-miscible ether solvents, and the addition of large amounts of aluminum powder to the resins prior to bonding. The addition of metal fillers, however, causes a drastic increase in weight and a less-flexible adhesive joint.

It has been discovered that the high-temperature strength of a polyimide adhesive can be improved (see table) by adding complexed aluminum ions without introducing excessive weight or embrittling the adhesive. In the process:

1. A polyamic acid solution is prepared in a solvent or mixture of solvents, one of which is a water- or alcohol-miscible ether.
2. Aluminum ions are added to the solution as tri(acetylacetonato)aluminum, $Al(acac)_3$.
3. The aluminum and polyamic acid solution is applied to a substrate prepared for bonding.

The aluminum-ion-containing adhesives can be applied to a suitably-prepared substrate surface as the neat resin with or without supports such as glass fabric. The substrates can be metal (titanium, steel, aluminum), composite (graphite/polyimide, graphite/epoxy, glass/polyimide, glass/epoxy), or polymeric film (either metalized or unmetalized). The coated substrates are allowed to stand for solvent evaporation or are prestaged to a certain temperature for solvent removal. They are then bonded together using heat (250° to 300° C) and, if necessary, pressure [50 to 200 psi (3.4×10^5 to 1.4×10^6 N/m^2)]. The heat evaporates any remaining solvent and converts the solution to a thermally-resistant cyclic polyimide containing aluminum ions. During this process, an excellent adhesive bond is formed.

The aluminum-ion-containing polyamic acid is prepared by adding an equimolar quantity of 3,3',4,4'-benzophenone tetracarboxylic acid dianhydride (BTDA) to a stirred solution of 3,3'-diaminobenzophenone (3,3'-DABP) in a water- or alcohol-miscible ether solvent or mixture of solvents, one being an ether. The $Al(acac)_3$ complex is then added to the solution at a concentration of 2 to 3 percent by weight. The reaction is carried out at room temperature, and the result is a viscous, homogeneous polymeric solution. The polyamic acid is characterized by a recurring unit with the structural formula illustrated.

Ultimate success of the adhesive at high temperature depends upon the presence of the $Al(acac)_3$ complex. The solvents useful for this process are of the aliphatic acyclic and cyclic ether types. Such solvents have a high affinity for the polar chemical groups of the aromatic polyamic acid intermediates, in contrast to aromatic water-immiscible solvents.

During the cure, the $Al(acac)_3$ maintains integrity as a metal complex rather than converting to a free metal. (This behavior has been confirmed by X-ray photoelectron spectroscopy.) This is believed to be the reason that the adhesive is able to maintain excellent strengths at high temperature. Other polyamic acid systems containing metal acetylacetonates are converted upon curing to the polyimide plus free metal and are essentially useless as high-temperature adhesives.

As opposed to a metal-powder-filled polymer, the polymer containing aluminum ions maintains the flexibility of a linear system without embrittlement caused by a free metal filler. This makes the adhesive an excellent candidate where flexibility of the bond line is required. In addition, at a metal-to-polymer weight loading of 2.5 percent, a considerable weight savings is realized compared to a polymer loaded with 80 percent aluminum powder.

This work was done by Anne K. St. Clair and Terry L. St. Clair of **Langley Research Center** *and Larry T. Taylor of Virginia Polytechnic Institute and State University. For further information, Circle 50 on the TSP Request Card.*

This invention is owned by NASA, and a patent application has been filed. Inquiries concerning nonexclusive or exclusive license for its commercial development should be addressed to the Patent Counsel, Langley Research Center [see page A5]. Refer to LAR-12640.

Simultaneous Measurement of Three Atmospheric Pollutants

Proposed method would enable simultaneous concentration monitoring of atmospheric SO_2, NO, and NO_2.

NASA's Jet Propulsion Laboratory, Pasadena, California

Although fluorescence is often used in separate measurements of atmospheric sulfur dioxide (SO_2), nitric oxide (NO), and nitrogen dioxide (NO_2), a sensitive and simultaneous measurement of these three pollutants is needed. Lasers have been used to detect NO_2, which has an absorption band in the visible part of the spectrum; but for SO_2 and NO, fluorescence is usually induced by discharge lamps, because of the lack of a suitable ultraviolet laser.

The three pollutants would be measured simultaneously by a proposed method that utilizes a dye laser with a fundamental output frequency in the visible spectral region and a second harmonic in the ultraviolet. Dye lasers with output wavelengths in the visible region and at 217 nm in the ultraviolet region are already in existence.

The method is illustrated in the figure. When both visible and ultraviolet frequencies from the dye laser are passed through the gas sample, the visible frequencies are absorbed by the NO_2 molecules while the ultraviolet frequencies are absorbed by SO_2 and NO. The subsequent fluorescence of these gases is detected by separate photomultipliers, each with optical filters to select the characteristic emissions of one of the three gases. The photomultiplier outputs are then fed to a signal processor unit for storage and subsequent analysis.

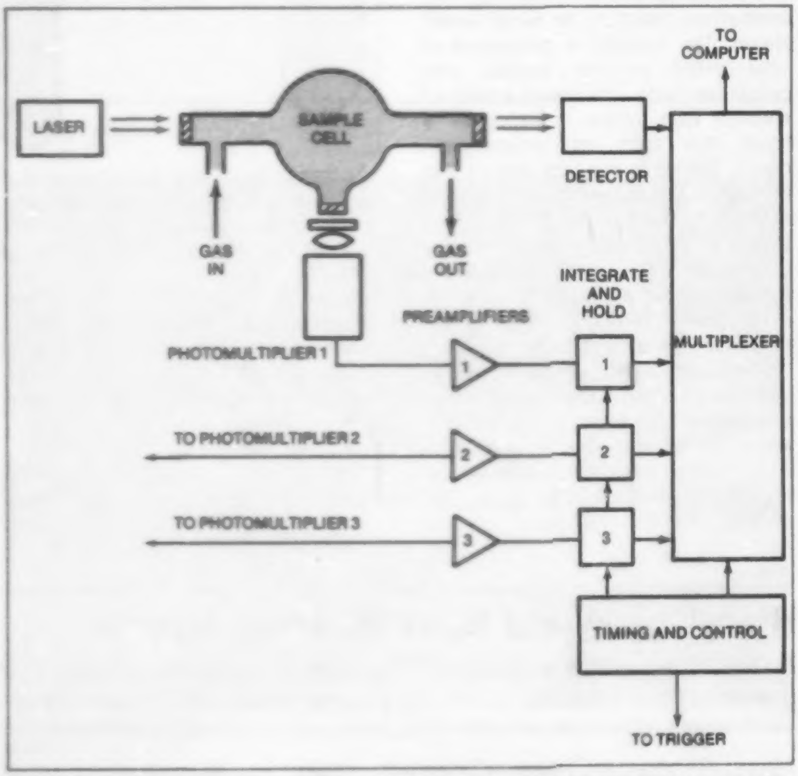

Fluorescing Pollutant Gases in the sample cell are excited by the visible output of a dye laser together with its second-harmonic ultraviolet frequencies. The fluorescence is viewed by three photomultipliers, each with suitable optical filters. For added sensitivity, the sample cell may be placed in a multipass cavity.

This method would eliminate the errors in sequential analysis that occur when the gas concentrations or flow characteristics are rapidly changing. It could be applied to the probe of ambient air, stack emissions, and highway automotive exhausts and may help to provide an understanding of the transport and dispersion properties of these gases.

This work was done by Mahadeva P. Sinha of Caltech for **NASA's Jet Propulsion Laboratory.** *For further information, Circle 51 on the TSP Request Card.*
NPO-14828

Aerosol Lasts up to Six Minutes

Catalytic generator ejects a high-visible lasting mist.

NASA's Jet Propulsion Laboratory, Pasadena, California

A simple, nonpolluting method for generating a highly visible aerosol aids in studying the wakes of aircraft and similar turbulent aerodynamic effects. The aerosol, a mist of dye and water vapor, lasts for as long as 6 minutes at ground level.

An aerosol is generated by the apparatus shown in the figure. Compressed hydrogen peroxide flowing over a catalyst bed is converted, in an exothermic reaction, to superheated steam. The catalyst is composed of silver-plated screens coated with potassium oxide. The steam enters an ejection tube where it vaporizes a liquid dye such as tetraethylene glycol. Baffles in the tube ensure that the dye is completely mixed with the steam before it is ejected. Tests show that the ejected mixture quickly condenses into a fog of particles approximately 1 μm in diameter — the most visible size — that remain suspended for as long as 6 minutes.

The superheated aerosol persists much longer than those produced by conventional aerosol generators, which last for only about a minute or less. Unlike aerosols produced by skywriting airplanes, it does not depend on the formation of ice crystals at cold high altitudes for visibility and is environmentally safe.

Because of its duration and visibility, the aerosol can be used to study turbulent aerodynamic effects, such as wakes produced by flying aircraft. One important application would be to study vortexes left behind moving aircraft. Though these last only several minutes, they are considered dangerous to following aircraft, particularly near ground level.

This work was done by Marshall A. Appel of Caltech for **NASA's Jet Propulsion Laboratory.** *For further information, Circle 52 on the TSP Request Card.*
NPO-14947

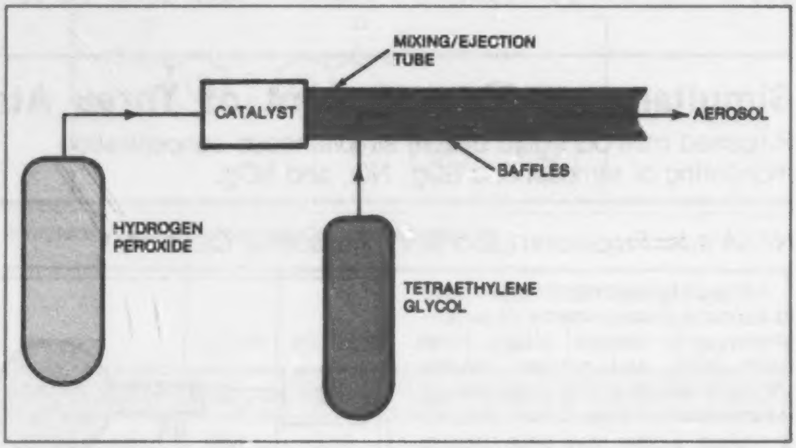

This **Simple Aerosol Generator** catalytically converts hydrogen peroxide to superheated steam and then mixes this steam with a dye. The highly visible mist can be used to study aerodynamic turbulence.

High-Char-Yield Epoxy Curing Agents

A new class of imide-amine curing agents preserves structural integrity, prevents fiber release, and is fully compatible with conventional epoxy resins.

Lewis Research Center, Cleveland, Ohio

Epoxy resins are the most widely used matrix resins in graphite-fiber-reinforced resin matrix composite materials because they are easy to process and because fiber-reinforced epoxies have excellent mechanical properties. However, the char yield of conventional epoxy resins is quite low, usually less than 25 percent. When exposed to a high heat flux such as produced by a fire, these composites lose their structural integrity, and free graphite fibers are released. A novel class of imide-amine curing agents has been synthesized, which more than double the char yield of cured epoxy resins, preserving structural integrity and preventing fiber release.

The imide-amine curing agents are fully compatible with conventional epoxy resins and do not detract from composite properties while greatly increasing char yield.

Conventional graphite-fiber/epoxy-resin composite specimens and neat (unreinforced) epoxy-resin specimens, both with and without the imide-amine curing agents, were fabricated and tested for mechanical properties, thermo-oxidative stability, and char yield. Processing characteristics with and without the imide-amine curing agents are similar. Mechanical properties are equivalent. All specimens exhibited essentially the same level of thermo-oxidative stability. In char yield tests, the epoxy resins with the imide-amine hardeners exhibited a 200- to 300-percent increase in aerobic char yield and as much as a 100-percent increase in anaerobic char yield.

The development of these imide-amine curing agents is a major breakthrough in achieving high-char-yield epoxy resins. Composite materials utilizing these curing agents can be used in aerospace, automotive, and other structural components where structural deterioration must be minimized and fiber release must be avoided in the event of fire.

This work was done by Peter Delvigs, Tito T. Serafini, and Raymond D. Vanucci of **Lewis Research Center.** *Further information may be found in NASA TM-79226 [N79-29240/NSP], "High Char Imide-Modified Epoxy Resins" [$5]. A copy may be purchased [prepayment required] from the National Technical Information Service, Springfield, Virginia 22161.*

This invention is owned by NASA, and a patent application has been filed. Inquiries concerning nonexclusive or exclusive license for its commercial development should be addressed to the Patent Counsel, Lewis Research Center [see page A5]. Refer to LEW-13226.

Cap Protects Aircraft Nose Cone

A polycarbonate cap protects aircraft nose cone from erosion.

Langley Research Center, Hampton, Virginia

An inexpensive, easily fabricated cap significantly reduces the costs of repairing nose-cone erosion on aircraft. Made of molded polycarbonate, the cap has been flight-tested and is in use on NASA T-38 aircraft (see figure).

Nose cones and other sections that house radar, radio, or other avionics equipment on some aircraft are usually made of fiberglass to allow transmission or reception of an electromagnetic signal. The fiberglass nose cones, which are especially vulnerable to rain, hail, or dust, eventually erode and must be replaced. For example, on the T-38 aircraft, the unprotected fiberglass nose cones had to undergo inspection twice a year. Roughly 50 percent of the cones had to be replaced annually, at a cost of material and labor for removal, inspection, and repair.

The polycarbonate caps are easily fabricated from commercially available 0.16-cm (1/16-in.) polycarbonate sheets by vacuum forming over a mold. Molding temperatures of only 464 K (375° F) are used. After molding, the interior concave surface of the cap is roughened to enhance adhesion, and the cap is applied to the nose cone with a polyester adhesive. Any required coloring is added to the adhesive resin.

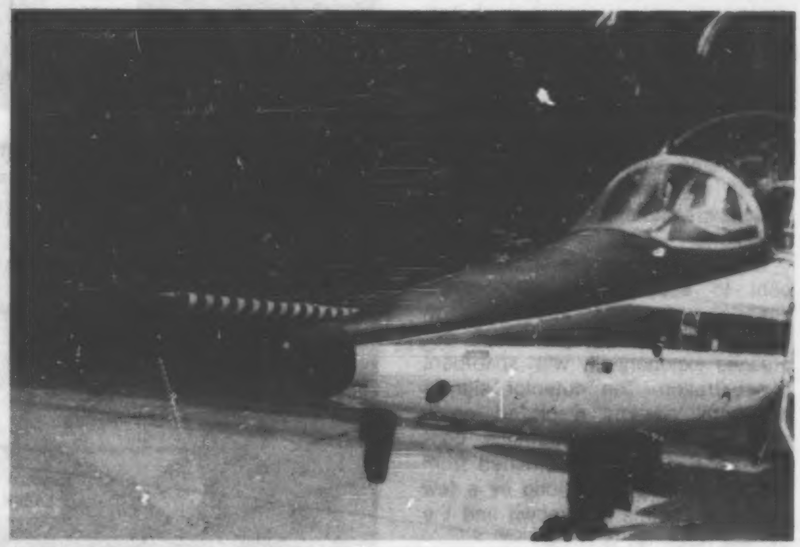

A **Polycarbonate Cap** on the T-38 nose cone protects the fiberglass cone from erosion.

The polycarbonate caps have been under development for several years. Their strength and erosion characteristics are superior to those of the fiberglass cones that the caps protect. Some caps have been tested in-place on T-38 aircraft for over 5 years. Thus far, not a single polycarbonate cap has required replacement. Polycarbonate caps have been tested at both subsonic and supersonic speeds, and a polycarbonate cap on the foresection of the T-38 luggage pod has also been tested. More extensive flight-testing of polycarbonate caps is planned.

This work was done by Charles F. Bryan, Jr., and Donald C. Bryan of **Langley Research Center.** *For further information, Circle 53 on the TSP Request Card.*
LAR-12367

Laser-Beam Methane Detector

Laser instrument determines methane concentration in liquid-natural-gas vapor.

NASA's Jet Propulsion Laboratory, Pasadena, California

A 3.39-μm wavelength helium/neon laser instrument determines the amount of methane in liquid-natural-gas (LNG) vapor. Methane concentration is measured by two InAs infrared detectors that monitor the intensity of the beam passing through the gas. The amount of radiation absorbed by methane at 3.39 μm is proportional to methane concentration. The instrument can be used in modeling the spread of LNG clouds, an important subject in studying the hazards of LNG spills in populated areas, and as a leak detector on LNG carriers and installations.

The laser and its power supply are contained in an enclosure (see photo). The detectors (designated as sensors 1 and 2) are mounted in a column alined with the laser beam. Sensor 1 is located at a height of 2.5 m; and sensor 2, at 1.5 m. A third detector at the column base monitors the laser output, to ensure that the measurements are not affected by power variations.

Gas enters adjustable airgaps adjacent to each sensor. The beam intensity remaining after passage through the absorbing medium decreases exponentially with absorbent concentration. The detector signals are amplified and displayed on a strip-chart recorder. Methane concentration is easily determined from the sensor outputs as long as a few calibration points are known and the system response is linear.

During the initial tests, the detectors remained within their linear-response range up to 6-mV output. The system was tested using a 1-cm-long calibration cell, with methane concentrations from 0 to 100 percent. Linearity and agreement between the two sensor channels were confirmed.

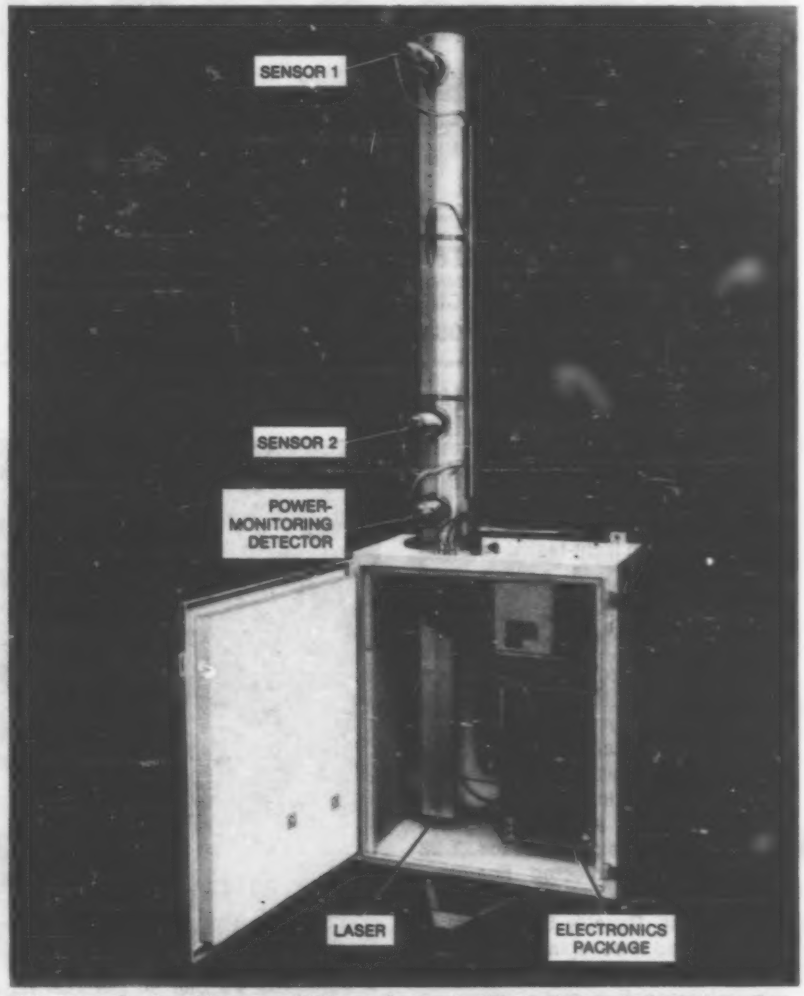

This **Laser System Measures Methane Concentration** by infrared absorption. Two sensors measure the intensity of the 3.39-μm laser beam after it passes through the gas; the absorption is proportional to the concentration of methane.

Though not essential to the detection of methane, several thermistors are mounted near the sensors and in the box near the laser and other electronic components to record the operating temperature. (This would be needed to monitor the system in a hot desert environment.) Provision is also made for air-conditioning to maintain stable temperature in hot environments. The unit includes wheels for mobility and can be operated vertically (as shown) or horizontally. A dynamic range of 10^6 is available, assuming operation at 6 mV, with an ultimate detector noise limit of 6 nV.

This work was done by Everett D. Hinkley, Jr., of Caltech for **NASA's Jet Propulsion Laboratory.** *For further information, Circle 54 on the TSP Request Card.*
NPO-14929

Reduced Hydrogen Permeability at High Temperatures

CO and CO_2 reduce hydrogen loss through iron-, nickel-, and cobalt-based alloy tubes.

Lewis Research Center, Cleveland, Ohio

Hydrogen gas is being used as a working fluid in a prototype automotive Stirling engine. Advantages may be achieved over the standard internal-combustion engine in terms of efficiency, fuel consumption, and emissions. The Stirling engine, which is being considered for automotive applications, uses hydrogen gas at high temperatures and high pressures in a closed system. At high temperatures, loss of hydrogen from permeability through the metal containers becomes a serious problem.

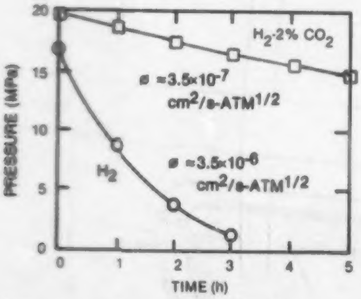

Hydrogen Pressure Loss at high temperatures in Incoloy-800H alloy tubes is up to an order of magnitude smaller when the hydrogen is doped with 2 percent carbon dioxide.

A method has been devised to reduce hydrogen permeability through iron-base, nickel-base, and cobalt-base alloys at high temperature. This method is based on the known concept that an oxide film on a metal surface reduces hydrogen permeability through the metal. The innovation is too add CO or CO_2 to the hydrogen in order to form oxide films continuously during operation. As a result, hydrogen containment at high temperatures is improved.

Tests were run with high-pressure containment tubes at temperatures of 1,400° F (760° C). The iron-, nickel-, and/or cobalt-base alloy tubes were filled with hydrogen gas that had been doped with 0.2 to 5 volume percent of CO or CO_2 gas. Hydrogen permeability rates were reduced by up to an order of magnitude. The necessary factors in reduced permeabilities in addition to an oxygen source such as CO or CO_2 in the hydrogen appear to be the presence of chromium and such other strong oxide formers as aluminum, columbium, or lanthanum in the alloys. The figure shows the reduction in hydrogen permeability, as indicated by loss in pressure, for Incoloy-800H alloy tubes using 2-percent-CO_2-doped hydrogen as compared to undoped H_2.

This research may act as a guide for the development of specific alloys to be used in conjunction with high-pressure, high-temperature hydrogen gas. This should in turn improve the prospects for increased utilization of the Stirling-engine system.

This work was done by J. R. Stephens, W. D. Klopp, and J. A. Misencik of **Lewis Research Center**. *No further documentation is available.*
LEW-13485

Chlorinolysis Reclaims Rubber of Waste Tires

A new process reclaims rubber and reduces sulfur content.

NASA's Jet Propulsion Laboratory, Pasadena, California

Disposing of or reclaiming the almost 100 million rubber tires scrapped annually in the United States presents many problems. Traditionally, the reclaim process consists of heating ground-up rubber tires in swelling agents after the cord and metal have been removed. Rubber reclaimed in this manner has poor hysteresis and abrasion resistance, making it unsuitable for premium radial tires.

A new process reclaims waste rubber by using chlorine gas to oxidize the sulfur bonds in preference to other bonds. At the same time, the chlorine gas adds chlorine atoms to the double bonds of the rubber molecules; this reduces depolymerization by preventing oxidation of the carbon/carbon bonds. The chlorinated rubber is less susceptible to swelling by oils and may be used as a paint ingredient. Rubber hydrochloride, a similar product, is an established packing film.

In a typical treatment, 50 grams of acetone-washed ground scrap rubber containing about 5 percent calcium carbonate are slurried with 400 grams of trichloroethane and 10 grams of water. The slurry is heated to boiling and chlorine gas is bubbled through at 0.18 liter/minute for from 1 to 4 hours. The liquid is then filtered through a Buchner funnel and washed with water to remove sulfates. The chlorinated product is washed with acetone to determine if other new compounds are

(continued on next page)

produced. The product is then vacuum-dried to remove all solvent.

Elemental analysis of the carbon, hydrogen, sulfur, and chlorine in rubber treated this way shows a large reduction in sulfur content and a sharp increase in the chlorine content. This process takes place without much depolymerization, though extensive chlorine addition at the rubber-polymer double bonds occurs. There is no measurable substitution of hydrogen atoms by chlorine atoms.

This work was done by Eugene R. du Fresne, Jan Harper Tervet, and Glen G. Hull of Caltech for **NASA's Jet Propulsion Laboratory.** *For further information, Circle 55 on the TSP Request Card.*

Inquiries concerning rights for the commercial use of this invention should be addressed to the Patent Counsel, NASA Resident Office-JPL [see page A5]. Refer to NPO-14935.

Reduced Gravity Favors Columnar Crystal Growth

In zero-gravity, alined columnar microstructures form at the expense of equiaxed growth.

Marshall Space Flight Center, Alabama

Alined columnar crystalline microstructures are preferred in castings for which the directional dependence of physical properties is beneficial (such as in turbine blades). However, many complex alloys preferentially form axial rather than columnar microstructures.

Recent experiments aboard sounding rockets indicate that in low gravity, it should be possible to produce completely columnar microstructures with no equiaxed crystal growth. Small samples of NH_4Cl-H_2O were tested as model systems. Experiments were performed during a 250-second free-fall period, when gravitational acceleration was less than 10^{-4} g.

The heart of the apparatus used in the experiment is a solidification chamber (see figure). A semicylindrical copper chill block has been brazed to a stainless-steel top plate. The plastic (Plexiglas or equivalent) front and rear faces are sealed with O-rings. A copper web transmits heat to and from the cell. The particular cell geometry was chosen to extract heat radially, to simulate weld bead solidification, and to allow a camera to observe the experiment.

At 1 g, depending on the amount of superheating and on the orientation of the chill block in the gravitational field, the columnar zone accounted for 25 to 100 percent of the structure. Equiaxed-grain multiplication occurred by showering and by convection-induced dendrites on remelting. These dendrites act as nuclei for the formation of equiaxed grains.

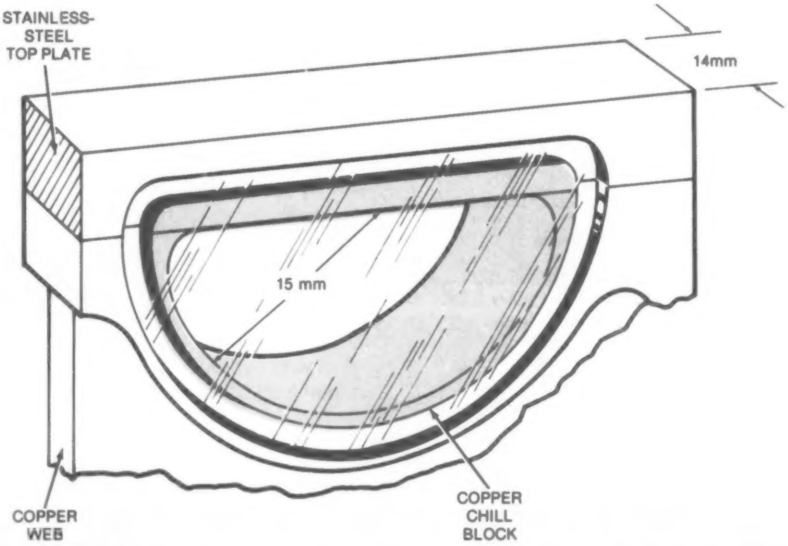

A Solidification Chamber, used to grow columnar structures preferentially, consists of a semicylindrical copper chill block brazed to a stainless-steel top plate. In experiments aboard sounding rockets, four chambers were symmetrically arranged about, and attached to, a copper web.

At low gravity, however, completely columnar structures were obtained; all equiaxed-grain multiplication mechanisms were suppressed. Reduced gravity apparently modified the thermal conditions and caused the liquid to cool more slowly. This resulted in steeper temperature gradients in the liquid ahead of the solidification interface. This interface is believed to be a determining factor in the columnar-to-equiaxed transition. The growth rate of the solid was not affected. Although in two cases a spring-loaded expansion piston jammed, causing "big-bang" nucleation and distributing nuclei throughout the liquid, an equiaxed zone did not form. Apparently, low gravity eliminates the columnar-to-equiaxed transition in this system; verification of the results with other metals and alloys is needed.

This work was done by Theodoulos Z. Kattamis and John M. Papazian of Grumman Aerospace Corp. for **Marshall Space Flight Center.** *For further information, Circle 56 on the TSP Request Card.*
MFS-25205

Life Sciences

Hardware, Techniques, and Processes

335 Flow Sensor for Biomedical Fluids
336 Treating Domestic Wastewater With Water Hyacinths
337 Compliant Transducer Measures Artery Profile
337 Improved Ureteral Stone Fragmentation Catheter
338 Miniaturized Physiological-Data Telemetry System

Books and Reports

339 Manual for Physical Fitness

Flow Sensor for Biomedical Fluids

Electronic sensor would accurately measure and control flow of plasma, whole blood, or drugs in solution.

Lyndon B. Johnson Space Center, Houston, Texas

A flow-rate sensor shows promise as an instrument for measuring the rate of injection of intravenous biomedical fluids. Originally developed for a water-quality measurement system [see "Meter for Very Slow Flows" (MSC-18112) on page 275 of *NASA Tech Briefs*, Vol. 3, No. 2], the sensor would noninvasively determine the amount of whole blood, plasma, or drug solutions administered to a patient. In combination with a valve or pump, the sensor would control the flow as well as measure it.

The complete apparatus (see figure) consists of intravenous delivery equipment with two metal segments in the delivery tubing, a thermal-flow sensor, control electronics, and a proportioning valve or peristaltic pump. The sensor uses thermistors to measure the temperature of the flowing biomedical fluid at two points in the delivery tube. Before the fluid passes the downstream thermistor, a small resistor heats the fluid just enough to keep the temperature sensed by the downstream thermistor at a predetermined level above that sensed by the upstream thermistor. The electric power consumed by the resistor to maintain the temperature difference is a measure of the flow rate.

The thermistors and resistor embedded in epoxy or other insulating material would contact curved metal plates in a groove on a plastic housing. The insulation insures that the heat from the resistor goes predominantly into the fluid. The fluid delivery tube would be placed in the groove so that its two metal segments, which could be stainless steel or a good thermal conductor such as copper or silver, contact the two metal plates in the housing. The resistor and thermistors thus have a low-thermal-resistance path to the fluid.

Electronic circuits measure the temperature difference between the thermistors, regulate power to the resistor, and calculate and indicate the flow rate. The circuitry also would generate a signal for the flow-control pump or valve.

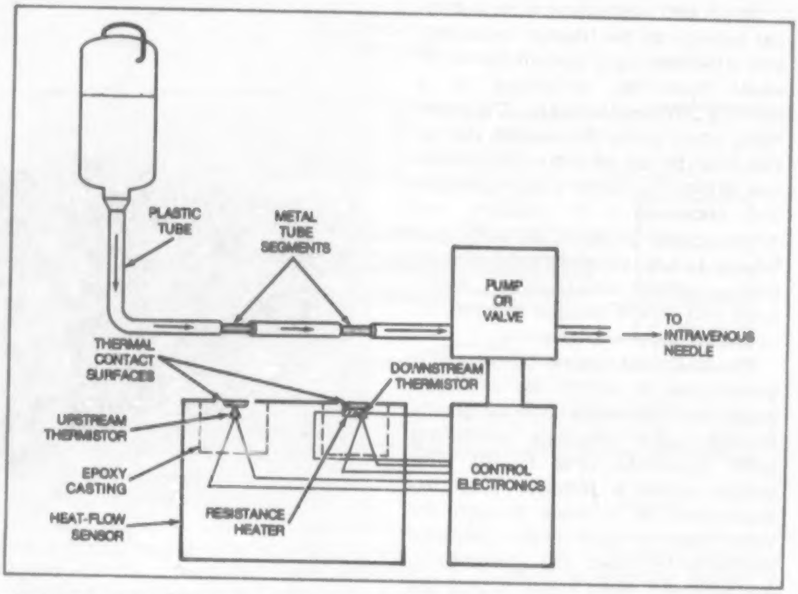

Upstream and Downstream Thermistors have a constant temperature difference maintained between them by a resistance heater. The electric power consumed by the heater in maintaining the constant temperature difference is a measure of the flow rate. This measure is used to control accurately the flow rate through the pump or valve.

The usual way to supply biomedical fluids is from a bottle, elevated to provide a gravity pressure head to force the fluid through a plastic tube and a hypodermic into the patient's body. A small pinch valve is used to control the fluid flow manually, the flow being estimated by counting the frequency of the drops of fluid at the mouth of the glass bottle. The error with this flow estimation method is ±15 percent.

With the new sensor, the fluid flow would be set and maintained at a precise rate. Since infusion-pump rates typically vary from 0.04 cc/hour to 4.00 cc/hour, the new sensor would have to function in this range. The pump would be controlled continuously to compensate for changes in upstream pressure as the bottle empties. Since the sensor responds to a temperature difference, rather than absolute temperature, it would not be very sensitive to the temperature at which the fluid is supplied — an important advantage since biomedical fluids are sometimes used directly as they come from the refrigerator. The sensor would also detect when air replaces liquid in the tube and could stop the pump to prevent air from being injected into the patient's veins when the bottle is empty.

Since the sensor would not directly contact the fluid, it would not have to be sterilized. It is compatible with disposable bottles, tubes, and the hypodermic needles widely used in hospitals. The only modification necessary is in the tube, which must contain two small metal inserts, spaced to fit in the curved thermistor plates.

This work was done by H. Eugene Winkler of **Johnson Space Center.** *For further information, Circle 57 on the TSP Request Card.*

Inquiries concerning rights for the commercial use of this invention should be addressed to the Patent Counsel, Johnson Space Center [see page A5]. Refer to MSC-18761.

Treating Domestic Wastewater With Water Hyacinths

Greenhouse system purifies water, extracts fertilizers, and generates fuel.

Marshall Space Flight Center, Alabama

Waste and wastewater from individual homes can be treated separately and effectively by a system based on water hyacinths, according to a recently proposed concept. The treatment would purify the wastewater so that it can be reused and would extract usable plant nutrients, rich in nitrogen and phosphorus. In addition, the system could produce methane gas for use as fuel. When fully developed, such a system may supplant septic tanks and central sewage systems for rural and undeveloped areas.

The treatment system consists of a greenhouse in which the domestic waste and wastewater flow by gravity through spiral channels containing water hyacinths (see figure). The soluble waste is removed from the wastewater as it flows through the water hyacinth roots where chemical elements (nitrogen and phosphorus) are removed. Solid waste settles out of the wastewater and decomposes in an anaerobic digestion tank, producing enough methane to heat the greenhouse during the winter months. After the solid waste is removed, the purified water is disinfected with ozone, ultraviolet light, or chlorine and recycled to the house.

The waste and wastewater are pumped to the top channel in the greenhouse, and a check valve in the main sewage line prevents backflow. Reflectors are positioned in the greenhouse to light the hyacinths in the bottom channels.

The number of square feet (meters) of plants needed varies according to their growth rate. Under controlled conditions, the water hyacinths grow rapidly, increasing their weight by 5 to 11 percent every day.

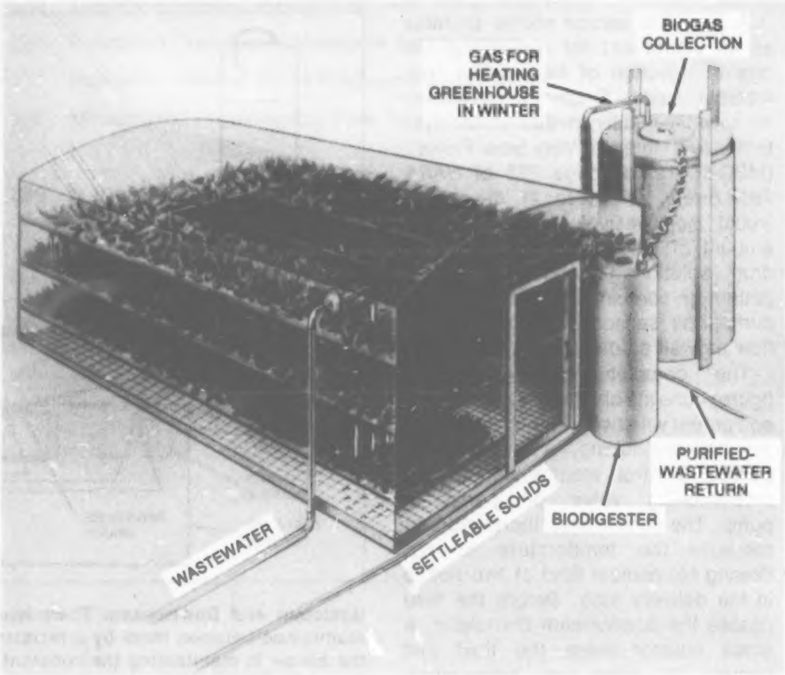
BIOGAS COLLECTION
GAS FOR HEATING GREENHOUSE IN WINTER
PURIFIED-WASTEWATER RETURN
BIODIGESTER
SETTLEABLE SOLIDS
WASTEWATER

This **Waste-Recycling System** uses water hyacinths to purify wastewater and generate methane gas as a byproduct. A system with 200 ft^2 (18.6 m^2) of water hyacinths would treat the wastewater of a family of four (1,500 liters/day) and would generate 600 to 850 ft^3 (17 to 24 m^3) of biogas.

The flow channels in the greenhouse should furnish 50 square feet (4.65 square meters) of plant surface area for every person or for 100 gallons (378 liters) of wastewater. The channel flow depth should be adjustable from 4 to 12 inches (10 to 31 centimeters) so that the retention time can be varied according to the water quality desired. Once the balance of nutrient loading to plant biomass produced is established, excess water-hyacinth growth can be harvested monthly and converted by anaerobic digestion to additional methane or by composting to organic fertilizer and soil conditioner.

This work was done by Rebecca C. McDonald and B. C. Wolverton of the National Space Technology Laboratory for **Marshall Space Flight Center.** *For further information, Circle 58 on the TSP Request Card.*
MFS-23964

Compliant Transducer Measures Artery Profile

Springy fingers give a continuous recording of artery diameter.

NASA's Jet Propulsion Laboratory, Pasadena, California

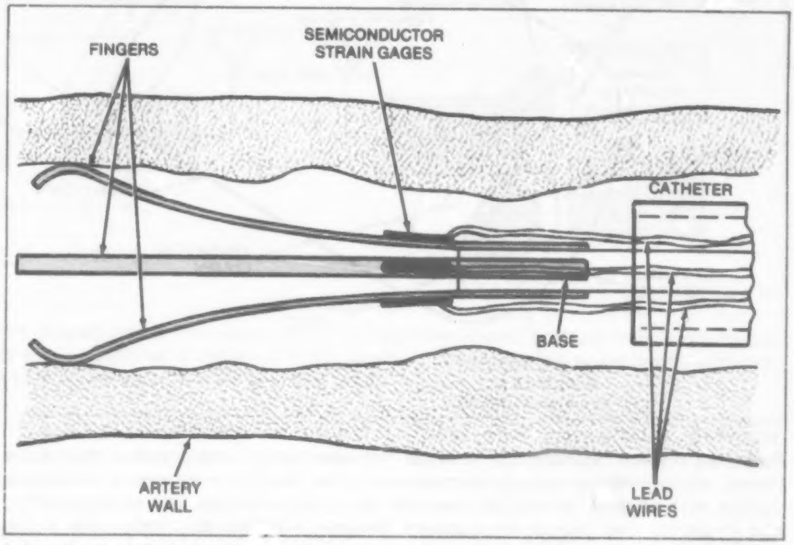

Artery Contour Transducer Has Fingers that move to conform to the walls. Semiconductor pickups convert the finger movements to proportional electrical signals. A catheter is used to place the instrument in an artery.

A new instrument accurately measures the inside contours of arteries without using X-rays or dyes. Consisting of compliant fingers with attached semiconductor sensors, the instrument is drawn through the artery to allow the fingers to follow the internal contours. Levels of stenosis and plaque can be quantified, along with the artery profile, from a continuous output on a pen recorder.

Two, three, or more compliant fingers may be used, each attached to a base and each with its own semiconductor pickup (see figure). Lead wires transmit electrical signals from the pickups to external processing equipment. The signals are converted to diameter data and displayed as a function of position along the artery.

The contour transducer is emplaced in a catheter, which is inserted in the artery by conventional methods. The catheter is then separated from the transducer, and both are pulled along the artery. As the transducer travels, its fingers press lightly against the artery wall and move in and out to reflect its contours. Because the fingers are thin, they do not interfere appreciably with blood flow.

Tests have shown that the finger pressure is so small that there is no visible enlargement of the artery as the transducer moves along. Reproducibility tests, in which recordings were made by repeatedly drawing the transducer along the same section of an artery, have shown that successive strip-chart traces match each other to a high degree.

This work was done by Cyril Feldstein and Virgil H. Culler of Caltech and Donald W. Crawford and James R. Spears of the University of Southern California for **NASA's Jet Propulsion Laboratory.** *For further information, Circle 59 on the TSP Request Card.*
NPO-14899

Improved Ureteral Stone Fragmentation Catheter

An improved catheter would include a fiber-optic viewer, a more reliable ultrasonic probe, and a better contact sensor.

NASA's Jet Propulsion Laboratory, Pasadena, California

Ureteral stones affect about 60,000 Americans every year. Many cases are treated nonsurgically by removing the stones with a Dornier stone basket or, more recently, by using ultrasonic catheters. Catheters using ultrasonically-driven wire probes have already been used with success; however, some improvements are needed.

One of the problems is in guiding the catheters with the assistance of X-rays or fluoroscopes. X-rays and fluoroscopes expose the patient to unnecessary radiation and are not very accurate in verifying when the probe is in contact with the stone. Another problem is the durability of the apparatus. The ultrasonic driver-to-probe coupling can overheat and break.

One suggested improvement is to use fiber-optic viewers to observe the stone directly at distances ranging between 0.5 and 1.0 cm. Two fiber bundles are needed (see figure): one to illuminate the path and the other for viewing.

(continued on next page)

best copy available

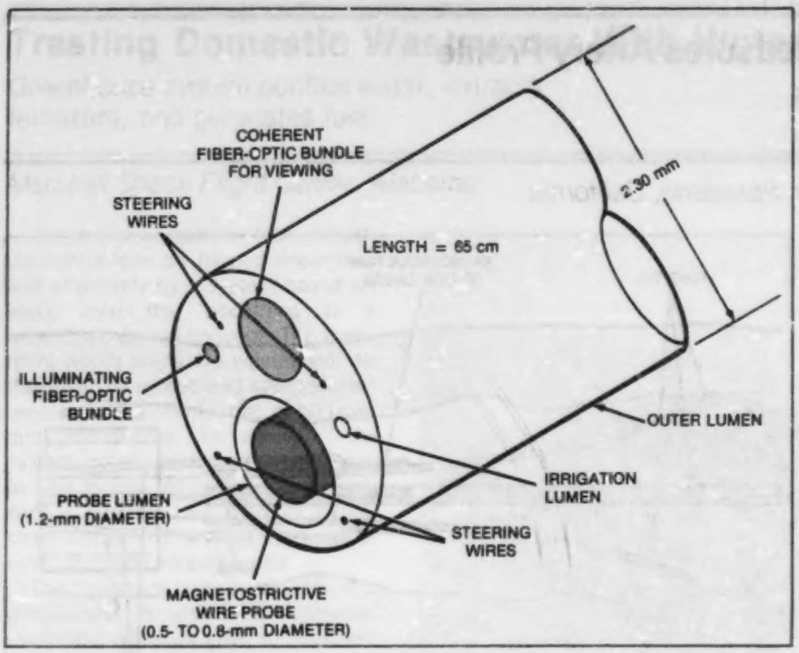
COHERENT FIBER-OPTIC BUNDLE FOR VIEWING
STEERING WIRES
LENGTH = 65 cm
2.30 mm
ILLUMINATING FIBER-OPTIC BUNDLE
OUTER LUMEN
IRRIGATION LUMEN
PROBE LUMEN (1.2-mm DIAMETER)
STEERING WIRES
MAGNETOSTRICTIVE WIRE PROBE (0.5- TO 0.8-mm DIAMETER)

Proposed Ureteral Stone Fragmentation Catheter would incorporate a fiber-optic viewer, a more-reliable magnetostrictive wire probe, and improved means of sensing contact with ureteral calculi. The catheter would be guided by four steering wires, and irrigation fluid would be supplied through a lumen to remove the stone fragments.

Another improvement is to energize the magnetostrictive probe along most of its length. This will help to distribute the stress and prevent probe breakage. To produce 25-μm axial sinusoidal displacements, the probe would be made from magnetostrictive material and wound with a coil that generates a magnetic-field intensity of 200-ampere turns/in.

Finally, contact with stones can be determined by sensing the change in mechanical impedance. This impedance can be sensed photoelectrically or electrically. In the first, an optical sensor comprised of light source, lens, and phototransistor can sense the mechanical displacement and produce a signal to increase the level of the ultrasound when the probe contacts the stone. The displacement could also be sensed electromechanically. In the second, the influence of the mechanical impedance upon the electrical impedance of the driving coils would be sensed.

All of these improvements can probably be incorporated into a 65-cm-long by 2.30-mm-diameter catheter. The catheter would be steered by four wires and equipped with an irrigation lumen. The lumen would supply fluids to remove the stone fragments.

This work was done by Paul M. Gammell of Caltech for **NASA's Jet Propulsion Laboratory.** *For further information, Circle 60 on the TSP Request Card.*
NPO-14745

Miniaturized Physiological-Data Telemetry System

Low-power portable unit has 13 data channels and two-way voice communication.

Lyndon B. Johnson Space Center, Houston, Texas

A portable digital physiological-data telemetry system uses less power, is more compact, and provides better data integrity than two previous systems designed to similar specifications. A block diagram of the portable unit (to be worn by the subject) and the base unit is shown in the figure.

The portable unit transmits 13 data channels to the base unit of which 6 are analog channels (350-Hz-bandwidth each) and 7 are dc data channels (30-Hz-bandwidth each). Three of the analog channels transmit electrocardiogram (ECG) signals (insulated electrodes can be used).

After signal conditioning, the analog data signals are converted to digital form and transmitted serially, using Manchester biphase-coded pulse code modulation (PCM). A modified phase-locked loop decodes the data. The loop has a narrow lock-in range and remains in operation even if the signal from the portable unit is momentarily interrupted.

The telemetry system also has two-way (narrow-band FM) voice communication. Voice transmission from the portable unit interrupts data transmission and is controlled by a voice-operated switch (VOX).

To reduce power drain and to prevent transmission interruption by the subject under crisis, the base unit controls power to most subsystems in the portable unit via a transponder. The base unit also selects the portable-unit operating modes, such as calibrate,

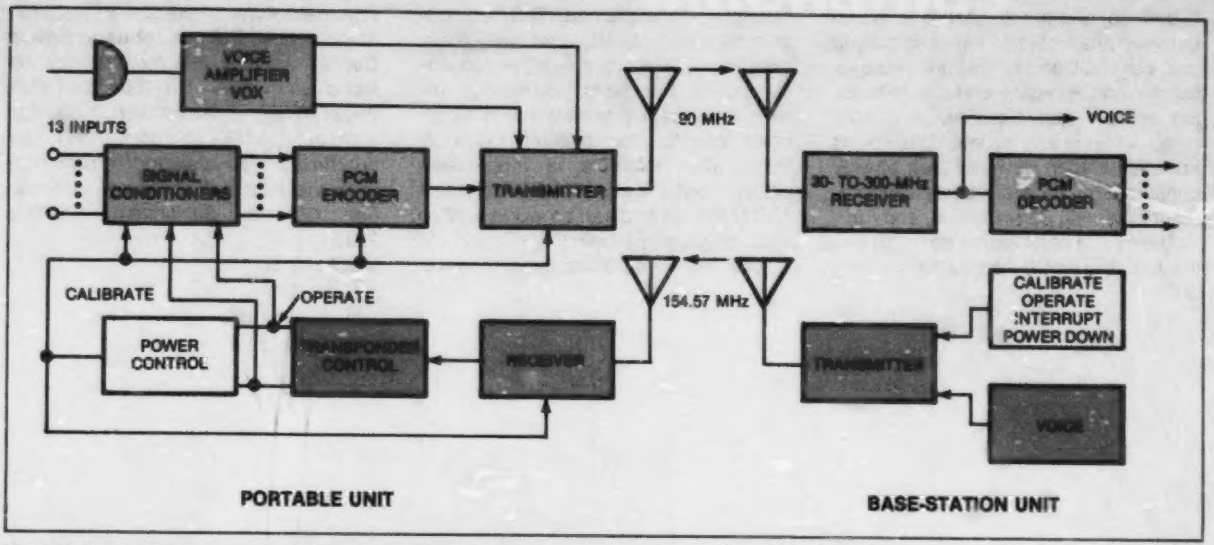

The **Miniaturized Physiological-Data Telemetry System** has a low-power-drain (1/3-watt-maximum) portable unit, worn by the subject, and a base-station unit. The portable-unit transmitter is mounted in the headset. The remaining portable-unit circuitry, measuring 2.5 by 4.5 by 1.25 inches (6.4 by 11.4 by 3.2 cm), is worn in a belt pack.

operate, interrupt (the portable unit receives but does not transmit), or power down (the portable unit samples received signals periodically, until directed to change mode).

All circuits use CMOS flat-pack integrated circuits for minimum power consumption and small size. The RF links in the portable unit operate between 8 and 10 volts and are powered by a standard 9-volt transistor-radio battery. The analog circuits operate at ± 5 and ± 2.5 volts from small nickel/cadmium batteries.

The base station uses a commercially available transmitter and receiver and converts the data received back into analog form. The system operates reliably in all modes at distances of up to 100 ft (30m).

This work was done by William M. Portnoy and Lawrence J. Stotts of Texas Tech University for **Johnson Space Center.** *Further information may be found in CR-160660 [N80-24357/NSP]. "A Miniaturized Digital Telemetry System for Physiological Data Transmission" [$7]. A copy may be purchased [prepayment required] from the National Technical Information Service, Springfield, Virginia 22161.*
MSC-18804

Books and Reports

These reports, studies, and handbooks are available from NASA as Technical Support Packages (TSP's) when a Request Card number is cited; otherwise they are available from the National Technical Information Service.

Manual for Physical Fitness

Personalized programs for becoming and staying fit are included in the *Astronaut Training Manual.*

The 250-page training manual used for preflight conditioning of NASA astronauts will be enjoyable and beneficial reading for anyone interested in physical fitness. Written for an audience with diverse backgrounds and interests, the *Astronaut Training Manual* suggests programs for various levels of fitness, including sample starter programs, safe progression schedules, and stretching exercises. Related information on equipment needs, environmental considerations, and precautions can help readers design safe and effective running programs.

A starter jogging program is recommended for people who can be classified as being in "fair or better" condition according to standards set forth in the manual. Lasting 21 weeks, this program allows beginners to build their cardiorespiratory endurance safely to the point where they can readily jog for 20 minutes continuously, four times a week. Swimming and cycling are among the other exercises for which sample training programs are given.

In addition to endurance training, strength training programs are suggested. The strength programs may be pursued concurrent with the endurance programs and may be performed by lifting free weights, doing isometric exercises, or working out on a mechanical gym. Stretching exercises (which make the body more flexible) are recommended for the morning, during work, before training, after training, during travel, before bed, and for relief of low-back tension. For all programs, performance norms for men and women are included.

The reader is amply furnished with the background needed to design and implement a personalized program. In a discussion of energy sources, fitness is defined, and the distinction is drawn between anaerobic activities (including golf, baseball, and tennis) and more-effective and efficient endurance-building aerobic activities (including running, cycling, and swimming). Sports are evaluated in terms of their energy consumption, hazard, fitness, development potential, convenience, and fun.

The nature of muscular strength and the principles of schemes for building strength are explained. The relationship between obesity, diet, and exercise is explored, and—in an appendix—busy but weight-conscious fitness trainees are provided with a calories counter for popular fast-food items. (For example, a three-piece crispy fried-chicken dinner furnishes 1,170 calories and can be worked off in a run of roughly 1 hour.)

This work was done by A. Eugene Coleman of the University of Houston at Clear Lake City for **Johnson Space Center**. *Further information may be found in NASA CR-160758 [N80-29024/NSP] "Astronaut Training Manual" [$15]. A copy may be purchased [prepayment required] from the National Technical Information Service, Springfield, Virginia 22161.*
MSC-18915

Mechanics

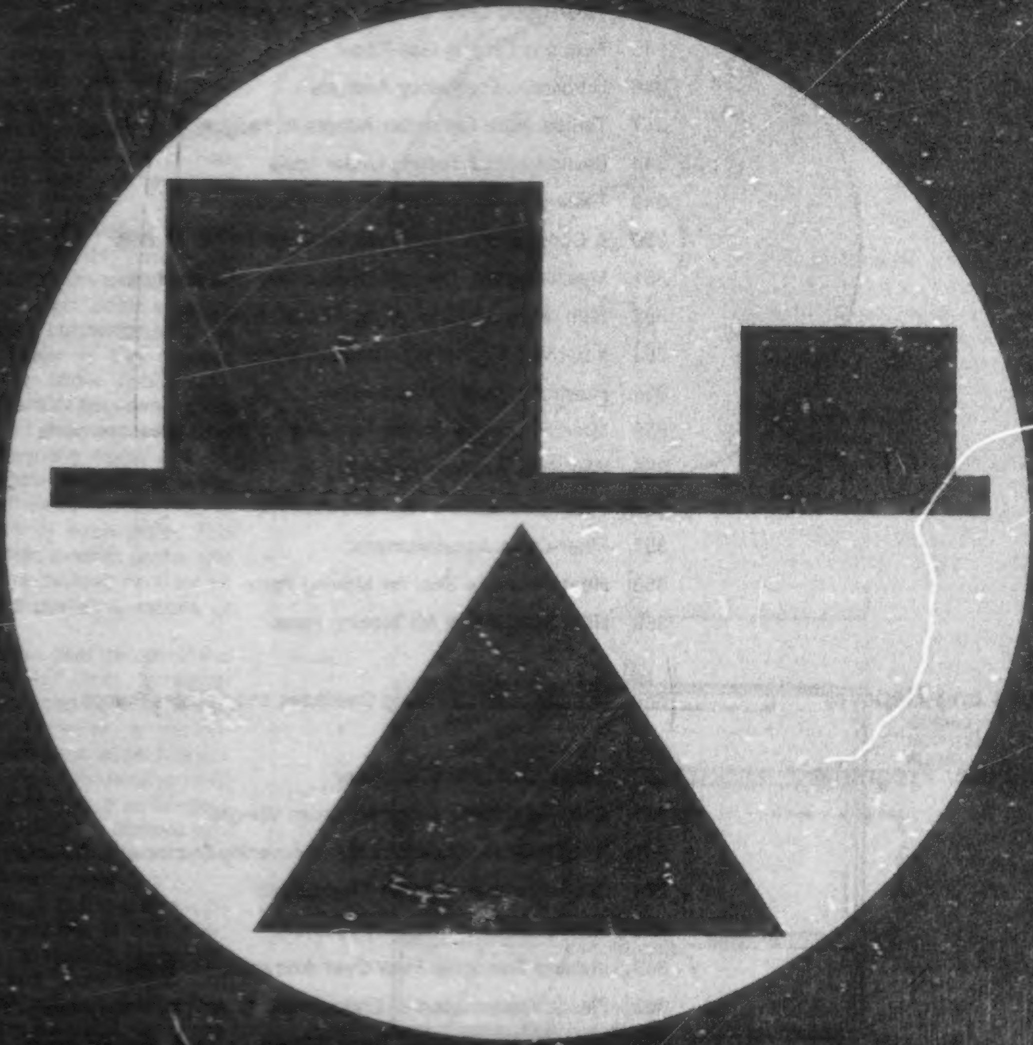

Hardware, Techniques, and Processes

343 Holes Help Control Temperature
344 Fast-Response Cryogen-Level Sensor
345 Fiber-Optic Level Sensor for Cryogens
345 Acoustic Lens is Gas-Filled
346 Ultrasonic Frequency Analysis
347 Temperature Controller Adapts to Fatigue Tester
348 Environmental Testing Under Load
349 Testing Panels in Tension and Flexure
350 A Construction Technique for Wind-Tunnel Models
351 Measuring the Thermal Conductivity of Insulation
352 Rain, Fog, and Clouds for Aircraft Simulators
353 Improved Magnetic Material Analyzer
354 Electronic Depth Micrometer
355 Interchangeable Spring Modules for Inertia Measurements
355 Wakeflow Analysis by COST
356 Integrated Material-Surface Analyzer
357 Fiber-Optic Accelerometer
358 Heat/Pressure Seal for Moving Parts
359 Heat Switch Has No Moving Parts

Books and Reports

359 Dynamics of Cavitating Cascades and Inducer Pumps

Computer Programs

360 Simplified Thermal Analyzer
361 Resizing Structures for Minimum Weight
361 NASTRAN Modifications for Recovering Strains and Curvatures
361 Cost-Minimized Aircraft Trajectories
362 Aerodynamic Preliminary Analysis
363 Inviscid Transonic Flow Over Axisymmetric Bodies
363 Plastic Deformation of Engines and Other Nonlinear Structures
364 Analysis of a Cooled, Turbine Blade or Vane With an Insert

Holes Help Control Temperature

Holes for radiative heat transfer assist in passive thermal control.

Goddard Space Flight Center, Greenbelt, Maryland

Completely-passive temperature control systems — those that use no fans, heaters, or other energy-consuming elements — are often considered for spacecraft because they save weight, cost, energy, and complexity. The same advantages could be realized in some Earthbound systems, particularly those for which convection effects are small.

A recent study of passive thermal control for the Solar Terrestrial Subsatellite (STSS) has found that an array of "see-through" holes substantially improves the performance of the system. The holes in the payload mounting plates allow line-of-sight radiative heat transfer between the hot and cold ends of the spacecraft and between the mounting plates and the ends. Temperature gradients between the plates are thereby reduced, as is the temperature of each plate. The holes and selected exterior paints and finishes keep the payload cool for all orientations and operating modes of the STSS.

Since convective heat transfer is the dominant mode for most terrestrial systems, some forced cooling is usually necessary. However, a passive system can sometimes substitute for some of the active elements; and in evacuated equipment such as flywheel energy-storage devices, a passive system can play a substantial role in controlling the temperature.

For the STSS, a cylindrical enclosure roughly 2 meters in diameter, heat transfer in the vacuum of space is all radiative and conductive. All orientations with respect to the Sun are possible, and the satellite may be spinning at 20 rpm about its axis of symmetry. The scientific payload, which dissipates up to 190 watts, in addition to a "housekeeping" load, is distributed on two interior "isogrid" mounting plates. Originally conceived as a way to save weight and to change modular payloads rapidly, the aluminum isogrid plates are perforated to accept spiderlike payload supports.

(continued on next page)

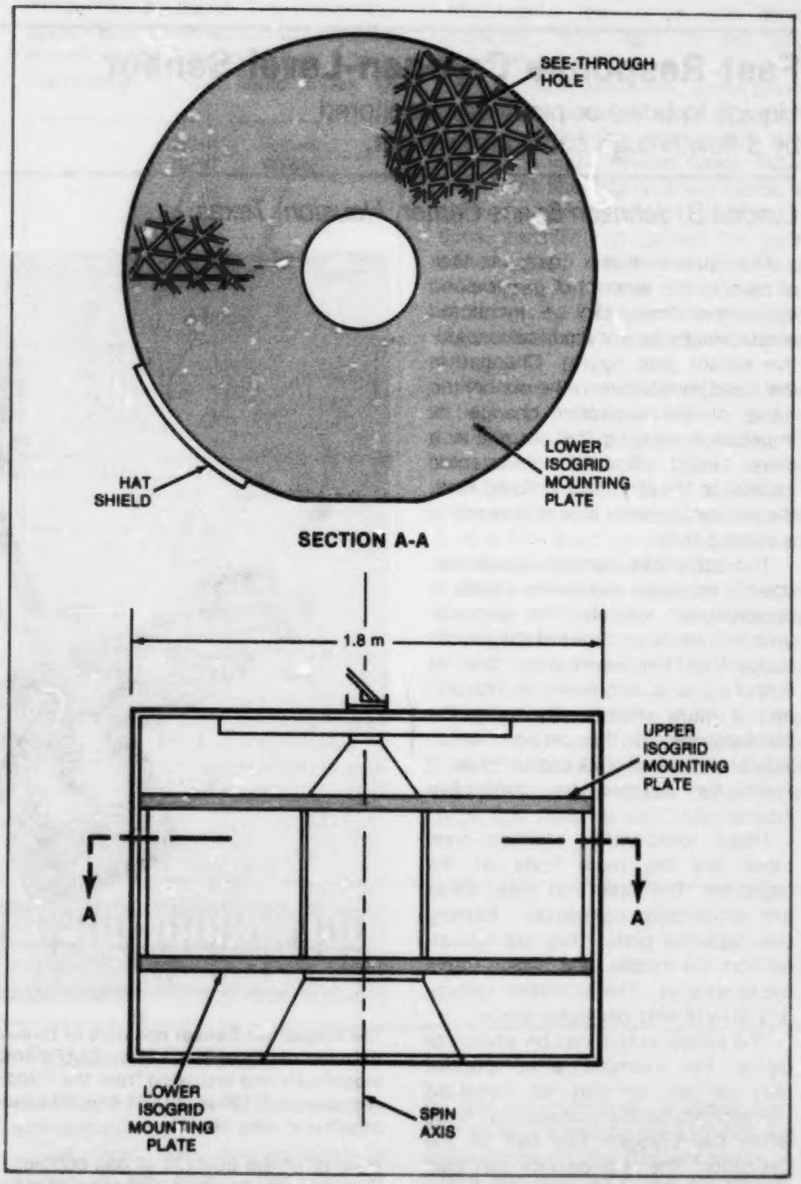
SEE-THROUGH HOLE
LOWER ISOGRID MOUNTING PLATE
HAT SHIELD
SECTION A-A
1.8 m
UPPER ISOGRID MOUNTING PLATE
A
A
LOWER ISOGRID MOUNTING PLATE
SPIN AXIS

The Solar Terrestrial Subsatellite (STSS) is a Space-Shuttle-launched-and-retrieved reusable satellite, operating at an altitude of 250 kilometers. Perforated "isogrid" mounting plates allow rapid interchange of scientific payload modules. A thermal analysis shows that the perforations are essential to effective temperature control.

Analysis of the STSS using a 52-node thermal model shows that the payload temperature can be held between 0° and 30° C for all operating conditions if the scientific instruments do not completely block the holes in the mounting plates. Nominal values for the absorptivity and emissivity of the exterior surfaces were chosen, although these parameters could be adjusted if necessary. Likewise, the total "see-through" area is a parameter that can also be varied. To insure that the radiative paths are not blocked, careful consideration is given to the placement of the payload. In such designs it is advantageous not to be constrained by the shape and size of the enclosure.

This work was done by Chandramohan K. Chhatpar of RCA Corp. for **Goddard Space Flight Center**. *No further documentation is available.*
GSC-12618

Fast-Response Cryogen-Level Sensor

Liquids in tanks or pipes are monitored by a flowthrough capacitive sensor.

Lyndon B. Johnson Space Center, Houston, Texas

The liquid level in a cryogenic tank or pipe, or the amount of gas trapped in pipeline flow, can be monitored electronically by a cylindrical capacitive sensor (see figure). Changes in the liquid level between the concentric tubes of the capacitor change its impedance, varying the current in a drive circuit. Since it is oriented parallel to the direction of liquid flow, the sensor presents little resistance to a moving fluid.

The capacitive sensor was developed to replace a warm-wire sensor in liquid-oxygen vessels. Its response time of 5 ms is an order of magnitude faster than the warm wire, and its output signal is also easier to interpret and is more reliable. By using the conductance of the sensor as an indicator, instead of its capacitance, it could be adapted for conductive liquids.

Three concentric stainless-steel tubes are the main body of the capacitor. The inner and outer tubes are electrically connected, forming one capacitor plate. They are insulated from the middle tube, which forms the other plate. The excitation voltage is a 20-V/6-kHz oscillator signal.

The sensor output can be analog or digital. For example, a comparator may be set so that its threshold corresponds to the current that flows when the cryogen fills half of the capacitor. The comparator can then open a valve if the liquid falls below that level.

For an analog readout, the drive current is monitored by an ammeter. The current gives a reading of liquid level or of the percent of gas bubbles in the liquid. The fast response of the sensor makes possible this quantitative evaluation of gas pockets.

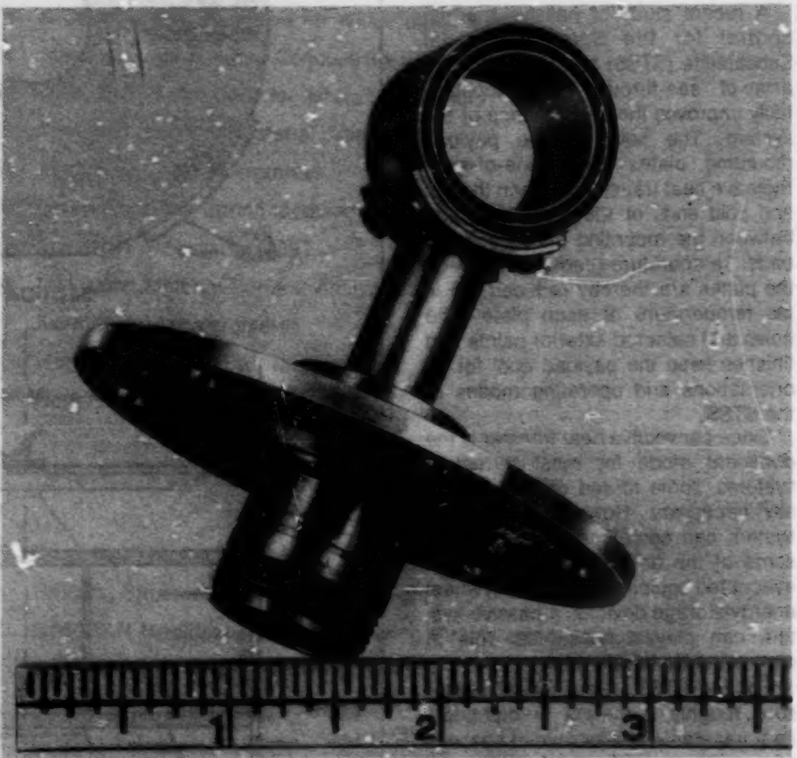

The Capacitive Sensor consists of three concentric tubes 0.825 in. (0.210 cm) long; its outer diameter is 1.125 in. (2.858 cm). The inner and outer tubes are connected electrically and insulated from the middle tube by polytetrafluoroethylene spacers. Airgaps are 0.100 in. (0.254 cm). The mounting flange for installing the sensor in a pipeline is also shown.

This work was done by Joel B. FitzPatrick and Lawrence C. Maier of Simmonds Precision Products, Inc., for **Johnson Space Center.** *For further information, including a detailed assembly drawing of the sensor, Circle 61 on the TSP Request Card.*
MSC-18697

Fiber-Optic Level Sensor for Cryogens

Sharp bends in the fiber improve sensitivity with liquids of low refractive index, such as liquid hydrogen.

Lyndon B. Johnson Space Center, Houston, Texas

A new fiber-optic liquid-level sensor is useful in cryogenic environments where liquids of very low index of refraction are encountered. It is a "yes/no" indicator of whether the liquid is in contact with the sensor.

In the new sensor (see figure), sharp bends in the fiber alter the distribution of light among the propagation modes. This amplifies the change in the light output observed when the sensor contacts liquid, without requiring a long fiber that would increase insertion loss. Tests of the sensor in liquid nitrogen show an insertion loss of 20 dB and a change in signal level of 8 dB when the sensor contacts the liquid. A change of 2 dB is expected for liquid hydrogen.

The fiber-optic level sensor uses a bare glass fiber coupled to a light source at one end and to a light detector at the other end. When the fiber contacts a liquid, light propagating in relatively oblique modes passes into the liquid rather than staying in the fiber, because the critical angle for total internal reflection is greater at the liquid interface than it is at the air interface. Thus, light that would remain trapped in the fiber if it were surrounded by air escapes when it is surrounded by liquid. The closer the liquid index of refraction approaches that of the fiber, the more light is lost. Conversely, if the liquid index of refraction is low — as with liquid hydrogen, little light is lost and sensitivity is poor.

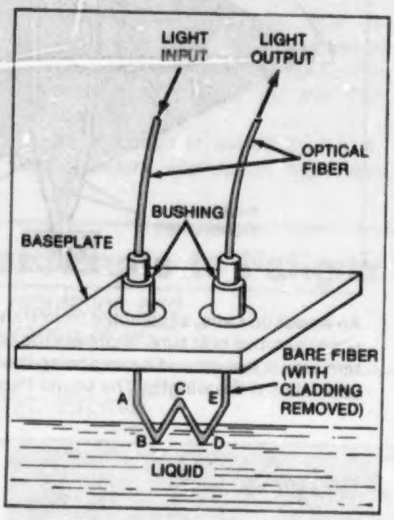

The Improved Fiber-Optic Liquid-Level Sensor has five sharp bends in the glass fiber. Contact with the liquid is sensed at bends B and D. It is driven by an LED that emits 0.2-ms pulses at 50 Hz, which are synchronously detected by a photodiode receiver.

To increase sensitivity, some previous sensors consist of a coil of smooth loops, so that the fiber enters and leaves the liquid several times. However, if the fiber has no sharp bends to generate oblique modes, little additional sensitivity is gained for each added loop, while insertion loss increases. Any mode that does not escape at the first entry into the liquid does not escape at subsequent entries either.

The new sensor uses a glass fiber 0.04 in. (1 mm) in diameter. Special low-loss seals (not shown in figure) are used where the fiber passes through holes in a metal baseplate. The seals have a bushing that assures a very fine band of contact between the epoxy sealant and the fiber.

This work was done by Madan Sharma of TRW, Inc., for **Johnson Space Center.** *For further information, Circle 62 on the TSP Request Card.*

Inquiries concerning rights for the commercial use of this invention should be addressed to the Patent Counsel, Johnson Space Center [see page A5]. Refer to MSC-18674.

Acoustic Lens Is Gas-Filled

A fluorocarbon gas contained by a plastic film makes an effective lens for sound waves.

NASA's Jet Propulsion Laboratory, Pasadena, California

A novel acoustic lens is fabricated by clamping together two membranes of thin plastic and filling the enclosed space with a fluorocarbon gas. In tests, the lens substantially improved the accuracy of sound "maps" of turbulent airflow. It could also be used to record sound-intensity patterns in the design of speakers, lecture halls, and auditoriums.

The basic lens configuration is shown in the figure. Two circular membranes of Mylar or equivalent plastic, 0.25 mil (0.06 mm) in thickness, are clamped together around their peripheries. At one point on the circumference, a small tube (not shown) is held by the same clamp and extends into the gastight space. A heavy gas such as Freon (or equivalent) is fed through the tube, stretching the plastic facesheets into the shape of a convex lens.

(continued on next page)

The speed of sound in the gas is considerably less than in air. Thus, the lens refracts and focuses sound waves, in analogy to the focusing of light by a glass lens. (The focal length is adjusted simply by changing the gas pressure, which changes the lens curvature.)

In previous efforts to map the sound from gas flow over an airfoil, a directional microphone was scanned over the flow area. When the new lens was interposed between the flow and the microphone, the sharpness of the sound "image" was improved by a factor of more than 2. The overall gain of the system is also increased because the source energy is focused onto a smaller image area. The inset to the figure is a typical sound map for a sweptwing model tested in a wind tunnel at an airspeed of 28 meters per second. The measurement grid is 1.25 cm between points.

This work was done by James M. Kendall, Jr., of Caltech for **NASA's Jet Propulsion Laboratory.** *For further information, Circle 63 on the TSP Request Card.*
NPO-14757

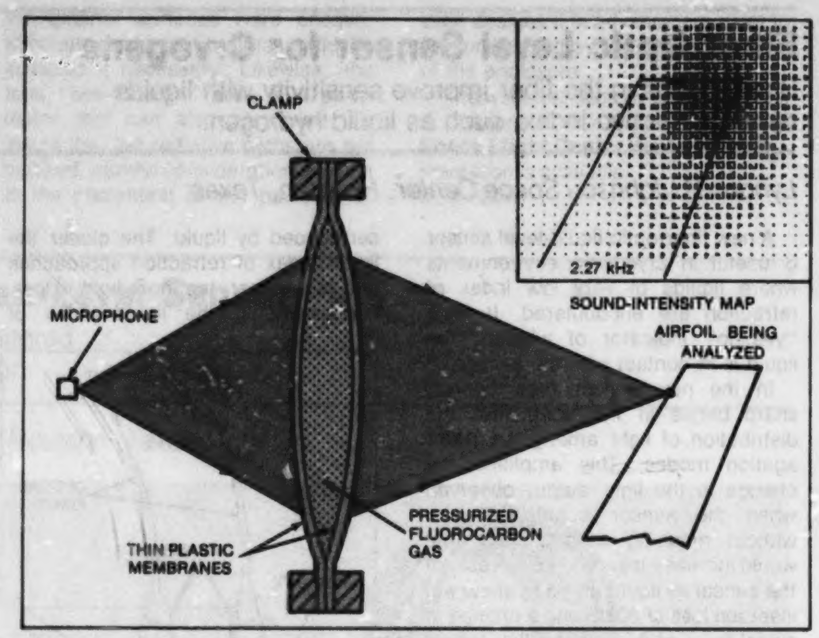

An **Acoustic Lens,** assembled from transparent plastic sheets and filled with Freon at slight positive pressure, improves the accuracy of sound-intensity maps. A typical pattern for airflow around a sweptwing is shown in the inset. It shows a noise source concentrated at the wingtip. The sound frequency is 2.27 kHz.

Ultrasonic Frequency Analysis

Frequency-tracked gated-pulse technique eliminates problems found with current techniques.

Langley Research Center, Hampton, Virginia

An improved technique developed at Langley Research Center for ultrasonic frequency analysis can be used for the evaluation and characterization of materials, fluids, and biological tissue. Normally, short, untuned voltage spikes from a pulser are used to shock-excite a highly-damped piezoelectric transducer. The transducer emits a sharp ultrasonic pulse with a relatively-wide frequency bandwidth, which interrogates the test sample. The signal from the sample is then fed into a spectrum analyzer that displays the magnitude of the Fourier transform of the signal. The spectra, however, are strongly influenced by the shape of the electrical spike used to generate the ultrasonic waveform. Further, the spikes produce unwanted nonlinearities in the emission waveform. This may complicate interpretation of the frequency spectra from the test sample.

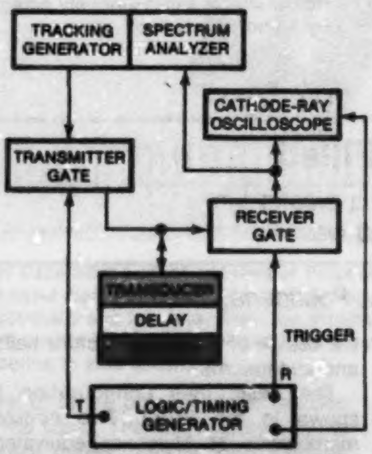

Figure 1. Frequency Control for an Ultrasonic Analyzer employs a tracking generator that is slaved to the local oscillator of the spectrum analyzer to produce spectra equivalent to shock-exciting the transducer with a true delta function excitation.

The new method eliminates the problem of the electrical drive-pulse shape by slaving a tracking generator to the local oscillator of the spectrum analyzer, as shown in Figure 1. A logic/timing generator is used to control the pulse transmission and receiving sequence, the pulse width, and the pulse repetition rate. With this arrangement the frequency of the RF input that is pulse-gated to the spectrum analyzer is locked to the frequency in the analyzer at which measurements are being made. Therefore, spectra are produced that are equivalent to shock-exciting the transducer with a true delta function (Figure 2). Since the drive voltages are typically two orders of magnitude lower than those of conventional methods, unwanted nonlinearities in the emission spectra are eliminated. Further, use of the frequency-tracking technique with the newly-developed phase-insensitive acoustic/electric transducer (AET) permits the AET to extract spectral information; this capability does not exist with the AET using conventional pulse methods.

The practical limitations of the frequency-tracking technique are associated with the frequency limitations of the spectrum analyzer and the electroacoustic bandwidth characteristics of the transducer. For most ultrasonic measurements the spectrum analyzer bandwidths, typically in the tens or hundreds of megahertz, impose little limitation. The development of broadband capacitive transducers should permit maximum exploitation of the frequency-tracking technique for ultrasonic frequency analysis.

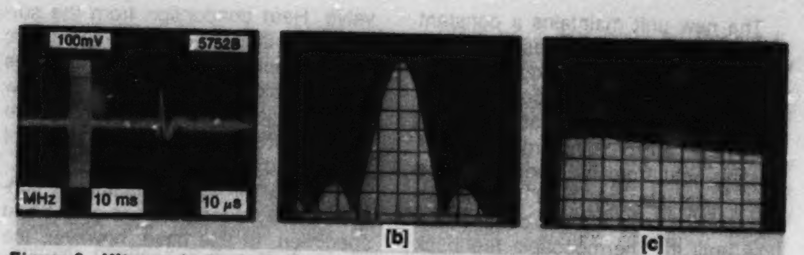

Figure 2. **Ultrasonic Analysis Spectra** are produced by gating an ultrasonic pulse (a) into a spectrum analyzer, using (b) a conventional technique and (c) the frequency-tracking technique.

This work was done by John H. Cantrell, Jr., and Joseph S. Heyman of **Langley Research Center**. *For further information, Circle 64 on the TSP Request Card.*

This invention is owned by NASA, and a patent application has been filed. Inquiries concerning nonexclusive or exclusive license for its commercial development should be addressed to the Patent Counsel, Langley Research Center [see page A5]. Refer to LAR-12697.

Temperature Controller Adapts to Fatigue Tester

Aluminum blocks allow accurate regulation and fast variation over a temperature range of 850° F.

Langley Research Center, Hampton, Virginia

A specimen of material undergoing fatigue tests is maintained at constant temperature or cycled over a wide temperature range by an electronic temperature controller. Cryogenic temperatures near the boiling point of liquid nitrogen and elevated temperatures to 600° F (315° C) are possible with the new unit, which consumes little power and coolant and has low thermal inertia so that rapid temperature changes may be programed.

The temperature controller (see figure) consists of two identical blocks of aluminum placed against the front and back of the test specimen and held together by spring clamps. Thermocouple wires pass through holes in the blocks to monitor the specimen temperature. The temperature signals control either electrical heaters or the valve in a liquid-nitrogen line to small cavities in the blocks.

In the past, relatively-massive commercial systems have been available as either heat sources or cryogenic sources. These, however, are incompatible with fatigue-testing machines designed to test small samples and, because of the large mass, temperature changes occur relatively slowly.

(continued on next page)

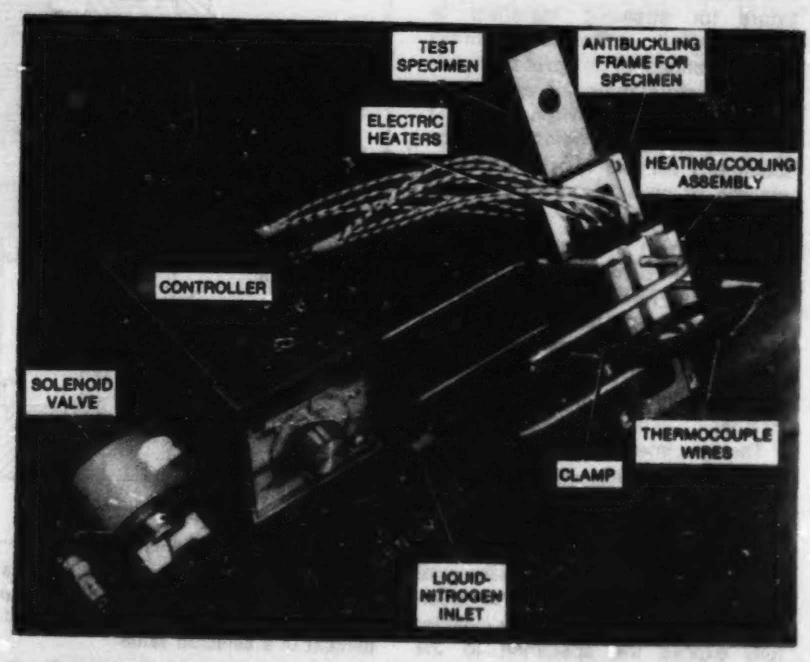

The **Temperature Controller**, designed for compatibility with fatigue-test machines, is shown mounted on a test specimen. Identical blocks of aluminum, held against the front and back of the specimen, each contain electrical heaters, a liquid-nitrogen cavity with input and exhaust tubes, and a thermocouple. The thermocouples are connected to the control unit, which adjusts the specimen temperature during fatigue tests.

The new unit maintains a constant cold temperature on the test specimen by introducing liquid nitrogen from a remote pressurized source through a solenoid valve. The liquid absorbs heat from the surrounding material, including heat from the specimen, and then exhausts the heat to the atmosphere. Liquid nitrogen continues to flow until the thermocouple feedback probe in contact with the specimen senses that the desired temperature has been reached. The solenoid valve controller then closes the solenoid valve. Heat conduction from the surroundings tends to warm the specimen; but the thermocouple probe actuates the solenoid valve controller to allow nitrogen flow, thus maintaining the temperature within a narrow range of the desired temperature.

A similar process maintains a constant elevated temperature on the test specimen. In this case, however, the thermocouple temperature controls electrical power to the heating cartridges. Using a simple timing device the controller was successfully tested over a temperature cycle from 600° F (315° C) to − 250° F (− 155° C).

This work was done by Leland A. Imig and Mickey R. Gardner of **Langley Research Center.** *For further information, Circle 65 on the TSP Request Card.*

This invention is owned by NASA, and a patent application has been filed. Inquiries concerning nonexclusive or exclusive license for its commercial development should be addressed to the Patent Counsel, Langley Research Center [see page A5]. Refer to LAR-12393.

Environmental Testing Under Load

An inexpensive fixture applies compression loads to specimens exposed to the environment.

Langley Research Center, Hampton, Virginia

Since environmental testing of materials under compressive stress usually requires rather elaborate equipment, engineers and others will be interested in a low-cost, compact test fixture for stressing materials to predetermined compressive stress levels. Intended for compressive loading of structural materials exposed to natural or simulated environments, the fixture can handle relatively large specimens suitable for postexposure analysis of physical, chemical, and mechanical properties.

As shown in the figure, the test specimen is contained in a guide cylinder between two horizontal plates. The plates are held together by two bolts. An adjustable loading bolt through the top plate transmits the load through a piston in the guide cylinder.

The specimen is held in place by adjustable retainers — one pair on the load piston and the other on the bottom plate. The ends of the guide cylinder fit snugly in recesses in the top and bottom plates to ensure axial alinement of the load and the specimen. Two cutouts in the guide cylinder fully expose the specimen to the environment.

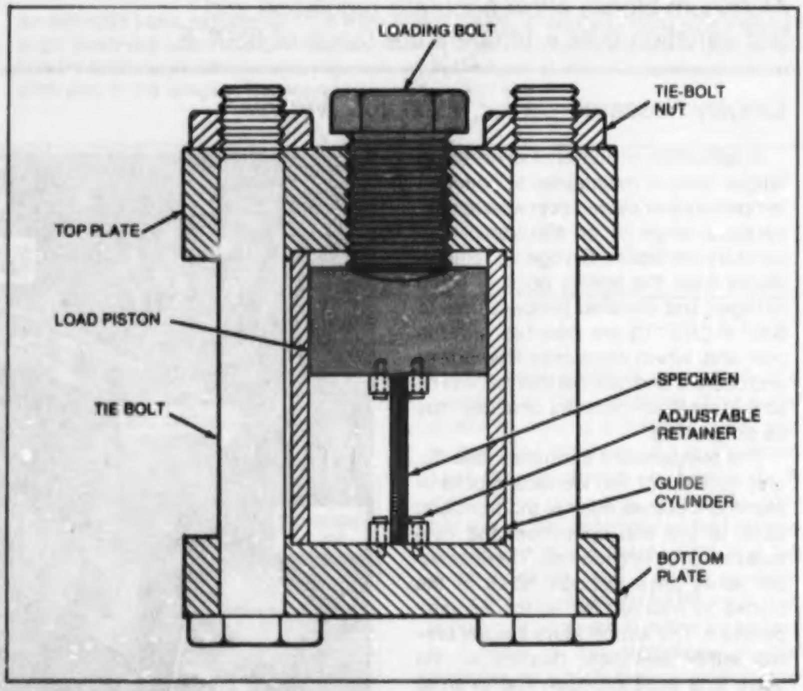

Piston Applies a Load to a specimen, as cutouts (not shown) in the cylinder expose the test sample to the environment. Specimens up to 1 in. (2.5 cm) in width and 1-1/2 in. in length are accommodated. The applied load can be set within ±10 percent of a selected value.

The adjustable loading bolt in the top plate allows the load to be varied; however, since rotation of the bolt could apply a torque to the specimen, the load is not increased simply by advancing the bolt. Instead, the tie-bolt nuts are loosened, the loading bolt is turned to the desired load setting, and a load-test machine applies a purely axial load. When the bolts are retightened, the desired load is locked in the specimen.

Calibration curves are taken to determine the appropriate position of the loading bolt. The curves are developed for a given material and specimen configuration with the aid of a strain-gaged specimen, the axial-load test machine, and a load/strain recorder. The strain and load on the specimen are correlated with the angular position of an index on the loading bolt, as indicated by an angular scale scribed on the top plate.

This work was done by Ronald K. Clark and W. Barry Lisagor of **Langley Research Center.** *For further information, Circle 66 on the TSP Request Card.*

Inquiries concerning rights for the commercial use of this invention should be addressed to the Patent Counsel, Langley Research Center [see page A5]. Refer to LAR-12602.

Testing Panels in Tension and Flexure

A simple jig adapts a tensile-test machine for the simultaneous application of tension and flexure.

Marshall Space Flight Center, Alabama

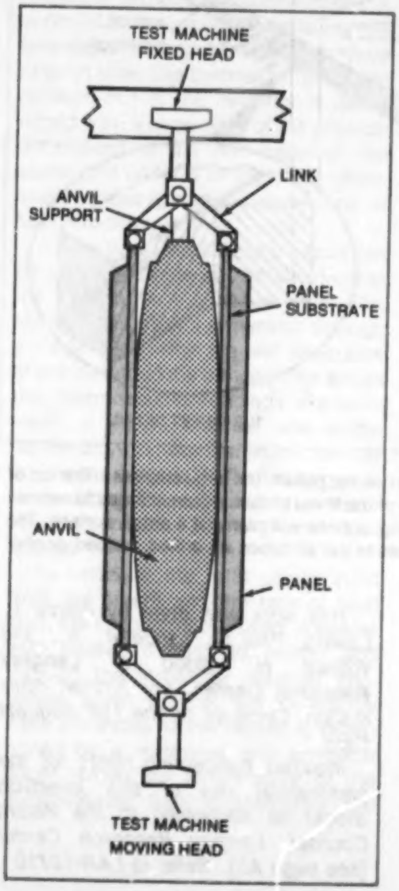

An Anvil Applies Flexure while linkages apply tension to panels under test. Loading of the test jig is along a single axis.

Multilayered panels are rapidly tested in both tension and flexure by a novel jig, shown in the figure. The panels are subjected to virtually any combination of tensile and flexural loads simultaneously, for evaluating the panel composition, processing, and design.

The jig is attached to a conventional tensile-test machine. An environmental test chamber can be added so that panel properties can be measured at extreme temperatures.

The tensile-test machine applies a load along a single vertical axis. In the jig, linkages support two panels on opposite sides of a curved anvil. As the panels are loaded by the tensile-test machine, they bend to follow the anvil contours. The bending creates the flexural component of stress.

Anvils having various curvatures — even sharp edges — are used. Smoothly curved anvils of radii from 100 to 500 inches (2.5 to 12.7 m) have been fabricated, as have anvils with more than one radius of curvature.

This work was done by Gustave K. Jung of Martin Marietta Corp. for **Marshall Space Flight Center.** *For further information, Circle 67 on the TSP Request Card.*
MFS-25421

Tracking Falling Objects

Objects in free fall are viewed at constant magnification by an optical carriage on a vertical track and a fixed telescope attached to a camera. A small motor supplies the power needed to overcome the drag on the carriage. The system has been used to study the formation of glass coatings on nuclear-fuel pellets.
(See page 306.)

Photometer Used for Response Time Measurement

In tests of servocontrol systems, a photometer has been used to measure system response time. When the photometer is sighted on a line on the system display screen, it senses output movement on the screen shortly after an operator activates a hand-controlled input. The response time is measured on an X/T recorder.
(See page 293.)

A Construction Technique for Wind-Tunnel Models

Integrally machined orifices and channels offer advantages over traditional miniaturized plumbing.

Langley Research Center, Hampton, Virginia

Miniature wind-tunnel models must satisfy stringent physical requirements, including high strength, good surface finish, and corrosion resistance. Some of the most troublesome problems result from the internal steel tubes that lead to small, pressure-sensing, surface orifices. These tubes may plug or leak, and the cavities they require weaken the model. Since the plumbing cannot be installed until late in the machining process, considerable fabrication time is wasted if defects arise at that point.

These problems are overcome by machining the pressure channels as an integral part of the model. As illustrated in Figure 1 for a sample airfoil built at Langley Research Center, the model with plumbing is assembled from two flat stainless-steel plates, which are joined face to face. The pattern of pressure channels is scribed, machined, or photoetched into the flat surface, and the pressure-sensing orifices are drilled before joining the two halves. The portion of the plates along the central cross section—where the orifice network pierces the airfoil surface—is premachined to minimize the orifice drilling depth.

The mating surfaces of the plates are flashed with a very thin ($8x10^{-4}$-cm) coat of copper. After they are diffusion-brazed together, the plumbing is checked for plugs or leaks. At that point the block is machined to its final contour. Figure 2 shows the airfoil, with the top surface complete. The tubing shown is brazed in place when the blocks are joined.

In addition to solving construction problems for wind-tunnel models, this technique should be useful in fuel injection, transpiration cooling, and similar applications involving small elements of fluid flow. Since the technique has been developed for 17-4 PH alloy stainless steel, it can be used for corrosive or high-temperature environments.

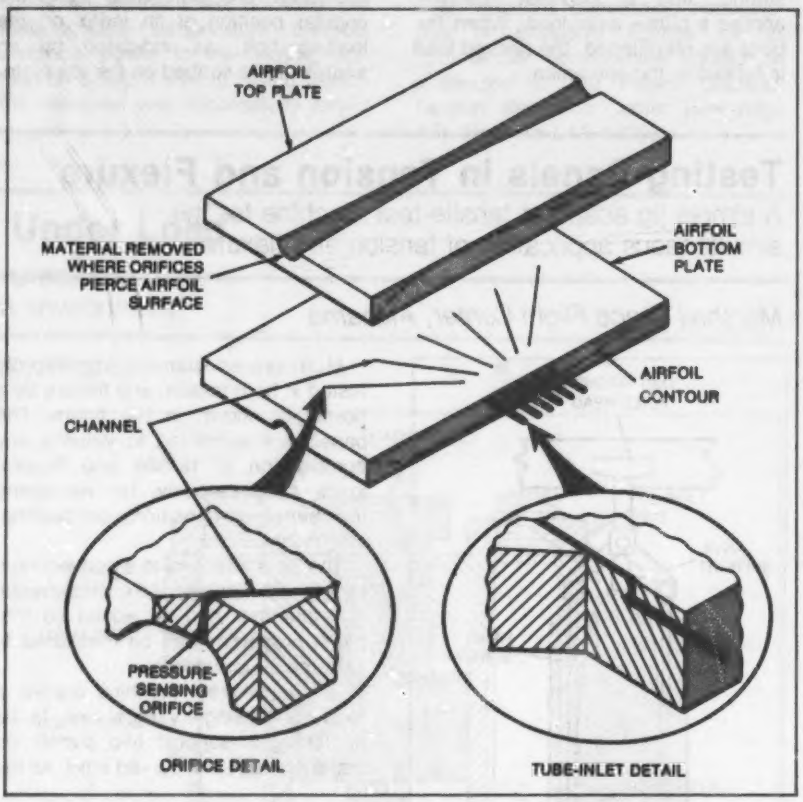

Figure 1. An Airfoil Model Is Constructed from two flat plates. The large channel in the top of the upper plate and the channel in the bottom of the lower plate are premachined to remove material along the line where pressure-sensing orifices will pierce the airfoil surface. The small interior channels leading from the orifices to the six tubes are drilled, scribed, or photoetched.

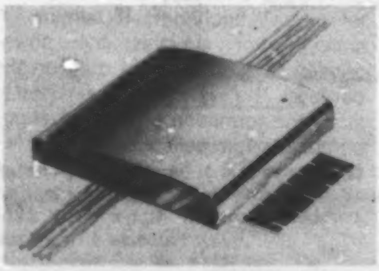

Figure 2. The Airfoil Has Been Machined to Contour along one surface in this view, after the plates have been brazed together. The tiny pressure-sensing orifices are too small to be visible in this photograph.

This work was done by Pierce L. Lawing, Paul G. Sandefur, Jr., and William H. Wood of **Langley Research Center.** *For further information, Circle 68 on the TSP Request Card.*

Inquiries concerning rights for the commercial use of this invention should be addressed to the Patent Counsel, Langley Research Center [see page A5]. Refer to LAR-12710

Measuring the Thermal Conductivity of Insulation

Two symmetrical heat sources help determine the thermal transmission properties of an insulating material.

NASA's Jet Propulsion Laboratory, Pasadena, California

The thermal transmission properties of many insulators can be measured with an apparatus that uses two symmetrical heat sources to match temperatures. The heat sources for the apparatus, which has accurately measured the thermal insulation properties of rocket insulation, are saturated steam (though other vapor heat sources can be used) and a wire heater.

To test the thermal transmission of an insulating material (see figure), it is packed in two identical copper tubes. A series of thermocouples measures the temperature along the exterior surface of each tube. The thermal transmission (in W/m °C) of the insulator is determined from a knowledge of the physical dimensions of the test material, the stable and uniform temperature differential across it, and the stable rate of heat flow through it.

In one tube, the constant saturation temperature of steam is maintained at the inner surface of the material. The steam flows from a generator through a copper tube within the test apparatus and is vented to the atmosphere. When the thermocouple readings are constant, a known uniform and stable temperature differential exists radially across the material (different temperatures along the tube could indicate inhomogeneous packing and end losses).

To measure the total power input from the steam and the rate of heat flow, the second tube is used. A heater wire passes through its center and through the insulating material contained within it. The rate of energy input (in watts) to the heater is determined by a voltmeter and ammeter shunt. When the temperature of the steam-heated tube is stabilized, the power output of the wire heater is adjusted until the two sets of thermocouples on the tubes indicate the same temperature. The thermal conductivity of the insulating material can then be determined.

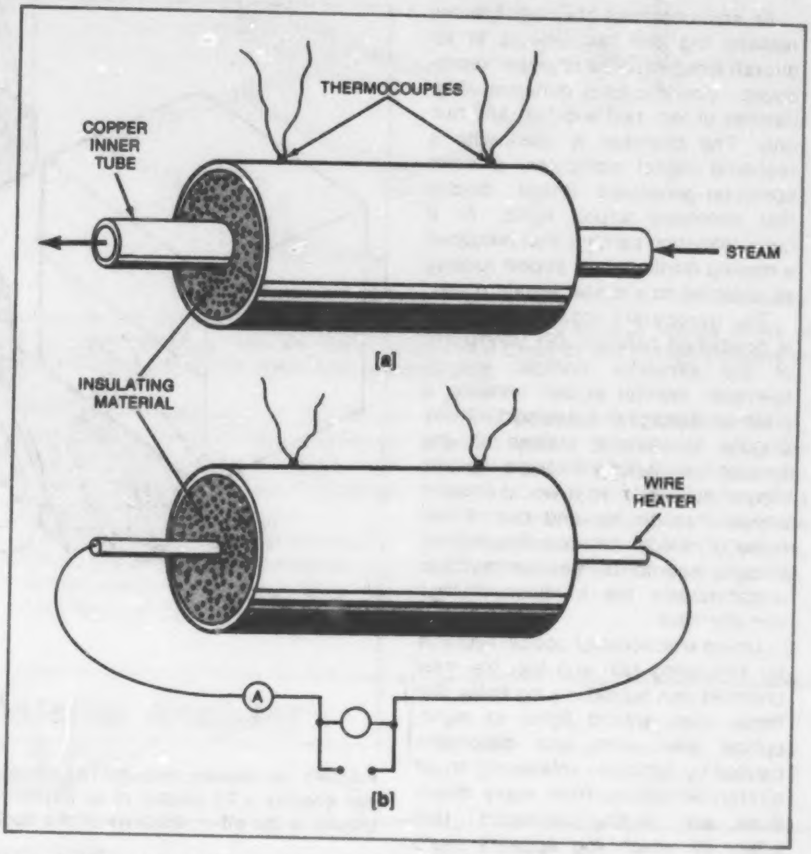

An Insulating Material is packed in two copper tubes to measure its thermal transmission properties. In one of the tubes (a), steam is the heat source; in the other tube (b), a wire heats the insulating material. When the thermocouples on the two tubes read the same stable temperature, the thermal transmission of the insulating material can be determined.

This work was done by Christine A. Wilkins, Robert Ash, and Warren L. Dowler of Caltech for **NASA's Jet Propulsion Laboratory**. *For further information, Circle 69 on the TSP Request Card.*
NPO-14671

Rain, Fog, and Clouds for Aircraft Simulators

Moisture chamber realistically reproduces airborne mists for pilot training.

Ames Research Center, Moffett Field, California

An environmental chamber creates realistic fog and rain effects in an aircraft simulator. The chamber reproduces clouds, homogeneous fog, patches of fog, rain and fog, and rain only. The chamber is used with a real-time digital computer, a color computer-generated image display that simulates airport lights, or a color-television camera that produces a moving display of an airport runway as depicted on a model terrain board.

The transparent fog/rain chamber is positioned between the windshield of the simulator cockpit and a television monitor screen showing a collimated image of the airport runway (Figure 1). A pilot trainee looking through the windshield sees a realistic view of the airport as it would actually appear through fog and rain. Other types of optical beam-splitter/mirror systems now in use can be made to accommodate the transparent fog/rain chamber.

Unlike electronic or optical systems for simulating rain and fog, the new chamber can reproduce fog halos like those seen around lights at night, optical attenuation and distortions caused by raindrops splattering on an aircraft windshield from many directions, and "veiling luminance" (the effect by which fog appears more dense when it is viewed in Sunlight, by backscattering as seen by the pilot due to the aircraft landing lights, or from nearby lightning discharges). Windshield wipers in the chamber add to the authenticity of its effects.

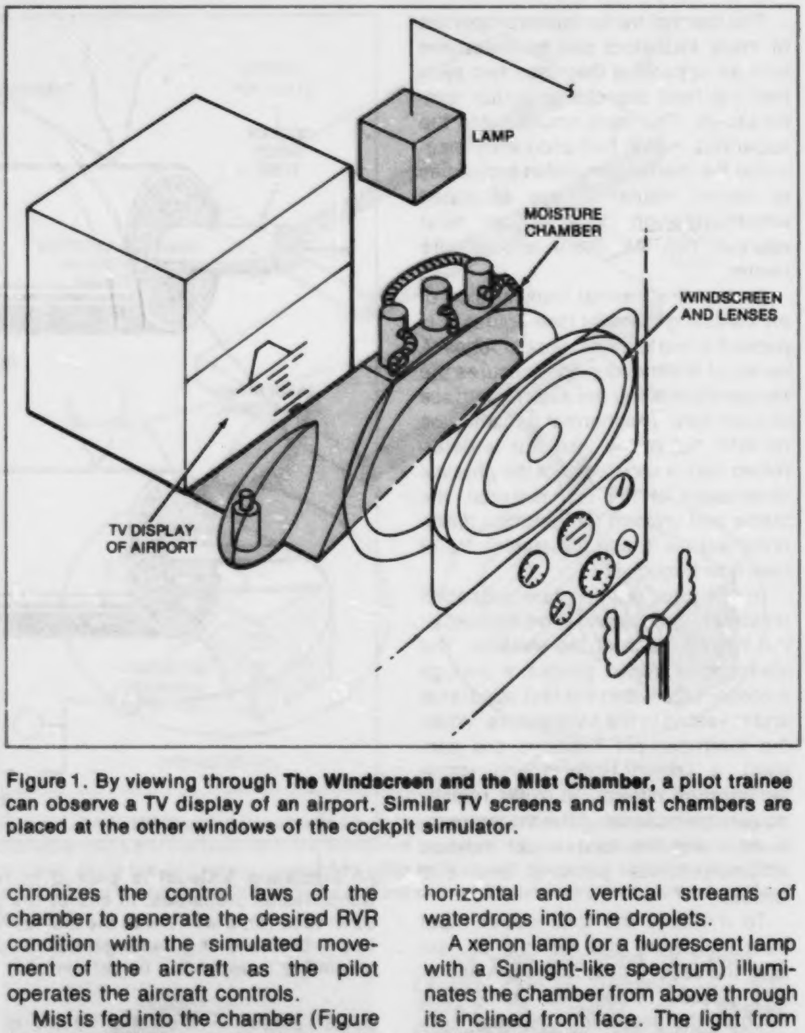

Figure 1. By viewing through The Windscreen and the Mist Chamber, a pilot trainee can observe a TV display of an airport. Similar TV screens and mist chambers are placed at the other windows of the cockpit simulator.

Aerosol generators in the chamber are controlled by the computer to produce water droplets in a variety of sizes — from 5 to 20 microns for fog and from 20 to 50 microns for clouds. The mist can be cleared out of the chamber almost instantly, or its density can be increased or decreased abruptly to represent the conditions of a specified runway visual range (RVR) from zero visibility to 30 miles (48.3 km), or that when an aircraft suddenly emerges from fog or clouds or enters a denser or lighter fog bank. The computer low-visibility algorithm synchronizes the control laws of the chamber to generate the desired RVR condition with the simulated movement of the aircraft as the pilot operates the aircraft controls.

Mist is fed into the chamber (Figure 2a) by two primary aerosol units at its sides and auxiliary aerosol generators at its top. To change the density of the mist for a specified RVR condition, two perforated tubes at the bottom inject computer-controlled bursts of high-pressure air to mix with the mist, which is exhausted out the top of the chamber. Rain is simulated by a combination of water and air ejected through orifices in horizontal and vertical tubes and by air alone ejected through a horizontal tube (Figure 2b). Jets from the air tube break up the horizontal and vertical streams of waterdrops into fine droplets.

A xenon lamp (or a fluorescent lamp with a Sunlight-like spectrum) illuminates the chamber from above through its inclined front face. The light from the lamp is visible only when there are water particles in the chamber to scatter it. Thus, the brightness of the haze as observed by the pilot becomes less intense as the simulated aircraft "descends" or as the mist density decreases in the chamber. Finally, when all mist is removed from the chamber, the pilot sees only the runway scene on the TV or computer-generated-image CRT screen. Even though the lamp is still on, its light is not scattered and therefore is not visible to the pilot.

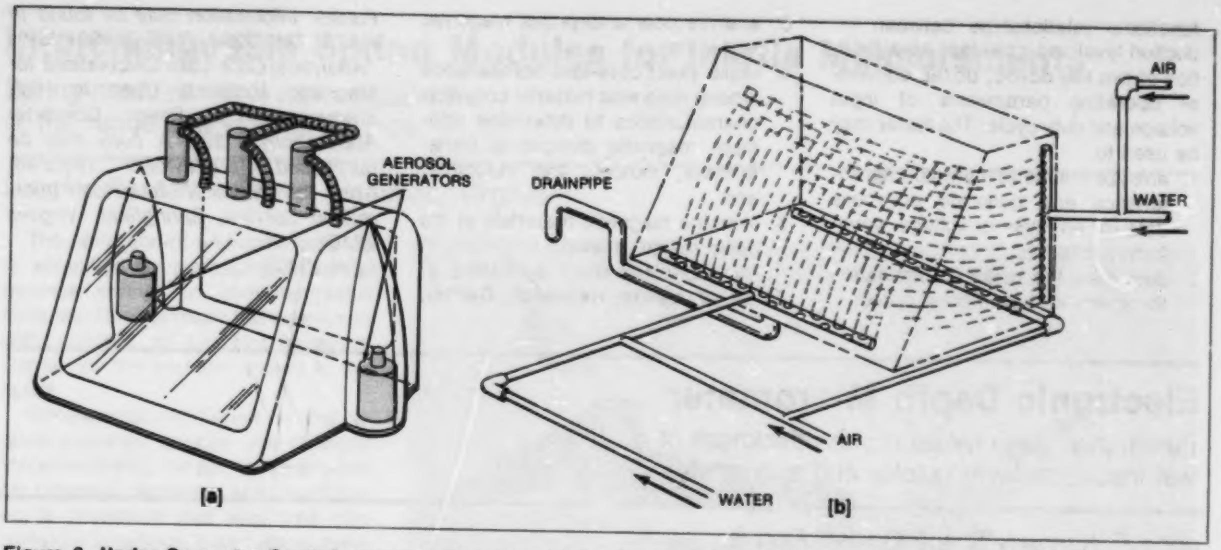

Figure 2. Under Computer Control, aerosol generators (a) at the top of the chamber and in side alcoves release mists of predetermined densities. Perforated tubes (b) eject "raindrops" that are broken up into finer drops by jets of high-pressure air from a tube at the bottom of the chamber. The drainpipe prevents water from accumulating.

The lamp can also be controlled by the computer to change brightness to simulate ascent or descent through variable-density clouds. The computer can also flash the lamp intermittently to simulate nearby lightning flashes in a cloud.

For greater realism, the computer controls the brightness of the TV or computer-generated image display so that ground objects are brightest when close to the pilot and gradually fade as they approach the horizon.

This work was done by Wendell D. Chase of **Ames Research Center.** *For further information, Circle 70 on the TSP Request Card.*

This invention is owned by NASA, and a patent application has been filed. Inquiries concerning nonexclusive or exclusive license for its commercial development should be addressed to the Patent Counsel, Ames Research Center [see page A5]. Refer to ARC-11158.

Improved Magnetic Material Analyzer

Core losses at frequencies up to 10 kHz or greater are measured instantaneously.

Lewis Research Center, Cleveland, Ohio

A flux-controlled magnetic-core-loss tester has been developed that produces high-frequency core-loss data (within 2 percent) for any desired waveform excitation and allows the magnetic characteristics of a material to be measured under symmetrical and asymmetrical excitation conditions. It allows the direct control of an additional loss variable, $d\varphi/dt$, rather than just the driving frequency as is the case for all previous sinusoidal core-loss measurements.

Existing core-loss test equipment can measure only sinusoidal low-frequency ($<$400-Hz) core-loss characteristics with respect to frequency and flux density. This new core-loss tester will directly measure core-loss characteristics at high frequency ($>$10 kHz), at saturation, for any type of voltage waveform, instantaneously.

The flux-controlled magnetic-core-loss tester is composed of a drive subsystem, an excitation subsystem, and an instrumentation subsystem. The excitation subsystem consists of a high-power wideband operational amplifier that allows the option of selecting either voltage, current, or the integral of voltage (magnetic flux) as the feedback parameter. This allows a high-frequency voltage source, current source, or flux control configuration to be simulated. Using the flux feedback option, true sinusoidal, square-wave, or impulse voltage excitation conditions may be easily generated. The instrumentation subsystem allows instantaneous core-loss measurements and analyses to be made.

The instrument allows the two core-loss variables, time rate of change of flux ($d\varphi/dt$) and the maximum flux density (B_m), to be directly measured. It also provides the data necessary to calculate Steinmetz coefficients exactly, experimentally verify Warburg's law, and allows examination of domain wall theories under constant and controlled $d\varphi/dt$ conditions.

The magnetic characteristics obtained from this new test unit are extremely useful to the power electronics designer in that they show the

(continued on next page)

functional relationships between induction level and core loss as a function of two key dc/dc, dc/ac converter operating parameters of input voltage and duty cycle. The tester may be used to:

1. analyze magnetic material characteristics and generate core-loss data for any type of voltage waveform excitation;
2. determine the optimum lamination thickness for tape-wound cores;
3. analyze new amorphous magnetic materials;
4. make exact core-loss comparisons among magnetic material core-loss characteristics to determine optimum magnetic designs in transformers, motors, and inductors; and
5. examine magnetic materials at the basic research level.

This work was done by James E. Triner of **Lewis Research Center.** *Further information may be found in NASA TM-79234 [N79-31499/NSP], "Analytical Core Loss Calculations for Magnetic Materials Used in High Frequency High Power Converter Applications" [$9]. A copy may be purchased [prepayment required] from the National Technical Information Service, Springfield, Virginia 22161.*
LEW-13493

Electronic Depth Micrometer

Penetration gage measures the thickness of a wet-insulation layer quickly and accurately.

John F. Kennedy Space Center, Florida

A novel device for measuring depth or thickness reads the distance of penetration by a small-diameter probe. The probe is fastened to the sliding contact on a linear 1,000-ohm potentiometer that has a travel of 1.000 inch (2.54 cm). Thus the resistance between the end of the potentiometer and the sliding contact increases by 1 ohm when the probe moves 1 mil (0.025 mm). The resistance is read on a digital ohmmeter. With the meter set on the 1-kilohm scale, direct readings in thousandths of an inch are obtained.

This device was developed specifically to measure the thickness of wet (uncured) insulation applied to Space Shuttle structures; the thin probe penetrates the wet insulation to the substrate, and the reference surface on the gage is then positioned against the outer surface of the insulation to measure its thickness. The gage is easy to use, even by workers wearing gloves or other protective clothing, and allows remote reading and recording of production data.

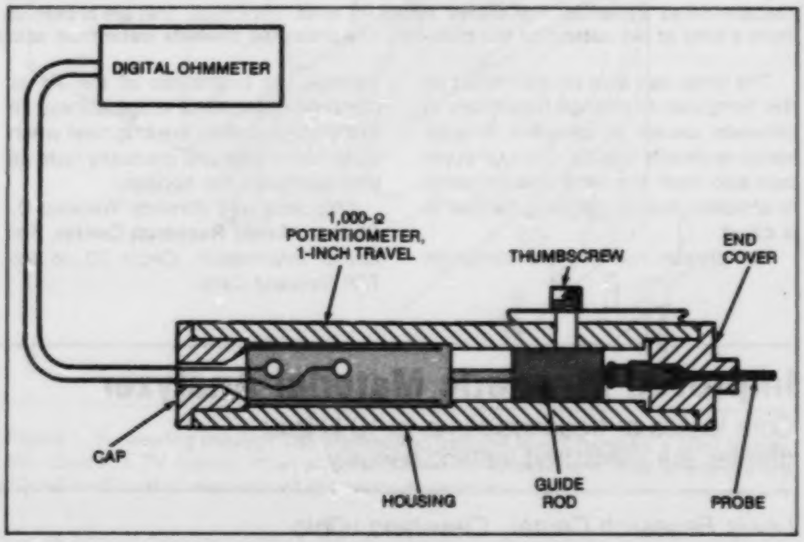

A 1-Kilohm Linear Potentiometer that is 1.000 inch long has a probe fastened to its moving contact. When the probe moves out of its housing, the resistance between the fixed and movable contacts on the potentiometer increases by 1 ohm per mil of probe projection. The digital ohmmeter thus reads probe extension directly when it is on the 1-kilohm scale.

As shown in the figure, the thickness-gage housing has a recess for the linear potentiometer; a cap threaded into the end of the housing has an opening for the potentiometer lead wires. The guide rod attached to the end of the potentiometer shaft is mated to the probe, which is trimmed to length and can project through a hole in the end cover. A thumbscrew applies friction to brake the guide rod so that thickness measurements can be made by placing the probe against the substrate and moving the gage until the end cover just touches the outer surface of the wet film being measured. The thickness measured is the distance from the tip of the probe to the surface of the end cover.

For the insulation thickness measurements, tests showed that a linear 1,000-ohm potentiometer with a tolerance of ±5 percent gives sufficient accuracy and repeatability. For other applications, a more accurate unit could be used.

This work was done by Richard K. Major of United Space Boosters, Inc., for **Kennedy Space Center.** *No further documentation is available.*

Inquiries concerning rights for the commercial use of this invention should be addressed to the Patent Counsel, Kennedy Space Center [see page A5]. Refer to KSC-11181.

Interchangeable Spring Modules for Inertia Measurements

Spring modules allow rapid adjustment of the range of an inertia balance.

Langley Research Center, Hampton, Virginia

The operation of an inertia balance is simplified by packaging a set of balance springs in interchangeable modules. This approach has been used with success at Langley Research Center for the balance shown in the figure.

Since models of different weights require crosshair springs with different force constants, the springs must often be removed, replaced, and recalibrated, a procedure that was time consuming and tedious. It was also subject to inaccuracy, since the recalibration step could not always be done reproducibly.

The new spring modules (one of which is shown in the inset to the figure) are prepackaged and precalibrated. They are held in place in the balance pedestal by just two fasteners, making removal and replacement fast and simple. With them, the balance can be readied for a model of different weight in less than 15 minutes, in contrast to more than 2 hours by the previous method.

This work was done by James W. McNamara and John W. Oakley of **Langley Research Center.** *No further documentation is available.*
LAR-12402

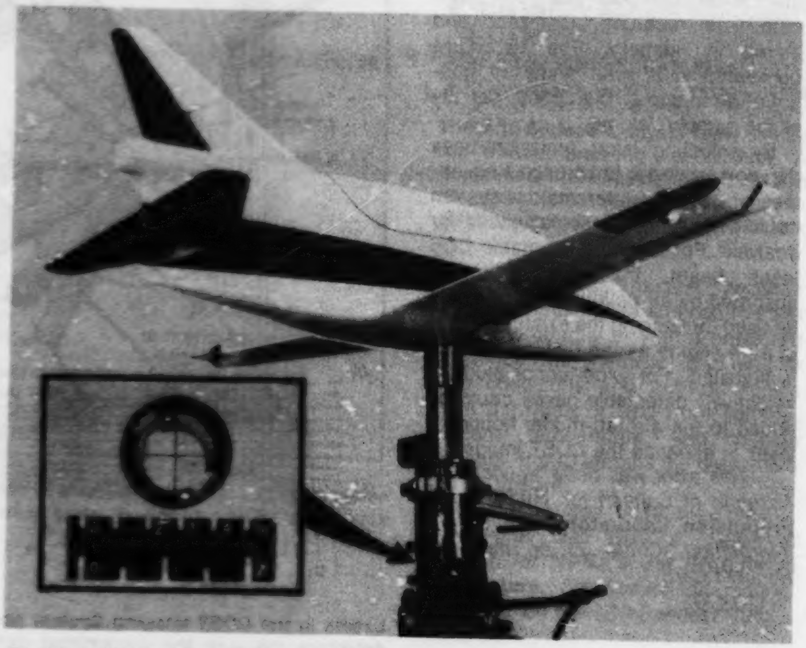

The **Precalibrated Crosshair-Spring Module** shown in the inset is used to determine the moment of inertia of this lightweight model of a low-altitude aircraft. A heavy-duty spring module is rapidly substituted when calibrating heavier models.

Wakeflow Analysis by COST

Turbulent airflow is imaged by computerized optical-scanning tomography.

NASA's Jet Propulsion Laboratory, Pasadena, California

COST — computerized optical-scanning tomography — is proposed for visualizing the wakeflows of aircraft and wind-tunnel models. Operating very close to real time, COST hardware could be installed at airports to monitor the turbulent flow trailing large aircraft, so that smaller aircraft could be directed to avoid the turbulence. The real-time analysis of jet-engine exhaust plumes, to reduce pollution and optimize performance, is also possible.

COST is similar to CAT (computerized axial tomography), an X-ray imaging technique that is becoming increasingly important as a medical diagnostic. However, COST uses laser radiation rather than X-rays as the probe. By recording the net absorption along different beam paths, the system generates a computer image of a cross section through a sample volume that may be constantly changing. It does so with a laser source (laser 1) and an array of detectors (D_1 through D_n) on opposite sides of the sample volume (see figure, typical for wind tunnels). The laser is pivoted so that the beam path can be changed,

(continued on next page)

falling on each detector in sequence. A second laser and detectors scan the sample at right angles to the first set. All laser sources and detectors are mounted on a mechanism that allows rotation of the beam paths about the sample volume.

The detector outputs, which measure the net absorption along the beam path, are recorded, digitized, and stored in memory. The data are correlated with scan angle to construct an image of the optical density of the sample volume.

By selecting laser emission lines that correspond to absorption frequencies of gases of interest, the system could select only particular gases for analysis. For example a tunable CO_2 laser beam that is selectively absorbed by air pollution gases could be used for imaging the exhaust plume of a jet engine as the fuel/air mixture is adjusted. For wind-tunnel studies, selectively detectable gases could be added to the aircraft-model boundary layer to enhance the COST image.

This work was done by Victor J. Anselmo of Caltech for **NASA's Jet Propulsion Laboratory.** *For further information, Circle 71 on the TSP Request Card.*
NPO-14705

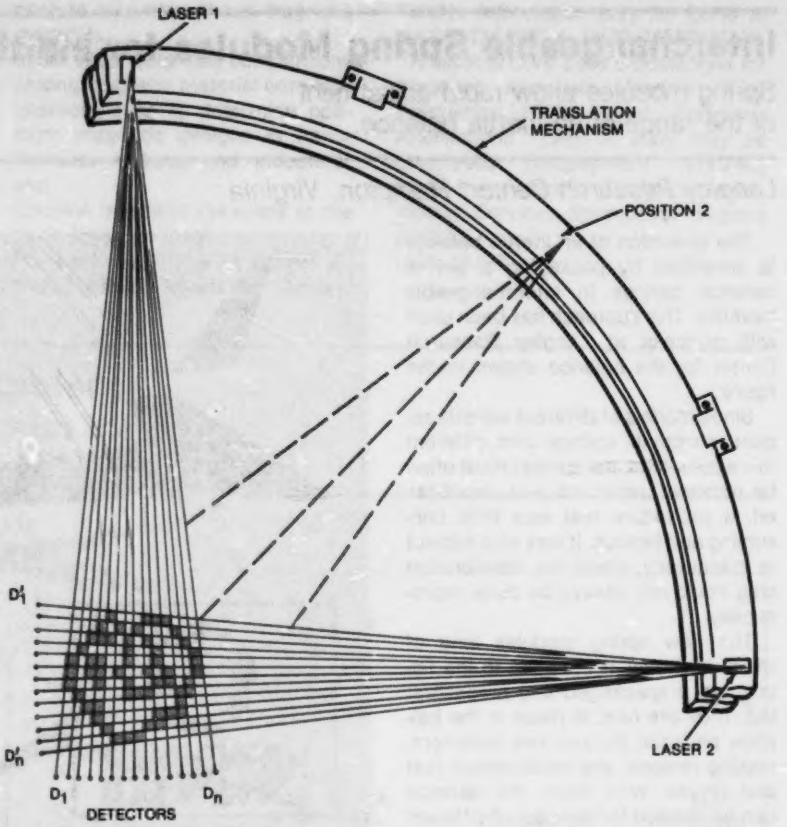

Lasers in the **COST Imaging System** scan a sample volume at right angles. The detectors measure the transmitted light. From these data, an image of the absorption characteristics of the sample is constructed. Scan position 2 would be used to enhance resolution.

Integrated Material-Surface Analyzer

Up to 10 in vacuo surface analyses are performed in one system.

NASA's Jet Propulsion Laboratory, Pasadena, California

Any or all of up to 10 in vacuo surface analyses would be carried out with the proposed module shown in the figure. Such a battery of tests (see table), used to study MOS and other devices, usually requires separate instruments. Combining the tests in one system would speed up testing and would reduce the possibility of sample contamination between tests.

The module concept combines a mass spectrometer, a charged-particle analyzer, and a multiple sample holder. Ultraviolet, X-ray, electron, and ion sources are directed at one sample at a time, as is the analyzer inlet lens. Also included are: a heater/cooler, an electron/ion multiplier, a Faraday cup detector, and digital control circuitry.

The two-section, hemispherical kinetic-energy analyzer is mounted between inlet and exit lenses. From the exit lens, ions ejected from the sample pass symmetrically between four parallel rods in the quadrupole mass spectrometer. When the module is used for one of the ion spectroscopies, an alternating potential superimposed on a steady potential filters out all ions except those of a particular mass. For the electron spectroscopies, the quadrupole mass spectrometer functions as an electron transfer lens between the kinetic-energy analyzer and the electron/ion multiplier.

The different analysis functions are selected by switching to the desired source, applying appropriate potentials to the kinetic-energy and mass analyzers, and controlling the inlet and exit lenses. (A Faraday cup at the spectrometer output is included primarily for calibration.) The potentials are programable and can be set accurately.

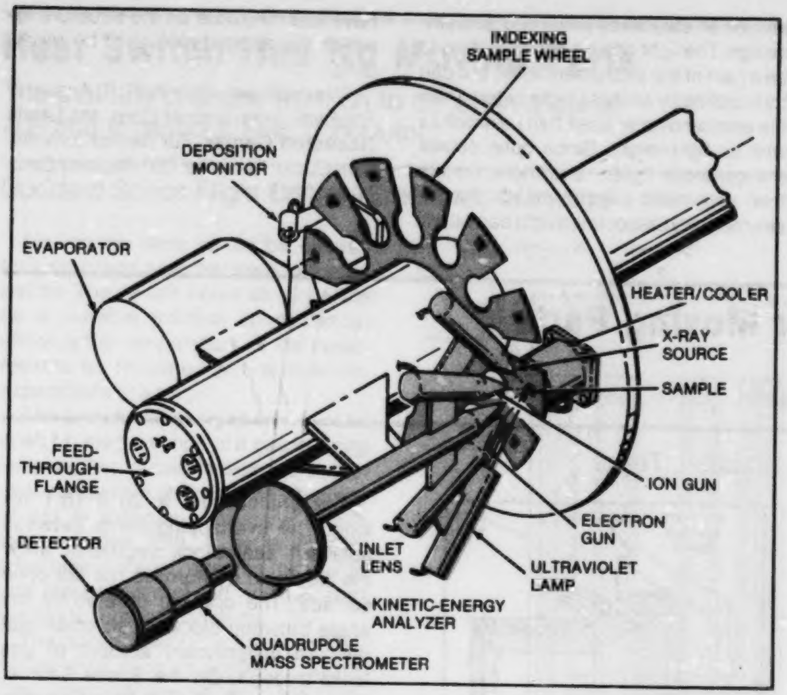

This **Surface-Analysis Module** for installation in a vacuum chamber can run a series of tests without breaking the vacuum between tests. Power for the different tests varies from 100 to 1,500 watts.

- Secondary-ion mass spectroscopy
- Ion-scattering spectroscopy
- Electron-stimulated desorption
- Residual-gas analysis
- Auger electron spectroscopy
- X-ray photoelectron spectroscopy
- Ultraviolet photoelectron spectroscopy
- Characteristic-electron energy-loss spectroscopy
- Scanning electron microscope
- Scanning low-energy electron probe

These **10 Surface-Analysis Tests** can be run without breaking the vacuum. A quadrupole mass spectrometer, used in the first four tests, serves as an electron transfer lens in the last six tests.

An electronics module decodes digital command data and controls the detectors directly or with a prestored sequence from memory. This module also conditions and buffers signals from the detector and from voltage, current, temperature, and position sensors. It also formats the data into a digital stream.

This work was done by Frank J. Grunthaner and Blair F. Lewis of Caltech for **NASA's Jet Propulsion Laboratory.** *For further information, Circle 72 on the TSP Request Card.*
NPO-14702

Fiber-Optic Accelerometer

Lightweight instrument would convert mechanical motion into digitized optical outputs.

Lewis Research Center, Cleveland, Ohio

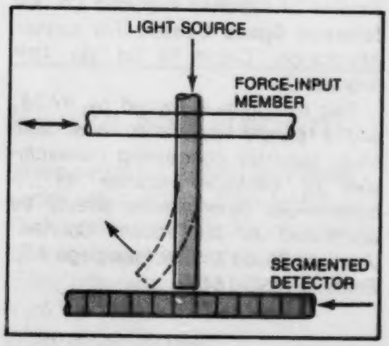

The **Optical Fiber Is Displaced** by the acceleration of the force-input member. The magnitude of the acceleration, which is related to the instantaneous position of the end of the fiber, is indicated as a digital output from the segmented detector.

A low-cost, rugged, lightweight accelerometer has been developed that converts mechanical motion into digitized optical outputs and is immune to electromagnetic and electrostatic interferences. This instrument can be placed in a hostile environment, such as an engine under test, and the output led out through a miscellany of electrical fields, high temperatures, etc., by optic fiber cables to the benign environment of a test panel. There, the digitized optical signals can be converted to electrical signals for use in standard electrical equipment or used directly in optical devices, such as an optical digital computer.

Basically as shown in the figure, a flexible optic fiber is suspended by one end fastened to the instrument case. A light source located at the fixed end introduces light into the suspended fiber. The other end of the fiber is free to move with respect to the case and directs the light onto an array of receptors, fixed with respect to the case. Acceleration applied to the case causes different receptors of the segmented detector to be activated by the light from the end of the oscillating fiber, providing a reading of the instantaneous positions of the fiber. The instantaneous position of the fiber is a direct measure of the acceleration being experienced by the case.

The fiber flexes in a single plane. Three orthogonally mounted instruments can produce three-axis acceleration data, which can, in turn, yield the total acceleration vector.

Variations in the instrument design are possible by controlling length, mass, and optical finish of the oscillating optic fiber, as well as clearance limits and detector design. The light source does not have to be a part of the instrument itself, but can be supplied by an input optic cable. Then the accelerometer itself can be small as well as lightweight. Since optic cables are generally lighter and more flexible than equivalent electric cables, the instrument and associated light cables will have less influence on the structure for which the acceleration is to be measured.

This work was done by R. R. August of Rockwell International Corp. for **Lewis Research Center**. *For further information, Circle 73 on the TSP Request Card. LEW-13219*

Heat/Pressure Seal for Moving Parts

Articulated graphite segments accommodate dimensional variations.

Lyndon B. Johnson Space Center, Houston, Texas

A prototype seal keeps hot gases from leaking between large, adjacent parts in relative motion. The seal withstands temperatures greater than 1,000° C (1,800° F) and accommodates heat- and pressure-caused distortion of the parts. It is nonabrasive, creates little resistance to the movement of parts, and causes minimal wear and damage to surface coatings.

The seal was developed for the tail of the Space Shuttle orbiter, where it protects rudder/speed-brake components from high temperatures during reentry. It could also find application in manufacturing processes requiring thermal barriers between large moving parts.

The seal (see figure) consists of a housing, for attachment to one of the two adjacent moving parts, and an articulated graphite seal block, located in a channel within the housing. There are two sealing surfaces on the seal block: a rubbing surface that is held against one of the moving parts by helical springs, and a sliding surface that is held against the seal housing by a cantilever spring and a roller. The helical-spring force varies only slightly with deflection so that essentially constant pressure is maintained on the rubbing surface. In addition, the spring force is low enough to minimize rubbing friction and high enough to ensure an adequate seal under atmospheric and aerodynamic pressures.

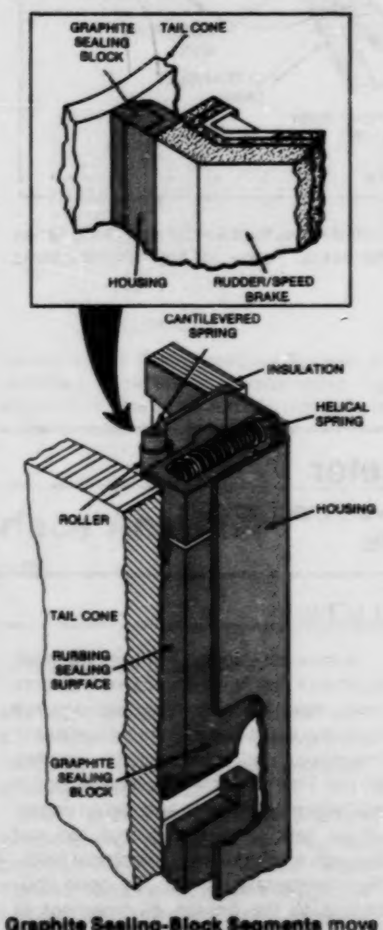

Graphite Sealing-Block Segments move on the Space Shuttle tail cones as the rudder/speed brake moves. Mounted on the rudder/speed brake, the housing contains springs that bias the block segments against the tail cone and housing sealing surface. The block segments accommodate dimensional changes caused by variations in temperature and pressure.

The Shuttle seal is 20 ft (6.1 m) long. The overlapping joints between adjacent seal block segments allow the blocks to conform to the tail cone surface. The opening created by the angle between blocks is so small that only an insignificant amount of gas leaks through. On the Space Shuttle, the seal permits 2-ft (0.61-m) relative rotational motion of the rudder/speed-brake leading edge around the tail cone.

Because of the high-temperature difference between the graphite blocks and the metal housing, each block is positioned by a guide slot and locating pin and is held against the housing by a cantilever spring. The locating pin is attached to the side of the housing, and the guide slot is between projections of the graphite blocks. This allows relative expansion and contraction of the housing without interrupting the seal.

This work was done by Martin L. Stevens of Fairchild Republic Co. for **Johnson Space Center.** *For further information, Circle 74 on the TSP Request Card.*

This invention is owned by NASA, and a patent application has been filed. Inquiries concerning nonexclusive or exclusive license for its commercial development should be addressed to the Patent Counsel, Johnson Space Center [see page A5]. Refer to MSC-18422.

Heat Switch Has No Moving Parts

Thermal link changes from on to off when a getter adsorbs a gaseous heat conductor.

Goddard Space Flight Center, Greenbelt, Maryland

No moving parts would be needed for a proposed new thermally actuated switch. The switch could also operate as a variable thermal conductance, allowing the temperature of the equipment to be regulated with a minimum expenditure of energy.

The switch is a gas-gap type — one in which the presence of a gas in a gap between two plates makes the switch heat-conductive (on) and the absence of gas in the gap makes the switch nonconductive (off). A getter (a gas-adsorbing material) adsorbs the gas to turn the heat switch off and releases the gas to turn the switch on.

The plates, made of a heat-conducting material such as copper or aluminum, are interleaved and are supported by a cylinder of an insulating material, such as fiberglass, nylon, or glass (see figure), which also serves to contain the gas. The gas gap is connected by a capillary tube to a small disk of getter material such as activated charcoal or a member of the zeolite mineral group. An electrical heater is positioned next to the getter. After the gas has been introduced into the switch through a fill tube, the tube is hermetically sealed.

A small current applied to the getter heater turns the heat switch on. The current raises the temperature of the getter enough to expel adsorbed gas into the gap. When the gas pressure in the gap reaches 100 to 200 μm of mercury (0.1 to 0.2 torr), the switch is fully conducting.

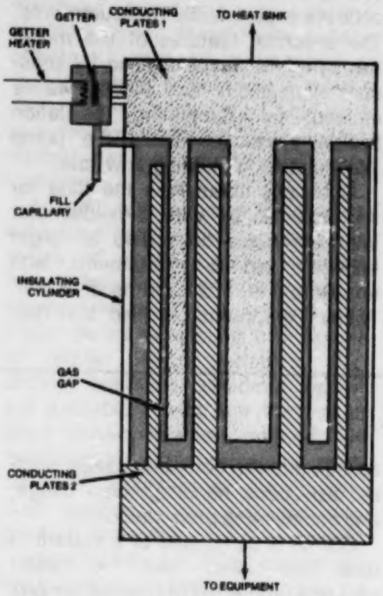

A Gap Between Interleaved Plates conducts heat when it is filled with gas and prevents heat transfer when the gas is absent. Controlled by a heater, a getter emits gas into the gap or adsorbs the gas from the gap.

If the heater is turned off and the getter is attached to a sufficiently-cold heat sink, it will adsorb the gas from the gap. When the gap pressure drops to about 10^{-5} torr, the heat switch is in its state of lowest conductance — its off state. In this state, the conductance of the gap is less than that of the insulating cylinder.

The amount of gas that the getter releases into the gap is determined by the magnitude of the heater current. Thus, the current can be regulated to control the amount of gas emitted and hence the conductance of the switch. The heat switch can then be operated as a heat valve with continuously-variable thermal conductance.

The choice of gas and getter depends on the temperature of the heat sink. Helium gas, for example, is the choice for temperatures between 1 and 8 K. The minimum and maximum gas pressures in this temperature range correspond to the required off and on conductances. At higher heat-sink temperatures, krypton (66 to 116 K) or water (233 to 373 K) can be used, for example.

This work was done by Stephen H. Castles of **Goddard Space Flight Center**. *For further information, Circle 75 on the TSP Request Card.*
GSC-12625

Books and Reports

These reports, studies, and handbooks are available from NASA as Technical Support Packages (TSP's) when a Request Card number is cited; otherwise they are available from the National Technical Information Service.

Dynamics of Cavitating Cascades and Inducer Pumps

Annotated bibliography summarizes 19 papers on the dynamics of cavitation.

A report chronicles the advances in understanding and predicting the unsteady dynamic characteristics of cavitating cascades and inducer pumps. It includes a bibliography of 19 papers authored between 1972 and 1980.

Cavitation is a phenomenon in which the fluid pressure of a liquid fluctuates slightly above and below the vapor pressure, causing the alternate formation and collapse of vapor bubbles. This in turn causes localized shock waves that can lead to the pitting of metal surfaces and a marked drop in efficiency. Cavitation phenomena, thus, have very significant

(continued on next page)

implications in liquid-handling and mixing systems.

In early papers simple L,R,C models were used for cavitating pumps, and the types of cavitation occurring in cascades and inducer pumps were identified. Compliance resulting from attached-blade cavities and compliance characteristics of bubbly cavitation were analyzed.

In later papers a more general dynamic-transfer-function concept was developed, and the contributions to the mass flow gain factor due to attached-blade cavities were presented. A test facility was constructed to study the unsteady dynamic response of cavitating inducer pumps. Using water and impellers 3 in. (7.6 cm) in diameter, complete dynamic transfer functions for various mean flow conditions (including cavitation number) were obtained at frequencies up to 42 Hz.

To understand better the dynamics of cavitation, the Bubbly Flow model was developed. It uses a bubbly, two-phase flow representation for the dynamics of cavitation pumps. Its transfer functions are in good qualitative and fair quantitative agreement with the experimental measurements. The essential features of the model are dynamic waves caused by pressure fluctuations and kinetic waves caused by fluctuating cavitation bubble production (near the pump inlet) due to fluctuating flow rate.

Questions about how the data for the test facility with 3-in.-diameter impellers could be scaled to larger impellers led to experiments with impellers 4 in. (10.2 cm) in diameter. These experiments verified that correct scaling behavior had been deduced. Under certain conditions and without external perturbations, flow in the test facility demonstrated large pressure and flow-rate fluctuations. This auto-oscillation instability was also investigated. Studies and theoretical analyses of flow details at or near the inlet to a cavitating impeller showed that the complicated swirling flow at the inlet is an important determinant of both the steady-state performance and the dynamic characteristics of the inducer.

This work was done by C. E. Brennen and A. J. Acosta of the California Institute of Technology for **Marshall Space Flight Center.** *To obtain a copy of the report, "Dynamics of Cavitating Cascades," Circle 76 on the TSP Request Card.*
MFS-25399

Computer Programs

These programs may be obtained at very reasonable cost from COSMIC, a facility sponsored by NASA to make new programs available to the public. For information on program price, size, and availability, circle the reference letter on the COSMIC Request Card in this issue.

Simplified Thermal Analyzer

Program for quick analysis of temperature and power balance is especially easy to use.

The Simplified Shuttle Payload Thermal Analyzer (SSPTA) aids in evaluating the thermal design of instruments to be flown in the Space Shuttle cargo bay. It is a collection of programs that are currently used in the thermal analysis of spacecraft, modified for quick, preliminary analysis of payloads. Although designed primarily to analyze the Shuttle payloads, it can easily be used for thermal analysis in other situations.

SSPTA includes a reduced math model of the Shuttle cargo bay. One of the prime objectives in developing SSPTA was to create an easily used program. With it, the user-required input is simple; and the user is free from many of the concerns normally associated with computer usage, such as disk-space handling, tape usage, and complicated program control.

SSPTA is comprised of a system of data files called "bins," a master program, and a set of thermal subprograms. The bin system is a collection of disk files that contain data required by or computed by the thermal subprograms. SSPTA currently handles 50 bins.

The master program serves primarily as a manager for the bins and their interaction with the thermal subprograms. Inputs to the master program are simple user commands that direct the data manipulation procedures, prepare the data for these procedures, and call the appropriate thermal subprograms. The subprograms of SSPTA are all based on programs that have been used extensively in the analysis of orbiting spacecraft and space hardware.

In subprogram CONSHAD, the user-supplied geometric radiation model computes blackbody view factors, shadow factors, and a description of the surface model. The subprogram WORKSHEET uses the surface-model description, optical-property data, and node-assignment data to prepare input for SCRIPTF, which computes the inverses of the infrared (IR) and ultraviolet (UV) radiation transfer equations. SCRIPTF also computes the radiation coupling between nodes in the thermal model.

Subprogram ORBITAL uses the shadow tables to compute incident flux intensities on each surface in the geometric model. In subprogram ABSORB, these flux intensities are combined with the IR and UV inverses to compute the IR and UV fluxes absorbed by each surface. The radiation couplings from SCRIPTF and the absorbed fluxes from ABSORB are used to compute the temperature and power balance for each node in the thermal model, in subprogram TTA.

Outputs consist of tabulated data from each of the subprograms executed during an analysis. Because SSPTA is modular, analyses may be run in whole or in part, and new subprograms may be added.

SSPTA is written in FORTRAN IV and Assembler for batch execution and has been implemented on an IBM 370-series computer with a central memory requirement of approximately 600K of 8-bit bytes. SSPTA was developed in 1977 and last updated in 1979.

This program was submitted by Michael J. Coyle of **Goddard Space Flight Center.** *For further information, Circle A on the COSMIC Request Card.*
GSC-12638

Resizing Structures for Minimum Weight

Approximation concepts and dual-method algorithms are combined in a new weight-minimization method.

Approximation concepts and dual-method algorithms are combined in a new method of minimum-weight design for structures. The Approximation Concepts Code for Efficient Structural Synthesis (ACCESS3) program is a powerful research tool in which mathematical programing and optimality criteria are coalesced in an efficient structural weight-minimization method.

Approximation concepts convert the general structural synthesis problem into a sequence of explicit problems of separable algebraic form. The dual method exploits this separable form to construct a sequence of explicit dual functions. These dual functions are maximized subject to nonnegativity constraints on the dual variables. This approach is very efficient because the dimensionality of the dual space, where most of the optimization effort is expended, is relatively low for most structural optimization problems of practical interest.

A rather general class of structural optimization problems can be concisely stated as a nonlinear programing (NLP) problem involving the minimization of an objective function subject to a set of inequality constraints. For practical structural design applications, the associated NLP problem is often very complicated due to the large number of design variables, the large set of inequality constraints, and the computational difficulties associated with the constraint functions. The ACCESS3 approach makes such an NLP problem tractable by replacing it with a sequence of relatively small, explicit mathematical programing problems that approximate the original problem while retaining important problem features. This is accomplished through the coordinated use of design variable linking, constraint deletion techniques, and explicit approximations for retained constraints.

Structures with prescribed configurations and given material properties are realized by modifying the dimensions of the finite elements, in particular their cross-sectional areas or thicknesses. Types of finite elements available in ACCESS3 include a truss, an isotropic constant-strain triangular membrane, a constant-strain triangular element with arbitrary orthotropic material properties, an isotropic shear panel, and a thermal shear panel. Thermal load analysis is included for problems involving load vectors that are dependent on design variables.

In addition to the usual Taylor-series expansion with respect to the reciprocals of linked design variables, natural-frequency constraints may be represented as first- or second-order Taylor-series expansions with respect to regular linked variables. Four distinct optimizer algorithm options are available. These are the interior point penalty-function method, the second-order primal-projection method, the second-order Newton-type dual method, and the first-order gradient projection-type dual method.

Input data for ACCESS3 consist of a finite-element model that exhibits the topological form, the geometrical configuration, and the structural materials of the structural system to be optimized, along with a set of structural loads and a selection of program options. Outputs include a description of the resizing of elements required to achieve minimum weight.

The ACCESS3 program is written in FORTRAN IV for batch execution and has been implemented on a CDC CYBER 70-series computer with a central memory requirement of approximately 74K (octal) of 60-bit words. The ACCESS3 program was developed in 1979.

This program was written by C. Fleury and L. A. Schmit of the University of California, Los Angeles, for **Langley Research Center.** *For further information, Circle B on the COSMIC Request Card.*
LAR-12699

NASTRAN Modifications for Recovering Strains and Curvatures

Where required, curvatures and strains can be retrieved in lieu of stresses.

NASTRAN, NASA's general-purpose finite-element structural analysis program, has been modified to allow recovery of surface strains, reference plane strains, and local curvatures at the nodes of the general plane elements. The NASTRAN routines that operate on element stress/strain/temperature relationships and strain/displacement relationships have been modified to incorporate the generation and return of strains and curvatures in lieu of stresses. The strains and curvatures are then transformed to the material axes and interpolated to generate the corresponding strains and curvatures at the nodes of the element. This interpolation is accomplished using a special surface-mapping function.

The recovery of strains and curvatures can be valuable in the performance of certain analyses. These variables are useful in comparing predicted strains with those measured via strain gages. Availability of this information can simplify the use of NASTRAN to solve nonlinear problems. Composite analysts can now couple NASTRAN with composite mechanics via 'pre' and 'post' processors and take advantage of NASTRAN's vast capabilities for designing and analyzing structures.

This program was written by C. C. Chamis of **Lewis Research Center** *and C. H. Hennrich of MacNeal-Schwendler Corp. For further information, Circle C on the COSMIC Request Card.*
LEW-12592

Cost-Minimized Aircraft Trajectories

Climb, cruise, and descent profiles for lowest operating costs

For an aircraft operating over a fixed range, the operating costs are basically a sum of fuel cost and time cost; but determining a minimum cost trajectory can be complex. A new program optimizes trajectories with respect to a cost function that is based on a weighted sum of fuel cost and time cost. Minimum fuel, minimum time, and various delay trajectories are obtained by specifying particular values for the fuel and time cost factors.

As a research tool, the program could be used to study characteristics of optimum trajectories and to compare them to standard trajectories. It might also be used to generate a model for the development of an airborne trajectory optimization system. The program could be incorporated into an airline flight-planning system, with optimum flight plans determined at takeoff time for the prevailing flight conditions. Trajectory optimization could significantly reduce the cost for a given aircraft mission.

The algorithm incorporated in the program assumes that a trajectory consists of climb, cruise, and descent segments. Each segment is not optimized independently, as in classical procedures, but is optimized to account for interactions between the segments. This is done with optimal control theory.

The climb and descent profiles are generated by integrating a set of kinematic and dynamic equations, where the total energy of the aircraft is the independent variable. At each energy level of the climb and descent profiles, the airspeed and power necessary for an optimal trajectory are determined. The variational Hamiltonian of the problem consists of the rate of change of cost with respect to total energy and a term dependent on the adjoint variable, which is identical to the optimum cruise cost at a specified altitude. This variable uniquely specifies the optimal cruise energy, cruise altitude, cruise mach number, and indirectly, the climb and descent profiles.

If the optimum cruise cost is specified, an optimum trajectory can easily be generated; however, the range obtained for a particular optimum cruise cost is not known a priori. For short-range flights, the program iteratively varies the optimum cruise cost (and therefore the cruise altitude) until the computed range converges to the specified range. For long-range flights, iteration is unnecessary since cruise flight always takes place at the optimum cruise altitude.

The user must supply the program with engine fuel flowrate and thrust data and an aircraft aerodynamic model. The program currently includes data for the Pratt-Whitney JT8D-7 engine and an aerodynamic model representative of the Boeing 727. Inputs to the program consist of the flight range to be covered and the prevailing flight conditions, including pressure, temperature, and wind profiles. Information output by the program includes: optimum cruise tables at selected weights, optimal climb and descent profiles, and a summary of the complete synthesized optimal trajectory.

This program is written in FORTRAN IV for batch execution and has been implemented on a CDC 6000-series computer with a central memory requirement of approximately 100K (octal) of 60-bit words. This aircraft trajectory optimization program was developed in 1979.

This program was written by Homer Lee and Heinz Erzberger of **Ames Research Center.** *For further information, NASA TP-1565, "Computer Algorithm for Fixed Range Optimal Trajectories" [1980], Circle D on the COSMIC Request Card.*
ARC-11282

Aerodynamic Preliminary Analysis

An interactive system for surveying alternative configurations and component geometries.

The computerization of aerodynamic theory has progressed to a state where the analysis of complete aircraft configurations can be performed by a single program. Currently existing programs of this nature abound with subtleties and difficulties attributable to the level of precision of the underlying theory and the sensitivity of the associated numerical solution techniques. In preliminary design stages, it is often desirable to accept some degree of approximation in the interest of faster turnaround, reduced computational costs, the simplification of input, and the stability of results while maintaining generality.

The Aerodynamic Preliminary Analysis System, APAS, is a comprehensive aerodynamic analysis system, based on linearized potential theory. Three-dimensional configurations (with or without jet flaps) having multiple nonplanar surfaces of arbitrary planform and open or closed slender bodies of noncircular contour may be analyzed with the APAS. As a preliminary design aid, APAS allows the designer to survey systematically a large number of alternative configurations and component geometries economically. When combined with realistic assessments of its limitations and estimated viscous characteristics, APAS is a valuable tool for analyzing general aircraft configurations and aerodynamic interactions.

The analysis technique employed by APAS is based on linearized aerodynamic theory. The configuration to be analyzed is simulated by a distribution of source and vortex singularities. Each of the singularities satisfies the linearized small-perturbation-potential equation of motion. The singularity strengths are obtained by satisfying the condition that the flow remains tangent to the local surface.

The bodies, interference shells, and aerodynamic surfaces are each simulated by different types of singularities. First, the strengths of singularities representing the fuselage and nacelles are determined by using a slender body thickness approach to predict the surface and near-field properties. Perturbation velocities induced on the aerodynamic surfaces are evaluated.

Singularity strengths representing aerodynamic surfaces are determined utilizing thin airfoil panel theory, which allows the effects of thickness and lift to be considered independently. A cylindrical, noncircular, interference shell, composed entirely of vortex panels, is used to account for the interference effects of the aerodynamic surfaces on the fuselage and nacelles.

Once all of the singularity strengths are determined, the resulting velocities and pressures throughout the flow are obtained. APAS also performs a drag analysis for determining skin friction, potential form drag, and trim drag.

APAS is a user-oriented interactive system. Once the system is accessed, it is a self-contained interactive environment where the analyst can input vehicle definitions, perform aerodynamic analysis, and display computed results without exiting the system. Geometry and analysis data may be saved for later sessions and are protected from loss due to machine failure. The interactive nature of APAS permits the user to quickly learn how to use the system.

The APAS is written in FORTRAN IV for interactive, or batch, execution and has been implemented on a CDC CYBER 175 computer. The largest program in the system has a central memory requirement of approximately 120K (octal) of 60-bit words. The computer on which APAS is installed must support segmentation and random-access files. The interactive and graphics capabilities of APAS require a Tektronix 4014 graphics terminal, a Tektronix 4096 graphics tablet, and the Tektronix Plot 10 and graphics tablet support software. The APAS was developed in 1978.

This program was written by E. Bonner, W. Clever, P. Divan, K. Dunn, and J. Kojima of Rockwell International Corp. for **Langley Research Center.** *For further information, Circle E on the COSMIC Request Card.*
LAR-12404

Inviscid Transonic Flow Over Axisymmetric Bodies

Outputs include pressure distribution, drag, and flow-field data.

Axisymmetric transonic flow is of interest not only because of its practical application to missile and launch vehicle aerodynamics but also because of its relation, in terms of the area rule, to fully three-dimensional flow. The RAXBOD computer program analyzes steady, inviscid, irrotational, transonic flow over axisymmetric bodies in free air. RAXBOD uses a finite-difference relaxation method to solve numerically the exact formulation of the disturbance velocity potential with exact surface boundary conditions. The nonconservative form of the potential equation is used. Agreement with available experimental results has been good in cases where viscous effects and wind-tunnel wall interference are not important.

The governing second-order partial differential equation describing the flow potential is replaced by a system of finite-difference equations, including Jameson's "rotated" difference scheme at supersonic points. A stretching is applied to both the normal and tangential coordinates, such that the infinite physical space is mapped onto a finite computational space. The boundary condition at infinity can be applied directly, and there is no need for an asymptotic far-field solution.

The system of finite-difference equations is solved by a column relaxation method. In order to obtain both rapid convergence and any desired resolution, the relaxation is performed iteratively on successively refined grids. Inputs to RAXBOD consist of a description of the body geometry, the free-stream conditions, and the desired resolution control parameters. Outputs from RAXBOD include computed geometric parameters in the normal and tangential directions, iteration history information, pressure distribution, drag coefficients, flow-field data in the computational plane, and coordinates of the sonic line.

This program is written in FORTRAN IV for batch execution and has been implemented on a CDC 6600 computer with an overlaid central memory requirement of approximately 40K (octal) of 60-bit words. Optional plotted output can be generated for the CALCOMP plotting system. The RAXBOD program was developed in 1976.

This program was written by Jerry C. South, Jr., and James D. Keller of **Langley Research Center.** *For further information, Circle F on the COSMIC Request Card.*
LAR-12499

Plastic Deformation of Engines and Other Nonlinear Structures

Program analyzes elastic, plastic, and creep deformation for high temperatures and cyclic loads.

The Plastic Analysis Capability for Engines (BOPACE3D) is a nonlinear stress-analysis program based on a very general family of isoparametric finite elements. Although the development of BOPACE3D has been heavily influenced by the requirements for engine analysis (in particular the Space Shuttle main engine), it is a general program applicable to many nonlinear structures.

BOPACE3D analyzes the stresses on structures subjected to very high temperatures, large plastic-creep effects, and geometric nonlinearities, while experiencing cyclic thermal and mechanical loads. It includes several such advanced features as substructuring, an out-of-core Gauss wave-front equation solver, multipoint constraints, combined material and geometric nonlinearities, automatic calculation of inertia effects, follower forces, singular crack-tip elements, and axisymmetric capabilities.

Classical constitutive theory in an elastoviscoplastic program such as BOPACE3D provides the incremental relations between stresses and strains. BOPACE3D uses these relations and the standard finite-element stiffness method to obtain an efficient solution approach for an important class of nonlinear structural-analysis programs.

Elastic, plastic, thermal, and creep deformations and the nonlinear dependence of all deformations on temperatures are accurately accounted for in the BOPACE3D solution. The material theory used includes a combined isotropic/kinematic plastic hardening theory and a generalized approach to cyclic load reversal. A family of isoparametric finite elements is provided for structure modeling. The simplest elements of this family are the two-node rod, the four-node quadrilateral, and the eight-node brick. Various higher order elements are available with each basic element edge containing up to five arbitrarily spaced nodes.

The ability to space edge nodes arbitrarily and to have different numbers of edge nodes on different edges of the same element provides versatility in representing complex geometries. To relieve the user of much of the effort required in developing a complex finite-element model, the program provides an automated data-generation capability.

The BOPACE3D program is written in FORTRAN IV for batch execution and has been implemented on a UNIVAC 1100-series computer with a segmented central memory requirement of approximately 56K of 36-bit words. Version 6 of the BOPACE3D program was released in 1978.

This program was written by R. G. Vos and J. L. Arnquist of The Boeing Co. for **Marshall Space Flight Center**. *For further information, Circle G on the COSMIC Request Card.*
MFS-23814

Analysis of a Cooled, Turbine Blade or Vane With an Insert

Transient thermal analysis of blades and vanes with a coolant insert

A computer program, TACTI, has been developed to calculate transient and steady-state temperatures, pressures, and flows in a cooled turbine blade or vane with an impingement insert. Coolant-side heat-transfer coefficients are calculated internally in the program, with the user specifying one of three modes of heat transfer at each station: (1) impingement, including the effect of crossflow; (2) forced-convection channel flow; or (3) forced convection over pin fins. A limited capability to handle film cooling is also available in the program. It is assumed that spent impingement air flows in a chordwise direction and is discharged through a split or drilled trailing edge and through film-cooling holes. The program does not allow for radial flow of the spent impingement air. The use of film cooling is restricted by a numerical model requirement for a continuous crossflow.

As turbine-engine core operating conditions became more severe, it was more difficult to effectively cool blades and vanes. Advanced transient thermal calculation techniques were needed to design reliable turbine blades. There was no generally-available computer program that used advanced techniques in combining the required heat-transfer and coolant-flow-distribution calculations. TACTI was developed to perform transient and steady-state heat-transfer and coolant-flow analyses for a cooled blade, given the outside hot-gas boundary conditions, the coolant inlet conditions, the geometry of the blade shell, and the cooling configuration. It can handle a turbine blade or vane that is equipped with a central coolant-plenum insert from which coolant air flows through holes to impinge on the inner surface of the blade shell. The blade is modeled by dividing it by chordwise planes into as many as 15 slices, with each slice having as many as 79 chordwise calculational stations. Temperatures at each station are calculated for four points through the wall and one in the coolant channel. Included in this model is the capability to analyze a blade with a ceramic thermal-barrier coating. The ability of the program to handle film cooling is limited by the numerical modeling of the coolant crossflow.

For inputs to the program, the following basic elements of the geometry are needed for each station: (1) the thicknesses of the wall coating and wall metal and the coolant-channel width, (2) the chordwise distance of each node from the adjacent upstream node, and (3) the radial span for this slice. In addition, depending on the mode of heat transfer specified, the user must supply diameter and spacing for impingement holes or pin fins and data for film-cooling holes. All input values except the radial span are assumed to be the values at the midspan of the slice. Program output includes the temperature at each node, the coolant pressures and flow rates, and the inside heat-transfer coefficients.

The numerical solution for the temperatures throughout the blade involves writing a transient energy equation for each node and forming a set of equations to be solved for the temperature distribution. The nodal energy balances are linearized, one-dimensional, heat-conduction equations at the wall-outer-surface node, at the junction of the cladding and the metal node, and at the wall-inner-surface node. At the midmetal node, a linear, three-dimensional, heat-conduction equation is used.

Similarly, the coolant pressure distribution is determined by writing the transient momentum equation for one-dimensional flow between adjacent fluid nodes and solving the resulting set of equations for static pressures. In the coolant channel, energy and momentum equations for one-dimensional compressible flow including friction and heat transfer are written for the elemental channel length between two coolant nodes.

This program was written in FORTRAN IV for use on an IBM TSS/360-67 computer.

This program was written by R. E. Gaugler of **Lewis Research Center**. *For further information, Circle H on the COSMIC Request Card.*
LEW-13293

Machinery

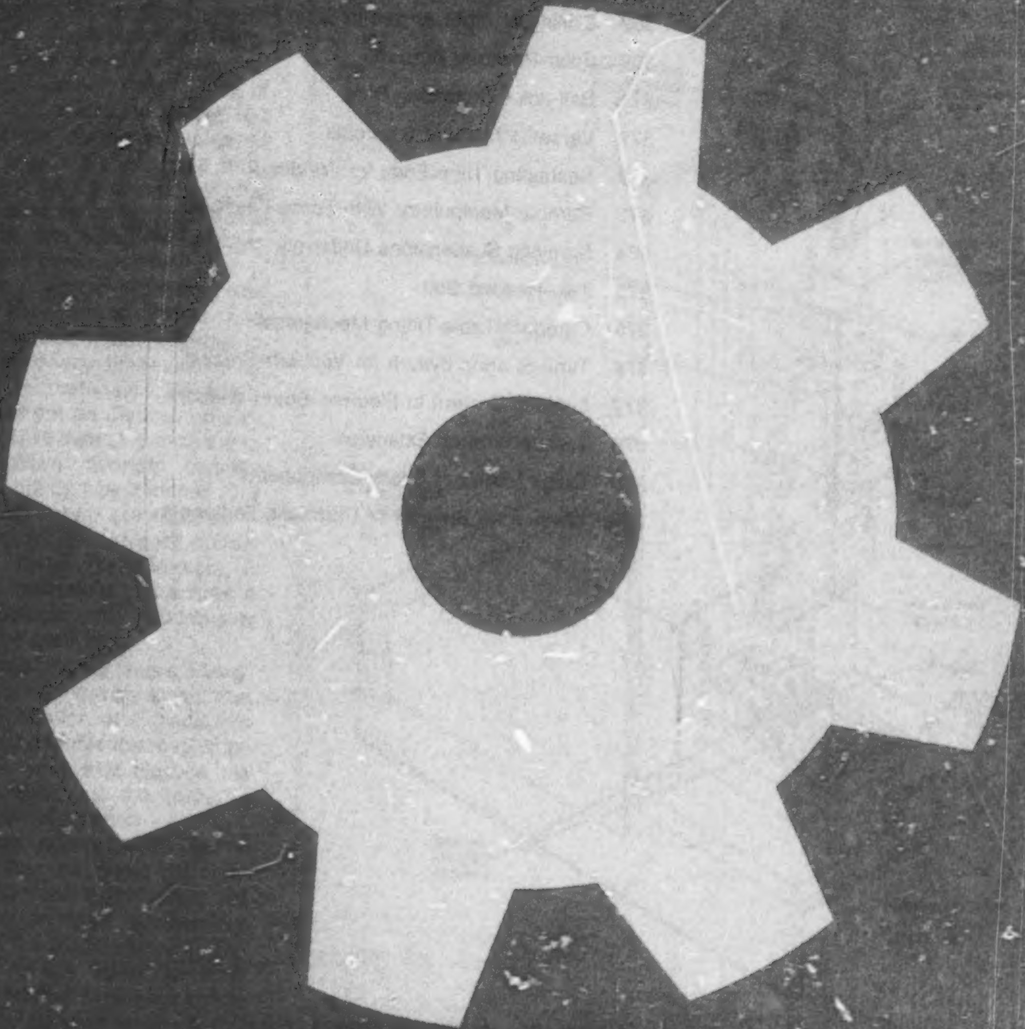

Hardware, Techniques, and Processes

367 Cleaving Machine for Hard Crystals
368 Abrasive Drill for Resilient Materials
369 Drilling at Right Angles in Blind Holes
369 Solar-Powered Aircraft
371 Ball-Joint Grounding Ring
372 Versatile Modular Scaffolds
373 Reshaping Tube Ends for Welding
373 Remote Manipulator With Force Feedback
374 Spraying Suspensions Uniformly
375 Two-Headed Bolt
376 Compact Table-Tilting Mechanism
376 Time-Sharing Switch for Vacuum Brazing
377 Limiting Current in Electron-Beam Welders
378 Torque-Wrench Extension
379 Quick Mixing of Epoxy Components
380 Wrench for Smooth or Damaged Fasteners

Cleaving Machine for Hard Crystals

Undistorted LiF slices for spectrometers can be prepared quickly and with little waste.

Goddard Space Flight Center, Greenbelt, Maryland

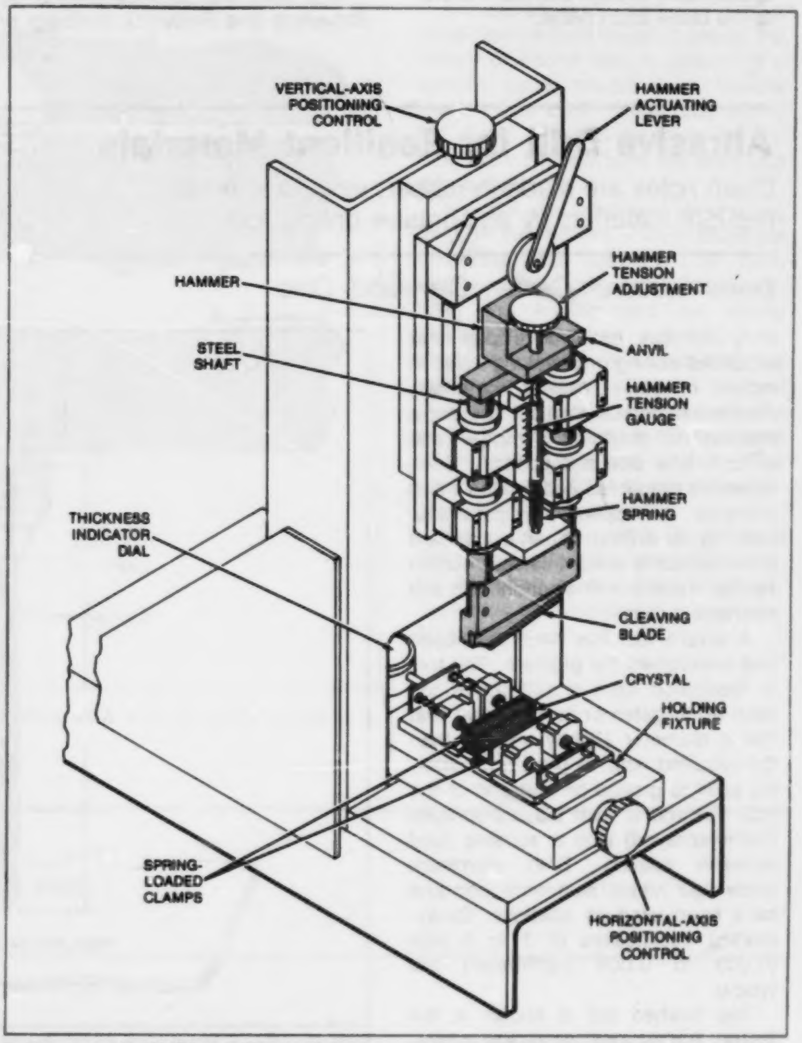

A Hammer/Anvil/Blade Mechanism transmits a shock wave that cleaves the crystal. The hard-crystal cleaving machine has controls for adjusting the position of the crystal block and the striking force of the hammer. The machine shown here can accommodate crystals up to 1 by 2 by 1/2 inches (25.4 by 50.8 by 12.7 mm) in size.

Hard crystalline materials such as lithium fluoride (LiF) can be cleaved in thin sections — precisely and reproducibly — with the aid of a semiautomatic machine. The yield of undistorted LiF crystals is almost 100 percent, even when the cleaved section is only 1/32 inch (0.8 mm) thick. Using the machine, a semiskilled operator can produce uniform crystal slices with greater speed than a skilled hand cleaver.

Previously, lithium fluoride was cleaved by hand with a hammer and knife or razor blade, but learning to cleave by hand was time-consuming and costly in materials. By hand, crystals could not be cleaved reliably to less than 1/16 inch (1.6 mm) thick. Although lithium fluoride crystals measuring 1/32 by 1 by 2 inches (0.8 by 25.4 by 50.8 mm) are required in substantial quantities for such optical devices as crystal spectrometers, it was almost impossible to produce a sufficient number of good-quality slices by hand cleaving.

The new machine contains a spring-activated hammering mechanism that limits the penetration of a blade into the crystal and controls the magnitude of the shock wave that cleaves the crystal. The tension in the spring is adjusted by turning a knob.

A fixture with spring-loaded clamps precisely locates and holds the crystal, restraining it only to the extent that it remains in an ideal position for cleaving until the blade strikes it. The crystal then splays apart as it is cleaved. The holding fixture minimizes damping of the shock wave so that it has full effect in breaking the crystal bonds.

To cleave a crystal, an operator:

- Measures the thickness of the crystal block;
- Places the block between the spring-loaded clamps on the holding fixture so that the crystal cleaving plane is alined parallel to the blade;
- Turns the horizontal-axis positioning control until a dial thickness indicator reads one-half the thickness of the crystal block (this step ensures that the blade will contact the block at its midpoint and that shock-wave forces are balanced; otherwise, the crystal may shatter);
- Raises the hammer by pulling the hammer-actuating lever;
- Turns the hammer tension-adjustment knob until the tension gage indicates the proper tension value for the crystal-block thickness (this experimentally determined adjustment ensures that the hammer strikes the blade with sufficient force to completely break the crystal bond along

(continued on next page)

the cleavage plane without shattering the crystal);

- Lowers the blade until it touches the crystal (blade penetration is limited by a fixed stop);
- Trips the hammer-actuating lever, releasing the hammer so that it strikes the anvil, which transfers the shock wave through two steel shafts to the blade and crystal;
- Raises the blade and removes the two crystal slices.

The procedure can be repeated to obtain progressively thinner slices. During a production run, crystals of a given thickness should be cleaved in sequence so that the hammer tension can be kept at a single setting.

This work was done by John S. J. Benedicto and Frederick Hallberg of **Goddard Space Flight Center.** *For further information, Circle 77 on the TSP Request Card.*

This invention is owned by NASA, and a patent application has been filed. Inquiries concerning nonexclusive or exclusive license for its commercial development should be addressed to the Patent Counsel, Goddard Space Flight Center [see page A5]. Refer to GSC-12584.

Abrasive Drill for Resilient Materials

Clean holes are made in rubber, vinyl, and other resilient materials by an abrasive drilling tool.

Lewis Research Center, Cleveland, Ohio

A tool has been developed that simplifies drilling or punching holes in rubber or other resilient materials. Resilient materials normally present a problem in obtaining accurate and uniform hole size and position. Such materials compress and stretch when pressure is applied in punching, piercing, or drilling. When a standard drill or punch is used, this deformation results in a hole that is nonuniform and nonreproducible.

A simple tool has been developed that overcomes the problem. The tool is fabricated from a stiff metal rod such as tungsten or carbon steel that has a diameter slightly smaller than the required hole. A piercing/centering point is ground on one end of the rod. The rod is then plasma-sprayed (flame-sprayed) with a suitable hard abrasive coating. Both aluminum oxide and nickel/aluminum powders have been used as coatings. Spray-coating thicknesses of 1 to 3 mils (0.003 to 0.008 centimeter) are typical.

The finished tool is shown in the figure. High-speed, slow-feed operation of the tool is necessary for accurate holes, and this can be done with a drill press, hand drill, or similar machines. The tool has been used to drill neoprene rubber, vinyl, and polytetrafluoroethylene with maximum deviation of approximately ±0.002 inch (±0.005 centimeter). It is expected that the drill would work well on other resilient materials.

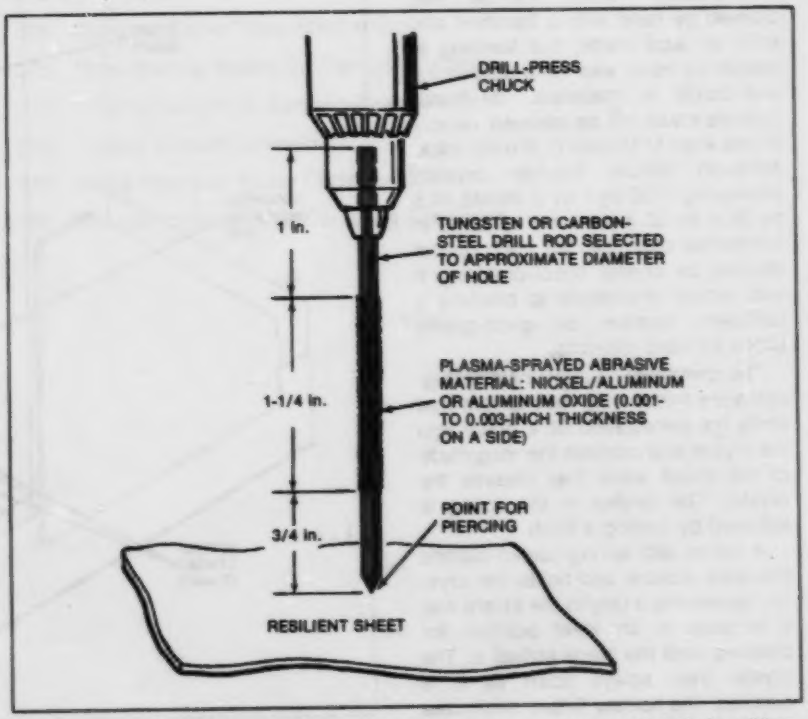
DRILL-PRESS CHUCK
1 in.
TUNGSTEN OR CARBON-STEEL DRILL ROD SELECTED TO APPROXIMATE DIAMETER OF HOLE
1-1/4 in.
PLASMA-SPRAYED ABRASIVE MATERIAL: NICKEL/ALUMINUM OR ALUMINUM OXIDE (0.001- TO 0.003-INCH THICKNESS ON A SIDE)
3/4 in.
POINT FOR PIERCING
RESILIENT SHEET

The Gritty Surface on the tool turning at high speed reams a smooth hole in rubber, vinyl, and other resilient materials

This work was done by A. J. Koch of **Lewis Research Center.** *No further documentation is available.*
LEW-13411

Drilling at Right Angles in Blind Holes

Flexible shaft in a metal tube guides a carbide cutter through the wall of a blind hole.

Marshall Space Flight Center, Alabama

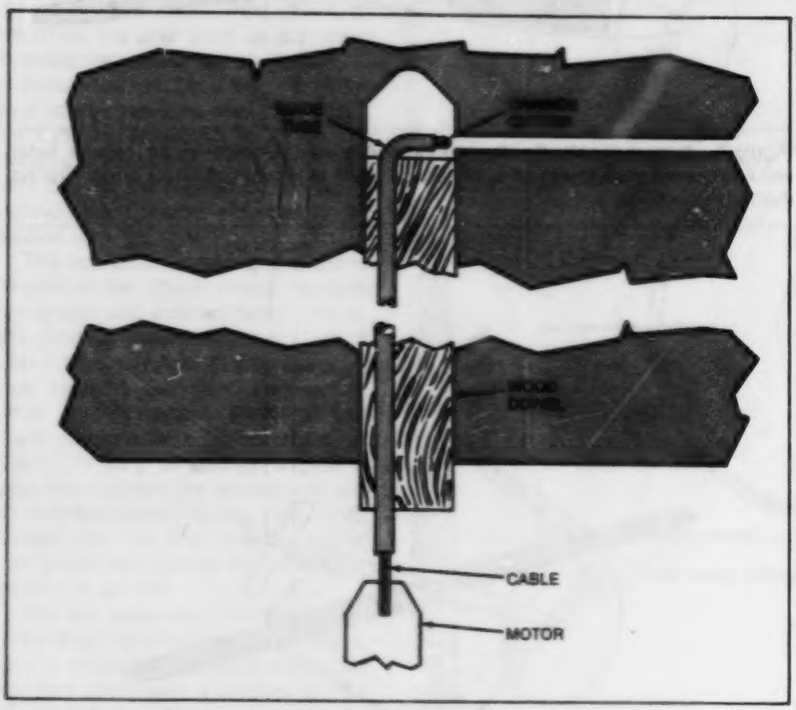

Drill for Hard-To-Reach Areas contains a flexible shaft that transmits torque to a carbide cutter at its tip.

The tool shown in the figure drills a small hole perpendicular to and at the bottom of a blind hole. It consists of a carbide cutter brazed to a flexible shaft, inside a thin metal tube with a 90° bend. A wood dowel holds the tube while a motor turns the shaft and drives the cutter.

The tool was developed for clearing plugged fuel orifices. With it, plugs are cleared on the Space Shuttle main engine without completely disassembling the engine part for offsite electrochemical or electrical-discharge machining. It is used to drill a 3/32-inch (2.4-mm) hole, 3/16 inch (4.8 mm) deep, normal to the wall of a hole 1 inch (2.54 cm) in diameter and 10 inches (25.4 cm) deep. The concept is adaptable to other hard-to-reach drilling situations.

This work was done by Richard Pessin of Rockwell International Corp. for **Marshall Space Flight Center.** *No further documentation is available.*
MFS-19535

Solar-Powered Aircraft

Cruciform wing allows aircraft to keep solar cells perpendicular to Sun.

Langley Research Center, Hampton, Virginia

A proposed solar-powered aircraft, driven by an electric motor, would have vertical and horizontal wings. This design would allow the aircraft to fly in a straight path while banked, permitting optimal exposure of its wing-mounted solar cells to the Sun. Such an aircraft would fly at an altitude high enough to be above the clouds and to avoid winds with velocities much greater than its own airspeed. Its most likely application would be as a pilotless aircraft to take advantage of its ability to remain aloft for long periods (for very long flights). Excess solar energy could be stored as increased altitude or in batteries or some other energy-storage system. The stored energy would be used to keep the vehicle aloft at night, eliminating fuel as a factor limiting endurance. Because of power limitations, the aircraft would need a very light wing loading.

At least two solar-powered aircraft have been flown successfully; one has an 81-inch (2.1-meter) wingspan, the other a 32-foot (9.8-meter) wingspan. These are conventionally configured with solar cells on top of the wing or fuselage. As a result, the energy available to fly these aircraft is maximum when the Sun is directly overhead, and they can operate only for a few hours near noon in seasons and latitudes in which the Sun is high in the sky.

(continued on next page)

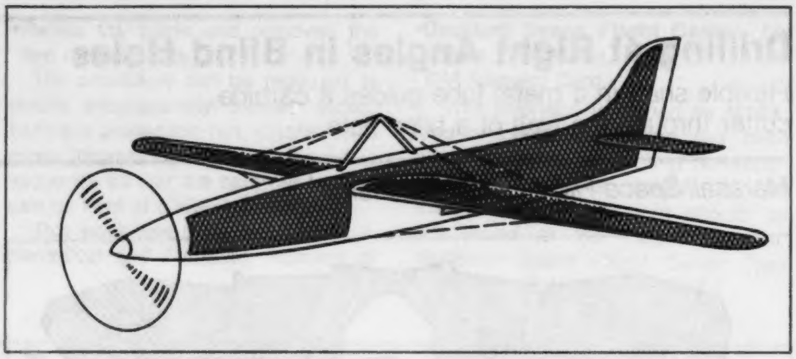

Figure 1. **Conventionally-Configured Solar-Powered Aircraft** would require solar cells (cross-hatched areas) on both vertical sides to provide constant output during daylight hours.

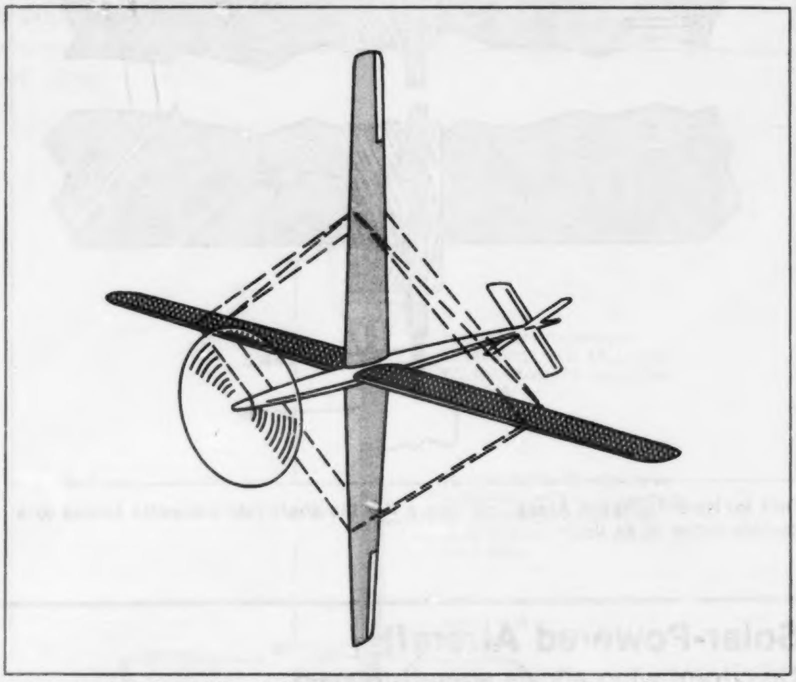

Figure 2. **Cruciform-Wing Solar-Powered Aircraft** could bank steeply to keep its solar cells perpendicular to the Sun line, yet fly a straight course.

A solar-powered aircraft, to be useful as a monitoring or surveillance platform, should be able to fly indefinitely over any part of Earth and to maintain a station over a desired location. To do this, the plane must be able to recover maximum solar energy throughout the day.

This would be possible, despite the angle of the Sun, if there were solar cells in both the vertical and horizontal planes. For station keeping, the aircraft would have to fly a racetrack pattern, and calculations show that the aircraft would require arrays of solar cells on the upper surface of the wing and an equal number of arrays on each vertical side as shown in Figure 1. However, the weight of the additional solar cells would greatly limit the payload of the aircraft.

One way to eliminate the need for additional cells in the vertical plane would be to bank the aircraft so that the normal to the wing lies along the Sun line, but a conventional aircraft cannot maintain straight flight at a large bank angle. However, by using a vertical wing in addition to the conventional horizontal wing, the aircraft could be flown in a straight line at any bank angle. Thus the solar cells could be kept normal to the Sun line by duplicating the wing rather than by tripling the area of solar cells. A cruciform-winged aircraft (Figure 2) would need solar cells on one wing only. This wing is kept normal to the Sun line.

The racetrack pattern required for station keeping could be flown by banking first in one direction, then in the other, keeping the solar cells normal to the Sun line, and taking full advantage of available solar energy anywhere on Earth throughout the daylight hours. A simplified theoretical analysis shows that as the cruciform aircraft is banked about an axis parallel to the zero lift line, the lift and induced drag remain constant.

In an alternate configuration, the tail and fuselage are eliminated, and the differential thrust of four propellers, one at each wingtip, supplies the pitching and yawing moments required for stability and control. Because of the critical importance of drag and weight in the design of solar-powered aircraft, elimination of the fuselage and tail may be an important factor in meeting the required performance goals.

Launching and landing for either configuration would be unconventional. The planes could be launched with a motorized dolly or carried aloft on a balloon; they could be recovered by parachute or could return to the motorized dolly.

This work was done by William H. Phillips of **Langley Research Center.** *No further documentation is available.*

This invention is owned by NASA, and a patent application has been filed. Inquiries concerning nonexclusive or exclusive license for its commercial development should be addressed to the Patent Counsel, Langley Research Center [see page A5]. Refer to LAR-12615.

Ball-Joint Grounding Ring

Spring-loaded fingers assure continuous electrical contact across a ball-and-socket joint.

Lyndon B. Johnson Space Center, Houston, Texas

In a ball-and-socket joint where an electrical insulator such as polytetrafluoroethylene is used as a liner to minimize friction, good electrical contact across the joint may be needed for lightning protection or to prevent static-charge buildup. Electrical contact can be maintained by a ring of spring-loaded fingers mounted in the socket (see figure).

This approach is used on the Space Shuttle at the attach points between the orbiter and external tanks. There, the principal hazard is lightning, which could falsely trigger the pyroseparation system. Beryllium copper, an alloy with excellent flexibility and hardness and high conductivity, is used. The ring of springy fingers is attached between the socket wall and its polytetrafluoroethylene liner. They extend over the liner into the socket cavity and bear against the bare-metal portion of the ball.

The full peripheral contact of the grounding ring should be more reliable than a single-path, lanyard connector and less costly than a bellows. It may be useful in industry for cranes, trailers, and other applications requiring a ball-and-socket joint.

This work was done by Peter J. A. Aperlo, Peter A. Buck, and Vincent A. Weldon of Rockwell International Corp. for **Johnson Space Center.** *No further documentation is available. MSC-18824*

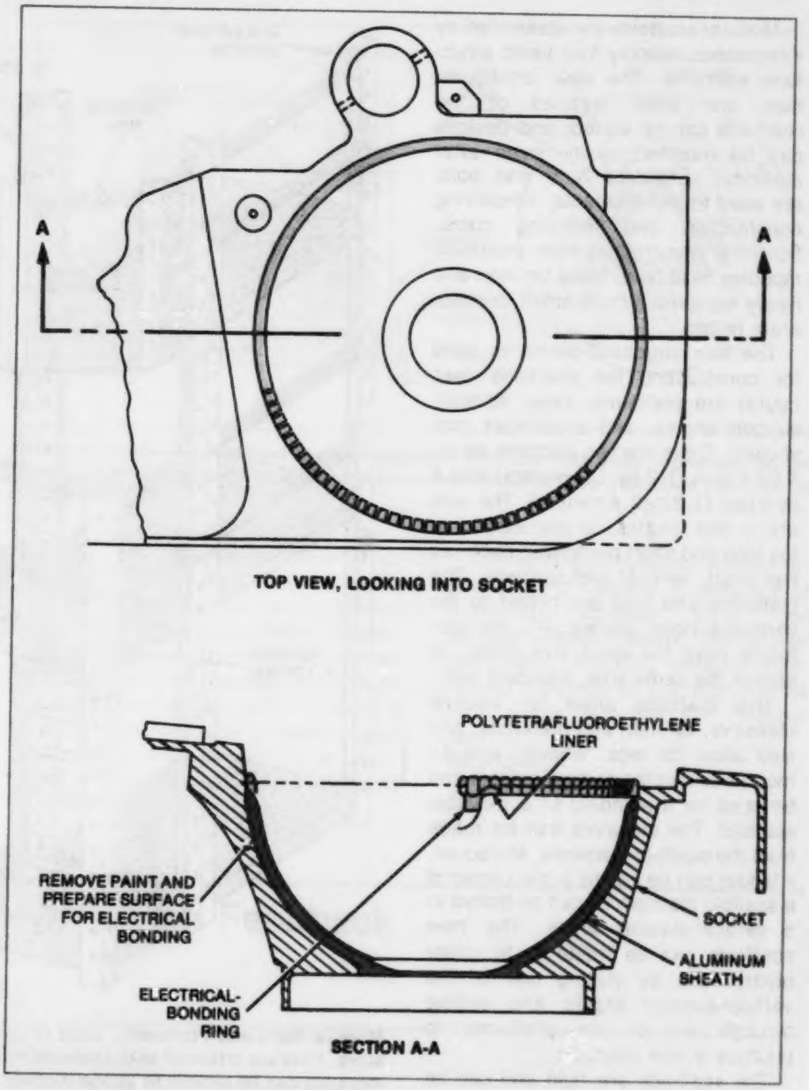
A
A
TOP VIEW, LOOKING INTO SOCKET
POLYTETRAFLUOROETHYLENE LINER
REMOVE PAINT AND PREPARE SURFACE FOR ELECTRICAL BONDING
SOCKET
ALUMINUM SHEATH
ELECTRICAL-BONDING RING
SECTION A-A

The Beryllium Copper Electrical-Bonding Ring (in color) is attached to the metal socket. Part of the polytetrafluoroethylene socket liner overlaps the ring. On the Space Shuttle, 100 equal-sized tabs were used. The ring dimensions are chosen for each application.

Versatile Modular Scaffolds

Movable and fixed modular scaffolds can be tailored to most scaffolding needs.

Goddard Space Flight Center, Greenbelt, Maryland

Modular scaffolds are assembled by interconnecting only four basic structural elements. The size, configuration, and other features of the scaffolds can be varied, and designs can be modified easily, even after assembly. Standard nuts and bolts are used to join elements, simplifying construction and reducing costs. Scaffolds constructed from prototype modules have been used for men and heavy equipment from small to moderate height.

The four structural elements used for constructing the scaffolds (see figure) are platforms, rails, vertical-support angles, and a stiffener (not shown). There are two platform sizes: 4 by 4 feet (1.2 by 1.2 meters) and 4 by 8 feet (1.2 by 2.4 meters). The rails are in two lengths, to correspond to the long and short platforms; each rail has short, vertical end sections. The platforms and rails are bolted to the vertical-support angles. All the elements have the same size holes, to accept the same size, standard bolt.

The scaffolds allow for internal elevators, for men and materials, and also allow for legs, wheels, and air mounts so that the same elements can be used for a standing or a movable scaffold. The elevators can be made from the scaffold elements. Moreover, a ladder can be added in the center of a scaffold platform or can be bolted to a vertical-support angle. The new scaffolds can be made to fit under obstructions by cutting one of the vertical-support angles and cutting through one of the platforms to produce a new platform.

The scaffolds are rigid and can be made any length. They are stable on unlevel ground and can extend to well over 50 feet (15 meters) in height.

This work was done by James Kerley of **Goddard Space Flight Center.** *For further information, Circle 78 on the TSP Request Card.*
GSC-12606

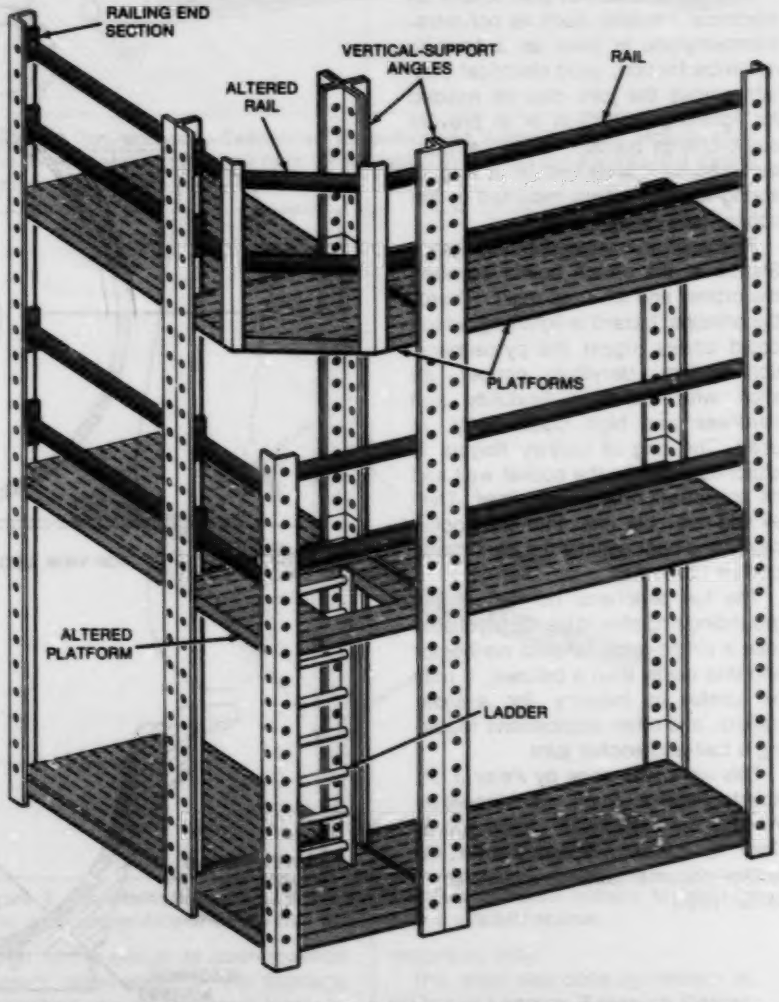

Modular Rails and Platforms, used in constructing scaffolds, come in two different sizes. They are attached with standard nuts and bolts to vertical-support angles. The modules can be altered to accommodate ladders and obstructions and can be used to construct elevators for the scaffolds. They allow easy access to the platforms because no diagonal supports are used.

Reshaping Tube Ends for Welding

A semiautomatic tool rounds deformed tube ends.

Lyndon B. Johnson Space Center, Houston, Texas

A semiautomatic tool rounds tube ends in preparation for welding. It was originally designed for tubes that have been trimmed close to a bend, where deformation is introduced by the bending process. Roundness is restored so that the tube ends can be welded.

The hydraulically operated tool (see figure) can be mounted on a workbench and is small enough to be moved easily from one factory area to another. It consists of two major parts: an "expander" that opens up the out-of-round tube so that a plug can be inserted and a "crimper" that compresses the tube into shape around the plug. Both parts are powered from a single pressurizing line.

An operator first squeezes the out-of-round tube in a vise to restore partially its original shape, then a steel plug is inserted into the tube end. The plug is selected to have the same diameter as the desired inside diameter of the tube. If necessary, the hydraulically actuated expander on the tool is used to enlarge the deformed tube end so that it can accommodate the plug.

Next, the operator inserts the tube end and its plug into the crimping end of the tool. Hydraulic pressure is applied, and the jaws of the crimper swage the tube around the plug so that it assumes the proper shape. Finally, the operator removes the tube from the tool, removes the plug, and places a cap over the tube end to protect it until it is welded. The present design handles a range of tube sizes, from 1/4 to 2-1/2 in. (0.635 to 6.350 cm) outside diameter.

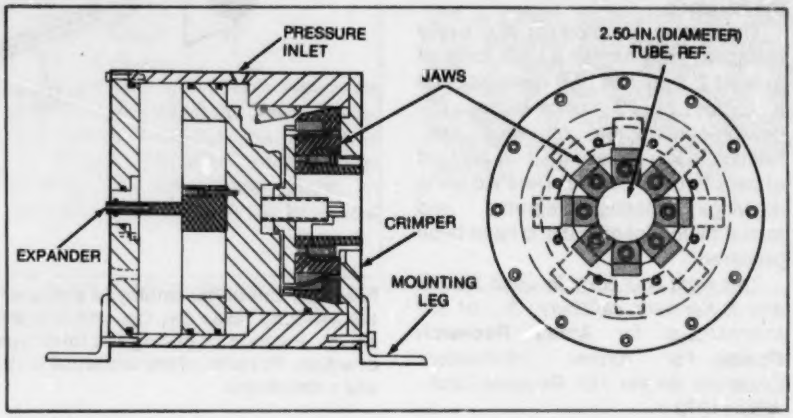

This **Hydraulically Actuated Tool** reshapes out-of-round tube ends in preparation for welding. Six sets of interchangeable jaws handle tube outside diameters from 1/4 to 2-1/2 inches.

This work was done by William H. Emanuel and Charles A. Headley of McDonnell Douglas Corp. for **Johnson Space Center.** *For further information, including detailed engineering drawings of the tool and its parts, Circle 79 on the TSP Request Card.*

MSC-18462

Remote Manipulator With Force Feedback

Controller gives the user a feel for the force and torque exerted on an object.

Ames Research Center, Moffett Field, California

A controller for a remote manipulator gives a user a "feel" for the forces required to lift, slide, turn, and otherwise handle objects. Because an operator experiences sensations similar to those he would perceive if he handled the objects directly, he needs much less skill and training for this manipulator than for one without force feedback.

The controller was developed to handle hazardous materials, such as radioactive substances, explosives, or corrosive chemicals. Other possible uses include tracking moving objects, vehicle control, and human interaction with computers (for example, via a three-dimensional display of a computer model).

The controller, now in the design stage, allows six degrees of freedom: the translation of an object along x, y, and z axes and the rotation of the object in pitch, roll, and yaw (see figure). It can follow all the angles and positions the hand can assume in a cubic volume about 12 inches (30 centimeters) on a side, while the operator is seated at a table.

A gimbaled handgrip is mounted on a telescopic extension. As the user moves and turns the handgrip, the controller senses its position and orientation with built-in potentiometers and sends appropriate commands to

(continued on next page)

the remote manipulator. At the same time, built-in electric torque motors feed back a force proportional to the force exerted on the object. Cables link the joints to the back-force motors at the end of the telescope joint, through a counterbalanced takeup mechanism. The motors themselves serve as counterweights for balancing the handgrip.

The motors are modular and easily replaced. They furnish a back force of at least 2.2 pounds (9.8 newtons) and a torque of 70 ounce-inches (50 newton-centimeters) on each axis. Friction is low — less than 10 percent of back force or torque. Detailed parts drawings, cabling diagrams, and torque motor specifications have been prepared.

This work was done by John W. Hill and J. Kenneth Salisbury, Jr., of SRI International for **Ames Research Center.** *For further information, Circle 80 on the TSP Request Card.* *ARC-11272*

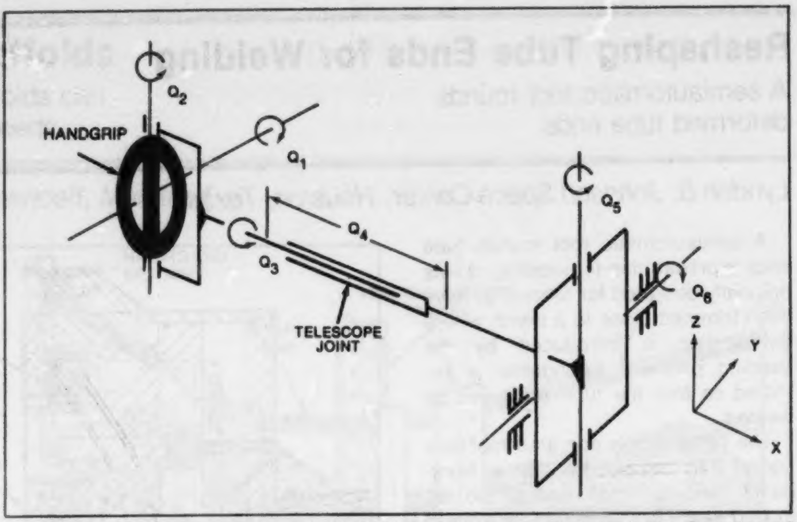

Feedback Controller employs a gimbaled handgrip and a telescope joint. Rotation of the handgrip (axes Q_1, Q_2, and Q_3) produces similar rotation of the manipulated object. Pushing or pulling the telescope joint (axis Q_4) moves the object in the x direction. Rotation of the telescope joint (axes Q_5 and Q_6) moves the object in the y and z directions.

Spraying Suspensions Uniformly

Nozzle contours suppress overspray while preventing suspension components from separating.

Marshall Space Flight Center, Alabama

Coarse, multi-ingredient suspensions can be sprayed on a surface smoothly, uniformly, and without overspray with the aid of a nozzle attachment for a commercial spray gun. The nozzle has been used to apply a protective coating to the aluminum and steel parts of the Space Shuttle rocket boosters, which are recovered from the ocean after they are used. The density of the ingredients in the spray liquid ranges from 0.64 to 1.08 g/cm^3.

In conventional spray nozzles, heavy particles become concentrated on the inside of the jet, and light particles form a fine mist on the outside of the jet. This fine mist drifts onto surface areas on which no spray coating is intended, causing an undesired overspray. As a result, the jet does not deposit a uniform layer on a surface. Removing the overspray can affect material properties, increase labor

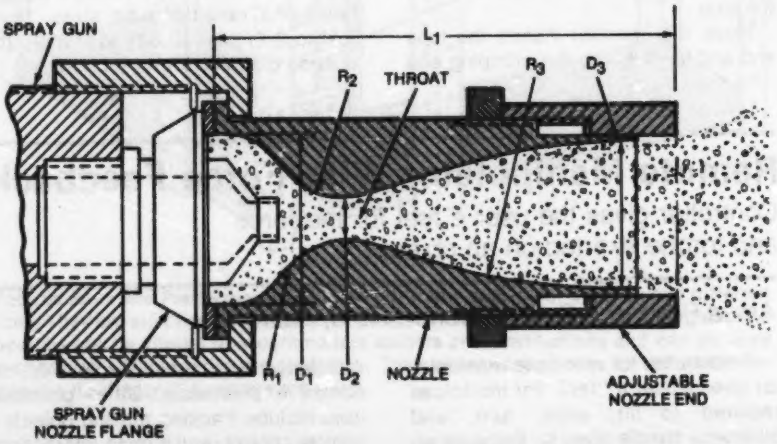

Smooth-Spraying Nozzle is attached to the conventional nozzle of a commercial spray gun. The gently curving contours within the attachment prevent the spray mixture from breaking up into low- and high-density components.

costs, and cause the debonding of subsequently sprayed layers.

The new nozzle attachment (see figure) is contoured internally to suppress overspray and to prevent the spray from segregating. From its conical inlet, the nozzle converges smoothly to a throat section, then diverges in a bell-shaped chamber that allows the suspension to flow uninterruptedly without building up turbulently in the nozzle. The end of the nozzle is adjustable and can be extended or retracted to avoid dripping when the inlet pressure, pump pressure, or density of the mixture changes slightly and to adjust for maximum smoothness on the deposited layer.

The shape and dimensions of the nozzle are critical. A smooth, homogeneous coating with good overspray control can be obtained with the following dimensions:

$D_1 = 2.56$ cm
$D_2 = 0.64$ cm
$D_3 = 2.18$ cm
$R_1 = 0.64$ cm
$R_2 = 1.28$ cm
$R_3 = 7.95$ cm
$L_1 = 6.41$ cm

A nozzle having a conical divergence chamber also deposits a homogeneous mixture. However, the deposit is not smooth and often requires hand sanding. The bell-shaped nozzle, in contrast, avoids the material waste and labor of finishing the coated surface. Furthermore, it can spray material continuously without stops for removing low-density edge deposits.

This work was done by Willibald P. Prasthofer of **Marshall Space Flight Center**. *For further information, Circle 81 on the TSP Request Card.*

This invention is owned by NASA, and a patent application has been filed. Inquiries concerning nonexclusive or exclusive license for its commercial development should be addressed to the Patent Counsel, Marshall Space Flight Center [see page A5]. Refer to MFS-25139.

Two-Headed Bolt

Machine bolt can be unscrewed from either end.

Marshall Space Flight Center, Alabama

With a head on each of its ends, a new bolt can be disengaged from its blind side. The bolt has a conventional hexagonal head on one end and a smaller hexagonal head on its threaded end (see figure). Since the reduced head is smaller than the bolt diameter, it does not interfere with insertion of the bolt shank in a bolthole. However, it can be turned by a wrench to release the bolt from its blind (threaded) end. The bolt should be tethered on its large-head end so that it does not drop away from the assembly.

The two-headed bolt makes it easier for mechanics to remove a Space Shuttle engine from its engine-handler adapter plate. Formerly, a mechanic had to lean over the edge of the adapter plate to reach the head of a conventional single-headed bolt. Now, the reduced head on the easily accessible side of the plate can be turned to disengage the bolt.

This work was done by G. W. Jeffers of Rockwell International Corp. for **Marshall Space Flight Center**. *No further documentation is available.*
MFS-19619

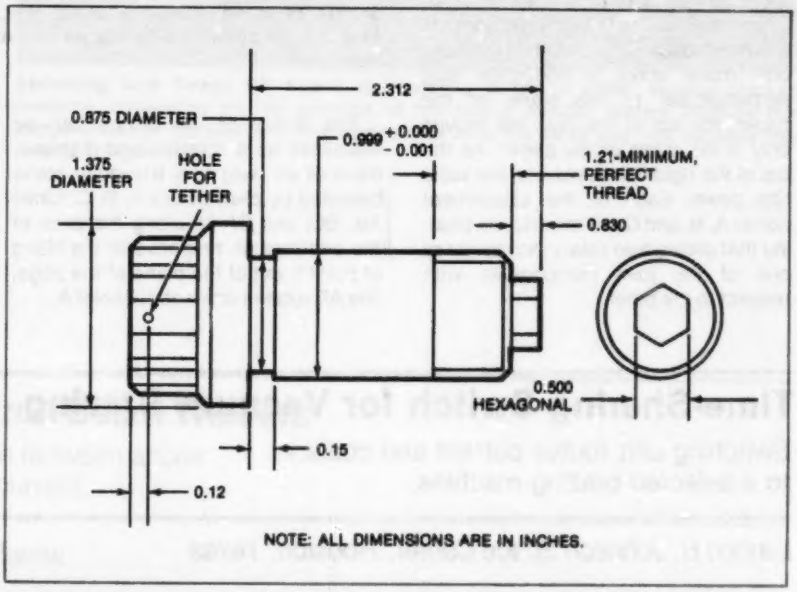

With a Conventional Head at One End and a smaller head at the other, this bolt can be unscrewed from either end. When it is unscrewed by the smaller head, a tether at the conventional head retains the bolt.

Compact Table-Tilting Mechanism

Optical components and other objects are oriented precisely by a simple motorized device.

NASA's Jet Propulsion Laboratory, Pasadena, California

A mechanism proposed for rotating a mirror through a precise angle aboard a spacecraft could have other applications in orienting, positioning, and alining equipment. Offering the advantages of compactness, simplicity, and low backlash, it can manipulate essentially any object that can be attached to a plane tilt table.

As shown in the figure, the device consists of a drive motor, a rotatable disk, a rigid link, and a table. The motor rotates about a vertical axis, and the motion is converted through the disk and rigid link to rotation of the table about a perpendicular axis.

When the motor is activated, the arm attached to the disk moves to the position shown in the illustration at the right of the figure. The bottom edge of the rigid link is carried with the arm. Since the top of the rigid link is attached to the table and the table can only move about a horizontal axis perpendicular to the plane of the paper, the top of the rigid link moves only in the plane of the paper. As the top of the rigid link descends, the table tilts down. Each of the attachment points A, B, and C is a low-friction bearing that allows free rotary movement of one of the joint components with respect to the other.

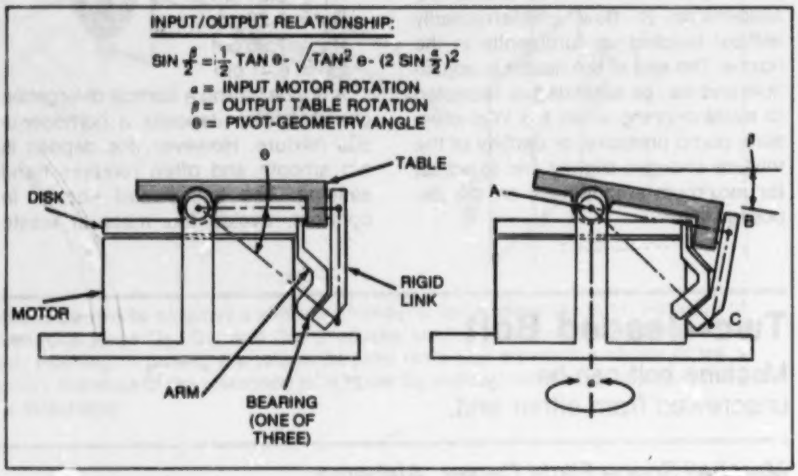
INPUT/OUTPUT RELATIONSHIP:
$\sin\frac{\beta}{2} = \frac{1}{2}\tan\theta - \sqrt{\tan^2\theta - (2\sin\frac{\alpha}{2})^2}$
α = INPUT MOTOR ROTATION
β = OUTPUT TABLE ROTATION
θ = PIVOT-GEOMETRY ANGLE
θ
TABLE
DISK
RIGID LINK
MOTOR
ARM
BEARING (ONE OF THREE)
β
A
B
C

The Table Is Tilted from the horizontal plane in the illustration at the left to the orientation in the illustration at the right. The rotation of the motor about a vertical axis through point A is translated into rotation of the table about a horizontal axis through A.

The action of the device can be visualized as a rotation and displacement of an imaginary triangular plane bounded by pivot points A, B, C. Lines AB, BC, and CA lie along the axes of the bearings. In response to the lifting of point C out of the plane of the page, line AB rotates down about point A.

This work was done by Frank R. Mitchell of Frank R. Mitchell and Associates for **NASA's Jet Propulsion Laboratory.** *For further information, Circle 82 on the TSP Request Card.*
NPO-14800

Time-Sharing Switch for Vacuum Brazing

Switching unit routes current and coolant to a selected brazing machine.

Lyndon B. Johnson Space Center, Houston, Texas

A switching unit changes power and cooling-water connections between two vacuum-brazing machines. The switch allows both units to be powered by a single radio-frequency (RF) generator. One of the machines can be used for brazing while the bell jar of the other is being evacuated (a 20-minute process) in preparation for brazing or is being cooled after brazing (a 10-minute process).

The switch, as shown in the figure, eliminates manual interchange of power cables from each brazing machine at the RF generator. The manual interchange operation is not only time-consuming but potentially hazardous as well, since some cooling water is inevitably spilled and can cause arcing around the cable coupling.

The unit is linked to the RF generator by a coaxial cable and to each of the vacuum-brazing machines by two square-cross-section copper conductors. Temperature indicators on the unit allow the operator to monitor pyrometers in the vacuum bell jars. A separate control box controls the RF generator output.

Cooling water flows through the coaxial cable from the RF generator through a tee fitting in the switching unit. From the tee, it passes through a flexible dielectric tube, a check valve, and one of the square copper tubes to the cooling coil on a bell jar. The water returns to the RF generator through a channel in the return square conductor, an on/off valve in the switching unit, and the coaxial cable.

The brazing-machine operator selects a machine for use by moving the switch handle to the left or right of its center position, thereby engaging the on/off valve so that water flows to the selected bell jar. At the same time, the handle completes the circuit for current from the RF generator to the selected bell jar. The current path is through a copper section on the handle, through the square copper conductors, the bell jar, and a jumper around the on/off water valve to the coaxial cable.

The square conductors offer greater surface area for the transmission of RF current than does the coaxial cable and allow the supply and return lines to be placed closer together so that power losses are minimized. Each tube is covered individually with insulating shrink tubing, and each pair of supply and return copper tubes is held together with another shrink tube.

For safety, an interlock cuts off RF power unless the bell jar is lowered, the switching-unit cover is in place, and the cooling water is flowing.

This work was done by John A. Stein of Rockwell International Corp. for **Johnson Space Center.** *For further information, including detailed engineering drawings, Circle 83 on the TSP Request Card.*
MSC-18600

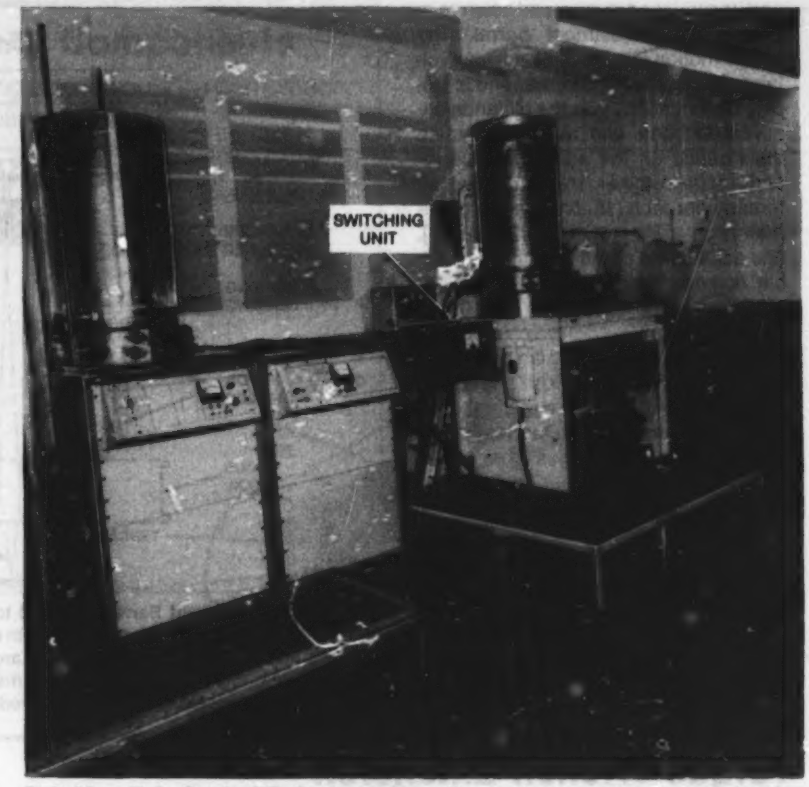

Switching Unit Sends RF Power and cooling water to either vacuum-brazing machine, depending on the position of the switch handle. Meters indicate the temperatures in the bell jars. The control box atop the switching unit controls the remote RF generator.

Limiting Current in Electron-Beam Welders

Mechanically adjustable separation between anode and cathode regulates maximum current.

Marshall Space Flight Center, Alabama

Damage to a workpiece by excessive current in an electron-beam welder is prevented by a mechanism that accurately adjusts the anode-to-cathode spacing. The mechanism is installed on a standard Sciaky (or equivalent) electron-beam gun with only minimal modification. By turning a knurled knob and observing a digital readout of anode/cathode separation, the machine operator adjusts the welder for a safe maximum current before welding begins.

The mechanism consists of an internally-threaded knurled adjustment barrel and an externally-threaded mating anode retainer (see figure). The adjustment barrel is press-fit in an acetyl copolymer roller bearing with nonmagnetic stainless-steel balls. The barrel is free to rotate clockwise or counterclockwise to move the anode retainer, and in turn the anode, toward and away from the cathode.

The electron-beam gun and cathode are rigidly mounted in a vacuum chamber, and the mechanism housing is attached to the lower part of the electron-beam gun. The anode retainer is fitted with either a standard or french anode and a focus coil. When the operator turns the adjustment barrel, the anode

(continued on next page)

and its retainer move up and down relative to the adjustment barrel. The anode motion is sensed by a linear voltage differential transformer and is displayed continuously as the distance between cathode and anode. Because the threads on the adjustment barrel and anode retainer are extra fine [40 threads per inch (16 threads per centimeter) on a 3-inch (7.6-cm) diameter], fine adjustment of the spacing is possible; one complete revolution of the barrel changes the spacing by only 0.025 inch (0.64 mm).

The anode retainer also holds an electron-beam focusing coil and a slipring, which provides an electrical contact for the anode. Tetrafluoroethylene vapor shields prevent gas from entering the vacuum chamber through the threads or bearing.

This work was done by Kirk W. Spiegel of Rockwell International Corp. for **Marshall Space Flight Center.** *No further documentation is available.*
MFS-19503

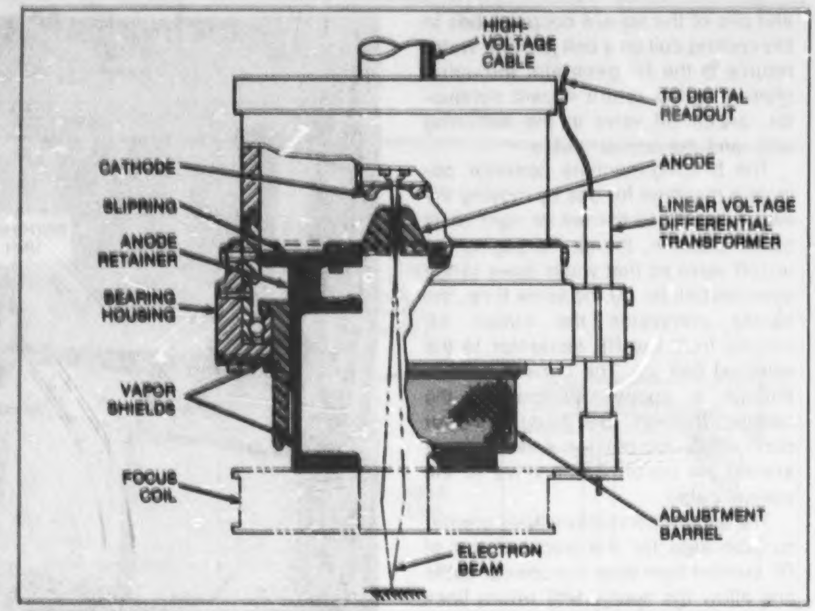

A Knurled Adjustment Barrel is turned to change the separation between anode and cathode and, thereby, alter the maximum electron-beam current. The section above the dashed line in this drawing is a standard electron-beam gun. The section below the dashed line is the new current-limiting mechanism. The shaded portion represents the anode-retainer assembly, which is moved vertically by rotation of the knurled barrel.

Torque-Wrench Extension

Tool made from two bevel gears and an extension shaft reaches difficult locations and allows accurate torque readings.

Lyndon B. Johnson Space Center, Houston, Texas

A novel torque-wrench extension makes it easy to install and remove fasteners that are beyond the reach of typical wrenches or are located in narrow spaces that prevent full travel of the wrench handle. At the same time the new tool allows the applied torque to be read accurately.

The figure shows a tool with an overall length of 28 inches (71 cm), although it could be scaled up or down in size for different applications. The drive system for torques up to 125 inch-pounds (14 N-m) uses two standard 1/4-inch (0.6-cm) drive-socket extensions in an aluminum frame that also holds a pair of 90° bevel gears.

The extensions are connected to one of the bevel gears, which turns the other bevel gear. The gears produce a 1:1 turns ratio through a 90° translation of the axis of rotation. The output bevel gear has a short extension that is used to attach a 1/4-inch drive socket.

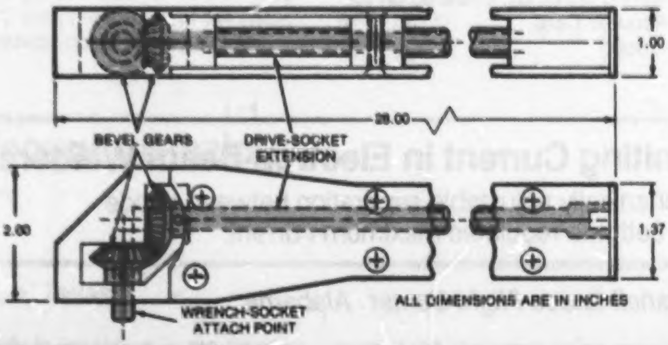

Drive-Socket Extensions and Bevel Gears are housed in the aluminum frame of a torque-wrench extension. The tool facilitates the installation and removal of fasteners that are difficult to reach. A short extension on one of the bevel gears is for the attachment of a wrench socket.

Some commercially available wrench extensions have a flexible shaft that can affect the accuracy of torque readings. The new design with bevel gears has a substantially-greater torque-drive range in addition to giving accurate readings. The torque-wrench extension should be useful in aircraft assembly and automated machine-equipment repair.

This work was done by David H. Peterson of Rockwell International Corp. for **Johnson Space Center.** *No further documentation is available.*
MSC-18769

Quick Mixing of Epoxy Components

In a proposed cartridge, the curing agent would be combined quickly and thoroughly with the base material.

Lyndon B. Johnson Space Center, Houston, Texas

Two materials would be mixed quickly, thoroughly, and in precise proportion by a proposed disposable cartridge. The cartridge would make it possible to mix components of fast-curing epoxy resins, with no mess, just before they are used. Developed to enable astronauts to mix epoxy for repairs in space, the cartridge would also be useful in the home and in industry for such jobs as caulking, sealing, and patching.

The materials (A and B) to be mixed are initially isolated within the cartridge by a cylindrical wall (see figure). The cylinder has vanes at one end and a handle at the opposite end. The vanes have holes through which material A, within the cylinder, can enter material B. To prevent premature mixing, the holes in the vanes are blocked by a gasket; the piston seals the cylinder at the other end.

To mix the materials, the handle on the cylinder is pulled, disengaging the vanes from the gasket. As the cylinder is pulled, material A extrudes through the holes in the vanes and into material B. The cylinder rides on a helically grooved shaft that rotates the vanes so that material A is homogeneously dispersed in material B in a single stroke of the piston. The shaft is rigidly attached to the cartridge by a diaphragm. Mixing would be easier for the user if the materials are formulated so that they are less viscous than usual.

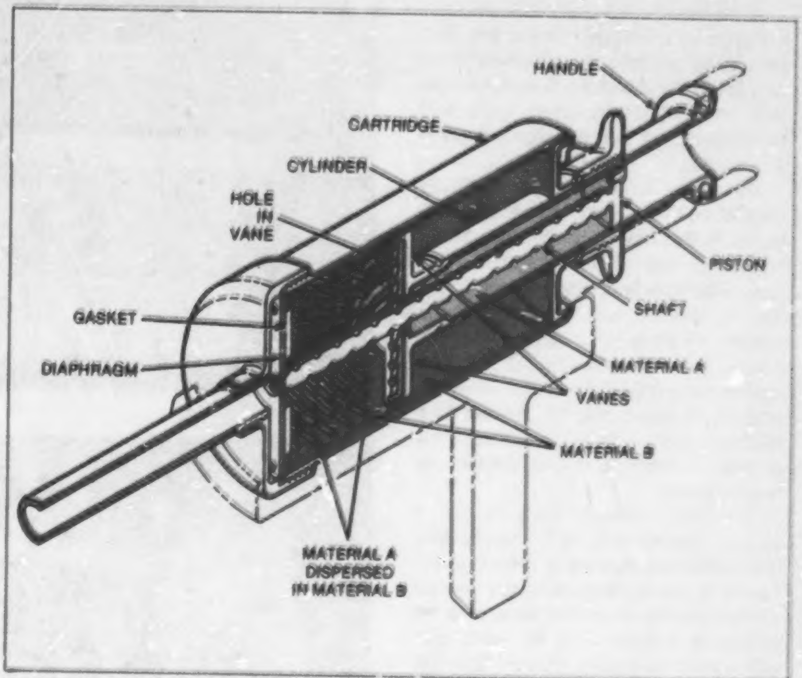

Material A is initially contained within the cylinder. When the handle on the cartridge is pulled back, materials A and B mix. The grooves on the shaft rotate the cylinder as it is pulled back so that the vanes rotate to extrude material A uniformly into material B.

Although mixer capsules have previously been available in which materials A and B are arranged in tandem, separated by a breakable diaphragm, repeated plunging or stirring is needed to ensure a homogeneous mixture. As many as 50 strokes of a plunger may be needed, whereas mixing and stirring would occur in one step with the proposed cartridge.

This work was done by David E. Dunlap, Jr., of McDonnell Douglas Corp. for **Johnson Space Center**. *No further documentation is available.*
MSC-18731

Cutting Holes in Fabric-Faced Panels

A new tool has two carbide inserts that bore clean holes through fibrous material with a knifelike slicing action. The cutting edge of the insert is curved, with a plane inner surface at a 30° angle to the tool axis. A drill press or a hand-held drill can be used to hold the cutting tool.

(See page 391.)

Contour-Measuring Tool for Composite Layups

A simple handtool helps to form contours and complex shapes from laminae of resin-impregnated fabric. The tool, which consists of a yoke having a ballpoint pen and a spindle and gage, is placed so that it straddles a model. As the tool is moved, the pen draws a constant-thickness locus that is used as a template.

(See page 383.)

Compliant Transducer Measures Artery Profile

An instrument consisting of compliant fingers with attached semiconductor pickups measures the inside contours of narrow vessels. The instrument, originally designed to monitor human arteries, is drawn through the vessel to allow the fingers to follow the contours. Lead wires transmit the electrical signals to external processing equipment.

(See page 387.)

Wrench for Smooth or Damaged Fasteners

Serrated tool removes fasteners that cannot be gripped by conventional wrenches.

Lyndon B. Johnson Space Center, Houston, Texas

A special wrench unscrews smooth-surfaced or damaged fasteners that cannot be gripped by a conventional wrench. It can be used in tight spaces and, in contrast to other tools and techniques, will not damage adjacent structures.

The new wrench was originally developed to remove commercial two-part nuts that have a round body and a hexagonal cap. The hexagonal section, needed only during installation so that a wrench can be applied, is broken off once the nut is tightened. Since the smooth round section cannot be gripped by a conventional wrench, it could only be removed by twisting with pliers, chiseling, or drilling — at some risk of damage to nearby parts.

The new wrench consists of a central handle and two independent jaws with serrated teeth (see figure). To use it, the serrated jaws are placed on the fastener to be removed, and the handle is rotated until its teeth grip with a positive locking action. Rotation of the wrench handle safely removes the fastener.

This work was done by Ray Carrillo of Rockwell International Corp. for **Johnson Space Center.** *No further documentation is available.*
MSC-18772

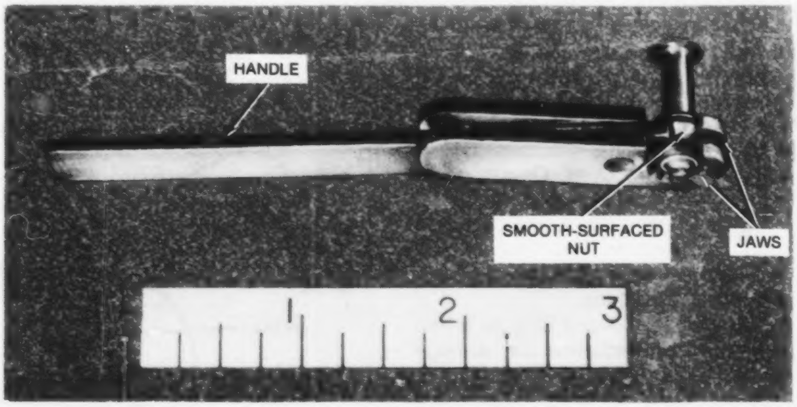

[a]

[b]

Three Sets of Teeth on the wrench clamp the smooth cylindrical surface of the nut in (a). The wrench is well suited for use in limited-access areas (b).

Fabrication Technology

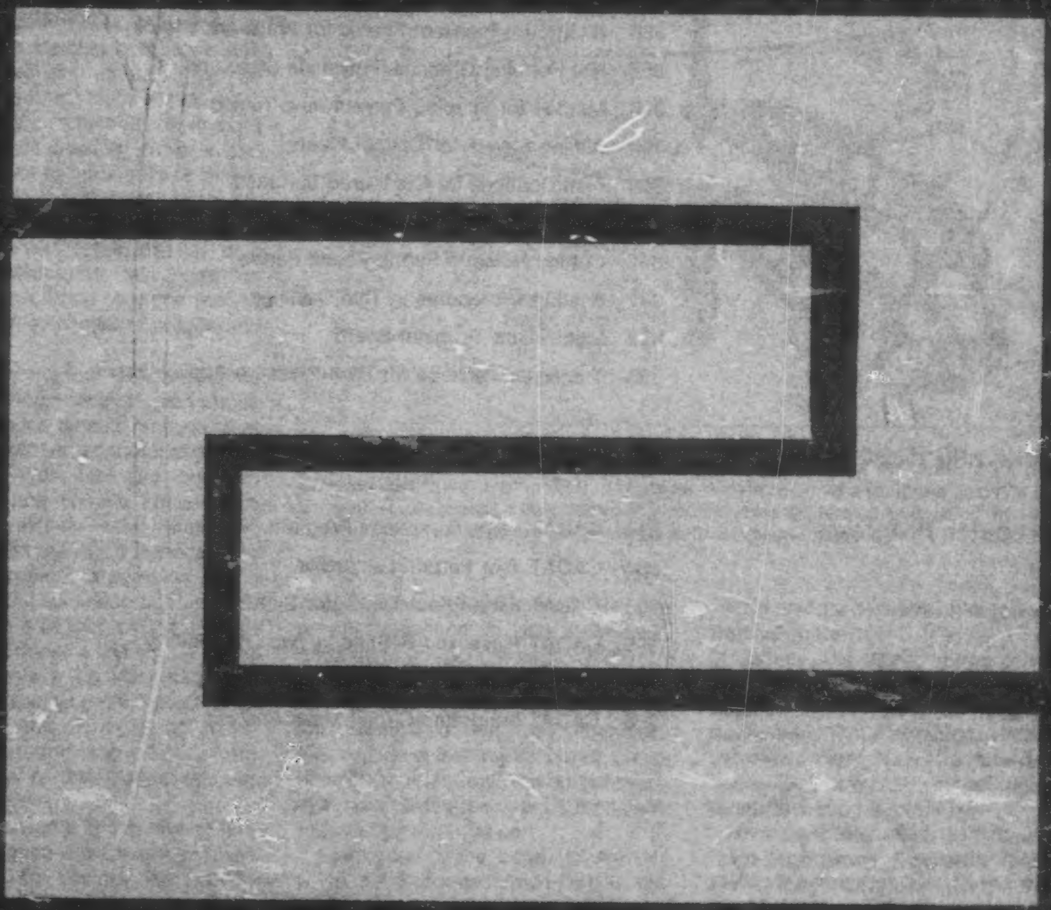

6

Hardware, Techniques, and Processes

383 Contour-Measuring Tool for Composite Layups
384 A New Family of Fire-Resistant Foams
385 Modified Fire-Resistant Foams for Seat Cushions
386 One-Step Microwave Foaming and Curing
386 Rigid Fire-Resistant Foams for Walls and Floors
387 Hot Forming Graphite/Polyimide Structures
388 Method for Shaping Polyethylene Tubing
389 Alining Sleeve for Optical Fibers
389 Film Coatings for Contoured Surfaces
390 Kilovolt Vacuum Feedthrough Is Less Noisy
391 Cutting Holes in Fabric-Faced Panels
391 Sealing Micropores in Thin Castings
392 Lightweight Terminal Board
393 Transistor Package for High-Pressure Applications

Books and Reports

393 Automatic Chemical Vapor Deposition

Computer Programs

394 CADAT Logic Simulation Program
394 CADAT Test Pattern Generator
395 CADAT Field-Effect-Transistor Simulator
395 CADAT Place-and-Routine in Two Dimensions
396 CADAT Multiport Placement and Routing
396 CADAT Integrated-Circuit Mask Analysis

Contour-Measuring Tool for Composite Layups

Resin-impregnated fabric is marked for cutting with the help of a simple handtool.

Ames Research Center, Moffett Field, California

Contours and complex shapes are formed from laminae of resin-impregnated fabric, with the help of a simple handtool. In the layup technique, sheets of carbon-fiber-reinforced fabric composite are cut into shapes that, when stacked and cured, give the proper contour to the finished part. The new tool, which resembles a micrometer, is used to make paper templates prior to cutting the laminae.

A model of the part (for example, the propeller shown in the figure) is first sprayed with a thin coating of a contact adhesive. A thin sheet of paper is then placed over the model. Care is taken to eliminate bulges and wrinkles.

The contouring tool, which consists of a yoke having a ballpoint pen at one extremity and a spindle and gage at the other, is placed so that it straddles the model. With the gap between writing ball and spindle adjusted so that it is slightly less than the maximum thickness of the model, the tool is moved along a path that keeps the pen and the spindle in contact with the opposite surfaces of the model. The pen thus draws a line on the paper that represents a constant-thickness locus. The paper is peeled away from the model, and a layer of resin-impregnated fabric is cut to conform to the shape of the closed contour line.

Next, the thimble and sleeve on the micrometer gage are rotated to close the gap by an amount that corresponds to the thickness of a single layer in the laminated composite. A new sheet of paper is stuck on the model, and the tool is moved so that it draws a new constant-thickness contour. A ply of fabric is then cut to the new contour. The procedure is repeated until all the plies needed for the composite have been cut.

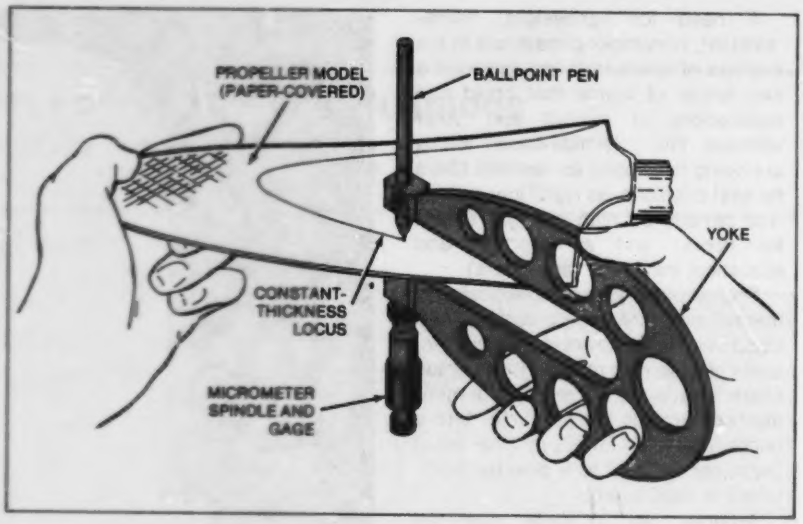

The User Moves the Handtool, scribing a locus of constant thickness on a paper-covered part (here, a propeller). The paper is then used as a template to cut a sheet of resin-impregnated fabric. Several such layers are stacked and cured to form a composite layup with the same shape as the original part.

The plies are assembled in the proper sequence in two half-molds and baked in vacuum bags at 250° F (121° C) for 1 hour. After the two halves have cooled, they are mated and heated so that they coalesce. Finally, the assembly is cured under controlled temperature and pressure in a mold having the exact dimensions required of the final part.

Even though the paper is not flat when a contour is drawn, but is flat when used as a template for a ply, there is enough "give" in the plies during curing to compensate for most distentions during patternmaking. If it is necessary to eliminate distentions completely, a pantograph can be used to transfer a contour from a paper while it is still on the model; or, the contour can be photographed from above and the negative enlarged to the correct scale.

Usually, the fabric will be oriented before each cut so that the fibers of adjacent layers make a 90° angle with each other. This alternating orientation increases strength and fracture resistance and ensures more uniform properties in all directions.

This work was done by Manuel J. Fontes of **Ames Research Center.** *For further information, Circle 84 on the TSP Request Card.*

This invention is owned by NASA, and a patent application has been filed. Inquiries concerning nonexclusive or exclusive license for its commercial development should be addressed to the Patent Counsel, Ames Research Center [see page A5]. Refer to ARC-11246.

A New Family of Fire-Resistant Foams

Polyimide-based foams have potential applications in the interiors of aircraft and other vehicles.

Lyndon B. Johnson Space Center, Houston, Texas

A need for lightweight, flame-resistant, nonsmoking materials in the interiors of spacecraft has spawned a new family of foams that could find applications in aircraft and other vehicles. The polyimide-based foams are being developed as resilient fillers for seat cushions, as rigid, low-density wall panels, as high-strength sheets for floors, and as thermal and acoustical insulation (see figure).

Foams of varying mechanical and thermal properties are prepared from liquid or powder polyimide precursors, some of which are mixed with selected fillers. Heating by microwaves or other method expands the precursor into a uniform cellular structure (the liquid precursor is dried to a powder first), which is then cured.

Aromatic and aliphatic diamines and tetracarboxylic acid dianhydrides are used as starting materials in preparing the precursors; the exact choices depend on the properties desired. For example, foams produced from heterocyclic aromatic/aliphatic diamines at high molecular ratios show good flexibility and compression set and are therefore good candidates for seat-cushion material; foams with various reinforcing fillers, such as carbon or glass, have potential as floor and wall materials; and glass fibers, glass microballoons, and other additives are combined with flexible foam precursors to produce thermal/acoustical insulation.

The many variables that affect foam properties have been examined during an extensive development program, with the objective of optimizing the process. Some significant developments, described in more detail in the articles that follow and in the reports cited at the end of this article, are:

- new terpolyimide precursors for use in seat-cushion foams;
- a continuous spray-drying process for producing large quantities of polyimide powder precursors;
- polyimide powder precursors mixed with conductive fillers are microwave foamed and cured in one step;
- constrained-rise microwave foaming has successfully produced rigid foams;
- the fire resistance of polyimide foams is significantly improved by adding ceramic fibers to the powder precursor; the foams produced from these mixtures are flexible and have good acoustical attenuation; and
- optimum foam compositions have been selected for each final product studied (seat-cushion material, wall material, floor material, thermal/acoustic insulation).

Early work on this fire-resistant-foam technology is reported in "Fire-Retardant Foams" (MSC-16222) on page 59 of *NASA Tech Briefs*, Vol. 3, No. 1.

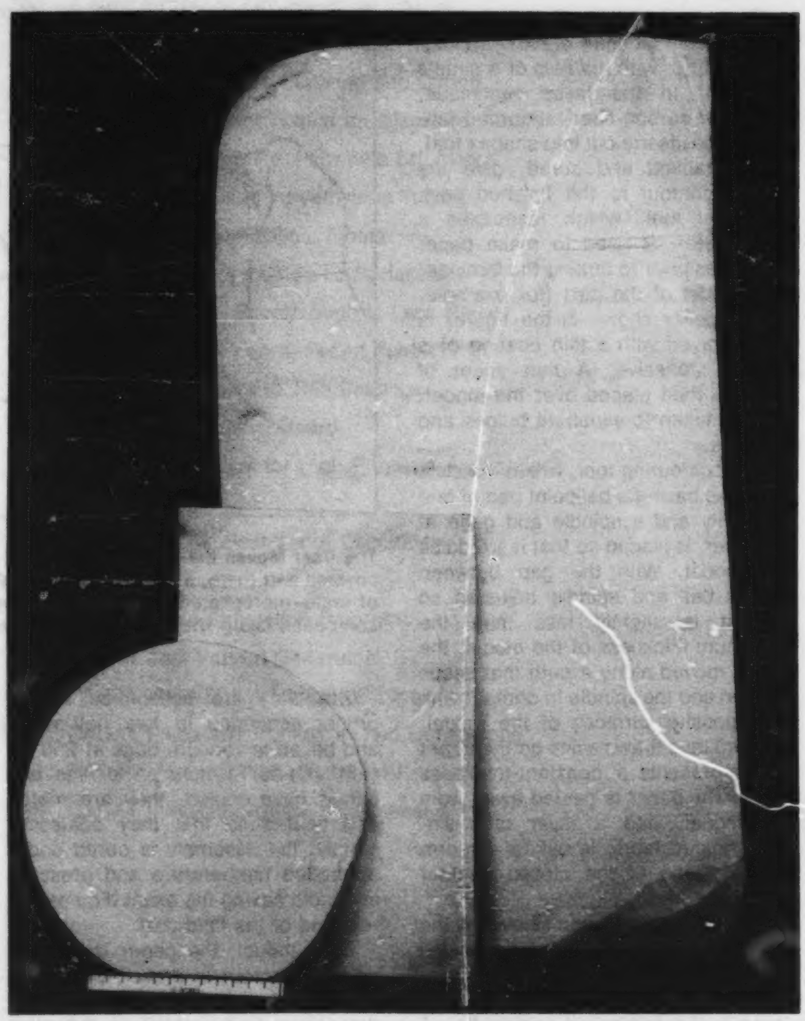

Finished Polyimide Foams such as these are prepared by heating a powder precursor in a 15-kW microwave oven. The large slab measures 160 by 89 by 18 cm. Final curing of the slabs was done in a conventional oven.

This work was done by John Gagliani of International Harvester Co. for **Johnson Space Center.** *Further information may be found in:*

NASA CR-160576 [N80-22492/NSP], "Development of Fire-Resistant, Low Smoke Generating, Thermally Stable End Items for Commercial Aircraft and Spacecraft Using a Basic Polyimide Resin" [$11], and

NASA CR-151472 [N77-28301/NSP], "Development of Fire-Resistant, Low Smoke Generating Thermally Stable End Items for Aircraft and Spacecraft" [$10].

Copies of these reports may be purchased [prepayment required] from the National Technical Information Service, Springfield, Virginia 22161.

Inquiries concerning rights for the commercial use of this invention should be addressed to the Patent Counsel, Johnson Space Center [see page A5]. Refer to MSC-16921.

Modified Fire-Resistant Foams for Seat Cushions

Aliphatic diamines improve the flexibility and resilience of polyimide foams.

Lyndon B. Johnson Space Center, Houston, Texas

Modified polyimide-polymer resins are the precursors for a new family of resilient fire-resistant foams (see preceding article). The terpolyimide foams containing long-chain aliphatic diamines withstand 50,000 cycles of compression under a 200-pound (890-N) load — an equivalent of 3 years of continuous use as seat-cushion filler.

Although terpolyimide resins usually increase the flexibility of polymers, this is not the case for totally-aromatic terpolyimide systems. When considered as possible seat-cushion material, foams derived from such terpolyimides do not meet minimum specifications for fatigue resistance or elasticity. In fact, the aromatic terpolyimide foams fail after less than 10,000 compression cycles, as do more-conventional copolyimide foams.

When the resin composition is modified by preparing terpolyimides with long-chain aliphatic diamines (see figure), the foam elastic properties improve markedly, although some flame resistance is lost. In trading off between flexibility and flame resistance, it is found that 0.2 mole of aliphatic diamine per mole of tetracid dianhydride give a good combination of properties. Foams produced from these precursors are flexible, do not burn, and meet fatigue requirements for seat-cushion material.

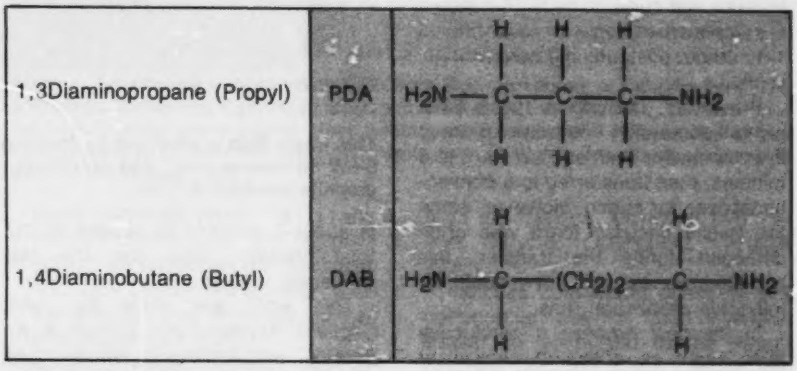

Aliphatic Diamines such as these are combined with aromatic diamines to form terpolyimide precursors for resilient fire-resistant foams. Precursors prepared at an aliphatic diamine ratio of 0.2 showed the best combination of mechanical and thermal properties.

This work was done by John Gagliani, Raymond Lee, Usman A. K. Sorathia, and Anthony L. Wilcoxson of International Harvester Co. for **Johnson Space Center.** *Further information may be found in:*

NASA CR-160576 [N80-22492/NSP], "Development of Fire-Resistant, Low Smoke Generating, Thermally Stable End Items for Commercial Aircraft and Spacecraft Using a Basic Polyimide Resin" [$11], and

NASA CR-151472 [N77-28301/NSP], "Development of Fire-Resistant, Low Smoke Generating, Thermally Stable End Items for Aircraft and Spacecraft" [$10].

Copies of these reports may be purchased [prepayment required] from the National Technical Information Service, Springfield, Virginia 22161.

Inquiries concerning rights for the commercial use of this invention should be addressed to the Patent Counsel, Johnson Space Center [see page A5]. Refer to MSC-18704.

One-Step Microwave Foaming and Curing

Simpler process scales up fire-resistant foam slabs to production sizes.

Lyndon B. Johnson Space Center, Houston, Texas

A process that combines microwave foaming and curing of polyimide precursors in a single step produces fire-resistant foam slabs of much larger volume than has previously been possible (see figure). By adding selected conductive fillers to the powder precursors and by using a high-power microwave oven, foam slabs with dimensions in excess of 61 by 61 by 7.6 cm are made. Typical foaming and curing time is 35 minutes in a microwave oven with an additional 1- to 2-hour postcure in a conventional oven.

Previously, polyimide precursors without conductive fillers were foamed in a microwave oven at 5 kW for 3 to 6 minutes, then transferred to a conventional oven for curing. However, since the fragile uncured foam was often damaged during the transfer, this two-step process was not suitable for full-scale production runs.

In the new process a conductive filler, such as activated carbon or graphite, is mixed with the powder precursor. The filler heats up in the microwave field, transferring more energy to the charge than is possible for the powder precursor alone. The additional energy is directly related to the concentration of the conductive filler and can be controlled to foam and cure the charge in one step. Typical loading of the conductive filler is about 5 percent by weight of the total charge. (Also see the two preceding articles.)

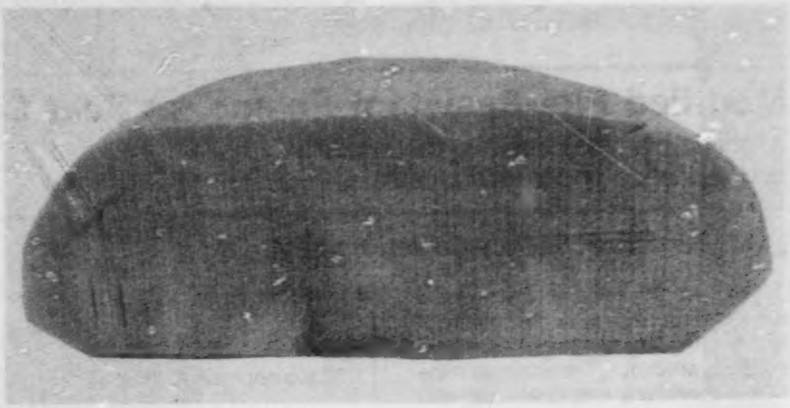

This Foam Slab is produced by foaming and curing 600 g of powder precursor in a 5-kW microwave oven. The polyimide precursor contained 5 percent by weight of graphite conductive filler.

This work was done by John Gagliani, Raymond Lee, Usman A. K. Sorathia, and Anthony L. Wilcoxson of International Harvester Co. for **Johnson Space Center.** *Further information may be found in:*

NASA CR-160576 [N80-22492/NSP], "Development of Fire-Resistant, Low Smoke Generating, Thermally Stable End Items for Commercial Aircraft and Spacecraft Using a Basic Polyimide Resin" [$11], and

NASA CR-151472 [N77-28301/NSP], "Development of Fire-Resistant, Low Smoke Generating, Thermally Stable End Items for Aircraft and Spacecraft" [$10].

Copies of these reports may be purchased [prepayment required] from the National Technical Information Service, Springfield, Virginia 22161.

Inquiries concerning rights for the commercial use of this invention should be addressed to the Patent Counsel, Johnson Space Center [see page A5]. Refer to MSC-18707.

Rigid Fire-Resistant Foams for Walls and Floors

Constrained-rise produces stronger foams than does compression.

Lyndon B. Johnson Space Center, Houston, Texas

Previous techniques for fabricating rigid fire-resistant polyimide foams by compressing an already-foamed precursor have been supplanted by a new one-step constrained-rise process. A precursor mixed with reinforcing fillers is placed between rigid substrates that constrain the expansion of the foam as it is heated by microwave energy. The process works for both liquid and powder precursors and can also be adapted to attach woven fiberglass skins at the same time as the precursor is being foamed.

Previously, rigid polyimide foams were produced by compounding fillers and fibers into a liquid or powder polyimide precursor, coating a substrate with the mixture, and drying it in a conventional oven at 120° to 130° F (49° to 71° C) for 6 to 8 hours. The dry composition would then be heated at 500° to 600° F (260° to 315° C) to foam the polyimide resin. The foam, which has very irregular cellular structure, thickness, and flatness at this stage, is compressed at 500° to 550° F (260° to 290° C) and 5 to 50 psi (34×10^3 to 340×10^3 N/m^2). When tested, such "rigid" foams were found to have poor compressive strength, since the cellular structure collapses in the press.

In the new process (see figure), the polyimide resin is spread on a substrate and dried in a microwave oven at a power of about 1.25 to 2.5 kW. The dried resin is placed between two rigid panels and is foamed at a power of 5 kW. Spacers between the substrates control the panel thickness. By eliminating the compression, this method prevents collapse of the cell structure and produces foams with higher compressive strength. (Also see the three preceding articles.)

This work was done by John Gagliani, Raymond Lee, Usman A. K. Sorathia, and Anthony L. Wilcoxson of International Harvester Co. for **Johnson Space Center.** *Further information may be found in:*

NASA CR-160576 [N80-22492/NSP], "Development of Fire-Resistant, Low Smoke Generating, Thermally Stable End Items for Commercial Aircraft and Spacecraft Using a Basic Polyimide Resin" [$11], and NASA CR-151472 [N77-28301/NSP], "Development of Fire-Resistant, Low Smoke Generating, Thermally Stable End Items for Aircraft and Spacecraft" [$10].

Copies of these reports may be purchased [prepayment required] from the National Technical Information Service, Springfield, Virginia 22161.

Inquiries concerning rights for the commercial use of this invention should be addressed to the Patent Counsel, Johnson Space Center [see page A5]. Refer to MSC-18708.

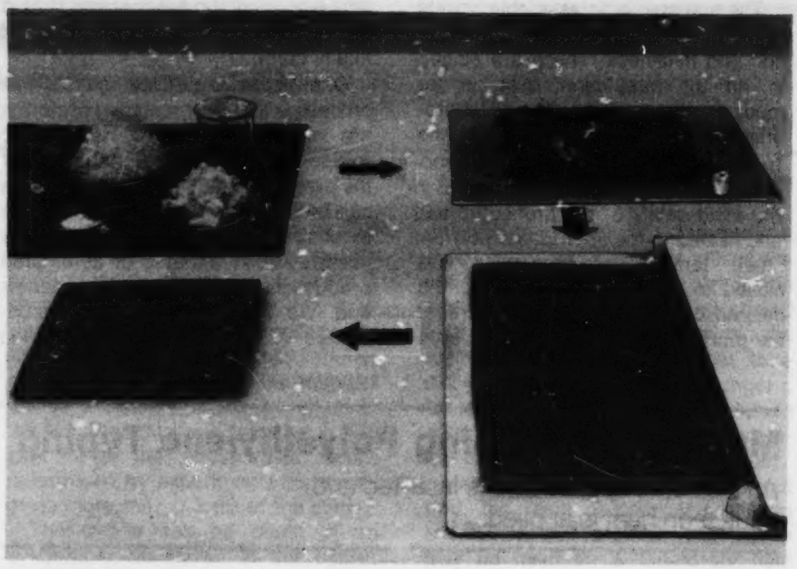

Steps in Fabricating a Rigid Foam Slab from liquid precursor are shown here. The precursor, containing rigidizing fibers and other additives (top left), is dried on a polytetrafluoroethylene-coated glass substrate (top right) and is then heated (by microwave energy) between two rigid sheets (bottom right). The completed slab is seen at the bottom, left.

Hot Forming Graphite/Polyimide Structures

Storable, stabilized preforms simplify fabrication.

Langley Research Center, Hampton, Virginia

Graphite/polyimide structures are generally fabricated by making the shaped structure out of graphite-fiber-reinforced polyimide prepreg. The shaped prepreg is then vacuum-bagged, staged in an oven or autoclave, rebagged, cured, and postcured. Most polyimide resins used for graphite/polyimide prepreg materials are chemically unstable and degrade when stored, which can significantly alter the processability of the material. In addition, the autoclave (or sometimes a captive environment press) can cause problems arising from vacuum bag systems, equipment control limitations, and layup movement.

A hot forming process has been developed in which structural shapes and panels are fabricated directly from stabilized graphite/polyimide preforms. The process can be used with thermosetting polymers that have a high-temperature melt phase just before final cure. This phase allows the fibers to move without destroying the matrix-to-fiber adhesion. It does not require such elaborate equipment as an autoclave or vacuum-augmented heated platen press. A heated platen press and simple matched metal tools are the only processing equipment required to mold the prestaged preforms into fully-cured graphite/polyimide shapes.

(continued on next page)

The first step is to assemble sheets of the prepreg in the desired orientation and thickness. These are staged in an air circulation oven under modest vacuum pressure and appropriate temperature to remove the free solvents and imidization byproducts. The flat preform is then placed in the mold cavity of the preheated tool and heated to the appropriate polymer "melt" temperature; then the tool is closed to shape the preform to the desired contour. The temperature of the tool is next increased to the cure temperature of the polymer and is held there until the structural shape is totally cured.

One of the key advantages of this process is that the prestaged preforms are very stable and do not require refrigerated storage. The flat shape of the preforms simplifies storage, which can be at ambient temperature for an indefinite time. The process lends itself to semiautomated or automated production of prestaged flat panels and has been successfully demonstrated in the manufacture of Celion 6000/PMR-15 and Celion 6000/LaRC-160 graphite/polymide structural sections.

This work was done by Robert M. Baucom of ***Langley Research Center*** *and Paul W. Kidder of LTV. No further documentation is available.*

Inquiries concerning rights for the commercial use of this invention should be addressed to the Patent Counsel, Langley Research Center [see page A5]. Refer to LAR-12547.

Method for Shaping Polyethylene Tubing

An insulated copper wire is inserted and bent, then heat is applied.

Lyndon B. Johnson Space Center, Houston, Texas

A new method forms polyethylene plastic tubing into configurations previously only possible with metal tubing. By using polyethylene in place of copper or stainless-steel tubing in low-pressure systems, fabrication costs are significantly reduced. The polyethylene tubing can be used wherever low-pressure tubing is needed in oil operations, aircraft and space applications, powerplants, and testing laboratories.

To shape the tubing, a tetrafluoroethylene-insulated stranded copper wire is inserted into it. When the tubing is bent to the desired shape, heat is applied with a 500° F (260° C) heat gun until the tubing is pliable to the touch. The heat gun is held about 12 inches (30 cm) from the tube. After about 3 minutes of cooling, the wire is removed, and the tubing retains its new shape. For ¼-inch (0.64-cm) tubing, for example, 12-gage stranded wire is used.

A pneumatic power supply using polyethylene tubing formed by this method is shown in the figure. After the tube is shaped, the end is heated and pressed on a 37° cone so that it will fit on a standard B-nut.

Previously, polyethylene tubing was conventionally used in simple shapes. Special plastic fittings were needed to provide bends between straight tubing sections. Otherwise, only large-radius bends were allowed, to avoid collapsing the tubing walls.

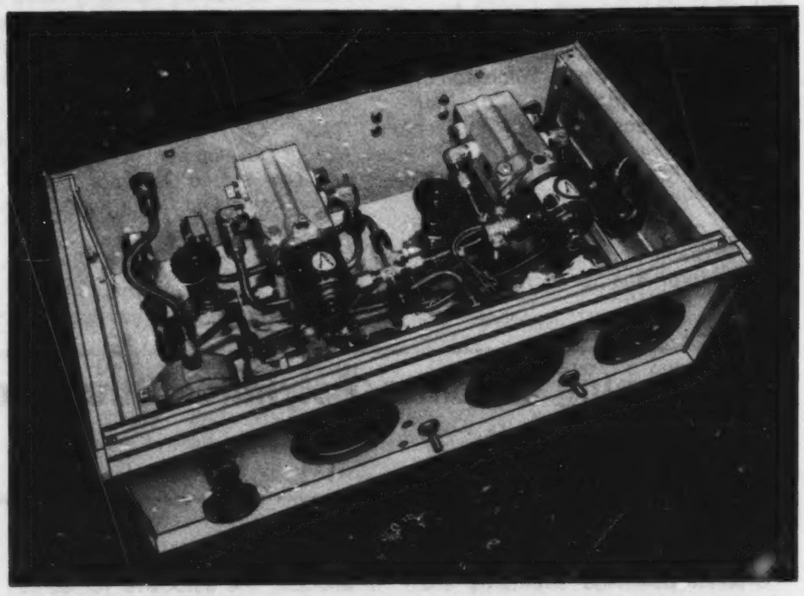

Shaped Polyethylene Tubing is used in this pneumatic power supply to minimize its weight and size. The bends in the tubing were formed by inserting a tetrafluoroethylene-insulated stranded copper wire and then applying heat until the tubing becomes pliable. Upon cooling, the tubing retains its shape.

This work was done by Ralph C. Kramer of Rockwell International Corp. for ***Johnson Space Center***. *No further documentation is available.*
MSC-18771

Alining Sleeve for Optical Fibers

Loss at a butt joint of two light-guide sections is only 0.3 dB when the fibers are slipped into a molded resin sleeve.

Lyndon B. Johnson Space Center, Houston, Texas

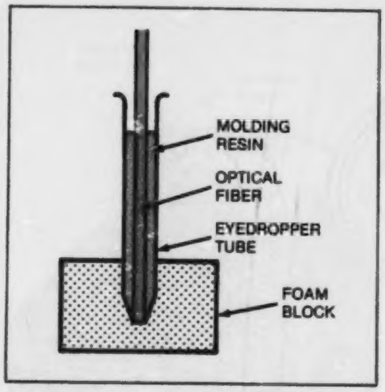

A Sleeve is Formed by letting resin set around a length of optical fiber that is used as a mandrel. The mandrel is removed while the resin is still slightly gellike; the sleeve is removed from its glass-eyedropper mold when completely hardened. A typical fiber length, in tests, was 5 inches (13 cm).

A sleeve for alining two optical fibers is made with precisely the correct inside diameter by using a section of the fiber as a mandrel. Because optical fiber is manufactured to very close tolerances, the diameter of the section serving as the mandrel will be the same as the diameters of the two fibers that are mated in a butt joint inside the sleeve. The result, determined by experiments, is a loss of no more than 0.3 dB at the joint.

The sleeve can be made in an eyedropper as shown in the figure. The glass tube of the eyedropper is inserted into a block of polystyrene foam to hold it vertically and to block the small end. A selected resin (a polyester, for example) mixed with its catalyst is poured into the vertical eyedropper, and then a length of the optical fiber (cleaned of its sizing with acetone or other solvent and coated with mold release) is inserted into the resin. After the resin has set to a strong gel (i.e., when it is no longer a liquid), the fiber is removed. Upon completing curing, the resin is removed from the eyedropper cylinder.

The required lengths can be cut from the resin cylinder and shaped and polished if desired. The sleeve may be used for a temporary field splice or even for a permanent joint.

This work was done by Kenneth L. Austin of Lockheed Electronics Co., Inc., for **Johnson Space Center**. *No further documentation is available.*
MSC-18756

Film Coatings for Contoured Surfaces

Spray process leaves thin-film coatings on convoluted surfaces.

Lyndon B. Johnson Space Center, Houston, Texas

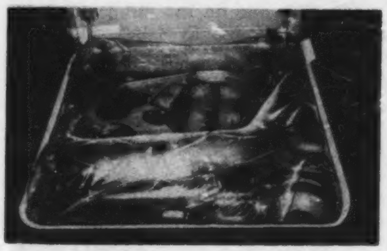

Contoured Fluorocarbon Film of uniform strength and thickness was spray-formed to cover the external tank umbilical cavity on the Space Shuttle.

The thickness of fluorocarbon elastomer films applied to contoured or convoluted shapes by vacuum forming is difficult to control at sharply curved areas. If the film is too thin in these regions, it may fail under applied pressure.

A process for spraying contoured fluorocarbon elastomer films of uniform strength and thickness has been used instead of vacuum forming to fabricate a curtain covering the external tank of the Space Shuttle (see figure). A solution of KEL-F-800 (or equivalent) fluorocarbon elastomer resin, dissolved in a ketone or other suitable solvent, is sprayed over a contoured form or mandrel. Conventional spray equipment may be used, and thicknesses are controlled to 0.003 ± 0.0005 in. (0.008 ± 0.001 mm).

While still on the mold, the film is air-dried by heating at 425° F (218° C) for 30 minutes. Two molds are used, each fabricating half of the curtain. The dried film is then placed on an assembly fixture to trim the periphery.

A rubber bead, installed along the perimeter of the film, is held in place by Kapton (or equivalent) tape. Polytetrafluoroethylene tape holds the two halves of the curtain together.

This work was done by Henry E. Flanery, Roger K. Frost, and Arnold J. Olson of Rockwell International Corp. for **Johnson Space Center**. *No further documentation is available.*
MSC-18784

Kilovolt Vacuum Feedthrough Is Less Noisy

Electrical feedthrough has low capacitance and low microphonic sensitivity.

NASA's Jet Propulsion Laboratory, Pasadena, California

A new electrical feedthrough connects both low-voltage and high-voltage signals between a cryogenic environment and the "outside world." Developed for a cooled germanium gamma-ray detector, the feedthrough has especially low capacitance and low sensitivity to microphonic noise. Its high-voltage lead is free of corona discharge and electrical breakdown to at least 5 kV.

As shown in the figure, the new feedthrough has two high-thermal-resistance leads, one for high voltage and one for low voltage. Each lead is supported by four insulating disks and an insulating rod (for the low-voltage lead) or an insulating tube (for the high-voltage lead). When the feedthrough is installed, the disks rest in alined holes in the parallel walls of the cooler. They are then epoxied in place to form vacuum-tight seals.

In the low-voltage lead, microphonic sensitivity is reduced by the disks and the insulating rod supporting the thin wire. The rod prevents vibration without seriously increasing the capacitance.

In the high-voltage lead, the conductor is shielded by a guard electrode, which is connected to the same voltage to prevent corona discharge and electrical breakdown. The guard electrode is a thin vapor-deposited coating on the inside surface of the insulating tube. The coating is thin enough to avoid increasing thermal conductance appreciably but thick enough to offer electrical continuity.

The strongest electric field in the vicinity of the high-voltage electrode occurs in the wall of the insulating tube; but even at 5 kV, the field is less than half the breakdown strength of the insulator. As in the low-voltage electrode, the stiff insulating tube and the disks prevent vibration and microphonic noise, and the small inner diameter and thin wall keep the capacitance low.

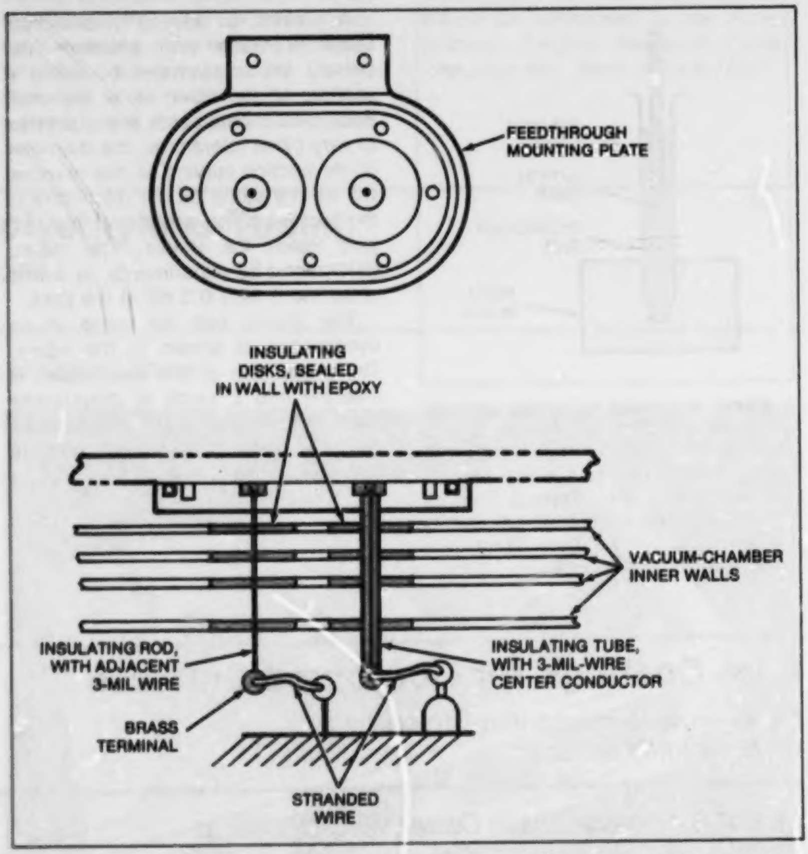
FEEDTHROUGH MOUNTING PLATE
INSULATING DISKS, SEALED IN WALL WITH EPOXY
VACUUM-CHAMBER INNER WALLS
INSULATING ROD, WITH ADJACENT 3-MIL WIRE
INSULATING TUBE, WITH 3-MIL-WIRE CENTER CONDUCTOR
BRASS TERMINAL
STRANDED WIRE

Cryogenic Electrical Feedthrough has two leads. The one on the left is for low-voltage signals; the one at the right is for high voltage (up to 5 kV). Electrical connections are soft-soldered to the terminals at the bottom of the figure. The conductors are 3 mils (7.6 μm) in diameter.

This work was done by Larry D. Howell of IT&T Corp. for **NASA's Jet Propulsion Laboratory**. *For further information, Circle 85 on the TSP Request Card.*
NPO-14802

Cutting Holes in Fabric-Faced Panels

A carbide cutter splices, rather than snags, fibrous material.

Lyndon B. Johnson Space Center, Houston, Texas

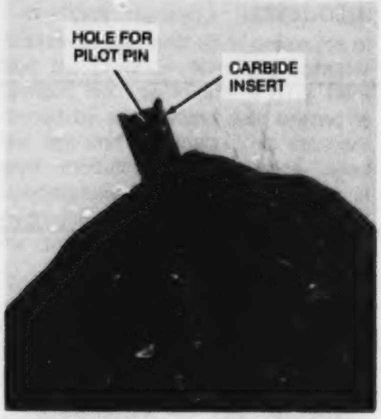

Carbide Inserts on the Cylindrical Tool have curved edges that cut cleanly through fibrous material. The outside diameter of the tool is ground to the required hole diameter. An existing model bores holes 0.561 in. (1.425 cm) in diameter; it is alined with a pilot pin 0.187 in. (4.75 mm) in diameter.

A new tool (see figure) has two carbide inserts that bore through fibrous material with a knifelike slicing action. The tool cuts clean holes in aramid fabric-faced sandwich panels and should be effective for other fabric- or fibrous-faced materials.

Conventional hole cutters have one or more teeth that can snag surface fibers rather than cut them cleanly. In contrast, the carbide inserts in the new boring tool cut like knives, pressing down on the fibers as they slice through them.

The cutting edge of the insert is curved, with a plane inner surface at a 30° angle to the tool axis. To aline the cutter perpendicularly to the work, a pilot pin or guide plate may be used. For a pilot pin, an axial hole is drilled in the body of the cutter.

The cutter can be placed in a drill press or a hand-held drill. To assure a clean hole on both sides of the panel, a backup plate may be required, or the hole can be cut about half way through from each side.

Previously, it took about 1 hour using a grinding jig to bore a clean hole through an aramid sandwich panel used in the Space Shuttle orbiter. It takes about 3 minutes to bore the hole using the new tool in a hand-held drill motor.

This work was done by Scott A. Peterson of Rockwell International Corp. for **Johnson Space Center.** *No further documentation is available.*
MSC-18786

Sealing Micropores in Thin Castings

A surface pretreatment produces hermetically sealed aluminum chassis.

Lyndon B. Johnson Space Center, Houston, Texas

Microscopic pores in thin-walled aluminum castings are sealed by an impregnation pretreatment. The pretreatment was developed for investment castings used in hermetically sealed chassis for electronic circuitry (see figure). Excessively high leakage rates were previously measured in some chassis.

The aluminum chassis are impregnated with a resin that fills the pores in the metal so that it can contain a pressurized gas. With the pretreatment, leakage is reduced below 1×10^{-4} atm-cm^3/s. The principle of the pretreatment is to open the micropores to accept more resin and to control the resin viscosity for maximum penetration.

(continued on next page)

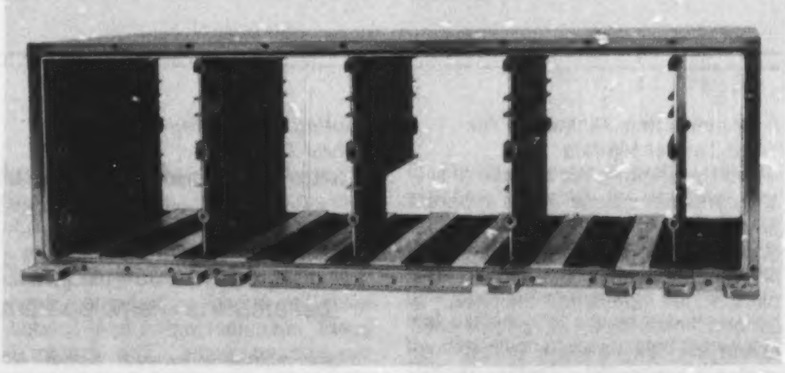

Aluminum Investment Castings like this one hold electronic circuit boards in space vehicles and aircraft. When the openings are sealed with cover plates and electrical connectors, the cast-aluminum chassis is leaktight.

The machined investment casting is first chemically etched in a solution of nitric acid and Actane 70 (or equivalent). With a solution temperature of 20° to 30° C and an immersion time of 3 to 5 minutes, 0.0001 to 0.0006 inch (0.0025 to 0.015 mm) of material are removed from the surfaces of the casting. This amount is small enough to keep the part within dimensional tolerance for most applications, but it is large enough to expose micropores that might have been smeared over by sandblasting and machining.

Next the casting is preheated to 65° C to expand the micropores. The impregnant resin is diluted so that its viscosity measures 15 seconds in a No. 4 Zahn cup. This value of viscosity ensures that the resin permeates deeply into the micropores. The resin impregnated casting is cured at 135° C for 45 minutes.

This work was done by George A. Mersereau, George O. Nitzschke, Hal L. Ochs, and Frank S. Sutch of Honeywell Inc. for **Johnson Space Center.** *For further information, Circle 86 on the TSP Request Card.*
MSC-18623

Lightweight Terminal Board

Sandwich construction
reduces cost and weight.

Lyndon B. Johnson Space Center, Houston, Texas

A new sandwich construction for terminal boards reduces fabrication time and produces thinner boards that have better insulation consistency, better appearance, and less weight. The new method also permits closer spacing of the terminal posts.

As the figure shows, the previous fabrication started with a thick (0.12-inch, or 3.0-mm) polyimide board. Slots were end-milled to a controlled depth, holes were drilled, and the terminal posts were inserted. After the "upset" ends of the posts were expanded, the slot was filled with epoxy for insulation.

The new method starts with a thin (0.031-inch, or 0.8-mm) sheet of polyimide and consists of drilling, inserting the terminal posts, upsetting the ends, and then bonding a second sheet to the upset side as a continuous insulation member. The resulting sandwich is lighter and much cheaper to fabricate than the single board.

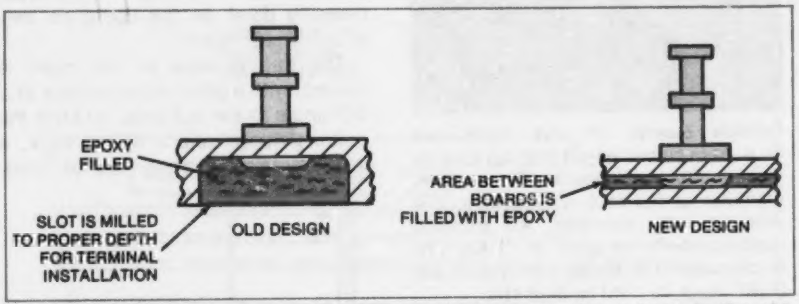
EPOXY FILLED
SLOT IS MILLED TO PROPER DEPTH FOR TERMINAL INSTALLATION
OLD DESIGN
AREA BETWEEN BOARDS IS FILLED WITH EPOXY
NEW DESIGN

The Old and New Methods for making terminal boards are shown here. In the old method (left), slots are end-milled in a thick board; after the posts are mounted, the slot is filled with epoxy. In the new technique (right), the posts are mounted on a thin sheet, and then a second sheet is epoxied to the upset side. The result is a lighter, cheaper product.

Thirty boards made by the new method saved an estimated 8 pounds (4 kg) in the weight of the Space Shuttle orbiter. Further reduction in size and weight is possible, because the elimination of slot milling allows terminal rows to be installed closer together.

This work was done by James D. Drechsler and Harry G. Eaton of Rockwell International Corp. for **Johnson Space Center.** *No further documentation is available.*
MSC-18787

A Construction Technique for Wind-Tunnel Models

High strength, good surface finish, and corrosion resistance are imparted to miniature wind-tunnel models by machining the pressure channels as an integral part of the model. The pattern for pressure channels is scribed, machined, or photoetched before the channels are drilled. The mating surfaces for the channels are flashed and then diffusion-brazed together.
(See page 350.)

Cooling/Grounding Mount for Hybrid Circuits

Extremely-short input and output connections, adequate grounding, and efficient heat removal for hybrid integrated circuits are possible with a new mounting. A rectangular clamp holds the hybrid on a printed-circuit board, in contact with a heat-conductive ground plane. The clamp is attached to the ground plane by bolts.
(See page 274.)

Reshaping Tube Ends for Welding

Tube ends are rounded in preparation for welding by a new semiautomatic tool. Tubes that have been trimmed close to a bend may be deformed by the process. To restore roundness, the out-of-round tube is opened, a plug is inserted, and a crimper compresses the tube into proper shape around the plug.
(See page 373.)

Transistor Package for High-Pressure Applications

With an alumina disk brazed to cap and terminals, a TO63 transistor package can withstand 200 psi.

Lyndon B. Johnson Space Center, Houston, Texas

A TO63 transistor package can operate in hydraulic oil at pressures of 200 psi (1.4×10^6 N/m^2) or greater without leakage failure if it is reinforced by an alumina disk brazed to the cap and terminals. This inexpensive modification has been used successfully on power transistors in hydraulic circulating-pump assemblies for the Space Shuttle orbiter and should be effective in other pressurized environments, such as in oil exploration equipment. The modified package has been proof-tested at 500 psi (3.5×10^6 N/m^2).

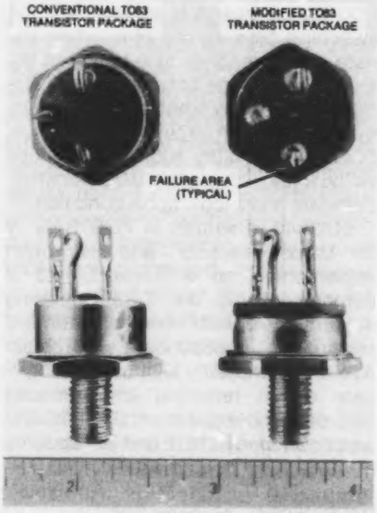
CONVENTIONAL TO63 TRANSISTOR PACKAGE
MODIFIED TO63 TRANSISTOR PACKAGE
FAILURE AREA (TYPICAL)
2
3
4

Figure 1. **Modification of a TO63 Transistor Package,** by brazing an alumina disk to the cap and terminals, prevents leaks at the terminals under high pressures.

The TO63 is a stud-mounted transistor package with three terminals emerging through the top cap (see Figure 1). When submerged in oil under high pressure, it was subject to failure at the base of the terminals where they enter the cap.

The alumina disk is added to the cap when the transistor is manufactured. As a preparatory step, molybdenum/manganese alloy is metal-screened (a process similar to silk screening) onto the areas to be brazed (see Figure 2). The disk is then heat-treated by raising its temperature to 1,300° C over 30 to 60 minutes, holding it at that temperature for 15 minutes, and then cooling it back to ambient temperature over another 30- to 60-minute period.

The three terminals are inserted through the holes in the disk and then brazed to the molybdenum/manganese pads. Following this, the disk with terminals is brazed to the transistor cap. For this step, a ring of preformed BT braze alloy that matches the screened area on the disk is used. This brazing operation is done over the same time cycle as in the preparatory step, but the temperature is held at 1,050° C, rather than 1,300° C. The modified cap is then ready for standard transistor assembly.

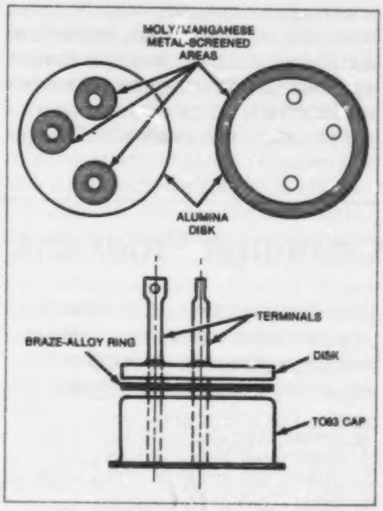

Figure 2. The **Brazing Process** begins (top) when molybdenum/manganese pads are metal-screened around the terminal holes on one side of the alumina disk and around the perimeter of the disk on the reverse side. After a heat treatment, the disk is brazed to the transistor cap, using a preformed braze-alloy ring (bottom).

This work was done by Peter J. Zantos of Rockwell International Corp. for **Johnson Space Center.** *No further documentation is available.*
MSC-18743

Books and Reports

These reports, studies, and handbooks are available from NASA as Technical Support Packages (TSP's) when a Request Card number is cited; otherwise they are available from the National Technical Information Service.

Automatic Chemical Vapor Deposition

Characteristics of the process and equipment are detailed.

A report reviews chemical vapor deposition (CVD) for processing integrated circuits and describes a fully automatic machine for CVD. In chemical vapor deposition, gases react next to the surface of a wafer (silicon, sapphire, or spinel, for example) and form a thin layer of solid material on the wafer. In integrated-circuit manufacturing, CVD is sometimes favored over such other methods as the thermal oxidation of silicon substrates or the deposition of evaporated materials. This is primarily because CVD proceeds at a relatively low temperature, allows a wide choice of film compositions (including graded or abruptly

(continued on next page)

changing compositions), and deposits uniform films of controllable thickness at a fairly high growth rate.

The report surveys CVD techniques for "glassing" chips — that is, for coating integrated-circuit chips with an impermeable protective layer of glass. Glasses composed of silicon dioxide, borosilicates, aluminosilicates, phosphosilicates, and laminates of these materials are considered. Methods of densifying glass films are reviewed, and appropriate substrate materials are surveyed.

The report also deals with CVD for applying insulating, conducting, and semiconducting films — that is, films that form part of the functional structure of an integrated circuit, in contrast to glass films, which are primarily protective.

The automatic CVD machine covered in the report is a continuous system under computer control. It automatically loads 3-inch (7.6-cm) substrates in a "boat," deposits a film on them, and unloads the substrates. Some of the preliminary considerations that go into the design of an automatic CVD machine are described in the report, though details of the system subcomponents are not included. The report gives an overview of hardware, reactants, and temperature ranges used with the CVD machine.

This work was done by Bobby W. Kennedy of **Marshall Space Flight Center**. *To obtain a copy of the report, "Chemical Vapor Deposition for Automatic Processing of Integrated Circuits," Circle 87 on the TSP Request Card.*
MFS-25459

Computer Programs

These programs may be obtained at very reasonable cost from COSMIC, a facility sponsored by NASA to make new programs available to the public. For information on program price, size, and availability, circle the reference letter on the COSMIC Request Card in this issue.

CADAT Logic Simulation Program

Program checks logic functional correctness, accounting for realistic propagation delays.

The CADAT Logic Simulation Program (LOGSIM) checks the functional correctness of an electronic logic circuit by simulating the circuit at the logic gate level. LOGSIM also checks the propagation delay through the logic nets and indicates any timing or "race" problems.

LOGSIM simulates very large logic networks within a modest amount of computer core memory. The program has an internal library of 15 logic elements, to which the user may add new elements by simply defining their operation. In addition, the user can define complex logic functions in terms of read-only memories, each with up to 15 inputs.

LOGSIM is divided into three phases: the preprocessor, the simulator, and the postprocessor. Each phase can run independently or in a stream. The preprocessor validates the input data and sends diagnostic messages whenever necessary. It also generates a connectivity list showing each gate and its loads, to aid the user in determining that the input data describe the circuit intended. The preprocessor also prepares a circuit data file for use by the simulator.

The simulator first establishes the initial levels of each of the logic elements. Next, the user-specified input signals are propagated through the circuit. Specified level changes are entered into an element status table. Each element loaded by the changed signals is then examined to determine if its output is changed. Appropriate logic delay and decay times are added to the current time to find the times at which future events are to be scheduled. When all loads have been examined, the current time is advanced to that of the next scheduled event, and the process is repeated. As the new levels of each scheduled event are entered in the element status table, the event is also recorded on tape for input to the postprocessor.

The postprocessor reads the list of input circuit element names and the initial conditions and prints a list of the output signals. A timing diagram may be printed with the initial condition of each element or a list of all initial conditions. Logic events are read from the simulator data tape, and the status of the user-selected elements is printed for each time within the specified interval at which an event occurs. The postprocessor is controlled by user directives and can generate any number of timing diagrams in any user-specified format during a single run.

For logic circuitry to be simulated on an ideal binary-valued basis, a relationship must be established between the ideal low and high levels and the realistic delayed level transitions. The LOGSIM approach is to establish the switching time as the time when the gate output reaches nine-tenths of the maximum change between levels. The rise and fall delay times are supplied by the user for each circuit element. Thus, LOGSIM simulates such occurrences as logic fall decay of an MOS transmission gate and a logic spike condition.

LOGSIM is written in FORTRAN IV for batch execution and has been implemented on a Xerox Sigma V computer using the CP-5 operating system. Program central memory requirement is dependent on problem size and complexity with a 5,000-logic-gate circuit requiring approximately 50K of 32-bit word memory. LOGSIM was developed in 1972 and last updated in 1976. [See related article, "CADAT Integrated-Circuit Mask Analysis" (MFS-25054), on page 396.]

This program was written by C. L. Mitchell and J. F. Taylor of M&S Computing, Inc., for **Marshall Space Flight Center**. *For further information, Circle J on the COSMIC Request Card.*
MFS-25183

CADAT Test Pattern Generator

Checkout and testing of complex digital circuits are reduced and done in a few days instead of months.

The CADAT test pattern generator (TPG) aids in the checkout, fault detection, and fault isolation of complex digital circuits. The time and the effort of manually generating digital test patterns can be a major limiting factor in effectively utilizing automatic testing. This time and effort are reduced from several months to several days by TPG.

TPG performs the three major tasks associated with test program design. After examining the circuit, it develops a set of stimulus-and-response patterns for checkout, fault detection, and fault isolation. TPG then verifies the diagnostic potential of the patterns, and finally, it creates a data file that can be interfaced with automated circuit-testing equipment.

Input to TPG consists of a nodal description of the digital configuration. A large, expandable digital component library is available for describing the circuit. Once the complete circuit has been introduced, TPG generates a NAND-gate equivalent circuit as the basic model for test pattern generation. The use of NAND equivalents facilitates a realistic failure simulation, which has proved more effective and efficient than individual component simulation. Signal propagation delay is simulated by using a fixed time delay across each NAND. This NAND-gate time accounting has higher resolution than fixed component delay, since nodes are processed simultaneously throughout the circuit. By checking for node-status oscillations, TPG has a high probability of spotting "race" conditions that might otherwise go undetected.

Once TPG has analyzed the model, generated a test pattern, and verified the validity of the pattern, the stimulus data for testing the actual device are prepared. In order actually to test or simulate the device accurately, the TPG-generated stimulus data must be transformed into acceptable inputs for logic test equipment or for a logic simulator. The TPG package includes an interface program (TPGITF) to utilize the TPG stimulus data to generate TOIL test sequences for the MACRODATA-200 LSI tester and to generate excitation input for the CADAT system logic-simulator program LOGSIM.

The TPG program is written in FORTRAN IV for batch execution and has been implemented on a Xerox Sigma V computer. The TPG program was originally developed in 1971 and was last updated in 1976.

This program was written by M&S Computing Co., for **Marshall Space Flight Center.** *For further information, Circle K on the COSMIC Request Card.*
MFS-25066

CADAT Field-Effect-Transistor Simulator

A versatile designer tool for analyzing MOS circuits

The CADAT field-effect-transistor simulator (FETSIM) analyzes the dc and transient behavior of metal-oxide-semiconductor (MOS) circuits. Both N-MOS and P-MOS transistor configurations in either bulk or silicon-on-sapphire (SOS) technology and almost any combination of R/C elements are analyzed.

As inputs, FETSIM requires the complete circuit topology and device, process, and control parameters. The user may also specify initial node conditions and the input pulse format. For example, pulse rise time, fall time, width, and time between succeeding pulses are all independently controlled.

FETSIM is based on a sophisticated mathematical model that can accurately handle N-MOS, P-MOS, bulk, and SOS devices. By considering doping of the ionized acceptors (or donors) in the substrate, several second-order physical effects are implicitly accounted for. They include the apparently-decreased carrier mobility resulting from heavy substrate doping and the gating effect associated with stacked devices. Sensitivity to process changes is maintained by requiring such data as threshold voltages and doping levels as inputs. Such intrinsic MOS phenomena as parasitic feedback capacitance and variation of threshold voltage with source potential are handled implicitly.

FETSIM transforms the input data into a set of nodal equations. These ordinary differential equations are numerically integrated. As outputs, FETSIM lists node voltages and all transistor currents as a function of time.

The FETSIM program is written in FORTRAN IV for batch execution and has been implemented on Xerox Sigma V with a central memory requirement of approximately 45K of 32-bit words. The FETSIM program was developed in 1974 and was last updated in 1977.

This program was written by RCA Corp. for **Marshall Space Flight Center.** *For further information, Circle L on the COSMIC Request Card.*
MFS-25067

CADAT Place-and-Routine in Two Dimensions

An interactive program for converting a logic design to final LSI/MOS chip artwork.

The CADAT place-and-route-in-two-dimensions program (PR2D) is a standard-cell automatic-layout program for generating large-scale-integrated/metal-oxide-semiconductor (LSI/MOS) arrays. PR2D translates the logic designer's cell interconnection requirements into a physically-defined MOS chip. Input data consist of program control parameters, logic pattern assignments, and the interconnecting nets. PR2D reads the input data, searches the pin data file for data on each pattern type, generates a placement of the patterns, and interconnects the patterns. As output, it generates the artwork for the layouts.

The program control parameters allow the individual functions of PR2D to be executed in separate steps. This increases the flexibility of the program and can reduce computer run time. By inspecting the output at each step, changes can be made to improve the placement and routing on the final chip design.

PR2D produces a map, or printer plot, that is assembled into the final chip layout. All pertinent data regarding the layout are shown on the map. In addition, a printout of chip statistics is generated for review by the designer. Once the design is finalized, an artwork data file is generated for fabricating the chip mask.

PR2D is written in FORTRAN IV for batch execution and has been implemented on a Xerox Sigma V CP-V computer with 64K of 32-bit memory. The program was developed in 1978.

This program was written by RCA Corp. for **Marshall Space Flight Center.** *For further information, Circle M on the COSMIC Request Card.*
MFS-25058

CADAT Multiport Placement and Routing

Substantial chip area is saved by unique multiport cells.

The CADAT multiport-in-two-dimensions program (MP2D) is a powerful placement and routing aid for processing double-ended cell equivalents of the high-speed silicon-on-sapphire (SOS) standard-cell family. The basic purpose of MP2D is to design high-density large-scale-integrated (LSI) arrays. Using inputs that consist of control parameters, logic pattern assignments, and node connectivity data, MP2D determines a two-dimensional placement of the cells and a two-dimensional routing of interconnections. The outputs include artwork-plotting instructions for generating the final mask. Innovative double-entry and "feedthrough" multiport cells allow MP2D to reduce substantially the chip area and wiring.

Two major innovations in LSI array design make MP2D substantially better than typical single-entry placement and routing programs. One of these innovations enables the program (1) automatically to route interconnections to either the top or bottom of each cell in such a way as to minimize total wire length and interconnection area and (2) to make connections between cells on nonadjacent rows by routing the interconnections directly across or through intermediate cell rows.

The other innovation relates to the unique feature of the circuit cell that permits the input/output connections to be accessed at either the top or the bottom of the cells. This multiport placement and routing can save substantial chip "real estate" because of the reduced requirements for wiring, which previously was the largest user of chip area.

MP2D is written in FORTRAN IV for batch execution, has been implemented on a Xerox Sigma V computer with the CP-V operating system, and has a central memory requirement of approximately 56K of 32-bit words. The program was developed in 1977.

This program was written by RCA Corp. for **Marshall Space Flight Center.** *For further information, Circle N on the COSMIC Request Card.*
MFS-25065

CADAT Integrated-Circuit Mask Analysis

Program verifies artwork, checks logic equations, and evaluates other mask design parameters.

The CADAT System Mask Analysis Program (MAPS2) is an automated software tool for analyzing integrated-circuit mask design. Included in MAPS2 functions are artwork verification, device identification, nodal analysis, capacitance calculation, and logic equation generation.

To simplify the data base, MAPS2 operates on mask data that have been converted from their original forms to orthogonal rectangles with identification numbers. MAPS2 accepts and automatically converts mask data in MAP, PRF, MANN, AIDS, and Banning Cell Library formats. The resultant rectangular mask data file allows MAPS2 to analyze circuit masks quickly and efficiently.

Once the mask data file is created, the user controls the analysis through a versatile command language. The user commands a wide range of processes, including qualitative and quantitative testing of selected mask areas, the modification of masks, the creation of new masks, and the computation and sorting of mask data.

MAPS2 processing is divided into two major processes: rectangular refinement and command execution. In the rectangular refinement processing, user-supplied mask data are converted into the orthogonal rectangle format that approximates the mask to any user-specified accuracy. Once the rectangular mask data have been generated and stored, user-supplied commands are processed one at a time. Data are read from the mask rectangle file, the requested processing is performed, output data files are generated, and any user-requested information is printed.

MAPS2 is written in FORTRAN IV for batch execution and has been implemented on a Xerox Sigma II computer with a central memory requirement of approximately 33K of 16-bit words. MAPS2 was developed in 1976. [See related article, "CADAT Logic Simulation Program" (MFS-25183), on page of this issue.]

This program was written by C. L. Mitchell of M&S Computing, Inc., for **Marshall Space Flight Center**. *For further information, Circle P on the COSMIC Request Card.*
MFS-25054

Mathematics and Information Sciences

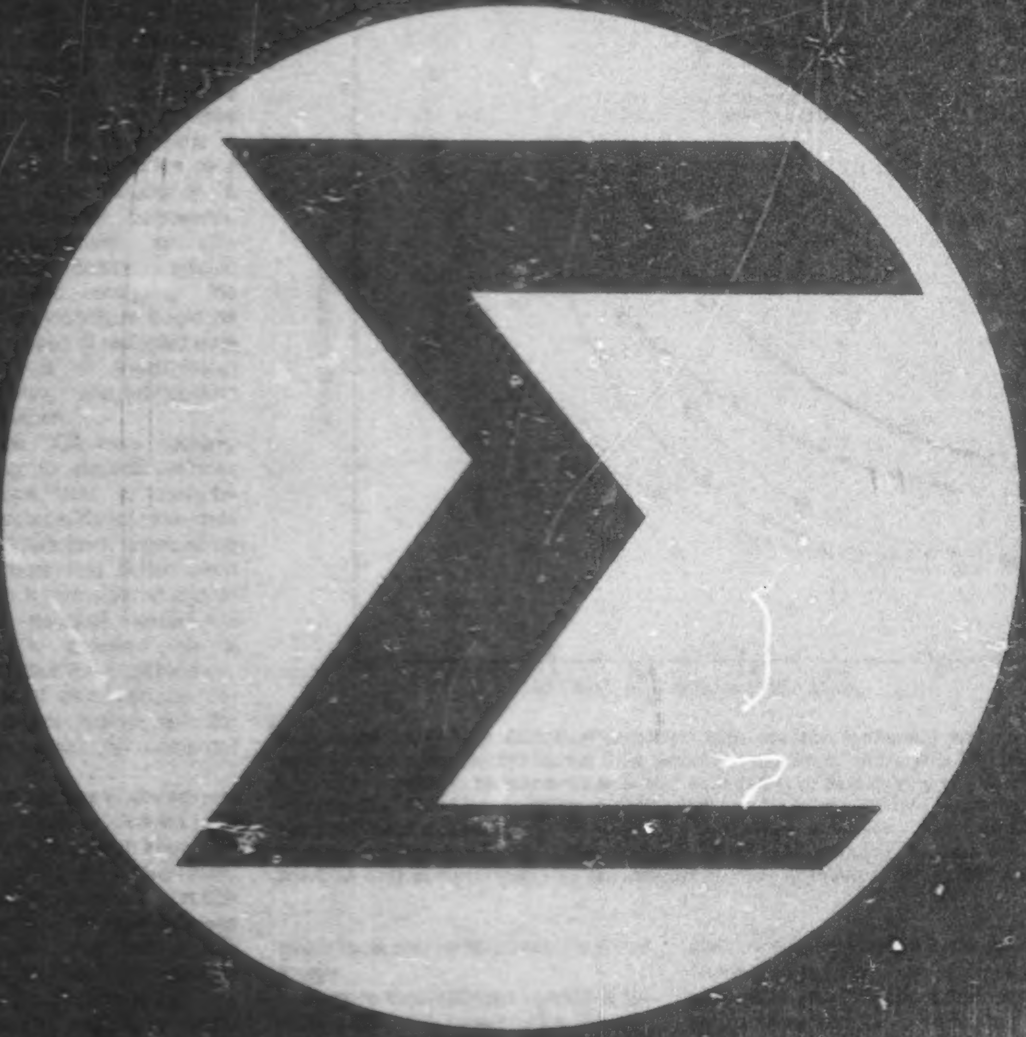

Hardware, Techniques, and Processes

399 An Image-Data-Compression Algorithm
400 Determining Manufacturing Cost From Product Complexity

An Image-Data-Compression Algorithm

A proposed algorithm simplifies image data processing.

NASA's Jet Propulsion Laboratory, Pasadena, California

A recently-proposed Cluster Compression Algorithm (CCA) preprocesses Landsat image data immediately following the satellite data sensor (receiver). The data are reduced by extracting pertinent image features and compressing this result into a concise format for transmission to a ground station. This results in a narrower transmission bandwidth, increased data-communication efficiency, and reduced computer time in reconstructing and analyzing the image. A similar technique could be applied to other types of recorded data to cut the costs of transmitting, storing, distributing, and interpreting complex information.

Basically, the CCA uses spatially local clustering to extract features from the image data to describe spectral characteristics of the data set. These features form a sequence of scalar numbers that define each picture element in terms of the cluster features. The sequence, called the feature map, is encoded into a compressed format for transmission. The preprocessed data can be decoded via a simple lookup table for image reconstruction or computer analysis.

The CCA can use any of the several clustering techniques all derived from the basic iterative approach known as the Basic Clustering Algorithm (BCA) for automatically grouping the multidimensional data. The BCA involves simple repetitive computations and can be structured in a highly parallel manner for very high data rates.

The BCA assigns each data vector to the closest cluster and generates a predetermined number of features per data set that correspond to a rate-controlled mode for a data compressor. There are many ways to modify the BCA to make it adaptive. For example, clusters might be split, combined, or deleted during the iterative clustering based on intracluster and intercluster distance measures.

The most basic version constitutes the Uncoded CCA. This version applies measurement vectors from every local source to cover the entire image.

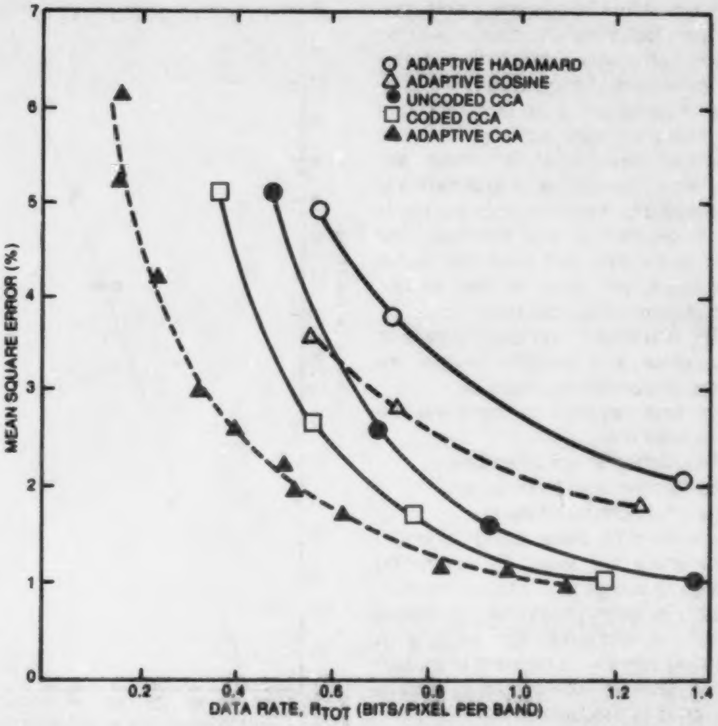

A Comparison of New CCA Configurations with adaptive Hadamard and Fourier techniques shows that the former CCA technique has fewer errors as a function of data rate. Algorithm performance was defined in terms of data quality as a function of data rate. The data quality was defined in the most commonly used terms of percent mean-square error (%MSE), classification accuracy, and subjective appearance. The results have shown that in addition to reducing the data volume, the CCA data compression also reduces the number of required classifications.

A more sophisticated version is the Coded CCA. It is based on the fact that in image data there is significant spectral correlation between spatially-close picture elements and correspondingly adjacent elements on the feature map. This correlation lends itself to entropy encoding techniques.

Other versions include the Adaptive CCA and the Cascaded CCA. The Adaptive form is as the Coded CCA except the clustering is adaptive. The clusters may be deleted, split, or combined according to the user supervision thresholds. The Cascaded CCA can modify the local source clustering based on the knowledge of clustering results from surrounding local sources. This characteristic can be used to reduce the spatial and spectral data rates.

The figure shows a comparison of the performances of the new CCA configurations. Performance is measured as the percentage of errors introduced at a given data rate.

This work was done by Edward E. Hilbert and Robert F. Rice of Caltech for **NASA's Jet Propulsion Laboratory.** *For further information, Circle 92 on the TSP Request Card. NPO-14496*

Determining Manufacturing Cost From Product Complexity

Analytical method exploits the special relationship between complexity and manufacturing improvement trends.

Marshall Space Flight Center, Alabama

A procedure allows the calculation of manufacturing complexity — the totality of cost elements that determine the cost of manufacturing a unit. The procedure is based on the premise that manufacturing follows a learning curve; that is, costs are assumed to decrease as experience is acquired and improvements are made in design, tooling, and methods. The cost of the first unit produced is the maximum unit cost of the series. Subsequent units cost less.

The first step in the procedure is to enumerate and tabulate several indexes of complexity, such as:

- The time required to complete the first assembly,
- The number of subassemblies,
- The number of fasteners, and
- The total number of parts.

The values of these design-oriented parameters are found by examining design drawings and production records. For each parameter, sufficient data are gathered for plotting a learning curve — a curve of manufacturing cost vs. the length of time a design is in production.

Learning curves are plotted on double logarithmic paper for at least six values of each parameter. This step is repeated for each of the subsystems (e.g., electrical, mechanical) in a production unit. For example, if a production unit consists of four subsystems, at least 24 learning curves must be plotted for the number of fasteners and for each of the other design parameters. The slopes of the learning curves for the various parameter values are plotted for each subsystem to give a trend curve (see Figure 1). In general, the slope will increase more or less along a straight line as the parameter value increases.

At that point, a decision is made about the parameters to be included in the calculation. If a parameter appears to be unrepresentative of the overall system, it is omitted from further consideration. Different subassemblies may have different parameters; for example, the set chosen for an electrical assembly may be different from that for a mechanical assembly.

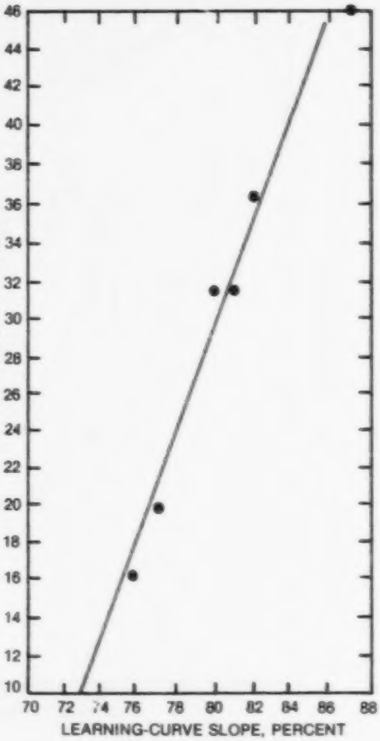

Figure 1. A **Trend Curve** shows how the learning-curve slope varies for different values of a manufacturing parameter (in this case, the number of fasteners).

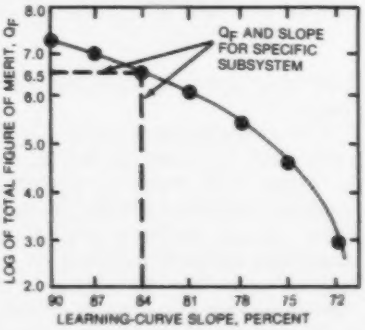

Figure 2. A **Figure-of-Merit Curve** shows how complexity varies with the learning-curve slope of a subsystem.

The next step is to determine a figure of merit representing the complexity of a specific subsystem design. The figure of merit, called Q_F, is found for each of the subsystems in the unit. Q_F is equal to the product of the parameter values at a given value of the learning-curve slope. The logarithm of Q_F is plotted as a function of slope (see Figure 2). This curve applies to a subsystem. The learning-curve slope for a specific subsystem design is found by interpolating from the known Q_F value for the design.

Finally, a composite slope for the complete unit is calculated by a formula that takes into account the slopes of the individual subsystems, the value in dollars of worker hours of each of the subsystems, and the total value of the complete unit. The formula weights the contribution of the individual subsystem slopes according to the value of the subsystem.

With the composite slope, it is possible to compute the cost of the nth unit turned out on the production line. The computation is reduced to finding the ordinate (cost of the nth unit) that corresponds to a particular abscissa (nth unit) on a straight line on double logarithmic paper. Both the slope and intercept (the cost of the first unit produced) are known.

This work was done by Leon M. Delionback of **Marshall Space Flight Center.** *For further information, Circle 88 on the TSP Request Card.*
MFS-25371

SUBJECT INDEX

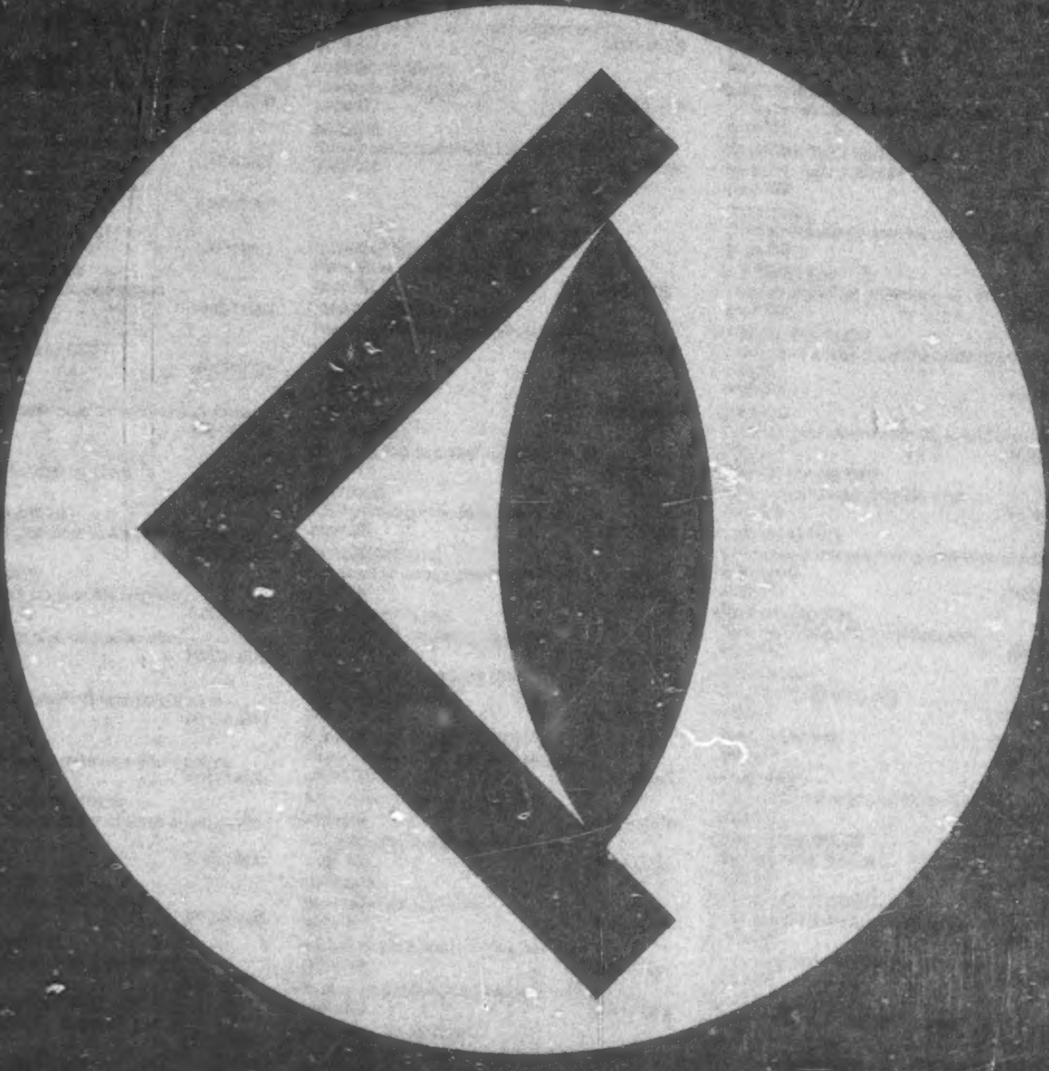

ACCELEROMETERS
Fiber-optic accelerometer
page 357 LEW-13219
ACOUSTIC PROPAGATION
Acoustic lens is gas-filled
page 345 NPO-14757
ACOUSTO-OPTICS
Acoustically-tuned optical filter
page 304 HQN-10924
ADHESIVES
Aluminum ions enhance polyimide adhesive
page 326 LAR-12640
AERODYNAMIC CONFIGURATIONS
Aerodynamic preliminary analysis
page 362 LAR-12404
AEROSOLS
Aerosol lasts up to six minutes
page 328 NPO-14947
AIRBORNE EQUIPMENT
Airborne meteorological data-collection system
page 290 LEW-13346
AIRCRAFT DESIGN
Aerodynamic preliminary analysis
page 362 LAR-12404
Cap protects aircraft nose cone
page 282 LAR-12367
Solar-powered aircraft
page 370 LAR-12615
AIRCRAFT MANEUVERS
Cost-minimized aircraft trajectories
page 362 ARC-11282
AIRCRAFT WAKES
Wakeflow analysis by COST
page 355 NPO-14705
AIRFOILS
A construction technique for wind-tunnel models
page 350 LAR-12710
ALIGNMENT
Alining sleeve for optical fibers
page 389 MSC-18756
ANALOG SIMULATION
Converting a digital filter to its analog equivalent
page 289 MSC-18587
ANTENNA ARRAYS
Arrayed receivers for low-rate telemetry
page 285 NPO-14590
Receiver array for high-rate telemetry
page 284 NPO-14579
ANTENNAS
Antenna feed for circular/linear polarization
page 270 NPO-14810
ARTERIES
Compliant transducer measures artery profile
page 337 NPO-14699
ATMOSPHERIC COMPOSITION
Simultaneous measurement of three atmospheric pollutants
page 327 NPO-14828
ATTITUDE [INCLINATION]
Compact table-tilting mechanism
page 376 NPO-14800
AUTOMATIC CONTROL
Automatic chemical vapor deposition
page 393 MFS-25459
AUTOMATIC FREQUENCY CONTROL
Ultrastable automatic frequency control
page 267 MSC-18679
AUTOMOBILE ENGINES
Reduced hydrogen permeability at high temperatures
page 331 LEW-13465
AXISYMMETRIC BODIES
Inviscid transonic flow over axisymmetric bodies
page 363 LAR-12499
BENDING
Method for shaping polyethylene tubing
page 388 MSC-18771
BIOMEDICAL DATA
Flow sensor for biomedical fluids
page 335 MSC-18761
BIOTELEMETRY
Miniaturized physiological-data telemetry system
page 338 MSC-18604
BLOOD VESSELS
Compliant transducer measures artery profile
page 337 NPO-14699
BOLTS
Two-headed bolt
page 375 MFS-19619
BORING MACHINES
Boring tool for aramid fabric-faced panels
page 391 MSC-18786
BUFFER STORAGE
Common data buffer
page 277 KSC-11048
BRAZING
Time-sharing switch for vacuum brazing
page 376 MSC-18600

CALIBRATING
Portable zero-delay assembly
page 292 NPO-14671
CAPACITIVE FUEL GAGES
Fast-response cryogen-level sensor
page 344 MSC-18697
CARBON
Carbon scrubber
page 324 MSC-16531
CARTRIDGES
Quick mixing of epoxy components
page 379 MSC-18731
CASTINGS
Sealing micropores in thin castings
page 391 MSC-18623
CATHETOMETERS
Improved ureteral stone fragmentation catheter
page 337 NPO-14745
CAVITATION FLOW
Dynamics of cavitating cascades
page 369 MFS-25399
CENTRAL PROCESSING UNITS
Common data buffer
page 277 KSC-11048
CHARGE COUPLED DEVICES
Four-quadrant CCD analog multiplier
page 279 LAR-12332
Monolithic CCD-array readout
page 282 LAR-12376
Monolithic four-quadrant multiplier
page 280 LAR-12330A
CHARRING
Heat-resistant polymers
page 319 ARC-11176
High-char-yield epoxy curing agents
page 328 LEW-13226
Resin char oxidation retardant for composites
page 322 LEW-13275
CHEMICAL ANALYSIS
Simultaneous measurement of three atmospheric pollutants
page 327 NPO-14828
CLEAVAGE
Precision cleaving machine for hard crystals
page 367 GSC-12584
COATINGS
Improved metallic and thermal-barrier coatings
page 321 LEW-13324
COMPOSITE MATERIALS
Boring tool for aramid fabric-faced panels
page 391 MSC-18786
Composites with nearly-zero thermal expansion
page 323 MSC-18724
Contour-measuring tool for composite layups
page 383 ARC-11246
High-char-yield epoxy curing agents
page 328 LEW-13226
Hot forming graphite/polyimide structures
page 387 LAR-12547
Resin char oxidation retardant for composites
page 322 LEW-13275
Testing panels in tension and flexure
page 349 MFS-25421
COMPRESSION TESTS
Environmental testing under load
page 348 LAR-12602
CONCENTRATORS
Offset paraboloidal solar concentrator
page 299 NPO-14846
CONSTRUCTION MATERIALS
Versatile, safe scaffolds
page 372 GSC-12606
CONTOURS
Contour-measuring tool for composite layups
page 383 ARC-11246
CONTROLLERS
Toggled signal for prevention of control errors
page 286 MSC-18779
CONVECTIVE FLOW
Analysis of a cooled turbine blade or vane with an insert
page 364 LEW-13293
COOLING
Cooling/grounding mount for hybrid circuits
page 274 MSC-18726
COPPER CHLORIDES
High-power copper chloride laser
page 308 NPO-14782
COST ANALYSIS
Determining manufacturing cost from product complexity
page 400 MFS-25371
COST REDUCTION
Cost-minimized aircraft trajectories
page 362 ARC-11282
COUPLINGS
Ball-joint grounding ring
page 371 MSC-18824
Two-headed bolt
page 375 MFS-19619
COVERINGS
Cap protects aircraft nose cone
page 282 LAR-12367
CRUCIFORM WINGS
Solar-powered aircraft
page 370 LAR-12615
CRYOGENIC EQUIPMENT
Fast-response cryogen-level sensor
page 344 MSC-18697
Fiber-optic level sensor for cryogens
page 345 MSC-18674
CRYSTALS
Alined columnar microstructures
page 332 MFS-25205
Precision cleaving machine for hard crystals
page 367 GSC-12584
CURING
High-char-yield epoxy curing agents
page 328 LEW-13226
One-step microwave foaming and curing
page 386 MSC-18707

CURVATURE
NASTRAN modifications for recovering strains and curvatures
page 361 LEW-1252

CURVED SURFACES
Contour-measuring tool for composite layups
page 383 ARC-11246

CUSHIONS
Modified fire-resistant foams for seat cushions
page 385 MSC-1870

DATA COMPRESSION
An image-data-compression algorithm
page 399 NPO-1449

Compressing TV-image data
page 286 NPO-1482

DATA STORAGE
Simultaneous disk storage and retrieval
page 278 KSC-1116

DECARBONATION
Carbon scrubber
page 324 MSC-1653

DEFORMATION
Reshaping tube ends for welding
page 373 MSC-1846

DEPOSITION
Automatic chemical vapor deposition
page 393 MFS-2545

DEPTH MEASUREMENTS
Direct-reading depth probe
page 354 KSC-1118

DIGITAL DATA
Real-time image enhancement
page 267 NPO-1426

DIGITAL FILTERS
Converting a digital filter to its analog equivalent
page 289 MSC-1856

DIMENSIONAL MEASUREMENT
Contour-measuring tool for composite layups
page 383 ARC-1124

Direct-reading depth probe
page 354 KSC-11181

DIPLEXERS
Diplexer for laser-beam-communication heterodyne receiver
page 307 GSC-12589

DISPERSING
Spraying suspensions uniformly
page 374 MFS-25139

DISPLAY DEVICES
Monolithic CCD-array readout
page 282 LAR-12376

Rain, fog, and clouds for aircraft simulators
page 352 ARC-11158

DOSIMETERS
Miniature personal UV solar dosimeter
page 300 LAR-12469

DRILL BITS
Abrasive drill for resilient materials
page 368 LEW-13411

DRILLING
Drilling at right angles in blind holes
page 369 MFS-19535

DUST STORMS
Predicting and monitoring duststorms
page 302 NPO-14277

ELASTIC DEFORMATION
Plastic deformation of engines and other nonlinear structures
page 363 MFS-23814

ELASTIC PROPERTIES
Composites with nearly-zero thermal expansion
page 323 MSC-18724

ELECTRIC CONDUCTORS
Electrically-conductive palladium-containing polyimide films
page 325 LAR-12629

ELECTRIC CONNECTORS
Kilovolt vacuum feedthrough is less noisy
page 390 NPO-14802

ELECTRICAL GROUNDING
Ball-joint grounding ring
page 371 MSC-18824

ELECTRICAL RESISTIVITY
Electrically-conductive palladium-containing polyimide films
page 325 LAR-12629

ELECTRON BEAM WELDING
Limiting current in electron-beam welders
page 377 MFS-19503

ELECTRONIC PACKAGING
Cooling/grounding mount for hybrid circuits
page 274 MSC-18725

Lightweight terminal board
page 392 MSC-18787

Transistor package for high-pressure applications
page 392 MSC-18743

ELECTRONIC SWITCHES
Fast microwave switching power divider
page 269 GSC-12420

ENERGY CONVERSION EFFICIENCY
Combined photovoltaic and thermal-storage module
page 305 NPO-14591

ENGINE DESIGN
Plastic deformation of engines and other nonlinear structures
page 363 MFS-23814

ENVIRONMENTAL TESTS
Data-acquisition and control system for severe environments
page 310 MFS-25471

Environmental testing under load
page 348 LAR-12602

EPOXY RESINS
High-char-yield epoxy curing agents
page 326 LEW-13226

Quick mixing of epoxy components
page 379 MSC-18731

EQUILIBRIUM FLOW
Analysis of a cooled turbine blade or vane with an insert
page 364 LEW-13293

EXERCISE [PHYSIOLOGY]
Manual for physical fitness
page 339 MSC-18915

EXTENSIONS
Torque-wrench extension
page 379 MSC-18769

EXTRACTION
Wrench for smooth or damaged fasteners
page 380 MSC-18772

FAILURE MODES
Toggled signal for prevention of control errors
page 288 MSC-18779

FALLING SPHERES
Tracking falling objects
page 306 NPO-14613

FASTENERS
Two-headed bolt
page 375 MFS-19619

FATIGUE TESTING MACHINES
Temperature controller adapts to fatigue tester
page 347 LAR-12393

FIBER OPTICS
Alining sleeve for optical fibers
page 389 MSC-18736

Fiber-optic accelerometer
page 357 LEW-13219

Fiber-optic level sensor for cryogens
page 345 MSC-18674

Improved ureteral stone fragmentation catheter
page 337 NPO-14745

FIELD EFFECT TRANSISTORS
CADAT field-effect-transistor simulator
page 395 MFS-25067

FILTRATION
Treating domestic wastewater with water hyacinths
page 336 MFS-23984

FIRE PREVENTION
A new family of fire-resistant foams
page 384 MSC-16921

Modified fire-resistant foams for seat cushions
page 385 MSC-18704

Rigid fire-resistant foams for walls and floors
page 386 MSC-18708

FIRE RESISTANCE
One-step microwave foaming and curing
page 386 MSC-18707

FLEXING
Testing panels in tension and flexure
page 349 MFS-25421

FLIGHT SIMULATORS
Rain, fog, and clouds for aircraft simulators
page 352 ARC-11158

FLOW DISTRIBUTION
Inviscid transonic flow over axisymmetric bodies
page 363 LAR-12499

Wakeflow analysis by COST
page 355 NPO-14705

FLOWMETERS
Flow sensor for biomedical fluids
page 335 MSC-18761

FLUID FLOW
Dynamics of cavitating cascades
page 359 MFS-25399

FLUORESCENCE
Simultaneous measurement of three atmospheric pollutants
page 327 NPO-14826

FLUX MEASUREMENT
Improved magnetic material analyzer
page 353 LEW-13493

FRAMES
Versatile, safe scaffolds
page 372 GSC-12606

FREE FALL
Tracking falling objects
page 306 NPO-14613

FREQUENCY ANALYZERS
Ultrasonic frequency analysis
page 346 LAR-12697

FREQUENCY MODULATION
Ultrastable automatic frequency control
page 267 MSC-18679

FREQUENCY STABILITY
Ultrastable automatic frequency control
page 267 MSC-18679

FOAMS
A new family of fire-resistant foams
page 384 MSC-16921

Modified fire-resistant foams for seat cushions
page 385 MSC-18704

One-step microwave foaming and curing
page 386 MSC-18707

Rigid fire-resistant foams for walls and floors
page 386 MSC-18708

FOCUSING
Acoustic lens is gas-filled
page 345 NPO-14757

GAS DETECTORS
Laser-beam methane detector
page 330 NPO-14929
GAS LASERS
High-power copper chloride laser
page 308 NPO-14782
GAS TURBINE ENGINES
Oxide-dispersion-strengthened superalloy
page 320 LEW-13569

HEATING EQUIPMENT
A high school is supplied with solar energy — Dallas, Texas
page 316 MFS-25514
Commercial-building solar-energy system — Stamford, Connecticut
page 310 MFS-25468
Costs and description of a solar-energy system — Austin, Texas
page 312 MFS-25472
Data-acquisition and control system for severe environments
page 310 MFS-25471
Heat for film processing from solar energy
page 309 MFS-25444
Multiplexed logic controls solar-heating system
page 297 MFS-25287
Municipal recreation center is heated and cooled by solar energy — Dallas, Texas
page 312 MFS-25478
Offset paraboloidal solar concentrator
page 299 NPO-14846
Residential solar-heating installation — Stillwater, Minnesota
page 315 MFS-25504
Residential solar hot-water system — Tempe, Arizona
page 315 MFS-25490
Residential system tested in an office — Huntsville, Alabama
page 314 MFS-25481
Solar energy in a historical city — Abbeville, South Carolina
page 312 MFS-25479
Solar energy meets 50 percent of motel hot-water needs — Key West, Florida
page 313 MFS-25454
Solar-energy workshop — Tucson, Arizona
page 314 MFS-25473
Solar-heated and cooled office building — Dalton, Georgia
page 310 MFS-25451
Solar-heated office complex — Greenwood, South Carolina
page 313 MFS-25458
Solar-heated two-level residence — Akron, Ohio
page 314 MFS-25480
Solar heater/cooler for mass market
page 309 MFS-25452
Solar-heating and hot-water system — St. Louis, Missouri
page 311 MFS-25453
Solar heating for an electronics manufacturing plant — Blue Earth, Minnesota
page 311 MFS-25469
Three-story residence with solar heat — Manchester, New Hampshire
page 315 MFS-25499
HEAT RESISTANT ALLOYS
Low-cost, high-temperature, duplex coating for superalloys
page 321 LEW-13497
Oxide-dispersion-strengthened superalloy
page 320 LEW-13569
HEAT SHIELDING
Heat/pressure seal for moving parts
page 358 MSC-18422
HEAT TRANSFER
Compact, reliable heat switch
page 358 GSC-12625
Holes help control temperature
page 343 GSC-12618
Simplified thermal analyzer
page 360 GSC-12638
HIGH PRESSURE
Transistor package for high-pressure applications
page 392 MSC-18743
HIGH TEMPERATURE GASES
Reduced hydrogen permeability at high temperatures
page 331 LEW-13485
HIGH VOLTAGES
Kilovolt vacuum feedthrough is less noisy
page 390 NPO-14602
HOT WORKING
Hot forming graphite/polyimide structures
page 387 LAR-12547
HYBRID CIRCUITS
Cooling/grounding mount for hybrid circuits
page 274 MSC-18726
HYDROGEN
Reduced hydrogen permeability at high temperatures
page 331 LEW-13485

IMAGE CONVERTERS
An image-data-compression algorithm
page 399 NPO-14496
Four-quadrant CCD analog multiplier
page 279 LAR-12332
Monolithic CCD-array readout
page 282 LAR-12376
Monolithic four-quadrant multiplier
page 280 LAR-12330A
IMAGE ENHANCEMENT
Real-time image enhancement
page 287 NPO-14281
IMAGING TECHNIQUES
Acoustically-tuned optical filter
page 304 HQN-10924
IMPINGEMENT
Analysis of a cooled turbine blade or vane with an insert
page 364 LEW-13293
INERTIA
Interchangeable spring modules for inertia measurements
page 356 LAR-12402
INFRARED REFLECTION
Reducing energy consumption in incandescent lamps
page 304 MSC-18757
INSULATION
Measuring the thermal conductivity of insulation
page 351 NPO-14871
INTEGRATED CIRCUITS
Automatic chemical vapor deposition
page 393 MFS-25459
CADAT field-effect-transistor simulator
page 395 MFS-25067
CADAT integrated-circuit mask analysis
page 396 MFS-25054
CADAT logic simulation program
page 394 MFS-25183
CADAT multiport placement and routing
page 396 MFS-25065
CADAT place-and-route in two dimensions
page 395 MFS-25058
CADAT test pattern generator
page 394 MFS-25066
Four-quadrant CCD analog multiplier
page 279 LAR-12332
Monolithic CCD-array readout
page 282 LAR-12376
Monolithic four-quadrant multiplier
page 280 LAR-12330A
INTERFEROMETERS
Diplexer for laser-beam-communication heterodyne receiver
page 307 GSC-12589
INTRAVENOUS PROCEDURES
Flow sensor for biomedical fluids
page 335 MSC-18761
INVISCID FLOW
Inviscid transonic flow over axisymmetric bodies
page 363 LAR-12499

JOINTS [JUNCTIONS]
Ball-joint grounding ring
page 371 MSC-18824

LAMINATES
Boring tool for aramid fabric-faced panels
page 391 MSC-18786
LASER APPLICATIONS
Laser-beam methane detector
page 330 NPO-14929
Simultaneous measurement of three atmospheric pollutants
page 327 NPO-14828
LASER DOPPLER VELOCIMETERS
Noise suppression in forward-scattering optical instruments
page 303 LAR-12730
LASERS
Diplexer for laser-beam-communication heterodyne receiver
page 307 GSC-12589
High-power copper chloride laser
page 308 NPO-14782
LENSES
Acoustic lens is gas-filled
page 345 NPO-14757
LEVEL [QUANTITY]
Fast-response cryogen-level sensor
page 344 MSC-18697
Fiber-optic level sensor for cryogens
page 345 MSC-18674
LIQUIFIED NATURAL GAS
Laser-beam methane detector
page 330 NPO-14929
LITHIUM FLUORIDES
Precision cleaving machine for hard crystals
page 367 GSC-12584
LOGIC CIRCUITS
CADAT field-effect-transistor simulator
page 395 MFS-25067
CADAT integrated-circuit mask analysis
page 396 MFS-25054
CADAT logic simulation program
page 394 MFS-25183
CADAT multiport placement and routing
page 396 MFS-25065
CADAT place-and-route in two dimensions
page 395 MFS-25058
CADAT test pattern generator
page 394 MFS-25066
LOW GRAVITY MANUFACTURING
Alined columnar microstructures
page 332 MFS-25206
LUMINAIRES
Reducing energy consumption in incandescent lamps
page 304 MSC-18757

MACHINE TOOLS
Abrasive drill for resilient materials
page 368 LEW-13411
MACHINING
A construction technique for wind-tunnel models
page 350 LAR-12710
MAGNETIC MATERIALS
Improved magnetic material analyzer
page 353 LEW-13493
MANIPULATORS
Remote manipulator with force feedback
page 373 ARC-11272
MANUFACTURING
Determining manufacturing cost from product complexity
page 400 MFS-25371
MASS DISTRIBUTION
Interchangeable spring modules for inertia measurements
page 355 LAR-12402
MATERIALS HANDLING
Remote manipulator with force feedback
page 373 ARC-11272
MATERIALS RECOVERY
Decomposition of waste tires through chlorinolysis
page 331 NPO-14935
MATERIALS TESTS
Temperature controller adapts to fatigue tester
page 347 LAR-12393
MECHANICAL DRIVES
Compact table-tilting mechanism
page 376 NPO-14800
MEDICAL ELECTRONICS
Improved ureteral stone fragmentation catheter
page 337 NPO-14745
METEOROLOGICAL FLIGHT
Airborne meteorological data-collection system
page 290 LEW-13346
METHANE
Laser-beam methane detector
page 330 NPO-14929
MICROMETERS
Direct-reading depth probe
page 354 KSC-11181
MICROPOROSITY
Sealing micropores in thin castings
page 391 MSC-18623
MICROSTRUCTURE
Alined columnar microstructures
page 332 MFS-25205
MICROWAVE EQUIPMENT
Fast microwave switching power divider
page 268 GSC-12420
High-power solid-state microwave transmitter
page 269 NPO-14603
Portable zero-delay assembly
page 292 NPO-14671
MINIATURIZATION
Miniature personal UV solar dosimeter
page 300 LAR-12469
MINICOMPUTERS
Common data buffer
page 277 KSC-11048
MINORITY CARRIERS
Improving MOS minority-carrier lifetime
page 273 NPO-14738
MIST
Aerosol lasts up to six minutes
page 328 NPO-14947
MIXING
Quick mixing of epoxy components
page 379 MSC-18731
MOS [SEMICONDUCTORS]
Improving MOS minority-carrier lifetime
page 273 NPO-14738
MOUNTING
Compact table-tilting mechanism
page 376 NPO-14800
MULTICHANNEL COMMUNICATION
28-channel rotary transformer
page 273 NPO-14661
MULTIPLIERS
Four-quadrant CCD analog multiplier
page 279 LAR-12332
Monolithic four-quadrant multiplier
page 280 LAR-12330A
MULTIPROCESSING [COMPUTER]
Simultaneous disk storage and retrieval
page 278 KSC-11167
MUSCULAR STRENGTH
Manual for physical fitness
page 339 MSC-18915

NOISE REDUCTION
Noise suppression in forward-scattering optical instruments
page 303 LAR-12730
NONLINEAR SYSTEMS
Plastic deformation of engines and other nonlinear structures
page 363 MFS-23814
NOSE CONES
Cap protects aircraft nose cone
page 282 LAR-12367
NUTS [FASTENERS]
Wrench for smooth or damaged fasteners
page 380 MSC-18772

OPTICAL COMMUNICATIONS
Diplexer for laser-beam-communication heterodyne receiver
page 307 GSC-12589
OPTICAL EQUIPMENT
Noise suppression in forward-scattering optical instruments
page 303 LAR-12730
OPTICAL FILTERS
Acoustically-tuned optical filter
page 304 HQN-10924
OPTICAL TRACKING
Tracking falling objects
page 308 NPO-14813
OXIDATION RESISTANCE
Resin char oxidation retardant for composites
page 322 LEW-13275

PANELS
Testing panels in tension and flexure
page 349 MFS-25421
PARABOLIC BODIES
Offset paraboloidal solar concentrator
page 299 NPO-14846
PARAMETERIZATION
Determining manufacturing cost from product complexity
page 400 MFS-25371
PERMEABILITY
Reduced hydrogen permeability at high temperatures
page 331 LEW-13465
PHOTOGRAPHIC PROCESSING
Heat for film processing from solar energy
page 309 MFS-25444
PHOTOMETERS
Photometer used for response time measurement
page 283 MSC-18712
PHOTOVOLTAIC CONVERSION
Combined photovoltaic and thermal-storage module
page 305 NPO-14591
PHYSICAL FITNESS
Manual for physical fitness
page 339 MSC-18915
PHYSIOLOGICAL TESTS
Miniaturized physiological-data telemetry system
page 338 MSC-18804
PIERCING
Abrasive drill for resilient materials
page 368 LEW-13411
PILOT TRAINING
Rain, fog, and clouds for aircraft simulators
page 352 ARC-11156
PIPES [TUBES]
Method for shaping polyethylene tubing
page 388 MSC-18771
Reshaping tube ends for welding
page 373 MSC-18462
PLASTIC DEFORMATION
Plastic deformation of engines and other nonlinear structures
page 363 MFS-23814
POLARIZED ELECTROMAGNETIC RADIATION
Antenna feed for circular/linear polarization
page 270 NPO-14610
Receiving signals of any polarization
page 291 NPO-14836
POLLUTION MONITORING
Simultaneous measurement of three atmospheric pollutants
page 327 NPO-14828
POLYCARBONATES
Cap protects aircraft nose cone
page 282 LAR-12367
POLYETHYLENES
Method for shaping polyethylene tubing
page 388 MSC-18771
POLYIMIDES
Aluminum ions enhance polyimide adhesive
page 326 LAR-12640
A new family of fire-resistant foams
page 384 MSC-16921
Electrically-conductive palladium-containing polyimide films
page 325 LAR-12629
Modified fire-resistant foams for seat cushions
page 385 MSC-18704
One-step microwave foaming and curing
page 386 MSC-18707
Rigid fire-resistant foams for walls and floors
page 386 MSC-18708
POLYMER CHEMISTRY
Heat-resistant polymers
page 319 ARC-11176
POWER CONDITIONING
Fast microwave switching power divider
page 268 GSC-12420
POWER SUPPLY CIRCUITS
Efficient, lightweight dc/dc switching converter
page 271 LEW-12609
PREFORMS
Hot forming graphite/polyimide structures
page 387 LAR-12547
PRODUCTION MANAGEMENT
Determining manufacturing cost from product complexity
page 400 MFS-25371
PROTECTIVE COATINGS
Film coatings for contoured surfaces
page 389 MSC-18784
Improved metallic and thermal-barrier coatings
page 321 LEW-13324
Low-cost, high-temperature, duplex coating for superalloys
page 321 LEW-13497
PULSE GENERATORS
Ultrasonic frequency analysis
page 348 LAR-12697

PUMPS
Dynamics of cavitating cascades
page 359 MFS-25399
PURIFICATION
Treating domestic wastewater with water hyacinths
page 336 MFS-23964

RADIATION MEASUREMENT
Miniature personal UV solar dosimeter
page 300 LAR-12469
Economical ultraviolet radiometer
page 301 NPO-14843
READOUT
Monolithic CCD-array readout
page 282 LAR-12376
RECEIVERS
Arrayed receivers for low-rate telemetry
page 285 NPO-14590
Receiver array for high-rate telemetry
page 284 NPO-14579
Receiving signals of any polarization
page 291 NPO-14836
RECLAMATION
Decomposition of waste tires through chlorinolysis
page 331 NPO-14935
REDUNDANCY
Toggled signal for prevention of control errors
page 288 MSC-18779
REMOTE HANDLING
Remote manipulator with force feedback
page 373 ARC-11272
RESILIENCE
Abrasive drill for resilient materials
page 368 LEW-13411
RESPONSE TIME [COMPUTERS]
Photometer used for response time measurement
page 293 MSC-18712
ROTATING SHAFTS
28-channel rotary transformer
page 273 NPO-14861
RUBBER
Decomposition of waste tires through chlorinolysis
page 331 NPO-14935
RUNNING
Manual for physical fitness
page 339 MSC-18915

SANDWICH STRUCTURES
Lightweight terminal board
page 392 MSC-18787
SCRUBBERS
Carbon scrubber
page 324 MSC-16531
SEALING
Heat/pressure seal for moving parts
page 358 MSC-18422
Sealing micropores in thin castings
page 391 MSC-18623
Translator package for high-pressure applications
page 392 MSC-18743
SENSORY FEEDBACK
Remote manipulator with force feedback
page 373 ARC-11272
SIMULATION
CADAT field-effect-transistor simulator
page 395 MFS-25067
CADAT logic simulation program
page 394 MFS-25183
SIZE DETERMINATION
Resizing structures for minimum weight
page 361 LAR-12699
SLEEVES
Alining sleeve for optical fibers
page 389 MSC-18756
SOLAR ENERGY
A high school is supplied with solar energy — Dallas, Texas
page 316 MFS-25514
Commercial-building solar-energy system — Stamford, Connecticut
page 310 MFS-25468
Costs and description of a solar-energy system — Austin, Texas
page 312 MFS-25472
Data-acquisition and control system for severe environments
page 310 MFS-25471
Four-cell solar tracker
page 298 NPO-14811
Heat for film processing from solar energy
page 309 MFS-25444
Miniature personal UV solar dosimeter
page 300 LAR-12469
Municipal recreation center is heated and cooled by solar energy — Dallas, Texas
page 312 MFS-25478
Multiplexed logic controls solar-heating system
page 297 MFS-25287
Offset paraboloidal solar concentrator
page 299 NPO-14846
Residential solar-heating installation — Stillwater, Minnesota
page 315 MFS-25504
Residential solar hot-water system — Tempe, Arizona
page 315 MFS-25490
Residential system tested in an office — Huntsville, Alabama
page 314 MFS-25481
Solar energy in a historical city — Abbeville, South Carolina
page 312 MFS-25479
Solar energy meets 50 percent of motel hot-water needs — Key West, Florida
page 313 MFS-25454
Solar-energy workshop — Tucson, Arizona
page 314 MFS-25473
Solar-heated and cooled office building — Dalton, Georgia
page 310 MFS-25451
Solar-heated office complex — Greenwood, South Carolina
page 313 MFS-25458
Solar-heated two-level residence — Akron, Ohio
page 314 MFS-25480
Solar heater/cooler for mass market
page 309 MFS-25452
Solar-heating and hot-water system — St. Louis, Missouri
page 311 MFS-25453
Solar heating for an electronics manufacturing plant — Blue Earth, Minnesota
page 311 MFS-25469
Solar-powered aircraft
page 370 LAR-12615
Three-story residence with solar heat — Manchester, New Hampshire
page 315 MFS-25499
SPECTROMETERS
Acoustically-tuned optical filter
page 304 HQN-10924
Integrated material-surface analyzer
page 356 NPO-14702
SPRAYED COATINGS
Film coatings for contoured surfaces
page 389 MSC-18784
SPRAYING
Spraying suspensions uniformly
page 374 MFS-25139
SPRINGS [ELASTIC]
Interchangeable spring modules for inertia measurements
page 355 LAR-12402
STRAIN DISTRIBUTION
NASTRAN modifications for recovering strains and curvatures
page 361 LEW-12592
STRAIN GAGES
Signal conditioner for nickel temperature sensors
page 270 MSC-18367
STRUCTURAL ANALYSIS
NASTRAN modifications for recovering strains and curvatures
page 361 LEW-12592
Plastic deformation of engines and other nonlinear structures
page 363 MFS-23814
Resizing structures for minimum weight
page 361 LAR-12699
SUPPORTS
Compact table-tilting mechanism
page 376 NPO-14800
Versatile, safe scaffolds
page 372 GSC-12606
SURFACE PROPERTIES
Integrated material-surface analyzer
page 356 NPO-14702
SURGICAL INSTRUMENTS
Improved ureteral stone fragmentation cathether
page 337 NPO-14745
SUSPENDING [MIXING]
Spraying suspensions uniformly
page 374 MFS-25139
SWITCHES
Compact, reliable heat switch
page 358 GSC-12625
Time-sharing switch for vacuum brazing
page 376 MSC-18600
SWIVELS
Ball-joint grounding ring
page 371 MSC-18824
SYNCHRONOUS SATELLITES
Predicting and monitoring duststorms
page 302 NPO-14277

TASK COMPLEXITY
Determining manufacturing cost from product complexity
page 400 MFS-25371
TELEMETRY
Arrayed receivers for low-rate telemetry
page 285 NPO-14590
Miniaturized physiological-data telemetry system
page 336 MSC-18804
Receiver array for high-rate telemetry
page 284 NPO-14579
Receiving signals of any polarization
page 291 NPO-14836
TELEVISION TRANSMISSION
Compressing TV-image data
page 286 NPO-14823
TEMPERATURE CONTROL
A high school is supplied with solar energy — Dallas, Texas
page 316 MFS-25514
Commercial-building solar-energy system — Stamford, Connecticut
page 310 MFS-25468
Compact, reliable heat switch
page 358 GSC-12625
Costs and description of a solar-energy system — Austin, Texas
page 312 MFS-25472
Data-acquisition and control system for severe environments
page 310 MFS-25471

Heat for film processing from solar energy
page 309 MFS-25444

Heat/pressure seal for moving parts
page 358 MSC-18422

Holes help control temperature
page 343 GSC-12616

Multiplexed logic controls solar-heating system
page 297 MFS-25287

Municipal recreation center is heated and cooled by solar energy — Dallas, Texas
page 312 MFS-25478

Residential solar-heating installation — Stillwater, Minnesota
page 315 MFS-25504

Residential solar hot-water system — Tempe, Arizona
page 315 MFS-25490

Residential system tested in an office — Huntsville, Alabama
page 314 MFS-25481

Solar energy in a historical city — Abbeville, South Carolina
page 312 MFS-25479

Solar energy meets 50 percent of motel hot-water needs — Key West, Florida
page 313 MFS-25454

Solar-energy workshop — Tucson, Arizona
page 314 MFS-25473

Solar-heated and cooled office building — Dalton, Georgia
page 310 MFS-25451

Solar-heated office complex — Greenwood, South Carolina
page 313 MFS-25456

Solar-heated two-level residence — Akron, Ohio
page 314 MFS-25480

Solar heater/cooler for mass market
page 309 MFS-25452

Solar-heating and hot-water system — St. Louis, Missouri
page 311 MFS-25453

Solar heating for an electronics manufacturing plant — Blue Earth, Minnesota
page 311 MFS-25469

Temperature controller adapts to fatigue tester
page 347 LAR-12393

Three-story residence with solar heat — Manchester, New Hampshire
page 315 MFS-25499

TEMPERATURE DISTRIBUTION
Simplified thermal analyzer
page 360 GSC-12636

TEMPERATURE GRADIENTS
Measuring the thermal conductivity of insulation
page 351 NPO-14871

TEMPERATURE SENSORS
Signal conditioner for nickel temperature sensors
page 270 MSC-18367

TENSILE TESTS
Testing panels in tension and flexure
page 349 MFS-25421

TEST FACILITIES
CADAT test pattern generator
page 394 MFS-25066

Environmental testing under load
page 348 LAR-12602

Testing panels in tension and flexure
page 349 MFS-25421

THERMAL CONDUCTIVITY
Measuring the thermal conductivity of insulation
page 351 NPO-14871

THERMAL CONTROL COATINGS
Improved metallic and thermal-barrier coatings
page 321 LEW-13324

THERMAL EXPANSION
Composites with nearly-zero thermal expansion
page 323 MSC-18724

THERMAL PROTECTION
Heat/pressure seal for moving parts
page 358 MSC-18422

THERMAL PROTECTION
Heat-resistant polymers
page 319 ARC-11176

THERMAL STRESSES
Simplified thermal analyzer
page 360 GSC-12636

THIN FILMS
Electrically-conductive palladium-containing polyimide films
page 325 LAR-12629

Film coatings for contoured surfaces
page 369 MSC-18784

TIME LAG
Portable zero-delay assembly
page 292 NPO-14671

TIME SHARING
Common data buffer
page 277 KSC-11048

Time-sharing switch for vacuum brazing
page 376 MSC-18600

TIRES
Decomposition of waste tires through chlorinolysis
page 331 NPO-14935

TOOLS
Boring tool for aramid fabricated-panels
page 391 MSC-18786

Drilling at right angles in blind holes
page 369 MFS-19536

Torque-wrench extension
page 379 MSC-18769

Wrench for smooth or damaged fasteners
page 380 MSC-18772

TORQUEMETERS
Torque-wrench extension
page 379 MSC-18769

TRACKING [POSITION]
Four-cell solar tracker
page 298 NPO-14811

TRAJECTORY OPTIMIZATION
Cost-minimized aircraft trajectories
page 362 ARC-11282

TRANSFORMERS
28-channel rotary transformer
page 273 NPO-14861

TRANSISTORS
Transistor package for high-pressure applications
page 392 MSC-18743

TRANSMITTERS
High-power solid-state microwave transmitter
page 289 NPO-14803

TRANSONIC FLOW
Inviscid transonic flow over axisymmetric bodies
page 363 LAR-12499

TURBINE BLADES
Analysis of a cooled turbine blade or vane with an insert
page 364 LEW-13293

TURBULENCE
Aerosol lasts up to six minutes
page 328 NPO-14947

TURBULENT WAKES
Wakeflow analysis by COST
page 355 NPO-14705

ULTRASONIC RADIATION
Acoustic lens is gas-filled
page 345 NPO-14757

Economical ultraviolet radiometer
page 301 NPO-14843

Miniature personal UV solar dosimeter
page 300 LAR-12469

Ultrasonic frequency analysis
page 346 LAR-12697

VACUUM APPARATUS
Kilovolt vacuum feedthrough is less noisy
page 390 NPO-14802

Time-sharing switch for vacuum brazing
page 376 MSC-18600

VACUUM TESTS
Integrated material-surface analyzer
page 356 NPO-14702

VAPOR DEPOSITION
Automatic chemical vapor deposition
page 393 MFS-25459

VOLTAGE CONVERTERS [DC to DC]
Efficient, lightweight dc/dc switching converter
page 271 LEW-12809

WAKES
Aerosol lasts up to six minutes
page 328 NPO-14947

WASTE UTILIZATION
Decomposition of waste tires through chlorinolysis
page 331 NPO-14935

WATER TREATMENT
Carbon scrubber
page 324 MSC-16531

WATER TREATMENT
Treating domestic wastewater with water hyacinths
page 336 MFS-23964

WEATHER FORECASTING
Airborne meteorological data-collection system
page 290 LEW-13346

Predicting and monitoring duststorms
page 302 NPO-14277

WEIGHT REDUCTION
Lightweight terminal board
page 392 MSC-18787

Resizing structures for minimum weight
page 361 LAR-12699

WELDING
Limiting current in electron-beam welders
page 377 MFS-19603

Reshaping tube ends for welding
page 373 MSC-18462

WIND TUNNEL MODELS
A construction technique for wind-tunnel models
page 350 LAR-12710

WRENCHES
Torque-wrench extension
page 379 MSC-18769

Wrench for smooth or damaged fasteners
Page 380 MSC-18772

National Aeronautics and
Space Administration

Washington, D.C.
20546

Official Business
Penalty for Private Use, $300

NO POSTAGE
NECESSARY
IF MAILED
IN THE
UNITED STATES

BUSINESS REPLY MAIL

FIRST CLASS PERMIT NO. 12028 WASHINGTON, D.C.

POSTAGE WILL BE PAID BY NASA

Director, Technology Transfer Division
P.O. Box 8757
Baltimore/Washington International Airport, MD 21240

NASA

National Aeronautics and
Space Administration

Washington, D.C.
20546

Official Business
Penalty for Private Use, $300

NO POSTAGE
NECESSARY
IF MAILED
IN THE
UNITED STATES

BUSINESS REPLY MAIL

FIRST CLASS PERMIT NO. 12028 WASHINGTON, D.C.

POSTAGE WILL BE PAID BY NASA

Director, Technology Transfer Division
P.O. Box 8757
Baltimore/Washington International Airport, MD 21240

NASA

National Aeronautics and
Space Administration

Washington, D.C.
20546

Official Business
Penalty for Private Use, $300

NO POSTAGE
NECESSARY
IF MAILED
IN THE
UNITED STATES

BUSINESS REPLY MAIL

FIRST CLASS PERMIT NO. 12028 WASHINGTON, D.C.

POSTAGE WILL BE PAID BY NASA

Director, Technology Transfer Division
P.O. Box 8757
Baltimore/Washington International Airport, MD 21240

NASA

TECH BRIEFS SUBSCRIPTIONS

☐ Please place me on the subscription list for NASA Tech Briefs (issued quarterly).
☐ I wish to change the delivery address for my current subscription.

FALL
1980

1. Please check any of the following that describe your organization:

☐ Federal Government
☐ State Government
☐ Municipal Government
☐ University/College
☐ Secondary School
☐ Trade/Vocational School
☐ Manufacturing
☐ Sales
☐ Research
☐ Consulting
☐ Medicine
☐ Professional Society
☐ News Media
☐ Information Sciences/Library

2. Please check the number of employees in your organization: ☐ Under 25 ☐ 25-100 ☐ 100-500 ☐ Over 500

3. Please indicate if your position is one of the following: ☐ Owner or Chief Executive Officer ☐ Administrator/Manager ☐ Scientist ☐ Engineer ☐ Other ____________

[PLEASE PRINT]

NAME ____________ TITLE ____________

COMPANY ____________ PHONE ____________
&
STREET ADDRESS ____________ CITY ____________ STATE ________ ZIP ________

TECH BRIEFS SUBSCRIPTIONS

☐ Please place me on the subscription list for NASA Tech Briefs (issued quarterly).
☐ I wish to change the delivery address for my current subscription.

FALL
1980

1. Please check any of the following that describe your organization:

☐ Federal Government
☐ State Government
☐ Municipal Government
☐ University/College
☐ Secondary School
☐ Trade/Vocational School
☐ Manufacturing
☐ Sales
☐ Research
☐ Consulting
☐ Medicine
☐ Professional Society
☐ News Media
☐ Information Sciences/Library

2. Please check the number of employees in your organization: ☐ Under 25 ☐ 25-100 ☐ 100-500 ☐ Over 500

3. Please indicate if your position is one of the following: ☐ Owner or Chief Executive Officer ☐ Administrator/Manager ☐ Scientist ☐ Engineer ☐ Other ____________

[PLEASE PRINT]

NAME ____________ TITLE ____________

COMPANY ____________ PHONE ____________
&
STREET ADDRESS ____________ CITY ____________ STATE ________ ZIP ________

FEEDBACK — YOUR COMMENTS

WE NEED YOUR HELP!

FALL
1980

Our ultimate goal is to provide you with solutions to your day-to-day technical problems. Are we meeting that goal? Tell us how Tech Briefs has helped you, or how it can be made more useful. We are especially interested in brief descriptions of specific instances where Tech Briefs has either helped you solve a problem or been applied to your product line.

If you need more space, write us a letter at the address on the front of this card.

[PLEASE PRINT]

NAME ____________ TITLE ____________

COMPANY ____________ PHONE ____________
&
STREET ADDRESS ____________ CITY ____________ STATE ________ ZIP ________

TSP REQUESTS

Please send me the Technical Support Package (TSP)
for the Tech Brief articles circled below:

FALL
1980

☐ I would like information about NASA's Industrial Applications Centers and other NASA TU services.

I am requesting these TSP's for:

☐ Current Awareness
☐ Product Development
☐ Other ______
☐ Process Improvement
☐ Problem Solving

Approximately how many TSP's have you requested from NASA in the last five years?

☐ 0 to 10 ☐ 11 to 25 ☐ over 25

[PLEASE PRINT]

NAME ______

TITLE ______

COMPANY & STREET ADDRESS ______ PHONE ______

CITY ______ STATE ______ ZIP ______

1	2	3	4	5	6	7	8	9	10	11	12	13	14	15	16
17	18	19	20	21	22	23	24	25	26	27	28	29	30	31	32
33	34	35	36	37	38	39	40	41	42	43	44	45	46	47	48
49	50	51	52	53	54	55	56	57	58	59	60	61	62	63	64
65	66	67	68	69	70	71	72	73	74	75	76	77	78	79	80
81	82	83	84	85	86	87	88	89	90	91	92				

TSP REQUESTS

Please send me the Technical Support Package (TSP)
for the Tech Brief articles circled below:

FALL
1980

☐ I would like information about NASA's Industrial Applications Centers and other NASA TU services.

I am requesting these TSP's for:

☐ Current Awareness
☐ Product Development
☐ Other ______
☐ Process Improvement
☐ Problem Solving

Approximately how many TSP's have you requested from NASA in the last five years?

☐ 0 to 10 ☐ 11 to 25 ☐ over 25

[PLEASE PRINT]

NAME ______

TITLE ______

COMPANY & STREET ADDRESS ______ PHONE ______

CITY ______ STATE ______ ZIP ______

1	2	3	4	5	6	7	8	9	10	11	12	13	14	15	16
17	18	19	20	21	22	23	24	25	26	27	28	29	30	31	32
33	34	35	36	37	38	39	40	41	42	43	44	45	46	47	48
49	50	51	52	53	54	55	56	57	58	59	60	61	62	63	64
65	66	67	68	69	70	71	72	73	74	75	76	77	78	79	80
81	82	83	84	85	86	87	88	89	90	91	92				

COSMIC REQUESTS

FALL
1980

I would like price and availability information about the computer program(s) circled below:

A B C D E F G H J K L M N P

Please send me further information about software and services available from COSMIC. I am particularly interested in programs in the following areas: ______

[PLEASE PRINT]

NAME ______ TITLE ______

COMPANY & STREET ADDRESS ______ PHONE ______

CITY ______ STATE ______ ZIP ______

National Aeronautics and
Space Administration

Washington, D.C.
20546

Official Business
Penalty for Private Use $300

NO POSTAGE
NECESSARY
IF MAILED
IN THE
UNITED STATES

BUSINESS REPLY MAIL

FIRST CLASS PERMIT NO. 12028 WASHINGTON, D.C.

POSTAGE WILL BE PAID BY NASA

Director, Technology Transfer Division
P.O. Box 8757
Baltimore/Washington International Airport, MD 21240

NASA

National Aeronautics and
Space Administration

Washington, D.C.
20546

Official Business
Penalty for Private Use $300

NO POSTAGE
NECESSARY
IF MAILED
IN THE
UNITED STATES

BUSINESS REPLY MAIL

FIRST CLASS PERMIT NO. 12028 WASHINGTON, D.C.

POSTAGE WILL BE PAID BY NASA

Director, Technology Transfer Division
P.O. Box 8757
Baltimore/Washington International Airport, MD 21240

NASA

National Aeronautics and
Space Administration

Washington, D.C.
20546

Official Business
Penalty for Private Use $300

NO POSTAGE
NECESSARY
IF MAILED
IN THE
UNITED STATES

BUSINESS REPLY MAIL

FIRST CLASS PERMIT NO. 12028 WASHINGTON, D.C.

POSTAGE WILL BE PAID BY NASA

COSMIC
Computer Software Management and Information Center
Suite 112, Barrow Hall
Athens, GA 30602

NASA

National Aeronautics and
Space Administration

Washington, D.C.
20546

Official Business
Penalty for Private Use $300

THIRD-CLASS BULK

THIRD-CLASS BULK RATE
POSTAGE & FEES PAID
NASA
WASHINGTON, D.C.
PERMIT No. P-154

New sound-absorbing products, such as the noise-blocking green wall in this light-socket manufacturing facility, are an outgrowth of an early NASA search for better vibration-absorbing encapsulants for spacecraft electronics. Based on a unique liquid plastic compound, the products could reduce noise in a variety of industrial and nonindustrial applications. [See the bottom of page A1.]

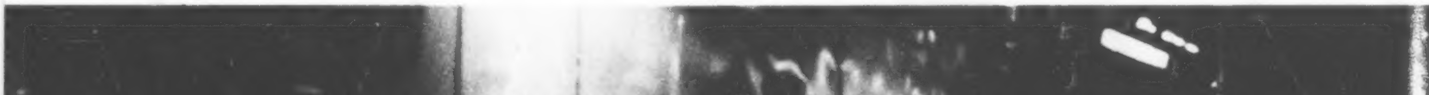

5/4

NASA Tech Briefs

National
Aeronautics and
Space
Administration

This fireplace-installed wood-burning heater is one of several commercial products protected by a coating originally developed for spacecraft. By reflecting rather than absorbing radiant energy, the coating keeps surfaces cool — even the metal surfaces exposed to 1,800° F in the wood burner. [See the bottom of page A1.]

Vol. 5, No. 4

Winter 1980

NAS 1.29/3:

About the NASA Technology Utilization Program

The National Aeronautics and Space Act of 1958, which established NASA and the United States civilian space program, requires that "The Administration shall provide for the widest practicable and appropriate dissemination of information concerning its activities and the results thereof."

To help carry out this objective, NASA's Technology Utilization (TU) Program was established in 1962. Now, as an element of NASA's Technology Transfer Division, this program offers a variety of valuable services to help transfer aerospace technology to nonaerospace applications, thus assuring American taxpayers maximum return on their investment in space research; thousands of spinoffs of NASA research have already occurred in virtually every area of our economy.

The TU program has worked for engineers, scientists, technicians, and businessmen; and it can work for you.

NASA Tech Briefs

Tech Briefs is published quarterly and is free to engineers in U.S. industry and to other domestic technology transfer agents. It is both a current-awareness medium and a problem-solving tool. Potential products . . . industrial processes . . . basic and applied research . . . shop and lab techniques . . . computer software . . . new sources of technical data . . . concepts . . . can be found here. The short section on New Product Ideas highlights a few of the potential new products contained in this issue. The remainder of the volume is organized by technical category to help you quickly review new developments in your areas of interest. Finally, a subject index makes each issue a convenient reference file.

Further Information on Innovations

Although some new technology announcements are complete in themselves, most are backed up by Technical Support Packages (TSP's). TSP's are available without charge and may be ordered by simply completing a TSP Request Card found at the back of this volume. Further information on some innovations is available for a nominal fee from other sources, as indicated. In addition, Technology Utilization Officers at NASA Field Centers will often be able to lend necessary guidance and assistance.

Patent Licenses

Patents have been issued to NASA on some of the inventions described, and patent applications have been submitted on others. Each announcement indicates patent status, if applicable.

Other Technology Utilization Services

To assist engineers, industrial researchers, business executives, city officials, and other potential users in applying space technology to their problems, NASA sponsors Industrial Applications Centers. Their services are described on page A7. In addition, an extensive library of computer programs is available through COSMIC, the Technology Utilization Program's outlet for NASA-developed software.

Applications Program

NASA conducts applications engineering projects to help solve public-sector problems in such areas as safety, health, transportation, and environmental protection. Applications teams, staffed by professionals from a variety of disciplines, assist in this effort by working with Federal agencies and health organizations to identify critical problems amenable to solution by the application of existing NASA technology.

Reader Feedback

We hope you find the information in *NASA Tech Briefs* useful. A reader-feedback card has been included because we want your comments and suggestions on how we can further help you apply NASA innovations and technology to your needs. Please use it; or if you need more space, write to the Director, Technology Transfer Division, P. O. Box 8757, Baltimore/Washington International Airport, Maryland 21240.

NASA Tech Briefs

National
Aeronautics and
Space
Administration

WINTER 1980
Volume 5, Number 4

NASA TU Services A3 Technology Utilization services that can assist you in learning about and applying NASA technology.

New Product Ideas A9 A summary of selected innovations of value to manufacturers for the development of new products.

Tech Briefs

409 Electronic Components and Circuits

417 Electronic Systems

425 Physical Sciences

445 Materials

455 Life Sciences

465 Mechanics

483 Machinery

493 Fabrication Technology

509 Mathematics and Information Sciences

Subject Index 515 Items in this issue are indexed by subject; a cumulative index will be published yearly.

COVERS: To find out more about the Reflecting Coating, Circle 79 on the TSP Request Card at the back of this issue of NASA Tech Briefs. Information on the Pipe Flexibility and Analysis Program [MEL-21] may be obtained from COSMIC [see page A8] by Circling R on the COSMIC Request Card.

About This NASA Publication

NASA Tech Briefs, a quarterly publication, is distributed free to qualified U.S. citizens to encourage commercial application of U.S. space technology. For information on publications and services available through the NASA Technology Utilization Program, write to the Director, Technology Transfer Division, P. O. Box 8757, Baltimore/Washington International Airport, Maryland 21240.

"The Administrator of National Aeronautics and Space Administration has determined that the publication of this periodical is necessary in the transaction of the public business required by law of this Agency. Use of funds for printing this periodical has been approved by the Director of the Office of Management and Budget."

Change of Address

If you wish to have NASA Tech Briefs forwarded to your new address, use one of the Subscriptions cards enclosed in the back of this volume of NASA Tech Briefs. Be sure to check the appropriate box indicating change of address.

Communications Concerning Editorial Matter

For editorial comments or general communications about NASA Tech Briefs, you may use the Feedback card in the back of NASA Tech Briefs, or write to: The Publications Manager, Technology Transfer Division (ETD-6), NASA Headquarters, Washington, DC 20546. Technical questions concerning specific articles should be directed to the Technology Utilization Officer of the sponsoring NASA Center (addresses listed on page A4).

Acknowledgements

NASA Tech Briefs is published quarterly by the National Aeronautics and Space Administration, Technology Utilization Branch, Washington, DC: Administrator: **Robert A. Frosch**; Director, Technology Transfer Division: **Floyd I. Roberson**; Publications Manager: **D. W. Orrick**. Prepared for the National Aeronautics and Space Administration by **Logical Technical Services Corp.**: Editor-in-Chief: **Jay Kirschenbaum**; Art Director: **Ernest Gillespie**; Senior Editor: **Jerome Rosen**; Chief Copy Editor: **Oden Browne**; Staff Editors: **Donald Blattner, Larry Grunberger, Ted Selinsky, George Watson**; Graphics: **Concetto Auditore, Conrad Carlock, Luis Martinez, Janet McCrie**; Editorial & Production: **Richard Johnson, Jeanne Bonner, Rose Giglietti, Marena Gutman, Kathi Norklun, Vincent Susinno, John Tucker, Ernestine Walker.**

This document was prepared under the sponsorship of the National Aeronautics and Space Administration.. Neither the United States Government nor any person acting on behalf of the United States Government assumes any liability resulting from the use of the information contained in this document, or warrants that such use will be free from privately owned rights.

NASA
TU SERVICES

NASA TECHNOLOGY UTILIZATION NETWORK

★ TECHNOLOGY UTILIZATION OFFICERS

Ben Padrick
Ames Research Center
Code AU: 240-2
Moffett Field, CA 94035
(415) 965-5151

Gussie Anderson
Hugh L. Dryden Flight Research Center
Code OD/TU Office - Room 2015
Post Office Box 273
Edwards, CA 93523
(805) 258-3311, Ext. 787

Donald S. Friedman
Goddard Space Flight Center
Code 702.1
Greenbelt, MD 20771
(301) 344-6242

John T. Wheeler
Lyndon B. Johnson Space Center
Code AT-3
Houston, TX 77058
(713) 483-3809

U. Reed Barnett
John F. Kennedy Space Center
Code PT-SPD
Kennedy Space Center, FL 32899
(305) 867-2780

John Samos
Langley Research Center
Mail Stop 139A
Hampton, VA 23665
(804) 827-3281

Harrison Allen, Jr.
Lewis Research Center
Mail Code 7-3
21000 Brookpark Road
Cleveland, OH 44135
(216) 433-4000, Ext. 6422

Aubrey D. Smith
George C. Marshall Space Flight Center
Code AT01
Marshall Space Flight Center, AL 35812
(205) 453-2224

D. W. Orrick
NASA Headquarters
Code ETD-6
Washington, DC 20546
(202) 755-2244

John H. Warden
NASA Resident Office-JPL
4800 Oak Grove Drive
Pasadena, CA 91103
(213) 354-6420

Gilmore H. Trafford
Wallops Flight Center
Code OD
Wallops Island, VA 23337
(804) 824-3411, Ext. 201

● INDUSTRIAL APPLICATIONS CENTERS

Aerospace Research Applications Center
1201 East 38th Street
Indianapolis, IN 46205
John M. Ulrich, director
(317) 264-4644

Computer Software Management and Information Center (COSMIC)
Suite 112, Barrow Hall
University of Georgia
Athens, GA 30602
Harold G. Hale, Jr., director
(404) 542-3265

Kerr Industrial Applications Center
Southeastern Oklahoma State University
Durant, OK 74701
Robert Oliver, director
(405) 924-0121, Ext. 413

NASA Industrial Applications Center
701 LIS Building
University of Pittsburgh
Pittsburgh, PA 15260
Paul A. McWilliams, executive director
(412) 624-5211

New England Research Applications Center
Mansfield Professional Park
Storrs, CT 06268
Daniel Wilde, director
(203) 486-4533

North Carolina Science and Technology Research Center
Post Office Box 12235
Research Triangle Park, NC 27709
Peter J. Chenery, director
(919) 549-0671

Technology Applications Center
University of New Mexico
Albuquerque, NM 87131
Stanley Morain, director
(505) 277-3622

NASA Industrial Applications Center
University of Southern California
Denny Research Building
University Park
Los Angeles, CA 90007
Robert Mixer, acting director
(213) 743-6132

■ STATE TECHNOLOGY APPLICATIONS CENTERS

NASA/University of Florida
State Technology Applications Center
311 Weil Hall
University of Florida
Gainesville, FL 32611
Ronald J. Thornton, director
Gainesville: (904) 392-6760
Orlando: (305) 275-2706
Tampa: (813) 974-2499

NASA/University of Kentucky
State Technology Applications Program
109 Kinkead Hall
University of Kentucky
Lexington, KY 40506
William R. Strong, manager
(606) 258-4632

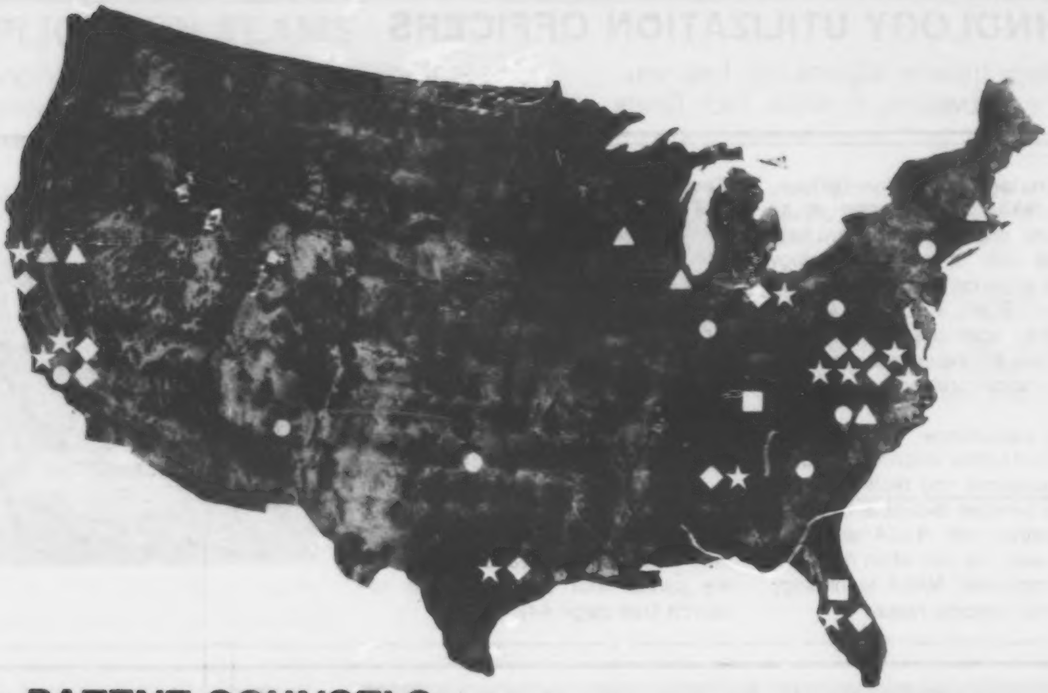

◆ PATENT COUNSELS

Robert F. Kempf
Asst. Gen. Counsel for patent matters
NASA Headquarters
Code GP-4
400 Maryland Avenue, SW.
Washington, DC 20546
(202) 755-3954

Darrell G. Brekke
Ames Research Center
Mail Code: 200-11A
Moffett Field, CA 94035
(415) 965-5104

Paul F. McCaul
Hugh L. Dryden Flight Research Center
Code OD/TU Office - Room 2015
Post Office Box 273
Edwards, CA 93523
(213) 354-2734

John O. Tresansky
Goddard Space Flight Center
Mail Code: 204
Greenbelt, MD 20771
(301) 344-7351

Marvin F. Matthews
Lyndon B. Johnson Space Center
Mail Code: AM
Houston, TX 77058
(713) 483-4871

James O. Harrell
John F. Kennedy Space Center
Mail Code: SA-PAT
Kennedy Space Center, FL 32899
(305) 867-2544

Howard J. Osborn
Langley Research Center
Mail Code: 279
Hampton, VA 23665
(804) 827-3725

Norman T. Musial
Lewis Research Center
Mail Code: 500-311
21000 Brookpark Road
Cleveland, OH 44135
(216) 433-4000, Ext. 346

Leon D. Wofford, Jr.
George C. Marshall Space Flight Center
Mail Code: CC01
Marshall Space Flight Center, AL 35812
(205) 453-0020

Monte F. Mott
NASA Resident Office-JPL
Mail Code: 180-601
4800 Oak Grove Drive
Pasadena, CA 91103
(213) 354-2700

▲ APPLICATION TEAMS

William N. Fetzner, director
Advisory Center for Medical Technology and Systems
University of Wisconsin
1500 Johnson Drive
Madison, WI 53706
(608) 263-2735

Edmund R. Bangs, director
IIT Research Institute
10 West 35th Street
Chicago, IL 60616
(312) 567-4191

Doris Rouse, director
Research Triangle Institute
Post Office Box 12194
Research Triangle Park, NC 27709
(919) 541-6256

Tom Anyos, director
SRI International
333 Ravenswood Avenue
Menlo Park, CA 94026
(415) 326-6200, Ext. 2864

Eugene Schmidt, program coordinator
Stanford University School of Medicine
Cardiology Division
Biomedical Technology Transfer
703 Welch Road, Suite E-4
Palo Alto, CA 94304
(415) 497-5353

David MacFadyen, project director
Technology + Economics
2225 Massachusetts Avenue
Cambridge, MA 02140
(617) 491-1500

TECHNOLOGY UTILIZATION OFFICERS

Technology transfer experts can help you apply the innovations in NASA Tech Briefs.

The Technology Utilization Officer at each NASA Field Center is an applications engineer who can help you make use of new technology developed at his center. He brings you NASA Tech Briefs and other special publications, sponsors conferences, and arranges for expert assistance in solving technical problems.

Technical assistance, in the form of further information about NASA innovations and technology, is one of the services available from the TUO. Together with NASA scientists and engineers, he can often help you find and implement NASA technology to meet your specific needs.

Technical Support Packages (TSP's) are prepared by the center TUO's. They provide further technical details for articles in NASA Tech Briefs. This additional material can help you evaluate and use NASA technology. You may receive most TSP's free of charge by using the TSP Request Card found at the back of this issue.

Technical questions about articles *in NASA Tech Briefs are answered in the TSP's. When no TSP is available, or you have further questions, contact the Technology Utilization Officer at the center that sponsored the research [see page A4].*

NASA INVENTIONS AVAILABLE FOR LICENSING

Over 3,500 NASA inventions are available for licensing in the United States — both exclusive and nonexclusive.

Nonexclusive licenses for commercial use of NASA inventions are encouraged to promote competition and to achieve the widest use of inventions. They must be used by a negotiated target date but are usually royalty-free.

Exclusive licenses may be granted to encourage early commercial development of NASA inventions, especially when considerable private investment is required. These are generally for 5 to 10 years and usually require royalties based on sales or use.

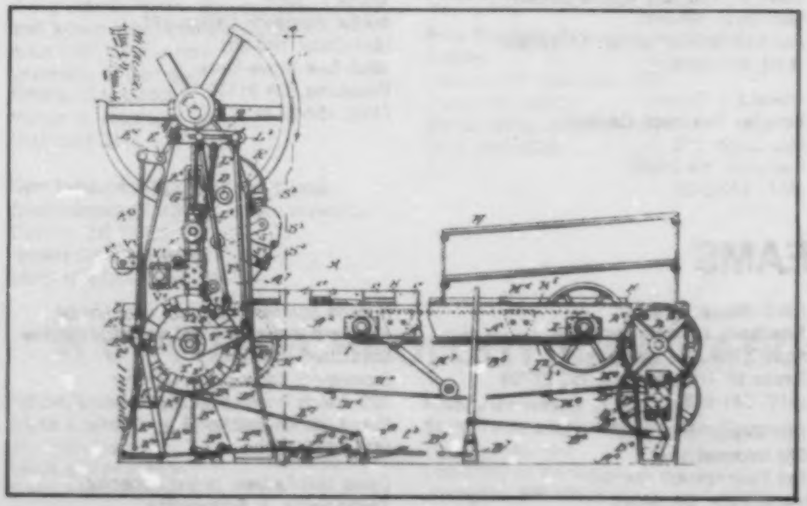

Additional licenses available include those of NASA-owned foreign patents. In addition to inventions described in NASA Tech Briefs, *"NASA Patent Abstract Bibliography"* (PAB), containing abstracts of all NASA inventions, can be purchased from National Technical Information Service, Springfield, VA 22161. The PAB is updated semiannually.

Patent licenses for Tech Briefs *are frequently available. Many of the inventions reported in NASA Tech Briefs are patented or are under consideration for a patent at the time they are published. The current patent status is described at the end of the article; otherwise, there is no statement about patents. If you want to know more about the patent program or are interested in licensing a particular invention, contact the Patent Counsel at the NASA Field Center that sponsored the research [see page A5]. Be sure to refer to the NASA reference number at the end of the Tech Brief.*

APPLICATION TEAMS

Technology-matching and problem-solving assistance to public-sector organizations

Application engineering projects are conducted by NASA to help solve public-sector problems in such areas as safety, health, transportation, and environmental protection. Some application teams specialize in biomedical disciplines; others, in engineering and scientific problems. Staffed by professionals from various disciplines, these teams work with other Federal agencies and health organizations to identify critical problems amenable to solution by the application of existing NASA technology.

Public-sector organization *representatives can learn more about application teams by contacting a nearby NASA Field Center Technology Utilization Office* [*see page A4*].

INDUSTRIAL APPLICATIONS CENTERS

Computerized access to nearly 10 million documents worldwide

Computerized information retrieval from one of the world's largest banks of technical data is available from NASA's network of Industrial Applications Centers (IAC's). The IAC's give you access to 1,800,000 technical reports in the NASA data base and to more than 10 times that many reports and articles found in 140 other computerized data bases.

The major sources include:

- *750,000 NASA Technical Reports*
- *Selected Water Resources Abstracts*
- *NASA Scientific and Technical Aerospace Reports*
- *Air Pollution Technical Information Center*
- *NASA International Aerospace Abstracts*
- *Chem Abstracts Condensates*
- *Engineering Index*
- *Energy Research Abstracts*
- *NASA Tech Briefs*
- *Government Reports Announcements*

and many other specialized files on food technology, textile technology, metallurgy, medicine, business, economics, social sciences, and physical science.

The IAC services range from tailored literature searches through expert technical assistance:

- *Retrospective Searches:* Published or unpublished literature is screened, and documents are identified according to your interest profile. IAC engineers tailor results to your specific needs and furnish abstracts considered the most pertinent. Complete reports are available upon request.
- *Current-Awareness Searches:* IAC engineers will help design a program to suit your needs. You will receive selected monthly or quarterly abstracts on new developments in your area of interest.
- *Technical Assistance:* IAC engineers will help you evaluate the results of your literature searches. They can help find answers to your technical problems and put you in touch with scientists and engineers at appropriate NASA Field Centers.

Prospective clients *can obtain more information about the services offered by NASA IAC's by contacting the nearest IAC [see page A4] or by checking the IAC box on a TSP Request Card in this issue.*

STATE TECHNOLOGY APPLICATIONS CENTERS

Technical information services for industry
and state and local government agencies

Local government and industry in Florida and Kentucky can utilize the services of NASA's State Technology Applications Centers (STAC's). The STAC's differ from the Industrial Applications Centers described on page A7, primarily in that they are integrated into existing state technical assistance programs and serve only the host state, whereas the IAC's serve multistate regions.

Many data bases, including the NASA base and several commercial bases, are available for automatic data retrieval through the STAC's. Other services such as document retrieval and special searches are also provided. (The STAC's normally charge a fee for their services.)

To obtain information *about the services offered by NASA STAC's, write or call the STAC in your state [see page A4].*

COSMIC®

An economical source of computer programs
developed by NASA and other government agencies

A vast software library is maintained by COSMIC — the Computer Software Management and Information Center. COSMIC gives you access to approximately 1,600 computer programs developed for NASA and the Department of Defense and selected programs for other government agencies. Programs and documentation are available at reasonable cost.

Available programs range from management (PERT scheduling) to information science (retrieval systems) and computer operations (hardware and software). Hundreds of engineering programs perform such tasks as structural analysis, electronic circuit design, chemical analysis, and the design of fluid systems. Others determine building energy requirements and optimize mineral exploration.

COSMIC services go beyond the collection and storage of software packages. Programs are checked for completeness; special announcements and an indexed software catalog are prepared; and programs are reproduced for distribution. Customers are helped to identify their software needs; and COSMIC follows up to determine the successes and problems and to provide updates and error corrections. In some cases, NASA engineers can offer guidance to users in installing or running a program.

Information about programs *described in NASA Tech Briefs articles can be obtained by completing the COSMIC Request Card at the back of this issue. Just circle the letters that correspond to the programs in which you are interested.*

NEW PRODUCT IDEAS

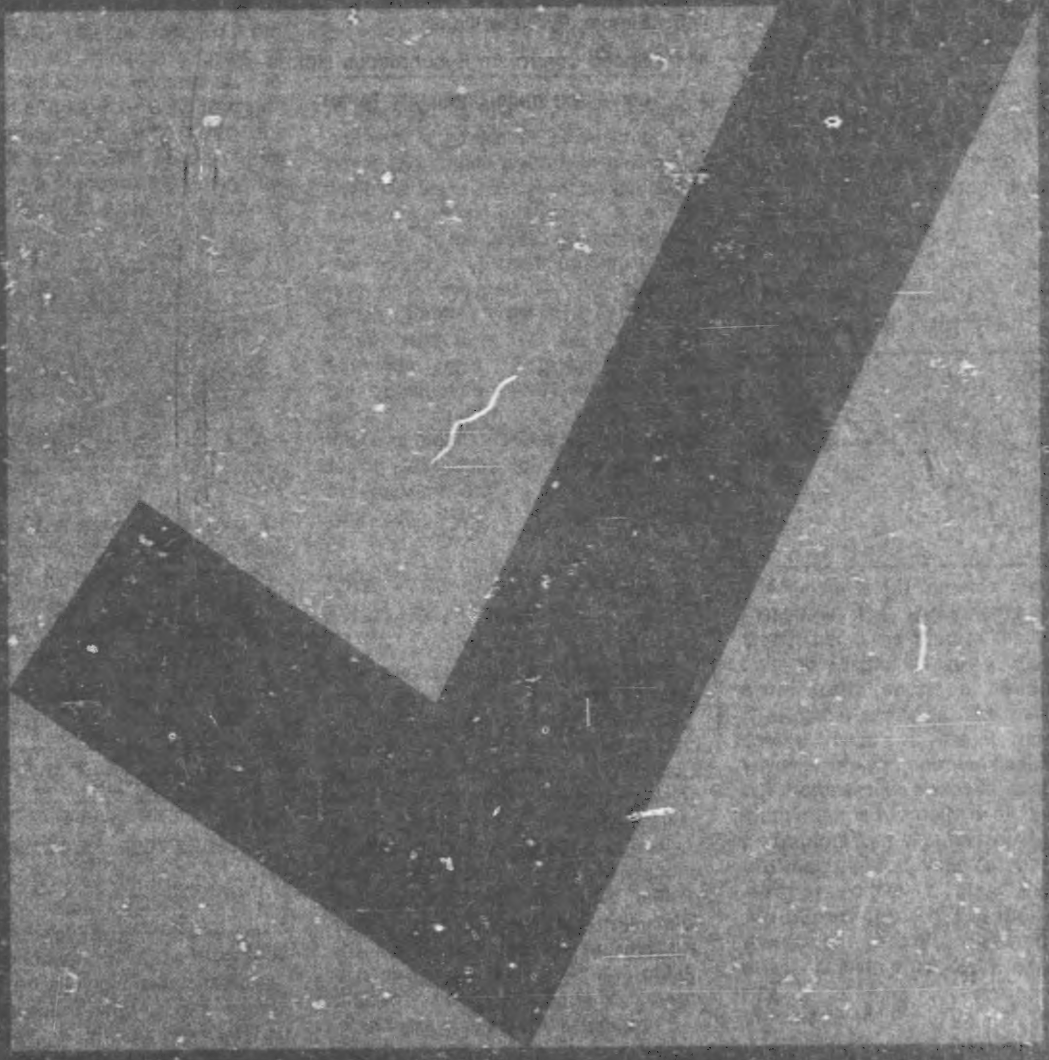

Hardware, Techniques, and Processes

411 Improved Battery Charger for Electric Vehicles
412 Multijunction High-Voltage Solar Cell
413 Solar Cell Is Housed in Light-Bulb Enclosure
413 Simple JFET Oscillator
414 Speed Control for Synchronous Motors
415 Low-Resistance Continuity Tester

of glass-filled material. Successive turns of the strip are spirally wrapped in a groove machined into one of the flange surfaces. Closing the joint compresses the gasket.
(See page 502.)

Pneumatic-Power Supply

A new portable compressed-air supply has two or more outputs at pressures that can be adjusted from 20 to 100 psi. It can be used to operate production equipment, to spray paint and lubricants, to pressurize refrigeration systems, and for other applications. The supply filters the air from a standard high-pressure line, reduces it to working pressure, and adds a lubricant if required. An accurate regulator supplies the low-pressure air to the output channels. On the channel lines, vernier-control valves select the output pressures.
(See page 486.)

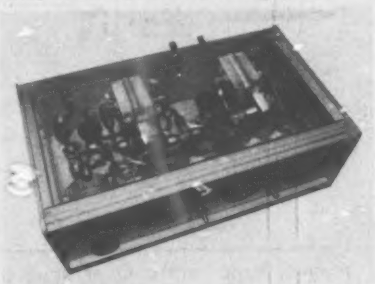

Multijunction High-Voltage Solar Cell

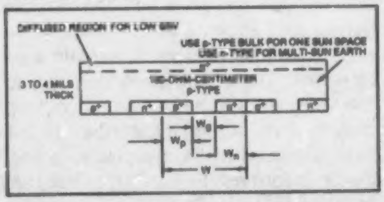
DIFFUSED REGION FOR LOW SRV
USE p-TYPE BULK FOR ONE SUN SPACE
USE n-TYPE FOR MULTI-SUN EARTH
3 TO 4 MILS THICK
100-OHM-CENTIMETER p-TYPE
W_g
W_p
W_n
W

The fabrication of a high-voltage solar cell on a single semiconductor wafer is possible with a new multijunction cell. A photovoltaic energy source using the new cell could be combined on a wafer with the circuit it is to power. For example, a computer module could be built on a silicon wafer with the energy for the internal information processing, and even readouts, derived from an external light source. The new cell consists of many voltage-generating regions that are interconnected internally or externally to give the desired voltage-and-current combination.
(See page 412.)

Gas-Laser Power Monitor

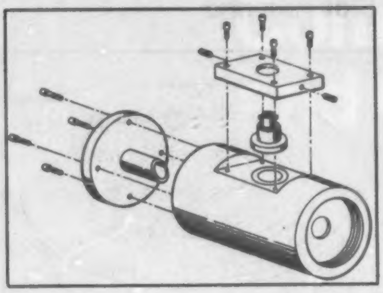

Attached to the front of a laser housing, a gas-laser power monitor reads the power output continuously while the laser is in use. It is calibrated to read either the total power output of the laser or the power generated in a test volume. No modifications to the laser are required — the monitor simply attaches to the laser end cap. It is fabricated from four black-anodized aluminum parts. A piece of crown glass positioned at the Brewster angle reflects a small fraction of the beam into a photodiode, which is calibrated for an electrical output proportional to the laser power.
(See page 430.)

New Pressure-Sensitive Silicone Adhesive

A new pressure-sensitive silicone adhesive for high or low temperatures does not stretch severely under load. The blend of silicone tackifier and cured rubbery silicone is used without solvents. It is produced by combining an intermediate-molecular-weight pressure-sensitive silicone adhesive, which does not cure, with a silicone resin, which generally cures with a catalyst to a rubbery tack-free state. The ratio of silicone tackifier to silicone resin is varied to obtain different degrees of tack, creep resistance, and tensile strength.
(See page 452.)

Cardiopulmonary Data-Acquisition System

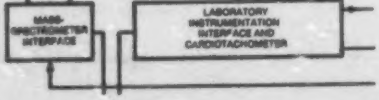
MASS SPECTROMETER
LABORATORY INSTRUMENTATION: TREADMILL OR BICYCLE ERGOMETER, BLOOD-PRESSURE MEASURING SYSTEM, VECTORCARDIOGRAPH
MASS-SPECTROMETER INTERFACE
LABORATORY INSTRUMENTATION INTERFACE AND CARDIOTACHOMETER

A computerized cardiopulmonary data-acquisition system controls and monitors bicycle and treadmill cardiovascular stress tests. It acquires and reduces stress data and displays in real time the heart rate, blood pressure, workload, respiratory rate, exhaled-gas composition, and other variables. The data are printed on a hard-copy terminal every 30 seconds so that the operator can quickly respond to the subject throughout the test. The ergometer workload is controlled in real time according to the experimental protocol, and the collected data are stored directly on tape in analog form and on floppy disks in digital form for posttest data processing.
(See page 457.)

Gage for Evaluating Rheumatoid Hands

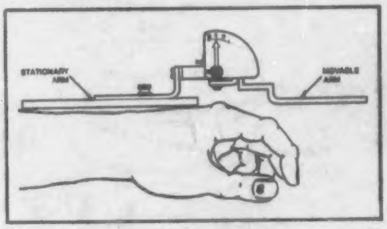

A two-axis goniometer accurately measures the movements of the fingers about the knuckle joints. It can help to diagnose hands that have structurally changed because of rheumatoid arthiritis. The new goniometer measures lateral movement which is small in normal knuckle joints but increases in diseased joints. The instrument is basically two connected protractors that simultaneously measure angles in perpendicular planes. Its dials are offset to clear the bony protuberances that result from rheumatoid arthritis. Extension and offset adjustments span any hand size.
(See page 461.)

Compact Infrared Detector

Compactness, high responsivity, and high noise immunity are among the advantages of a new broadband IR detector that could be integrated into a compact package for pollution monitoring and weather prediction. The sensing material is a transparent sheet, metalized with a reflecting coating and then overcoated with a

(continued on next page)

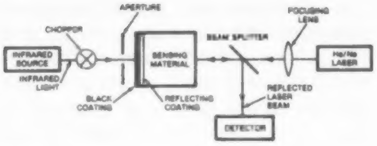
APERTURE
CHOPPER
FOCUSING LENS
BEAM SPLITTER
INFRARED SOURCE
SENSING MATERIAL
He/Ne LASER
INFRARED LIGHT
BLACK COATING
REFLECTING COATING
REFLECTED LASER BEAM
DETECTOR

black material on the same side. Each pulse produced by chopping the infrared source beam with a shutter creates a transient "thermal lens" that temporarily defocuses a reflected laser-beam probe. The defocusing increases as the infrared intensity increases. A detector monitors the probe beam, which weakens as the infrared light becomes more intense. (See page 475.)

Improved Microbe Detection in Water Samples

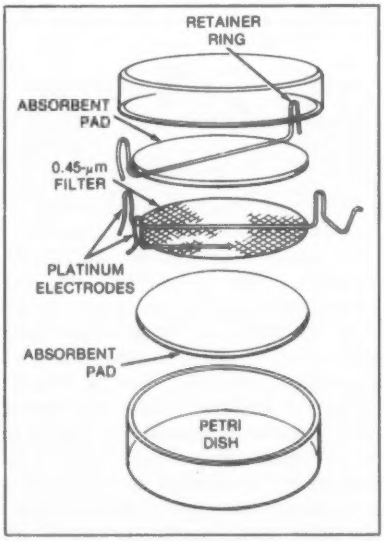
RETAINER RING
ABSORBENT PAD
0.45-μm FILTER
PLATINUM ELECTRODES
ABSORBENT PAD
PETRI DISH

Membrane filtration and electrochemical microbial detection are combined in a new method for detecting micro-organisms in water samples. Combined, the techniques give fast response and better detection of low concentrations. Cells are collected by a membrane filter placed on a moistened absorbent pad; platinum-wire electrodes are positioned on the surface of the filter. Another moistened pad is placed on top of the electrodes and filter. A retainer ring maintains constant pressure and close contact between pads, filter, and electrodes, which are contained in a petri dish to reduce moisture loss. (See page 460.)

Cavity-Backed Spiral-Slot Antenna

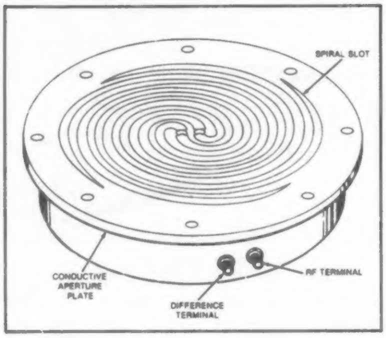
SPIRAL SLOT
CONDUCTIVE APERTURE PLATE
RF TERMINAL
DIFFERENCE TERMINAL

A new flush-mounted antenna can be switched to give either a radiation peak or a null on the axis, with circular polarization in either case. It is compact and can withstand severe mechanical and thermal loads. The radiating elements consist of two pairs of center-fed interleaved spiral slots in a conductive plane. Each slot in each pair lies between the slots of the other pair. At the center feedpoint of each pair of slots, a balanced feed assembly drives the slot from a split-tube coaxial balun. The entire apparatus is reciprocal, so that the circularly polarized patterns represent received signals as well as transmitted signals. (See page 421.)

Improved Cell for Water-Vapor Electrolysis

Water vapor in such gases as steam or ordinary room air is decomposed into hydrogen and oxygen by improved continuous-flow electrolytic cells. A new sintered iridium oxide catalytic anode coating yields dissociation rates over a hundredfold greater than those obtained using conventional platinum black. Each cell consists of two mirror-image cells, with a dual cathode sandwiched between two anodes.

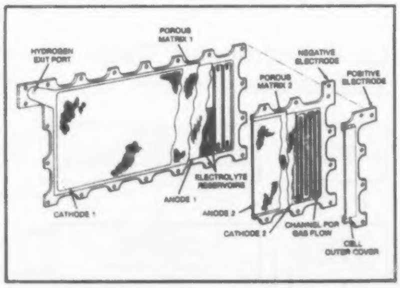
HYDROGEN EXIT PORT
POROUS MATRIX 1
NEGATIVE ELECTRODE
POROUS MATRIX 2
POSITIVE ELECTRODE
ELECTROLYTE RESERVOIRS
ANODE 1
ANODE 2
CATHODE 1
CATHODE 2
CHANNEL FOR GAS FLOW
CELL OUTER COVER

Vapor-laden gas traverses serpentine channels within each cell and is dissociated at the anode into hydrogen ions and free oxygen. The oxygen mingles with the gas stream, while the hydrogen migrates through a porous, electrolyte-saturated matrix and is liberated as hydrogen gas at the cathode. (See page 447.)

Hand-Held Coupler for Arthroscope

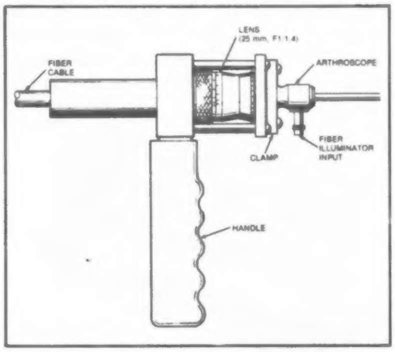
LENS (25 mm, F1:1.4)
FIBER CABLE
ARTHROSCOPE
FIBER ILLUMINATOR INPUT
CLAMP
HANDLE

A new, hand-held coupler images the output of an arthroscope onto a coherent fiber bundle. The arthroscope allows surgeons to examine internal structures and organs through a small incision or natural opening in the body. The coupler also can be used for engine inspection, instrument repair, and visual inspection through small openings. The image from the arthroscope travels along the flexible bundle and appears at the other cable end, where the image is recollimated by a lens. The image seen looking into the lens is the same as if looking directly into the arthroscope. If the lens is placed at the eyepiece, a real image is formed. Projection of the real image on a color-TV camera increases the image size and makes it easier to view, enchancing the surgical procedure. The hand-held portion of the coupler permits easy positioning and rotation of the arthroscope. (See page 462.)

Electronic Components and Circuits

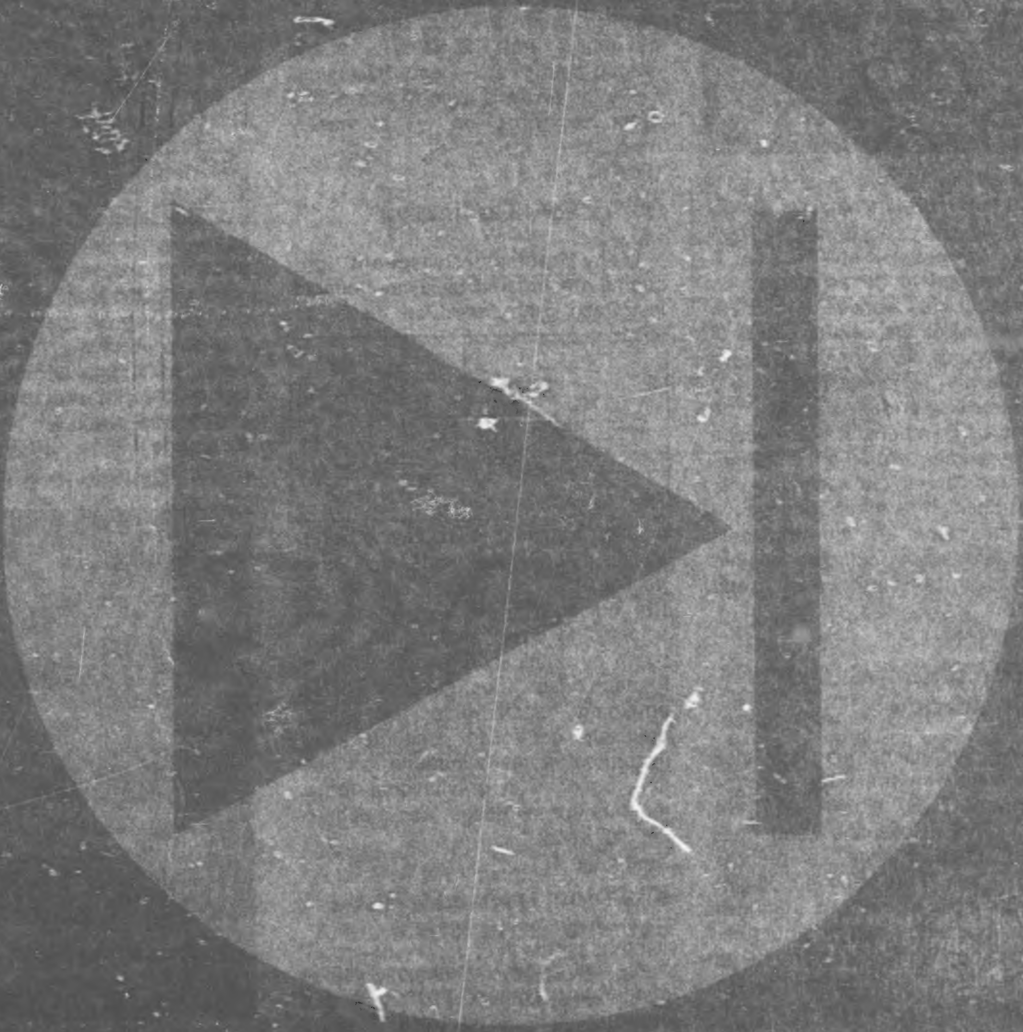

NEW PRODUCT IDEAS are just a few of the many innovations described in this issue of NASA Tech Briefs and having promising commercial applications. Each is discussed further on the referenced page in the appropriate section in this issue. If you are interested in developing a product from these or other NASA innovations, you can receive further technical information by requesting the TSP referenced at the end of the full-length article or by writing the Technology Utilization Office of the sponsoring NASA center (see page A4). NASA's patent-licensing program to encourage commercial development is described on page A8.

Interlocking Wedge Joint Is Easily Assembled

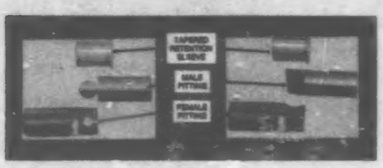

Two structural members in manual-, remote-, or automated-assembly operations are linked by a new interlocking wedge joint. The joint is simple enough to be assembled by undersea divers, workers in nuclear reactors, and others wearing gloves or bulky clothing. An expanding sleeve and male and female endpieces are joined in a single locking stroke. The joint has a high mechanical advantage that overcomes structural misalinements and forces the assembly into the true position as the locking sleeve moves into place. The joint transmits all structural loads, including tension, compression, bending moments, and torsion.
(See page 485.)

Microprocessor-Based Cardiotachometer

A new cardiotachometer operates reliably even with stress-test electrocardiogram (ECG) signals that are subject to noise, baseline wandering, and amplitude change. It records heart rate from a preamplified, single-lead ECG input signal and produces digital and analog heart-rate outputs, which can be fed to other instruments or computers. Analog hardware processes the ECG input signal, producing a 10-ms pulse for each heartbeat. The resulting pulse train is analyzed by a microprocessor computer program that identifies irregular heartbeats and maintains a stable output during ECG lead switching. Since the analysis logic is part of the computer program, it is easily modified.
(See page 459.)

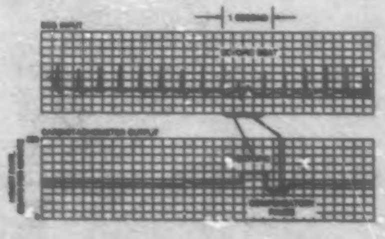

Multibeam Collimator

Many precisely-divergeant light beams are created by a new optical instrument that can be used to measure angles in surveying land, alining machine elements, and other applications. The angles and refractive indices of a stack of prisms are selected to divert an incoming laser beam by small increments, different for each prism. Thus, the angles of the emerging beams differ by small, precisely controlled amounts. The instrument is nearly immune to vibration, changes in gravitational force, temperature variations, and mechanical distortion.
(See page 427.)

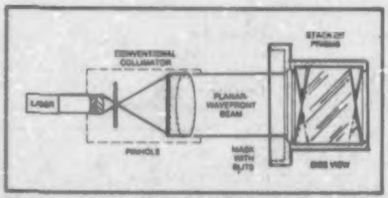

Vibration Transducer for Extreme Environments

An improved transducer with a temperature limit of 500° C and a pressure limit of up to 10 kilobars responds to mechanical vibrations up to 20 kHz. Constructed of high-temperature-resistant materials, the new vibration pickup should perform well in nuclear reactors, turbines, and other extreme environments. Outgassing and "virtual" leakage, problems experienced at very low pressures with previous transducers potted in epoxy, are eliminated by using only glass and metal supports. The interior is open to the atmosphere to prevent the buildup of pressure-induced stresses. A spring holds the transducer parts against the housing to reduce distortion due to pressurization and thermal strain.
(See page 471.)

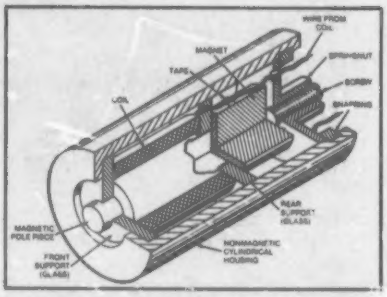

Low-Temperature Seal

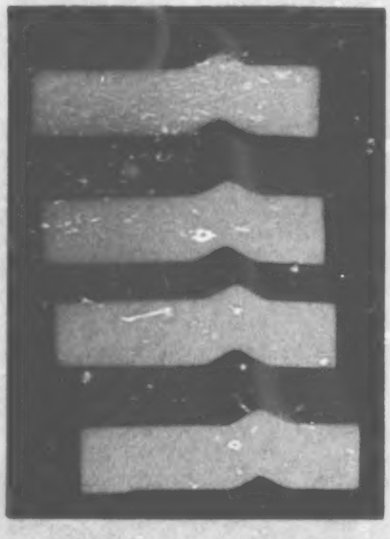

A spiral-wound cryogenic gasket is made from just one component, requires no encapsulant, and can be produced with self-locking or other features. Fabricated from a continuous strip, the seal can be "active" (be opened and closed), or it can be permanent. It is made by skiving a strip from the circumference of a disk

Improved Battery Charger for Electric Vehicles

Polyphase chopper circuit would significantly reduce ripple and EMI.

NASA's Jet Propulsion Laboratory, Pasadena, California

While the single-phase "boost chopper" is already superior to most conventional battery chargers for electric vehicles, a proposed polyphase version is expected to give even better performance. Calculations show that when the number of choppers is increased to two, three, or more, ripple and electromagnetic interference (EMI) are substantially reduced and efficiency is improved. The basic advantages of the boost chopper — compactness, high efficiency, and power factors approaching unity — are retained.

The elementry boost chopper has a bridge-based power circuit and a drive circuit that adjusts the rate of charge in response to changes in key battery parameters. An inductor, a transistor, and a diode in the power circuit make up the chopper, which boosts the bridge output so that current is delivered to the battery. The drive circuit adjusts the chopper duty cycle to give a near-unity power factor.

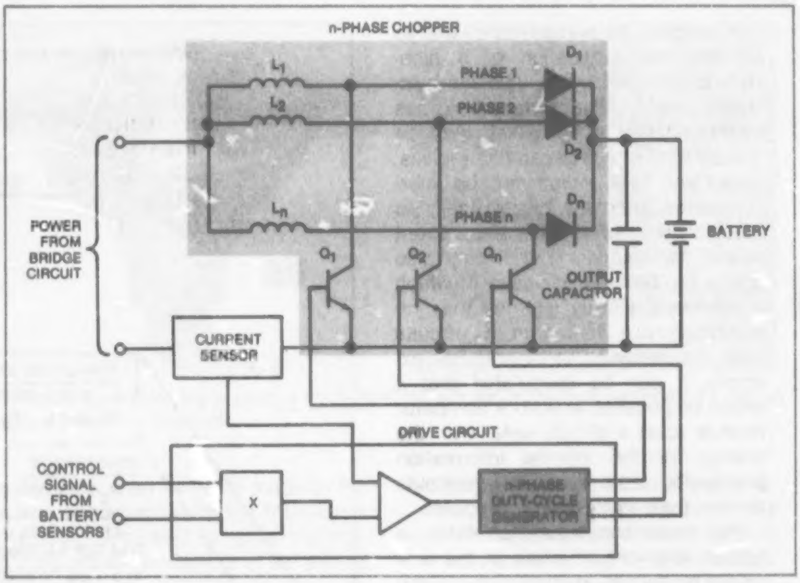

Drive circuit of **n-Phase Boost Chopper** incorporates an n-phase duty-cycle generator. Each chopper is composed of an inductor, a transistor, and a diode.

In the n-phase chopper, diagramed in the figure, each inductor carries 1/n of the current handled by the inductor of the analogous single-phase circuit. A modulator controls the duty cycle of the transistors, making the instantaneous current through the inductors proprtional to the instantaneous bridge output voltage. With this proportionality, the charger operates at a power factor near unity.

Because the ripple in the different chopper phases tends to cancel, the net ripple is low, as is the EMI produced by the charger. Switching spikes are lowered, because the current steps are reduced below that of the single-phase chopper.

For example, a three-phase chopper reduces ripple to one-ninth its single-phase value. At the same time, the ripple frequency is increased three times, and the ripple can therefore be more easily filtered out by small inductors and capacitors. The value of capacitance used to clamp switching spikes and protect the switching transistors is reduced to one-ninth its single-phase value. Thus a smaller and less-expensive capacitor can be used.

In general, an n-phase chopper reduces the ripple magnitude by a factor of n^2 while increasing the ripple fundamental frequency n times. The output capacitance is reduced by at least 1/n. Although ripple theoretically falls rapidly with increasing phases, it is probably not practical to increase n beyond three or four, because the inductors must be more closely matched as n increases, the transistor drive signals must be more closely matched, and the polyphase generator becomes more expensive.

The charger can be operated by single-phase or three-phase alternating current, at 115 or 230 volts, for example, or by direct current. With dc, it is possible for one electric vehicle to charge another in a road emergency.

This work was done by Wally E. Rippel of Caltech for **NASA's Jet Propulsion Laboratory.** *For further information, Circle 1 on the TSP Request Card.*

Inquiries concerning rights for the commercial use of this invention should be addressed to the Patent Counsel, NASA Resident Office-JPL [see page A5]. Refer to NPO-14964.

Multijunction High-Voltage Solar Cell

Integrated unit cells could yield 50 volts per linear inch on a single semiconductor wafer.

Lewis Research Center, Cleveland, Ohio

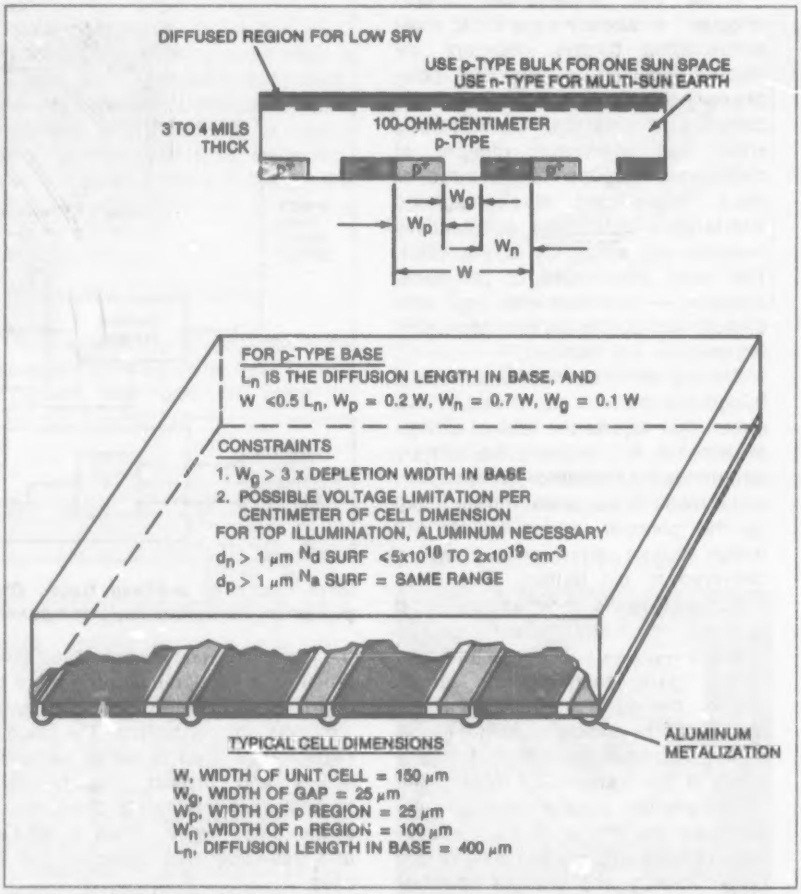
DIFFUSED REGION FOR LOW SRV
USE p-TYPE BULK FOR ONE SUN SPACE
USE n-TYPE FOR MULTI-SUN EARTH
3 TO 4 MILS THICK
100-OHM-CENTIMETER p-TYPE
p+
p+
p+
W_g
W_p
W_n
W
FOR p-TYPE BASE
L_n IS THE DIFFUSION LENGTH IN BASE, AND
$W < 0.5\ L_n$, $W_p = 0.2\ W$, $W_n = 0.7\ W$, $W_g = 0.1\ W$
CONSTRAINTS
1. $W_g > 3 \times$ DEPLETION WIDTH IN BASE
2. POSSIBLE VOLTAGE LIMITATION PER CENTIMETER OF CELL DIMENSION
FOR TOP ILLUMINATION, ALUMINUM NECESSARY
$d_n > 1\ \mu m$ N_d SURF $< 5 \times 10^{18}$ TO 2×10^{19} cm^{-3}
$d_p > 1\ \mu m$ N_a SURF = SAME RANGE
ALUMINUM METALIZATION
TYPICAL CELL DIMENSIONS
W, WIDTH OF UNIT CELL = 150 μm
W_g, WIDTH OF GAP = 25 μm
W_p, WIDTH OF p REGION = 25 μm
W_n, WIDTH OF n REGION = 100 μm
L_n, DIFFUSION LENGTH IN BASE = 400 μm

The **Planar Multijunction Solar Cell** is shown with doped regions and gaps (not to scale). Unit cells are combined in series, using aluminum metalization bars, to yield the required output voltage and current.

A recent innovation now makes possible the fabrication of a high-voltage solar cell on a single semiconductor wafer. Experimentation has confirmed that a solar cell may be divided into voltage-generating regions, called unit cells, which may be interconnected internally or externally to result in desired voltage and current output combination. The finding also opens up the field of usage in which photovoltaic energy sources may be combined on a wafer with the circuits they are designed to power. For example, it can be speculated that it would be possible to build a computer module upon a silicon wafer with the energy for the internal information processing and even the readouts derived from an external light source.

The accompanying sketch details a typical solar-cell structure of the new planar multijunction (PMJ) high-voltage cell. The starting material for the cited example is high-lifetime, single-crystal, Czochralski-grown silicon. As shown, the device has a thickness of 3 to 4 mils with a textured or planar surface and with an antireflection coating applied to the illuminated surface. In this surface, divided into regions located over the unit voltage-generating unit cells, are implanted or diffused dopants resulting in a front-surface field or a front junction, depending upon the chosen dopant type. When p-type silicon of any resistivity from 1 to 20,000 ohm-cm is used for the base material, a front junction of n+ dopant such as phosphorus or front surface field of p+ material such as boron or aluminum may be used. Some benefit is derived from the use of high-resistivity and high-lifetime material for the base.

In any unit voltage-generating unit cell, as shown, a p+ diffused or implanted region approximately 25 micrometers wide is diffused into a junction depth of 1 micrometer. Next to this narrow band of dopant, an undoped band of the same width is left. Next to the undoped region a wide band of n+ dopant is inserted to a depth of 1 micrometer. The width of the n+ region is 100 micrometers, bringing the unit cell width to a total of 150 micrometers. Since the nominal voltage of each such unit cell is one-half volt, it may be possible to produce approximately 50 volts per linear inch of the solar cell while still maintaining optimized size. Smaller or larger unit cells may be used with some penalties, if higher voltages or currents are desired. The overall output voltage of the solar cell is the sum of the unit cell voltages and is collected at the opposite edges of the cell with metal contacting bars as shown on the first p+ bar and the last n+ region.

This work was done by John C. Evans, Jr., Chandra Goradia, and An Ti Chai of **Lewis Research Center**. *Further information may be found in NASA TM-81389 [N80-16914/NSP], "Planar Multijunction High Voltage Solar Cells" [$5]. A copy may be purchased [prepayment required] from the National Technical Information Service, Springfield, Virginia 22161.*

Inquiries concerning rights for the commercial use of this invention should be addressed to the Patent Counsel, Lewis Research Center [see page A5]. Refer to LEW-13400.

Solar Cell Is Housed in Light-Bulb Enclosure

An inexpensive solar-cell module uses a standard outdoor light-bulb enclosure.

Lewis Research Center, Cleveland, Ohio

With the advent of a recently announced innovation in solar cell fabrication, the planar multijunction (PMJ) high voltage solar cell [see preceding article "Multijunction High Voltage Solar Cell" (LEW-13400)], a number of uses for the new cell have been found. Shown in the accompanying photographs is the first working model of the "light-electric bulb," which uses the focusing principle of the electric lamp in reverse to produce electric power from Sunlight.

Housed in a conventional weatherproof outdoor or yard light enclosure, the new cell, located within the concentrated circle of Sunlight where the lamp filament is conventionally placed, converts radiant energy to electricity. Use of this standard outdoor light enclosure provides a relatively low-cost housing, and one which serves to concentrate Sunlight in the solar cell. A unit as shown is capable of producing approximately 1 watt of electric power.

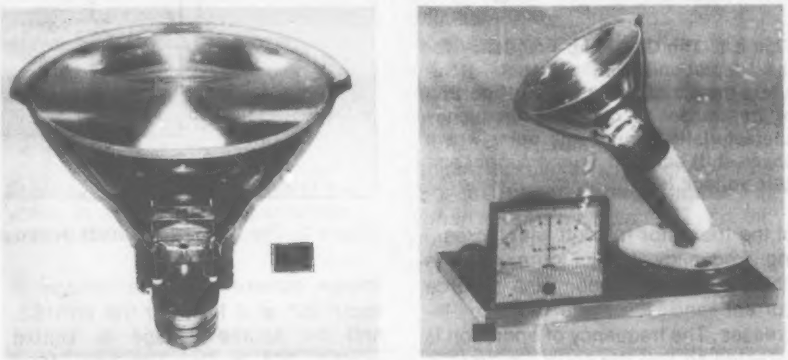

The Low-Cost Housing is seen in the bulb at the left and in the bulb generating 1 watt at about 5 volts on the right.

The new solar cells are made by the same microminiaturization techniques presently employed to make the integrated circuits so familiar in the pocket calculator.

This work was done by John C. Evans, Jr., of **Lewis Research Center.**

No further documentation is available.

Inquiries concerning rights for the commercial use of this invention should be addressed to the Patent Counsel, Lewis Research Center [see page A5]. Refer to LEW-13418.

Learning High-Quality Soldering

Soldering techniques for high-reliability electronic equipment are taught in a 5-day course. Among the areas covered are: new circuit assembly; reworking printed-wiring boards; parts replacement; and making circuit changes by cutting traces, changing wiring, and adding terminals.

(See page 499.)

CADAT Integrated-Circuit Artwork Program

Artwork data are converted into mask patterns by the CADAT integrated-circuit artwork program. The program generates signals for controlling mask-fabricating equipment. An extensive utility package enables the user to create new pattern libraries.

(See page 508.)

Trislot-Cavity Microstrip Antenna

A disk radiator sandwiched between conducting planes, so that it is enclosed in a cavity, has greater bandwidths and beamwidths than an unenclosed disk radiator. The cavity antenna, fabricated by conventional microstrip techniques, can be flush mounted on the surface of a moving vehicle.

(See page 422.)

Simple JFET Oscillator

Stable high-frequency signal source is compatible with integrated-circuit techniques.

Goddard Space Flight Center, Greenbelt, Maryland

A junction field-effect transistor (JFET) connected in a simple circuit makes a stable sine-wave oscillator for such applications as mixers, modulators, and function generators. The oscillation frequency can be tuned over a narrow band about the design value. The JFET circuit is convenient for either compact discrete-component assemblies or integrated circuits.

The frequency of this oscillator is in the rolloff portion of the JFET characteristic curve, somewhat above the 3-dB point. As the transconductance

(continued on next page)

best copy available

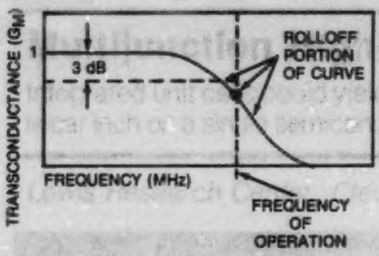

Figure 1. The Operating Frequency for the depletion-mode, junction field-effect transistor is in the rolloff portion of its transconductance-vs.-frequency characteristic, around the point where phase shift between source current and gate voltage is 90°.

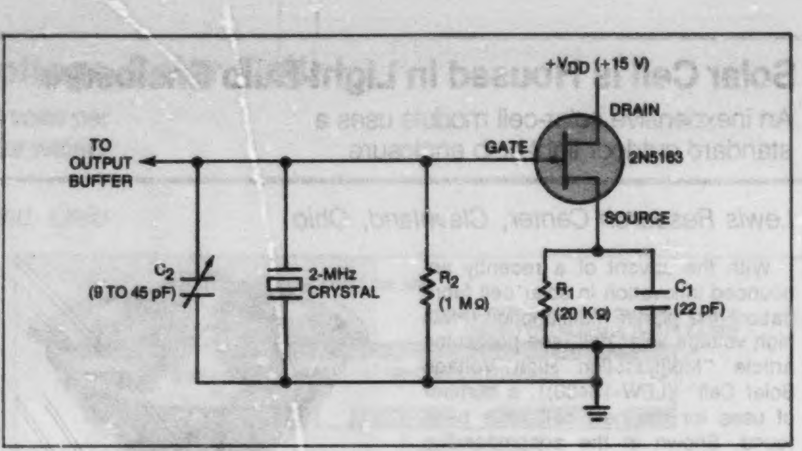

Figure 2. The Oscillator Circuit is compact, and has low power consumption.

of the transistor rolls off with increasing frequency (see Figure 1), the phase angle between the source current and the gate voltage increases. The frequency of operation is selected so that the source current is about 90° out of phase with the voltage at the gate and a source capacitor produces an additional 90° of phase shift. Positive feedback then occurs that causes oscillation.

An example of this circuit design is the 2-MHz oscillator shown in Figure 2. The 2N5163 is a depletion-mode JFET that is normally operated at frequencies well below 2 MHz. The drain of the transistor is connected directly to a power supply of +15 volts. The source terminal of the JFET is connected to one end of the parallel combination of resistor R_1 (20 k Ω) and capacitor C_1 (22 pF). The other end of the combination is connected to ground. The phase angle between source current and gate voltage is about 90° at 2 MHz for the 2N5163, and the source voltage is shifted another 90° in C_1. The total 180° phase shift provides positive feedback that drives a 2-MHz crystal (or a 2-MHz LC tank circuit) at resonance. A variable capacitor, C_2, connected across the resonator allows fine tuning, and a 1-M Ω resistor supplies a dc return path around the crystal.

The circuit of Figure 2 oscillates at 2.0009255 MHz, without varying more than 0.1 hertz. Its waveform is sinusoidal, with low distortion. The signal is 0.6 volt peak-to-peak at the source and 1.8 volts peak-to-peak at the gate. Outputting from the JFET gate, as shown, is preferred to outputting from the JFET source.

The frequency range, stability, linearity, and low power drain of this oscillator make it particularly suitable for use in communications receivers and transmitters and in such digital systems as microprocessors, computers, and displays. Its circuit simplicity also allows for ease of monolithic construction. The only components external to the chip would be the crystal or coil and the tuning capacitor.

This work was done by Leonard L. Kleinberg of **Goddard Space Flight Center.** *For further information, Circle 2 on the TSP Request Card.*

This invention is owned by NASA, and a patent application has been filed. Inquiries concerning nonexclusive or exclusive license for its commercial development should be addressed to the Patent Counsel, Goddard Space Flight Center [see page A5]. Refer to GSC-12555.

Speed Control for Synchronous Motors

Hunting is either suppressed or enhanced by a phase-sensitive feedback circuit.

Lyndon B. Johnson Space Center, Houston, Texas

A feedback circuit controls fluctuations in the speed of an ac synchronous motor. Small speed variations are detected and either suppressed or enhanced by applying a correction voltage to the motor excitation circuit. Among possible applications of the new speed control is reducing the wow and flutter of audio turntables and tape recorders.

Although an ideal synchronous motor runs at constant speed, small changes in loading, for example, in bearing resistance, cause the speed to "hunt" about the synchronous value at a fairly-constant low frequency. The hunting may be compared to the vibration of a spring, with the motor inertia analogous to the spring mass and the magnetic flux lines equivalent to the elastic spring.

To control hunting in a polyphase motor, the circuit senses the phase difference between the line currents in the motor windings. The phase angle varies in step with the speed variation. A voltage proportional to the angle is developed by a phase detector, rectified, amplified, compared to a threshold, and applied back to the motor excitation circuit. If the correction

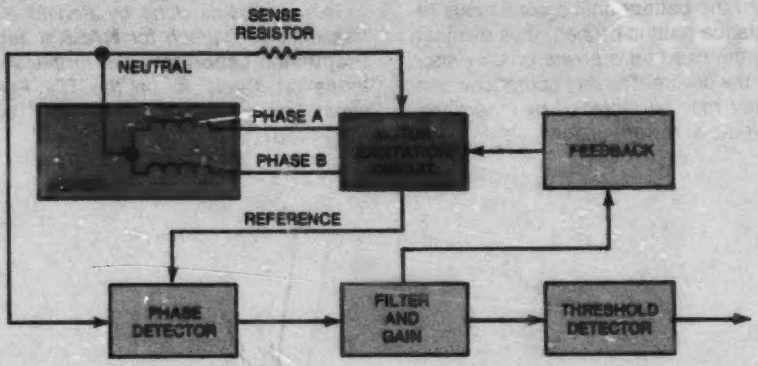
SENSE RESISTOR
NEUTRAL
PHASE A
PHASE B
MOTOR EXCITATION CIRCUIT
FEEDBACK
REFERENCE
PHASE DETECTOR
FILTER AND GAIN
THRESHOLD DETECTOR

Hunting in a Polyphase Synchronous Motor Is Detected by sensing the phase of the current through the neutral line, relative to the phase on one of the motor windings. A similar circuit is used for a split-capacitor synchronous motor.

signal is applied as negative feedback, it suppresses hunting. In some applications, such as gyroscope motors, enhanced hunting may be needed. In those cases, positive feedback is used.

In effect, the feedback alters the motor magnetic field, which is analogous to altering the stiffness of a spring. It is not necessary to apply the feedback to all the windings of a polyphase motor; applying it to just one winding is sufficient. An analogous circuit is used for split-capacitor synchronous motors.

This work was done by Henry Packard and James Schott of Northrop Corp. for **Johnson Space Center**. *For further information, Circle 3 on the TSP Request Card.*
MSC-18680

Low-Resistance Continuity Tester

A low-current-drain continuity tester measures resistances as low as 0.1 ohm.

NASA's Jet Propulsion Laboratory, Pasadena, California

Continuity checks of integrated-circuit socket connections with their many parallel paths frequently involve measuring resistances less than 1 ohm. A tester has been devised that measures resistances as low as 0.1 ohm while using little power. The circuit utilizes the inexpensive 741 operational amplifier operating on an 11.2-volt battery.

The operational amplifier controls an audio oscillator that drives a small loudspeaker or an LED visible display for indicating continuity. The probes are applied across the path for which continuity is to be checked. A low resistance across the input probes (see figure) unbalances the operational amplifier to produce a positive output. Threshold response is set by a 10-kilohm potentiometer. When setting the desired threshold resistance by means of the 10-kilohm potentiometer, a 0.5-ohm precision resistor may be used for calibration. A Zener diode in series with the output of the operational amplifier and the base of the bipolar switch transistor prevents the oscillator from operating until the positive output of the operational amplifier has sufficient amplitude, when the probe circuit is closed.

(continued on next page)

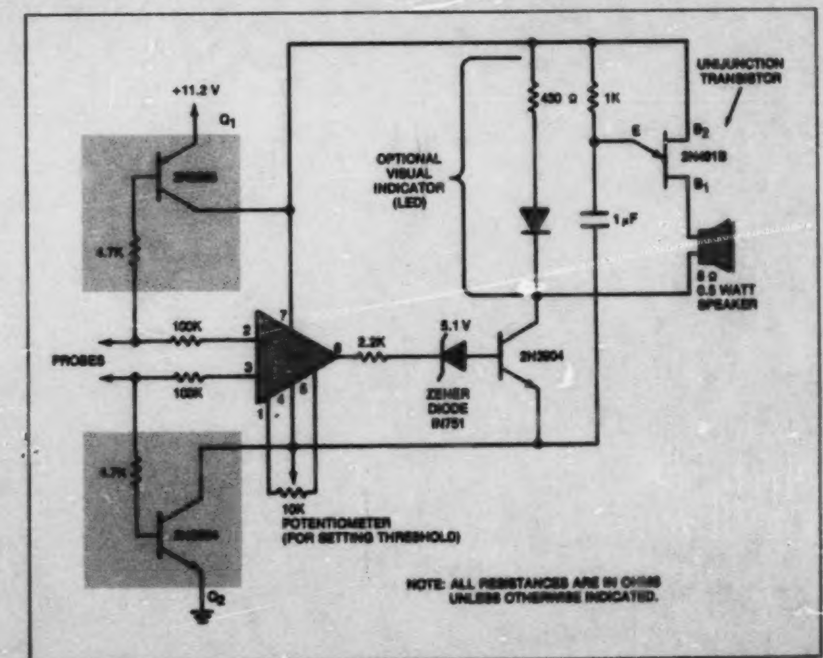
+11.2 V
Q1
4.7K
100K
PROBES
100K
2
3
7
6
4
5
1
4.7K
Q2
10K POTENTIOMETER (FOR SETTING THRESHOLD)
2.2K
5.1 V
ZENER DIODE IN751
2N3904
OPTIONAL VISUAL INDICATOR (LED)
430 Ω
1K
1 μF
UNIJUNCTION TRANSISTOR
E
B2
2N4919
B1
8 Ω 0.5 WATT SPEAKER
NOTE: ALL RESISTANCES ARE IN OHMS UNLESS OTHERWISE INDICATED.

The **Low-Resistance Continuity Tester** can be used to check IC printed-circuit boards. Two 4.7-kilohm resistors and the transistors connected to them prevent current flow through the operational amplifier until the probe circuit is completed. The Zener diode in series with the operational amplifier output prevents audio oscillator operation until the positive output of the operational amplifier has sufficient amplitude.

The oscillator uses a unijunction transistor to generate an audio tone. No current is drawn by the unijunction and switch transistors until the collector of the switch transistor goes low. Transistors Q_1 and Q_2 prevent current flow through the operational amplifier from the battery until a continuous resistance path is probed, thus eliminating the need for a power on/off switch for the device. The 741 operational amplifier may be replaced by others that operate at lower voltages.

This work was done by Ronald B. Reasoner of Caltech for **NASA's Jet Propulsion Laboratory.** *For further information, Circle 4 on the TSP Request Card.*
NPO-14881

Electronic Systems

Hardware, Techniques, and Processes

419 Superconducting Gyrocon Would Be Very Efficient
420 High-Power Dual-Directional Coupler
421 Cavity-Backed Spiral-Slot Antenna
422 Timing Signal Propagates Without Phase Shift
422 Trislot-Cavity Microstrip Antenna

Computer Programs

423 Developing Experiment Instrument Packages

Superconducting Gyrocon Would Be Very Efficient

Cryogenic operation of a gyrocon can increase gain and efficiency.

NASA's Jet Propulsion Laboratory, Pasadena, California

A theoretical analysis shows that the gyrocon can be a very efficient microwave amplifier, oscillator, or frequency multiplier when built with superconducting materials and operated at liquid-helium (4.2 K) temperature. Whereas room-temperature operation limits gyrocon gain to less than 15 dB and overall efficiency to about 80 percent despite excellent dc-to-RF conversion efficiency (at least 90 percent), superconductors would up this gain to more than 50 dB and increase the efficiency to more than 90 percent.

As shown in the figure, a gyrocon consists of five parts: the electron gun, the deflection cavity, the output cavity, the collector, and the output coupler. In the superconducting version, the cavities are made of lead or niobium, and are immersed in a cryostat. The electron gun generates a collimated electron beam that acquires very large kinetic energy from the high accelerating voltage between cathode and anode. The beam passes through the deflection cavity, where the field produced by the input RF signal causes the beam to follow an expanding helical path.

The gyrating beam traverses the output cavity through slots in the top and bottom of the cavity waveguide. The phase velocity of the waveguide field and the gyration velocity of the beam can be made to match, so that the beam experiences the same fields each time it sweeps around. The beam energy is thereby converted into waveguide-field RF energy, and the beam slows down almost to a halt. The RF power is taken out through the output coupler, and the electron beam continues on to the collector.

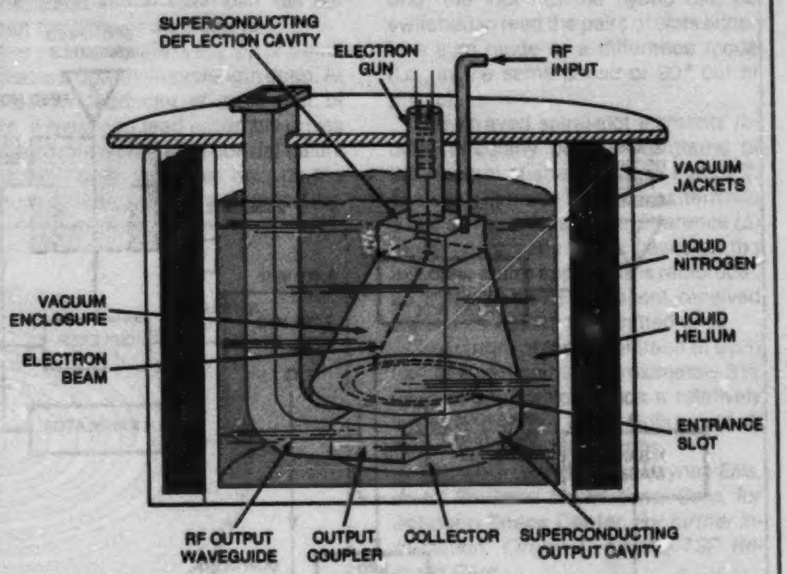

The **Superconducting Gyrocon** would have input and output cavities made of superconducting lead or niobium. Operation at frequencies to 50 GHz appear practical.

Performance is improved in the superconducting gyrocon because the RF surface resistance for superconducting materials is smaller than that of room-temperature copper by a factor of at least 10^4 to 10^6, depending on the surface conditions. Thus, for the same field strength, the RF losses in a superconducting cavity are substantially reduced. Calculations using an optimized gyrocon operated at 2.45 GHz with a dc beam power of 1.809 MW show that room-temperature overall efficiency is 0.818 and RF power gain is 13.4 dB; whereas, at superconducting temperature, the overall efficiency is 0.916 and RF power gain is 53.8 dB.

Another advantage of the superconducting gyrocon is that continuous operation becomes practical at very high power levels, and the efficiency does not suffer when the tube is operated at levels as low as 10 kW. Room-temperature gyrocons are practical only for pulsed operation and have to be operated at beam power levels near 1 MW.

This work was done by Huan-Chun Yen of Caltech for ***NASA's Jet Propulsion Laboratory****. For further information, Circle 5 on the TSP Request Card.*

This invention is owned by NASA, and a patent application has been filed. Inquiries concerning nonexclusive or exclusive license for its commercial development should be addressed to the Patent Counsel, NASA Resident Office-JPL [see page A5]. Refer to NPO-14975.

High-Power Dual-Directional Coupler

A water-cooled coupler can pass 400 kW of CW microwave energy without arcing.

NASA's Jet Propulsion Laboratory, Pasadena, California

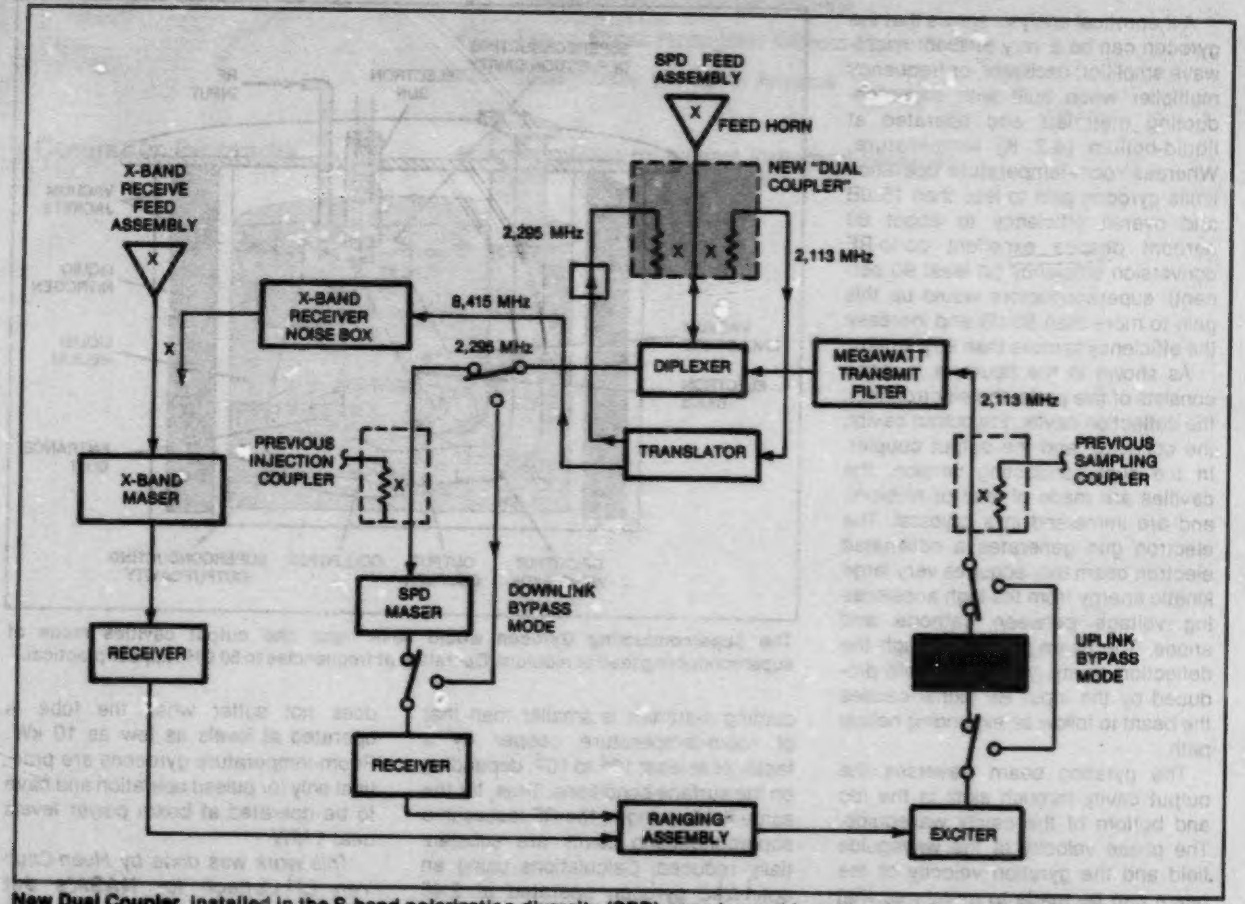
SPD FEED ASSEMBLY
X
FEED HORN
NEW "DUAL COUPLER"
X-BAND RECEIVE FEED ASSEMBLY
X
2,295 MHz
X
X
2,113 MHz
X-BAND RECEIVER NOISE BOX
8,415 MHz
X
2,295 MHz
DIPLEXER
MEGAWATT TRANSMIT FILTER
2,113 MHz
PREVIOUS INJECTION COUPLER
X
TRANSLATOR
PREVIOUS SAMPLING COUPLER
X
X-BAND MASER
SPD MASER
DOWNLINK BYPASS MODE
UPLINK BYPASS MODE
RECEIVER
RECEIVER
RANGING ASSEMBLY
EXCITER

New Dual Coupler installed in the S-band polarization diversity (SPD) cone is used in calibrating the receiving-station relay. The coupler operates successfully at 400 kW and permits accurate calibration of the entire system below the antenna feed horn.

During the Voyager near-Earth calibration sequence, the power levels received at the traveling-wave maser (TWM) inputs were high enough to saturate the ground station receivers, and the high-power uplink could have saturated the spacecraft receiver. A solution to this problem was to bypass the klystron (see figure); i.e., to use the exciter only and to bypass both the S-band and the X-band TWM's.

To calibrate the station delay for this bypass, as well as for the normal configuration, it was necessary to move the calibration sampling-injection points for the system closer to the S-band feed horn from their positions near the klystron and maser. Installation of the two existing couplers close to the feed horn was physically unfeasible, and a single compact dual coupler was therefore developed. This compact coupler was fitted with two 54-dB loop coupler modules, each only 5 cm in length, and was water-cooled. Tests showed that the coupler had good directivity, contributed less than 0.01 K to the system noise temperature, and was able to pass 400 kW of CW microwave energy without arcing.

The coupler was installed near the feed horn in the SPD (S-band polarization diversity) cone and has since been used as part of the range-delay calibration system. In the previous configuration, some of the component delays below the feed horn had to be calculated or precalibrated before installation into the system. In the new configuration, the test translator signal is injected at a point as near the feed horn as possible, allowing a direct range-delay measurement at that point of all parts of the system below the feed horn. As a result, the system is more accurately calibrated.

This work was done by Tommy Y. Otoshi and Kenneth B. Wallace of Caltech for **NASA's Jet Propulsion Laboratory.** *For further information, Circle 6 on the TSP Request Card. NPO-14713*

Cavity-Backed Spiral-Slot Antenna

A compact, rugged, flush-mounted antenna operates in sum or difference modes with circular polarization.

Lyndon B. Johnson Space Center, Houston, Texas

A new flush-mounted antenna can be switched to give either a radiation peak or a null on the axis, with circular polarization in either case. The structure is compact and can withstand severe mechanical and thermal loads.

The radiating elements (see Figure 1) consist of two pairs of center-fed interleaved spiral slots in a conductive plane. Each slot in each pair lies between the slots of the other pair.

The aperture plate is the top of a cavity that is a quarter-wavelength deep. At the center feedpoint of each pair of slots, a balanced feed assembly drives the slot from a split-tube coaxial balun. Both baluns extend down through the bottom of the cavity to a four-port hybrid; the input to the hybrid can be switched to feed the pairs of slots either in a sum mode or a difference mode (i.e., in the same phase or 90° out of phase).

The arrayed spiral-slot elements radiate circularly polarized patterns of the general shape shown in Figure 2. The sum (Σ) mode radiation pattern has a null on the axis, and the difference (Δ) mode has a pattern that peaks on the axis. The entire apparatus is reciprocal, so these patterns represent received signals as well as transmitted ones.

The length of the spiral trace of each half of a slot pair is approximately 3½ wavelengths, which yields a relatively large bandwidth. Longer slots would afford still greater bandwidths.

This work was done by Haynes Ellis, Jr., of Rockwell International Corp. for **Johnson Space Center.** *For further information, Circle 7 on the TSP Request Card.*

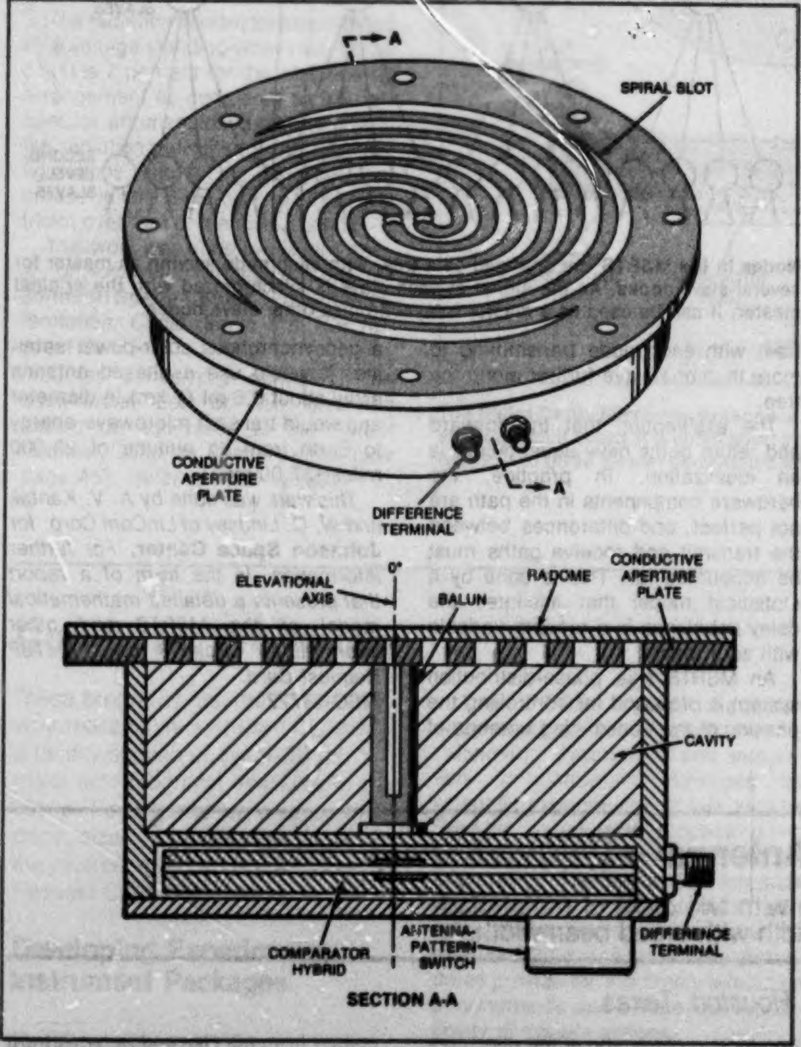

Figure 1. A Spiral-Slot Antenna consists of two pairs of center-fed interleaved spiral slots in a conductive aperture plane. At the center feedpoint of each slot pair is a balanced feed assembly. Each of these center points is fed from a split-tube coaxial balun, which passes through a cavity that is a quarter-wavelength deep. A radome covers the aperture plate.

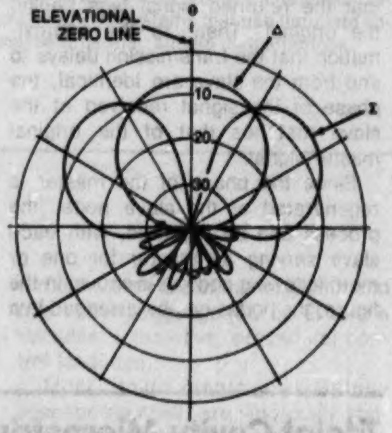

Figure 2. Radiation Patterns differ, depending on whether the antenna is in the sum (Σ) mode or the difference (Δ) mode.

This invention is owned by NASA, and a patent application has been filed. Inquiries concerning nonexclusive or exclusive license for its commercial development should be addressed to the Patent Counsel, Johnson Space Center [see page A5]. Refer to MSC-18532.

Timing Signal Propagates Without Phase Shift

Continuous monitoring of transmission delay corrects for phase shift.

Lyndon B. Johnson Space Center, Houston, Texas

In synchronized electronic systems, such as the phased microwave antenna array a solar-power satellite would use or the accurate clock-distribution systems in avionics and computers, performance depends critically on fixing the phase relationship between system components, or nodes. To maintain synchronization, a master timing signal at a fixed phase and frequency must be available at each node.

Such a timing signal is propagated without phase shift through an array of nodes by the master/slave returnable timing system (MSRTS). The MSRTS actively compensates for phase-shift drift caused by changing transmission delay between nodes.

The basic idea of the MSRTS is to cancel the transmission delay by returning back to the master a sample of the signal received at the slave. The phase transmitted from the master is then advanced until it leads the original phase by the same amount that the returned signal lags behind the original. Then, to the approximation that the transmission delays to and from the slave are identical, the phase of the signal received at the slave matches that of the original master signal.

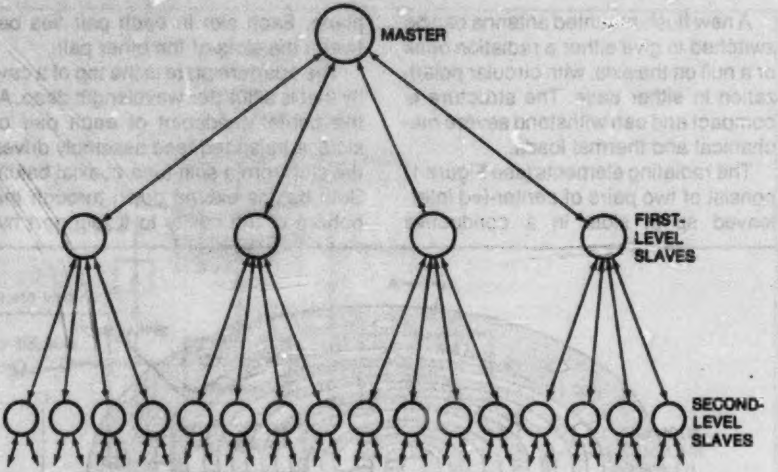

Nodes in the MSRTS are arranged as a tree, with each node serving as master for several slave nodes. As the signal at each slave is synchronized with the original master, it can be used as a master to synchronize other slave nodes.

Since the phase of the master is regenerated at the slave node, the process can be repeated, with each slave serving as master for one or more following nodes. As shown in the figure, the nodes can be arranged in a tree, with each node transmitting to more than one slave further along the tree.

The assumption that the forward and return paths have equal delays is an idealization. In practice, the hardware components in the path are not perfect, and differences between the transmit and receive paths must be accounted for. This is done by a statistical model that assumes the delay imbalance is a random variable with zero mean.

An MSRTS tree phase-distribution system is proposed for controlling the phasing of the transmitting antenna of a geosynchronous solar-power satellite. It would use a phased antenna array about 0.6 mi (1 km) in diameter and would transmit microwave energy to Earth from an altitude of 23,000 miles (37,000 km).

This work was done by A. V. Kantak and W. C. Lindsey of LinCom Corp. for **Johnson Space Center.** *For further information, in the form of a report that presents a detailed mathematical model of the MSRTS and other information, Circle 8 on the TSP Request Card.*
MSC-18777

Trislot-Cavity Microstrip Antenna

Flush-mountable assembly, made with two disks of metal-clad dielectric board, has wide bandwidth with broad beamwidth.

Lyndon B. Johnson Space Center, Houston, Texas

A simple disk radiator mounted over a conducting plane can be used as a flush-mounted microwave antenna. However, better antenna characteristics are achieved by placing another conducting plane above the disk, connecting the top and bottom planes so that the disk is enclosed in a cavity, and cutting a Y-shaped slot in the top plane. The cavity is excited by the microwave energy from the disk and radiates from the trislot aperture in the top plate.

The figure shows details of the trislot-cavity antenna, including the arrangement for feeding the signal to the disk.

The three slots are 120° apart, are $\lambda_0/4$ long (where λ_0 is the free-space wavelength at the center frequency of the microwave signal), and are $\lambda_0/40$ wide. The conductors that pass through the dielectric boards to connect the top and bottom metal planes are spaced 30° apart, at a radius that is greater than the slot length by the thickness of the antenna.

The excitation disk has a radius of $\lambda_0/4\varepsilon$; i.e., less than the slot length by a factor equal to the dielectric constant ε of the construction boards. A conducting post connects the center of the disk to the bottom conducting plane. Two feedpoints are located off-center and driven by a quadrature hybrid RF circuit.

The radiation bandwidth (determined by a voltage standing-wave ratio below 1.5:1) is 2 percent for the trislot-cavity arrangement as compared to 0.5 percent for an unenclosed disk. A plot of the radiation patterns for the two configurations shows a 25-percent increase in the 3-dB beamwidth of the trislot over that of the disk antenna.

This work was done by Haynes Ellis, Jr., of Rockwell International Corp. for **Johnson Space Center**. *For further information, Circle 9 on the TSP Request Card.*

Inquiries concerning rights for the commercial use of this invention should be addressed to the Patent Counsel, Johnson Space Center [see page A5]. Refer to MSC-18793.

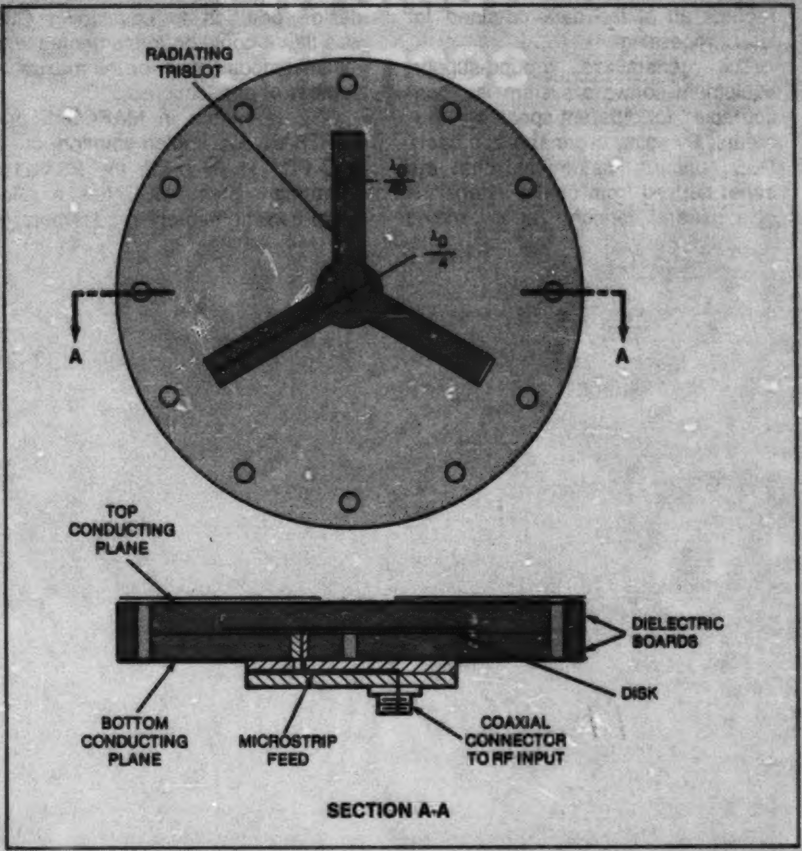

The **Trislot-Cavity Microstrip Antenna** is made from two circular pieces of metal-clad dielectric circuit board. It is applicable to communications systems that use flat-plate antennas and gives greater bandwidths and beamwidths than simple disk antennas.

Computer Programs

These programs may be obtained at very reasonable cost from COSMIC, a facility sponsored by NASA to make new programs available to the public. For information on program price, size, and availability, circle the reference letter on the COSMIC Request Card in this issue.

Developing Experiment Instrument Packages

Software support for development, calibration, and testing of experiment packages

The GSE (ground-support equipment) system supports the development, calibration, and integration of instrument packages for scientific experiments. It can also be used for "quick-look" processing and for data analysis once the experiment is operating. The user of GSE interacts with incoming telemetry data, performs computations, and controls the execution of procedures. The procedures provide for the timely execution of commands and assure the repeatability of system actions.

Facilities to command GSE, to command the scientific instruments, and to configure the system for different operational environments are provided through the Experiment Command Interactive Language (ECIL). ECIL is a versatile, interactive, procedural control language.

Most instruments, especially spaceborne ones, are vigorously tested to assure that their performances meet specifications. Usually they are precalibrated against known data sources. Once the instrument is calibrated, its electronics package is placed in its final enclosure and is installed at the experiment site. When the instrument is operating, its behavior under severe environmental conditions must often be analyzed quickly. These complex processes are monitored and supported by GSE, which

(continued on next page)

records all of the data obtained for later processing.

The generalized ground-support equipment software system is "configurable" for different specific instruments. By using a general approach, GSE supports instruments that are either derived from or are extensions of a general version. The overriding design criterion in developing GSE was that it could be implemented with minimal modification for the maximum number of applications.

GSE is written in MARCO II and FORTRAN for implementation on a DEC PDP-11/34 using the RSX-11M operating system. GSE has a minimum central memory requirement of approximately 42K of 16-bit words. It was developed in 1979.

This program was written by Rodney Herreid of **Goddard Space Flight Center.** *For further information, Circle A on the COSMIC Request Card.*
GSC-12536

Physical Sciences

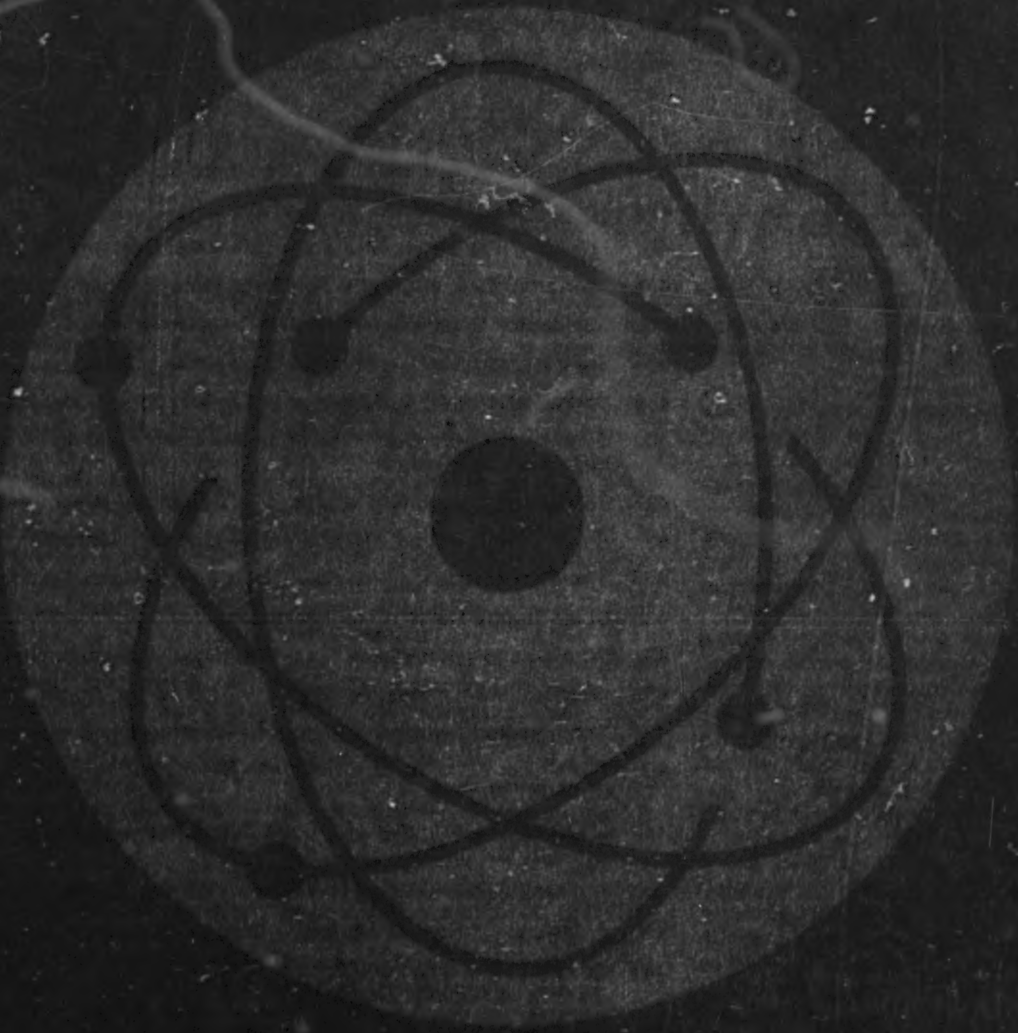

Hardware, Techniques, and Processes

427 Multibeam Collimator Uses Prism Stack
428 Pulse-Shaping Circuit for Laser Excitation
429 Field Limiter for Solar Radiometer
430 Gas-Laser Power Monitor
430 Fiber Optics Transmit Clock Signal More Reliably
431 Reduced Viscosity Interpreted for Fluid/Gas Mixtures
432 Tunable Pulsed Carbon Dioxide Laser
433 Short-Range Self-Pulsed Optical Radar

Books and Reports

433 Solar-Site Test Module
434 Evaluation of an Evacuated-Tube Liquid Solar Collector
434 Solar Water Heater Design Package
434 Five-City Economics of a Solar Hot-Water System
435 Economic Evaluation of a Solar Hot-Water System
435 Residential Solar-Heating System Uses Pyramidal Optics
436 Solar-Heated Bank — Marks, Mississippi
436 Solar Water-Heating Performance Evaluation — San Diego, California
436 Solar-Heated and Cooled Savings and Loan Building — Leavenworth, Kansas
437 Solar-Energy Landmark Building — Columbia, Missouri
437 Solar Heating for an Observatory — Lincoln, Nebraska
438 Two-Story Residence With Solar Heating — Newnan, Georgia
438 Solar-Energy Heats a Transportation Test Center — Pueblo, Colorado
438 Single-Family-Residence Solar Heating — Carlsbad, New Mexico
439 Multimode Solar-Heating System — Columbia, South Carolina
439 Solar-Heated Swimming School — Wilmington, Delaware
439 Winter Performance of a Domestic Solar-Heating System — Duffield, Virginia
440 One-Year Assessment of a Solar Space/Water Heater — Clinton, Mississippi
440 Fire-Station Solar-Energy System — Kansas City, Missouri
440 Solar-Heated Ranger Station — Glendo, Wyoming
441 Economic Evaluation of a Solar Hot-Water System — Palm Beach County, Florida
441 Residential System — Lansing, Michigan
442 Solar Space-Heating System — Yosemite National Park, California
442 Motel Solar-Hot-Water System — Dallas, Texas
442 Motel Solar-Hot-Water System With Nonpressurized Storage — Jacksonville, Florida
443 Closed-Circulation System for Motel Hot Water — Savannah, Georgia
443 Solar Heating for a Restaurant —North Little Rock, Arkansas
443 Motel Solar Hot-Water Installation — Atlanta, Georgia
444 Building With Integral Solar-Heat Storage — Starkville, Missippi

Multibeam Collimator Uses Prism Stack

A stack of prisms at minimum angular deviation generates divergent light beams for surveying.

Goddard Space Flight Center, Greenbelt, Maryland

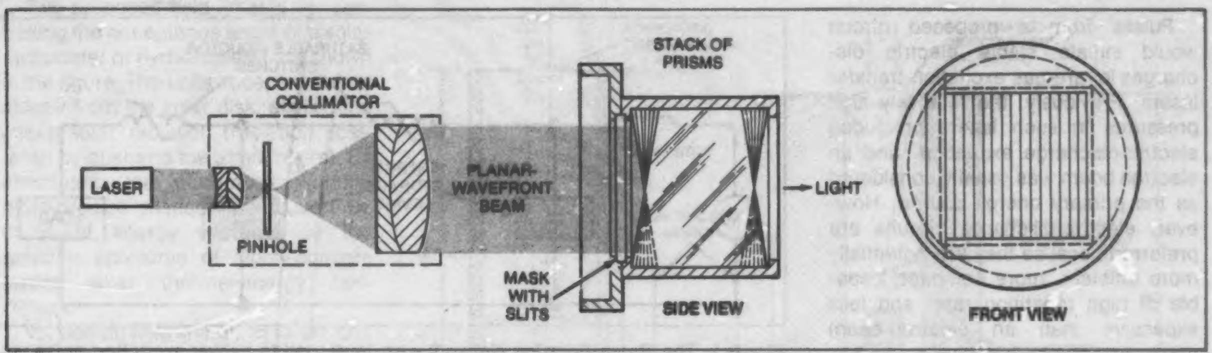

A Fanlike Stack of Prisms separates a beam of light into many beams, each having a precise directional relationship to the others. The light source, a helium/neon laser, was selected for its high intensity and the ease with which it can be collimated. A mask with alined parallel slits is mounted at the entrance to the prism stack.

Many precisely divergent beams are created from a single laser beam by a stack of prisms in a new optical instrument. Each beam points in a slightly different direction with a precise angular relationship to the others. The multiprism collimator can be used to measure angles in surveying land and alining machine elements.

Unlike many other devices for measuring angles, the multiprism collimator is nearly immune to vibration, changes in gravitational force, temperature variations, and mechanical distortion. It is accurate within 1 microradian in its present form, and it would be even more accurate if it were built in larger sizes.

As shown in the figure, the beam from a helium/neon laser is expanded and collimated by a conventional optical collimator. The beam is then directed onto a stack of prisms, so that each prism intercepts a different portion of the wave front. The angles of the front and rear prism faces and their refractive indices are selected to divert the beam by a given amount, different for each prism. The angle of the emerging beam thus changes by increments from one end of the prism array to the other. For example, the direction may vary from +7° to -7° from one side of the array to the other, with the prisms providing 1° increments and the deviation of the center wedge being 0°.

The prisms are mounted at their positions of minimum deviation. This means that the angle of incident light is at the minimum of the deviation-vs.-incidence-angle curve. In this region, the directions of the emerging beams are least sensitive to changes in incidence angle. The accuracy of the deviation, therefore, is relatively unaffected by dimensional distortions. Mechanical motion of the collimator causes all the beams to shift in unison but does not change the angular separation between the beams.

The glass used for the prisms is selected for its low-temperature coefficient of refractive index. This property ensures that the instrument accuracy is hardly affected by temperature changes.

In a collimator that has been built, the prisms are 4.7 mm thick and 82.5 mm wide. A stack of 15 such prisms in the mounting fixture provides a clear aperture 70.7 mm high and slightly more than 70.7 mm wide.

Prism arrays can be designed to produce various increments and ranges of deviation, since the parameters are determined chiefly by the angles of the entrance and exit faces for a given index of refraction. The important constraint is that the deviation of an individual prism should approximate the minimum deviation.

This work was done by Peter O. Minott of **Goddard Space Flight Center.** *For further information, Circle 10 on the TSP Request Card.*

This invention is owned by NASA, and a patent application has been filed. Inquiries concerning nonexclusive or exclusive license for its commercial development should be addressed to the Patent Counsel, Goddard Space Flight Center [see page A5]. Refer to GSC-12308.

Pulse-Shaping Circuit for Laser Excitation

Narrower, impedance-matched pulses would initiate stabler electric discharges for gas lasers.

NASA's Jet Propulsion Laboratory, Pasadena, California

Pulses from a proposed circuit would initiate stable electric discharges in rare-gas excitation-transfer lasers. Previously, the relatively high pressures in such lasers precluded electric-discharge excitation, and an electron beam was usually considered as the primary energy source. However, electric-discharge circuits are preferred because they are potentially more efficient, more compact, capable of high repetition rate, and less expensive than an electron-beam apparatus.

Self-sustained discharges in high-pressure rare-gas mixtures are difficult to control because the gas tends to break down and form localized arcs. In addition, high-voltage and high-energy charging circuits usually have large inductances that reduce voltage rise times below that required for optimum gas excitation.

The proposed network compresses the width of high-voltage pulses from a relatively-slow rise-time voltage generator and gradually grades the circuit impedance from the inherent high impedance of the generator to the low impedance of the gas.

As shown in the block diagram (Figure 1), the network consists of two saturable inductor switches, each with a distributed-capacitance energy-storage device at its input. Each inductance switch has a core formed of nonmagnetic material with a laminate wrapped around it. The laminate is formed of a thin layer of high-permeability material (>2,000μ_0) deposited on a flexible backing. Possible energy-storage devices are coaxial cables, multiple coaxial cables, or parallel-plate transmission lines.

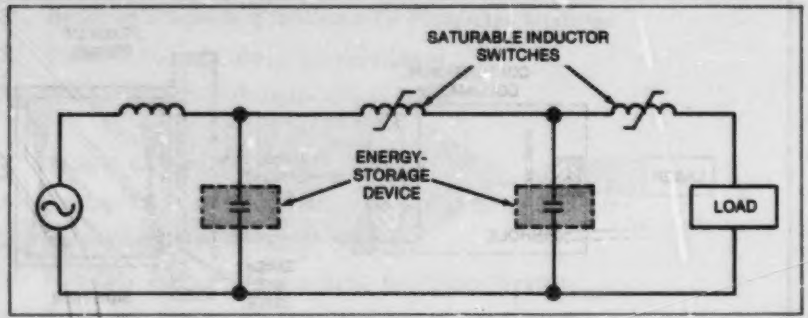

Figure 1. The **Pulse-Forming Network** was developed to deliver excitation pulses to a high-pressure rare-gas laser. The proposed circuit would generate pulses greater than 100 kilovolts, having energies of the order of hundreds of joules. Pulse durations would be less than 100 nanoseconds and rise times on the order of a few nanoseconds. Output impedance would be 1.0 Ω or less.

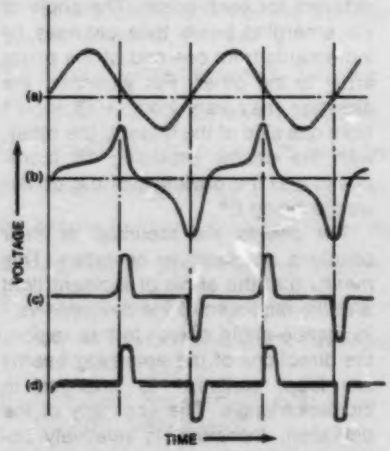

Figure 2. The **Change in the Waveform** as it passes through the circuit of Figure 1 is shown here.

The output from the primary voltage source as shown in Figure 2(a) is a sinusoidal wave that is slightly compressed, as in (b), prior to the time of switch saturation. When the first inductor switch saturates, the energy stored in the first distributed-capacitance storage device is transferred to the second distributed-capacitance energy-storage device as shown in waveform (c). As this occurs, the second inductor switch saturates, impressing a highly compressed voltage, shown in waveform (d), across the load.

The high-permeability material wound on the saturable inductor switch core has a thickness within an order of magnitude of the skin depth at a frequency corresponding to a desired rise time of the output pulse. For a 10-nanosecond-rise-time pulse-shaping network, the skin depth would be on the order of 1 to 2 microns.

This work was done by James B. Laudenslager and Thomas J. Pacala of Caltech for **NASA's Jet Propulsion Laboratory.** *For further information, Circle 11 on the TSP Request Card.*

This invention is owned by NASA, and a patent application has been filed. Inquiries concerning nonexclusive or exclusive license for its commercial development should be addressed to the Patent Counsel, NASA Resident Office-JPL [see page A5]. Refer to NPO-14556.

Field Limiter for Solar Radiometer

Lenses project the solar image onto an aperture to exclude circumsolar radiation.

NASA's Jet Propulsion Laboratory, Pasadena, California

Two proposed field limiters for controlling the acceptance angle of a solar radiometer or pyrheliometer are shown in the figure. The units accept radiation strictly from the solar disk, eliminating circumsolar radiation (radiation scattered by dust and the atmosphere). By eliminating the circumsolar inputs, more-precise measurements can be made of energy captured by the receiver apertures of highly-concentrating solar thermal-energy converters.

Version (a) field limiter, 16 in. (41 cm) long, uses an achromatic objective lens (similar to those used in small refractor telescopes) to form an image of the Sun at an aperture just ahead of the radiometer cavity. Version (b) is shorter, 7.4 in. (18.8 cm), and hence more convenient. Its shorter-focal-length achromatic objective forms a smaller image that is magnified by another lens and imaged onto an aperture.

The diameter of the image at the aperture (3.8 mm) is the same in both versions. Aperture diameter determines the instrument acceptance angle; i.e., the aperture is a field stop. An aperture the same diameter as the solar image would prevent circumsolar radiation from entering the radiometer cavity.

Concentrating or focusing solar-energy collectors form an image of the Sun on the collecting element. The Sun subtends an angle of 32 arc minutes. Practical solar collectors accept radiation from a somewhat larger angle to avoid having the intense solar image fall on anything but the collector element. The angle required depends on collector aiming accuracy and image definition.

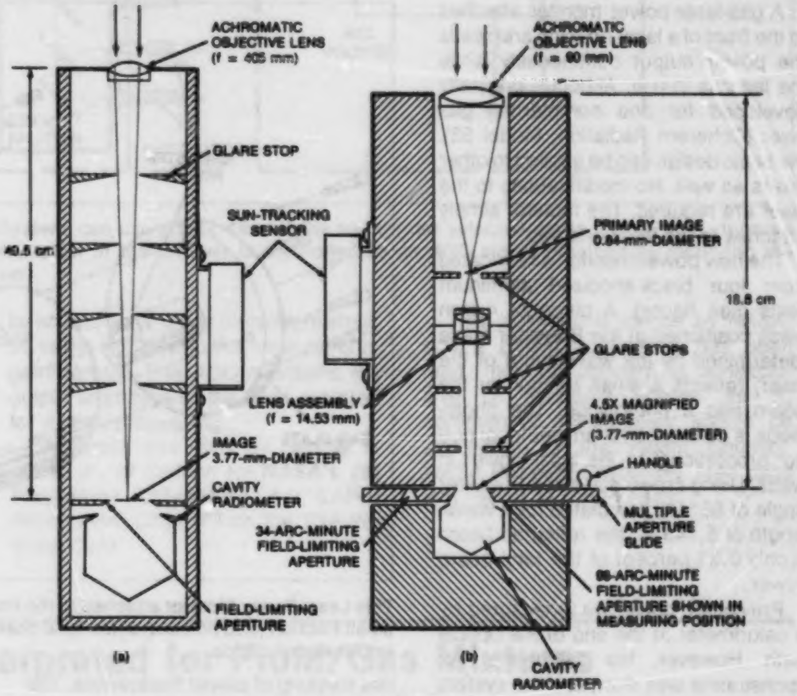
ACHROMATIC OBJECTIVE LENS (f = 405 mm)
GLARE STOP
40.5 cm
SUN-TRACKING SENSOR
IMAGE 3.77-mm-DIAMETER
CAVITY RADIOMETER
FIELD-LIMITING APERTURE
(a)
ACHROMATIC OBJECTIVE LENS (f = 90 mm)
PRIMARY IMAGE 0.84-mm-DIAMETER
18.8 cm
GLARE STOPS
LENS ASSEMBLY (f = 14.53 mm)
4.5X MAGNIFIED IMAGE (3.77-mm-DIAMETER)
HANDLE
MULTIPLE APERTURE SLIDE
34-ARC-MINUTE FIELD-LIMITING APERTURE
86-ARC-MINUTE FIELD-LIMITING APERTURE SHOWN IN MEASURING POSITION
CAVITY RADIOMETER
(b)

The Cavity Radiometer Field Limiters are designed for use with a standard 5°-field-angle radiometer with a cavity aperture 0.44 inch (1.13 cm) in diameter. The drawings are not to scale. Both radiometers give the same size image and have the same cavity sizes. The lengths, though, are different.

A collector performance evaluation requires accurate radiation measurements with the same acceptance angle as the collector. Measurements of radiation from the solar disk alone are also needed for comparison. Either type of measurement can be made by placing an aperture of the proper diameter in the field limiter.

Either version of the field limiter would require calibration against a standard radiometer because reflection and absorption losses in the lenses prevent accurate sensitivity calculations from geometry alone. A solar-tracking mount keeps the Sun image centered on the field-limiting aperture.

This work was done by C. Martin Berdahl of Caltech for **NASA's Jet Propulsion Laboratory.** *For further information, Circle 12 on the TSP Request Card.*
NPO-14781

Gas-Laser Power Monitor

Power output is continuously monitored while the laser is in use.

Langley Research Center, Hampton, Virginia

A gas-laser power monitor attaches to the front of a laser housing and reads the power output continuously while the laser is in use. Although originally developed for one commercial gas laser (Coherent Radiation, Model 53), the basic design can be applied to other lasers as well. No modifications to the laser are required. The monitor simply attaches to the laser end cap.

The new power monitor is fabricated from four black-anodized aluminum parts (see figure). A piece of crown glass positioned at the Brewster angle (determined by the wavelength of the laser) reflects a small fraction of the beam into a photodiode. The photodiode is calibrated for an electrical output proportional to the laser power in watts. Using crown glass at a Brewster angle of 56°41′, calculated for a wavelength of 5,145 Å, the reflected beam is only 0.33 percent of the total beam power.

Previously, power was measured by a calorimeter at the end of the optical path. However, the calorimeter response time was slow, and the system was susceptible to optical misalinement. The built-in power monitor does not interrupt the laser beam, as did the calorimeter; and the diode has much faster response, allowing instantaneous tracking of power fluctuations. The monitor can be calibrated to read either the total power output of the laser or the power generated in a test volume, making it more convenient for data reductions.

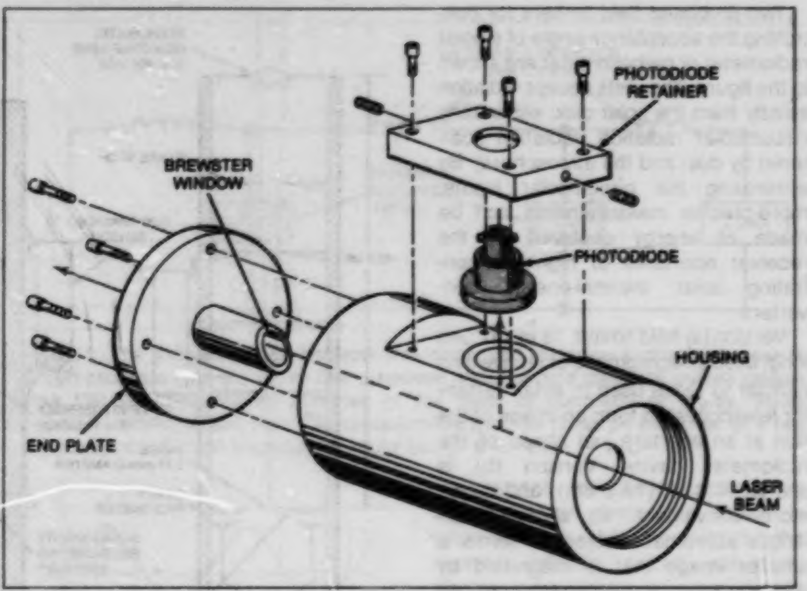

This **Laser Power Monitor** attaches to the front end cap of a high-power gas laser. Only a small fraction (0.33 percent) of the total beam power is diverted by the Brewster window into the photodiode.

This work was done by Courtney E. Russ, Jr., of **Langley Research Center.** *No further documentation is available. LAR-12682*

Fiber Optics Transmit Clock Signal More Reliably

Optical automatic gain control smooths maser clock amplitude fluctuations without introducing phase shift.

NASA's Jet Propulsion Laboratory, Pasadena, California

A proposed fiber-optic system would distribute a precise reference signal from a hydrogen maser frequency standard over 1 kilometer. The signal is propagated with near-zero phase shift as a function of automatic gain control (AGC) and with constant amplitude. The optical system, developed for the Deep Space Station complex to deliver reference signals to receiver and signal-processing equipment, is less complex and more reliable than electrical transmission circuits, which introduce phase shifts as a function of attenuation and require compensating phase-locked loops.

The maser, as shown in the block diagram, feeds the reference signal to a linear fiber-optic analog transmitter that emits a modulated laser beam, which is directed to an optical beam splitter. The beam splitter consists of dichroic mirrors and associated lenses for distributing the beam to several output ports. Fiber-optic cables attached to each port then guide the signals to the receiving station.

The cables up to 1 km long are terminated in a closed-loop automatic-gain-

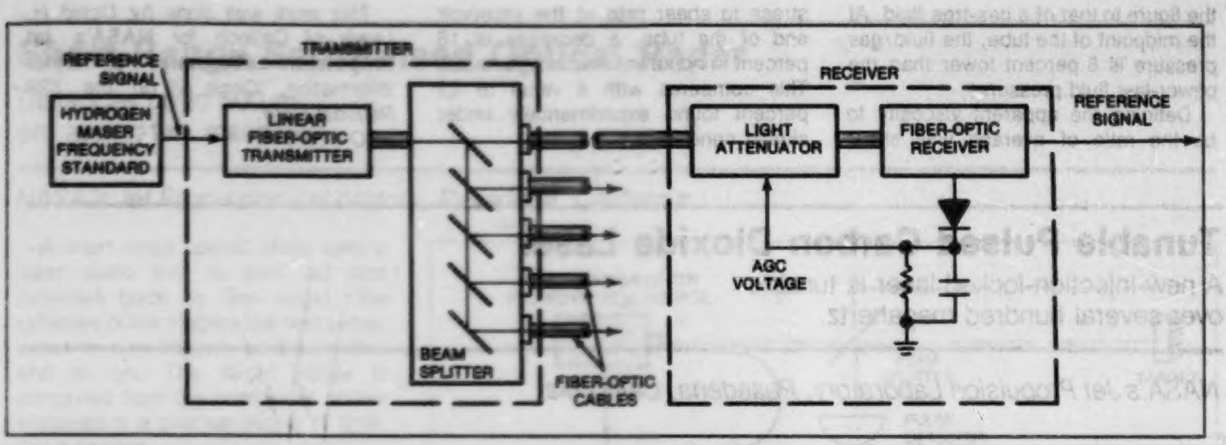

The Fiber-Optic Clock-Signal Distribution System can use plastic fiber if the transmitter selected emits visible light. Infrared transmitters are also available. The light attenuator in the receiver is controlled by an AGC signal obtained by rectifying the clock-signal output of the fiber-optic receiver.

controlled fiber-optic receiver utilizing a light attenuator, such as a Kerr cell (or a servo with a tapered opacity disk), that varies the transmitted light amplitude in response to a dc variable voltage.

The variable optical output of the attenuator is applied to the receiver. A part of the receiver output is rectified by an additional diode circuit furnishing dc to the light attenuator for automatic gain control. This AGC maintains the output amplitude at the level required for further processing.

This work was done by George F. Lutes, Jr., of Caltech for **NASA's Jet Propulsion Laboratory.** *For further information, Circle 13 on the TSP Request Card.*

This invention is owned by NASA, and a patent application has been filed. Inquiries concerning nonexclusive or exclusive license for its commercial development should be addressed to the Patent Counsel, NASA Resident Office/JPL [see page A5]. Refer to NPO-14749.

Reduced Viscosity Interpreted for Fluid/Gas Mixtures

An analysis predicts the decrease in fluid viscosity with gas admixture.

NASA's Jet Propulsion Laboratory, Pasadena, California

A theoretical analysis predicts the observed decrease in viscosity of a non-Newtonian fluid when the fluid is mixed with a gas. The understanding of this effect can assist in the design of flow systems for petroleum, coal, chain, polymers, paints, food products, and other materials.

In the analysis, the fluid is taken to be viscous, non-Newtonian, and incompressible; the gas, to be an ideal gas; and the flow, to be inertia-free, isothermal, and one-dimensional. The gas is assumed to be homogeneously dispersed as bubbles in the fluid as the mixture flows in a tube of constant radius. Surface tension is neglected.

The problem is formulated by introducing the equation of state of the gas, equations of conservation of mass and momentum, and a relationship between the wall shear stress and the fluid/gas velocity. Combining these equations yields a differential equation for the pressure. The exponent n in a relationship between the fluid viscosity and the shear rate is taken to be 1/2, a value typical of polyethylene plastics. When the boundary-value pressures are imposed, discrete solutions are obtained for the axial pressure, velocity, density, volumetric flow rate, and shear-stress profiles.

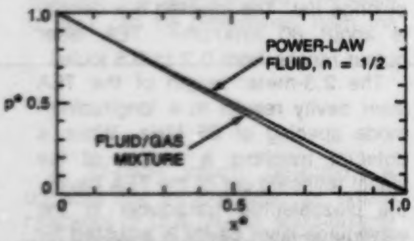

The **Pressure Profile of a Fluid/Gas Mixture** is compared with that of a power-law fluid; p^* is the normalized pressure p/p_0, and x^* is the normalized axial distance x/L, where p_0 is the reservoir pressure and L is the tube length.

Values of typical constants for low-density polyethylene are chosen for a representative calculation. The predicted pressure profile is compared in the figure to that of a gas-free fluid. At the midpoint of the tube, the fluid/gas pressure is 8 percent lower than the power-law fluid pressure.

Defining the apparent viscosity to be the ratio of average wall shear stress to shear rate at the reservoir end of the tube, a decrease of 16 percent in apparent viscosity is found. This compares with a value of 22 percent found experimentally under similar conditions.

This work was done by David H. Lewis of Caltech for **NASA's Jet Propulsion Laboratory.** *For further information, Circle 55 on the TSP Request Card.*
NPO-14976

Tunable Pulsed Carbon Dioxide Laser

A new injection-locked laser is tunable over several hundred megahertz.

NASA's Jet Propulsion Laboratory, Pasadena, California

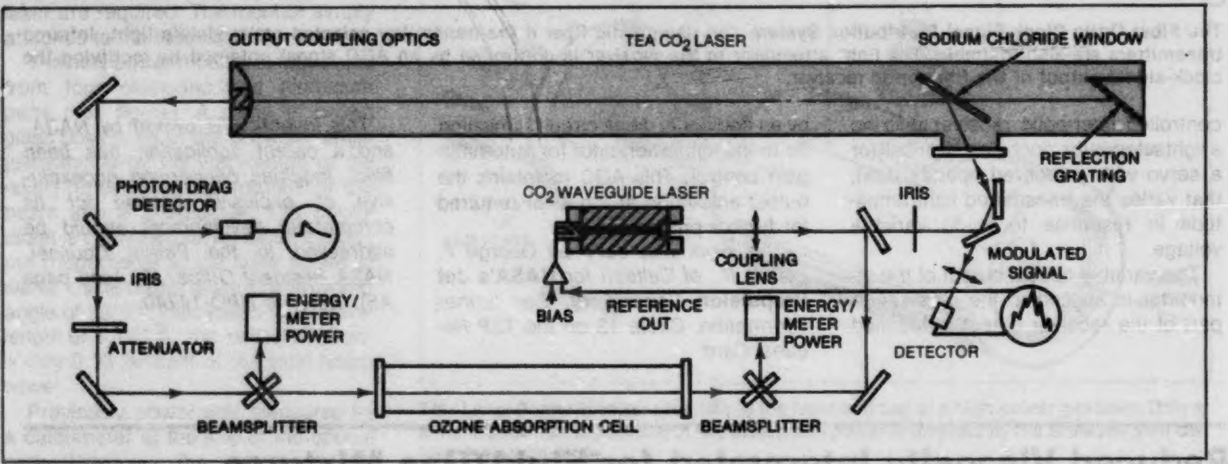

A Tunable Laser is used to measure an absorption line of ozone. The beam splitters at either end of the absorption cell are in one orientation for the observation of waveguide laser absorption and are in the orthogonal orientation for observation of the pulsed TEA-laser absorption.

A transverse electrically-excited-atmosphere (TEA) laser is continuously tunable over more than 300 MHz about the centers of various spectral lines of CO_2. It is operated in a single longitudinal mode (SLM) by injection of the beam from a continuous-wave, tunable-waveguide CO_2 laser, which serves as a master frequency-control oscillator.

The laser is diagramed in the figure. A diffraction grating in the CO_2 waveguide laser selects the spectral line of interest. A piezoelectric transducer varies the cavity length of the waveguide laser to tune it within its pressure-dependent gain bandwidth. Average continuous-wave output power is typically around 300 mW. The beam passes through a collimating lens and enters the TEA laser cavity by partial reflection from a sodium chloride flat. The injected flux density is about 60 mW/cm^2. TEA laser output ranges from 0.2 to 0.6 joule.

The 2.3-meter length of the TEA laser cavity results in a longitudinal-mode spacing of 65 MHz. While a detector monitors a portion of the signal reflected out of the TEA cavity, the piezoelectric transducer in the waveguide-laser cavity is adjusted for maximum detected signal, thus matching the two cavity resonances.

The output of the TEA CO_2 laser can be scanned across absorption features of molecules in the 9- to 12-micron spectral region. For example, it has been used to record absorption about the 9.488-micron line of ozone. With improvements in frequency control of the TEA cavity and in the waveguide tuning range, the new laser could be used to monitor atmospheric trace species.

This work was done by Gerard J. Megie and Robert T. Menzies of Caltech for **NASA's Jet Propulsion Laboratory.** *For further information, Circle 14 on the TSP Request Card.*

This invention is owned by NASA, and a patent application has been filed. Inquiries concerning nonexclusive or exclusive license for its commercial development should be addressed to the Patent Counsel, NASA Resident Office-JPL [see page A5]. Refer to NPO-14984.

Short-Range Self-Pulsed Optical Radar

Distances up to 500 m are accurately measured.

NASA's Jet Propulsion Laboratory, Pasadena, California

A short-range optical radar uses a laser pulse that is sent out and reflected back by the target; the reflected pulse triggers the next pulse, which in turn triggers another pulse, and so on. The target range is computed from the number of pulses triggered in a precise period of time, say 1 second.

Typical optical radar for measuring longer distances determines range by measuring the time of flight of a single pulse. The new radar, shown in the figure, would accurately measure distances up to about 500 m. It could be used for measuring the surface shape of reflectors in large, high-gain, highly directional antennas and for other short-range surveying.

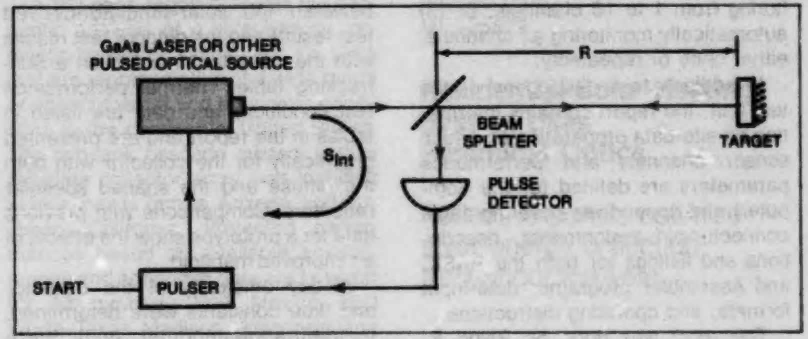

The Laser for an Optical Radar is retriggered when the previous laser pulse is reflected back from the target. The target range R is computed from the number of pulses triggered in a time interval.

For a typical target range, say 150 m, the range-measurement accuracy of the new optical radar can be estimated as follows: Knowing the speed of light, (3×10^8 m/s), the range R of 150 m (pulse round-trip distance 300 m) would produce a pulse frequency $f = c/2R = 10^6$ Hz. If the frequency is measured by counting pulses for 1 second and the count is accurate to 1 pulse, the frequency — and hence the range — will be known to an accuracy of 1 part in 10^6. For a range of 150 m, the range error would be 0.15 mm. The accuracy of the frequency-measuring equipment sets an ultimate limit on how well the range is measured.

The distance determined from the frequency measurement includes not only the external distance 2R covered by the pulse but an effective internal distance S_{int} due to pulse travel and propagation delay inside the radar. The true range R is therefore

$$R = \frac{c}{2f} - S_{int}$$

The internal range S_{int} can be determined by rotating the beam splitter through 90° so that it reflects the laser pulse directly to the detector. In effect, this sets R to zero. The value of S_{int} can be determined from the resulting pulse frequency f_{int}; i.e., $S_{int} = c/2f_{int}$.

This setup may overtax the laser or may produce a frequency that is inconvenient to measure. This can be dealt with by introducing a known delay into the system and modifying the range relation accordingly. Otherwise, S_{int} could be determined by measuring the frequency for an accurately known range and solving the range relation for S_{int}.

This work was done by C. Martin Berdahl of Caltech for **NASA's Jet Propulsion Laboratory.** *For further information, Circle 15 on the TSP Request Card.*
NPO-14901

Books and Reports

These reports, studies, and handbooks are available from NASA as Technical Support Packages (TSP's) when a Request Card number is cited; otherwise they are available from the National Technical Information Service.

Solar-Site Test Module

Small test set interrogates solar-energy data-acquisition systems.

A 32-page report describes a portable test module used for onsite checkout of DOE/NASA solar-energy demonstration installations. Although the report and the module are specific to the DOE/NASA application, the report nonetheless contains some general information and ideas that may assist engineers and others designing similar units.

A commercial portable microcomputer is the basic hardware of the test module. It is custom programed to monitor the status of an operating solar-energy installation. The site is fully instrumented with temperature sensors, flow-rate monitors, and other transducers; and data are collected and stored by an instrument called the SDAS (site data acquisition system). The portable unit interfaces with the SDAS.

The test unit consists of a microcomputer with keyboard, alphanumeric display, and printer; a cassette recorder/player for storing programs and data; and a cable for connecting to the SDAS. It weighs only about 10 lb (4.5 kg), including integral power supply and carrying case.

(continued on next page)

The unit is operated by a taped program written in BASIC (for ease of communication with the trouble shooter) and Assembly language (for speed of communication with the SDAS). The program gives the troubleshooter the option of (1) manually monitoring any sensor channel; (2) periodically and automatically monitoring from 1 to 10 channels; or (3) automatically monitoring all channels, either once or repeatedly.

In addition to a description of the test unit, the report contains information on site-data preparation (in which sensor channels and performance parameters are defined for the computer) and appendixes covering cable connector-pin assignments, descriptions and listings for both the BASIC and Assembler programs, data-input formats, and operating instructions.

This work was done by Ralph R. Kissel and Donald R. Scott of **Marshall Space Flight Center.** *Further information may be found in DOE/NASA TM-78291 [N80-30899/NSP], "Solar Site Test Module" [$6]. A paper copy may be purchased [prepayment required] from the National Technical Information Service, Springfield, Virginia 22161. The report is also available on microfiche at no charge. To obtain a microfiche copy, Circle 16 on the TSP Request Card.*

MFS-25543

Evaluation of an Evacuated-Tube Liquid Solar Collector

Indoor and outdoor thermal performances are compared.

The thermal performance of an evacuated-tube solar collector described in several previous NASA Tech Brief articles [see for example "Indoor Tests of the Concentric-Tube Solar Collector" (MFS-25390) on page 39 of Vol. 5, No. 1] is documented in a 42-page report. Tests were conducted outdoors and indoors, on an indoor solar simulator, and data were obtained for diffuse and specular reflectors.

The evacuated-tube collector uses water or water/glycol as the working fluid. Liquid flows in series through the 24 evacuated tubes (concentric glass tubes with an evacuated space between the cylinders) and the collector manifold. The external dimensions of the collector are 4 by 8 ft (1.2 by 2.4 m). The tubes are 44 in. (112 cm) in length and 2 in. (5 cm) in diameter. When filled with approximately 9 gallons (34 liters) of water, the unit weighs 185 lb (84 hg).

Excellent correlation was found between the solar-simulator-derived test results and the outdoor test results with the collector mounted on a Sun-tracking table. Thermal performance test conditions and data are listed in tables in the report and are presented graphically for the collector with both the diffuse and the shaped specular reflectors. Comparisons with previous data for a prototype show the effects of an improved manifold.

All-day efficiency of the collector and time constants were determined. Incident-angle-modifier tests were made for angles of 0°, 10°, 20°, 30°, 40°, 50°, and 60° from normal to the collector surface. All-day efficiency with a diffuse reflector was comparable to the performance with the standard shaped specular reflector.

This work was done by the Solar Energy Systems Division of Wyle Laboratories for **Marshall Space Flight Center.** *Further information may be found in DOE/NASA CR-161421 [N80-24745/NSP], "Comparison of Indoor-Outdoor Thermal Performance for the Sunpak Evacuated Tube Liquid Collector" [$6]. A paper copy may be purchased [prepayment required] from the National Technical Information Service, Springfield, Virginia 22161. The report is also available on microfiche at no charge. To obtain a microfiche copy, Circle 17 on the TSP Request Card.*

MFS-25450

Solar Water Heater Design Package

Documentation for preliminary design review

A 112-page design package contains documents pertaining to the preliminary design of a commercial domestic-hot-water heater. The system has roof- or rack-mounted solar collectors. It is adaptable to specific needs and may be installed in a new dwelling or fitted to an existing gas or electric hot-water system. Two systems are currently being installed: one in Tempe, Arizona, and the other in San Diego, California.

Each collector (a system may have more than one) weighs 100 lb (45.5 kg) when filled with water. System elements include a storage tank of 50 to 120 gallons (190 to 450 liters), an automatic control system, a pump, cascade (two-position diverter) valves, and associated plumbing. Automatic circulation of stored hot water and an automatic "dump" insure protection against freezing.

The design package includes:

- A list of drawings of system configurations, elements, parts, and installation methods;
- A description of the automatic control logic;
- Definitions of measurements that will be used to evaluate system performance;
- A description of proposed changes in the initial design;
- A list of materials in contact with potable water;
- A list of special tools for handling, installation, and maintenance;
- A manual for installation, operation, and maintenance; and
- An analysis of hazards from pressure, electricity, toxicity, flammability, gas, and hot water or steam.

This work was done by Elcam, Inc., for **Marshall Space Flight Center.** *Further information may be found in DOE/NASA CR-150605 [N80-27518/NSP], "Preliminary Design Package for Sunspot Domestic Hot Water Heating System" [$9]. A paper copy may be purchased [prepayment required] from the National Technical Information Service, Springfield, Virginia 22161. The report is also available on microfiche at no charge. To obtain a microfiche copy, Circle 18 on the TSP Request Card.*

MFS-25521

Five-City Economics of a Solar Hot-Water System

Energy savings and system costs are projected for five sites.

An analysis based on technical and economic models for a solar-energy, domestic hot-water (DHW) system for single-family residences at five sites provides such data as estimated year of payback and cumulative savings for replacing a conventional hot-water system with the solar-energy system. The system was actually installed at a site in Togus, Maine. Alternative parameters were evaluated for Albuquerque, Fort Worth, Madison (Wisconsin), and Washington, D.C. System design variables were derived from operation of the system at Togus.

Water is heated by circulating a silicone fluid through a flat-plate solar-collector array. The fluid then circulates through a double-walled heat exchanger, which transfers solar energy to water from a 120-gallon (454-liter) preheat tank. This tank services a standard electric DHW heater. One operating mode is used: The system turns on when the collector outlet temperature climbs 25° F (14° C) above the temperature of the water in the bottom of the preheat tank; it turns off when this difference falls below 8° F (4° C).

The solar-heating system can supply approximately 75 percent of the domestic hot water needed for a single-family residence in Togus, Maine. The economic payback period for the system at this site is estimated at 19 years.

Economic benefits from this solar-energy system depend primarily on two factors: the maintenance or decrease of the initial investment required and the continuing increase in the cost of conventional energy. The report includes an economic uncertainty analysis that weighs, for all 5 sites, the effect of uncertainty on the 15 variables used to evaluate profitability in the use of the solar-energy system.

This work was done by the Federal Systems Division of IBM Corp. for **Marshall Space Flight Center.** *Further information may be found in DOE/NASA CR-161510 [N80-29854/NSP], "Solar Energy System Economic Evaluation—Final Report for IBM System 2, Togus, Maine" [$8]. A paper copy may be purchased [prepayment required] from the National Technical Information Service, Springfield, Virginia 22161. The report is also available on microfiche at no charge. To obtain a* *microfiche* *copy, Circle 19 on the TSP Request Card.*
MFS-25532

Economic Evaluation of a Solar Hot-Water System

An analysis shows economic benefits at six representative sites.

A 103-page report presents the economic analysis of a solar-energy, domestic-hot-water system for six sites that are representative of a wide range of environmental and economic conditions in the continental United States. The two-tank cascade system with a flat-plate collector array, was installed at locations in Tempe, Arizona, and San Diego, California. Projected performances based on available environmental and economic data are forecast for Albuquerque, New Mexico, Fort Worth, Texas, Madison, Wisconsin, and Washington, D.C.

The report can be used to estimate the economic performance of the system for other parts of the country. For example, if it is noted that the environmental parameters of a locale are similar to those of Fort Worth, but that the conventional-energy cost is different, the savings can be scaled accordingly.

The four-mode solar-energy system that heats water for a single-family residence. Water is pumped directly from either the domestic-hot-water tank or the storage tank, through the collectors, and back into the same tank. Also included are freeze protection and auxiliary electrical heating.

Life-cycle costs, including hardware, installation, maintenance, and operating costs, are compared to net energy savings. The model for each site includes variables for long-term average environmental conditions, loads, fuel costs, and other economic factors. Federal tax credits for solar-energy systems and an economic uncertainty analysis are included. The year in which the installation begins to yield positive yearly savings and the year when cumulative savings will have paid back the original investment in the solar system are calculated.

This work was done by the Federal Systems Division of IBM Corp. for **Marshall Space Flight Center.** *Further information may be found in DOE/NASA CR-161492 [N80-31872/NSP], "Solar Energy System Economic Evaluation—Final Report for Elcam-Tempe, Tempe, Arizona, and Elcam-San Diego, San Diego, California" [$9]. A paper copy may be purchased [prepayment required] from the National Technical Information Service, Springfield, Virginia 22161. The report is also available on microfiche at no charge. To obtain a* *microfiche* *copy, Circle 20 on the TSP Request Card.*
MFS-25529

Residential Solar-Heating System Uses Pyramidal Optics

Reflective panels optimize solar-energy collection throughout the year.

A new report describes the operation, installation, and maintenance of a residential solar space-heating and domestic-hot-water system that features pyramidal optics for solar-energy collection. Subsystems include collection, storage, distribution, and control. Required construction and the proper sequence of installation are detailed in the report.

The solar-energy-collecting subsystem uses a partially variable reflector to optimize energy collection annually as the solar altitude changes. Weekly adjustments are made by motor in a moving reflector that concentrates light on a glazed absorber panel; heat is transferred to liquid flowing through the panel. The combination of fixed reflectors and the moving reflector varies the net optical gain, from 3.0 in the winter down to 1.0 in the summer. The entire collector subsystem is fitted into an attic.

Solar-heated fluid flows from the collector panel through a water tank where energy is transferred to storage. Heat exchangers for hot-water preheating and space heating are located in the storage tank. A temperature-differential controller selects among four modes of operation: direct solar heat, solar heat augmented by a heat pump, outside air heated by the same heat pump, and electrical-resistance heat. The pyramidal-optics solar-energy system can heat single-family and multifamily dwellings.

This work was done by Wormser Scientific Corp. for **Marshall Space Flight Center.** *Further information may be found in DOE/NASA CR-161203 [N80-33864/NSP], "Installation, Operation, and Maintenance for the Pyramidal Optics Solar System Installed at Yacht Cove, Columbia, South Carolina" [$9]. A paper copy may be purchased [prepayment required] from the National Technical Information Service, Springfield, Virginia 22161. The report is also available on microfiche at no charge. To obtain a microfiche copy, Circle 21 on the TSP Request Card.*
MFS-25567

Solar-Heated Bank — Marks, Mississippi

Air solar-energy collectors supply 60 percent of the space-heating load.

A 119-page report describes a solar-heating system installed in a full-service bank. The new building is a contemporary structure with a roof supporting 468 square feet (43.5 square meters) of flat-plate air solar-energy collectors. As the first solar-energy system in the geographical area, the installation has promoted much interest and features onsite temperature- and power-measurement readouts.

Problems of maintenance, system deterioration, freezeup, and control failure are minimized by using air rather than liquid solar collectors. The design also eliminates the need for a heat exchanger for space-heating.

A rock bin stores thermal solar energy. Temperature stratification is maintained by rock storage; thus, the highest available temperature, at the top of the storage bed, is used for space heating. Return air to the collectors is from the bottom of storage at a reduced temperature.

Solar-heated air is distributed to the space-heating load or to storage by an air-handling unit with both motorized and gravity-operated dampers. The solar-heating system is integrated to function with a backup heat pump and electric-resistance heating. A thermostatically-controlled exhaust fan vents the attic in hot weather.

This work was done by the First National Bank of Clarksdale for **Marshall Space Flight Center.** *Further information may be found in DOE/NASA CR-161549 [N80-33858/NSP], "Solar Heating System at Quitman County Bank, Marks, Mississippi — Final Report" [$9]. A paper copy may be purchased [prepayment required] from the National Technical Information Service, Springfield, Virginia 22161. The report is also available on microfiche at no charge. To obtain a microfiche copy, Circle 22 on the TSP Request Card.*
MFS-25558

Solar Water-Heating Performance Evaluation — San Diego, California

Energy is saved by replacing a domestic, conventional natural-gas heater with a solar-energy system.

A recently released report describes the 6-month performance of a solar-energy system that heats domestic hot water for a single-family residence in Encinitas, California, near San Diego. Energy savings for the test period averaged 1.089 million Btu (1.149 billion joules) per month. After the operating energy required for energy collection and storage is deducted, an average net monthly savings of 1.026 million Btu (1.083 billion joules) or 301 kWh is obtained.

A light load on the system prevented energy savings from reaching their potential during the test season; on the average as much as twice the hot water could have been used. Collector efficienty was 40 percent.

Solar energy from the 65-square-foot (6-square-meter) collector array is supplied to either a 66-gallon (250-liter) preheat tank (solar storage) or a 40-gallon (151-liter) domestic-hot-water tank. The temperatures of the water in the collectors, the preheat tank, and the domestic-hot-water tank are measured, and a programable controller pumps water from one of the tanks through the collectors and back to the same tank. At preset tank temperatures or at preset temperature differences between the tank and collector water, the controller switches the cascade valve to divert the flow to the proper tank.

The collector cover is 1/8-inch (3-millimeter) tempered glass. Freeze protection is provided by circulating hot water from the domestic-hot-water tank through the collectors when necessary. Auxiliary energy is supplied by natural gas.

This work was done by the Federal Systems Division of IBM Corp. for **Marshall Space Flight Center.** *Further information may be found in DOE/NASA CR-161481 [N80-27806/NSP], "Solar Energy System Performance Evaluation — Seasonal Report for Elcam San Diego, San Diego, California" [$7]. A paper copy may be purchased [prepayment required] from the National Technical Information Service, Springfield, Virginia 22161. The report is also available on microfiche at no charge. To obtain a microfiche copy, Circle 23 on the TSP Request Card.*
MFS-25502

Solar-Heated and Cooled Savings and Loan Building — Leavenworth, Kansas

A heating and cooling system for a two story building

A 310-page report describes a solar-heating and cooling system installed in the Citizens Mutual Savings and Loan Association, Leavenworth, Kansas. The system is expected to furnish 90 percent of the annual heating load, 70 percent of the cooling load, and all of the domestic hot-water load of the two-story structure. The building has two floors with 9,000 square feet (836 square meters) of conditioned space.

Flat-plate solar-energy collectors are roof-mounted and oriented to face south with a slope 40° to the horizontal. Nine computer-run comparisons were made to determine the optimum collector type and area. The building contains fully-automated temperature controls and is divided into five separate temperature-load zones, each with an independent heat pump.

Three different rates of flow are possible through the collector panels.

The lowest rate produces hot water for the absorption chillers, and the other two collect energy for heating. Two storage tanks are provided: one tank for summer use and both tanks for winter use when maximum storage is needed.

The control system is pneumatic and includes step controllers for sequential control of the five absorption-chilling units. A fan system cools from outdoor air until outside temperatures become too high. Also, the high vaulted ceiling of the main banking area results in temperature stratification, permitting the installation of dual return-air dampers. One near the roof peak recovers hot air for winter recycling, and the other near the floor recovers cooler air for summer.

This work was done by the Citizens Mutual Savings & Loan Association of Leavenworth, Kansas, for **Marshall Space Flight Center.** *Further information may be found in DOE/NASA CR-161484 [N80-29848/NSP], "Solar Heating and Cooling System Installed at Leavenworth, Kansas — Final Report" [$17]. A paper copy may be purchased [prepayment required] from the National Technical Information Service, Springfield, Virginia 22161. The report is also available on microfiche at no charge. To obtain a microfiche copy, Circle 24 on the TSP Request Card.*
MFS-25520

Solar-Energy Landmark Building — Columbia, Missouri

An attractive installation supplies space heating for a four-story, camput Visitors Center.

The 299-page final report on a solar-energy system at the Visitors Center on the Stephens College campus in Columbia, Missouri, includes design, cost, installation, maintenance, and performance details of the project. The four-story center will house the Admissions Office, the Faculty Lounge, a two-story art gallery, and nine rooms for guests of the college. The building is situated adjacent to a well-traveled intersection and is a highly visible landmark.

The solar-energy system, designed to meet 71 percent of the heating load for the building, includes 176 hydronic flat-plate collectors and a water-to-water heat exchanger. Solar-heated water is stored in a 5,000-gallon (18,900-liter) water-storage tank located in the basement equipment room. A natural-gas-fired boiler supplies hot water to the heating system when the solar-heat supply fails to meet the demand.

The collector array is mounted several inches (centimeters) off the roof on brackets that reduce the number of roof penetrations required, thereby minimizing the chance of roof leaks. The roof slopes 50° from the horizontal and faces south.

Building construction started in November 1977 and was completed in January 1979. The solar-energy-system installation and acceptance test were completed in May 1979. With the exception of some problems in the control system, performance has been exceptional. Although the site is not fully instrumented, an operating panel with various readouts, including an integration (British thermal unit) meter, gives interested visitors a quick summary of the system operation.

This work was done by the Building and Grounds Department of Stephens College for **Marshall Space Flight Center.** *Further information may be found in DOE/NASA CR-161485 [N80-29849/NSP], "Solar Space Heating For the Visitors Center, Stephens College, Columbia, Missouri — Final Report" [$17]. A paper copy may be purchased [prepayment required] from the National Technical Information Service, Springfield, Virginia 22161. The report is also available on microfiche at no charge. To obtain a microfiche copy, Circle 25 on the TSP Request Card.*
MFS-25524

Solar Heating for an Observatory — Lincoln, Nebraska

Most of the space heating for a 50-seat observatory is supplied by solar energy.

A new report describes a solar-energy system that provides 60 percent of the space heating for the 50-seat Hyde Memorial Observatory in Lincoln, Nebraska. The system includes nine flat-plate collectors, a rock-storage bin, blowers, controls, and ducting. A natural-gas furnace supplies additional energy when Sunlight cannot meet the space-heating demand.

The system has five modes of operation: supplying heat directly from the collectors, supplying heat from storage, storing solar energy, auxiliary heating, and summer venting to protect against high temperatures that are damaging to the collectors.

A total of 224.74 million Btu (237.11 billion joules) was measured in the plane of the collector array during the reporting period. The system collected 35.8 million Btu (37.8 billion joules) of the available energy, for a collector-array efficiency of 16 percent. During periods when the collector array was active, a total of 103.92 million Btu (109.64 billion joules) was measured in the plane of the collector array. Therefore, the operational collector efficiency was 35 percent.

Definitions of performance factors, solar-energy-system performance equations, and long-term average weather conditions are collected in appendixes to the report. Although the insolation was below the long-term average for the Lincoln, Nebraska, site, the net fossil-energy savings for the 12-month report period were measured at 11.31 million Btu (11.93 billion joules) or the equivalent of 1.9 barrels (300 liters) of oil. Unquantified system losses into the heated space from the storage bin and ductwork increase the actual savings beyond this figure.

This work was done by the Federal Systems Division of IBM Corp. for **Marshall Space Flight Center.** *Further information may be found in DOE/NASA CR-161495 [N80-29851/NSP], "Solar Energy System Performance Evaluation — Seasonal Report for SEECO Lincoln, Lincoln, Nebraska" [$7]. A paper copy may be purchased [prepayment required] from the National Technical Information Service, Springfield, Virginia 22161. The report is also available on microfiche at no charge. To obtain a microfiche copy, Circle 26 on the TSP Request Card.*
MFS-25525

Two-Story Residence With Solar Heating — Newnan, Georgia

A warm-air-collector system delivers heat to a two-story building.

A solar-energy system installed in a two-story dwelling about 40 miles (65 kilometers) southwest of Atlanta in Newnan, Georgia, was evaluated over the period from June 1979 through April 1980. The system consists of 14 warm-air collectors with a total area of 392 square feet (36.4 square meters), a rock-thermal-storage bin, an air handler, heat exchangers, a domestic-hot-water (DHW) preheat tank, and associated controls, plumbing, and air ducting. A report featuring an overall performance assessment as well as details on operation and maintenance is now available.

Air-handler blowers deliver hot air either directly from the solar collectors or from the rock-bin storage. Summer venting and DHW preheating is also included; a 40-gallon (151-liter) electric hot-water tank is supplied water from the 80-gallon (303-liter) preheat tank. When outdoor temperatures drop below 15° F (−9° C), auxiliary heating is available from electric resistance heaters and an electric heat pump.

An average building temperature of 72° F (22° C) was maintained during the 11-month reporting period. The measured space-heating load was 23.06 million Btu (24.33 billion joules), with the solar fraction totaling 47 percent. When accounted for, unmeasured losses from the solar-heating system into the heated space approximately doubled the measured net electrical savings for the test period, which were the equivalent of 0.9 barrel (140 liters) of oil.

This work was done by The Federal Systems Division of IBM Corp. for **Marshall Space Flight Center.** *Further information may be found in DOE/NASA CR-161494 [N80-29853/NSP], "Solar Energy System Performance Evaluation — Seasonal Report for Contemporary Newnan, Newnan, Georgia" [$8]. A paper copy may be purchased [prepayment required] from the National Technical Information Service, Springfield, Virginia 22161. The report is also available on microfiche copy. Circle 27 on the TSP Request Card.*

MFS-25526

Solar-Energy Heats a Transportation Test Center—Pueblo, Colorado

Warehouses and similar buildings could be heated by this flat-plate-collector system.

A petroleum-base, thermal-energy transport fluid circulating through 583 square feet (54 square meters) of flat-plate solar collectors accumulates much of the energy needed for space heating and domestic hot water at the U.S. Department of Transportation Test Center in Pueblo, Colorado. A report that is now available describes the operation, maintenance, and performance for this system, possibly suitable for warehouses and similar buildings, along with the energy savings for the test period from February 1979 to January 1980.

The measured daily average incident insolation in the plane of the collector array for the test period was about 10 percent below the long-term daily average for the area. The measured average outdoor ambient temperature for the period when solar heating was necessary was 51° F (11° C). For the report period, the solar-heating fraction was 31 percent, and the hot-water solar fraction was 79 percent. Since losses from transport piping that actually went toward heating the building were not measured and since much stored energy was lost because of the low hot-water consumption, the actual performance of the system can be above these figures.

This work was done by the Federal Systems Division of IBM Corp. for **Marshall Space Flight Center.** *Further information may be found in DOE/NASA CR-161493 [N-80-29850/NSP], "Solar Energy System Performance Evaluation — Seasonal Report for Colt Pueblo, Pueblo, Colorado" [$8]. A paper copy may be purchased [prepayment required] from the National Technical Information Service, Springfield, Virginia 22161. The report is also available on microfiche at no charge. To obtain a microfiche copy, Circle 28 on the TSP Request Card.*

MFS-25527

Single-Family-Residence Solar Heating — Carlsbad, New Mexico

About half of the space-heating and hot-water energy requirement is supplied by the Sun.

A solar-energy system described in a recent report is located in a single-family residence at Carlsbad Caverns National Park, New Mexico. This hot-air, solar-heating and hot-water system includes 408 square feet (38 square meters) of flat-plate air collectors, a rock-storage bin, an energy-transport system, an air-to-water heat exchanger, controls, and a hot-water preheat tank that supplies preheated water to an electric hot-water tank. An oil, hot-air furnace supplies auxiliary space heating. Electricity powers the air-handler blower and hot-water preheat pump.

Measured average daily insolation at the test site for the 12 months of the reporting period was 9 percent below the long-term average for the area, indicating a few more cloudy days than normal. However, space-heating and hot-water loads were near expected values based on results derived from a modified f-chart analysis, which uses measured weather and subsystem loads as inputs. Solar energy provided 43 percent of the space-heating and 53 percent of the hot-water energy. The total net energy savings during the reporting period amounted to 23.072 million Btu (24.34 billion joules or 6,761 kWh).

This work was done by the Federal Systems Division of IBM Corp. for **Marshall Space Flight Center.** *Further information may be found in DOE/NASA CR-161508 [N80-29856/NSP], "Solar Energy System Performance Evaluation — Seasonal Report for IBM System 1B, Carlsbad, New Mexico" [$7]. A paper copy may be purchased [prepayment required]*

from the National Technical Information Service, Springfield, Virginia 22161. The report is also available on microfiche at no charge. To obtain a microfiche copy, Circle 29 on the TSP Request Card.
MFS-25528

Multimode Solar-Heating System — Columbia, South Carolina

Operating-energy needs and control problems reduced winter energy savings.

A six-mode pyramidal-optics solar-energy system in a four-unit townhouse in Columbia, South Carolina, netted unexpectedly-low winter energy savings. Its performance over a 12-month period (from June 1979 through May 1980) is described in a report that is now available.

Control failures, occurring most severely in February, caused electrical strip heaters to turn on unnecessarily while solar heat was available. Consequently, almost 5 million Btu (5 billion joules) were wasted in 1 month.

Even if the controls had operated correctly, fossil-fuel savings would not have been impressive; much of the energy accumulated by the solar collectors was dissipated in losses through heat exchangers and ductwork, while operating-energy requirements for the many motors and lengths of tubing were high.

For this site and solar-energy application, more net energy could have been realized with a system utilizing only a direct space-heating mode or a hot-water-preheating mode. The most inefficient mode of the tested system was the one in which heat pumps mingled alternatively storage or collector energy with electric-heat-strip energy to satisfy the space-heating demand. The direct-solar-heating mode of the same system performed very well in comparison.

This work was done by The Federal Systems Division of IBM Corp. for ***Marshall Space Flight Center.*** *Further information may be found in DOE/NASA CR-161546 [N80-31880/NSP], "Solar Energy System Performance Evaluation — Seasonal Report for Wormser, Columbia, South Carolina" [$9]. A paper copy may be purchased [prepayment required] from the National Technical Information Service, Springfield, Virginia 22161. The report is also available on microfiche at no charge. To obtain a microfiche copy, Circle 30 on the TSP Request Card.*
MFS-25552

Solar-Heated Swimming School — Wilmington, Delaware

An energy alternative to natural gas pool heating.

During the winter of 1977, with the low availability of natural gas, the Wilmington Swim School in Wilmington, Delaware, was judged to be a nonessential user and as such faced possible cutbacks or the elimination of its gas allocation. Solar energy now supplies much of the total annual building energy load at this school, thus alleviating the dependence on natural gas. A new report describes the operation, installation, and performance of the solar-energy system.

The active solar-energy system is composed of 2,500 square feet (230 square meters) of liquid flat-plate collectors connected to a 3,600-gallon (13,600-liter), concrete storage tank located belowground near the building. An extension of the building completed in 1979 incorporates a vertical-wall, passive collection system that provides about 25 percent of the heated-fresh-air for the office area. The active collector area is the maximum that could fit on the building roofs.

A microcomputer-based control system selects the optimal application of stored energy among the space-heating, domestic-hot water, and pool-heating alternatives. Selection is based on seasonal energy availability and the specific thermal requirements of each load. For example, if winter space heating requires water in excess of 120° F (49° C), stored water below this temperature will be used for pool heating, which only requires temperatures in excess of 85° F (29° C); any heat stored below this temperature may be used for domestic water preheating.

This work was done by Cooperson Brack Associates for ***Marshall Space Flight Center.*** *Further information may be found in DOE/NASA CR-161538 [N80-31878/NSP], "Solar Energy System Demonstration Project at Wilmington Swim School, New Castle, Delaware — Final Report" [$8]. A paper copy may be purchased [prepayment required] from the National Technical Information Service, Springfield, Virginia 22161. This report is also available on microfiche at no charge. To obtain a microfiche copy, Circle 31 on the TSP Request Card.*
MFS-25548

Winter Performance of a Domestic Solar-Heating System — Duffield, Virginia

Sunlight supplies 39 percent of the heat load, saving 9 barrels of fuel oil in one heating season.

The wintertime performance of a solar-energy system in a Virginia home is described in a report that covers the period from October 1979 through March 1980. The house is a two-story, single-family residence with a floor area of approximately 1,940 square feet (180 m^2). Solar energy is collected with roof-mounted air flat-plate collectors. It is stored in a rock bin on the lower level of the house and is transferred to a water-preheat tank whenever the system is storing energy. The water is heated to its final temperature by electrical heaters in another tank. A heat pump supplies heat to the house when necessary.

Although the system was designed to furnish 24 percent of the space heating and heat for domestic hot water, it furnished 39 percent, even though the average daily insolation was 34 percent below normal and the average outdoor temperature was 5° F (2.8° C) below normal. The net energy saved by the use of solar energy instead of electricity was the equivalent of approximately 9 barrels (1,400 liters) of oil.

The solar-energy system was designed with the aid of system-solar-fraction charts (f-charts). The discrepancy between the measured system

(continued on next page)

solar fraction of 39 percent and the expected value of 24 percent possibly show that the f-chart simulation is not valid for the Duffield installation. Reasons for the discrepancy are under investigation.

This work was done by the Federal Systems Division of IBM Corp. for **Marshall Space Flight Center.** *Further information may be found in DOE/NASA CR-161507 [N80-30892/NSP], "Solar Energy System Performance Evaluation — Seasonal Report for Solaron-Duffield, Duffield, Virginia [$8]. A paper copy may be purchased [prepayment required] from the National Technical Information Service, Springfield, Virginia 22161. The report is also available on microfiche at no charge. To obtain a microfiche copy, Circle 32 on the TSP Request Card.*
MFS-25540

One-Year Assessment of a Solar Space/Water Heater — Clinton, Mississippi

Unit is integrated into the space-heating and hot-water systems of a dormitory building.

System 4, a solar-energy system for space heating and domestic-hot-water preheating, was evaluated during 1 year of operation at a training-center dormitory in Mississippi. As stated in a new report, the system satisfied 32 percent of the building heating load.

The system is designed to supply 48 percent of heating needs. The relatively low contribution of solar energy in the installed system is explained by a combination of correctable and uncontrollable factors: The solar array, which is close to a dirt road, became coated with dust during dry spells and did not receive full insolation. Air leakage into the collector array and an open bypass valve also reduced efficiency. In addition, the winter was somewhat cooler than usual.

System 4 is a prepackaged unit. Solar energy is absorbed in flat-plate collectors with air as the heat-transport medium. The collector area for the unit evaluated in the report is 259 ft^2 (24 m^2). A blower circulates air from the collector array to a rock storage bed. Another blower circulates air to the building from either the collector array or the rock storage bed. A heat exchanger at the bed absorbs heat for domestic hot-water use. Auxiliary heat is furnished by a 4-kW electric heater in each of two hot-water tanks and a 20-kW strip heater in an air duct.

The report describes the performance of the system and each of its subsystems (collector array, storage, hot water, and space heating). It presents operating energy requirements (the energy needed to transport solar energy to the point of use) and energy savings. Appendixes contain definitions of performance factors and solar terms, a listing of equations used in performance assessment, and a tabulation of long-term average weather conditions.

This work was done by the Federal Systems Division of IBM Corp. for **Marshall Space Flight Center.** *Further information may be found in DOE/NASA CR-161509 [N80-30893/NSP], "Solar Energy System Performance Evaluation — Seasonal Report for IBM System 4 at Clinton, Mississippi" [$8]. A paper copy may be purchased [prepayment required] from the National Technical Information Service, Springfield, Virginia 22161. The report is also available on microfiche at no charge. To obtain a microfiche copy, Circle 33 on the TSP Request Card.*
MFS-25539

Fire-Station Solar-Energy System — Kansas City, Missouri

Screen-walled solar collectors are part of an award-winning architectural design.

About half of the space heating and 75 percent of the heat for domestic hot water at a Kansas City fire station are provided by a solar-energy system, described in a 157-page report. A historical narrative of the project is included, along with detailed drawings, charts, and product literature.

The fire station has two areas: an operations area occupied by the firemen and the apparatus bay occupied by the fire equipment. The operations area covers 2,800 square feet (260 square meters) and has a winter design temperature of 70° F (21° C); the apparatus bay covers 6,000 square feet (560 square meters) with a winter design temperature of 50° F (10° C). The solar collectors, are an integral part of the apparatus bay. Two arrays of flat-plate, air solar collectors are mounted on the roof, and one large array extends from the roof to the ground, forming the south wall. Ninety-six collectors are integrated into the wall.

East and west screen walls create an attractive profile for the fire station without significantly affecting collector performance. A regional association awarded a certificate of design excellence to the architect for the conception of these screens. A concrete-box storage subsystem, a domestic-hot-water preheat tank, blowers, pumps, heat exchangers, air ducting, controls, and plumbing complete the solar-energy system.

This work was done by the city of Kansas City, Missouri, for **Marshall Space Flight Center.** *Further information may be found in DOE/NASA CR-161513 [N80-30895/NSP], "Solar Heating and Domestic Hot Water System Installed at Kansas City Fire Station, Kansas City, Missouri — Final Report" [$11]. A paper copy may be purchased [prepayment required] from the National Technical Information Service, Springfield, Virginia 22161. The report is also available on microfiche at no charge. To obtain a microfiche copy, Circle 34 on the TSP Request Card.*
MFS-25538

Solar-Heated Ranger Station — Glendo, Wyoming

Solar energy heats a Wyoming residential ranger station.

The Glendo Reservoir Ranger Station in Wyoming, occupying 1,078 square feet (100 square meters), is the residence of a State park ranger. A solar-energy system to provide 46 percent of the space-heating and 80 percent of the building domestic-hot-water energy requirements was installed in the existing building, and system performance was monitored from January through December 1979. A report that is now available describes the system and each of its subsystems: collector-array, storage, hot-water, and space-heating. Long-term average and actual weather conditions are included in the report for the test site, as well as system performance values and energy savings.

Water is the only heat-transfer medium used at the installation. A 1,000-gallon (3,785-liter) hot-water-storage tank is supplied with energy from 294 square feet (27.3 square meters) of flat-plate collectors. A domestic-hot-water tank, pumps, heat exchangers, and a controller complete the five-mode solar-energy system. A gas furnace supplies auxiliary space heating, and electrical-resistance elements supplement the hot-water supply.

An abnormally high number of cloudy days reduced the measured average daily insolation for the test year. The solar-energy system was able to supply 22 percent of the space-heating and 58 percent of the hot-water energy demand. Net energy savings for the year were about 30 million Btu (32 billion joules).

This work was done by The Federal Systems Division of IBM Corp. for **Marshall Space Flight Center.** *Further information may be found in DOE/NASA CR-161520 [N80-30896/NSP] "Solar Energy System Performance Evaluation — Seasonal Report for IBM System 3, Glendo, Wyoming" [$8]. A paper copy may be purchased [prepayment required] from the National Technical Information Service, Springfield, Virginia 22161. The report is also available on microfiche at no charge. To obtain a microfiche copy, Circle 35 on the TSP Request Card.*

MFS-25537

Economic Evaluation of a Solar Hot-Water System — Palm Beach County, Florida

Solar-energy costs and savings for a residential hot-water system are projected over a 20-year life cycle.

A solar-energy system designed to supply 90 percent of the domestic-hot-water energy requirements for the home of the refuge manager of the Loxahatchee National Wildlife Refuge in Palm Beach County, Florida, is the subject of a recent report. An economic evaluation of the system at this site uses technical and economic models with inputs based on the actual working characteristics of the installed system and on local conditions. The analysis relates system cost to anticipated savings over a 20-year period. Based on the analysis of the Loxahatchee site, economic viability is calculated for four other sites in the continental United States.

Tables of variables enable the prediction of the economic performance of the solar hot-water system at various locations, with different values for insolation and fossil-fuel cost. For example, at an Albuquerque, New Mexico, site, the total initial cost of the system in 1980 dollars, before adjustment for Federal tax credit, is $2,604. The 1980 value of fuel costs and other costs anticipated over a 20-year period without solar energy is $6,282; with solar energy, it is $2,364. The figures indicate positive savings with the solar installation in 1 year and total payback of investment costs after 10 years of operation.

This work was done by the Federal Systems Division of IBM Corp. for **Marshall Space Flight Center.** *Further information may be found in DOE/NASA CR-161512 [N80-30894/NSP], "Solar Energy System Economic Evaluation — Final Report for Semco-Loxahatchee, Loxahatchee National Wildlife Refuge, Palm Beach County, Florida" [$8]. A paper copy may be purchased [prepayment required] from the National Technical Information Service, Springfield, Virginia 22161. The report is also available on microfiche at no charge. To obtain a microfiche copy, Circle 36 on the TSP Request Card.*

MFS-25536

Residential System — Lansing, Michigan

Air collectors are combined with water storage.

A performance evaluation of a solar-energy system supplying space heating and hot water to a 1,300-square foot (121-square-meter) residence in Lansing, Michigan, is featured in an 87-page report, along with a discussion of typical system operation, operating energy, energy savings, and maintenance. During the reporting period from April 1979 to March 1980, the measured average outdoor ambient temperature was 48° F (9° C). Solar energy supplied 15 percent of the measured load for hot water and space heating.

The Lansing installation uses 278 square feet (25.8 square meters) of hot-air flat-plate collectors, three 120-gallon (454-liter) meter storage tanks, a liquid/air heat exchanger, an energy transport module, pumps, controls, and transfer lines. The unusual combination of water storage with an air collecting medium stores heat in about one-third the space of a rock-bin system, but with consequent loss of heat-exchanging efficiency.

Unusual operating conditions during the report period made it difficult to assess performance. A large amount of hot-water was consumed in the final 7 months — generally over 225 gallons (852 liters) per day, and as a result almost all the solar energy collected during this period was used in support of the hot-water subsystem. Solar-energy support was greatly reduced for the space-heating subsystem, contrary to design expectations. Nonetheless, net savings were approximately 21 million Btu (22 billion joules).

This work was done by the Federal Systems Division of IBM Corp. for **Marshall Space Flight Center.** *Further information may be found in DOE/NASA CR-161491 [N80-29855/NSP], "Solar Energy System Performance Evaluation — Seasonal Report for Fern Lansing, Lansing, Michigan" [$8]. A paper copy may be purchased [prepayment required] from the National Technical Information Service, Springfield, Virginia 22161. The report is also available on microfiche at no charge. To obtain a microfiche copy, Circle 37 on the TSP Request Card.*

MFS-25530

Solar Space-Heating System — Yosemite National Park, California

Performance over 12 months suffered from low insolation and equipment breakdown.

A report on a solar-heating system in the Visitors Center at Yosemite National Park, California, assesses system performance from May 1979 through April 1980. The installation has 980 square feet (91 square meters) of liquid flat-plate solar collectors, water energy storage, heat exchangers, pumps, controls, and plumbing.

Design expectations that over half the annual heating demand would be supplied by solar energy were not met due to large building-heat loss, below-average insolation, and maintenance downtime during the test period. Several large pine trees that add to the attractiveness of the Visitors Center also shade the building and cause significant performance penalties. Nonetheless, fossil-energy savings amounted to 109 million Btu (116 billion joules); the potential savings with fewer equipment failures is higher.

The system has four modes of operaton:

- Collector to storage via a heat exchanger, when the temperature difference between the two is sufficient;
- Storage to space heating via a second heat exchanger upon demand, when storage temperature exceeds 105° F (58° C);
- Mixed solar and conventional heating, at storage temperatures down to 90° F (32° C); and
- Conventional heating, using an oil-fired boiler to deliver hot water for building space heating to a third heat exchanger.

This work was done by the Federal Systems Division of IBM Corp. for **Marshall Space Flight Center.** *Further information may be found in DOE/NASA CR-161539 [N80-31883/NSP], "Solar Energy System Performance Evaluation — Seasonal Report for Colt Yosemite, Yosemite National Park, California" [$8]. A paper copy may be purchased [prepayment required] from the National Technical Information Service, Springfield, Virginia 22161. The report is also available on microfiche at no charge. To obtain a microfiche copy, Circle 38 on the TSP Request Card.*
MFS-25553

Motel Solar-Hot-Water System — Dallas, Texas

Solar energy meets most of the hot-water requirements of a large motel.

A report describes a solar-energy system designed to satisfy up to 64 percent of the hot-water demands of a 120-room motel. Key system components include a 1,000-square-foot (93-square-meter) roof-mounted collector array, a 1,000-gallon (3,800-liter) storage tank, a tube-in-shell heat exchanger, and three domestic hot-water tanks.

The collector array comprises 30 water-filled units in a series/parallel arrangement. A pump circulates water from the bottom of the storage tank, through the collectors, and back into the storage tank. A second pump circulates water from the storage tank, through the shell side of the heat exchanger, and back into the storage tank. A third pump circulates water between the domestic hot-water tanks and the tube side of the heat exchanger.

The pumps and valves are automatically controlled at preset temperature differences between the collectors and storage tank and between the storage tank and one of the domestic hot-water tanks. Pressure gages are installed for performance monitoring and manual valves are included for maintenance.

The report contains calibration instructions for the differential-temperature controllers, emergency-shutdown instructions, maintenance procedures, and a suggested form for operating records and performance analysis. Manufacturers' data sheets on system components are also included.

This work was done by Day's Inn of America, Inc., for **Marshall Space Flight Center.** *Further information may be found in DOE/NASA CR-161570 [N81-10521/NSP], "Solar Hot Water System Installed at Day's Inn Motel, Dallas, Texas [Valley View]" [$6]. A paper copy may be purchased [prepayment required] from the National Technical Information Service, Springfield, Virginia 22161. The report is also available on microfiche at no charge. To obtain a microfiche copy, Circle 39 on the TSP Request Card.*
MFS-25575

Motel Solar-Hot-Water System With Nonpressurized Storage — Jacksonville, Florida

Energy is transferred to pressurized domestic-hot-water tanks.

A solar-energy system providing 65 percent of the domestic-hot-water (DHW) demand at a Jacksonville, Florida, motel uses a 1,000-gallon (3,780-liter) nonpressurized storage tank to supply solar energy to existing motel hot-water lines, which are pressurized. Heat is transferred to each of three domestic-hot-water tanks by circulating water from these tanks through the tube side and water from the storage tank through the shell side of a tube-and-shell heat exchanger. The parts and operation of this system are described, along with maintenance, performance, and warranty information, in a report that is available upon request.

The modular roof-mounted solar-energy collectors have copper absorber plates. They are painted flat black, glazed, and insulated on the back. The collector array and piping are graded to drain into the storage tank whenever the collector circulating pump is not operating. The storage tank is vented to the atmosphere, and two vacuum breakers for the collectors admit air during draindown to speed drainage and prevent vapor problems.

When the absorber plate of one collector becomes 12° F (7° C) warmer than the bottom of the storage tank, the collector circulating pump turns on to fill all the collectors and begin their operation. When the temperature difference drops to a predetermined level, the pump turns off and the collectors drain back into storage.

If the temperature at the top of the storage tank is 30° F (17° C) greater than the temperature at the bottom of any of the three DHW tanks, water from the cold tanks is circulated through the heat exchanger, along with hot water from the storage tank. This heat-exchanger system, operating independently of the solar-collector system, shuts off again when the temperature differences decrease to 15° F (8° C).

This work was done by Day's Inn of America, Inc., for **Marshall Space Flight Center.** *Further information may be found in DOE/NASA CR-161560 [N81-10523/NSP], "Solar Hot Water System Installed at Day's Inn Motel, Jacksonville, Florida" [$6.50]. A paper copy may be purchased [prepayment required] from the National Technical Information Service, Springfield, Virginia 22161. The report is also available on microfiche at no charge. To obtain a microfiche copy, Circle 40 on the TSP Request Card.*
MFS-25569

Closed-Circulation System for Motel Hot Water — Savannah, Georgia

Solar-energy collectors are supported by guy wires.

A solar-energy hot-water-supply system installed in a Savannah, Georgia, motel has roof-mounted solar collectors supported by guy wires. The collectors circulate a 50-percent ethylene glycol solution rather than relying on a drain system for freeze protection. A heat exchanger transfers energy to the domestic hot water. A recent report describes the equipment and its operation and maintenance. The system is well tested, and at the Savannah installation no major problems were encountered with its operation.

The 1,000-gallon (3,780-liter) fiberglass storage tank contains two heat exchangers: One heats water in the storage tank with fluid from the solar collectors; and the other preheats the cold-water supply as it passes through to the domestic hot-water heaters, which have electrical elements for supplementing energy from the Sun. Temperature sensors are located in the collector plates and in the storage tank, and controller pumps are turned on or off according to the measured temperature differential.

Costly structural-steel mounting for the solar collectors was bypassed by using guy wires to secure the collector array to the roof. Although no roof penetrations were required over the occupied space, the mounting system is rated to withstand 120-mile-per-hour (193-kilometer-per-hour) winds. The solar-energy system provides an average of 2,440 gallons (9,240 liters) of 140° F (60° C) water at the installation.

This work was done by Day's Inn of America, Inc., for **Marshall Space Flight Center.** *Further information may be found in DOE/NASA CR-161561 [N81-10522/NSP], "Solar Hot Water System Installed at Day's Inn Motel, Savannah, Georgia" [$6.50]. A paper copy may be purchased [prepayment required] from the National Technical Information Service, Springfield, Virginia 22161. The report is also available on microfiche at no charge. To obtain a microfiche copy, Circle 41 on the TSP Request Card.*
MFS-25572

Solar Heating for a Restaurant — North Little Rock, Arkansas

Large building hot-water consumption affects solar-energy-system design.

A solar-heating system designed to supply a major portion of the space heat and water heat for a restaurant in North Little Rock, Arkansas, was installed in December 1979. The system uses flat-plate liquid collectors circulating an antifreeze solution. Equipment specifications and modifications to existing building heating and hot-water systems are described along with other information in a report that is now available.

Four rows of roof-mounted solar collectors at the North Little Rock site are surrounded by an architectural screen for an attractive building profile. Solar-collector area was determined by optimizing building load, collector output, and cost. Architectural considerations led to two of the collectors being tilted at an angle of only 25°, although the optimum is greater; the performance penalty for this modification is slight.

Because of the continual demand for domestic hot water at the restaurant, storage is less important than at other sites; storage capacity is equal to the estimated daily hot-water requirement. Two heat exchangers between the collector fluid and the potable hot-water supply prevent water contamination from the antifreeze solution flowing through the collectors. Water is pumped directly from storage through a coil for space heating. A purge coil in the collector loop protects against failure when more heat is collected than can be used or stored.

This work was done by Shoney's South, Inc., for **Marshall Space Flight Center.** *Further information may be found in DOE/NASA CR-161557 [N81-10520/NSP], "Solar Heating and Hot Water System Installed at Shoney's Restaurant, North Little Rock, Arkansas — Final Report" [$11]. A paper copy may be purchased [prepayment required] from the National Technical Information Service, Springfield, Virginia 22161. The report is also available on microfiche at no charge. To obtain a microfiche copy, Circle 42 on the TSP Request Card.*
MFS-25568

Motel Solar Hot-Water Installation — Atlanta, Georgia

An analysis of motel hot-water requirements insures compatibility with solar-energy system design.

Such considerations as the hardness of local water, average insolation for the site, and daily hot-water requirements are studied in a report describing two new solar-energy hot-water units at a motel in Atlanta, Georgia. The two units are designed to supply 61 percent of the total motel hot-water demand annually. Demand is based on an anticipated 85 percent

(continued on next page)

occupancy in the two buildings, each of which is served by a separate solar-energy system.

The report includes drawings, operating and maintenance instructions, and test results for 1 day of system operation.

Both buildings use 16 liquid flat-plate solar-energy collectors; the systems differ only in having slightly different controllers. Each includes a cement-lined steel tank for hot-water storage. As domestic hot water is consumed, water flows into them from the storage tanks.

Electric resistance units in the hot-water tanks heat the solar-heated water, if necessary, to reach the thermostat setting. When collector temeratures approach freezing or when there is an interruption in electrical power, the collectors drain to prevent failure. When working conditions are reinstated, the collectors are automatically refilled.

This work was done by Day's Inn of America, Inc., for **Marshall Space Flight Center.** *Further information may be found in DOE/NASA CR-161559 [N81-10519/NSP], "Solar Hot Water System Installed at Day's Lodge, Atlanta, Georgia" [$5]. A paper copy may be purchased [prepayment required] from the National Technical Information Service, Springfield, Virginia 22161. The report is also available on microfiche at no charge. To obtain a microfiche copy, Circle 43 on the TSP Request Card.*
MFS-25564

Building With Integral Solar-Heat Storage — Starkville, Mississippi

The roof-supporting column houses a rock-storage bin.

A solar space-heating system in a Starkville, Mississippi, bank has a rock thermal-storage bin that is an integral part of the building design. The bin is a steel container, with the exterior insulated and plastered, that runs from floor to ceiling in the bank lobby. Roof-supporting trusses are cantilevered from the steel column. A description of the system, including technical installation and operation data, is included in a report that is now available.

The solar-energy system supplies more than half the building space-heating load. Since very little hot water is used, hot water is supplied by conventional heaters. A special air-handling unit, with low-leakage dampers and a motor with high-temperature insulation, moves air over the solar collectors and into storage and connects to the conventional building cooling and air-duct distribution system. A two-stage electric-resistance heater in the ductwork makes up any additional building heat required.

The rock-storage bin in the lobby column is deeper and narrower than is normally recommended, due to its unusual location. To keep the airflow resistance at a minimum, individual pebble size was increased from the standard 3/4 to 1-1/2 in. (2 to 4 cm) to 2 in. (5 cm). A building thermostat integrates the following modes of operation: heating from collectors, heating from storage, storing heat, conventional backup heat, and conventional cooling.

This work was done by Security State Bank, Starkville, Mississippi, for **Marshall Space Flight Center.** *Further information may be found in DOE/NASA CR-161550 [N81-10518/NSP], "Solar Heating System at Security State Bank, Starkville, Mississippi — Final Report" [$9.50]. A paper copy may be purchased [prepayment required] from the National Technical Information Service, Springfield, Virginia 22161. The report is also available on microfiche at no charge. To obtain a microfiche copy, Circle 44 on the TSP Request Card.*
MFS-25559

Materials

Hardware, Techniques, and Processes

447 Improved Cell for Water-Vapor Electrolysis
448 Applying the Helium Ionization Detector in Chromatography
449 Photoproduction of Halogens Using Platinized TiO_2
450 Recycling Paper-Pulp Waste Liquors
451 User Chooses Coating Properties
452 Removing Freon Gas From Hydraulic Fluid
452 New Pressure-Sensitive Silicone Adhesive
453 Driving Bubbles Out of Glass

Books and Reports

453 Less-Toxic Corrosion Inhibitors

Computer Programs

454 Diffusion in Single-Phase Binary Alloys

Improved Cell for Water-Vapor Electrolysis

A sintered iridium oxide anode coating sharply increases the rate of dissociation of water vapor.

Lyndon B. Johnson Space Center, Houston, Texas

Water vapor in such gases as steam or ordinary room air is decomposed into hydrogen and oxygen by improved continuous-flow electrolytic cells akin to fuel cells. A new iridium oxide catalytic anode coating, demonstrated in over 1,000 hours of testing, yields dissociation rates over a hundredfold greater than those obtained using conventional platinum black (see Figure 1). Conversely, at equal current density, the iridium cell operates at approximately 0.45 volt lower potential, allowing practical dissociation rates at voltages below the threshold (2.1 volts) for significant ozone production. Power consumption is correspondingly reduced.

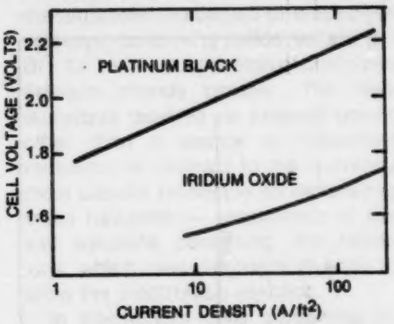

Figure 1. **Comparative Performance** of iridium oxide catalyst and conventional platinum black is shown in these I/V curves. The difference is a factor of over 100 in current density at fixed voltage, or about 0.45 volt at fixed current density.

A typical cell, originally developed for continuous oxygen enrichment of the atmosphere in manned space vehicles, is shown in Figure 2. Each unit actually consists of two mirror-image cells, with a dual cathode sandwiched between two anodes. Any number of dual cells can be stacked in parallel to handle the volume of water vapor at the input.

Vapor-laden gas traverses the serpentine channels within each cell and is dissociated at the anode into hydrogen ions and free oxygen. The oxygen mingles with the gas stream, while the hydrogen migrates through a porous, electrolyte-saturated matrix and is liberated as hydrogen gas at the cathode, exiting by a separate port.

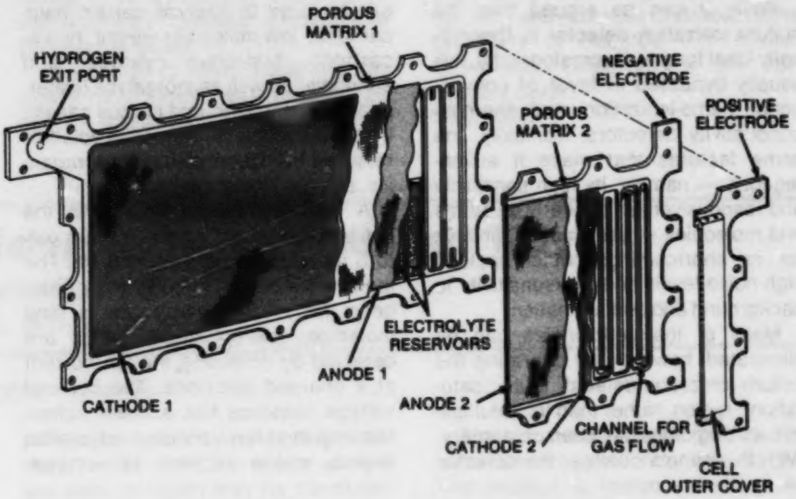

Figure 2. A **Dual-Cell Element** such as this would be part of a multicell stack, with blower, power supply, and control instrumentation.

Porous-metal electrolyte reservoirs lie against the anode. With variations in the humidity of the gaseous stream, electrolyte passes back and forth through the anode to the matrix to maintain the proper electrolyte level.

The anode substrate is a foraminous metal screen or expanded mesh, containing from 500 to over 1,500 pores/in.^{2} (80 to over 230 pores/cm^2). It may be titanium, gold, or tantalum (the latter is best, as it is inexpensive, inert, and resistant to hydrogen embrittlement). The matrix is made from a compounded asbestos such as blue asbestos, which will not decompose in the electrolyte — a mixture of sulfuric and phosphoric acid — yet will be adequately wetted.

The catalytic anode coating consists of 70 to 85 percent iridium oxide; the remainder is a high-temperature binder such as polytetrafluoroethylene resin. A soluble iridium compound, such as chloroiridic acid or iridium chloride, is dissolved in water and applied to sodium nitrate; after drying, the mixture is oxidized at 400° C. The fused cake is leached with water, and iridium oxide is filtered out and mixed in water with polytetrafluoroethylene. After another filtration, the mesh is pressed into the mixture to receive a coating of about 20 mg/cm^2. It is then sintered at 310° C for 5 minutes, producing a highly adherent coating on one side and in the pores of the mesh.

In a prototype cell, efficiencies greater than 99 percent are obtained at ambient temperatures, using atmospheric air and a current density of about 60 A/ft^2 (650 A/m^2). The cell may be operated at superatmospheric pressures and elevated temperatures, such as with steam.

This work was done by John R. Aylward of United Technologies Corp. for **Johnson Space Center**. *For further information, Circle 45 on the TSP Request Card.*

This invention is owned by NASA, and a patent application has been filed. Inquiries concerning nonexclusive or exclusive license for its commercial development should be addressed to the Patent Counsel, Johnson Space Center [see page A5]. Refer to MSC-16394.

Applying the Helium Ionization Detector in Chromatography

When modified to operate in its saturation region, the helium ionization detector can be ideal for gas chromatography.

Lyndon B. Johnson Space Center, Houston, Texas

While it can be argued that the helium ionization detector is theoretically ideal for gas chromatography, it is usually bypassed in favor of conventional flame-ionization and thermal-conductivity detectors. Ironically, the same features that make it advantageous — namely, its high sensitivity and responsiveness to nearly all atoms and molecules — are also responsible for its shortcomings, which include high noise levels and oversensitivity to background and contamination.

Many of the deficiencies can be eliminated, however, by operating the helium ionization detector in its "saturation" region, rather than its "multiplication" region as has been customary. With this simple change, the detector can be used to analyze certain halocarbons, low-molecular-weight hydrocarbons, hydrogen cyanide, and ammonia, as well as inorganics (water, phosphorus, sulfur, and nitrous gases). It is also suitable for detecting volatiles released from pyrolyzed metals, organics, and geological samples.

A radioactive beta emitter in the ionization detector excites helium gas to a metastable state at 19.8 eV. The metastable helium is sufficiently energetic to ionize nearby atoms and molecules (except neon), which are detected by collecting the ion current at a charged electrode. The current/voltage response has a linear collection region at low voltage, a saturation region where current is voltage-independent, and an exponential multiplication region at high voltage, resulting from the participation of secondary electrons.

Conventionally, the detector is operated in the multiplication region, where response is high; but so too are background current and noise. To minimize background current induced by atmospheric diffusion, some experimenters have even gone so far as to operate the entire chromatograph in a helium atmosphere.

In contrast, when the detector is operated in its saturation region — where its current output is independent of applied voltage, the result is low background current, low noise, high stability, and high sensitivity. To

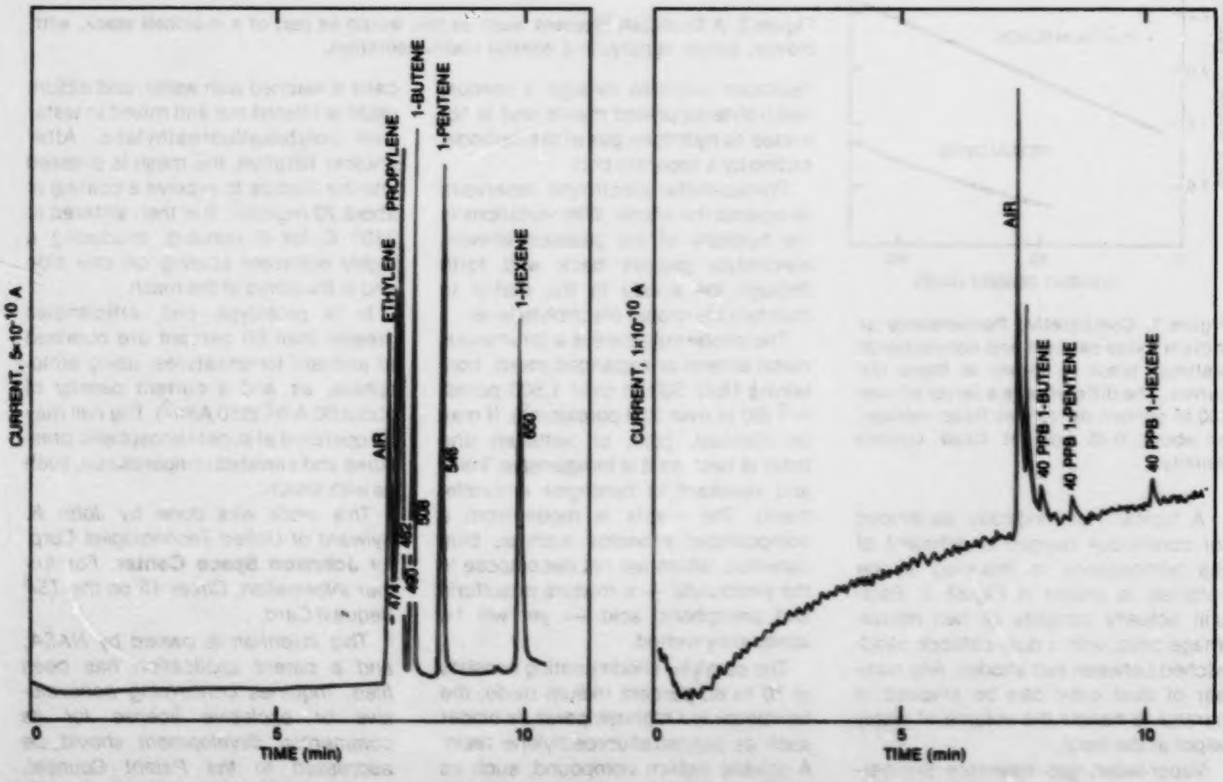

The Detector Response, when operating in its saturation region, to 17 parts per million of ethylene, propylene, 1-butene, 1-pentene, and 1-hexene is shown in the curve at the left. The curve on the right shows the response to 40 parts per billion. Chromatograph column temperature is 60° C; detector temperature is 175° C; and sample size is 100 microliters.

achieve these conditions, the bucking circuit of a commercial detector is modified for operation in the 20- to 200-volt saturation range and is calibrated to allow absolute measurement of the detector output current. The modified detector has a detection limit in the picogram range for organic compounds (see figure), and its response is linear over more than six orders of magnitude of concentration.

While a conventional detector is operated at a flow rate exceeding 45 cm^3/min to suppress the background and increase stability, the modified detector is stable at flow rates below 20 cm^3/min. Moreover, the system does not require expensive research-grade (99.9995-percent-purity) helium; standard high-purity-grade (99.995-percent-purity) helium, most often used in chromatography, gives excellent results while eliminating problems of signal-polarity reversal experienced with certain gases.

Many organic compounds are liquids at room temperature and must be directly injected with a syringe. This requires a simple modification to a standard commercial injection port to avoid introducing air that could overload the detector and obscure parts of the chromatogram.

This work was done by Everett K. Gibson of **Johnson Space Center**, *Fikry F. Andrawes of Lockheed Engineering and Management Services Co., Inc., and Roswitha S. Brazell of the University of Houston. For further information, Circle 46 on the TSP Request Card.*
MSC-18835

Photoproduction of Halogens Using Platinized TiO_2

A powdered photocatalyst dramatically increases the rate of production of I_2, Br_2, and Cl_2.

Langley Research Center, Hampton, Virginia

The halogen molecules, I_2, Br_2, and Cl_2, are produced efficiently by the ultraviolet irradiation of electrolyte solutions containing halide anions (I^-, Br^-, Cl^-) and a suspension of platinized titanium dioxide powder. The new technique requires no external power other than a source of ultraviolet radiation, in contrast to the currently most popular technique for generating these halogens — electrolysis of the salt solutions containing the halide ions, which uses electricity directly to drive the electrolysis reaction.

In electrolysis cells containing n-type semiconductors, light having energy greater than the band-gap energy initiates oxidation processes at the semiconductor/electrolyte interface at smaller (more-negative) potentials than at metal electrodes. This allows the oxidation/reduction reactions, which normally occur at very low rates or which may be thermodynamically unfavorable, to occur at higher rates in the presence of semiconductors and light. Platinized, powdered TiO_2 can photocatalyze some reactions that otherwise proceed slowly. Such powders are analogous to a system of many short-circuited photoelectrolysis cells; but the powder is less expensive than commercial electrodes, and it has a much higher surface-area-to-weight ratio — an important criterion for a good catalyst.

Halogen	Micromoles of Halogen Produced After 1 Hour of Illumination	Suspension
I_2	120	Pt/TiO_2
I_2	1	TiO_2 (anatase)
Br_2	80	Pt/TiO_2
Br_2	0	TiO_2
Cl_2	56	Pt/TiO_2
Cl_2	0	TiO_2

Halogen Photoproduction is compared for platinized and unplatinized TiO_2 powder. The technique, using platinized TiO_2, produces halogen molecules easily and inexpensively, without using electricity directly.

The Pt/TiO_2 powder is prepared by illuminating with ultraviolet radiation a solution of 15 ml platinic acid (H_2PtCl_6), 15 ml glacial acetic acid, and 2 grams of TiO_2 powder. The powder is of the anatase phase and can be doped or undoped. In a typical preparation, the resulting catalytic powder is 1:10 by weight of doped $Pt:TiO_2$.

Typically, 100 to 200 mg of this catalyst are suspended in a solution containing 35 ml of I^-, Br^-, or Cl^- salts (about 2M concentration) and irradiated with ultraviolet light from a 1,000-watt high-pressure mercury lamp. After several hours of irradiation, the color typical of the halogen molecule of interest appears in the solution: brown for I_2; yellow-brown for Br_2; yellow-green for Cl_2.

The amount of halogen produced is determined by two methods. In the first method, a known amount of As (III) is introduced into the halide solution. After irradiation, the solution is titrated with iodine in the presence of starch. The difference in the amount of As (III) before and after irradiation indicates the amount of halogen produced. In the second method, the solution is first saturated with O_2, and the reaction cell is closed. After irradiation, the amount of halogen produced is determined by titration in the presence of starch. (In the cases of Br_2 and Cl_2, KI is added before titration.)

The rate of production of halogen is summarized in the table. For comparison, the rate of production of halogen is also given in the presence of unplatinized TiO_2 powders.

The reduction of O_2 molecules occurs simultaneously with the halide oxidation. While the halide oxidation occurs on the illuminated side of the particle according to

$$2X^- \rightarrow X_2 + 2e^- \qquad (1)$$

(where X is the halide ion) oxygen is being reduced on the "dark" side of the particle according to

$$\frac{1}{2}O_2 + 2e^- + 2H^+ \rightarrow H_2O \qquad (2)$$

(continued on next page)

The overall reaction, therefore, is

$$2X^- + \frac{1}{2}O_2 + 2H^+ \rightarrow X_2 + H_2O \quad (3)$$

The half reaction in equation (2) determines the overall rate of the reaction in equation (3). The Pt on the powders affects the overall rate by decreasing the overvoltage for oxygen reduction.

Other useful reactions could possibly be photocatalyzed or photosynthesized effectively by the plantinized semiconductor powders. The technique can use light, such as solar radiation, and a brine solution containing a suspension of platinized semiconductor powder to produce halogen molecules; or it can be used to oxidize hazardous materials such as CN^- in wastewater or to convert carbon monoxide to CO_2.

This work was done by Benjamin Reichman of Christopher Newport College and Charles E. Byvik of **Langley Research Center.** *For further information, Circle 47 on the TSP Request Card.*

Inquiries concerning rights for the commercial use of this invention should be addressed to the Patent Counsel, Langley Research Center [see page A5]. Refer to LAR-12713.

Recycling Paper-Pulp Waste Liquors

Lignosulfonates are converted to an ion-exchange resin and sugars are recovered.

NASA's Jet Propulsion Laboratory, Pasadena, California

Papermills in the United States annually produce about 3 million tons (1978 figure) of sulfite waste-liquor solids. Although about 10 percent of the solids can be used, disposal of the remainder poses a serious environmental problem for the woodpulp industry. The sulfite waste liquor contains 10 to 15 percent solids, of which approximately 25 percent are monomeric sugars and the balance are lignosulfonates.

Sugars are recovered, and the lignosulfonates are converted to a useful ion-exchange resin in a new pulp-waste-liquor treatment now under development. In the new process, the sugars are converted to ethanol/single-cell protein and removed by distillation; a gelatin or a polymer similar to polyethyleneimine precipitates the lignosulfonates, which are then cross-linked to form the ion-exchange resin (see figure). Because of its high cost and potential environmental hazard, polyethyleneimine is being considered only as a model for identifying other, more practical, candidates for the process.

In laboratory tests, a 50-percent aqueous solution of sulfite waste liquor containing 13 percent sodium lignosulfonate was mixed with a 10-percent aqueous solution of gelatin. The precipitate, which was highly swollen and rubbery, was separated by centrifugation and vacuum-dried to obtain a 40-percent yield of lignosulfonate/gelatin resin (based on the weight of gelatin added). The swelling and rubberiness of the precipitate are attributed to only the high-molecular-weight lignosulfonates forming a complex with the gelatin. The precipitate was then cross-linked by heating with 37 percent formaldehyde at the boiling point of the aqueous solution for 5 minutes to form a lignosulfonate/

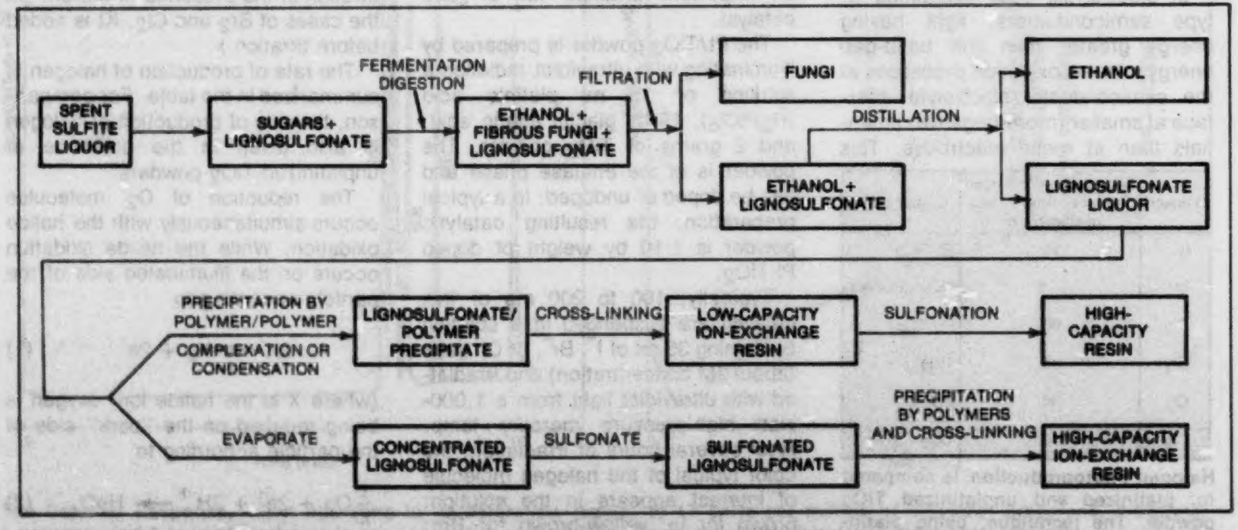
FERMENTATION DIGESTION
FILTRATION
FUNGI
ETHANOL
SPENT SULFITE LIQUOR
SUGARS + LIGNOSULFONATE
ETHANOL + FIBROUS FUNGI + LIGNOSULFONATE
DISTILLATION
ETHANOL + LIGNOSULFONATE
LIGNOSULFONATE LIQUOR
PRECIPITATION BY POLYMER/POLYMER COMPLEXATION OR CONDENSATION
LIGNOSULFONATE/POLYMER PRECIPITATE
CROSS-LINKING
LOW-CAPACITY ION-EXCHANGE RESIN
SULFONATION
HIGH-CAPACITY RESIN
EVAPORATE
CONCENTRATED LIGNOSULFONATE
SULFONATE
SULFONATED LIGNOSULFONATE
PRECIPITATION BY POLYMERS AND CROSS-LINKING
HIGH-CAPACITY ION-EXCHANGE RESIN

The Recovery of Lignosulfonates from sulfite waste liquor involves cross-linking the lignosulfonates to form a solid ion-exchange resin. Contamination of the sugars in the waste liquor is avoided by first converting them to ethanol and removing the ethanol by distillation.

gelatin/formaldehyde ion-exchange resin. The resin formed this way has a relatively-low exchange capacity of 1.3 milliequivalents per gram (dry).

Still better results were obtained when the procedure was repeated using a polyethyleneimine in place of the gelatin. All the lignosulfonates separated, and the supernatant was colorless. The complex that formed was stable and had an exchange capacity of 1.6 to 1.9 milliequivalents per gram (meg) (compared to about 4.5 meg for commercial resins). The precipitate weight increased as the molecular weight of polyethyleneimine increased. The exchange capacity of the resin was doubled by further sulfonation by a simple heat treatment in 98 percent sulfuric acid (or 30 percent oleum) in the presence of about 20 percent alumina at 250° to 270° C.

This work was done by Mohammad N. Sarbolouki of Caltech for **NASA's Jet Propulsion Laboratory.** *For further information, Circle 48 on the TSP Request Card.*
NPO-14797

User Chooses Coating Properties

Anodizing technique allows the independent selection of coating thermal emittance and solar absorption.

Langley Research Center, Hampton, Virginia

A versatile thermal-control coating is prepared by modified chromic acid anodizing of aluminum. The coating, with ranges of 0.10 to 0.72 for thermal emittance (ϵ_T) and 0.2 to 0.4 for solar absorptance (α_S), allows the selection of any value of ϵ_T or α_S in the specified range to within an accuracy of ±0.02.

Other thermal-control coatings include conversion coating (Alodine), other anodic coatings, and dielectric films and paints. These, however, have limited ranges of ϵ_T and α_S and do not allow the independent selection of these properties.

The variable anodic thermal-control coating process has three phases: initial material processing, anodizing, and material postprocessing. The initial processing prepares the material for anodizing and establishes the initial values of ϵ_T and α_S. The aluminum is immersed in a metal-cleaning bath, rinsed, immersed in a deoxidizer solution, and rinsed by physical agitation to remove all particulates from the aluminum surface.

The aluminum is anodized by immersing it in a chromic acid solution containing 3 to 10 percent CrO_3 (by weight) balanced with water. The voltage is applied between the aluminum and the chromic acid solution at a predetermined rate up to a selected voltage and is maintained for a selected period of time. The rate, voltage, and time, along with the initial values of ϵ_T and α_S, temperature of the chromic acid solution, acid concentration, and material to be anodized, determine the final values of ϵ_T and α_S. Material postprocessing involves rinsing with water, placing in a sealing bath of clear water at 180° F (82° C), and drying with filtered forced air.

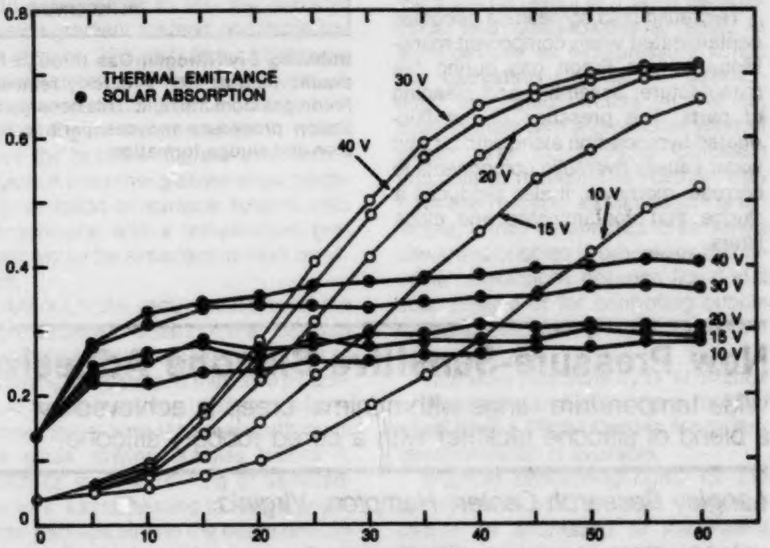

Thermal Emittance and Solar Absorptance of the anodic thermal-control coating are shown for various anodizing times and voltages. The cell voltage is increased to the operating voltage in 30 seconds in these examples. Solution temperature is 95° F (35° C), and the pH is 0.5.

Typical results are shown in the figure, where ϵ_T and α_S are plotted for various anodizing voltages and times. The anodic process has been applied on 6061, 1145, and 2024 aluminum with thicknesses as low as 0.001 inch (0.003 cm). Preliminary stability tests in vacuum have shown less than 15 percent degradation over a 2,000-hour solar exposure. The technique is sensitive to voltage, the rate of voltage application, time, temperature, acid concentration, material pretreatment, and sealing. However, consistent results are obtained if the processing parameters remain constant.

This work was done by Charles S. Gilliland and Roy J. Duckett of **Langley Research Center.** *For further information, Circle 49 on the TSP Request Card.*

Inquiries concerning rights for the commercial use of this invention should be addressed to the Patent Counsel, Langley Research Center [see page A5]. Refer to LAR-12719.

Removing Freon Gas From Hydraulic Fluid

Sparging the heated fluid with dry nitrogen speeds removal and lowers the final level of contamination.

Lyndon B. Johnson Space Center, Houston, Texas

Dissolved Freon gas can be removed from hydraulic fluid by raising the temperature to 150° F (66° C) and bubbling dry-nitrogen gas through the fluid reservoir (see figure). The procedure can be carried out while the fluid is circulating through the hydraulic system. Agitating a liquid with piped-in gas is called sparging; the dry-nitrogen sparging of the hydraulic fluid not only removes gas faster than simple heating does but also results in a lower final level of contamination.

Hydraulic fluid sometimes becomes contaminated when component manufacturers use Freon gas during the manufacture, assembly, and cleaning of parts. The presence of the fluorinated hydrocarbon along with air and water causes hydraulic components to corrode; moreover, it also produces a sludge that contaminates and clogs filters.

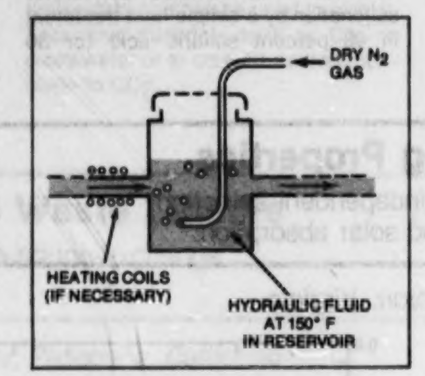
DRY N_2 GAS
HEATING COILS (IF NECESSARY)
HYDRAULIC FLUID AT 150° F IN RESERVOIR

Bubbling Dry-Nitrogen Gas through hydraulic fluid at 150° F quickly removes Freon gas from the fluid. This decontamination procedure reduces parts corrosion and sludge formation.

Specifications for Space Shuttle ground-support equipment limit the content of fluorinated hydrocarbon in hydraulic fluid to less than 100 parts per million. In the past, high temperatures were used to reduce the contamination to this level, but other design constraints now limit the fluid temperature to 165° F (74° C) at the most.

An application of the procedure successfully prevented corrosion and sludge resulting from dissolved Freon. The sparging was accomplished simply by immersing a tube in the hydraulic fluid after removal of the reservoir cover.

This work was done by Billy B. Williams, Shirley M. Mitchell, and Theodore S. State of Rockwell International Corp. for **Johnson Space Center.** *No further documentation is available.*
MSC-18740

New Pressure-Sensitive Silicone Adhesive

Wide temperature range with minimal creep is achieved by a blend of silicone tackifier with a cured rubbery silicone.

Langley Research Center, Hampton, Virginia

A new pressure-sensitive silicone adhesive can be used at high or low temperatures with minimal creep. A blending of silicone tackifier and cured rubbery silicone, the new adhesive can be used without solvents.

Pressure-sensitive adhesives are typically made from a polymer above its glassy transition temperature. The polymers usually have intermediate molecular weight (if they were of lower molecular weight, they would be liquid; and if of higher molecular weight, they would be solid with no tack). The adhesives are prepared from the tacky resins alone or from a blend with other polymers and/or fillers. For silicone systems, the only available pressure-sensitive adhesives are those for which the tacky intermediate-molecular-weight silicone is used alone or in conjunction with mineral fillers. Polymer binders other than silicones have also been used.

Conventional pressure-sensitive silicone adhesives have a tendency to creep or stretch severely when they are placed under a stress or load. Other polymeric binders can alleviate this problem in some instances; however, no other polymer systems have the unique properties of the silicones when temperature extremes (between -115° and 250° C) are experienced.

The new adhesive system is produced by blending an intermediate-molecular-weight pressure-sensitive silicone adhesive, which does not cure, with a silicone resin, which generally cures with a catalyst to a rubbery tack-free state. The result is a pressure-sensitive silicone adhesive that can be used for structural or load-bearing applications without creeping. The ratio of silicone tackifier to silicone resin can be varied to obtain different degrees of tack, creep resistance, and tensile strength. Various formulations were tested:

- 50/50 (tackifier/cured resin) — tack remains for up to 48 hours, low creepage under load;
- 75/25 (tackifier/cured resin) — tack remains over 3 months, low creepage under load; and
- 80/20 (tackifier/cured resin) — tack remains for over 3 months, creeps under load.

Flatwise tensile strengths of various formulations range from 10 to 19 psi (69×10^3 to 131×10^3 N/m^2) at room temperature.

The pressure-sensitive silicone adhesive has been successfully tested at temperatures from -45° to 232° C with minimal creep under structural loading. It can also be used without solvents in both atmospheric and vacuum environments.

This work was done by James L. Leiffer, William E. Stoops, Jr., Terry L. St. Clair, Vernon E. Watkins, Jr., and Thomas P. Kelly of ***Langley Research Center.*** *No further documentation is available.*

Inquiries concerning rights for the commercial use of this invention should be addressed to the Patent Counsel, Langley Research Center [see page A5]. Refer to LAR-12737.

Driving Bubbles Out of Glass

A surface-tension gradient forces gas bubbles to the surface.

Marshall Space Flight Center, Alabama

Gas bubbles have been eliminated from molten glasses by a surface-tension gradient in the melt. The bubbles move to a region of lower surface tension. Since surface tension decreases with increasing temperature in most molten glasses, bubbles rise to the surface if the temperature of the melt increases from bottom to top. Although developed by NASA for possible materials processing in space, the same technique should work for glasses and other liquids in normal gravity.

Traditionally, bubbles have been removed by buoyant "fining," in which the denser glass sinks, forcing the bubbles to move to the surface and burst. In chemical fining, also used to remove bubbles, chemicals are added to the melt to dissolve the gas contained in the bubbles so that they shrink and disappear.

Buoyant fining can be exceedingly slow in viscous glasses. (It does not occur at all in the absence of gravity.) Chemical fining is even slower, especially for large bubbles, since a sizable volume of gas must be absorbed.

In experiments to test the surface-tension-gradient method on simple borax glasses, 250-μm bubbles have been moved at rates as high as 30 μm/s. A few glasses have greater surface tension at higher temperatures, in which case the bubbles migrate to a cooler region. A few other glasses show hardly any variation in surface tension with temperature, and a temperature gradient would be expected to have no effect.

Although the requisite heat for the high-temperature part of the melt can be furnished by stationary electrical or natural-gas heaters, it may also be possible to use induction heating to create a moving hot zone that sweeps through the glass, driving bubbles before it, much as in zone refining of semiconductors. Laser heating is also a possibility, perhaps aiming the beam directly at a bubble to move it along.

The new method could remove the gases that are inevitably generated in glass processing and which reduce strength and transparency. It may therefore be useful in making glass-to-metal and glass-to-ceramic seals in such devices as high-pressure lamps and cathode-ray tubes; in "gassivating" integrated circuits — that is, coating them with a protective layer of glass; and in applying porcelain enamels to metals. The method may have even broader applications. For example, it may be adapted to removing unwanted bubbles in processes that involve conversions between liquid and solid phases or for controlling bubble formation in flowing fluids to prevent turbulence.

This work was done by D. M. Mattox of Westinghouse Electric Corp. for ***Marshall Space Flight Center.*** *No further documentation is available.*

Inquiries concerning rights for the commercial use of this invention should be addressed to the Patent Counsel, Marshall Space Flight Center [see page A5]. Refer to MFS-25414.

Books and Reports

These reports, studies, and handbooks are available from NASA as Technical Support Packages (TSP's) when a Request Card number is cited; otherwise they are available from the National Technical Information Service.

Less-Toxic Corrosion Inhibitors

Combinations of low-toxicity inhibitors effectively protect aluminum from corrosion in water.

Various combinations of borates, nitrates, nitrites, phosphates, silicates, and sodium mercaptobenzothiazole (NaMBT) were tested for their effectiveness in preventing or reducing the corrosion of aluminum parts immersed in corrosive freshwater. The inhibitors are intended to replace chromates and other water additives that are effective against corrosion but are subject to governmental restrictions.

The inhibitors were tested in combination because when used individually, they are only partly effective.

(continued on next page)

The chemicals were added to a corrosive test solution of distilled water containing 138 parts per million (ppm) sodium bicarbonate, 148 ppm sodium sulfate, and 165 ppm sodium chloride. Also present in some of the tests were 0.2 ppm copper sulfate. Test specimens of 2219-T87 aluminum were cut into small sheets, immersed in 300 ml (10 oz) of solution, and stored at room temperature. Exposure times varied from 1 to 14 months, depending upon the amount of corrosion observed and upon the nature of the solution.

Of 50 inhibitor combinations tested, 8 are effective and compare favorably with sodium chromate. While highly alkaline solutions are normally corrosive to aluminum, it was nevertheless observed that the most effective inhibitor combinations contained trisodium phosphate and were alkaline.

One disadvantage of the successful inhibitor combinations is that each must be formulated with the prescribed amounts of four to six of the chemicals mentioned above, with a total concentration of 500 to 1,000 ppm, whereas only 100 to 200 ppm of sodium chromate are required for effective inhibition. Under extended service (longer than 6 months) or the nonmonitoring of concentrations, the inhibitor dosage should be increased to allow for depletion. From an economic point of view, inhibitors that are effective at low concentration are preferred.

This work was done by T. S. Humphries of **Marshall Space Flight Center.** *Further information may be found in NASA TP-1279 [N78-28226/NSP], "Low Toxic Corrosion Inhibitors for Aluminum in Fresh Water" [$5]. A paper copy may be purchased [prepayment required] from the National Technical Information Service, Springfield, Virginia 22161. The report is also available on microfiche at no charge. To obtain a microfiche copy, Circle 50 on the TSP Request Card.*
MFS-25496

Computer Programs

These programs may be obtained at very reasonable cost from COSMIC, a facility sponsored by NASA to make new programs available to the public. For information on program price, size, and availability, circle the reference letter on the COSMIC Request Card in this issue.

Diffusion in Single-Phase Binary Alloys

Exact solutions for systems with planar, cylindrical, or spherical interfaces

The DBAS 1 computer program provides the analyst with a set of simple algorithms for exact solutions of diffusion in single-phase binary/alloy systems with planar, cylindrical, or spherical interfaces. This exact approach typically takes much less time than finite-difference calculations.

The analysis of diffusion-controlled processes requires the prediction of the interaction between different components for a given set of exposure equations. Exact solutions are available in the literature for diffusion in single-phase binary-alloy systems with constant diffusion coefficient and zero-flux boundary conditions. These solutions, however, have not been widely utilized because of their complexity and convergence problems.

Two algorithms are provided for each of the three interface geometries. One algorithm converges rapidly for short diffusion times; the other algorithm converges rapidly for long diffusion times. The algorithms in the DBAS 1 program, along with an established methodology for selecting the appropriate algorithm for a given situation, can rapidly solve diffusion problems.

For planar geometry, the long-tme algorithm is a trigonometric solution. The short-time algorithm is the classical double-error-function solution generalized to account for multiple reflections.

For cylindrical geometry, the long-time algorithm is based on Bessel functions and the roots of a Bessel equation. The short-time algorithm involves integration, using a Gauss-Legendre quadrature formula, over a modified Bessel function.

For spherical geometry, the long-time algorithm is based on roots of a trigonometric equation. The short-time algorithm involves error functions.

DBAS 1 is written in FORTRAN IV for batch execution and has been implemented on a CDC 6600 computer with a central memory requirement of approximately 33K (octal) of 60-bit words. The program was developed in 1979.

This program was written by Darrel R. Tenney of **Langley Research Center** *and Jalaiah Unnam of VPI and State University. For further information, Circle B on the COSMIC Request Card.*
LAR-12665

Life Sciences

Hardware, Techniques, and Processes

457 Cardiopulmonary Data-Acquisition System
458 Microprocessor-Controlled Ultrasonic Plethysmograph
459 Microprocessor-Based Cardiotachometer
460 Improved Microbe Detection in Water Samples
461 Gage for Evaluating Rheumatoid Hands
462 Fiber-Optics Couple Arthroscope to TV
463 Beef Grading by Ultrasound

Cardiopulmonary Data-Acquisition System

A computerized system controls stress tests and displays real-time physiological data.

Lyndon B. Johnson Space Center, Houston, Texas

A computerized cardiopulmonary data-acquisition system controls and monitors bicycle and treadmill cardiovascular stress tests. It acquires and reduces stress data and displays in real time the heart rate, blood pressure, workload, minute volume, respiratory rate, exhaled-gas composition, and other variables.

A block diagram of the microcomputer-based system is shown in the figure. The data are printed on a hard-copy terminal every 30 seconds so that the operator can quickly respond to the subject throughout the test. The ergometer workload is controlled in real time according to the experimental protocol, and the collected data are stored directly on tape in analog form and on floppy disks in digital form for posttest data processing.

One of the main advantages of the system is its simplicity. Many conventional near-real-time data-collection systems are more difficult to use or lack automatic calibration and accurate exhaled-gas analysis. Others have no real-time data display or are not as easily adapted to changing test requirements.

Major system components include a microcomputer operating with assembly-language and higher-level-language programs, a custom analog signal interface and control unit, a

(continued on next page)

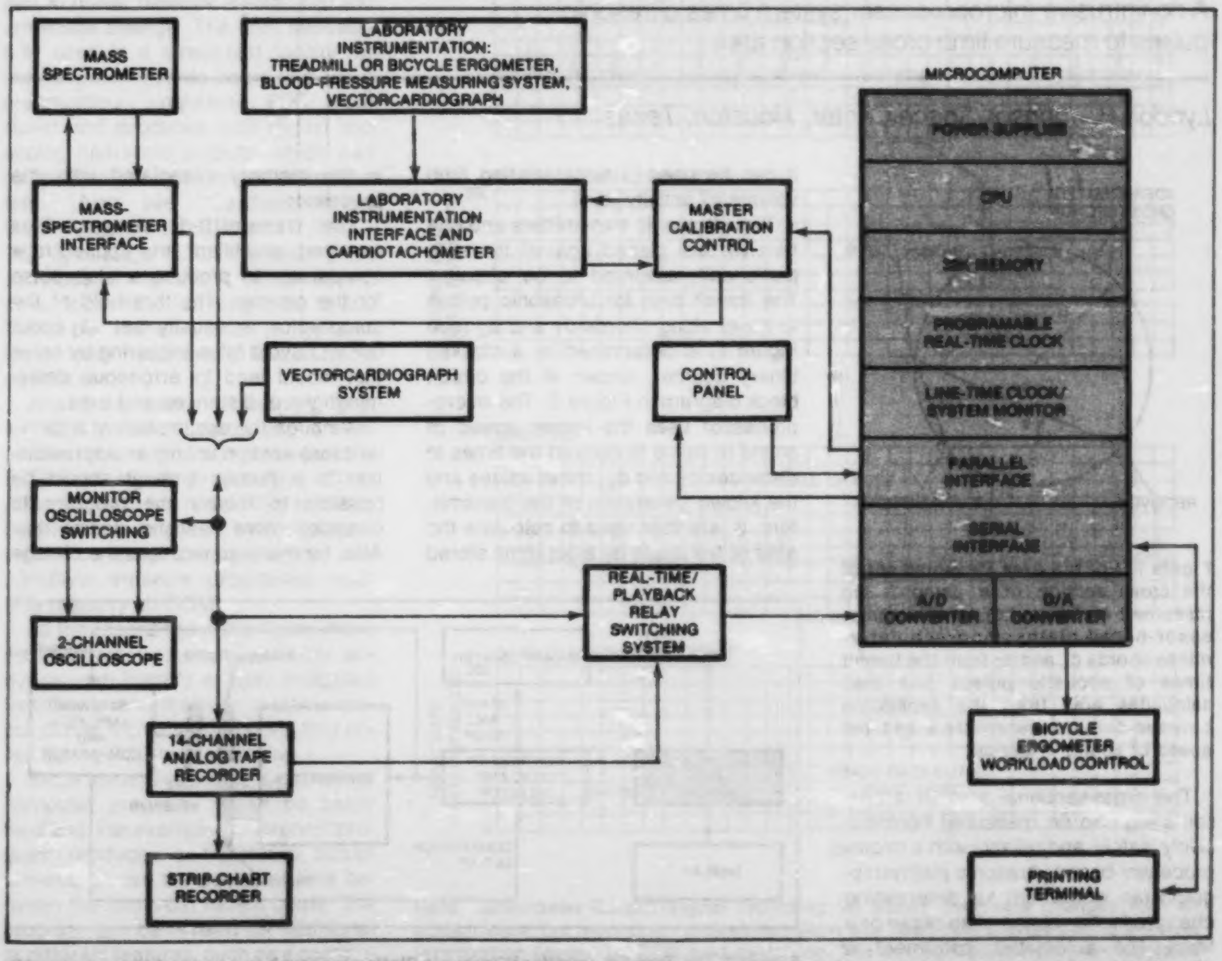
MASS SPECTROMETER
LABORATORY INSTRUMENTATION: TREADMILL OR BICYCLE ERGOMETER, BLOOD-PRESSURE MEASURING SYSTEM, VECTORCARDIOGRAPH
MICROCOMPUTER
POWER SUPPLIES
CPU
32K MEMORY
PROGRAMABLE REAL-TIME CLOCK
LINE-TIME CLOCK/ SYSTEM MONITOR
PARALLEL INTERFACE
SERIAL INTERFACE
A/D CONVERTER
D/A CONVERTER
MASS-SPECTROMETER INTERFACE
LABORATORY INSTRUMENTATION INTERFACE AND CARDIOTACHOMETER
MASTER CALIBRATION CONTROL
VECTORCARDIOGRAPH SYSTEM
CONTROL PANEL
MONITOR OSCILLOSCOPE SWITCHING
REAL-TIME/ PLAYBACK RELAY SWITCHING SYSTEM
2-CHANNEL OSCILLOSCOPE
14-CHANNEL ANALOG TAPE RECORDER
BICYCLE ERGOMETER WORKLOAD CONTROL
STRIP-CHART RECORDER
PRINTING TERMINAL

The Block Diagram of the Cardiopulmonary Data-Acquisition System shows the flow of data and control signals. A self-calibrating function compensates for drift or small changes in gain. The most critical calibrations (mass-spectrometer calibratons for the three respiratory gases) are checked through the entire system before each test and during the automatic calibration sequence.

beat-by-beat (nonaveraging) cardiotachometer [also see "Microprocessor-Based Cardiotachometer" (MSC-18775) on page 459 of this issue], and a mass-spectrometer interface/control. Many of the components are commercially available.

The system includes a multipole latching relay panel for switching to backup operating modes. All automatic functions can be overridden at the flip of a switch, and testing can continue even if major components fail, including the microcomputer.

A computer control panel with seven labeled pushbutton switches is used for executing a stress test. Once the stress program is started, only those switches that are illuminated under program control can be used. (Unilluminated buttons are deactivated). The only electrical connections to the test subject are those of the ECG machine.

This work was done by William G. Crosier and Roy A. Reed of Technology Inc. for **Johnson Space Center.** *Further information may be found in:*

NASA CR-160608 [N80-33083/NSP], "Final Report on the Cardiopulmonary Data Acquisition System, Version 2.0, Volume 1, User's Guide" [$7]; and

NASA CR-160609 [N80-33084/NSP], "Final Report on the Cardiopulmonary Data Acquisition System, Version 2.0, Volume 2, Detailed Software/Hardware Documentation" [$12].

Copies of these reports may be purchased [prepayment required] from the National Technical Information Service, Springfield, Virginia 22161.

MSC-18783

Microprocessor-Controlled Ultrasonic Plethysmograph

A nonintrusive microprocessor system times ultrasonic pulses to measure limb cross-section area.

Lyndon B. Johnson Space Center, Houston, Texas

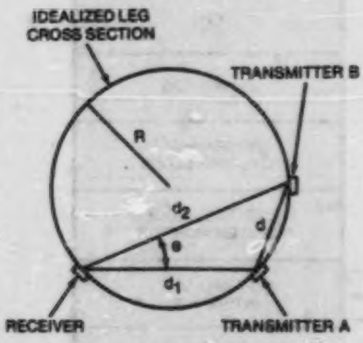

Figure 1. For the **Area Measurement** of the cross section of a person's leg (assumed to be round), a microprocessor-based plethysmograph determines chords d_1 and d_2 from the transit times of acoustic pulses and then calculates area from the separation between the two transmitters and the speed of sound in tissue.

The cross-sectional area of a person's leg can be measured nonintrusively, safely, and reliably with a microprocessor-based ultrasonic plethysmograph (an instrument for determining changes in the volume of an organ or a limb). The automated instrument is easy to operate and requires no calibration. Since the new plethysmograph does not confine leg movement, it can be used in tests relating limb volume to activity level.

Two ultrasonic transmitters and one receiver are placed against the subject's calf, assumed to be circular. The transit time for ultrasonic pulses to travel along chords d_1 and d_2 (see Figure 1) is determined by a clocked binary counter, shown in the circuit block diagram in Figure 2. The microprocessor uses the known speed of sound in tissue to convert the times to distances d_1 and d_2; these values and the known separation of the transmitters, d, are then used to calculate the area of the circle by algorithms stored in the memory associated with the processor.

The transmitted ultrasound is received, amplified, and applied to a comparator to produce a stop pulse for the counter. The threshold of the comparator is usually set at about 0.2 V to avoid false triggering by noise that would lead to erroneous determinations of distances and area.

Although the assumption of a circular cross section is only an approximation to a human limb, it should be possible to modify the program to consider more realistic geometries. Also, for many applications the change

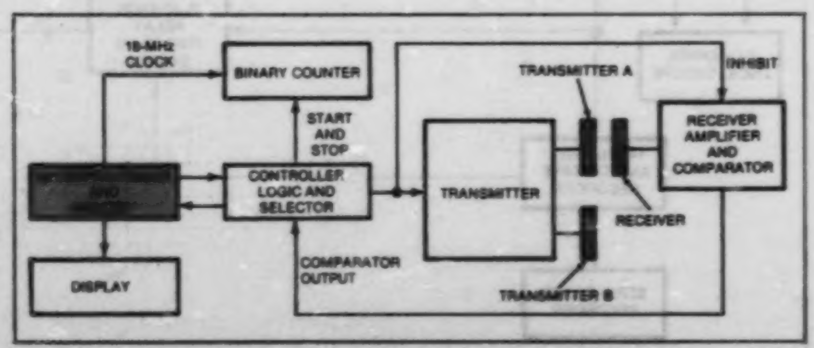

Figure 2. The **Two-Transmitter Ultrasonic Plethysmograph** is designed around an 8080 microprocessor. The controller logic and selector control the flow of information through the system, select a transmitter for a chord length measurement, and provide a count proportional to the measured transit time for display. The transmitted ultrasound is received and used by the comparator to stop the binary counter.

in area rather than the absolute area is of interest, and in these cases the error introduced by assuming a circular cross section is not very large.

Analysis of other factors affecting the system accuracy shows that errors due to body-temperature changes and timing roundoff are insignificant. Also, the uncertainty in chord length caused by variations of the comparator threshold affects the area precision by less than 1 percent.

This work was done by P. K. Bhagat and V. C. Wu of the University of Kentucky for **Johnson Space Center**. *For further information, including circuit diagrams and equations for calculating limb area, Circle 51 on the TSP Request Card.*

Inquiries concerning rights for the commercial use of this invention should be addressed to the Patent Counsel, Johnson Space Center [see page A5]. Refer to MSC-18759.

Microprocessor-Based Cardiotachometer

Heart rate is measured with better than 1 percent accuracy in rest or exercise stress testing.

Lyndon B. Johnson Space Center, Houston, Texas

A new cardiotachometer operates reliably even with stress-test electrocardiogram (ECG) signals that are subject to noise, baseline wandering, and amplitude change. The unit, successfully used in a stress-test facility for over a year, records heart rate via a preamplified, single-lead ECG input signal and produces both digital and analog heart-rate outputs, which can be fed to other instruments or computers. [Also see "Cardiopulmonary Data-Acquisition System" (MSC-18783) on page 457 of this issue.] The accuracy of the unit is better than 2 percent over the full range, 30 to 300 beats per minute, and is typically better than 1 percent up to 230 beats per minute.

Analog hardware, including a filter for ECG noise rejection and an improved R-wave detector, processes the ECG input signal, producing a 10-ms pulse for each heartbeat. The resulting pulse train is analyzed by a microprocessor computer program stored in a 2-kilobyte erasable programed read-only memory (EPROM).

As the recordings in the figure show, the program, written in Assembly language, can identify ectopic (irregular) heartbeats and maintain a stable output during signal interruptions that occur during ECG lead switching.

Since the analysis logic is part of the computer program, it can be easily modified. For example, the present program produces a heart-rate output computed from the period of time between the two most recent beats. The program can be revised for additional or different features, such as a continuously-updated averaged heart-rate output or digital filtering.

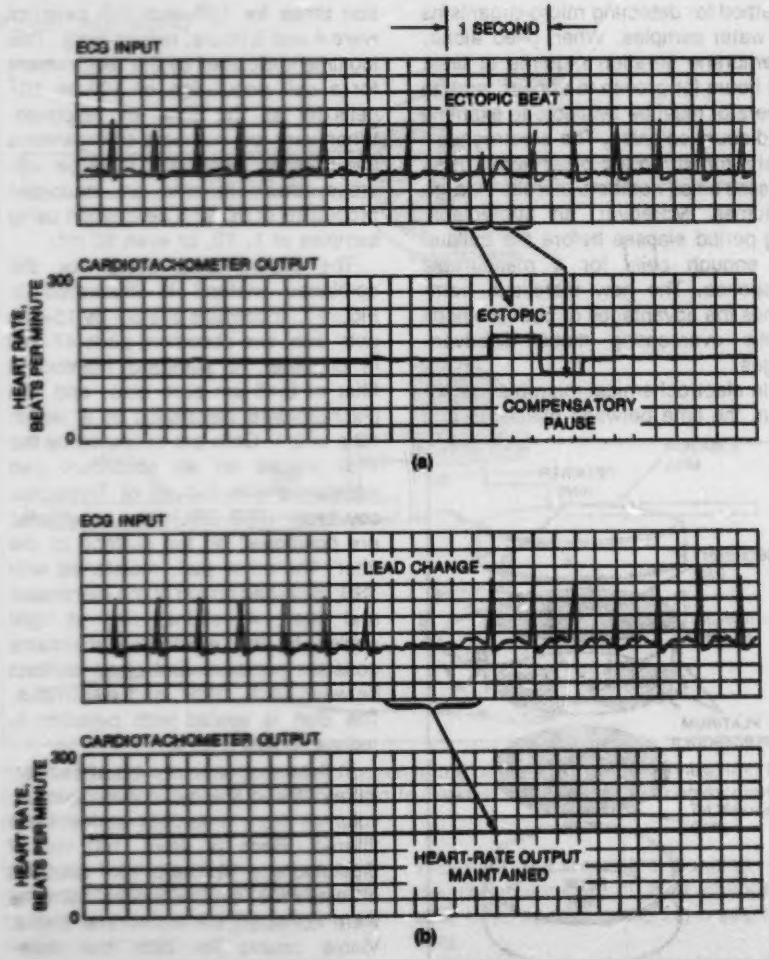

Cardiotachometer Output Signal recording (a) shows heart-rate changes with an ectopic beat, but recording (b) does not show any heart-rate change during a longer interruption caused by ECG lead switching. The microprocessor program contains the decisionmaking logic for interpreting such ECG signal artifacts. The time intervals interpreted as indicating various artifacts depend on the current heart rate, on when an early ectopic beat has occurred, and the like. The program updates these reference values with each heartbeat.

The unit also includes internal heart-rate calibration signals of 60 and 180 beats per minute. These are derived from the crystal-controlled clock controlling the microprocessor.

This work was done by William G. Crosier and John A. Donaldson of Technology Inc. for **Johnson Space Center.** *Further information may be found in NASA CR-160607 [N80-33082/NSP], "Final Report — A Microprocessor-Based Cardiotachometer" [$8]. A copy may be purchased [prepayment required] from the National Technical Information Service, Springfield, Virginia 22161.*
MSC-18775

Improved Microbe Detection in Water Samples

Combined membrane filtration and electrochemical detection give fast response and better detection of low concentrations.

Langley Research Center, Hampton, Virginia

Two techniques, membrane filtration and electrochemical microbial detection, are combined in a new method for detecting micro-organisms in water samples. When used alone, membrane filtration requires at least 24 hours for growth to appear, and an operator must be available to examine and count colonies. The electrochemical method, on the other hand, often misses small numbers of cells in large volumes. Moreover, an appreciable lag period elapses before the buildup of enough cells for a measurable response. The new technique combines the advantages of both methods while overcoming these disadvantages.

In electrochemical microbial detection, the time between challenge and the initial increase in voltage is a function of the number of cells in the inoculum. For *Escherichia coli*, detection times for 10^5 and 10^1 cells/ml were 4 and 8 hours, respectively. This lag time is dictated by the requirement for a cell population of 10^6 to 10^7 cells/ml at the time of response. When very low numbers of organisms are present, especially in large volumes, there is also an increased probability of missing cells when using samples of 1, 10, or even 50 ml.

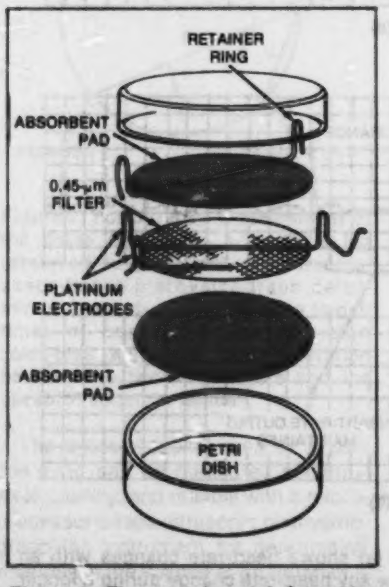

Figure 1. The experimental Apparatus for the Combined Technique requires only standard, commercially-available laboratory items.

The experimental setup for the combined method is illustrated in Figure 1. It consists of a 60- by 15-mm petri dish, two absorbent pads 47 mm in diameter, a standard membrane filter of 0.45-μm pore size, and two platinum-wire electrodes in a length ratio of 2:1. Cells are collected by the filter placed on an absorbent pad moistened with 2.0 ml of Trypticase soy broth (TSB,BBL); the electrodes are positioned on the surface of the filter. The other pad, moistened with TSB, is placed on top of the electrodes and filter. A retainer ring at right angles to the electrodes maintains constant pressure and close contact between pads, filter, and electrodes. The dish is sealed with parafilm to reduce moisture loss.

In dose-response studies of *Escherichia coli* and *Staphylococcus aureus*, volumes from a tenfold series were filtered. Bacteria from 100 ml of undiluted and 10^{-1} and 10^{-2} dilutions of estuarine or freshwater samples were collected on membrane filters. Viable counts for both the dose-response studies and the water samples were made by spreading appropriate dilutions from a tenfold series on Trypticase soy agar (BBL) and counting colonies after 24 hours incubation at 35° C.

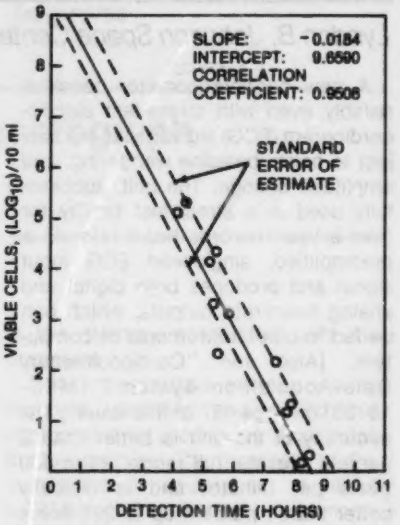

Figure 2. The relationship between the Number of "Escherichia coli" Cells retained on membrane filters and detection times obtained with the platinum electrode electrochemical method is shown here.

Prior to connecting the electrodes to the strip-chart recorder, each channel was set at a zero reference point. The 25-mm and 50-mm electrodes were connected to the positive and negative terminals, respectively, of the recorder. The electrodes were allowed to equilibrate for 60 to 80 minutes before establishing a baseline that was generally offset slightly from the recorder zero reference point in the positive direction. Responses upward from the baseline were considered positive and downward as negative. Detection time endpoints (lag time) were recorded as the time between challenge and the initial increase in voltage.

The dose-response curve for *Escherichia coli* is illustrated in Figure 2, and the linear regression parameters are shown. These results compare favorably with previously published data in which platinum electrodes were tested in a broth/test-tube experiment. Favorable results were also achieved with 50 estuarine and 46 freshwater samples tested with the combined technique. Results with *Staphylococcus aureus*, however, were erratic and not reproducible. The overall results indicate that the combined technique can be an effective and rapid method for estimating the microbial loading of water samples.

This work was done by Judd R. Wilkins and David C. Grana of **Langley Research Center** *and Susan C. Fox of The Bionetics Corp. For further information, Circle 52 on the TSP Request Card.*

Inquiries concerning rights for the commercial use of this invention should be addressed to the Patent Counsel, Langley Research Center [see page A5]. Refer to LAR-12709.

Gage for Evaluating Rheumatoid Hands

Lateral mobility of knuckle joints is measured simply and reliably.

Goddard Space Flight Center, Greenbelt, Maryland

A two-axis goniometer accurately measures the movements of the fingers about the metacarpophalangeal (knuckle) joints. It can be used to help diagnose hands that have structurally changed because of rheumatoid arthritis. The new goniometer measures lateral movement of a knuckle joint when it is flexed 70° to 90°. This lateral movement is small in normal joints but increases in diseased joints.

The new diagnostic instrument, constructed of stainless steel and brass, basically consists of two connected protractors that simultaneously measure angles in perpendicular planes. The goniometer dials are offset to clear the bony protuberances that result from rheumatoid arthritis. Extension and offset adjustments span any size hand. The pivots are friction damped, so that readings are retained even if the goniometer is accidently jostled. The unit weighs about 4.5 ounces (128 grams).

The movable arm of the goniometer operates in two mutually perpendicular planes (see figure), a plane perpendicular to the back of the hand (dorsal-volar plane) and a plane through the bones of the forearm (radio-ulnar plane). The measurement procedure begins by drawing a line on the middle of the back surface of each finger, along its axis. The stationary platform arm of the goniometer rests on the back of the hand in alinement with the bones between the knuckle and wrist of the fingers being measured. It is held in position by the measurer.

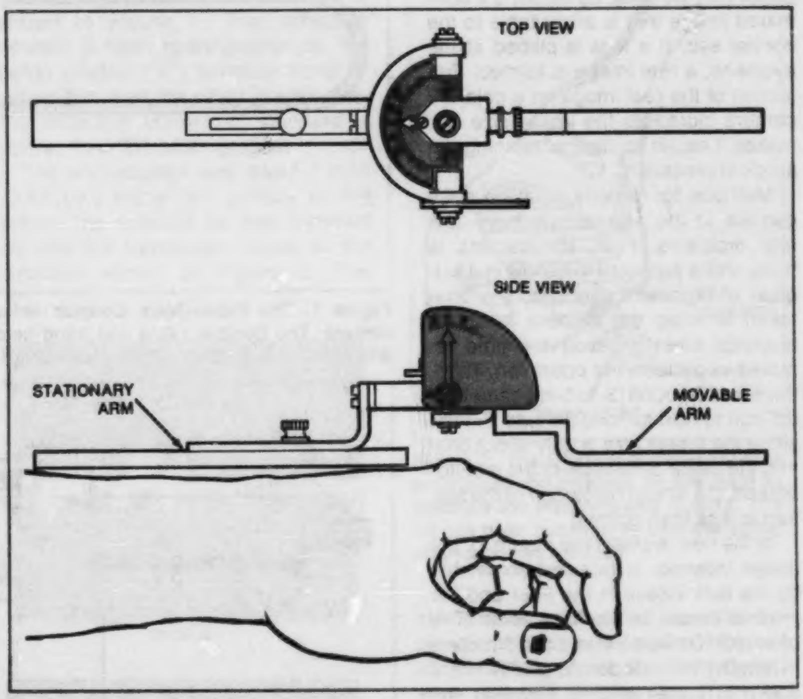

The Two-Axis Goniometer measures flection in the radio-ulnar plane (top view) and in the dorsal-volar plane (side view). The dial offset shown in the side view accommodates protuberances at the joint.

The knuckle joint is flexed 70° to 90° with the movable goniometer arm alined with the line drawn on the finger. With the joint flexed the finger and goniometer are passively moved in the radio-ulnar plane, and the total range of motion is recorded.

The two-axis goniometer and measurement procedure can be used with a minimum of training. Reliability studies show very good agreement of measurements by the same and by different measurers. The accuracy and reliability of measurement are important in assessment and treatment planning, in the documentation of joint changes over time, and for gathering research data.

This work was done by James C. Houge and Kenneth A. Plautz of the University of Wisconsin for **Goddard Space Flight Center.** *For further information, Circle 53 on the TSP Request Card.*

GSC-12610

Fiber-Optics Couple Arthroscope to TV

A hand-held flexible coupler links the arthroscope to a color-TV camera.

Langley Research Center, Hampton, Virginia

A new, hand-held coupler images the output of an arthroscope onto a coherent fiber bundle. The image travels along the flexible bundle and appears at the other cable end, where the image is recollimated by a lens. The image seen looking into this lens is the same as if looking directly into the arthroscope.

The arthroscope allows surgeons to examine internal structures and organs through a small incision or natural opening in the body. Its output is a collimated image that is acceptable to the normal eye. If a lens is placed at the eyepiece, a real image is formed. Projection of the real image on a color-TV camera increases the image size and makes it easier to view, enhancing the surgical procedure.

Methods for directly coupling a TV camera to the arthroscope have several problems. First, the camera is bulky and is awkward to handle in a surgical environment. Second, the time taken to wrap the camera in sterile drapings often exceeds the time required to perform the operation. Third, the 6- to 10-pound (3- to 5-kg) camera is difficult to hold for long periods. Finally, since the image size is only about one-fifth the major dimension of the monitor screen, the actual resolution of the system is less than optimal.

In the new system (see Figure 1), the image intensity is reduced somewhat by the bulk losses in the fiber and the Fresnel losses at the fiber ends. (The oriented 10-micron fibers are 3 meters in length.) With moderate quality fibers and short cable lengths, however, the losses are not significant. The collimated output is directed into the lens of the TV camera. The camera-lens focal length is chosen so that the image will fill the monitor screen.

The hand-held portion of the coupler is shown in Figure 2. The handle permits easy positioning and rotation of the

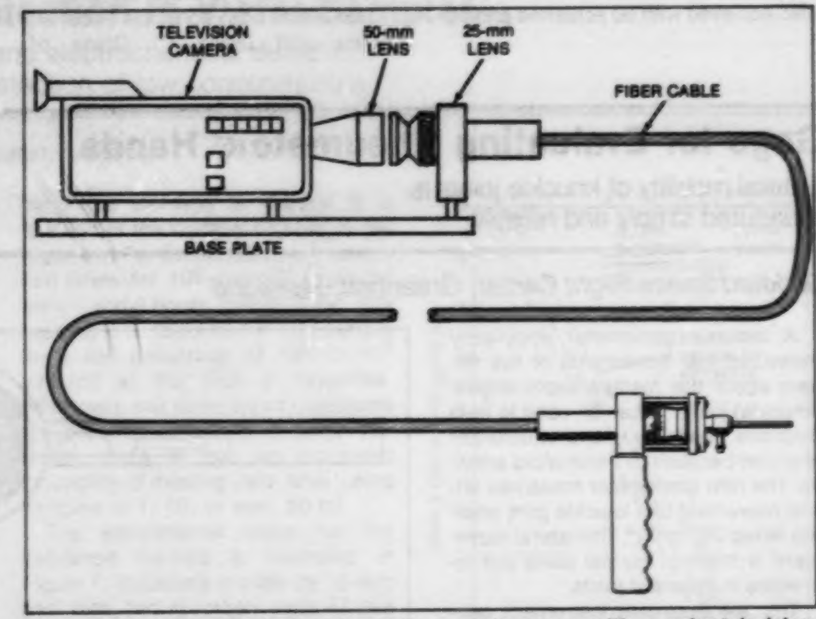

Figure 1. The **Fiber-Optic Coupler** links an arthroscope with a color-television camera. The flexible cable and hand-held coupler make it easy to manipulate the arthroscope in surgery, while displaying the arthroscope image on the TV monitor.

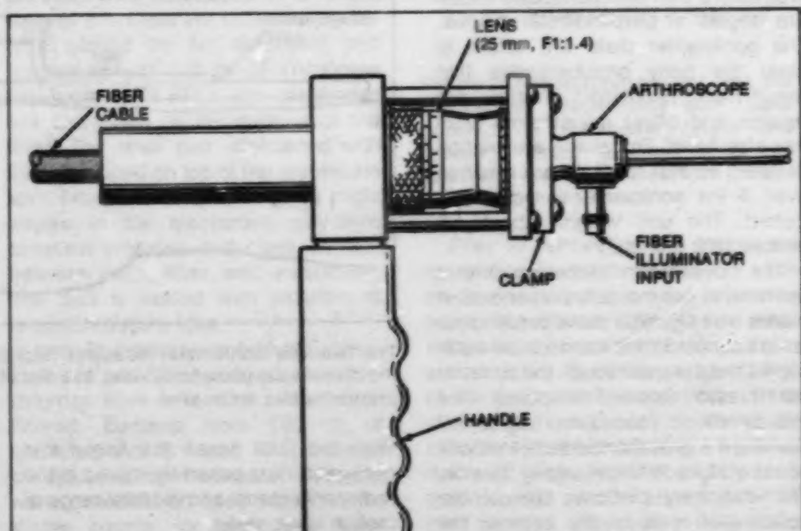

Figure 2. The **Hand-Held Portion** of the coupler has a pistol grip and a lens for imaging the arthroscope output on the fiber bundle.

arthroscope. The ultimate resolution of the system is limited by the resolution of the arthroscope and TV monitor (routine resolution is better than 100 microns). In addition to its medical applications, the coupler can be used for engine inspection, instrument repair, and visual inspection through small openings.

This work was done by John M. Franke and David B. Rhodes of **Langley Research Center.** *No further documentation is available.*
LAR-12718

Beef Grading by Ultrasound

The richness of reflections in ultrasonic A-scan signatures indicates the USDA grade of beef.

NASA's Jet Propulsion Laboratory, Pasadena, California

A proposed method for grading beef quality uses ultrasonic inspection. In the method, the grade of beef carcasses is determined by analysis of the ultrasonic A-scan signatures from the marbling within the muscle. Since the reflections from within the muscle are determined primarily by the fat/muscle interface, the richness of such reflections is a direct indication of the degree of marbling and quality. The method is intended to replace the present subjective method of sight and feel of individual USDA graders and ultimately to yield both the grade and yield of live cattle.

Though no work has been done on live animals, tests on butchered-beef specimens indicate a definite trend between ultrasonic signatures and grade. A typical scan of each grade is shown in Figure 1. The reflection content is seen to be greater for the better grades; i.e., prime is richer in reflections than the other grades, and the reflection content of standard is poorer than the other grades.

The area studied was about 1 inch (2.54 cm) below the surface of the steak. The external fat was trimmed off and the transducer aimed in the direction shown in Figure 2. The electronics were gated so that the picture displayed covers the range of 20 to 70 mm from the transducer, each graticule division being 5 mm. The reflection content or the density of moderate-amplitude (about 1-graticule-high) reflections is an indication of the fine structure of a specimen.

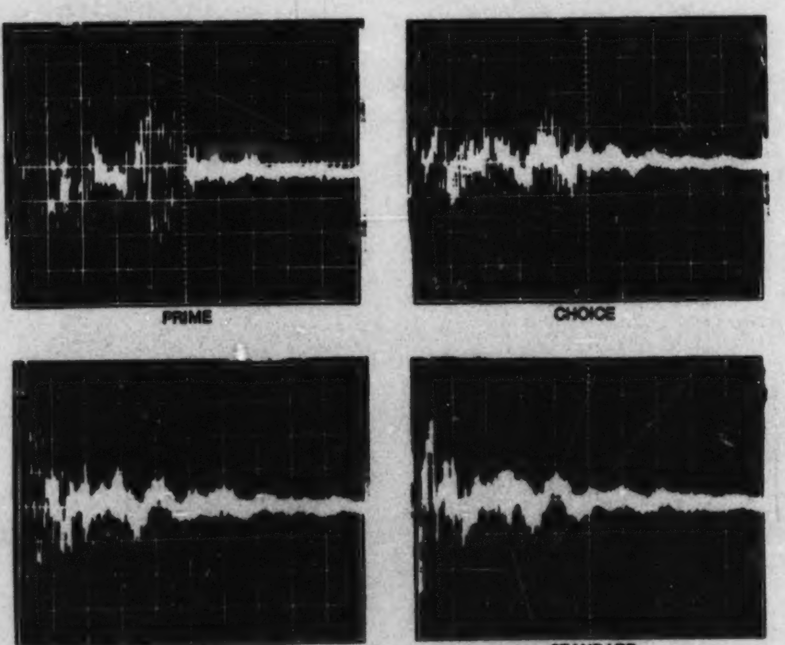
PRIME
CHOICE
GOOD
STANDARD

Figure 1. **Typical Ultrasound Patterns** for four USDA grades show the decrease in richness of reflections from best quality (prime) to lesser quality (standard) beef.

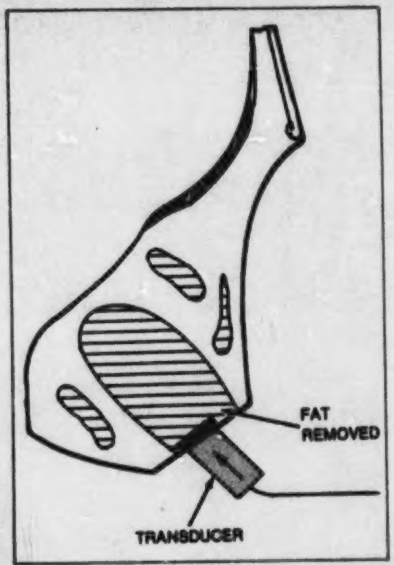

Figure 2. The **Ultrasonic Transducer** is positioned and oriented on the meat to measure the marbling and quality. The fat has been removed so that the signal attenuation is reduced.

As the sound wave propagates through fluid and soft tissues of the body, about 0.01 to 1 percent of the energy is reflected back toward the transducer at each interface. If the interface is approximately perpendicular to the transducer, a strong specular reflection is received, and the distance of the interface from the transducer can be measured with an

(continued on next page)

A-scan instrument.

In the feasibility experiments performed, a 2.25-MHz unfocused ultrasonic transducer of 0.5 in. (1.27 cm) diameter and moderate damping was used to transmit and receive direct and specular reflections from different tissue areas of marbled beef. The 2.25-MHz ultrasonic bursts were 20 milliwatts in power and lasted about 1 microsecond. A wideband receiver without a rectifying detector was used in order not to reduce the information content of the signal.

This work was done by Paul M. Gammell of Caltech for **NASA's Jet Propulsion Laboratory.** *For further information, Circle 54 on the TSP Request Card.*
NPO-14812

Mechanics

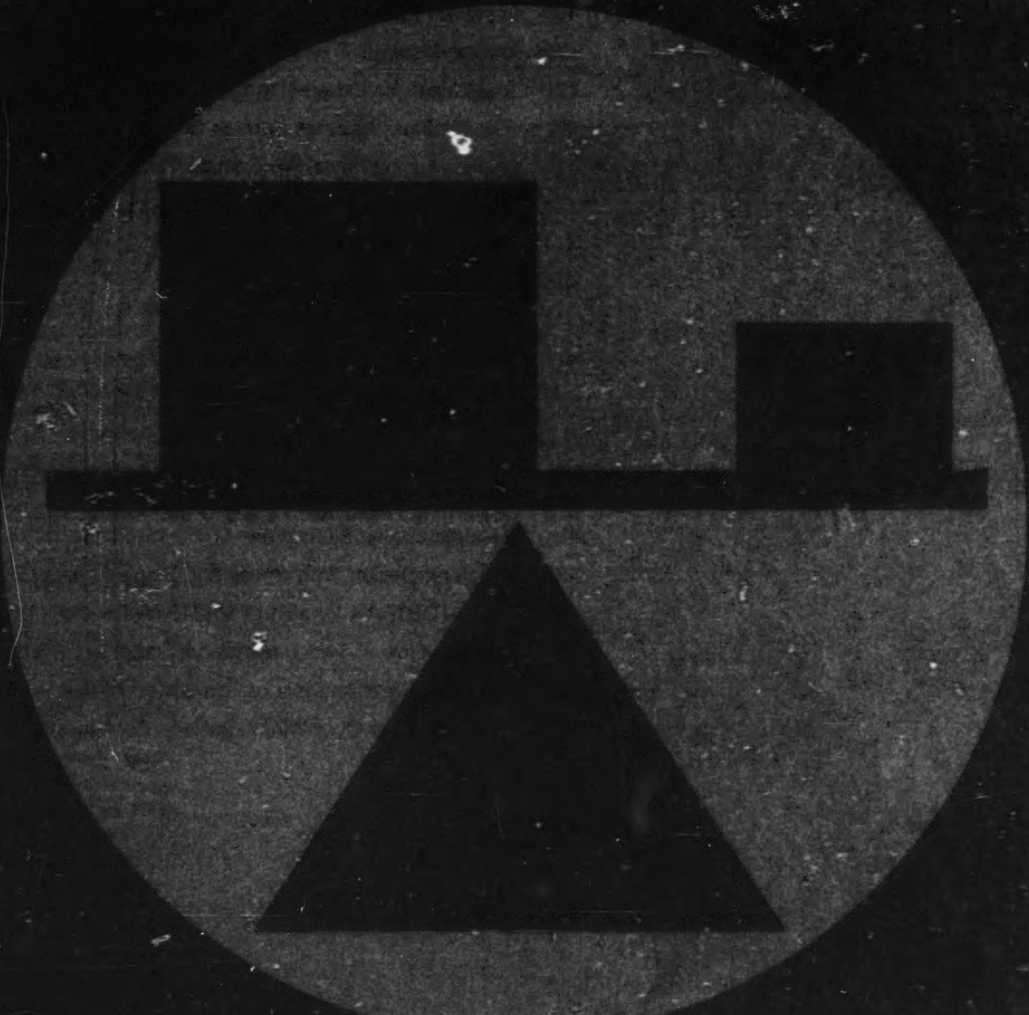

Hardware, Techniques, and Processes

467 An Oven for Many Thermocouple Reference Junctions
468 Isolation and Measurement of Rotor Vibration Forces
469 Improved LEEM Ranges Over Four Decades
470 Imager Displays Free Fall in Stop Action
471 Transducer for Extreme Temperatures and Pressures
471 Bulk Lifetime Indicates Surface Contamination
472 Biaxial Method for In-Plane Shear Testing
474 Gas Absorption/Desorption Temperature-Differential Engine
474 Instrument Measures Cloud Cover
475 Compact Infrared Detector
476 Fast Calibration of Gas Flowmeters
477 Wind-Simulation Tester for Solar Modules
478 Heat Pipes Cool Probe and Sandwich Panel

Computer Programs

479 Thermodynamic and Transport Properties of Air/Water Mixtures
479 Calculating Linear A,B,C, and D Matrices From a Nonlinear Dynamic Engine Simulation
480 Structural Design With Stress and Displacement Constraints
481 An All-FORTRAN Version of NASTRAN for the VAX
481 Potential Flow in Two-Dimensional Deflected Nozzles
481 The Design and Analysis of Low-Speed Airfoils
482 Transonic Flow Over Wing/Fuselage Configurations

An Oven for Many Thermocouple Reference Junctions

A compact oven holds many junctions at a stable temperature.

Dryden Flight Research Center, Edwards, California

Thermocouples are widely used for temperature measurement because they are inexpensive and reliable. They are accurate if their reference junctions are held at a constant known temperature. When many reference junctions are mounted in an oven for stable temperature control, temperature gradients in the oven or among the junctions may require special heating arrangements or special calibration measures.

To prevent nonuniformity in junction temperature, a compact, lightweight, multijunction oven has been designed with a symmetry of geometry, heating, and thermocouple-junction location (see figure). The oven has a cylindrical wall made of a material that is a good thermal conductor, such as brass. Inside the cylinder is a cylindrical heating coil, wound on a spool that is also made of brass. The end cap that closes the cylinder extends into the spool, with a temperature-sensing element (shown here as a control thermocouple). The sensor controls the power supplied to the heating coils so as to maintain the cylinder wall at a constant temperature.

Numerous holes are bored radially into the cylinder wall, and the thermocouple junctions are inserted in these holes. Because of their common distance from a common heating coil in a good conductor, the junctions are held at a common temperature.

This oven was originally developed for an airborne data-acquisition system used in flight tests. Its light weight, compactness, and low-power requirements, compared to other ovens for the same purpose, allowed the use of more thermocouples than would have been possible otherwise.

This work was done by Louis P. LeBlanc of **Dryden Flight Research Center.** *For further information, Circle 56 on the TSP Request Card.*

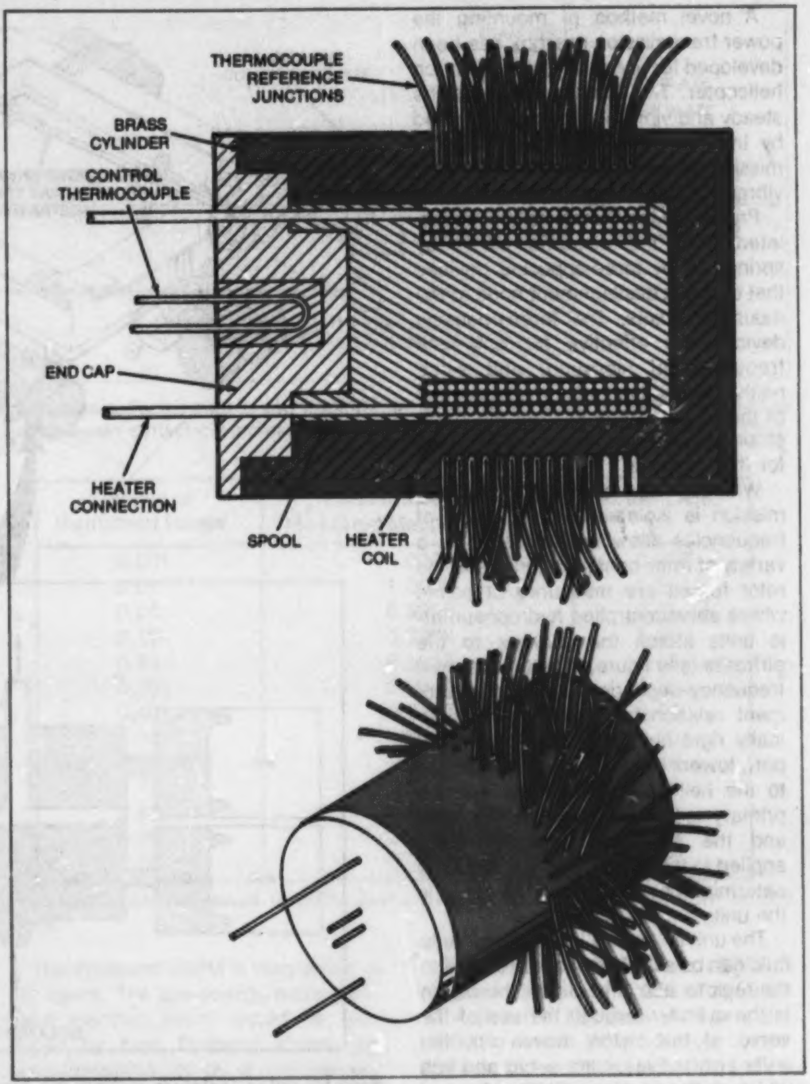

All of the Thermocouple Reference Junctions mounted in this cylindrically symmetrical oven are held at the same stable temperature.

This invention is owned by NASA, and a patent application has been filed. Inquiries concerning nonexclusive or exclusive license for its commercial development should be addressed to the Patent Counsel, Dryden Flight Research Center [see page A5]. Refer to FRC-10112.

Isolation and Measurement of Rotor Vibration Forces

Active vibration isolators couple transmission gearbox to helicopter frame and provide load measurement.

Langley Research Center, Hampton, Virginia

A novel method of mounting the power transmission gearbox has been developed for use on a NASA research helicopter. This system measures the steady and vibratory forces generated by the rotor and isolates the transmission from the airframe so that rotor vibrations are substantially reduced.

Previously the transmission was isolated from the airframe either by springs or by force-opposing devices that create a displacement node at the mounting points. The force-opposing devices are effective for only one frequency of vibration; and since neither method includes measurement of the vibration forces from the rotor, strain gages would have to be installed for that purpose.

With the new mounting, the transmission is isolated over a range of frequencies allowing the testing of a variety of rotor configurations, and the rotor forces are measured at points where servocontrolled hydropneumatic units attach the gearbox to the airframe (see figure). The units have a frequency-dependent load/displacement relationship that gives a statically rigid but dynamically soft support, lowering the vibration transferred to the helicopter. The units are the primary load path between the rotor and the airframe; thus the loads applied to the airframe by the rotor are determined by measuring the loads in the units.

The unit is "active" in that hydraulic fluid can be supplied under pressure to the regions above or below the piston in the cylinder through the use of the servo. If the piston moves up, the lever arm activates the servo and lets oil into the top region and lets oil out of the lower region. High-pressure fluid is pumped into the top of the cylinder until the piston is recentered — hence the static rigidity of the mounting. At frequencies above about 2 Hz, however, too little fluid can be pumped in to change loads, so the air in the air reservoirs acts as a simple pneumatic spring — hence the dynamic softness. Load is measured simply by measuring the differential pressure across the piston.

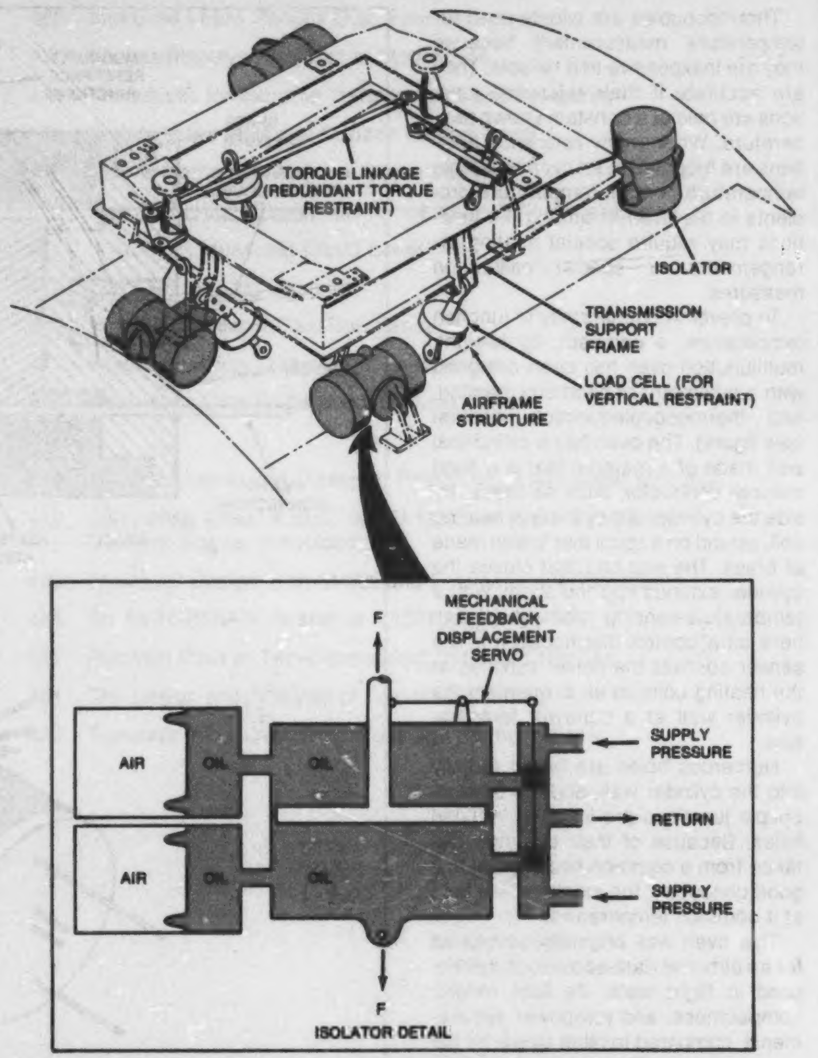
TORQUE LINKAGE (REDUNDANT TORQUE RESTRAINT)
ISOLATOR
TRANSMISSION SUPPORT FRAME
LOAD CELL (FOR VERTICAL RESTRAINT)
AIRFRAME STRUCTURE
MECHANICAL FEEDBACK DISPLACEMENT SERVO
F
AIR
OIL
OIL
AIR
OIL
OIL
SUPPLY PRESSURE
RETURN
SUPPLY PRESSURE
F
ISOLATOR DETAIL

Four Vibration Isolators restrain the transmission support frame against in-plane motion. For the current configuration, standard load cells are used for vertical restraint; however, they could be replaced by vibration isolators.

This work was done by Irwin Kenigsberg and John F. Madden of United Technologies Corp. for **Langley Research Center.** *Further information may be found in "The RSRA Active Isolation/Rotor Balance System." A copy may be purchased [$7, paper copy; $3, microfiche] from the Technical Information Service, American Institute of Aeronautics and Astronautics, Inc., 555 West 57th Street, New York, New York 10017. [Request document A79-18654.]*
LAR-12476

Improved LEEM Ranges Over Four Decades

A low-energy electron magnetometer would be suitable for terrestrial and aerial magnetic-field measurements.

Langley Research Center, Hampton, Virginia

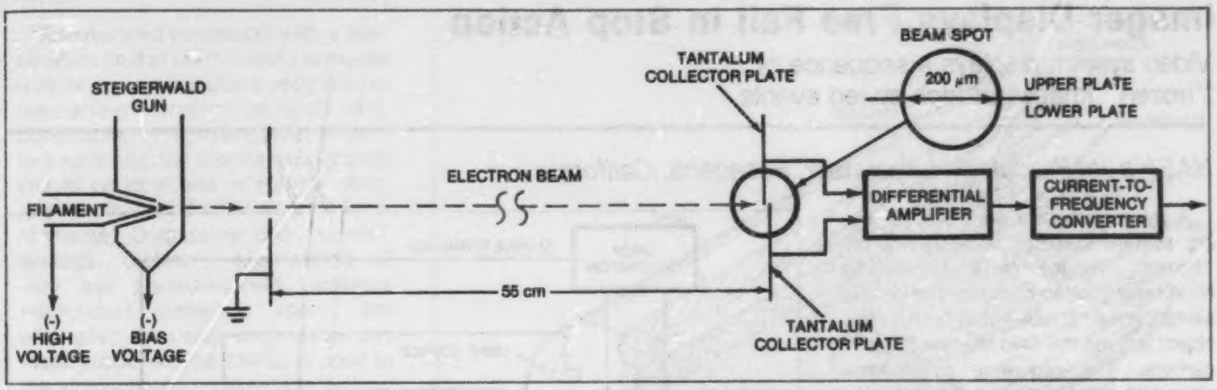

A **Beam of Low-Energy Electrons** strikes two tantalum collector plates, and the differential current is amplified and converted to frequency. The current difference increases as the beam deflection increases, providing a measure of the local magnetic field. The drawing is not to scale.

A proposed new low-energy-electron magnetometer (LEEM) would measure magnetic fields as low as 10^{-3} nanotesla. Its anticipated performance in selected applications compares favorably with that of more-complex high-resolution magnetometers.

Other magnetometers currently available include pivoted needle instruments, compensation-type variometers, fluxgate instruments, proton precession magnetometers, optically pumped magnetometers, and the highly-sensitive superconducting quantum interference device (SQUID) magnetometer. A SQUID magnetometer is essentially a superconducting flux transformer tightly coupled to a SQUID.

The SQUID and the optically pumped magnetometers can meet the 0.01-nT sensitivity requirement of many geomagnetic and interplanetary field measurements. However, the SQUID requires liquid helium for its operation and thus seems more appropriate for laboratory measurements. The sensitivity of the LEEM compares favorably with that of optical absorption magnetomers. Using modern solid-state technology, LEEM response time can be reduced to the microsecond range for analyzing fast magnetic transients and for magnetic-signature analysis in large engineering systems.

Fraction of Instrument Range	Ratio of Actual to Measured Magnetic Field	Actual Field, nT
0.001	1.0000	0.059
0.01	1.0000	0.59
0.05	0.9996	2.95
0.10	0.9983	5.90
0.20	0.9933	11.80
0.30	0.9848	17.70
0.40	0.9727	23.60
0.50	0.9566	29.50
0.60	0.9363	35.40
0.70	0.9109	41.30
0.80	0.8796	47.20
0.90	0.8400	53.00
1.00	0.7854	59.00

Predicted LEEM Response to fields over a range of four decades is shown in this table.

The improved LEEM is diagramed in the figure. The low-energy monoenergetic electron beam would be produced by high Rydberg atoms, by photoionization, or by a hot-filament source. Calculations show that if the current from each collector plate is fed to a current-to-frequency converter with a conversion factor of 1 Hz/10^{-14} A, the system sensitivity would be about 4.31×10^4 Hz/nT. Thus, a measurement of magnetic fields as low as 0.01 nT could be made with high accuracy in a 1-second counting time. A measurement of 0.1 nT could be made with moderate accuracy in a counting time of 10 milliseconds.

The response of the new LEEM to magnetic fields from 0.059 nT to 59.00 nT is shown in the table. As seen, the LEEM is linear to ±1 percent over three decades, from under 10^{-2} nT to over 10^1 nT. Since the nonlinearity of the instrument is known, it is easily corrected for, extending the useful range to four decades, from 5.9×10^{-3} nT to 5.9×10^1 nT.

This work was done by Jag J. Singh and George M. Wood, Jr., of **Langley Research Center,** *Grayson H. Rayborn of the University of Southern Mississippi, and Frederick A. White of Rensselaer Polytechnic Institute. Further information may be found in*

(continued on next page)

NASA TM-80172 [N80-13429/NSP], "A Low Energy Electron Magnetometer" [$4], a copy of which may be purchased [prepayment required] from the National Technical Information Service, Springfield, Virginia 22161.

This invention is owned by NASA, and a patent application has been filed. Inquiries concerning nonexclusive or exclusive license for its commercial development should be addressed to the Patent Counsel, Langley Research Center [see page A5]. Refer to LAR-12706.

Imager Displays Free Fall in Stop Action

Video system displays a sequence of "frozen" images of high-speed events.

NASA's Jet Propulsion Laboratory, Pasadena, California

A microprocessor-controlled imaging system displays a sequence of "frozen" images of a free-falling object using video cameras positioned along the fall. Strobe lights flash as the object passes the field of view of each camera. The sequence of images stored on video disk and displayed on a television monitor is a stop-action record of the dynamics of the falling object. With appropriate modifications, the system can monitor other high-speed phenomena using one or several cameras.

The basic configuration, developed to observe the dynamics of hollow liquid glass pellets formed by a drop generator, is shown in the diagram. As the generator releases a molten bubble, it generates an enable pulse that initiates the camera sequence.

As the object enters the field of view of each camera, photosensors detect light reflected from its surface and fire the strobe light. The photosensor signals also activate the video multiplexer and establish the connection to the first track on the video disk. At the beginning of the next available television frame, determined by the sync generator, a scan of the camera commences, and the video information is written on the disk. The arrival of the object in the field of view of the next camera initiates an analogous sequence, resulting in a series of single-frame exposures recorded on disk and displayed on the TV screen.

The enable pulse creates an erase scan in the camera to clear the system and establishes the black level. The beam or scan drive can be returned to x and y = 0 to wait the next command. This prevents loss of the image by leakage if the object arrives midframe.

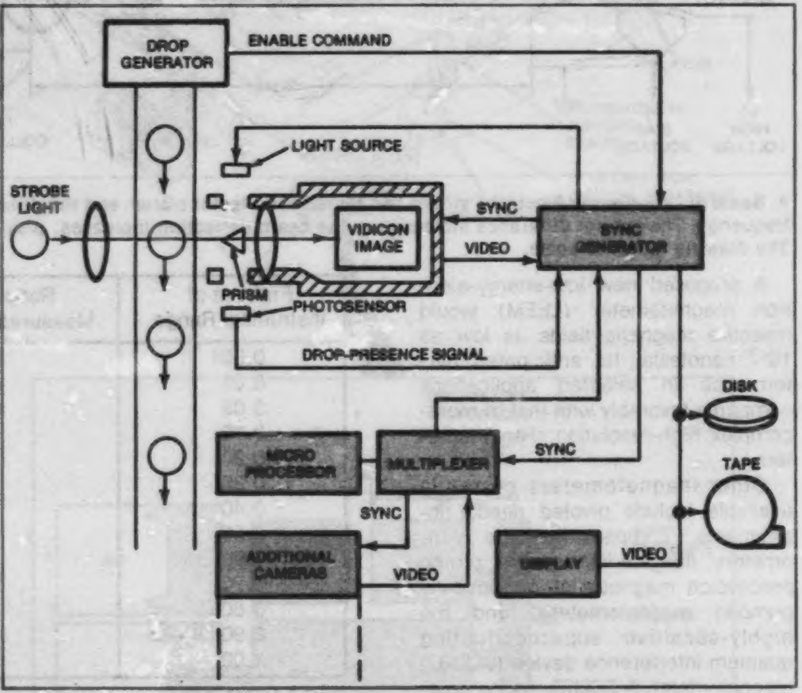

In the High-Speed Imager the drop generator outputs an enable command that initiates the sequence for visualizing the moving bubble. Each strobe light is controlled to flash during the camera retrace period. The system utilizes the intrinsic capability of the vidicon or CCD camera to store the image until it is scanned.

A microprocessor accepts the enable command from the drop generator and controls the cameras. It also supervises the writing of the image pixels on the video disk. The strobe light is triggered by sync pulses from the microprocessor. Similarly, the multiplexer function of the microprocessor enables the cameras in sequence and synchronizes the video format. The microprocessor can also be programed to image a single object in a train of objects by rejecting objects that arrive at the cameras at the wrong time.

The system can be modified to use a charge-coupled-device (CCD) camera and a strobed circular LED array arranged around the camera lens instead of the strobe light. In addition the image can be digitized by the microprocessor.

This work was done by Robert E. Frazer of Caltech for **NASA's Jet Propulsion Laboratory.** *For further information, Circle 58 on the TSP Request Card.*
NPO-14779

Transducer for Extreme Temperatures and Pressures

Transducer functions under high pressure and in vacuum.

Lyndon B. Johnson Space Center, Houston, Texas

An improved transducer with a temperature limit of 500° C and a pressure limit of up to 10 kilobars responds to mechanical vibrations up to 20 kHz. Constructed of high-temperature-resistant materials, the new vibration pickup should perform well in nuclear reactors, turbines, and other extreme environments. Outgassing and "virtual" leakage, problems experienced at very low pressures with previous transducers potted in epoxy, are eliminated by using only glass and metal supports. The interior is open to the atmosphere to prevent the buildup of pressure-induced stresses.

As with other transducers of this type, the new pickup senses the motion of a magnetic material attached to the test object. The motion changes the flux in a magnetic pole piece within a pickup coil, which generates an emf and current in the external circuit. A magnet attached to the pole piece biases the transducer at its operating point.

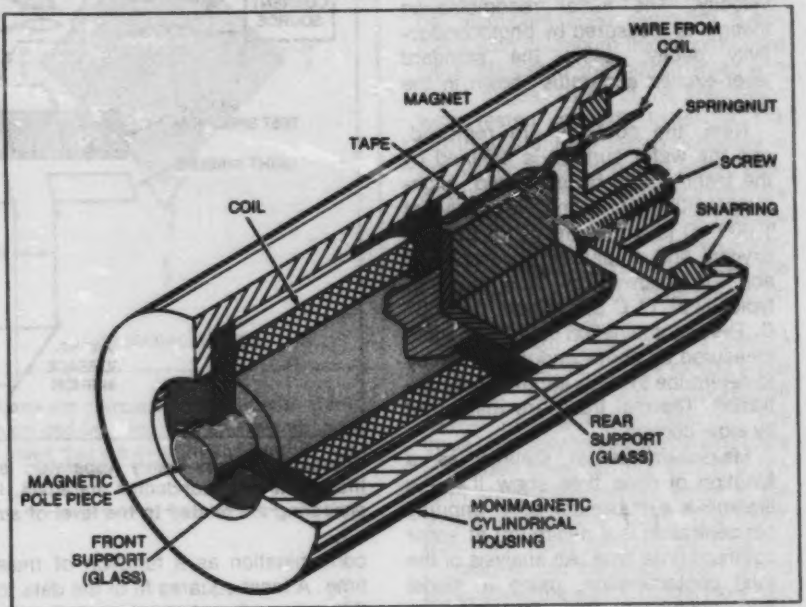

The Pole Piece of the transducer is attached to the test object and measures its mechanical vibration. By holding the parts against the housing with a spring, distortion due to pressurization and thermal strain is eliminated.

The transducer parts (see figure) are supported and positioned in a nonmagnetic housing. Glass supports orient the magnetic pole piece centrally and axially. Since the supports are open to the external atmosphere, there is no differential pressure on them. The magnet, which is Alnico 8 or similar material, clamps to the pole piece magnetically. All of the parts are held firmly against the housing shoulder by a snapring, a springnut (a flanged nut that can apply a bending load to a mating shoulder), and a screw. The coil, which is held in place by the glass spacers, is made of ceramic-insulated copper wire, or similar material.

To relieve strain on the electrical connection, insulated copper leads are welded to the coil terminations, taped to the magnet, and exit through the springnut. Holding the parts against the housing with a spring also reduces distortion due to pressurization and thermal strain.

This work was done by Harry Nadler of Rockwell International Corp. for **Johnson Space Center.** *No further documentation is available.*
MSC-18778

Bulk Lifetime Indicates Surface Contamination

An indirect measurement of wafer surface impurities has a sensitivity of 300 monolayers.

NASA's Jet Propulsion Laboratory, Pasadena, California

A new method of determining the level of surface contamination on semiconductor wafers has a sensitivity of approximately 10^{10} impurities per cm^2. Surface contamination of this magnitude results, on heat treatment, in a bulk impurity concentration of 10^{12} cm^{-3} (for a sample 0.02 cm in thickness), which is sufficient to degrade the minority-carrier recombination lifetime.

In the new technique, a sample is annealed at high temperature to redistribute the surface impurities uniformly throughout the bulk. The bulk impurity concentration is determined before and after annealing by measuring the recombination lifetime. The method can be used to evaluate wafer-cleaning techniques, to qualify

(continued on next page)

the purity of chemicals and deionized water used in these techniques, or to monitor a production process.

In tests to evaluate cleaning procedures, specimens are cut from high-resistivity silicon. Contacts are applied, and the surface is etched to control the surface recombination velocity. The initial recombination lifetime is measured by photoconductivity decay, using the standard laser-excited apparatus shown in the figure.

Next, the contacts are removed, and the wafer surface is cleaned by the technique to be evaluated. High-temperature annealing, typically at 1,000° C in a mixture of 95 percent oxygen and 5 percent hydrochloric acid, is followed by slow cooling, typically at 1° C per minute, to 200° C. The recombination lifetime is again measured by photoconductivity decay to determine the bulk impurity concentration. Thermal traps are minimized by slow cooling.

Measurements of lifetime as a function of rinse time show that the lifetime is a maximum (i.e., impurity concentration is a minimum) at some optimum rinse time. An analysis of the total contamination, using a model that postulates that the cleaning solution leaves a residue of salts, yields an expression for the net contamination as a function of rinse time. A least-squares fit of the data to this expression determines the optimum rinse time.

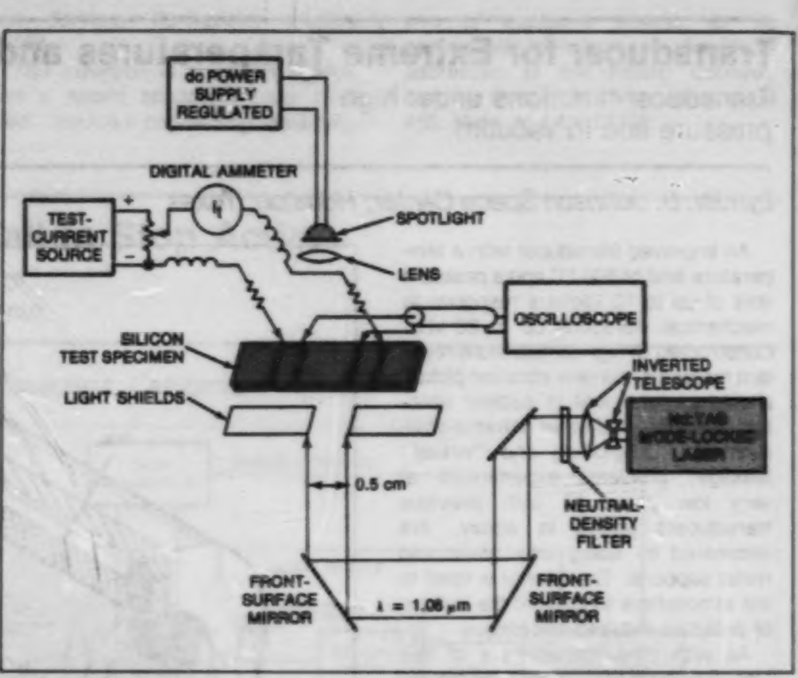

Photoconductivity-Decay Apparatus is used to determine the bulk recombination lifetime in semiconductor materials. Impurity levels in the bulk before and after annealing are related to the level of surface contamination.

This work was done by Phillip D. Blais of Westinghouse Electric Corp. for ***NASA's Jet Propulsion Laboratory.*** *For further information, Circle 59 on the TSP Request Card.*
NPO-14966

Biaxial Method for In-Plane Shear Testing

A method for obtaining uniform shear deformation yields more accurate values for material mechanical properties.

Langley Research Center, Hampton, Virginia

A biaxial method for measuring in-plane shear properties applies a more-uniform shearing deformation to orthotropic and isotropic materials than uniaxial picture-frame techniques. The forces applied by the biaxial method are one-half the magnitude required by the uniaxial method, reducing the transmitted force and consequently reducing pin deformations.

In the biaxial method, shown in Figure 1, a square sandwich specimen is installed in a very stiff fixture with pinned corners. Equal tensile and compressive forces are applied along the frame diagonals through the corner pins. The frame deformation, depicted in Figure 2b, creates a parallelogram with sides that are straight and unchanged in length. With the conventional, uniaxial method of loading, the sides are extended and bent, as shown in Figure 2a.

The deformation caused by the biaxial method is that required to subject the test specimen to a uniform shear strain. For orthotropic or isotropic materials, this is equivalent to subjecting the material to a uniform shear stress.

The tensile load is applied vertically by a standard tensile-test machine, and the compressive load is applied horizontally by a hydraulic cylinder, load cell, and tension bar. The compressive

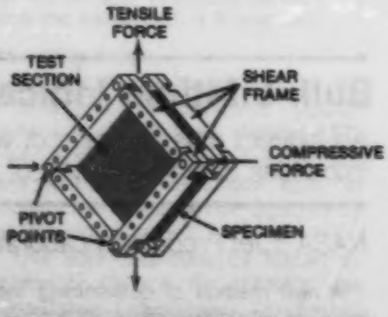

Figure 1. In the **Biaxial Method,** the square sandwich specimen is installed in a very stiff frame with pinned corners. Applied loads are one-half those required in the uniaxial method.

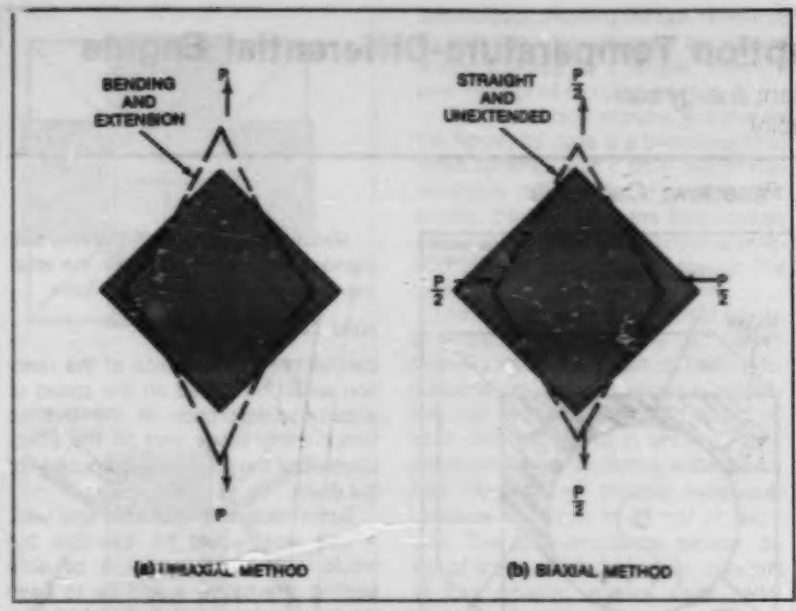

Figure 2. The Uniaxial and Biaxial Deformations are compared. The unaxial method (a) causes the edges to undergo both extension and bending; the biaxial method (b) deforms the frame into a parallelogram with sides that are straight and unchanged in length.

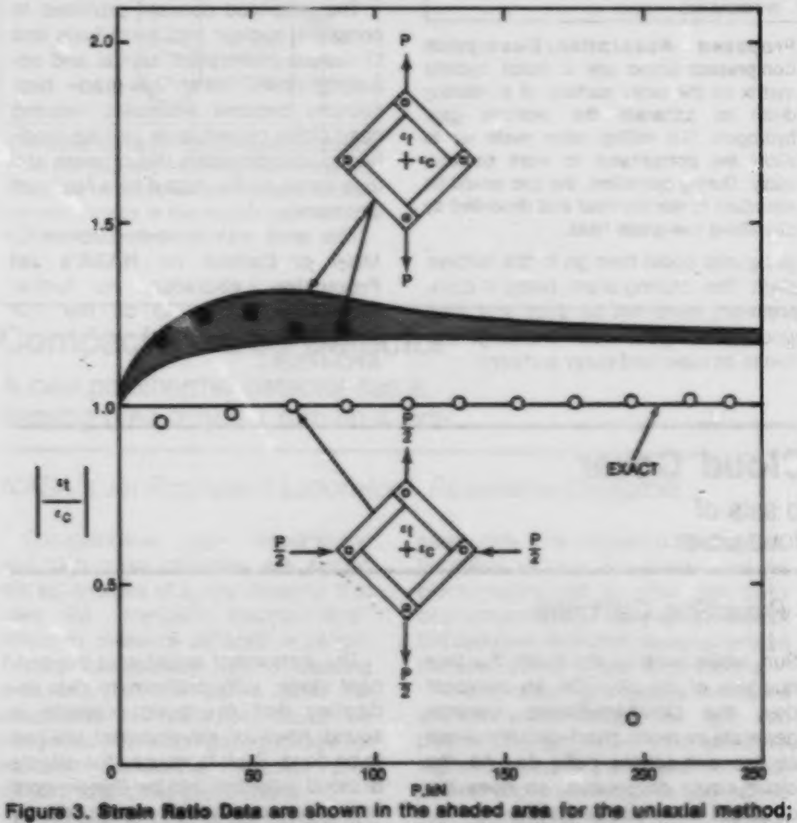

Figure 3. Strain Ratio Data are shown in the shaded area for the uniaxial method; biaxial data falls along the straight line $|\epsilon_t/\epsilon_c| = 1$, indicating a uniform shearing deformation.

load is measured by the load cell, while the tensile load is measured by a similar transducer built into the tensile-test machine. Output from both load cells is recorded electronically. A test machine with biaxial load capability (tension and compression) could also be used.

To quantify the difference between uniaxial and biaxial loading, four identical aluminum-faced sandwich specimens with aluminum honeycomb core were fabricated and instrumented with strain gages. Three of the specimens were tested uniaxially to failure. The fourth was initially tested uniaxially in the elastic range and then tested biaxially to failure. Results of these tests are shown in Figure 3, where the average value of the principal tensile-to-compressive strain ratio $|\epsilon_t/\epsilon_c|$ over the specimen face is plotted as a function of total applied load.

A specimen subjected to a uniform shearing deformation will exhibit equal principal tensile and compressive strains, yielding a strain ratio of 1. The three uniaxially tested specimens (date in shaded area) did not exhibit a uniform shear deformation, either in the elastic or inelastic range. The fourth specimen (data denoted by squares) showed similar behavior when tested uniaxially in the elastic range. However, when tested biaxially to failure, a uniform shearing deformation was achieved in both the elastic and inelastic regions (circles along $|\epsilon_t/\epsilon_c| = 1$).

In addition, tests showed that frictional effects in the shear frame and loading apparatus had a negligible effect on the experimental results. Also, the stiffening effect of honeycomb core on the in-plane shear response of a sandwich panel was identified, and a method was found for considering this effect.

This work was done by Harold G. Bush of **Langley Research Center** *and Tanchum Weller of the National Academy of Sciences. Further information may be found in NASA TM-74070 [N78-21489/NSP], "A Biaxial Method for Inplane Shear Testing" [$5]. A copy may be purchased [prepayment required] from the National Technical Information Service, Springfield, Virginia 22161.*
LAR-12680

Gas Absorption/Desorption Temperature-Differential Engine

Almost 90 percent of gas-turbine-plant energy can conceivably be converted to electricity.

NASA's Jet Propulsion Laboratory, Pasadena, California

A compressor concept is proposed that would be well suited to work in conjunction with a continuous Brayton-cycle gas-turbine plant for converting high-temperature energy to electricity. The compressor operating in a continuous mode would assist the plant in converting almost 90 percent of heat to electricity. Conventional turbine plants work in a batch mode and operate at 40 percent efficiency.

The compressor would utilize a reversible metal hydride reaction to supply hydrogen that would serve as the working fluid. The hydrogen gas would be compressed by cyclic absorption/desorption in a metal hydride matrix embedded on a rotating drum (see figure). The absorption process would release heat, and the desorption process would absorb low-grade heat.

Two thermal inputs could be used to operate the hydride compressor: a low-temperature input ($T \approx 100^\circ$ C), supplied by low-grade solar, geothermal, or waste heat; and a cold low-pressure gas input. For a continuous-acting heat pump that would replace a batch process, fixed locations for the heat would be maintained, and the absorbent material would be moved on a drum from one temperature region to the other and back. The compressed hot gas from the continuous-acting temperature-differential absorption/desorption gas pump could then go to the turbine plant. The rotating drum, being in compression, need not be thick and thus would allow good heat exchange between its inner and outer surfaces.

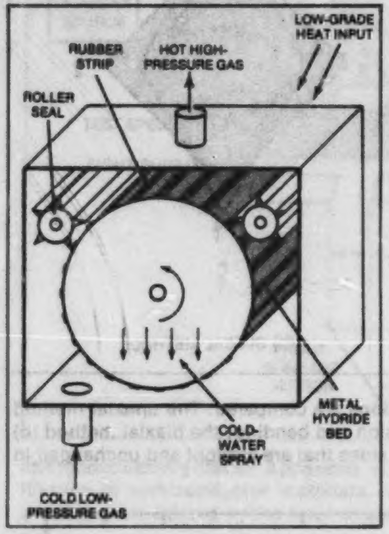

Proposed Absorption/Desorption Compressor would use a metal hydride matrix on the outer surface of a rotating drum to generate the working gas, hydrogen. The rolling valve seals would allow the compressor to work continuously. During operation, the gas would be absorbed to release heat and desorbed by absorbing low-grade heat.

Metal hydrides are not the only substances that can be used on the rotating drum. Any reactant of the form:

$$\text{solid} \rightleftarrows \text{solid} + \text{gas}$$

can be used. The choice of the reaction would be based on the speed of absorption/desorption in the desired temperature range and on the effectiveness of the roll seal used outside of the drum.

Some materials would not seal well. A gas leak would be tolerable but would reduce efficiency. A possible sealing alternative would be to have the roller in the form of a toothed star, as shown, that meshes with rubber seal strips on the drum. The active material on the drum would then be between the rubber strips.

The proposed concept promises to conserve nuclear and fossil fuels and to reduce powerplant capital and operating costs. When low-grade heat sources become abundant, existing gas-turbine powerplants can be modified to accommodate this process and thus increase the output by a factor of 2 or more.

This work was done by Charles G. Miller of Caltech for **NASA's Jet Propulsion Laboratory**. *For further information, Circle 60 on the TSP Request Card.*
NPO-14528

Instrument Measures Cloud Cover

The voltage ratio derived from two sets of solar cells equals the fractional cloud cover.

NASA's Jet Propulsion Laboratory, Pasadena, California

The outputs of eight solar cells are utilized in an instrument that makes an instantaneous measurement of cloud cover—a factor that is of interest to meteorologists as an aid in weather forecasting. The instrument includes a tracking mechanism so that one of the set of four solar cells always faces the Sun, while another set faces the four quarters of the sky. On an overcast day, the cloud-irradiance sensors generate as much short-circuit current as the sun-sensor cells do. As the cloud cover decreases, so does the output of the cloud sensors.

The instrument is just past the concept stage, with preliminary data indicating that the basic principle is sound; however, development still has to be done. Such factors as the effects of cloud reflection into the Sun sensors and erroneous readings caused by

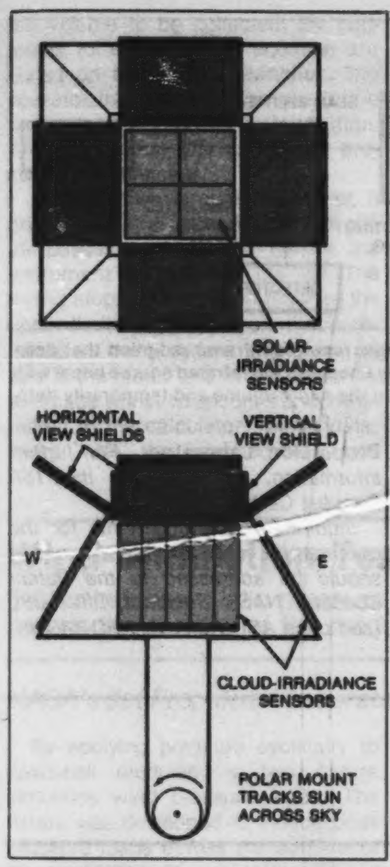

The Solar Cells (in color) sense radiation from the Sun and from the rest of the sky. The ratio of cloud-sensor voltage to Sun-sensor voltage is the numerical measure of the cloud cover.

small clouds blocking the Sun remain to be evaluated. Nonetheless, the sensor shows promise as a simple, inexpensive monitor of cloud cover.

The cloud-cover monitor is shown in the figure. Its base is a truncated four-sided pyramid, with a polar mount that rotates at 15° per hour to track the Sun across the sky. Thus the Sun-sensing solar cells on top of the truncated pyramid always face directly toward the Sun.

The four sides of the pyramid are at an angle of approximately 60° to the central axis of the pyramid. Each side supports one square silicon photovoltaic cell, with the electrical output of each cell connected in series. These cloud-irradiance sensors are loaded so that 100 mW/cm^2 (normal incidence) produce an output of 25 mV on each cell. The solar-irradiance sensor, on top of the truncated pyramid, consists of four smaller, square solar cells, also connected in series and also loaded so that 100 mW/cm^2 produce an output of 25 mV on each cell. Cloud cover is obtained by dividing the total series voltage obtained from the cloud-irradiance cells by the total series voltage obtained from the solar-irradiance cells.

View-limiting shields separate the fields of view of the two sets of solar cells. The nearly vertical limiters shield the solar-irradiance sensors from infrared radiation reflected by the clouds, while the horizontal limiters shield the cloud-irradiance sensors from direct or reflected solar irradiance. Horizontal limiters may also be needed near the bottom edges of the cloud-irradiance sensors to shield them from energy reflected from the ground.

This work was done by Eric G. Laue of Caltech for **NASA's Jet Propulsion Laboratory**. *For further information, Circle 61 on the TSP Request Card.*

This invention is owned by NASA, and a patent application has been filed. Inquiries concerning nonexclusive or exclusive license for its commercial development should be addressed to the Patent Counsel, NASA Resident Office-JPL [see page 5]. Refer to NPO-14936.

Compact Infrared Detector

A new potothermal detector has a sensing area only 0.1 mm on a side.

NASA's Jet Propulsion Laboratory, Pasadena, California

Compactness, high responsivity, and high noise immunity are among the advantages of a new detector that uses the "transient thermal lens" effect to measure infrared radiation. Tested successfully with a sensing area only 0.1 mm on a side, the broadband IR detector could be integrated into a compact package for pollution monitoring, weather prediction, and other applications.

The sensing material is a transparent sheet (plastic, for example), metalized with a reflecting coating and then overcoated with a black material on the same side. The reflecting coating can be either silver or aluminum, and the black coating can be either gold black or platinum black. The spectral range of the radiation detected depends only on the absorptivity of the black coating.

The infrared light passes through a shutter, which chops the light into pulses. The light strikes the black coating on the plastic sheet, where it is absorbed and transmitted to the plastic (see figure). Each pulse thus creates a transient region of hot material with an altered index of refraction in the plastic microvolume.

A beam of laser light is directed into the sensing material from a direction opposite to that of the infrared light. The laser beam is reflected by the metal coating under the black infrared-absorptive coating and is directed by a beam splitter into a detector.

The hot transient region generated by an infrared pulse acts as a lens that defocuses the laser beam. The defocusing increases as the infrared intensity increases. Thus the detector monitors a probe beam that weakens as the infrared light becomes more

(continued on next page)

intense. The detector could be a point detector such as a photomultiplier or an area detector such as a vidicon or a charge-coupled device. For the area detector, a two-dimensional profile of the IR beam is imaged. It is possible to pack a 20by20 matrix within a 1-cm^2 area detector.

Because the black absorbent layer on the sensing material absorbs equally well over a wide range of wavelengths, the infrared meter is sensitive over a broad band. Electrical noise is virtually eliminated because the sensor is nonelectronic, except for the last stage. Noise is also reduced because the infrared light is chopped and its transient rather than steady-state effects are measured.

The responsivity of the tested detector — the volts produced per unit flux — is $2x10^9$ $V/W/cm^2$ for a detector 0.1 mm on a side. Responsivity potentially can be further improved by substituting a transparent, highly polarizable material for the plastic sensing material. Such polarizable materials experience a higher change in index of refraction for a given change in temperature.

This work was done by Amitava Gupta, Su-Don Hong, and Jovan Moacanin of Caltech for **NASA's Jet Propulsion Laboratory.** *For further information, Circle 62 on the TSP Request Card.*

Inquiries concerning rights for the commercial use of this invention should be addressed to the Patent Counsel, NASA Resident Office-JPL [see page A5]. Refer to NPO-14864.

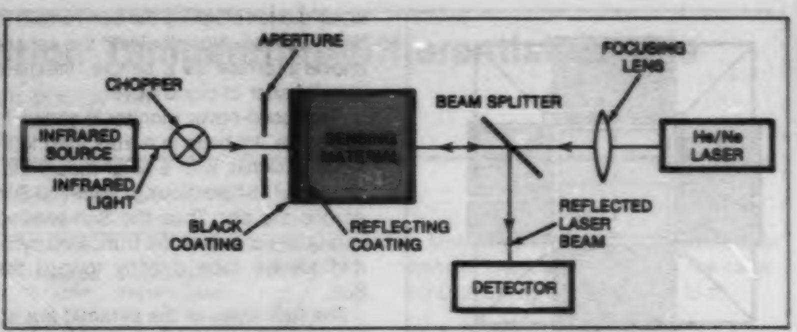
APERTURE
CHOPPER
FOCUSING LENS
BEAM SPLITTER
INFRARED SOURCE
SENSING MATERIAL
He/Ne LASER
INFRARED LIGHT
REFLECTED LASER BEAM
BLACK COATING
REFLECTING COATING
DETECTOR

The Sensing Material, only 0.1 mm on an edge, receives infrared radiation that defocuses the laser beam. Each pulse produced by chopping the infrared source beam with a shutter creates a transient "thermal lens" in the microvolume and temporarily defocuses the reflected laser beam.

Fast Calibration of Gas Flowmeters

Digital unit automates the calibration sequence.

John F. Kennedy Space Center, Florida

Digital logic and memory (see figure) are the key elements of an instrument that calibrates gas flowmeters quickly and accurately. The new instrument uses a calculator IC and a programable read-only memory (PROM) to solve the calibration equations. Infrared sensors start and stop the calibration sequence.

The instrument collects a known volume of gas, which displaces a piston, while simultaneously measuring the elapsed time. It calculates the meter flow rate from the volume, the time, and preset constants. Measured values of temperature and pressure in the instrument and in the flowmeter are entered in the calculations to adjust the calibration for differences in these variables at the two locations. The instrument calibrates either mass flowmeters or rotameters, in which flow measurement is based on mass or volume, respectively.

To calibrate, the operator connects a flowmeter to one of three cylinders and adjusts the piston upper-limit sensor for

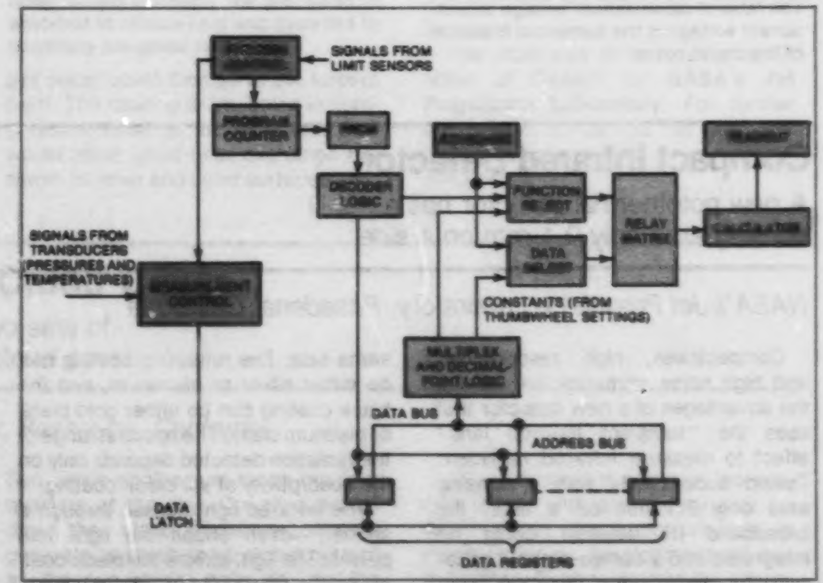
SIGNALS FROM LIMIT SENSORS
PROGRAM COUNTER
PROM
DECODER LOGIC
FUNCTION SELECT
DATA SELECT
RELAY MATRIX
CALCULATOR
SIGNALS FROM TRANSDUCERS (PRESSURES AND TEMPERATURES)
MEASUREMENT CONTROL
CONSTANTS (FROM THUMBWHEEL SETTINGS)
MULTIPLEX AND DECIMAL-POINT LOGIC
DATA BUS
ADDRESS BUS
DATA LATCH
DATA REGISTERS

Flowmeter Calibration Instrument Circuitry consists of hard-wired transistor/transistor logic (TTL) IC's, except for the calculator set, which are of metal-oxide-semiconductor (MOS) devices. The calibration program is stored in a programable read-only memory (PROM). Data are fed to the calculator serially from the data registers.

the volume to be collected. Six constants for the flow-rate equation are dialed on thumbwheel switches. The operator then turns on the gas to the flowmeter and presses a start button. From that point, the calibration proceeds automatically.

As gas flows through the meter, it drives the piston upward. When the piston passes the lower-limit sensor, the instrument starts timing the run. The timing stops as the piston reaches the upper-limit sensor. Four measurements — the pressure and temperature in the meter and in the prover — are made within 15 seconds and transmitted to the calculator. These data, along with the elapsed-time and volume measurements, are used to compute the flow rate in the flowmeter.

Each piston limit sensor is an infrared light-emitting-diode source and a phototransistor detector. The infrared energy from the source is reflected into the detector by the mercury seal on the moving piston. The pressure transducers are solid-state devices. Their outputs are digitized before they are processed by the calculator. The temperatures are measured by a multichannel digital thermometer. Pressures, temperatures, and the calculated flow rate are displayed on the instrument panels.

By controlling the procedure and performing the calculations automatically, the instrument has reduced operator time by 80 percent. It is more reliable than previous instruments using magnetic-pickup sensors because its components are solid-state devices. Also, because the instrument is digital, its accuracy is determined primarily by the accuracy of the transducers.

This work was done by R. V. Lisle and T. L. Wilson of **Kennedy Space Center.** *For further information, Circle 63 on the TSP Request Card.*

Inquiries concerning rights for the commercial use of this invention should be addressed to the Patent Counsel, Kennedy Space Center [see page A5]. Refer to KSC-11076.

Wind-Simulation Tester for Solar Modules

Tester induces cyclic pressure loads across the surface of the module.

NASA's Jet Propulsion Laboratory, Pasadena, California

By applying pressure cyclically to solar-cell modules, a test fixture simulates wind pressure loads. The fixture was developed to induce peak pressure loads across the surface of the modules at a predetermined pressure, typically 2,400 pascals (0.35 psi). Through gentle test pressure loads upon the solar module, the fixture guarantees the mechanical integrity of the module. The fixture operates at relatively high speed, completing a cycle in 5 seconds.

The module is sandwiched between two stiffened aluminum plates covered with 1/64-in. (0.4-mm) rubber sheets (see figure). To insure that the air pressure is transmitted uniformly to the module, the rubber sheets are slack. All the spaces and nonuniformities between the module and the sheets are filled with foam rubber until the foam is flush to within 5 mm of the module frame.

Automatic front-side and back-side pressure loading is cycled by a pneumatic system on a separate stand. Two loading valves and two exhaust valves alternately pressurize each side of the fixture. The controller for the valves is motor-driven. The applied load is uniform to within 10 percent, as measured by indicators mounted on a bar across the test

(continued on next page)

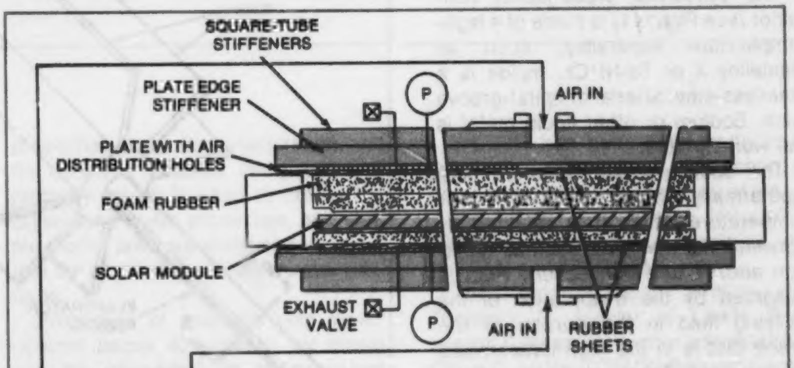

The Solar-Cell Module, to be tested, is sandwiched between two stiffened aluminum sheets that are covered with rubber sheets. Automatic front- and back-side pressure loading is cycled by a pneumatic system on a separate stand. Relief valves prevent overpressurizing.

frame that sense module frame deflections.

To reduce the air pressure from the line level to the desired pressure load, two regulators are used. Relief valves prevent overpressurizing. As an extra precaution, the air supply lines to the fixture have vents in them that are immersed in a can of water. The water in the can is only slightly deeper than the desired pressure, expressed in inches of water.

This work was done by John S. Griffith of Caltech for **NASA's Jet Propulsion Laboratory.** *For further information, Circle 64 on the TSP Request Card.*
NPO-14837

Heat Pipes Cool Probe and Sandwich Panel

Two new concepts integrate heat-pipe technology.

Langley Research Center, Hampton, Virginia

Heat pipes are incorporated in two new design concepts at Langley Research Center: a heat-pipe-cooled jacket for a probe used in hostile high-temperature environments, such as those encountered in the measurement of combustion-gas parameters, and a heat-pipe sandwich panel that combines the structural efficiency of sandwich construction with the thermal efficiency of the heat pipe.

The cylindrical probe-jacket container (see Figure 1) is made of a high-temperature superalloy, such as Hastelloy X or Td-Ni/Cr. Inside is a stainless-steel arterial or spiral-groove wick. Sodium or other liquid metal is the working fluid.

The cooling jacket transfers heat isothermally to an area of lower temperature where it is rejected by conventional methods, such as radiation and/or free convection. Heat is absorbed by the evaporation of the working fluid in the portion of the probe that is in the high-temperature environment. The heated vapor flows to the finned condenser where it condenses and rejects heat. From there, the liquid condensate flows back to the evaporator region by the action of gravity and by the capillary action of the wick.

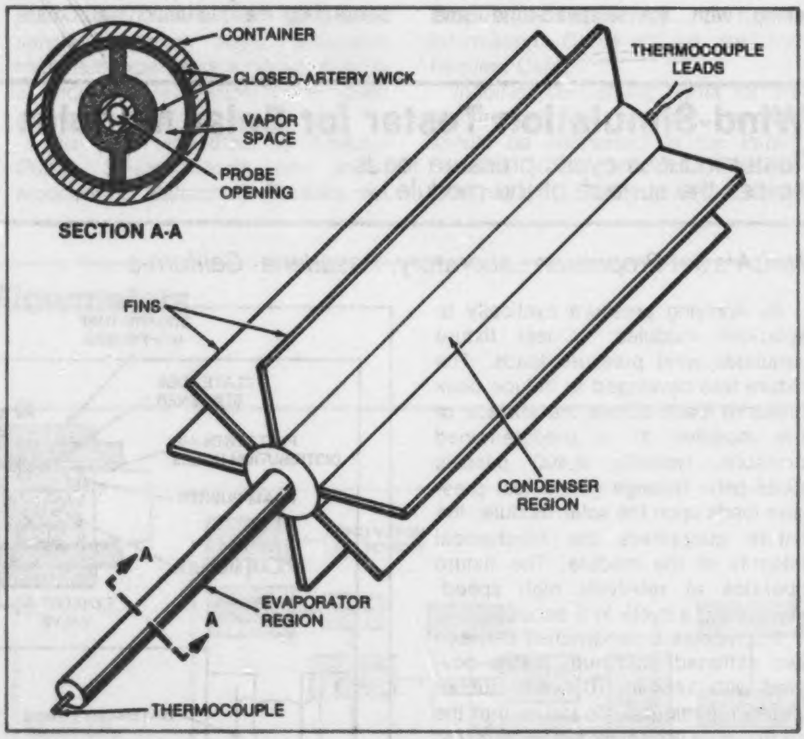

Figure 1. The **Heat-Pipe-Cooled Probe** could be used to measure temperature in a hostile environment.

The system is self-contained, passive, and has no moving parts, unlike conventional air- and water-cooled probes. An alternate wick configuration consists of narrow spiral grooves running the length of the internal surface of the pipe. The heat-pipe-cooled jacket can be used to cool probes for measuring temperatures or pressures in high-heating environments, such as wind tunnels and powerplants. It can also be used on high-speed research vehicles or hypersonic cruise vehicles.

The heat-pipe sandwich panel reduces thermal gradients, hence stresses, in a honeycomb sandwich panel that is heated or cooled along one face. Conventional honeycomb structures have a very low transverse thermal conductivity and consequently are often used as insulation. The heat-pipe sandwich panel concept retains this feature, yet it can also operate as a thermal diode. The sandwich is an insulating barrier when the heat pipes are not operating, and it is a thermally conducting panel that transfers heat efficiently from one face to the other when the heat pipes are operating.

The panel consists of a metallic honeycomb core, two facesheets, and a working fluid. Heat is transferred from the heated face to the cooler face by the evaporation and condensation of the working fluid. The fluid evaporates at the heated face and condenses at the cooler face, and the condensate returns to the evaporator region by the capillary action of the wick. In this application, the wick is the honeycomb and inner surfaces of the facings, which are either scored, etched, or grooved (see Figure 2).

An alternate concept uses a sintered-metal foil-gage screen formed to the honeycomb shape and spot-welded to the facings; or, arbitrary cells can be used as wicking columns. The faces are etched for capillary flow, and the honeycomb cells are notched at both ends to allow flow to cells not in direct contact with the wicking columns.

The heat-pipe sandwich panel can be applied in any situation where it is necessary to transfer heat from one face of the panel to the other, to eliminate thermal gradients and stresses, and/or to minimize thermal distortions. Possible applications include reducing thermal stresses in the walls of jet engines, cooling electronic components, limiting thermal distortions in large structures, and operating as a thermal diode for cryogenic storage vessels.

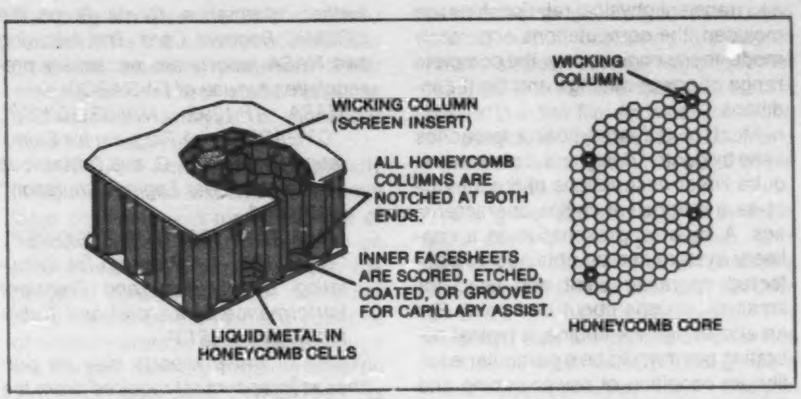
WICKING COLUMN (SCREEN INSERT)
ALL HONEYCOMB COLUMNS ARE NOTCHED AT BOTH ENDS.
INNER FACESHEETS ARE SCORED, ETCHED, COATED, OR GROOVED FOR CAPILLARY ASSIST.
LIQUID METAL IN HONEYCOMB CELLS
WICKING COLUMN
HONEYCOMB CORE

Figure 2. **Heat-Pipe Sandwich Panel combines sandwich strength with heat-pipe thermal efficiency. Either the honeycomb walls are used as the wicking medium; or, as shown, selected honeycomb cells can contain the wick material.**

This work was done by Charles J. Camarda, Lana M. Couch, and H. Neale Kelly of **Langley Research Center.** *No further documentation is available.*

Inquiries concerning rights for the commercial use of this invention should be addressed to the Patent Counsel, Langley Research Center [see page A5]. Refer to LAR-12588 and LAR-12637.

Computer Programs

These programs may be obtained at very reasonable cost from COSMIC, a facility sponsored by NASA to make new programs available to the public. For information on program price, size, and availability, circle the reference letter on the COSMIC Request Card in this issue.

Thermodynamic and Transport Properties of Air/Water Mixtures

Properties of mixtures are calculated up to nearly 1,500 K and 4,500 atmospheres.

The thermodynamic and transport properties of air/water mixtures are calculated by the subroutine WETAIR. Inputs required are the assigned values of either temperature and density, pressure and density, temperature and pressure, pressure and entropy, or pressure and enthalpy. Outputs are the properties of dry air, water (steam), and the air/water mixtures. Interpolation of property tables is used to obtain the dry-air and water properties, and simple mixing laws are then used to calculate the properties of the air/water mixtures.

Properties of mixtures with water content below 40 percent (by mass) can be calculated at temperatures from 273.2 to 1,497 K and at pressures to 450 MN/m^2 (4,500 atmospheres). Dry-air properties can be calculated at temperatures as low as 150 K. Water properties can be calculated at temperatures to 1,747 K and at pressures to 100 MN/m^2. The precision of the air properties is approximately 0.01 percent, and that of the water properties is approximately 0.05 percent, although both show maximums of up to 1 percent for extreme conditions.

Experimental data on air/water-mixture properties are generally lacking in the literature, with the exception of viscosity measurements. Until such data become available, WETAIR represents the state-of-the-art in the calculation of thermodynamic and transport properties of air/water mixtures.

WETAIR has been used in testing gas-turbine engines and components operating in relatively humid air at pressures to 40 atmospheres (40×10^5 N/m^2). The program is available in SFTRAN and FORTRAN.

This program was written by Theodore E. Fessler of **Lewis Research Center.** *For further information, Circle C on the COSMIC Request Card.*
LEW-13432

Calculating Linear A, B, C, and D Matrices From a Nonlinear Dynamic Engine Simulation

Program generates linear state-space models for simulating turbofan and turbojet engines.

Digital computers can accurately simulate the steady-state and transient performance of turbojet and turbofan engines. When nonlinear steady-state

(continued on next page)

and transient physical relationships are included, the computations accurately model these engines over the complete range of power settings and flight conditions.

Most of the analytical approaches used by control designers, however, require linear descriptions of the steady-state and transient engine characteristics. A linear approximation to a nonlinear system can be obtained at a selected operating point and used for small excursions about that point. For an aircraft turbine engine, a typical operating point would be a particular equilibrium condition of power setting and flight condition.

For a system as complex as an aircraft engine, the linear description usually consists of a number of coupled linear algebraic and differential equations. These equations can be written in the so-called "state-space" form, using vector-matrix notation. At an operating point, the linear model is fully described by the set of matrices, commonly designated as: a system matrix A, a control matrix B, an output matrix C, and a feed-forward matrix D. To describe an engine over its complete operating envelope, a number of operating points are defined, and a set of matrices is obtained for each point.

A digital computer program DYGABCD generates linear state-space models of simulated turbofan and turbojet engines. DYGABCD also contains DYNGEN, a program that simulates nonlinear steady-state and transient cases for one-spool and two-spool turbojet engines or two-spool and three-spool turbofan engines. Consequently, DYGABCD can be used exactly as DYNGEN to simulate nonlinear engine steady-state and transient performance. In addition, DYGABCD calculates the state-space matrices A, B, C, and D for any turbine engine that can be simulated with DYNGEN. The method used in DYGABCD to generate A, B, C, and D could also be used in any other transient simulation that uses a backward difference integration technique.

DYGABCD is written in FORTRAN IV for batch execution and has been implemented on an IBM 360-series computer with a central memory requirement of approximately 314K of 8-bit bytes. DYGABCD was completed in 1977.

This work was done by Lucille C. Geyser of **Lewis Research Center.** *For further information, Circle D on the COSMIC Request Card. The following two NASA reports are necessary prerequisites for use of DYGABCD:*

NASA TP-1295 [N78-33110/NSP], "DYGABCD — A Program for Calculating Linear A, B, C, and D Matrices from a Nonlinear Engine Simulation" [$13]; and

NASA TN D-7901 [N75-25620/NSP], "DYNGEN — A Program for Calculating Steady-State and Transient Performance of Turbojet and Turbofan Engines" [$13].

Copies of these reports may be purchased [prepayment required] from the National Technical Information Service, Springfield, Virginia 22161.

LEW-13250

Structural Design With Stress and Displacement Constraints

A program for synthesizing minimum-weight linear elastic structures with upper limits on stresses and displacements

Every structural design task is either directly or indirectly governed by certain optimality criteria. The designer is seldom required to create a structure that will only serve its primary function. Instead, the design is usually expected to meet such objectives as minimum weight and cost.

The DESAP1 program synthesizes linear elastic structures under static loads. Its design objective is to find the element sizes that minimize the total weight without changing the layout of the structure. The primary constraints in the synthesis algorithm are upper limits on stresses and displacements. These stress limits are prescribed as yield criteria and local instability criteria. DESAP1 also allows secondary constraints consisting of minimum allowable element sizes and size-proportion constraints.

An iterative process is used in the synthesis, with each iterative step consisting of three parts: First, the current structure is analyzed. Next, the results of that analysis are evaluated in terms of structure optimization. Finally, the results of the evaluation are used to redesign the structure.

The classical stress-ratio method is employed in the redesign with respect to stress constraints. This procedure drives the final design to the fully stressed design, which may not coincide with the design having minimum weight. For the displacement constraints, the redesign formula is obtained from the minimum-weight criterion with element sizes being driven toward a design having optimal weight. In the presence of both stress and displacement constraints, each iterative redesign operation first determines the element sizes from the stress-ratio method. These results are then used as minimum-size constraints during the application of the displacement-constrained redesign formulas. The result of the synthesis is a minimum-weight structure adhering to the prescribed constraints.

Inputs to DESAP1 consist of an initial finite-element model of the structure and a set of constraints. Basic structural elements available in DESAP1 include three-dimensional bars, three-dimensional beams, quadrilateral shear panels, anisotropic plane-stress quadrilaterals and triangles, and anisotropic quadrilateral and triangular plates.

A set of boundary elements is included to represent elastic supports and to apply constraints. The design procedure assumes that the loading is independent of element sizes. Allowances have been made for such size-dependent loads as thermal stresses and gravity loading. Outputs from DESAP1 consist of a redesign history, the final structural weight, and the redesigned element sizes.

The DESAP1 program is written in FORTRAN IV for batch execution and has been implemented on an IBM 360 computer with a central memory requirement of approximately 300K of 8-bit bytes. The DESAP1 program was developed in 1977.

This program was written by J. Kiusalaas and G. B. Reddy of Pennsylvania State University for **Marshall Space Flight Center.** *For further information, Circle E on the COSMIC Request Card.*

MFS-25235

An All-FORTRAN Version of NASTRAN® for the VAX

A general-purpose finite-element program for structural analysis

An all-FORTRAN version of the level 17.6 NASA structural analysis program NASTRAN® was developed for implementation on the DEC VAX-series computer under the VAX/VMS operating system. The minimum configuration includes half a megabyte of central memory and 50 megabytes of disk space. A recommended configuration incides 4 megabytes of central memory, two 256-megabyte disk drives, two 1,600-bpi tape drives, and the optional floating-point accelerator.

Developed in the mid-1960's, NASTRAN is a general-purpose finite-element computer program for structural analysis. Besides being efficient, versatile, and convenient to use, NASTRAN can be modified easily and expanded to accommodate new problems and new computer configurations without major redevelopment.

Applications of NASTRAN extend to almost every type of linear structure and construction. Structural elements provide for the specific representation of the more-common types of construction, including rods, beams, shear panels, plates, and shells of revolution. More general structures are analyzed by using combinations of these elements and by the use of "general" elements. Control systems, aerodynamic transfer functions, and other nonstructural features can be incorporated by the engineer into the structural analysis problem. A complex structure can be represented as a set of substructures to decrease processing time. NASTRAN includes plotting interforces that permit the display of structure and substructures with or without deformations.

The range of analysis that can be performed using NASTRAN includes: static response to concentrated or distributed loads, thermal expansion, and enforced deformation; dynamic response to transient loads, steady-state sinusoidal loads, and random excitation; the determination of real and complex eigenvalues for use in vibration analysis; dynamic stability analysis; and elastic stability analysis. The program also includes a limited capability for the solution of nonlinear problems, including piecewise linear analysis of nonlinear static response and transient analysis of nonlinear dynamic response.

NASTRAN has been specifically designed to treat and solve efficiently large problems with many degrees of freedom. The only limitations on problem size are those imposed by the practical considerations of computer run time and by the ultimate capacity of auxiliary storage devices. To reduce the central memory requirements on the VAX computer, NASTRAN is organized into 16 sections called links. One of these links is a control program that pulls the other links into core only as they are needed. This structure allows NASTRAN to offer the user a large selection of capabilities while requiring only a moderate amount of core resources.

Two new NASTRAN features are available in the VAX version. The program can be executed from a terminal in a manner that permits use of the VAX interactive debugger, and any link can be interactively restarted as often as desired by making a copy of all NASTRAN work files before executing that link for the first time.

This program was written by Lloyd Purves of **Goddard Space Flight Center.** *For further information, Circle F on the COSMIC Request Card.*
GSC-12600

Potential Flow in Two-Dimensional Deflected Nozzles

An informative approximation to three-dimensional nozzle flow.

Potential flow in two-dimensional deflected-flow nozzles is calculated by three programs: SCIRCL, a geometry definition program; 24Y, an incompressible two-dimensional potential-flow program; and NOZZLEC, a program that combines incompressible potential-flow solutions into solutions of interest and applies a compressibility correction.

SCIRCL uses nozzle geometry segments as input, with each segment introduced as an analytic curve. The printed output, containing the coordinates, slopes, curvatures, and other features of the entire nozzle surface, is placed in a disk file. An initial screening of candidate nozzles can be made from the printout from this stage of the computation.

Using the results of SCIRCL as input, plus desired points of output, 24Y generates simple two-dimensional basic potential-flow solutions for both on-body and off-body points. The velocity fields are placed on disk files for use as input to NOZZLEC. Since a full three-dimensional nozzle analysis does not now exist, the simpler but more approximate methods of 24Y were developed to analyze real nozzles. Even though actual nozzles are three-dimensional, there are sections of the nozzles for which a two-dimensional analysis is an informative approximation.

The final routine, NOZZLEC, combines the basic solutions from 24Y into solutions of interest having specified values of nozzle mass flow and, if desired, free-stream velocity and angle of attack. NOZZLEC output includes velocities, pressures, flow angles, and mach numbers. If desired, compressibility corrections are also applied.

The program group is written in FORTRAN V and has been implemented on a UNIVAC 1100/42. It requires a memory having approximately 52K of 36-bit bytes. The program was completed in 1979.

This program was written by J. Dennis Hawk and Norbert O. Stockman of **Lewis Research Center.** *For further information, Circle G on the COSMIC Request Card.*
LEW-13461

The Design and Analysis of Low-Speed Airfoils

Direct and inverse airfoil-flow problems are solved by the program PROFILE.

The flow about an airfoil in free air can be described approximately by a boundary-layer flow near the surface of the airfoil and by a potential flow everywhere else. Boundary-layer theory can be applied to the flow about an airfoil in two ways. First, the boundary-layer development can be determined for a given potential-flow velocity distribution. This is the direct, or analysis, problem. Second, the potential-flow field, or at least some of its properties, can be determined for a given boundary-layer development. This is the inverse, or design, problem. Both the direct and inverse problems are solved by the program PROFILE.

A conformal-mapping method for the design of airfoils with prescribed velocity-distribution characteristics, a panel method for the analysis of the potential flow about given airfoils, and a boundary-layer method are combined in the PROFILE program. The conformal-mapping method, similar to that of Lighthill, solves most multipoint design problems very simply. The potential-flow analysis method is required for comparison with wind-tunnel tests of given airfoils and for analyses of airfoils generated by the design method and then modified by a flap deflection. This analysis method employs a distributed surface-singularity technique. The boundary-layer method uses integral momentum and energy equations but does not contain a boundary-layer displacement iteration.

PROFILE is written in FORTRAN IV and has been implemented on a CDC 6000-series computer with a central memory requirement of approximately 110K (octal) 60-bit words. The program was developed in 1980.

This program was written by Richard Eppler of the University of Stuttgart and Dan M. Somers of **Langley Research Center.** *For further information, Circle H on the COSMIC Request Card.*
LAR-12727

Transonic Flow Over Wing/ Fuselage Configurations

Flow-field analysis in the transonic region

The Wing Body Code (WIBCO) simulates the aerodynamics of wing/ fuselage configurations at transonic speeds. It can reduce the design cost and improve the performance of high-speed aircraft.

The transonic flow field is characterized by mixed subsonic and supersonic regions, shock waves, and complicated viscous effects. The complexity of such flow often makes a purely experimental approach impractical for solving aircraft design problems in this regime. WIBCO obtains a numerical finite-difference solution of a modified (extended) small-disturbance flow equation on a multiple embedded mesh system. This approach gives high computational resolution and coordinate-system flexibility for treating complex realistic aircraft shapes.

The WIBCO flow equation is a modified extension of the classical transonic small-disturbance equation. This modification includes crossflow terms for resolving shock waves with large sweep angles. The computational space used in solving the flow equation is divided into a global crude grid and embedded fine grids about the wing and body where the gradients are large and the details are important.

The simplicity of the approximate flow equation and planar boundary conditions permit the use of Cartesian coordinates for all grids. The resulting numerical efficiency permits a very dense computational mesh, a benefit in both the resolution of shock waves and the calculation of configuration forces and moments. The embedded meshes are independent and optimized for a particular geometric component, facilitating applications to complex configurations. The flow-field equation is of mixed type for supercritical flow and is solved using a type-dependent finite-difference approximation with planar boundary conditions. A successive-line overrelaxation method is used where vertical columns of mesh points are relaxed starting at the first line (plane) upstream and ending at the last line (plane) downstream in each grid system.

Inputs to WIBCO consist of ambient flow conditions and geometric configuration data, the grid control and relaxation parameters are internally set. Outputs include input data echo; grid system verification; relaxation-solution convergence history; and computed velocities, pressures, forces, moments, reference lengths, and areas. Plotted output for geometry verification is also available. Plotted output can be generated for any offline X/Y plotter.

WIBCO is written in FORTRAN IV for batch execution and has been implemented on a CDC CYBER 175 with a central memory requirement of approximately 226K (octal) of 60-bit words. WIBCO was developed during 1977 to 1979.

This program was written by Charles W. Boppe of Grumman Aerospace Corp. for **Langley Research Center.** *For further information, Circle J on the COSMIC Request Card.*
LAR-12702

Machinery

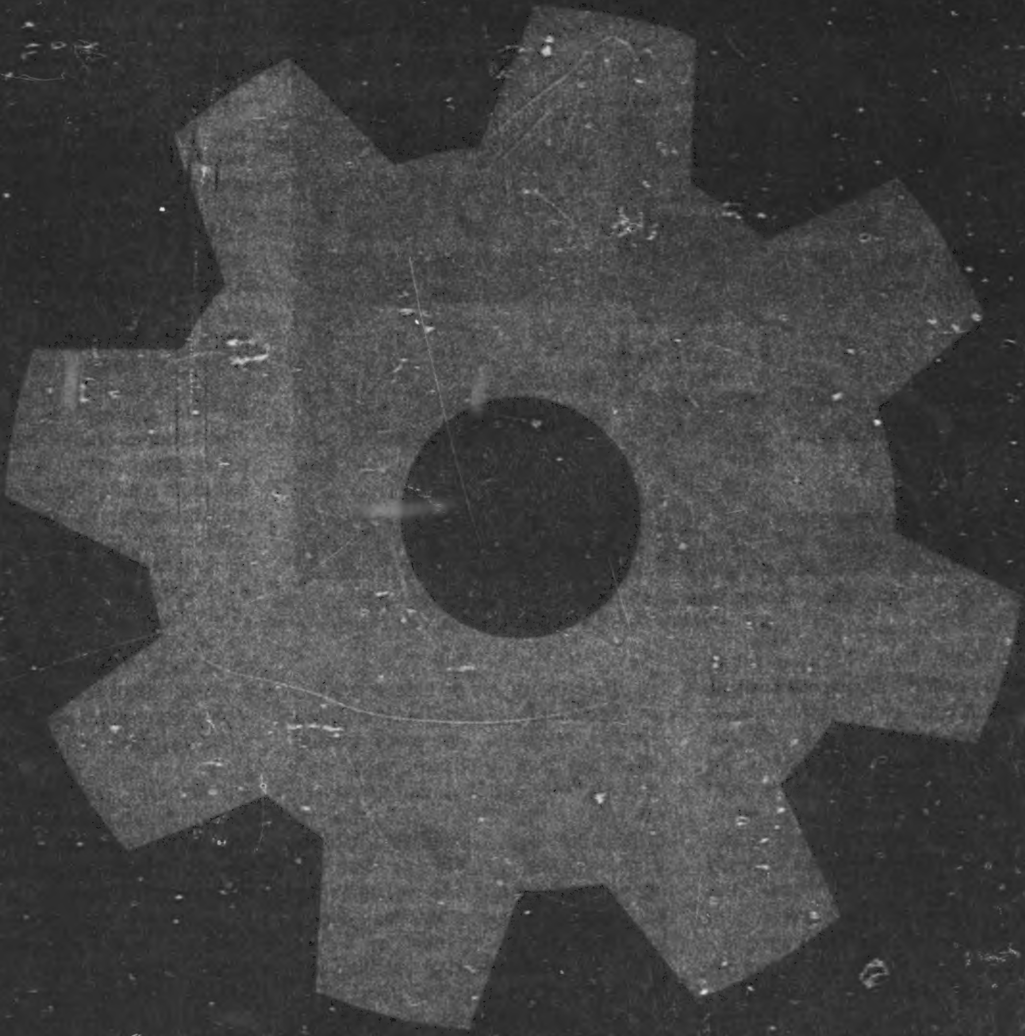

Hardware, Techniques, and Processes

485 Interlocking Wedge Joint Is Easily Assembled
486 Pneumatic-Power Supply
487 Sidewall Penetrator for Oil Wells
488 Four-Wheel Dual Braking for Automobiles
489 Lock for Hydraulic Actuators
490 Gentle Arrester for Moving Bodies
491 Soft Container for Explosive Nuts

Computer Programs

491 Cylindrical Bearing Analysis

Interlocking Wedge Joint Is Easily Assembled

Structural joint is simple enough to be used by workers wearing gloves or bulky clothing.

Langley Research Center, Hampton, Virginia

A new interlocking wedge joint links two structural members in manual-, remote-, or automated-assembly operations. It transmits all structural loads, including tension, compression, bending moments, and torsion. If necessary, electrical powerlines and data-transmission lines can be incorporated within the joint. Originally developed for use by astronauts, the joint is simple enough to be assembled by undersea divers, workers in nuclear reactors, and others wearing gloves or bulky clothing.

The joint consists of a male endpiece, a female endpiece, and a sleeve (see figure). The small end of the male taper is inserted into the large end of the female tapered hole and pressed in until the sleeve slides over the two pieces; then the sleeve is forced up the conical surface to lock the joint. In moving up the conical surface, the sleeve expands to near its yield point or beyond, resulting in a clamping action that holds it in place. The necessary force is furnished by the operator with a special tool or by special mechanisms built into a manipulator or other automated equipment. For release, the assembly steps are reversed.

In large structures, one of the endpieces could be attached to (or an integral part of) a column or strut, and the other endpiece could be an integral part of a cluster with connections for several such members. If electrically nonconductive materials are used for the endpieces, metal inserts cast or molded in place may be used to conduct electrical power or data signals across the joint. Multiple electrical paths are feasible without a separate connecter.

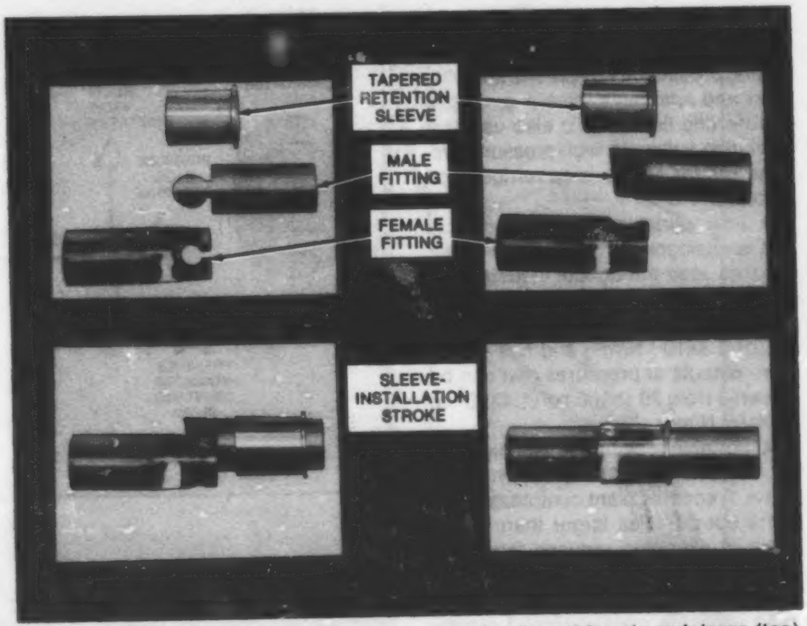

In the **New Wedge Joint**, an expanding sleeve and male and female endpieces (tcp) are joined in a single locking stroke (bottom).

Comparable joints are usually expensive machined mechanisms requiring extremely close tolerances. Few carry bending or torsional loads. The components of the new joint may be formed by machining, casting, or molding. If many are required, casting or molding should reduce costs substantially. The overall size, wedge angle, and conical taper may be varied to handle unusual loads or special assembly problems.

The joint is inherently insensitive to thermal excursions, vibration, and the buildup of machining tolerances. Joints assembled from injection-molded composites, using qualified materials, should withstand severe environments. The combination of wedging angles on the male/female parts and the sleeve create high mechanical advantages that overcome structural misalinements and force the assembly into the true position as the locking sleeve moves into place.

This work was done by Moses J. Long of **Langley Research Center.** *No further documentation is available.*

Inquiries concerning rights for the commercial use of this invention should be addressed to the Patent Counsel, Langley Research Center [see page A5]. Refer to LAR-12729.

Pneumatic-Power Supply

A pneumatic analog of the portable electric-power supply has adjustable pressure outputs.

Lyndon B. Johnson Space Center, Houston, Texas

Compressed air is used in industrial plants, shops, and laboratories for operating production equipment, spraying paint and lubricants, cleaning, drying, and moving liquids. It is also used for activating valves in high-pressure systems and for pressurizing refrigeration systems.

A new portable pneumatic supply that is analogous to the electric-power supplies used throughout industry simplifies these operations. It connects to a standard high-pressure air line (120 psi, or 8.3×10^5 N/m^2) and has two or more outputs at pressures that can be adjusted from 20 to 100 psi (1.4×10^5 to 6.9×10^5 N/m^2).

A portable pneumatic supply with two adjustable outputs is shown in the figure. It accepts plant compressed air, filters out particles larger than 10 microns in diameter, reduces the air to working pressure, and adds a lubricant if required.

An accurate constant-bleed regulator supplies the reduced-pressure air to both output channels. On the channel lines, vernier-control valves select the output pressures. Gages show inlet and channel pressures.

A "momentary-on" toggle switch controls channel selection through two solenoid-operated four-way valves (converted to three-way operation). Safety and convenience features are included, such as a pressure-relief valve, a stand, a carrying handle, and mode-of-operation indicator lights.

This work was done by Ralph C. Kramer of Rockwell International Corp. for **Johnson Space Center.** *No further documentation is available.*
MSC-18855

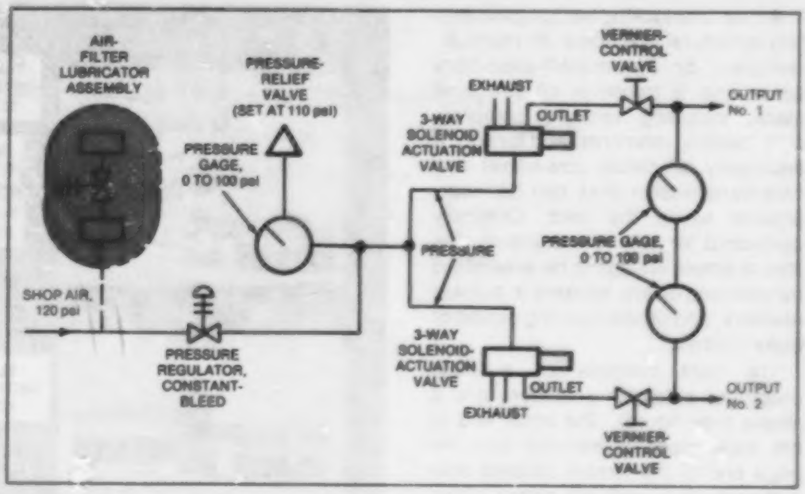
AIR-FILTER LUBRICATOR ASSEMBLY
PRESSURE-RELIEF VALVE (SET AT 110 psi)
PRESSURE GAGE, 0 TO 100 psi
SHOP AIR, 120 psi
PRESSURE REGULATOR, CONSTANT-BLEED
EXHAUST
3-WAY SOLENOID ACTUATION VALVE
OUTLET
VERNIER-CONTROL VALVE
OUTPUT No. 1
PRESSURE
PRESSURE GAGE, 0 TO 100 psi
3-WAY SOLENOID-ACTUATION VALVE
OUTLET
EXHAUST
OUTPUT No. 2
VERNIER-CONTROL VALVE

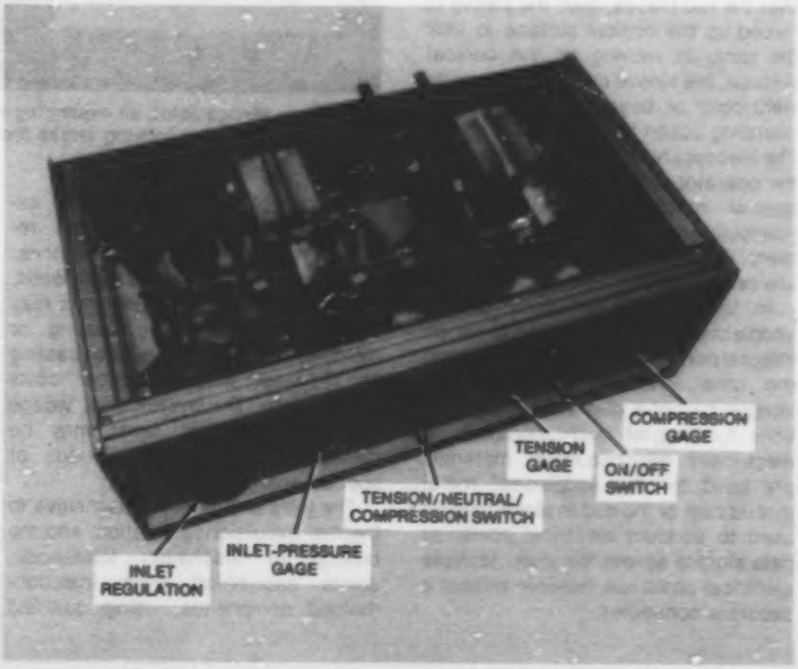
COMPRESSION GAGE
TENSION GAGE
ON/OFF SWITCH
TENSION/NEUTRAL/COMPRESSION SWITCH
INLET-PRESSURE GAGE
INLET REGULATION

Two Adjustable-Pressure Outputs of filtered compressed air are available from the compact portable pneumatic supply shown here in a schematic diagram (top) and a photograph (bottom). The primary source is high-pressure air from a main air line. The actuator valves and indicator lights require standard 120-volt ac electricity.

Sidewall Penetrator for Oil Wells

New penetrator bores horizontal holes in the well casing to increase oil drainage.

NASA's Jet Propulsion Laboratory, Pasadena, California

A sidewall penetrator (see figure) bores horizontal holes 6 in. (15 cm) in diameter, 15 in. (37.5 cm) deep, to extract oil trapped in the adjacent strata. A common drive mechanism turns several penetrators at once to cut multiple holes simultaneously. The penetrators are more efficient than the more-commonly-used armor-piercing bullets and shaped explosive charges, none of which pierces the sidewalls as deeply.

Each penetrator drill bit is turned by a flexible shaft. The shaft, made from a spiraling cable, rotates and thrusts simultaneously through a rigid curvilinear guide tube forcing the bit through the well casing and into the strata.

The shaft is driven by a series of interlocking thrust segments confined in the tube and connected to a drive motor at the mouth of the well. Each segment contains a rotatable hollow sleeve that interlocks with the next one. Drilling fluid feeding through these sleeves flows through ports in the drill bit to cool and lubricate the cutting teeth and to flush chips and debris from the drilled hole. When the drill is retracted, the sleeves disconnect.

Power is applied to the thrust segments via a feeding mechanism coupled to the drive motor. The motor drives several of these feeding mechanism at once. Each feeding mechanism operates in the manner of a lead screw/nut arrangement. A threaded rod, analogous to a lead screw, is thrust forward by a rotating nut driven by a gear reduction mechanism. Simultaneously a rotary drive gear turns the thrust segments.

The rotating segments surge forward, interlock, and apply power to the shaft. The feeding-mechanism gears advance the drill bit slowly in relation to its high rotary speed.

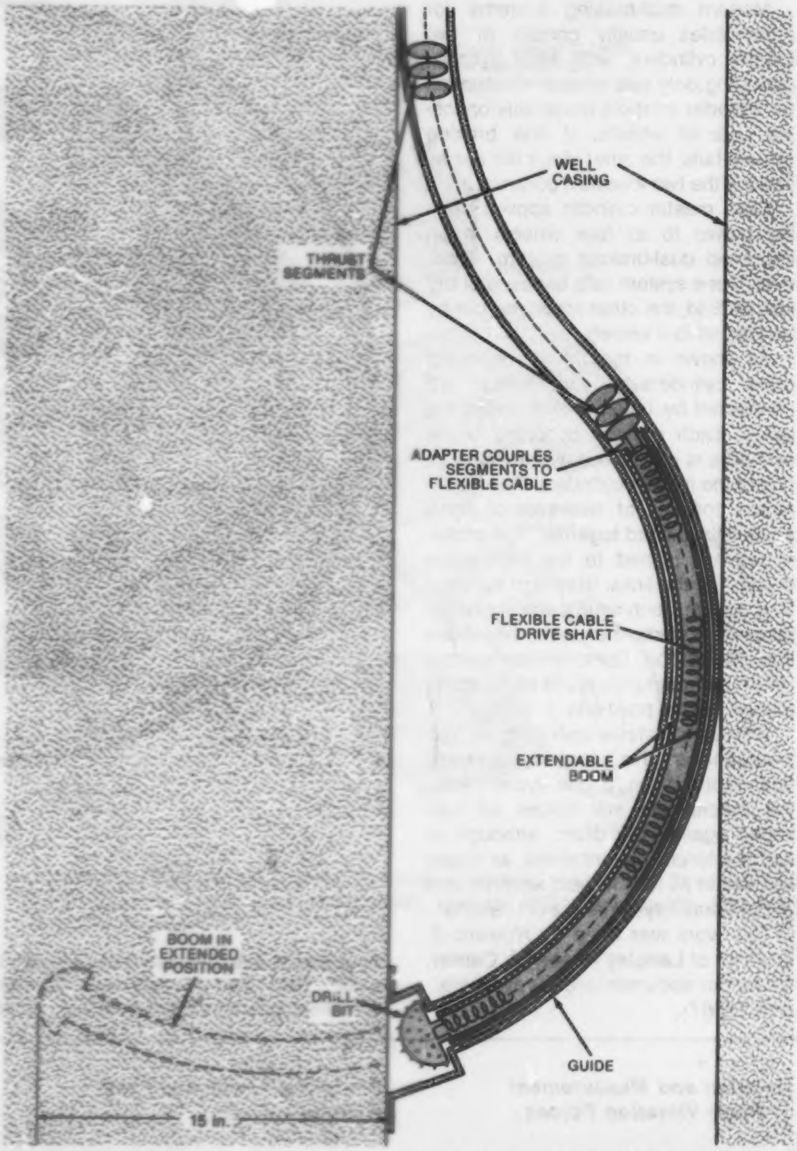
WELL CASING
THRUST SEGMENTS
ADAPTER COUPLES SEGMENTS TO FLEXIBLE CABLE
FLEXIBLE CABLE DRIVE SHAFT
EXTENDABLE BOOM
BOOM IN EXTENDED POSITION
DRILL BIT
GUIDE
15 in.

Sidewall Penetrator cuts horizontal holes in oil wells to release oil trapped in the adjacent strata. A number of these penetrators operated by a common drive is inserted into the well at once. The drill bits advance simultaneously in several directions, releasing trapped oil into the well.

This work was done by Earl R. Collins of Caltech for **NASA's Jet Propulsion Laboratory.** *For further information, Circle 67 on the TSP Request Card.*

Title to this invention has been waived under the provisions of the National Aeronautics and Space Act [42 U.S.C. 2457(f)], to the California Institute of Technology/Jet Propulsion Laboratory, Pasadena, CA 91103.
NPO-14306

Four-Wheel Dual Braking for Automobiles

All four wheels are braked by either of two master cylinders.

Langley Research Center, Hampton, Virginia

Modern dual-braking systems for automobiles usually consist of two master cylinders, with each cylinder operating only two wheels. Each master cylinder controls diagonally opposing sets of wheels. If one braking system fails, the other stops the car by braking the two wheels it controls.

Each master cylinder applies braking power to all four wheels in an improved dual-braking system. Thus, even if one system fails because of the loss of fluid, the other stops the car by braking all four wheels.

As shown in the figure, opposing brake cylinders at each wheel are connected by holes drilled through a block. Each pair of opposing brake cylinders is connected hydraulically to one of the master cylinders. The mechanism consists of two sets of right-angle links pinned together. The brakeshoes are pinned to the right-angle corners of the links. Standard automotive design techniques are used to place the studs that lock the shoes against rotation. Compression springs return the mechanism and brakeshoes to their neutral positions.

With both systems operating, all four brakeshoes are forced outward against the drum. If one system fails, the mechanism still forces all four shoes against the drum, although at half the force. Nevertheless, all shoes operate in all four wheels whether one or both brake systems are operational.

This work was done by Howard B. Edwards of **Langley Research Center**. *No further documentation is available.*
LAR-12687

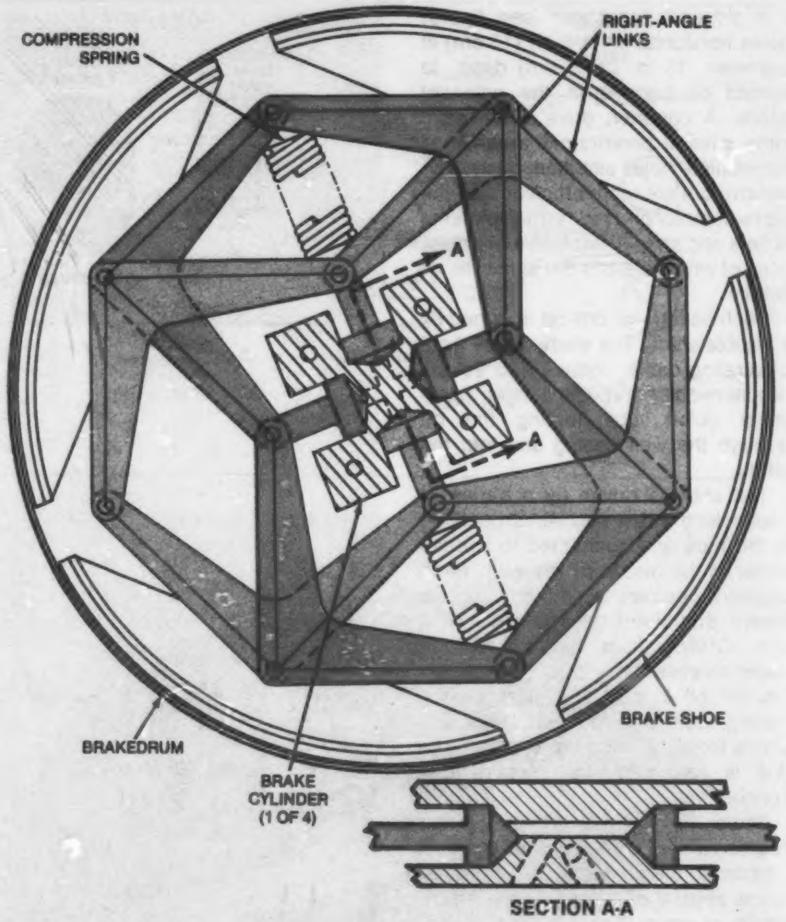

Opposing Brake Cylinders are connected to each other by a hole drilled through the block. Each pair of cylinders, connected hydraulically to one of the master cylinders, operates independently. A model of the linkage has been built.

Isolation and Measurement of Rotor Vibration Forces

A mounting for a helicopter gearbox measures forces generated by the rotor and isolates the transmission from the airframe. The mountings have a frequency-dependent load/displacement relationship that gives a statically rigid but dynamically soft support, which lowers vibratory transfer.
(See page 468.)

Removing Freon Gas From Hydraulic Fluid

Dissolved Freon gas can be removed from hydraulic fluid by raising the temperature to 150° F and bubbling dry-nitrogen gas through it, even while the fluid is circulating through the hydraulic system. This decontamination procedure reduces parts corrosion and sludge formation.
(See page 452.)

Speed Control for Synchronous Motors

A feedback circuit controls fluctuations in the speed of synchronous motor. A voltage proportional to the phase angle is developed by a phase detector, rectified, amplified, compared to a threshold, and applied back to the motor excitation circuit.
(See page 414.)

Lock for Hydraulic Actuators

Two clamps prevent rod travel in deenergized actuators.

Lyndon B. Johnson Space Center, Houston, Texas

In a hydraulic actuator, a rod is thrust out from a cylinder or is retracted into the cylinder. As long as hydraulic pressure is maintained, the actuator holds the rod at the desired extension. When power is removed, however, the rod can move under the load.

A pair of clamps developed for hydraulic actuators on the Space Shuttle engines prevents the unwanted movement. The clamps are fastened to the rod and cylinder and are then locked together with bolts. Besides preventing the travel of deenergized actuators, the clamps might also serve as a temporary rigid link in a hydraulic system under repair.

A prototype of the locking device is shown in the figure. Both the rod and cylinder are threaded. Each clamp consists of two threaded halves that are assembled around the rod and cylinder threads. The two clamps are then fastened together by bolts that prevent both retraction and extension of the rod. An important feature of the mechanism is that the spacing between the clamps is adjustable through use of the bolts. Thus the actuator can be locked at any rod extension.

The clamps can lock an actuator to be used as a mechanical support or linkage — for example, to support a platform. The mechanism may also be useful as a fail-safe device in case of loss of hydraulic pressure. Potential applications include manufacturing processes and specialized handling and holding devices.

This work was done by Robert H. Wood of Rockwell International Corp. for **Johnson Space Center.** *No further documentation is available.*
MSC-18853

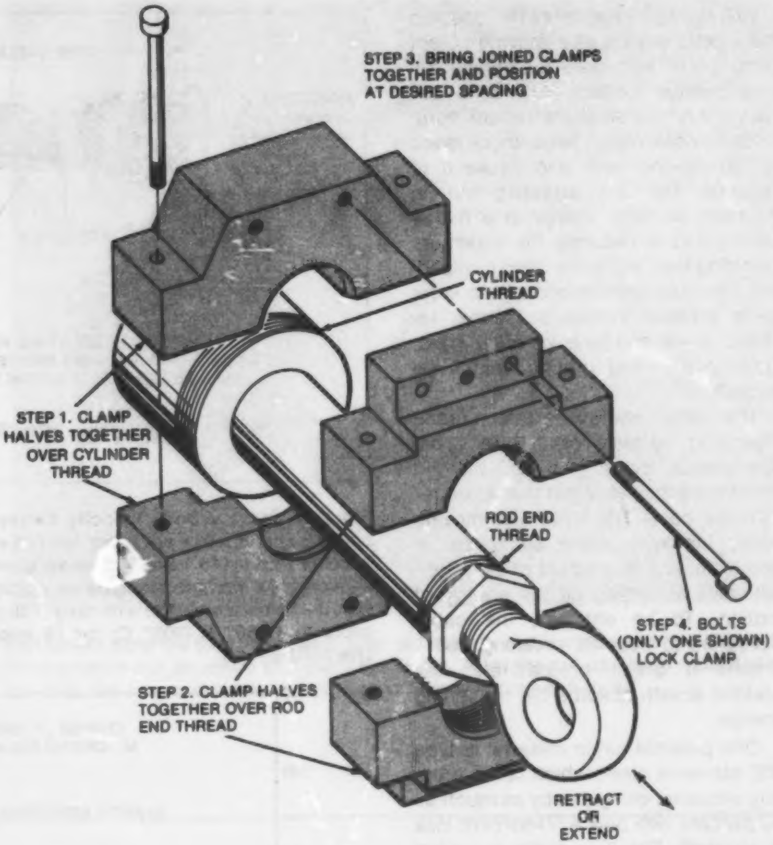
STEP 3. BRING JOINED CLAMPS TOGETHER AND POSITION AT DESIRED SPACING
CYLINDER THREAD
STEP 1. CLAMP HALVES TOGETHER OVER CYLINDER THREAD
ROD END THREAD
STEP 4. BOLTS (ONLY ONE SHOWN) LOCK CLAMP
STEP 2. CLAMP HALVES TOGETHER OVER ROD END THREAD
RETRACT OR EXTEND

This Adjustable Lock for a hydraulic actuator can hold the rod in a fixed extension from the cylinder even when power is off, thus converting the actuator into a stiff structural member.

Gentle Arrester for Moving Bodies

A wire cable absorbs energy with reduced shock and rebounding.

Langley Research Center, Hampton, Virginia

An elongating wire cable absorbs the kinetic energy of a moving object more gently than does a conventional elastic-arrest system, such as a coil spring, a net, or an aircraft shock cord. Such devices impart large shock loads to the moving body and cause it to rebound. The new arresting line, in contrast, absorbs energy at a nearly constant rate, reducing the maximum arresting load and minimizing rebounding. Possible applications of the wire-cable arrester include passenger restraint in air and land vehicles, parachute risers, and ground snatch by aircraft.

The new energy arrester (see Figure 1) consists of a wire cable surrounded by a tubular braided sheath of polyester cloth that is longer than the cable. To arrest the moving body, the wire cable elongates to approximately 90 percent of its potential while absorbing all the energy of motion. To be efficient, the cable elongates to near its breaking point. Should it break prematurely, the braided sheath absorbs the remaining energy.

One possible cable material is type 302 stainless steel, which when properly annealed elongates by as much as 40 percent with only a 50-percent loss in strength. The wire cable is routed through the longer tubular suspension line to prevent chafing against adjacent structures during elongation and to prevent a catastrophic failure should the wire cable break. Figure 2 compares the maximum shock loads imparted to the arrested body by the elongating cable and by typical elastic arresters, for equivalent energy absorption.

This work was done by Reid A. Hull of **Langley Research Center.** *No further documentation is available.*

This invention is owned by NASA, and a patent application has been filed. Inquiries concerning nonexclusive or exclusive license for its commercial development should be addressed to the Patent Counsel, Langley Research Center [see page A5]. Refer to LAR-12372.

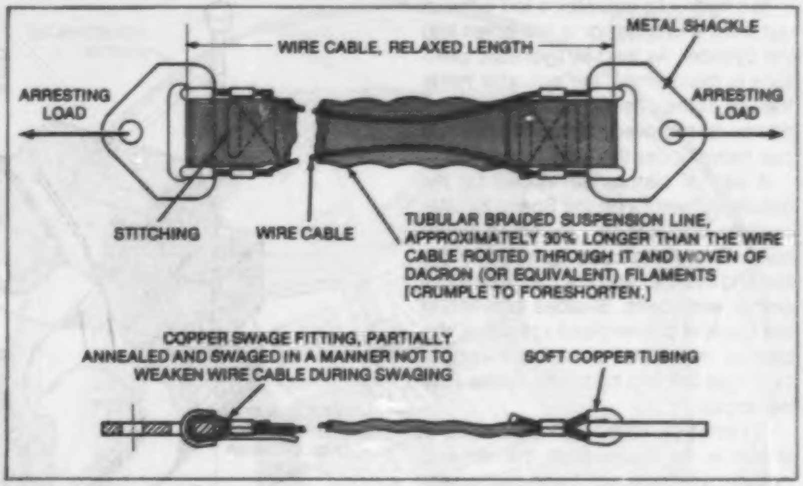
WIRE CABLE, RELAXED LENGTH
METAL SHACKLE
ARRESTING LOAD
ARRESTING LOAD
STITCHING
WIRE CABLE
TUBULAR BRAIDED SUSPENSION LINE, APPROXIMATELY 30% LONGER THAN THE WIRE CABLE ROUTED THROUGH IT AND WOVEN OF DACRON (OR EQUIVALENT) FILAMENTS [CRUMPLE TO FORESHORTEN.]
COPPER SWAGE FITTING, PARTIALLY ANNEALED AND SWAGED IN A MANNER NOT TO WEAKEN WIRE CABLE DURING SWAGING
SOFT COPPER TUBING

Figure 1. **Moving-Body Velocity Arrester** consists of wire cable surrounded by a braided sheath. The stitching reinforces the assembly. The wire cable is partially annealed so as to have increased elongation potential. [Type 302 stainless-steel cable can be made to elongate as much as 40 percent if cleaned and annealed in a vacuum furnace and that with only a 50 percent loss in strength; subjecting the wire cable to 1,650° F (900° C) for 15 minutes is required to achieve these physical characteristics.]

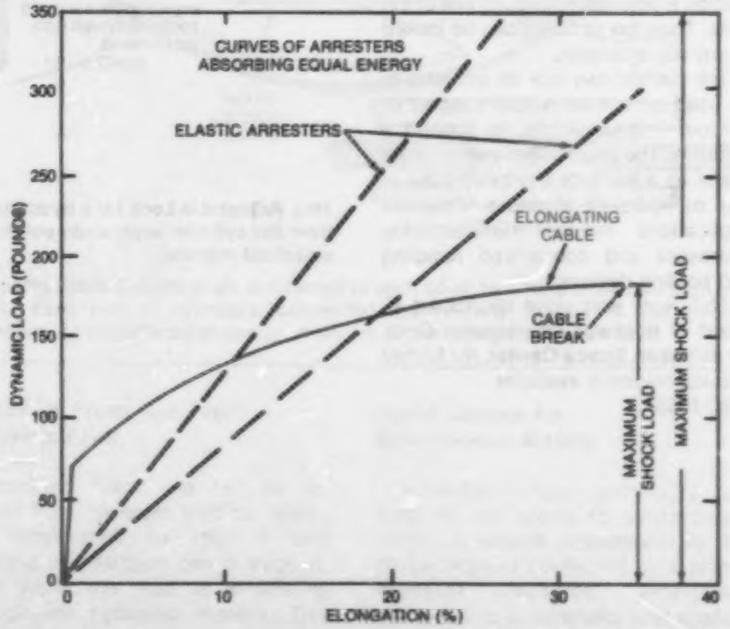

Figure 2. **Dynamic Load Is Compared** for an elongating cable, 1/16 in. (0.16 cm) in diameter, and typical elastic-arrest systems. The cable data were obtained experimentally.

Soft Container for Explosive Nuts

Flexible fabric bag fits over a variety of assembly shapes.

Lyndon B. Johnson Space Center, Houston, Texas

Blasts from explosive nuts and other pyrotechnic devices are contained by a bag sewn from fabric. Unlike conventional metal vessels for blast containment, the bag is light and flexible and readily fits around odd shapes. It could be used to contain not only the debris produced by explosive-nut detonations but also that from safety tests.

The material for the bag is woven aramid (a multifilament polyamide) fabric. Belt loops of the same fabric attach the bag to a three-piece clamp, which retains the bag on a rigid ring. The ring supports the structure for the explosive nut inside the bag. The clamp makes a sewn-on top unnecessary, and the bag can therefore easily be placed over the nut structure and removed after the nut has been detonated.

Thread is stitched around the bag in parallel rings (see figure). The stitches help to absorb energy as the threads break from the shock of the explosion.

This work was done by Dean C. Glenn, William E. Drummond, and Gordon Miller of **Johnson Space Center.** *For further information, Circle 68 on the TSP Request Card.*
MSC-18871

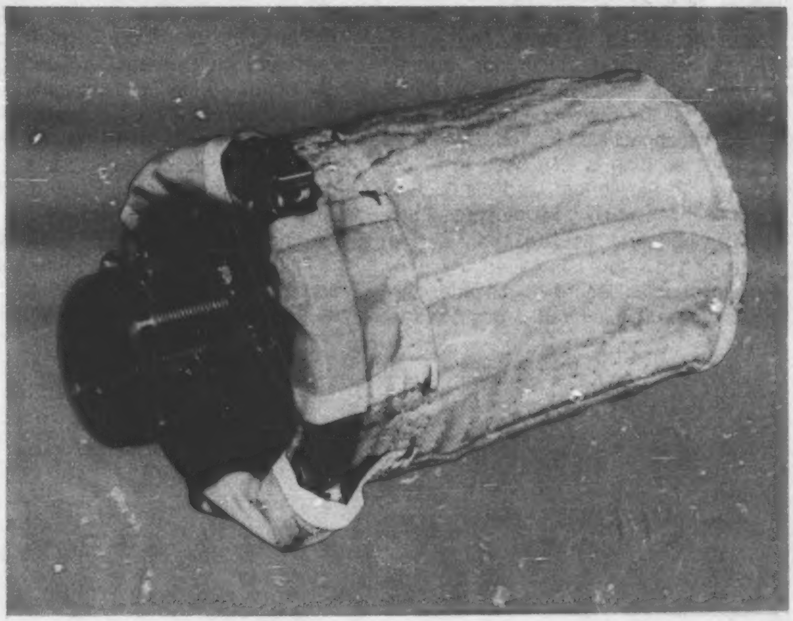

Belt Loops Hold the Blast-Container Bag to a clamp. A threaded-neck ring supports the explosive-nut structure and detonator wires. After the nut has been mounted in the ring, the bag and clamp are slipped over it and fastened to it.

Computer Programs

These programs may be obtained at very reasonable cost from COSMIC, a facility sponsored by NASA to make new programs available to the public. For information on program price, size, and availability, circle the reference letter on the COSMIC Request Card in this issue.

Cylindrical Bearing Analysis

Including the effects of bearing geometry, shaft misalinement, and temperature

CYBEAN computes the behavior of cylindrical rolling-element bearings under conditions that may include high speed and misalined shafts. Accurate assessment of geometry-induced roller preload is possible for various outer-ring and housing configurations. The analysis considers a flexible outer ring and housing and treats cases where the outer-ring outer surface is not in contact with the housing around its entire perimeter. This would be the case when a two- or three-point out-of-round ring is pressed into a circular mounting hole in the housing.

CYBEAN is structured for the coordinated execution of modules that perform specific analytic tasks. It initiates a computation with geometry, lubricant, and material definitions. To economize on computation, constants are evaluated in structure locations external to iterative calculations.

A repetitive loop is used that addresses the computation of geometry fits. Arbitrary housing and outer-ring profile interactions are considered. Rolling-element load distribution is obtained for the mode of bearing preload defined by the user. Interference-fit effects, including rotation, temperature, and roller-load-induced ring displacements, are evaluated and used to compute the operating diametral clearance. The field-equation set is evaluated for the bearing, which can contain up to 50 rollers. The set of values for the independent variables that satisfies all

(continued on next page)

the equations of equilibrium simultaneously is considered to be a solution.

An accurate initial guess of the variable values can save considerable execution time. However, the nonlinear coupling of the large set of unknowns within a typical physical system makes it difficult to guess accurately. This problem is overcome by first solving the simpler elastic case. The set of variables that satisfy the equilibrium of elastic forces is then used as an initial guess for the more complicated solution, which includes friction. This initial elastic solution is also used to determine the equilibrium load distribution that defines housing-fit pressures.

The general field-equation set is partitioned before it is solved. Independent variables describing the inner-ring position and roller radial position are addressed in conjunction with field equations governing ring and roller radial equilibrium. Equation cross coupling is established through the roller radial position. This subset is brought to equilibrium by Newton-Raphson iteration.

Once inner-ring equilibrium is satisfied, the field-equation set is again partitioned to include roller axial, radial, skew, and tilt moment equations of equilibrium. Coupling is maintained through the associated displacement variables. At this portion of the analysis, roller end-flange contact forces are equilibrated with raceway-induced loading.

A final partition is made such that the field equations defining force equilibrium in the direction tangent to the pitch circle, moments about the roller axis, and radial cage equilibrium are considered. Associated variables are: radial position, rotational and orbital speeds, and cage displacements. The set of values of independent variables that simultaneously satisfy these equations is considered a solution.

Satisfactory convergence of the iterative procedure allows the definition of results of a specific temperature. The remaining program structure addresses the computation of steady state and the time-transient system thermal performance.

This program is written in FORTRAN V for use on the UNIVAC 1100/40 computer.

This program was written by R. J. Kleckner and J. Pirvics of SKF Industries for **Lewis Research Center**. *For further information, Circle K on the COSMIC Request Card.*
LEW-13393

Fabrication Technology

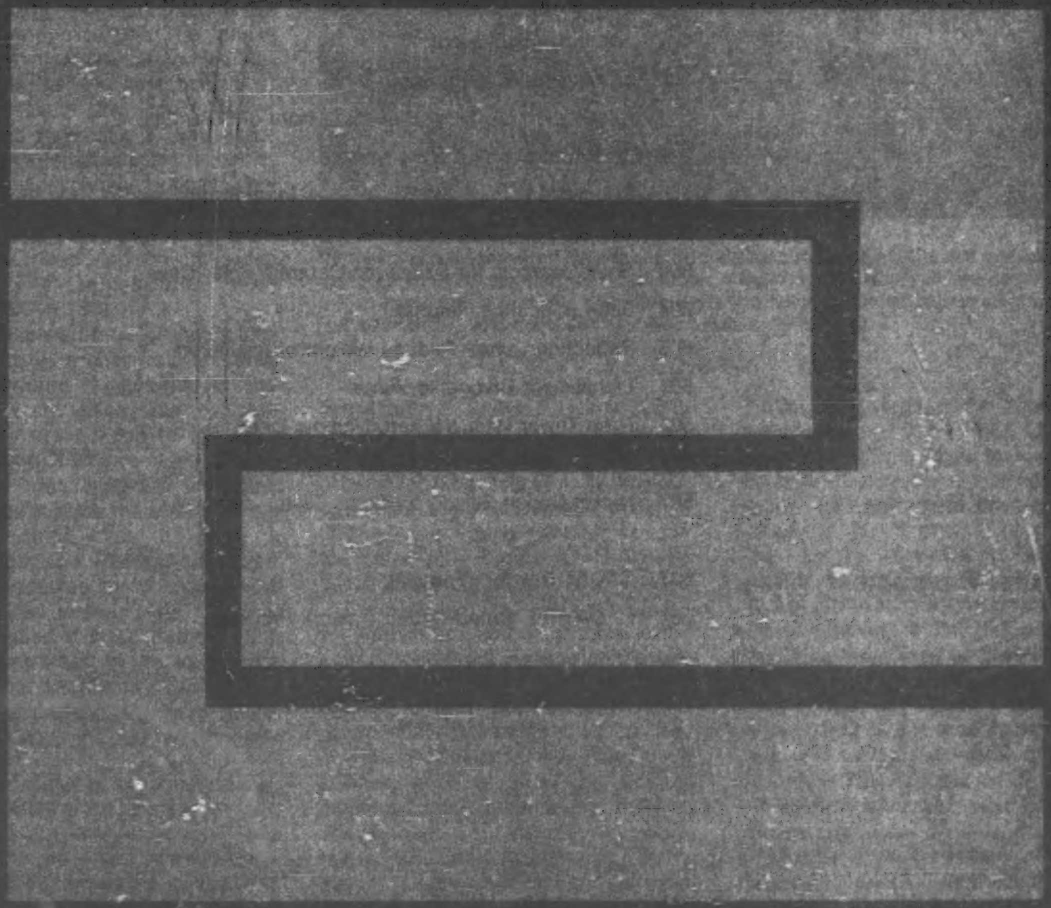

Hardware, Techniques, and Processes

495 "Densified" Tiles Form Stronger Bonds
495 Tile Densification With TEOS
496 Repairing High-Temperature Glazed Tiles
497 Producing Silicon Continuously
498 Mobile Glazing Unit
499 Learning High-Quality Soldering
500 Eliminating Gaps in Split Rings
501 Passivation Layer for Steel Substrate of Solar Cell
502 Low-Cost Concentrating Mirrors
502 Spiral-Wound Gasket Forms Low-Temperature Seal
503 Arc Spraying Solderable Tabs to Glass
504 Back Contacts for Silicon-on-Ceramic Solar Cells
504 Self-Lubricating Gearset
505 Reflecting Layers Reduce Weight of Insulation
505 Lightweight Cryogenic Vessel
506 Drop Tower With No Aerodynamic Drag

Books and Reports

507 Nickel-Doped Silicon for Solar Cells

Computer Programs

507 CADAT Network Translator
508 CADAT Integrated-Circuit Artwork Program

"Densified" Tiles Form Stronger Bonds

A one-step application of colloidal silica more than doubles the bond strength.

Lyndon B. Johnson Space Center, Houston, Texas

The technique selected for strengthening the Space Shuttle surface-tile/substrate bond could be applied to similar ceramic-tile-attachment problems in other applications. The "densification" process strengthens the surface where the tile attaches to a felt strain-isolator pad, redistributing stresses and preventing failures at that point. Those interested in the technology of bonding delicate ceramics to nonrigid materials should also consider the Shuttle backup tile-strengthening technique, described in the following article, "Tile Densification With TEOS" (MSC-18737).

Densified and Undensified Tiles fail at different locations and at different stresses. The undensified specimen (left) failed at about 11 psi (7.5×10^4 N/m^2) at its interface with the stress-isolation pad. The densified tile (right) failed at a much higher stress, 23 psi (1.6×10^5 N/m^2), and the break occurred in the bulk material.

The reusable surface-insulation tiles that protect the orbiter from repeated high-temperature plunges through the atmosphere are susceptible to failure where they are bonded to felt pads that separate them from the Shuttle frame. In densification, a binder mixture impregnates the bottom of the fibrous ceramic tiles to form a high-strength skin. The platelike layer more than doubles the strength of the tile-to-felt-pad bond. In tests, tiles that were densified did not fracture until they were stressed to the limit of the bulk material (see figure). Undensified tiles, in comparison, fractured at the bond interface and at much lower stresses.

The process uses an aqueous mixture of colloidal silica as a cement and ball-milled silica particles, which — like sand in concrete — act as a reinforcement. Brushing forces the mixture into the interstices of the tile. The depth of densification is 0.06 to 0.11 inch (1.5 to 2.8 mm), depending on the original tile density. The outer 0.035 inch (0.9 mm) of densified tile are three to six times as strong as the bulk material. The densified layer is still porous and allows volatile materials to escape as the Shuttle heats up in the atmosphere.

The first step in densification is an application of isopropyl alcohol to the bottom (unglazed) surface of the tile. The alcohol allows the densifying agents to wet and penetrate the water-repellent treatment on the tile. The slurry of colloidal silica and silica powder, with a small amount of pigment added, is painted on the tile. The pigment, an inert ceramic (tetraboron silicide), makes the slurry easier to see and aids in an even application.

After air-drying for 24 hours and oven-drying at 150° F (66° C) for 2 hours, the tile is weighed to determine the amount of material that has been added. Usually the amount is about 0.5 g/in.^{2} (0.078 g/cm^2) of surface area. Finally, the tile is rewaterproofed by exposure to vapors or methyltrimethoxysilane and acetic acid (a catalyst) at 350° F (1.77° C). The tile is then ready for installation.

This work was done by Robert L. Dotts of **Johnson Space Center** *and Jack W. Holt of Rockwell International Corp. For further information, Circle 69 on the TSP Request Card.*

Inquiries concerning rights for the commercial use of this invention should be addressed to the Patent Counsel, Johnson Space Center [see page A5]. Refer to MSC-18741.

Tile Densification With TEOS

Tetraethyl orthosilicate is another effective tile densifier.

Lyndon B. Johnson Space Center, Houston, Texas

The alternate densification process for Space Shuttle surface-insulation tiles (see preceding article) uses a brushed or sprayed coating of tetraethyl orthosilicate (TEOS), a commercial bonding agent for refractory brick and constituent of high temperature paint. When applied to the tile surface, TEOS is absorbed and deposits a relatively pure form of silica within the tile. The thermal expansion of the deposit matches that of the tile closely; and the surface tension of TEOS liquid is low enough that it

(continued on next page)

readily penetrates into the tile, even if the tile has been waterproofed. A TEOS-densified layer in the tile, about 0.2 inch (0.5 cm) deep with a minimum density of 2.5 g/in.^{3} (0.15 g/cm^3), strengthens the tile/pad combination to a level consistent with the full strength of the tile alone.

The liquid is generally applied and cured in three steps, after which the tile is allowed to cool and is weighed. The weight increase will usually average 0.15 g per square centimeter.

The TEOS liquid is prepared by mixing TEOS with 0.05N hydrochloric acid in the correct volume ratio. A dye added to the mixture helps to determine when the constituents are fully mixed; it also makes the TEOS easier to see when it is applied to the tile. The liquid should be used within 48 hours after preparation.

The TEOS liquid can be applied by brush, spray, or any other means that will ensure an even coating. If the area to be densified is less than the total area of the tile base, the boundary may be marked by a soft pencil (for brush application) or masked (for spraying).

The versatility of TEOS gives it a wide range of applications. Selected areas of tile can be densified to provide stiffer and stronger tile properties; also, a more durable surface is provided for additional coatings. The penetration of TEOS into a tile can be adjusted from full penetration (saturation) to a controlled localized densification. There is no surface buildup from the use of TEOS; thus, there are no dimensional changes when densifying.

This work was done by Glenn M. Ecord and Calvin Schomburg of **Johnson Space Center.** *For further information, Circle 70 on the TSP Request Card.*

Inquiries concerning rights for the commercial use of this invention should be addressed to the Patent Counsel, Johnson Space Center [see page A5]. Refer to MSC-18737.

Repairing High-Temperature Glazed Tiles

Chips and cracks in glaze are fixed quickly and dependably with a mixture containing tetraethyl orthosilicate.

Lyndon B. Johnson Space Center, Houston, Texas

Surface-damaged insulation tiles (see preceding articles) survive exposure to hostile sonic and temperature environments when they are repaired according to a new procedure. The new method consists of filling damaged areas on the glazed surface of the tile after proper preparation. The primary ingredient in the filler material is tetraethyl orthosilicate (TEOS).

The filler is prepared by mixing hydrolyzed TEOS, silicon tetraboride powder, and pulverized tile material. The silicon tetraboride gives the filler a black color; for white tiles it can be omitted.

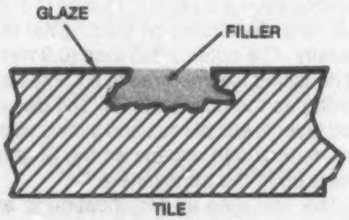

Undercutting the Edge of a Surface Crack, as shown in this cross section, helps to anchor filler material securely. The filler is carefully built up to the level of the tile glaze. The procedure can be performed in less than 1-1/2 hours.

To repair a tile, the damaged area is first cleaned. With the aid of dental tools, the edges of the damaged area are undercut (see figure), and any residue is removed. The area is coated with liquid TEOS and dried with heat lamps or a heat gun. After another coat of liquid TEOS is applied to the damaged area, the filler paste is applied to the crack with a spatula. The paste is carefully worked into the damaged area, including the undercut edges. Packed gently but firmly so as not to crack the surrounding coating, the pase is built up to the surface of the tile. The surface then is heated to dry and cure the filler. Finally, excess filler is sanded off the tile surface, and a final coat of liquid TEOS is brushed on.

Tiles repaired in this manner survived tests in which they were subjected to intense acoustic emissions, arc jets, and intense heat radiation. The new method is not only more reliable but also is less time-consuming than previously used methods. It can be performed in less than 1-1/2 hours with the tile in any orientation — even facing downward; the tile does not have to be removed for repair.

This work was done by Glenn M. Ecord and Calvin Schomburg of **Johnson Space Center.** *For further information, Circle 71 on the TSP Request Card.*

Inquiries concerning rights for the commercial use of this invention should be addressed to the Patent Counsel, Johnson Space Center [see page A5]. Refer to MSC-18736.

Producing Silicon Continuously

Fluid-bed vaporization followed by chemical vapor deposition generates large, semiconductor-grade silicon particles.

NASA's Jet Propulsion Laboratory, Pasadena, California

Chunks of semiconductor-grade silicon suitable as "seeds" for single-crystal growth and other applications is harvested continuously from an apparatus that combines a vaporizer with a fluidized bed or riser bed. Now undergoing laboratory development, the apparatus generates only dense silicon particles (no powder) from $(SiF_2)_x$ polymer feedstock. It shows promise as a more economical, higher volume alternative to previous batch-processing methods.

The apparatus, as shown in the figure, includes a fluid-bed vaporizer, consisting of silicon particles ranging from 1/2-in. (13-mm) to 5-mesh, with a $(SiF_2)_x$ polymer feed, and a SiF_4 inlet. The temperature of the vaporizer is maintained between 200° and 400° C by controlling the temperature of the inlet SiF_4. At these temperatures the $(SiF_2)_x$ is in equilibrium with Si_xF_y homologs that distill out of the vaporizer. Si_xF_y exits the vaporizer and contacts 5-to-80-mesh silicon in heaters at 500° to 1,000° C in the fluidized bed or riser bed. The flow rate and diameter of the reactor tube determine the mode of operation (fluidized or riser). On contacting the hot silicon, the Si_xF_y homologs disproportionate into silicon (which deposits on the hot silicon) and SiF_4.

The pure silicon is separated from the Si_xF_y in a cyclone separator, and the SiF_4 is recycled after cooling to 250° C. Part of the SiF_4 is stored, and the balance is recycled.

The addition of SiF_4 is regulated in the vaporizer to ensure that the partial pressure of Si_xF_y in the fluidized bed is less than 7 torr. At this low pressure, no silicon powder forms.

The $(SiF_2)_x$ polymer can be introduced into the duplex vaporizer/harvester by several methods. It could be formed in a heat exchanger/condenser and scraped into a displacement pump, which would force-feed the $(SiF_2)_x$ polymer into the vaporizer. Alternatively, the polymer could be scraped into a storage hopper and then added to the vaporizer.

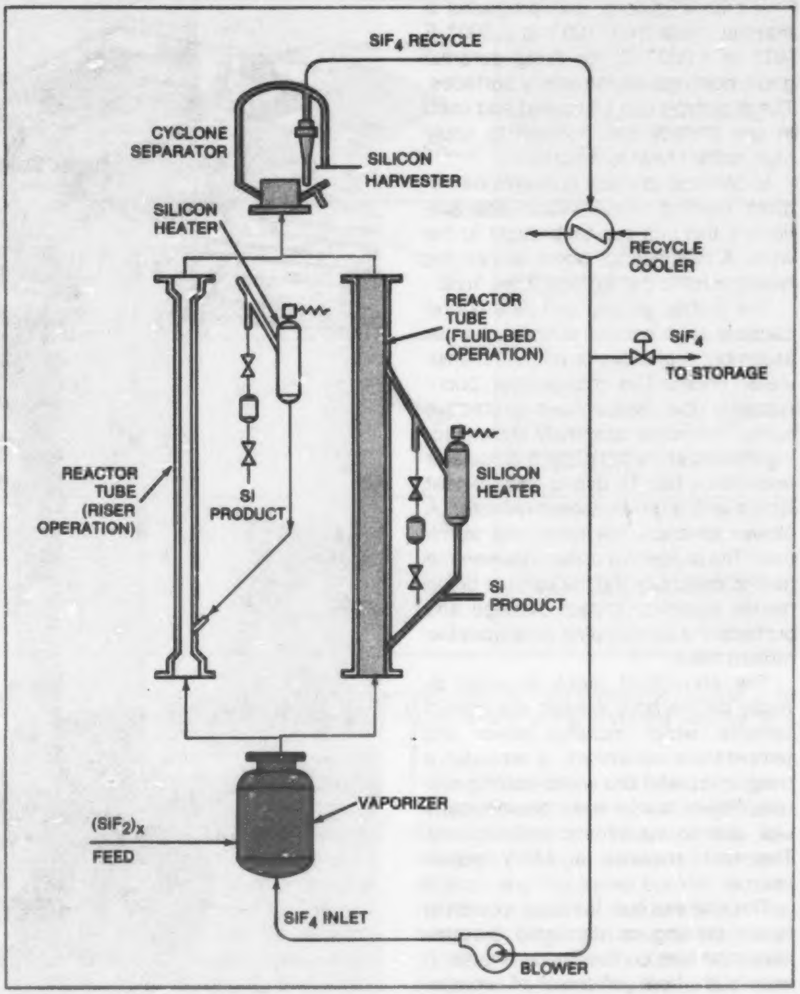

Semiconductor-Grade Silicon Chunks, roughly 1 cm in diameter, are produced continuously in a process based on the vaporization of feedstock, chemical vapor deposition in a fluidized bed, the extraction of silicon chunks, and the recycling of SiF_4.

The product fluidized-bed particles are approximately 0.03 to 0.5 cm in diameter; and the harvested chunks, extracted in a cyclone separator, are about 0.5 to 1.3 cm in diameter. The process is not limited to $(SiF_2)_x$ polymer feedstock; it can utilize virtually any halosilane intermediate used in silicon production.

This work was done by William M. Ingle, Richard S. Rosler, and Stephen Thompson of Motorola, Inc., for **NASA's Jet Propulsion Laboratory.** *For further information, Circle 72 on the TSP Request Card.*
NPO-14796

Mobile Glazing Unit

The unit provides a programed thermal cycle for in situ repair of ceramic coatings.

John F. Kennedy Space Center, Florida

A mobile glazing unit programs a thermal cycle from 100° to 2,300° F (40° to 1,260° C) for firing ceramic glaze coatings on refractory surfaces. The prototype can be moved and used in any attitude and position to apply high radiant heat to a surface.

In contrast to many conventional radiant heating units, which are stationary, this unit can be brought to the work. A manipulator boom places the heater next to the surface to be fired.

The mobile glazing unit (see figure) consists of a control console, heater assembly, protective cover, and manipulator boom. The manipulator boom supports the heater and protective cover. The heater assembly, shown facing upward at the top of the manipulator boom arm, has 18 quartz radiant-heat lamps with a water-cooled reflector. A blower air-cools the lamp end terminals. The protective cover between the heater assembly and the surface being heated prevents thermal damage and protects the surrounding area from the radiant heat.

The equipment racks mounted directly on the dolly contain the control console, which includes power and temperature controllers, a recorder, a programer, and the water-cooling system. Fail-safe interlocks prevent damage due to equipment malfunctions. The unit requires a 480-V power source.

The unit was built for firing a ceramic repair coating on damaged thermal-insulation tiles on the Space Shuttle. It was built from off-the-shelf components. The unit should be useful industrially for in situ repair applications of glazing on ceramics or for curing individual refractory blocks during the maintenance of furnaces.

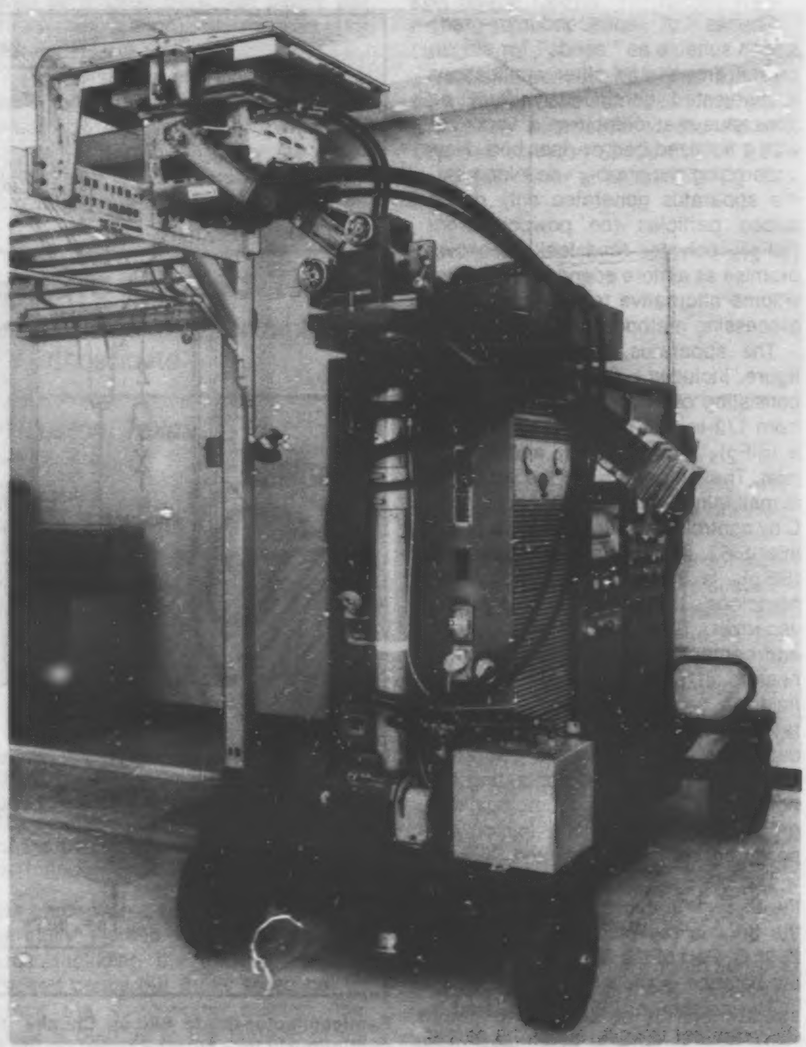

The Mobile Glazing Unit consists of a control console, heater assembly, protective cover, and manipulator boom. The heater assembly has 18 quartz radiant-heat lamps and a water-cooled reflector that provide thermal cycling in the temperature range of 100° to 2,300° F.

This work was done by Jack W. Holt of Rockwell International Corp. for **Kennedy Space Center.** *Further information may be found in NASA N81-70850/NSP, "Model 1023/8. Mobile Tile Glazing High Density Radiant Heating System—Preliminary Manual" and "Instruction Manual" [$20]. A copy may be purchased [prepayment required] from the National Technical Information Service, Springfield, Virginia 22161.*

Inquiries concerning rights for the commercial use of this invention should be addressed to the Patent Counsel, Kennedy Space Center [see page A5]. Refer to KSC-11171.

Learning High-Quality Soldering

A 5-day course teaches ultra-high-reliability electronic assembly.

NASA's Jet Propulsion Laboratory, Pasadena, California

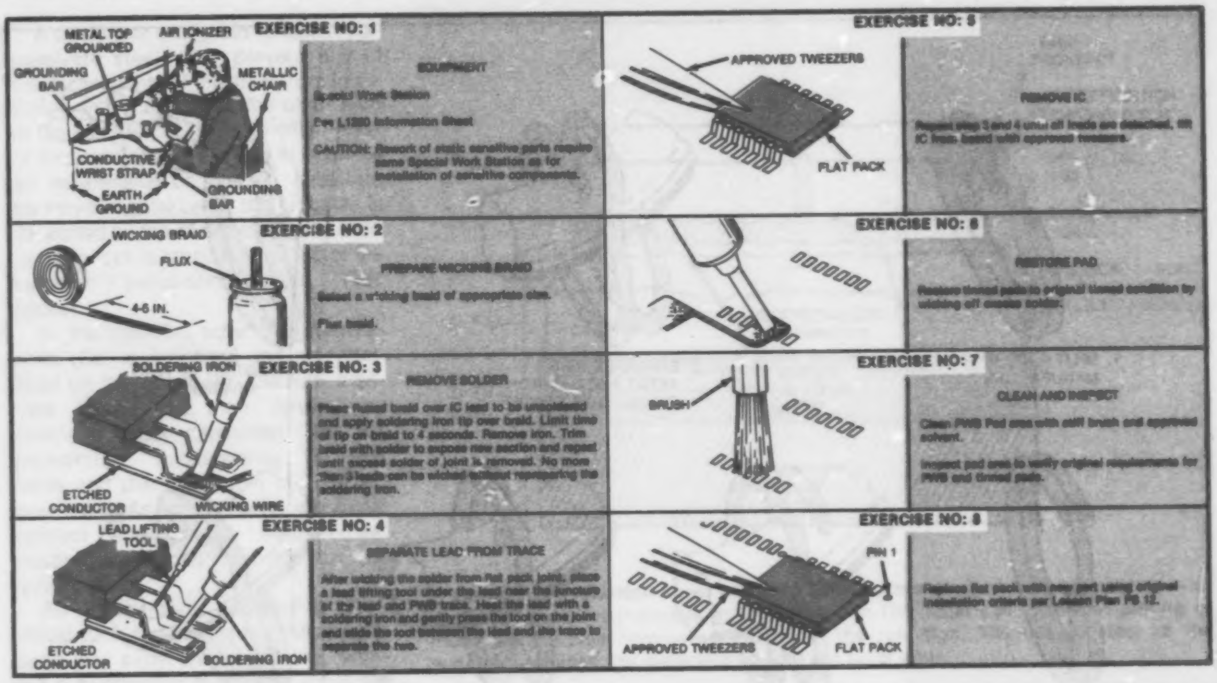

EQUIPMENT

Special Work Station

See L1280 Information Sheet

CAUTION: Rework of static sensitive parts require same Special Work Station as for installation of sensitive components.

PREPARE WICKING BRAID

Select a wicking braid of appropriate size.

Flux braid.

REMOVE SOLDER

Place fluxed braid over IC lead to be unsoldered and apply soldering iron tip over braid. Limit time of tip on braid to 4 seconds. Remove iron. Trim braid with solder to expose new section and repeat until excess solder of joint is removed. No more than 3 leads can be wicked without repreparing the soldering iron.

SEPARATE LEAD FROM TRACE

After wicking the solder from flat pack joint, place a lead lifting tool under the lead near the juncture of the lead and PWB trace. Heat the lead with a soldering iron and gently press the tool on the joint and slide the tool between the lead and the trace to separate the two.

REMOVE IC

Repeat step 3 and 4 until all leads are detached, lift IC from board with approved tweezers.

RESTORE PAD

Restore tinned pads to original tinned condition by wicking off excess solder.

CLEAN AND INSPECT

Clean PWB Pad area with stiff brush and approved solvent.

Inspect pad area to verify original requirements for PWB and tinned pads.

Replace flat pack with new part using original installation criteria per Lesson Plan PS 12.

Exercises in a Lesson Plan show in detail the approved steps for assembly or disassembly operations for electronic circuits — in this case, the removal of an integrated-circuit flat pack. Each step is presented in a simple and straightforward fashion in a training booklet and a video-tape demonstation.

A training course teaches soldering techniques to technicians who work on high-reliability electronic equipment. The course develops student awareness of soldering practices that assure long, failure-free equipment life.

At NASA's Jet Propulsion Laboratory, students attend the course for 5 days, from 8:15 in the morning to 4:15 in the afternoon. Part of their time is spent listening to lectures and watching video-tape demonstrations, but most of their time is devoted to performing step-by-step procedures under the guidance of an instructor.

Topics covered include:

- Hand Soldering;
- Wire and Component-Lead Preparation;
- Eyelet, Hook, Bifurcated, and Turret Terminal Soldering;
- Soldering of Flat and Round Conductors;
- Wire Routing; and
- Component Installation.

In addition to learning how to assemble new circuits, the students learn how to rework printed-wiring boards, to replace parts, and to make circuit changes by cutting traces, changing wiring, and adding terminals. The students are taught the benefits of using approved and calibrated instruments and tools and of performing the operations at properly-equipped and grounded work stations, particularly for complementary metal-oxide-semiconductor (CMOS) integrated circuits.

The instructor demonstrates — and the students practice — the use of flux; cleaning before and after soldering; joint inspection; soldering-iron care, maintenance, and calibration; and wire stripping and forming. The procedures and practices are organized as lesson plans, each plan consisting of step-by-step instructions for a complete assembly or disassembly operation.

For example, one lesson plan covers the removal of an integrated-circuit flat pack. The student is instructed (through video-tape demonstration and illustrated booklet — see figure) to select a soldering-iron tip and a wicking braid and to apply the iron and braid to each of the flat-pack leads in turn, removing the solder from each. Then the student is told to select a soldering-iron tip of the proper size and shape for the leads, to select a lead-lifting tool as well, and to use these tools to detach each lead in turn from the circuit board. Throughout, the student is shown methods that will prevent damage to the parts and ensure cleanliness.

This work was done by William S. Read of Caltech for **NASA's Jet Propulsion Laboratory.** *For further information, Circle 73 on the TSP Request Card.*
NPO-14869

Eliminating Gaps in Split Rings

A simple installation method allows smaller, lighter tether rings for cables.

Lyndon B. Johnson Space Center, Houston, Texas

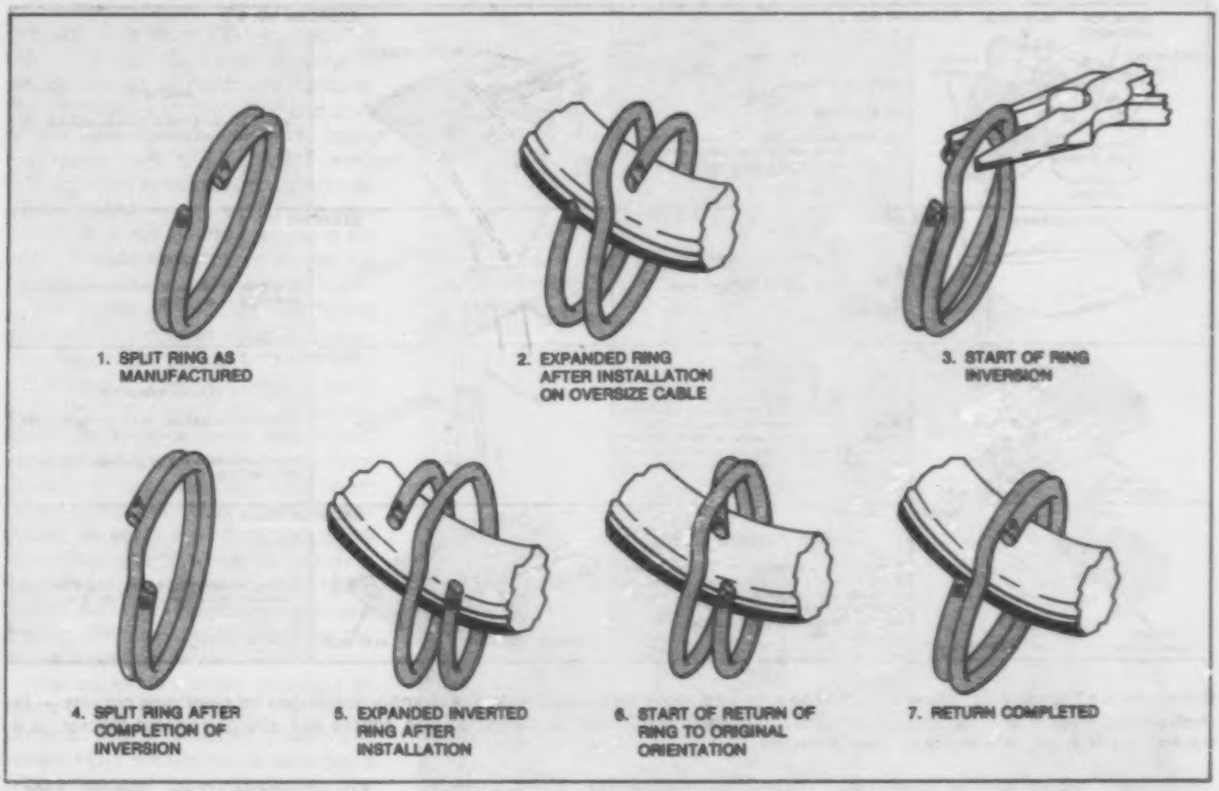
1. SPLIT RING AS MANUFACTURED
2. EXPANDED RING AFTER INSTALLATION ON OVERSIZE CABLE
3. START OF RING INVERSION
4. SPLIT RING AFTER COMPLETION OF INVERSION
5. EXPANDED INVERTED RING AFTER INSTALLATION
6. START OF RETURN OF RING TO ORIGINAL ORIENTATION
7. RETURN COMPLETED

A Split Ring Is Expanded (views 1 and 2) if it is installed on too large a cable. However, the procedure shown in views 3 through 7 inverts the coils and then returns them to their original position so that the coil gap disappears.

Ordinarily, the split-ring wire coils used to tether objects to a cable or rope have a wire diameter greater than some minimum determined by the cable diameter. Below this thickness, the elastic limit of the wire will be exceeded when its coils are opened wide enough to pass over the cable. The coils then will not snap together after they have passed over the cable, but will remain expanded, with a gap between adjacent coils. In this condition, the ring is not a reliable fastener.

A simple method of attaching split-ring coils to cables prevents such gaps from forming. The method makes it possible to use thinner coils without gaps forming and thus saves cost and weight. In the method, a ring is inverted before it is installed and returned to its original position after it is installed.

The coil installation is shown in the figure. The installer inverts the ends of the ring with a small pair of pliers, pulling one end through the ring and allowing the coils to follow. The coils are spread, and the ring slides over the cable. This procedure expands the inverted ring, leaving gaps between the coils. Finally, the installer reverses the inversion, pulling one end through the ring so that the coils follow it. The ring is then in its original orientation, and the coils are tightly compressed.

This work was done by Richard W. Gould of Rockwell International Corp. for **Johnson Space Center.** *No further documentation is available.*
MSC-18854

Passivation Layer for Steel Substrate of Solar Cell

Thin-film solar cell can be fabricated on commercial sheet-steel substrate passivated with tungsten layer.

NASA's Jet Propulsion Laboratory, Pasadena, California

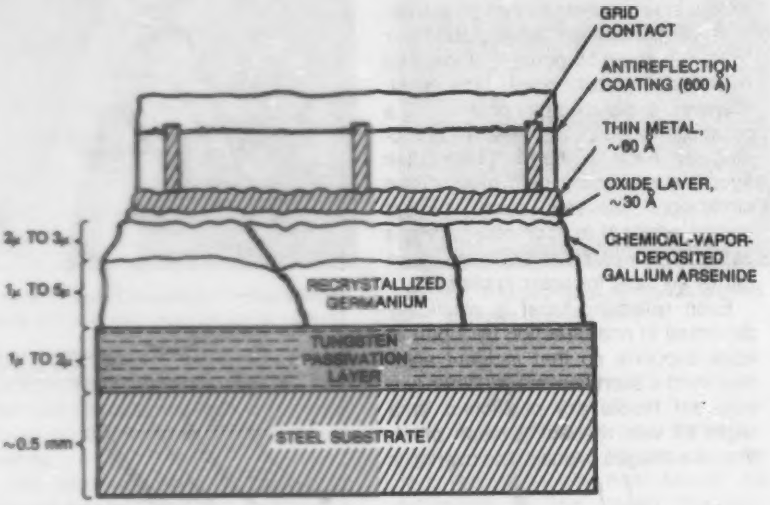

A Tungsten Passivation Layer prevents constituents of steel from interacting with the semiconductor materials in this MOS thin-film solar cell. The thin plating of nickel on the steel improves bonding of the tungsten. The use of steel as the substrate reduces the materials cost of the solar cell.

A coating of fine-grain tungsten can passivate steel; i.e., prevent any of the constituents of the steel from interacting with material on the other side of the tungsten. This passivation layer of tungsten allows the use of steel as an inexpensive conducting substrate for thin-film solar cells; the tungsten is deposited on top of the steel, and then the solar cell is fabricated on top of the tungsten passivation layer (see figure).

In the thin-film solar cell, germanium (Ge) is deposited and recrystallized on the substrate. Gallium arsenide (GaAs) is then formed by chemical vapor deposition over the germanium. Subsequently, a thin oxide and thin metal film are formed over the GaAs layer. A conducting grid contact and a top antireflection coating are added to complete the solar cell.

An inexpensive conducting substrate such as steel makes these solar cells less expensive. However, without a passivation layer, the substrate can alloy with the germanium or diffuse into the germanium and gallium arsenide.

The characteristics desired in a passivation layer are:

- thermal and electrical conduction,
- low contact resistance with the adjacent materials,
- strong adhesion to the adjacent materials,
- low interdiffusion of the substrate and Ge/GaAs through the passivation layer, and
- low loss of the passivating material into the adjacent materials.

Because Ge bonds, wets, and crystallizes well on tungsten, vapor-deposited coatings of tungsten and of tungsten with 1 percent carbon were tested for passivation. The steel was first plated with a thin nickel coating to improve the bonding of the tungsten layer.

Studies with various growth temperatures and power levels for the laser-beam recrystallization of the germanium show no evidence of nickel or iron contamination of the Ge/GaAs. Also, the studies show that the high background temperatures and long-duration laser pulses used to melt and recrystallize the germanium cause small clumps of tungsten to appear in the upper regions of the germanium. The appearance of the tungsten clumps, however, is not expected to affect the electrical performance of the cells. The clumps could be prevented by using lower background temperatures and higher-power-density, intermittent laser pulses to melt and recrystallize the germanium.

This work was done by Richard J. Stirn and Yea-Chuan M. Yeh of Caltech for **NASA's Jet Propulsion Laboratory.** *For further information, Circle 74 on the TSP Request Card. NPO-14961*

Low-Cost Concentrating Mirrors

Cost-effective concentrator mirrors are constructed from flat stock.

NASA's Jet Propulsion Laboratory, Pasadena, California

Parabolic mirrors used as concentrators in solar-energy systems are relatively expensive to manufacture. Their costs run about 15 percent of the total solar-concentrator costs. The cost, however, is reduced by constructing a parabolic reflector from many flat rectangular mirrors. Each mirror (see figure) is elastically deformed in one dimension. Several such mirrors placed adjacent to each other along a parabolic curve form an inexpensive mirror suitable for solar application.

Each reflecting facet is elastically deformed in one direction by a pair of edge supports so that incident solar rays form a short line image. When two adjacent facets are positioned at a slight tilt with respect to each other, their line images overlap. The overlap is somewhat smeared because the focal planes for the two facets are not identical; but if the radius of curvature of the mirrors is large, the images are far away from the mirrors, the smearing is slight, and the tilt of adjacent facets for image overlap is small. By this principle, many facets can be assembled to form a concentrating mirror approximating a parabolic reflector.

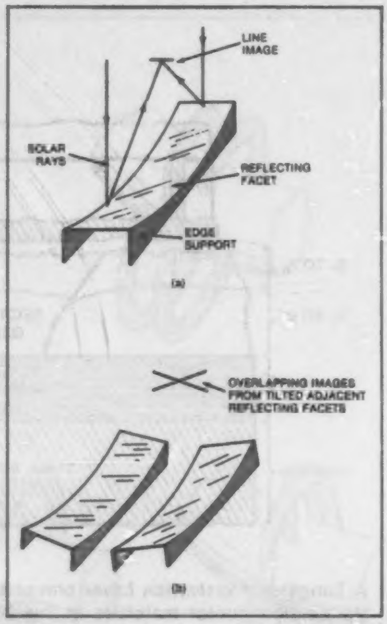

Rectangular Mirror Facets are slightly curved (a) by edge supports to produce line images of incident solar rays. When adjacent curved facets are tilted (b), the line images overlap to concentrate energy for solar-cell or solar-heating applications.

This simple, low-cost reflector may be fabricated from commercially available flat stock. The edge-supports may be integrated into the mounting arrangement.

This work was done by Timothy R. Carroll of Caltech for ***NASA's Jet Propulsion Laboratory.*** *No further documentation is available.*
NPO-14962

Spiral-Wound Gasket Forms Low-Temperature Seal

Small when stored, a new seal is formed in place into large-diameter seal.

Langley Research Center, Hampton, Virginia

A new cryogenic seal has been tested between −320° F (77 K) and room temperature against chamber pressures up to 130 psig (896×10^3 N/m^2). Seal pressure loads between 500 psig (3.45×10^6 N/m^2) and 2,500 psig (17.23×10^3 N/m^2) are applied. Fabricated from 25 percent glass-filled Teflon (or equivalent) material formed into a continuous strip gasket, the seal can be "active" (be opened and closed), or it can be permanent. It is made from just one component, requires no encapsulant, and can be easily produced with self-locking or other features.

The seal is made by skiving a thin continuous strip from the circumference of a disk of the glass-filled material. The disk is prepared by planing both surfaces to a smooth, parallel finish. When machining the strip, a lathe turns the disk, and the lathe crossfeed is adjusted to give the required thickness to the skived strip.

The seal is installed in a groove machined into one of the flange surfaces by wrapping successive turns of the strip spirally until the groove is filled. The thickness of the disk is the height of the seal, part of which protrudes above the groove. Closing the joint compresses the gasket, forming a tight seal. Figure 1 shows two concentric seals, and Figure 2 shows a cross section of a self-locking seal.

The new strip seal eliminates several design weaknesses of large-diameter cryogenic pressure seals. Since it is not fabricated to its final diameter by the manufacturer, as are conventional gaskets, problems of shipping and storage are minimized. Furthermore, because the seal is so small before installation, access to its location can be limited (relative to the seal final diameter), eliminating overdesign and unnecessary cost.

In contrast to large-diameter segmented seals, the new strip seal does not have radial leak paths. With the continuous strip, the potential leak-path length between the spiral windings is several times the circumference; thus, the chance for leakage is only a fraction of that of a conventional segmented seal. In addition, the seal allows for the relief of thermal stresses, and cracking would not necessarily cause the seal to fail.

A variation of the basic seal has an adhesive between the strips, resulting in a bonded solid piece of material. Other forms are a tubular strip with ends that allow for pressurization after assembly and a thermally controlled seal with a heated wire embedded in the strip. Large-diameter bearings, using a suitable material, could also be constructed in the same way. The strip seal can be custom-fitted to irregular flange surfaces and to different flange shapes.

This work was done by Stephen C. Irick of **Langley Research Center**. *For further information, Circle 75 on the TSP Request Card.*

This invention is owned by NASA, and a patent application has been filed. Inquiries concerning nonexclusive or exclusive license for its commercial development should be addressed to the Patent Counsel, Langley Research Center [see page A5]. Refer to LAR-12315.

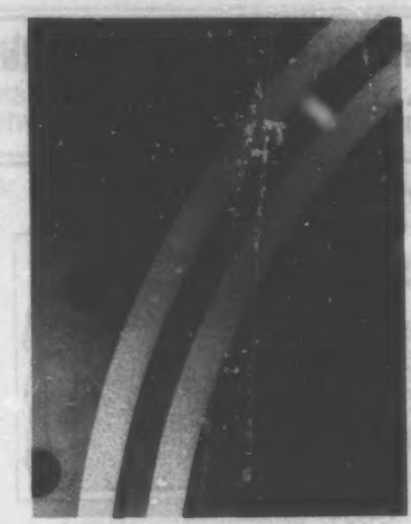

Figure 1. **Two Concentric Spiral-Wound Seals** are shown in their grooved flange.

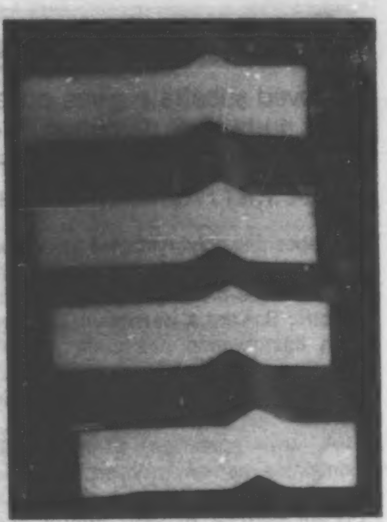

Figure 2. The **Self-Locking Spiral-Wound Seal** is shown in cross section.

Arc Spraying Solderable Tabs to Glass

Solder wets copper, copper bonds to aluminum, and aluminum adheres to glass.

NASA's Jet Propulsion Laboratory, Pasadena, California

Solderable tabs suitable for electrical or mechanical connections in such devices as solar cells and integrated circuits can be made by arc spraying aluminum and then copper onto glass. Arc spraying can be automated and integrated with encapsulation, eliminating hand tabbing, improving reliability, and reducing cost.

In an arc sprayer, two wires of the metal being sprayed are fed through hollow electrodes. An electric arc between the wires melts the metal; compressed air sprays the molten metal toward the surface being coated.

Adhesion tests of various metals arc sprayed on glass showed that aluminum adheres strongly but that copper can be peeled off. On the other hand, copper solders easily, but aluminum does not.

Thus, the key to making firmly-adhered solderable tabs is strongly bonding aluminum and copper so that both metals can be used. Copper and aluminum have different thermal expansion properties; the copper must be sprayed lightly, or the tab will curl like a bimetallic strip and warp. Good adhesion is obtained by spraying copper for only 2 to 3 seconds at minimum feed rate.

After soldering a tab to the copper, adhesion was tested by pulling on the tab at a 45° angle. It took a force of about 0.4 lb (2N) or more to pull a tab off. The tabs did not peel off the glass; rather, the glass beneath the tab fractured.

The excellent adhesion is believed due to a chemical reaction between the glass and the aluminum: Glass is primarily silicon dioxide, and aluminum bonds readily to oxygen. Also, glass softens around the melting point of aluminum, 1,200° F (660° C).

This work was done by Joseph Lindmayer of Solarex Corp. for **NASA's Jet Propulsion Laboratory.** *For further information, Circle 76 on the TSP Request Card.*
NPO-14853

Back Contacts for Silicon-on-Ceramic Solar Cells

Grooved substrate gives access to back surface of photovoltaic cells.

NASA's Jet Propulsion Laboratory, Pasadena, California

Depositing polycrystalline silicon on a ceramic substrate is an economical way of mass-producing cells for solar electric power. A persistent problem with this method has been making electrical contact with the back surface of the silicon layer — the surface next to the substrate.

A new substrate configuration, containing narrow grooves, exposes part of the back surface so that a dopant can be diffused into it and electrical contact can be made without weakening the substrate. When the substrate is coated first with carbon and then with molten silicon, silicon bridges form, leaving open channels in the grooves (see figure).

Liquid silicon containing a high concentration of boron is injected into the grooves. The liquid diffuses p^+ dopant (that is, a large quantity of boron ions) into the silicon. The p^+-doped silicon creates a back-surface field effect.

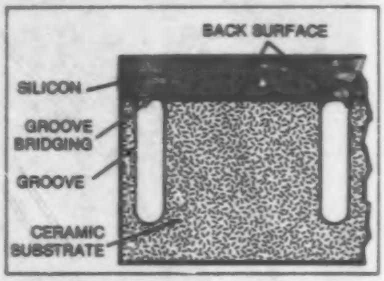

Polycrystalline-Silicon Bridges form over grooves in a ceramic substrate to expose the back surface of a solar cell. The back surface can be impregnated with dopants and can be contacted electrically. The groove spacing is 65 mils (1.6 mm).

After removal of the oxide that forms on the silicon bridges during diffusion, contact with p^+ silicon is made by any of several methods, such as electrolytic plating or solid-metal deposition by the decomposition of a liquid. Contacts to the front surface are made by conventional methods.

For best adhesion, the substrate grooves should run perpendicular to the direction in which the liquid-silicon layer is applied. The grooves should be closely spaced to maximize the back-contact area.

This work was done by Terry L. Schuller and Shirley Marquardt of Honeywell, Inc., for **NASA's Jet Propulsion Laboratory.** *For further information, Circle 77 on the TSP Request Card.*
NPO-14809

Self-Lubricating Gearset

Self-lubricating material allows attention-free operation in a vacuum and at extreme temperatures.

Lyndon B. Johnson Space Center, Houston, Texas

A skewed-axis gearset (see figure) can operate unattended for long periods if it is fabricated from a molybdenum sulfide filled polyimide (such as du Pont Vespel-SP1 or an equivalent material). The filled-polyimide gearset does not require lubrication, and it can be used in vacuum or at extreme temperatures.

Skewed-axis gearsets are often selected for slow-rotation high-torque drives because their rugged, multitooth contacts are compatible with gear ratios from as little as 10:1 to as much as 500:1. However, when the gears are fabricated of metal, the need for a lubricant restricts their use. In vacuum, for example, a lubricant would evaporate; and at extreme temperatures it can burn or freeze. The metal gears are also impractical in remote installations where it is difficult to do routine maintenance.

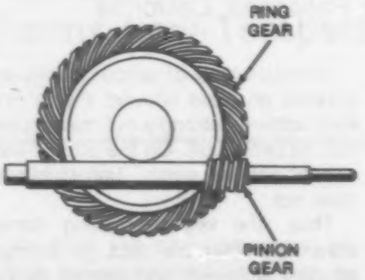

Ring Gear Drives Pinion Gear on a shaft in a skewed-axis arrangement. Because loads are shared among multiple meshing teeth, the molybdenum sulfide filled polyimide material is strong enough to handle a high gear ratio.

In contrast, a skewed-axis gearset fabricated of the self-lubricating polyimide plastic retains its ruggedness and efficiency, while allowing reliable attention-free operation in environments inappropriate for metal gears. Although originally developed for use in space, the self-lubricating gearset could also be used in remote installations on Earth.

This work was done by Derek S. Binge of RCA Corp. for **Johnson Space Center.** *No further documentation is available.*
MSC-18801

Reflecting Layers Reduce Weight of Insulation

The density of insulation blankets can be halved if metalized films are placed between layers.

Lyndon B. Johnson Space Center, Houston, Texas

The weight of insulating blankets is reduced 40 percent by interleaving gold-metalized films of plastic between the layers of fibrous material. Use of the lighter weight material with the "goldized" film in the Space Shuttle orbiter has saved approximately 710 pounds (320 kg). It should also be useful in commercial aircraft to reduce weight and increase cargo space.

Previously, thermal conductivity was reduced in fibrous-batting insulation blankets by increasing their density (and thus increasing their weight). However, the new insulation design (see figure) reduces density and weight while maintaining equivalent thermal conductivity. Development tests indicate that insulation with a density of 1 lb/ft^3 (17 kg/m^3), plus reflectors of goldized film spaced between the layers of insulation, has a thermal conductivity comparable to that of 2 lb/ft^3 (34 kg/m^3) insulation without the films.

This work was done by James D. Cole, Edward D. Schlessinger, and Harley J. Rockoff of Rockwell International Corp. for **Johnson Space Center.** *No further documentation is available.*
MSC-18785

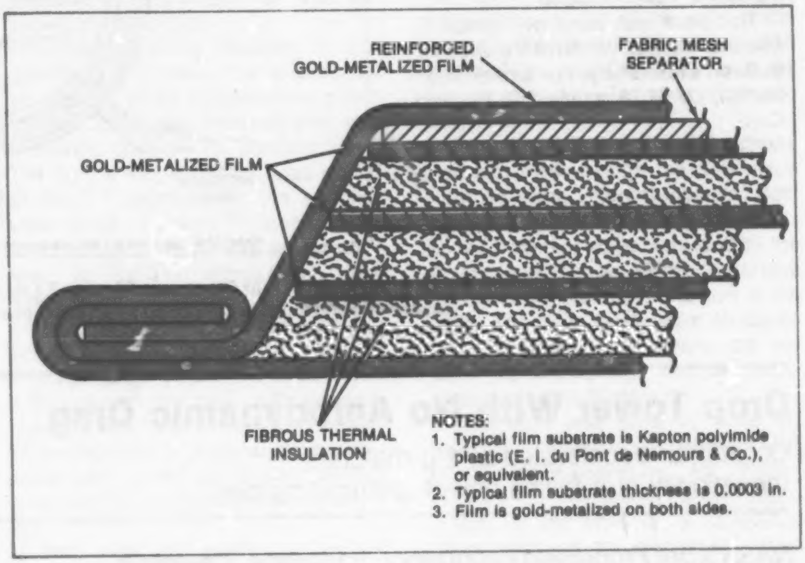

NOTES:
1. Typical film substrate is Kapton polyimide plastic (E. I. du Pont de Nemours & Co.), or equivalent.
2. Typical film substrate thickness is 0.0003 in.
3. Film is gold-metalized on both sides.

Lightweight Insulation batting is formed by interleaving gold-metalized films between layers of fibrous material. Because only half the density of fibrous material is required for a given thermal protection when the film is used, this construction saves 40 percent in weight.

Lightweight Cryogenic Vessel

A thin cooling jacket is contained by relatively thin walls.

NASA's Jet Propulsion Laboratory, Pasadena, California

A concept in the design of cryogenic cooling vessels would allow much lighter and more-easily fabricated vessels than are possible with conventional Dewar construction. The concept requires recirculating liquid nitrogen in a thin cooling jacket, but it does away with the evacuated insulating spaces normally required. This eliminates the need for heavy-walled shells to contain the vacuum.

The new cryogenic vessel was originally proposed for maintaining liquid fluorine, a cryogenic rocket fuel, while a spacecraft is on its launch pad. (After launch, the vacuum of space completes a Dewar-flask structure.) Since the design saves weight, it reduces fuel consumption (at the expense of increased consumption of liquid nitrogen).

The proposed design is shown in the figure, where the thickness of the outer shell has been exaggerated for clarity. The actual thickness is only about 5 mils (0.13 mm) or less. The inner shell, which holds the primary cryogenic fluid, is of conventional design.

The thin wall of the outer shell is possible because it contains recirculating liquid nitrogen at only a slight *positive*

(continued on next page)

pressure. In conventional Dewar design, the outer shell has to withstand full atmospheric negative pressure. It must therefore be thick enough to prevent buckling.

The new design is not limited to cryogenics. It could also be used to keep liquids hot by circulating a hotter fluid instead of liquid nitrogen.

This work was done by Joseph C. Lewis of Caltech for **NASA's Jet Propulsion Laboratory.** *For further information, Circle 78 on the TSP Request Card.*
NPO-14794

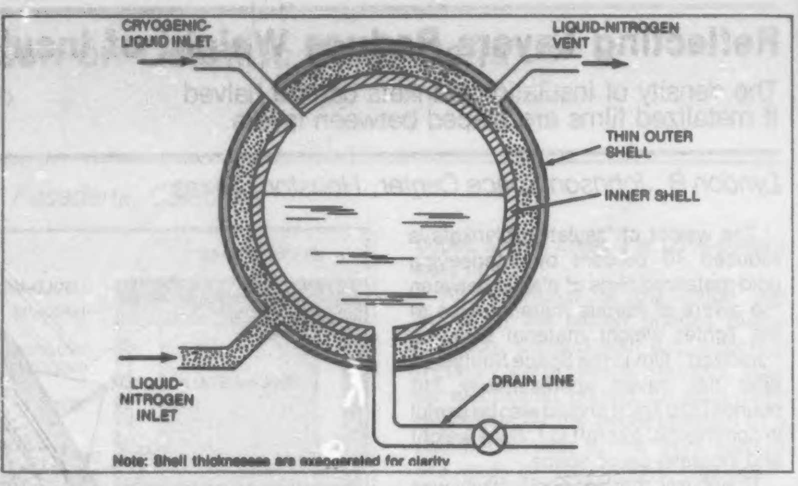

A Lightweight Cryogenic Storage Tank is kept cool by recirculating liquid nitrogen. The nitrogen is contained by an outer shell that can be less than 5 mils in thickness.

Drop Tower With No Aerodynamic Drag

Cooling air accelerated at 1 g matches the velocity of a falling object, eliminating drag.

NASA's Jet Propulsion Laboratory, Pasadena, California

A prototype 3-meter drop tower has air cooling but no aerodynamic drag. The drag is eliminated by forcing cooling air downward at 1 g with a suction fan so the air velocity matches the velocity of the falling drops. The tower geometry (see figure) causes the air to accelerate downward at 1 g.

Drop towers have long been used to make lead shot. Drops of molten material released at the top of the air-filled tower cool and solidify as they fall. However, aerodynamic drag tends to distort the drops, preventing them from assuming the spherical shape that would result from surface tension.

The drag-free tower was tested with hollow waterdrops. The time of fall was 0.7 second. Photographs confirm that the drops are more nearly spherical and the bubbles within more concentric than when drag is present.

A full-scale drop tower is planned for making spherical fuel capsules for thermonuclear fusion reactors. The tower must be taller than one with drag because the spheres continue to accelerate rather than approach a limiting velocity. Thus they fall farther in a given time interval. The spheres also cool more slowly because the surrounding air moves with them, lowering the heat-transfer rate.

This work was done by James M. Kendall, Jr., of Caltech for **NASA's Jet Propulsion Laboratory.** *For further information, Circle 57 on the TSP Request Card.*

This invention is owned by NASA, and a patent application has been filed. Inquiries concerning nonexclusive or exclusive license for its commercial development should be addressed to the Patent Counsel, NASA Resident Office-JPL [see page A8]. Refer to NPO-14845.

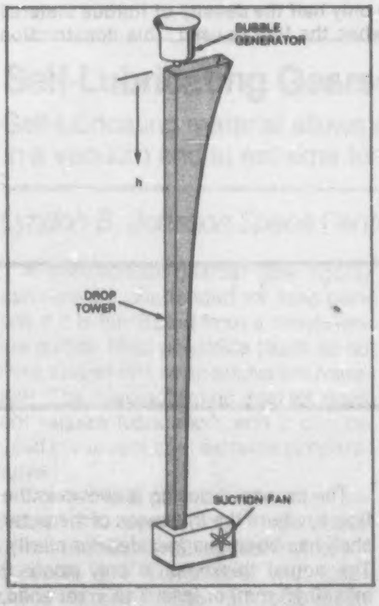

The Drop Tower with no aerodynamic drag has a fan that expels air from the bottom of the tower. Ideally, the tower cross-sectional area would be proportional to $1/\sqrt{h}$ where h is the height measured from the top of the tower. In practice, an area increment is added to correct for the effects of air friction on the wall of the channel.

Books and Reports

These reports, studies, and handbooks are available from NASA as Technical Support Packages (TSP's) when a Request Card number is cited; otherwise they are available from the National Technical Information Service.

Nickel-Doped Silicon for Solar Cells

Large grain boundaries act as gettering centers for nickel precipitates and improve cell performance.

When a p-type semiconductor crystal is grown from silicon doped with nickel, Ni precipitates in star-shaped clumps in the crystal. Heavier doping produces a higher density of larger clumps. However, in polycrystals the Ni precipitates along the grain boundaries without forming large clumps.

If the nickel-doped silicon is used for a solar cell (by the diffusion of a donor material into a wafer of the silicon, to form a pn junction), the clumps of precipitated Ni degrade the performance of the cell. The larger the size of the precipitate clumps, the more the conversion efficiency of the cell is degraded. However, a grain boundary around the effective area of the cell acts as a gettering center for the precipitates and impurities and improves the efficiency.

These effects in Ni-doped Si are described in a report that is available on request. Three crystals were grown (by the Czochralski method) with successively greater Ni concentration. The first, a single crystal, was doped at 5×10^{14} atoms/cm^3; the second, also single, at 4×10^{15} atoms/cm^3; and the third, which was polycrystalline, at 8×10^{15} atoms/cm^3. The examination of wafers cut from the crystals showed that the first had 400 precipitation clumps per cm^2, with an average size of 12 μm. The second had 1,500 clumps per cm^2, with an average size of 17 μm. However, in wafers of the third, the polycrystal, the precipitates were alined along grain boundaries and had an average size of only 5 μm.

Solar cells were made from wafers of each crystal by diffusing phosphorus into the top surface to form an n^+ region. The qualities of the n^+p junctions were determined by measurements of the electrical properties of the cells.

Data on open-circuit voltage, short-circuit current, maximum power, and conversion efficiency for the illuminated cells were compared with values for baseline (undoped) cells. The efficiencies of the solar cells made from the Ni-doped Si were lower than those of the baseline cells, with the heavier-doped single crystal degraded the most.

Dark forward current versus voltage was also measured for the cells made from the three different crystals. Both cells made from single-crystal silicon showed current leakage caused by the presence of the closely spaced arrays of precipitate clumps in the bulk of the cells. The cells made from Ni-doped polycrystalline Si, however, did not show current leakage and had near-ideal perfection factors.

This work was done by Amal M. Salama of Caltech for **NASA's Jet Propulsion Laboratory**. *For further information, including X-ray topographs of the crystals, a SEM/EBIC micrograph of an electrically-active star-shaped precipitate clump, and a photomicrograph of a Sirtl-etched solar cell, Circle 66 on the TSP Request Card.*
NPO-14780

Computer Programs

These programs may be obtained at very reasonable cost from COSMIC, a facility sponsored by NASA to make new programs available to the public. For information on program price, size, and availability, circle the reference letter on the COSMIC Request Card in this issue.

CADAT Network Translator

Cell-net data are converted to logic-gate models for test and simulation.

The CADAT network translator (NTRAN) converts cell-net data, as used by automatic layout programs, into logic-gate models for use by test and simulation programs. NTRAN input consists of either a Place, Route, and Fold (PRF) or a Place-and-Route-in-Two-Dimensions (PR2D) layout data deck. Output consists of either a Test Pattern Generator (TPG) or Logic-Simulation (LOGSIM) logic-circuitry data deck.

NTRAN reduces the workload of the integrated-circuit designer. Instead of having to build both the cell-net-data circuit description and the logic-gate-model circuit description, the designer needs only to build the former. Both describe the same circuit, and NTRAN acts as a translator. Thus, once the layout cell-net data are developed, they are translated and used as inputs for logic simulation and test pattern generation.

NTRAN is written in FORTRAN IV for batch execution and has been implemented on a Xerox Sigma V computer. It was developed in 1975. (Also see the related series of articles on the CADAT programs on pages 394 through 396 of *NASA Tech Briefs*, Vol. 5, No. 3.)

This program was written by E. R. Pitts of M&S Computing, Inc., for **Marshall Space Flight Center**. *For further information, Circle L on the COSMIC Request Card.*
MFS-25055

CADAT Integrated-Circuit Artwork Program

A versatile, ready-to-use mask-generator package

The CADAT integrated-circuit artwork program (ARTWORK) converts high-level artwork data into mask patterns. ARTWORK generates commands for a Gerber 1200 plotter or for a Mann pattern generator that select the appropriate apertures and completely expose, or "fill in," the specified areas of a circuit mask. The program generates the commands required to produce the artwork on a "one-mask-at-a-time" basis with up to nine mask levels. The commands are written to tape, with each level being written in a separate file.

ARTWORK also contains an extensive utility package. This enables the user to create new pattern libraries, to develop new cells, to incorporate new cells into the pattern library, and to perform system orientation functions, such as pattern-library display and tape handling. Included with the COSMIC distribution package for ARTWORK is an extensive PMOS, CMOS, and SOS pattern library.

ARTWORK is written in FORTRAN IV for batch execution and has been implemented on a Xerox Sigma V computer with a central memory requirement of approximately 20K of 32-bit words. It was developed in 1976. (Also see the preceding article.)

This program was written by **Marshall Space Flight Center,** *RCA Corp., and R. L. Kuelthau of M&S Computing, Inc. For further information, Circle M on the COSMIC Request Card.*
MFS-25017

Mathematics and Information Sciences

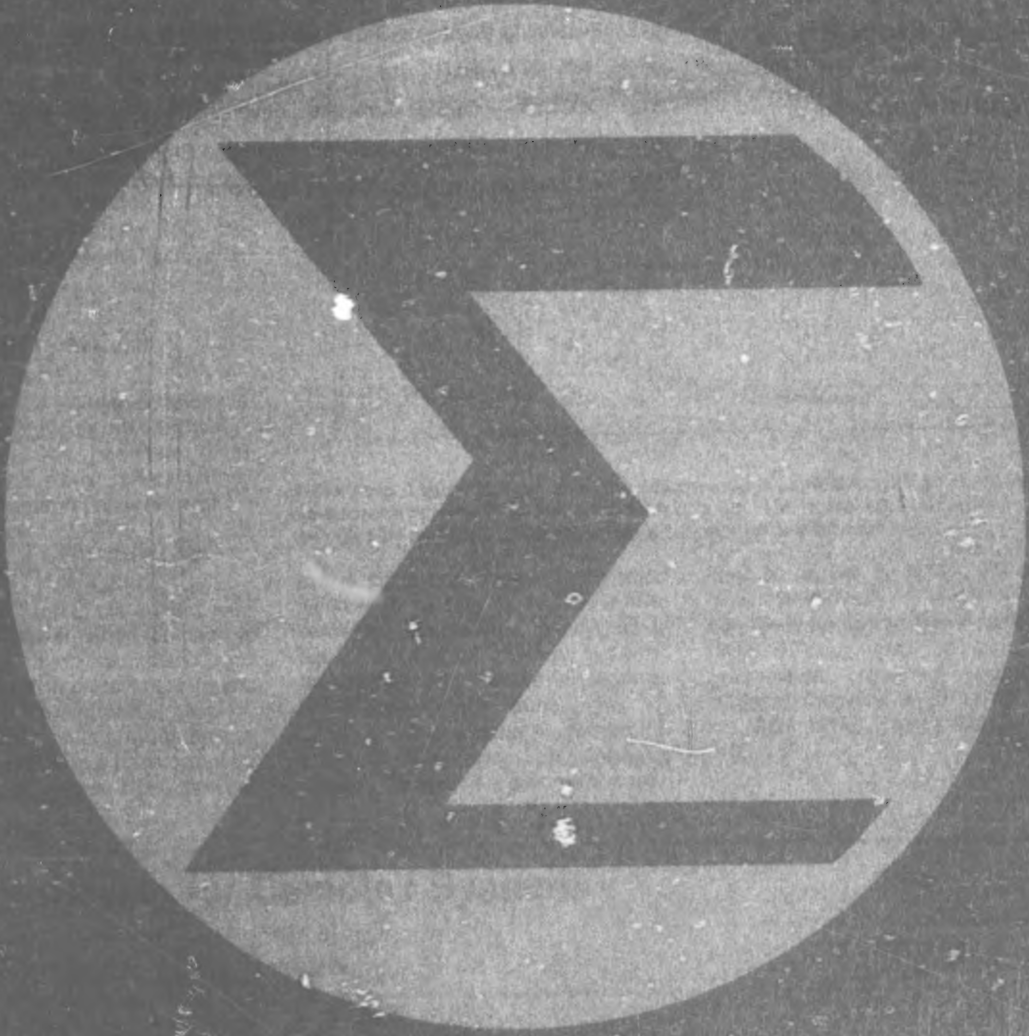

Hardware, Techniques, and Processes

511 An Approximation for Inverse Laplace Transforms
511 Safety Analysis for Complex Systems

Books and Reports

512 Evaluating Computer-Drawn Ground-Cover Maps

Computer Programs

512 OCCULT — ORSER Complete Conversational User-Language Translator
513 Selecting Optimum Algorithms for Image Processing
513 A Universal Structured-Design Diagramer

An Approximation for Inverse Laplace Transforms

A finite-series approximation can be run on a programable calculator.

Lyndon B. Johnson Space Center, Houston, Texas

A finite-series approximation for Laplace transform inversions is simple enough to run on a programable calculator. Utilizing a new family of orthonormal functions, the approximation can be used for a wide range of transforms, including those encountered in feedback-control problems.

For a Laplace transform F(s), the N-term approximation to its inverse F(t) is given by

$$_NF(t) = \sum_{n=1}^{N} A_n L_n(st)$$

where the A_n are Fourier coefficients and the $L_n(st)$ are the new orthonormal functions. The parameter s is chosen to give the best approximaton, such that the integral square error

$$E(s) = \int_0^\infty \left[{}_NF(t) - F(t) \right]^2 dt$$

is minimized. Each of the orthonormal functions is a power series, containing terms that are readily calculated from recursion relations given in the report referenced at the end of this article.

The new method approximates the Laplace transform by a transform with a series of simple poles along the real axis in the left-half plane. The method works well as long as F(t) decays to zero as t approaches infinity, as is often the case for physical systems. An example of a six-term approximation is shown in the figure.

This work was done by William M. Lear of TRW, Inc., for **Johnson Space Center.** *Further information may be found in NASA TM-81064 [N80-25056/NSP], "Inversion and Approximation of Laplace Transforms" [$6]. A copy may be purchased [prepayment required] from the National Technical Information Service, Springfield, Virginia 22161. MSC-18867*

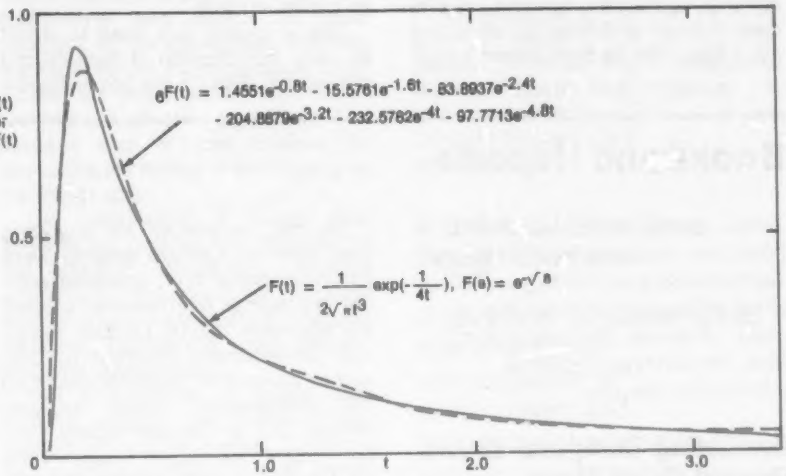

A Six-Term Approximation using the new method is compared with an exact Laplace transform inversion F(t). The parameter s is 0.8. The agreement is excellent, even though F(t) does not at all resemble a function of the form $e^{-0.8t}$.

Safety Analysis for Complex Systems

Hardware, environment, and human factors are considered in operational risk assessment.

Lyndon B. Johnson Space Center, Houston, Texas

A technique for assessing the possible failure modes of a complex system accounts for factors introduced by the presence of human operators and by the environment. The effects of hardware failures are considered for all phases of a mission.

Some risks or hazards are inherent in a configuration; high voltages and pressurized vessels are examples. These hazards can be identified and resolved in a design-phase hazard analysis. Hazards resulting from improper performance of a function at a time when its consequences become adverse, however, are analyzed in an operating-phase or mission-phase analysis.

The mission-phase hazard analysis technique starts with the division of a postulated mission into segments.

(continued on next page)

best copy available

Each segment is then subdivided into events that must occur during the segment. The events are further broken down into operational steps (such as crew actions, hardware responses, software instructions, and data feedback required) that must occur to allow execution of the event without adverse effects on the system. For large-scale complex operations, the division process may be simplified by sketching out a logic flow diagram showing each event in relation to preceding and/or parallel events.

The consequences of each event, nonoccurrence, premature operation, out-of-sequence operation, and inadvertent execution are all examined at the subevent, event, and phase levels. Any indication of a hazardous consequence is identified and treated on an individual basis.

This technique was used to obtain an early identification of hazards and operational risks for the Space Shuttle mission. It has also been applied in hazard analysis for aircraft flight tests. Analysts in the fields of energy and transportation should find it of value.

This work was done by Joseph P. Onesty and Robert L. Peercy, Jr., of Rockwell International Corp. for **Johnson Space Center**. *To obtain a copy of a report, "Risk Assessment Process as Applied to the Space Shuttle," Circle 65 on the TSP Request Card.*
MSC-18745

Books and Reports

These reports, studies, and handbooks are available from NASA as Technical Support Packages (TSP's) when a Request Card number is cited; otherwise they are available from the National Technical Information Service.

Evaluating Computer-Drawn Ground-Cover Maps

Plots of remote-sensing data were compared with photos of actual ground cover.

Computer-generated character maps from Landsat data were compared to aerial photos (and actual ground cover) for two test sites in Florida. The success in extracting ground features by two analytical techniques is the subject of a 113-page report.

The test sites were each about 20 miles (32 km) square. One was characterized by hardwood forests, softwood forests, grazing lands, cultivated fields, rivers, lakes, small towns, and scattered residential areas. The other had similar features, plus part of a city and some mining areas.

The two techniques for analyzing data from the Landsat satellite were an unsupervised (i.e., operated without any human interference) clustering algorithm, called Landsat Signature Development Program (LSDP), and an interactive algorithm based on the multispectral image analyzer (Image 100) at Kennedy Space Center. LSDP computer maps were produced at a scale of 1:24,000 (the scale of U.S. Geological Survey maps). The Image 100 plots were printed at the same scale. The most promising computer maps for both test sites were compared to geological survey maps and to aerial photos. In making comparisons, attention was given to determining whether the computer-generated maps could depict characteristic ground features.

In this study the LSDP maps provided good results when the features of interest had distinct spectral signatures. Successful characterization of Landsat scenes on the Image 100 depends heavily on firsthand knowledge of ground-cover conditions and on the ability to locate features on the display console.

The exact location of such specific ground features as small residential areas, roads, small rivers, and lakes could not be determined from any of the evaluated computer-generated maps in the study. Due to edge effects, such features were classified in one of the surrounding-cover categories. The study also found that the smaller the number of classifications used, the easier the maps were to interpret and the higher the accuracy of the maps.

Overall, the report concludes that the Landsat-generated maps are satisfactory depictions of actual ground conditions. The study was convincing that computer classification of digital Landsat multispectral data, supplemented with certain ground-cover information, may be a valuable tool in the hands of qualified scientists for the analysis of renewable resources.

This work was done by L. G. Arvanitis, R. Newburne, and R. Reich of the University of Florida for **Kennedy Space Center.** *Further information may be found in NASA CR-154635 [N80-32805/NSP], "Evaluation of Remote Sensing Techniques on Selected Forest Sites in Florida" [$10]. A copy may be purchased [prepayment required] from the National Technical Information Service, Springfield, Virginia 22161.*
KSC-11195

Computer Programs

These programs may be obtained at very reasonable cost from COSMIC, a facility sponsored by NASA to make new programs available to the public. For information on program price, size, and availability, circle the reference letter on the COSMIC Request Card in this issue.

OCCULT — ORSER Complete Conversational User-Language Translator

A "friendly" translator for non-computer-oriented users of satellite imagery and other remotely sensed data

The ORSER Complete Conversational User-Language Translator (OCCULT) assists non-computer-oriented users to set up and submit jobs for the ORSER system developed and distributed by Pennsylvania State University. OCCULT is designed for those who would like to use ORSER but cannot justify the effort of acquiring and maintaining the necessary proficiency in Remote Job Entry Language, Job Control Language (JCL), and control-card formats. For such users, OCCULT provides a "friendly" conversational front end to the ORSER software. OCCULT includes a data-management system and an output retrieval system.

ORSER is a collection of image-processing programs for analyzing remotely sensed data, such as those from Landsat satellites. Its use requires proficiency in editing JCL procedure files and in the details of ORSER control-card formats.

OCCULT is a set of "user-friendly" conversational programs that assists the new, or infrequent, ORSER user to set up and run ORSER jobs. OCCULT prompts the user for information, checks the validity of the answers, automatically creates the JCL and control cards, and submits the job to the computer. It also helps to retrieve the job output and provides a data-management system for storing image names and other pertinent data. OCCULT currently supports six of the available ORSER programs: SUBSET, NMAP, UMAP, STATS, CLUS, and CLASS.

OCCULT is written in FORTRAN IV and OS Assembler for interactive execution. It has been implemented on an IBM 360 computer under OS/MVT with a central memory requirement of approximately 230K of 8-bit bytes. The use of OCCULT requires interactive execution capability (e.g., with the time-sharing option, TSO). The OCCULT program was developed in 1979.

This program was written by H. K. Ramapriyan of **Goddard Space Flight Center** *and Kenneth Young of Computer Sciences Corp. For further information, Circle S on the COSMIC Request Card.*

Selecting Optimum Algorithms for Image Processing

An evaluation of registration, compression, and classification algorithms

Several algorithms process digital imagery such as Landsat data. The most common of these perform registration, compression, and classification. Because different techniques are available for registration, compression, and classification, image-data users need a rationale for selecting one approach over others.

A collection of registration, compression, and classification algorithms allows users to evaluate the different approaches and select the best approach for an application. Routines are included for six registration algorithms, six compression algorithms, and two classification algorithms. The package also includes routines for evaluating the effects of processing on the image data.

The registration of image data involves the geometrical alteration of the imagery. Registration routines available in the evaluation package include image magnification, mapping functions, partitioning, map overlay, and data interpolation.

The compression of image data involves reducing the volume of data needed for a given image. Compression routines available include adaptive differential-pulse-code modulation, two-dimensional transforms, clustering, vector reduction, and picture segmentation.

The classification of image data involves analyzing the uncompressed or compressed image data to produce inventories and maps of areas of similar spectral properties within a scene. The classification routines include a sequential linear technique and a maximum-likelihood technique.

The choice of the appropriate evaluation criteria is quite important in evaluating the image-processing functions. The user is therefore given a choice of evaluation criteria. All of the available criteria basically compare the observed results with the expected results. For the image reconstruction processes of registration and compression, the expected results are usually the original data or some selected characteristics of the original data. For classification processes the expected result is the ground truth of the scene.

Thus, the comparison process consists of determining what changes occur in processing, where the changes occur, how much change occurs, and the amplitude of the change. The package includes evaluation routines for performing such comparisons as average uncertainty, average information transfer, chi-square statistics, multidimensional histograms, and the computation of contingency matrices.

This collection of routines is written in FORTRAN IV for batch execution and has been implemented on an IBM 360 computer with a central memory requirement of approximately 662K of 8-bit bytes. The collection was developed in 1979.

This program was written by R. R. Jaroe, J. Hodges, R. E. Atkinson, B. Gaggini, L. Callas, and J. Peterson of **Marshall Space Flight Center.** *For further information, Circle N on the COSMIC Request Card.*
MFS-25367

A Universal Structured-Design Diagramer

A generator of standardized flow charts and concordances for development and debugging of programs in virtually any language

The Universal Structured-Design Diagramer (FLOWCHARTER) is a tool for documenting and understanding computer programs. FLOWCHARTER is "universal" because it produces flow charts and concordances for any program written in any language that can be described according to a defined set of rules. Because the generated flow charts are presented in a concise treelike format appropriate for representing the flow of control in a structured program, FLOWCHARTER is termed a "structured-design diagramer."

To flow-chart a program, the user provides FLOWCHARTER with a description of the programing-language grammar. Three sets of rules are needed: The first is a list of syntax rules in Backus-Naur form (BNF). These rewrite rules allow FLOWCHARTER to do a bottom-up parse of the input program. The next set is a list of semantic rules, in one-to-one correspondence with the syntactic rules, which specify how a particular construct is to be diagramed. Last is a set of concordance rules, again in one-to-one correspondence with the syntactic rules, which are used to isolate positions where identifiers may appear and to classify these identifiers as variables or as procedure names. Preparing this list is not trivial;

(continued on next page)

however, the list is only prepared once for each language. (A grammar description for PASCAL is included with the FLOWCHARTER package.)

Once the grammar is described, the user supplies only the source code of the program to be diagramed. FLOWCHARTER automatically produces a flow diagram and a concordance. The diagram is quite different from traditional flow charts. The structured-design diagram represents the main flow of the program in the top-down format, with increasing levels of detail explicitly indicated. This structured-design diagram approach is particularly appropriate for languages with higher level constructs, such as case, iterative loops, or logical dependent execution blocks.

The source code for FLOWCHARTER is written for the PASCAL Release 2 compiler, as distributed by the University of Minnesota. FLOWCHARTER is intended for batch execution and has been implemented on a CDC 6000-series computer with a central memory requirement of approximately 100K (octal) of 60-bit words. FLOWCHARTER was developed in 1979.

This program was written by Higher Order Software, Inc., for **Langley Research Center.** *For further information, Circle P on the COSMIC Request Card.*
LAR-12548

SUBJECT INDEX

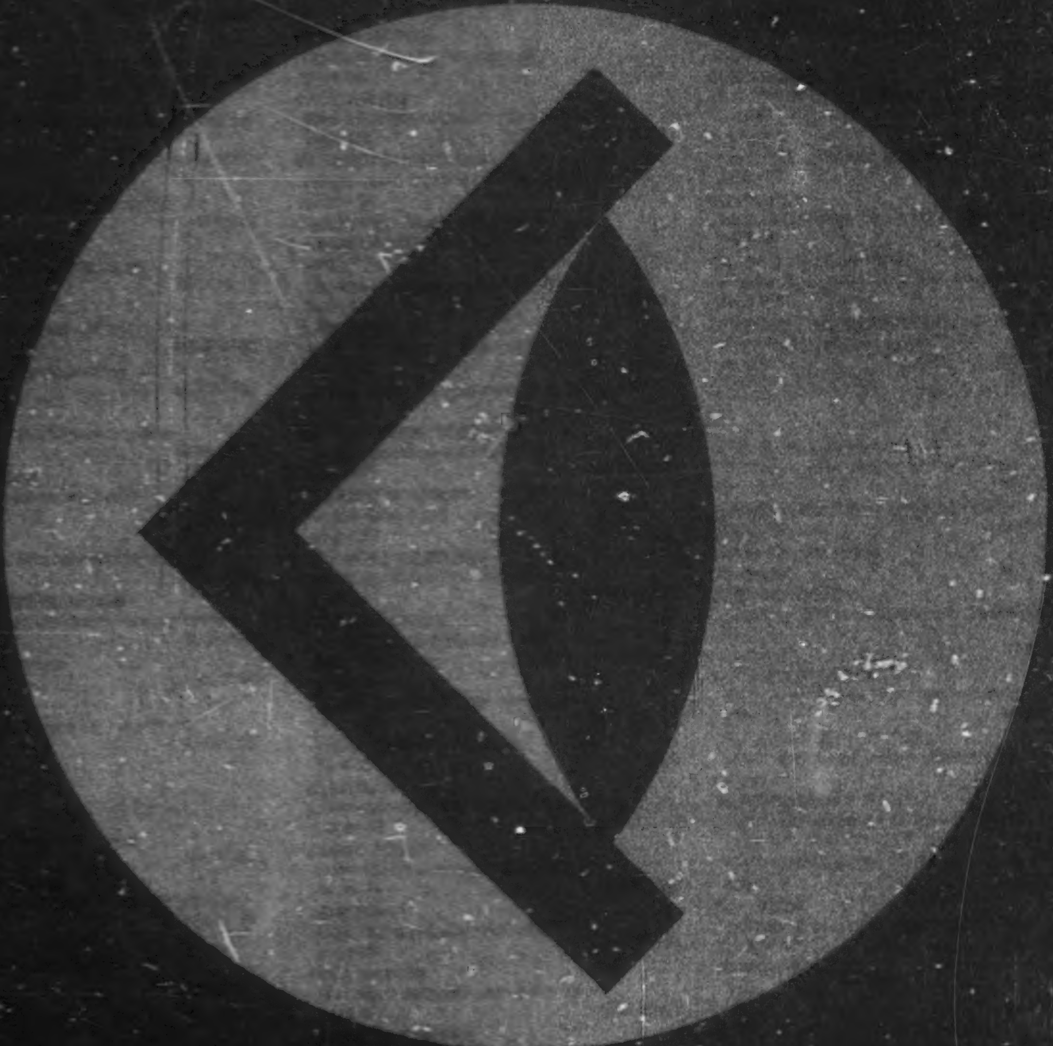

ACTUATORS
Lock for hydraulic actuators
page 489 MSC-18853
ADHESIVES
New pressure-sensitive silicone adhesives
page 452 LAR-12737
AERODYNAMICS
The design and analysis of low-speed airfoils
page 481 LAR-12727
Transonic flow over wing/fuselage configurations
page 482 LAR-12702
AIR WATER INTERACTIONS
Thermodynamic and transport properties of air/water mixtures
page 479 LEW-13432
AIRFOILS
The design and analysis of low-speed airfoils
page 481 LAR-12727
ALGORITHMS
Selecting optimum algorithms for image processing
page 513 MFS-25367
ANODIZING
User chooses coating properties
page 451 LAR-12719
ANTENNA COUPLERS
High-power dual-directional coupler
page 420 NPO-14713
ANTENNAS
Cavity-backed spiral-slot antenna
page 421 MSC-18532
Trislot-cavity microstrip antenna
page 422 MSC-18793
ARC SPRAYING
Arc spraying solderable tabs to glass
page 503 NPO-14853
ARRESTING GEAR
Gentle arrester for moving bodies
page 490 LAR-12372
ARTHRITIS
Gage for evaluating rheumatoid hands
page 461 GSC-12610
AUTOMATIC TEST EQUIPMENT
Developing experiment instrument packages
page 423 GSC-12536
Solar-site test module
page 433 MFS-25543
AUTOMOBILES
Four-wheel dual braking for automobiles
page 488 LAR-12687

BAGS
Soft container for explosive nuts
page 491 MSC-18871
BATTERY CHARGERS
Improved battery charger for electric vehicles
page 411 NPO-14964
BEARINGS
Cylindrical bearing analysis
page 491 LEW-13393
BINARY ALLOYS
Diffusion in single-phase binary alloys
page 454 LAR-12665
BIOINSTRUMENTATION
Cardiopulmonary data-acquisition system
page 457 MSC-18783
Microprocessor-based cardiotachometer
page 459 MSC-18775
BONDING
Arc spraying solderable tabs to glass
page 503 NPO-14853
"Densified" tiles form stronger bonds
page 495 MSC-18741
Tile densification with TEOS
page 495 MSC-18737
BRAKES (FOR ARRESTING MOTION)
Four-wheel dual braking for automobiles
page 488 LAR-12687
Gentle arrester for moving bodies
page 490 LAR-12372
BRAYTON CYCLE
Gas absorption/desorption temperature-differential engine
page 474 NPO-14528
BUBBLES
Driving bubbles out of glass
page 453 MFS-25414

CABLES (ROPES)
Gentle arrester for moving bodies
page 490 LAR-12372
CALIBRATING
Fast calibration of gas flowmeters
page 476 KSC-11076
CARDIOTACHOMETERS
Microprocessor-based cardiotachometer
page 459 MSC-18775
CARDIOVASCULAR SYSTEM
Cardiopulmonary data-acquisition system
page 457 MSC-18783
Microprocessor-based cardiotachometer
page 459 MSC-18775
CATALYSTS
Improved cell for water-vapor electrolysis
page 447 MSC-16394
Photoproduction of halogens using platinized TiO_2
page 449 LAR-12713
CAVITY RESONATORS
Cavity-backed spiral-slot antenna
page 421 MSC-18532
CERAMIC COATINGS
Mobile glazing unit
page 498 KSC-11171
CHEMICAL REACTORS
Producing silicon continuously
page 497 NPO-14796
CIRCUIT BOARDS
Low-resistance continuity tester
page 415 NPO-14881
CLAMPS
Eliminating gaps in undersized split rings
page 500 MSC-18854
Lock for hydraulic actuators
page 489 MSC-18853
CLOCKS
Fiber-optic clock-signal distribution system
page 430 NPO-14749
CLOUD COVER
Instrument measures cloud cover
page 474 NPO-14936
COATINGS
User chooses coating properties
page 451 LAR-12719
COLLIMATORS
Multibeam collimator uses prism stack
page 427 GSC-12606
COMPLEX SYSTEMS
Safety analysis for complex systems
page 511 MSC-18745
COMPRESSED AIR
Pneumatic-power supply
page 486 MSC-18855
COMPUTER PROGRAMS
A universal structured-design diagramer
page 513 LAR-12548
COMPUTERIZED SIMULATION
CADAT integrated-circuit artwork program
page 508 MFS-25017
CADAT network translator
page 507 MFS-25055
Calculating linear A,B,C, and D matrices from a nonlinear dynamic engine simulation
page 479 LEW-13250
CONCENTRATORS
Low-cost parabolic mirrors
page 502 NPO-14962
CONNECTORS
Interlocking wedge joint is easily assembled
page 485 LAR-12729
CONTAINMENT
Soft container for explosive nuts
page 491 MSC-18871
CONTAMINATION
Bulk lifetime indicates surface contamination
page 471 NPO-14966
COOLING
Heat pipes cool probe and sandwich panel
page 478 LAR-12588
COUPLINGS
Interlocking wedge joint is easily assembled
page 485 LAR-12729
CRYOGENIC EQUIPMENT
Spiral-wound gasket forms low-temperature seal
page 503 LAR-12315
CRYOGENIC FLUID STORAGE
Lightweight cryogenic vessel
page 505 NPO-14794

DATA ACQUISITION
Cardiopulmonary data-acquisition system
page 457 MSC-18783
Microprocessor-based cardiotachometer
page 459 MSC-18775
Solar-site test module
page 433 MFS-25543
DATA ANALYSIS
Selecting optimum algorithms for image processing
page 513 MFS-25367
DECONTAMINATION
Removing Freon gas from hydraulic fluid
page 452 MSC-18740
DEFORMETERS
Biaxial method for in-plane shear testing
page 472 LAR-12680
DENSIFICATION
"Densified" tiles form stronger bonds
page 495 MSC-18741
Tile densification with TEOS
page 495 MSC-18737
DIFFUSION
Diffusion in single-phase binary alloys
page 454 LAR-12665
DISPLAY DEVICES
Imager displays free fall in stop action
page 450 NPO-14779
DISTANCE MEASURING EQUIPMENT
Short-range self-pulsed optical radar
page 432 NPO-14901
DOPING (ADDITIVES)
Nickel-doped silicon for solar cells
page 507 NPO-14780
DRILLING
Sidewall penetrator for oil wells
page 487 NPO-14306
DROP TOWER
Drop tower with no aerodynamic drag
page 506 NPO-14845

DYNAMIC RESPONSE
An all-FORTRAN version of NASTRAN for the VAX
page 481 GSC-12600
DYNAMIC STABILITY
Isolation and measurement of rotor vibration forces
page 466 LAR-12476

ELECTRIC CONTACTS
Back contacts for silicon-on-ceramic solar cells
page 504 NPO-14809
ELECTRIC DISCHARGES
Pulse-shaping circuit for laser excitation
page 428 NPO-14556
ELECTRICAL RESISTANCE
Low-resistance continuity tester
page 415 NPO-14881
ELECTROLYTIC CELLS
Improved cell for water-vapor electrolysis
page 447 MSC-16394
ENDOSCOPES
Fiber-optic coupler for arthroscope
page 462 LAR-12718
ENERGY CONVERSION
Solar cell is housed in light-bulb enclosure
page 413 LEW-13418
ENGINE DESIGN
Calculating linear A,B,C, and D matrices from a nonlinear dynamic engine simulation
page 479 LEW-13250
Gas absorption/desorption temperature-differential engine
page 474 NPO-14528
ENVIRONMENT POLLUTION
Recycling paper-pulp waste liquors
page 450 NPO-14797
EXPLOSIVES
Soft container for explosive nuts
page 491 MSC-18871

FASTENERS
Eliminating gaps in undersized split rings
page 500 MSC-18854
Interlocking wedge joint is easily assembled
page 485 LAR-12729
FEEDBACK CONTROL
Speed control for synchronous motors
page 414 MSC-18680
FIBER OPTICS
Fiber-optic coupler for arthroscope
page 462 LAR-12718
FIELD-EFFECT TRANSISTORS
Simple JFET oscillator
page 413 GSC-12555
FILLERS
Repairing high-temperature glazed tiles
page 496 MSC-18736
FLOW CHARTS
A universal,structured-design diagramer
page 513 LAR-12548
FLOW DISTRIBUTION
The design and analysis of low-speed airfoils
page 481 LAR-12727
FLOW MEASUREMENT
Fast calibration of gas flowmeters
page 476 KSC-11076
FLUID FLOW
Potential flow in two-dimensional deflected nozzles
page 481 LEW-13461
Reduced viscosity interpreted for fluid/gas mixtures
page 431 NPO-14976
Transonic flow over wing/fuselage configurations
page 482 LAR-12702
FLUIDIZED BED PROCESSORS
Producing silicon continuously
page 497 NPO-14796
FORTRAN
An all-FORTRAN version of NASTRAN for the VAX
page 481 GSC-12600
FREE FALL
Drop tower with no aerodynamic drag
page 506 NPO-14845
Imager displays free fall in stop action
page 450 NPO-14779
FREON
Removing Freon gas from hydraulic fluid
page 452 MSC-18740

GAS CHROMATOGRAPHY
Applying the helium ionization detector in chromatography
page 448 MSC-18835
GAS FLOW
Fast calibration of gas flowmeters
page 476 KSC-11076
GAS LASERS
Gas-laser power monitor
page 430 LAR-12682
GAS TURBINE ENGINE
Gas absorption/desorption temperature-differential engine
page 474 NPO-14528
GAS-LIQUID INTERACTIONS
Driving bubbles out of glass
page 453 MFS-25414
GASKETS
Spiral-wound gasket forms low-temperature seal
page 503 LAR-12315
GEARS
Self-lubricating gearset
page 504 MSC-18801
GEOMAGNETISM
Improved LEEM ranges over four decades
page 469 LAR-12706
GLASS
Arc spraying solderable tabs to glass
page 503 NPO-14853
Driving bubbles out of glass
page 453 MFS-25414
GLAZES
Mobile glazing unit
page 498 KSC-11171
GOLD COATINGS
Reflecting layers reduce weight of insulation
page 505 MSC-18785
GONIOMETERS
Gage for evaluating rheumatoid hands
page 461 GSC-12610
GROUND SUPPORT EQUIPMENT
Developing experiment instrument packages
page 423 GSC-12536

HALOGENS
Photoproduction of halogens using plantinized TiO_2
page 449 LAR-12713
HAND (ANATOMY)
Gage for evaluating rheumatoid hands
page 461 GSC-12610
HEART RATE
Microprocessor-based cardiotachometer
page 459 MSC-18775
HEAT PIPES
Heat pipes cool probe and sandwich panel
page 478 LAR-12586
HEAT TREATMENT
Mobile glazing unit
page 498 KSC-11171
HEATING EQUIPMENT
Building with integral solar-heat storage—Starkville, Mississippi
page 444 MFS-25559
Closed-circulation system for motel hot water—Savannah, Georgia
page 443 MFS-25572
Economic evaluation of a solar hot-water system
page 435 MFS-25529
Economic evaluation of a solar hot-water system —Palm Beach County, Florida
page 441 MFS-25536
Evaluation of an evacuated-tube liquid solar collector
page 434 MFS-25450
Fire-station solar-energy system—Kansas City, Missouri
page 440 MFS-25538
Five-city economics of a solar hot-water system
page 434 MFS-25532
Motel solar-hot-water installation — Atlanta, Georgia
page 443 MFS-25564
Motel solar-hot-water system—Dallas, Texas
page 442 MFS-25575
Motel solar-hot-water system with nonpressurized storage—Jacksonville, Florida
page 442 MFS-25569
Multimode solar-heating system—Columbia, South Carolina
page 439 MFS-25552
One-year assessment of a solar space water heater—Clinton, Mississippi
page 440 MFS-25539
Residential solar-heating system—Lansing, Michigan
page 441 MFS-25530
Residential solar-heating system uses pyramidal optics
page 436 MFS-25567
Single-family-residence solar heating—Carlsbad, New Mexico
page 438 MFS-25526
Solar-energy heats a transportation test center—Pueblo, Colorado
page 438 MFS-25527
Solar-energy landmark building—Columbia, Missouri
page 437 MFS-25524
Solar-heated and cooled savings and loan building —Leavenworth, Kansas
page 436 MFS-25520
Solar-heated bank—Marks, Mississippi
page 436 MFS-25558
Solar-heated ranger station—Glendo, Wyoming
page 440 MFS-25537
Solar-heated swimming school—Wilmington, Delaware
page 439 MFS-25548
Solar heating for a restaurant—North Little Rock, Arkansas
page 443 MFS-25568
Solar heating for an observatory—Lincoln, Nebraska
page 437 MFS-25525
Solar space-heating system—Yosemite National Park, California
page 442 MFS-25553
Solar water heater design package
page 434 MFS-25521

Solar water-heating performance evaluation—San Diego, California
page 436 MFS-25502
Two-story residence with solar heating—Newnan, Georgia
page 438 MFS-25526
Winter performance of a domestic solar-heating system—Duffield, Virginia
page 439 MFS-25540
HELICOPTER DESIGN
Isolation and measurement of rotor vibration forces
page 468 LAR-12476
HIGH PRESSURE
Vibration transducer for high temperatures and pressures
page 471 MSC-18778
HYDRAULIC EQUIPMENT
Lock for hydraulic actuators
page 489 MSC-18853
HYDRAULIC FLUIDS
Removing Freon gas from hydraulic fluid
page 452 MSC-18740

IMAGE ENHANCEMENT
OCCULT—ORSER complete conversational user-language translator
page 512 GSC-12604
IMAGERY
Evaluating computer-drawn ground-cover maps
page 512 KSC-11195
Imager displays free fall in stop action
page 450 NPO-14779
Selecting optimum algorithms for image processing
page 513 MFS-25367
INFRARED DETECTORS
Compact infrared detector
page 475 NPO-14864
INSTRUMENT PACKAGES
Developing experiment instrument packages
page 423 GSC-12536
INSULATION
Reflecting layers reduce weight of insulation
page 505 MSC-18765
INTEGRAL TRANSFORMATIONS
An approximation for inverse Laplace transforms
page 511 MSC-18867
INTERFACIAL TENSION
Driving bubles out of glass
page 453 MFS-25414
IONIZATION COUNTERS
Applying helium ionization detector in chromotography
page 448 MSC-18835

JOINTS (ANATOMY)
Gage for evaluating rheumatoid hands
page 461 GSC-12610
JOINTS (JUNCTIONS)
Interlocking wedge joint is easily assembled
page 485 LAR-12729
JUNCTION TRANSISTORS
Simple JFET oscillator
page 413 GSC-12555

LANDSAT SATELLITES
Evaluating computer-drawn ground-cover maps
page 512 KSC-11195
LAPLACE TRANSFORMATION
An approximation for inverse Laplace transforms
page 511 MSC-18867

LASER RANGE FINDERS
Short-range self-pulsed optical radar
page 432 NPO-14901
LASERS
Gas-laser power monitor
page 430 LAR-12682
Tunable pulsed carbon dioxide laser
page 432 NPO-14984
LIGHT BEAMS
Multibeam collimator uses prism stack
page 427 GSC-12608
LIVESTOCK
Beef grading by ultrasound
page 463 NPO-14812
LOCKS (FASTENERS)
Lock for hydraulic actuators
page 489 MSC-18853
LOGIC CIRCUITS
CADAT integrated-circuit artwork program
page 506 MFS-25017
CADAT network translator
page 507 MFS-25055

MACHINE-INDEPENDENT PROGRAMS
A universal structured-design diagramer
page 513 LAR-12548
MAGNETIC TRANSDUCERS
Vibration transducer for high temperatures and pressures
page 471 MSC-18778
MAGNETOMETERS
Improved LEEM ranges over four decades
page 469 LAR-12706
MAINTENANCE
Repairing high-temperature glazed tiles
page 496 MSC-18736
MAPS
Evaluating computer-drawn ground-cover maps
page 512 KSC-11195
MATERIALS HANDLING
Lightweight cyrogenic vessel
page 505 NPO-14794
Soft container for explosive nuts
page 491 MSC-18871
MATERIALS RECOVERY
Recycling paper-pulp waste liquors
page 450 NPO-14797
MATRICES (MATHEMATICS)
Calculating linear A,B,C, and D matrices from a nonlinear dynamic engine simulation
page 479 LEW-13250
MEDICAL EQUIPMENT
Cardiopulmonary data-acquisition system
page 457 MSC-18783
Fiber-optic coupler for arthroscope
page 462 LAR-12718
Microprocessor-based cardiotachometer
page 459 MSC-18775
Microprocessor-controlled ultrasonic plethysmograph
page 458 MSC-18759
METEOROLOGY
Instrument measures cloud cover
page 474 NPO-14936
MICROORGANISMS
Improved microbe detection in water samples
page 460 LAR-12709
MICROWAVE ANTENNAS
Cavity-backed spiral-slot antenna
page 421 MSC-18532
Trislot-cavity microstrip antenna
page 422 MSC-18793
MICROWAVE COUPLING
High-power dual-directional coupler
page 420 NPO-14713
MICROWAVE TUBES
Cooling microwave tube for enhanced performance
page 419 NPO-14975
MIRRORS
Low-cost parabolic mirrors
page 502 NPO-14962
MOLYBDENUM SULFIDES
Self-lubricating gearset
page 504 MSC-18801
MULTIPHASE FLOW
Reduced viscosity interpreted for fluid/gas mixtures
page 431 NPO-14976

NONNEWTONIAN FLOW
Reduced viscosity interpreted for fluid/gas mixtures
page 431 NPO-14976
NOZZLE FLOW
Potential flow in two-dimensional deflected nozzles
page 461 LEW-13461

OIL RECOVERY
Sidewall penetrator for oil wells
page 487 NPO-14306
OPTICAL COMMUNICATION
Fiber-optic clock-signal distribution system
page 430 NPO-14749
OPTICAL EQUIPMENT
Multibeam collimator uses prism stack
page 427 GSC-12608
OPTICAL RADAR
Short-range self-pulsed optical radar
page 432 NPO-14901
OPTIMIZATION
Selecting optimum algorithms for image processing
page 513 MFS-25367
Structural design with stress and displacement constraints
page 480 MFS-25235
ORTHONORMAL FUNCTIONS
An approximation for inverse Laplace transforms
page 511 MSC-18867
OSCILLATORS
Simple JFET oscillator
page 413 GSC-12555
OVENS
An oven for many thermocouple reference junctions
page 467 FRC-10112

PAPERS
Recycling paper-pulp waste liquors
page 450 NPO-14797
PARABOLIC REFLECTORS
Low-cost parabolic mirrors
page 502 NPO-14962
PASSIVATION
Passivation layer for steel substrate of solar cell
page 501 NPO-14961
PHASE LOCKED SYSTEMS
Fiber-optic clock-signal distribution system
page 430 NPO-14749
Timing signal propagates without phase shift
page 422 MSC-18777
PHOTOELECTRIC CELLS
Solar cell is housed in light-bulb enclosure
page 413 LEW-13418

PHOTOMETERS
Compact infrared detector
page 475 NPO-14864
Gas-laser power monitor
page 430 LAR-12682
PHOTOPRODUCTION
Photoproduction of halogens using platinized TiO_2
page 449 LAR-12713
PHOTOVOLTAIC CELLS
Multijunction high-voltage solar cell
page 412 LEW-13400
PLETHYSMOGRAPHY
Microprocessor-controlled ultrasonic plethysmograph
page 458 MSC-18759
PNEUMATIC EQUIPMENT
Pneumatic-power supply
page 486 MSC-18655
POLLUTION MONITORING
Improved microbe detection in water samples
page 460 LAR-12709
POTENTIAL FLOW
Potential flow in two-dimensional deflected nozzles
page 481 LEW-13461
PRISMS
Multibeam collimator uses prism stack
page 427 GSC-12608
PROGRAMMING LANGUAGES
OCCULT—ORSER complete conversational user-language translator
page 512 GSC-12604
PROTECTIVE COATINGS
Passivation layer for steel substrate of solar cell
page 501 NPO-14961
PULSE GENERATORS
Pulse-shaping circuit for laser excitation
page 428 NPO-14556
PURIFICATION
Driving bubbles out of glass
page 453 MFS-25414

RADAR
Short-range self-pulsed optical radar
page 432 NPO-14901
RADIANT HEATING
Mobile glazing unit
page 498 KSC-11171
RADIOMETERS
Compact infrared detector
page 475 NPO-14864
Field limiter for cavity solar radiometer
page 429 NPO-14781
RANGE FINDERS
Short-range self-pulsed optical radar
page 432 NPO-14901
RECYCLING
Recycling paper-pulp waste liquors
page 450 NPO-14797
REDUNDANT COMPONENTS
Four-wheel dual braking for automobiles
page 488 LAR-12687
REFLECTORS
Low-cost parabolic mirrors
page 502 NPO-14962
REMOTE SENSORS
Evaluating computer-drawn ground-cover maps
page 512 KSC-11195
RING STRUCTURES
Eliminating gaps in undersized split rings
page 500 MSC-18654
ROLLING CONTACT LOADS
Cylindrical bearing analysis
page 491 LEW-13393
RUGGEDNESS
Self-lubricating gearset
page 504 MSC-18801

SAFETY FACTORS
Safety analysis for complex systems
page 511 MSC-18745
SANDWICH STRUCTURES
Heat pipes cool probe and sandwich panel
page 478 LAR-12588
SEALING
Spiral-wound gasket forms low-temperature seal
page 503 LAR-12315
SELF LUBRICATING MATERIALS
Self-lubricating gearset
page 504 MSC-18801
SHEAR PROPERTIES
Biaxial method for in-plane shear testing
page 472 LAR-12680
SILICON
Back contacts for silicon-on-ceramic solar cells
page 504 NPO-14809
Producing silicon continuously
page 497 NPO-14796
SILICONES
New pressure-sensitive silicone adhesives
page 452 LAR-12737
SIMULATION
Wind-simulation tester for solar modules
page 477 NPO-14837
SLOT ANTENNAS
Cavity-backed spiral-slot antenna
page 421 MSC-18532
Trislot-cavity microstrip antenna
page 422 MSC-18703
SOLAR CELLS
Back contacts for silicon-on-ceramic solar cells
page 504 NPO-14809
Multijunction high-voltage solar cells
page 412 LEW-13400
Nickel-doped silicon for solar cells
page 507 NPO-14780
Passivation layer for steel substrate of solar cell
page 501 NPO-14961
Solar cell is housed in light-bulb enclosure
page 413 LEW-13418
Wind-simulation tester for solar modules
page 477 NPO-14837
SOLAR ENERGY
Building with integral solar-heat storage—Starkville, Mississippi
page 444 MFS-25559
Closed-circulation system for motel hot water—Savannah, Georgia
page 443 MFS-25572
Economic evaluation of a solar hot-water system
page 435 MFS-25529
Economic evaluation of a solar hot-water system—Palm Beach County, Florida
page 441 MFS-25536
Evaluation of an evacuated-tube liquid solar collector
page 434 MFS-25450
Fire-station solar-energy system—Kansas City, Missouri
page 440 MFS-25538
Five-city economics of a solar hot-water system
page 434 MFS-25532
Low-cost parabolic mirrors
page 502 NPO-14962
Motel solar-hot-water installation—Atlanta, Georgia
page 443 MFS-25564
Motel solar-hot-water system—Dallas, Texas
page 442 MFS-25575
Motel solar-hot-water system with nonpressurized storage—Jacksonville, Florida
page 442 MFS-25569
Multijunction high-voltage solar cells
page 412 LEW-13400
Multimode solar-heating system—Columbia, South Carolina
page 439 MFS-25552
Nickel-doped silicon for solar cells
page 507 NPO-14780
One-year assessment of a solar space water heater—Clinton, Mississippi
page 440 MFS-25539
Residential solar-heating system—Lansing, Michigan
page 441 MFS-25530
Residential solar-heating system uses pyramidal optics
page 436 MFS-25567
Single-family-residence solar heating—Carlsbad, New Mexico
page 438 MFS—25528
Solar-energy heats a transportation test center—Pueblo, Colorado
page 438 MFS-25527
Solar-energy landmark building—Columbia, Missouri
page 437 MFS-25524
Solar-heated and cooled savings and loan building—Leavenworth, Kansas
page 436 MFS-25520
Solar-heated bank—Marks, Mississippi
page 436 MFS-25558
Solar-heated ranger station—Glendo, Wyoming
page 440 MFS-25537
Solar-heated swimming school—Wilmington, Delaware
page 439 MFS-25548
Solar heating for a restaurant—North Little Rock, Arkansas
page 443 MFS-25568
Solar heating for an observatory—Lincoln, Nebraska
page 437 MFS-25525
Solar-site test module
page 433 MFS-25543
Solar space-heating system—Yosemite National Park, California
page 442 MFS-25553
Solar water heater design package
page 434 MFS-25521
Solar water-heating performance evaluation—San Diego, California
page 436 MFS-25502
Two-story residence with solar heating—Newnan, Georgia
page 438 MFS-25526
Winter performance of a domestic solar-heating system—Duffield, Virginia
page 439 MFS-25540
SOLAR RADIATION
Field limiter for cavity solar radiometer
page 429 NPO-14781
SOLDERING
Learning high-quality soldering
page 499 NPO-14869
SPEED CONTROL
Speed control for synchronous motors
page 414 MSC-18680
SPRAYING
Pneumatic-power supply
page 486 MSC-18655
STORAGE TANKS
Lightweight cyrogenic vessel
page 505 NPO-14794
STRESS ANALYSIS
Structural design with stress and displacement constraints
page 480 MFS-25235
STRESS MEASUREMENT
Biaxial method for in-plane shear testing
page 472 LAR-12680

STRUCTURAL ANALYSIS
An all-FORTRAN version of NASTRAN for the VAX
page 481 GSC-12600
Structural design with stress and displacement constraints
page 480 MFS-25235
SYNCHRONISM
Fiber-optic clock-signal distribution system
page 430 NPO-14749
Timing signal propagates without phase shift
page 422 MSC-18777
SYNCHRONOUS MOTORS
Speed control for synchronous motors
page 414 MSC-18680

TEA LASERS
Tunable pulsed carbon dioxide laser
page 432 NPO-14984
TEMPERATURE CONTROL
An oven for many thermocouple reference junctions
page 467 FRC-10112
Building with integral solar-heat storage—Starkville, Mississippi
page 444 MFS-25559
Closed-circulation system for motel hot water—Savannah, Georgia
page 443 MFS-25572
Economic evaluation of a solar hot-water system
page 435 MFS-25529
Economic evaluation of a solar hot-water system—Palm Beach County, Florida
page 441 MFS-25536
Evaluation of an evacuated-tube liquid solar collector
page 434 MFS-25450
Fire-station solar-energy system—Kansas City, Missouri
page 440 MFS-25538
Five-city economics of a solar hot-water system
page 434 MFS-25532
Motel solar hot-water installation—Altanta, Georgia
page 443 MFS-25564
Motel solar-hot-water system—Dallas, Texas
page 442 MFS-25575
Motel solar-hot-water system with nonpressurized storage—Jacksonville, Florida
page 442 MFS-25569
Multimode solar-heating system—Columbia, South Carolina
page 439 MFS-25552
One-year assessment of a solar space water heater—Clinton, Mississippi
page 440 MFS-25539
Residential solar-heating system—Lansing, Michigan
page 441 MFS-25530
Residential solar-heating system uses pyramidal optics
page 436 MFS-25567
Single-family-residence solar heating—Carlsbad, New Mexico
page 438 MFS-25528
Solar-energy heats a transportation test center—Pueblo, Colorado
page 438 MFS-25527
Solar-energy landmark building—Columbia, Missouri
page 437 MFS-25524
Solar-heated and cooled savings and loan building—Leavenworth, Kansas
page 436 MFS-25520
Solar-heated bank—Marks, Mississippi
page 436 MFS-25558
Solar-heated ranger station—Glendo, Wyoming
page 440 MFS-25537
Solar-heated swimming school—Wilmington, Delaware
page 439 MFS-25548
Solar heating for a restaurant—North Little Rock, Arkansas
page 443 MFS-25568
Solar heating for an observatory—Lincoln, Nebraska
page 437 MFS-25525
Solar space-heating system—Yosemite National Park, California
page 442 MFS-25553
Solar water heater design package
page 434 MFS-25521
Solar water-heating performance evaluation—San Diego, California
page 436 MFS-25502
Two-story residence with solar heating—Newnan, Georgia
page 438 MFS-25526
Winter performance of a domestic solar-heating system—Duffield, Virginia
page 439 MFS-25540
TEST EQUIPMENT
Solar-site test module
page 433 MFS-25543
TETRAETHYL ORTHOSILICATE
Repairing high-temperature glazed tiles
page 496 MSC-18736
Tile densification with TEOS
page 495 MSC-18737
THERMAL INSULATION
Reflecting layers reduce weight of insulation
page 505 MSC-18785
THERMOCOUPLES
An oven for many thermocouple reference junctions
page 467 FRC-10112
THERMODYNAMIC PROPERTIES
Thermodynamic and transport properties of air/water mixtures
page 479 LEW-13432
TILES
"Densified" tiles form stronger bonds
page 495 MSC-18741
Repairing high-temperature glazed tiles
page 496 MSC-18736
Tile densification with TEOS
page 495 MSC-18737
TIME SIGNALS
Fiber-optic clock-signal distribution system
page 430 NPO-14749
Time signal propagates without phase shift
page 422 MSC-18777
TRACE CONTAMINANTS
Bulk lifetime indicates surface contamination
page 471 NPO-14966
TRANSDUCERS
Vibration transducer for high temperatures and pressures
page 471 MSC-18778
TRANSLATING
OCCULT—ORSER complete conversational user-language translator
page 512 GSC-12604
TRANSONIC FLOW
Transonic flow wing/fuselage configurations
page 482 LAR-12702
TRANSPORT PROPERTIES
Thermodynamics and transport properties of air/water mixtures
page 479 LEW-13432

ULTRASONIC TESTS
Beef grading by ultrasound
page 463 NPO-14812
Microprocessor-controlled ultrasonic plethysmograph
page 458 MSC-18759

VAPOR DEPOSITION
Producing silicon continuously
page 497 NPO-14796
VIBRATION MEASUREMENT
Vibration transducer for high temperatures and pressures
page 471 MSC-18778
VIDEO EQUIPMENT
Imager displays free fall in stop action
page 450 NPO-14779
VISCOSITY
Reduced viscosity interpreted for fluid/gas mixtures
page 431 NPO-14976

WASTE ENERGY UTILIZATION
Gas absorption/desorption temperature-differential engine
page 474 NPO-14528
WASTES
Recycling paper-pulp waste liquors
page 450 NPO-14797
WATER QUALITY
Improved microbe detection in water samples
page 460 LAR-12709
WATER VAPOR
Improved cell for water-vapor electrolysis
page 447 MSC-16394
WEATHER FORECASTING
Instrument measures cloud cover
page 474 NPO-14936
WEIGHT REDUCTION
Reflecting layers reduce weight of insulation
page 505 MSC-18785
Structural design with stress and displacement constraints
page 460 MFS-25235
WHEEL BRAKES
Four-wheel dual braking for automobiles
page 488 LAR-12687
WIND PRESSURE
Wind-simulation tester for solar modules
page 477 NPO-14837
WIRING
Learning high-quality soldering
page 499 NPO-14869

National Aeronautics and
Space Administration

Washington, D.C.
20546

Official Business
Penalty for Private Use $300

NO POSTAGE
NECESSARY
IF MAILED
IN THE
UNITED STATES

BUSINESS REPLY MAIL

FIRST CLASS PERMIT NO. 12028 WASHINGTON, D.C.

POSTAGE WILL BE PAID BY NASA

Director, Technology Transfer Division
P.O. Box 8757
Baltimore/Washington International Airport, MD 21240

NASA

National Aeronautics and
Space Administration

Washington, D.C.
20546

Official Business
Penalty for Private Use $300

NO POSTAGE
NECESSARY
IF MAILED
IN THE
UNITED STATES

BUSINESS REPLY MAIL

FIRST CLASS PERMIT NO. 12028 WASHINGTON, D.C.

POSTAGE WILL BE PAID BY NASA

Director, Technology Transfer Division
P.O. Box 8757
Baltimore/Washington International Airport, MD 21240

NASA

National Aeronautics and
Space Administration

Washington, D.C.
20546

Official Business
Penalty for Private Use $300

NO POSTAGE
NECESSARY
IF MAILED
IN THE
UNITED STATES

BUSINESS REPLY MAIL

FIRST CLASS PERMIT NO. 12028 WASHINGTON, D.C.

POSTAGE WILL BE PAID BY NASA

Director, Technology Transfer Division
P.O. Box 8757
Baltimore/Washington International Airport, MD 21240

NASA

TECH BRIEFS SUBSCRIPTIONS

WINTER
1980

☐ Please place me on the subscription list for NASA Tech Briefs (issued quarterly).
[New subscribers should allow 6 to 10 weeks for delivery for first issue.]

☐ I wish to change the delivery address for my current subscription. The identification number at the top right of my current mailing label is T________.

1. Please check any of the following that describe your organization:
   - ☐ Federal Government
   - ☐ State Government
   - ☐ Municipal Government
   - ☐ University/College
   - ☐ Secondary School
   - ☐ Trade/Vocational School
   - ☐ Manufacturing
   - ☐ Sales
   - ☐ Research
   - ☐ Consulting
   - ☐ Medicine
   - ☐ Professional Society
   - ☐ News Media
   - ☐ Information Sciences/Library
2. Please check the number of employees in your organization: ☐ Under 25 ☐ 25-100 ☐ 100-500 ☐ Over 500
3. Please indicate if your position is one of the following: ☐ Owner or Chief Executive Officer ☐ Administrator/Manager ☐ Scientist ☐ Engineer ☐ Other ________

[PLEASE PRINT]

NAME ________ TITLE ________

COMPANY ________ PHONE ________

&

STREET ADDRESS ________ CITY ________ STATE ________ ZIP ________

TECH BRIEFS SUBSCRIPTIONS

WINTER
1980

☐ Please place me on the subscription list for NASA Tech Briefs (issued quarterly).
[New subscribers should allow 6 to 10 weeks for delivery for first issue.]

☐ I wish to change the delivery address for my current subscription. The identification number at the top right of my current mailing label is T________.

1. Please check any of the following that describe your organization:
   - ☐ Federal Government
   - ☐ State Government
   - ☐ Municipal Government
   - ☐ University/College
   - ☐ Secondary School
   - ☐ Trade/Vocational School
   - ☐ Manufacturing
   - ☐ Sales
   - ☐ Research
   - ☐ Consulting
   - ☐ Medicine
   - ☐ Professional Society
   - ☐ News Media
   - ☐ Information Sciences/Library
2. Please check the number of employees in your organization: ☐ Under 25 ☐ 25-100 ☐ 100-500 ☐ Over 500
3. Please indicate if your position is one of the following: ☐ Owner or Chief Executive Officer ☐ Administrator/Manager ☐ Scientist ☐ Engineer ☐ Other ________

[PLEASE PRINT]

NAME ________ TITLE ________

COMPANY ________ PHONE ________

&

STREET ADDRESS ________ CITY ________ STATE ________ ZIP ________

FEEDBACK — YOUR COMMENTS

WINTER
1980

WE NEED YOUR HELP!

Our ultimate goal is to provide you with solutions to your day-to-day technical problems. Are we meeting that goal? Tell us how Tech Briefs has helped you, or how it can be made more useful. We are especially interested in brief descriptions of specific instances where Tech Briefs has either helped you solve a problem or been applied to your product line.

____

____

____

____

If you need more space, write us a letter at the address on the front of this card.

[PLEASE PRINT]

NAME ________ TITLE ________

COMPANY ________ PHONE ________

&

STREET ADDRESS ________ CITY ________ STATE ________ ZIP ________

TSP REQUESTS

WINTER
1980

Please send me the Technical Support Package (TSP) for the Tech Brief articles circled below:

☐ I would like information about NASA's Industrial Applications Centers and other NASA TU services.

I am requesting these TSP's for:

☐ Current Awareness
☐ Product Development
☐ Other ____________
☐ Process Improvement
☐ Problem Solving

Approximately how many TSP's have you requested from NASA in the last five years?

☐ 0 to 10 ☐ 11 to 25 ☐ over 25

[PLEASE PRINT]

NAME ____________
TITLE ____________
COMPANY & STREET ADDRESS ____________ PHONE ____________
CITY ____________ STATE ______ ZIP ______

1	2	3	4	5	6	7	8	9	10	11	12	13	14	15	16
17	18	19	20	21	22	23	24	25	26	27	28	29	30	31	32
33	34	35	36	37	38	39	40	41	42	43	44	45	46	47	48
49	50	51	52	53	54	55	56	57	58	59	60	61	62	63	64
65	66	67	68	69	70	71	72	73	74	75	76	77	78	79	

TSP REQUESTS

WINTER
1980

Please send me the Technical Support Package (TSP) for the Tech Brief articles circled below:

☐ I would like information about NASA's Industrial Applications Centers and other NASA TU services.

I am requesting these TSP's for:

☐ Current Awareness
☐ Product Development
☐ Other ____________
☐ Process Improvement
☐ Problem Solving

Approximately how many TSP's have you requested from NASA in the last five years?

☐ 0 to 10 ☐ 11 to 25 ☐ over 25

[PLEASE PRINT]

NAME ____________
TITLE ____________
COMPANY & STREET ADDRESS ____________ PHONE ____________
CITY ____________ STATE ______ ZIP ______

1	2	3	4	5	6	7	8	9	10	11	12	13	14	15	16
17	18	19	20	21	22	23	24	25	26	27	28	29	30	31	32
33	34	35	36	37	38	39	40	41	42	43	44	45	46	47	48
49	50	51	52	53	54	55	56	57	58	59	60	61	62	63	64
65	66	67	68	69	70	71	72	73	74	75	76	77	78	79	

COSMIC REQUESTS

WINTER
1980

I would like price and availability information about the computer program(s) circled below

A B C D E F G H J K L M N P R S

[PLEASE PRINT]

NAME ____________
TITLE ____________
COMPANY & STREET ADDRESS ____________
CITY ____________ STATE ______ ZIP ______

Please send me further information about software and services available from COSMIC. I am particularly interested in programs in the following areas:

____
____
____
____

National Aeronautics and
Space Administration

Washington, D.C.
20546

Official Business
Penalty for Private Use $300

NASA

NO POSTAGE
NECESSARY
IF MAILED
IN THE
UNITED STATES

BUSINESS REPLY MAIL

FIRST CLASS PERMIT NO. 12028 WASHINGTON, D.C.

POSTAGE WILL BE PAID BY NASA

Director, Technology Transfer Division
P.O. Box 8757
Baltimore/Washington International Airport, MD 21240

National Aeronautics and
Space Administration

Washington, D.C.
20546

Official Business
Penalty for Private Use $300

NASA

NO POSTAGE
NECESSARY
IF MAILED
IN THE
UNITED STATES

BUSINESS REPLY MAIL

FIRST CLASS PERMIT NO. 12028 WASHINGTON, D.C.

POSTAGE WILL BE PAID BY NASA

Director, Technology Transfer Division
P.O. Box 8757
Baltimore/Washington International Airport, MD 21240

National Aeronautics and
Space Administration

Washington, D.C.
20546

Official Business
Penalty for Private Use $300

NASA

NO POSTAGE
NECESSARY
IF MAILED
IN THE
UNITED STATES

BUSINESS REPLY MAIL

FIRST CLASS PERMIT NO. 12028 WASHINGTON, D.C.

POSTAGE WILL BE PAID BY NASA

COSMIC
Computer Software Management and Information Center
Suite 112, Barrow Hall
Athens, GA 30602

National Aeronautics and
Space Administration

Washington, D.C.
20546

Official Business
Penalty for Private Use, $300

THIRD-CLASS BULK

THIRD-CLASS BULK RATE
POSTAGE & FEES PAID
NASA
WASHINGTON, D.C.
PERMIT No. P-154

NASA

An engineer for a Kansas City, Missouri, corporation peers through a maze of steam and water lines — a model of a flow network that will eventually be part of a powerplant. The MEL-21 computer program, available from NASA's Computer Software Management and Information Center [COSMIC], saves design time and effort in this and other projects by analyzing pipe stresses due to temperature, weight, and flow pressure. [See the bottom of page A1.]